THEORY OF AUTOMATIC CONTROL

General Editor A. NETUSHIL, D.Sc.

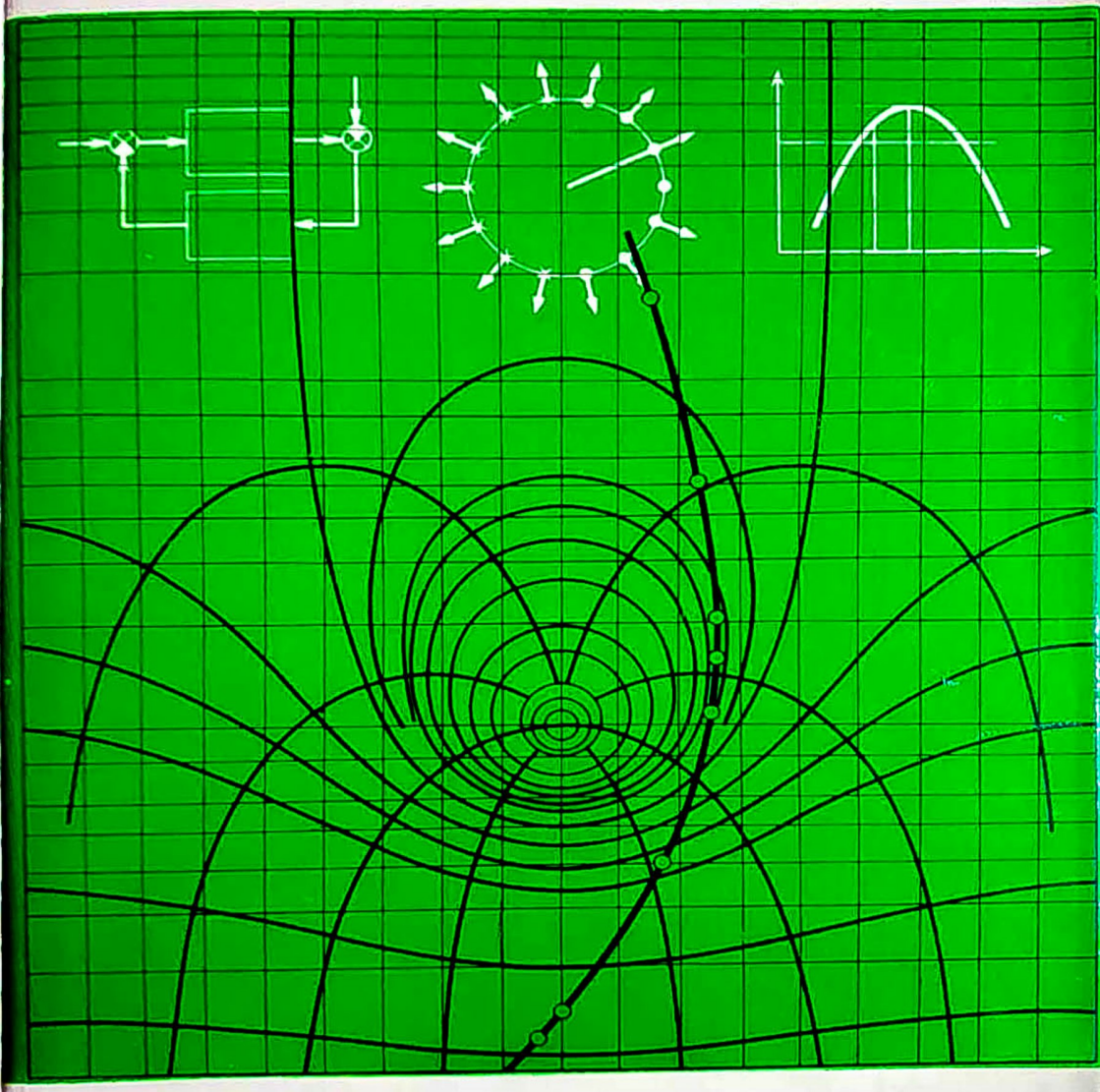

MIR PUBLISHERS

THEORY OF AUTOMATIC CONTROL

This book is meant for students specializing in automation and telemechanics, computational, informational and measuring techniques. It includes the theory of linear, continuous and sampled-data automatic systems, theory of nonlinear and optimal automatic systems under deterministic actions, automatic control systems under random actions and elements of the theory of self-adjusting systems. The book is richly illustrated with examples and drawings. The text may be of use to engineers working with automatic control and regulation systems.

Gen.Ed.
A.NETUSHIL
D.Sc.

ИЗДАТЕЛЬСТВО
МИР

ТЕОРИЯ АВТОМАТИЧЕСКОГО УПРАВЛЕНИЯ

Под общей редакцией А. В. НЕТУШИЛА

Издательство «Высшая школа»

Москва

THEORY OF AUTOMATIC CONTROL

General Editor

A. NETUSHIL, D.Sc.(Eng.)

Contributors:

L. GOLDFARB

A. BALTRUSHEVICH

G. KRUG

A. NETUSHIL

E. PASTERNAK

N. ALEKSANDROVSKY

R. KUZIN

V. BURLYAEV

MIR PUBLISHERS MOSCOW

UDC 62-50(075.8)=20

Translated from the Russian
by
ALEKSANDR PARNAKH

Translation editor
VALERY SOKOLOV, Cand.Sc.(Eng.)

First published 1973
Revised from the 1972 Russian edition

На английском языке

© English translation, Mir Publishers, 1973

H $\frac{3313-219}{041(01)-73}$

PREFACE

This book is an extension and refinement of the lectures delivered by the authors in the Moscow Power Institute for students specializing in Automation and Remote Control, Computer Engineering, Information and Measurement Technology, Electric Drives and Automation of Industrial Facilities.

It is a textbook on Automatic Control Theory written to implement a program approved by the Ministry of Higher and Secondary Specialized Education of the USSR.

The selection and presentation of the material was greatly influenced by lectures delivered by Professors L. S. Goldfarb and Ya. Z. Tsypkin in the Moscow Power Institute over many years. The subject matter of some of Goldfarb s lectures is included in the book.

The sequence of presentation is the result of studying the logical relations between the various parts of the curriculum. In this book the material is presented so as to minimize the time gaps between logically related parts of the curriculum.

The readers are presumed to be familiar with the relevant parts of the curriculae on Theoretical Fundamentals of Electrical Engineering, Higher Mathematics, Theoretical Mechanics, and Computer Engineering. They are also supposed to know the plants and some principles of automatic control as described in the curriculae on Electrical Machines, Electrical Measurements, Magnetic and Electronic Elements of Control Hardware.

The curriculum on Automatic Control underlies the subsequent curriculae on Automatic Measuring Devices, Controllers and Servo Systems, Information-and-Control Systems, etc.

Programs are to be carefully coordinated to prevent duplication. Apart from the required branches of higher mathematics, students of the theory of automatic control should know the mathematical description of processes in electrical machines, measuring devices, electronic and magnetic amplifiers and be familiar with analog computers.

This is abridged translation of the two parts of the textbook published by the Higher School Publishing House in 1968 and 1972, respectively.

CONTENTS

Chapter I

GENERAL DESCRIPTION OF PLANTS AND AUTOMATIC CONTROL SYSTEMS

1.1. Introduction 13
1.2. The Plant 14
1.3. Examples of Plants 17
1.4. Functional and Structural Diagrams of Plants 27
1.5. Principles of Automatic Control 30
1.6. Examples of Continuous Control Systems and Their Functional Diagrams 35
1.7. General Considerations on Methods of Process Study in Automatic Control Systems 40

Chapter II

PROPAGATION OF REGULAR SIGNALS THROUGH LINEAR ELEMENTS

2.1. General Characteristics of Regular Signals and Linear Elements 42
2.2. Regular Signals 43
2.3. Equations of a Linear Element 45
2.4. Characteristics of a Linear Element 46
2.5. Examples of Transfer Functions 53
2.6. A Common Property of Minimal-Phase Stable Elements 57
2.7. Transformation of an Arbitrary Signal by a Linear Element 60

Chapter III

TYPICAL ELEMENTS OF LINEAR CONTROL SYSTEMS

3.1. Typical Linear Elements. General 63
3.2. Simple Elements 64
3.3. First-Order Elements 70
3.4. An Oscillator 81

Chapter IV

SPECIAL ELEMENTS OF LINEAR AUTOMATIC CONTROL SYSTEMS

4.1. Special Features of Linear Element Responses 86
4.2. Stable Nonminimal-Phase Elements 86

4.3. Unstable Elements 89
4.4. Irrational Elements 91
4.5. Delay Elements 98

Chapter V

LINEAR ELEMENTS CONNECTION

5.1. General 102
5.2. Series Connection of Elements 103
5.3. Determining the Parameters of a Minimal-Phase System by Its Amplitude-Frequency Response 107
5.4. Parallel Concordant (Feedforward) Connection 112
5.5. Parallel Contrary (Feedback) Connection 115
5.6. Models of Standard Linear Elements 118

Chapter VI

EQUATIONS OF AUTOMATIC CONTROL SYSTEMS

6.1. Structural Diagrams and Transfer Functions of Elementary Control Systems 121
6.2. Transformations of Structural Diagrams 130
6.3. Structural Diagrams and Transfer Functions of Two-Variable Control Systems 135
6.4. Transfer Function of a Circuit Between Any Points 140

Chapter VII

STABILITY OF CONTROL SYSTEMS

7.1. Stability of Linear Control Systems. Statement of the Problem . . 142
7.2. Algebraic Criteria of Stability 143
7.3. Frequency Criteria of Stability 150
7.4. The Extension of the Nyquist Criterion to Irrational and Transcendental Systems 164
7.5. Comparison of Stability Criteria 169

Chapter VIII

THE EFFECT OF SYSTEM'S PARAMETERS ON ITS STABILITY

8.1. Statement of the Problem 170
8.2. The Root Locus Method 170
8.3. *D*-Decomposition Method 178
8.4. Decomposition by One (Complex) Parameter 179

Chapter IX

CONTROL PERFORMANCE: DIRECT METHODS OF STUDY

9.1. Performance Indices 183
9.2. Control Performance with Standard Actions 188
9.3. Forced Component of the Error 199
9.4. Astatic Order of Control Systems 203
9.5. Frequency Technique for Calculating Control Processes 207

Chapter X

CONTROL PERFORMANCE: INDIRECT METHODS OF STUDY

10.1. General 217
10.2. Frequency Methods of Studying Control Performance 218
10.3. Integral Estimates of Transient Performance 229

Chapter XI

DESIGN OF LINEAR CONTROL SYSTEMS

11.1. General Description of Problems 241
11.2. Compensating Units Based on Logarithmic Responses 244

Chapter XII

SAMPLED-DATA CONTROL SYSTEMS. EQUIVALENT CIRCUITS, SPECTRA AND IMAGES OF PULSE SIGNALS

12.1. Examples of Sampled-Data Control Systems 260
12.2. Equivalent Diagram of a Sampled-Data Control System 266
12.3. Discrete Signal Spectra and Images 270

Chapter XIII

SAMPLED-DATA CONTROL SYSTEMS. SIGNAL PROPAGATION. COMPLEX GAINS. TRANSFER FUNCTIONS

13.1. Signal Propagation Through a Sampled-Data Control System . . 283
13.2. Complex Gains and Transfer Functions of Open-Loop Sampled-Data Control Systems 285
13.3. Complex Gains and Transfer Functions of Closed-Loop Sampled-Data Systems 299

Chapter XIV

SAMPLED-DATA CONTROL SYSTEMS. STABILITY, TRANSIENT AND STEADY-STATE PROCESSES

14.1. Stability of Sampled-Data Control Systems 305
14.2. Determining Signal Variation Laws in Sampled-Data Control Systems 316
14.3. Indirect Methods of Performance Estimation, and Synthesis of Sampled-Data Control Systems 330

Chapter XV

NONLINEARITIES IN CONTROL SYSTEMS: GENERAL

15.1. Introduction 337
15.2. Examples of Inherent Nonlinearities 338
15.3. Systems with Deliberately Introduced Nonlinearities 345
15.4. Examples of Systems Controlling Plants with Nonmonotonic (Extremal) Responses 349
15.5. Nonlinear Elements of Control Systems 354

15.6. Standard Nonlinear Elements 356
15.7. Linearization of Standard Nonlinear Elements by Periodic Oscillations (Vibrational Linearization) 367
15.8. Nonstandard (Singular) Elements of Nonlinear Systems 370

Chapter XVI

NONLINEAR SYSTEM STATICS. CONNECTION AND TRANSFORMATION OF NONLINEAR ELEMENTS

16.1. Specific Features of Response of Nonlinear Element Connections 378
16.2. Series Connection 380
16.3. Parallel Feedforward Connection 385
16.4. Parallel Feedback Connection 387
16.5. Steady-State Misalignment (SSM) of Nonlinear Control Systems 390
16.6. Transformation of Nonlinear System Structural Diagrams 392
16.7. Equivalent Circuits of Multivalued Nonlinearities 395
16.8. Small Parameters of Actual Inertialess Elements 396
16.9. Models of Nonlinear Elements 399

Chapter XVII

NONLINEAR SYSTEM DYNAMICS. PHASE PLANE

17.1. Equations of Nonlinear Dynamic Systems. State Space 402
17.2. The Phase Plane and Its Properties 408
17.3. System Behaviour at Small Deflections from Equilibrium 415
17.4. System Behaviour at Large Deflections. Self-Oscillations 434
17.5. Piecewise-Linear Systems 454
17.6. Point Transformation Method 470

Chapter XVIII

HARMONIC LINEARIZATION

18.1. The Method of Harmonic Linearization. General 484
18.2. Complex Gain of a Nonlinear Element 486
18.3. Analysis of Symmetrical Self-Oscillations in Nonlinear Systems 494
18.4. Analysis of Nonsymmetrical Self-Oscillations in Nonlinear Systems 499
18.5. Conditions for Absence of Monoharmonic Self-Oscillations in Nonlinear Systems 504
18.6. Improvement of Harmonic Linearization Accuracy 506
18.7. Application of the Harmonic Linearization Method in the Presence of Several Nonlinearities 512
18.8. The Use of the Harmonic Linearization Method in the Studies of Nonlinear Sampled-Data Systems 517

Chapter XIX

STABILITY OF NONLINEAR SYSTEMS

19.1. Concept of Stability in Nonlinear Systems 530
19.2. Lyapunov's Direct Method 537

19.3. The Criterion for Absolute Stability of Equilibrium 542
19.4. Extension of the Absolute Stability Criterion to Certain Multivalued Nonlinearities 549
19.5. Absolute Stability of Processes 553
19.6. Absolute Stability of Sampled-Data Systems 555
19.7. Comparison of Stability Analysis Methods in Nonlinear Systems 558

Chapter XX

CONTROL PERFORMANCE IN NONLINEAR SYSTEMS

20.1. Specific Features of Nonlinear Systems Performance 561
20.2. The Method of "Passing Solutions" in Construction of Transient Processes in Nonlinear Systems 561
20.3. Difference Methods of Constructing Transient Processes in Nonlinear System 566
20.4. The Effect of Nonlinearities on Transient Processes 574
20.5. Harmonic Linearization as a Tool in Analyzing Control Performance 584
20.6. Criterion for Absolute Stability as an Aid in Analyzing Control Performance 587
20.7. Specific Features of Synthesis of Nonlinear Control Systems . . . 589

Chapter XXI

PROBLEMS AND METHODS OF OPTIMAL CONTROL: GENERAL

21.1. Statement of the Problem 591
21.2. Examples of Optimal-Control Problems 594
21.3. Design of Simple Response-Optimal Second-Order Systems . . . 601
21.4. Quasi-Optimal Control Techniques 607

Chapter XXII

THEORETICAL METHODS OF OPTIMAL CONTROL

22.1. General 613
22.2. The Euler Equation in Solving Optimal-Control Problems 614
22.3. The Maximum Principle in Solution of Optimal Control Problems 629
22.4. Dynamic Programming and Its Application to Optimal Control . 649
22.5. Comparison of Optimal Control Methods 660

Chapter XXIII

RANDOM SIGNALS IN CONTROL SYSTEMS

23.1. General 661
23.2. Examples of Random Signals and Their Characteristics 663
23.3. Mean Correlation Time and Mean Frequency Band of Random Signals 677
23.4. Cross-Correlation Functions and Spectral Densities of Random Signal 678
23.5. Determining Statistical Characteristics of Random Signals by Their Samples on an Interval of Length T_s 681

Chapter XXIV

LINEAR SYSTEMS SUBJECTED TO RANDOM STATIONARY SIGNALS

24.1. A Random Signal Propagating Through a Linear Element 690
24.2. Problems Involved in Study of Linear Systems Subjected to Stationary Random Signals 696
24.3. Finding the Parameters of an Optimal (in Terms of Minimal R.M.S. Error) Servo System 703
24.4. Synthesis of Accuracy-Optimal Systems Subjected to Stationary Random Actions 706
24.5. Transformation of a Distribution Law by a Linear Element . . . 710

Chapter XXV

NONLINEAR SYSTEMS SUBJECTED TO RANDOM STATIONARY SIGNALS

25.1. Random Signal Propagation Through a Nonlinear Element . . . 716
25.2. Distribution Density Transformation 716
25.3. Transformation of Mean Value (First-Order Moment or Mathematical Expectation) 724
25.4. Transformation of Dispersion (Second-Order Moment) 725
25.5. Transformation of Correlation Functions 727
25.6. Input-Output Cross-Correlation Function for a Nonlinear Element 731
25.7. Statistical Linearization of Nonlinear Elements 732
25.8. Statistical Linearization of Nonlinear Feedback Systems 735

Chapter XXVI

ADAPTIVE CONTROL SYSTEMS

26.1. Basic Concepts, Definitions, Classification 741
26.2. Searching Systems. General 742
26.3. Methods to Determine the Objective Function Gradient 747
26.4. Search Methods with Separation of Trial and Operational Steps 752
26.5. Search Methods with Combined Trial and Operational Steps . . . 758
26.6. Extremal System Dynamics 762
26.7. General Characteristics of Systems with Models 771
26.8. Systems with a Reference Model 773
26.9. Systems with an Adjustable Model 775
Appendix 782
References 797
Subject Index 801

Chapter I

GENERAL DESCRIPTION OF PLANTS AND AUTOMATIC CONTROL SYSTEMS

1.1. INTRODUCTION

The course in the theory of automatic control is intended to familiarize the student with the general principles underlying the design of automatic control systems, with the processes taking place therein and methods employed to study these processes. The design principles are related to general laws of control, the significance of which extends far beyond the confines of technical problems. The theory of automatic control, however, has developed into a science in its own right, primarily through studying the control processes in technological facilities. In this book the principles of system study and control are presented as applied to control of various industrial facilities. The principles of control to be considered have broad implications and can be applied to studies of processes in entirely different cybernetic systems—biological, economic, social, and others.

Cybernetics, the science of optimal and purposeful control of complex systems, is based on studies of plants subjected to external disturbances, acquisition of the necessary data on processes inside the plants and generation of control actions ensuring a state of the plants optimal in a specified sense.

These "plants" may be living beings (animals and/or vegetation), groups of people, industrial enterprises, factories, workshops, machine tools, machines. Depending on the particular plant and the purpose of control, control systems may vary from simple regulators maintaining some quantity (for instance, voltage, temperature or pressure) at a constant level to complex systems incorporating dozens of computers which solve problems of optimal control for a set of plants.

The plants considered in this book are technical facilities, above all the simplest ones.

The science dealing with the control of technical facilities is referred to as *control engineering*.

The constituent parts of control engineering are the theory of information systems and the theory of automatic control. The for-

mer studies the acquisition and processing of data necessary for human control of a system, while the latter is concerned with control of a system without direct activity of man.

The problem of man's activity in a system controlling technical facilities is a separate field of control engineering known as Man-Machine interface problems.

The theory of automatic control is based on the theory of automatic regulation, which developed into a self-sustained field as late as 1940. *Regulation* is the simplest variety of control and may be defined as *maintaining a specified quantity characterizing the process at a given level* or as *variation of this quantity in accordance with a specified law.* In the latter case the plant's states or disturbances acting on the plant are measured so as to generate action on the plant's regulating unit (Ref. 5).

Control is a much more comprehensive concept. It is usually understood as *automatic implementation of a group of actions selected from among a set of feasible actions on the basis of available data and intended to maintain or improve the functioning of the plant in keeping with the goal of control* (Ref. 5).

A comparison of the definitions for regulation and control shows that all problems of regulation are essentially simpler cases of control problems.

Furthermore, the problems of automatic control include adaptation or self-adjustment of control systems to cope with the changes in their parameters or external disturbances, the problems of optimal operation in various conditions, automatic selection of the best operating model from among several possible ones, and other problems which are outside the scope of automatic regulation.

The theory of automatic control incorporates the theory of automatic regulation as the basic and most thoroughly elaborated part but it poses additional, more complicated problems, which will be discussed later.

In the beginning of the course the terms regulation and control are often synonymous but in the final part a clear distinction is drawn between them.

The theory of automatic control as a scientific subject is still in the making. Some problems which are outside the scope of automatic regulation remain obscure at this juncture.

1.2. THE PLANT

An automatic control system may be regarded as consisting of two main parts, the plant to be controlled and the control unit.

A plant may be either a controlled technical facility or a simpler control system. In the latter case we deal with a hierarchical control system, where a more complex control system incorporates a

simpler one or a subsystem as a plant. These elementary systems are usually regulation systems.

The state of the plant depends on a set of parameters which characterize both the effects of the environment and the control facilities and the processes inside the plant itself.

Some of these parameters are monitored during operation and are termed *observable variables*. Others, while exerting an effect on the operating mode of the plant, are not measured and are referred to as *unobservable variables*.

Those parameters which represent the effects of the environment on the plant are called *external actions*.

The external actions generated by the control unit are *control variables* or *control actions*.

The external actions coming from sources other than the control unit are termed *disturbances*. These may be classified into *loads* and *noises*. The presence of a time-variable load results from plant operation and a plant in principle cannot be made immune to it. Noises may be caused by undesirable side-effects and their reduction always improves the operation of the plant.

The observable variables which are subject to control are known as *controlled* or *output variables*. They normally define to a certain degree the qualitative characteristics of the process in the plant.

Generally a plant, P, can be shown as in Fig. 1.1*a* and *b*, where the set of observable variables is represented by the vector $\mathbf{Z} = \{z_1, z_2, \ldots, z_r\}$, the set of unobservable variables by the vector $\mathbf{F} = \{f_1, f_2, \ldots, f_k\}$, the set of control actions by the vector $\mathbf{U} = \{u_1, u_2, \ldots, u_n\}$, the set of output variables by the vector $\mathbf{Y} = \{y_1, y_2, \ldots, y_m\}$. If the mathematical description of the plant is given, then the set of equations which relate the controlled variables with all external actions is known as well.

The initial conditions being given, this set of equations permits finding the output controlled variables Y in terms of external actions U, Z, F.

If a plant has one control and one output variable, in other words, if the vectors U and Y have one coordinate each, the plant is a *simple*, or *single variable*. If there are several interrelated coordinates, the plant is termed *multivariable*.

Each plant can be regarded in statics or in dynamics. In the former case both the external uncontrollable actions Z and F and the control actions U are assumed constant and independent of time. The plant is then characterized by the relations of the output variables and external actions

$$\mathbf{Y} = \mathbf{Y}\{\mathbf{U}, \mathbf{Z}, \mathbf{F}\} \tag{1.1}$$

If a plant is subjected to harmonic external actions, then in steady state it may be described also by relations between time-

invariable quantities such as amplitudes and phases of harmonic actions. In this case it can be regarded as quasi-static, or stationary, and may be described by Eq. (1.1).

In studying the dynamics, the value of $Y(t)$ is investigated as a function of variable external actions $Z(t)$, $F(t)$, and $U(t)$. In this case Eq. (1.1) takes the form of a set of differential equations.

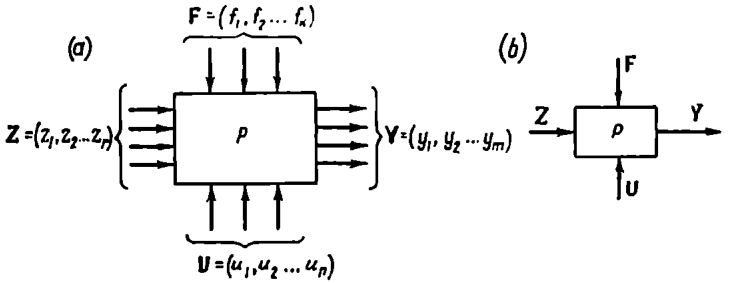

Fig. 1.1.

If this set can be reduced to a set of linear differential equations, the plant is referred to as *linear*, otherwise it is *nonlinear*.

In studying the statics, attention is focused on the relation of the controlled variable Y to the control action U. This characteristic

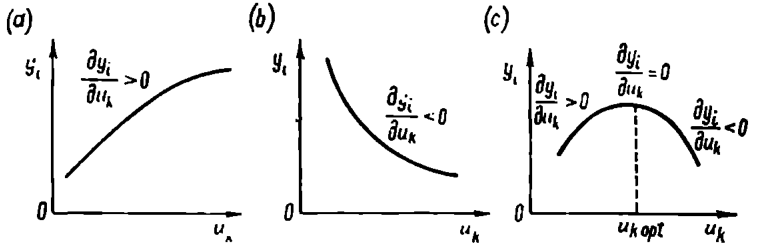

Fig. 1.2.

is called the *static control response*. The responses $y_i = y_i(u_k)$ may be either *monotonic* when $\frac{\partial y_i}{\partial u_k}$ never changes sign (Fig. 1.2*a* and *b*), or *extremal* when at a certain (usually optimal) value of the control variable $u_k = u_{k\,opt}$ the derivative $\frac{\partial y_i}{\partial u_k} = 0$ and changes sign.

A plant can be *stable*, *unstable*, or *neutral*.

A plant is *stable* if, following a short external action, it eventually returns to the initial state or to a state close to the initial one.

Nonlinear plants may be stable "in the small", that is at small external actions, but unstable "in the large", that is at large actions.

Static responses are meaningful for stable plants only. If in a stable plant the action, for instance Δu_k, continues for a period τ (Fig. 1.3), then the controlled variable y_i will within a certain time (for $t < \tau$) return to the initial state or one close to it.

Mechanically, plants of this kind can be simulated by a ball in a hole. The ball can be displaced but returns to its original position when the action responsible for the displacement ceases (Fig. 1.3*a*, bottom). Stable plants are sometimes described as *self-stabilizing.*

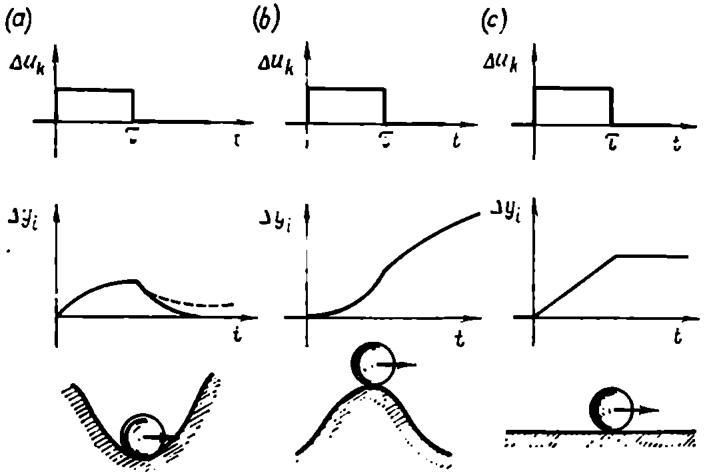

Fig. 1.3.

In an *unstable plant* the controlled variable continues changing even when the external action is removed, no matter how small it is. Mechanically, such plants are represented as a ball on the top of a hill (Fig. 1.3*b*, bottom). Even when the impulse ceases, the ball is still moving away from the equilibrium point.

Neutral plants are plants where, following the action, a new equilibrium is attained different from the initial one and depending on the action that has occurred. A ball on a horizontal plane is the mechanical analogy of this type of plant (Fig. 1.3*c*, bottom). Neutral plants are sometimes called *plants without self-stabilization.*

Depending on the operational conditions, the same plant with nonlinear response can be in a stable, unstable or neutral state.

Steady-state and transient processes in plants can be studied under regular and random external actions.

1.3. EXAMPLES OF PLANTS

Let us consider some simple examples of plants which will be used in further discussion to describe different principles of automatic control.

These are basically plants with monotonic response which are used in the control systems studied in the first part of the course.

Plants with extremal responses and more complex plants for which no mathematical description is available are discussed only

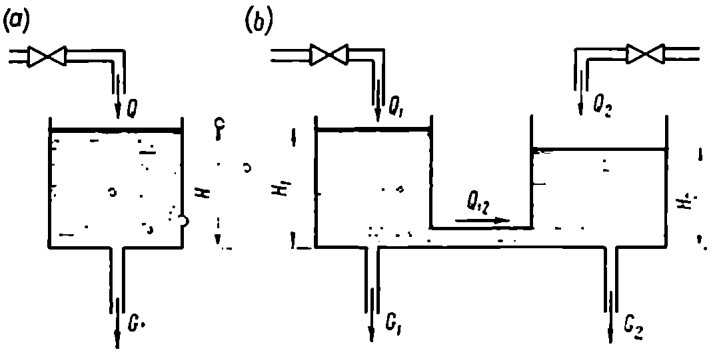

Fig. 1.4.

to the extent required for students to get a general idea of more involved control systems.

Hydraulic, electromechanical, thermal, and aeromechanical plants with monotonic response are considered in the order of increasing complexity of their mathematical description.

Examples of plant equations are given for simplest cases. A number of less important variables are neglected. Stability or instability is asserted without proof and in simple cases follows from first-order differential equations.

A hydraulic tank. An example of a simple plant is shown in Fig. 1.4*a*. The control action u is the rate of water inflow Q into the tank, the controlled variable y is the water level H in the tank, and external disturbance is the water outflow G.

The variables Q, H, and G are interrelated by the equation

$$S\frac{dH}{dt} = Q - G \tag{1.2}$$

where S is the tank cross section.

Equation (1.2) is the mathematical description of the simple plant under consideration. It is easy to see that the plant is neutral since at $Q = 0$, $G = 0$, and $H = H_0$ a short-term increase of Q (following the decrease of Q to zero) would lead to an increase in the level H and a transition to a new state, $H_0' > H_0$. This situation corresponds to the graph of Fig. 1.3*c*. The response of the plant is monotonic because $\frac{dH}{dt}$ increases with Q.

If there are two communicating tanks (Fig. 1.4*b*) the plant will be described by the set of equations

$$\left.\begin{aligned} S_1 \frac{dH_1}{dt} &= Q_1 - G_1 - Q_{12} \\ S_2 \frac{dH_2}{dt} &= Q_2 - G_2 + Q_{12} \end{aligned}\right\} \qquad (1.3)$$

where $Q_{12} = Q_{12}(H_1 - H_2)$ is generally a nonlinear monotonic function.

Equations (1.3) are a mathematical description of the plant. In this case each vector of controlled variables and actions has two components:

$$\mathbf{U} = \{Q_1, Q_2\}, \qquad \mathbf{Y} = \{H_1, H_2\}, \qquad \mathbf{F} = \{G_1, G_2\}$$

Each of the levels H_1 and H_2 depends on the quantities Q_1, Q_2, G_1, and G_2. Consequently, the plant is multivariable.

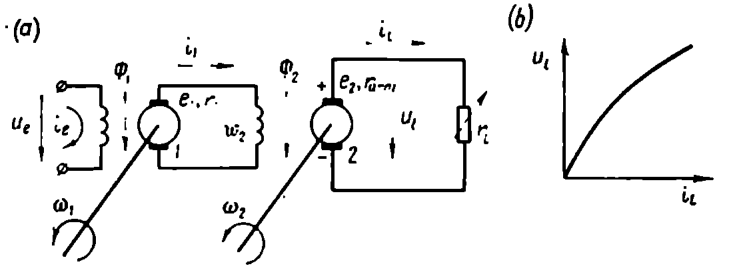

Fig. 1.5

A d.c. generator. In this example the controlled variable may be, depending on the problem, the current, the voltage or the power at the generator output.

In most cases it is the voltage at the generator terminals that must be maintained constant. The controlled variable is then the load voltage $y_1 = u_l$ (Fig. 1.5*a*).

The generator is controlled by the excitation winding. If main generator *2* has an auxiliary exciter *1* (see Fig. 1.5*a*), then the control variable u_1 is the excitation current i_e of the exciter. The external actions for the generator are: (1) changes in the rotation rate of the generator (ω_2) and the exciter (ω_1) shafts, (2) variations in the load resistance r_l or load current i_l, (3) the displacement of brushes relative to the generator poles, (4) the collector wear, (5) variations in the magnetic characteristics of the steel and the air gaps, etc. Some of these actions such as the load current i_l or rotation rates ω_1 and ω_2 are measurable and consequently may be classed with observable variables, while others are not measurable and therefore belong to the category of unobservable variables.

If the variable i_l is measured, while the variables ω_1 and ω_2 are not, then for the plant under consideration $z_1 = i_l$, $f_1 = \omega_1$, $f_2 = \omega_2$. The differential equations which relate u_l, i_l, ω_1, ω_2 and i_e thus give the mathematical description of the plant.

For the circuit of Fig. 1.5 these equations have the form

$$\left.\begin{aligned} \Phi_1 &= \Phi_1(i_e) \\ e_1 = c_1\omega_1\Phi_1 &= i_1 r_1 + w_2 \frac{d\Phi_2}{dt} \\ \Phi_2 &= \Phi_2(i_1) \\ e_2 = c_2\omega_2\Phi_2 &= u_l + i_l r_{arm} \end{aligned}\right\} \qquad (1.4)$$

where e_1 and e_2 are the emf's in the armatures of the auxiliary and the main generator, respectively; $\Phi_1(i_e)$ and $\Phi_2(i_1)$ are excitation characteristics of the generators.

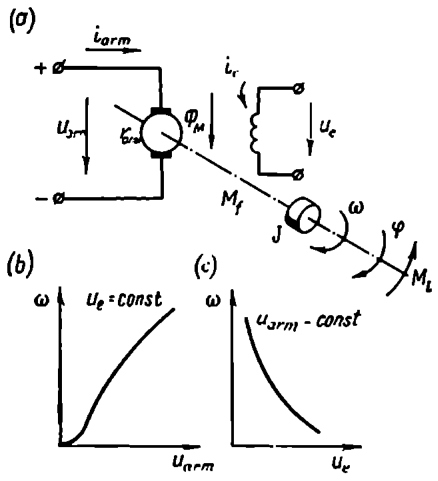

Fig. 1.6

These equations neglect the armature response, magnetic dissipation, eddy currents in the magnetic system, and a number of less important variables.

The proportionality coefficients c_1 and c_2 are the plant parameters and depend on the characteristics of armature windings and the position of the brushes relative to the generator poles.

With the initial conditions specified the set of equations (1.4) completely describes u_l as a function of i_e, i_l, ω_1, and ω_2 and can be used as a mathematical description of the plant.

For an electric generator with independent excitation the control response $u_l = u_l(i_e)$ is monotonic and the load voltage increases with excitation current (Fig. 1.5*b*).

The generator in question is a stable plant and its pulse response coincides with the one shown in Fig. 1.3*a*. If there is a hysteresis, then at the end of an excitation pulse the voltage at the generator terminals may be somewhat different from the initial value (see the dotted line in Fig. 1.3*a*).

A d.c. motor. The shaft rotation rate of a d.c. motor may be controlled by the armature or the excitation winding supply (Fig. 1.6*a*).

In the former case the control variable is the voltage u_{arm} or the current i_{arm} in the armature circuit and in the latter case, the voltage u_e or the current i_e in the excitation winding.

The controlled variable of the motor is normally the shaft rotation angle φ or the rotation rate $\omega = \frac{d\varphi}{dt}$, so $y_1 = \varphi$ or $y_1 = \omega$, respectively.

The external actions are forces acting on the motor shaft and caused by friction and inertia of the mechanism driven by the motor. If the motor is controlled by the armature supply, then changes in the voltage or the current of the excitation winding may be regarded as external actions and, conversely, if the control is by the excitation winding supply, it is changes in the voltage or in supply current of the armature that should be regarded as external actions.

If the control action u_1 is the armature supply voltage u_{arm}, then the value of the armature current can serve as an index of the load on the motor shaft, so the armature current i_{arm} may be used as the observable variable which characterizes the external actions z_1.

Unobservable actions for the motor are forces acting on the motor shaft, variations in the motor parameters caused by heating, mechanical action, wear, displacement of brushes, etc.

The processes in an electric motor may be described mathematically. The system of differential equations is

$$\left.\begin{aligned} \Phi_M &= \Phi_M(i_e) \\ u_{arm} &= i_{arm} r_{arm} + c_1 \omega \Phi_M \\ a_1 i_{arm} \Phi_M &= J \frac{d\omega}{dt} + M_f + M_l \\ M_f &= M_f(\omega) \end{aligned}\right\} \qquad (1.5)$$

Here $\Phi_M(i_e)$ and $M_f(\omega)$ are usually nonlinear functions.

J = the load mechanism inertia torque reduced to the motor axis

M_l = the load torque on the motor shaft

M_f = the friction torque on the motor shaft.

The proportionality coefficients c_1 and a_1 are the motor parameters and depend on its design. As in the case of a generator, the armature response, the magnetic dissipation, and the effect of eddy currents were neglected.

If control is provided by the armature supply, the motor control response $\omega = \omega(u_{arm})$ is monotonic and the shaft rotation rate increases with the armature supply voltage (Fig. 1.6*b*). When control is effected by excitation winding supply, the motor control response $\omega = \omega(u_e)$ is also monotonic, but the shaft rotation rate falls with increasing voltage on the excitation winding (Fig. 1.6*c*). Both phenomena follow directly from consideration of the set of equations (1.5) at $\frac{d\omega}{dt} = 0$ with monotonic functions $\Phi_M(i_e)$, $M_l(\omega)$, and $M_f(\omega)$.

Analysis of dynamic processes for an armature-controlled motor is much simpler than for an excitation-controlled motor since in the latter case Eqs. (1.5) include a variable coefficient, Φ_M, of the unknown variable ω.

In both methods of motor rate control, however, the plant is stable and its pulse response is similar to that shown in Fig. 1.3*a* (the dotted line represents the existence of friction in the system).

For an armature-controlled motor the value of $\frac{\partial y_t}{\partial u_h} = \frac{\Delta\omega}{\Delta u_{arm}}$ is positive, while for an excitation-controlled motor this value is negative.

As regards the changes in the angle φ

$$\varphi = \varphi_0 + \int_0^t \omega\, dt \tag{1.6}$$

the motor is a neutral system.

Let us assume that the initial position of the shaft is $\varphi_0 = 0$. Then a control voltage pulse will rotate the motor shaft by a certain angle. When this pulse ceases, the motor shaft will stop in a new position, $\varphi_1 = \int_0^t \omega\, dt$. Approximate plots of $u_{arm}(t)$ and $\varphi(t)$ for that case are given in Fig. 1.7.

An asynchronous motor. An asynchronous motor may be a stable or an unstable plant, depending on its operating point.

The control of an asynchronous motor in different operational conditions may proceed in different ways.

Let us examine the case of an asynchronous motor (Fig. 1.8*a*) with the load on the shaft characterized by inertial masses with an inertia moment J and load momentum M_l.

The motor is controlled by varying the three-phase supply voltage U having a frequency f.

The dependence of the momentum developed on the motor shaft, M_M, on the angular rotation rate, ω, is shown in Fig. 1.8*b*.

At a certain value of the rate, the momentum reaches a maximum value and then, with the rate approaching the synchronous one, reduces to zero at

$$\omega = \omega_0 = \frac{2\pi f}{n}$$

where n is the number of pole pairs.

The control variable in this case is the supply voltage, while the controlled variable is the motor shaft rotation rate.

The processes in a motor may be approximately described by the motion equation

$$M_M = J\frac{d\omega}{dt} + M_l \tag{1.7}$$

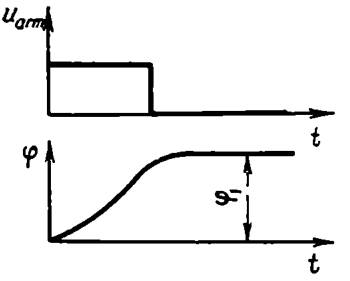

Fig. 1.7

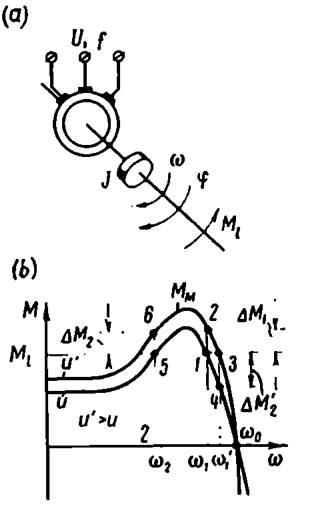

Fig. 1.8

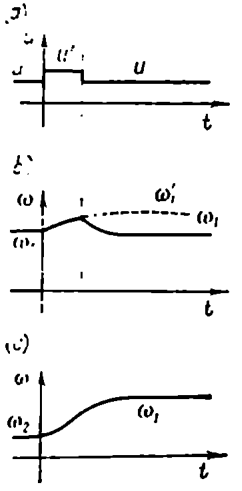

Fig. 1.9

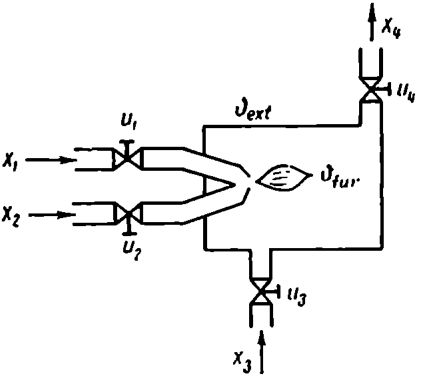

Fig. 1.10

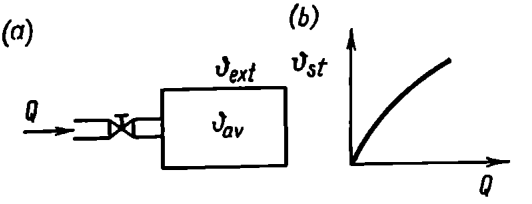

Fig. 1.11

or

$$J\frac{d\omega}{dt}=M_M-M_l=\Delta M \tag{1.7a}$$

If ΔM decreases with increasing motor rotation rate, the operation is stable. Conversely, if an increase in ω increases ΔM and, consequently increases the rate still further, then the operation is unstable.

Let us now consider the parameters of a plant characterized by the function shown in Fig. 1.8*b*. Assume for simplicity that M_l is independent of ω. Points *1* and *5* where $\Delta M=0$ $\left(\text{and consequently } \frac{d\omega}{dt}=0\right)$ correspond to stationary operation.

In point *1* and at rotation rate ω_1 an increase in voltage to $U_1'>U_1$ makes the motor accelerate at the rate $\frac{d\omega}{dt}=\frac{\Delta M_1}{J}$. The value of initial acceleration is defined by the segment *1-2* corresponding to ΔM_1 in a proper scale.

The rotation rate will increase until it reaches the value ω_1' (point *3* on the curve). The subsequent reduction of the control voltage to the initial value makes the value of $\Delta M_2'$ negative (segment *3-4*) and decelerates the motor to the initial rate ω_1.

The transient responses corresponding to this operation mode are shown schematically in Fig. 1.9*a*, *b* and are typical responses of stable plants.

In point *5* at $\omega=\omega_2$ a rise in voltage leads to increasing acceleration of the motor. The value of initial acceleration $\frac{d\omega}{dt}$ depends on the segment *5-6* representing ΔM_2. With the motor accelerating and the rate ω increasing, this value increases until the rate ω exceeds the value for which the momentum is maximal. Then $\frac{d\omega}{dt}$ decreases until the rate reaches the value ω_1' in point *3*. A reduction of voltage to the initial value does not affect the nature of the process. In this case the rate increases to ω_1. The transient responses of this unstable operation are displayed in Fig. 1.9*a*, *b*.

Furnaces (fuel- and electricity-powered). One of the more complex plants is a furnace heated by burning fuel (Fig. 1.10).

The controlled variable is the temperature in given points ϑ_{fur}. The control variables are the positions of valves u_1, u_2, u_3, u_4, which regulate the feeding of fuel, air, and the draught of exhaust gases. The external actions are variations in fuel composition and consumption, in air pressure, in the heating parameters, which depend on the furnace loading and unloading. Some of these values, such as consumption and temperature, can be measured but most of them cannot.

The thermal conditions of a furnace are described by a complex set of partial differential equations which usually give a rough idea of the nature of processes in the furnace.

The mathematical description of systems controlled exclusively by the fuel feed rate (in fuel furnaces) or by the power of electric heaters (in electric furnaces) may be approximated by first-order differential equations.

If Q is the amount of heat dissipated inside the furnace per unit time and ϑ_{av} is the average temperature of the furnace (Fig. 1.11*a*), then the heat balance equation can be approximately represented as

$$Q = g(\vartheta_{av} - \vartheta_{ext}) + C\frac{d\vartheta_{av}}{dt} \qquad (1.8)$$

where C = thermal capacity of the furnace
g = total thermal conductivity of the furnace-environment system (the environmental temperature is ϑ_{ext}).

The distributed nature of the system furnace-ingot is approximately represented by introducing a certain delay between the average temperature of the furnace, ϑ_{av}, and the temperature of the ingot or at a certain point of the furnace, ϑ, which is the controlled variable. Thus

$$\vartheta(t) = \vartheta_{av}(t - \tau) \qquad (1.9)$$

where τ is an equivalent delay time.

The furnace parameters g and C generally depend on temperature and may be assumed constant only in approximate calculations.

Unobservable variables are changes in the environmental temperature, ϑ_{ext}, in the thermal capacity of the furnace, C, and in the total thermal conductivity, g.

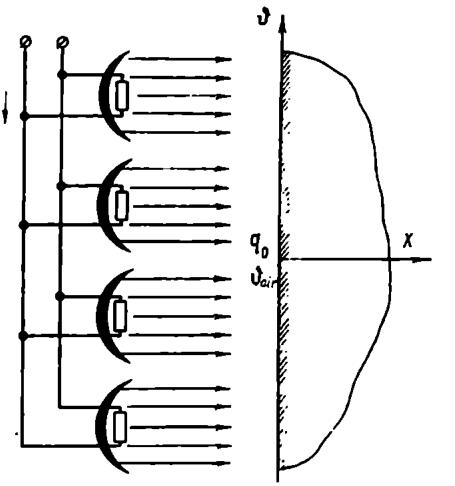

Fig. 1.12

The interrelation of the steady-state temperature, ϑ_{st}, of the furnace and the amount of heat, Q, dissipated in the furnace per unit time is expressed as a monotonic static control response (Fig. 1.11*b*).

To describe mathematically the process in electric furnaces with radiation-type heating of ingots is a somewhat more complicated matter. Figure 1.12 is a schematic representation of radiation heaters which raise the temperature of a massive body. The power dissipated per unit surface of an ingot in thermal units is

$$q_0 = kUI$$

where U and I = heater voltage and current, respectively
k = a factor depending on the heater and inversely proportional to the ingot surface.

The control action is the supply voltage U. The unit power

$$q_0 = q_0(U) \tag{1.10}$$

is a nonlinear function of supply voltage.

The controlled variable is the ingot surface temperature.

The external (chiefly unobservable) actions are the difference in the parameters of ingots, changes in the parameters of heat radiators and in the conditions of heat dissipation on the ingot surface.

The thermal conditions of surface heating are approximately described by the one-dimensional Fourier equation for a semibounded body

$$\lambda \frac{\partial^2 \vartheta}{\partial x^2} = c \frac{\partial \vartheta}{\partial t} \tag{1.11}$$

at the initial conditions

$$\vartheta(x, 0) = \vartheta_0(x) \tag{1.12}$$

and at the boundary conditions depending on heat exchange on the ingot surface

$$q_0 = -\lambda \frac{\partial \vartheta}{\partial x}(0, t) + q_{fl}[\vartheta(0, t), \vartheta_{air}] \tag{1.13}$$

In Eqs. (1.11-1.13) the following notation is used: c and λ are the unit thermal capacity and thermal conductivity of the ingot, respectively; x is the coordinate of the ingot point with reference to its surface; ϑ_{air} is the temperature of the air over the ingot surface; q_{fl} is the density of the heat flow from the surface of the ingot to the environment. The latter parameter depends on the surface temperature $\vartheta(0, t)$ and the environmental temperature ϑ_{air}.

The solution to these equations gives a rough idea of the transient processes in heating.

The furnaces described above are self-stabilizing stable plants.

Plants with extremal static response. Far from all plants have a monotonic control response. There are many plants for which the relation between the control and controlled variables has a clearly defined maximum or minimum. For instance, the relation between the speed of a car and the fuel consumption per kilometre or mile has a minimum at a certain optimal speed. A lower or a higher speed would lead to overconsumption of fuel. This minimum may be somewhat shifted depending on the engine adjustment or the road conditions.

Another example of a plant with extremal response is a system controlling the feed of the drill in well drilling. The rate of drill feed v depends on the pressure P on the drill, so that there is a certain

pressure P_{opt} at which the rate is maximal. At pressures lower or higher than P_{opt} the feed is below the maximum.

The control response is extremal in electrical facilities operating in resonance. Let us take the output stage of a radio transmitter as an example. A simplified diagram of the stage is shown in Fig. 1.13*a*.

The grid of the vacuum tube receives a voltage $u_1 = U_{1m} \sin 2\pi ft$. The voltage u_2 fed to the transmitting aerial depends on the resonant tuning of the load circuit of the tube.

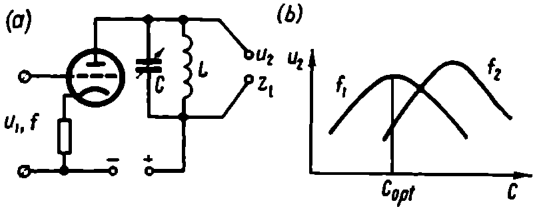

Fig. 1.13

The control parameter may be the variable capacity C. The controlled variable is the voltage u_2 across the aerial. At a certain optimal value of C this voltage across the aerial and consequently the radiation power at a specified frequency f_1 is maximal.

The control response of such a plant is shown in Fig. 1.13*b*.

With changes in frequency or in aerial capacity the response also changes (see the response curve at the frequency f_2). The external disturbing actions for this plant will be variations in the frequency f, in the complex radiation resistance z_1 of the aerial, in the supply voltage, and in other parameters of the system. Frequency may be either observable or unobservable. Parameter variations in the uncontrollable part of the circuit are normally unobservable.

The effect of the resonant circuit parameter variations is the greatest if the load is not the transmitter aerial, but a capacitor filled with a material heated by high-frequency currents. With the material parameters varying during the heating the control response changes noticeably and the maximum of the curve shifts.

1.4. FUNCTIONAL AND STRUCTURAL DIAGRAMS OF PLANTS

Control systems can be represented functionally or structurally, so their diagrams are subdivided into functional and structural.

A *functional* diagram is one where each functional element of the system is associated with a definite block.

A *structural* diagram is one where each mathematical operation of signal transformation is associated with a definite block.

All examples of plants given above can be represented by the general functional diagram shown in Fig. 1.1.

Each type of external action (U, Z, F) and the controlled variable Y can be represented by one arrow (see Fig. 1.1*b*).

Depending on the completeness of the mathematical description and on the mathematical operations performed by the different blocks, different structural diagrams can be drawn for each of these plants.

Let us consider structural diagrams that would represent some of the plants.

In order to give a structural representation of the hydraulic tank of Fig. 1.4*a* described by Eq. (1.2), it is sufficient to introduce the concepts of an integrator and an adder. The structural diagram of this plant is shown in Fig. 1.14*a*. Adder *1* is represented by a circle divided into four sectors. The sector receiving a positive addend is not darkened, while the one receiving a negative addend is.

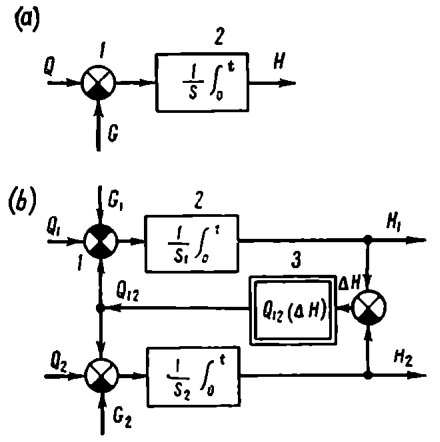

Fig. 1.14

The integrator is represented by block *2*.

Using the same principle to represent Eqs. (1.3) for two communicating tanks, we will have a more complex diagram of a two-variable plant shown in Fig. 1.14*b*. Apart from integrators and adders this figure shows (in a double frame) a nonlinear element, which transforms the quantity $\Delta H = H_1 - H_2$ into the outflow Q_{12}.

For the two-stage d.c. generator of Fig. 1.5*a* described by the system of four equations (1.4) the structural diagram is shown in Fig. 1.15, where the nonlinear relations $\Phi_1(i_e)$ and $\Phi_2(i_1 r_1)$ are represented by nonlinear elements *1* and *4*. The multiplication of the quantity Φ_1 by $c_1\omega_1$ and Φ_2 by $c_2\omega_2$ is represented by multipliers *2* and *5* marked by multiplication signs ($\times$). The subtraction of the quantity $w_2 \frac{d\Phi_2}{dt}$ from e_1 and $i_1 r_1$ from e_2 is effected by adders *3* and *6*. The operation of differentiation and multiplication by w_2 is represented by differentiator *7*. The diagram of Fig. 1.15 includes nonlinear elements, multipliers, differentiators, and adders.

For the d.c. motor of Fig. 1.6*a* described by the system of differential equations (1.5), the structural diagram of Fig. 1.16*a* is valid. This consists of adders and elements representing the operations of multiplication, nonlinear transformation and integration.

The two inputs, u_{arm} and i_e are to distinguish between armature-controlled and excitation-controlled motors. The output quantity is the rotation rate ω of the motor shaft.

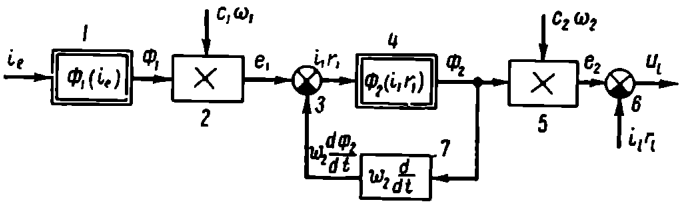

Fig. 1.15

The effects of the motor parameters a_1, r_{arm}, c_1 and the load moment M_l are represented in the diagram by the corresponding actions fed to the adders and multipliers.

For the asynchronous motor of Fig. 1.8 and described by Eq. (1.7) the structural diagram is given in Fig. 1.16*b*.

Since the motor moment is a nonlinear function of two variables (supply voltage U and the generator shaft rotation rate ω), the structural diagram of the plant contains a corresponding nonlinear element, $M_M(U, \omega)$.

If the load moment depends on the shaft rotation rate, then this dependence is expressed by the nonlinear element $M_l(\omega)$.

By using the above method one can construct an appropriate structural diagram for any plant with a given mathematical description. As an exercise the reader may construct structural diagrams for plants of Figs. 1.11 and 1.12.

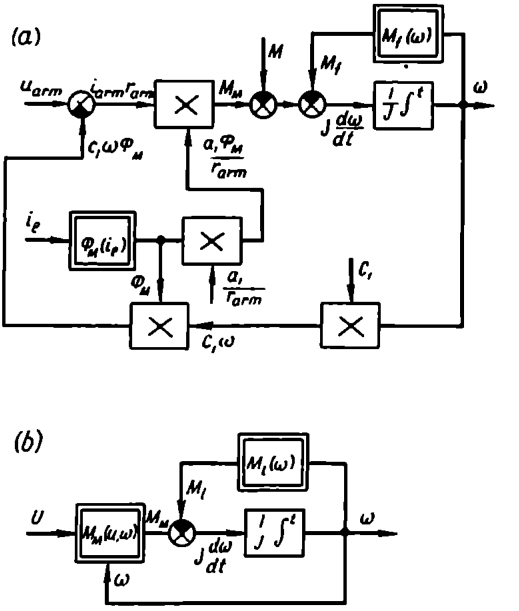

Fig. 1.16

The representation of the mathematical description of a plant as structural diagrams is very important for calculation and simulation of automatic control systems.

Most of the above plants have been described by nonlinear equations and their analysis is very difficult. The consideration of small increments of actions enables one to linearize the equations and considerably simplify them and the structural diagrams of the plants.

1.5. PRINCIPLES OF AUTOMATIC CONTROL

The principles of automatic control differ substantially depending on the nature of data characterizing the plant and obtained in the course of its operation, on the availability of the mathematical description of the plant, the static responses and, above all, on the problem facing the automatic control system.

If studies of the plant give an answer to the question, what to control, then new questions are posed, for what purpose, how, by what means the control is to be implemented.

The problems faced by the control system can be divided into the following groups:

1. *Stabilization of a controlled variable.* In this case some controlled variables should be maintained constant with a given accuracy.

2. *Program control of one controlled variable.* The law of the variation of a controlled quantity may be either known *a priori* and set by the operator of the system or it may automatically follow the variation law of a quantity unknown *a priori* but measurable. In the former case we have program control, in the latter case, servocontrol.

3. *System's self-adjustment to the optimal value of plant or system parameter.* The purpose of adjustment may be the achievement of either the extremal value of the controlled variable or the maximal speed of control or plant operating conditions optimal in a specified sense. Self-adjustment can be combined with stabilization and program control.

The control systems are classified into open-loop and closed-loop.

In *open-loop systems* the control action is set on the basis of the control purpose, the plant characteristics, and external actions without regard for the actual value of the controlled variable. This control is referred to as *hard.*

In *closed-loop systems* the control action is generated in direct relation to the controlled variable.

Open-loop control systems require that unobservable disturbances have no effect. These systems are used for stabilization and program control. The theory of open-loop systems, which is related to the theory of relay circuits and finite automata, is outside the scope of this curriculum, which is chiefly concerned with closed-loop systems.

Stabilization. Depending on the knowledge of the plant and external actions the stabilization problem can be solved in different ways. If all external actions are observable and measurable while the properties and dynamic responses of the plant are known, then control can be implemented on the basis of measurements of observable external actions. This control is referred to as *disturbance compensation* and is an example of an open-loop control system as shown in Fig. 1.17*a* where no unobservable actions are present ($F \approx 0$) and the problem of control is solved by finding the function

$$U = U(Z) \qquad (1.14)$$

with which the condition

$$Y = Y_0 = \text{const}$$

is satisfied. Y_0 is the setpoint of the controlled variable.

A controller solving this problem makes the controlled variables *stable* or *invariant* with respect to external actions.

If there are unobservable disturbances or the plant mathematical description is incomplete, disturbance compensation control cannot make the controlled variable stable. In this case a closed-loop *proportional control* is used. A schematic diagram of proportional control is shown in Fig. 1.17*b*.

The variation of the control variable depends on the difference between the controlled variable and the desired value and acts to reduce this difference.

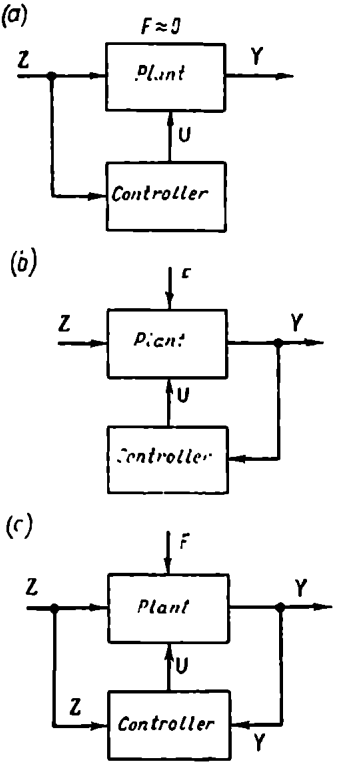

Fig. 1.17

To increase the accuracy of automatic control systems, both proportional and disturbance compensation controls (Fig. 1.17*c*) are often used at the same time.

In further discussion we will be chiefly concerned with control systems in the presence of unobservable disturbances since they require using the principle of proportional control so as to make the controlled variable practically independent of external actions.

Program control. Depending on the presence or absence of a mathematical description and unobservable external actions, program control can be performed by *open-loop* or *closed-loop systems.*

If an accurate mathematical description of a plant exists, while all external actions are observable and reducible to zero through

control by disturbance compensation, the program control can be performed by an *open-loop control system.* The law of the control variable variation will be specified so that the desired law of variation of the controlled variable is followed.

Let us require that the controlled variable y change in time by the law

$$y = y_0(t) \tag{1.15}$$

Then, by using equations describing the plant, the desired law of the control variable variation can be calculated

$$u = u_0(t) \tag{1.16}$$

A program facility setting this dependence ensures implementation of the desired law of the controlled variable variation.

The dependence $u_0(t)$ can be found automatically by a special computing unit. Figure 1.18*a* shows the diagram of an open-loop program control system. One of the system inputs is the desired control law $y_0(t)$. The dependence $u_0(t)$ is computed by the model and fed to the plant control.

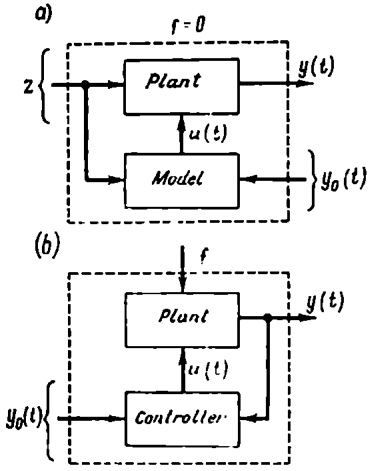

Fig. 1.18

Any inaccuracy in the mathematical description of the plant or the presence of an unobservable action disturbs the correspondence of $y(t)$ and $y_0(t)$ so that the desired law of controlled parameter variation is not obeyed.

In the presence of unobservable actions the principle of *program proportional control* is used. Systems where this approach is used are *closed-loop control systems.* In such systems the controller has two inputs, the desired law for changing of variation of $y_0(t)$ (setpoint) and the real value of the controlled variable $y(t)$ (Fig. 1.18*b*). These inputs are compared and a control action $u(t)$ is generated such that ensures the minimal value of the error

$$\varepsilon(t) = y_0(t) - y(t) \tag{1.17}$$

The smaller the error, the higher the performance of the controller.

In program controllers the function $y_0(t)$ is set by a certain program facility, while in servo systems this function is generally a certain (not known *apriori*) rotation angle of a shaft, the rate of shaft rotation or changes in any other physical quantity which should be reproduced with the minimum possible error.

In the latter case the control system, which consists of a plant and a controller, can be regarded as a plant of an open-loop control system (enclosed within the dotted line) where the input is $y_0(t)$ and the output is $y(t)$.

The above systems of automatic stabilization are particular cases of program control systems where the program is independent of time, i.e. $y_0(t) = \text{const}$.

Self-adjustment. Problems facing self-adjustment control systems are much more involved and versatile than those solved by program control systems.

The first problem is to maintain the extremal value of the controlled variable. To solve this problem, the plant receives trial

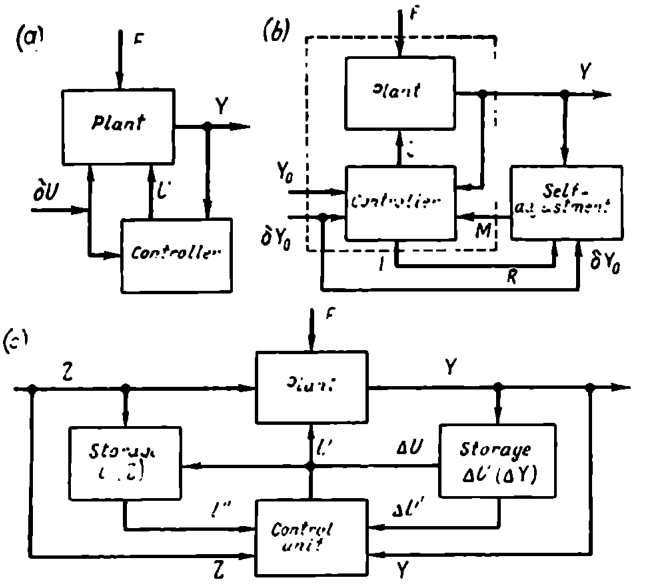

Fig. 1.19

control signals δU. The sign of variation of the controlled variable Y is analyzed and a control action is generated so that the operating conditions approach the extremum point. In this way the control system automatically maintains a near-optimal operating mode at which $\frac{\partial y_i}{\partial y_k} \approx 0$. Facilities providing near-optimal operating conditions are known as *automatic optimizers* or *extremal controllers.*

A diagram of extremal control is shown in Fig. 1.19*a*. This type of control is used with plants having extremal characteristics when there are substantial, but slowly changing unobservable actions resulting in variation of extremal characteristics.

Another problem requiring self-adjustment is the design of a control system which must operate at a maximal speed. In this case the index of the extremum is the time within which the system responds to changes in the setpoint. This time can be analyzed by a special self-adjustment facility. Receiving the analysis data the facility changes the controller parameters so that the control time is minimized. Such a system is shown schematically in Fig. 1.19*b*. The action which changes the controller parameters is denoted as M. In order to determine the control time trial variation of the controller setpoint δY_0 can be made.

The control time may be determined by using a plant model operating on a compressed time scale. In this case the model parameters are automatically aligned with those of the plant. The model may help to find a time-optimal control U, which is later implemented by the controller.

In the self-adjusting system of Fig. 1.19*b* the plant with a controller may be regarded as a new higher level plant having an extremal characteristic and controlled by a self-adjustment unit. The controlled variable of the system is the process transient performance computed by the self-adjustment unit on the basis of the quantities Y and R while the control variable is a certain adjustable parameter M of the controller. A self-adjusting system of this type can be represented as two systems where one controls the other.

To find optimal operating conditions in complex systems having many unobservable variables and no mathematical description various control conditions must be memorized. Experience is thus accumulated in learning how to control, as in self-learning systems of automatic control where different situations of control are stored in special facilities. Depending on the input and output, automatic facilities can select from the system's storage the appropriate controls and apply them to the plant. The control principle used may be either disturbance compensation or proportional control. At small values of unobservable variables F the control U is selected by using the values of Z, while at high values of F the variation ΔU of the control action is selected in accordance with the required variation ΔY of the controlled variable. A diagram of a self-learning system incorporating both control principles is shown in Fig. 1.19*c*.

Since self-adjusting systems combine the study and the control of the plant, they are termed *dual control facilities.*

Because of their complexity, self-adjusting systems have not been used extensively thus far. But the rapid progress in developing methods for making reliable computers and models for signal storage and transformation, the application of digital computers to control and manufacture of special-purpose control computers will give an impetus to construction of self-adjusting systems, which will probably be extensively used in the near future.

1.6. EXAMPLES OF CONTINUOUS CONTROL SYSTEMS AND THEIR FUNCTIONAL DIAGRAMS

Any control system can be represented by a set of elements performing specific functions: *1*—plant, *2*—measuring unit, *3*—setpoint unit, *4*—comparator, *5*—amplifier, *6*—actuator, *7*—correcting (compensating) unit.

All these elements except a correcting unit are shown in Fig. 1.20.

Plants have already been discussed in Section 1.3. A plant essentially differs from other elements of the system in that it is normally given and cannot be changed in developing the control system, while all other elements are specifically selected to solve the problem at hand.

All elements of a system apart from the plant constitute a *control unit* (or *regulator*).

Measuring units receive a signal which corresponds to the controlled variable. This signal is subtracted in the *comparator* from the *setpoint* given by a *setpoint unit*. The difference, termed the misalignment (error), is fed to the *amplifier*, whose output is fed to the *actuator* acting on the control variable.

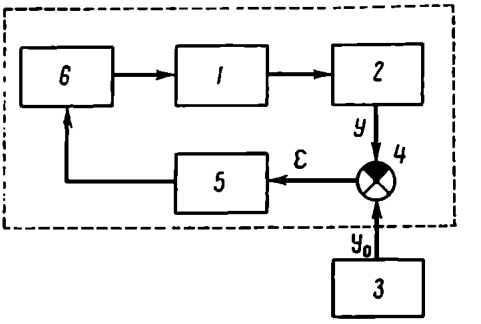

Fig. 1.20

Depending on the physical nature of the control and controlled variable, measuring units and an actuator may be left out of a control system. If the amplifier output is a control variable, then there is no actuator. If the output controlled variable can be fed directly to the comparator, then there is no measuring unit.

Aside from the above elements, systems sometimes include *compensating units*, which improve the system's characteristics (not shown in the figure).

Measuring units and amplifiers may be continuous or discrete, and comparators may be of the analog or digital type, respectively. In the former case all variables that are processed in the system elements are continuous in time; in the latter case they are discontinuous time functions and the sampling time is either specified by a special pulse unit (sampled data systems) or depends on the nonlinear characteristics of the elements in question (relay systems and variable structure systems). In this section we will deal with examples of continuous systems only.

Ball float level controller. One of the first controllers was a ball float level controller constructed by I. I. Polzunov in 1765 to maintain the water level in a steam boiler. Nowadays controllers of this

type are widely used in technology. A simple modern level controller is the float chamber of a car carburettor (Fig. 1.21*a*). The plant is chamber *1* where the gasoline level H is directly measured by the position of float *2*. A system of levers connects the float to needle valve *3* which regulates the gasoline inflow Q into the chamber. At $H = H_0$ the needle valve stops the inflow ($Q = 0$).

The external unobservable action is the gasoline outflow G to the carburettor jets.

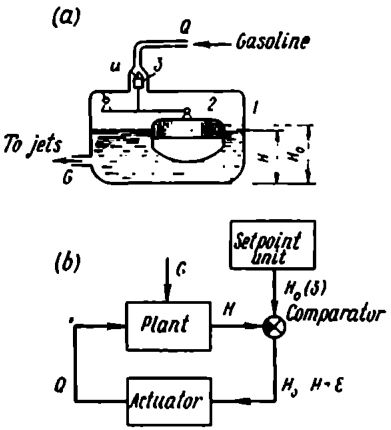

Fig. 1.21

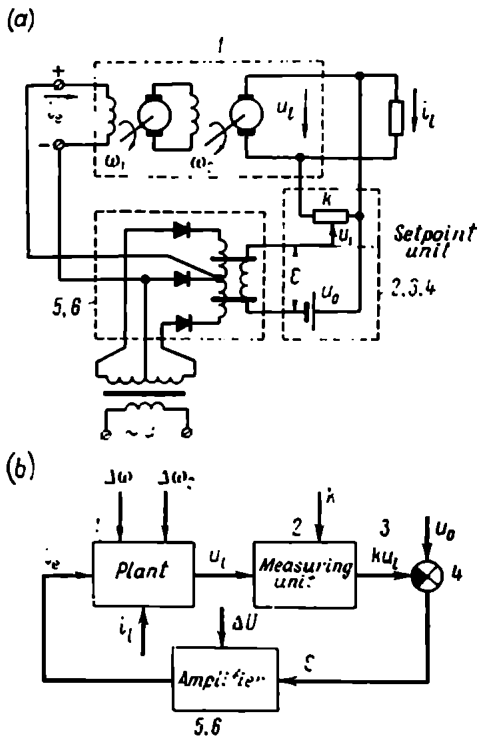

Fig. 1.22

A functional diagram of the controller is Fig. 1.21*b* illustrating two elements of the system: (1) the float chamber, which is a combination of a plant and a measuring unit receiving the difference $Q - G$ at the input and yielding the gasoline level H at the output, and (2) an actuator, which is the gasoline inflow channel setting the magnitude of Q and controlled by the position of the float and the movement of the needle valve.

Stabilization of a d.c. generator terminal voltage. Figure 1.22*a* is a flowchart of voltage stabilization at the terminals of a d.c. generator by a self-magnetizing magnetic amplifier. The control winding of the amplifier receives the value of the error, the difference between a reference voltage u_0 and a voltage u_1 obtained from a divider in proportion to the voltage at the generator terminals u_t. Thus

$$\varepsilon = u_0 - u_1 = u_0 - ku_t \qquad (1.18)$$

The load of the magnetic amplifier is current i_e in the excitation winding of the generator auxiliary exciter.

A setpoint is given by a coefficient k of the voltage divider.

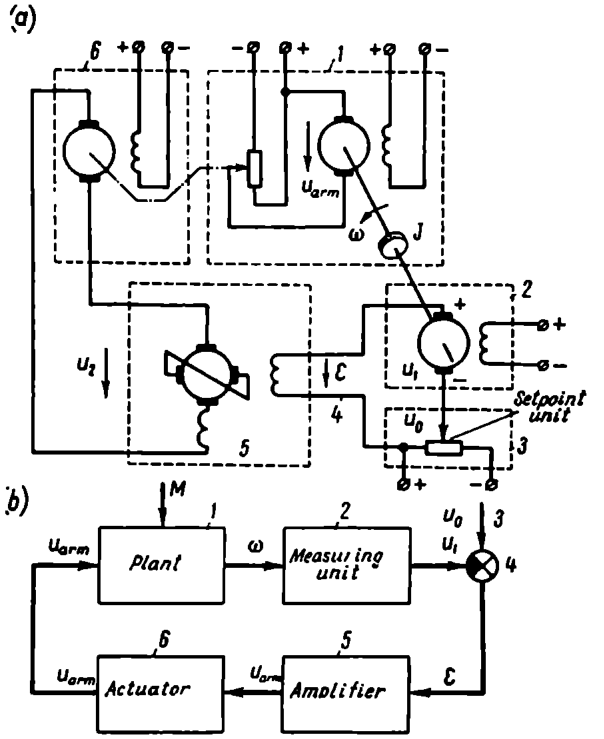

Fig. 1.23

The functional diagram of the control system is shown in Fig. 1.22*b*.

The controller combines measuring and setpoint units, while there is no actuator in the circuit since the load current of the magnetic amplifier is the control variable.

The disturbing unobservable actions are: voltage drop at the generator winding induced by the load current i_l; noises due to changes in the rotation rates $\Delta\omega_1$ and $\Delta\omega_2$ of the generator shafts, and in the magnetic amplifier supply voltage, etc.

Electric motor rotation rate controller. An amplidyne-based system controlling the rotation rate of an electric motor is shown in Fig. 1.23*a*.

The plant is a mechanism, *1*, driven by a d.c. motor. The shaft rotation rate of the motor should change by a specified law or it should be maintained constant. The rotation rate is measured by a

tachometric generator, *2*; the voltage u_1 at its terminals is proportional to the shaft rotation rate. This voltage is compared with the setpoint u_0, and the error $\varepsilon = u_0 - u_1$ generated in the loop *4-2-3* is fed to the excitation winding of amplidyne *5*. The amplidyne feeds the armature of motor-actuator *6*, which moves the voltage divider slide. The position of the slide is a control variable.

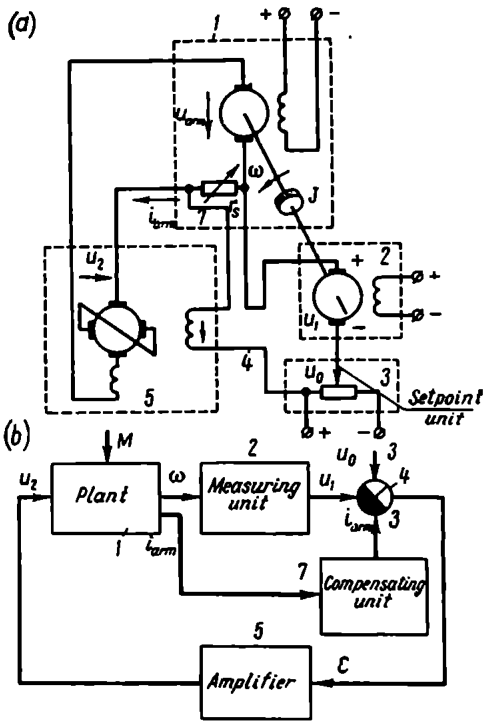

Fig. 1.24

A functional diagram of the system is shown in Fig. 1.23*b*. The external disturbance is a change in the load moment M on the shaft of the work motor.

At any load the actuator moves the voltage divider slide until the work motor gathers speed exactly equal to the setpoint and the actuating motor then stops. Under stationary conditions the error of an ideal system would be zero, or $u_0 = u_1$. In practice, due to friction the actuating motor has a dead zone which is a function of its start-up voltage. The difference between u_1 and u_0 depends on this zone and is insensitive to the external disturbance M.

If the power of the amplidyne is sufficient to feed the work motor of the system, then the control circuit can be somewhat simplified by eliminating the actuating motor and voltage divider and connecting the output terminals of the amplidyne directly to the armature of the work motor (Fig. 1.24*a*). In this case, as in the system of voltage control (see Fig. 1.22), each value of the controlled rate ω is associated with a certain value of the error. The error increases with the load moment M on the motor shaft.

With a view to decreasing this effect and improving the dynamic characteristics of the system, compensating loop *7* is used to introduce an additional voltage $r_s i_{arm}$ into the comparator loop in proportion to the armature current of the motor. The voltage increases with the load moment on the motor shaft. With appropriate choice of

the armature resistance r_s (see the flowchart), a high accuracy may be obtained in the control system. Because in this system the control action u_2 depends not only on the controlled variable ω but on the external action M monitored by the armature current i_{arm},

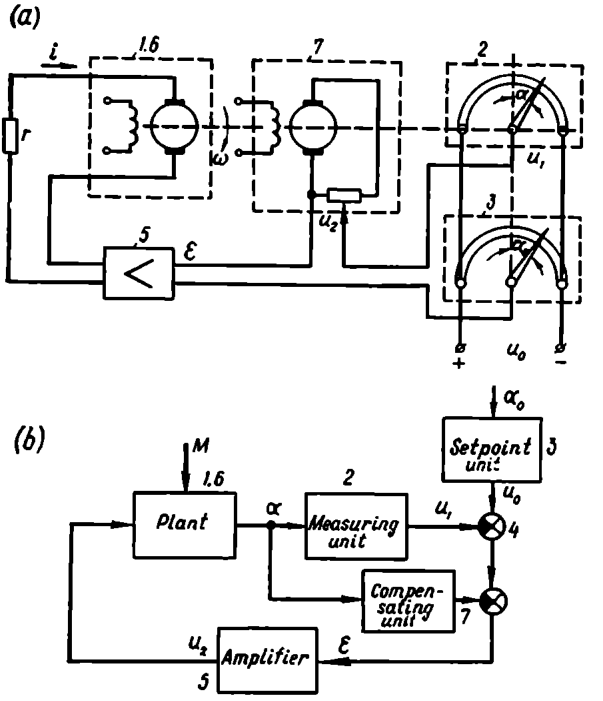

Fig. 1.25

the system combines proportional control and disturbance compensation control (see Fig. 1.18*c*). A functional diagram of the system is shown in Fig. 1.24*b*.

A servo system. A servo system controls the motor shaft (output axis) rotation angle. The setpoint is given by rotation of the reference shaft (reference axis). A simple diagram of the servo system is portrayed in Fig. 1.25*a*. Two voltage dividers, *2* and *3*, are connected with the reference and output axes. The voltages u_0 and u_1 taken from each of the dividers are proportional to the rotation angle α_0 or α of the axis. The difference of these voltages $u_0 - u_1$ in loop *4* is fed to amplifier *5*, which feeds the armature winding of actuating motor *1*, *6*. With any misalignment between the positions of the reference and output axes, an error voltage ε is generated at the amplifier input and induces a current in the armature winding of the actuating motor. The motor shaft rotates until the angle of the output

axis becomes equal to that of the reference axis and the error voltage drops to zero.

The stability of the entire system and the transient performance is improved by using compensating circuit 7, which includes a tachometric generator to measure the rotation rate ω of the motor shaft. The voltage u_2, which is proportional to ω, is fed to the comparator and added to the voltage u_1. In a static case, where $\omega = 0$, $u_0 = \text{const}$, $u_1 = \text{const}$, u_2 is zero. In a dynamic case, where $\omega \neq 0$, the compensating circuit slightly slows down the motor acceleration but suppresses self-oscillations in the system.

A functional diagram of the system in question is shown in Fig. 1.25*b*.

1.7. GENERAL CONSIDERATIONS ON METHODS OF PROCESS STUDY IN AUTOMATIC CONTROL SYSTEMS

We have heretofore discussed several primitive control systems for plants that were described by equations in Section 1.3 and by structural diagrams in Sec. 1.4. The specific pattern of a control system structural diagram may vary with the degree of idealization in the system equations and processes. Most of the above equations are nonlinear and their analysis is rather involved.

The characteristics of controllers may also be described nonlinearly. With small deviations of controlled variables from initial values and with insignificant nonlinearities of characteristics, however, actual nonlinear systems can be described by linear differential equations with accuracy sufficient for practical purposes. In these cases the analysis and synthesis of control systems is greatly simplified since these equations are a well-developed mathematical tool.

Processes described by nonlinear equations are much harder to study, but the knowledge of solutions for linear systems often facilitates solution for nonlinear ones.

Therefore methods of studying control systems will be considered first for linear and then for nonlinear control systems.

Depending on the nature of external actions and their mathematical description these actions can be classified into deterministic, or regular, described by definite time functions, and random, or stochastic, described by random functions.

Mathematical methods of system analysis and synthesis with different descriptions of external actions have a number of specific features and require somewhat different mathematical tools. Therefore methods for investigation of deterministic and random actions will be treated separately.

Control systems have already been shown to differ considerably as functions of control problems and plant characteristics. For those

plants having monotonic characteristics in the specified control range where the control problem is to reduce the difference between the desired and the actual value of some variable to zero or a minimum, stabilization or program control systems are used which can be referred to as *null-systems*. If control is to provide the extremum of a certain index with the system parameters varying, self-adjusting or adaptive control systems are used. These systems can be termed *extremal*. We will first take up null-systems with program control and then extremal systems with self-adjustment.

The first part of the curriculum deals theoretically with the most thoroughly elaborated problems related to linear systems of program control under deterministic external actions. Continuous systems will precede discontinuous linear systems.

Chapter II

PROPAGATION OF REGULAR SIGNALS THROUGH LINEAR ELEMENTS

2.1. GENERAL CHARACTERISTICS OF REGULAR SIGNALS AND LINEAR ELEMENTS

Any part of an automatic control system may be regarded as an element which converts an input signal into an output signal. If this element is a plant, then the input signals are control actions and external disturbances, while the output signals are controlled variables. If an elementary control system is regarded as part of a more complicated system, then the input signal is the setpoint and the output signal is the controlled variable.

An element which transforms a signal going in one direction only is a *directed action* or a *unilateral element*. Both a plant and an elementary control system are unilateral elements because variations

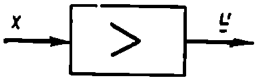

Fig. 2.1

of the controlled variable have no effect on the setpoint or the external actions.

Let us see how a signal goes through a unilateral element (Fig. 2.1) with an input x and an output y. With regular signals, x and y are definite time functions.

A differential equation relating x and y determines the characteristics of the element. For linear elements this differential equation is linear, and the corresponding relation can be expressed in terms of an operator function. Since actual systems are nonlinear and must be described by nonlinear differential equations, their linear representation is possible only in the case of smooth nonlinearities and small variations of x and y.

Let us first consider the problems of analysis and synthesis. The problem of analysis is stated in this way: given a signal $x(t)$ and the differential equation of the element, find the signal $y(t)$ at specified initial conditions.

Synthesis solves inverse problems, e.g. with the input signal $x(t)$ known it is required to find the element's characteristic satisfying given conditions and generating an output signal $y(t)$ meeting the desired requirements.

Whereas analysis problems for linear elements are unambiguous synthesis problems may be ambiguous and their solution is more involved. An important condition in the synthesis of linear systems is the feasibility of the element implementing the required equation.

2.2. REGULAR SIGNALS

Any complex signal can be represented as a set of simpler signals. We will use the following simple signals:

(a) a harmonic signal $\sin(\omega t + \psi)$;

(b) unit step $1_0(t) = \begin{cases} 0 \text{ at } t \leqslant 0 \\ 1 \text{ at } t > 0; \end{cases}$

(c) unit pulse $\delta(t) = \frac{d1_0(t)}{dt}$.

Let a signal be expressed by a time function $x(t)$. Then it can be represented as a set of harmonic signals by using a Fourier series for periodic signals and a Fourier transform for nonperiodic signals.

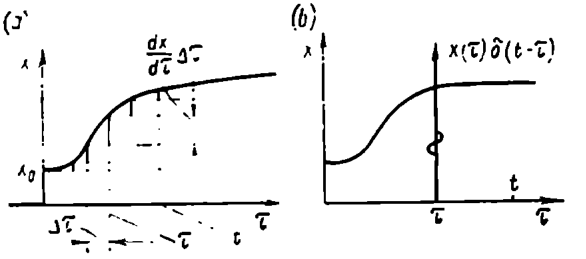

Fig. 2.2

By using the Duhamel integral in different forms the signal can also be represented as a set of unit steps

$$x(t) = x(\alpha)\, 1_0(t) + \int_0^t \frac{dx(\tau)}{d\tau} 1_0(t-\tau)\, d\tau \qquad (2.1)$$

as $\alpha \to 0$;
or as a set of unit pulses

$$x(t) = \int_0^t x(\tau)\, \delta(t-\tau)\, d\tau \qquad (2.2)$$

The expressions (2.1) and (2.2) are graphically illustrated in Fig. 2.2. Here $x(t)$ is represented as a set of steps with magnitude

$\frac{dx}{d\tau}\Delta\tau$ acting at times $\tau < t$ (Fig. 2.2*a*) or as the integral of the δ-function multiplied by the value of x at the time τ (Fig. 2.2*b*).

A linear system can be better studied with any signals if the signals are represented as a set of simple components. Then, using the superposition principle, the system response to each of the components can be found and the resulting output components summed up. For example, a signal can be represented as a set of integrals of unit steps acting either at the time $t = 0$

$$x(t) = A_0 1_0(t) + A_1 \int_0^t 1_0(t)\,dt + A_2 \int_0^t \int_0^t 1_0(t)\,dt^2 + \\ + A_3 \int_0^t \int_0^t \int_0^t 1_0(t)\,dt^3 + \ldots = 1_0(t) \sum_{i=0}^{n} \frac{A_i}{i!} t^n \qquad (2.3)$$

or at the time t_k

$$x(t) = 1_0(t - t_k) \sum_{i=0}^{n} \frac{A_i}{i!} (t - t_k)^n \qquad (2.4)$$

The plots for each of these components are given in Fig. 2.3.

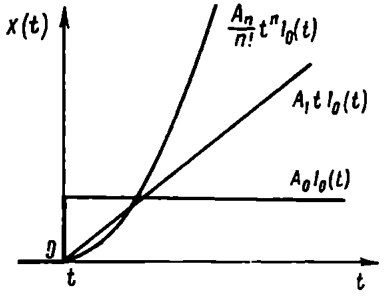

Fig. 2.3

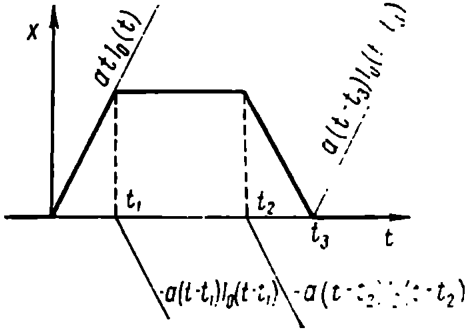

Fig. 2.4

We can also use a set of addends expressed by Eq. (2.4) for different t_k.

Example 2.1. Let the signal $x(t)$ be represented by the plot of Fig. 2.4. Find its expression as a set of unit steps.

By decomposing the signal into four components, each expressed by the function

$$x_k(t) = \pm a(t - t_k)\,1_0(t - t_k)$$

we obtain

$$x(t) = a\,[t1_0(t) - (t - t_1)\,1_0(t - t_1) - \\ - (t - t_2)\,1_0(t - t_2) + (t - t_3)\,1_0(t - t_3)] \qquad (2.5)$$

2.3. EQUATIONS OF A LINEAR ELEMENT

Generally a conventional differential equation of a simple single-variable element is given in the form

$$F(x, x', x'', \ldots, x^{(m)}, y, y', \ldots, y^{(n)}, t) = 0 \qquad (2.6)$$

where

$$x^{(i)} = \frac{d^i x}{dt^i} \quad \text{and} \quad y^{(i)} = \frac{d^i y}{dt^i}$$

If system parameters do not vary in time the function F is time independent.

For linear systems the function F is expressed by a linear relation and Eq. (2.6) takes the form

$$(b_0 x + b_1 x' + \ldots + b_m x^{(m)}) - (a_0 y + a_1 y' + \ldots \\ \ldots + a_n y^{(n)}) = 0 \qquad (2.7)$$

If the function F is smooth and arguments variations are small then the nonlinear relation between x and y can be reduced to a linear one.

Assume that at $t = 0$

$$x = x_0, \quad y = y_0, \quad x^{(i)} = x_0^{(i)} = 0 \quad \text{and} \\ y^{(i)} = y_0^{(i)} = 0 \quad \text{at } i \neq 0$$

Then Eq. (2.6) takes the form

$$F(x_0, x_0', \ldots, x_0^{(m)}, y_0, y_0', \ldots, y_0^{(m)}) = 0$$

Expanding the function F into a Taylor series in the vicinity of the points x_0, y_0 and $x^{(i)} = 0$, $y^{(i)} = 0$ for $i \neq 0$ and neglecting the higher-order terms of the expansion at $x = x_0 + \Delta x$ and $y = y_0 + \Delta y$ gives

$$k_0 \Delta x + k_1 \frac{d\Delta x}{dt} + \ldots + k_m \frac{d^m \Delta x}{dt^m} = d_0 \Delta y + d_1 \frac{d\Delta y}{dt} + \ldots + d_n \frac{d^n \Delta y}{dt^n} \qquad (2.8)$$

where

$$k_i = \left[\frac{\partial F}{\partial x^{(i)}}\right]_0, \qquad d_i = -\left[\frac{\partial F}{\partial y^{(i)}}\right]_0$$

The sign of F is assumed to be selected so that $d_n > 0$.

If the initial values of x and y are equal to x_0 and y_0, respectively, then Eq. (2.8) can be given in the form

$$\sum_{i=0}^{m} k_i \frac{d^{(i)} x}{dt^{(i)}} = \sum_{i=0}^{n} d_i \frac{d^{(i)} y}{dt^{(i)}} \qquad (2.9)$$

where x and y are understood as the increments Δx and Δy.

Direct Laplace transformation gives

$$K(p)\,X(p) = D(p)\,Y(p) \tag{2.10}$$

$$\left.\begin{aligned} K(p) &= \sum_{i=0}^{m} k_i p^i \\ D(p) &= \sum_{i=0}^{n} d_i p^i \end{aligned}\right\} \tag{2.11}$$

and the relation between frequency spectra $X(j\omega)$ and $Y(j\omega)$

$$K(j\omega)\,X(j\omega) = D(j\omega)\,Y(j\omega) \tag{2.12}$$

If the problem has nonzero initial conditions and at the time $t = 0$ both x and y and their derivatives may be nonzero, then direct Laplace transformation gives

$$X(p)\sum_{i=0}^{m} k_i p^i - \sum_{i=1}^{m} k_i \sum_{r=1}^{i} p^{r-1} x^{(i-r)}(0) =$$

$$= Y(p)\sum_{i=0}^{n} d_i p^i - \sum_{i=1}^{n} d_i \sum_{r=1}^{i} p^{r-1} y^{(i-r)}(0) \tag{2.13}$$

Most problems handled in control theory by the superposition principle reduce to zero condition problems. This is also facilitated by considering each action as a signal which starts to act only at $t > 0$, while at $t = 0$ it is zero, as are its derivatives. Naturally, allowance must be made for function discontinuities occurring immediately after the transition from zero to a region where $t > 0$.

A similar linearization of equations can be performed for complex (multivariable) elements. Depending on the number of input and output signals the element is described by sets of equations of the type (2.6), (2.9), (2.10). If, for instance, the element has two input signals, x_1 and x_2, and two output signals, y_1 and y_2, then Eq. (2.10) takes the form of the set of equations

$$\left.\begin{aligned} K_{11}(p)\,X_1(p) + K_{12}(p)\,X_2(p) &= D_1(p)\,Y_1(p) \\ K_{21}(p)\,X_1(p) + K_{22}(p)\,X_2(p) &= D_2(p)\,Y_2(p) \end{aligned}\right\} \tag{2.14}$$

2.4. CHARACTERISTICS OF A LINEAR ELEMENT

Depending on the statement of the problem linear element properties may be quantitatively described by the following interrelated characteristics: complex gain, transfer function, transient function, and weighting function.

Let us define each of these.

Complex gain of an element. The *complex gain of an element*, $\tilde{W} = W(j\omega)$, is the ratio of the complex amplitude of the output signal to that of the input signal in the case of a sine wave at the input.

From Eq. (2.12) the complex gain of a linear element is obtained as

$$\tilde{W} = W(j\omega) = \frac{\dot{Y}_m}{\dot{X}_m} = \frac{Y(j\omega)}{X(j\omega)} = \frac{K(j\omega)}{D(j\omega)} \tag{2.15}$$

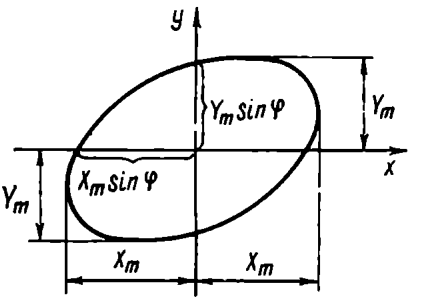

Fig. 2.5

An element is completely described by giving variations of its complex gain as the frequency varies from zero to infinity.

The locus made by the head of the complex gain vector as frequency varies from zero to infinity is the *frequency-gain locus* or *complex frequency response*. This quantity is sometimes referred to as the *amplitude-phase response* of the element.

The complex gain can be found experimentally if a sine voltage of definite amplitude and frequency is fed at the input and the signal amplitude and phase are measured at the output. For instance, if

$$x = X_m \sin \omega t$$
$$y = Y_m \sin(\omega t + \varphi)$$

then the complex amplitude of the input signal $\dot{X}_m = X_m$, while that of the output signal $\dot{Y}_m = Y_m e^{j\varphi}$. Consequently

$$\tilde{W} = W(j\omega) = \frac{\dot{Y}_m}{\dot{X}_m} = \frac{Y_m}{X_m} e^{j\varphi} = W e^{j\varphi} \tag{2.16}$$

The ratio of amplitudes and the phase shift are found from the plot of y versus x obtained at steady state with x varying sinusoidally in time (Fig. 2.5).

If the system receives at its input a unit pulse whose frequency spectrum is unity, then the frequency spectrum of the output signal coincides with the complex frequency response of the system. Indeed, in this case $W(j\omega) = Y(j\omega)$ by formula (2.12) and consequently the *complex frequency response of an element can be defined as the frequency spectrum of the output signal with a unit pulse as the input.*

This definition of $W(j\omega)$ is purely theoretical since in practice a signal cannot be obtained as a unit pulse.

An example of a complex gain locus (complex frequency response) is shown in Fig. 2.6*a*. The differential equation of actual elements normally has $m < n$ and the order of the numerator in the expression (2.15) is below that of the denominator. In the locus this is seen in the fact that as $\omega \to \infty$ the value of $W(j\omega)$ goes to zero. Instead of a frequency-gain locus the amplitude-frequency $W(\omega)$ and the

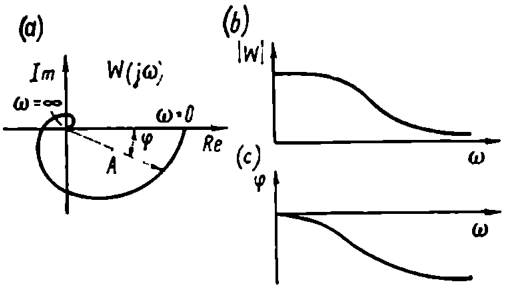

Fig. 2.6

phase-frequency $\varphi(\omega)$ characteristics are often used (Fig. 2.6*b* and *c*). The amplitude is understood as the output amplitude with a unit amplitude sine input or as the gain magnitude.

These characteristics are conveniently expressed in a logarithmic scale with the decimal logarithm of the frequency on the x-axis (a unit division corresponds to a 10-fold variation of frequency). In this case the frequency is said to be measured in *decades* relative to a specified frequency corresponding to the reference point. The values of ω can be conveniently set on the x-axis.

The module of the gain $W(\omega) = |W(j\omega)|$ is then measured in *decibels*

$$L(\omega) = 20 \log W(\omega) \tag{2.17}$$

The relation $L(\log \omega)$ is the logarithmic amplitude-frequency response while $\varphi(\log \omega)$ is the logarithmic phase-frequency response. The response $L(\omega)$ is negative at $|W| < 1$, zero at $|W| = 1$, and positive at $|W| > 1$. Since as $\omega \to \infty$ in real systems $W \to 0$, the value of L tends to $-\infty$.

Element transfer function. The *transfer function $W(p)$ of an element* is the ratio of the output signal image to the input signal image at zero initial conditions.

By virtue of Eq. (2.10) a transfer function is defined as

$$W(p) = \frac{Y(p)}{X(p)} = \frac{K(p)}{D(p)} \tag{2.18}$$

The notation of the transfer function used in structural diagrams of a linear element is shown in Fig. 2.7*a*.

Transition from a transfer function to a complex gain consists in replacing p by $j\omega$.

In the poles (p_i) and zeroes (q_i) of the function $W(p)$ corresponding to roots of the equations $D(p) = 0$ and $K(p) = 0$ are known, then Eq. (2.18) can be rearranged as

$$W(p) = \frac{K(p)}{D(p)} = \frac{k_m \prod_{i=1}^{m} (p - q_i)}{d_n \prod_{i=1}^{n} (p - p_i)} \tag{2.19}$$

The polynomials $D(p)$ and $K(p)$ are assumed to have no common roots and the fraction (2.19) cannot be reduced.

By decomposing the function $W(p)$ into elementary fractions formula (2.19) can be transformed

$$W(p) = \sum_{i=1}^{n} \frac{K(p_i)}{D'(p_i)(p - p_i)} = \frac{K(0)}{D(0)} + \\ + \sum_{i=1}^{n} \frac{pK(p_i)}{p_i D'(p_i)(p - p_i)} \tag{2.20}$$

It is assumed that the function $W(p)$ has no multiple poles and that $n > m$.

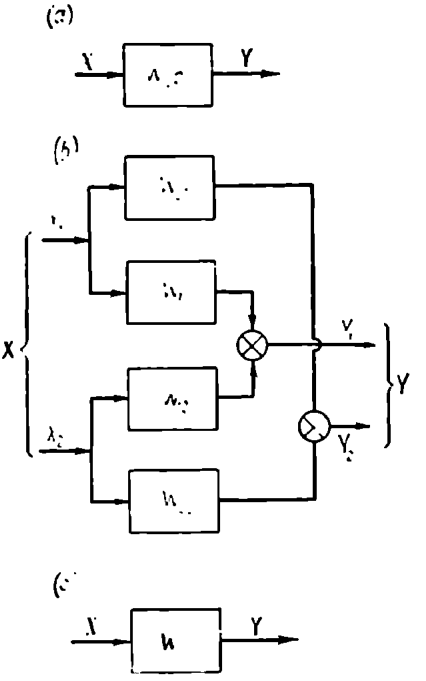

Fig. 2.7

A multivariable element is described by a matrix of transfer functions which relate input and output signals. For instance, for an element with two inputs and two outputs, by virtue of Eq. (2.14)

$$\left.\begin{aligned} Y_1(p) &= W_{11}(p)\, X_1(p) + W_{12}(p)\, X_2(p) \\ Y_2(p) &= W_{21}(p)\, X_1(p) + W_{22}(p)\, X_2(p) \end{aligned}\right\} \tag{2.21}$$

where

$$\left.\begin{aligned} W_{11}(p) &= \frac{K_{11}(p)}{D_1(p)} \\ W_{12}(p) &= \frac{K_{12}(p)}{D_1(p)} \\ W_{21}(p) &= \frac{K_{21}(p)}{D_2(p)} \\ W_{22}(p) &= \frac{K_{22}(p)}{D_2(p)} \end{aligned}\right\} \tag{2.22}$$

In this case the transfer function is a matrix

$$\mathbf{W}(p) = \begin{vmatrix} W_{11}(p) & W_{12}(p) \\ W_{21}(p) & W_{22}(p) \end{vmatrix} \tag{2.23}$$

and Eq. (2.21) can be written in the vectorial form as

$$\mathbf{Y}(p) = \mathbf{W}(p)\,\mathbf{X}(p) \tag{2.21a}$$

The notation for this kind of element is shown in Fig. 2.7*b* and *c*.

For simplicity the transfer function will hereafter be denoted where possible by W instead of $W(p)$.

The transient function. The *transient function of an element*, $h(t)$, is the element output at a unit step input $1_0(t)$. In this case the Laplace image of the input signal $X(p) = \frac{1}{p}$ and, by virtue of Eq. (2.18), the image of the output signal is

$$H(p) = Y(p) = \frac{W(p)}{p} \tag{2.24}$$

Inverse Laplace transformation gives

$$h(t) = y(t) = L^{-1}\left[\frac{W(p)}{p}\right] \tag{2.25}$$

A transient function can be calculated by the operator technique and conventional techniques and, as seen from Eq. (2.25), is in univalent relation with the element's transfer function.

Using Eq. (2.20) and inverse Laplace transformation, we have

$$h(t) = \sum_{i=1}^{n} \frac{K(p_i)}{p_i D'(p_i)} (e^{p_i t} - 1)\, 1_0(t) \tag{2.26}$$

or

$$h(t) = \left[\frac{K(0)}{D(0)} + \sum_{i=1}^{n} \frac{K(p_i)}{p_i D'(p_i)} e^{p_i t}\right] 1_0(t) \tag{2.26a}$$

The steady-state (forced) component of the transient function

$$h_{st} = h(\infty) = \frac{K(0)}{D(0)} = W(0) \tag{2.27}$$

characterizes the static properties of the element.

The transient (free) component is defined as the difference

$$h_t(t) = h(t) - h(\infty) = L^{-1}\left[\frac{W(p) - W(0)}{p}\right] = \sum_{i=1}^{n} \frac{K(p_i)}{p_i D'(p_i)} e^{p_i t} \tag{2.28}$$

If we assume that $K(p) = 1$ and define the transfer function $h_0(t)$, then at any

$$K(p) = k_0 + k_1 p + k_2 p^2 + \ldots + k_m p^m$$

the transient function

$$h(t) = k_0 h_0(t) + k_1 \frac{d}{dt} h_0(t) + \ldots + k_m \frac{d^m}{dt^m} h_0(t) \qquad (2.26b)$$

The weighting, or pulse, transient function. The *weighting* or *pulse function* $w(t)$ is a signal at the element output when the input is a unit pulse $\delta(t)$. In this case the Laplace image of the input signal $X(p) = 1$, while that of the output signal coincides with the transfer function

$$Y(p) = W(p) \qquad (2.29)$$

By inverse Laplace transformation we obtain for the weighting function

$$w(t) = y(t) = L^{-1}[W(p)] \qquad (2.30)$$

in other words the *weighting function is the original of the transfer function*. Since the image of the weighting function $W(p)$ differs from the image of the transfer function $H(p)$ only by the multiplier p,

$$w(t) = \frac{dh(t)}{dt} \qquad (2.31)$$

Consequently, knowing the transfer function we can always find the weighting function of an element. For $h(t)$ expressed by formula (2.26) we have

$$w(t) = \sum_{i=1}^{n} \frac{K(p_i)}{D'(p_i)} e^{p_i t} 1_0(t) \qquad (2.32)$$

Formulae (2.26) and (2.32) have been obtained for nonmultiple roots of the equation $D(p) = 0$. Formulae for multiple roots can be obtained from these expressions by limit transition as the difference between the corresponding roots goes to zero.

Element stability. Expression (2.32) leads to the conclusion that the system stability depends on the region where the roots p_i are located.

For linear systems the definition of the plant stability can be more stringent than for the general case.

A linear element is stable if it eventually returns to the initial state after a short-term external action.

A unit pulse can be regarded as a short-term action. Whether a linear element is stable in this case depends on the value of $w(t)$ as $t \to \infty$; an element is stable if

$$\lim_{t \to \infty} w(t) = 0 \qquad (2.33a)$$

unstable if

$$\lim_{t\to\infty} w(t) = \infty \tag{2.33b}$$

and neutral if

$$\lim_{t\to\infty} w(t) \neq \begin{Bmatrix} 0 \\ \infty \end{Bmatrix} \tag{2.33c}$$

Each real value of $p_i = \alpha_i$ has in expression (2.32) a corresponding addend of the form

$$w_i(t) = c_i e^{\alpha_i t} \tag{2.34}$$

where

$$c_i = \frac{K(p_i)}{D'(p_i)}$$

A complex pair of roots of the characteristic equation

$$p_i = \alpha_i + j\omega_i$$

and

$$p_{i+1} = \alpha_i - j\omega_i$$

has a corresponding addend of the form

$$w_k(t) = w_i(t) + w_{i+1}(t) = c_i e^{(\alpha_i + j\omega_i)t} + c_{i+1} e^{(\alpha_i - j\omega_i)t} =$$

$$= 2Me^{\alpha_i t} \cos(\omega_i t + \varphi_i) \tag{2.35}$$

The position of the roots depends on whether
(1) the real part is positive ($\alpha_i > 0$),
(2) the real part is negative ($\alpha_i < 0$),
(3) the real part is zero ($\alpha_i = 0$).

In the first case the roots are in the right-hand half-plane, or to the right of the imaginary axis, in the second case, in the left-hand half-plane, or to the left of the imaginary axis (Fig. 2.8), and in the third case, on the imaginary axis.

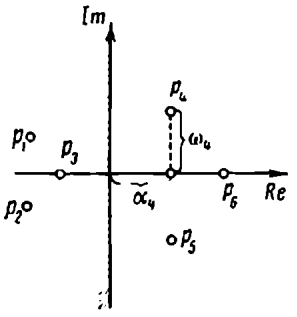

Fig. 2.8

The nature of time variations of the components of $w_i(t)$ depends on the position of the roots relative to the imaginary axis. When $\alpha_i > 0$ (Fig. 2.9*a*) the appropriate component goes to infinity as $t \to \infty$ and, consequently, so does the total value of $w(t)$ and the element is unstable.

At $\alpha_i < 0$ (Fig. 2.9*b*) the appropriate component tends to zero as $t \to \infty$. Consequently, if all components, whose number is finite, satisfy this condition, $w(t)$ also tends to zero and the element is stable.

With $\alpha_i = 0$ (Fig. 2.9*c*) the component remains finite and nonzero as $t \to \infty$, so the element is neutral.

Figure 2.9 shows characteristics for each case of root positions with the real root above and a pair of conjugate complex roots below.

Thus, the necessary and sufficient condition for stability of a linear element is that the real part of all poles of the function $W(p)$

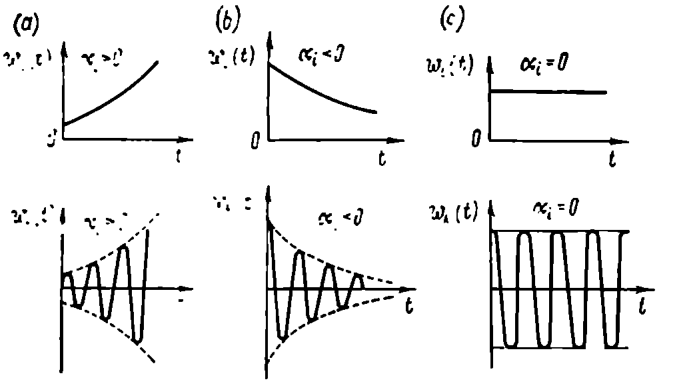

Fig. 2.9

be negative; in other words, all poles should lie in the left half of the p plane.

The above four kinds of linear element characteristics are in one to one correspondence; if one is known, any other can always be found. In further discussion the transfer function $W(p)$ will be used in mathematical description of a linear element, and all other characteristics can be found from this function.

2.5. EXAMPLES OF TRANSFER FUNCTIONS

The equations for all plants discussed in Sections 1.2 and 1.4 can be linearized so that the plants are represented as linear elements with transfer functions $W(p)$.

Example 2.2. A hydraulic tank (see Fig. 1.4*a*). For a hydraulic tank described by Eq. (1.2) the input is the variation in liquid inflow $x = Q - G$ and the output is the change of liquid level $y = \Delta H$. In operator form Eq. (1.2) is

$$SpY(p) = X(p) \tag{2.36}$$

and, consequently,

$$W(p) = \frac{Y(p)}{X(p)} = \frac{1}{Sp} \tag{2.37}$$

Because the equation for $W(p)$ has one pole $p = 0$, the plant is neutral.

Example 2.3. Communicating tanks (see Fig. 1.4*b*). For a plant described by Eqs. (1.3) the input quantities x_1 and x_2 are $(Q_1 - G_1)$ and $(Q_2 - G_2)$, while the outputs y_1 and y_2 are ΔH_1 and ΔH_2.

Linearizing the dependence of Q_{12} on $(H_1 - H_2)$, we can write

$$Q_{12} = b_0 (y_1 - y_2) \tag{2.38}$$

where $b_0 = \frac{\partial Q_{12}}{\partial y_1} = -\frac{\partial Q_{12}}{\partial y_2}$ at specified values of H_1 and H_2. Following the substitution of these notations and the application of direct Laplace transformation Eqs. (1.3) take the form

$$\left.\begin{aligned} S_1 p Y_1 &= X_1 - b_0 (Y_1 - Y_2) \\ S_2 p Y_2 &= X_2 + b_0 (Y_1 - Y_2) \end{aligned}\right\} \tag{2.39}$$

Solving these equations for Y_1 and Y_2, we have

$$\left.\begin{aligned} Y_1 &= W_{11} X_1 + W_{12} X_2 \\ Y_2 &= W_{21} X_1 + W_{22} X_2 \end{aligned}\right\} \tag{2.40}$$

where

$$W_{11} = \frac{b_0 + S_2 p}{p [b_0 (S_1 + S_2) + S_1 S_2 p]}$$

$$W_{22} = \frac{b_0 + S_1 p}{p [b_0 (S_1 + S_2) + S_1 S_2 p]}$$

$$W_{12} = W_{21} = \frac{b_0}{p [b_0 (S_1 + S_2) + S_1 S_2 p]}$$

In each of these equations X_i, Y_i and W_{ih} are functions of p.

The structural diagram of the resultant linearized plant is as in Fig. 2.7*b* (cf. Fig. 1.14*b*).

Example 2.4. A d.c. generator (see Fig. 1.5*a*). For a plant described by Eqs. (1.4) the control variable is the variation of the excitation current $u = \Delta i_e$, the external disturbances are the variations of generator shaft rotation rates $f_1 = \Delta\omega_1$, $f_2 = \Delta\omega_2$, and of the load current $f_3 = \Delta i_l$; the controlled variable is the change of voltage at the generator terminals, $y = \Delta u_l$.

Linearizing the functions $\Phi_1 (i_e)$ and $\Phi_2 (i_l)$ at the values of i_e and i_l close to those corresponding to the initial conditions and at small increments $\Delta\Phi_1$, $\Delta\Phi_2$, Δi_e, Δi_l, Δe_1, Δe_2, Δu_l, $\Delta\omega_1$, $\Delta\omega_2$, and Δi_l, we can neglect the terms of the second order of smallness and then obtain

$$\left.\begin{aligned} \Delta\Phi_1 &= a_1 \Delta i_e \\ \Delta e_1 &= c_1 \omega_1 \Delta\Phi_1 + c_1 \Phi_1 \Delta\omega_1 = r \Delta i_1 + w_2 \frac{d\Delta\Phi_2}{dt} \\ \Delta\Phi_2 &= a_2 \Delta i_1 \\ \Delta e_2 &= c_2 \omega_2 \Delta\Phi_2 + c_2 \Phi_2 \Delta\omega_2 = \Delta u_l + r_{arm} \Delta i_l \end{aligned}\right\} \tag{2.41}$$

where a_1 and a_2 are $\frac{\partial \Phi_1}{\partial i_e}$ and $\frac{\partial \Phi_2}{\partial i_1}$, respectively, at a specified point of the characteristic $\Phi_1(i_e)$, $\Phi_2(i_1)$.

By direct Laplace transformation and eliminating $\Delta\Phi_1$, $\Delta\Phi_2$, and Δi_1 from the equations we have

$$Y = \frac{k_1}{1+pT_1} U + \frac{k_1 b_1}{1+pT_1} F_1 + b_2 F_2 - b_3 F_3 \tag{2.42}$$

where

$$k_1 = \frac{a_1 a_2 c_1 c_2 \omega_1 \omega_2}{r_1}, \qquad T_1 = \frac{a_2 w_2}{r_1},$$

$$b_1 = \frac{\Phi_1}{a_1 \omega_1}, \qquad b_2 = c_2 \Phi_2 \quad \text{and} \quad b_3 = r_{arm}$$

while U, Y, F_1, F_2, and F_3 are the images of u, y, f_1, f_2, and f_3.

In the absence of external disturbances ($F_1 = F_2 = F_3 = 0$) the relation of the control and the controlled variables is given by the transfer function

$$W_1 = \frac{Y}{U} = \frac{k_1}{1+pT_1}$$

For this case $W(p)$ has one pole at the point $p_1 = -\frac{1}{T_1}$; consequently, the element is stable. The structural diagram for this case is given in Fig. 2.7*a* (cf. Fig. 1.15).

Example 2.5. A d.c. motor (see Fig. 1.6*a*). For a plant described by Eqs. (1.5) the inputs are the variations of armature supply voltage and excitation current $x_1 = \Delta u_{arm}$ and $x_2 = \Delta i_e$ and the output is the change of the shaft rotation rate $y = \Delta\omega$. Linearizing Eqs. (1.5) near the point of the initial conditions, we obtain

$$\left.\begin{aligned} &\Delta\Phi_M = a\Delta i_e = ax_2 \\ &\Delta u_{arm} = x_1 = r_{arm}\Delta i_{arm} + c_1\omega\Delta\Phi_M + c_1\Phi_M\Delta\omega \\ &a_1 i_{arm}\Delta\Phi_M + a_1\Phi_M\Delta i_{arm} = J\frac{d\Delta\omega}{dt} + b\Delta\omega \end{aligned}\right\} \tag{2.43}$$

where

$$a = \frac{\partial\Phi_M}{\partial i_e}, \quad b = \frac{\partial M}{\partial\omega}, \quad M = M_f + M_l$$

Eliminating Δi_{arm} and $\Delta\Phi_M$ from the equation gives

$$k_1 x_1 + k_2 x_2 = y + T\frac{dy}{dt}$$

where

$$\left.\begin{aligned} k_1 &= \frac{a_1\Phi_M}{r_{arm}b + c_1\Phi_M^2 a_1} \\ k_2 &= \frac{a_1 i_{arm} a - a_1\Phi_M a\omega c_1/r_{arm}}{b + c_1\Phi_M^2 a_1/r_{arm}} \\ T &= \frac{J}{b + c_1\Phi_M^2 a_1/r_{arm}} \end{aligned}\right\} \qquad (2.44)$$

The small ranges of input and output variations permit considering the parameters k_1, k_2, and T approximately constant. In this case direct Laplace transformation gives

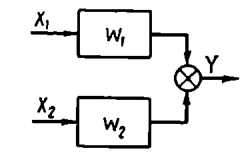

Fig. 2.10

$$Y = W_1X_1 + W_2X_2 \qquad (2.45)$$

where

$$W_1 = \frac{k_1}{1 + pT}, \qquad W_2 = \frac{k_2}{1 - pT}$$

The structural diagram of the plant under consideration is shown in Fig. 2.10*a* (cf. Fig. 1.16*a*).

In the case where the plant is controlled only by the armature supply voltage, $x_2 = 0$ and the motor is a simple element with parameters k_1 and T, which can be assumed independent of ω.

Example 2.6. An asynchronous motor (see Fig. 1.8*a*). For an asynchronous motor operating almost in an equilibrium state Eq. (1.7*a*) has the form

$$J\frac{d\omega}{dt} = \Delta M \qquad (2.46)$$

where ΔM is a function of the mains voltage U and the rotation rate ω shown in Fig. 1.8*b*.

Expanding ΔM into a series of increments of ω and U and neglecting higher-order terms, we obtain

$$\Delta M = a\Delta\omega + b\Delta U \qquad (2.47)$$

where $a = \frac{\partial\Delta M}{\partial\omega}$, $b = \frac{\partial\Delta M}{\partial\Delta U}$. In stable points *1*, *2*, *3*, *4* $a < 0$, and in unstable points *5*, *6* $a > 0$. The values of b and J are always positive.

Considering (2.46) and (2.47) simultaneously, we have

$$kx = y + T\frac{dy}{dt} \qquad (2.48)$$

where

$$T = -\frac{J}{a}, \quad k = -\frac{b}{a}, \quad x = \Delta U, \quad y = \Delta\omega$$

Direct Laplace transformation gives:

$$W = \frac{Y}{X} = \frac{k}{1+pT} \tag{2.49}$$

At $a < 0$, k and T are positive, the root of the equation $1 + pT = 0$ is negative and the motor is a stable element. At $a > 0$, the root $p_1 = -\frac{1}{T} = \frac{a}{J}$ is positive and the motor is an unstable element. The structural diagram of the plant is given in Fig. 2.7*a* (cf. Fig. 1.16*b*).

2.6. A COMMON PROPERTY OF MINIMAL-PHASE STABLE ELEMENTS

One important problem characterizing all elements is whether the transfer function zeroes belong to the left half-plane p. If the transfer function is given by Eq. (2.19), then the complex gain may be expressed as

$$W(j\omega) = \frac{k_m}{d_n} \frac{\prod_{i=1}^{m} (j\omega - q_i)}{\prod_{i=1}^{n} (j\omega - p_i)} \tag{2.50}$$

Let us take up one multiplier $(j\omega - q_i)$ of the numerator. This is a vector with the origin at the point q_i and the end on the imaginary

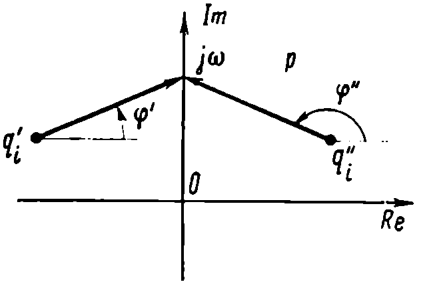

Fig. 2.11

axis at the point $j\omega$. The phase of this vector determines its counterclockwise rotation around the real axis.

Figure 2.11 represents two such vectors for different positions of the point q_i denoted as q_i' and q_i''. At the same magnitude of the complex $(j\omega - q_i)$ its phase φ is seen to be smaller when q_i is located in the left half-plane. Therefore elements having all zeroes of transfer functions in the left half-plane ($\mathrm{Re}\, q_i < 0$) are referred to as *minimal-phase* elements.

Elements having at least one zero of the transfer function in the right half-plane (Re $q_i > 0$) are called *nonminimal-phase* elements.

For minimal-phase stable elements there is an unambiguous relation between the amplitude-frequency and phase-frequency responses and consequently the amplitude-frequency response determines the transfer function unambiguously.

This fact, very important for the synthesis of linear systems, follows from the Gilbert transformation, well known in the theory of functions of a complex variable and consisting in the following.

If the analytical function of a complex variable $F(p)$ is known and all poles lie in the left half of the p plane, then the imaginary and real components of this function of the imaginary argument $F(j\omega) = F_1(\omega) + jF_2(\omega)$ are related as follows:

$$F_1(\omega) = -\frac{1}{\pi}\int_{-\infty}^{+\infty}\frac{F_2(v)}{v-\omega}\,dv \tag{2.51}$$

and

$$F_2(\omega) = \frac{1}{\pi}\int_{-\infty}^{+\infty}\frac{F_1(v)}{v-\omega}\,dv \tag{2.52}$$

The Gilbert transformation enables one to find the frequency dependence of the imaginary part of a complex variable function provided the frequency dependence of the real part is known and, conversely, to find the frequency dependence of the real part if the frequency dependence of the imaginary part is given.

Let $W(j\omega)$ be a complex gain of a minimal-phase stable system. Then the analytical function

$$\begin{aligned} F(j\omega) &= \ln W(j\omega) = \ln W(\omega) + j\varphi(\omega) = \\ &= F_1(\omega) + jF_2(\omega) \end{aligned} \tag{2.53}$$

satisfies the requirements for the Gilbert transformation since the condition of the minimal phase of $W(j\omega)$ ensures the absence of poles of the function $F(p)$ in the right half of the p plane. Then, knowing the logarithmic amplitude-frequency response

$$L(\omega) = 20 \log W(\omega) = 8.7 \ln W(\omega) = 8.7F_1(\omega) \tag{2.54}$$

we can find by formula (2.52) the phase-frequency response

$$\varphi(\omega) = \frac{1}{\pi}\int_{-\infty}^{+\infty}\frac{\ln W(v)}{v-\omega}\,dv = \frac{1}{8.7\pi}\int_{-\infty}^{+\infty}\frac{L(v)}{v-\omega}\,dv \tag{2.55}$$

Introducing the variable $u = \ln \frac{v}{\omega}$, the integral (2.55) can be represented as

$$\varphi(\omega) = \frac{1}{\pi} \int_{-\infty}^{+\infty} \frac{d[\ln W(v)]}{du} \ln \coth \left| \frac{u}{2} \right| du \qquad (2.56)$$

The latter expression can often be conveniently used in finding $\varphi(\omega)$ when $L(\omega)$ is known.

Consequently, if the amplitude-frequency response of an element is given and the element is stable and minimal-phase, this information is sufficient to find all frequency responses and thus describe completely the behaviour of the system at any inputs.

Example 2.7. Assume that the gain of a stable minimal-phase element does not depend on frequency, i.e.

$$W(\omega) = \text{const} = k$$

Let us find $\varphi(\omega)$.

Substitute $W(\omega) = k$ into Eq. (2.55)

$$\varphi(\omega) = \frac{1}{\pi} \int_{-\infty}^{+\infty} \frac{\ln k}{v - \omega} dv$$

since the value of $\int_{-\infty}^{+\infty} \frac{dv}{v - \omega}$ on the real axis is zero, $\varphi(\omega) = 0$.

Thus the minimal-phase element for which the gain is independent of frequency is an element with a transfer function $W(p) = k$.

Example 2.8. Let a minimal-phase stable element have the amplitude-frequency response

$$W(\omega) = \sqrt{1 + (\omega T)^2}$$

Find $\varphi(\omega)$.

We have

$$F_1(\omega) = \ln W(\omega) = \frac{1}{2} \ln [1 + (\omega T)^2] \qquad (2.57)$$

and

$$\varphi(\omega) = \frac{1}{2\pi} \int_{-\infty}^{+\infty} \frac{\ln [1 + (vT)^2]}{v - \omega} dv \qquad (2.58)$$

The value of the above definite integral on the real axis is 2π arc tan ωT. Consequently

$$\varphi = \text{arc tan } \omega T \qquad (2.59)$$

This example refers to an element with a transfer function $W(p) = 1 + pT$.

Example 2.9. Find $\varphi(\omega)$ of a minimal-phase stable element if

$$W(\omega) = [1 + (\omega T)^2]^a \tag{2.60}$$

We have

$$F_1(\omega) = \ln W(\omega) = a \ln [1 + (\omega T)^2] \tag{2.61}$$

and

$$\varphi(\omega) = \frac{a}{\pi} \int_{-\infty}^{+\infty} \frac{\ln [1+(vT)^2]}{v-\omega} dv = 2a \arctan \omega T \tag{2.62}$$

This corresponds to an element with a transfer function

$$W(p) = [1 + pT]^{2a} \tag{2.63}$$

where a may be either positive or negative.

2.7. TRANSFORMATION OF AN ARBITRARY SIGNAL BY A LINEAR ELEMENT

Knowing the responses of an element, we can find its output signal at any input signal. Indeed, as shown in Sec. 2.2, any signal can be represented as a set of elementary sine wave, unit step, or unit pulse signals. An output signal can be found corresponding to each of the elementary input components. By the superposition principle the output signal of a linear element may be regarded as a set of components, each corresponding to a particular elementary input signal.

If thus an input signal is given as a frequency spectrum $X(j\omega)$, the frequency spectrum of the output signal is found using the complex gain

$$Y(j\omega) = W(j\omega)\, X(j\omega) \tag{2.64}$$

If an input signal is given as the image $X(p)$, the image of the output signal is found via the transfer function

$$Y(p) = W(p)\, X(p) \tag{2.65}$$

If an input signal is given as a time function $x(t)$, the output signal can be found via either the transfer or the weighting function.

Expanding $x(t)$ into a set of unit steps $1_0(t-\tau)$ by formula (2.1) and finding the response of the element to each step, we have

$$y(t) = x(0)\, h(t) + \int_0^t h(t-\tau) \frac{dx(\tau)}{d\tau} d\tau \tag{2.66}$$

In a similar way, decomposing $x(t)$ into a set of unit pulses $\delta(t-\tau)$ by formula (2.2) and finding the response to each pulse, we have

$$y(t) = \int_0^t w(t-\tau)\, x(\tau)\, d\tau \tag{2.67}$$

Thus, the above responses completely define the element output if the input is known at zero initial conditions.

The calculation of the output is somewhat more complicated if the initial conditions are nonzero. In this case in calculating the output signal by the operator method formula (2.13) should be used.

By appropriate choice of the time reference to calculate processes caused by incrementation of x relative to the initial value, $x^{i-r}(0)$ can be reduced to zero.

An allowance should be made, however, for the initial values of $y^{i-r}(0)$. In that case from formula (2.13) we have

$$Y(p) = \frac{K(p)}{D(p)} X + Y_{in}(p) \tag{2.68}$$

where

$$D(p) - Y_{in}(p) = \sum_{i=1}^{n} d_i \sum_{r=1}^{i} p^{r-1} y^{i-r}(0) \tag{2.69}$$

Let us assume that the image of a typical input, $X(p)$, is a fractional rational function

$$X(p) = \frac{N(p)}{M(p)} \tag{2.70}$$

where $N(p)$ and $M(p)$ are polynomials in p.

Then

$$Y(p) = W(p) X(p) + \frac{Y_{in}(p)}{D(p)} = \frac{R(p)}{D(p) M(p)} \tag{2.71}$$

where

$$R(p) = K(p) N(p) + Y_{in}(p) M(p) D(p) \tag{2.72}$$

At zero initial conditions $Y_{in}(p) = 0$ and the expression (2.68) transforms into (2.65)

Note that by virtue of Eq. (2.71) nonzero initial conditions change only the numerator of the output signal image. The roots of the denominator (poles) of this image are, at any initial conditions, determined from the equations

$$D(p) = 0 \tag{2.73}$$

$$M(p) = 0 \tag{2.74}$$

To find the original $y(t)$ we can use decomposition of Eq. (2.68) into elementary fractions corresponding to n roots of Eq. (2.73) and s roots of Eq. (2.74).

If all roots of Eqs. (2.73) and (2.74) are different, then

$$y(t) = \sum_{l=1}^{n} \frac{R(p_l)}{D'(p_l) M(p_l)} e^{p_l t} + \sum_{k=1}^{s} \frac{K(p_k) N(p_k)}{D(p_k) M'(p_k)} e^{p_k t} \tag{2.75}$$

where p_i = roots of Eq. (2.73)
p_k = roots of Eq. (2.74).

The components of the first sum in Eq. (2.75) are found with an accuracy to coefficients on the basis of the roots of Eq. (2.73) and in the case of stable elements damp out with time. The first sum is termed the *transient* (or *free*) *component of the process*

$$y_t(t) = \sum_{i=1}^{n} \frac{R(p_i)}{D'(p_i) M(p_i)} e^{p_i t} \tag{2.76}$$

In particular, at zero initial conditions

$$y_t(t) = \sum_{i=1}^{n} \frac{K(p_i) N(p_i)}{D'(p_i) M(p_i)} e^{p_i t} \tag{2.77}$$

Note that since the summation in Eq. (2.76) uses weighting coefficients which depend on coefficients of the characteristic equation, the numerator of the element transfer function $K(p)$, initial conditions $Y_{in}(p)$, and the action parameters $N(p)$ and $M(p)$ (Eq. (2.75)), the transient process is largely a function of all these factors.

Transient processes can be usefully compared for common (standard) input actions under standard (usually zero) initial conditions.

With the same reservations the components of the second sum in Eq. (2.75) are defined by the roots of Eq. (2.74), or by the poles of the input action image. The second sum is termed the *forced component of the process*

$$y_{fo}(t) = \sum_{k=1}^{s} \frac{K(p_k) N(p_k)}{D(p_k) M'(p_k)} e^{p_k t} \tag{2.78}$$

Note that the forced component depends on the input action and the variables of the system transfer function but is independent of the initial conditions $Y_{in}(p)$.

After a time interval sufficient for the transient component of Eq. (2.76) to damp out with a required accuracy the process is assumed a steady-state one.

At steady state $y(t)$ depends on the forced component and is independent of initial conditions.

If the roots of Eq. (2.73) or (2.74) are multiple, decomposition into simple fractions should allow for the multiplicity.

Chapter III

TYPICAL ELEMENTS OF LINEAR CONTROL SYSTEMS

3.1. TYPICAL LINEAR ELEMENTS. GENERAL

In actual systems processes are described by using idealized diagrams which give an accurate mathematical description but just an approximate characteristic of actual elements behaviour in a specified frequency range.

As in electric circuits, where the concepts of r, L, and C are introduced, although actual resistors, capacitors, and inductors are representable by these concepts only within certain frequency ranges, theory of automatic control uses the concept of *typical elements* whose transfer functions correspond to those of actual elements only in a specified frequency range.

Disregarding the function of the elements, the operational principle, signal power and frequency, we can distinguish some typical elements which can be described by usual first- and second-order linear differential equations:

(a) simple: proportional, integrating, and differentiating;

(b) first-order: inertial (lag), inertial-differentiating, lead, and lag-lead;

(c) oscillatory second-order.

All typical elements have a transfer function, which is a rational fraction

$$W(p) = \frac{K(p)}{D(p)}$$

The zeroes and poles of the function $W(p)$ which correspond to the equations $K(p) = 0$ and $D(p) = 0$ are in the left half of the p plane or on its boundary, which coincides with the imaginary axis.

Complex linear elements can be treated as combinations of typical elements.

When an actual element is classed with a certain type, the frequency range within which the responses are studied should be indicated. Beyond that range more variables would come into the picture and make the mathematical description more complicated.

In the following pages we will discuss the responses of typical elements and give several examples of elements themselves.

Unstable and nonminimal-phase elements as well as elements described by transcendental or irrational transfer functions are not typical and will be discussed in Chapter IV.

3.2. SIMPLE ELEMENTS

Proportional element. The simplest element is one where the output is directly proportional to the input. The equation of such an element is

$$y = kx \tag{3.1}$$

where k is the gain.

This type includes a voltage divider (Fig. 3.1*a*), a d.c. amplifier (Fig. 3.1*b*), lever transmission (Fig. 3.1*c*), reduction gear (Fig. 3.1*d*), etc.

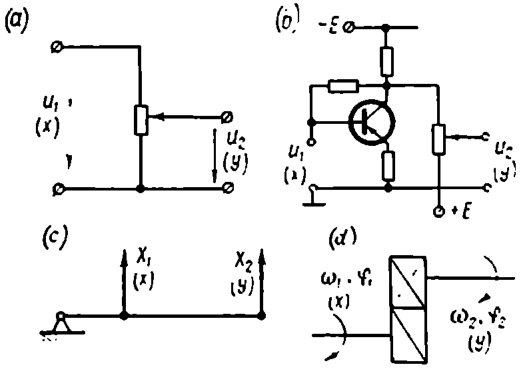

Fig. 3.1

The signal is assumed to propagate from the input to the output instantaneously without any inertia. Therefore such elements are known as *inertialess*.

If a proportional element has a sine input:

$$x = X_m \sin \omega t$$

then the output signal will be

$$y = Y_m \sin \omega t$$

where

$$Y_m = kX_m$$

In the complex form

$$\dot{Y} = k\dot{X} \quad \text{or} \quad Y(j\omega) = kX(j\omega) \tag{3.2}$$

and the complex gain is

$$W(j\omega) = \frac{Y(j\omega)}{X(j\omega)} = k \tag{3.3}$$

The locus of the complex gain $W(j\omega)$ at $0 < \omega < \infty$ is a point shifted along the real axis by the distance k from zero (Fig. 3.2*a*).

This description of input-output relation is completely true for an ideal element and is valid for an actual element only at frequencies below a certain maximum, ω_{max}.

At higher frequencies the accepted mathematical description ceases to be true and the small variables neglected in the model reduce the gain to zero. For a voltage divider (see Fig. 3.1*a*) this variable may be the capacity of output leads; for an amplifier (see Fig. 3.1*b*) it is the distributed capacities and inductances of the circuit; for a mechanical transmission (see Fig. 3.1*c* and *d*), the elasticity of levers and shafts. Therefore with ω increasing to infinity, the gain of any actual element reduces to zero and the locus of the gain at $\omega_{max} < \omega < \infty$ is a curve of the type shown in Fig. 3.2*a* by a dotted line. In control systems, however, one usually considers the range of relatively low frequencies where $\omega < \omega_{max}$ and all facilities in question can be classified with proportional (inertialess) elements, while the locus of the gain is the point k.

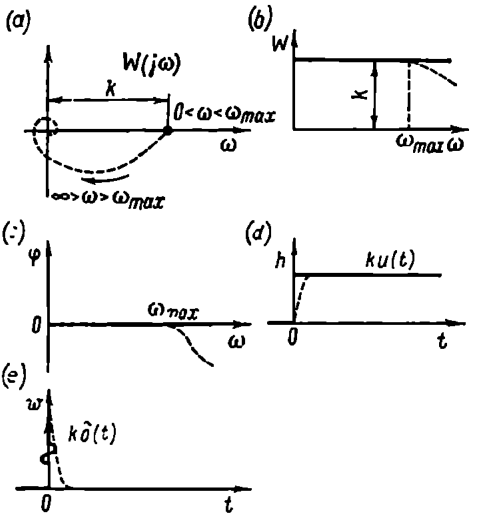

Fig. 3.2

The respective amplitude-frequency and phase-frequency characteristics are shown in Fig. 3.2*b* and *c*.

In further discussion a *proportional element* is an ideal element whose gain is constant in the whole frequency range $0 < \omega < \infty$.

Going over from the gain to the transfer function and then to the transient and the weighting functions we have

$$W(p) = k \tag{3.4}$$

$$h(t) = k1_0(t) \tag{3.5}$$

and

$$w(t) = k\delta(t) \tag{3.6}$$

A graphical representation of the transient and weighting functions is shown in Fig. 3.2*d* and *e*. Both these functions correspond to an ideal proportional element. Actual elements, whose diagrams are shown in Fig. 3.1, have responses which can be described by these

plots only approximately. The divergence between actual and ideal responses is shown by dotted lines (see Fig. 3.2).

A number of control systems use a.c. amplifiers with modulation and demodulation or phase detection where the carrier frequency is much higher than the maximum input frequency. Such circuits ensure stable operation at large gains. A block diagram of an amplifier with a modulator M and a demodulator DM is shown in Fig. 3.3.

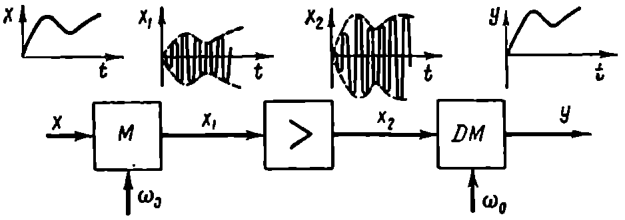

Fig. 3.3

At signal frequencies much below the carrier frequency ω_0 such amplifiers may be classified with proportional elements and all responses shown in Fig. 3.2 for ideal elements are valid for them.

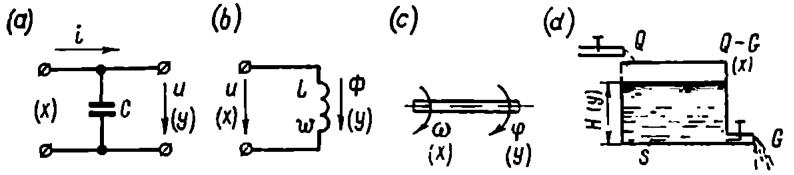

Fig. 3.4

Integrator. There are many elements where the output variable is proportional or equal to the time integral of the input

$$y = k \int_0^t x(t)\,dt + y_0 \tag{3.7}$$

where k is a proportionality coefficient.

Such elements are termed *integrators*.

Example 3.1. Real elements whose equivalent circuits reduce to an integrator include an electric capacitor (Fig. 3.4*a*), an inductor (Fig. 3.4*b*), a rotating shaft (Fig. 3.4*c*), a hydraulic tank (Fig. 3.4*d*), a hydraulic amplifier (Fig. 3.5*a*).

Indeed, the voltage at the capacitor

$$u = \frac{1}{C} \int_0^t i\,dt + u_0 \tag{3.8}$$

the magnetic flow in the inductor

$$\Phi = \frac{1}{w} \int_0^t u\,dt + \Phi_0 \tag{3.9}$$

the shaft rotation angle

$$\varphi = \int_0^t \omega\,dt + \varphi_0 \tag{3.10}$$

the water level in the hydraulic tank

$$H = \frac{1}{S} \int_0^t (Q - G)\,dt + H_0 \tag{3.11}$$

Equations (3.8)-(3.11) use the following notation:

i = current in capacitor C

u = voltage at coil with w turns

ω = angular velocity of shaft

$Q - G$ = resulting water inflow in tank with surface area S.

A hydraulic amplifier can also be described as an integrator. The displacement x_1 of the piston of the valve leads to changes in

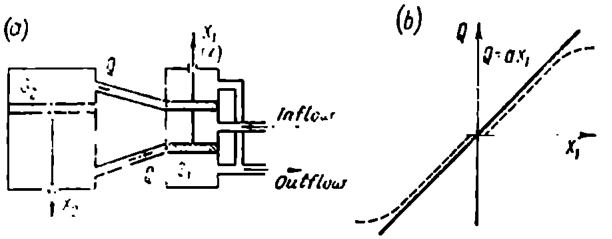

Fig. 3.5

liquid inflow and outflow Q in the working cylinder and consequently to displacement x_2 of the working piston relative to the initial position x_{20}.

The relation between x_1 and Q at a constant pressure in the cylinders is represented by dotted lines in Fig. 3.5*b*. This plot can be approximated by a straight line $Q = ax_1$ (the solid line in Fig. 3.5*b*).

Since the liquid is incompressible we have

$$Q = S_2 \frac{dx_2}{dt} = ax_1 \tag{3.12}$$

where S_2 is the working piston surface area.

Consequently

$$x_2 = \frac{1}{S_2} \int_0^t Q_1\,dt + x_{20} \approx \frac{a}{S_2} \int_0^t x_1\,dt + x_{20} \tag{3.13}$$

If the input of an integrator is a sine wave, $x = X_m \sin \omega t$, then from Eq. (3.7) it follows directly that

$$y = -\frac{k}{\omega} X_m \cos \omega t \tag{3.14}$$

or

$$\dot{Y} = \frac{k}{j\omega} \dot{X} \quad \text{and} \quad Y(j\omega) = \frac{k}{j\omega} X(j\omega) \tag{3.15}$$

The complex gain of the integrator is

$$W(j\omega) = \frac{Y(j\omega)}{X(j\omega)} = \frac{k}{j\omega} = \frac{k}{\omega} e^{-j\frac{\pi}{2}} \tag{3.16}$$

The frequency locus and the frequency responses of the integrator are shown in Fig. 3.6*a* and *b*.

The logarithmic amplitude-frequency response $L = 20 \log |W|$ (as a function of log ω) has the form of a straight line with a slope

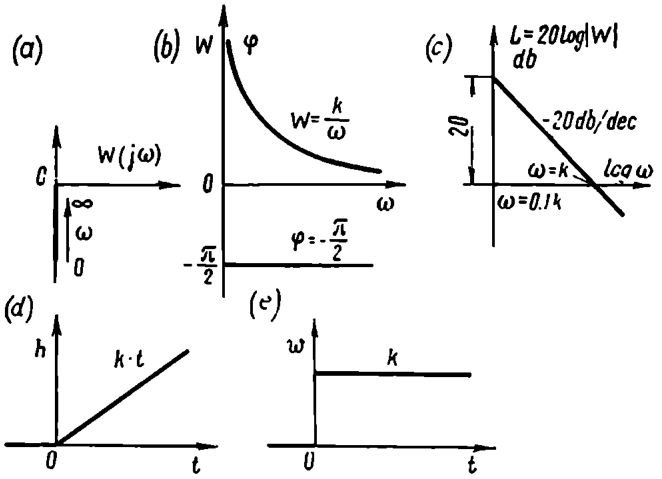

Fig. 3.6

—20 db/dec; in other words L reduces by 20 db at a 10-fold frequency variation (Fig. 3.6*c*). The plot of $L(\omega)$ for an integrator crosses the x-axis at $\omega = k$.

Going over from the gain to the transfer function and then to the transient and weighting functions, we have

$$W(p) = \frac{k}{p} \tag{3.17}$$

$$h(t) = kt1_0(t) \tag{3.18}$$

and

$$w(t) = k1_0(t) \tag{3.19}$$

(Fig. 3.6*d* and *e*).

Differentiator. There is no actual element which would accurately reproduce at its output a derivative of any input signal. In developing the structural diagram of a system, however, it can be divided

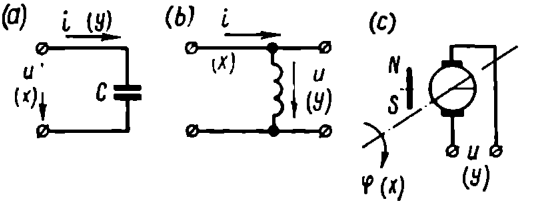

Fig. 3.7

into elements so that the concept of a *differentiator* will be completely justified (Fig. 1.15).

In this case the output variable y depends on the input variable x as follows

$$y = k\frac{dx}{dt} \tag{3.20}$$

where k is the proportionality coefficient.

Example 3.2. A differentiating element may be an electric capacitor, inductor, electric tachometer (Fig. 3.7).

The current in the capacitor

$$i = C\frac{du}{dt} \tag{3.21}$$

the voltage at the inductor

$$u = L\frac{di}{dt} \tag{3.22}$$

and the voltage at the terminals of a tachometric d.c. generator

$$u = a\omega = a\frac{d\varphi}{dt} \tag{3.23}$$

are proportional to derivatives of the voltage, current and shaft rotation angle.

The complex gain is

$$W(j\omega) = \frac{Y(j\omega)}{X(j\omega)} = jk\omega = k\omega e^{j\frac{\pi}{2}} \tag{3.24}$$

All frequency responses of the elements are shown in Fig. 3.8*a*, *b*, *c*.

The logarithmic amplitude-frequency response has a positive slope of 20 db/dec.

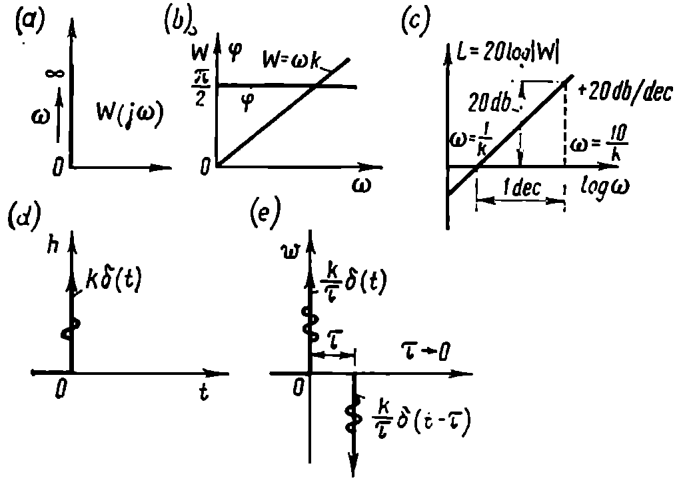

Fig. 3.8

The transfer function of a differentiator

$$W(p) = pk \tag{3.25}$$

and the transient and weighting functions

$$h(t) = k\delta(t) \tag{3.26}$$

$$w(t) = k\delta'(t) \tag{3.27}$$

(Fig. 3.8*d* and *e*). The derivative of the δ-function or the second-order δ-function δ′ is shown in Fig. 3.8*e* as two pulses with the interval τ between them tending to zero.

3.3. FIRST-ORDER ELEMENTS

An inertial (lag) element. One of the most widespread elements of control systems is an *inertial element* described by the equation

$$y + T\frac{dy}{dt} = kx \tag{3.28}$$

where k and T are the gain and time constant of the element, respectively.

Example 3.3. Many of the plants discussed in Ch. I (Fig. 3.9), actuators, electronic and magnetic amplifiers and four-terminal elements including inductors or capacitors (Fig. 3.10) may be classified

with inertial elements provided their equations are linearized. Examples 2.4, 2.5, and 2.6 show that a generator and a motor can be represented as inertial elements.

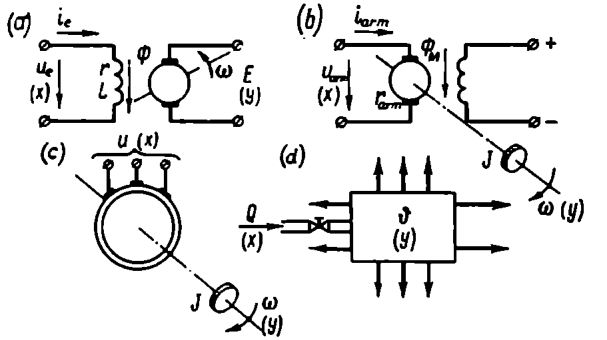

Fig. 3.9

Similarly, from Eq. (1.8) for a furnace it follows that

$$g\Delta\vartheta + C\frac{d\Delta\vartheta}{dt} = \Delta Q \tag{3.29}$$

Assuming $\Delta Q = x$, $\Delta\vartheta = y$, $\frac{1}{g} = k$ and $\frac{C}{g} = T$, we reduce Eq. (3.29) to Eq. (3.28).

The analysis of the four-terminals of Fig. 3.10 shows that Eq. (3.28) is valid for them as well with $k = 1$, $T = rC$ or $T = \frac{L}{r}$, while $x = u_1$ and $y = u_2$.

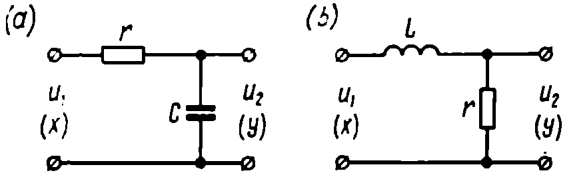

Fig. 3.10

Using frequency spectra or harmonic signals instead of instantaneous values of variables in Eq. (3.28), we have

$$W(j\omega) = \frac{Y(j\omega)}{X(j\omega)} = \frac{k}{1 + j\omega T} \tag{3.30}$$

The frequency responses for this function are shown in Fig. 3.11*a*, *b*, *c*. In this case

$$W(\omega) = \frac{k}{\sqrt{1+(\omega T)^2}} \tag{3.31}$$

and

$$\varphi(\omega) = -\arctan \omega T \tag{3.32}$$

Along with the response $W(j\omega)$ it is sometimes convenient to use the inverse response $\frac{1}{W(j\omega)} = \frac{1}{k} + j\omega \frac{T}{k}$. For an inertial element this response is shown in Fig. 3.11*b*. If the response $W(j\omega)$ is a

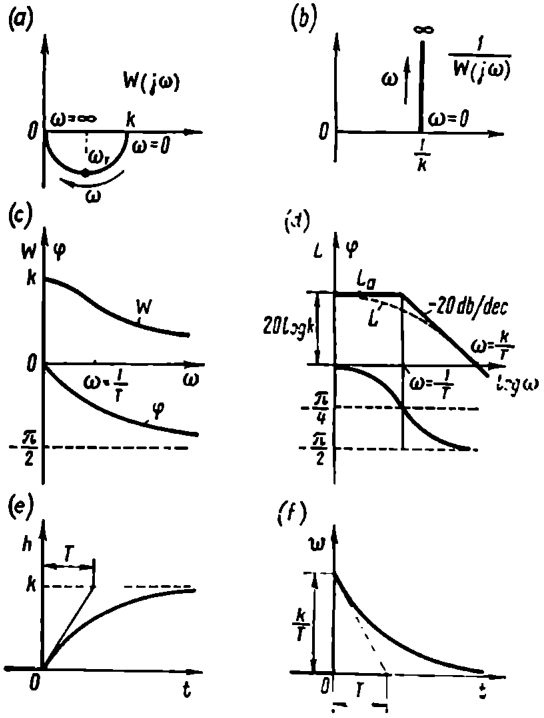

Fig. 3.11

typical circle diagram located in the fourth quadrant and supported by the diameter $0 \rightarrow k$, then the inverse response is a straight line which goes from the point $\frac{1}{k}$ into infinity parallel to the imaginary axis.

In order to plot a logarithmic amplitude-frequency response let us use the following expression

$$L(\omega) = 20 \log |W| = 20 \log k - 10 \log [1 + (\omega T)^2] \tag{3.33}$$

This relation is shown in Fig. 3.11*d* by a dotted line and denoted as L.

Logarithmic responses are also constructed via their asymptotic approximations. For an inertial element an asymptotic approximation is obtained by replacing an accurate response by two asymptotes at $0 < \omega T \leqslant 1$ and at $\omega T \geqslant 1$. The first asymptote is obtained

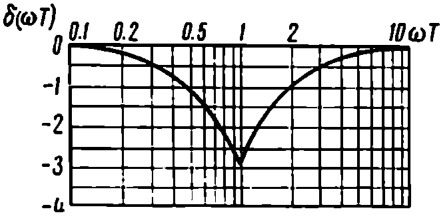

Fig. 3.12

by eliminating $(\omega T)^2$ in Eq. (3.33) and the second one, by eliminating the unit term.

The asymptotic response is thus described by two equations

$$L_a(\omega) = \begin{cases} 20 \log k & \text{at } 0 < \omega T \leqslant 1 \\ 20 \log k - 20 \log \omega T & \text{at } \omega T \geqslant 1 \end{cases} \tag{3.34}$$

In Fig. 3.11*d* the response L_a is shown as a solid line parallel to the x-axis at $0 < \omega T < 1$ and having a slope of 20 db/dec at $\omega T > 1$.

The difference between an accurate response $L(\omega T)$ and the asymptotic one $L_a(\omega T)$ is a correction to the asymptotic response

$$\delta(\omega T) = L(\omega T) - L_a(\omega T) \tag{3.35}$$

Figure 3.12 gives a graphical representation of that function. The greatest error is at $\omega T = 1$, where

$$\delta(\omega T) = -10 \log 2 \cong -3 \text{ db}$$

At frequencies differing from $\frac{1}{T}$ by more than an order of magnitude this error is negligible.

The transfer function of an inertial element, by virtue of Eq. (3.30), is

$$W(p) = \frac{k}{1 + pT} \tag{3.36}$$

The transient function is

$$h(t) = L^{-1}\left[\frac{k}{1+pT}\frac{1}{p}\right] = k\left(1 - e^{-\frac{t}{T}}\right) 1_0(t) \tag{3.37}$$

The weighting function is

$$w(t) = \frac{dh}{dt} = \frac{k}{T} e^{-\frac{t}{T}} 1_0(t) \tag{3.38}$$

The plots of the transient and weighting functions are shown in Fig. 3.11*e* and *f*.

A lead element. An element described by the differential equation

$$y = k\left(x + T\frac{dx}{dt}\right) \tag{3.39}$$

is a *lead element.*

Such an element is the result of different parallel connections between a proportional and a differentiating or inertial element (see Ch. V).

For a lead element we have

$$W(j\omega) = \frac{Y(j\omega)}{X(j\omega)} = k(1 + j\omega T) \tag{3.40}$$

$$W(\omega) = k\sqrt{1 + (\omega T)^2} \tag{3.41}$$

$$\varphi(\omega) = \arctan \omega T \tag{3.42}$$

$$L(\omega) = 20 \log k + 10 \log [1 + (\omega T)^2] \tag{3.43}$$

$$L_a(\omega) = \begin{cases} 20 \log k & \text{at } 0 < \omega T \leqslant \\ 20 \log k + 20 \log \omega T & \text{at } \omega T \geqslant 1 \end{cases} \tag{3.44}$$

The frequency responses of a lead element are shown in Fig. 3.13. The direct amplitude-phase response of a lead element is seen to

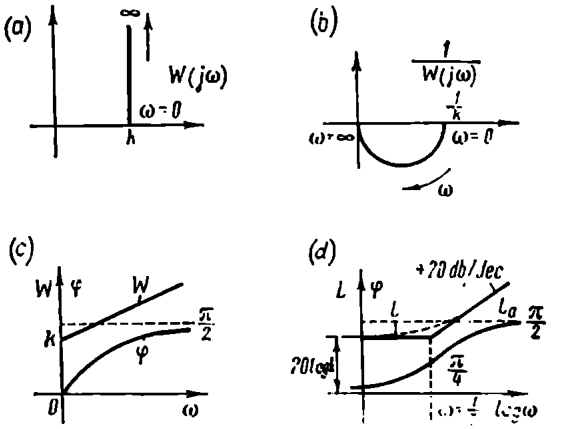

Fig. 3.13

be similar to the inverse response of an inertial element, while its inverse response coincides with the direct response of an inertial element.

This is also valid for the amplitude and phase responses.
The transfer function of a lead element is

$$W(p) = k(1 + pT) \tag{3.45}$$

and can be represented as the sum of the transfer functions of the proportional and differentiating elements (see Sec. 3.2).

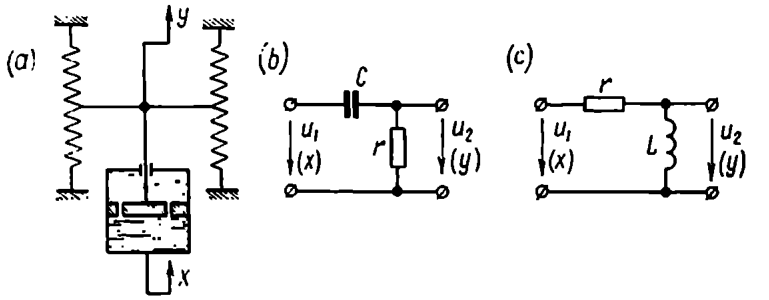

Fig. 3.14

The transient and weighting functions of a lead element are sums of the corresponding functions of simple elements

$$h(t) = k1_0(t) + kT\delta(t) \tag{3.46}$$

$$w(t) = k\delta(t) + kT\delta'(t) \tag{3.47}$$

An inertial-differentiating element. An element described by the differential equation

$$y + T\frac{dy}{dt} = k\frac{dx}{dt} \tag{3.48}$$

is termed a *real differentiating*, or an *inertial-differentiating element.*
Among such elements are a mechanical system with a flexible hydraulic link and four-terminals made up of active and reactive resistors (Fig. 3.14).
Replacing the instantaneous values of variables in Eq. (3.48) by frequency spectra, we have

$$W(j\omega) = \frac{Y(j\omega)}{X(j\omega)} = \frac{kj\omega}{1 + j\omega T} = \frac{\frac{k}{T}}{1 + \frac{1}{j\omega T}} \tag{3.49}$$

The frequency responses for this function are shown in Fig. 3.15*a*, *b*, *c*, *d*:

$$W(\omega) = \frac{k\omega}{\sqrt{1 + (\omega T)^2}} \tag{3.50}$$

$$\varphi(\omega) = \frac{\pi}{2} - \arctan \omega T \tag{3.51}$$

$$\frac{1}{W(j\omega)} = \frac{T}{k} - j\frac{1}{k\omega} \tag{3.52}$$

$$L(\omega) = 20 \log |W| = 20 \log k\omega - 10 \log [1 + (\omega T)^2] \tag{3.53}$$

The asymptotic responses consist of two half-lines

$$L_a(\omega) = \begin{cases} 20 \log k\omega & \text{at} \quad \omega T \leqslant 1 \\ 20 \log \frac{k}{T} & \text{at} \quad \omega T \geqslant 1 \end{cases} \tag{3.54}$$

As in inertial elements, the correction to the asymptotic characteristic is a curve of Fig. 3.12 with the appropriate sign.

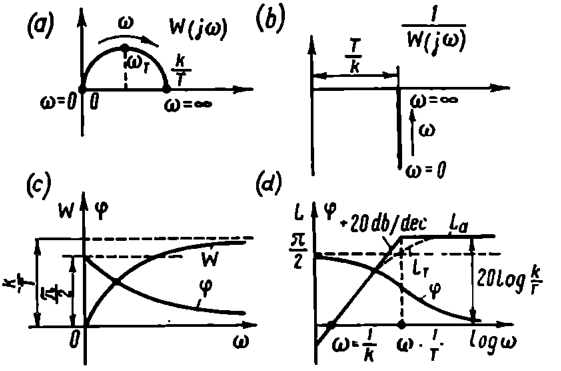

Fig. 3.15

By virtue of (3.49) the transfer function of an inertial-differentiating element is

$$W(p) = \frac{kp}{1 + pT} \tag{3.55}$$

A reverse Laplace transformation gives

$$h(t) = L^{-1}\left[\frac{kp}{1 + pT}\,\frac{1}{p}\right] = \frac{k}{T} e^{-\frac{t}{T}} 1_0(t) \tag{3.56}$$

Differentiating Eq. (3.56) gives

$$w(t) = \frac{k}{T}\delta(t) - \frac{k}{T^2} e^{-\frac{t}{T}} 1_0(t) \tag{3.57}$$

If the frequency responses of an inertial or inertial-differentiating element have been obtained experimentally, then the values of k and T can readily be found.

From Figs. 3.11*a* and 3.15*a* the phase shift between the input and output signals is seen to be equal to $\frac{\pi}{4}$ at $\omega = \omega_T = \frac{1}{T}$ when

$\omega T = 1$. The value of T is found from this condition. The coefficient k is obtained via the diameter of the frequency response circle.

Much more often it is required to find element parameters using a transient response measured experimentally. In this case it is advisable to find $w = \frac{dh}{dt}$ by numerical or graphical differentiation and to plot a curve of the transient process in the coordinates h, w. As follows from Eqs. (3.28) and (3.48), for both elements this will be a straight line going through the origin of coordinates for an inertial-differentiating element (*1* in Fig. 3.16) and through the point $h = k$, for an inertial element (*2* in Fig. 3.16).

The tangent of the slope angle of this line equals T. The value of k for an inertial element is found from the value of h as $t \to \infty$, and for an inertial-differentiating element, from the initial value of $h_0 = \frac{k}{T}$.

The practical applicability of an equation to the description of real elements depends on the degree of correspondence between the desired response and the experimental curve.

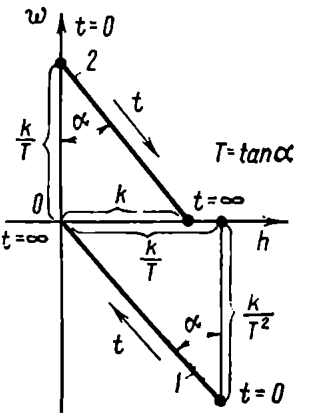

Fig. 3.16

A lag-lead element. A *lag-lead* (or *elastic*) *element* is one described by a first-order differential equation in the most general form

$$y + T\frac{dy}{dt} = k\left(x + T_0\frac{dx}{dt}\right) \tag{3.58}$$

An important parameter of a lag-lead element is the coefficient $\tau = \frac{T_0}{T}$. If $\tau < 1$, then the properties of the element are approaching those of an integrator and an inertial element. If $\tau > 1$, then the element properties are closer to a differentiator and an inertial-differentiating element.

The complex gain of a lag-lead element is

$$W(j\omega) = \frac{Y(j\omega)}{X(j\omega)} = \frac{k(1+j\omega T_0)}{1+j\omega T} \tag{3.59}$$

and the transfer function

$$W(p) = k\frac{(1+pT_0)}{(1+pT)} \tag{3.60}$$

Examples of electric circuits acting as lag-lead elements are shown in Fig. 3.17.

Example 3.4. Considering the gain of the circuits shown in Fig. 3.17 as the transfer coefficient of a voltage divider

$$W = \frac{Z_2}{Z_1 + Z_2} \tag{3.61}$$

we have:

for circuit (*a*)

$$\left.\begin{aligned} Z_1 = r_1, \quad Z_2 = r_2 + \frac{1}{j\omega C} = \frac{1 + j\omega C r_2}{j\omega C} \\ W(j\omega) = \frac{1 + j\omega C r_2}{1 + j\omega C (r_1 + r_2)} = \frac{1 + j\omega T_0}{1 + j\omega T} \end{aligned}\right\} \tag{3.62}$$

where

$$T_0 = Cr_2, \qquad T = C(r_1 + r_2), \quad \text{and} \quad k = 1$$

for circuit (*b*)

$$\left.\begin{aligned} Z_1 = \frac{r_1}{1 + j\omega C r_1}, \quad Z_2 = r_2 \\ W(j\omega) = \frac{r_2 (1 + j\omega C r_1)}{(r_1 + r_2)\left(1 + j\omega C \dfrac{r_1 r_2}{r_1 + r_2}\right)} = k \frac{1 + j\omega T_0}{1 + j\omega T} \end{aligned}\right\} \tag{3.63}$$

where

$$T_0 = Cr_1, \qquad T = C \frac{r_1 r_2}{r_1 + r_2}, \qquad k = \frac{r_2}{r_1 + r_2}$$

and

$$\tau = \frac{r_1 + r_2}{r_2} > 1$$

Circuit (*a*) is sometimes referred to as an *elastic integrating element* and circuit (*b*), an *elastic differentiating element.*

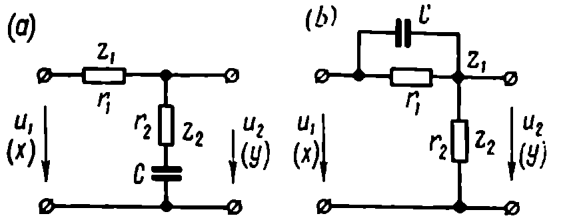

Fig. 3.17

Figure 3.18 gives frequency responses at $\tau < 1$ (*a*, *c*, *e*, *g*) and $\tau > 1$ (*b*, *d*, *f*, *h*). The responses are plotted for normalized values of

$$W_0(j\Omega) = \frac{1}{k} W(j\Omega)$$

versus relative dimensionless frequency $\Omega = \omega T$. In this case

$$W_0(j\Omega) = \frac{1 + j\Omega\tau}{1 + j\Omega} \tag{3.64}$$

$$W_0(\Omega) = \sqrt{\frac{1 + (\Omega\tau)^2}{1 + \Omega^2}} \tag{3.65}$$

$$\varphi(\Omega) = \arctan \Omega\tau - \arctan \Omega \tag{3.66}$$

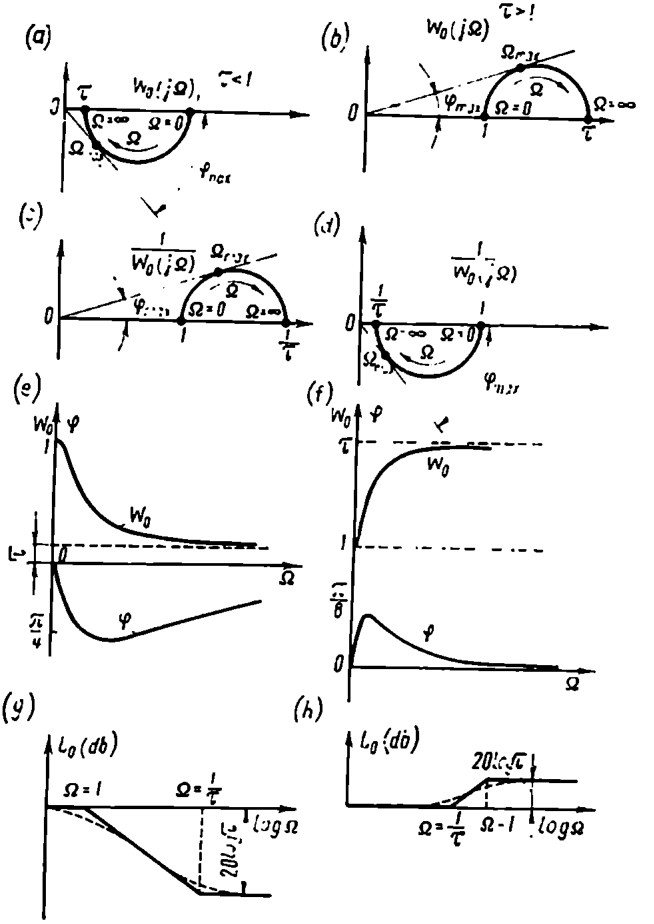

Fig. 3.18

Solving Eq. $\frac{d\varphi}{d\Omega} = 0$, we find that the maximal phase shift

$$\varphi_{max} = \arcsin \frac{\tau - 1}{\tau + 1} \tag{3.67}$$

occurs at

$$\Omega_{max} = \frac{1}{\sqrt{\tau}} \tag{3.68}$$

The logarithmic responses are given by the equation

$$L_0(\Omega) = 20 \log |W_0| = 10 \log [1 + (\Omega\tau)^2] - 10 \log [1 + \Omega^2] \tag{3.69}$$

The asymptotic responses are expressed in different ways depending on τ:

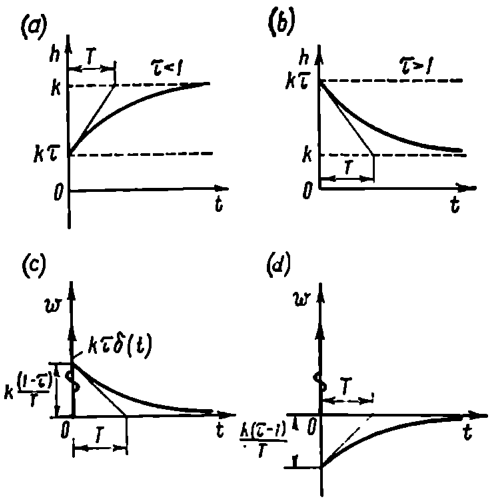

Fig. 3.19

at $\tau < 1$

$$L_{0a} = \begin{cases} 0 & \text{for } \Omega \leqslant 1 \\ -20 \log \Omega & \text{for } 1 \leqslant \Omega \leqslant \frac{1}{\tau} \\ -20 \log \tau & \text{for } \Omega \geqslant \frac{1}{\tau} \end{cases} \tag{3.70}$$

at $\tau > 1$

$$L_{0a} = \begin{cases} 0 & \text{for } \Omega \leqslant \frac{1}{\tau} \\ 20 \log \Omega\tau & \text{for } \frac{1}{\tau} \leqslant \Omega \leqslant 1 \\ 20 \log \tau & \text{for } \Omega \geqslant 1 \end{cases} \tag{3.71}$$

The transient function is determined from Eq. (3.60) as

$$h(t) = L^{-1}\left[\frac{k(1+pT_0)}{1+pT}\frac{1}{p}\right] = k\left[1+(\tau-1)\,e^{-\frac{t}{T}}\right]1_0(t) \qquad (3.72)$$

and consequently

$$w(t) = \frac{dh}{dt} = \frac{k}{T}(1-\tau)\,e^{-\frac{t}{T}}1_0(t) + k\tau\delta(t) \qquad (3.73)$$

The transient and weighting functions of lag-lead elements are given in Fig. 3.19 at $\tau < 1$ (*a* and *c*) and at $\tau > 1$ (*b* and *d*).

3.4. AN OSCILLATOR

An oscillator is described by a second-order equation

$$y + 2\zeta T\frac{dy}{dt} + T^2\frac{d^2y}{dt^2} = kx \qquad (3.74)$$

for a damping ratio $\zeta < 1$, which corresponds to complex roots of the characteristic equation

$$1 + 2\zeta pT + (pT)^2 = 0 \qquad (3.75)$$

The time constant T of an oscillator is related to its resonance frequency ω_0 as

$$T = \frac{1}{\omega_0} \qquad (3.76)$$

and is $\frac{1}{2\pi}$ times the period of resonance oscillations:

$$T_0 = \frac{2\pi}{\omega_0} \qquad (3.77)$$

Equation (3.74) is sometimes rearranged as

$$\frac{d^2y}{dt^2} + 2\zeta\omega_0\frac{dy}{dt} + y\omega_0^2 = k_1x \qquad (3.78)$$

where

$$k_1 = k\omega_0^2$$

Example 3.5. Examples of an oscillator may be an elastic mechanical system with a substantial effect of the mass, an electric oscillating circuit (Fig. 3.20), and other systems.

Indeed, in the elastic mechanical system of Fig. 3.20*a* the forces acting on a body with a mass M may be described as

$$a(x-y) = M\frac{d^2y}{dt^2} + b\frac{dy}{dt} \qquad (3.79)$$

where a and b are the coefficients of the spring and the damper. For the oscillating circuit of Fig. 3.20b

$$u_1 = u_2 + rC\frac{du_2}{dt} + LC\frac{d^2u_2}{dt^2} \tag{3.80}$$

Equation (3.79) at $\zeta = \frac{b}{2\sqrt{aM}} < 1$ describes an oscillating element with parameters $k = 1$, $T^2 = \frac{M}{a}$, and $2\zeta T = \frac{b}{a}$. Equation (3.80) at

$$\frac{r}{2}\sqrt{\frac{L}{C}} < 1$$

describes an oscillating element with parameters

$$T^2 = LC, \quad 2\zeta T = rC, \quad k = 1$$

Substituting harmonic signals in Eq. (3.74), we have a complex gain of the oscillator

$$W(j\omega) = \frac{Y(j\omega)}{X(j\omega)} = \frac{k}{1 + 2\zeta j\omega T + (j\omega T)^2} \tag{3.81}$$

By introducing the dimensionless frequency $\Omega = \omega T$, $W(j\Omega)$ can be expressed in the following way

$$W(j\Omega) = kW_0(j\Omega) = \frac{k}{1 + 2\zeta j\Omega + (j\Omega)^2} \tag{3.82}$$

Figure 3.21a, b, c, d illustrates frequency responses of an oscillator. As shown in Fig. 3.21a, the frequency response locus intersects two quadrants, IV and III, and crosses the imaginary axis at $\Omega = 1$ when $1 + (j\Omega)^2 = 0$ in Eq. (3.82). Then

$$W(j) = \frac{k}{2j\zeta}$$

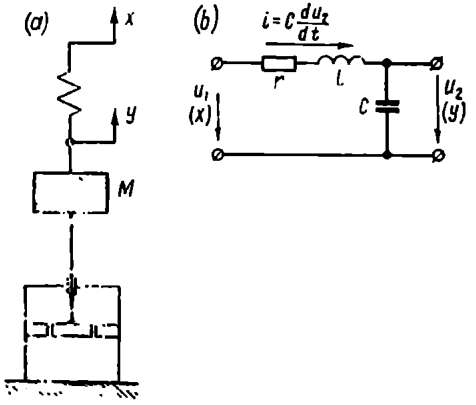

Fig. 3.20

With decreasing ζ the loop of the locus expands (see the dotted line) and at $\zeta = 0$ the response degenerates into two half-lines: I—from $W(j\Omega) = k$ to $W(j\Omega) \to \infty$ at $0 < \Omega < 1$ and II—from $W(j\Omega) = -\infty$ to $W(j\Omega) = 0$ at $1 < \Omega < \infty$. The inverse response $[W(j\Omega)]^{-1}$ intersects two quadrants, I and II, and as $\Omega \to \infty$ goes to infinity parallel to the real axis.

If a frequency locus of a real element, close to an oscillator, has been obtained experimentally, then the parameters of the corres-

ponding oscillating element can be found from the points of the response on the real and imaginary axes (points *1* and *2* in Fig. 3.21*a*). Point *1* gives k and point *2*, $\omega_0 = \frac{1}{T}$ and ζ.

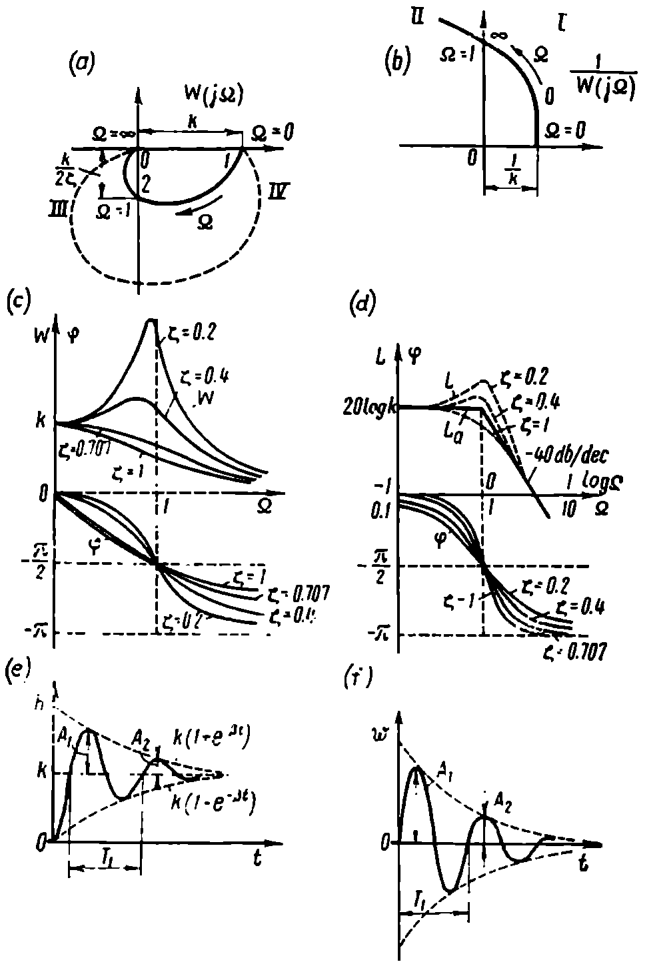

Fig. 3.21

The amplitude-frequency and phase-frequency responses are expressed by equations

$$W(\Omega) = \frac{k}{\sqrt{(1-\Omega^2)^2 + 4\zeta^2\Omega^2}} \tag{3.83}$$

$$\varphi(\Omega) = -\arctan\frac{2\zeta\Omega}{1-\Omega^2} \tag{3.84}$$

At $\Omega = 1$ these responses go through the points $W = \frac{k}{2\zeta}$ and $\varphi = -\frac{\pi}{2}$, respectively. At $\zeta < \frac{1}{\sqrt{2}} = 0.707$ the curve $W(\Omega)$ has a maximum

$$W_{max} = \frac{k}{2\zeta\sqrt{1-\zeta^2}} \tag{3.85}$$

with

$$\Omega_{max} = \sqrt{1-2\zeta^2} \tag{3.86}$$

The logarithmic amplitude-frequency response of an oscillator is

$$L(\Omega) = 20 \log k - 10 \log [(1 - \Omega^2)^2 + 4\zeta^2\Omega^2] \tag{3.87}$$

This response is strongly dependent on the damping ratio ζ near the resonance point ($\omega T = \Omega = 1$), but away from the resonance frequency the responses are practically independent of ζ.

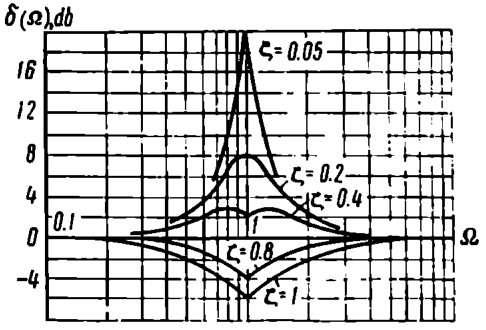

Fig. 3.22

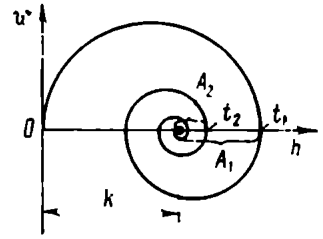

Fig. 3.23

For oscillators the following asymptotic responses are used

$$L_a(\Omega) = \begin{cases} 20 \log k & \text{at} \quad \Omega \leqslant 1 \\ 20 \log k - 40 \log \Omega & \text{at} \quad \Omega \geqslant 1 \end{cases} \tag{3.88}$$

The correction to the asymptotic response

$$\delta(\Omega) = L(\Omega) - L_a(\Omega) \tag{3.89}$$

depends on the damping ratio ζ. Plots of corrections at different ζ are shown in Fig. 3.22.

According to Eq. (3.81) the transfer function of the oscillator is

$$W(p) = \frac{k}{1 + 2\zeta pT + (pT)^2} \tag{3.90}$$

The roots of the characteristic equation $1+2\zeta pT+(pT)^2=0$ are

$$p_{1,2}=\frac{-\zeta\pm\sqrt{1-\zeta^2}}{T}=-\beta\pm j\omega_1 \tag{3.91}$$

where

$$\beta=\frac{\zeta}{T}=\omega_0\zeta=\text{damping coefficient}$$

$$\omega_1=\omega_0\sqrt{1-\zeta^2}=\frac{\sqrt{1-\zeta^2}}{T}=\text{oscillator natural frequency.}$$

The transient function

$$h(t)=L^{-1}\left[\frac{k}{1+2\zeta pT+(pT)^2}\frac{1}{p}\right]=$$

$$=k1_0(t)\left[1-e^{-\beta t}\left(\cos\omega_1 t+\frac{\beta}{\omega_1}\sin\omega_1 t\right)\right] \tag{3.92}$$

The weighting function

$$w(t)=\frac{dh}{dt}=\frac{k\omega_0^2}{\omega_1}1_0(t)\,e^{-\beta t}\sin\omega_1 t \tag{3.93}$$

The oscillator transient and weighting functions are shown in Fig. 3.21*e* and *f*. Knowing the experimental transient responses of a real element one can find the parameters of the corresponding oscillator. The values of k, A_1, A_2 and T_1 are found from $h(t)$ (see Fig. 3.21*e*) and all parameters of the element are calculated by the formulae

$$\omega_1=\frac{2\pi}{T_1} \tag{3.94}$$

$$\beta T_1=\ln\frac{A_1}{A_2} \tag{3.95}$$

$$\omega_0=\sqrt{\omega_1^2+\beta^2}=\frac{1}{T} \tag{3.96}$$

$$\zeta=\beta T \tag{3.97}$$

The same parameters can be found from the plot of the transient process in the phase plane $w(h)$ (Fig. 3.23), for which $T_1=t_2-t_1$.

Chapter IV

SPECIAL ELEMENTS OF LINEAR AUTOMATIC CONTROL SYSTEMS

4.1. SPECIAL FEATURES OF LINEAR ELEMENT RESPONSES

There are elements of control systems whose responses differ essentially from those of the typical elements described in the preceding chapter. These include *nonminimal-phase elements*, whose transfer functions are fractional rational and have zeroes in the right half-plane; *unstable elements* with poles in the right half-plane; *distributed elements*, which can be subdivided into *irrational elements*, described by irrational transfer functions, and *transcendental elements*, described by transcendental transfer functions.

4.2. STABLE NONMINIMAL-PHASE ELEMENTS

Many units, for instance those having differential or bridge circuits, incorporate elements which are described by differential equations having negative coefficients in the right-hand part and therefore zeroes in the right half-plane. The phase shift between the input and output signals may exceed $\frac{\pi}{2}$.

The differential equation of a stable nonminimal-phase first-order element is

$$y + T\frac{dy}{dt} = k\left(x - T_0\frac{dx}{dt}\right) \tag{4.1}$$

The complex gain is

$$W(j\omega) = \frac{k(1 - j\omega T_0)}{1 + j\omega T} \tag{4.2}$$

while the transfer function is

$$W(p) = k\frac{1 - pT_0}{1 + pT} \tag{4.3}$$

Example 4.1. The bridge circuits of Fig. 4.1 exemplify such elements. In the case (*a*) the equation is of the form

$$y + rC\frac{dy}{dt} = x - r_0C\frac{dx}{dt} \tag{4.4}$$

and in the case (*b*)

$$ry + r_1 r_2 C \frac{dy}{dt} = r_0 x - r_1 r_2 C \frac{dx}{dt} \qquad (4.5)$$

where $r = r_1 + r_2$, while $r_0 = r_2 - r_1$. In both cases it is implied that $r_2 > r_1$.

For the circuit (*a*) $k = 1$, $T_0 = r_0 C$, $T = rC$, $\tau = \frac{T_0}{T} < 1$.

For the circuit (*b*) $k = \frac{r_0}{r} < 1$, $T_0 = \frac{r_1 r_2}{r_1 - r_2} C$, $T = \frac{r_1 r_2}{r_2 + r_1} C$, $\tau = \frac{T_0}{T} > 1$.

Figure 4.2 represents the frequency responses of the element plotted for $\tau < 1$ and $\tau > 1$ in normalized form, where $W_0 = \frac{1}{k} W$ and $\Omega = \omega T$.

At $\tau < 1$ and at $\tau > 1$ the frequency loci are seen to lie in the third and fourth quadrants and have the form of semi-circles. Consequently, the inverse responses are semi-circles located in the first and second quadrants.

Although the loci of $W(j\Omega)$ have different positions for the lag-lead (see Fig. 3.18) and the nonminimal-phase elements, their amplitude-frequency responses are similar. Indeed, in the case under consideration

$$W_0(\Omega) = \frac{\sqrt{1 + (\Omega\tau)^2}}{\sqrt{1 + \Omega^2}} \qquad (4.6)$$

which completely coincides with Eq. (3.65).

The logarithmic amplitude-frequency responses are also similar (see Figs. 3.18 and 4.2*e* and *g*).

For phase-frequency responses

$$\varphi = -\arctan \Omega\tau - \arctan \Omega \qquad (4.7)$$

which differs considerably from Eq. (3.66).

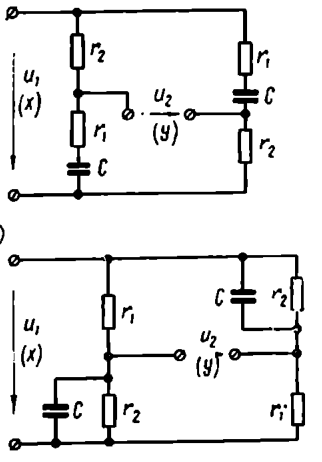

Fig. 4.1

Thus, *while amplitude-frequency responses of minimal- and nonminimal-phase elements coincide their phase-frequency responses are different.*

This is a very important fact which should always be borne in mind in determining the phase-frequency response on the basis of the amplitude-frequency response (see Sec. 2.6).

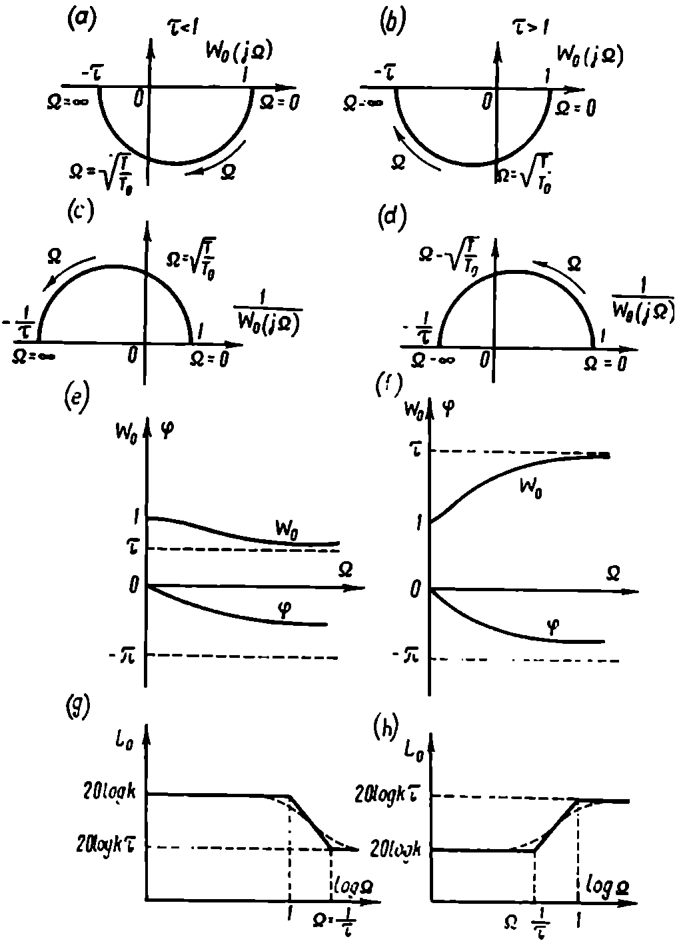
(a)
τ<1
W0(jΩ)
-τ
1
Ω=∞
0
Ω=0
Ω=√(T/T0)
Ω
(b)
τ>1
W0(jΩ)
-τ
1
Ω=∞
0
Ω=0
Ω
Ω=√(T/T0)
(c)
Ω
Ω=√(T/T0)
-1/τ
1/W0(jΩ)
1
Ω=∞
0
Ω=0
(d)
Ω=√(T/T0)
Ω
-1/τ
1/W0(jΩ)
1
Ω=∞
0
Ω=0
(e)
W0
φ
1
τ
W0
Ω
0
φ
-π
(f)
W0
φ
τ
1
W0
Ω
0
φ
-π
(g)
L0
20logk
20logkτ
logΩ
1
Ω=1/τ
(h)
L0
20logkτ
20logk
logΩ
Ω
1/τ
1

Fig. 4.2

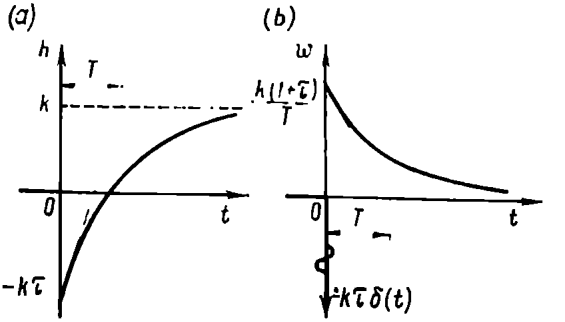
(a)
h
T
k
0
1
t
-kτ
(b)
w
k(1+τ)/T
0
T
t
kτδ(t)

Fig. 4.3

Knowing the transfer function (4.3), the transient function (Fig. 4.3*a*)

$$h(t) = k\left[1 - (1+\tau)\, e^{-\frac{t}{T}}\right] 1_0(t) \tag{4.8}$$

and the weighting function (Fig. 4.3*b*)

$$w(t) = \frac{dh}{dt} = -k\tau\delta(t) + \frac{(1+\tau)}{T} e^{-\frac{t}{T}} 1_0(t) \tag{4.9}$$

can be found.

Figure 4.3 shows that $h(t)$ changes sign with time, but the value of τ does not affect so substantially the shape of the curves $h(t)$ and $w(t)$ as in the case of minimal-phase elements.

4.3. UNSTABLE ELEMENTS

The equation of an unstable first-order element in the most general form can be given as

$$y = T\frac{dy}{dt} = k\left(x + T_0\frac{dx}{dt}\right) \tag{4.10}$$

The transfer function is

$$W(p) = \frac{k(1+pT_0)}{1-pT} \tag{4.11}$$

Equations (4.10) and (4.11) differ from (3.58) and (3.60) only in the sign of T. All kinds of first-order elements can be described

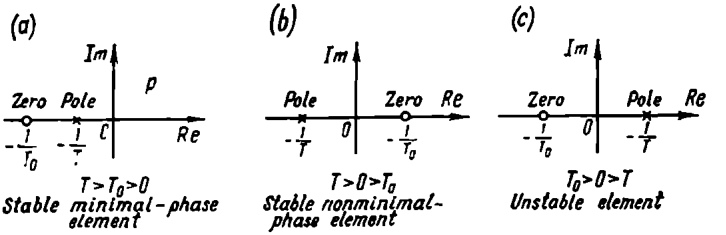

Fig. 4.4

by Eq. (3.58) if we assume that at $T > 0$ and $T_0 > 0$ the element is a standard minimal-phase one; at $T > 0$ and $T_0 < 0$ it is a nonminimal-phase stable one; at $T < 0$ it is unstable with either sign of T_0.

Figure 4.4 shows examples of zeroes and poles of first-order element transfer functions with different signs of T and T_0 in Eq. (3.58).

The most popular unstable element is a quasi-inertial element for which $T_0 = 0$. For this element we obtain, depending on the

choice of the positive directions of x and y,

$$y - T\frac{dy}{dt} = kx \tag{4.12}$$

or

$$-y + T\frac{dy}{dt} = kx \tag{4.13}$$

Example 4.2. An example of an unstable element is an asynchronous motor whose operation is represented by points *5* and *6* on the characteristic (Fig. 1.8*b*), where $a > 0$ (see Example 2.6). Choosing the positive direction of ΔU so that $b > 0$, we obtain from Eq. (2.47) the equation of an unstable element (4.13), where

$$T = \frac{J}{a}, \qquad k = \frac{b}{a}$$

The complex gain of an unstable quasi-inertial element is

$$W(j\omega) = \frac{k}{j\omega T - 1} \tag{4.14}$$

and the transfer function is

$$W(p) = \frac{k}{pT - 1} \tag{4.15}$$

The loci of the amplitude-phase response of an unstable quasi-inertial element are shown in Fig. 4.5*a* and *b*. The direct and inverse loci of the complex gain are seen to be mirror images of the inertial element loci (see Fig. 3.11) relative to the imaginary axis.

The amplitude-frequency response has the same expression as for a typical inertial element

$$W(\omega) = \frac{k}{\sqrt{1 + (\omega T)^2}} \tag{4.16}$$

Thus, the plots of $W(\omega)$ and $L(\log \omega)$ for the unstable element in question do not differ from those of a standard inertial element.

The phase-frequency response is

$$\varphi(\omega) = -\pi + \arctan \omega T \tag{4.17}$$

This relation (Fig. 4.5*c* and *d*) is a mirror image of the phase-frequency response of an inertial element relative to the straight line $\varphi = -\frac{\pi}{2}$, which corresponds to the imaginary axis.

The frequency responses discussed above allow us to conclude that *unstable elements can have the same amplitude-frequency responses as stable elements but their phase-frequency responses differ substantially from those of stable elements.*

The transfer function (4.15) can lead to the transient function (Fig. 4.5*e*)

$$h(t) = k\left[e^{\frac{t}{T}} - 1\right] 1_0(t) \tag{4.18}$$

and the weighting function (Fig. 4.5*f*)

$$w(t) = \frac{dh}{dt} = \frac{k}{T} e^{\frac{t}{T}} 1_0(t) \tag{4.19}$$

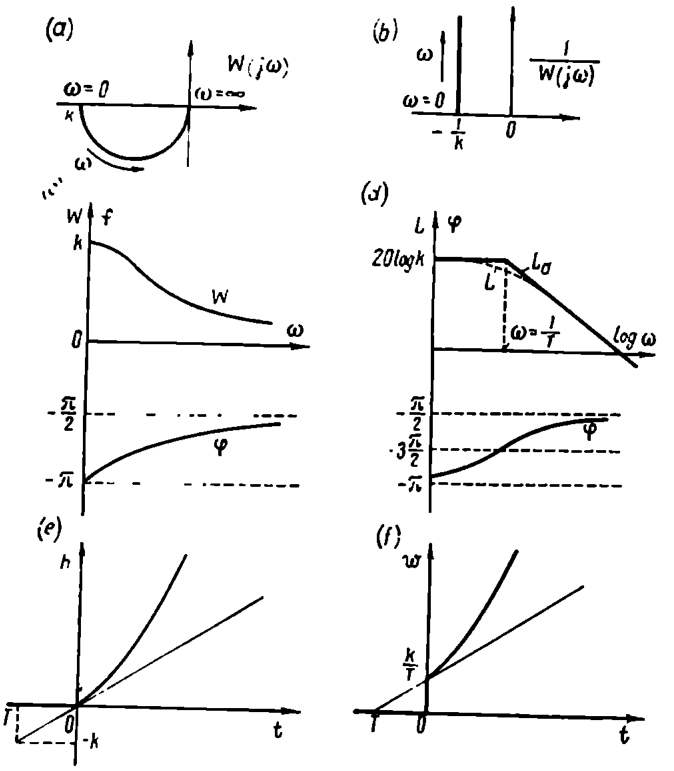

Fig. 4.5

There is no steady state for linear unstable elements and with time the output tends to infinity at any input.

4.4. IRRATIONAL ELEMENTS

A distributed element described by a one-dimensional thermal conduction equation of Fourier

$$\frac{\partial^2 v}{\partial r^2} = a \frac{\partial v}{\partial t} \tag{4.20}$$

where $v = v(r, t)$ is a function of the space coordinate r and time t and has an irrational transfer function whose form is essentially dependent on boundary conditions which allow for the points where the input signal is fed and the output signal taken out.

Assuming that v is a sine function of ω, i.e. $v = \operatorname{Im} V(j\omega t)$ where

$$V(j\omega t) = \dot{V}_m e^{j\omega t} \tag{4.21}$$

Eq. (4.20) can be transformed into

$$\frac{d^2\dot{V}_m}{dr^2} - j\omega a\dot{V}_m = 0 \tag{4.22}$$

This is a homogeneous differential equation. The roots of its characteristic equation ($\gamma^2 - j\omega a = 0$) are

$$\gamma_{1,2} = \pm\sqrt{j\omega a} \tag{4.23}$$

A solution to Eq. (4.22) has the form

$$\dot{V}_m = \dot{A}e^{-r\sqrt{j\omega a}} + \dot{B}e^{r\sqrt{j\omega a}} \tag{4.24}$$

where $\dot{A}$ and $\dot{B}$ are coefficients dependent on the boundary conditions.

If the boundary condition is $\dot{V}_m = 0$ as $r \to \infty$, then $\dot{B} = 0$ and

$$\dot{V}_m = \dot{A}e^{-r\sqrt{j\omega a}} \tag{4.25}$$

There are three most characteristic cases of feeding input and obtaining output signals

$$\left.\begin{aligned} &\text{(a)}\ \dot{X}_m = \dot{V}_m \text{ at } r = 0 \\ &\qquad \dot{Y}_m = \dot{V}_m \text{ at } r = l \end{aligned}\right\} \tag{4.26}$$

which corresponds to boundary conditions of the first type;

$$\left.\begin{aligned} &\text{(b)}\ \dot{X}_m = -b\frac{d\dot{V}_m}{dr} \text{ at } r = 0 \\ &\qquad \dot{Y}_m = \dot{V}_m \qquad \text{at } r = 0 \text{ or } r = l \end{aligned}\right\} \tag{4.27}$$

which corresponds to boundary conditions of the second type;

$$\left.\begin{aligned} &\text{(c)}\quad \dot{X}_m = -b\frac{d\dot{V}_m}{dr} + \alpha\dot{V}_m \text{ at } r = 0 \\ &\qquad \dot{Y}_m = \dot{V}_m \qquad\qquad \text{at } r = 0 \text{ or } r = l \end{aligned}\right\} \tag{4.28}$$

which corresponds to boundary conditions of the third type.

The element complex gain $W(j\omega)$ is defined as $\frac{\dot{Y}_m}{\dot{X}_m}$ with due regard for Eq. (4.25). The constant $\dot{A}$ is reduced and for the three above cases we have

for (a)

$$W(j\omega) = \frac{\dot{Y}_m}{\dot{X}_m} = e^{-l\sqrt{j\omega a}} \tag{4.29}$$

for (b)

$$W(j\omega) = \frac{\dot{Y}_m}{\dot{X}_m} = \frac{1}{b\sqrt{j\omega a}} \tag{4.30}$$

or

$$W(j\omega) = \frac{\dot{Y}_m}{\dot{X}_m} = \frac{1}{b\sqrt{j\omega a}} e^{-l\sqrt{j\omega a}} \tag{4.31}$$

for (c)

$$W(j\omega) = \frac{\dot{Y}_m}{\dot{X}_m} = \frac{1}{\alpha + b\sqrt{j\omega a}} \tag{4.32}$$

or

$$W(j\omega) = \frac{\dot{Y}_m}{\dot{X}_m} = \frac{1}{\alpha + b\sqrt{j\omega a}} e^{-l\sqrt{j\omega a}} \tag{4.33}$$

In all cases the complex gain is expressed as an irrational function of $j\omega$.

Examples of irrational elements include all kinds of diffusion and heat plants (Fig. 4.6*a*), in particular plants heated by radiation

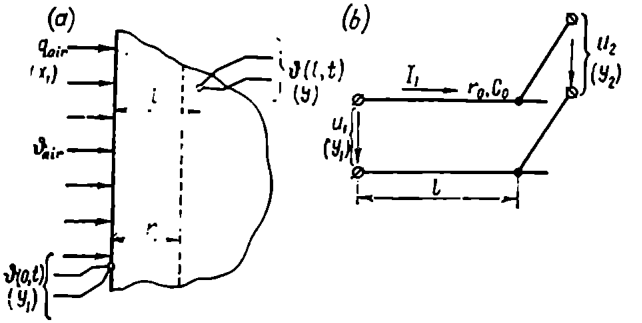

Fig. 4.6

(see Ch. I, Sec. 1.3, Fig. 1.12); induction-heated plants; a telephone cable (Fig. 4.6*b*) with distributed resistance and capacitance.

Example 4.3. Let a body of infinite thickness (Fig. 4.6) be heated by radiation with no heat emission from the surface ($q_s = 0$). Then Eq. (1.13) becomes

$$q_0 = -\lambda \frac{\partial \vartheta (0, t)}{\partial r} \tag{4.34}$$

provided that, by virtue of Eq. (1.11),

$$\frac{\partial^2 \vartheta}{\partial r^2} = \frac{c}{\lambda} \frac{\partial \vartheta}{\partial t} \tag{4.35}$$

These equations coincide with Eqs. (4.27) and (4.20), respectively, at

$$\dot{Q}_{0m} = \dot{X}_m, \quad \dot{\Theta}_m (0) = \dot{V}_m (0) = \dot{Y}_m, \quad \lambda = b \quad \frac{c}{\lambda} = a$$

Consequently, for a radiation furnace

$$W_1 (j\omega) = \frac{\dot{\Theta}_m (0)}{\dot{\Theta}_{0m}} = \frac{1}{\lambda \sqrt{j\omega a}} \tag{4.36}$$

If heat is dissipated by the body surface by Newton's law, i.e.

$$q_s = \alpha [\vartheta (0, t) - \vartheta_{air}] \tag{4.36a}$$

where α is the coefficient of heat exchange between the surface and air and the air temperature ϑ_{air} is assumed to be zero, then the complex gain is given by the equation

$$W_2 (j\omega) = \frac{\dot{\Theta}_m (0)}{\dot{Q}_{0m}} = \frac{1}{\alpha + \lambda \sqrt{j\omega a}} \tag{4.37}$$

If the input is the body surface temperature $\dot{X}_m = \dot{\Theta}_m (0)$ and the output is the temperature at a depth l, i.e. $\dot{Y}_m = \dot{\Theta}_m (l)$, then

$$W_3 (j\omega) = \frac{\dot{\Theta}_m (l)}{\dot{\Theta}_m (0)} = e^{-l \sqrt{j\omega a}} \tag{4.38}$$

Denoting $\frac{1}{\lambda \sqrt{a}} = k_1$, $\frac{1}{\alpha} = k$, $\left(\frac{\lambda}{\alpha}\right)^2 a = T$, and $l^2 a = T_0$, Eqs. (4.36)-(4.38) can be rearranged as

$$W_1 (j\omega) = \frac{k_1}{\sqrt{j\omega}} \tag{4.39}$$

$$W_2 (j\omega) = \frac{k}{1 + \sqrt{j\omega T}} \tag{4.40}$$

$$W_3 (j\omega) = e^{-\sqrt{j\omega T_0}} \tag{4.41}$$

which corresponds to Eqs. (4.30), (4.32), and (4.29).

The transfer functions which correspond to Eqs. (4.30), (4.32), and (4.29) at $k_1 = \frac{1}{b\sqrt{a}}$, $k = \frac{1}{\alpha}$, $T = \frac{ab^2}{\alpha^2}$, and $T_0 = al^2$ are

$$W(p) = \frac{k_1}{\sqrt{p}} \tag{4.42}$$

$$W(p) = \frac{k}{1+\sqrt{pT}} \tag{4.43}$$

$$W(p) = e^{-\sqrt{pT_0}} \tag{4.44}$$

Equations (4.42) and (4.43) differ from the transfer functions of an integrating and an inertial element only by the square root. By analogy with integrating and inertial elements the elements under consideration can be termed *semi-integrating* and *semi-inertial*. The third expression is transcendental as well as irrational.

Let us now take a closer look at characteristics of irrational elements described by Eqs. (4.42) and (4.43).

A semi-integrating element. The frequency responses of a semi-integrating element given by Eq. (4.39) are shown in Fig. 4.7. The frequency locus (*a*) is a straight line located in the fourth quadrant and running at an angle of $-\frac{\pi}{4}$, which is half that for an integrating element. The inverse response (*b*) is in the first quadrant and has a slope of $+\frac{\pi}{4}$.

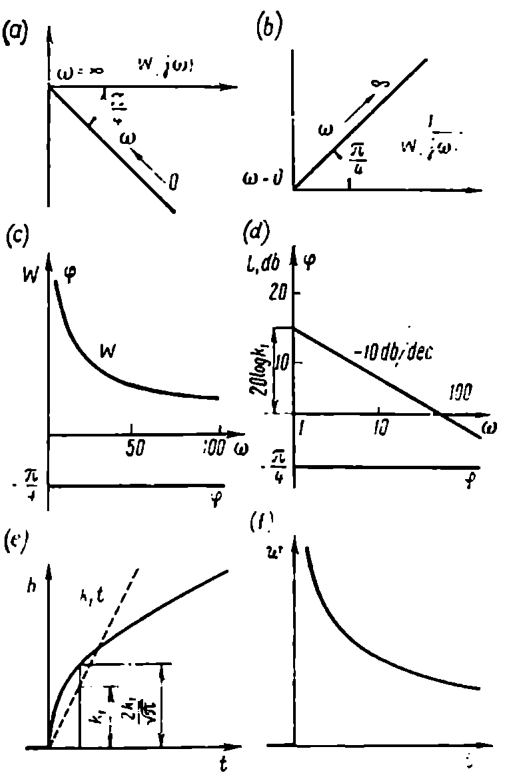

Fig. 4.7

The amplitude and phase of the complex gain

$$W(\omega) = \frac{k_1}{\sqrt{\omega}} \tag{4.45}$$

and

$$\varphi(\omega) = -\frac{\pi}{4} \tag{4.46}$$

The logarithmic amplitude-frequency response is

$$L(\omega) = 20 \log W(\omega) = 20 \log k_1 - 10 \log \omega \qquad (4.47)$$

The plots of amplitude-frequency and phase-frequency responses are shown in Fig. 4.7*c* and *d*. The logarithmic amplitude-frequency response is seen to be half as steep as the response of an integrating element and its slope is 10 db/dec.

Knowing the transfer function (4.42), the transient and weighting functions (see Fig. 4.7*e* and *f*) can be obtained through Laplace transformation tables

$$h(t) = L^{-1}\left\{\frac{k_1}{\sqrt{p}}\frac{1}{p}\right\} = 2k_1\sqrt{\frac{t}{\pi}}\,1_0(t) \qquad (4.48)$$

and

$$w(t) = \frac{dh}{dt} = \frac{k_1}{\sqrt{\pi t}}\,1_0(t) \qquad (4.49)$$

While in the integrating element the value of h reaches k_1 over a time $t = 1$ (dotted line in Fig. 4.7*e*), the process in the semi-integrating element goes faster at the beginning and over a time $t = 1$ the value of h reaches $\frac{2}{\sqrt{\pi}}k_1 \cong 1.13k_1$. However, in both cases $h \to \infty$ with time.

Semi-inertial element. The frequency responses of a semi-inertial element plotted by Eq. (4.40) are shown in Fig. 4.8*a*, *b*, *c*, *d*. In all cases

$$W(j\omega) = \frac{k}{1+\sqrt{j\omega T}} = \frac{k}{1+e^{j\frac{\pi}{4}}\sqrt{\omega T}} = \frac{k\sqrt{2}}{(\sqrt{2}+\sqrt{\omega T})+j\sqrt{\omega T}} \qquad (4.50)$$

The locus of a semi-inertial element (*a*) differs from that of an inertial element. It is not a half but a quarter of a circle with centre in point O and supported by a chord of length k. The tangents to the locus at points $\omega = 0$ and $\omega = \infty$ intersect the real axis at an angle of $\frac{\pi}{4}$ and each other at an angle of $\frac{\pi}{2}$.

The inverse response (*b*) is a half-line issuing from point $\frac{1}{k}$ at $\omega = 0$ at an angle of $\frac{\pi}{4}$ to the real axis.

The magnitude and phase of the complex gain will be, respectively,

$$\left.\begin{aligned} W(\omega) &= \frac{k\sqrt{2}}{\sqrt{|\sqrt{2}+\sqrt{\omega T}|^2+\omega T}} = \frac{k}{\sqrt{1+\sqrt{2\omega T}+\omega T}} \\ \varphi(\omega) &= -\arctan\frac{\sqrt{\omega T}}{\sqrt{2}+\sqrt{\omega T}} \end{aligned}\right\} \qquad (4.51)$$

As $\omega \to \infty$, $\varphi = -\arctan 1 = -\frac{\pi}{4}$.

Consequently, the logarithmic amplitude-frequency response is

$$L(\omega) = 20 \log k - 10 \log [1 + \sqrt{2\omega T} + \omega T] \qquad (4.52)$$

The asymptotic response for this case may be given by two

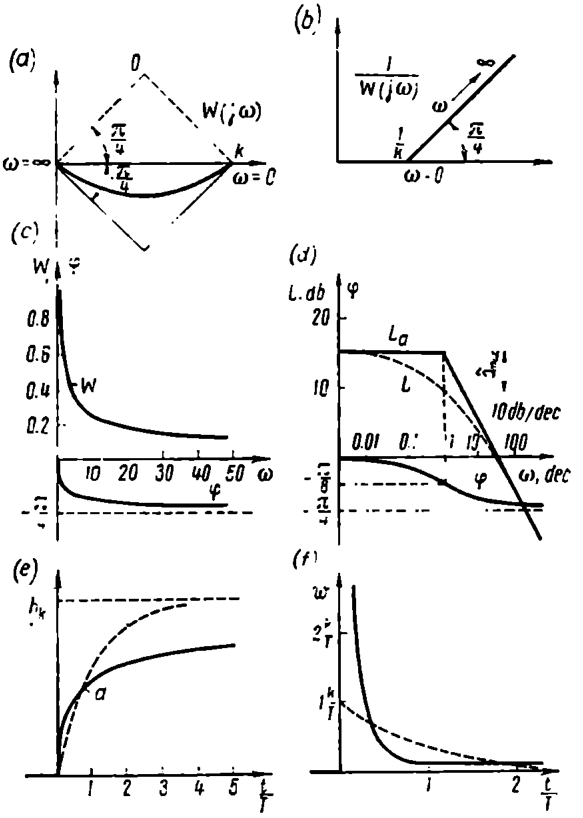

Fig. 4.8

half-lines

$$L_a(\omega) = \begin{cases} 20 \log k & \text{at } \omega T \leqslant 1 \\ 20 \log k - 10 \log \omega T & \text{at } \omega T \geqslant 1 \end{cases}$$

and at $\omega T > 1$ it has a slope of -10 db/dec.

The maximum error is in the breaking point at $\omega T = 1$

$$\delta_{max} = L\left(\frac{1}{T}\right) - L_a\left(\frac{1}{T}\right) = -10 \log (2 + \sqrt{2}) \approx -5.3 \text{ db}$$

Thus, for a semi-inertial element the phase shift and the slope of the logarithmic frequency response is half that for an inertial element and the maximum error of asymptotic response is appreciably higher (5.3 db instead of 3 db).

The transient function is obtained from the transfer function (4.43) by inverse Laplace transformation, which can be found in handbooks

$$h(t) = L^{-1}\left\{\frac{k}{1+\sqrt{pT}}\frac{1}{p}\right\} = k\left[1 - e^{\frac{t}{T}}\operatorname{erfc}\sqrt{\frac{t}{T}}\right]1_0(t) \qquad (4.53)$$

where

$$\operatorname{erfc}(x) = \frac{2}{\sqrt{\pi}}\int_x^\infty e^{-u^2}du = 1 - \operatorname{erf}(x)$$

is a tabulated probability integral.

The weighting function is

$$w(t) = \frac{dh}{dt} = \frac{k}{T}\left[\sqrt{\frac{T}{\pi t}} - e^{\frac{t}{T}}\operatorname{erfc}\sqrt{\frac{t}{T}}\right]1_0(t) \qquad (4.54)$$

Both these functions are plotted in Fig. 4.8*e* and *f* where the dotted lines show similar characteristics for an inertial element.

As evidenced by the plots, a semi-inertial element is stable but, unlike an inertial element with the same time constant T, its transient process goes faster at the beginning and then approaches the steady state more slowly. The value of the semi-inertial and inertial element output is $h = 0.5k$ at $t = 0.7T$ (see intersection point *a* in Fig. 4.8*e*).

4.5. DELAY ELEMENTS

A distributed element described by a one-dimensional telegraphic equation of D'Alembert

$$\frac{\partial^2 v}{\partial r^2} = a\frac{\partial^2 v}{\partial t^2} \qquad (4.55)$$

where $v = v(r, t)$ is a function of the space coordinate r and the time t, has a transcendental transfer function, which depends on the boundary conditions and the point where the output signal is taken out.

Introducing a phaser (which depends on the space coordinate)

$$V(j\omega t) = \dot{V}_m e^{j\omega t} \qquad (4.56)$$

Eq. (4.55) can be reduced to the form

$$\frac{d^2\dot{V}_m}{dr^2} + \omega^2 a\dot{V}_m = 0 \qquad (4.57)$$

The roots of the characteristic equation $\gamma^2 + a\omega^2 = 0$ are imaginary

$$\gamma_{1,2} = \pm j\omega\sqrt{a} = \pm j\omega\alpha \tag{4.58}$$

where $\alpha = \sqrt{a}$.

The solution to Eq. (4.57) can be given as

$$\dot{V}_m = \dot{A}e^{-j\omega\alpha r} + \dot{B}e^{j\omega\alpha r} \tag{4.59}$$

where $\dot{A}$ and $\dot{B}$ are coefficients depending on the boundary conditions. The first addend represents a wave moving in the direction of increasing r, the second addend, a reverse wave.

Let us restrict our attention to plants with just one wave moving in the direction of increasing r. Then $\dot{B} = 0$ and

$$\dot{V}_m = \dot{A}e^{-j\omega\alpha r}. \tag{4.60}$$

The most widespread case is an input action at $r = 0$, or $\dot{X}_m = \dot{V}_m(0)$ and an output signal at $r = l$, or $\dot{Y}_m = \dot{V}_m(l)$. In this case $\dot{X}_m = \dot{A}$, $\dot{Y}_m = \dot{A}e^{-j\omega\alpha l}$ and

$$W(j\omega) = \frac{\dot{Y}_m}{\dot{X}_m} = e^{-j\omega\tau} \tag{4.61}$$

where $\tau = \alpha l$ is the delay time.

If $x = X_m \sin \omega t$, or $X(j\omega t) = \dot{X}_m e^{j\omega t}$, then $Y(j\omega t) = \dot{X}e^{j\omega(t-\tau)}$, or $y(t) = X_m \sin \omega(t - \tau)$; in other words the output reproduces the input signal with a delay τ. Therefore such elements are called *delay elements*, or *delays*.

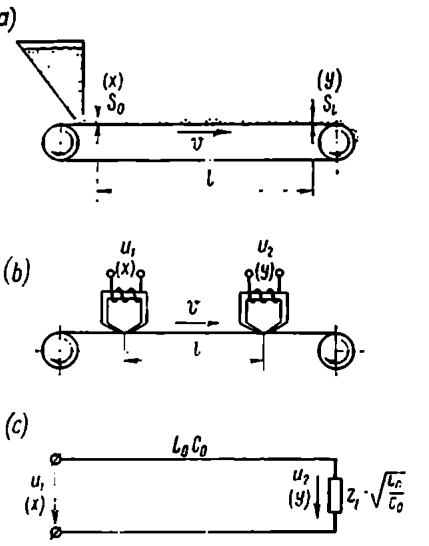

Fig. 4.9

Delays are used in most diverse technological lines, in tape recorders, in hydraulic systems, and electric circuits without losses and with distributed inductance L_0 and capacitance C_0.

Some examples of actual delays are shown in Fig. 4.9. When dry material is fed on a line (*a*) moving at the rate v, the thickness S_l of the layer at a distance l falls behind the thickness S_0 at the beginning by the time $\tau = \frac{l}{v}$. The voltage u_2 at the reading head (*b*) of a tape recorder reproduces the voltage u_1 at the writing head with

a delay $\tau = \frac{l}{v}$. The voltage u_2 at the end of the line without losses (*c*) loaded with a matched resistance $z_l = z_m = \sqrt{\frac{L_0}{C_0}}$ reproduces the voltage u_1 at the input terminals with a delay $\tau = l\sqrt{L_0 C_0}$.

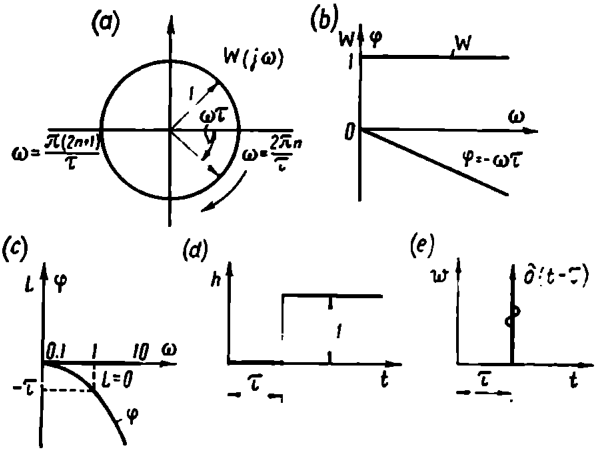

Fig. 4.10

The frequency responses of the complex gain calculated by formula (4.61) are shown in Fig. 4.10*a*, *b*, *c*. The amplitude-phase response is a circle of unit radius with centre in the origin of coordinates (*a*). The circle intersects the real axis in point $+1$ at $\omega = \frac{2\pi n}{\tau}$ and in point -1 at $\omega = \frac{\pi(2n+1)}{\tau}$.

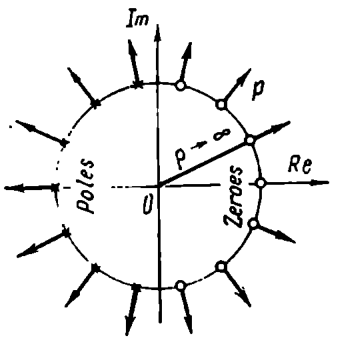

Fig. 4.11

The amplitude-frequency and phase-frequency responses (*b*) and (*c*) are given by the following relations

$$|W| = 1, \quad L = 0, \quad \varphi = -\omega\tau$$

The transfer function of the delay is

$$W(p) = e^{-p\tau} \qquad (4.62)$$

A delay is a nonminimal-phase stable element and has an infinite number of poles in the left half-plane with the magnitude tending to infinity, and an infinite number of zeroes in the right half-plane with the magnitude tending to infinity as well. Indeed, the equation $e^{-p\tau} = 0$ has a solution $p_l = \rho e^{j\varphi}$ if $\rho \to \infty$ and $-\frac{\pi}{2} < \varphi <$

$< +\frac{\pi}{2}$, while the equation $e^{p\tau} = 0$ has a solution if $\rho \to \infty$ and $\frac{\pi}{2} < \varphi < 3\frac{\pi}{2}$ (see Fig. 4.11).

The transient and weighting functions (Fig. 4.10*d* and *e*) are found from the transfer function

$$h(t) = L^{-1}\left\{\frac{e^{-p\tau}}{p}\right\} = 1_0(t-\tau) \tag{4.63}$$

$$w(t) = \frac{dh}{dt} = \delta(t-\tau) \tag{4.64}$$

Of all the elements treated in this chapter, the delay is of greatest practical importance, especially in sampled data systems.

Chapter V

LINEAR ELEMENTS CONNECTION

5.1. GENERAL

If the mathematical description of all the control system elements is known, one can readily draw a structural diagram of the elements connection as was done for the plants.

When making an analysis of different connections the effect of a particular connection on element transfer functions should

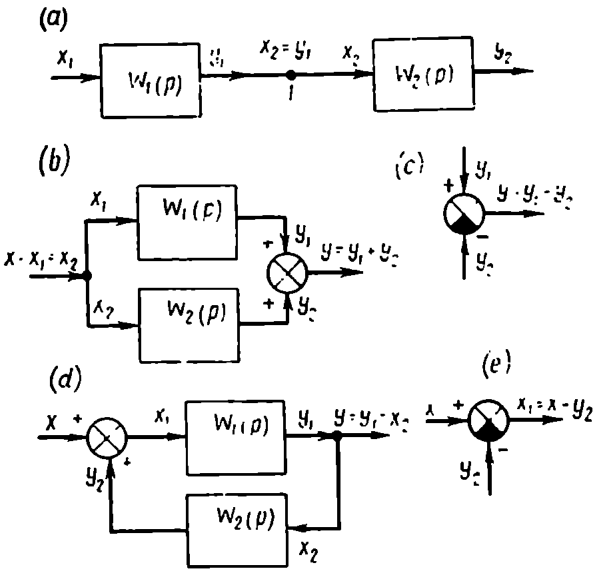

Fig. 5.1

be taken into account. For example, if the output of a four-terminal is connected to the input of an amplifier with a resistance r, the resistance should be introduced into the four-terminal diagram and allowed for in determining its transfer function. In order to eliminate the effect of elements connection on the individual transfer functions

the input resistance of the subsequent element or the output signal power of the preceding element must be infinitely large.

It is assumed hereafter that the elements are *unilateral* (i.e. they transmit a signal in one direction) and the transfer functions of the particular elements do not depend on their connection (i.e. the transfer functions are found with due regard for the elements connection).

There are three basic types of elements connections: *series* (Fig. 5.1*a*), *parallel concordant*, or *feedforward* (Fig. 5.1*b*, *c*), and *parallel contrary*, or *feedback* (Fig. 5.1*d*, *e*). Let us consider the specific features of each connection.

5.2. SERIES CONNECTION OF ELEMENTS

In series connection the output of one element is the input of another. If elements i and k are connected in series, then

$$y_i = x_k \tag{5.1}$$

When n elements having transfer functions W_1, W_2, . . ., W_n are connected in series (Fig. 5.2), the interconnection equations have the form

$$x_{i+1} = y_i \quad \text{or} \quad X_{i+1}(p) = Y_i(p) \tag{5.2}$$

Since for each element

$$Y_i(p) = W_i(p)\, X_i(p) \tag{5.3}$$

then

$$X_{i+1}(p) = W_i(p)\, X_i(p) \tag{5.4}$$

Writing such equations for all elements and eliminating all intermediate variables (leaving the input $X(p) = X_1(p)$ and the output

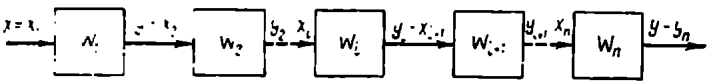

Fig. 5.2

$Y(p) = Y_n(p)$ variables only), we obtain

$$Y(p) = W_1(p)\, W_2(p) \ldots W_n(p)\, X(p) \tag{5.5}$$

Consequently, *the transfer function of a system consisting of elements connected in series is*

$$W(p) = \frac{Y(p)}{X(p)} = \prod_{i=1}^{r} W_i(p) \tag{5.6}$$

i.e. *it is the product of element transfer functions.* The magnitudes of complex coefficients are multiplied and the arguments added up.

The logarithmic amplitude-frequency and phase-frequency responses of individual elements are added up.

When minimal-phase elements are connected in series the resultant system is also a minimal-phase one, i.e. its transfer function has neither zeroes nor poles in the right half-plane. Indeed, if none of the terms of the product (5.6) have zeroes or poles in the right half of the p plane, the same is true for the entire product.

If at least one of the elements connected in series is nonminimal-phase or unstable, the entire system can be shown to be nonminimal-phase or unstable.

Example 5.1. A series connection of an integrator and an inertial element (inertial integrator).

If two elements with transfer functions $W_1(p) = \frac{1}{p}$ and $W_2(p) = \frac{k}{1+pT}$ are connected in series, the transfer function of the resulting system is

$$W = W_1 W_2 = \frac{k}{p(1+pT)} \tag{5.7}$$

This system represents a d.c. motor with an inertial load on the shaft if the armature supply voltage is the input and the shaft rotation angle is the output (see Sec. 2.3).

The complex gain of the system is

$$W(j\omega) = \frac{k}{j\omega(1+j\omega T)} \tag{5.8}$$

At $0 < \omega < \infty$ it is represented by the locus of Fig. 5.3*a*.

This locus is constructed by multiplying the appropriate complex values found for each specified frequency from the loci of an integrator (see Fig. 3.6*a*) and an inertial (see Fig. 3.11*a*) element.

Transforming the expression (5.8) and separating the real and imaginary parts, we get

$$W(j\omega) = -\frac{kT}{1+(\omega T)^2} - j\frac{\frac{k}{\omega}}{1+(\omega T)^2} \tag{5.9}$$

Hence follows that as ω tends to 0 the complex $W(j\omega)$ tends to infinity along a vertical straight line which passes through the point $-kT$. This straight line is an asymptote for the locus in question.

An inverse locus (Fig. 5.3*b*) can be constructed in a similar way.

Logarithmic amplitude-frequency and phase-frequency responses (Fig. 5.3*c*) are obtained by summing the corresponding curves of Figs. 3.6*b* and *c*, and 3.11*c* and *d*.

The transient and weighting functions of a system of elements connected in series are found from its transfer function and cannot

be obtained by direct summing of the responses of individual elements

$$h(t) = L^{-1}\left\{\frac{k}{p(1+pT)}\frac{1}{p}\right\} = k\left[t - T\left(1 - e^{-\frac{t}{T}}\right)\right] 1_0(t) \qquad (5.10)$$

$$w(t) = \frac{dh}{dt} = k\left(1 - e^{-\frac{t}{T}}\right) 1_0(t) \qquad (5.11)$$

These responses are shown in Fig. 5.3*d* and *e*. The dotted lines show the asymptotes $h_a(t) = k(t - T)$ and $w_a = k$.

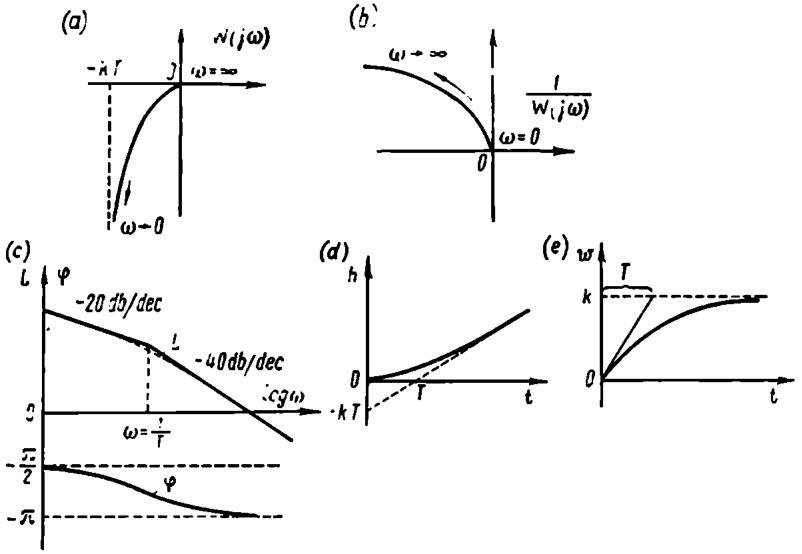

Fig. 5.3

A series connection of a differential and an inertial element gives an inertial-differentiating element, while that of a lead and an inertial element gives a lag-lead element (see Secs. 3.3 and 3.4).

Example 5.2. A series connection of two inertial elements. The transfer function of two elements connected in series and having transfer functions $W_1 = \frac{k_1}{1+pT_1}$ and $W_2 = \frac{k_2}{1+pT_2}$ has the form

$$W(p) = W_1 W_2 = \frac{k_1 k_2}{(1+pT_1)(1+pT_2)} \qquad (5.12)$$

The complex gain is

$$W(j\omega) = \frac{k}{(1+j\omega T_1)(1+j\omega T_2)} \qquad (5.13)$$

where $k = k_1 k_2$.

Equations (5.12) and (5.13) coincide with the corresponding equations of an oscillator for $\zeta \geqslant 1$.

The frequency responses of such a series connection are shown in Fig. 5.4. The locus (*a*) of complex gain has the same form as for

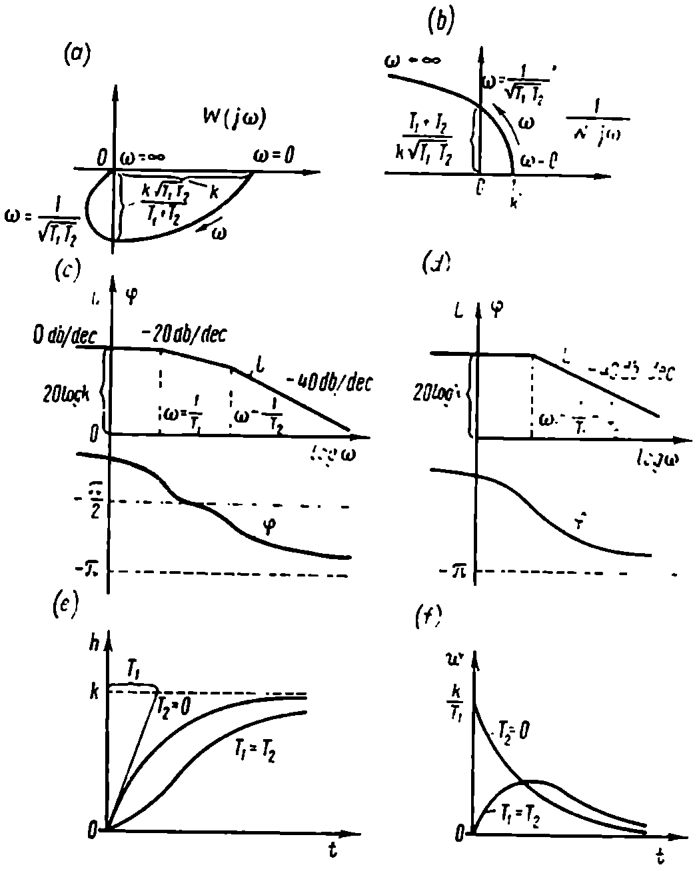

Fig. 5.4

an oscillator, but the point of intersection with the imaginary axis is closer to the origin of coordinates.

The inverse locus (*b*) also has the same form as for an oscillator. The logarithmic amplitude-frequency and phase-frequency responses are obtained by direct summation of the ordinates of the corresponding element responses for the two cases, $T_2 < T_1$ (*c*) and $T_2 = T_1$ (*d*).

Knowing the transfer function (5.12), one can find the transient and weighting functions

$$h(t) = k\left[1 - \frac{T_1 e^{-\frac{t}{T_1}} - T_2 e^{-\frac{t}{T_2}}}{T_1 - T_2}\right] 1_0(t) \qquad (5.14)$$

$$w(t) = \frac{k}{T_1 - T_2}\left(e^{-\frac{t}{T_1}} - e^{-\frac{t}{T_2}}\right) 1_0(t) \qquad (5.15)$$

At $T_1 = T_2$ or $\xi = 1$ the solution is obtained by limit transition $T_2 \to T_1$ and evaluating the indeterminate form $\frac{0}{0}$. In that case

$$h(t) = k\left[1 - \left(1 + \frac{t}{T_1}\right) e^{-\frac{t}{T_1}}\right] 1_0(t) \qquad (5.16)$$

and

$$w(t) = \frac{k}{T_1^2} t e^{-\frac{t}{T_1}} 1_0(t) \qquad (5.17)$$

If $T_2 \to 0$, the system degenerates into one inertial element with a time constant T_1 (see Sec. 3.3).

At $0 < T_2 < T_1$ the transient and weighting functions are located in the intermediate region between the curves obtained for $T_2 = 0$ and $T_2 = T_1$ (Fig. 5.4*e* and *f*).

5.3. DETERMINING THE PARAMETERS OF A MINIMAL-PHASE SYSTEM BY ITS AMPLITUDE-FREQUENCY RESPONSE

If the frequency response of a system has been obtained for the entire frequency range from 0 to ∞, then the equivalent circuit of a minimal-phase system having the same response can be found.

Let us find the equivalent circuit of a series connection of integrating, inertial, and lead elements. The complex gain of such a system is

$$W(j\omega) = \frac{k}{(j\omega)^{n_0}} \prod_{i=1}^{m} (1 + j\omega T_i)^{n_i} \qquad (5.18)$$

where n_0 is the number of integrating elements and $|n_i|$, the total number of identical elements.

When $n_i > 0$ the elements are of a lead type, when $n_i < 0$, they are inertial.

For an equivalent circuit to be implementable with standard, easy-to-construct elements, n_i must be an integer.

If time constants T_i differ by more than one decade, then the regions of the overall response $L(\omega) = 20 \log |W(j\omega)|$ may be

specified where the asymptotic logarithmic response obtained for the frequency range $\frac{1}{T_i} < \omega < \frac{1}{T_{i+1}}$ fits well the real (accurate) response. Thus, for the whole response $L(\omega)$ the asymptotic response may be constructed as a broken line with a slope variation $20n_i$ db/dec.

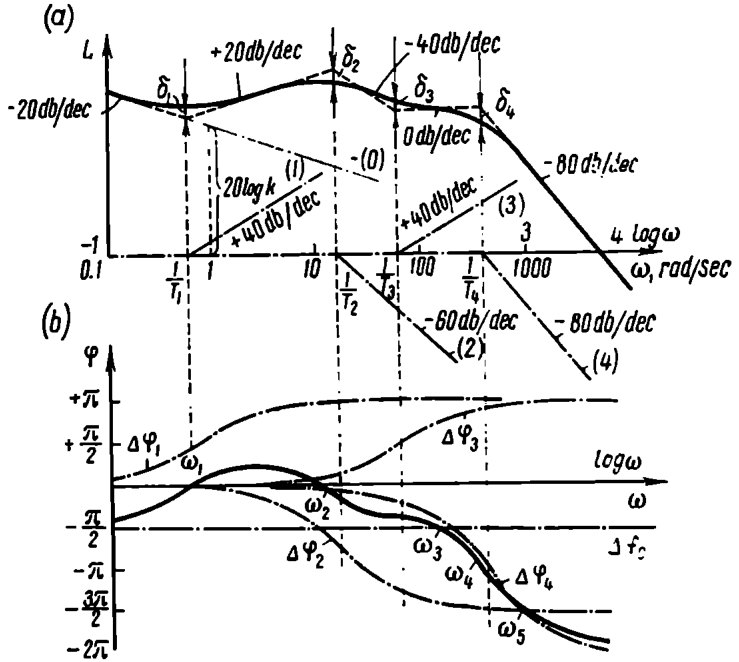

Fig. 5.5

When $n_i > 0$, this variation is positive and the slope of $L(\omega)$ grows with frequency. When $n_i < 0$, it decreases with frequency.

When Eq. (5.18) holds, the analytical expressions of accurate amplitude-frequency and phase-frequency responses have the form

$$L(\omega) = 20 \log k - n_0 20 \log \omega + \sum_{i=1}^{m} n_i 10 \log [1 + (\omega T_i)^2] \qquad (5.19)$$

and

$$\varphi(\omega) = -n_0 \frac{\pi}{2} + \sum_{i=1}^{m} n_i \arctan \omega T_i \qquad (5.20)$$

The breaking points of the asymptotic response permit determining T_i, while the difference in slope angles yields the power of n_i.

Example 5.3. The response $L(\omega)$ of a system is given in Fig. 5.5*a*. The smooth curve $L(\omega)$ can be approximated by a broken line

with slopes of —20 db/dec, +20 db/dec, —40 db/dec, 0 db/dec, —80 db/dec. It is required to find a minimal-phase equivalent circuit and construct a phase-frequency response.

An asymptotic broken curve can be represented as consisting of a set of components which correspond to asymptotic responses of standard elements. For the case under consideration these are one integrator (straight line 0 with a slope of —20 db/dec), two identical lead elements with a time constant T_1 (line *1* with slopes

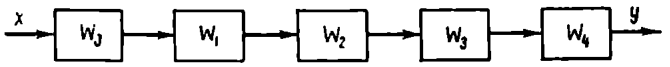

Fig. 5.6

of 0, +40 db/dec), three identical inertial elements with a time constant T_2 (line *2* with slopes of 0, —60 db/dec), two identical lead elements with a time constant T_3 (line *3* with slopes of 0, +40 db/dec), and four identical inertial elements with a time constant T_4 (line *4* with slopes of 0, —80 db/dec).

The equivalent circuit is a series connection of elements with transfer functions

$$W_0 = \frac{k}{p}, \quad W_1 = (1 + pT_1)^2,$$

$$W_2 = \frac{1}{(1 + pT_2)^3},$$

$$W_3 = (1 + pT_3)^2 \quad \text{and} \quad W_4 = \frac{1}{(1 + pT_4)^4}$$

which corresponds to $n_0 = 1$, $n_1 = 2$, $n_2 = -3$, $n_3 = 2$, $n_4 = -4$, and $m = 4$ in formulae (5.18) and (5.19). This circuit is shown in Fig. 5.6.

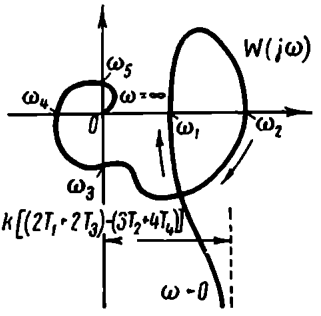

Fig. 5.7

Knowing the parameters of the equivalent circuit, the phase-frequency responses can be obtained by formula (5.20) (see Fig. 5.5*b*). The equivalent circuit was found using asymptotic characteristics which assume an error $\delta_i = n_i$ 3 db in breaking points. If the values of errors assumed in the approximation (δ_1, δ_2, δ_3, and δ_4 in Fig. 5.5*a*) satisfy this condition, then the curve $\varphi(\omega)$ is in full correspondence with the initial curve $L(\omega)$.

The locus of $W(j\omega)$ for this case is shown in Fig. 5.7.

The frequency response $\varphi(\omega)$ must be found in some practical cases on the knowledge of $L(\omega)$ without constructing a readily implementable equivalent circuit. Then the initial curve $L(\omega)$

can be approximated by an arbitrary broken line the straight sections of which have slopes of n_i 20 db/dec, where n_i can be any number, either integral or fractional. In this case, too, $\varphi(\omega)$ is calculated by formula (5.20). If there is a sharp peak in the breaking points of the response $L(\omega)$, while the slope change in the vicinity of the

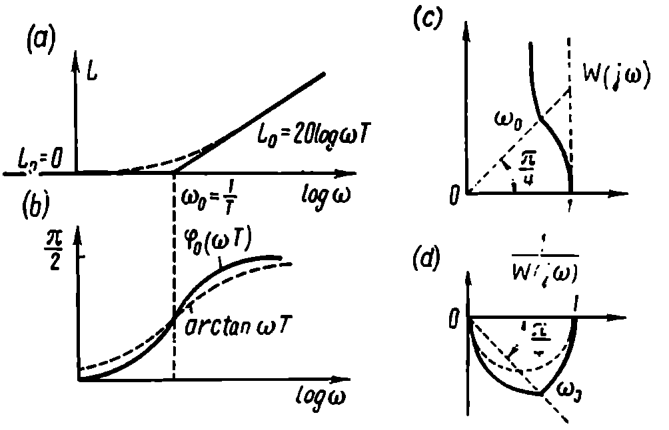

Fig. 5.8

breaking point is —40 db/dec, then the response of an oscillator (see Sec. 3.4) can be conveniently used for approximating $L(\omega)$ in this region.

If the logarithmic response is a broken line, then the response $\varphi(\omega)$ of the minimal-phase systems can be obtained rigorously without the assumption of smoothing in the vicinity of the breaking points. To do this one must find phase-frequency responses which completely correspond to the logarithmic amplitude-phase response given as a broken line.

Let us consider a logarithmic response described by Eq. (3.54) at $k = 1$ (solid line in Fig. 5.8*a*):

$$L_0(\omega) = \begin{cases} 0 & \text{at } 0 < \omega T \leqslant 1 \\ 20\log\omega T & \text{at } \omega T \geqslant 1 \end{cases} \qquad (5.21)$$

A minimal-phase element having such a response is known as an *asymptotic lead element*. Let us find by formula (2.55) the phase-frequency response of the minimal-phase element if the amplitude-frequency response is given by (5.21)

$$\varphi(\omega) = \frac{1}{\pi}\int_1^\infty \frac{\ln \nu T}{\nu T - \omega T}\, d\nu T = \frac{1}{\pi}\int_1^\infty \frac{\ln x}{x - \omega T}\, dx = \varphi_0(\omega T) \qquad (5.22)$$

This definite integral has been tabulated, and the function $\varphi_0(\omega T)$ is given in Ref. 77 and shown in Figs. 5.8*b* and 5.9. A comparison of $\varphi_0(\omega T)$ with the curve $\arctan \omega T$ shows that these functions have much in common: they are valued in the same range and go through the point $\varphi = \frac{\pi}{4}$ at $\omega T = 1$. But the curve $\varphi_0(\omega T)$ is

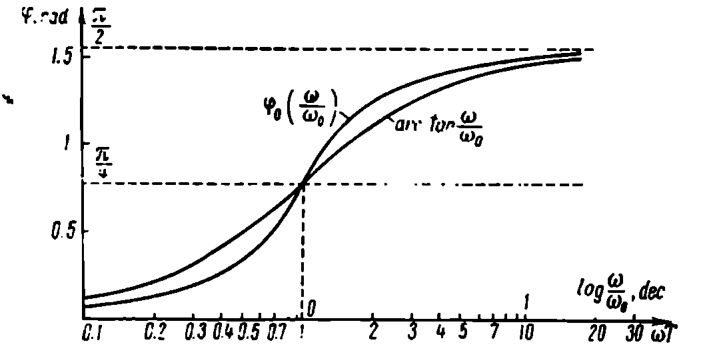

Fig. 5.9

much steeper near the frequency $\omega = \frac{1}{T}$ than the curve $\arctan \omega T$.

If a frequency locus is constructed by using the curves $L(\omega)$ and $\varphi_0(\omega T)$, it will differ perceptibly from that of a lead element. Figure 5.8*c* and *d* shows the accurate (dotted line) and asymptotic (solid line) responses of a lead element. The difference is at its greatest near the frequency $\omega = \frac{1}{T}$.

The function $\varphi_0(\omega T)$ is used extensively to find the phase-frequency response of a minimal-phase system when the broken-line logarithmic response is known.

Figure 5.10 shows the decomposition of the logarithmic response into half-infinite straight lines corresponding to the asymptotic responses of a lead or inertial element, having an arbitrary slope angle and obtainable by multiplying the appropriate response by n_i.

The same figure shows the construction of $\varphi(\omega)$ as a sum of products $n_i\varphi_0(\omega_i T)$ found for each of the half-infinite straight lines.

The described method of finding the phase-frequency responses from amplitude responses was first applied by Bode for the synthesis of feedback amplifiers.

A comparison of the curves $\varphi_0(\omega T)$ and $\arctan \omega T$ also demonstrates that the methods of decomposing logarithmic responses into accurate (see Fig. 5.5) or asymptotic (see Fig. 5.10) responses of inertial

or lead elements are very much alike and give almost the same results.

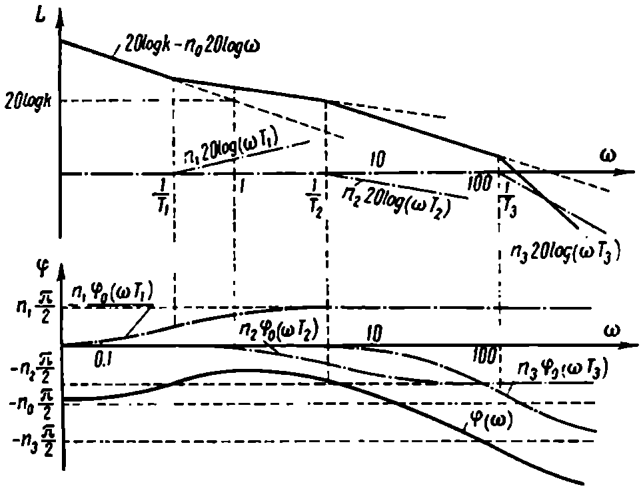

Fig. 5.10

The first method is simpler and permits using the amplitude-frequency response to find an equivalent circuit consisting of standard elements connected in series, and estimate the resulting approximation error.

5.4. PARALLEL CONCORDANT (FEEDFORWARD) CONNECTION

In the case of *feedforward connection* of elements the inputs of all the elements are the same, while the outputs are summed (with appropriate signs). If n elements are connected in parallel, the input is

$$x = x_1 = x_2 = \ldots = x_n \tag{5.23}$$

and the output is

$$y = \sum_{i=1}^{n} y_i \tag{5.24}$$

Using images, we find that the transfer function of a feedforward connection is

$$W(p) = \frac{Y(p)}{X(p)} = \sum_{i=1}^{n} \frac{Y_i(p)}{X_i(p)} = \sum_{i=1}^{n} W_i(p) \tag{5.25}$$

Consequently, the transient function is

$$h(t) = \sum_{i=1}^{n} h_i(t) \tag{5.26}$$

and the weighting function is

$$w(t) = \sum_{i=1}^{n} w_i(t) \tag{5.27}$$

The flowchart of a feedforward connection of n elements is shown in Fig. 5.11.

The transfer, transient and weighting functions are summed up in this case. To obtain a complex gain the separate complex variable

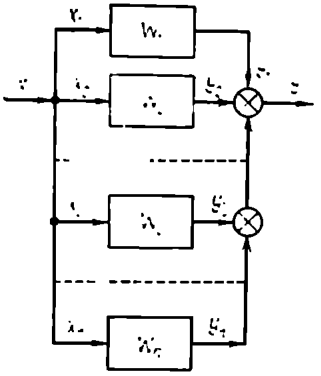

Fig. 5.11

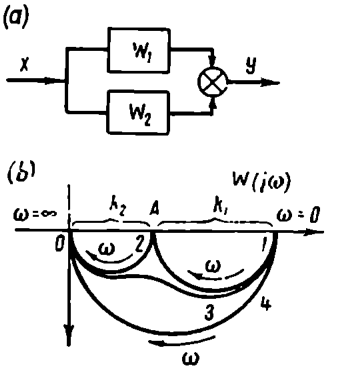

Fig. 5.12

must be represented as a real and an imaginary part rather than as the magnitude and argument. For example, if

$$W_i(j\omega) = P_i(\omega) + jQ_i(\omega) \tag{5.28}$$

then

$$W(j\omega) = \sum_{i=1}^{n} W_i(j\omega) = \sum_{i=1}^{n} P_i(\omega) + j \sum_{i=1}^{n} Q_i(\omega) \tag{5.29}$$

The system resulting from parallel connection of stable elements is also found to be stable because the common denominator of the sum of fractions cannot have roots other than the roots of the addends, and consequently the lack of poles of addends in the right half-plane rules out the appearance of the poles in the sum.

The situation with minimal-phase elements is different. The sum of minimal-phase transfer functions may have zeroes in the right half-plane and consequently feedforward connection of minimal-phase elements may give a nonminimal-phase system. Conversely,

feedforward connection of nonminimal-phase stable elements may result in a minimal-phase stable system.

Example 5.4. Let us determine the frequency response of a feedforward connection of two inertial elements with the same sign of the outputs (Fig. 5.12*a*)

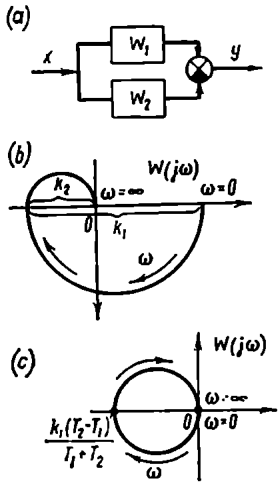

Fig. 5.13

$$W(j\omega) = \frac{k_1}{1+j\omega T_1} + \frac{k_2}{1+j\omega T_2} \qquad (5.30)$$

Depending on the relation of T_1 and T_2, the locus of the complex gain may have different forms. If $T_1 \gg T_2$, the frequencies at which the complex gain goes along the circles of the loci to be added up are different; the final locus is made up of two half-circles of diameters k_1 and k_2 (Fig. 5.12*b*, curves *1* and *2*). Where frequencies vary from 0 to about $\frac{10}{T_1}$, the head of the complex gain vector describes a half-circle *1* of diameter k_1. If the frequencies range from $\frac{10}{T_1}$ to $\frac{0.1}{T_2}$, the head of this vector shifts slightly near point A and if the frequencies range from $\frac{0.1}{T_2}$ to ∞ it describes half-circle *2* of diameter k_2.

If the time constants T_1 and T_2 do not differ much, the vector describes a smooth curve *3* (see Fig. 5.12*b*).

If $T_1 = T_2$, the locus is a half-circle of diameter $k_1 + k_2$ (curve *4*).

Example 5.5. Let us find the frequency response of two inertial elements in a feedforward connection with opposite signs of the outputs (Fig. 5.13*a*)

$$W(j\omega) = \frac{k_1}{1+j\omega T_1} - \frac{k_2}{1+j\omega T_2} = \frac{(k_1-k_2)+j\omega(k_1T_2-k_2T_1)}{(1+j\omega T_1)(1+j\omega T_2)} \qquad (5.31)$$

If $k_1 > k_2$ and $k_1T_2 < k_2T_1$, then this system is a nonminimal-phase one and has a zero in the right half-plane. The locus of the complex gain for this case is shown in Fig. 5.13*b*.

If $k_1 = k_2$, then

$$W(j\omega) = \frac{j\omega(k_1T_2-k_2T_1)}{1+j\omega(T_1+T_2)+(j\omega)^2T_1T_2} \qquad (5.32)$$

The locus is a complete circle (Fig. 5.13*c*) of diameter $k_1\frac{T_1-T_2}{T_1+T_2}$. It goes through the point $k_1\frac{T_2-T_1}{T_1+T_2}$ at a frequency $\omega = \frac{1}{\sqrt{T_1T_2}}$.

Example 5.6. Let us find the frequency response of the feedforward connection of the proportional element ($W = 1$) and the delay [$W_2(j\omega) = e^{-j\omega\tau}$] having the same signs of the outputs. We have

$$W(j\omega) = (1 + e^{-j\omega\tau}) = 2e^{-j\frac{\omega\tau}{2}} \cos\frac{\omega\tau}{2} \quad (5.33)$$

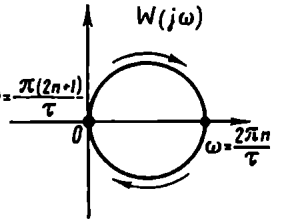

Fig. 5.14

The corresponding locus is shown in Fig. 5.14. This system is seen to be a filter rejecting all frequencies $\omega = \frac{\pi(2n+1)}{\tau}$ for which the gain is zero.

A lead element consisting of a proportional and a differentiating element and a lag-lead element, which can be obtained by parallel connection of an inertial and an inertial-differentiating element or an inertial and a proportional element, are examples of systems made up of parallel-connected simple elements.

5.5. PARALLEL CONTRARY (FEEDBACK) CONNECTION

Two elements make a *feedback connection* if the output signal of the first element is fed to the input of the second one, and the output signal of the second element is summed (with the appropriate sign) with the common input signal and fed to the input of the first element. The common output signal is the output of the first element (see Fig. 5.1*d* and *e*).

The element where the direction of signal propagation coincides with that of the common signal (the first element) is termed a *forward element*, while the element where the direction of signal propagation is opposite to that of the common signal (the second element) is a *feedback element*.

If the sign of the feedback signal is positive, i.e. the signal is added to the common input signal (see Fig. 5.1*d*), the feedback is termed *positive*. If the sign of the feedback is negative, i.e. the signal is subtracted from the common input signal (see Fig. 5.1*e*), the feedback is termed *negative*.

In a feedback connection the feedforward and feedback elements are connected as a closed ring and the external signal is fed to the common point of the first element input and the second element output. The equations of a feedback connection are

1) input equations:

a) for positive feedback

$$x_1 = x + y_2 \quad (5.34)$$

b) for negative feedback

$$x_1 = x - y_2 \tag{5.35}$$

these are *closing equations*;

2) output equation

$$y = y_1 = x_2 \tag{5.36}$$

The theory of oscillations normally deals with positive feedback circuits and uses Eq. (5.34).

The control theory deals mainly with negative feedback circuits and uses Eq. (5.35), which will be the basis of further discussion. Considering Eqs. (5.35) and (5.36) simultaneously and bearing in mind that

$$Y(p) = W(p)\,X(p), \quad Y_1(p) = W_1(p)\,X_1(p) \quad \text{and}$$
$$Y_2(p) = W_2(p)\,X_2(p)$$

we obtain

$$X_1(p) = \frac{Y(p)}{W_1(p)} = X(p) - W_2(p)\,Y(p)$$

whence

$$Y(p) = \frac{W_1(p)}{1 + W_1(p)\,W_2(p)}\,X(p) \tag{5.37}$$

or

$$W(p) = \frac{Y(p)}{X(p)} = \frac{W_1(p)}{1 + W_1(p)\,W_2(p)} \tag{5.38}$$

For elements with a fractional rational transfer function

$$W_1(p) = \frac{K_1(p)}{D_1(p)} \quad \text{and} \quad W_2(p) = \frac{K_2(p)}{D_2(p)}$$

Eq. (5.38) can be rearranged as

$$W(p) = \frac{K_1(p)\,D_2(p)}{K_1(p)\,K_2(p) + D_1(p)\,D_2(p)} \tag{5.39}$$

The last equation leads to the conclusion that the zeroes of $W(p)$ coincide with the zeroes of $W_1(p)$ and the poles of $W_2(p)$, but the poles of the function $W(p)$ differ from the poles of $W_1(p)$ and $W_2(p)$. Consequently, a feedback connection of stable elements may result in an unstable system, and conversely, a feedback connection of elements which include unstable ones may prove stable. With harmonic signals the complex gain is

$$W(j\omega) = \frac{W_1(j\omega)}{1 + W_1(j\omega)\,W_2(j\omega)} \tag{5.40}$$

If a feedback circuit is a proportional element [$W_2(p) = k_2$], the feedback is referred to as *proportional*.

If the feedback circuit is a differentiating element $\left(W_2 = pT \right.$ or $\left. W_2 = \frac{pT}{1+pT}\right)$, then the feedback is termed *rate*, or *differentiating feedback.*

If a feedback circuit is an integrator $\left(W_2 = \frac{1}{pT}\right)$, the feedback is *integrating.*

Some of the standard elements can be visualized as feedback connections of simpler elements.

Example 5.7. An integrating element with a proportional feedback.

The transfer functions of such elements are

$$W_1 = \frac{k_1}{p}, \quad W_2 = k_2$$

Substituting W_1 and W_2 into formula (5.38), we have

$$W(p) = \frac{k_1}{k_1 k_2 + p} = \frac{k}{1+pT}$$

where

$$T = \frac{1}{k_1 k_2} \quad \text{and} \quad k = \frac{1}{k_2}$$

Consequently, a feedback connection of an integrator and a proportional element gives an inertial element (see Sec. 3.3).

Example 5.8. A proportional element with an integrating feedback.

The transfer functions of such elements are

$$W_1 = k_1, \quad W_2 = \frac{k_2}{p}$$

Substituting into (5.38), we have

$$W(p) = \frac{k_1 p}{k_1 k_2 + p} = \frac{kp}{1+pT}$$

where

$$k = \frac{1}{k_2} \quad \text{and} \quad T = \frac{1}{k_1 k_2}$$

An inertial-differentiating element (see Sec. 3.3) can thus be obtained by a feedback connection of a proportional and an integrating element.

Example 5.9. An inertial-integrating element with a proportional feedback.

The transfer functions of such elements are

$$W_1 = \frac{k_1}{p(1+pT_2)}, \quad W_2 = k_2$$

Substituting into (5.38), we have

$$W(p) = \frac{k_1}{k_1 k_2 + p + p^2 T_1} = \frac{k}{1 + 2\zeta T p + p^2 T^2} \tag{5.41}$$

where

$$k=\frac{1}{k_2},\quad T=\sqrt{\frac{T_1}{k_1k_2}},\quad \zeta=\frac{1}{2\sqrt{k_1k_2T_1}}$$

An oscillator (Sec. 3.4) can thus be obtained by introducing a proportional feedback loop into an inertial-integrating element.

Example 5.10. A high-gain feedback amplifier.

If we assume that in Eq. (5.38) $W_1(p)=k_1W_0(p)$ and $k_1\to\infty$, then

$$W(p)=\frac{1}{W_2(p)} \tag{5.42}$$

Consequently, if the gain of a forward element is very high the transfer function of a feedback connection is independent of the frequency response of the forward path and is the inverse transfer function of the feedback element. Thus, the introduction of an integrating element into the feedback path may yield a system equivalent to a differentiating element; by introducing an inertial feedback element, a system analogous to a lead element can be obtained.

The examples of this chapter lead to the conclusion that all standard elements of Ch. III are reducible to different connections of two simple elements: a proportional and an integrating element.

5.6. MODELS OF STANDARD LINEAR ELEMENTS

In studying various processes in control systems, models of standard elements are used extensively to form more involved structures.

These models are usually based on operational d.c. amplifiers whose transfer function corresponds to a proportional element with a very high gain (normally thousands and tens of thousands).

The diagram of a model incorporating an operational amplifier is shown in Fig. 5.15. The amplifier is assumed ideal with input resistance between the terminals *1-0* infinitely high and the output voltage $Y(p)=kU_1(p)$ independent of the load. This implies that the internal resistance between the terminals *2-0* is zero.

Using the superposition principle, we have

$$U_1(p)=X(p)\frac{Z_2(p)}{Z_1(p)+Z_2(p)}-Y(p)\frac{Z_1(p)}{Z_1(p)+Z_2(p)} \tag{5.43}$$

For an amplifier

$$Y(p)=kU_1(p) \tag{5.44}$$

Solving these equations for $Y(p)$, we have

$$Y(p)=\frac{kZ_2(p)}{(1+k)Z_1(p)+Z_2(p)}X(p) \tag{5.45}$$

whence the transfer function is

$$W(p) = \frac{Y(p)}{X(p)} = \frac{kZ_2(p)}{(1+k)Z_1(p) + Z_2(p)} \tag{5.46}$$

If $k \gg 1$ (which is true for operational amplifiers), then Eq. (5.45) can be simplified by assuming $k \to \infty$. Then

$$W(p) = \frac{Z_2(p)}{Z_1(p)} \tag{5.47}$$

By selecting appropriate values of $Z_1(p)$ and $Z_2(p)$, models of different elements can be obtained from this equation.

Example 5.11. Using active resistors r_1 and r_2 for $Z_1(p)$ and $Z_2(p)$, we will have a proportional element. Selecting $Z_1(p) = r_1$ and

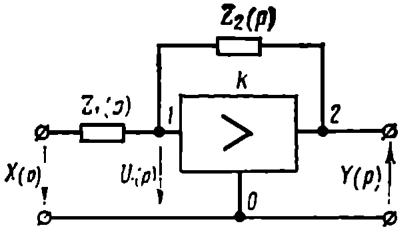

Fig. 5.15

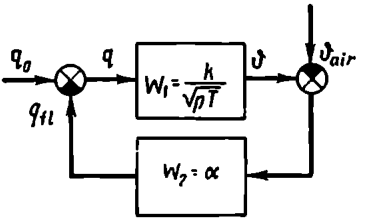

Fig. 5.16

$Z_2(p) = \frac{1}{pC}$, an integrator with a transfer function $W_1 = \frac{1}{pT}$ can be obtained, where $T = r_1C$. Using a parallel connection of the capacitor C and the resistor r_2 as $Z_2(p)$ gives an inertial element with a transfer function

$$W_2(p) = \frac{Z_2(p)}{Z_1(p)} = \frac{1}{\left(\frac{1}{r_2} + pC\right) r_1} = \frac{\frac{r_2}{r_1}}{1 + pCr_2} \tag{5.48}$$

An oscillator can be obtained by using a parallel connection of the inductor L_2, resistor r_2, and capacitor C as $Z_2(p)$ and the inductor L_1 as $Z_1(p)$. Then

$$W(p) = \frac{Z_2(p)}{Z_1(p)} = \frac{1}{\left(\frac{1}{r_2} + pC + \frac{1}{pL_2}\right) pL_1} = \frac{\frac{L_2}{L_1}}{1 + p\frac{L_2}{r_2} + p^2CL_2} \tag{5.49}$$

Consequently, models of all standard elements of linear control systems can be obtained. By connecting these models, control systems of any complexity can be investigated.

Example 5.12. Operational amplifiers can be used in constructing nonstandard elements as well. For instance, if $Z_2(p)$ is represented

by a model of a long line which is a chain-like circuit consisting of resistors and capacitors, then with a sufficient number of chain links its input resistance in the operator form is

$$Z_2(p) \cong \sqrt{\frac{r_0}{pC_0}}$$

where r_0 and C_0 are the resistance and capacitance of the chain elements.

If $Z_1 = r_1$, the model's transfer function is

$$W_1(p) = \frac{Z_2(p)}{Z_1(p)} = \sqrt{\frac{r_0}{pC_0 r_1^2}} \tag{5.50}$$

This model corresponds to a semi-integrating element. If, for instance, radiation heating of a massive body has to be modelled and the relation of the heat flux density q and the temperature ϑ at the surface is described by a semi-integrating element, given that the heat flux density is the difference between the density of the incident flux and heat dissipation from a unit surface [see Eq. (4.36a)],

$$q_{fl} = \alpha (\vartheta - \vartheta_{air}) \tag{5.51}$$

then the plant model can be constructed of two elements, a proportional one with a gain α and a semi-integrating one with a transfer function as given by Eq. (5.50). The density of the incident heat flux q_0 and the ambient air temperature ϑ_{air} are given in the appropriate scale by input signals fed to the operational amplifiers.

The block diagram of such a model is shown in Fig. 5.16.

Chapter VI

EQUATIONS OF AUTOMATIC CONTROL SYSTEMS

6.1. STRUCTURAL DIAGRAMS AND TRANSFER FUNCTIONS OF ELEMENTARY CONTROL SYSTEMS

In Ch. I functional diagrams of elementary control systems were considered. For these systems *structural diagrams* can be composed which correspond to equations describing the processes in each of the functional elements.

Let us discuss structural diagrams and transfer functions for the examples of control systems given in Sec. 1.6.

Float level controller. If we assume that in a certain operating range of the obturating needle the rate Q of petrol influx into the

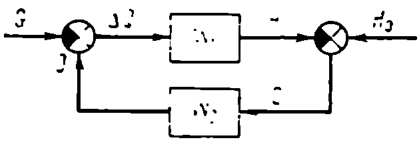

Fig. 6.1

carburettor (see Fig. 1.21*a*) is proportional to the needle motion u, which is in turn proportional to the float displacement ε relative to the desired level H_0, then the level controller can be represented as a combination of an integrator and a proportional element which correspond to the plant (W_1) and the actuator (W_2) on the functional diagram (see Fig. 1.21*b*). The transfer function of a floating chamber as a hydraulic tank is determined in Example 2.2. The external disturbance G is subtracted from the petrol influx rate.

The structural diagram of the system in question is given in Fig. 6.1, where

$$W_1 = \frac{k_1}{p} \quad \text{and} \quad W_2 = k_2$$

The relation between the variation of petrol outflow $f = \Delta G$ and the variation of the petrol level $y = \Delta H$ is expressed, following formula (5.38), as

$$Y(p) = -\frac{W_1}{1 + W_1 W_2} F(p) \tag{6.1}$$

The transfer function of the system relating the disturbance to the output is

$$W(p) = \frac{Y(p)}{F(p)} = \frac{-k_1}{k_1 k_2 + p} \tag{6.1a}$$

Automatic voltage stabilization at the terminals of a d.c. generator (see Fig. 1.22). In a d.c. generator control system the generator load current i_l, the rotation rates $\Delta\omega_1$ and $\Delta\omega_2$ of the generator

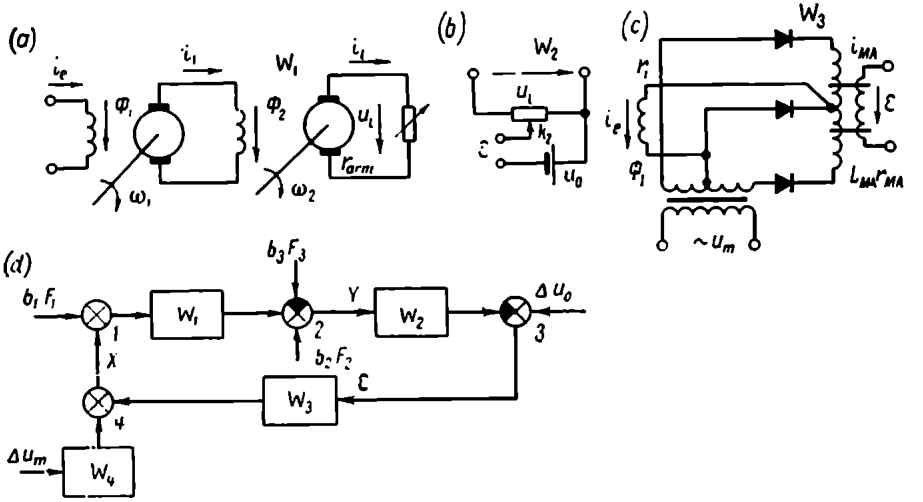

Fig. 6.2

shafts, and the supply voltage ΔU_{MA} of the magnetic amplifier are external disturbances, whose effect necessitates the presence of a controller.

To evaluate the effect of different disturbances on the operation of the system, a structural diagram specifying the points where the disturbances act may prove useful. This diagram can be obtained by using the transfer functions of three basic elements of the functional diagram (see Fig. 1.22*b*): the generator (Fig. 6.2*a*), the measuring unit (Fig. 6.2*b*), and the amplifier (Fig. 6.2*c*).

Equation (2.42) establishes a relation between the load voltage and external controls and disturbances. Giving it in the form

$$Y = W_1 (X + b_1 F_1) + b_2 F_2 - b_3 F_3 \tag{6.2}$$

where

$$W_1 = \frac{k_1}{1 + pT_1} \tag{6.3}$$

allows one to represent the plant and the actions as in the structural diagram of Fig. 6.2*d*. Here the images of increments Δi_e, Δu_l, $\Delta\omega_1$, $\Delta\omega_2$, and Δi_l are denoted as X, Y, F_1, F_2, and F_3, respectively.

The external actions are applied in accordance with Eq. (6.2) at nodes *1* and *2*.

The measuring unit and the comparator (which compares the controlled variable and the reference $\frac{u_0}{k_2}$) are shown on the diagram as element W_2 and summing point *3*. Since the equation of the comparator circuit is (see Fig. 6.2*b*)

$$\varepsilon = u_0 - k_2 u_l$$

then the transfer function

$$W_2 = -\frac{\Delta\varepsilon}{\Delta u_l} = k_2 \tag{6.4}$$

The magnetic amplifier of Fig. 6.2*c* is an a.c. system with modulation and demodulation. To consider signal conversion by the amplifier in full detail would be a rather involved task. If the frequency spectrum of the magnetic amplifier input current i_{MA} is below the supply frequency, then a transient process is mainly determined by time constants of the excitation winding both of the amplifier and the generator (the latter winding acts as the load of the magnetic amplifier).

In this case the following approximate equations are valid

$$\varepsilon = r_{MA} i_{MA} + L_{MA} \frac{di_{MA}}{dt} \tag{6.5}$$

$$e_{MA} = r_1 i_e + w_1 \frac{d\Phi_1}{dt} \tag{6.6}$$

Here L_{MA} is the equivalent inductance of the magnetic amplifier excitation winding, r_{MA} and i_{MA}, the resistance and the excitation circuit current, and e_{MA} and ε, the unloaded output voltages of the magnetic amplifier and the comparator.

If

$$e_{MA} = e_{MA}(u_{MA}, i_{MA}) \tag{6.7}$$

where u_{MA} is the magnetic amplifier supply voltage (the amplitude value), then for increments of variables in linearized regions we obtain

$$\Delta e_{MA} = \left(\frac{\partial e_{MA}}{\partial u_{MA}}\right)_0 \Delta u_{MA} + \left(\frac{\partial e_{MA}}{\partial i_{MA}}\right)_0 \Delta i_{MA} \tag{6.8}$$

$$\Delta e_{MA} = r_1 \Delta i_e + w_1 \left(\frac{\partial \Phi_1}{\partial i_e}\right)_0 \frac{d\Delta i_e}{dt} \tag{6.9}$$

By direct Laplace transformation we obtain

$$\Delta I_e(p) = \frac{\Delta E_{MA}(p)}{r_1 + w_1 \left(\frac{\partial \Phi_1}{\partial i_e}\right)_0 p} \tag{6.10}$$

$$\Delta I_{MA}(p) = \frac{\Delta E(p)}{r_{MA} + L_{MA} p} \tag{6.11}$$

Solving Eqs. (6.8), (6.10), and (6.11) simultaneously, we obtain for images of increments

$$\Delta I_c(p) = \left(\frac{\partial e_{MA}}{\partial u_{MA}}\right)_0 \frac{\Delta U_{MA}(p)}{r_1 + w_1\left(\frac{\partial \Phi_1}{\partial i_e}\right)p} + \\ + \left(\frac{\partial e_{MA}}{\partial i_{MA}}\right)_0 \frac{\Delta E(p)}{(r_{MA} + L_{MA}p)\left[r_1 + w_1\left(\frac{\partial \Phi_1}{\partial i_e}\right)_0 p\right]}$$

or

$$X = W_3 \Delta E + W_5 \Delta U_{MA} \tag{6.12}$$

where

$$\left.\begin{aligned} W_3 &= \frac{k_3}{(1+pT_2)(1+pT_3)} \\ W_4 &= \frac{k_4}{1+pT_2} \end{aligned}\right\} \tag{6.13}$$

Here

$$k_3 = \frac{1}{r_1 r_{MA}}\left(\frac{\partial e_{MA}}{\partial i_{MA}}\right)_0, \qquad k_4 = \frac{1}{r_1}\left(\frac{\partial e_{MA}}{\partial u_{MA}}\right)_0,$$
$$T_2 = \frac{w_1}{r_1}\left(\frac{\partial \Phi_1}{\partial i_e}\right)_0, \quad \text{and} \quad T_3 = \frac{L_{MA}}{r_{MA}}$$

The additional noise caused by mains voltage oscillations, Δu_{MA}, is shown in the diagram of Fig. 6.2*d* as the action in summing point *4*.

If the variation of voltage at the armature of the generator caused by the variation of the generator load current, $r_{arm}\Delta i_l$, is treated as an external action $b_3 f_3$, while the variation of voltage at the generator terminals, $\Delta u_l = y$, as the controlled action, then, according to Eq. (5.38), we have

$$Y(p) = \frac{-1}{1+W_{o-l}} b_3 F_3(p) \tag{6.14}$$

where $W_{o-l} = W_1 W_2 W_3$ is the transfer function of the open-loop system.

By formulae (6.3), (6.4), and (6.13)

$$W_{o-l} = \frac{k}{(1+pT_1)(1+pT_2)(1+pT_3)} \tag{6.15}$$

where $k = k_1 k_2 k_3$.

Substituting (6.15) into (6.14) gives

$$Y(p) = -\frac{(1+pT_1)(1+pT_2)(1+pT_3)}{k+(1+pT_1)(1+pT_2)(1+pT_3)} b_3 F_3(p) \tag{6.16}$$

The transfer function of the closed-loop system relating the external disturbance, which is the voltage drop across the armature

circuit, to the output is found from Eq. (6.14):

$$W_e = -\frac{1}{1+W_{o-l}} = \frac{(1+pT_1)(1+pT_2)(1+pT_3)}{k+(1+pT_1)(1+pT_2)(1+pT_3)} \qquad (6.17)$$

In a similar way the transfer functions relating any other external actions and changes of the setpoint to the output can be found.

A d.c. motor rate controller. In an electric motor rate control system of Fig. 1.23 the plant is a d.c. motor with an inertial load

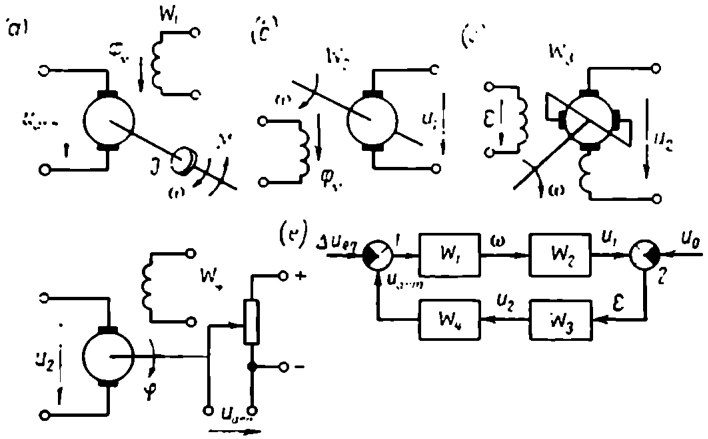

Fig. 6.3

(Fig. 6.3*a*), whose equations under the above assumptions correspond to an inertial element (see Example 2.5).

If the torque M on the shaft varies spontaneously and the excitation flux Φ_M is constant, the set of equations (1.5) takes the form

$$\omega + \frac{r_{arm}J}{a_1 c_1 \Phi_M^2}\frac{d\omega}{dt} = \frac{u_{arm}}{c_1\Phi_M} - \frac{r_{arm}M}{a_1 c_1 \Phi_M^2} \qquad (6.18)$$

where $M = M_f + M_l$ and consequently the effect of the shaft torque is similar to reduction of the armature voltage by the value of equivalent voltage

$$\Delta u_{eq} = \frac{r_{arm}}{a_1\Phi_M} M \qquad (6.19)$$

The motor in question can be represented by an element with a transfer function

$$W_1 = \frac{k_1}{1+pT_1} \qquad (6.20)$$

where

$$k_1 = \frac{1}{c_1\Phi_M}, \qquad T_1 = \frac{r_{arm}J}{a_1 c_1 \Phi_M^2}$$

The second element of the control system having a transfer function

$$W_2 = \frac{U_1}{\Omega} = k_2 \tag{6.21}$$

is a tachometric generator (Fig. 6.3*b*).

The third element is an amplidyne (Fig. 6.3*c*), which has the same transfer function as two different cascaded d.c. generators, i.e.

$$W_3 = \frac{U_2(p)}{E(p)} = \frac{k_3}{(1+pT_2)(1+pT_3)} \tag{6.22}$$

where $E = U_0 - U_1$.

The last element is the actuator which is a motor driving the slide of the voltage divider (Fig. 6.3*d*). The output voltage of this element is proportional to the shaft rotation angle of an armature-controlled motor. As shown in Examples 2.5 and 5.1, this results in an inertial-integrating element, whose transfer function is

$$W_4 = \frac{k_4}{p(1+pT_4)} \tag{6.23}$$

The structural diagram of a complete control system is shown in Fig. 6.3*e* as a combination of W_1, W_2, W_3, and W_4.

If one allows for the variations of the amplidyne shaft rotation rate or the voltage of the excitation winding of the motors, then it is necessary to introduce additional external actions, which are calculated as in the preceding example.

Let the external action be the variation of the torque on the motor shaft and the corresponding variation of the armature voltage found by Eq. (6.19)

$$f = \Delta u_{eq} = \frac{r_{arm}}{a_1 \Phi_M} M$$

Then the image of the variation of the controlled variable $y = \omega$ is, according to the structural diagram of Fig. 6.3*e*,

$$Y(p) = \frac{W_1}{1+W_1W_2W_3W_4} F(p) =$$

$$= \frac{k_1(1+pT_2)(1+pT_3)(1+pT_4)pF(p)}{(1+pT_1)(1+pT_2)(1+pT_3)(1+pT_4)p+k} = W_3F(p) \tag{6.24}$$

The transfer function of the closed-loop system is

$$W_{cl-l} = \frac{W_1}{1+W_1W_2W_3W_4} \tag{6.25}$$

where W_1, W_2, W_3, W_4 are given by formulae (6.20)-(6.23), the product of k_1, k_2, k_3, k_4 is denoted as k.

For the system of rate control shown in Fig. 1.24, the structural diagram is more involved because it includes a compensating loop with a supplementary resistor, r_s.

In this case Eqs. (1.5) take the form

$$\left.\begin{aligned} u_2 &= i_{arm}(r_{arm}+r_s)+c_1\omega\Phi_M \\ a_1 i_{arm}\Phi_M &= J\frac{d\omega}{dt}+M \end{aligned}\right\} \tag{6.26}$$

Thence we have

$$\omega+T_1\frac{d\omega}{dt}=k_1(u_2-\Delta u_{eq}) \tag{6.27}$$

and

$$i_{arm}r_s=\frac{\alpha T_1}{k_1}\frac{d\omega}{dt}+\alpha\Delta u_{eq} \tag{6.28}$$

where

$$T_1=\frac{(r_{arm}+r_s)J}{a_1c_1\Phi_M^2}, \qquad k_1=\frac{1}{c_1\Phi_M},$$

$$\Delta u_{eq}=\frac{r_{arm}+r_s}{a_1\Phi_M}M, \qquad \alpha=\frac{r_s}{r_{arm}+r_s}$$

The comparator subtracts the voltage $u_1 = k_2\omega$ from the setpoint voltage u_0 and adds the voltage $i_{arm}r_s$ to the result; by Eq. (6.28)

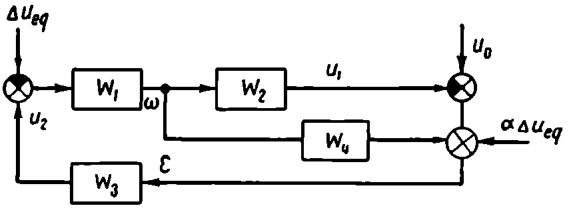

Fig. 6.4

the voltage $i_{arm}r_s$ consists of two components of which one is proportional to the derivative of the controlled variable $\frac{d\omega}{dt}$ and the other, to the external action Δu_{eq}.

The structural diagram of the system in question, according to Eqs. (6.27), (6.28), (6.21), and (6.22), is shown in Fig. 6.4. Here

$$W_1=\frac{k_1}{1+pT_1}, \qquad W_2=k_2,$$

$$W_3=\frac{k_3}{(1+pT_2)(1+pT_3)}, \qquad W_4=\frac{\alpha T_1}{k_1}p$$

If the control action x is given by the setpoint voltage u_0, the external disturbance f by a voltage Δu_{eq} equivalent to variation

of the torque on the motor shaft, and the controlled variable y by the shaft rotation rate ω, then following the structural diagram of Fig. 6.4 the transfer functions relating the control action and the disturbance to the output can be given in the form

$$W_c = \frac{Y}{X} = \frac{W_3 W_1}{1 + W_3 W_1 (W_2 - W_4)} \tag{6.29}$$

$$W_d = \frac{Y}{F} = \frac{W_1 (-1 + \alpha W_3)}{1 + W_1 W_3 (W_2 - W_4)} \tag{6.30}$$

If an inertialess amplifier is used in the control circuit, then the parameters can be selected so that $\alpha W_3 = 1$. The transfer function

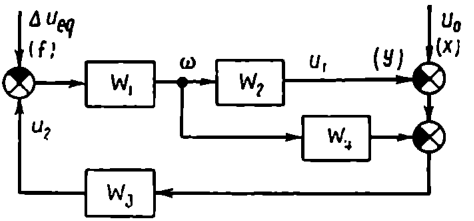

Fig. 6.5

relating the external action to the output W_d is in this case zero and the system is insensitive to the external action or, in other words, invariant to it.

A servo system. The servo system of Fig. 1.25*a* consists of elements similar to those given in the above examples. Knowing the functional diagram of Fig. 1.25*b* and the equations of each portion of the diagram, a structural diagram can be constructed (Fig. 6.5), where

$$W_1 = \frac{k_1}{1 + pT_1} \tag{6.31}$$

If the active resistance r of the armature circuit is high, the first term in the left-hand part of Eq. (6.27) is negligible and Eq. (6.31) degenerates into

$$W_1 = \frac{k_1}{p} \tag{6.32}$$

which is equivalent to an integrator.

The voltage u_1 of the divider is proportional to the integral of the motor shaft rotation rate ω, and so the transfer function is

$$W_2 = \frac{k_2}{p} \tag{6.33}$$

Depending on its circuit the amplifier of the servo system can be approximately described by equations of the proportional element

(electronic amplifier), inertial element (magnetic amplifier), or two inertial elements (amplidyne). Consequently, in the general case it can be assumed that

$$W_3 = \frac{k_3}{(1+pT_2)(1+pT_3)} \tag{6.34}$$

The transfer function of the tachometer correcting circuit corresponds to a proportional element, or

$$W_4 = k_4 \tag{6.35}$$

With $f = \Delta u_{eq}$ taken as the disturbing action, the setpoint variation $x = \Delta u_0$ as the control action, and the position of the output axis characterized by the voltage u_1 as the controlled variable y, one can obtain from the structural diagram transfer functions relating x and f to y:

$$W_c = \frac{Y}{X} = \frac{W_2 \dfrac{W_1 W_3}{1+W_1 W_3 W_4}}{1+W_2 \dfrac{W_1 W_3}{1+W_1 W_3 W_4}} = \frac{W_1 W_2 W_3}{1+W_1 W_3 (W_4+W_2)} \tag{6.36}$$

$$W_d = \frac{Y}{F} = -\frac{W_1 W_2}{1+W_1 W_3 (W_2+W_4)}. \tag{6.37}$$

Substituting into Eqs. (6.36) and (6.37) the values of W_1, W_2, W_3, and W_4 from Eqs. (6.31) and (6.33)-(6.35), we have

$$W_c = \frac{k_1 k_2 k_3}{p(1+pT_1)(1+pT_2)(1+pT_3)+k_1 k_3 (k_2+k_4 p)} \tag{6.38}$$

$$W_d = -\frac{k_1 k_2 (1+pT_2)(1+pT_3)}{p(1+pT_1)(1+pT_2)(1+pT_3)+k_1 k_3 (k_2+k_4 p)} \tag{6.39}$$

The denominators of Eqs. (6.38) and (6.39) coincide. By equating to zero the denominator of the transfer function relating any external action to the output, the characteristic equation of a closed-loop system is obtained, which in the case under consideration has the form

$$A(p) = p(1+pT_1)(1+pT_2)(1+pT_3)+k_1 k_3 (k_2+k_4 p) = 0 \tag{6.40}$$

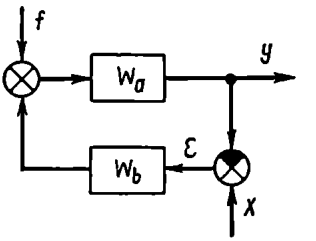

Fig. 6.6

All the above examples are reducible to the same structural diagram of Fig. 6.6. Here f is the external action, or the noise, y is the controlled variable, x is the controlled variable setpoint, ε is the error, W_a and W_b are the transfer functions of the appropriate portions of the closed-loop system defined by the sites where the setpoint and the noise are applied.

For servo systems and programmed controllers x is a function of time.

In order to calculate the system behaviour under different external actions those transfer functions are determined which express the dependence of the controlled variable and the error ε on the noise f or the setpoint x:

$$W_d = W_{yf} = \frac{Y(p)}{F(p)} = \frac{W_a}{1+W_aW_b} = \frac{W_a}{1+W_{o-l}} \tag{6.41}$$

$$W_c = W_{yx} = \frac{Y(p)}{X(p)} = \frac{W_aW_b}{1+W_aW_b} = \frac{W_{o-l}}{1+W_{o-l}} \tag{6.42}$$

$$W_\varepsilon = W_{\varepsilon x} = \frac{E(p)}{X(p)} = \frac{1}{1+W_aW_b} = \frac{1}{1+W_{o-l}} \tag{6.43}$$

Here $W_{o-l} = W_aW_b$ is the transfer function of an open-loop system.

With the transfer functions and external actions known, the variations of y or ε can be calculated.

6.2. TRANSFORMATIONS OF STRUCTURAL DIAGRAMS

Different structural diagrams may have the same transfer functions, or be dynamically equivalent. It is therefore very important to find general rules whereby one diagram can be transformed into another while its dynamic properties are retained. The theory of such transformations was developed by B. N. Petrov.

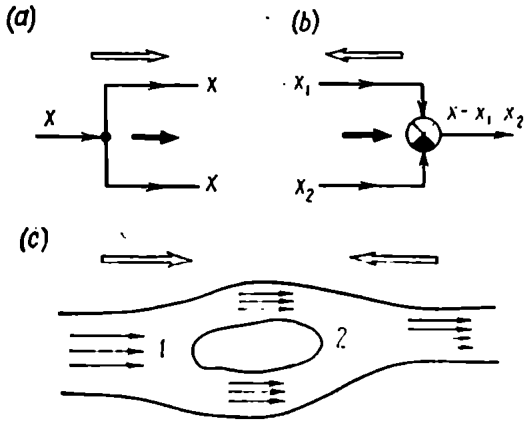

Fig. 6.7

Let us take up three elements of the structural diagram: a fanning node, an adder (summing element), and a converter.

We will introduce the concept of the *direction of fanning*. This direction may be coincident with or opposite to the direction of signal propagation as in a fanning node or an adder, respectively. Figure 6.7 represents a fanning node (*a*) and an adder (*b*); the heavy arrow denotes the signal propagation direction and the light arrow, the direction of fanning.

The direction of fanning is a concept applicable both to signal and matter propagation. Figure 6.7*c* shows a liquid flowing around

a body. The direction of fanning upstream of the body coincides with the direction of the flow (region *1*) and that downstream of the body (region *2*) is opposite to the flow.

Let us consider two kinds of transformation of structural diagrams:

(a) transposition of the adder beyond the fanning node;

(b) transposition of the converter beyond the node.

The rules of transformation of structural diagrams in both cases depend on whether the direction of transposition is coincident with or opposite to the direction of fanning.

The transposition of the adder beyond a fanning node. Let the direction of the adder transposition coincide with the direction of

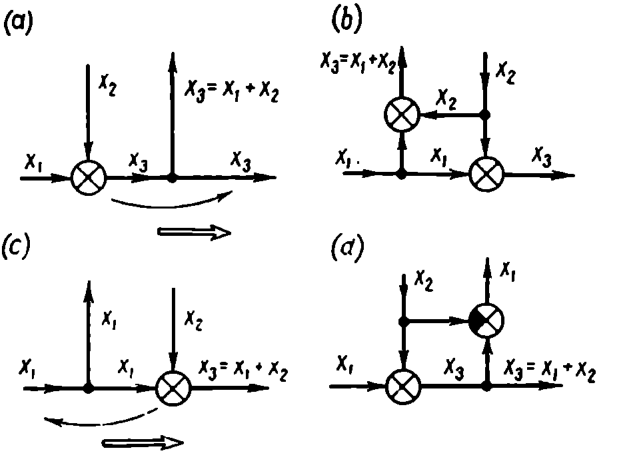

Fig. 6.8

fanning (Fig. 6.8*a*). Then the transposition will change the signal in the fanning node and, consequently, in all other branches issuing from the node. In order to compensate for that change, the outcoming branch should include an adder identical with the one being transposed (Fig. 6.8*b*).

The structural diagrams of Fig. 6.8*a* and *b* are equivalent. This follows from the equation

$$x_3 = x_1 + x_2 \tag{6.44}$$

which is valid for both diagrams.

Now, *the first transformation rule* can be formulated. *With an adder transposed through a fanning node along the direction of fanning adders identical with the one being transposed should be added to the outgoing branches of the node* (see Fig. 6.8*a* and *b*).

If the direction of adder transposition is opposite to the direction of fanning (Fig. 6.8*c*), then in order to compensate for the effect

of transposition the input of the adder should be subtracted from the branch signals rather than added to them (Fig. 6.8*d*).

For the diagrams (*c*) and (*d*) to be equivalent and the input and output values to be preserved, a value (x_2) equal to that added in adder transposition should be subtracted from the value outgoing from the fanning node.

The second transformation rule (corresponding to this case) is formulated as follows. *When an adder is transposed beyond the fanning node in a direction opposite to fanning, the outgoing branches should be supplemented with adders differing from the one being transposed in the sign of the added values* (see Fig. 6.8*c* and *d*).

Transposition of a converter beyond a fanning node. The direction of fanning is also important in transposing a converter beyond a node. Let us consider converter transposition in the direction of fanning. If a converter W_1 is transposed beyond a node with outgoing signals y_1 (Fig. 6.9*a*), then for retaining these signals it is necessary that

$$Y_1 = W_1 X_1 \tag{6.45}$$

For this condition to be satisfied, elements with a transfer function W_1 should be added to all outgoing branches. The diagrams

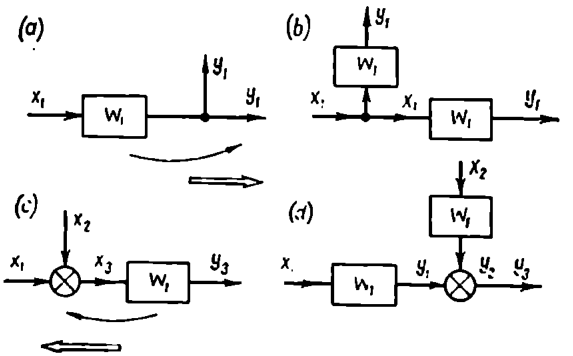

Fig. 6.9

of Fig. 6.9*a* and *b* are seen to be equivalent with respect to external connections.

If a converter is transposed beyond an adder along the direction of fanning, then the equation

$$Y_3 = (X_1 + X_2)\, W_1 = Y_1 + Y_2 \tag{6.46}$$

is valid provided that all input branches of the adder are supplemented with the transfer function W_1. The equivalence condition for such circuits is illustrated by Fig. 6.9*c* and *d*.

The third transformation rule is formulated as follows. *When a converter is transposed beyond a node along the direction of fanning, the branches connected to the node should be supplemented with elements with the transfer function of the converter being transposed* (see Fig. 6.9).

If the direction of converter transposition is opposite to the direction of fanning, then in order to compensate for the effect of the

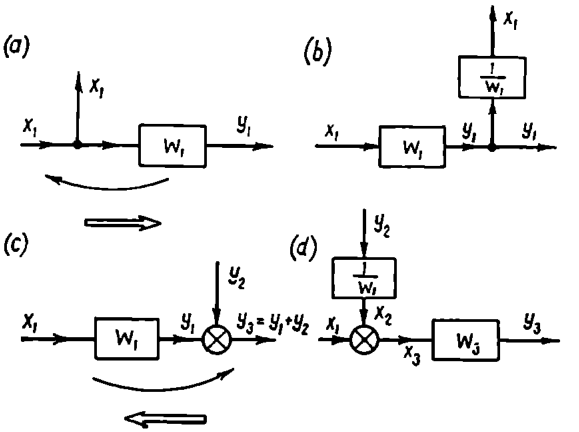

Fig. 6.10

transposition on the outgoing signals of the fanning node the branches of the node should include elements with inverse transfer functions.

The equivalence condition follows from Eq. (6.45) for the transposition of a converter beyond the fanning node (Fig. 6.10*a* and *b*) and from Eq. (6.46) for the transposition of a converter beyond the adder (Fig. 6.10*c* and *d*).

The fourth transformation rule is as follows. *With a converter transposed beyond a node in a direction opposite to the direction of fanning, the branches connected to the node should incorporate elements with a transfer function inverse to that of the element being transposed* (see Fig. 6.10).

The application of the above rules permits most diverse transformations of structural diagrams. It should be remembered that the transposition of a converter or a node from one branch into another is possible only if the directions of signal propagation in these branches coincide.

We will now give some examples illustrating these rules.

Example 6.1. Find the relations between the transfer functions under which the diagrams of Fig. 6.11*a* and *b* are equivalent. Let us transform the diagram (*b*) by moving adder *1* along the direction

of fanning beyond fanning node *2*. By the first transformation rule, adders *1* will appear in two branches issuing from node *2*, as shown in diagram (*c*). Then we move the converter beyond the newly-formed fanning node *3* along the direction of fanning; this will lead to the

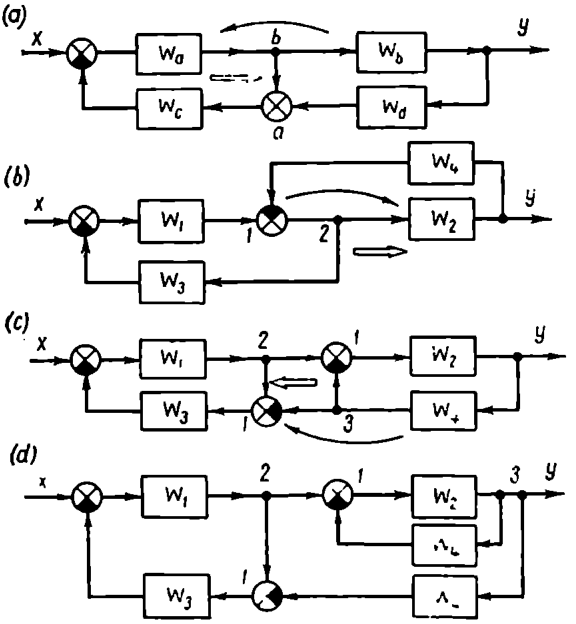

Fig. 6.11

appearance of converters in two branches as specified by the third rule. This transformation is shown in diagram (*d*). For diagrams (*a*) and (*b*) to be equivalent it is necessary that

$$W_a = W_1, \quad W_b = \frac{W_2}{1 + W_2 W_4}, \quad W_c = W_3, \text{ and } W_d = -W_4 \qquad (6.47)$$

The same result can be obtained by transforming diagram (*a*) using the second and fourth rules (transposition of adder *a* beyond node *b*).

Example 6.2. Using the transformation rules, simplify the diagram of Fig. 6.12*a* by reducing all the disturbances to one node.

This diagram corresponds to a voltage control system (see Fig. 6.2). By combining elements *1* and *2* we obtain the diagram of Fig. 6.12*b*; then, transposing element W_1 beyond node *3*, we will have circuit (*c*), where one common equivalent disturbance acts

$$F_{eq} = F_3 W_4 + F_1 + \frac{F_2}{W_1} \qquad (6.48)$$

The diagram obtained corresponds to the general diagram of Fig. 6.6.

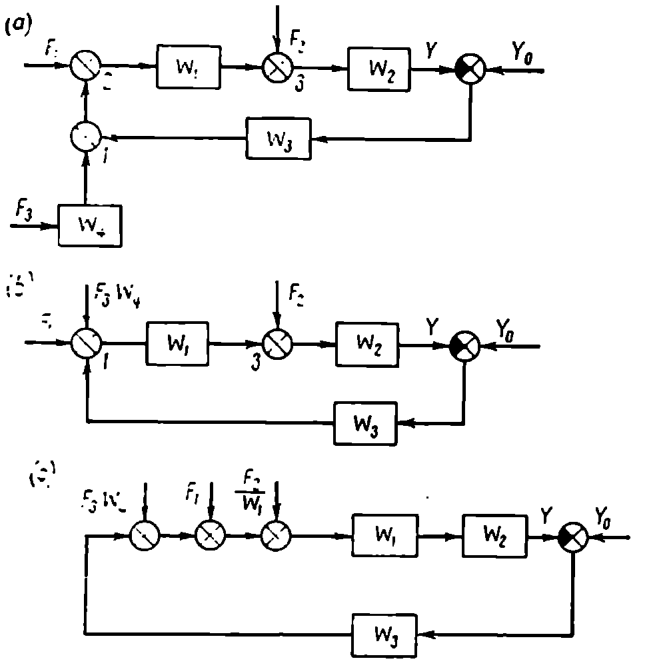

Fig. 6.12

The above example shows that, depending on the problem formulation, the totality of actions in the different nodes of a circuit can always be reduced to a single action applied to any one point of the circuit.

6.3. STRUCTURAL DIAGRAMS AND TRANSFER FUNCTIONS OF TWO-VARIABLE CONTROL SYSTEMS

We have thus far dealt with systems controlling simple single-variable plants, or plants with one controlled input and one controlled output variable. Control of multivariable plants with several input and output variables is more involved.

Let us consider a plant with two inputs, x_1 and x_2, and two outputs, y_1 and y_2, related by linear equations (2.14) or (2.40). An example of such a plant is a system of communicating tanks discussed in Example 2.3.

The equations of a two-variable plant in the operator form are

$$\left.\begin{aligned} Y_1(p) &= W_{11}X_1(p) + W_{12}X_2(p) \\ Y_2(p) &= W_{21}X_1(p) + W_{22}X_2(p) \end{aligned}\right\} \qquad (6.49)$$

The two-variable plant in question is shown schematically in Fig. 6.13*a*, while its equivalent circuit corresponding to Eq. (6.49) is depicted in Fig. 6.13*b*.

Apart from the hydraulic system described above, examples of multivariable plants are an air conditioning system (temperature and humidity), a turbine (rotation rate and pressure), a distillation column (temperature and level), etc.

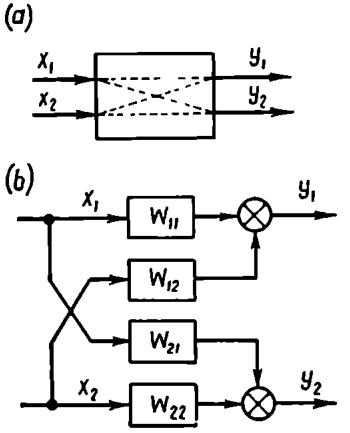

Fig. 6.13

To maintain constant output quantities of multivariable plants, multivariable proportional control systems are used. For instance, in two-variable systems the controlled quantities Y_1 and Y_2 are compared with the setpoints Y_{10} and Y_{20} and the results of comparison (errors ε_1 and ε_2) are fed to the plant input (x_1 and x_2) through the control system (elements W_{c11}, W_{c12}, W_{c21}, and W_{c22}).

The schematic of such a control applied to a hydraulic system is shown in Fig. 6.14*a* and its structural diagram in Fig. 6.14*b*. If, for instance, the effect of the first controlled variable setpoint variation on the second variable or on the error ε_2 is to be found, the transfer function relating these quantities must be calculated

$$W_{102}(p) = \frac{E_2(p)}{\Delta Y_{10}(p)} \tag{6.50}$$

If it is zero, the first controller setpoint variation does not change the second controlled variable, and *the control is termed autonomous.*

To facilitate calculation of W_{102}, the elements of the control system connected in series or in parrallel are to be found and replaced by their equivalents using the formulae given in Ch. V.

The diagram of Fig. 6.14*b* or its version given in Fig. 6.14*c*, which is more convenient for calculations, does not clearly resemble any familiar type of connection.

Transformation simplifies the structural diagram of Fig. 6.14*c*, reducing it to a set of elements connected in parallel and in series.

Let us restrict ourselves to the case where the flows f_1 and f_2 do not vary. In order to simplify the diagram of Fig. 6.14*c*, adders *1* and *2* are transposed beyond fanning nodes *3* and *4* (the first rule). The resultant transformed diagram is shown in Fig. 6.15*a*. This diagram can be further transformed if all the eight elements are transferred along the direction of fanning (the third rule) beyond nodes *1*, *2*, *3*, *4*, *5*, *6*, *7*, and *8* as shown by arrows in Fig. 6.15*a*.

Each branch will then include two series-connected elements replaceable by a single element whose transfer function is equal to the product of transfer functions of two elements shifted into the branch.

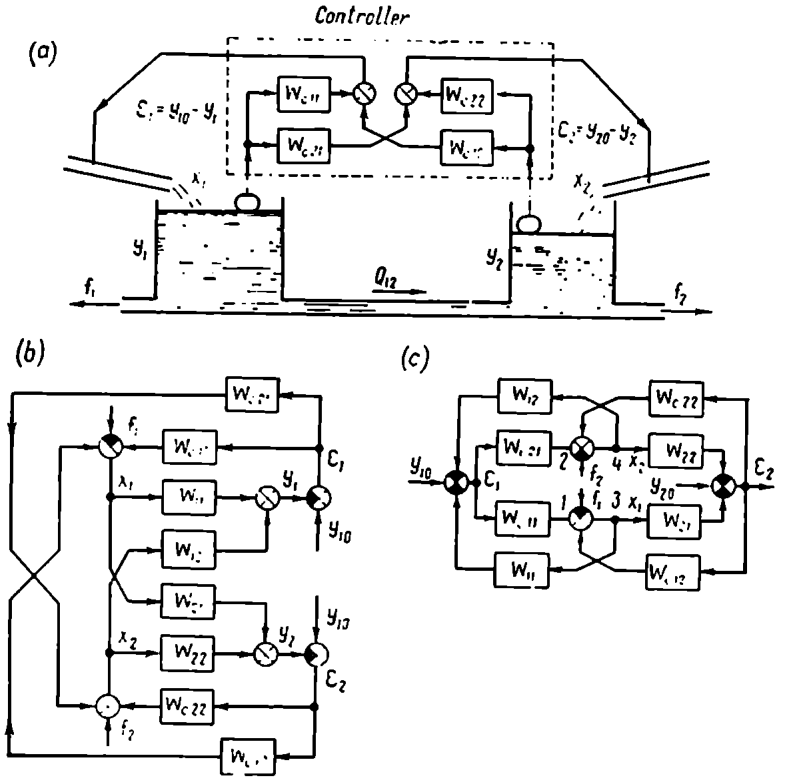

Fig. 6.14

The resultant structural diagram is given in Fig. 6.15*b*, where the conventional parallel connections can be easily seen.

Replacing each parallel connection of elements by one element with an equivalent transfer function the whole diagram can be reduced to a connection of four elements given in Fig. 6.15*c*, where

$$\left.\begin{aligned} W_a &= \frac{1}{1+W_{11}W_{c11}+W_{12}W_{c21}} \\ W_b &= \frac{1}{1+W_{22}W_{c22}+W_{21}W_{c12}} \\ W_c &= W_{c21}W_{22}+W_{21}W_{c11} \\ W_d &= W_{12}W_{c22}+W_{11}W_{c12} \end{aligned}\right\} \qquad (6.51)$$

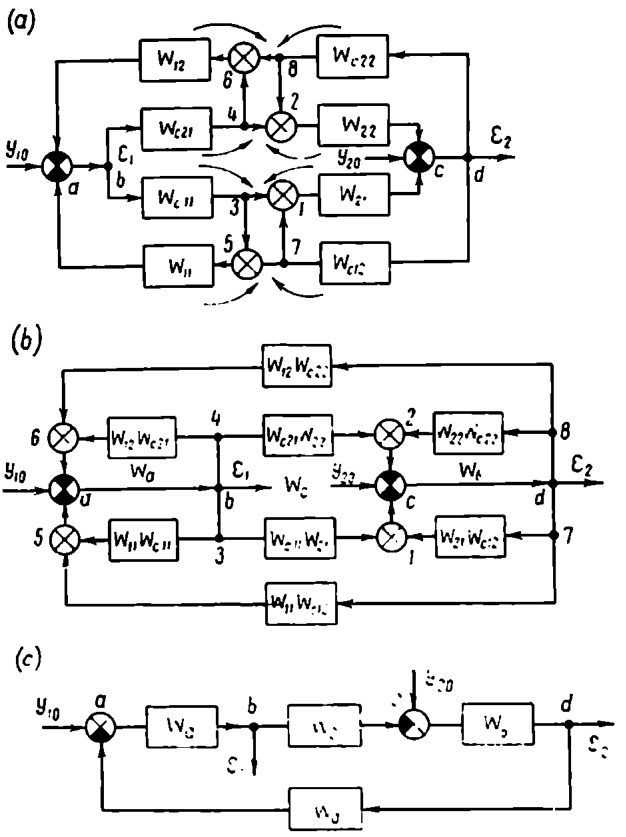

Fig. 6.15

With the transfer functions of each of these four elements known, the transfer functions can be found

$$\left.\begin{aligned} W_{101} &= \frac{E_1(p)}{Y_{10}(p)} = \frac{W_a}{1 - W_a W_b W_c W_d} \\ W_{102} &= \frac{E_2(p)}{Y_{10}(p)} = \frac{W_a W_c W_b}{W_a W_b W_c W_d - 1} \end{aligned}\right\}$$

and, consequently,

$$\left.\begin{aligned} W_{202} &= \frac{E_2(p)}{Y_{20}(p)} = \frac{W_b}{1 - W_a W_b W_c W_d} \\ W_{201} &= \frac{E_1(p)}{Y_{20}(p)} = \frac{W_b W_d W_a}{W_a W_b W_c W_d - 1} \end{aligned}\right\} \qquad (6.52)$$

The condition of autonomy is satisfied if $W_c - W_d = 0$ and the controller transfer functions meet the condition

$$\left.\begin{aligned} W_{c21} &= -W_{c11}\frac{W_{21}}{W_{22}} \\ W_{c12} &= -W_{c22}\frac{W_{12}}{W_{11}} \end{aligned}\right\} \tag{6.53}$$

In this case

$$\left.\begin{aligned} W_{101} &= \frac{E_1(p)}{Y_{10}(p)} = W_a \\ W_{202} &= \frac{E_2(p)}{Y_{20}(p)} = W_b \end{aligned}\right\} \tag{6.54}$$

The variation of the setpoint of one controlled variable (y_{10}) does not then entail a variation in the second one (y_2) as in the case where both control systems are completely independent, or autonomous. The general theory of autonomous control as applied to control of boiler installations was developed by Professor N. N. Voznesensky in 1934.

Example 6.3. Find the condition of autonomous control for a circuit controlling automatically the levels in two communicating tanks whose transfer functions are given in Example 2.3:

$$W_{11}(p) = \frac{b_0 + S_2 p}{p\,[b_0(S_1+S_2)+S_1S_2p]}, \quad W_{22}(p) = \frac{b_0 + S_1 p}{p\,[b_0(S_1+S_2)+S_1S_2p]}$$

and

$$W_{12}(p) = W_{21}(p) = \frac{b_0}{p\,[b_0(S_1+S_2)+S_1S_2p]}$$

To obtain autonomy, the condition (6.53) should be observed. Substituting into Eq. (6.53) the values of $W_{11}(p)$, $W_{22}(p)$ and $W_{12}(p) = W_{21}(p)$ we find

$$W_{c12} = -W_{c11}\frac{1}{1+pT_1} \quad \text{and} \quad W_{c21} = -W_{c22}\frac{1}{1+pT_1}$$

where

$$T_1 = \frac{S_1}{b_0}, \qquad T_2 = \frac{S_2}{b_0}$$

The relations thus obtained show that if control is autonomous, then every action on liquid influx into the first tank should be accompanied by a reverse action on influx into the second tank with a certain inertia depending on the channel between the tanks (b_0). This reverse action offsets the supplementary influx into the second tank caused by the increased level in the first tank. The inertia in the action on influx into the second tank should correspond exactly to that inherent in the process of level raising in that tank due to its communication with the first tank.

6.4. TRANSFER FUNCTION OF A CIRCUIT BETWEEN ANY POINTS

Using algebraic equations describing the structural diagram of a linear system, Mason suggested in 1953 a rule for calculating the transfer function between two specified nodes of a circuit. This rule can be given by the following formula

$$W_{mn} = \frac{\left[\left(\sum_{k=1}^{r} W_{ff\,k}\right) \prod_{i=1}^{s} (1 + W_{o\text{-}l\,i})\right]^*}{\left[\prod_{i=1}^{s} (1 + W_{o\text{-}l\,i})\right]^*} \tag{6.55}$$

where $\sum_{k=1}^{r} W_{ff\,k}$ is the sum of r transfer functions of different forward paths from the node m to the node n; $W_{o\text{-}l\,i}$ is the transfer function of an open-loop circuit taken with a sign corresponding to the negative feedback; the product $\prod$ includes all s closed-loop circuits of the system; the asterisk denotes elimination of all terms containing the products of transfer functions of the same elements (including elements with a transfer function equal to unity).

Example 6.4. Calculate the transfer function $W(p) = \frac{Y(p)}{X(p)}$ in the diagram of Fig. 6.11*a*. For this diagram we have in formula (6.55) one ($r = 1$) forward path with a transfer function $W_a W_b$ and two ($s = 2$) closed-loop circuits with transfer functions $W_a W_b W_d W_c$ and $W_a W_c$ corresponding to open negative feedback loops. Substituting these values into Eq. (6.55), we have

$$W(p) = \frac{[W_a W_b (1 + W_a W_c)(1 + W_a W_b W_d W_c)]^*}{[(1 + W_a W_c)(1 + W_a W_b W_d W_c)]^*} \tag{6.56}$$

Removing the parenthesis and eliminating all terms containing the products of transfer functions of common branches, we have

$$W(p) = \frac{W_a W_b}{1 + W_a W_c + W_a W_b W_d W_c} \tag{6.57}$$

Example 6.5. Find the transfer function

$$W_{102} = \frac{E_2}{Y_{10}}$$

in the diagram of Fig. 6.14*c*. There are two ($r = 2$) forward paths with transfer functions $-W_{c12} W_{22}$ and $-W_{c11} W_{12}$ and six ($s = 6$) closed-loop circuits with transfer functions $W_{c12} W_{21}$, $W_{22} W_{c22}$, $W_{c11} W_{11}$, $W_{12} W_{c21}$, $-W_{c12} W_{22} W_{c21} W_{11}$, and $-W_{c11} W_{12} W_{c22} W_{21}$. Substituting these values into Eq. (6.55) and eliminating terms

containing the products of transfer functions of closed-loop circuits and branches having a common part, we have

$$W_{102}=\frac{-(W_{c21}W_{22}+W_{c11}W_{21})}{1+W_{c12}W_{21}+W_{22}W_{c22}+W_{c11}W_{11}+W_{12}W_{c21}+}\rightarrow$$
$$\rightarrow\frac{}{+(W_{c12}W_{c21}-W_{c11}W_{c22})(W_{21}W_{12}-W_{11}W_{22})} \tag{6.58}$$

Here, when eliminating the products, an allowance was made for branches with a transfer function equal to unity (branches issuing from the adders in Fig. 6.14*c*).

Equation (6.58) coincides with the solution obtained by formulae (6.51) and (6.52).

Chapter VII

STABILITY OF CONTROL SYSTEMS

7.1. STABILITY OF LINEAR CONTROL SYSTEMS. STATEMENT OF THE PROBLEM

When describing various plants we indicated that their equilibrium state may be stable, unstable or neutral (see, for instance, Sec. 2.4). The same is true for automatic control systems.

An unstable plant may be part of a stable control system. In this case the stability of systems is artificial. Unstable linear control systems cannot, however, be put to practical service without facilities ensuring artificial stability. Therefore, to be workable at all, a linear control system must be stable.

It was shown in Ch. II that the necessary and sufficient condition for a linear element to be stable is that the real part of all poles of the transfer functions be negative.

By virtue of Eq. (2.18), for an open-loop control system

$$W_{o\text{-}l}(p) = \frac{K(p)}{D(p)} \tag{7.1}$$

where $K(p)$ and $D(p)$ are algebraic polynomials in p (Eq. 2.11). The stability condition for an open-loop system is the negative sign of the real part of the roots of the characteristic equation

$$D(p) = 0 \tag{7.2}$$

In order to ascertain the stability of a closed-loop system, any function relating the signals at the input and output of the system ((6.41), (6.42) or (6.43)) may be regarded as the transfer function.

We will treat the transfer function relating the control variable to the output (6.42) as the transfer function of a closed-loop system

$$W_{cl\text{-}l}(p) = \frac{Y(p)}{X(p)} = \frac{W_{o\text{-}l}(p)}{1 + W_{o\text{-}l}(p)} \tag{7.3}$$

By substituting the expression for $W_{o\text{-}l}(p)$ from Eq. (7.1) we have

$$W_{cl\text{-}l}(p) = \frac{K(p)}{D(p) + K(p)} \tag{7.4}$$

Any other transfer function of a closed-loop system (for instance, (6.41), (6.43)) differs from the function given by Eq. (7.4) only in the numerator, while the denominator remains the same for all functions of a closed-loop system. Introducing common notation for the transfer function

$$W_{cl\text{-}l}(p) = \frac{B(p)}{A(p)} \tag{7.5}$$

we will at any time have for the denominator of a closed-loop system

$$A(p) = D(p) + K(p) \tag{7.6}$$

The stability condition for a closed-loop system is the negative sign of the real parts of all roots of the characteristic equation

$$A(p) = 0 \tag{7.7}$$

This condition of stability, which has been proved for linear systems, was extended to linearized equations of nonlinear systems by A. M. Lyapunov in 1892.

Stability analysis therefore consists merely in finding the signs of the real parts of the characteristic equation roots, i.e. in studying the distribution of the roots relative to the imaginary axis in the complex p plane.

Equations up to the fourth order are solvable since there are analytical expressions to determine their roots. No such expressions exist for equations of a higher order. To ascertain stability, however, the knowledge of the values of roots is unnecessary, since it is sufficient to know the sign of their real part.

It is therefore important to find rules which would make it possible, without calculating the roots themselves, to answer the question how the roots are distributed in the complex plane relative to the imaginary axis. These rules are called *stability criteria.*

There are several stability criteria; they are mathematically equivalent, since they answer the question whether or not all roots of the characteristic equation are positioned in the left half-plane. The selection of a criterion depends on the problem at hand.

The following criteria are currently in use: *algebraic criteria* (a) of Routh and (b) of Hurwitz; *frequency criteria* (a) of Mikhailov and (b) of Nyquist.

7.2. ALGEBRAIC CRITERIA OF STABILITY

The problem of finding the relations between the coefficients of the characteristic equation of a linear system which ensure its stability has been attracting the attention of engineers and mathematicians for a long time. Back in 1860 I. A. Vyshnegradsky, who

studied the control system of a steam engine, formulated the conditions relating the coefficients of a third-order characteristic equation at which the system is stable. G. Maxwell and A. Stodola were also intrigued by this problem. Routh and Hurwitz, whose services were enlisted in solving the problem for an arbitrary order of the equation, obtained solutions to the problem in slightly different forms.

Routh published his findings in 1875 in the form of what was later named the Routh table. Hurwitz published his criterion in 1895 in the form of a system of determinants. Both these criteria lead to the same algebraic inequalities and differ practically only in the general method of obtaining them. For this reason they are often combined under the name of the *Routh-Hurwitz criterion.*

Omitting the proof of each criterion, we will give their mathematical formulation and illustrate some of their applications.

The Routh criterion. Let the characteristic equation of a system be

$$A(p) = a_n p^n + a_{n-1} p^{n-1} + \ldots + a_0 = 0 \qquad (7.8)$$

Let us compile Table 7.1, referred to as the *Routh table.*

Table 7.1

	$c_{11}=a_n$	$c_{21}=a_{n-2}$	$c_{31}=a_{n-4}$	$c_{41}=a_{n-6}$
	$c_{12}=a_{n-1}$	$c_{22}=a_{n-3}$	$c_{32}=a_{n-5}$	$c_{42}=a_{n-7}$
$\lambda_3=\frac{c_{11}}{c_{12}}$	$c_{13}=c_{21}-\lambda_3 c_{22}$	$c_{23}=c_{31}-\lambda_3 c_{32}$	$c_{33}=c_{41}-\lambda_3 c_{42}$	$c_{43}=c_{51}-\lambda_3 c_{52}$
$\lambda_4=\frac{c_{12}}{c_{13}}$	$c_{14}=c_{22}-\lambda_4 c_{23}$	$c_{24}=c_{32}-\lambda_4 c_{33}$	$c_{34}=c_{42}-\lambda_4 c_{43}$	$c_{44}=c_{52}-\lambda_4 c_{53}$
$\lambda_5=\frac{c_{13}}{c_{14}}$	$c_{15}=c_{23}-\lambda_5 c_{24}$	$c_{25}=c_{33}-\lambda_5 c_{34}$	$c_{35}=c_{43}-\lambda_5 c_{44}$	$c_{45}=c_{53}-\lambda_5 c_{54}$

The rule for the compilation of the table can easily be deduced from its structure. Any entry of the table, c_{kl}, at $|\, i \geqslant 3 \,|$ (k denotes the number of the column, and i, the number of the row) can be found by the formula

$$c_{kl} = c_{k+1,\, i-2} - \lambda_l c_{k+1,\, i-1} \qquad (7.9)$$

where

$$\lambda_l = \frac{c_{1,\, i-2}}{c_{1,\, i-2}} \quad \text{at} \quad i \geqslant 3$$

The number of rows in the Routh table is equal to the order of the equation plus one, or $(n + 1)$. Entries with negative subscripts are denoted by zeroes.

The Routh stability criterion is formulated as follows. *For a system to be stable it is necessary and sufficient that the entries of the first column of the Routh table be positive, i.e.*

$$c_{11} > 0, \quad c_{12} > 0, \quad c_{13} > 0, \quad c_{14} > 0, \ldots, \quad c_{1,\, n+1} > 0 \quad (7.10)$$

When the Routh table with equation coefficients is given in numerical form, the calculations can be simplified by multiplying or dividing the rows by a positive number. This does not affect the result.

If the entries of the first column are not all positive, or the system is unstable, the number of roots in the right half-plane is equal to the number of sign alterations in the first column of the table.

Example 7.1. Let

$$A(p) = p^6 + 6p^5 + 21p^4 + 44p^3 + 62p^2 + 52p + 100 = 0$$

It is required to determine the number of roots in the right half-plane.

Let us make up a Routh table (Table 7.2). The first column is seen to include two sign alterations, from plus to minus and from minus to plus. Consequently, the characteristic equation has two roots in the right half-plane and represents an unstable system.

The Hurwitz criterion. Let the characteristic equation (7.7) of a system be given. Compile a table of coefficients referred to as *Hurwitz table*

a_{n-1}	a_{n-3}	a_{n-5}	.			0
a_{n-2}	a_{n-2}	a_{n-4}	.			
0	a_{n-1}	a_{n-3}	.			
0	a_n	a_{n-2}	.	.	.	.
0	0	a_{n-1}	.	.	.	.
.	.	.	.	.	.	.
.	.	.	.	.	.	.
0	.	.	.	a_1	a_2	a_0

The rule of table filling is seen from the structure of the table. The first row is formed of the coefficients of the equation with subscripts $n - 1$, $n - 3$, $n - 5$, etc., the second row is formed of the coefficients of the equation with subscripts n, $n - 2$, $n - 4$, etc. Each subsequent row is formed of coefficients of the equation with subscripts exceeding by one those of the preceding row; the coefficients with subscripts below zero and above n are replaced by

Table 7.2

	$a_6=1$	$a_4=21$	$a_2=62$	$a_0=100$
	$a_5=6$	$a_3=44$	$a_1=52$	0
$\lambda_3=\frac{1}{6}=0.167$	$21-0.167\times 44=13.65$	$62-0.167\times 52-53.3$	$100-0.167\times 0=100$	0
$\lambda_4=\frac{6}{13.65}=0.44$	$44-0.44\times 53.3$ 20.6	$52-0.44\times 100=8$	$0-0.44\times 0=0$	$0-0.44\times 0$ -0
$\lambda_5=\frac{13.65}{20.6}=0.662$	$53.3-0.662\times 8=48.0$	$100-0.662\times 0=100$	0	0
$\lambda_6=\frac{20.6}{48.0}=0.43$	$8-0.43\times 100=-35.0$	0	0	0
$\lambda_7=\frac{48.0}{-35.0}=-1.37$	$100+1.37\times 0=100$	0	0	0

zeroes. The table contains n rows, where n is the order of the equation.

Determinants of the kth order Δ_k are formed by isolating k rows and k columns in the Hurwitz table

$$\Delta_1 = a_{n-1}, \quad \Delta_2 = \begin{vmatrix} a_{n-1} & a_{n-3} \\ a_n & a_{n-2} \end{vmatrix},$$
$$\Delta_3 = \begin{vmatrix} a_{n-1} & a_{n-3} & a_{n-5} \\ a_n & a_{n-2} & a_{n-4} \\ 0 & a_{n-1} & a_{n-3} \end{vmatrix}, \text{ etc.} \tag{7.11}$$

These determinants are called *Hurwitz determinants.*

The Hurwitz stability criterion is defined as follows. *A system is stable if* $a_n > 0$ *and all Hurwitz determinants are positive, i.e.* $\Delta_k > 0$, *where* $1 \leqslant k \leqslant n$.

Consider in more detail cases where $n = 1, \ldots, 4$.

(1) $n = 1$,

$$a_1 p + a_0 = 0 \tag{7.12}$$

The stability conditions are

$$a_1 > 0, \qquad \Delta_1 = a_0 > 0$$

(2) $n = 2$,

$$a_2 p^2 + a_1 p + a_0 = 0$$

The stability conditions are

$$\left.\begin{array}{l} a_2 > 0, \\ \Delta_1 = a_1 > 0, \end{array} \qquad \Delta_2 = \begin{vmatrix} a_1 & 0 \\ a_2 & a_0 \end{vmatrix} = a_1 a_0 > 0 \right\} \tag{7.13}$$

The latter condition, if combined with the preceding one, is equivalent to $a_0 > 0$.

Consequently, the stability conditions for second-order equations reduce to the requirements

$$a_0 > 0, \qquad a_1 > 0, \qquad a_2 > 0 \tag{7.14}$$

(3) $n = 3$,

$$a_3 p^3 + a_2 p^2 + a_1 p + a_0 = 0$$

The stability conditions are

$$\left.\begin{array}{l} a_3 > 0, \\ \Delta_1 = a_2 > 0, \end{array} \qquad \Delta_3 = \begin{vmatrix} a_2 & a_0 & 0 \\ a_3 & a_1 & 0 \\ 0 & a_2 & a_0 \end{vmatrix} = a_0 \Delta_2 > 0 \right.$$

$$\Delta_2 = \begin{vmatrix} a_2 & a_0 \\ a_3 & a_1 \end{vmatrix} = a_2 a_1 - a_3 a_0 > 0,$$

The latter condition, if combined with the preceding one, is equivalent to $a_0 > 0$.

The condition $\Delta_2 > 0$ at $a_3 > 0$, $a_0 > 0$, and $a_2 > 0$ is feasible only if $a_1 > 0$.

Thus, the stability conditions for third-order equations reduce to the requirements

$$a_0 > 0, \quad a_1 > 0, \quad a_2 > 0, \quad a_3 > 0 \tag{7.15}$$

$$a_1 a_2 - a_0 a_3 > 0 \tag{7.16}$$

(4) $n = 4$,

$$a_4 p^4 + a_3 p^3 + a_2 p^2 + a_1 p + a_0 = 0$$

The stability conditions are

$$a_4 > 0, \qquad \Delta_1 = a_3 > 0,$$

$$\Delta_2 = \begin{vmatrix} a_3 & a_1 \\ a_4 & a_2 \end{vmatrix} = a_3 a_2 - a_4 a_1 > 0,$$

$$\Delta_3 = \begin{vmatrix} a_3 & a_1 & 0 \\ a_4 & a_2 & a_0 \\ 0 & a_3 & a_1 \end{vmatrix} = a_1 (a_3 a_2 - a_4 a_1) - a_3^2 a_0 > 0,$$

$$\Delta_4 = \begin{vmatrix} a_3 & a_1 & 0 & 0 \\ a_4 & a_2 & a_0 & 0 \\ 0 & a_3 & a_1 & 0 \\ 0 & a_4 & a_2 & a_0 \end{vmatrix} = a_0 \Delta_3 > 0$$

The latter condition, if combined with the preceding one, is equivalent to $a_0 > 0$.

The condition $\Delta_3 > 0$ at $a_0 > 0$ is feasible only at $a_1 > 0$ and $\Delta_2 > 0$. The condition $\Delta_2 > 0$ at $a_4 > 0$, $a_1 > 0$, and $a_3 > 0$ is feasible at $a_2 > 0$.

The stability conditions for fourth-order equations reduce to the requirements

$$a_0 > 0, \quad a_1 > 0, \quad a_2 > 0, \quad a_3 > 0, \quad a_4 > 0 \tag{7.17}$$

$$a_1 (a_3 a_2 - a_4 a_1) - a_3^2 a_0 > 0 \tag{7.18}$$

Thence follows that *for systems described by equations of the first and second order to be stable, the coefficients of the characteristic equation must be positive.*

For third- and fourth-order equations, the above condition must be combined with the validity of inequalities (7.16) *and* (7.18).

From the structure of Hurwitz determinants it follows that

$$\Delta_n = a_0 \Delta_{n-1} \tag{7.19}$$

By virtue of the Hurwitz stability criterion the system is stable if all Hurwitz determinants are positive and, in particular, $\Delta_n > 0$.

The system is on the stability boundary when

$$\Delta_n = a_0 \Delta_{n-1} = 0 \tag{7.20}$$

This is only possible if either $a_0 = 0$ or $\Delta_{n-1} = 0$.

In the first case the system is said to be on the boundary of deadbeat (aperiodic) stability (one of the characteristic equation roots is zero). In the second case the system is said to be on the boundary of oscillatory stability (two conjugate roots of the characteristic equation are on the imaginary axis).

In most cases $a_0 \neq 0$ and therefore if the system is on the boundary of stability, this implies the boundary of oscillatory stability.

Example 7.2. Let the characteristic equation be

$$(1 + pT_1)(1 + pT_2)(1 + pT_3) + k = 0 \tag{7.21}$$

This equation corresponds to a control system incorporating three inertial elements with time constants T_1, T_2, and T_3 and having an overall gain k. It is required to find the limit value of k at which the system ceases to be stable, i.e. k_{lim} as a function of T_i ($i = 1, 2, 3$). We rearrange the equation

$$T_1T_2T_3p^3 + (T_1T_2 + T_1T_3 + T_2T_3)\,p^2 + (T_1 + T_2 + T_3)\,p + 1 + k = 0$$

By the Hurwitz criterion the system is stable if the inequalities (7.15) and (7.16) are satisfied, i.e. if all the coefficients of the equation are positive and the inequality

$$(T_1T_2 + T_2T_3 + T_3T_1)(T_1 + T_2 + T_3) > (1 + k)\,T_1T_2T_3 \tag{7.22}$$

is valid. That the coefficients are positive follows from the problem statement. Inequality (7.22) can be rearranged as

$$(1 + \tau_2 + \tau_3)\left(1 + \frac{1}{\tau_2} + \frac{1}{\tau_3}\right) > 1 + k \tag{7.23}$$

where

$$\tau_2 = \frac{T_2}{T_1}, \qquad \tau_3 = \frac{T_3}{T_1}$$

The resultant inequality does not hold if

$$k \geqslant k_{lim} = (1 + \tau_2 + \tau_3)\left(1 + \frac{1}{\tau_2} + \frac{1}{\tau_3}\right) - 1 \tag{7.24}$$

It follows from Eq. (7.24) that the limit gain k_{lim} of the system does not depend on the magnitude of the elements' time constants, but on their relative values, and k_{lim} increases with the values of τ_2 and τ_3, or with the difference between the time constants. In the particular case where $\tau_2 = \tau_3 = 1$, i.e. $T_1 = T_2 = T_3 = T$ the value of k_{lim} is minimal and equal to 8.

7.3. FREQUENCY CRITERIA OF STABILITY

The argument principle. The frequency criteria are based on the argument principle well-known in the theory of complex variable functions.

Assume that we have an algebraic equation with real coefficients

$$A(p) = a_n p^n + a_{n-1} p^{n-1} + \ldots + a_0 = 0 \qquad (7.25)$$

The polynomial $A(p)$ can be represented in the form

$$A(p) = a_n (p - p_1)(p - p_2) \ldots (p - p_n) \qquad (7.26)$$

where p_i are the roots of the equation $A(p) = 0$.

Assume that $p = j\omega$, then

$$A(j\omega) = a_n (j\omega - p_1)(j\omega - p_2) \ldots (j\omega - p_n) \qquad (7.27)$$

Consider the geometric representation of the complex number $(j\omega - p_i)$ on the complex p plane. The origin of the vector repre-

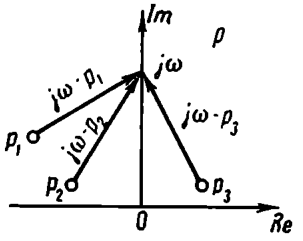

Fig. 7.1

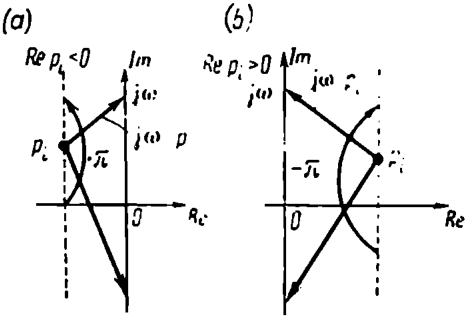

Fig. 7.2

senting this complex number is the point p_i and the end lies on the imaginary axis at the point $j\omega$ (Fig. 7.1).

Let us find the argument of the complex number

$$\arg A(j\omega) = \sum_{i=1}^{n} \arg (j\omega - p_i) \qquad (7.28)$$

If ω varies within the range $-\infty$ to $+\infty$ we have for the argument variation $A(j\omega)$

$$\Delta \arg A(j\omega) = \sum_{i=1}^{n} \Delta \arg (j\omega - p_i) \qquad (7.29)$$
$$-\infty < \omega < +\infty$$

By virtue of Eq. (7.29) the variation of the argument is calculated as the sum of variations of arguments of the complex numbers $(j\omega - p_i)$. This argument variation depends on where (in the right or left half-plane) the root p_i lies. Consider these two cases.

The root p_i is in the left half-plane (Fig. 7.2*a*). With ω varying from $-\infty$ to $+\infty$ the head of the vector $(j\omega - p_i)$ slides up the

imaginary axis, turning counterclockwise through 180°; consequently, the argument variation is

$$\Delta \arg (j\omega - p_l) = +\pi \qquad (7.30)$$
$$-\infty < \omega < +\infty$$

The root p_l is in the right half-plane (Fig. 7.2*b*). In this case, we have by similar reasoning

$$\Delta \arg (j\omega - p_l) = -\pi \qquad (7.31)$$
$$-\infty < \omega < +\infty$$

Let us assume that the equation $A(p) = 0$ has m roots in the right and l roots in the left half-plane, and $l + m = n$. Then, by virtue of Eqs. (7.27), (7.30), and (7.31),

$$\Delta \arg A(j\omega) = \pi (l - m) = (n - 2m)\pi \qquad (7.32)$$

Equation (7.32) is a representation of the argument principle, which is formulated as follows. *The variation of the argument $A(j\omega)$ with ω varying from $-\infty$ to $+\infty$ is equal to the difference between the number l of roots (of the equation $A(p) = 0$) in the left half-plane and the number m of roots in the right half-plane multiplied by π.*

The Mikhailov criterion. The Mikhailov stability criterion formulated in 1938 is essentially a geometric interpretation of the argument principle. Assume that the characteristic equation of the system (7.7) is

$$A(p) = a_n p^n + a_{n-1} p^{n-1} + \ldots + a_0 = 0 \qquad (7.33)$$

The polynomial $A(p)$ is in this case referred to as a *characteristic polynomial*. For the system to be stable all roots of the characteristic equation must be in the left half-plane, i.e. $m = 0$. Then, by virtue of Eq. (7.32), the equation

$$\Delta \arg A(j\omega) = n\pi \qquad (7.34)$$
$$-\infty < \omega < +\infty$$

must be valid. From this condition it follows that all the roots of the equation $A(p) = 0$ are in the left half-plane.

The locus of the head of the vector $A(j\omega)$ when $-\infty < \omega < +\infty$ is referred to as the *locus of the vector $A(j\omega)$* or the *Mikhailov locus*. According to Eq. (7.33) the equation of the Mikhailov locus is

$$A(j\omega) = a_n (j\omega)^n + \ldots + a_0 = U(\omega) + jV(\omega) \qquad (7.35)$$

where the real and imaginary parts of the complex $A(j\omega)$ will be, respectively,

$$U(\omega) = a_0 - a_2\omega^2 + a_4\omega^4 - \ldots \qquad (7.36)$$
$$V(\omega) = a_1\omega - a_3\omega^3 + a_5\omega^5 - \ldots \qquad (7.37)$$

From Eqs. (7.36) and (7.37) it follows that the real part of $A(j\omega)$ is an even function of ω

$$U(-\omega) = U(+\omega) \qquad (7.38)$$

while the imaginary part of $A(j\omega)$ is an odd function of ω

$$V(-\omega) = -V(\omega) \tag{7.39}$$

Consequently

$$A(-j\omega) = U(\omega) - jV(\omega) \tag{7.40}$$

This means that $A(j\omega)$ and $A(-j\omega)$ are conjugate complex quantities, and therefore

$$\Delta \underset{-\infty<\omega<0}{\arg} A(j\omega) = \Delta \underset{0<\omega<+\infty}{\arg} A(j\omega) \tag{7.41}$$

With an allowance for Eq. (7.41), Eq. (7.34) can be given as

$$\Delta \underset{0<\omega<+\infty}{\arg} A(j\omega) = n\frac{\pi}{2} \tag{7.42}$$

Equation (7.42) leads to the formulation of the Mikhailov stability criterion. *An automatic control system is stable if, with* ω *varying from* 0 *to* $+\infty$, *the vector* $A(j\omega)$ *turns through an angle of* $n\frac{\pi}{2}$, *where* n *is the order of the characteristic equation* $A(p) = 0$, or, in other words, *if the locus of* $A(j\omega)$, *with* ω *increasing from* 0 *to* $+\infty$, *traverses successfully* n *quadrants in the positive direction (counterclockwise) with the starting point on the real axis.*

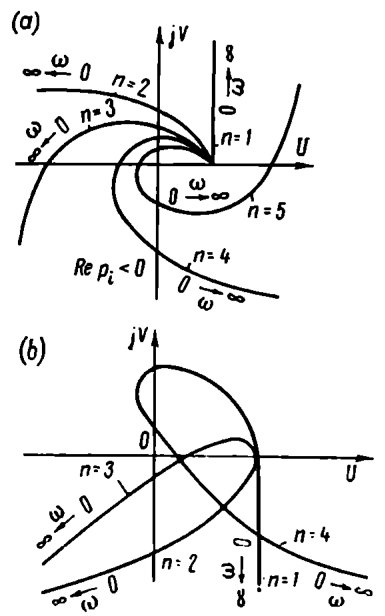

Fig. 7.3

Figure 7.3*a* shows the loci of stable systems at different values of n. All of them traverse the corresponding number of quadrants in the positive direction.

Figure 7.3*b* shows the loci of unstable systems which do not go through n quadrants in the positive direction.

The locus of $A(j\omega)$ can be plotted by using Eqs. (7.36) and (7.37) with the values of ω given and U and V calculated.

The locus can also be constructed geometrically using Eq. (7.35) with the vector $A(j\omega)$ being the closing side of a polygon whose other sides are equal to $a_k\omega^k$ and make an angle of 90° if they are adjacent. In Fig. 7.4 this is shown for one point $\omega = \omega_1$, where

$$A(j\omega_1) = a_3(j\omega_1)^3 + a_2(j\omega_1)^2 + a_1(j\omega_1) + a_0 \tag{7.43}$$

The whole locus is constructed in the same way with the values of ω assumed within the range from zero to infinity.

As follows from Eq. (7.6), the characteristic polynomial of a closed-loop system can be represented as a sum of $K(p)$ and $D(p)$. The loci of $D(j\omega)$ and $K(j\omega)$ can be represented as a product of loci that are usually known and have a simpler form for standard elements. Thence it follows that in order to construct the locus of $A(j\omega)$ it is necessary to construct the loci of $D(j\omega)$ and $K(j\omega)$ and add up the vectors of $D(j\omega)$ and $K(j\omega)$ for each value of ω.

If $K(j\omega) = k$ and does not depend on the frequency ω, the plotting is simplified. The latter two operations are replaced by merely

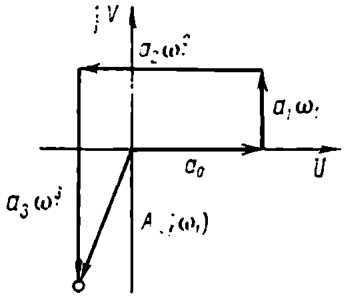

Fig. 7.4

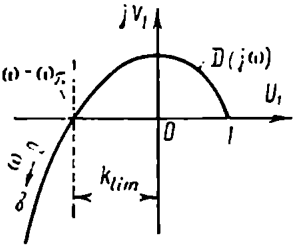

Fig. 7.5

shifting the locus of $D(j\omega)$ rightwards along the real axis by the value of k or, which is the same, by shifting the imaginary axis leftwards by the value of k.

Example 7.3. Determine the limit gain k_{lim} of a voltage stabilization system of a generator whose structural diagram is shown in Fig. 6.2.

The transfer function of the open-loop system is

$$W_{o\text{-}l}(p) = \frac{k}{(1+pT_1)(1+pT_2)(1+pT_3)} = \frac{k}{D(p)}$$

where $k = k_1k_2k_3$.

The characteristic equation of the closed-loop system is

$$A(p) = D(p) + k = (1 + pT_1)(1 + pT_2)(1 + pT_3) + k = 0$$

To solve the problem, one should construct a Mikhailov locus

$$\underset{0<\omega<+\infty}{A(j\omega)} = \underset{0<\omega<+\infty}{D(j\omega)} + k$$

For this, first construct the locus

$$D(j\omega) = (1 + j\omega T_1)(1 + j\omega T_2)(1 + j\omega T_3) = U_1(\omega) + jV_1(\omega)$$

Assume that $T_1 = 2.0$ sec, $T_2 = 0.5$ sec, $T_3 = 0.1$ sec. Then

$$\left.\begin{aligned} U_1(\omega) &= 1 - (T_1T_2 + T_2T_3 + T_3T_1)\omega^2 = 1 - 1.25\omega^2 \\ V_1(\omega) &= \omega(T_1 + T_2 + T_3 - T_1T_2T_3\omega^2) = \omega(2.6 - 0.1\omega^2) \end{aligned}\right\} \quad (7.44)$$

and the locus of $D(j\omega)$ has the form of Fig. 7.5.

In order to obtain the locus of $A(j\omega)$ it is sufficient to shift the imaginary axis leftwards by the value of k. From Fig. 7.5 it follows that the system will be on the stability boundary if k is equal to k_{lim} at which the locus of $A(j\omega)$ goes through the origin of coordinates. As can be seen from Fig. 7.5, the value of k_{lim} can be found from the equations

$$V_1(\omega_\pi) = 0, \qquad -U_1(\omega_\pi) = k_{lim} \tag{7.44'}$$

where ω_π is the intersection frequency, or the frequency corresponding to the intersection point of the locus of $D(j\omega)$ with the real axis.

Solving Eqs. (7.44) and (7.44') at $\omega = \omega_\pi$ we have

$$\left.\begin{aligned} \omega_\pi &= \sqrt{\frac{T_1+T_2+T_3}{T_1T_2T_3}} = \sqrt{\frac{2.6}{0.1}} = 5.1\,\frac{1}{\text{sec}} \\ k_{lim} &= (T_1T_2 + T_2T_3 + T_1T_3)\,\omega_\pi^2 - 1 = 1.25\,\frac{2.6}{0.1} - 1 = 31.5 \end{aligned}\right\} \tag{7.45}$$

It is easily seen that with the substitution of the expressions describing ω_π, τ_2, τ_3 Eqs. (7.45) and (7.24) coincide.

The Nyquist criterion. In order to study the stability of feedback amplifiers, a frequency stability criterion was suggested by Nyquist in 1932. According to this criterion the frequency locus of an open-loop system should be known for studying the stability of a closed-loop system. It can be obtained either analytically or experimentally. The latter fact is an advantage of this criterion over the preceding ones.

The Nyquist criterion is physically meaningful in that it relates stationary frequency properties of an open-loop system with non-stationary properties of a closed-loop system.

Stability criterion based on the construction of the frequency locus of an open-loop system. Assume that the transfer function of an open-loop system is $W_{o\text{-}l}(p) = \frac{K(p)}{D(p)}$. Form the function

$$F(p) = 1 + W_{o\text{-}l}(p) = \frac{D(p)+K(p)}{D(p)} \tag{7.46}$$

The numerator of this function is the characteristic polynomial of a closed-loop system, the denominator is that of an open-loop system. Let the degree of $D(p)$ be n and that of $K(p)$, r. Physically it follows that

$$r < n \tag{7.47}$$

At $r > n$ the addends with p raised to a positive power can be isolated from the transfer function $W(p)$; this corresponds to differentiating elements, which were shown in Ch. III to be unimplementable in practice.

With an allowance for inequality (7.47), the degree of the polynomial $D(p) + K(p)$ can also be shown to be equal to n.

Let us consider the three possible states of an open-loop system: stable, unstable, and neutral.

In the first case, by the Mikhailov stability criterion the variation of an argument of the open-loop system characteristic polynomial is

$$\Delta \underset{0<\omega<\infty}{\arg} D(j\omega) = n\frac{\pi}{2}$$

If we require that in the closed-loop state a system be stable, the following equation should be valid

$$\Delta \underset{0<\omega<\infty}{\arg} [D(j\omega) + K(j\omega)] = n\frac{\pi}{2}$$

Then from (7.46) it follows that

$$\Delta \underset{0<\omega<\infty}{\arg} F(j\omega) = \Delta \underset{0<\omega<\infty}{\arg} [D(j\omega) + K(j\omega)] - \Delta \underset{0<\omega<\infty}{\arg} D(j\omega) = 0 \quad (7.48)$$

A control system is thus stable if the variation of an argument of the vector $F(j\omega)$ is zero as ω varies from 0 to ∞.

Figure 7.6*a* shows two loci of $F(j\omega) = 1 + W_{o-l}(j\omega)$; *I* represents a stable system and does not encircle the point (0, 0), *II* represents an unstable system and encircles the point (0, 0). Since $F(j\omega)$ differs from $W_{o-l}(j\omega)$ by +1, the above can be directly formulated for the response $W_{o-l}(j\omega)$ (see Fig. 7.6*b*).

A closed-loop system is stable if the locus of the open-loop system $W_{o-l}(j\omega)$ *does not encircle the point* $(-1, j0)$.

Example 7.4. Let us use the Nyquist criterion to determine the limit gain of the control system treated in Example 7.3, for which

$$W_{o-l}(p) = \frac{k}{(1+pT_1)(1+pT_2)(1+pT_3)}$$

The frequency loci for this system at different values of k are shown in Fig. 7.7. By the Nyquist criterion the system is stable at $k = k_I$ and unstable at $k = k_{II}$.

In order to find the value of k_{lim} one should find the value of k at which the locus goes through the point $(-1, j0)$, or solve the following equation

$$W_{o-l}(j\omega_\pi) = \frac{k_{lim}}{(1+j\omega_\pi T_1)(1+j\omega_\pi T_2)(1+j\omega_\pi T_3)} = -1$$

or

$$(1 + j\omega_\pi T_1)(1 + j\omega_\pi T_2)(1 + j\omega_\pi T_3) = -k_{lim}$$

Composing equations for real and imaginary parts of this equation, we find ω_π and k_{lim}

$$\left.\begin{aligned} \omega_\pi &= \sqrt{\frac{T_1+T_2+T_3}{T_1T_2T_3}} \\ k_{lim} &= (T_1+T_2+T_3)\left(\frac{1}{T_1}+\frac{1}{T_2}+\frac{1}{T_3}\right) - 1 \end{aligned}\right\} \quad (7.49)$$

The solution obtained coincides with Eqs. (7.45) and (7.24) found by using the Mikhailov and Hurwitz criteria.

In the second case, the system is unstable in the open-loop state.

A system having single or multiple loops and containing unstable elements may be found unstable in the open-loop state.

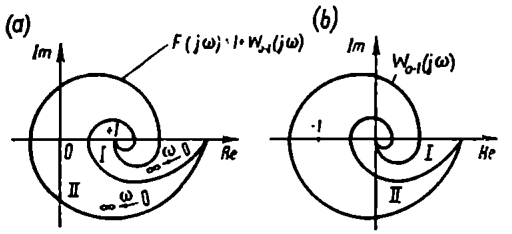

Fig. 7.6

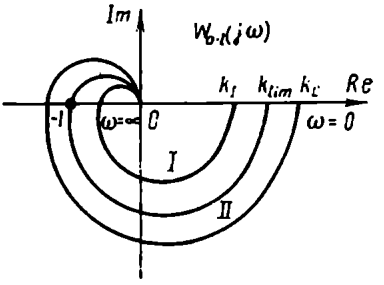

Fig. 7.7

Let a system be unstable in the open-loop state; then the characteristic equation of the open-loop system has m roots in the right half-plane. According to the argument principle (7.32)

$$\underset{-\infty<\omega<+\infty}{\Delta \arg} D(j\omega) = (n-2m)\pi$$

or, with an allowance for the symmetry of characteristics for $+\omega$ and $-\omega$,

$$\underset{0<\omega<\infty}{\Delta \arg} D(j\omega) = (n-2m)\frac{\pi}{2}$$

If we require that the system in the closed-loop state be stable, the following equality must be valid

$$\underset{0<\omega<\infty}{\Delta \arg} [D(j\omega)+K(j\omega)] = n\frac{\pi}{2}$$

Then, by virtue of Eq. (7.46)

$$\underset{0<\omega<\infty}{\Delta \arg} F(j\omega) = \underset{0<\omega<\infty}{\Delta \arg} [D(j\omega)+K(j\omega)] - \underset{0<\omega<\infty}{\Delta \arg} D(j\omega) =$$

$$= n\frac{\pi}{2} - (n-2m)\frac{\pi}{2} = \frac{m}{2}2\pi \qquad (7.50)$$

Consequently, *a control system is stable if, with* ω *varying from zero to infinity, the locus of the open-loop system* $W_{o-l}(j\omega)$ *encircles* $\frac{m}{2}$ *times the point* $(-1, j0)$ *in the positive direction, where* m *is the number of roots of the characteristic equation of an open-loop system in the right half-plane.*

The number of times the locus encircles the point can be determined in an illustrative way from the number of revolutions made by a vector connecting the point $(-1, j0)$ to the current point of the locus.

Figure 7.8 shows the locus of a stable closed-loop system which is unstable in the open-loop state; the number of roots is $m = 2$. The locus encircles the point $(-1, j0)$ only once $\left(\frac{m}{2} = 1\right)$ in the positive direction and consequently, by Eq. (7.50), the system is stable in the closed-loop state.

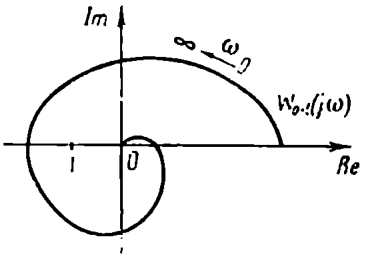

Fig. 7.8

Example 7.5. Let us apply the Nyquist criterion to find the limit gain of a simple stabilization system operating with an unstable plant.

Let

$$W_{o\text{-}l}(p) = \frac{k}{(pT_1 - 1)(1 + pT_2)}$$

The frequency loci of this system at different values of k and at $\tau = \frac{T_1}{T_2}$ are shown in Fig. 7.9*a*.

For this system $n = 2$ and $m = 1$; therefore, for the system to be stable as ω varies from zero to infinity the point -1 should be

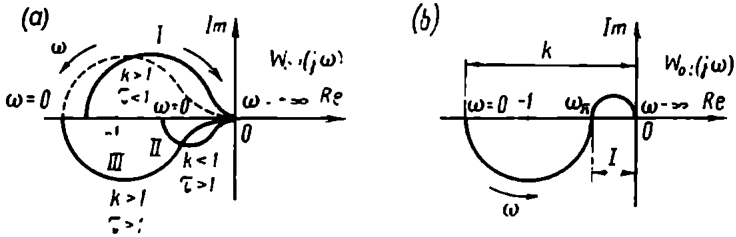

Fig. 7.9

encircled by the locus in the positive direction 0.5 times or once with ω varying from $-\infty$ to $+\infty$. This condition is satisfied by locus *III* alone.

Locus *I* encircles the point -1 only in the negative direction, and locus *II*, not at all.

Therefore, the stability condition is $k > k_{lim} = 1$ at $T_1 > T_2$.

Example 7.6. Let us take the problem of Example 7.5, but with

$$W_{o\text{-}l}(p) = \frac{k}{(pT_1 - 1)(1 + pT_2)(1 + pT_3)}$$

In this case the fulfilment of the conditions $k > 1$ and $T_1 > T_2$ will not always make the system stable. Considering the locus

of Fig. 7.9*b* for this case, we can see that the additional condition of stability is that at the frequency ω_π the locus should intersect the real axis to the right of point -1.

The mathematical formulation of this condition is obtained by finding the intersection frequency ω_π at which the imaginary part of the numerator of $W_{o\text{-}l}(j\omega)$ is zero. Here, this is true at

$$\operatorname{Im} D(j\omega) = j\omega_\pi [(T_1 - T_2 - T_3) - \omega_\pi^2 T_1 T_2 T_3] = 0$$

whence

$$\omega_\pi = \sqrt{\frac{T_1 - T_2 - T_3}{T_1 T_2 T_3}} \tag{7.51}$$

Consequently, the intercept cut off by the locus

$$I = \frac{k}{\omega_\pi^2 (T_1 T_2 + T_1 T_3 - T_2 T_3) - 1}$$

should be less than unity. In this case stability is obtained if the inequality

$$1 < k < \omega_\pi^2 (T_1 T_2 + T_1 T_3 - T_2 T_3) - 1 \tag{7.52}$$

is valid.

In the third case, the system is neutral in the open-loop state. The transfer function of an open-loop system is

$$W_{o\text{-}l}(p) = \frac{K(p)}{p^\nu D_1(p)} \tag{7.53}$$

where ν = the number of integrators in the system

$K(p)$ and $D_1(p)$ = polynomials in p, and $D_1(p)$ has no zeroes in the right half-plane and on the imaginary axis.

From Eq. (7.53) it follows that $W_{o\text{-}l}(j\omega)$ tends to ∞ as $\omega \to 0$, and therefore the shape of the locus of $W_{o\text{-}l}(j\omega)$, which has a discontinuity point at $\omega = 0$, does not clearly indicate whether it encircles the point $(-1, j0)$ and whether the system is stable. Therefore the locus should be specifically studied near the point corresponding to $\omega = 0$.

By limit transition this case can be obtained from the first or the second one. Solve this problem by applying the results obtained for a system stable in the closed-loop state. Let $\nu = 1$.

Then

$$W_{o\text{-}l}(j\omega) = \frac{K(j\omega)}{j\omega D_1(j\omega)} \tag{7.54}$$

At $j\omega = 0$ the value of $W_{o\text{-}l}$ goes to infinity by virtue of Eq. (7.54): therefore to preserve the formulation of the criterion which is true for systems stable in the open-loop state the locus is constructed either by circumventing the point (0, 0) from the right along a half-circle of infinitesimal radius $\rho \to 0$ when going along the imaginary axis from $-\infty$ to $+\infty$ (Fig. 7.10*a*) or regarding the zero root as the limit of a negative real root (Fig. 7.10*b*) $p_n = -\beta$ as $\beta \to 0$.

Let us use the second version of the limit transition from a stable open-loop system to a neutral one. In this case we replace the function $W_{o\text{-}l}(j\omega)$ by the function $W'_{o\text{-}l}(j\omega)$, which reduces to $W_{o\text{-}l}(j\omega)$ as $\beta \to 0$

$$W'_{o\text{-}l}(j\omega) = \frac{K(j\omega)}{(j\omega+\beta)D_1(j\omega)} \tag{7.55}$$

with

$$\lim_{\omega\to 0} W'_{o\text{-}l}(j\omega) = \frac{b_0}{\beta d_0} = R \tag{7.56}$$

where b_0 and d_0 are the values of the polynomials $K(j\omega)$ and $D_1(j\omega)$ at $\omega = 0$, and R is the value of $W'_{o\text{-}l}(j\omega)$ at $\omega = 0$.

At low frequencies the locus of $W'_{o\text{-}l}(j\omega)$ differs from the locus of $W_{o\text{-}l}(j\omega)$, taking the form of the dotted line of Fig. 7.10*c*. As β tends

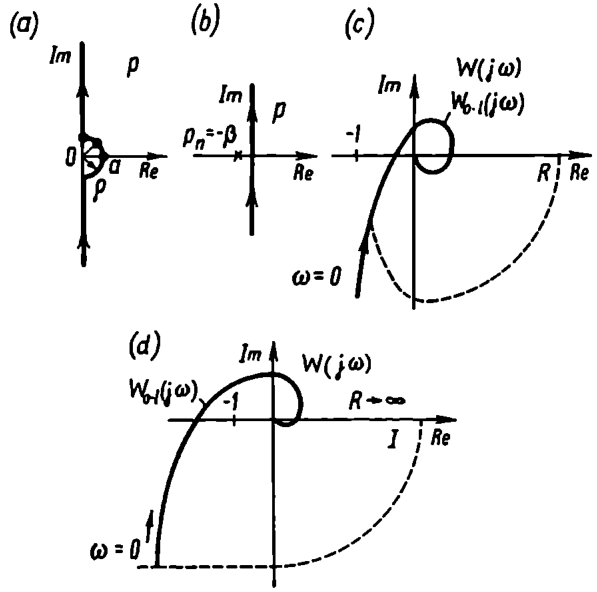

Fig. 7.10

to zero $R \to \infty$ and the locus of $W'_{o\text{-}l}(j\omega)$ differs from the locus of $W_{o\text{-}l}(j\omega)$ only by a quarter of a circle of infinitely large radius complemented as $\omega \to 0$. We will refer to this part of a circle as "a complement at infinity".

For $\nu = 1$ a complement at infinity is a quarter of a circle of infinitely large radius, for $\nu = 2$ this is already half of a circle, while for an arbitrary value of ν a complement of a locus at infinity is an arc containing ν quarters of a circle of infinitely large radius,

starting at a frequency $\omega = 0$ on the real axis and, with increasing frequency, making an angle of $\frac{\nu}{2}$ in the negative direction around the origin of coordinates.

Thus the system with one integrator, whose locus and its complement at infinity shown in Fig. 7.10*c* do not encircle the point $(-1, j0)$, is stable.

Fig. 7.10*d* illustrates the locus of an unstable system which encircles the point $(-1, j0)$.

Thence it follows that *a control system neutral in the open-loop state is stable if the locus of the open-loop system with its complement at infinity does not encircle the point* $(-1, j0)$.

Example 7.7. Let us use the Nyquist criterion to determine the limit gain of a control system with an open-loop transfer function

$$W_{o\text{-}l}(p) = \frac{k}{p(1+pT_1)(1+pT_2)}$$

The frequency loci of this system at different values of k are shown in Fig. 7.11. Curve I represents an unstable system ($k > k_{lim}$) and

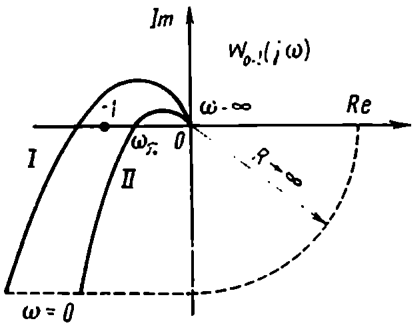

Fig. 7.11

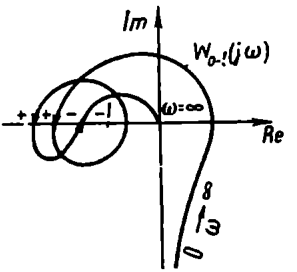

Fig. 7.12

curve II, a stable system ($k < k_{lim}$). The value of k_{lim} is found from the gain at the intersection frequency

$$\omega_\pi = \sqrt{\frac{1}{T_1 T_2}}$$

and therefore

$$k_{lim} = \frac{T_1 + T_2}{T_1 T_2} = \frac{1}{T_1} + \frac{1}{T_2} \qquad (7.57)$$

For practical applications a somewhat different formulation of the Nyquist criterion can be conveniently used which combines all the three above-discussed cases. If the transition of the locus of $W_{o\text{-}l}(j\omega)$ from the upper half-plane into the lower one with increasing ω is

regarded as positive and the reverse transition, negative, then the Nyquist criterion can be reformulated as follows. *A control system is stable if the difference between the numbers of positive and negative transitions of the locus of an open-loop system through the interval* $(-\infty, -1)$ *of a real axis is* $\frac{m}{2}$, *where m is the number of roots of the characteristic equation of an open-loop system in the right half-plane.*

In the particular case where $m = 0$ (which is equivalent to a stable or neutral open-loop system) the system is stable if the difference between the numbers of positive and negative transitions of the locus of $W_{o\text{-}l}(j\omega)$ through the interval $(-\infty, -1)$ is zero.

Figure 7.12 illustrates the locus $W_{o\text{-}l}(j\omega)$ of a system unstable in the open-loop state for which $m = 2$. The locus has two positive and one negative transitions; therefore the difference is $2 - 1 = 1$. By the above formulation of the stability criterion this system, although unstable in the open-loop state ($m = 2$), is stable in the closed-loop state.

Stability criterion based on plotting an inverse frequency locus of an open-loop system. In practice use is often made of a stability criterion based on plotting an inverse frequency locus

$$W_{o\text{-}l}^{-1}(j\omega) = \frac{1}{W_{o\text{-}l}(j\omega)} = \frac{D(j\omega)}{K(j\omega)} \tag{7.58}$$

In this case calculations are considerably simplified, especially for complex systems, since the order of $D(j\omega)$ is usually greater than that of $K(j\omega)$

$$W_{o\text{-}l}^{-1}(j\omega) = \frac{1}{W_{o\text{-}l}(\omega)} e^{-j\varphi(\omega)} \tag{7.59}$$

and consequently all points inside (outside) the circle of unit radius in the $W_{o\text{-}l}(j\omega)$ plane have corresponding points outside (inside) a circle of unit radius in the $W_{o\text{-}l}^{-1}(j\omega)$ plane (Fig. 7.13). In particular, the points of intersection with the interval $(-\infty, -1)$ of the real axis in the $W_{o\text{-}l}(j\omega)$ plane are associated with the points of intersection with the interval $(0, -1)$ in the $W_{o\text{-}l}^{-1}(j\omega)$ plane, while the sign of transition in the latter points is reversed.

Therefore the stability criterion based on using the inverse characteristic can be formulated as follows. *A control system is stable if the difference between the numbers of negative and positive transitions of an inverse frequency locus of an open-loop system through the interval* $(0, -1)$ *of a real axis is* $\frac{m}{2}$, *where m is the number of roots of the characteristic equation of an open-loop system in the right half-plane.*

At $m = 0$, which is the case in a stable or neutral open-loop system, the system is stable if the difference between the numbers

of negative and positive traversals of the interval (0, —1) by the locus of $W_{o\text{-}l}^{-1}(j\omega)$ is zero.

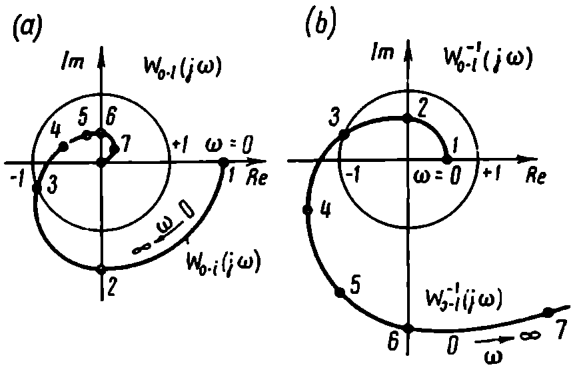

Fig. 7.13

Example 7.8. Assume that

$$W_{o\text{-}l}(j\omega) = \frac{k}{(1+j\omega T_1)(1+j\omega T_2)(1+j\omega T_3)}$$

Figure 7.14 is a plot of the loci of $W_{o\text{-}l}(j\omega)$ and $W_{o\text{-}l}^{-1}(j\omega) = \frac{1}{W_{o\text{-}l}(j\omega)}$. The former does not intersect the interval $(-\infty, -1)$ and, consequently, the system is stable in the closed-loop state at the given value of k.

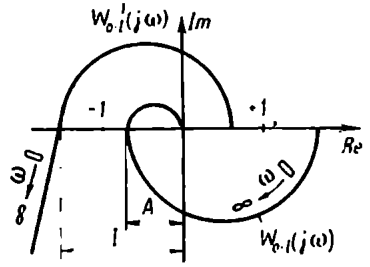

Fig. 7.14

Using the loci it is required to find the limit gain k_{lim}. As in Example 7.4, using the locus of $W_{o\text{-}l}(j\omega)$ one finds

$$k_{lim} = \frac{1}{A}k$$

The same result is obtained by studying the inverse locus $W_{o\text{-}l}^{-1}(j\omega)$. This cuts off the intercept $I = \frac{1}{A}$. With increasing gain the locus contracts, whereas if k increases I times the locus goes through the point $(-1, j0)$, the system being on the stability boundary. Thence

$$k_{lim} = kI = k\frac{1}{A} \tag{7.60}$$

Estimating the stability from the system logarithmic response. The Nyquist stability criterion can be formulated for logarithmic responses of a system in the open-loop state. The points where the locus

$W_{o\text{-}l}(j\omega)$ intersects the interval $(-\infty, -1)$ of the real axis are associated with points for which $L(\omega) = 20 \log |W_{o\text{-}l}(j\omega)| > 0$ and $\varphi(\omega) = \arg W_{o\text{-}l}(j\omega) = -\pi, -3\pi, -5\pi, \ldots$. The points of the logarithmic phase response $\varphi(\omega)$ for which $L(\omega) > 0$ and where it intersects (with increasing ω) the straight lines $-\pi$, -3π, -5π from below will be referred to as *positive transitions*, and from above, *negative transitions* of the logarithmic response (Fig. 7.15*a*).

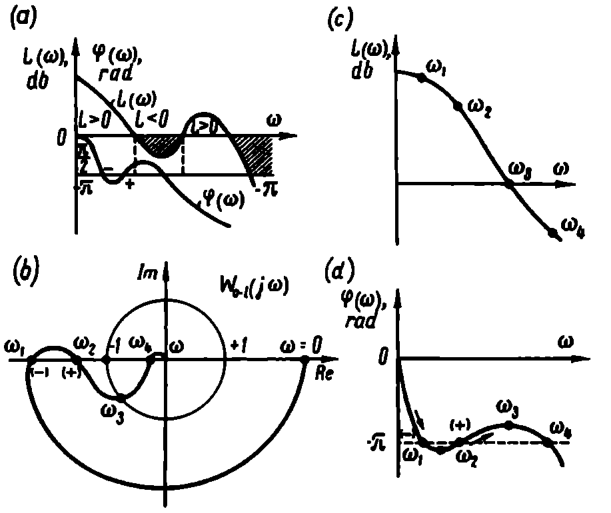

Fig. 7.15

Then the stability criterion can be formulated as follows. *A control system is stable if the difference between the numbers of positive and negative transitions of the logarithmic response is* $\frac{m}{2}$, *where m is the number of roots of the characteristic equation of an open-loop system in the right half-plane.*

At $m = 0$ (the system is stable or neutral in the open-loop state) the formulation changes to: *a system is stable if the difference between the numbers of positive and negative transitions of the logarithmic response is zero.*

Figure 7.15*b*, *c*, *d* is the plot of responses of a system stable in the open-loop state ($m = 0$). The logarithmic responses and the frequency loci show that the system is stable in the closed-loop state.

Using frequency techniques, a number of general conclusions can be made concerning the stability of systems consisting of integrating, inertial (stable and unstable) and oscillatory elements. For example, if a system has two integrators, the frequency locus is found to be turned clockwise by an angle greater than π relative to the real axis; the system is therefore permanently unstable.

Systems unstable at any values of the variables are known as *structurally unstable.*

In a similar way it can be shown that two unstable inertial elements or one integrator and one unstable inertial element are sufficient to make a system structurally unstable.

The problems of structural stability have been treated by M.A. Aizerman (Ref. 1).

The introduction of differentiating and lead elements distorts the locus by turning it counterclockwise and can make the system stable at certain values of parameters. How systems are corrected by means of additional elements is shown in Ch. XI.

7.4. THE EXTENSION OF THE NYQUIST CRITERION TO IRRATIONAL AND TRANSCENDENTAL SYSTEMS

The Nyquist stability criterion proved for systems described by rational transfer functions is also applicable to systems neutral or stable in the open-loop state, which are described by irrational, exponential or transcendental transfer functions, which, when expanded in a series, are reducible to fractional rational functions where the powers of the numerator and denominator tend to infinity. Without proving the Nyquist criterion for each case, we will dwell on its application to certain problems of the class defined.

Stability of systems with irrational elements. Let us consider the applicaton of the Nyquist criterion to systems containing elements with irrational transfer functions using a specific example.

Example 7.9. A control system of a radiant heater with a transfer function

$$W_1 = \frac{k_1}{\sqrt{p}}$$

has a controller with a transfer function

$$W_2 = \frac{k_2}{(1+pT_1)(1+pT_2)}$$

It is required to find the limit gain $k = k_1k_2$ of an open-loop system at which the system becomes unstable.

The reduction of a neutral system to a stable one is achieved by introducing a small parameter β and replacing W_1 by the transfer function

$$W_1' = \frac{k_1}{\sqrt{p}+\beta}$$

as $\beta \to 0$. If we plot the locus of W_1' for $\beta \to 0$, we obtain its complement at infinity.

The locus of

$$W_{o\text{-}l}(j\omega) = W_1(j\omega)\, W_2(j\omega) = \frac{k}{\sqrt{j\omega}\,(1+j\omega T_1)\,(1+j\omega T_2)} \qquad (7.61)$$

is shown in Fig. 7.16. The dotted line represents its complement at infinity.

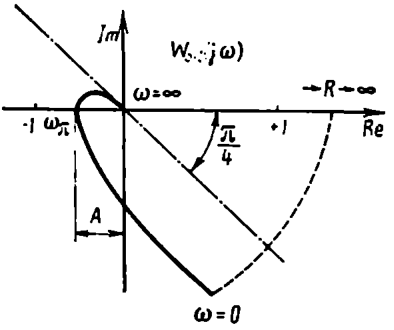

Fig. 7.16

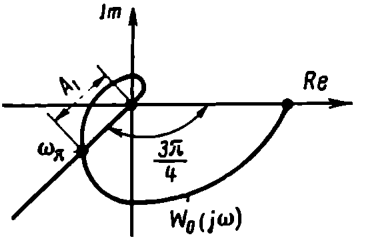

Fig. 7.17

The limit gain $k = k_{lim}$ and the intersection frequency ω_π are found from the equations

$$W_{o\text{-}l}(j\omega_\pi) = -1 \qquad (7.62)$$

or

$$\sqrt{j\omega_\pi}\,(1+j\omega_\pi T_1)\,(1+j\omega_\pi T_2) = -k_{lim} \qquad (7.62')$$

By substituting $\sqrt{j} = \frac{1+j}{\sqrt{2}}$ and isolating the equations for imaginary and real parts

$$\sqrt{\omega_\pi}\,[1-\omega_\pi(T_1+T_2)-\omega_\pi^2 T_1 T_2] = -\sqrt{2}k_{lim}$$

and

$$1+\omega_\pi(T_1+T_2)-\omega_\pi^2 T_1 T_2 = 0$$

we find

$$\omega_\pi = \frac{T_1+T_2+\sqrt{T_1^2+6T_1T_2+T_2^2}}{2T_1T_2} \qquad (7.63)$$

and

$$k_{lim} = \sqrt{2}\,\omega_\pi^{2/2}\,(T_1+T_2) \qquad (7.64)$$

For any kind of function W_2 Eq. (7.62) can be solved graphically. If $W_{o\text{-}l}(j\omega_\pi)$ is represented in the form

$$W_{o\text{-}l}(j\omega_\pi) = \frac{k_{lim}}{\sqrt{j\omega_\pi}}\, W_0(j\omega_\pi) \qquad (7.65)$$

where $W_0 = \frac{W}{k}$, then Eq. (7.62) can be given as

$$W_0(j\omega_\pi) = -\frac{\sqrt{j\omega_\pi}}{k_{lim}} \tag{7.66}$$

The values of ω_π and k_{lim} can be found from the intersection points of the locus $W_0(j\omega_\pi)$ and a straight line inclined at an angle $\arg(-\sqrt{j}) = -\frac{3\pi}{4}$ to the real axis (Fig. 7.17).

A segment of that line, A_1, is $\frac{\sqrt{\omega_\pi}}{k_{lim}}$ and consequently

$$k_{lim} = \frac{\sqrt{\omega_\pi}}{A_1} \tag{7.67}$$

Stability of systems with delays. The applicability of the Nyquist criterion to systems with a delay was substantiated by Ya. Z. Tsypkin in 1947.

Given a control system with a delay (Fig. 7.18). The transfer function $W_1(p)$ of element I is expressed by a fractional rational

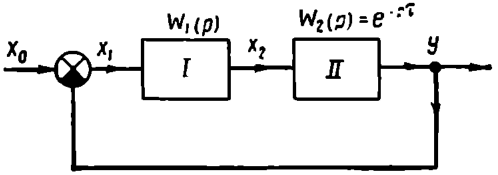

Fig. 7.18

function of p, the transfer function $W_2(p)$ corresponds to delay II with delay time τ and has the form $e^{-p\tau}$.

The transfer function of the system in the open-loop state is

$$W_{o\text{-}l}(p) = W_1(p)\, e^{-p\tau} \tag{7.68}$$

A system without a delay ($\tau \to 0$) is referred to as a *limit system*. Its transfer function in the open-loop state is

$$W_1(p) \tag{7.69}$$

The frequency responses of a system with and without a delay are given, respectively, by the expressions

$$W_{o\text{-}l}(j\omega) = W_1(j\omega)\, e^{-j\omega\tau} \tag{7.70}$$

and

$$W_1(j\omega)$$

It is evident from Eq. (7.70) that to obtain a frequency locus for a system with a delay a locus for a limit system should be constructed

and each vector of this locus must be turned clockwise through an angle $\omega\tau$. If ω increases, so does $\omega\tau$ (points *1-1'* in Fig. 7.19). Since at large values of ω the magnitude of $W_1(j\omega)$ is normally small, the locus of a system with a delay spirals around zero.

Assume that a limit system is stable. Then by the Nyquist criterion for systems stable in the open-loop state, the locus should not

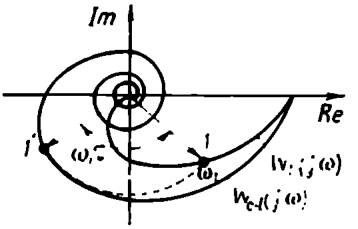

Fig. 7.19

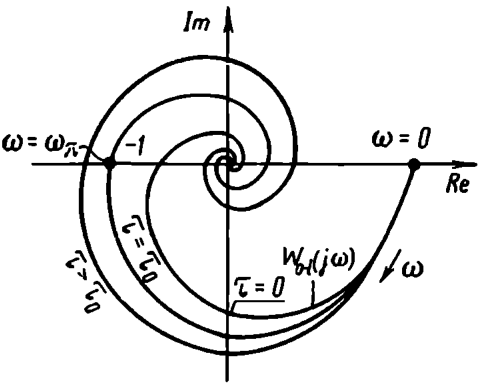

Fig. 7.20

encircle the point $-1, j0$ (Fig. 7.20). Increase τ from zero and observe the shape of the locus $W_{o-l}(j\omega)$.

For a certain value of $\tau = \tau_0$ at $\omega = \omega_\pi$ the locus may go through the point $(-1, j0)$. At $\tau < \tau_0$ the locus $W_{o-l}(j\omega)$ will not encircle the point $(-1, j0)$, and at $\tau > \tau_0$ it will. So the system is on the stability boundary at $\tau = \tau_0$.

With further increase of τ the point $(-1, j0)$ will be found inside the locus, and the system will be unstable.

If τ is increased still further, the deforming response $W_{o-l}(j\omega)$ will not encircle the point $(-1, j0)$ again, and the system will regain stability. If τ is increased still further, the system may become unstable again. The values of τ at which $W_{o-l}(j\omega)$ goes through the point $(-1, j0)$ are known as *limit*. These limit values of τ_0 and of the frequency ω_π are found from the equation

$$W_{o-l}(j\omega_\pi) = W_1(j\omega_\pi)\, e^{-j\tau_0\omega_\pi} = -1 \tag{7.71}$$

which is equivalent to the equations

$$\operatorname{mod} W_{o-l}(j\omega_\pi) = \operatorname{mod} W_1(j\omega_\pi) = 1 \tag{7.72}$$

$$\arg W_{o-l}(j\omega_\pi) = \arg W_1(j\omega_\pi) - \omega_\pi\tau_0 = -\pi(2m+1) \tag{7.73}$$

From Eq. (7.73) it follows that the limit values of τ_0 can be found from the condition

$$\tau_0 = \frac{\pi - \varphi}{\omega_\pi} + \frac{2m\pi}{\omega_\pi} = \frac{\gamma}{\omega_\pi} + \frac{2m\pi}{\omega_\pi} \tag{7.74}$$

where $\varphi = -\arg W_1(j\omega_\pi)$

γ = angle between the vector $W_{o\text{-}l}(j\omega_\pi)$ and the negative direction of the real axis.

Equation (7.71) can be solved graphically. To do this, draw a circle of unit radius in the $W(j\omega)$ plane (Fig. 7.21).

The points of intersection between the locus $W_1(j\omega)$ and this circle determine the intersection frequencies ω_π, and the ratios of the angles γ to the values of ω_π determine the limit times of delay.

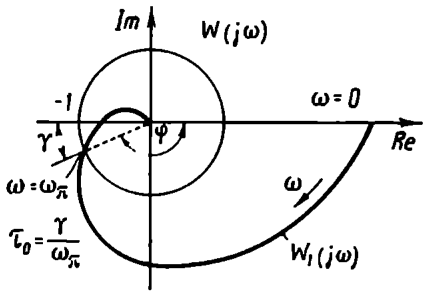

Fig. 7.21

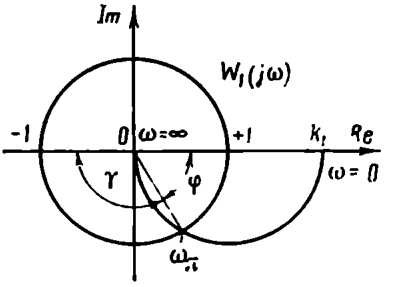

Fig. 7.22

For systems with a delay the minimal limit delay time τ_{01} is often of primary importance. The stability condition for such systems may be given in the form $\tau < \tau_{01}$.

Note that if the locus $W_1(j\omega)$ is completely within the unit radius circle, i.e. there are no intersection points, then the system is stable at any value of τ.

Example 7.10. A control system consists of an inertial element with a transfer function

$$W_1(p) = \frac{k_1}{1 + pT_1}$$

and a delay with a transfer function

$$W_2(p) = e^{-p\tau}$$

Find the limit delay time τ at which the system is stable at $k_1 > 1$.

Equation (7.72) for this case has the form

$$k_1^2 = 1 + \omega_\pi^2 T_1^2$$

whence

$$\omega_\pi^2 = \frac{k_1^2 - 1}{T_1^2} \tag{7.75}$$

Knowing ω_π, we can find

$$\varphi = -\arg W_1(j\omega_\pi) = \arctan(\omega_\pi T_1) \tag{7.76}$$

and by Eq. (7.74) determine the limit delay time. The locus of $W_1(j\omega)$ for this case is shown in Fig. 7.22, where

$$\tau_0 = \frac{\pi - \varphi}{\omega_\pi} = \frac{\pi - \arctan \omega_\pi T_1}{\omega_\pi} \tag{7.77}$$

At $\tau < \tau_0$ the system is stable, and at $\tau > \tau_0$, unstable.

7.5. COMPARISON OF STABILITY CRITERIA

Each of the above criteria has its own scope of application.

The Hurwitz criterion is the most expedient if the order of the characteristic equation is up to four inclusive ($n \leqslant 4$).

The Routh criterion gives a quick answer if coefficients are given numerically and $n > 4$.

The Mikhailov criterion is best suited for studying complex multiloop systems where it is necessary to determine the effect of changes in the system structure and of stabilizers on the system stability.

The Nyquist stability criterion in its inverse and normal form is best applied to complex systems study and is the only feasible criterion when some or all responses of elements are given experimentally. It is useful in analysis of systems described by analytical functions other than fractional rational, e.g. irrational, exponential, transcendental, etc., and it can also be conveniently used in analysis of systems with a delay.

Chapter VIII

THE EFFECT OF SYSTEM'S PARAMETERS ON ITS STABILITY

8.1. STATEMENT OF THE PROBLEM

The stability criteria of Ch. VII enable one to see whether the system is stable or not if its parameters are known. They may help to show the effect of certain parameters on the system stability and determine the limit values of the system gain and delay time.

There are special methods that facilitate analysis of the effect of the various parameters on the system stability. The main of them are based on analysis of displacement of the characteristic equation roots in the root plane and analysis of the number of characteristic equation roots in the right half-plane in the system parameter space. The former method is known as the *method of root locus*, and the latter, as *D-decomposition of the parameter space*. The root locus method was suggested by Teodorchik in 1948 and developed by Uderman (Moscow) in 1949 (Ref. 83) and Evans (USA) in 1950. *D*-decomposition was suggested by Neimark (Gorky City, USSR) in 1948.

8.2. THE ROOT LOCUS METHOD

The root locus is the locus of the characteristic equation roots when one of the system parameters changes from zero to infinity.

Let the characteristic equation of an nth-order system be given in the form

$$A(p) = P(p) + vQ(p) = 0 \tag{8.1}$$

where

v = variable parameter of the system

$P(p)$ and $Q(p)$ = polynomials in p.

Then to find the root locus it is necessary to find the displacement of all n roots of the characteristic equation when $0 < v < \infty$.

Without loss of generality, the unit of measurement of the parameter v can always be selected so as to make the coefficients of highest powers of p in the expressions $P(p)$ and $Q(p)$ equal to 1, i.e.

$$P(p) = p^n + a_1 p^{n-1} + \ldots + a_n \tag{8.2}$$

while

$$Q(p) = p^r + b_1 p^{r-1} + \ldots + b_r \tag{8.3}$$

Then, finding the roots of the equations $P(p) = 0$ denoted as z_1, z_2, ..., z_n and $Q(p) = 0$ denoted as q_1, q_2, ..., q_r, Eq. (8.1) can be rearranged as

$$\prod_n (p - z_i) + v \prod_r (p - q_i) = 0 \tag{8.4}$$

or for $v \neq 0$

$$\frac{1}{v} \prod_n (p - z_i) + \prod_r (p - q_i) = 0 \tag{8.5}$$

By appropriate selection of the variable v the condition $n \geqslant r$ can always be guaranteed.

If the roots of Eq. (8.1) or (8.4) and (8.5) are denoted as p_i, then the latter two equations lead to the conclusion that at $v = 0$ the roots p_i coincide with the roots z_i, while at $v = \infty$ they coincide with q_i or go to infinity.

Since all complex roots of the characteristic equation are symmetrical relative to the real axis in the root plane, the above considerations lead to the following rule for the construction of a root locus.

Rule 1. *A root locus is symmetrical relative to the real axis and consists of n branches issuing from n zeroes of the equation* $P(p) = 0$ *at* $v = 0$, *of which r branches end in r zeroes of the equation* $Q(p) = 0$, *while* $n - r$ *branches go to infinity as* $v \to \infty$.

Let us consider $n - r$ asymptotic curves of a root locus at $r < n$ and $v \to \infty$. Represent Eq. (8.4) in the form

$$-v = \frac{\prod_n (p - z_i)}{\prod_r (p - q_i)} = \frac{P(p)}{Q(p)} \tag{8.6}$$

The numerator and denominator of Eq. (8.6) have the form of polynomials (8.2) and (8.3), while $a_1 = -\sum_n z_i$ and $b_1 = -\sum_r q_i$. Dividing the numerator by the denominator, we have

$$-v = p^{n-r} + c_1 p^{n-r-1} + c_2 p^{n-r-2} + \ldots \tag{8.7}$$

where

$$c_1 = a_1 - b_1 = \sum_r q_i - \sum_n z_i \tag{8.8}$$

In the general case Eq. (8.7) is a sum of an infinite series of terms with the powers of the variable p decreasing to $-\infty$.

As $|p| \to \infty$, which is true for asymptotic curves, only the first two terms of the series are of importance. Therefore we will consider the coefficients of these two terms only.

As $|p| \to \infty$ Eq. (8.7) degenerates into the equation of an $(n-r)$-pointed symmetrical star. Indeed, the parametric equation of such a star with centre in the point x_0 has the form

$$-v = (p - x_0)^{n-r} \tag{8.9}$$

where v varies from zero to infinity.

At $n - r = 1$ this star is a half-line going along the real axis in the negative direction from the point x_0 to infinity (Fig. 8.1*a*).

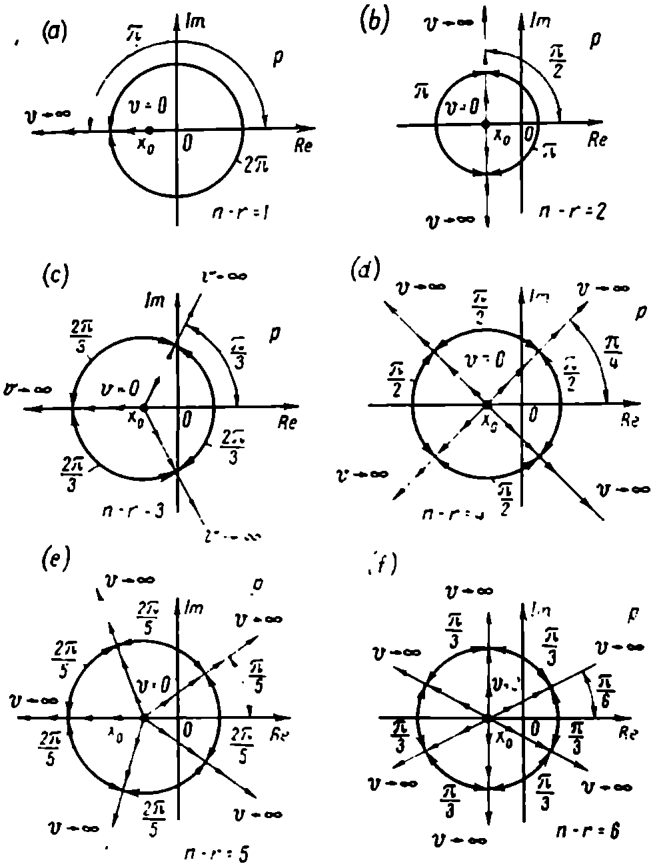

Fig. 8.1

At $n - r = 2$ the star has two rays issuing from the point x_0 and going in the directions $+j$ and $-j$ to infinity (Fig. 8.1*b*). With increasing $n - r$ the number of rays increases (Fig. 8.1*c*, *d*, *e* and *f*).

With the equations of modules and arguments written down we have, in place of Eq. (8.9),

$$\text{mod}\,(p - x_0) = \sqrt[n-r]{v} \tag{8.10}$$

and

$$\arg(p-x_0)=\frac{\pi(2k+1)}{n-r} \tag{8.11}$$

It is assumed that $-1=e^{-j\pi(2k+1)}$, where k is any integer.

From Eq. (8.11) it follows that the angle between two adjacent rays of the star is $\frac{2\pi}{n-r}$, while the angle between the real axis and the nearest ray is $\frac{\pi}{n-r}$.

By using the Newton binomial formula Eq. (8.9) can be rearranged in a form closer to Eq. (8.7):

$$-v=p^{n-r}-(n-r)\,p^{n-r-1}x_0+\frac{(n-r)\,(n-r-1)}{2!}\,p^{n-r-2}x_0^2-\ldots \tag{8.12}$$

Comparing Eqs. (8.12) and (8.7), we can see that as $|p|\to\infty$ and, accordingly, $v\to\infty$, i. e. when we can restrict ourselves to the first two terms, the equations coincide if $c_1=-(n-r)\,x_0$.

Expressing c_1 through z_i and q_l by Eq. (8.8) and solving the resulting equation for x_0, we find

$$x_0=\frac{\sum\limits_{n} z_l-\sum\limits_{r} q_l}{n-r} \tag{8.13}$$

Equation (8.13) yields the centre of gravity for a system of bodies with weights of $+1$ and -1.

Therefore, the following rule may be applied in constructing an asymptotic root locus.

Rule 2. *An asymptotic root locus as $v\to\infty$ is a symmetrical $(n-r)$-pointed star with centre in the point corresponding to the centre of gravity of the roots of the equations $P(p)=0$ and $Q(p)=0$ if the roots of the first equation are denoted as $+1$ and those of the second, as -1. The angles between the rays of the star are $\frac{2\pi}{n-r}$, while the ray closest to the real axis forms an angle of $\frac{\pi}{n-r}$ with it.*

The above rules permit finding the origins and ends of the root locus branches as $v\to 0$ and $v\to\infty$. At intermediate values of the parameter the roots are displaced, with variation in v, either along the real axis or in the complex plane.

In constructing the root locus it is important to know the direction of displacement of the roots and the points where they break away from the real axis. To this end Eq. (8.6) is represented in the form

$$\frac{P(p)}{Q(p)}=f(p)=-v \tag{8.14}$$

and, with p assumed real, $f(p)$ is plotted. The points where this curve meets the straight line $-v$ yield the values of the roots at specified values of v. The extremum points where $\frac{df(p)}{dp} = 0$ or $Q(p)\frac{dP(p)}{dp} - P(p)\frac{dQ(p)}{dp} = 0$ determine the breakaway points from the real axis and transition to the region of complex values.

An example of the function $f(p)$ is shown in Fig. 8.2. At $v = 0$ all the three roots of the characteristic equation are on the real axis in the points z_1, z_2, and z_3. With increasing v the displacement of these roots depends on the points where the curve $f(p)$ intersects the straight line $f = -v$. Thus at $v = v_1$ the roots of the characteristic equation are expressed by the abscissas of points *1*, *2*, and *3*. Roots *2* and *3* are seen to go to the right and root *1*, to the left. At $v = v_0$ roots *1* and *2* in point *4* coincide and are equal ($p_1 = p_2 = p_0$) and a further increase of v breaks the roots away from the real axis. At $v > v_0$ only the root p_3 (point *6*) will stay on the real axis and with increasing v it approaches the point q_1 arriving at this point as $v \to \infty$.

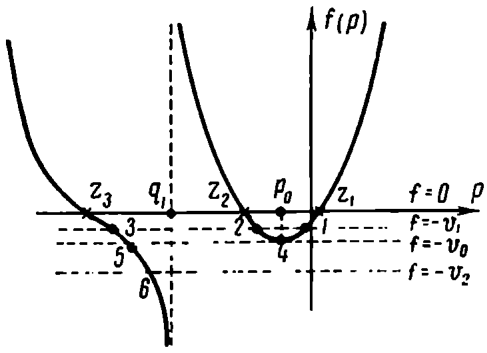

Fig. 8.2

Similar considerations lead to the following rule for the construction of a root locus.

Rule 3. *The displacement of roots along the real axis can be determined from the intersection points of the auxiliary function* $f(p) = \frac{P(p)}{Q(p)}$ *and the straight line* $f = -v$. *The root locus breaks away from the real axis in the point where* $\frac{df}{dp} = 0$.

The value of the parameter v *at which the system ceases to be stable is found from the intersection points of the root locus and the imaginary axis of the p plane.*

The above rules may yield root loci for different variations of control system parameters.

Example 8.1. Plot a root locus for a control system with a transfer function

$$W(p) = \frac{k}{p(1+pT_1)(1+pT_2)}$$

with k varying from zero to infinity, assuming $T_1 = 0.1$ sec and $T_2 = 0.02$ sec.

Equation (8.1) for this case has the form

$$A(p)=p\left(p+\frac{1}{T_1}\right)\left(p+\frac{1}{T_2}\right)+\frac{k}{T_1T_2}=0$$

Therefore

$$P(p)=p\left(p+\frac{1}{T_1}\right)\left(p+\frac{1}{T_2}\right)$$

$$Q(p)=1$$

$$v=\frac{k}{T_1T_2}$$

In this way

$$n=3,\quad r=0,\quad z_1=0,\quad z_2=-\frac{1}{T_1}=-10\frac{1}{\text{sec}},$$

$$z_3=-\frac{1}{T_2}=-50\frac{1}{\text{sec}}$$

Since $n-r=3$, the asymptotic root locus has the form of a three-pointed star (see Fig. 8.1*c*) with centre in a point determined by Eq. (8.13)

$$x_0=\frac{-10-50}{3}=-20\frac{1}{\text{sec}}$$

To find the root displacements and the breakaway point let us plot the graph $f(p)=p(p+10)(p+50)$ shown in Fig. 8.3*a*.

The breakaway point is found from the condition

$$\frac{df}{dp}=0$$

or

$$3p^2+120p+500=0$$

Solving this equation, we find

$$p_0=-20+\sqrt{400-\frac{500}{3}}\cong-5\frac{1}{\text{sec}}$$

Here, from among the two extremum points of the function $f(p)$ the one is selected which corresponds to $f(p)=-v<0$.

In the breakaway point the value

$$v_0=-p_0(p_0+10)(p_0+50)=1{,}125\frac{1}{\text{sec}^3}$$

The value of v in the intersection points of the locus and the imaginary axis v_{lim} is found from the equation $A(j\omega)=0$

$$v_{lim}=\frac{k_{lim}}{T_1T_2}=\frac{T_1+T_2}{T_1^2T_2^2}=30{,}000\frac{1}{\text{sec}^3}$$

for which

$$p=\pm j\omega_0=\pm j\sqrt{z_2z_3}\cong\pm j\,22.4\frac{1}{\text{sec}}$$

The locus plotted on the basis of three asymptotes, three roots at $v = 0$, the breakaway point at $v = v_0$ and intersection points with the imaginary axis at $v = v_{lim}$ is shown in Fig. 8.3*b*.

Example 8.2. Plot a root locus for the same system with T_2 varying from zero to infinity if $T_1 = 0.1$ sec and $k = 1.6 \frac{1}{\text{sec}}$.

For this case Eq. (8.1) has the form

$$A(p) = p^2\left(p + \frac{1}{T_1}\right) + \frac{1}{T_2}\left(p^2 + p\frac{1}{T_1} + \frac{k}{T_1}\right) = 0$$

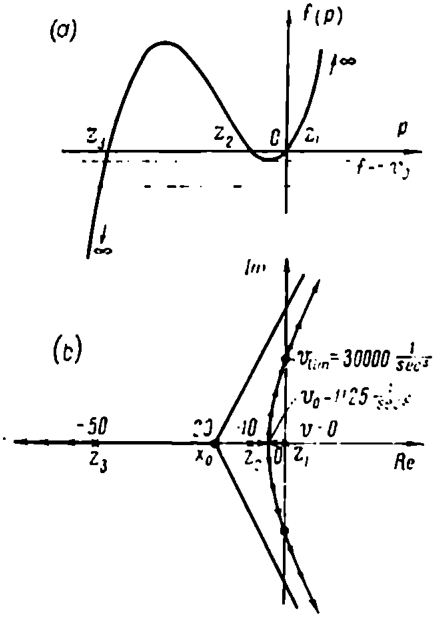

Fig. 8.3

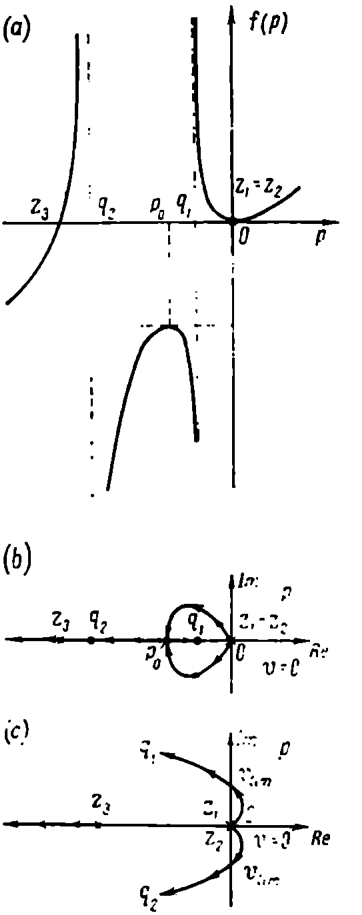

Fig. 8.4

Therefore

$$P(p) = p^2\left(p + \frac{1}{T_1}\right)$$

and

$$Q(p) = p^2 + p\frac{1}{T_1} + \frac{k}{T_1} = (p - q_1)(p - q_2)$$

$$v = \frac{1}{T_2}$$

Consequently

$$n=3, \quad r=2, \quad z_1=z_2=0, \quad z_3=-\frac{1}{T_1}=-10\frac{1}{\text{sec}},$$

$$q_1q_2=\frac{k}{T_1}=16\frac{1}{\text{sec}}, \quad q_1+q_2=\frac{-1}{T_1}=-10\frac{1}{\text{sec}}$$

whence

$$q_1=-2\frac{1}{\text{sec}} \quad \text{and} \quad q_2=-8\frac{1}{\text{sec}}$$

Since $n-r=1$, the asymptotic root locus has the form of a ray going from the point z_3 to $-\infty$. In order to find the displacement of roots and the breakaway points, we plot the graph

$$f(p)=\frac{p^2(p+10)}{(p+2)(p+8)}$$

shown in Fig. 8.4*a*.

The breakaway point is seen to be in the origin of coordinates, where two roots go at once to the complex region. For the specified parameters of the system at a certain value of $v=v_0$ these roots meet on the real axis in the point p_0 and on further increase of v they go along the real axis towards the poles of the function $f(p)$ (in the points q_1 and q_2). The meeting point p_0 of these poles is determined by the equation $\frac{df}{dp}=0$ and located between the points q_1 and q_2.

The value of v in the points where the locus intersects the imaginary axis v_{lim} is found from the equation $A(j\omega)=0$

$$v_{lim}=\frac{1}{T_{2lim}}=k-\frac{1}{T_1}$$

For the specified parameters of the system $v_{lim}=k-\frac{1}{T_1}=-8.2<0$ and consequently at any positive values of v the system remains stable and the locus lies in the left half-plane (Fig. 8.4*b*).

If in our example $k>\frac{1}{T_1}$, the locus will be displaced into the right half-plane at some values of v and intersect the imaginary axis at $v=v_{lim}=k-\frac{1}{T_1}$. This is illustrated in Fig. 8.4*c*. Here the roots of the equation $Q(p)=0$ are complex, and as $v\to\infty$, both branches of the locus terminate in the points q_1 and q_2 which do not lie on the real axis. The function $f(p)$, in contrast to the plot of Fig. 8.4*a*, has no U-shaped branch located in the lower half-plane.

8.3. D-DECOMPOSITION METHOD

Assume a characteristic equation of the nth order

$$A(p) = p^n + a_{n-1}p^{n-1} + \ldots + a_0 = 0$$

Generally, with given values of the coefficients it has m roots in the right half-plane and $(n - m)$ roots in the left half-plane. If the coefficients vary the roots move in the root plane, describing root loci. At some values of the coefficients one of the roots arrives at the origin of coordinates or a pair of roots arrive at the imaginary axis. Consequently these values satisfy the equation

$$A(j\omega) = (j\omega)^n + a_{n-1}(j\omega)^{n-1} + \ldots + a_0 = 0 \qquad (8.15)$$

In the n-dimensional space of the coefficients with axes a_0, a_1, ... , a_{n-1} Eq. (8.15) is represented by a hypersurface as ω varies in the range $-\infty$ to $+\infty$.

If one moves in the space of coefficients by changing the coefficients of the equation, then at some of their values the hypersurface $A(j\omega) = 0$ is met and therefore a pair of roots or one root goes from one half-plane to the other.

Let us consider in more detail the case where $n = 3$ and the characteristic equation has the form

$$A(p) = p^3 + a_2p^2 + a_1p + a_0 = 0$$

Each set of values of the coefficients a_0, a_1, and a_2 is represented by a point in the three-dimensional space of coefficients (Fig. 8.5). There is a specific position of the equation roots in the plane of roots (Fig. 8.5*b*) which corresponds to a given set of coefficient values. The point M is associated with the roots m_1, m_2, and m_3, the point N, with the roots n_1, n_2, and n_3. At certain values of coefficients one root or a pair of roots will arrive at the imaginary axis; in other words, the roots will have the form 0 or $\pm j\omega_1$ and consequently the corresponding point in the space of coefficients will satisfy the equation

$$A(j\omega_1) = (j\omega_1)^3 + a_2(j\omega_1)^2 + a_1(j\omega_1) + a_0 = 0$$

When $-\infty < \omega_1 < +\infty$ this equation is represented by the surface S partially shown in Fig. 8.5*a*. As coefficients vary the roots of the characteristic equation also change and arrive at the imaginary axis only when the point in the space of coefficients arrives at the surface S. When the point crosses the surface the roots leave one half-plane and shift to the other. Thence the surface S divides the space of coefficients into regions each point of which is represented by a 3rd-order characteristic equation with a definite number of roots in the right and left half-planes. Let us denote these regions

as $D(m)$, where m is the number of roots in the right half-plane. For a 3rd-order equation the space of coefficients may have four regions $D(3)$, $D(2)$, $D(1)$, $D(0)$. The last is the stability region. *This decomposition of a space into regions with different values of m is referred to as D-decomposition.*

For equations of a higher order ($n > 3$) a multidimensional space and hypersurfaces decomposing this space into regions have to be investigated.

This complicates the problem a good deal and the investigation loses its illustrativeness. If only some of the coefficients change,

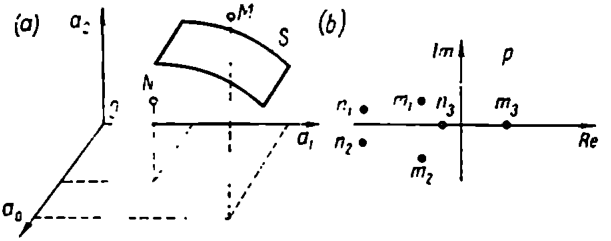

Fig. 8.5

e.g. a_1 and a_2, while $a_0 = \text{const}$, then instead of a surface we have a curve which is a cross section of the surface S by the plane $a_0 = \text{const}$.

It has been shown that a transition across the boundary of a D-decomposition is equivalent to a transition of the equation roots across the imaginary axis. Consequently, by virtue of the above, the equation of a D-decomposition boundary has the form of Eq. (8.15) and thus it can be obtained from the characteristic equation $A(p) = 0$ by substituting $j\omega$ for p. Using equations obtained in the parametric form the boundary of the D-decomposition can be plotted assuming the values of ω from $-\infty$ to $+\infty$.

In a similar way a D-decomposition can be obtained not in the space of coefficients but in the space of system parameters on which the coefficients of the characteristic equation depend, e.g. in the coordinates T_1, T_2, k, etc.

8.4. D-DECOMPOSITION BY ONE (COMPLEX) PARAMETER

Sometimes the effect of a certain parameter, v, on the system stability has to be ascertained. Assume, as in the plotting of a root locus, that this parameter is a linear term of the characteristic equation which can be given the form of Eq. (8.1)

$$A(p) = P(p) + vQ(p) = 0 \qquad (8.16)$$

According to Eq. (8.15) the boundaries of the D-decomposition are found by the equation

$$A(j\omega) = P(j\omega) + vQ(j\omega) = 0 \tag{8.17}$$

Thence

$$v = -\frac{P(j\omega)}{Q(j\omega)} = X + jY \tag{8.18}$$

$$-\infty < \omega < +\infty$$

When constructing the boundary of a D-decomposition it is sufficient to find and plot it for positive values of ω ($0 < \omega < +\infty$) only and then complete the construction by a mirror image of the plotted part relative to the real axis. In practice only the D-decomposition of the real axis of the complex v plane to which the real values of v correspond is of importance, rather than the decomposition of the whole plane.

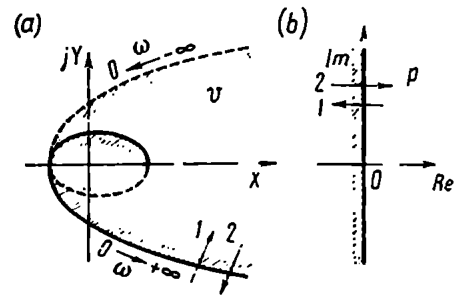

Fig. 8.6

Figure 8.6 shows the view of the D-decomposition boundary in the $v = x + jy$ plane. With ω varying from $-\infty$ to $+\infty$ in the p plane the imaginary axis goes vertically up with the left half-plane remaining on the left. Let us hatch the imaginary axis from the left (Fig. 8.6*b*). The movement along the imaginary axis is associated with a movement along the D-decomposition boundary in the v plane (Fig. 8.6*a*), which will also be hatched from the left as ω varies from $-\infty$ to $+\infty$.

If one crosses the boundary of the D-decomposition in the v plane in the direction of hatching (arrow *1*, Fig. 8.6*a*), then one root goes from the right to the left half-plane in the plane of roots. If one crosses in the opposite direction (arrow *2*, Fig. 8.6*a*), then in the plane of roots one root goes from the left to the right half-plane.

The direction and amount of hatching determine the number of roots crossing the imaginary axis and the direction of crossings. Therefore to obtain the D-decomposition it is sufficient to know the distribution of roots relative to the imaginary axis at any value of the parameter. Changing the value of the parameter v in the v plane in an arbitrary way, the number of boundary crossings and the direction of hatching can be used to find the value of m in any point. It should be remembered that the stability region is $D(0)$ and the runner-up is a region or segment to which the hatching is directed.

In linear problems the variable parameter is normally real (gain, time constant) and the region of D-decomposition adjoining the

x-axis is of practical interest. Consideration of the whole region of the complex parameter is of interest for nonlinear problems, where the result obtained can be used.

Example 8.3. Assume that the characteristic equation is

$$(1 + pT_1)(1 + pT_2)(1 + pT_3) + k = 0 \qquad (8.19)$$

where T_1, T_2, T_3 are specified time constants and k is the overall gain. The system thus consists of three inertial elements. Find the value of k at which the system is stable.

To solve the problem, we construct the boundary of the D-decomposition in the plane of the complex parameter k and concentrate on the decomposition of the real axis only, or on the real values of k.

From Eq. (8.19) it follows that the boundary of the D-decomposition is described by the equation

$$v = k = -(1 + j\omega T_1)(1 + j\omega T_2)(1 + j\omega T_3) = x + jy \qquad (8.20)$$

This boundary is shown in Fig. 8.7*a*. The runner-up is the region S to which the hatching of the boundary is directed. It can be shown that this region is not only the runner-up but the stability region itself. Indeed, the point (0, 0), i.e. $k = 0$, which is in the region S, belongs to the stability region D (0) also, because when $k = 0$ the characteristic equation (8.19) becomes

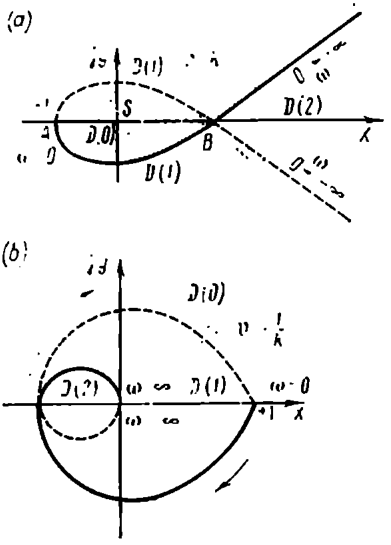

Fig. 8.7

$$(1 + pT_1)(1 + pT_2)(1 + pT_3) = 0$$

all the three roots at which $\left(p_1 = -\frac{1}{T_1};\ p_2 = -\frac{1}{T_2};\ p_3 = -\frac{1}{T_3}\right)$ are in the left half-plane. The system is thus stable if the real values of k vary within the limits set by the segment AB. The limit value of k is determined by the point B. The system is stable also at negative values of k if $k \geqslant -1$.*

In order to find k_{lim} (point B) the value of ω should be found at which

$$\bar{y}(\omega) = 0 \qquad (8.21)$$

* Negative values of k represent a positive feedback.

Let the root of this equation be different from zero ($\omega = \omega_0$). Then

$$k_{lim} = x(\omega_0) \tag{8.22}$$

Neglecting the calculation from (8.20), we have

$$\omega_0^2 = \frac{T_1+T_2+T_3}{T_1T_2T_3}$$

$$k_{llm} = x(\omega_0) = (1+\tau_2+\tau_3)\left(1+\frac{1}{\tau_2}+\frac{1}{\tau_3}\right)-1 \tag{8.23}$$

where $\tau_2 = \frac{T_2}{T_1}$; $\tau_3 = \frac{T_3}{T_1}$. This solution coincides with the results of Examples 7.2 and 7.3.

Figure 8.7*a* shows the regions $D(0)$, $D(1)$, $D(2)$. The region $D(3)$ is absent in this case; this means that at positive values of T_1, T_2 and at any value of k all the three roots of Eq. (8.19) cannot be in the right half-plane.

If the variable is $-\frac{1}{k}$ rather than k, then the boundary of the D-decomposition can be constructed by using the normalized frequency locus of an open-loop system. Indeed, by denoting

$$v = W_0 = -\frac{1}{k} = \frac{1}{(1+j\omega T_1)(1+j\omega T_2)(1+j\omega T_3)} = X+jY \tag{8.24}$$

the boundary will be obtained as a locus similar to Fig. 7.7 at $k = 1$. This locus is shown in Fig. 8.7*b*. By hatching on the left of the boundary and labelling the regions we can see that the system is stable only if the point $-\frac{1}{k}$ is outside the closed loop of Fig. 8.7*b*.

Chapter IX

CONTROL PERFORMANCE: DIRECT METHODS OF STUDY

9.1. PERFORMANCE INDICES

Stability is a necessary but far from sufficient condition for a a control system to be justified. A stable system responding to different actions may prove insufficiently accurate, the transient processes may damp out too slowly (response is too sluggish), the output variation may happen to be lacking in smoothness; in other words the automatic control may be deficient.

The set of requirements for system behaviour at steady state and in transient processes when responding to a given action is covered by the term *control performance* (*system performance*). These requirements arise from practical experience.

To analyze control processes means to ascertain the effect of the system structure and the values of its parameters on the control process and its performance indices and to find to what extent a particular system satisfies the requirements.

Selection of the control system structure and parameters to suit the performance requirements is a design synthesis problem.

Let us consider control processes in stable systems assuming that the most frequent or most unfavourable actions can be given in advance as certain (determined) functions of time. Determined actions pre-assigned with due regard for the specific features of the system are referred to as *standard.*

In most practical cases the system study is restricted to the standard cases discussed in Ch. II such as a single pulse, a single step signal or a harmonic signal.

For these elementary cases direct performance indices of transient processes have been developed.

Studies of program control systems sometimes require determination of the system response to an arbitrary signal which can be represented as a power series (2.3) or (2.4).

Let us consider the structural diagram of Fig. 9.1. A control system with a transfer function W_{cl-l} consisting of the plant W_p, the controller in the feedforward circuit W_{ff}, and the controller W_{fb} in the feedback circuit is acted on by the control signal x and the disturbance f.

The system performance when responding to standard signals x or f is estimated either directly via the controlled variable (the output y) or via the system error $\delta(t)$, which is the difference between

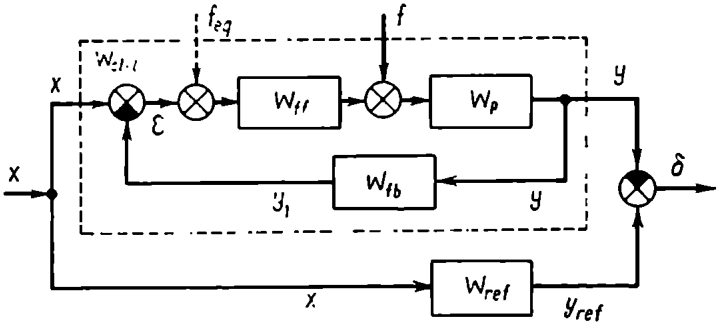

Fig. 9.1

the outputs of the system under test and of a certain reference linear system W_{ref}

$$\delta = y_{ref} - y \tag{9.1}$$

According to Fig. 9.1 the image of the error is

$$\Delta(p) = \left[W_{ref} - \frac{W_{ff}W_p}{1+W_{ff}W_pW_{fb}}\right] X - \frac{W_p}{1+W_{ff}W_pW_{fb}} F = W_\delta X - W_f F \tag{9.2}$$

where

$$W_\delta = W_{ref} - \frac{W_{ff}W_p}{1+W_{ff}W_pW_{fb}}, \qquad W_f = \frac{W_p}{1+W_{ff}W_pW_{fb}}$$

The reference transfer function should correspond to a specified linear dynamic transformation of the input signal $x(t)$ into the desired signal $y(t)$ of the closed-loop system. For a control system, in the ideal case, y should be equal to x, whence $W_{ref}(p) = 1$; for a copying system with scale change $y = kx$, whence $W_{ref} = k$; for an integrator $y = \frac{1}{T_0}\int_0^t x\,dt$ and therefore $W_{ref} = \frac{1}{T_0 p}$. If we are interested in the system response to a disturbance, then normally $W_{ref} = 0$, since it is required that $y = \varepsilon = 0$ for any variations of $x(t) = f(t)$.

Such extremely rigorous idealized requirements should not be always imposed on a system. An inertialess system with a transfer function $W_{cl\text{-}l}(p) = 1$ cannot be obtained physically since signals

of infinite power would generate there; furthermore, there is no nee for such a system because noises cannot be filtered there.

Reasonable selection of the reference, $W_{ref} = W_{opt}$, with du regard for the control problems at hand and the hardware capabilitie is treated in the theory of optimal systems the fundamentals o

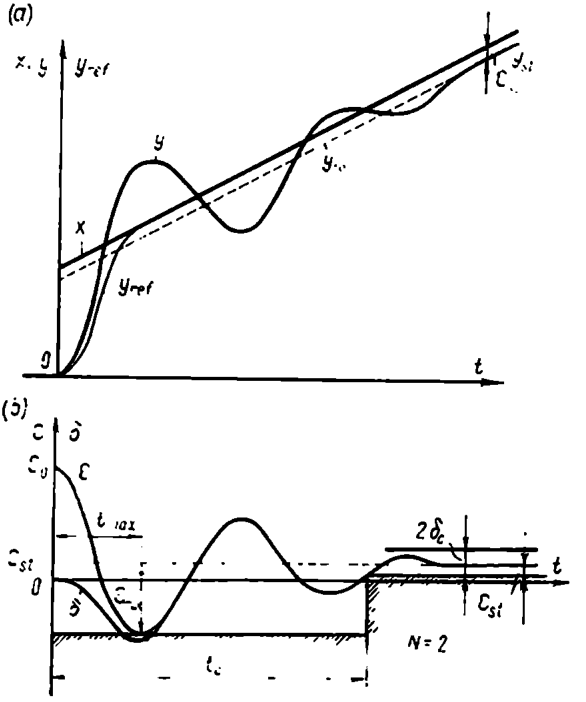

Fig. 9.2

which will be given in the second part of the book when we come to random actions.

The difference between the control signal x and the system output y_1 is the system misalignment

$$\varepsilon(t) = x(t) - y_1(t) \tag{9.3}$$

According to Fig. 9.1

$$E(p) = [1 - W_{cl-l}]X - W_f F =$$

$$= \left(1 - \frac{W_{ff}W_p}{1 + W_{ff}W_pW_{fb}}\right)X - \frac{W_p}{1 + W_{ff}W_pW_{fb}}F = W_e X - W_f F \tag{9.4}$$

Figure 9.2*a* illustrates the control system response to a control action $x(t)$. The graphs for the system error $\delta(t)$ and the misalign-

ment $\varepsilon(t)$ for $W_{fb} = 1$, and hence $y = y_1$, are given in Fig. 9.2*b*. The function y_{ref} is represented by a smooth curve.

Consider the direct performance indices of this process as applied to the system misalignment. Distinction is made between the following indices:

(1) Steady-state misalignment which determines the system accuracy

$$\varepsilon_{st}(t) = \lim_{t \to \infty} \varepsilon(t) \tag{9.5}$$

In the particular case in question $\varepsilon_{st} = \text{const}$.

(2) Control time t_c, which is the main index of the system speed and is found from the condition of smallness of the transient component

$$|\varepsilon(t) - \varepsilon_{st}| \leqslant \delta_c \quad \text{at } t \geqslant t_c \tag{9.6}$$

where δ_c is a specified value depending on the system accuracy.

(3) Maximal overshoot ε_{max}, which, in combination with indices (4) and (5), characterizes the smoothness of transient processes (system damping). It is defined as the greatest overshoot of the control process $y(t)$ relative to the steady-state process $y_{st}(t)$ (Fig. 9.2*b*). A relative (dimensionless) overshoot characteristic is often introduced

$$\sigma = \frac{\varepsilon_{max}}{y_0} 100\%$$

where y_0 is some reference value.

(4) The time of maximal overshoot t_{max} at which

$$\varepsilon(t_{max}) = \varepsilon_{max} \tag{9.7}$$

(5) The number of overshoots N in the interval $0 < t \leqslant t_c$ defined as the number of overshoots for which

$$\varepsilon_{st} - \varepsilon_{max} > \delta_c > 0 \tag{9.8}$$

Figure 9.2*b* shows that the first three indices determine the zone limiting the system misalignment in the process of control. The boundary of this zone is shown by hatching.

Similar indices may define the system performance in terms of the output $y(t)$ or the error $\delta(t)$.

If, in studying a control system, one adopts $W_{ref} = 1$ and $W_{fb} = 1$, then

$$\varepsilon(t) = \delta(t) \tag{9.9}$$

or the system error is equal to its misalignment and the structural diagram of Fig. 9.1 can be represented as in Fig. 9.3. This is the reason why the system error is often identified with the misalignment. In Fig. 9.3 $W_{o\text{-}l}(p) = W_{ff}(p) W_0(p)$ is the transfer function of the open-loop system ($W_{fb}(p) = 1$) and f_{eq} is an equivalent disturbance reduced to the input of the feedforward circuit. From

Fig. 9.1 and the rules for the transformation of structural diagrams given in Ch. VI it follows that

$$F_{eq}(p) = W_{eq}(p) F(p) = \frac{1}{W_{ff}(p)} F(p) \qquad (9.10)$$

and

$$W_{eq}(p) = \frac{1}{W_{ff}(p)}$$

In order to estimate the control process by direct performance indices the process should be represented mathematically or recorded experimentally.

Methods of direct calculation of a process under study are known as direct methods of performance analysis. As shown in Ch. VI, control processes in a closed-loop system with specified action are described

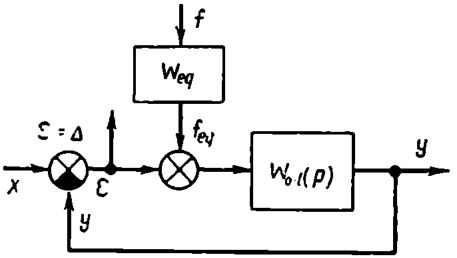

Fig. 9.3

by nonhomogeneous linear differential equations with constant coefficients; therefore, direct methods coincide with methods of solving equations of this type.

The *classical method* involves cumbersome operations of solving the characteristic equation of a closed-loop system, the calculation of arbitrary constants corresponding to specified initial conditions, and the variation of arbitrary constants.

The *operator method* considerably simplifies the solution by reducing it to finding the original of the right-hand part of the operator equation (9.4). Detailed tables of transformations facilitate the calculations to a considerable degree but the most unwieldy operation, the solution of the characteristic equation of the closed-loop system $A(p) = 0$, still has to be coped with.

The control process in a linear system known to be stable can be calculated by the *frequency method* based on the inverse Fourier transformation. For this purpose use is made of the same calculated or experimental frequency responses that serve for stability studies. The characteristic equation need not be solved. The practical graph-analytic methods of calculation make this approach as easy as can be (Sec. 9.5).

Analog simulators completely mechanize the calculation of control processes. A control system can be modelled directly from its structural diagram (Sec. 5.7).

The above-listed direct methods permit one only to determine the control process with a specified action and specified parameters. Here, the relation between the system parameters and the control process performance can be established only for elementary systems described by a second-order differential equation. Consequently, the main problem in studing the transient process performance cannot be solved completely by direct methods and requires indirect analysis methods developed in the control theory with this specific purpose. These methods are discussed in Ch. X.

Following a time interval sufficient for the transient processes ($t > t_c$) to damp out, a control system operates at steady state and its behaviour depends on the forced component in the solution of the differential equation.

The dynamic accuracy of a system is measured by the steady-state error of the response to the external action, i.e. by the forced component $\delta_{fo}(t)$ of the system error. Different estimates of the error are possible, of which the most widespread are:
the maximal error

$$\delta_{max} = |\delta_{fo}(t)|_{max} \tag{9.11}$$

and the root mean square (r.m.s.) error

$$\delta_{r.m.s.} = \lim_{T \to \infty} \sqrt{\frac{1}{T} \int_0^T [\delta_{fo}(t)]^2 \, dt} = \sqrt{\overline{\delta^2}} \tag{9.12}$$

Forced operation can be analyzed by using direct methods of performance analysis.

9.2. CONTROL PERFORMANCE WITH STANDARD ACTIONS

Transient function and static error. The wide use of the transient function as a measure of system performance is chiefly attributed to the simplicity and illustrativeness of obtaining this characteristic both on a system model and in actual conditions. In the latter case, however, the magnitude of the action must be small enough lest the responding system leave the boundaries of the region where linearized equations correspond, with the desired accuracy, to the mathematical description of the physical (nonlinear) system. At a low level of useful action various noises may completely distort the experimental results. In this case a system model is tested, the transient function is determined indirectly via frequency responses, or $h(t)$ is found by statistical processing of many experimental results.

The various transient functions of control systems can be divided into three types: oscillatory with overshoot, oscillatory without overshoot, and monotonic.

Let us consider the application of performance indices to estimation of the system transient function.

Example 9.1. Estimate the performance of a response to a unit step control action in a servo system the structural diagram of which is given in Fig. 9.4.

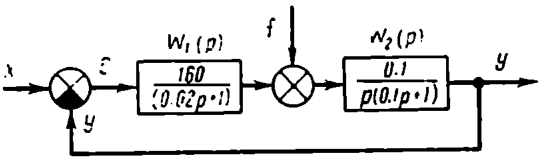

Fig. 9.4

The system response to the control action $X(p)$ is given as

$$Y(p) = H_x(p) = \frac{K(p)}{A(p)} X(p) = \frac{k}{p(1+pT_1)(1+pT_2)+k} X(p)$$

where

$$K(p) = k = 16, \quad T_1 = 0.1 \text{ sec}, \quad T_2 = 0.02 \text{ sec}$$

and

$$X(p) = \frac{1}{p}$$

The roots of the characteristic equation $A(p) = 0 = p^3 + 60p^2 + 500p + 8.000$ are calculated by the Cardan formula

$$p_1 = -53.4, \quad p_2 = -3.29 + j11.8, \quad p_3 = -3.29 - j11.8$$

and therefore

$$H_x(p) = \frac{8,000}{p(p+53.4)(p+3.29-j11.8)(p+3.29+j11.8)}$$

Expanding $H_x(p)$ into common fractions and using inverse Laplace transformation, we obtain

$$h_x(t) = 1 - 0.0545e^{-53.4t} + 1.08e^{-3.29t} \sin(11.8t + 1.064)$$

Estimating the transient function for $\delta_c = 0.05$ as shown in Fig. 9.5, we find that

$$h_{st} = 1, \quad t_c = 0.85 \text{ sec}, \quad \Delta h_{max} = 0.39, \quad t_{max} = 0.26 \text{ sec}, \quad N = 2$$

The accuracy of a control system responding to a step signal, $A_0 1_0(t)$, is estimated from the static error of the system, Δ_{stat}.

Static error to control action. By Eq. (9.2) the error in response to a control action is

$$\delta_x(t) = L^{-1}\left\{W_\delta(p)\frac{A_0}{p}\right\}$$

and by the limit value theorem the static error is

$$\Delta_{x_{stat}} = \lim_{t\to\infty}\delta_x(t) = \lim_{p\to 0}\left[pW_\delta(p)\frac{A_0}{p}\right] = W_\delta(0)\,A_0 \qquad (9.13)$$

Evidently, $\Delta_{x_{stat}} = 0$ provided that in Eq. (9.13)

$$W_\delta(0) = \lim_{p\to 0}[W_{ref}(p) - W_{cl\text{-}l}(p)] = 0 \qquad (9.14)$$

Systems with this property are termed *astatic with respect to the control action.*

If $W_\delta(0) \neq 0$ the system is termed *static.* By virtue of Eq. (9.13) the difference between the steady-state output of this system with

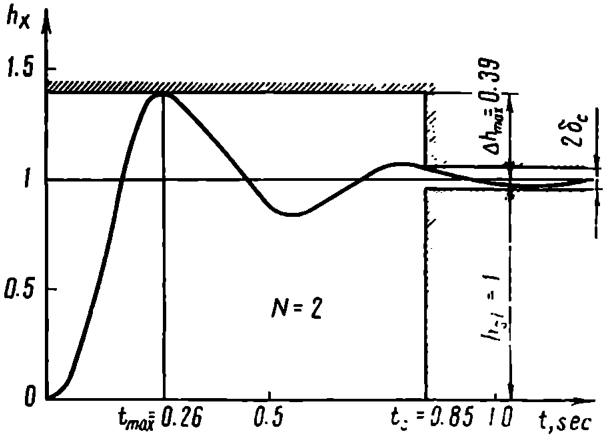

Fig. 9.5

constant control action and the required (reference) value increases with the input signal level.

In control systems for which the condition (9.9) is valid

$$\Delta_{x_{stat}} = \varepsilon_{stat} = [1 - W_{cl\text{-}l}(0)]\,A_0 = \frac{1}{1+k}A_0 \qquad (9.15)$$

where k is the gain of an open-loop system.

Static error disturbance. In estimating the accuracy relative to a disturbance, one can obtain from Eqs. (9.2) and (9.10)

$$\delta_f(t) = L^{-1}\left\{W_{cl\text{-}l}(p)\frac{1}{W_{ff}(p)}\frac{A_0}{p}\right\} \qquad (9.16)$$

where $W_{ff}(p) = \dfrac{K_{ff}(p)}{D_{ff}(p)}$ is the transfer function between the control input and the input of the disturbance under study.

The static error is

$$\Delta_{f_{stat}} = \lim_{t\to\infty} \delta_f(t) = \lim_{p\to 0} \left[pW_{cl\text{-}l}(p) \frac{1}{W_{ff}(p)} \frac{A_0}{p} \right] = \frac{W_{cl\text{-}l}(0)}{W_{ff}(0)} A_0 \quad (9.17)$$

For a system astatic with respect to disturbance

$$\frac{W_{cl\text{-}l}(0)}{W_{ff}(0)} = \lim_{p\to 0} \frac{W_{cl\text{-}l}(p)}{W_{ff}(p)} = 0 \quad (9.18)$$

For a system to respond to a constant control signal it is necessary that $W_{cl\text{-}l}(0) \neq 0$, and hence the condition (9.18) is equivalent to the requirement

$$\lim_{p\to 0} \frac{1}{W_{ff}(p)} = 0 \quad (9.18a)$$

If the condition (9.18) is not met, the system is referred to as *static relative to a disturbance*, and the static error is calculated by the formula

$$\Delta_{f_{stat}} = W_{cl\text{-}l}(0) \frac{1}{k_{ff}} A_0 \quad (9.19)$$

where $k_{ff} = W_{ff}(0)$.

As evidenced by the structural diagram of Fig. 9.1 the portion W_{ff} is a feedback loop relative to the disturbance in question (from the system output to the disturbance input), therefore it follows from Eq. (9.19) that the accuracy of a static system increases with the gain of the feedback loop (of the proportional controller). However the increase of the gain in a static system with a view to improving the accuracy of response to the input and to disturbances is limited by the transient performance requirements, and in the limit case, by the stability condition

$$k = k_p k_{ff} < k_{lim} \quad (9.20)$$

Consequently, control systems need compensation, or modification of the structure and parameters to enable obtaining both a high accuracy and the required performance of transient processes.

We will illustrate the calculation of static accuracy with examples of control systems the equations of which were discussed in Ch. VI.

Example 9.2. Float-type level controller. By the structural diagram of Fig. 6.1 and the Eq. (6.1*a*)

$$\Delta_{f_{stat}} = -y_\infty = -\lim_{p\to 0} pY(p) = -\frac{1}{k_2} \Delta G$$

The slope of the system static response $y(G)$ is given by the relation

$$\frac{\Delta_{f_{stat}}}{\Delta G} = -\frac{1}{k_2}$$

the magnitude of which characterizes the steady-state static error of the loaded system. The error is inversely proportional to the feedback loop gain.

Example 9.3. A servo system. By the structural diagram of Fig. 6.5 and Eq. (6.37) with the disturbance (load) $f = f_0 1_0(t)$ acting in node *1*

$$Y(p) = W_d F(p)$$

and for W_d expressed by Eq. (6.39)

$$\Delta_{f_{stat}} = \frac{f_0}{k_{cl\text{-}l}}$$

Consequently, the servo system in question is static with respect to the load torque on the shaft which causes a disturbance in node *1*.

The servo system is astatic with respect to the control action $x = u_0$ acting in node *2*. Indeed, in this case the misalignment ε_1 with the setpoint $x = x_0 1_0(t)$ varying stepwise

$$E_1(p) = W_\varepsilon(p) X(p) = (1 - W_c) X(p)$$

From Eq. (6.38) $W_\varepsilon(0) = 0$ in this case, and the astatic condition (9.14) is satisfied. The steady-state misalignment is zero, which implies accurate response to the constant control signal.

Pulse transient function. The performance of systems subjected to impulse action and of systems whose output is to reproduce the integral of the input signal can be conveniently estimated by the system response to a pulse. Control systems operating in this way are widespread (see Chs. XII to XIV); besides, a pulse action can often be conveniently used in experimental determination of the performance of actual systems and their models.

In determining the performance by the pulse transient function $w(t)$ the same estimates can be used as in case of the system misalignment.

Note that for stable closed-loop systems of Sec. 2.4 the static deviation of the weighting function is

$$w_{st} = \lim_{t \to \infty} w(t) = 0 \tag{9.21}$$

If this condition is not satisfied, we have an integrating (neutral) system for which

$$A(p) = pA_1(p) \tag{9.22}$$

and Eq. (2.32) can be given in the form

$$w(t) = \frac{B(0)}{A_1(0)} + \sum_{i=1}^{n-1} \frac{B(p_i)}{p_i A_1'(p_i)} e^{p_i t} \qquad (9.23)$$

whence the weighting function of a neutral system (integrator) characterizes its performance in the same way as the transient function describes the performance of a stable system.

Example 9.4. Determine the response to a unit control pulse (weighting function) for the servo system of Example 9.1 and for

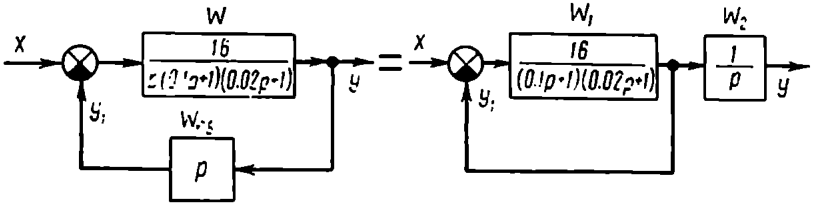

Fig. 9.6

a constant rate drive (electromechanical integrator) the structural diagram of which is given in Fig. 9.6.

Since the transient function of a servo system with respect to the control input has been determined in Example 9.1, let us now find the weighting function as a derivative of the transient function

$$w_x(t) = \frac{dh_x}{dt} = 2.9e^{-53.4t} + 13.2e^{-3.29t} \sin(11.8t - 0.23)$$

The plot of $w_x(t)$ given in Fig. 9.7*a* demonstrates that

$$t_c = 0.98 \text{ sec} \quad (\text{at } \delta_c = 0.5), \quad \Delta w_{max} = w_{max} = 8,$$
$$t_{max} = 0.13, \quad N = 2$$

Evidently, $w_x(\infty) = 0$.

For an electromechanical integrator, as follows from the structural diagram of Fig. 9.6,

$$W_{cl\text{-}I}(p) = \frac{16}{p[(0.1p+1)(0.02p+1)+16]} = \frac{8{,}000}{p(p^2+60p+8{,}500)}$$

The roots of the characteristic equation

$$p_1 = -30 + j87.2, \qquad p_2 = -30 - j87.2$$

whence

$$W_{cl\text{-}I}(p) = \frac{8{,}000}{p[(p+30)^2+(87.2)^2]}$$

and by inverse Laplace transformation

$$w_{cl\text{-}I}(t) = 0.941 + 0.993e^{-30t} \sin(87.2t - 1.24)$$

According to the $w(t)$ plot given in Fig. 9.7*b*

$$t_c = 0.105 \text{ sec}, \quad \Delta w = 0.38, \quad t_{max} = 0.029 \text{ sec}, \quad N = 2$$

In this neutral system $w_{st} = \frac{16}{17} = 0.941$.

Kinetic error. The accuracy of astatic systems is found via the steady-state error in response to a constant rate signal, i.e. to the

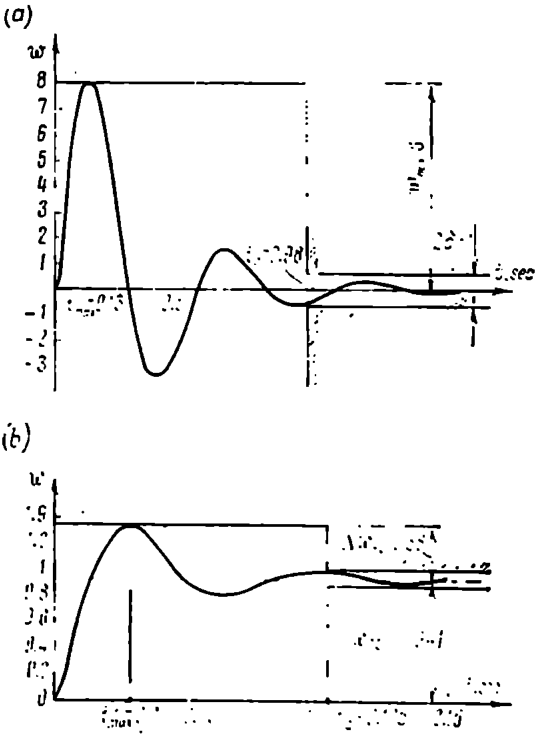

Fig. 9.7

action

$$x(t) = A_1 t 1_0(t)$$

whence

$$X(p) = \frac{1}{p^2} A_1 \tag{9.24}$$

The steady-state error in these conditions is referred to as the kinetic error Δ_{kin}.

The kinetic error relative to a control action, $\Delta_{x\,kin}$, is the basic accuracy characteristic of many automatic systems, in particular, of a servo drive.

From Eqs. (9.2) and (9.24)

$$\delta(t) = L^{-1}\left\{W_\delta(p)\frac{A_1}{p^2}\right\} \tag{9.25}$$

By the final value theorem the kinetic error is

$$\Delta_{x\,kin} = \lim_{t\to\infty}\delta(t) = \lim_{p\to\infty}\left[pW_\delta(p)\frac{A_1}{p^2}\right] = \lim_{p\to 0}\frac{W_\delta(p)}{p}A_1$$

Since the system in question is astatic, then, as $p \to 0$, $W_\delta(p) \to 0$ at least to the same extent as p does. Evaluating the indeterminate form by the L'Hopital rule, we have

$$\Delta_{x\,kin} = W'_\delta(0)\,A_1 \tag{9.26}$$

where

$$W'_\delta(0) = \frac{d}{dp}W_\delta(p)\Big|_{p=0}$$

Let us consider an astatic control system at $W_{ref} = 1$ and $W_c(p) = \frac{K(p)}{D(p)}$, where

$$K(p) = k_m p^m + k_{m-1}p^{m-1} + \ldots + k_1 p + k_0$$

and

$$D(p) = d_n p^n + d_{n-1}p^{n-1} + \ldots + d_1 p + d_0$$

are polynomials in p, while $m \leqslant n$.

The transfer function

$$W_\delta(p) = W_e(p) = 1 - W_{cl}(p) = \frac{D(p)}{K(p)+D(p)}$$

satisfies the condition (9.14) if at least $d_0 = 0$, whence

$$D(p) = pD_1(p), \quad D_1(0) \neq 0$$

It is evident that

$$W'_e(0) = \frac{D_1(0)}{K(0)} = \frac{d_1}{k_0} = \frac{1}{k_{as}}$$

where $k_{as} = \frac{k}{T_{ff}}\,\text{sec}^{-1}$ is the *gain of an open-loop astatic system*, or *its figure of merit*. Then from Eq. (9.26)

$$\Delta_{kin} = \frac{1}{k_{as}}A_1 \tag{9.27}$$

In other words, the kinetic error of an astatic control system is directly proportional to the constant rate of the action and inversely proportional to the figure of merit of the system. With present-day requirements for the accuracy of a servo drive the figure of merit

amounts to several thousand. Consequently, such systems cannot be implemented without compensating facilities.

The kinetic error relative to disturbance is found in the same way with $W_\delta(p)$ replaced by $W_{cl\text{-}l}(p)\frac{1}{W_{lf}(p)}$.

Dynamic error. *The steady-state system error when responding to an arbitrary standard action is known as the system dynamic error.* In most cases this involves a monoharmonic (sine) action

$$x(t) = A_1 \sin \omega_1 t 1_0(t)$$

As shown in Ch. II, the steady-state (forced oscillation) output of a dynamic linear system with constant parameters can be fully characterized by the complex quantity

$$Y(j\omega_1) = W(j\omega_1) A_1$$

where $W(j\omega_1)$ is complex gain at the frequency ω_1.

From Eq. (9.2) the dynamic error relative to the control action is

$$\Delta_{x\,dyn}(j\omega_1) = W_\delta(j\omega_1) A_1 = \Delta_{x\,dyn}(\omega_1) e^{j\varphi_\delta(\omega_1)} \qquad (9.28)$$

where the magnitude

$$\Delta_{x\,dyn}(\omega_1) = |\Delta_{x\,dyn}(j\omega)| = |W_\delta(j\omega_1)| A_1 = \Delta_{xm}(\omega_1) \qquad (9.29)$$

is equal to the amplitude value of the system dynamic error or to the amplitude error, and the argument

$$\varphi_\delta(j\omega_1) = \arg \Delta(j\omega_1) = \arg W_\delta(j\omega_1) \qquad (9.30)$$

is equal to the phase shift between the dynamic error and oscillations at the system input.

Using a time function, we have

$$\delta_{x\,dyn}(t) = \Delta_{xm}(\omega_1) \sin [\omega_1 t + \varphi_\delta(\omega_1)] \qquad (9.31)$$

The dynamic error relative to disturbance f is found in a similar way with $W_\delta(j\omega_1)$ replaced by $\frac{W_{cl\text{-}l}(j\omega_f)}{W_{lf}(j\omega_f)}$, whence

$$E_{f\,dyn}(j\omega_f) = \frac{W_{cl\text{-}l}(j\omega_f)}{W_{lf}(j\omega_f)} A_f \qquad (9.32)$$

where A_f is the amplitude of the sine disturbance f

$$\Delta_{f\,dyn}(\omega_f) = \left| \frac{W_{cl\text{-}l}(j\omega_f)}{W_{lf}(j\omega_f)} \right| A_f = \Delta_{fm}(\omega_f) \qquad (9.33)$$

$$\varphi_\delta(\omega_f) = \arg W_{cl\text{-}l}(j\omega_f) = \arg W_{lf}(j\omega_f) \qquad (9.34)$$

and

$$\delta_{f\,dyn}(t) = \Delta_{fm}(\omega_f) \sin [\omega_f t + \varphi_\delta(\omega_f)] \qquad (9.35)$$

Since the oscillations under consideration are sinusoidal, the r.m.s. error or its effective value is

$$\Delta_{r.m.s.} = \Delta = \frac{\sqrt{2}}{2}\Delta_m \tag{9.36}$$

Let us estimate the dynamic accuracy of an automatic control system for which $W_\delta(j\omega) = W_\varepsilon(j\omega)$. The structural diagram of the system is given in Fig. 9.8.

Analytical calculation of the magnitude and phase of $W_\varepsilon(j\omega)$ for a specified frequency is rather cumbersome and is not always

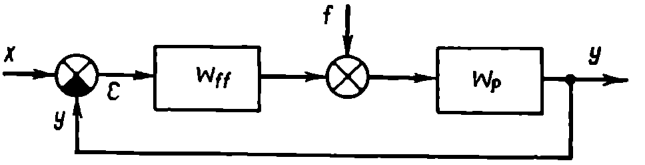

Fig. 9.8

possible because frequency responses of the plant W_p are often given as experimental curves.

Rigorous graphical and analytical solution to the problem is obtained by using a special nomogram (see Fig. 10.8) enabling one to construct a $W_x(j\omega)$ plot of magnitude and phase from the plot (logarithmic locus) of $W_{o\text{-}l}(j\omega)$.

In the operational frequency range

$$|W_{o\text{-}l}(j\omega)| \gg 1 \qquad \text{at} \quad 0 < \omega < \omega_b \tag{9.37}$$

where ω_b is the uniform passband boundary frequency of a closed-loop system found from the conditions of admissible amplitude distortions (Fig. 9.9) as the least positive root of the equation

$$\frac{|1 - W_{cl\text{-}l}(\omega)|}{W_{cl\text{-}l}(0)} = \delta_c \tag{9.38}$$

where δ_c is given in advance. Normally $\delta_c = 0.05$ to 0.1.

Inequality (9.37) leads to a simple approximate estimate of the dynamic accuracy of a closed-loop system based on the knowledge of the open-loop frequency response. Indeed, in this case

$$|W_\delta(j\omega)| = \frac{1}{|1 + W_{o\text{-}l}(j\varphi)|} \approx \frac{1}{|W_{o\text{-}l}(j\omega)|} \tag{9.39}$$

Substituting into (9.29) we have

$$\Delta_{xm} \approx \frac{A_1}{|W_{o\text{-}l}(\omega_1)|} \tag{9.40}$$

where $W_{o\text{-}l}(\omega_1)$ is the magnitude of the open-loop system gain when the frequency of control is ω_1. Using the logarithmic response, we have

$$20 \log \Delta_{xm} \approx 20 \log A_1 - L(\omega_1) \tag{9.41}$$

The dynamic error relative to disturbance (load) f is found in a similar way; then in the operational frequency range $0 < \omega_f < \omega_b$

$$\Delta_{fm} \approx \frac{A_f}{|W_{o\text{-}l}(\omega_f)|} \tag{9.42}$$

From Eqs. (9.40) and (9.42) the dynamic accuracy of a control system responding to an action the frequency of which is in the ope-

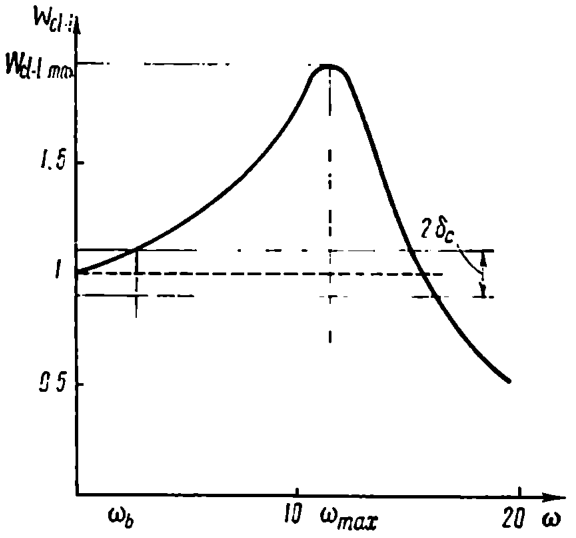

Fig. 9.9

rational frequency range of the system increases with the complex gain of the system feedback at the frequency of that action.

Example 9.5. Determine the dynamic accuracy of the servo system (Example 9.1) with a harmonic action x (control input).

The transfer function of a closed-loop system where the output is the system's misalignment is

$$W_\varepsilon(p) = \frac{p(T_1p+1)(T_2p+1)}{p(T_1p+1)(T_2p+1)+k}$$

The dynamic error relative to x is

$$\Delta_{xm} = |W_x(j\omega_1)| A_1 = \left| \frac{j\omega_1(j\omega_1T_1+1)(j\omega_1T_2+1)}{j\omega_1(j\omega_1T_1+1)(j\omega_1T_2+1)+k} \right| A_1$$

The accurate relation of $\frac{\Delta_{xm}}{A_1}$ versus ω_1 at $T_1 = 0.1$ sec, $T_2 = 0.02$ sec, and $k = 20$ is plotted in Fig. 9.10*a* (curve *1*). Δ_{xm} is approximately estimated by Eq. (9.40)

$$\Delta_{xm} \approx \frac{A_1}{|\Phi_{o\text{-}l}(j\omega)|} = \frac{A_1}{\frac{k}{\omega_1 \sqrt{[(T_1\omega_1)^2+1][(T_2\omega_1)^2+1]}}}$$

whereby curve *2* is plotted for the given parameters.

Finally, rough estimation by the asymptotic characteristic gives

$$\Delta_{xm}(\omega_1) = \frac{A_1\omega_1}{k}, \qquad 0 < \omega_1 < \frac{1}{T_1}$$

$$\Delta_{xm}(\omega_1) = \frac{A_1\omega_1^2 T_1}{k}, \qquad \frac{1}{T_1} < \omega_1 < \frac{1}{T_2}$$

$$\Delta_{xm}(\omega_1) = \frac{A_1\omega_1^2 T_1 T_2}{k}, \qquad \frac{1}{T_2} < \omega_1$$

These approximate relations yield curve *3*. The results coincide with an accuracy $\Delta = 0.1$ at

$$0 < \omega_1 < \omega_b = 2.8\,\frac{1}{\text{sec}}$$

(Fig. 9.10*b*).

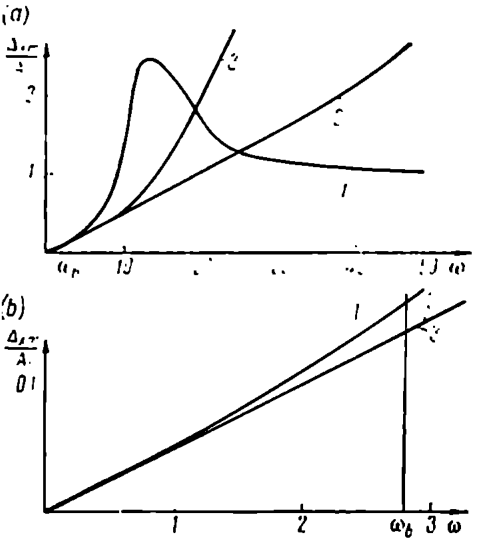

Fig. 9.10

9.3. FORCED COMPONENT OF THE ERROR

In case of more complicated actions it may be important to find the forced component of the error, which characterizes the system behaviour when the transient component expressing the free process (2.77) decays.

If the image of the external action is expressed by a fractional rational function of p having no multiple roots, then the forced component can be found by Eq. (2.78). In the case of multiple roots this expression complicates somewhat and involves unwieldy calculations as does Eq. (2.78).

The calculations can be considerably simplified if the external action is expressed as the power series (2.3). Below we describe the method for computing the forced component of the error in this case, which is termed the *method of error coefficient.*

If the action $x(t)$ is approximated by the polynomial

$$x(t)=\left[A_0+A_1t+\ldots+\frac{A_l}{l!}t^l\right]1_0(t) \tag{9.43}$$

then its image is

$$X(p)=A_0\frac{1}{p}+A_1\frac{1}{p^2}+\ldots+A_l\frac{1}{p^{l+1}}=\frac{N(p)}{p^{l+1}} \tag{9.44}$$

where

$$N(p)=\sum_{k=0}^{l}A_kp^{l-k}$$

contains just one multiple root $p=0$.

The image of the error is

$$\Delta(p)=W(p)\sum_{0}^{l}A_k\frac{1}{p^{k+1}}=W(p)\frac{N(p)}{p^{l+1}} \tag{9.45}$$

where $W(p)$ is the transfer function relating the error to the given action.

If the influence of the setpoint is studied, then $W(p)=W_\delta(p)$, and if the effect of the disturbance is investigated, then $W(p)=\frac{W_{cl-l}(p)}{W_{ff}(p)}$.

The image of the forced component of a stable system error is obtained by decomposing Eq. (9.45) into common fractions corresponding to the zero $(l+1)$-tuple pole. In decomposing we will use the method of indefinite coefficients

$$\frac{W(p)}{p^{l+1}}=\frac{C_0}{p^{l+1}}+\frac{C_1}{p^l}+\ldots+\frac{C_l}{p}+S(p) \tag{9.46}$$

where $C_0, C_1, \ldots, C_l$ are indefinite coefficients of decomposition, and $S(p)$ is a component given by the poles of $W(p)$. It is presumed that $W(p)$ has no poles in the point $p=0$ and that $W(0)\neq\infty$.

To determine the coefficients C, we will represent Eq. (9.46) in the form

$$W(p)=C_0+C_1p+\ldots+C_lp^l+S(p)\,p^{l+1} \tag{9.47}$$

Differentiating successively with respect to p and substituting $p=0$, we find

$$C_0=W(0),\quad C_1=\left[\frac{dW}{dp}\right]_{p=0},\quad C_2=\frac{1}{2}\left[\frac{d^2W}{dp^2}\right]_{p=0},\ \ldots,$$
$$C_k=\frac{1}{k!}\left[\frac{d^kW}{dp^k}\right]_{p=0},\ \ldots,\quad C_l=\frac{1}{l!}\left[\frac{d^lW}{dp^l}\right]_{p=0} \tag{9.48}$$

Consequently, the image of the error $\Delta(p)$ can be given as any one of two components, viz. a transient (or free) one

$$\Delta_t(p) = S(p)\,N(p) \tag{9.49}$$

which decays as $t \to \infty$, and a forced one

$$\Delta_{fo}(p) = [C_0 + C_1 p + C_2 p^2 + \ldots + C_l p^l]\,X(p) \tag{9.50}$$

where

$$C_k = \frac{1}{k!}\frac{d^k W(p)}{dp^k}\Big|_{p=0} \qquad (k = 0, 1, 2, \ldots)$$

Each addend $C_k p^k X(p)$ at $t > 0$ is associated with a term of the error's forced component

$$C_k \frac{d^k x(t)}{dt^k} = C_k x^{(k)}(t)$$

Therefore the forced component can be given as a sum

$$\delta_{fo}(t) = C_0 x(t) + C_1 \frac{dx(t)}{dt} + \ldots + C_l \frac{d^l x(t)}{dt^l}$$

or

$$\delta_{fo}(t) = \sum_{k=0}^{l} C_k x^{(k)}(t) \tag{9.51}$$

Equation (9.51) is the basic formula of the error coefficients method. It is difficult to determine the coefficients C_k by Eqs. (9.48). They are easier to obtain by expanding the transient function $W(p)$ into a power series of p:

$$W(p) = \frac{b_0 + b_1 p + \ldots + b_m p^m}{a_0 + a_1 p + \ldots + a_n p^n} = C_0 + C_1 p + C_2 p^2 + \ldots = \sum_0^\infty C_k p^k \tag{9.52}$$

In order to determine the coefficients C_k, the right- and left-hand parts of the above equality should be multiplied by the denominator of the left-hand part and, equating the coefficients of equal powers of p, we have

$$\left.\begin{aligned}
b_0 &= C_0 a_0 \\
b_1 &= C_1 a_0 + C_0 a_1 \\
b_2 &= C_2 a_0 + C_1 a_1 + C_0 a_2 \\
&\ldots\ldots\ldots\ldots\ldots \\
b_m &= C_m a_0 + C_{m-1} a_1 + \ldots + C_0 a_m \\
0 &= C_{m+1} a_0 + C_m a_1 + \ldots + C_0 a_{m+1} \\
&\ldots\ldots\ldots\ldots\ldots
\end{aligned}\right\} \tag{9.53}$$

whence follows the recurrence formula

$$C_k = \frac{1}{a_0}\left\{b_k - \sum_{r=1}^{k} C_{k-r}a_r\right\} \tag{9.54}$$

where $b_k \equiv 0$ if $k > m$; $a_r \equiv 0$ if $r > n$.

Example 9.6. Determine the forced error of a servo system the

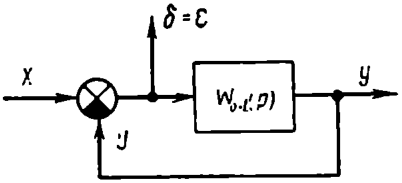

Fig. 9.11

transfer function of which in the open-loop state is

$$W_{o\text{-}t}(p) = \frac{k_{as}}{p(1+T_1p)(1+T_2p)}$$

where

$$k_{as} = 100\,\frac{1}{\text{sec}}, \quad T_1 = 0.1 \text{ sec}, \quad T_2 = 0.01 \text{ sec}$$

when the control action is

$$x_1(t) = 20 + 2t - 0.5t^2 \text{ rad}$$

By the structural diagram of Fig. 9.11 and Eq. (9.9) we find

$$\Delta(p) = E(p) = W_\varepsilon(p)\,X$$

where

$$W_\varepsilon(p) = \frac{p(1+T_1p)(1+T_2p)}{p(1+T_1p)(1+T_2p)+k_{as}} = \frac{T_1T_2p^3+(T_1+T_2)p^2+p}{T_1T_2p^3+(T_1+T_2)p^2+p+k_{as}}$$

To obtain a solution it would be sufficient to find the first three error coefficients which are given by Eq. (9.54)

$$C_0 = \frac{b_0}{a_0} = 0, \quad C_1 = \frac{b_1 - C_0a_1}{a_0} = \frac{1}{k_{as}} = 0.01 \text{ sec},$$

$$C_2 = \frac{b_2 - C_1a_1 + C_0a_2}{a_0} = \frac{1}{k_{as}}\left(T_1 + T_2 - \frac{1}{k_{as}}\right) = 0.001 \text{ sec}^2$$

The derivatives of the control action are

$$x_1'(t) = 2 - t\,\frac{\text{rad}}{\text{sec}}$$

$$x_1''(t) = -1\,\frac{\text{rad}}{\text{sec}^2}$$

The forced error, the control action is

$$\varepsilon_{fo}(t) = \delta_{fo}(t) = C_0 x_1(t) + C_1 x_1'(t) + C_2 x_1''(t) = \\ = 0.01(2 - t) - 0.001 = 0.019 - 0.01t \text{ rad}$$

The forced component of the system output is

$$y_{fo}(t) = x_1 - \varepsilon_{fo} = 19.981 + 2.01t - 0.5t^2 \text{ rad}$$

From the above example it follows that

(a) the servo system forced error, the control action is independent of the signal constant component ($A_0 = 20$ rad) since $C_0 = 0$;

(b) the signal component proportional to time ($A_1 t = 2t$ rad—uniform setting) leads to a constant forced error, which is inversely proportional to the servo system figure of merit since $C_1 = \frac{1}{k_{as}}$;

(c) the signal component proportional to squared time $\left(\frac{A_0}{2} t^2 = 0.5t^2 \text{ rad}\right.$—acceleration setting$\left.\right)$ causes an error of infinitely increasing magnitude. The servo system in question does not manage to respond properly to the increasing control signal.

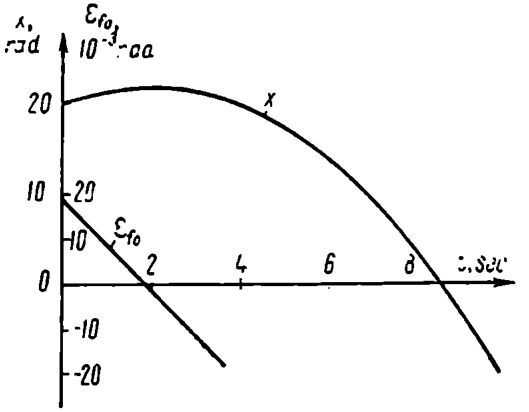

Fig. 9.12

The plots of the control action x and forced error ε_{fo} are given in Fig. 9.12. A full picture of the error in response to the action $x(t)$ can only be obtained if an allowance for the transient (free) component is made.

9.4. ASTATIC ORDER OF CONTROL SYSTEMS

With the same standard action the accuracy of steady-state motion of the control system depends on the coefficients of a power series expansion of the transfer function relating the error, the given

action, i.e., the error coefficients. This fact may be used as a basis for the system classification according to the accuracy of steady-state motion.

The main classification feature in this case is the *astatic order* ν.

A system with zero astatic order with respect to a specified action x *(a static system) is one which has a forced (systematic) error proportional to the magnitude of the constant action* $x = A_0 = \text{const}$. From Eq. (9.51) it follows that this can be the case only at $C_0 \neq 0$.

A first-order astatic system (an astatic system) is one the forced (systematic) error of which in response to a constant action is zero and is constant and proportional to the rate A_1 *of an action* $x(t) = A_0 + A_1(t)$ *linearly variable in time (constant rate setting).* From Eq. (9.51) it follows that this can occur only at $C_0 = 0$. $C_1 \neq 0$.

A ν*th order astatic system is a system the forced systematic error of which in response to an action given as a polynomial of the* ν*th degree in* t

$$x(t) = A_0 + A_1(t) + \ldots + \frac{A\nu}{\nu!} t^{\nu}$$

is constant and proportional to the value of A_ν. If the action is described by a polynomial of lower degree the forced error of such a system is zero. From Eq. (9.51) it follows that in this case

$$C_0 = C_1 = \ldots = C_{\nu-1} = 0, \quad C_\nu \neq 0$$

The astatic order of a system is thus the ordinal number of the first nonzero coefficient of the error relative to the given action.

Let us have a look at the structural premises that ensure astatic conditions for a closed-loop proportional control system responding

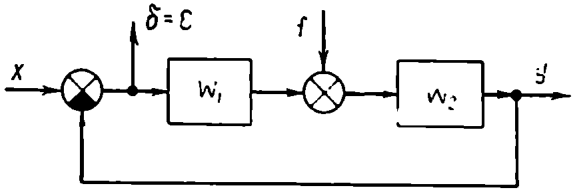

Fig. 9.13

to variations of control actions and disturbances. Figure 9.13 is a typical structure of a control system. In an actual control system W_1 would be a controller the input of which results from comparison of the control signal (setpoint) x and the control system output y. The plant W_2 is subject to disturbances f reduced to its output. The

transfer function of an open-loop control system is

$$W_{o\text{-}l}(p) = W_1(p)\,W_2(p) = \frac{K_1(p)\,K_2(p)}{D_1(p)\,D_2(p)} = \frac{K(p)}{D(p)} \tag{9.55}$$

where

$$K(p) = k_m p^m + k_{m-1}p^{m-1} + \ldots + k_1 p + k_0$$

$$D(p) = d_n p^n + d_{n-1}p^{n-1} + \ldots + d_1 p + d_0$$

Physically, $n \geqslant m$ and $k_0 \neq 0$ at $d_0 \neq 0$.

A system without integrators (static system). If a system has no integrators at all, then $d_0 \neq 0$ and we can assume without limiting generality that

$$d_0 = d_{01} \cdot d_{02} = d_{01} = d_{02} = 1$$

Then $k_0 = k_{01} \cdot k_{02} = k$ is the gain of an open-loop system.

By virtue of Eq. (9.4) the image of the error is

$$\Delta(p) = \mathrm{E}(p) = W_e(p)\,X(p) - W_{cl\text{-}l}(p)\,\frac{1}{W_1(p)}\,F(p) = \mathrm{E}_1(p) + \mathrm{E}_f(p) \tag{9.56}$$

At constant actions, $x(t) = x_0 = \text{const}$ and $f(t) = f_0 = \text{const}$, the steady-state error, according to Eq. (9.51), depends on the coefficient C_0. The transfer function error to the control action is

$$W_e(p) = \frac{1}{1 + \dfrac{K(p)}{D(p)}} = \frac{D(p)}{K(p) + D(p)} = \frac{d_n p^n + d_{n-1}p^{n-1} + \ldots + d_1 p + 1}{a_n p^n + a_{n-1}p^{n-1} + \ldots + a_1 p + a_0} \tag{9.57}$$

where $a_i = k_i + d_i$; in particular, $a_0 = 1 + k_0 = 1 + k$.

From (9.53) we have

$$C_{0x} = \frac{1}{1+k} \quad \text{and} \quad \Delta_{stat} = \frac{1}{1+k}\,x_0 \tag{9.58}$$

The transfer function of a system relating the disturbance and the error is

$$W_f(p) = \frac{\dfrac{K(p)}{D(p)}}{1 + \dfrac{K(p)}{D(p)}}\,\frac{D_1(p)}{K_1(p)} = \frac{K_2(p)\,D_1(p)}{K(p) + D(p)} \tag{9.59}$$

or

$$W_f(p) = \frac{b_r p^r + b_{r-1}p^{r-1} + \ldots + b_1 p + b_0}{a_n p^n + a_{n-1}p^{n-1} + \ldots + a_1 p + a_0} \tag{9.60}$$

Evidently $b_0 = k_{20}$ is the plant gain.

From Eq. (9.53)

$$C_{0f} = \frac{k_{20}}{1+k} \quad \text{and} \quad \Delta_{stat\,f} = -\frac{1}{1+k}\,k_{20} f_0 \tag{9.61}$$

The total static error of a closed-loop system is

$$\Delta_{stat\ cl\text{-}l} = \Delta_{stat\ x} + \Delta_{stat\ f} = \frac{1}{1+k}[x_0 - k_{20} f_0] \qquad (9.62)$$

Residual nonuniformity of the control response δ_c *is the percentage ratio of the static error to the rated value of the system output.*

From Eqs. (9.57) and (9.60)

$$\delta_{x\ cl\text{-}l} = C_{0x}\frac{x_0}{y_0}100\%, \qquad \delta_{f\ cl\text{-}l} = C_{0f}\frac{f_0}{y_0}100\% \qquad (9.63)$$

Let us open the system loop at the controller input. It is easy to see that under the same actions the static error of an open-loop system is

$$\Delta = \Delta_{stat\ o\text{-}l} = x_0 - k_{20} f_0 \qquad (9.64)$$

The ratio of static errors of a closed-loop and an open-loop system

$$\frac{\Delta_{stat\ cl\text{-}l}}{\Delta_{stat\ o\text{-}l}} = \frac{\delta_{cl\text{-}l}}{\delta_{o\text{-}l}} = \frac{1}{1+k} \qquad (9.65)$$

Consequently, *a static (proportional) controller reduces the static error* $\frac{1}{1+k}$ *times, where* k *is the gain of an open-loop system.*

The limit static accuracy $\delta_{cl\text{-}l\ min}$ depends on the stability condition $k < k_{lim}$.

A system with ν integrators (astatic control system). If a system includes ν integrators, then $d_0 = d_1 = \ldots = d_{\nu-1} = 0$; $d_\nu = d_{\nu_1} \cdot d_{\nu_2} \neq 0$, and $\nu = \nu_1 + \nu_2$, where ν_1 is the number of integrators in $W_1(p)$ and ν_2 is the number of integrators in $W_2(p)$. It can be assumed that $d_\nu = d_{\nu_1} = d_{\nu_2} = 1$, and $k_0 = k_{10} \cdot k_{20} = k \neq 0$.

By virtue of Eq. (9.57), the transfer function of a system relating the error to the control action is in this case

$$W_\delta = W_e(p) = \frac{d_n p^n + \ldots + d_{\nu+1} p^{\nu+1} + p^\nu}{a_n p^n + \ldots + a_1 p + a_0} = \frac{d_n p^{n-\nu} + \ldots + d_{\nu+1} p + 1}{a_n p^n + \ldots + a_1 p + a_0} p^\nu \qquad (9.66)$$

where

$$a_0 = k_0 = k, \quad a_1 = k_1, \quad \ldots, \quad a_{\nu-1} = k_{\nu-1}, \quad a_\nu = k_\nu + 1$$

By Eq. (9.51)

$$C_0 = C_1 = \ldots = C_{\nu-1} = 0, \qquad C_\nu = \frac{1}{k} \qquad (9.67)$$

Consequently, the astatic order of a system with respect to the control action is equal to the number of integrators in the system loop.

The value of a constant error due to an action containing a senior power of t^{ν} (at $\nu = 1$ this is known as the kinetic error Δ_{kin}) is inversely proportional to the gain of an open-loop system with νth astatic order.

By Eq. (9.59) the transfer function of a system relating the disturbance to the error is

$$W_f(p) = \frac{K_2(p) D_1(p)}{K(p) + D(p)}$$

Consider the numerator. As noted above, $W_1(p)$ includes ν_1 integrators and so the polynomial $D_1(p)$ has a term p^{ν_1}. Since $k_0 = k_{10} \cdot k_{20} \neq 0$, in this case

$$W_f(p) = \frac{b_r p^{r-\nu_1} + b_{r-1} p^{r-(\nu_1+1)} + \ldots + b_{\nu_1}}{a_n p^n + a_n p^{n-1} + \ldots + a_1 p + a_0} p^{\nu_1} \qquad (9.68)$$

where $b_{\nu_1} = k_{20} d_{\nu_1} = k_{20}$, $a_0 = k_{20} \cdot k_{10} = k$.

By Eq. (9.51)

$$C_0 = C_1 = C_2 = \ldots = C_{\nu_1 - 1} = 0, \qquad C_{\nu_1} = \frac{k_{20}}{k} = \frac{1}{k_{10}} \qquad (9.69)$$

Consequently, the astatic order of a system relative to the disturbance (load) fed to the input of the plant W_2 is equal to the number of integrators in the controller W_1 and is independent of the number of integrators in the plant.

The value of the constant error caused by the disturbance containing a senior power of t^{ν_1} is inversely proportional to the gain k_{10} of a controller with ν_1th astatic order [$\sec^{-\nu_1}$].

The above-described study permits formulation of the general structural feature to be used in determining the astatic order of a closed-loop system (Fig. 9.13).

The astatic order of a system with respect to the action x is equal to the number of integrators in the feedback loop between the input of the action and the point where the error is measured (output) and is independent of the number of integrators in the feedforward loop. In relation to the control action the whole circuit of the system is a feedback loop.

Note that closed-loop systems with a high astatic order are hard to implement since a control system with just two integrators is structurally unstable and cannot be implemented without the use of compensating units.

9.5. FREQUENCY TECHNIQUE FOR CALCULATING CONTROL PROCESSES

Let us find the transient process in a system with a transfer function $W(p)$ when there is a unit step at the input. The transfer function $W(p)$ has no poles in the right half and on the imaginary axis of the p plane.

Thence it follows that the pulse transient (weighting) function $w(t)$ of a stable system satisfies the condition of absolute integrability and can be computed by inverse Fourier transformation, which in this case takes the form

$$w(t) = \frac{1}{2\pi} \int_{-\infty}^{\infty} W(j\omega)\, e^{j\omega t}\, d\omega = \frac{1}{2\pi} \int_{-\infty}^{\infty} W(j\omega)\, (\cos \omega t + j \sin \omega t)\, d\omega$$

When the real part of $W(j\omega)$ is an even and the imaginary part, an odd function of ω, we have

$$w(t) = \frac{1}{\pi} \int_{0}^{\infty} \operatorname{Re} W(j\omega) \cos \omega t\, d\omega - \frac{1}{\pi} \int_{0}^{\infty} \operatorname{Im} W(j\omega) \sin \omega t\, d\omega$$

With negative values of time the original is identically zero. Since $\sin \omega t$ is an odd function of time, then

$$w(-t) = \frac{1}{\pi} \int_{0}^{\infty} \operatorname{Re} W(j\omega) \cos \omega t\, d\omega + \frac{1}{\pi} \int_{0}^{\infty} \operatorname{Im} W(j\omega) \sin \omega t\, d\omega = 0$$

and

$$\int_{0}^{\infty} \operatorname{Re} W(j\omega) \cos \omega t\, d\omega = - \int_{0}^{\infty} \operatorname{Im} W(j\omega) \sin \omega t\, d\omega$$

Thence in the final form the original $w(t)$ is given by the relation

$$w(t) = \frac{2}{\pi} \int_{0}^{\infty} \operatorname{Re} W(j\omega) \cos \omega t\, d\omega \tag{9.70}$$

or by the equivalent relation

$$w(t) = -\frac{2}{\pi} \int_{0}^{\infty} \operatorname{Im} W(j\omega) \sin \omega t\, d\omega \tag{9.71}$$

Assume that the image of the transient function is given in the form $H(p) = \frac{1}{p} W(p)$.

Then the original $h(t)$ can be computed by integrating Eq. (9.70)

$$h(t) = \int_{0}^{t} \left[\frac{2}{\pi} \int_{0}^{\infty} \operatorname{Re} W(j\omega) \cos \omega t\, d\omega \right] dt$$

or, changing the order of integration,

$$h(t) = \frac{2}{\pi} \int_{0}^{\infty} \operatorname{Re} W(j\omega) \frac{\sin \omega t}{\omega}\, d\omega \tag{9.72}$$

Consider a control system the transfer function of which in the open-loop state is $W_{o\text{-}l}(p)$. Then the image of the system output $y(t)$ is defined as

$$Y = \frac{W_{o\text{-}l}(p)}{1+W_{o\text{-}l}(p)} X = W_{cl\text{-}l}(p) X$$

and that of the system error is

$$\Delta(p) = \frac{1}{1+W_{o\text{-}l}(p)} X = W_{\delta}(p) X$$

By Eq. (9.70) we have, respectively,

$$y(t) = \frac{2}{\pi} \int_0^{\infty} \operatorname{Re}[W_{cl\text{-}l}(j\omega) X(j\omega)] \cos \omega t \, d\omega \tag{9.73}$$

$$\delta(t) = \frac{2}{\pi} \int_0^{\infty} \operatorname{Re}[W_{\delta}(j\omega) X(j\omega)] \cos \omega t \, d\omega \tag{9.74}$$

The quantities $\operatorname{Re}[W_{cl\text{-}l}(j\omega) X(j\omega)]$ and $\operatorname{Re}[W_{\delta}(j\omega) X(j\omega)]$ are known as *generalized real frequency responses of the system.* If $X = \frac{1}{p}$, then Eq. (9.72) is more convenient, and we have

$$y(t) = h(t) = \frac{2}{\pi} \int_0^{\infty} \frac{\operatorname{Re} W_{cl\text{-}l}(j\omega)}{\omega} \sin \omega t \, dt = \frac{2}{\pi} \int_0^{\infty} \frac{P_{cl\text{-}l}(\omega)}{\omega} \sin \omega t \, d\omega \tag{9.75}$$

where

$$P_{cl\text{-}l}(\omega) = \operatorname{Re} W_{cl\text{-}l}(j\omega)$$

In a similar way

$$\delta(t) = h_{\delta}(t) = \frac{2}{\pi} \int_0^{\infty} \frac{P_{\delta}(\omega)}{\omega} \sin \omega t \, d\omega \tag{9.76}$$

where

$$P_{\delta}(\omega) \operatorname{Re} W_{\delta}(j\omega)$$

From Eqs. (9.75) and (9.76) it follows that the system transient functions $h(t)$ and $h_{\delta}(t)$ relating the input to the output and the error, respectively, depend on *proper real frequency responses of the system* $P_{cl\text{-}l}(\omega)$ and $P_{\delta}(\omega)$*.

* In further discussion the word "proper" will be omitted from the term "proper real frequency responses", and the subscript at $P(\omega)$ will be dropped for generality sake.

Plotting transient functions by using standard responses. When the real frequency response is given as an experimental graph or table, or where analytical calculation of the integral (9.75) or (9.76) is difficult, graphical calculation is used. For this purpose the real frequency response is decomposed into standard, trapezoidal or triangular responses for which the transient processes are tabulated. This method has been developed by V.V. Solodovnikov (Ref. 75) and A.A. Voronov (Ref. 87).

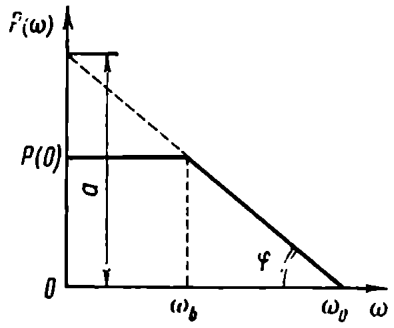

Fig. 9.14

Let us assume that the system has a real response of trapezoidal form (Fig. 9.14). Denote by ω_0 the *passband frequency* and by ω_b the *uniform passband frequency.*

Now we introduce the coefficient

$$\lambda = \frac{\omega_b}{\omega_0} \text{ and assume } 0 \leqslant \lambda \leqslant 1$$

The transient function is

$$h(t) = \frac{2}{\pi} \int_0^\infty \frac{P(\omega)}{\omega} \sin \omega t \, d\omega =$$

$$= \frac{2}{\pi} \int_0^{\omega_b} \frac{P_0}{\omega} \sin \omega t \, d\omega + \frac{2}{\pi} \int_{\omega_b}^{\omega_0} \frac{a - b\omega}{\omega} \sin \omega t \, d\omega \qquad (9.77)$$

where a and b are given by the following relations

$$a = P(0) \frac{\omega_0}{\omega_0 - \omega_b} = P(0) \frac{1}{1 - \lambda}$$

$$b = P(0) \frac{1}{\omega_0 - \omega_b} = \frac{P(0)}{\omega_0} \frac{1}{1 - \lambda}$$

Integration in Eq. (9.77) gives, for $P(0) = 1$ (unit trapezium),

$$h_\lambda(\tau) = \frac{2}{\pi} \frac{1}{1 - \lambda} \left[\operatorname{si} \tau - \lambda \operatorname{si} \lambda\tau + \frac{\cos \tau - \cos \lambda\tau}{\tau} \right] \qquad (9.78)$$

where $\operatorname{si} \tau = \int_0^\tau \frac{\sin x}{x} dx$ is the tabulated function of the integral sine plotted in Fig. 9.15, and $\tau = \omega_0 t$.

From Eq. (9.78) it follows that $h_\lambda(\tau)$ is a function of dimensionless time τ and of the coefficient λ. This function has been tabulated (Ref. 77).

Let us consider the function $h_\lambda(\tau)$ for two extreme cases.

At $\lambda = 0$ the real frequency response $P(\omega)$ and the corresponding transient function $h_0(\tau)$ are shaped as in Fig. 9.16. The transient process is monotonic in this case.

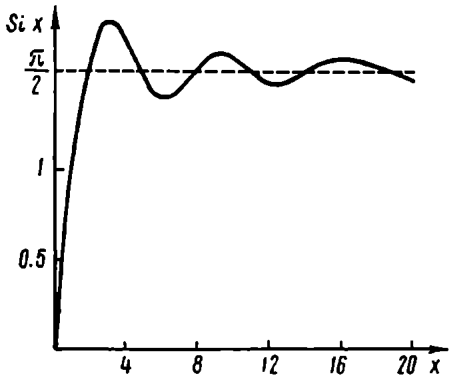

x	Si x	x	Si x
0	0	2π	1.4182
0.1	0.09994	7.0	1.4546
0.25	0.2491	8.0	1.5742
0.5	0.4931	9.0	1.6650
0.75	0.7270	13.0	1.4994
1.0	0.9461	15.0	1.6182
π/2	1.3699	20.0	1.5482
2.0	1.6054	25.0	1.5315
2.3	1.7785	35.0	1.5963
3.0	1.8487	55.0	1.5707
π	1.8519	60 0	1.5867
3.5	1.8331	75.0	1.5586
4.0	1.7582	80.0	1.5723
1.5π	1.6089	85.0	1.5824
5.0	1.5499	100	1.5622
6.0	1.4247	110	1.5799
		130	1.5737

Fig. 9.15

At $\lambda = 1$ the real frequency response is rectangular and the corresponding transient response is oscillatory (Fig. 9.17).

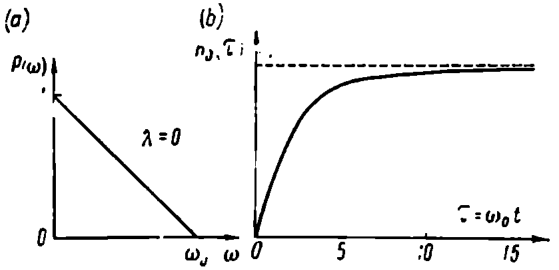

Fig. 9.16

The response time (established with an accuracy of $\delta_c = 0.05$) for trapezoidal real frequency responses is within

$$\frac{\pi}{\omega_0} < t_c < \frac{4\pi}{\omega_0} \tag{9.79}$$

and can be estimated from Fig. 9.18.

The overshoot σ can be estimated from Fig. 9.19.

Example 9.7. Consider the plotting of a transient function from a trapezoidal real frequency response.

Assume $P(0) = 5$; $\omega_0 = 100 \frac{1}{\text{sec}}$; $\omega_b = 60 \frac{1}{\text{sec}}$.

Let us find the coefficient $\lambda = \frac{\omega_b}{\omega_0} = 0.6$. By using the table of $h_\lambda(\tau)$ (Ref. 77) find the values of $h_{0.6}(\tau)$.

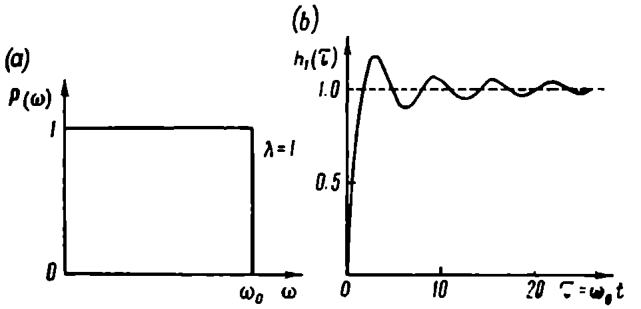

Fig. 9.17

Fig. 9.18

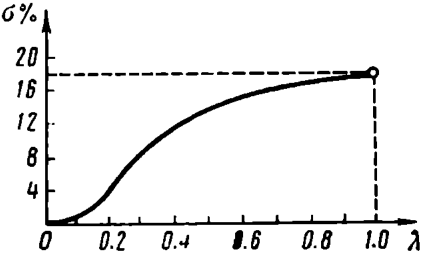

Fig. 9.19

Now, using the usual measurable time $t = \frac{\tau}{\omega_0}$, we finally find the transient function

$$h(t) = P(0) \cdot h_\lambda(t) \qquad (9.80)$$

The results are given in Table 9.1.

Table 9.1

τ	0	0.5	1	2	3
$h_{0.6}(\tau)$	0	0.255	0.490	0.878	1.1
t, sec	0	$\frac{0.5}{100}$	$\frac{1}{100}$	$\frac{2}{100}$	$\frac{3}{100}$
$h(t)$	0	5×0.255	5×0.490	5×0.878	5×1.1

Example 9.8. Consider the plotting of the transient process on the basis of the real frequency response.

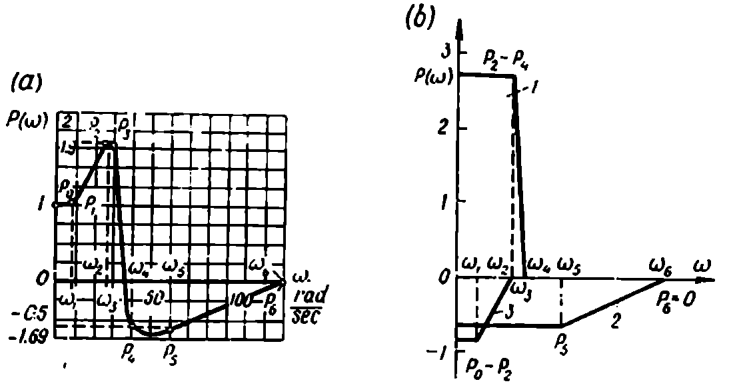

Fig. 9.20

Let the real frequency response have the shape shown in Fig. 9.20*a*. We approximate it as a broken line and decompose it into three trapezia (Fig. 9.20*b*):

1st trapezium $P(0)=P_2-P_4$; $\omega_0=\omega_4$; $\omega_b=\omega_3$;
2nd trapezium $P(0)=P_4$; $\omega_0=\omega_6$; $\omega_b=\omega_5$;
3rd trapezium $P(0)=P_0-P_2$; $\omega_0=\omega_2$; $\omega_b=\omega_1$.

Using the table of $h_\lambda(\tau)$, find for each trapezium the transient process, $h_1(t)$, $h_2(t)$, and $h_3(t)$ (Fig. 9.21). Adding them up, we obtain the desired transient process $h(t)=h_1+h_2+u_3$.

The real frequency response can be used to plot the system response to a unit pulse, or the system pulse transient (or weighting) function. According to Eqs. (9.70) and (9.75)

$$w(t)=\frac{2}{\pi}\int_0^\infty P(\omega)\cos\omega t\,d\omega \qquad (9.81)$$

If $P(\omega)$ has a trapezoidal shape (Fig. 9.22), Eq. (9.81) gives

$$w(t)=\frac{2}{\pi}P(0)\,\Omega\frac{\sin\Omega t}{\Omega t}\frac{\sin\omega_1 t}{\omega_1 t} \qquad (9.82)$$

where

$$\Omega=\frac{\omega_0+\omega_b}{2}, \qquad \omega_1=\frac{\omega_0-\omega_b}{2}$$

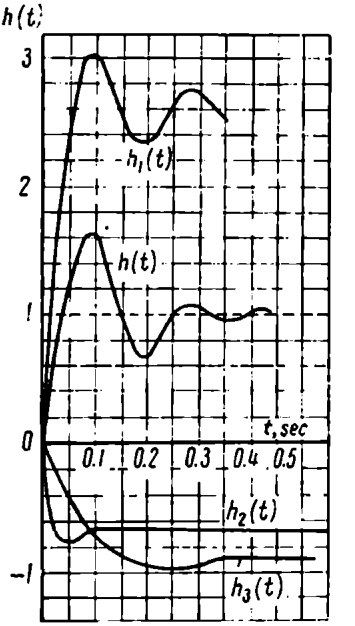

Fig. 9.21

Thence the function $w(t)$ is seen to be defined by a function of the form $\frac{\sin x}{x}$.

If the real frequency response is given as a sum of n trapezia, then

$$w(t) = \frac{2}{\pi} \sum_{i=1}^{n} P_i(0)\, \Omega_i \frac{\sin \Omega_i t}{\Omega_i t} \frac{\sin \omega_i t}{\omega_i t} \qquad (9.83)$$

Plotting a real frequency response $P_{cl\text{-}l}(\omega)$ of a closed-loop system from frequency responses of an open-loop system. A real frequency response of a closed-loop system can be plotted by using the frequency locus of an open-loop system. The plotting technique follows from the relation

$$P(\omega) = \operatorname{Re} W_{cl\text{-}l}(j\omega) = \operatorname{Re} \frac{W_{o\text{-}l}(j\omega)}{1 + W_{o\text{-}l}(j\omega)} \qquad (9.84)$$

which has a simple geometric meaning.

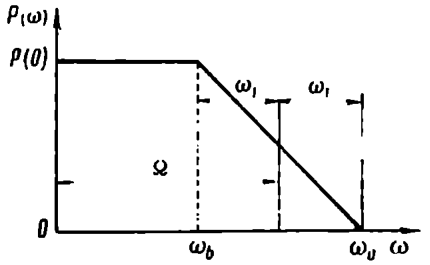

Fig. 9.22

Fig. 9.23 shows such a frequency locus of an open-loop system:

$$W_{o\text{-}l}(j\omega) = x(\omega) + jy(\omega)$$

At a certain frequency $\omega = \omega_1$ the numerator of Eq. (9.84) represents the vector $\vec{ob}$, and the denominator, the vector $\vec{ab}$. Therefore

$$P(\omega) = \operatorname{Re} \frac{\vec{ob}}{\vec{ab}} = \operatorname{Re} \frac{ob}{ab} e^{j(\theta_1 - \theta_2)} = \frac{ob}{ab} \cos\theta = \frac{cb}{ab} \qquad (9.85)$$

where cb is the projection of the vector $\vec{ob}$ on the vector $\vec{ab}$.

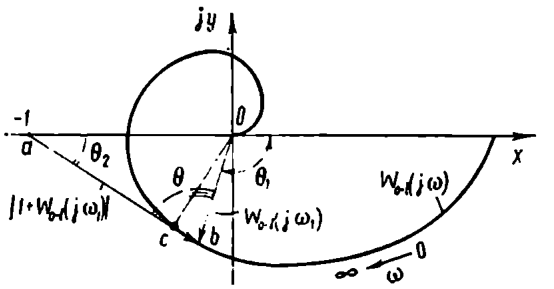

Fig. 9.23

$P_{cl\text{-}l}(\omega)$ can be most conveniently obtained by using the lines representing the constant values of a real frequency response of a closed-loop system (P-nomogram) plotted in advance in the complex $W_{o\text{-}l}(j\omega)$ plane.

The lines satisfy the condition $P(\omega) = \text{const} = c$, where c is the parameter of a family of curves.

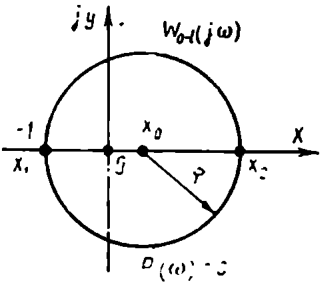

Fig. 9.24

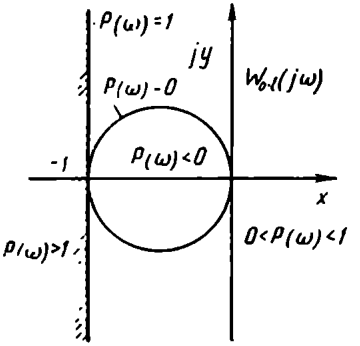

Fig. 9.25

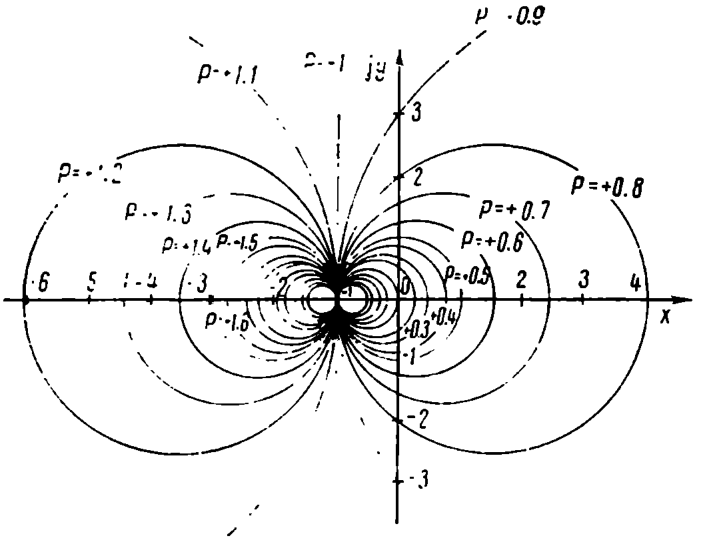

Fig. 9.26

By Eq. (9.84), for these lines

$$P(\omega) = \operatorname{Re} \frac{x+jy}{1+x+jy} = c$$

or

$$\frac{x(1+x)+y^2}{(1+x)^2+y^2} = c \qquad (9.86)$$

Find the points where the curves of Eq. (9.86) intersect the real axis. Substituting the condition $y = 0$ into Eq. (9.86) gives the equation

$$x(1 + x) = c(1 + x)^2$$

whence $x_1 = -1$; $x_2 = \frac{c}{1-c}$. All curves thus have a common tangential point, $(-1 + j0)$. They are circles with centres in the points $x_0 = \frac{x_1+x_2}{2} = \frac{1}{2}\left(\frac{c}{1-c} - 1\right)$ as shown in Fig. 9.24. A circle supported by the segment $(-1, 0)$ of the real axis corresponds to the parameter value $P(\omega) = c = 0$, and a vertical straight line $x = -1$ corresponds to $P(\omega) = c = 1$. The decomposition of the plane $W_{o\text{-}l}(j\omega)$ into regions of characteristic values of $P(\omega)$ is shown in Fig. 9.25. Assuming the values of the parameter c and calculating x_0, the P-nomogram of Fig. 9.26 can be easily plotted.

A comparison of the frequency technique of plotting the transient process (Examples 9.7 and 9.8) with the operator (or classical) technique, which uses the values of the characteristic equation roots (Example 9.1), leads to the conclusion that the frequency technique is best suited for characteristic equations of the fourth and higher orders. For first-, second-, and third-order systems the transient process can be easily calculated by determining the roots of the characteristic equation.

Analog computers facilitate the solution.

Chapter X

CONTROL PERFORMANCE: INDIRECT METHODS OF STUDY

10.1. GENERAL

The basic performance indices of control transients are the speed at which the initial deviations are offset (speed of response) and the process smoothness (zero or small overshoot). They can far from always be determined directly. It should be noted, however, that wide application of analog models increases the potential of the direct approach to studying the performance and, if combined with a reasonable method of simulation and processing the results, increases still more its practical value.

The main goal of performance studies is to ascertain the effect of the structure and parameters on the speed and smoothness of transients. In linear systems this goal is easily achieved by indirect methods developed rather recently (chiefly in the period from 1945 to 1960). We shall discuss two groups of them.

Frequency methods. The main advantage of frequency methods is the use of experimental as well as calculated responses of an open-loop system in order to determine the performance of the system after a feedback loop is closed. This is combined with the simplicity and illustrativeness of estimating the changes in responses due to structure and parameter variations.

The most rational approach to estimating transients in a closed-loop system and thus to synthesizing this system is the study of its amplitude-frequency response and of the relations between its parameters and the frequency responses of the open-loop system.

Integral methods. The most succinct and clear-cut idea of a process is evidently achieved when this process can be characterized by a single number which gives a relatively complete characteristic of the process over a specified time interval $0 \leqslant t \leqslant T$. In mathematics estimates of this type are known as functionals and can be given as a definite integral

$$J = \int_0^T F[f(t)]\,dt$$

the numerical value of which for a given function F depends on the whole course of the process, $f(t)$, at $0 \leqslant t \leqslant T$.

If the problem of minimizing such estimates, which is normally treated by the variational methods, is solved, then optimal (or best in a specified sense) systems can be obtained (Ref. 14).

A quantitative (numerical) representation of the performance index permits automatic solution of this problem and development of self-optimizing systems with a specified algorithm (program) of automatic adjustment. This makes such estimates especially important in the theory of automatic control.

10.2. FREQUENCY METHODS OF STUDYING CONTROL PERFORMANCE

Oscillation index. Using Eq. (3.92), the normalized transient function of an oscillator can be given in the form

$$\frac{h(\tau)}{k} = \left[1 - e^{-\zeta\tau}\left(\cos\sqrt{1-\zeta^2}\,\tau + \frac{\zeta}{\sqrt{1-\zeta^2}}\sin\sqrt{1-\zeta^2}\,\tau\right)\right] 1_0(t) \quad (10.1)$$

where $\tau = \omega_0 t$.

From (10.1) it follows that the direct performance indices of an oscillator are unambiguously defined by two parameters, the damping ratio ζ and the resonance frequency ω_0.

Let us define the oscillation index M as the relative maximum value of the closed-loop system amplitude-frequency response:

$$M = \frac{[W_{cl\text{-}l}(\omega)]_{max}}{W_{cl\text{-}l}(0)} \quad (10.2)$$

By Eqs. (3.85) and (3.86) for an oscillator

$$M = \frac{W(\omega_{max})}{W(0)} = \frac{1}{2\zeta\sqrt{1-\zeta^2}}, \quad \zeta \leqslant \frac{\sqrt{2}}{2} \quad (10.3)$$

where $\omega_{max} = \omega_0\sqrt{1-2\zeta^2}$.

Equations (10.1) and (10.3) establish the dependence of the transient performance indices Δh_{max}, t_{max}, t_c, and N on the oscillation index M of the oscillator amplitude-frequency response. This dependence is plotted in Fig. 10.1.

A system with the oscillator transfer function

$$W_{cl\text{-}l}(p) = \frac{\omega_0^2}{p^2 + 2\zeta\omega_0 p + \omega_0^2} \quad (10.4)$$

is obtained if the series-connected circuit of inertial and integrating elements is closed by a unit negative feedback and consequently

$$W_{o\text{-}l} = \frac{k_{as}}{p(pT+1)} \quad (10.5)$$

and

$$W_{cl\text{-}l} = \frac{\frac{k_{as}}{T}}{p^2 + \frac{1}{pT} + \frac{k_{as}}{T}} \tag{10.6}$$

Equations (10.4) and (10.6) establish the relation between the

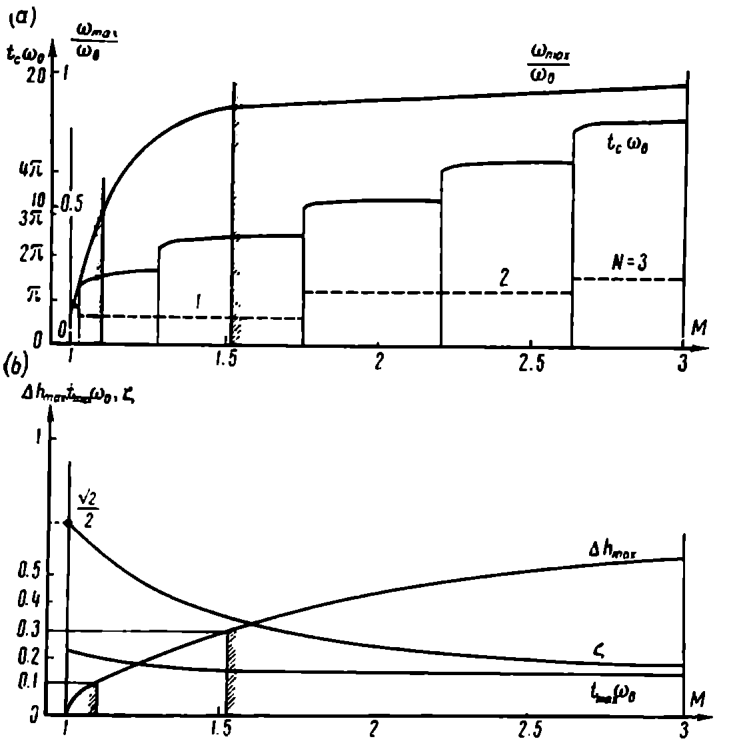

Fig. 10.1

system parameters in an open-loop and a closed-loop state

$$\omega_0 = \sqrt{\frac{k_{as}}{T}} \quad \text{and} \quad \zeta = \frac{1}{2\sqrt{k_{as}T}} \tag{10.7}$$

and also between the closed-loop system oscillation index and the phase margin of the open-loop system at the cutoff frequency

$$\gamma_{cf} = 180° + \varphi_{o\text{-}l}(\omega_{cf}) \tag{10.8}$$

This relation is plotted in Fig. 10.2.

Figure 10.3 gives examples of the asymptotic logarithmic amplitude-frequency response of an open-loop system with transfer function

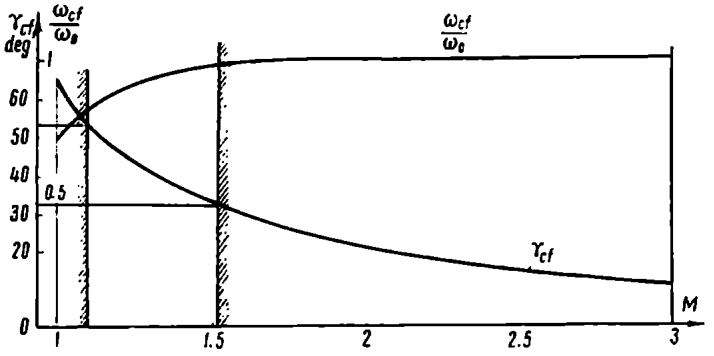

Fig. 10.2

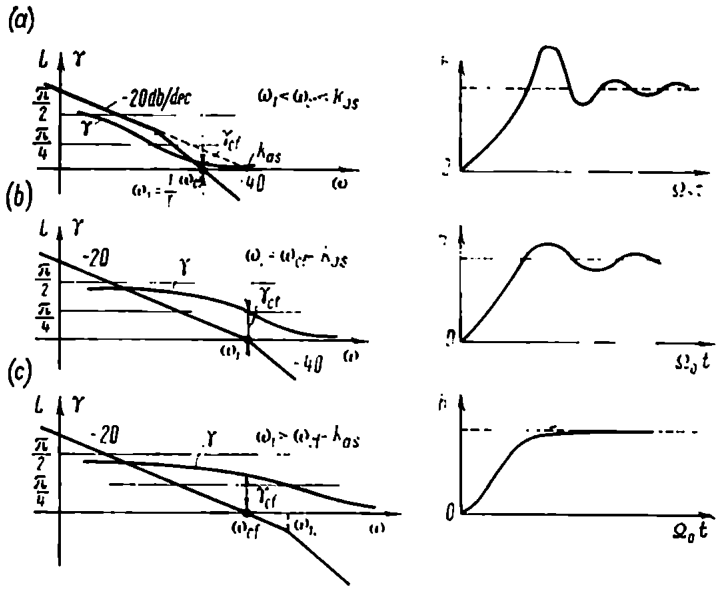

Fig. 10.3

(10.5) at different values of the figure of merit. The corresponding transfer functions of a closed-loop system are also plotted in this figure.

An increased figure of merit k_{as} clearly leads to increased oscillation frequency in the system and higher overshoot. An increased oscillation index M reduces the phase margin γ_{cf}. It is thought that

for satisfactory transient performance one must have

$$\left.\begin{array}{c}\Delta h = 0.1 \text{ to } 0.3\\ \text{Then, by Fig. 10.1, it is necessary that}\\ M = 1.1 \text{ to } 1.5\\ \text{which corresponds in Fig. 10.2 to}\\ \gamma_{cf} = 30^\circ \text{ to } 50^\circ\end{array}\right\} \quad (10.9)$$

If the amplitude-frequency response of the system, irrespective of the system complexity, is close to that of an oscillator with oscillation index M and resonance peak frequency ω_{max}, then the transients of the system will be close to those of the oscillator. This presumption permits estimating the transient functions of many complex control systems from the amplitude-frequency response of a closed-loop system (oscillation index M) and from the frequency response of an open-loop system (phase margin γ_{cf}). It should be noted that in most cases transient performances can be suitably described by the indices M, ω_{max}, ω_{cf}, ω_0, and γ_{cf}.

Plotting a closed-loop system amplitude-frequency response from the open-loop system frequency locus. In order to determine the oscillation index M and the resonance peak frequency ω_{max}, the closed-loop system amplitude-frequency response should be plotted or estimated. This may be done by using the same calculated or experimental frequency responses of an open-loop system which are employed in studying its stability.

The relation between frequency responses of a system in the open-loop and closed-loop states is given by the formula

$$W_{cl\text{-}l}(j\omega) = \frac{W_{o\text{-}l}(j\omega)}{1 + W_{o\text{-}l}(j\omega)} \quad (10.10)$$

whence it follows that in the $W_{o\text{-}l}(j\omega)$ plane we can plot in advance a family of lines representing equal magnitudes of the closed-loop frequency response.

The intersection points of the locus (the values of the frequency ω must be marked on the curve) with the family lines $W_{cl\text{-}l} = \text{const} = c$ will readily lead to a plot of $W_{cl\text{-}l} = f(\omega)$ or a direct estimate of the closed-loop system performance by determining M and ω_{max}.

Let us consider the plotting of curves $W_{cl\text{-}l} = c$ in the $W_{o\text{-}l}(j\omega) = P + jQ$ plane. From Eq. (10.10) it follows that

$$W_{cl\text{-}l} = \frac{|W_{o\text{-}l}(j\omega)|}{|1 + W_{o\text{-}l}(j\omega)|} = \frac{|P + jQ|}{|(1+P) + jQ|} = c \quad (10.11)$$

Squaring gives

$$\frac{P^2 + Q^2}{(1+P)^2 + Q^2} = c^2$$

whence

$$P^2-2P\frac{c^2}{1-c^2}+Q^2=\frac{c^2}{1-c^2} \tag{10.12}$$

Following elementary transformations equality (10.12) is reduced to the form

$$\left(P-\frac{c^2}{1-c^2}\right)^2+Q^2=\left(\frac{c}{1-c^2}\right)^2 \tag{10.13}$$

This is the equation of a family of circles, centres of which are on the real axis at a distance

$$P_0=\frac{c^2}{1-c^2} \tag{10.14}$$

from the origin of coordinates.

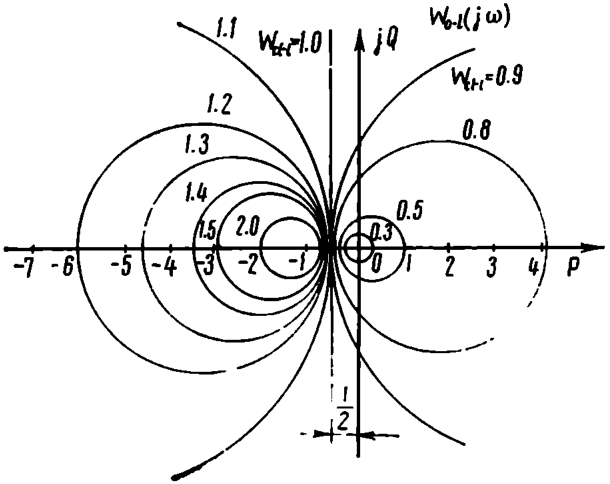

Fig. 10.4

The intersection points of each circle with the real axis are

$$P_1=-\frac{c}{1+c} \quad \text{and} \quad P_2=\frac{c}{1-c} \tag{10.15}$$

and the radius is

$$R=\left|\frac{c}{1-c^2}\right| \tag{10.16}$$

where $c = W_{cl-l} = \text{const}$ is the parameter of the family.

A diagram plotted according to Eqs. (10.13) to (10.16) is given in Fig. 10.4.

The point $(-1 + j0)$ corresponds to $W_{cl-l} = \infty$, and the origin of coordinates to $W_{cl-l} = 0$. At $W_{cl-l} = 1$ we have a vertical straight

line $P_1 = -\frac{1}{2}$. Circles for which $W_{cl-l} < 1$ are on the right, and those for which $W_{cl-l} > 1$, on the left of the straight line.

Similar to the diagram of Fig. 10.4 (Hall diagram) we can plot a family of lines of equal phases of the closed-loop complex gain

$$\varphi_{cl-l} = \arg W_{cl-l}(j\omega) = \text{const} = c.$$

This plot is given in Fig. 10.5.

If the maximum value of a closed-loop amplitude-frequency response is confined by a specified oscillation index (10.2)

$$W_{cl-l\ max} \leqslant M W_{cl-l}(0) = M_{tr} \tag{10.17}$$

then the frequency locus of the open-loop system $W_{o-l}(j\omega)$ at $M_{tr} \geqslant 1$ cannot be inside a circle with parameter $W_{cl-l} = c = M_{tr}$ (see Fig. 10.4). Therefore the curve $W_{o-l}(j\omega)$ can just touch the circle $W_{cl-l} = M_{tr}$ in one or several points. This condition is met by the use of special compensating units, which change the filtering properties of an open-loop system and distort the locus of its frequency response.

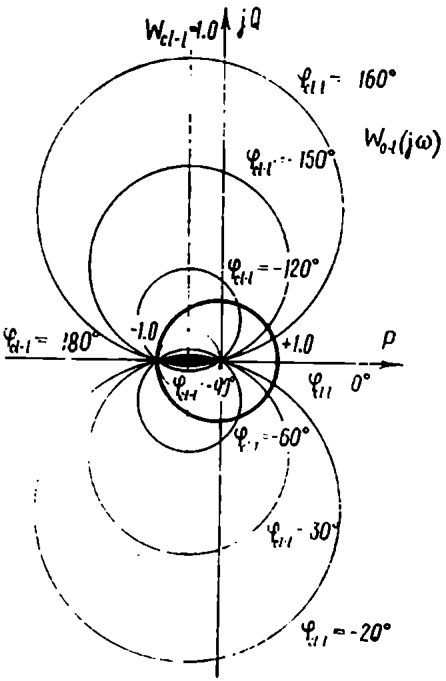

Fig. 10.5

The statement and solution of the system compensation problem (it will be treated in more detail in Ch. XI) are considerably simplified if we use the constraint on the magnitude of W_{o-l} and the phase margin γ of an open-loop complex gain instead of the constraint (10.17) imposed on the response of a closed-loop system.

Figure 10.6*a* shows one of the circles from the diagram of Fig. 10.4. In order to obtain the equation of this boundary circle $W_{cl-l} = c = M_{tr}$ in the polar coordinates W_{o-l}, γ, substitute $W_{o-l} = P^2 + Q^2$ and $P = -W_{o-l} \cos \gamma$ into equality (10.12). Then

$$W_{o-l}^2 + 2W_{o-l} \cos \gamma \frac{M_{tr}^2}{1 - M_{tr}^2} = \frac{M_{tr}^2}{1 - M_{tr}^2}$$

or

$$2W_{o-l} \cos \gamma = \left(1 + W_{o-l}^2 \frac{M_{tr}^2 - 1}{M_{tr}^2}\right)$$

The final equation for the boundary circle in polar coordinates is

$$\cos\gamma = \frac{1}{2W_{o\text{-}l}}\left[1 + \frac{W_{o\text{-}l}^2}{M_{tr}^2}(M_{tr}^2 - 1)\right] \qquad (10.18)$$

As follows from Eq. (10.18) and Fig. 10.6*a*, to keep the oscillation index of a closed-loop system down to a certain limit it is sufficient

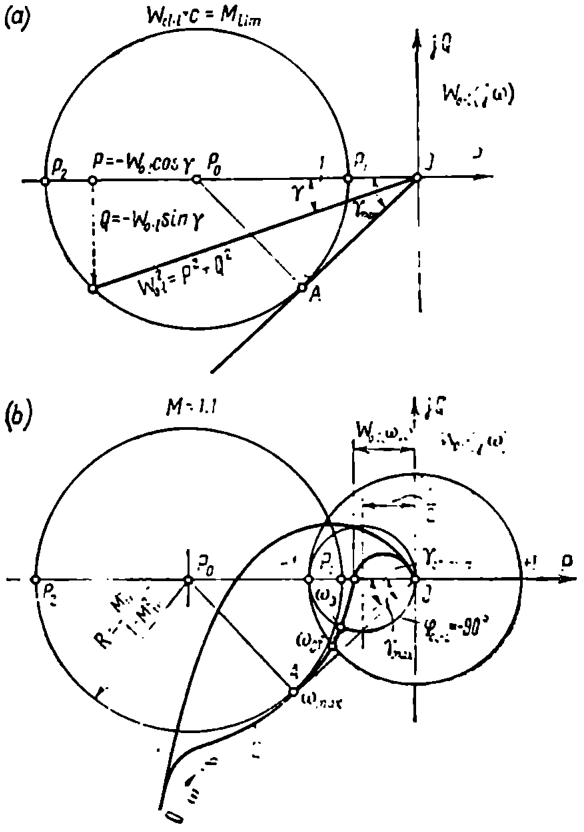

Fig 10.6

that in the interval

$$|P_2| = \frac{M_{tr}}{M_{tr}-1} \geqslant M_{o\text{-}l}(\omega) \geqslant \frac{M_{tr}}{M_{tr}+1} = |P_1|$$

the phase margin satisfy the inequality

$$\gamma \geqslant \arccos\frac{1}{2W_{o\text{-}l}}\left(1 + W_{o\text{-}l}^2\frac{M_{tr}^2 - 1}{M_{tr}^2}\right) \qquad (10.19$$

From Fig. 10.6*a* it is seen that the locus $W_{o\text{-}l}(j\omega)$ should be distorted by a compensating circuit so that in the resonance peak region $W_{cl\text{-}l}(\omega_{max}) = \max$, or in the average frequency range, the system phase margin γ satisfy the inequality

$$\gamma \geqslant \gamma_{max}$$

Since the system filtering properties are changed by using special compensating units, which increase the system complexity, efforts are always made to achieve the desired performance with the minimum possible phase lead introduced by compensating units. This requirement is met when the locus $W_{o\text{-}l}(j\omega)$ touches the boundary circle in just one point, A. In this case

$$\gamma(\omega_{max}) = \gamma_{max}$$

and, as follows from Fig. 10.6*a* and Eqs. (10.14) to (10.16),

$$\sin\gamma_{max} = \frac{R}{|P_0|} = \frac{1}{c} = \frac{1}{M_{tr}}$$

i.e.

$$\gamma_{max} = \arcsin\frac{1}{M_{tr}}, \qquad M_{tr} \gg 1 \tag{10.20}$$

Figure 10.6*b* gives the loci of uncompensated system *1* and the same system after a compensation satisfying the minimal phase lead requirement (curve *2*).

The phase and gain margin of an open-loop system. In most practical problems satisfactory performance is achieved when simple (necessary) requirements following from the condition (10.19) are met, in particular when the required phase margin γ_{cf} at the cutoff frequency and the gain margin L_{mr} are provided. Using Fig. 10.6*b*, let us see what these parameters are.

1. The phase margin γ_{cf} at the cutoff frequency $\omega = \omega_{cf}$ when $W_{o\text{-}l} = 1$. From Eq. (10.18) it follows that the minimal phase margin at the cutoff frequency

$$\gamma_{cf\,min} = \arccos\left(1 - \frac{1}{2M_{tr}^2}\right) = \arcsin\frac{1}{M_{tr}}\sqrt{1 - \frac{1}{4M_{tr}^2}} \tag{10.21}$$

Figure 10.7 gives the plots of $\gamma_{max}(M_{tr})$ and $\gamma_{cf\,min}(M_{tr})$ according to Eqs. (10.20) and (10.21).

Evidently, when the condition (10.20) is valid, $\omega_{max} < \omega_{cf}$ and $\gamma_{max} > \gamma_{cf\,min}$. The greater is M_{tr}, the smaller is the difference between γ_{max} and $\gamma_{cf\,min}$.

2. The gain margin (magnitude margin) is understood as the logarithm of the ratio of the limit gain (defined from the stability considerations) to the real system gain. According to the Nyquist

criterion this ratio is inversely proportional to the length of the segment intercepted by the locus $W_{o\text{-}l}(j\omega)$ on the negative real axis at $\omega = \omega_\pi$

$$\frac{k_{ltm}}{k} = \frac{1}{W_{o\text{-}l}(\omega_\pi)}$$

where ω_π is the intersection frequency given by the condition

$$Q(\omega_\pi) = 0 \quad \text{when} \quad P(\omega_\pi) < 0$$

Consequently, the magnitude margin given in decibels

$$L_{mr} = 20 \log \frac{1}{W_{o\text{-}l}(\omega_\pi)} \tag{10.22}$$

Equation (10.18) and Fig. 10.6*b* lead to the conclusion that the minimal value of the gain margin at a given M_{tr} is

$$L_{mr\,min} = 20 \log \frac{1}{|P_1|} = 20 \log \frac{M_{tr}+1}{M_{tr}} \tag{10.23}$$

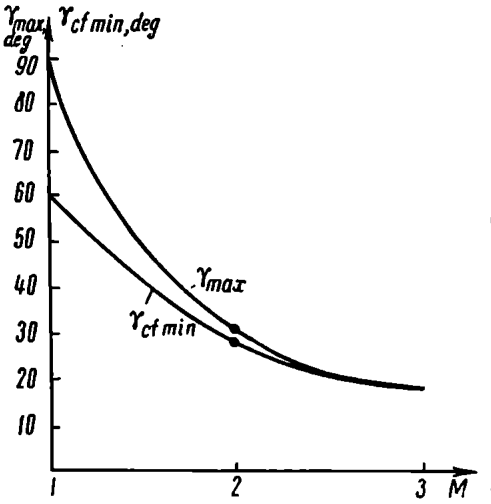

Fig. 10.7

The gain margin of practical systems is normally higher than the minimal necessary value of Eq. (10.23) and is selected within the range

$$L_{mr} = 8 \text{ to } 12 \text{ db}$$

The resonance frequency of undamped oscillations ω_0 of a closed-loop system is found from the condition $\varphi_{cl\text{-}l} = -90°$, which corresponds to the intersection point of the locus $W_{o\text{-}l}(j\omega)$ with the circle the diameter of which is the segment $[-1, 0]$ of the real axis (see Fig. 10.6*b*). From this figure and from Figs. 10.1 and 10.2 it follows that at $M > 1$ the frequencies $\omega_{max} < \omega_{cf} < \omega_0$ are as a rule rather close to each other and the greater is M, the closer they are. The frequency of free damping oscillations ω_t of a closed-loop system is also between ω_{max} and ω_0. Thus, for an oscillator

$$\frac{\omega_{max}}{\omega_0} = \sqrt{1-2\zeta^2} < \sqrt{1-\zeta^2} = \frac{\omega_t}{\omega_0}$$

Therefore in approximate estimates it is assumed that

$$\omega_t \approx \omega_{cf} \tag{10.24}$$

i.e. *the damping frequency of a closed-loop transient process is approximately equal to the cutoff frequency of an open-loop system.*

Performance estimate from logarithmic frequency responses. Typical responses. An open-loop system is as a rule given as elements connected in series. The frequency responses of some of these can be given by an experimental table or a graph, and others, by formulae. To plot the loci $W_{c\text{-}l}(j\omega)$ or $W_{o\text{-}l}^{-1}(j\omega)$, the magnitudes of vectors at the same value of frequency should be multiplied. If the polar coordinates

$$W_{o\text{-}l}(j\omega) = W_{o\text{-}l}(\omega)\, e^{j\varphi_{o\text{-}l}(\omega)}$$

are replaced by the rectangular logarithmic ones

$$\ln W_{o\text{-}l}(j\omega) = \ln W_{o\text{-}l}(\omega) + j\varphi_{o\text{-}l}(\omega)$$

multiplication is replaced by addition, which considerably simplifies the plotting. Also the change from the response $W_{o\text{-}l}(j\omega)$ to the response $W_{o\text{-}l}^{-1}(j\omega)$ in these coordinates is achieved by simply changing the signs of the axes. This is especially convenient when not only the closed-loop system output performance but also the misalignment performance must be studied, because

$$W_{\varepsilon}(j\omega) = \frac{1}{1+W_{o\text{-}l}(j\omega)} = \frac{W_{o\text{-}l}^{-1}(j\omega)}{1+W_{o\text{-}l}^{-1}(j\omega)}$$

depends on $W_{o\text{-}l}^{-1}(j\omega)$ as $W_{cl\text{-}l}(j\omega)$ on $W_{o\text{-}l}(j\omega)$.

The magnitude axis of the logarithmic diagram normally goes vertically (a Nichols diagram) as shown in Fig. 10.8. The main, uniform, scale for that axis is given in decibels: $L_{o\text{-}l} = 20 \log W_{o\text{-}l}$. For convenience the logarithmic scale $W_{o\text{-}l} = |W_{o\text{-}l}(j\omega)|$ can also be used. The horizontal axis of the diagram represents the phase shift $\varphi_{o\text{-}l}$ (in degrees) or the phase margin $\gamma_{o\text{-}l}$ of an open-loop system.

The equal-magnitude ($W_{cl\text{-}l}$) and equal-phase ($\varphi_{cl\text{-}l}$) lines for a closed-loop system given in the nomogram permit plotting the frequency responses of a closed-loop system from those of an open-loop one.

By way of illustration, the locus of a specific open-loop system with indicated values of the parameter ω is superimposed on the nomogram of Fig. 10.8. A change in the gain shifts the curve vertically relative to the coordinate grid.

The figure shows how easy it is to determine the phase and gain margins.

In studying minimal-phase systems which in the open-loop state can be represented as a series connection of simple elements, the use of frequency techniques is especially simplified. The phase-frequency response of such systems is defined unambiguously by their amplitude-frequency response, while the asymptotic logarithmic amplitude-frequency response consists of segments whose slope is a multiple of 20 db/dec.

According to the condition (10.9) acceptable transient performance is achieved if the phase margin at the cutoff frequency $\gamma_{cf} \geqslant 30°$. Then, by the condition (2.55) for minimal-phase systems, the segment of the asymptotic logarithmic amplitude-frequency response of an

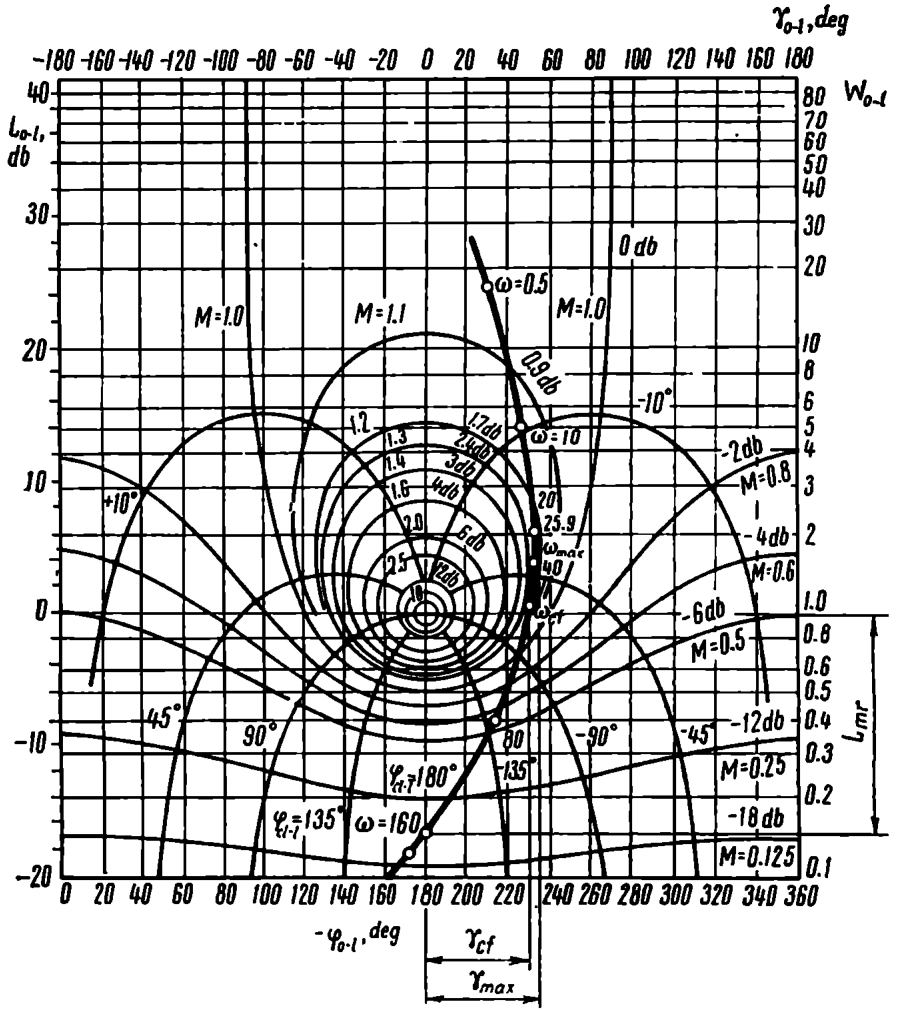

Fig. 10.8

open-loop system which contains the cutoff frequency ω_{cf} should be inclined at —20 db/dec. The longer this segment, the greater (other conditions being equal) the open-loop system phase margin and the lower the closed-loop system oscillation index M. This is illustrated, in particular, by Fig. 10.3.

The possible configurations of the response of such systems in the average frequency range are practically limited to typical characteristics, which correspond to the open-loop transfer function of the form

$$W_{o\text{-}l}(p) = \frac{k(T_0 p+1)^l}{p^\nu (T_1 p+1)^r (T_2 p+1)^l}, \quad l=1,\ 2, \quad r=1,\ 2, \quad \nu=0,\ 1,\ 2 \tag{10.25}$$

The parameters of a typical frequency response are given in Fig. 10.9*a*. The relatively low number of versions to be studied made

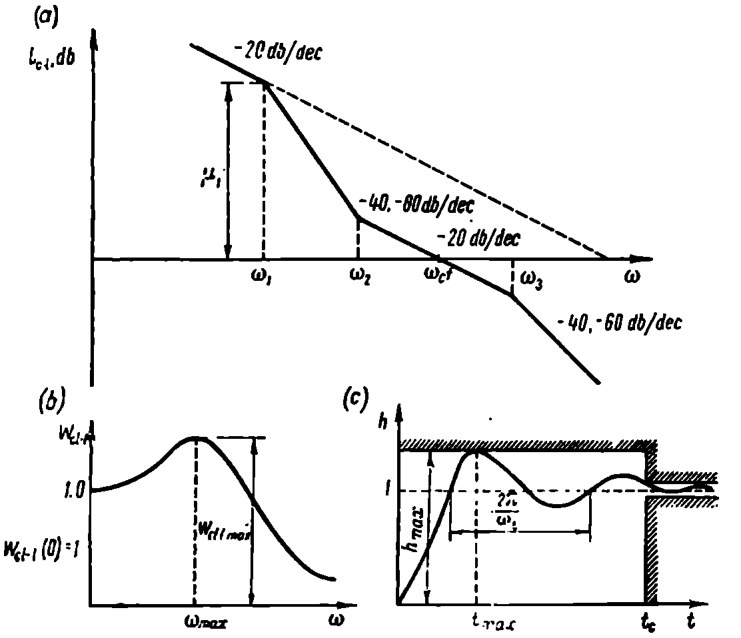

Fig. 10.9

it possible to calculate and plot a set of nomograms relating the parameters of typical open-loop response with indices of the closed-loop amplitude-frequency response (Fig. 10.9*b*) and transient function (Fig. 10.9*c*). The nomograms of Ref. 15 greatly simplify performance studies for systems of this type.

10.3. INTEGRAL ESTIMATES OF TRANSIENT PERFORMANCE

Let us consider integral estimates of increasing complexity that characterize the control process transient component defined as in Fig. 10.10

$$y_t(t) = -y_{fr}(t) = y_{fo}(t) - y(t) = \varepsilon_{fr}(t) \tag{10.26}$$

where y_{fr} is the control process free component over the whole theoretical interval of its existence $0 < t < \infty$.

Naturally, before integral estimates can be calculated, the system structure and parameters should be given (as a differential equation, structural diagram or transfer function), input actions specified

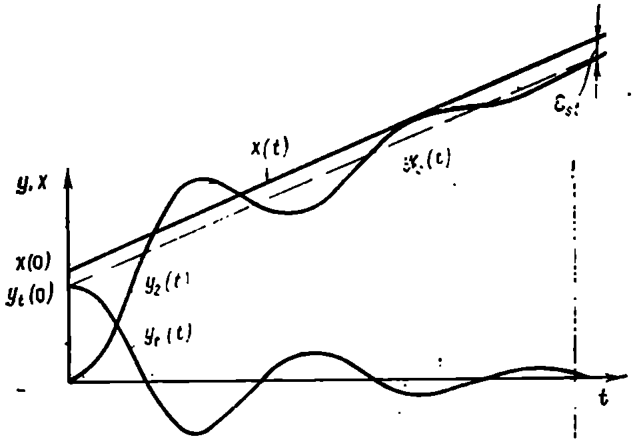

Fig. 10.10

(as the time function or its Laplace transform), and initial conditions known. There is no need to solve the differential equation.

Linear integral estimates. A *linear integral estimate* of the transient component y_t is a definite integral of the form

$$S = \int_0^\infty \varphi(t)\, y_t(t)\, dt \qquad (10.27)$$

where $\varphi(t)$ is a given time funcion (which should not be confused with $w(t)$, the system weighting function).

Of practical significance are linear integral estimates

$$S_{\alpha l} = \int_0^\infty e^{-\alpha t} t^l y_t(t)\, dt$$

chiefly of the form

$$S_{0l} = \int_0^\infty t^l y_t(t)\, dt \qquad (10.28)$$

with $\varphi(t) = t^l$.

The simplest of these estimates

$$S_{00} = \int_0^\infty y_t(t)\,dt \tag{10.29}$$

is equal to the transient process area hatched in Fig. 10.11 with due regard for the sign of y_t. For monotonic processes (Fig. 10.11*a*) this estimate can be the performance index of the system.

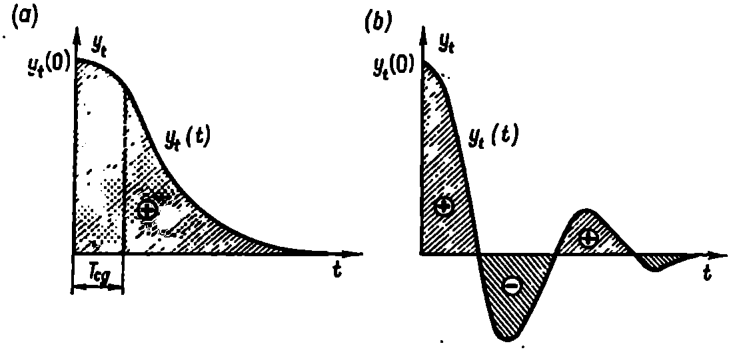

Fig. 10.11

The estimate

$$S_{01} = \int_0^\infty t y_t(t)\,dt \tag{10.30}$$

is equal to the moment of the area S_{00} relative to the origin of coordinates. The relation

$$T_{cg} = \frac{S_{01}}{S_{00}}$$

determines the position of the centre of gravity for the figure hatched in Fig. 10.11 and characterizes the system speed of response under monotonic control processes (see Fig. 10.11*a*).

Senior estimates of (10.28) determine the lth order moments of the function $y_t(t)$, where $l = 2, 3, \ldots$.

Linear integral estimates are very easy to calculate. Differentiating the image of $y_t(t)$ with respect to the complex parameter p, we have

$$\frac{d^l}{dp^l} Y_t(p) = \frac{d^l}{dp^l} \int_0^\infty y_t(t)\, e^{-pt}\,dt = \int_0^\infty (-1)^l t^l y_t(t)\, e^{-pt}\,dt =$$

$$= (-1)^l L\{t^l y_t(t)\}$$

where $Y_t(p)$ is the image of $y_t(t)$.

By the final value theorem

$$S_{0l} = \int_0^\infty t^l y_t(t)\,dt = (-1)^l \lim_{p\to 0} \frac{d^l}{dp^l} Y_t(p) \qquad (10.31)$$

Equality (10.31) is equivalent to Eq. (9.80) for the method of error coefficients. One should take into consideration, however, that the transfer function, which relates the transient component and the system input, does not generally coincide with the transfer function of the system. By Eq. (10.31) the estimate

$$S_{00} = \lim_{p\to 0} Y_t(p) = Y_t(0) \qquad (10.32)$$

The use of linear integral estimates is limited in practice, since they are applicable to monotonic processes only. Figure 10.11*b* clearly shows that for an oscillatory process the value of S_{00} and of other linear estimates can be small at poor damping and at large overshoot. Unfortunately, to establish in advance the monotonic character of processes in a system under study is rather difficult, which further limits the direct use of these estimates. Quadratic integral estimates are free from this disadvantage.

Quadratic integral estimates. Quadratic integral estimates of the form

$$J = \int_0^\infty [y_t^{(l)}(t)]^2\,dt$$

were suggested in 1909 by Academician L.I. Mandelshtam and N.D. Papalexi for a wide range of problems in the theory of oscillations. An estimate of this type was applied to instrumentation problems by A.A. Kharkevich in 1937. In the theory of automatic control quadratic estimates were applied and extended by A.A. Krasovsky (1946) and A.A. Feldbaum (1948).

The elementary quadratic integral estimate

$$J_0 = \int_0^\infty y_t^2(t)\,dt \qquad (10.33)$$

characterizes the transient process as shown in Fig. 10.12. Its numerical value, equal to the hatched area in this figure, makes an allowance for the magnitude of deviation of y_t, which makes the estimate J_0 applicable to oscillatory systems.

The integral is most easily determined by the Rayleigh theorem, whence

$$J_0 = \int_0^\infty y_t^2(t)\,dt = \frac{1}{\pi}\int_0^\infty |Y_t(j\omega)|^2\,d\omega \qquad (10.34)$$

where $|Y_t(j\omega)|$ is the amplitude spectrum of the transient component at the output of the control system.

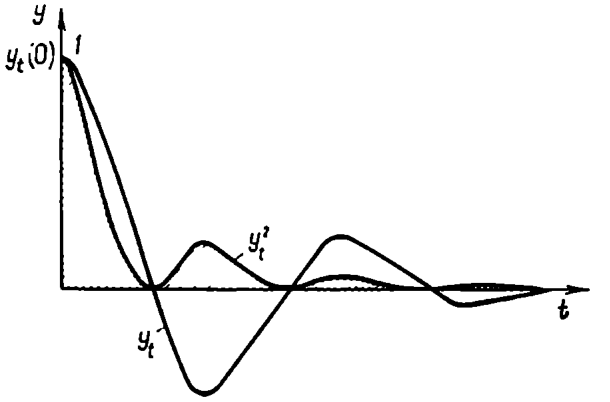

Fig. 10.12

In most cases the image $Y_t(p)$ is a fractional rational function

$$Y_t(p) = \frac{B(p)}{C(p)} = \frac{b_m p^m + b_{m-1} p^{m-1} + \ldots + b_1 p + b_0}{c_n p^n + c_{n-1} p^{n-1} + \ldots + c_1 p + c_0} \qquad (10.35)$$

and Eq. (10.34) can be rearranged as

$$J_0 = \frac{1}{\pi} \int_0^\infty \frac{B(j\omega) B(-j\omega)}{C(j\omega) C(-j\omega)} d\omega \qquad (10.36)$$

Integrals of the form (10.36) as functions of the coefficients b_k and c_k were originally calculated by McLenn for $m = n - 1$ and $n = 1, 2, 3, \ldots, 7$. There are tables for up to $n = 10$ (Ref. 57), which is more than enough for practical purposes.

Thus, in estimating a pulse response of a stable control system

$$y_t(t) = W_{cl\text{-}l}(t), \quad Y_t(p) = W_{cl\text{-}l}(p), \quad \text{and}$$
$$|Y_t(j\omega)|^2 = W_{cl\text{-}l}(j\omega) W_{cl\text{-}l}(-j\omega) = W_{cl\text{-}l}^2(\omega)$$

If we are concerned with the system transient function, then

$$y_t(t) = h_{st} - h(t), \quad Y_t(p) = \frac{W_{cl\text{-}l}(0) - W_{cl\text{-}l}(p)}{p}, \quad \text{and}$$

$$|Y_t(j\omega)|^2 = \frac{[W_{cl\text{-}l}(0) - W_{cl\text{-}l}(j\omega)][W_{cl\text{-}l}(0) - W_{cl\text{-}l}(-j\omega)]}{-\omega^2} = \frac{B(j\omega) B(-j\omega)}{C(j\omega) C(-j\omega)}$$

Example 10.1. Determine the quadratic integral estimate J_0 for the transient function of a system where

$$W_{cl\text{-}l}(p) = \frac{1}{p^3 + Ap^2 + Bp + 1}$$

and calculate the values of the parameters A and B minimizing J_0. Since $W_{cl-l}(0) = 1$, then

$$Y(p) = \left[1 - \frac{1}{p^3 + Ap^2 + Bp + 1}\right] \frac{1}{p} = \frac{p^2 + Ap + B}{p^3 + Ap^2 + Bp + 1}$$

For $n = 3$

$$J_0 = \frac{b_2^2 c_0 c_1 + (b_1^2 - 2b_0 b_2)\, c_0 c_3 + b_0^2 c_2 c_3}{2c_0 c_3 (c_1 c_2 - c_0 c_3)}$$

In the case under study

$$b_0 = c_1 = B, \quad b_1 = c_2 = A, \quad b_2 = c_3 = c_0 = 1$$

whence

$$J_0 = \frac{B + (A^2 - 2B) + B^2 A}{2(AB - 1)} = \frac{B(AB - 1) + A^2}{2(AB - 1)} = \frac{B}{2} + \frac{A^2}{2(AB - 1)}$$

Let us determine partial derivatives

$$\frac{\partial J_0}{\partial A} = \frac{2A(AB - 1) - A^2 B}{2(AB - 1)^2}, \quad \frac{\partial J_0}{\partial B} = \frac{1}{2}\left[1 - \frac{A^3}{(AB - 1)^2}\right]$$

and, equating them to zero, we have $A = 1$, $B = 2$, and $J_{0\,min} = 1.5$.

The transient process corresponding to the minimal J_0 is found to be oscillatory in the system under study, and the value of the

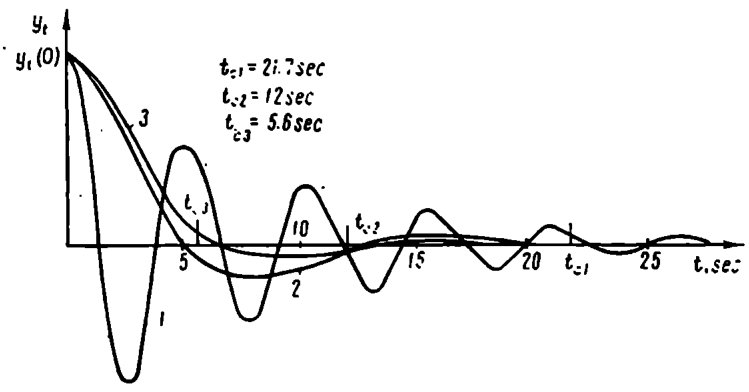

Fig. 10.13

oscillation index $M = 1.34$ is evidence of a large overshoot. This is not surprizing because the estimate J_0 does not characterize the smoothness of control.

Figure 10.13 shows three different processes corresponding to the same value of the integral quadratic estimate J_0. Process *1* is evidently hardly applicable in practice, process *2* is satisfactory, and process *3* represents good performance of the system.

The least (zero) value of the estimate J_0 by Eq. (10.33) is attained at $y_t(t)=0$ in all points except $t=0$. This process cannot be taken as reference because excessive speed of response in a linear system leads to inadmissible and unfeasible overtensions and overloads.

The quadratic integral estimate

$$J_1=\int_0^\infty [y_t^2(t)+\tau_1^2\dot{y}^2(t)]\,dt \tag{10.37}$$

has no such disadvantages.

If an allowance is made for the rate of the process, $\dot{y}(t)=\frac{dy_t(t)}{dt}$ with weight τ_1, this estimate acquires qualitatively new properties.

The integral (10.37) can be represented in the form

$$J_1=\int_0^\infty [y_t(t)+\tau_1\dot{y}(t)]^2\,dt-2\tau_1\int_0^\infty y_t(t)\,\dot{y}(t)\,dt=$$

$$=\int_0^\infty [y_t(t)+\tau_1\dot{y}(t)]^2\,dt-2\tau_1\int_0^\infty y_t(t)\,dy_t(t)$$

Since by definition $y_t(\infty)=0$, then

$$J_1=\int_0^\infty [y_t(t)+\tau_1\dot{y}(t)]^2\,dt+\tau_1 y_t^2(0)$$

whence it follows that

$$J_{1min}=\tau_1 y_t^2(0) \tag{10.38}$$

is associated with the process described by the equation

$$\tau_1\frac{dy_t}{dt}+y_t=0 \tag{10.38a}$$

with the initial condition $y_t(0)$.

Therefore the optimal process in terms of minimal estimate J_1 is given by the exponent of Fig. 10.14 representing the solution to Eq. (10.38a)

$$y_{t\,min}(t)=y_t(0)\,e^{-\frac{t}{\tau_1}} \tag{10.39}$$

Giving the numerical value of the weight coefficient limits the speed of the optimal (reference) system and thus provides the smoothness of the control process. It is normally assumed that $\frac{1}{6}t_c<\tau_1<\frac{1}{3}t_c$, where t_c is the required recovery time.

As shown by A.A. Feldbaum the integral J_1 and senior quadratic integral estimates J_k have a very important property, namely if the extremal (minimal) value of the estimate $J_{k\ min}$ $(k = 1, 2, 3, \ldots)$

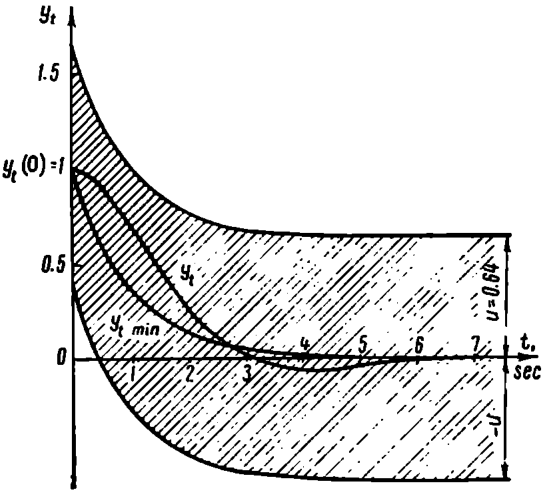

Fig. 10.14

differs from the value of J_k calculated for the system under study by an amount

$$\varepsilon_k = J_k - J_{k\ min} > 0$$

then the transient process in this system $y_t(t)$ differs at any time from the extremal $y_{t\ opt}(t)$ by less than

$$u = \sqrt{w_k \varepsilon_k} \tag{10.40}$$

where w_k can be calculated for any integral J_k. This is illustrated in Fig. 10.14. In particular, for J_1

$$w_1 = \frac{1}{\tau_1}$$

and

$$|y_t(t) - y_{t\ min}(t)| < u = \sqrt{\frac{\varepsilon_1}{\tau_1}} \tag{10.41}$$

With increasing order of the differential equation of the system under study the value of the difference ε_1 attainable even with the best selected parameters increases as does the bandwidth $\pm u$. How close the transient process is to the specified reference one cannot be estimated with desired accuracy. Increased accuracy of judgement

is obtained by using one of the senior quadratic integral estimates

$$J_k = \int_0^\infty \{y_t^2(t) + \tau_1^2 \dot{y}^2(t) + \ldots + \tau_k^2 [y^{(k)}(t)]^2\}\, dt \qquad (10.42)$$

whose extremal is the solution to the linear differential equation

$$a_k y^{(k)}(t) + a_{k-1} y^{(k-1)}(t) + \ldots + a_1 \dot{y}(t) + a_0 y(t) = 0 \qquad (10.43)$$

at $a_0 = 1$ and with specified initial conditions. It is normally assumed that

$$y(0) = y_t(0), \quad \dot{y}(0) = \ddot{y}(0) = \ldots = y^{(k-1)}(0) = 0 \qquad (10.44)$$

In order to determine the relation between the weight coefficients in Eq. (10.42) and the coefficients of Eq. (10.43) the following identity is used

$$\int_0^\infty [y_t^2(t) + \tau_1^2 \dot{y}^2(t) + \ldots + \tau_k^2 (y^{(k)}(t))^2]\, dt =$$

$$= \int_0^\infty (y + a_1 \dot{y} + \ldots + a_k y^{(k)})^2 dt + C$$

Expanding the integrand squared sum in the right-hand part and integrating the doubled products in parts with an allowance for the initial conditions (10.44), we have

$$\left.\begin{aligned} C &= a_1 y_t^2(0) \\ \tau_1^2 &= a_1^2 - 2a_0 a_2 \\ \tau_2^4 &= a_2^2 - 2a_1 a_3 + a_0 a_4 \\ \tau_3^6 &= a_3^2 - 2a_2 a_4 + 2a_1 a_5 - 2a_0 a_6 \\ &\ldots\ldots\ldots\ldots\ldots\ldots \\ \tau_k^{2k} &= a_k^2 \end{aligned}\right\} \qquad (10.45)$$

The estimate J_k is calculated as the sum

$$J_k = J_0 + \sum_{i=1}^{k} \tau_i^2 J_{0i}$$

the components of which

$$J_{0i} = \int_0^\infty [y^{(i)}(t)]^2\, dt$$

are found from the image $L\{y^{(i)}(t)\}$ as is the estimate J_0.

Example 10.2. Calculate the quadratic integral estimate J_0 and J_1 for the transient function of the system with a transfer function

$$W_{cl\text{-}l}(p) = \frac{1}{p^2 + 2\zeta p + 1}$$

Determine the value of ζ at which J_1 is minimal. Compare the resultant transient process with the extremal.

The image

$$L\{y_t(t)\} = Y_t(p) = \frac{1}{p}\left[1 - \frac{1}{p^2 + 2\zeta p + 1}\right] = \frac{p + 2\zeta}{p^2 + 2\zeta p + 1}$$

$$L\{\dot{y}_t(t)\} = pY_t(p) - Y_t(0) = -\frac{1}{p^2 + 2\zeta p + 1}$$

For $n = 2$

$$J_0 = \frac{b_1^2 c_0 + b_0^2 c_2}{2c_0 c_1 c_2}$$

The values of coefficients for $Y_t(p)$ are:

$$b_1 = c_2 = c_0 = 1; \quad b_0 = c_1 = 2\zeta$$

whence

$$J_0 = \frac{1 + 4\zeta^2}{4\zeta}$$

for $pY_t(p) - Y_t(0)$

$$b_1 = 0, \quad b_0 = c_2 = c_0 = 1, \quad c_1 = 2\zeta$$

whence

$$J_{01} = \frac{1}{4\zeta} \quad \text{and} \quad J_1 = \frac{1 + 4\zeta^2}{4\zeta} + \tau_1^2 \frac{1}{4\zeta} = \frac{(1 + \tau_1^2) + 4\zeta^2}{4\zeta}$$

From the equation

$$\frac{\partial J_1}{\partial \zeta} = \frac{4\zeta^2 - (1 + \tau_1^2)}{4\zeta^2} = 0$$

we have

$$\zeta = \frac{1}{2}\sqrt{1 + \tau_1^2}$$

and

$$J_1 = \sqrt{1 + \tau_1^2}$$

Since at $y_t(0) = 1$ by Eq. 10.38 $J_{1min} = \tau_1$, then

$$\varepsilon_1 = \sqrt{1 + \tau_1^2} - \tau_1$$

As could be expected, ε_1 reduces with increasing τ_1. In particular, at

$$\tau_1 = 1, \quad \zeta = \frac{\sqrt{2}}{2}, \quad \varepsilon_1 = \sqrt{2} - 1 = 0.414, \quad u = \sqrt{\frac{\varepsilon_1}{\tau_1}} = 0.64$$

The transient process obtained and the extremal for this case are shown in Fig. 10.14.

Integral quadratic estimate of deviation from the reference. When discussing the quadratic integral estimates J_k we found that the reference transient process (extremal) for these is the solution of the linear differential equation (10.43). The system is optimized relative to these estimates by finding the local minimum of J_k in the space of system variables. The result of the optimization is evaluated by the difference of the local minimum obtained and the global one, $J_{k\ min}$.

The expansion of the class of processes used as references and a more rigorous statement of the system optimization problem are achieved by using the integral quadratic estimate J_{ref} of the deviation from the specified (reference) function y_{ref}.

The estimate J_{ref} is given by the equality

$$J_{ref} = \int_0^\infty \delta^2(t)\,dt = \int_0^\infty [y_{ref}(t) - y(t)]^2\,dt \quad (10.46)$$

and is the area bounded by the curve of quadratic deviation δ^2 of the control process y_t in the system studied from the rationally specified best pocess y_{ref} (Fig. 10.15). The necessary condition for convergence of the estimate J_{ref} is the equality

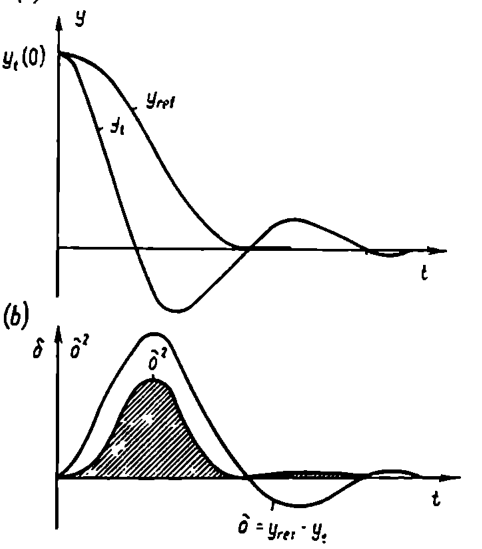

Fig. 10.15

$$\lim_{t\to\infty} |\,y_{ref}(t) - y(t)\,| = 0$$

J_{ref} is calculated from the image $\Delta(p) = Y_{ref}(p) - Y(p)$ exactly as J_0 is calculated from the image $Y_t(p)$, in particular, from the table of integrals.

Example 10.3. Determine the damping ratio ζ optimal in terms of J_{ref} in a second-order system with transfer function

$$W_{cl}(p) = \frac{2\zeta p + 1}{p^2 + 2\zeta p + 1}$$

using as reference the inertial element transient function

$$h_{ref} = y_{ref}(t) = 1 - e^{-t}$$

Let us determine

$$\Delta(p) = \frac{1}{p(p+1)} - \frac{1}{p}\,\frac{2\zeta p+1}{p^2+2\zeta p+1} = \frac{(1-2\zeta)p-1}{p^3+(2\zeta+1)p^2+(2\zeta+1)p+1} = \frac{(1-a)p-1}{p^3+(a+1)p^2+(a+1)p+1}$$

where

$$a = 2\zeta$$

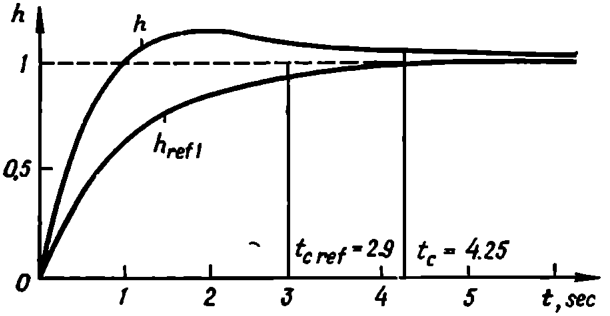

Fig. 10.16

Using the table of integrals (A.3), we can see that

$$J_{ref} = \frac{a^2-a+2}{2a(a+2)}$$

From the condition

$$\frac{\partial J_{ref}}{\partial a} = \frac{3a^2-4a-4}{2a^2(a+2)^2} = 0$$

we calculate $a = 2$, $\zeta = 1$, and $J_{ref\ min} = 0.25$. The resultant process $h(t)$ and the reference process $h_{ref}(t)$ are given in Fig. 10.16.

Chapter XI

DESIGN OF LINEAR CONTROL SYSTEMS

11.1. GENERAL DESCRIPTION OF PROBLEMS

Statement of the problem. The automatic control systems design is understood as the problem of selecting and calculating the parameters of compensators ensuring the desired static and dynamic properties of the system. The basic functional elements are assumed already selected to suit the given specifications and make up the unchangeable part of the system. The general design problem involves the selection and calculation of both the compensators and the unchangeable part of the system and is treated in special curricula (Ref. 9).

Design of control systems used in automation of industrial processes is a problem in its own right. The specific features of these systems are:

(a) strict division of the system into two parts, the plant and the controller; the inertia of individual functional parts in the controller is negligible in comparison with the inertia of the plant proper,

(b) use of standard controllers.

The general design problem for such systems therefore reduces to the selection of a standard controller which would ensure the desired control law and to the adjustment of its parameters to suit the plant dynamic responses.

Figure 11.1 shows the most popular structural diagrams of compensation.

In a simplest cascade (series) compensation (Fig. 11.1*a*), the compensator is incorporated directly into the control loop. The transfer function of an open-loop compensated system is

$$W_{com}(p) = W_{unc}(p)\, W_{cc}(p) \tag{11.1}$$

where $W_{unc}(p)$ = transfer function of an open-loop uncompensated system

$W_{cc}(p)$ = transfer function of the cascade compensating unit.

In parallel compensation the compensating unit is in the special feedback loop (Fig. 11.1*b*). The open-loop transfer function of this

system is

$$W_{com}(p) = \frac{W_{in}(p)\, W_{out}(p)}{1 + W_{in}(p)\, W_{pc}(p)} \tag{11.2}$$

where $W_{in}(p)$ = transfer function of the system part inside the compensating feedback

$W_{out}(p)$ = transfer function of the system part outside the compensating feedback

$W_{pc}(p)$ = transfer function of the parallel compensating unit.

Formally, parallel compensation can always be selected so as to obtain the same result as in series compensation, and conversely.

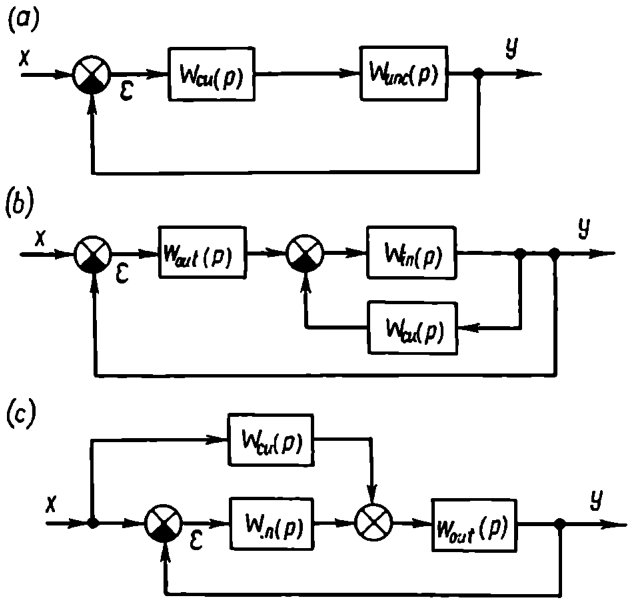

Fig. 11.1

Equating the right-hand parts of Eqs. (11.1) and (11.2), bearing in mind that $W_{in}(p)\, W_{out}(p) = W_{unc}(p)$, we have the transfer functions of compensating units of two identical systems one of which has a parallel and the other, a cascade, compensation:

$$\left.\begin{aligned} W_{cc}(p) &= \frac{1}{1 + W_{in}(p)\, W_{pc}(p)} \\ W_{pc}(p) &= \frac{1 - W_{cc}(p)}{W_{in}(p)\, W_{cc}(p)} \end{aligned}\right\} \tag{11.3}$$

In practice the choice of a compensating circuit depends on the operational characteristics of the functional elements.

The use of parallel compensation is known to increase the stability of the system responses, which follows directly from expression (11.2) for complex gain of an open-loop compensated system.

In the frequency range where $|W_{in}(j\omega)\ W_{cu}(j\omega)| \gg 1$ the transfer function

$$W_{com}(j\omega) \approx \frac{W_{out}(j\omega)}{W_{cu}(j\omega)} \tag{11.4}$$

where W_{cu} = transfer function of the compensating unit; the system responses as a whole are practically independent of those of the main functional elements inside the compensating feedback.

The third structural diagram (Fig. 11.1*c*) shows disturbance compensation. The compensating unit is included in this case in a supplementary feedforward loop along which the disturbing signal x to be measured is introduced into the system. In its principle of action the disturbance compensation differs substantially from the two above. The structural diagram shows that such compensation cannot affect the free oscillations and stability of a closed-loop system; it improves the system performance by reducing dynamic errors induced by a disturbing action which is to be compensated.

Let us see how the image of the system dynamic error is related with the transfer functions of individual units when using disturbance compensation. By the superposition principle, which is valid for linear systems, we can write down the expression for the image of a misalignment

$$E(p) = \frac{1}{1+W_{in}(p)\,W_{out}(p)}\,X(p) - \frac{W_{cu}(p)\,W_{out}(p)}{1+W_{in}(p)\,W_{out}(p)}\,X(p) =$$

$$= \frac{1-W_{cu}(p)\,W_{out}(p)}{1+W_{in}(p)\,W_{out}(p)}\,X(p) \tag{11.5}$$

This expression leads to the unexpected conclusion that by selecting the compensating unit transfer function from the condition

$$W_{cu}(p) = \frac{1}{W_{out}(p)} \tag{11.6}$$

the dynamic error of the system can be eliminated irrespective of the kind of action X.

The use of this method of compensation involves technical difficulties which prevent complete elimination of the dynamic error. This is attributable, in particular, to the fact that the transfer function $W_{out}(p)$ represents, as a rule, an integrating, inertial or oscillatory element, or a combination of the three. Thence the compensating element transfer function should correspond to differentiating elements, whose practical implementation is difficult.

The above classification of automatic control system compensation methods does not imply that they are mutually exclusive.

On the contrary, for example in systems with disturbance compensation, the desired stability margin is achieved by using either cascade or parallel compensation.

Methods of design. How is a circuit selected and parameters for a compensating unit calculated?

A large number of chiefly approximate methods of compensating unit design are available now of which the most widespread (in engineering) are *graph-analytical methods* using the inverse and logarithmic frequency responses of an open-loop system. Indirect estimates of transient performance (not requiring solution of a system of differential equations) such as the phase margin, magnitude margin, oscillation index, cutoff frequency, which can be determined in a straightforward way from frequency responses (see Ch. X), are widely used.

Another group includes *analytical methods*. A function is found which analytically relates the system performance index with the parameters of the compensating unit, and those values of the parameters are to be found that correspond to the extremal value of the function. These methods may use integral criteria of transient performance and the r.m.s. error criterion.

Computers, especially analog computers, simplify to a great extent direct solution of differential equations and construction of transient processes. Therefore there is a trend to avoid approximate methods and solve the design problem by directed examination of solutions of the initial system of differential equations with variable-parameters of the compensating unit. The design reduces then to the problem of search; the basic difficulty here is the elaboration of a program or an algorithm whereby one could find the most suitable parameters of system adjustment as fast as possible.

The appropriate algorithms are discussed elsewhere in this course.

This chapter treats the design methods using logarithmic frequency responses of a system.

11.2. COMPENSATING UNITS BASED ON LOGARITHMIC RESPONSES

Selection of desired logarithmic amplitude-frequency response (LAFR). Asymptotic logarithmic amplitude-frequency and phase-frequency responses were shown (see Ch. III) to be easy to obtain and therefore widely used in engineering calculations. These responses can be used to estimate the performance as well as to check the stability of a system. One of the basic problems in the design of a compensating unit is to build the desired logarithmic amplitude and phase responses of a compensated system.

For minimal-phase systems the logarithmic amplitude-frequency response would be sufficient; it will be referred to in further discussion as the *system response*.

The design of the desired response cannot be completely formalized but certain general recommendations can be made.

1. The response of an uncompensated system and the desired response of a compensated system should coincide in the widest possible range, otherwise the implementation of compensating units becomes very complicated, especially if the cutoff frequency and the high-frequency gain are to be increased.

2. At low frequencies the slope of the response should be -20ν db/dec, where ν is the astatic order of the system.

The low-frequency asymptote at a frequency $\omega = 1$ has an ordinate $20 \log k$, where k is the overall system gain.

If the system dynamic error Δ_1 is given at low-frequency harmonic oscillations of the control action (frequency ω_1), then the reference point can be calculated above which the desired response should pass.

As shown in Sec. 9.2, the system dynamic error at low frequencies is

$$\Delta_{dyn} \approx | W_{o-l}^{-1} (j\omega_1) | A_1 \tag{11.7}$$

where A_1 = amplitude of the input control action $x = A_1 \sin \omega_1 t$;
$| W_{o-l} (j\omega_1) |$ = magnitude of the open-loop gain.

Equation (11.7) gives

$$L(\omega_1) = 20 \log \frac{A_1}{\Delta_{dyn}} \tag{11.8}$$

By drawing the desired response 3 db above the point with the coordinates $L(\omega_1)$, ω_1 we ensure that the dynamic error does not exceed the predetermined value.

If the maximal rate $\dot{x}_{1max}$ and the acceleration $\ddot{x}_{1max}$ are constrained by the condition $\dot{x}_{1max} \leqslant v$ and $\ddot{x}_{1max} \leqslant a$, the limit values of the harmonic oscillation amplitude and frequency are found from the equations

$$\left.\begin{aligned} A_1 &= \frac{v^2}{a} \\ \omega_1 &= \frac{a}{v} \end{aligned}\right\} \tag{11.9}$$

and the coordinates of the reference point are equal, respectively, to

$$\left.\begin{aligned} L(\omega_1) &= 20 \log \frac{v^2}{a\Delta_{dyn}} \\ \omega_1 &= \frac{a}{v} \end{aligned}\right\} \tag{11.10}$$

3. At a cutoff frequency equal to ω_{cf} or when

$$20 \log | W_{o-l} (\omega_{cf}) | = 0$$

the slope of the desired LAFR should be selected equal to —20 db/dec, which as a rule ensures a sufficient phase margin (see Sec. 10.2).

The desired cutoff frequency can be approximately estimated by the formula

$$\omega_{cf} \geqslant \frac{k\pi}{t_c} \tag{11.11}$$

where t_c = specified transient time

k = coefficient, which is found from the graph of Fig. 11.2 from the specified value of overshoot ε_{max}.

Relation (11.11) has been obtained by graphical plotting of transient processes attributable to standard real frequency responses.

4. The desired response of the entire compensated system or its separate conjugation frequencies can be selected by using the nomograms given in Ref. 15 and the specified values of ε_{max}, t_c, t_{max}, ω_t, M (see Fig. 10.9).

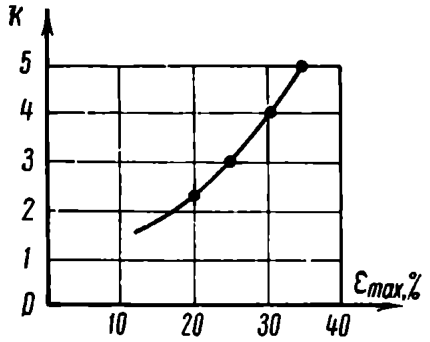

Fig. 11.2

Design of a cascade compensation based on logarithmic responses. When a cascade compensation is used (see Fig. 11.1*a*), the amplitude and phase responses of a compensated system are given by the following equations

$$\left.\begin{aligned} L_{com}(\omega) &= L_{unc}(\omega) + L_{cu}(\omega) \\ \varphi_{com}(\omega) &= \varphi_{unc}(\omega) + \varphi_{cu}(\omega) \end{aligned}\right\} \tag{11.12}$$

It follows from this equation that the responses of a compensating unit are found by subtracting the logarithmic responses of the uncompensated system from those of the desired compensated system

$$\left.\begin{aligned} L_{cu}(\omega) &= L_{com}(\omega) - L_{unc}(\omega) \\ \varphi_{cu}(\omega) &= \varphi_{com}(\omega) - \varphi_{unc}(\omega) \end{aligned}\right\} \tag{11.13}$$

Using the logarithmic frequency responses, one must find a proper electric circuit of compensation and calculate the numerical values of its parameters.

By way of illustration, Fig. 11.3*a* shows the response $L_{unc}(\omega)$ of a system consisting of three inertial elements with time constants

$$T_1 = \frac{1}{\omega_1}, \qquad T_2 = \frac{1}{\omega_2}, \qquad T_3 = \frac{1}{\omega_3}$$

The compensated system response, $L_{com}(\omega)$, for this case is plotted with an allowance for the desired phase margin γ_{cf}.

The compensating loop response of Fig. 11.3*b* resulting from Eq. (11.13) can be given as a sum of two components one of which, $L'_{cu}(\omega)$, represents an inertialess amplifier with a gain of 20 log k_{cu}, and the other, $L''_{cu}(\omega)$, an electric circuit the parameters of which

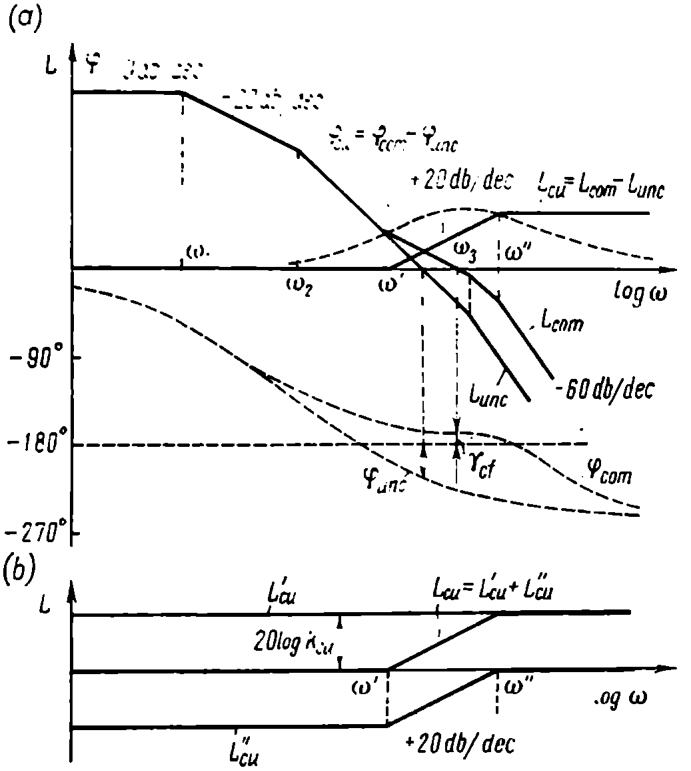

Fig. 11.3

correspond to an elastic element (see Ch. III) and can be calculated from conjugation frequencies ω' and ω''.

Example 11.1. Let a control system be given which consists of an inertial element and an integrator. The numerical values of the parameters are $T_M = 0.25$ sec, $k = 200$.

It is required to design a system with a cutoff frequency of at least $40\frac{1}{\text{sec}}$ and a phase margin equal to 30°. The overall open-loop gain should remain unchanged.

Figure 11.4*a* gives the $L_{unc}(\omega)$ of the specified system, for which $\omega_{cf} = 30\frac{1}{\text{sec}}$, $\gamma_{cf} = 6°$. The phase margin is clearly insufficient. The desired response $L_{com}(\omega)$ must be traced so as to coincide

with $L_{unc}(\omega)$ in the low-frequency range $\omega < \omega_1$, to have a slope of -20 db/dec in the medium-frequency range, pass through the cutoff frequency

$$\omega_{cf} = 40 \frac{1}{\text{sec}}$$

and go parallel to $L_{unc}(\omega)$ in the high-frequency range $\omega > \omega_2$.

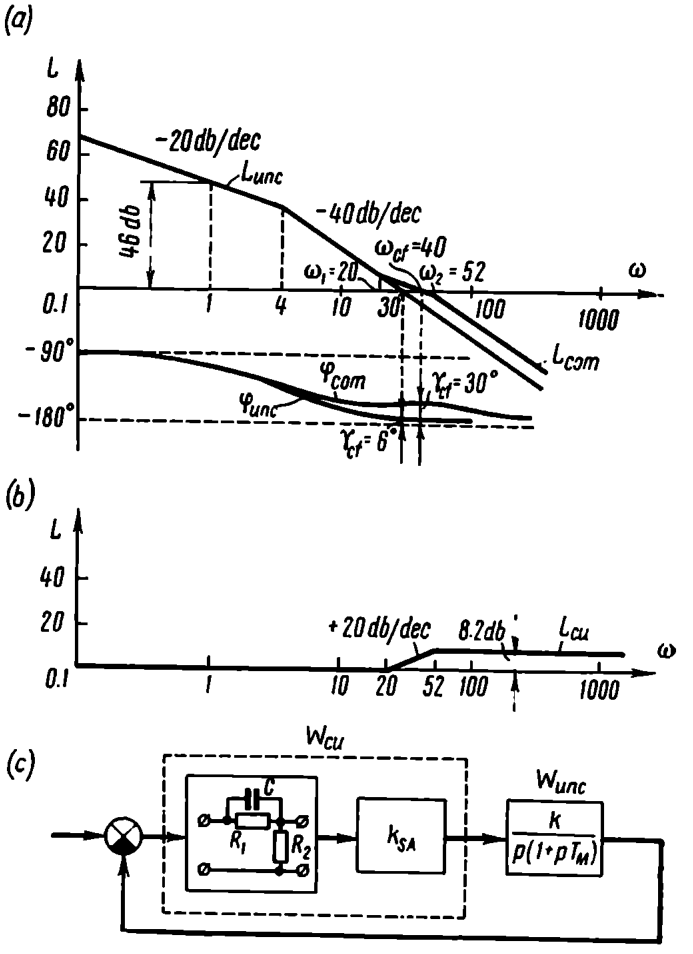

Fig. 11.4

The conjugation frequencies of $L_{com}(\omega)$ breaking points can be found in the following way: $\omega_1 = 20 \frac{1}{\text{sec}}$ is determined directly from the plotting of $L_{com}(\omega)$, ω_2 from the expression for the phase-

frequency response at the cutoff frequency

$$30° - 180° = -150° = -90° - \arctan 40 \cdot 0.25 + \\ + \arctan 40 \cdot \frac{1}{20} - \arctan 40 \frac{1}{\omega_2}$$

From this equation we find $\omega_2 = 52 \frac{1}{\text{sec}}$.

The compensating unit response is given in Fig. 11.4*b* and it corresponds to series connection of an elastic differentiating loop and a supplementary amplifier (Fig. 11.4*c*). The transfer function of this unit is

$$W_{cu}(p) = \frac{k_{SA}(1+pT_1)}{1+pT_2}$$

The numerical values of the parameters are found from the response and from Eq. (3.63):

$$T_1 = R_1 C = \frac{1}{\omega_1} = 0.05 \text{ sec}, \qquad T_2 = \frac{R_1 C R_2}{R_1 + R_2} = \frac{1}{\omega_2} = 0.019 \text{ sec},$$

$$\frac{T_1}{T_2} = \frac{R_1 + R_2}{R_2} = \frac{\omega_2}{\omega_1} = k_{SA} = 2.6 \qquad (20 \log 2.6 = 8.2 \text{ db})$$

Example 11.2. Given an uncompensated control system with a transfer function

$$W_{unc}(p) = \frac{2}{p(1+0.25p)(1+0.0625p)}$$

It is required to increase the open-loop gain 20 times over (by 26 db) without substantial deterioration in the system transient performance. The admissible decrease of the phase margin is 5°.

The response $L_{unc}(\omega)$ of Fig. 11.5*a* shows that the phase margin of the uncompensated system at the cutoff frequency $\omega = 2 \frac{1}{\text{sec}}$ is $\gamma_1 = 56°$.

The desired response should be increased by 26 db at low frequencies and coincide with $L_{unc}(\omega)$ at medium and high frequencies.

The phase of the compensated system can be written as (Fig. 11.5*a*)

$$\varphi_{com}(\omega) = -90° - \arctan \frac{\omega}{\omega_1} + \arctan \frac{\omega}{\omega_2} - \\ - \arctan \omega \cdot 0.25 - \arctan \omega \cdot 0.0625$$

Substituting into this equation $\omega = \omega_{cf} = 2 \frac{1}{\text{sec}}$ and bearing in mind that $\omega_1 = \frac{\omega_2}{20}$ and $\varphi_{com}(\omega_{cf}) = -180 + 51 = -129°$, we have

$$-6° = -\arctan 2 \frac{20}{\omega_2} + \arctan \frac{2}{\omega_2}$$

From this equation $\omega_2 = 0.22 \frac{1}{\text{sec}}$, $\omega_1 = 0.011 \frac{1}{\text{sec}}$. The response $L_{cu}(\omega) = L_{com}(\omega) - L_{unc}(\omega)$ is plotted in Fig. 11.5*b*.

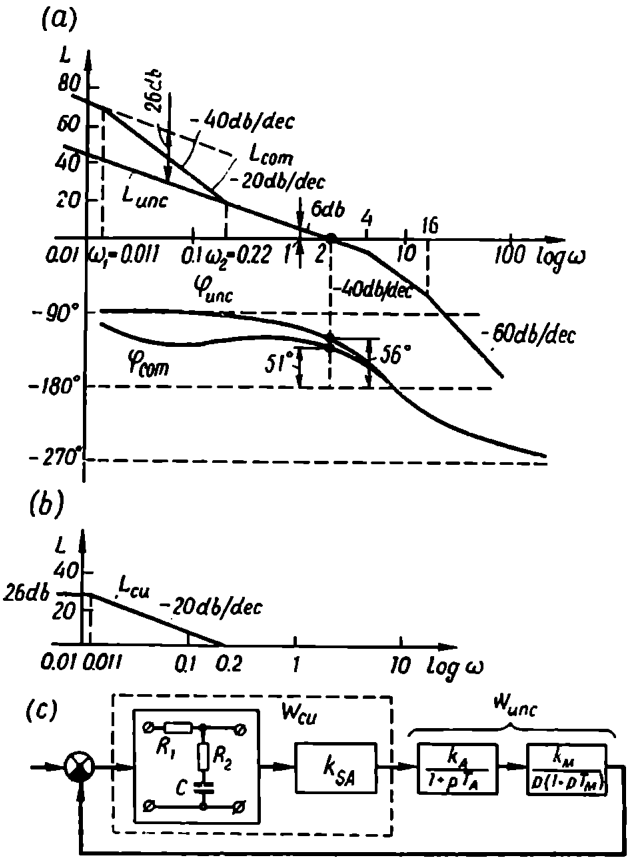

Fig. 11.5

The compensating unit can be represented as a series connection of an elastic integrating loop (see Ch. III) and a supplementary amplifier (Fig. 11.5*c*).

The transfer function of the compensating unit is

$$W_{cu}(p) = \frac{k_{SA}(1+pT_2)}{1+pT_1}$$

The numerical values of the parameters are found from the response $L_{cu}(\omega)$ by Eqs. (3.62)

$$T_1 = \frac{1}{\omega_1} = R_2 C \frac{R_1 + R_2}{R_2} = 90 \text{ sec},$$

$$T_2 = \frac{1}{\omega_2} = R_2 C = 4.5 \text{ sec},$$

$$k_{SA} = \frac{T_1}{T_2} = \frac{R_1 + R_2}{R_2} = 20$$

Design of a parallel compensating unit by means of LAFR. This problem is not so simple as in the case of cascade compensation. The starting point for plotting $L_{cu}(\omega)$ is Eq. (11.2).

In the frequency range where $|W_{cu}(j\omega) W_{in}(j\omega)| \ll 1$ Eq. (11.2) takes the form

$$W_{com}(j\omega) \approx W_{out}(j\omega) W_{in}(j\omega) = W_{unc}(j\omega) \qquad (11.14)$$

or, for logarithmic frequency responses,

$$\left.\begin{aligned} L_{com}(\omega) &\approx L_{unc}(\omega) \\ \varphi_{com}(\omega) &\approx \varphi_{unc}(\omega) \end{aligned}\right\} \qquad (11.15)$$

In the frequency range where the inequality $|W_{cu}(j\omega) W_{in}(j\omega)| \gg 1$ is valid we have

$$W_{com}(j\omega) \approx \frac{W_{unc}(j\omega)}{W_{cu}(j\omega) W_{in}(j\omega)} = \frac{W_{out}(j\omega)}{W_{cu}(j\omega)} \qquad (11.16)$$

whence

$$\left.\begin{aligned} L_{com}(\omega) &\approx L_{unc}(\omega) - L_{cu}(\omega) - L_{in}(\omega) \\ \varphi_{com}(\omega) &\approx \varphi_{unc}(\omega) - \varphi_{cu}(\omega) - \varphi_{in}(\omega) \end{aligned}\right\} \qquad (11.17)$$

Consequently, $L_{com}(\omega)$ in parallel correction can be approximately given for each frequency range by two approximate expressions

$$\left.\begin{aligned} L'_{com}(\omega) &\approx L_{com}(\omega) \quad \text{at} \quad |W_{cu}(j\omega) W_{in}(j\omega)| \ll 1 \\ L''_{com}(\omega) &\approx L_{unc}(\omega) - L_{cu}(\omega) - L_{in}(\omega) \quad \text{at} \quad |W_{cu}(j\omega) W_{in}(j\omega)| \gg 1 \end{aligned}\right\} \qquad (11.18)$$

Thus $L_{cu}(\omega)$ is given by the equation

$$L_{cu}(\omega) = L_{unc}(\omega) - L_{com}(\omega) - L_{in}(\omega) \qquad (11.19)$$

when $L_{cu}(\omega) + L_{in}(\omega) \gg 0$.

The conjugation frequencies at which the transition from one response to another occurs are given by the equation

$$|W_{in}(j\omega) W_{cu}(j\omega)| = 1$$

or

$$L_{in}(\omega) + L_{cu}(\omega) = 0 \qquad (11.20)$$

Graphically this frequency is given by the intersection points of the resulting response $L_{in}(\omega) + L_{cu}(\omega)$ with the axis 0 db. Considering $L_{com}(\omega)$ as two conjugate responses, the following sequence can be suggested for the design of the parallel compensating unit parameters:

(a) the LAFR of the uncompensated system is plotted on the basis of principal functional unit parameters;

(b) the desired LAFR of the compensated system, $L_{com}(\omega)$, is plotted according to the recommendations of this chapter;

(c) the overall response $L_{cu}(\omega) + L_{in}(\omega)$ is found by subtracting $L_{com}(\omega)$ from the response $L_{unc}(\omega)$;

(d) with an allowance for the requirements imposed on the system and for feasibility, the structural diagram of the compensated

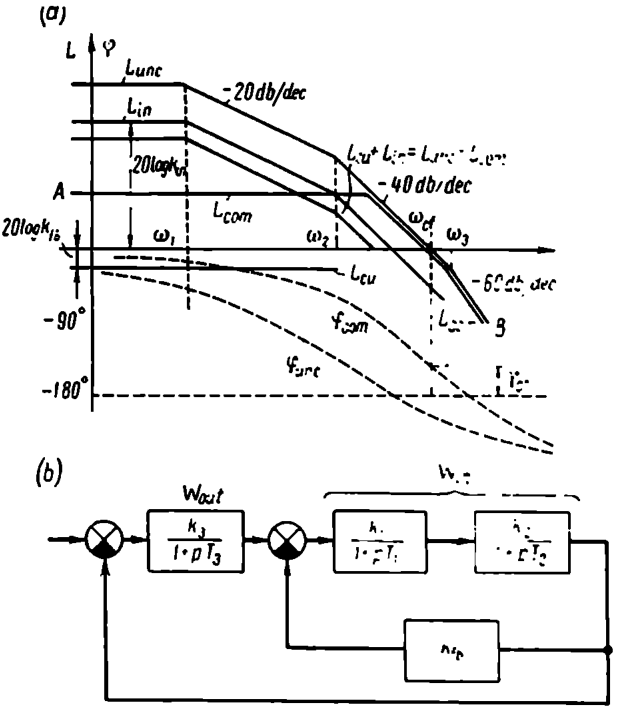

Fig. 11.6

system is found (i.e. the input and output points of parallel compensation are determined), following which the logarithmic response $L_{in}(\omega)$ of system elements in the compensation loop is plotted;

(e) subtracting the response $L_{in}(\omega)$ from the response $L_{cu}(\omega) + L_{in}(\omega)$ (in the frequency range where $L_{cu}(\omega) + L_{in}(\omega) > 0$) we find the logarithmic frequency response of the desired compensating unit in the compensating feedback loop;

(f) using the shape of $L_{cu}(\omega)$, the electric circuit is selected and the compensating unit parameters calculated.

Figure 11.6*a* shows some LAFR explaining the design of parallel compensation by the above method. The initial system consists of three inertial elements. The feedback loop encloses two of them with the largest time constants

$$T_1 = \frac{1}{\omega_1} \quad \text{and} \quad T_2 = \frac{1}{\omega_2}$$

In this example the desired response L_{com} (the broken line AB) is selected, contrary to the general recommendation, with a slope of 40 db/dec at ω_{cf}. Calculations show that this may yield the desired phase margin γ_{cf} (see the curve φ_{com}).

The response $L_{cu}(\omega)$ obtained is a horizontal straight line with a y-line value equal to 20 log k_{fb}, where k_{fb} is the gain of less-than-unity proportional feedback.

The structural diagram of the compensated system is given in Fig. 11.6*b*.

Example 11.3. Determine the parameters of a parallel compensating unit of a servo system whose structural diagram is given

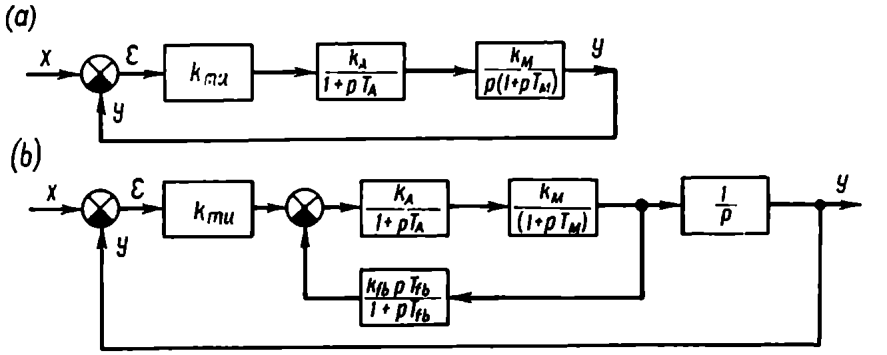

Fig. 11.7

in Fig. 11.7*a*. Here

$$k_{mu} = 855 \frac{V}{\text{rad}}, \quad k_A = 26, \quad k_M = 0.0092 \frac{\text{rad}}{\text{sec} \cdot V},$$
$$T_A = 0.02 \text{ sec}, \qquad T_M = 1.53 \text{ sec}$$

Parallel compensation should be introduced in order to keep the transient time down to 0.8 sec and the overshoot down to 50%. The total gain should be retained

$$D = k_{mu} k_A k_M = 200 \frac{1}{\text{sec}}$$

The uncompensated system responses $L_{unc}(\omega)$ and $\varphi_{unc}(\omega)$ are given in Fig. 11.8.

The desired response $L_{com}(\omega)$ is plotted so as to coincide at low and high frequencies with $L_{unc}(\omega)$ (to retain the value of D). In the

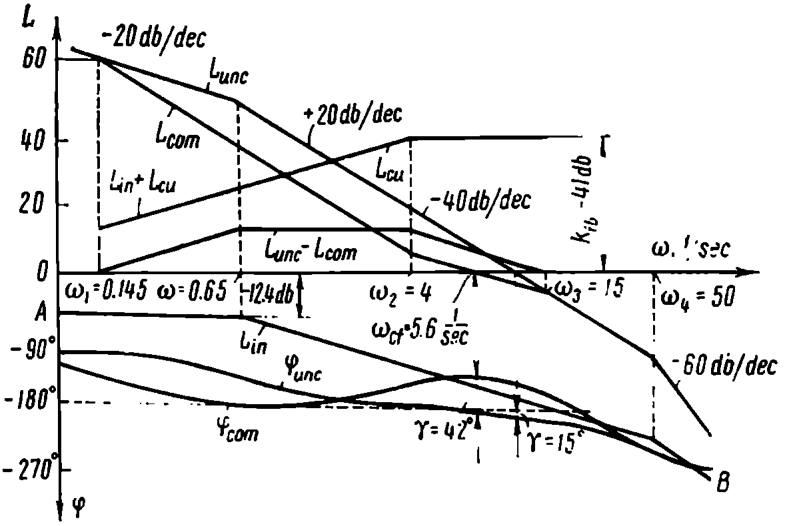

Fig. 11.8

region of the cutoff frequency it goes below $L_{unc}(\omega)$ with a slope of —20 db/dec.

Figure 11.8 shows the response $L_{in}(\omega) + L_{cu}(\omega)$ resulting from the subtraction $L_{unc}(\omega) - L_{com}(\omega)$.

For elements included in the rate feedback we select an amplifier and a motor with the overall transfer function (Fig. 11.7*b*)

$$W_{in}(p) = \frac{0.23}{(1+p0.02)(1+p1.5)}$$

The response L_{in} is given as a broken line, AB, which corresponds to this transfer function, and has a gain of 12.4 db in the low-frequency range $\omega \leqslant 0.65$.

The compensating unit response

$$L_{cu}(\omega) = L_{unc}(\omega) - L_{com}(\omega) - L_{in}(\omega)$$

consists of a part with a slope of +20 db/dec and a horizontal part with a gain of 41 db. The pattern of $L_{cu}(\omega)$ leads to a rate feedback as a compensating circuit: $k_{fb} = 105 \frac{V \cdot \text{sec}}{\text{rad}}$ [41 db]

$$T_{fb} = \frac{1}{\omega_2} = 0.25 \text{ sec}$$

The structural diagram of the compensated system is given in Fig. 11.7*b*.

Automatic control systems are more often than not compensated by passive d.c. four-terminal networks whose typical electric circuits, complex gains, and responses are given in Table 11.1. Using this table and knowing the shape of the compensating unit response resulting from the design of cascade or parallel compensation, the necessary electric circuit can be selected and its parameters calculated.

In a.c. carrier-frequency-operated control systems, d.c. four-terminal networks are not expedient since they require a supplementary modulator and demodulator.

A.c. systems can be compensated by carrier-frequency-operated four-terminal networks. The best circuit is a double T-bridge. The different versions of its connection are shown in Table 11.2. It should be remembered that the values of complex gains and responses given in the table are approximate and valid only in the range $\omega \ll \omega_{car}$, where ω_{car} is the carrier frequency.

Table 11.1 **Basic Passive Four-Terminals Used as Compensators**

Diagram	Complex Gain	Logarithmic Amplitude-Frequency and Phase-Frequency Responses
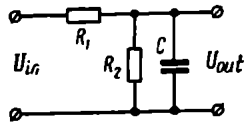	$W(j\omega)=k$ $k=\dfrac{R_2}{R_1+R_2}\ll 1$	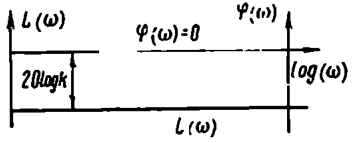
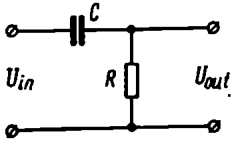	$W(j\omega)=\dfrac{j\omega T}{1+j\omega T}$ $T=RC$	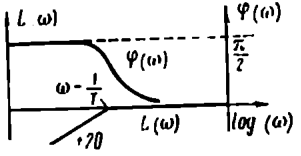
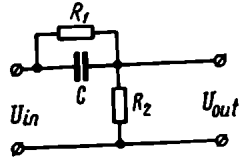	$W(j\omega)=\dfrac{k(1+j\omega T)}{1+j\omega Tk}$ $T=CR_1$ $k=\dfrac{R_2}{R_1+R_2}\ll 1$	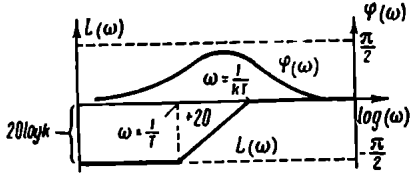

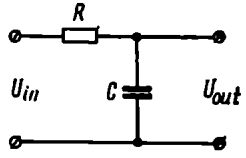	$W(j\omega) = \frac{1}{1+j\omega T}$ $T = RC$	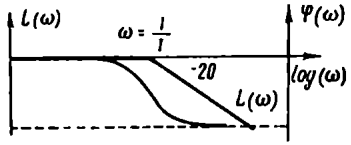
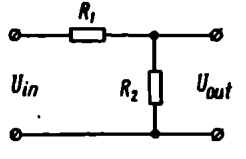	$W(j\omega) = \frac{k}{1+j\omega T}$ $k = \frac{R_2}{R_1+R_2} \ll 1$ $T = C\frac{R_1R_2}{R_1+R_2}$	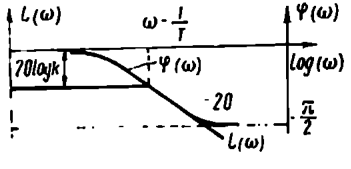
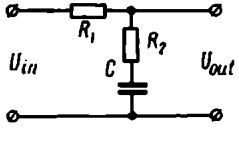	$W(j\omega) = \frac{1+j\omega T}{1+j\omega Tk}$ $T = R_2C$ $k = \frac{R_1+R_2}{R_2}$	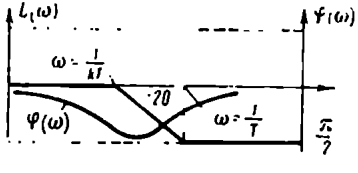

Table 11.1 (cont'd)

Diagram	Complex Gain	Logarithmic Amplitude-Frequency and Phase-Frequency Responses
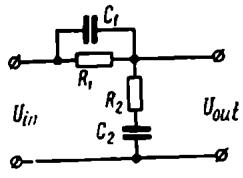	$W(j\omega)=\dfrac{(1+j\omega T_1)(1+j\omega T_2)}{(1+j\omega T_3)(1+j\omega T_4)}$ $T_1=R_1C_1,\ T_2=R_2C_2,\ T_3T_4=T_1T_2$ $T_3+T_4=T_1+T_2\left(1+\dfrac{R_1}{R_2}\right)$	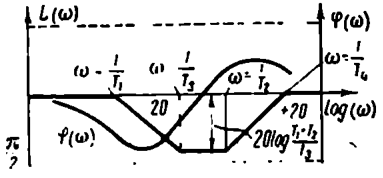
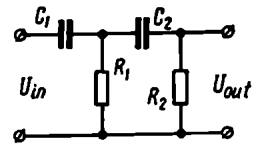	$W(j\omega)=\dfrac{-T_1T_2\omega^2}{1+(T_1+T_2+R_1C_2)\,j\omega+T_1T_2(j\omega)^2}$ $T_1=R_1C_1,\ T_2=R_2C_2$	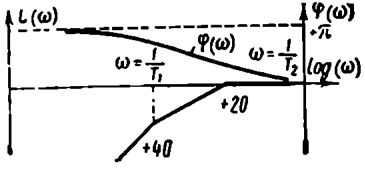
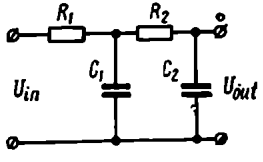	$W(j\omega)=\dfrac{1}{1+(T_1+T_2+R_1C_2)\,j\omega+T_1T_2\omega^2}$ $T_2=R_1C_1,\ T_1=R_2C_2$	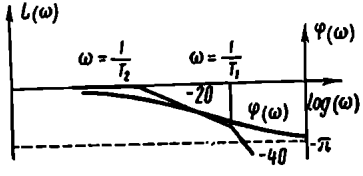

Table 11.2. **A.C. Compensating Circuits**

Diagram	Complex Gain	Logarithmic Amplitude-Frequency and Phase-Frequency Responses
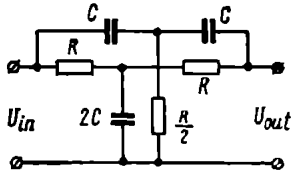	$W(j\omega) = j\omega T_{eq}$ $T_{eq} = \frac{1}{2\omega_{car}} = \frac{RC}{2}$	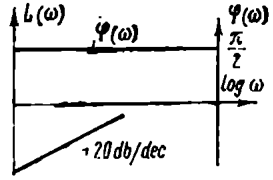
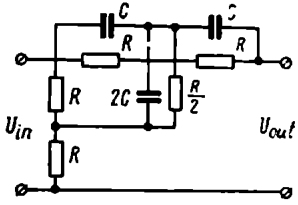	$W(j\omega) = k(1 + j\omega T'_{eq})$ $T'_{eq} = \frac{1}{2\omega_{car}} \frac{R_1}{R_2}$ $k = \frac{R_2}{R_1 + R_2}$	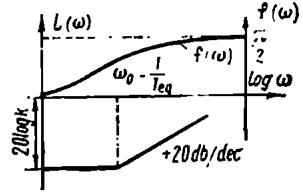
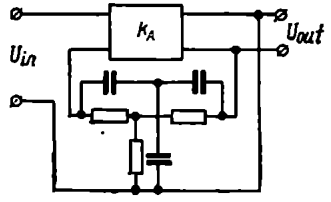	$W(j\omega) = \frac{k_A}{1 + jk_A\omega T_{eq}}$ as $k_A \to \infty$ $W(j\omega) \approx \frac{1}{j\omega T_{eq}}$ $T_{eq} = \frac{1}{2\omega_{car}} = \frac{RC}{2}$	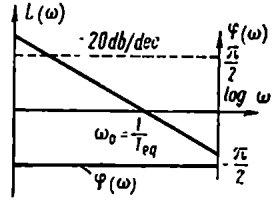

Chapter XII

SAMPLED-DATA CONTROL SYSTEMS. EQUIVALENT CIRCUITS, SPECTRA AND IMAGES OF PULSE SIGNALS

12.1. EXAMPLES OF SAMPLED-DATA CONTROL SYSTEMS

Sampled-data control systems (also known as *discontinuous control systems*) are a specific class of systems which sometimes can be described by linear equations. In these systems the misalignment (error) between the reference and the controlled variable is not measured continuously but at discrete time instants known as *sampling points*. These points are, as a rule, equally spaced in time. Within the intervals between the sampling points the control system functions in accordance with the previously measured values of error. The theory of sampled-data control systems was developed by Ya. Z. Tsypkin (Ref. 81).

The representation of a signal by its discrete values $x_0, x_1, x_2, \ldots$ $\ldots, x_l$ shown in Fig. 12.1*a* is sometimes referred to as *time sampling*. In sampled-data control systems a time-sampled signal of error modulates a sequence of control pulses. Any pulse shape and any kind of modulation such as amplitude, pulse-width, phase, and frequency modulation may be used. This chapter will cover the widely used amplitude-modulation system which, as will be shown below, can be described by linear equations.* If the control system includes nonlinear elements, then linearization should be used and small increments considered. In further discussion, however, we will deal with control systems consisting of linear elements only.

Figure 12.1*b* shows rectangular pulses the amplitude of which is modulated by the discrete sequence $x_0, x_1, x_2, \ldots, x_l$. The period of pulse sequencing is denoted as T_p, the pulse width as γT_p, the duty factor as γ, and the modulation coefficient as k_p.

The time sampling of signals generally leads to loss of some information since discrete values do not give any idea of signal varia-

* Pulse-width modulation systems with short pulse duration are equivalent to amplitude modulation systems since the action of a very short pulse depends on its area (see Ch. II). In some systems control pulses are modulated by current rather than instantaneous, values of the error signal, which vary over the pulse duration so that the pulse shape changes in the course of modulation. Such systems are essentially *systems with variable parameters* (variable gain) and are not treated in this book.

tions between sampling points. Different continuous signals can lead to the same sequences of discrete values as shown in Fig. 12.2. In order to better represent the nature of a signal by means of its discrete values the sampling frequency $\omega_p = \frac{2\pi}{T_p}$ should be taken as high as possible.

The principle of sampled-data control is used in digital computer control systems, in multichannel systems of automatic control, in radars, and some other systems.

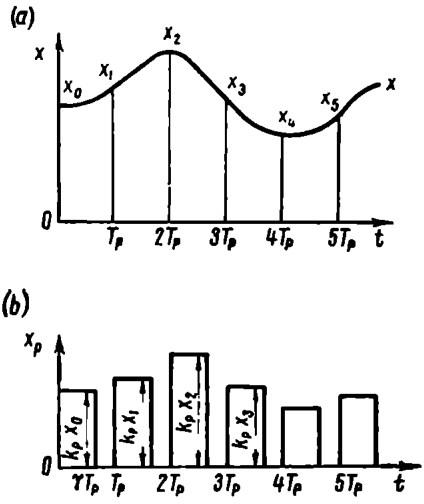

Fig. 12.1

In most cases time-sampled signals have to be used. In digital computer systems this is caused by the fact that most digital computers deliver solutions periodically. In multichannel control systems one controller serves several plants, which also necessitates discontinuous measurements and control in each particular system. In radar systems the input and output signals are pulses and thus the systems themselves are discontinuous or sampled-data systems.

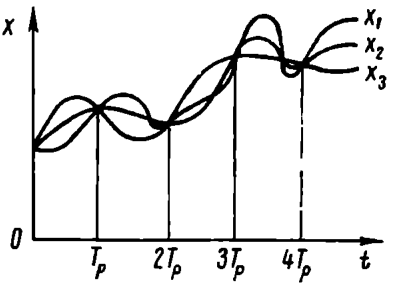

Fig. 12.2

It should be noted that in certain cases (see Ch. XIV) sampled-data control has certain advantages over continuous one and may be preferable.

Let us consider several examples of sampled-data control systems.

Digital servo system. The functional diagram of such a system is shown in Fig. 12.3. The digital servo system serves for proportional conversion, in a certain scale, of the digital input x_d to the rotation angle of the output shaft, y. The input signal is periodically fed to the digital comparator DC as a parallel pulse code. At the same time instants DC receives the parallel digital code y_d, which results from digital measurement of the rotation angle y. The measurement is performed by the analog-to-digital converter AD, which

is designed, for instance, as a code disc. DC subtracts y_d from x_d and delivers at the output the digital error ε_d with a certain delay τ

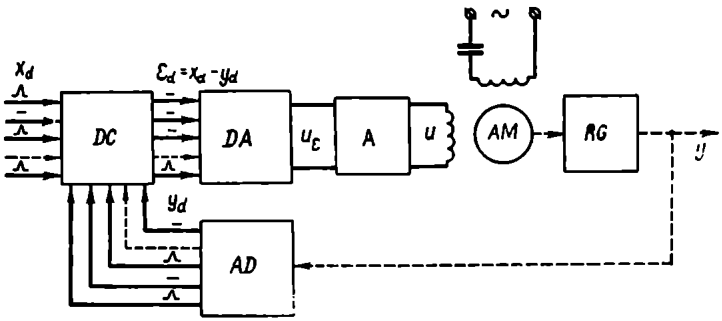

Fig. 12.3

with respect to the time when x_d and y_d are fed. The value of τ depends on the time required for the subtraction in DC; τ is often much smaller than T_p and can be neglected.

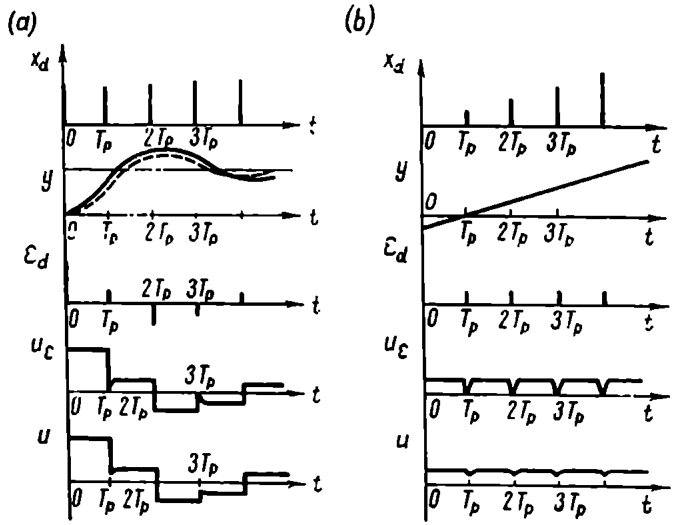

Fig. 12.4

The parallel code of the digital error ε_d is fed to the digital-to-analog converter DA, which includes a register storing ε_d during the time T_p. Directly before the subsequent value of ε_d is fed zeroes are set in all digits of the register. The DA output is an analog value (the a.c. voltage u_ε), which is then amplified by the amplifier A.

The control voltage u is fed to the actuating motor AM (an asynchronous two-phase motor). Using a reducing gear RG the latter rotates the output axis so as to reduce the error ε_d. As a result, the output y "follows up" the input x_d.

Figure 12.4*a* shows time diagrams which characterize the transient process in a digital servo system responding to a step action $x_d(t)$. For comparison, the time diagram of $y(t)$ includes a dotted line for a process in a continuous servo system with the same parameters but with a continuous transmission of signals x_d, y_d, ε_d. With decreasing T_p the difference between the processes in both systems reduces; in the limit, as $T_p \to 0$, the sampled-data system becomes continuous.

Figure 12.4*b* shows steady-state time diagrams corresponding to a linear input signal x_d. As in normal servo systems, y and y_d vary linearly, while the error ε_d is constant. The voltage u_ε is constant except for short pulses, which represent setting the register in DA to zero. In the voltage u these pulses are largely smoothed out.

Digital servo systems are used for conversion of calculation results given by control computers to movements of plant actuators. In addition to generating the signal x_d a digital computer sometimes determines the difference $x_d - y_d$; therefore a digital comparator is unnecessary. Since the computer has to handle quite a number of problems, the period T_p may be rather large ($T_p = 0.1$ to 1 sec). The delay τ can be about 1 msec.

Range tracking radar (automatic ranging radar). The functional diagram of a ranging radar is shown in Fig. 12.5*a*; it includes a strobing unit SU, two integrators I_1 and I_2, time modulator TM, and strobing pulse generator SPG. Figure 12.5*b* shows time diagrams illustrating the operation of the radar over one period T_p.

The sounding pulse SOP (which is sent towards the target) is fed to the time modulator TM, where it is delayed for a time interval depending on the control voltage u. The time modulator may be, for instance, a phantastron. The delayed SOP starts up the strobing pulse generator SPG made up, say, of blocking generators. The SPG generates two strobing pulses SP of opposite polarities, which follow in succession. The shift of the strobing pulse boundary relative to the SOP, τ_y, is proportional to u. The strobing pulses and the echo pulse EP shaped by the shaping unit SPU (e.g. an amplifier with saturation) are fed to the strobing unit SU. The shift of the middle of the EP relative to the SOP, τ_x, is proportional to the target range.

The SU contains two gate circuits. At the output of SU two pulses, P_1 and P_2, with the same amplitude and different polarities are obtained, which are parts of the EP coinciding with the first and second strobing pulses. The difference of P_1 and P_2 duration is proportional to the error $\tau_\varepsilon = \tau_x - \tau_y$. The pulses P_1 and P_2 are fed

to the first integrator I_1, which consists of two diode gates and an integrating RC circuit with a large time constant. The voltage u_C across the capacitor C may be assumed linear when P_1 or P_2 terminates. As a result the increment of the voltage u_C after the cessation

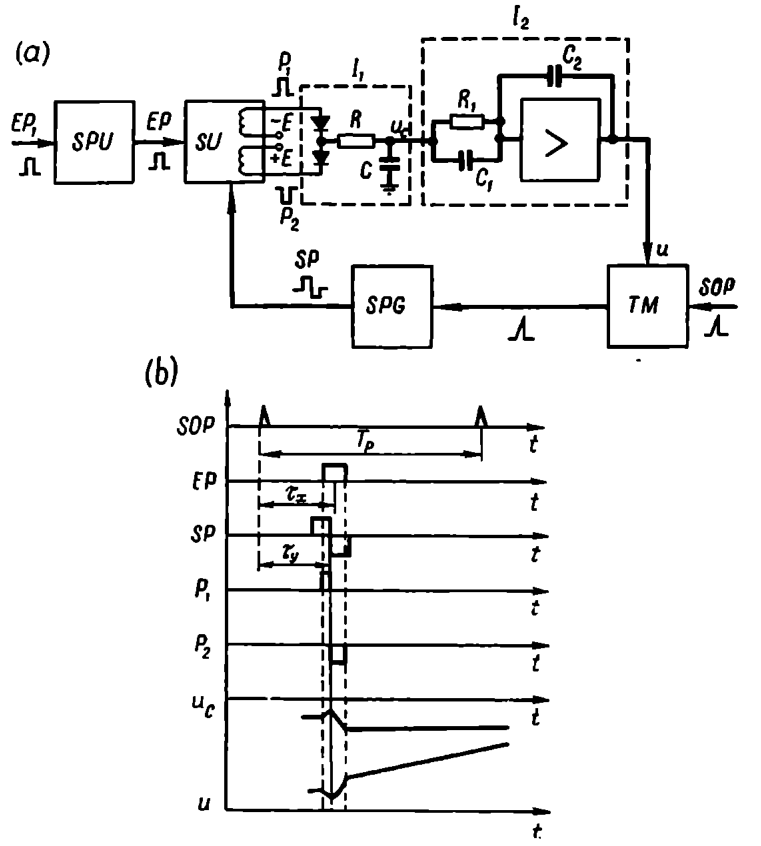

Fig. 12.5

of P_1 and P_2 is proportional (with the opposite sign) to the difference of P_1 and P_2 durations, or to the error τ_ε. The voltage at the output of the I_1 is proportional to the sum of errors τ_ε at all preceding sampling times; the I_1 is thus an adder of discrete values (pulse integrator).

The voltage u_C is fed to the second integrator I_2, which is actually an operational amplifier with a transfer function

$$W(p) = -\frac{1+pT_1}{pT_2}$$

where $T_1 = R_1C_1$, $T_2 = R_1C_2$. The resistor R_1 is selected sufficiently large so that the input of the operational amplifier does not load

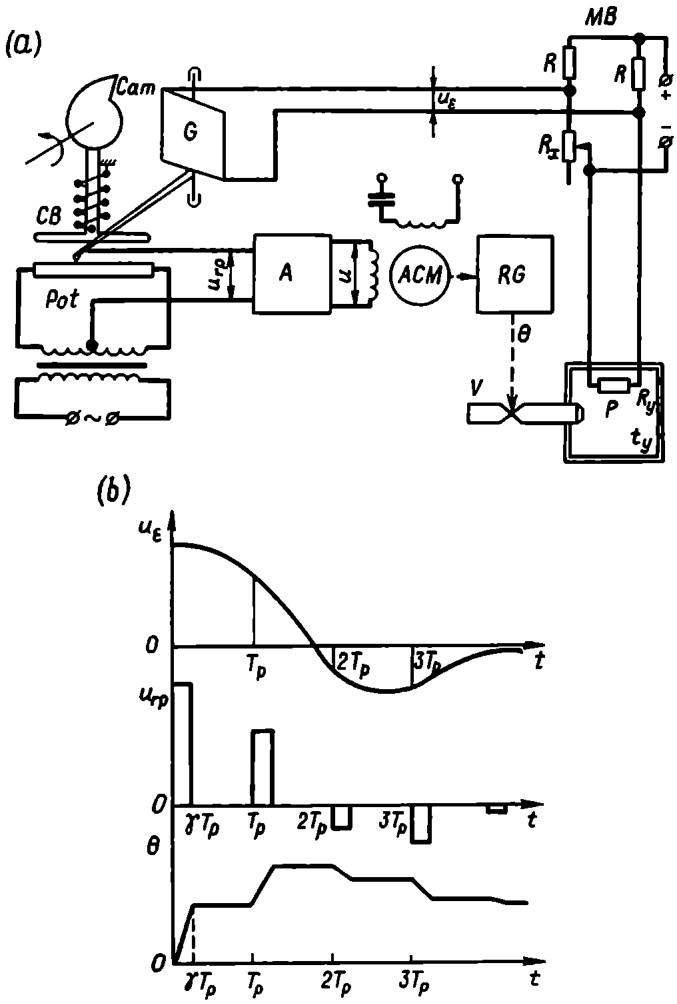

Fig. 12.6

the RC circuit. If the operational amplifier transfer function is given in the form

$$W(p) = -\left(\frac{T_1}{T_2} + \frac{1}{pT_2}\right)$$

its output voltage u is seen to have two components of which one is proportional to u_C and the other, to the integral of u_C. When

P_1 and P_2 cease, the voltage u changes by the linear law. If, as shown in Fig. 12.5*b*, $\tau_x > \tau_y$ ($\tau_\varepsilon > 0$), u increases; as a result τ_y increases by the next sampling, tending to τ_x. If $\tau_\varepsilon < 0$, then u and τ_y decrease.

Consequently, an automatic ranging radar is a sampled-data system which automatically controls the time shift τ_y (and the voltage u which is proportional to it). The input is the time shift τ_x, which varies with the range. The two integrators make the tracking of a constant velocity target a flawless operation. The sounding pulse frequency is normally 100 to 1,000 Hz (T_p = 1 to 10 msec).

Chopper-bar temperature controller. The functional diagram of an automatic temperature control circuit (Fig. 12.6*a*) includes a plant P (a furnace), a measuring bridge MB, a galvanometer G with a chopper-bar CB driven by a cam, an actuating motor AM, a reducing gear RG, a valve V controlling the fuel inflow into the furnace.

The temperature inside the furnace is measured by a thermally-sensitive resistor R_y, which is incorporated in the measuring bridge MB along with the setpoint resistor R_x.

The out-of-balance voltage u_ε is fed to the galvanometer G. The chopper-bar CB performs periodical movements under the effect of a synchronous motor (not shown in the figure) acting through the cam and a leverage system. It periodically presses the galvanometer needle to the potentiometer Pot for a time γT_p. The amplifier A receives rectangular voltage pulses u_{rp} of constant duration γT_p. The amplitude of the pulse is proportional to the values of misalignment measured at the times when the chopper-bar acts (sampling times). The pulses u_{rp} are amplified and fed to the asynchronous two-phase actuating motor AM. Via the reducing gear RG the motor turns the valve V by an angle θ to increase or reduce the fuel feeding rate.

In such a galvanometer power is amplified to a considerable degree; the intermittent contacts between the galvanometer needle and the potentiometer preclude any friction error. The period T_p normally amounts to minutes, since a thermal plant has a high inertia. The chopper-bar controller was one of the first discontinuous controllers.

Figure 12.6*b* shows time diagrams of the signals in the system.

12.2. EQUIVALENT DIAGRAM OF A SAMPLED-DATA CONTROL SYSTEM

Figure 12.7*a* shows a structural diagram of a sampled-data control system, which includes, in addition to a comparator, a control pulse generator or pulse element PE and a continuous part CP with a transfer function $W_{CP}(p)$. The PE block exhibits the shape of control pulses, which is generally arbitrary and is characterized by the function $s(t)$ equal to zero outside the interval $0 < t \leqslant T_p$.

In all practical cases the function $s(t)$ has a finite height and can be normalized by including the modulation coefficient k_p into the gain of the CP, so that $s_{max} = 1$ (Fig. 12.7*b*).

The error signal $\varepsilon(t)$ is sampled in time and its discrete values modulate the amplitude of the PE pulses. If we assume that $\varepsilon(t) = 0$ at $t < 0$, then the pulse signal is

$$\varepsilon_p(t) = \sum_{l=0}^{\infty} \varepsilon(lT_p)\, s(t - lT_p) \qquad (12.1)$$

at $0 \leqslant t < \infty$.

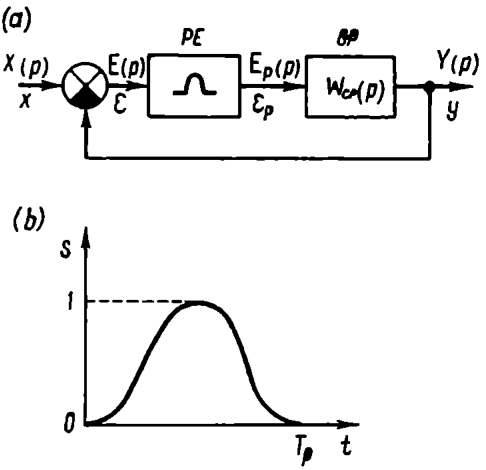

Fig. 12.7

A PE with modulated pulses of arbitrary shape at the output can be conveniently replaced for investigation purposes by a series-connected PE with modulated unit pulses at the output and a shaping element. The response of the latter to a unit pulse (the weighting function)

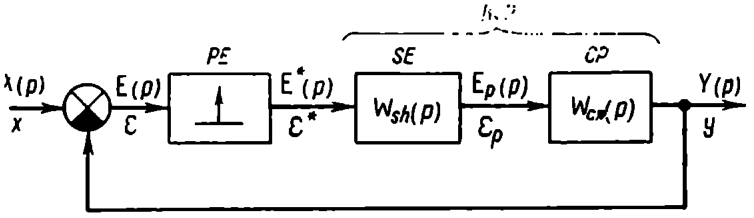

Fig. 12.8

should be identical in its shape to the pulses in the system

$$w_{sh}(t) = s(t) \qquad (12.2)$$

If this is to be achieved, the transfer function of the shaping element must be equal to the image of the function $s(t)$, since the image of a unit pulse is 1, i.e.

$$W_{sh}(p) = S(p) \qquad (12.3)$$

Figure 12.8 is an equivalent diagram of a control system with a simplest possible PE. A unit pulse inside a PE is represented as an arrow of unit length. The shaping element and the continuous part are connected in series to form a reduced continuous part RCP

with the transfer function

$$W_{RCP}(p) = W_{sh}(p)\, W_{CP}(p) \tag{12.4}$$

A modulated pulse train, $\varepsilon^*(t)$, at the output of a simple PE is shown in Fig. 12.9; it can be described as

$$\varepsilon^*(t) = \sum_{l=0}^{\infty} \varepsilon(lT_p)\, \delta(t - lT_p) \tag{12.5}$$

The shaping element transforms this sequence into a sequence of real pulses $\varepsilon_p(t)$ (see Eq. (12.1)) acting on the continuous part of the system.

A simple PE is typical of linear sampled-data systems. Its presence in structural diagrams distinguishes sampled-data systems from continuous ones.

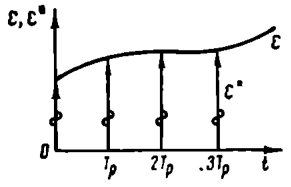

Fig. 12.9

It is an important feature of sampled-data systems that *a PE and a continuous element cannot interchange their places in structural diagram transformations*; in other words, *the commutative law is not observed in the presence of a PE.*

In continuous systems where linear elements with transfer functions W_1 and W_2 are connected in series these elements can be interchanged, with no variations in signal transformation, i.e.

$$W(p) = W_1(p)\, W_2(p) = W_2(p)\, W_1(p)$$

In sampled-data systems the interchange of a PE and a continuous element changes the properties of a circuit (an inertialess element is an exception). Thus in the diagram of Fig. 12.8 the connection of the element W_{sh} before the PE leads to a considerable change in the system characteristics. This subject is treated in more detail in the concluding part of Ch. XIV.

Example 12.1. Let us consider an equivalent circuit of the digital servo system discussed in Sec. 12.1. We will neglect for simplicity the nonlinearities which occur in analog-to-digital conversion and arise from the rounding of the digitalized quantities. The rounding error is normally small and has but a slight impact on the system behaviour. As was shown in Fig. 12.4, the control pulses are of rectangular form and the duty factor is equal to one. A rectangular pulse of unit height and of duration T_p can be represented as a sum of $1_0(t)$ and $1_0(t - T_p)$, as shown in Fig. 12.10. Then the image $S(p)$ and the transfer function $W_{sh}(p)$ are equal

$$W_{sh}(p) = S(p) = \frac{1 - e^{-pT_p}}{p} \tag{12.6}$$

The shaping unit complex gain is

$$W_{sh}(j\omega) = \frac{1-e^{-j\omega T_p}}{j\omega} = T_p \frac{\sin \frac{\omega T_p}{2}}{\frac{\omega T_p}{2}} e^{-j\omega \frac{T_p}{2}} \qquad (12.7)$$

Figure 12.11 portrays frequency responses of a shaping unit giving rectangular pulses of duration T_p. The shaping unit reduces the

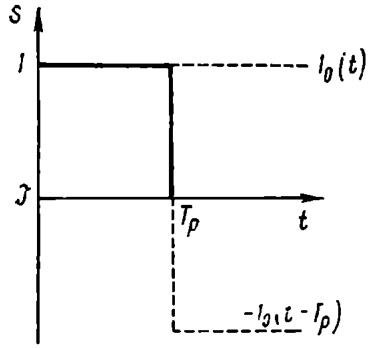

Fig. 12.10

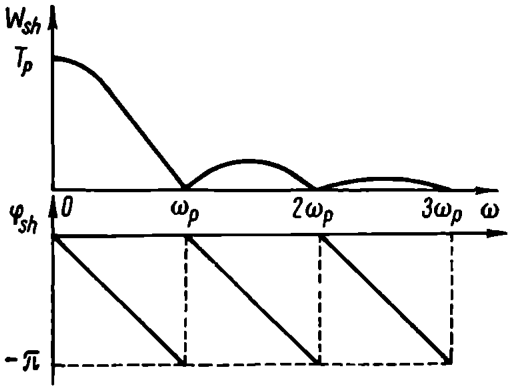

Fig. 12.11

high-frequency components of the signal $\varepsilon^*(t)$. At low frequencies, when $\omega T_p \ll 1$, the properties of the shaping unit are close to those of a delay element with delay time $\frac{T_p}{2}$

$$W_{sh}(j\omega) \approx T_p e^{-j\omega \frac{T_p}{2}} \qquad (12.8)$$

This is illustrated in Fig. 12.12, where the signals $\varepsilon(t)$ and $\varepsilon_p(t)$ are shown and the latter is seen to fall behind the former.

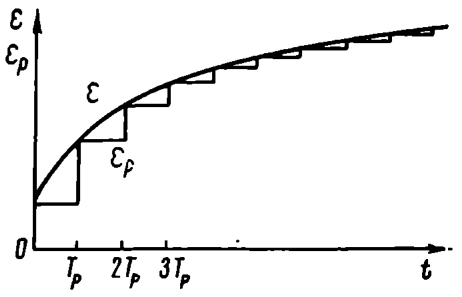

Fig. 12.12

If the electromechanical time constant of the motor T alone is of importance, then the reduced continuous part of a digital servo system will have the transfer function

$$W_{RCP}(p) = \frac{1-e^{-pT_p}}{p} \frac{k}{p(1+pT)} \qquad (12.9)$$

where k is the gain of the continuous part, and the complex gain is

$$W_{RCP}(j\omega) = \frac{-k(1-e^{-j\omega T_p})}{\omega^2(1+j\omega T)} \tag{12.10}$$

12.3. DISCRETE SIGNAL SPECTRA AND IMAGES

Application of Fourier and Laplace transformations to discrete signals. Let us look at the spectrum and image of a discrete signal $x^*(t)$ obtained at the output of a simple PE the input of which is

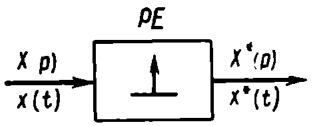

Fig. 12.13

the signal $x(t)$ (Fig. 12.13). We assume that all signals are zero if $t < 0$; all expressions for signals are valid at $t \geqslant 0$. The signal $x^*(t)$ has already been shown to be equal to a sum of modulated and shifted unit pulses

$$x^*(t) = \sum_{l=0}^{\infty} x(lT_p)\,\delta(t - lT_p)$$

The Fourier transform, or the spectrum for one pulse $\delta(t - lT_p)$, is equal to $e^{-j\omega lT_p}$, so the signal spectrum is

$$X^*(j\omega) = \sum_{l=0}^{\infty} x(lT_p)\,e^{-j\omega lT_p} \tag{12.11}$$

The Laplace image of the signal $x^*(t)$ is

$$X^*(p) = \sum_{l=0}^{\infty} x(lT_p)\,e^{-plT_p} \tag{12.12}$$

In Eqs. (12.11) and (12.12) both the spectrum and image of the signal $x^*(t)$ depend on discrete values of $x(lT_p)$. In the literature the transformation (12.12) is often referred to as *discrete Laplace transformation* (Ref. 81).

With substitution $e^{pT_p} = z$ the expression (12.12) takes the form

$$X(z) = \sum_{l=0}^{\infty} x(lT_p)\,z^{-l} \tag{12.13}$$

The resultant formula is called the *z-transformation for discrete values of the signal x*. This notation and the term are also found in the literature (Ref. 31).

One important feature of the discrete signal spectrum is that it is periodic along the frequency axis and its period is $\omega_p = \frac{2\pi}{T_p}$. This fact follows from Eq. (12.11), since

$$e^{-j(\omega+r\omega_p)lT_p} = e^{-j\omega lT_p}\, e^{-jrl2\pi} = e^{-j\omega lT_p}$$

The spectra of discrete signals can therefore be considered in the frequency range $-\frac{\omega_p}{2} < \omega \leqslant \frac{\omega_p}{2}$; for other ranges the pattern is repeated periodically. The range can be halved $0 \leqslant \omega \leqslant \frac{\omega_p}{2}$ if an allowance is made for the property (common for all spectra) that the values of the spectrum for a negative frequency can be obtained from that for the respective positive frequency by conjugation.

The image $X^*(p)$ is also periodic in the p plane along the imaginary axis with period ω_p. Therefore in studying the images $X^*(p)$ we can restrict ourselves to a horizontal band of width ω_p which is symmetrically disposed relative to the real axis (Fig. 12.14)

$$-\frac{\omega_p}{2} < \operatorname{Im} p \leqslant \frac{\omega_p}{2} \qquad (12.14)$$

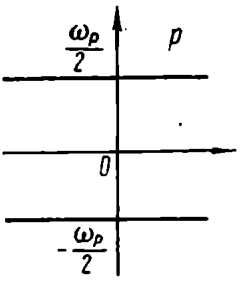

Fig. 12.14

Let us examine several examples of images for simple discrete signals.

Example 12.2. The discrete signal $x^*(t)$ is a single unit pulse

$$x^*(t) = \delta(t)$$

Such a pulse is obtained in feeding an arbitrary $x(t)$ equal to one at $t = 0$ and to zero at $t \geqslant T_p$ (Fig. 12.15*a*) to the input of a *PE*. The signal image is

$$X^*(p) = 1 \qquad (12.15)$$

Example 12.3. The signal $x(t)$ is a unit function $1_0(t)$, $x^*(t)$ is a discrete unit function (Fig. 12.15*b*)

$$x^*(t) = \sum_{l=0}^{\infty} \delta(t - lT_p) \qquad (12.16)$$

By the formula of a sum of an infinite geometric progression with the first term equal to one and the denominator e^{-pT_p} the image $X^*(p)$ is equal to

$$X^*(p) = \sum_{l=0}^{\infty} e^{-plT_p} = \frac{1}{1-e^{-pT_p}} = \frac{e^{pT_p}}{e^{pT_p}-1} \qquad (12.17)$$

Example 12.4. The signal $x(t)$ is an exponent $e^{\alpha t}$, $x^*(t)$ is a discrete exponent (Fig. 12.5*c*)

$$x^*(t) = \sum_{l=0}^{\infty} e^{\alpha l T_p} \delta(t - l T_p) \qquad (12.18)$$

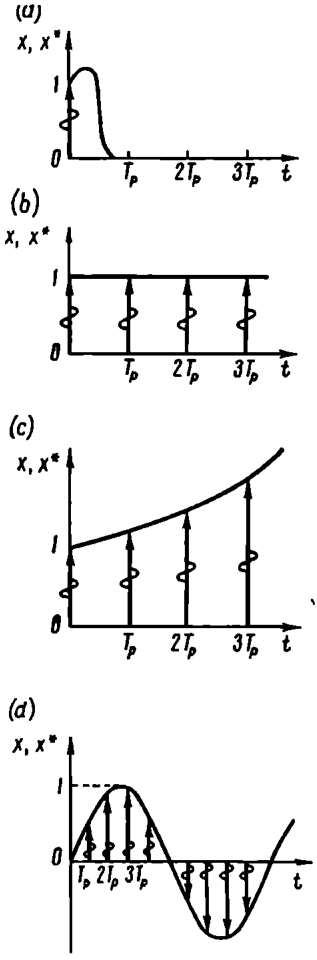

Fig. 12.15

As before, the image is

$$X^*(p) = \sum_{l=0}^{\infty} e^{\alpha l T_p} e^{-p l T_p} =$$

$$= \sum_{l=0}^{\infty} e^{-(p-\alpha) l T_p} = \frac{1}{1 - e^{-(p-\alpha) T_p}} =$$

$$= \frac{e^{pT_p}}{e^{pT_p} - e^{\alpha T_p}} \qquad (12.19)$$

In a particular case, at $\alpha = j\omega$ (a harmonic signal, whose imaginary part is given in Fig. 12.15*d*)

$$X^*(p) = \frac{e^{pT_p}}{e^{pT_p} - e^{j\omega T_p}} \qquad (12.20)$$

Table 12.1 presents the images $X^*(p)$ for $x^*(t)$ obtained by feeding signals $x(t)$ described by some typical functions to the input of a PE. Images $X(p)$ are also given there.

Relation between spectra and images of discrete and continuous signals.

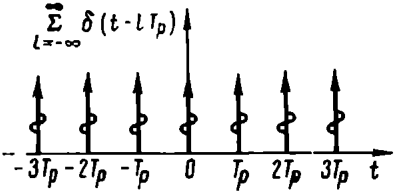

Fig. 12.16

Let us find the relation between the spectra of the discrete signal $x^*(t)$ at the output of a PE and of the signal $x(t)$ at its input. For this purpose we will consider a periodic function formed by unit pulses appearing after every T_p interval over the entire time range $-\infty < t < \infty$ (Fig. 12.16). This function can be given by a Fourier

Table 12.1

	$x(t)$ at $t \geqslant 0$	$X(p)$	$X^*(p)$
1	$1_0(t)$	$\frac{1}{p}$	$\frac{e^{pT_p}}{e^{pT_p}-1}$
2	t	$\frac{1}{p^2}$	$T_p \frac{e^{pT_p}}{(e^{pT_p}-1)^2}$
3	$\frac{1}{2!}t^2$	$\frac{1}{p^3}$	$\frac{T_p^2}{2}\frac{e^{pT_p}(e^{pT_p}+1)}{(e^{pT_p}-1)^3}$
4	$\frac{1}{3!}t^3$	$\frac{1}{p^4}$	$\frac{T_p^3}{2}\frac{e^{pT_p}(e^{pT_p}+1)}{(e^{pT_p}-1)^4} + \frac{T_p^3}{6}\frac{e^{pT_p}(e^{pT_p}+2)}{(e^{pT_p}-1)^3}$
5	$\frac{1}{n!}t^n$	$\frac{1}{p^n}$	$\frac{T_p^n e^{pT_p}}{(e^{pT_p}-1)^{n+1}} R_n^*(p)$, where $R_n^*(p) = \begin{vmatrix} 1 & 1-e^{pT_p} & 0 & \cdots & 0 \\ \frac{1}{2!} & 1 & 1-e^{pT_p} & \cdots & 0 \\ \frac{1}{3!} & \frac{1}{2!} & 1 & \cdots & 0 \\ \cdots & \cdots & \cdots & \cdots & \cdots \\ \frac{1}{n!} & \frac{1}{(n-1)!} & \frac{1}{(n-2)!} & \cdots & 1 \end{vmatrix}$
6	$e^{-\alpha t}$	$\frac{1}{p+\alpha}$	$\frac{e^{pT_p}}{e^{pT_p}-e^{\alpha T_p}}$
7	$te^{-\alpha t}$	$\frac{1}{(1+\alpha)^2}$	$T_p \frac{e^{-\alpha T_p} \cdot e^{pT_p}}{(e^{pT_p}-e^{-\alpha T_p})^2}$
8	$\frac{1-e^{-\alpha t}}{\alpha}$	$\frac{1}{p(p+\alpha)}$	$\frac{(1-e^{-\alpha T_p})e^{pT_p}}{\alpha(e^{pT_p}-1)(e^{pT_p}-e^{\alpha T_p})}$

Table 12.1 (cont'd)

9	$\frac{t}{\alpha}-\frac{1-e^{-\alpha t}}{\alpha^2}$	$\frac{1}{p^2(p+\alpha)}$	$\frac{T_p}{\alpha}\frac{e^{pT_p}}{(e^{pT_p}-1)^2}-\frac{(1-e^{-\alpha T_p})e^{pT_p}}{\alpha^2(e^{pT_p}-1)(e^{pT_p}-e^{-\alpha T_p})}$
10	$\sin \beta t$	$\frac{\beta}{p^2+\beta^2}$	$\frac{\sin \beta T_p e^{pT_p}}{e^{2pT_p}-2\cos \beta T_p e^{pT_p}+1}$
11	$\cos \beta t$	$\frac{p}{p^2+\beta^2}$	$\frac{e^{pT_p}(e^{pT_p}-\cos \beta T_p)}{e^{2pT_p}-2\cos \beta T_p e^{pT_p}+1}$
12	$e^{-\alpha t}\sin \beta t$	$\frac{\beta}{(p+\alpha)^2+\beta^2}$	$\frac{e^{-\alpha T_p}\sin \beta T_p e^{-pT_p}}{e^{2pT_p}-2e^{-\alpha T_p}\cos \beta T_p e^{pT_p}+e^{-2\alpha T_p}}$
13	$e^{-\alpha t}\cos \beta t$	$\frac{p+\alpha}{(p+\alpha)^2+\beta^2}$	$\frac{e^{pT_p}(e^{pT_p}-e^{-\alpha T_p}\cos \beta T_p)}{e^{2pT_p}-2e^{-\alpha T_p}\cos \beta T_p e^{pT_p}+e^{-2\alpha T_p}}$

eries in the complex form

$$\sum_{t=-\infty}^{\infty}\delta(t-lT_p)=\sum_{r=-\infty}^{\infty}C_r e^{ir\omega_p t} \tag{12.21}$$

where

$$\omega_p=\frac{2\pi}{T_p} \tag{12.22}$$

and the expansion coefficients determined by the formula

$$C_r=\frac{1}{T_p}\int_{-\frac{T_p}{2}}^{\frac{T_p}{2}}\left[\sum_{l=-\infty}^{\infty}\delta(t-lT_p)\right]e^{-jr\omega_p t}\,dt \tag{12.23}$$

are equal to $\frac{1}{T_p}$ for any r. Therefore

$$\sum_{l=-\infty}^{\infty}\delta(t-lT_p)=\frac{1}{T_p}\sum_{l=-\infty}^{\infty}e^{jr\omega_p t} \tag{12.24}$$

A discrete signal $x^*(t)$ can be given in the form

$$x^*(t)=\sum_{l=0}^{\infty}x(lT_p)\,\delta(t-lT_p)=x(t)\sum_{l=-\infty}^{\infty}\delta(t-lT_p) \tag{12.25}$$

since $x(t)=0$ at $t<0$ and $\delta(t-lT_p)=0$ at $t\neq lT_p$.

Following substitution of Eq. (12.24) we have

$$x^*(t) = x(t)\frac{1}{T_p}\sum_{r=-\infty}^{\infty} e^{jr\omega_p t} \tag{12.26}$$

The spectrum of the signal $x^*(t)$ is expressed as follows

$$X^*(j\omega) = \frac{1}{T_p}\int_0^{\infty}\left[x(t)\sum_{r=-\infty}^{\infty} e^{jr\omega_p t}\right]e^{-j\omega t}\,dt =$$

$$= \frac{1}{T_p}\sum_{r=-\infty}^{\infty}\int_0^{\infty} x(t)\,e^{-j(\omega - r\omega_p)t}\,dt$$

The integral which follows the sigma is

$$\int_0^{\infty} x(t)\,e^{-j(\omega - r\omega_p)t}\,dt = X[j(\omega - r\omega_p)] \tag{12.27}$$

Therefore

$$X^*(j\omega) = \frac{1}{T_p}\sum_{r=-\infty}^{\infty} X[j(\omega - r\omega_p)]$$

or, replacing $-r$ by r and changing the order of summation, we obtain

$$X^*(j\omega) = \frac{1}{T_p}\sum_{r=-\infty}^{\infty} X[j(\omega + r\omega_p)] \tag{12.28}$$

The components of a series at $r \neq 0$ are known as *transposed components.*

This result can be shown to be rigorously valid for functions $x(t)$ equal to zero at $t = 0$. If $x(0) \neq 0$, the sum in the right-hand part must be complemented by the term $\frac{1}{2}x(0)$, i.e.

$$X^*(j\omega) = \frac{1}{T_p}\sum_{r=-\infty}^{\infty} X[j(\omega + r\omega_p)] + \frac{1}{2}x(0) \tag{12.29}$$

For images, similar expressions have the form:
at $x(0) = 0$

$$X^*(p) = \frac{1}{T_p}\sum_{r=-\infty}^{\infty} X(p + jr\omega_p) \tag{12.30}$$

at $x(0) \neq 0$

$$X^*(p) = \frac{1}{T_p}\sum_{r=-\infty}^{\infty} X(p + jr\omega_p) + \frac{1}{2}x(0) \tag{12.31}$$

The principal value of the formulae relating the spectra and images of discrete and continuous signals is not so much in that they provide another tool for calculating $X^*(j\omega)$ and $X^*(p)$ as in illustrative interpretation of the phenomena in sampled-data systems. Figure 12.17 shows real and imaginary components of the spectra $\frac{1}{T_p}X(j\omega)$ and $X^*(j\omega)$, the latter being obtained by adding up the components of the spectrum $\frac{1}{T_p}X(j\omega)$ transposed over $r\omega_p$ $(-\infty < r < \infty)$. As a result the spectrum $X^*(j\omega)$ is found to be periodic along the frequency axis with period ω_p, as was noted above. The spectrum $X^*(j\omega)$ differs from $\frac{1}{T_p}X(j\omega)$ not only at high frequencies but generally also at low frequencies in the range $-\frac{\omega_p}{2} < \omega \leqslant \frac{\omega_p}{2}$ owing to the addition of high-frequency "tails" of the transposed components. The latter fact is traceable to the so-called *stroboscopic effect* and can be better understood by considering two harmonic components of the signal $x(t)$ $(-\infty < t < \infty)$

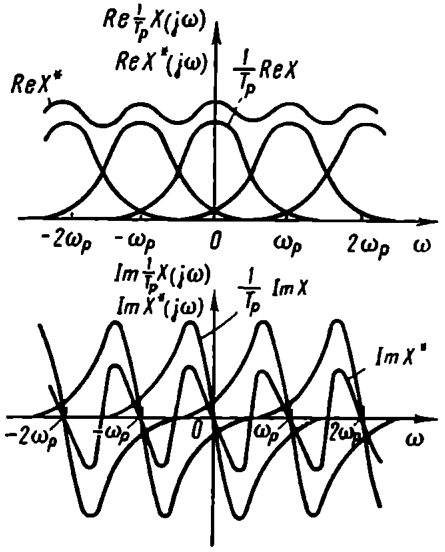

Fig. 12.17

$$x_1(t) = e^{j(\omega t+\varphi)} \quad \text{and} \quad x_2(t) = e^{j[(\omega+r\omega_p)t+\varphi]}$$

where r is an integer.

At the sampling times $t = lT_p$ both components have identical values (Fig. 12.18)

$$x_1(lT_p) = e^{j(\omega lT_p+\varphi)}$$

$$x_2(lT_p) = e^{j[(\omega+r\omega_p)lT_p+\varphi]} = e^{j(\omega lT_p+\varphi)}e^{jrl2\pi} = e^{j(\omega lT_p+\varphi)} = x_1(lT_p)$$

Consequently, $x_1(t)$ and $x_2(t)$ give identical discrete components at the PE output; as a result, the low- and high-frequency components of the signal $x(t)$ have the same effect on the behaviour of a sampled-data system.

As noted above and as follows from Eq. (12.31), the image $X^*(p)$ of a discrete signal is periodic in the p plane along the imaginary axis. Therefore, if $X^*(p)$ has singular points (poles), these are periodically repeated in the vertical direction (Fig. 12.19) and infinite in number.

Let us consider the number of poles of the image $X^*(p)$ in the horizontal band $-\frac{\omega_p}{2} < \operatorname{Im} p \leqslant \frac{\omega_p}{2}$. By Eq. (12.31) the poles of $X^*(p)$ are above all the poles of $X(p)$ from the same band (due to the addend corresponding to $r = 0$). All other poles of $X(p)$ from other parts of the p plane also find themselves in this band (due to the other addends). Consequently, the total number of poles in the band in question, with due regard for their multiplicity, is equal to the total number of poles of the image $X(p)$.

One exception is the case where two or more poles of $X(p)$ lie on a straight line parallel to the imaginary axis and differ in their

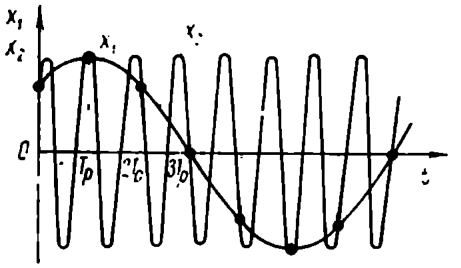

Fig. 12.18

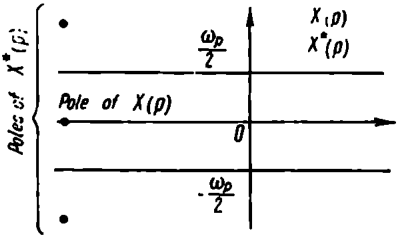

Fig. 12.19

imaginary parts by $jk\omega_p$, where k is an integer. In $X^*(p)$ these poles can be mutually compensated when summing the transposed components in Eq. (12.31). For instance, the continuous signal $x(t) = \sin \omega_p t$ has an image $X(p) = \frac{\omega_p}{p^2 + \omega_p^2}$, which has two poles, $j\omega_p$ and $-j\omega_p$. The sampling values of the signal $x(lT_p) = \sin \omega_p l T_p$ are zero; therefore $X^*(p) = 0$, and thus $X^*(p)$ has no poles.

Reconstruction of continuous signals from discrete ones. The distortion of $X^*(j\omega)$ at low frequencies by high-frequency "tails" generally prevents the reconstruction of the initial signal $x(t)$ from $x^*(t)$ even with the use of a low-frequency filter to chop off the periodic spectrum $X^*(j\omega)$ at high frequencies. This is caused by the fact that the modulation of a pulse sequence uses only disrete values of the signal x, while the nature of signal changes between sampling times is neglected; as a result, some information on the signal is lost.

There are, however, conditions in which no information loss occurs. If the spectrum of the signal $x(t)$ is limited by a frequency ω_b and if the *PE* frequency is taken large enough, so that

$$\omega_p \geqslant 2\omega_b \tag{12.32}$$

then, as can be seen from Fig. 12.20, the transposed components of the spectrum $X^*(j\omega)$ do not overlap; as a result, the spectra $X^*(j\omega)$ and $\frac{1}{T_p} X(j\omega)$ coincide in the frequency range $-\frac{\omega_p}{2} < \omega \leqslant \frac{\omega_p}{2}$. If an ideal low-pass filter having a unit gain and uniform passband $-\frac{\omega_p}{2} < \omega \leqslant \frac{\omega_p}{2}$ is applied, then its output will be the reconstructed signal $\frac{1}{T_p} x(t)$.

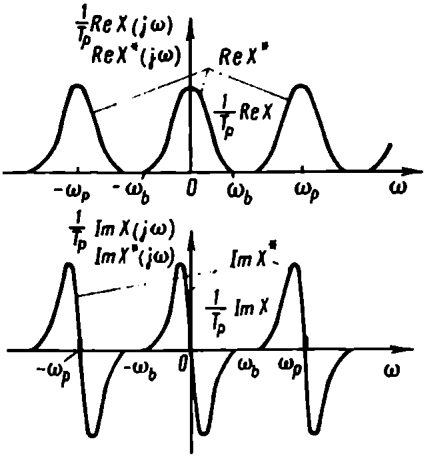

Fig. 12.20

This result has been formulated in the well-known *Kotelnikov pulse theorem.*

Images of discrete signals in case of fractional rational $X(p)$ and in the presence of delay. Reverting to the relation between the spectra and images of continuous $x(t)$ and discrete $x^*(t)$ signals, let us consider the case where the image of the continuous function $x(t)$ at the input of a PE is a fractional rational function of p

$$X(p) = \frac{B(p)}{A(p)} \tag{12.33}$$

The denominator order n is greater than the numerator order m and the polynomial in the denominator, $A(p)$, has no multiple roots. If the roots P_ν of the polynomial are known, then $X(p)$ can be represented as a sum of simple (common) fractions

$$X(p) = \sum_{\nu=1}^{n} \frac{B(p_\nu)}{\dot{A}(p_\nu)} \frac{1}{p - p_\nu} \tag{12.34}$$

where $\dot{A}(p) = \frac{dA(p)}{dp}$.

This implies that the signal $x(t)$ can be represented as a linear combination of exponential signals.

Using the result of Example 12.4, we have

$$X^*(p) = \sum_{\nu=1}^{n} \frac{B(p_\nu)}{\dot{A}(p_\nu)} \frac{e^{pT_p}}{e^{pT_p} - e^{p_\nu T_p}} \tag{12.35}$$

A similar formula can be obtained for multiple roots of $A(p)$ but it is not given, being extremely cumbersome. In specific cases

multiple roots can be eliminated, e.g. by adding small increments to the roots. After this we can find the image $X^*(p)$ by Eq. (12.35) and then implement a limit transition, making the increments tend to zero. There are also other ways to obtain $X^*(p)$ with multiple roots; one of them will be treated in Example 13.2 (Sec. 13.2).

Equation (12.35) leads to the conclusion that for fractional rational $X(p)$ the image $X^*(p)$ is a fractional rational function of e^{pT_p}, which will be further on denoted as

$$X^*(p) = \frac{B^*(p)}{A^*(p)} \tag{12.36}$$

where

$$A^*(p) = a_n e^{npT_p} + a_{n-1} e^{(n-1)pT_p} + \ldots + a_0 \tag{12.37}$$

$$B^*(p) = b_m e^{mpT_p} + b_{m-1} e^{(m-1)pT_p} + \ldots + b_0 \tag{12.38}$$

The degree n of the polynomials $A^*(p)$ and $A(p)$ is the same.

Example 12.5. The image of a continuous signal is

$$X(p) = \frac{k}{p(1+pT)}$$

which implies $X(t) = k(1 - e^{-\frac{t}{T}})$. Let us find $X^*(p)$.

The roots of the denominator $p_1 = 0$, $p_2 = -\frac{1}{T}$.

Using Eq. (12.35), we can write

$$X^*(p) = k\left(\frac{e^{pT_p}}{e^{pT_p}-1} - \frac{e^{pT_p}}{e^{pT_p}-e^{-\frac{T_p}{T}}}\right) =$$

$$= \frac{k(1-e^{-\frac{T_p}{T}})\,e^{pT_p}}{(e^{pT_p}-1)(e^{pT_p}-e^{-\frac{T_p}{T}})} \tag{12.39}$$

Let us have a look at the image of the discrete signal $x_\tau^*(t)$ which is obtained at the output of PE when there is a delayed signal $x(t-\tau)\,1_0(t-\tau)$ at its input (Fig. 12.21). The delay τ is within the interval $(k-1)\,T_p < \tau \leqslant kT_p$.

In this case

$$x_\tau^*(t) = \sum_{l=k}^{\infty} x(lT_p - \tau)\,\delta(t - lT_p) \tag{12.40}$$

$$X_\tau^*(p) = \sum_{l=k}^{\infty} x(lT_p - \tau)\,e^{-plT_p} \tag{12.41}$$

since samplings are still made at times lT_p.

If the delay is equal to an integral number of periods $\tau = kT_p$, then

$$X_\tau^*(p) = \sum_{l=k}^{\infty} x[(l-k)T_p]\, e^{-plT_p}$$

Replacing $(l-k)$ by l, we have

$$X_\tau^*(p) = e^{-kpT_p} \sum_{l=0}^{\infty} x(lT_p)\, e^{-plT_p} = e^{-kpT_p} X^*(p) \qquad (12.42)$$

Example 12.6. The signal $x(t)$ is an exponent $e^{\alpha t}$ with the image

$$X(p) = \frac{1}{p-\alpha}$$

The image of the delayed signal $x(t-\tau)\,1_0(t-\tau)$ is

$$X_\tau(p) = \frac{1}{p-\alpha}\, e^{-p\tau}$$

According to Eq. (12.41) $X_\tau^*(p) = \sum_{l=k}^{\infty} e^{\alpha(lT_p-\tau)} e^{-plT_p}$,

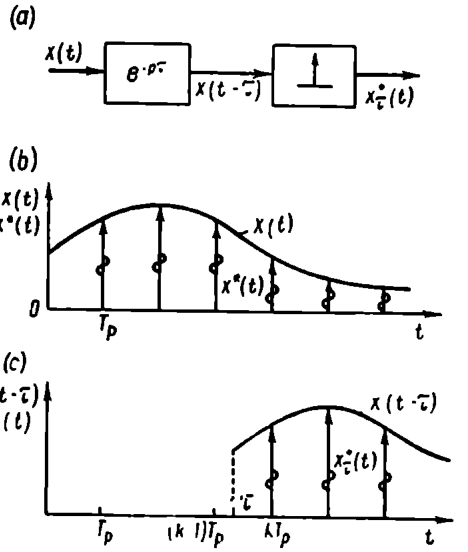

Fig. 12.21

The latter expression is a sum of a geometric progression with the first term $e^{\alpha(kT_p-\tau)} e^{-pkT_p}$ and the denominator $e^{\alpha T_p} e^{-pT_p}$

$$X_\tau^*(p) = \frac{e^{\alpha(kT_p-\tau)}}{e^{kpT_p}} \cdot \frac{e^{pT_p}}{e^{pT_p} - e^{\alpha T_p}} = \frac{e^{\alpha(kT_p-\tau)}}{e^{kpT_p}}\, X^*(p) \qquad (12.43)$$

where $X^*(p)$ is the image of a discrete exponential signal without delay (12.19).

At $\tau = kT_p$

$$X_\tau^*(p) = e^{-kpT_p} X^*(p)$$

which is equivalent to Eq. (12.42).

Example 12.7. An undelayed signal is a linear combination of exponential signals, and its image is a fractional rational function

$$X(p) = \frac{B(p)}{A(p)} = \sum_{\nu=1}^{n} \frac{B(p_\nu)}{\dot{A}(p_\nu)} \frac{1}{p - p_\nu}$$

The image of a delayed signal is

$$X_\tau(p) = \sum_{\nu=1}^{n} \frac{B(p_\nu)}{\dot{A}(p_\nu)} \frac{1}{p - p_\nu} e^{-p\tau}$$

The image of a discrete delayed signal with an allowance for Eq. (12.43) is

$$X_\tau^*(p) = \frac{1}{e^{kpT_p}} \sum_{\nu=1}^{n} \frac{B(p_\nu)}{\dot{A}(p_\nu)} e^{p_\nu(kT_p - \tau)} \frac{e^{pT_p}}{e^{pT_p} - e^{p_\nu T_p}} \qquad (12.44)$$

Thence it follows that the image of a discrete delayed signal is in this case a fractional rational function of e^{pT_p}, and its denominator differs from that of a discrete undelayed signal image (12.35) only by the presence of the multiplier e^{kpT_p}

$$X_\tau^*(p) = \frac{B_\tau^*(p)}{e^{kpT_p} A^*(p)} \qquad (12.45)$$

Tables for images of discrete delayed signals $x_\tau^*(t)$ are given, for instance, in Ref. 73.

The reverse problem, i.e. finding the discrete values $x(lT_p)$ when the image $X^*(p)$ is known can be solved by conversion formulae for discrete signals similar to conversion formulae for continuous signals. These formulae will be given without proof. The most general conversion formula is of the form

$$x(lT_p) = \frac{T_p}{2\pi j} \int_{c - j\frac{\omega_p}{2}}^{c + j\frac{\omega_p}{2}} X^*(p) e^{plT_p} dp \qquad (12.46)$$

where the range of integration, which depends on the distance c, is such that all singular points of the image $X^*(p)$ are on its left.

If we denote $e^{pT_p} = z$, then Eq. (12.46) is given as

$$x(lT_p) = \frac{1}{2\pi j} \oint_{\Gamma} X(z)\, z^{l-1}\, dz \qquad (12.47)$$

where Γ is a circle of radius e^{cT_p}, and the left-hand part of the band $\operatorname{Re} p \leqslant c$, $-\frac{\omega_p}{2} < \operatorname{Im} p \leqslant \frac{\omega_p}{2}$ is converted into the interior of the circle Γ.

Using the Residue Theorem, we can say that

$$x(lT_p) = \sum_{\nu} \operatorname{Res}_{z_\nu} [X(z)\, z^{l-1}] \qquad (12.48)$$

where $\operatorname{Res}_{z_\nu} [X(z)\, z^{l-1}]$ is the residue of the function $X(z)\, z^{l-1}$ at the pole $z_\nu = e^{p_\nu T_p}$.

In a particular case where $X^*(p)$ is a fractional rational function of e^{pT_p}

$$X^*(p) = \frac{B^*(p)}{A^*(p)} = \frac{b_m e^{mpT_p} + b_{m-1} e^{(m-1)pT_p} + \ldots + b_0}{a_n e^{npT_p} + a_{n-1} e^{(n-1)pT_p} + \ldots + a_0}$$

$(m < n)$, and the roots of the denominator $A^*(p)$ are simple, Eq. (12.48) takes the form

$$x(lT_p) = \sum_{\nu=1}^{n} \frac{B^*(p_\nu)}{\dot{A}^*(p_\nu)} e^{p_\nu (l-1) T_p} = \sum_{\nu=1}^{n} \frac{B^*(p_\nu)}{e^{p_\nu T_p} \dot{A}^*(p_\nu)} e^{p_\nu l T_p} \qquad (12.49)$$

Here

$$\dot{A}^*(p) = \frac{dA^*(p)}{d(e^{pT_p})}$$

p_ν are the roots of the denominator $A^*(p)$ in the half-band $\operatorname{Re} p \leqslant c$, $-\frac{\omega_p}{2} < \operatorname{Im} p \leqslant \frac{\omega_p}{2}$ (their number is n).

Equation (12.49) is an analog of the well-known expansion formula for continuous functions. A similar but more cumbersome formula can be obtained for multiple roots of $A^*(p)$.

The conversion formulae (12.46) and (12.49) give only discrete values of the signal x at the input of a PE; the values of this signal in the interval between sampling points can be obtained with the knowledge of $x(lT_p)$ only if the conditions of the pulse theorem are valid. Thus if the conversion formula, say, leads to the result

$$x(lT_p) = lT_p$$

then it would be erroneous to write

$$x(t) = t$$

since a linear law of discrete signal variations can be obtained also at signals other than the linear signal $x(t)$. This remark also holds for inverse conversion with the use of Table 12.1 when the original is found from a known image $X^*(p)$. In the function $x(t)$, found in the first column, $t = lT_p$ should be substituted.

Chapter XIII

SAMPLED-DATA CONTROL SYSTEMS. SIGNAL PROPAGATION. COMPLEX GAINS. TRANSFER FUNCTIONS

13.1. SIGNAL PROPAGATION THROUGH A SAMPLED-DATA CONTROL SYSTEM

Let us see how a signal $\varepsilon(t)$ propagates through the sampled-data control system of Fig. 12.8. Let us find the spectrum of the output variable y assuming for simplicity that $\varepsilon(0) = 0$ and that zero initial conditions hold in the system

$$Y(j\omega) = W_{RCP}(j\omega)\, E^*(j\omega) \tag{13.1}$$

where, according to Eq. (12.28),

$$E^*(j\omega) = \frac{1}{T_p} \sum_{r=-\infty}^{\infty} E[j(\omega + r\omega_p)] \tag{13.2}$$

If we isolate, in the expression for $Y(j\omega)$, the addend corresponding to $r = 0$, then

$$Y(j\omega) = \frac{1}{T_p} W_{RCP}(j\omega)\, E(j\omega) + \frac{1}{T_p} W_{RCP}(j\omega) \sum_{\substack{r=-\infty \\ r \neq 0}}^{\infty} E[j(\omega + r\omega_p)] \tag{13.3}$$

In this expression the first addend is the output signal spectrum which would exist in a continuous system with a frequency response $\frac{1}{T_p} W_{RCP}(j\omega)$. The second addend, which includes a sum of transposed spectral components $E[j(\omega - r\omega_p)]$, represents the effect of the *PE*. Figure 13.1 illustrates how the signal spectrum $E(j\omega)$ changes in accordance with Eq. (13.3) when the signal propagates through a sampled-data system. For pictorialness we selected a case where the conditions of the pulse theorem are valid, i.e. the spectrum is bounded by the frequencies ω_b and $\omega_p \geqslant 2\omega_b$. The presence of the *PE* leads to the appearance in the output signal of high-frequency components which were not observed in the signal spectrum $E(j\omega)$. As a result, a complex gain cannot generally be used to relate

the spectra $E(j\omega)$ and $Y(j\omega)$ in a sampled-data system, as is done in continuous systems; this is seen from Eq. (13.3).

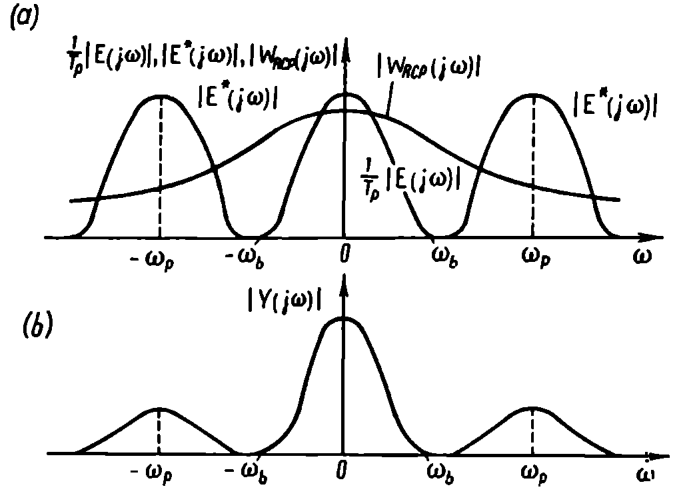

Fig. 13.1

A case can be specified, however, where such relationship does exist. Figure 13.2 represents the spectrum $E(j\omega)$ limited by the

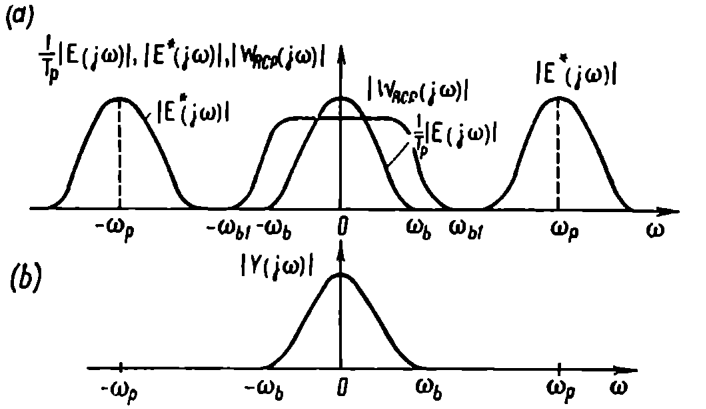

Fig. 13.2

frequency ω_b; and the frequency response W_{RCP} limited by the frequency ω_{bl}; $\omega_p > \omega_b + \omega_{bl}$. As a result, Eq. (13.3) preserves only the first addend

$$Y(j\omega) = \frac{1}{T_p} W_{RCP}(j\omega) E(j\omega) \qquad (13.4)$$

and the sampled-data system becomes equivalent to a continuous system with the open-loop complex gain $\frac{1}{T_p} W_{RCP}(j\omega)$. Consequently, with increasing sampling frequency ω_p the properties of a sampled-data system tend (with an accuracy to a factor $\frac{1}{T_p}$) to those of a reduced continuous part; if the condition

$$\omega_p \geqslant \omega_b + \omega_{b1} \tag{13.5}$$

is observed, their properties become identical. In practice this is often assumed to take place where the largest time constant of the continuous part greatly exceeds the operating period T_p of a *PE*.

The expression for the output variable image is in the general case similar to Eqs. (13.1) and (13.2)

$$Y(p) = W_{RCP}(p)\, E^*(p) = \frac{1}{T_p} W_{RCP}(p) \sum_{r=-\infty}^{\infty} E(p + jr\omega_p) \tag{13.6}$$

13.2. COMPLEX GAINS AND TRANSFER FUNCTIONS OF OPEN-LOOP SAMPLED-DATA CONTROL SYSTEMS

Complex gains of open-loop sampled-data systems. In Sec. 13.1 it was established that there is generally no proportional relation between the spectra and images of the signal $\varepsilon(t)$ and of the output

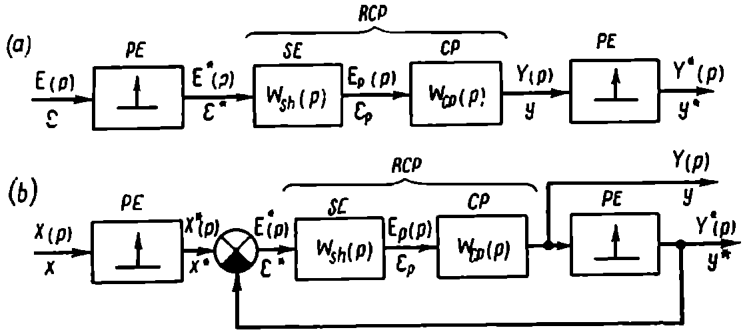

Fig. 13.3

signal $y(t)$ in a sampled-data control system. Such a relation has been discovered, however, between the spectra and images of discrete signals $\varepsilon^*(t)$ and $y^*(t)$. The latter signal is obtained from $y(t)$ in propagating it through a simple *PE* as shown in Fig. 13.3*a*.

That the knowledge of this relation is useful follows from the possibility of representing an equivalent diagram of the sampled-data control system given in Fig. 12.8 in the form of Fig. 13.3*b*. This

conversion of diagrams follows from the obvious relation

$$\varepsilon^* = (x-y)^* = x^* - y^* \tag{13.7}$$

In order to find the relation between the spectra and images of $\varepsilon^*(t)$ and $y^*(t)$ let us have another look at the signals $y(t)$ and $y^*(t)$. The signal $y(t)$ at zero initial conditions is made up of the response of the reduced continuous part to pulses $\varepsilon^*(t)$ (Fig. 13.4*a*). The system response to a pulse acting at the ith sampling point and having an area $\varepsilon(iT_p)$ is shown in Fig. 13.4*b*

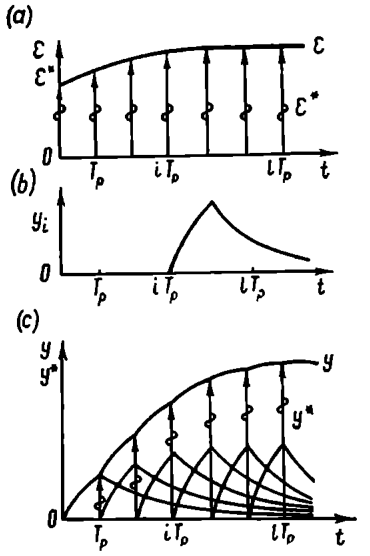

Fig. 13.4

$$y_i(t) = \varepsilon(iT_p)\, w_{RCP}(t-iT_p), \quad t \geqslant iT_p \tag{13.8}$$

where $w_{RCP}(t)$ is the weighting function of the reduced continuous part.

The complete output signal $y(t)$ of the system obtained by adding up the components $y_i(t)$ is shown in Fig. 13.4*c*; for $lT_p \leqslant t < (l+1)\,T_p$

$$y(t) = \sum_{i=0}^{l} \varepsilon(iT_p)\, w_{RCP}(t-iT_p) \tag{13.9}$$

where l is the integral part of $\frac{t}{T_p}$.

The discrete value $y(lT_p)$ is obtained from Eq. (13.9) by substituting $t = lT_p$

$$y(lT_p) = \sum_{i=0}^{l} \varepsilon(iT_p)\, w_{RCP}[(l-i)\,T_p] \tag{13.10}$$

The weighting function $w_{RCP}(t)$, which is the response of the reduced continuous part to the unit pulse $\delta(t)$, is essentially the response of the continuous part to one pulse $s(t)$, which is the transform of the unit pulse given by the shaping unit.

The signal $y^*(t)$ is obtained from $y(t)$ by sampling in time

$$y^*(t) = \sum_{l=0}^{\infty} y(lT_p)\, \delta(t-lT_p) \tag{13.11}$$

or, after the substitution of Eq. (13.10),

$$y^*(t) = \sum_{l=0}^{\infty} \left\{ \sum_{i=0}^{l} \varepsilon(iT_p)\, w_{RCP}[(l-i)\,T_p] \right\} \delta(t-lT_p) \tag{13.12}$$

Since the weighting function $w_{RCP}(t)$ at $t<0$ is identically zero, then l in the upper limit of the internal sum can be replaced by ∞

$$y^*(t) = \sum_{l=0}^{\infty} \left\{ \sum_{i=0}^{\infty} \varepsilon(iT_p)\, w_{RCP}[(l-i)\,T_p] \right\} \delta(t-lT_p) \qquad (13.13)$$

Changing the order of summation, we have

$$y^*(t) = \sum_{i=0}^{\infty} \varepsilon(iT_p) \left\{ \sum_{l=0}^{\infty} w_{RCP}[(l-i)\,T_p]\, \delta(t-lT_p) \right\} \qquad (13.14)$$

Assuming $l-i=k$,

$$y^*(t) = \sum_{i=0}^{\infty} \varepsilon(iT_p) \left\{ \sum_{k=-i}^{\infty} w_{RCP}(kT_p)\, \delta[t-(i+k)\,T_p] \right\} \qquad (13.15)$$

or, assuming that $w_{RCP}(t)=0$ at $t<0$,

$$y^*(t) = \sum_{i=0}^{\infty} \varepsilon(iT_p) \left\{ \sum_{k=0}^{\infty} w_{RCP}(kT_p)\, \delta[t-(i+k)\,T_p] \right\} \qquad (13.16)$$

Let us find the spectrum of the signal $y^*(t)$ using the Fourier transformation. The spectrum of $\delta[t-(i+k)\,T_p]$ is $e^{-j\omega(i+k)T_p}$, therefore

$$Y^*(j\omega) = \sum_{i=0}^{\infty} \varepsilon(iT_p) \left\{ \sum_{k=0}^{\infty} w_{RCP}(kT_p)\, e^{-j\omega(i+k)T_p} \right\} =$$

$$= \sum_{i=0}^{\infty} \varepsilon(iT_p)\, e^{-j\omega iT_p} \sum_{k=0}^{\infty} w_{RCP}(kT_p)\, e^{-jk\omega T_p} \qquad (13.17)$$

The first multiplier in Eq. (13.17) is the spectrum $E^*(j\omega)$; consequently, we can write

$$Y^*(j\omega) = W^*_{o\text{-}l}(j\omega)\, E^*(j\omega) \qquad (13.18)$$

where the proportionality coefficient $W^*_{o\text{-}l}(j\omega)$ showing the relation between the spectra $Y^*(j\omega)$ and $E^*(j\omega)$ is called the *complex gain of an open-loop sampled-data control system*. This gain is

$$W^*_{o\text{-}l}(jw) = \sum_{k=0}^{\infty} w_{RCP}(kT_p)\, e^{-j\omega kT_p}$$

or, if k is replaced by l,

$$W^*_{o\text{-}l}(jw) = \sum_{l=0}^{\infty} w_{RCP}(lT_p)\, e^{-j\omega lT_p} \qquad (13.19)$$

Thence the complex gain $W^*_{o\text{-}l}(j\omega)$ is seen to be the spectrum of the signal $w^*_{RCP}(t)$, which can be represented as the result of the propagation of a signal equal to the weighting function of the reduced

continuous part $w_{RCP}(t)$ through a simple PE. Therefore Eq. (12.29) can be used to express $W^*_{o\text{-}l}(j\omega)$ through the spectrum $W_{RCP}(j\omega)$, which is the complex gain of the reduced continuous part

$$W^*_{o\text{-}l}(j\omega) = \frac{1}{T_p}\sum_{r=-\infty}^{\infty} W_{RCP}[j(\omega + r\omega_p)] + \frac{1}{2} w_{RCP}(0) \qquad (13.20)$$

If the power of the continuous part transfer function denominator is below that of the numerator, then the weighting function $w_{RCP}(t)$, which is the response of the continuous part to one pulse $s(t)$ at a finite height of the latter (both conditions practically always hold), is zero at $t = 0$; therefore we will use a simplified expression for $W^*_{o\text{-}l}(j\omega)$ (see Eq. (12.28))

$$W^*_{o\text{-}l}(j\omega) = \frac{1}{T_p}\sum_{r=-\infty}^{\infty} W_{RCP}[j(\omega + r\omega_p)] \qquad (13.21)$$

Sometimes to simplify the analysis of a sampled-data control system the small parameters of the reduced continuous part transfer function are neglected; as a result, the weighting function of the reduced continuous part may prove to be nonzero at $t = 0$. The situation can be remedied by introducing a small delay. In this case the weighting function is given in the form

$$w_{RCP}(t) = w_{RCP1}(t-\tau) \qquad (13.22)$$

where $w_{RCP1}(t)$ is the weighting function with a discontinuity at

$$t = 0 \quad (w_{RCP1}(0) \neq 0)$$

τ is a very small delay ($\tau \approx 0$).

The weighting functions $w_{RCP}(t)$ and $w_{RCP1}(t)$ differ only at $t = 0$. Therefore

$$w^*_{RCP}(t) = w^*_{RCP1}(t) - w_{RCP1}(0)\,\delta(t) \qquad (13.23)$$

Then

$$W^*_{RCP}(j\omega) = W^*_{RCP1}(j\omega) - w_{RCP1}(0) =$$

$$= \left\{\frac{1}{T_p}\sum_{r=-\infty}^{\infty} W_{RCP1}[j(\omega + r\omega_p)] + \frac{1}{2} w_{RCP1}(0)\right\} - w_{RCP1}(0) =$$

$$= \frac{1}{T_p}\sum_{r=-\infty}^{\infty} W_{RCP1}[j(\omega + r\omega_p)] - \frac{1}{2} w_{RCP1}(0) \qquad (13.24)$$

where $W_{RCP1}(j\omega)$ is a simplified complex gain of the reduced continuous part with a weighting function $w_{RCP1}(t)$, which is nonzero at $t > 0$.

The complex gain $W^*_{o\text{-}l}(j\omega)$, which is the spectrum of the function $w^*_{RCP}(t)$, has all the properties of discrete signal spectra; in particular, it is periodic along the frequency axis with a period ω_p

and its values for negative frequencies can be obtained from those for positive frequencies by conjugation. Therefore the amplitude-phase responses of sampled-data control systems are discussed only for the frequency range $-\frac{\omega_p}{2} < \omega \leqslant \frac{\omega_p}{2}$ or even $0 \leqslant \omega \leqslant \frac{\omega_p}{2}$.

The series in Eq. (13.21) for $W^*_{o\text{-}l}(j\omega)$ converges at a rate increasing with the decrease of the complex gain $W_{RCP}(j\omega)$ when ω increases.

In the case of fast decrease the number of addends in the sum can be assumed to be equal to the two largest addends (for the lowest frequency magnitudes); then

$$W^*_{o\text{-}l}(j\omega) \approx \frac{1}{T_p}\{W_{RCP}(j\omega) + W_{RCP}[j(\omega - \omega_p)]\} \qquad (13.25)$$

Figure 13.5 illustrates graphical plotting of the amplitude-phase response $W^*_{o\text{-}l}(j\omega)$ based on the latter formula for two frequencies,

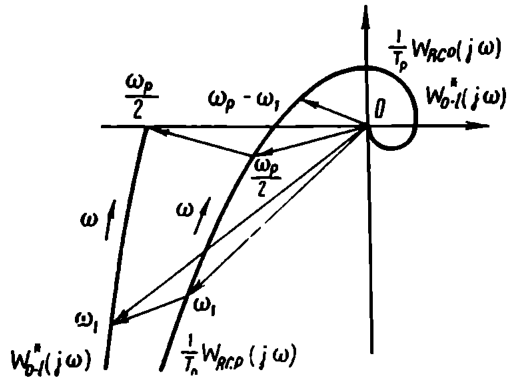

Fig. 13.5

$\omega = \omega_1$ and $\omega = \frac{\omega_p}{2}$. The vector which connects the origin of coordinates with the point of the locus $\frac{1}{T_p}W_{RCP}(j\omega)$ where $\omega = \omega_1$ is added up with the vector which is conjugate with the one taken for $\omega = \omega_p - \omega_1$.

$W^*_{o\text{-}l}(j\omega)$ for the frequency $\omega = \frac{\omega_p}{2}$ is obtained by adding up the vector $\frac{1}{T_p}W_{RCP}\left(j\frac{\omega_p}{2}\right)$ with its conjugate; as a result, the point of the amplitude-phase response is found on the real axis.

If the reduced continuous part has a limited passband, ω_{b1}, and $\omega_{b1} \leqslant \frac{\omega_p}{2}$ (i. e. the band is narrower than halved frequency of the

PE), then all addends, except one in the sum (13.21) (at $r=0$), are zero and therefore in the frequency range $-\frac{\omega_p}{2} < \omega \leqslant \frac{\omega_p}{2}$

$$W^*_{o\text{-}l}(j\omega) = \frac{1}{T_p} W_{RCP}(j\omega) \tag{13.26}$$

Transfer functions of open-loop sampled-data systems. Let us have a look at signal images in sampled-data systems. Applying Laplace transformations to the signal $y^*(t)$, as was done for the spectra (13.17), we have

$$Y^*(p) = W^*_{o\text{-}l}(p)\, E^*(p) \tag{13.27}$$

$$W^*_{o\text{-}l}(p) = \sum_{l=0}^{\infty} w_{RCP}(lT_p)\, e^{-plT_p} \tag{13.28}$$

where $W^*_{o\text{-}l}(p)$ is the transfer function of an open-loop sampled-data system and is the image of the signal $w^*_{RCP}(t)$; therefore expressions similar to Eqs. (13.20), (13.21), and (13.24) can be written for it:

at $w_{RCP}(0) \neq 0$

$$W^*_{o\text{-}l}(p) = \frac{1}{T_p} \sum_{r=-\infty}^{\infty} W_{RCP}(p + jr\omega_p) + \frac{1}{2} w_{RCP}(0) \tag{13.29}$$

at $w_{RCP}(0) = 0$

$$W^*_{o\text{-}l}(p) = \frac{1}{T_p} \sum_{r=-\infty}^{\infty} W_{RCP}(p + jr\omega_p) \tag{13.30}$$

at $w_{RCP}(t) = w_{RCP1}(t-\tau)$, $w_{RCP1}(0) \neq 0$, $\tau \approx 0$

$$W^*_{o\text{-}l}(p) = \frac{1}{T_p} \sum_{r=-\infty}^{\infty} W_{RCP1}(p + jr\omega_p) - \frac{1}{2} w_{RCP1}(0) \tag{13.31}$$

In specific cases the transfer function $W^*_{o\text{-}l}(p)$ can be obtained from $W_{RCP}(p)$ and $w_{RCP}(t)$ using Table 12.1.

The transfer function $W^*_{o\text{-}l}(p)$ is periodic along the imaginary axis in the p plane and can thus be studied in a band $-\frac{\omega_p}{2} < \mathrm{Im}\, p \leqslant \frac{\omega_p}{2}$ of width ω_p symmetric relative to the real axis (see Fig. 12.14).

If $W_{RCP}(p)$ is a fractional rational function

$$W_{RCP}(p) = \frac{K(p)}{D(p)}$$

which is true when $W_{sh}(p) = 1$ (the control pulse is described by δ-function) and $W_{RCP}(p) = W_{CP}(p)$, then $W^*_{o\text{-}l}(p)$ can be found

via Eq. (12.35); in this case

$$W^*_{o-l}(p) = \sum_{\nu=1}^{n} \frac{K(p_\nu)}{\dot{D}(p_\nu)} \frac{e^{pT_p}}{e^{pT_p} - e^{p_\nu T_p}} \tag{13.32}$$

where p_ν are simple roots of the polynomial $D(p)$.

From this equation it follows that the transfer function $W^*_{o-l}(p)$ is in this case a fractional rational function of e^{pT_p}. Formula (13.32) can also be used in order to find the complex gain

$$W^*_{o-l}(j\omega) = \sum_{\nu=1}^{n} \frac{K(p_\nu)}{\dot{D}(p_\nu)} \frac{e^{j\omega T_p}}{e^{j\omega T_p} - e^{p_\nu T_p}} \tag{13.33}$$

The transfer function $W^*_{o-l}(p)$ can be shown (Ref. 81) to be a fractional rational function of e^{pT_p} at $W_{CP}(p) = \frac{K_{CP}(p)}{D_{CP}(p)}$ and $W_{sh}(p) \neq \neq 1$, i.e. at any shape of the control pulses. The order of the transfer function $W^*_{o-l}(p) = \frac{K^*(p)}{D^*(p)}$ (the power of its denominator $D^*(p)$) is at any shape of control pulses equal to the order of the continuous part of the system, or to the power n of the denominator $D_{CP}(p)$ of the transfer function of the continuous part. An exception is possible when the poles of $W_{CP}(p)$ include poles differing only in the imaginary parts by $jk\omega_p$ (k an integer). The order of the transfer function $W^*_{o-l}(p)$ in this case may be below n. In practice this situation occurs very rarely.

If the height of control pulses is finite, and the power of the continuous part transfer function denominator is greater than that of the numerator (both conditions practically always persist), then the power of the numerator $K^*(p)$ of the transfer function $W^*_{o-l}(p)$ is one unit below the power of its denominator $D^*(p)$, or is equal to $n-1$.

A delay element in the continuous part of a sampled-data system shifts the weighting function of the reduced continuous part by the delay time τ: $(k-1)\,T_p < \tau \leqslant kT_p$.

By virtue of Eqs. (13.28) and (12.45) the transfer function of an open-loop sampled-data system with a delay is

$$W^*_{p\tau}(p) = \frac{K^*_\tau(p)}{e^{kpT_p} D^*(p)} \tag{13.34}$$

where $D^*(p)$ = denominator of the transfer function of a system without a delay

$K^*_\tau(p)$ = polynomial in $e^{\nu T_p}$, which can be shown to have a degree n in the same conditions as indicated for the polynomial $K^*(p)$ (i.e. practically always).

According to Eqs. (13.28) and (12.38), if a delay is equal to an integral number of periods $\tau = kT_p$ the transfer function is

$$W^*_{p\tau}(p) = e^{-kpT_p} W^*_{o\text{-}l}(p) = \frac{K^*(p)}{e^{kpT_p} D^*(p)} \tag{13.35}$$

where $W^*_{o\text{-}l}(p)$ is the transfer function of a system without a delay.

Consequently, sampled-data control systems with lumped parameters and delay elements in the continuous part are described by transfer functions $W^*_{o\text{-}l}(p)$ or $W^*_{p\tau}(p)$, which are fractional rational functions of e^{pT_p}; the power of the denominator in these functions practically always exceeding that of the numerator.

The meaning of the complex gain of a sampled-data control system can be refined in terms of the transfer function. Take up the case of propagation of a harmonic signal with a phasor $\varepsilon(t) = Ae^{j\omega t}$ through the open-loop system of Fig. 13.3*a*. The corresponding discrete signal $\varepsilon^*(t)$, by virtue of Eq. (12.20), has an image

$$\mathrm{E}^*(p) = A \frac{e^{pT_p}}{e^{pT_p} - e^{j\omega T_p}}$$

The image of the output signal $y^*(t)$ is represented in terms of the transfer function as

$$Y^*(p) = W^*_{o\text{-}l}(p)\,\mathrm{E}^*(p) = W^*_{o\text{-}l}(p)\,A \frac{e^{pT_p}}{e^{pT_p} - e^{j\omega T_p}} \tag{13.36}$$

The discrete values of the output signal can be obtained from $Y^*(p)$ using Eq. (12.48)

$$y(lT_p) = \sum_{\nu} \mathrm{Res}_{e^{p_\nu T_p}} [Y^*(p)\, e^{p(l-1)T_p}] =$$

$$= \sum_{\nu} \mathrm{Res}_{e^{p_\nu T_p}} \left[W^*_{o\text{-}l}(p)\, A \frac{1}{e^{pT_p} - e^{j\omega T_p}} e^{plT_p} \right] \tag{13.37}$$

Isolating the addend corresponding to the pole of the input action $p = j\omega$ (for simplicity $W^*_{o\text{-}l}(p)$ is assumed to have no poles at that point), we have

$$y(lT_p) = W^*_{o\text{-}l}(j\omega)\, Ae^{j\omega lT_p} +$$

$$+ \sum_{\substack{\nu \\ p_\nu \neq j\omega}} \mathrm{Res}_{e^{p_\nu T_p}} \left[W^*_{o\text{-}l}(p)\, A \frac{1}{e^{pT_p} - e^{j\omega T_p}} e^{plT_p} \right] \tag{13.38}$$

The second addend in the latter expression is a transient component, which tends to zero if the open-loop sampled-data system is stable. (The conditions for stability of sampled-data control systems will be discussed in Ch. XIV.) Therefore the steady-state (or forced) component of discrete values of the output signal is

in this case a discrete harmonic function

$$y_{fo}(lT_p) = W^*_{o\text{-}l}(j\omega)\, Ae^{j\omega lT_p} \qquad (13.39)$$

Figure 13.6*a* and *b* displays imaginary components of the phasors of the input, $\varepsilon(t)$, and steady-state output, $y_{fo}(t)$, signals and of their corresponding signals $\varepsilon^*(t)$ and $y^*_{fo}(t)$.

Although the output signal $y_{fo}(t)$ is not harmonic, its discrete values at sampling points can be connected by a harmonic envelope (Fig. 13.6*c*), the relation of whose amplitude and phase to those of the input signal being defined by a complex gain $W^*_{o\text{-}l}(j\omega)$.

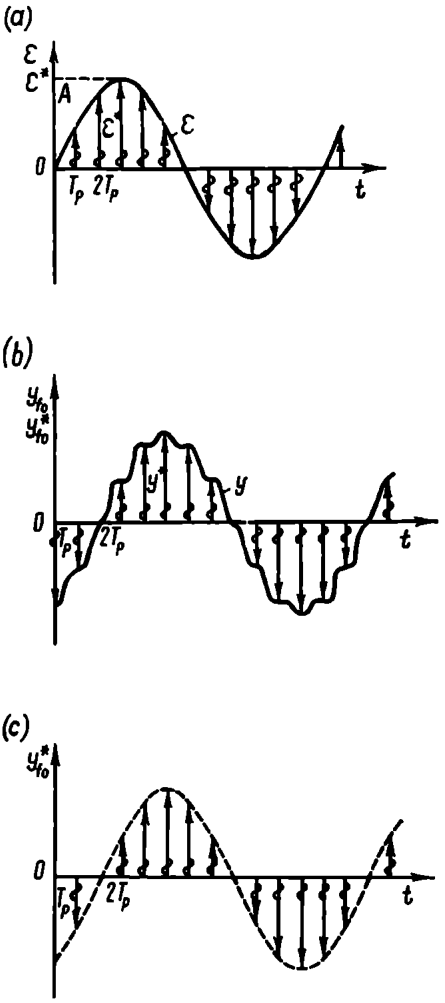

Fig. 13.6

Poles of transfer functions of open-loop sampled-data control systems. Consider the poles of the transfer function $W^*_{o\text{-}l}(p)$ of an open-loop sampled-data control system in the band $-\frac{\omega_p}{2} < \mathrm{Im}\, p \leqslant \frac{\omega_p}{2}$ (see Fig. 12.14). As follows from Eq. (13.29) and from Sec. 12.3, the number of poles of $W^*_{o\text{-}l}(p)$ in this band is equal to the total number of poles of the transfer function $W_{o\text{-}l}(p)$; the poles of these two transfer functions either coincide (for those poles of $W_{RCP}(p)$ which are located within the given band) or differ by an integer $j\omega_p$ (for poles of $W_{RCP}(p)$ outside the band).*

The poles of the reduced continuous part transfer function $W_{RCP}(p) = W_{sh}(p)\, W_{CP}(p)$ are in their turn the poles of the continuous part transfer function $W_{CP}(p)$. This follows from the fact that the shaping element transfer function $W_{sh}(p)$, which by Eq. (12.3) is equal to the image of the function $s(t)$ describing

* A possible exception is the very rare case of Sec. 12.3.

the shape of control pulses, has no poles if the height and duration of the pulses are finite. The poles of $W^*_{o-l}(p)$ thus coincide with those of $W_{CP}(p)$ in the band under consideration with an accuracy to $jr\omega_p$ (r an integer).

If the denominator of the transfer function $W_{CP}(p)$ can be given as the product

$$D_{CP}(p) = \prod_{\nu=1}^{n} (p - p_\nu) \tag{13.40}$$

where p_ν are the poles of $W_{CP}(p)$, then each multiplier $(p - p_\nu)$ is associated with a corresponding multiplier

$$e^{pT_p} - e^{(p_\nu - jr\omega_p)T_p} = e^{pT_p} - e^{p_\nu T_p - jr2\pi} \tag{13.41}$$

in the denominator $D^*(p)$ of the transfer function $W^*_{o-l}(p)$.

An inertial element connected in series in the continuous part of the system is represented by the multiplier

$$e^{pT_p} - e^{-\frac{T_p}{T}} \tag{13.42}$$

where T is an inertial element time constant.

An integrating element is given by the multiplier

$$e^{pT_p} - 1 \tag{13.43}$$

Series-connected ν integrating elements are represented by the multiplier

$$(e^{pT_p} - 1)^\nu \tag{13.44}$$

An oscillator is represented by a product of two first-order multipliers

$$[e^{pT_p} - e^{-\xi\omega_0 T_p + j(\omega_0 T_p \sqrt{1-\xi^2} - r2\pi)}] \times [e^{pT_p} - e^{-\xi\omega_0 T_p - j(\omega_0 T_p \sqrt{1-\xi^2} - r2\pi)}] =$$
$$= e^{2pT_p} - 2e^{-\xi\omega_0 T_p} \cos\omega_0 T_p \sqrt{1-\xi^2} e^{pT_p} + e^{-2\xi\omega_0 T_p} \tag{13.45}$$

where ξ = damping ratio

ω_0 = oscillating element resonance frequency.

As has been shown above, an element with delay τ at $(k-1)T_p < \tau \leqslant kT_p$ is representable by the multiplier e^{kpT_p} in $D^*(p)$.

These relations permit monitoring the denominator of the transfer function W^*_{o-l} for cases where the roots of the polynomial $D_{CP}(p)$ are known.

Examples of transfer functions and complex gains of open-loop sampled-data systems.

Example 13.1. Let us find the transfer function $W^*_{o-l}(p)$ for a sampled-data system with rectangular pulses having a unit duty factor. A continuous part contains an inertial element

$$W_{CP}(p) = \frac{k}{1+pT}$$

The reduced continuous part transfer function is

$$W_{RCP}(p) = W_{sh}(p)\, W_{CP}(p) = \frac{(1-e^{-pT_p})}{p} \frac{k}{(1+pT)} \qquad (13.46)$$

An open-loop sampled-data system may be represented by the equivalent diagram of Fig. 13.7*a* and, following obvious transformation, by that of Fig. 13.7*b*.

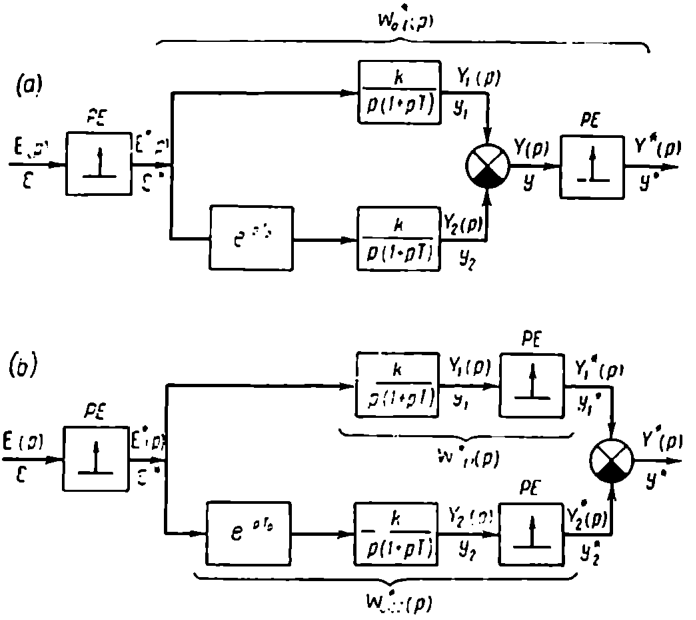

Fig. 13.7

The transfer function is

$$W^*_{o\text{-}l}(p) = W^*_{o\text{-}l1}(p) - W^*_{o\text{-}l2}(p) = W^*_{o\text{-}l1}(p) - e^{-pT_p} W^*_{o\text{-}l1}(p) = \\ = (1-e^{-pT_p})\, W^*_{o\text{-}l1}(p) \qquad (13.47)$$

The transfer function $W^*_{o\text{-}l1}(p)$ can be found from Eq. (13.32) for

$$W_{RCP1}(p) = \frac{k}{p(1+pT)}$$

Equation (12.39) obtained in Example 12.5 for the image $X(p) = \frac{k}{p(1+pT)}$ can also be used. Then

$$W^*_{o\text{-}l1}(p) = \frac{k\left(1-e^{-\frac{T_p}{T}}\right)e^{pT_p}}{(e^{pT_p}-1)\left(e^{pT_p}-e^{-\frac{T_p}{T}}\right)}$$

Substituting $W^*_{o\text{-}l1}(p)$ into Eq. (13.47), we have

$$W^*_{o\text{-}l}(p) = \frac{e^{pT_p}-1}{e^{pT_p}} W^*_{o\text{-}l1}(p) = \frac{k\left(1-e^{-\frac{T_p}{T}}\right)}{e^{pT_p}-e^{-\frac{T_p}{T}}} \tag{13.48}$$

The system complex gain is

$$W^*_{o\text{-}l}(j\omega) = \frac{k\left(1-e^{-\frac{T_p}{T}}\right)}{e^{j\omega T_p}-e^{-\frac{T_p}{T}}} \tag{13.49}$$

In order to obtain the locus of $W^*_{o\text{-}l}(j\omega)$, let us consider the inverse complex gain

$$W^{*-1}_{o\text{-}l}(j\omega) = \frac{1}{k\left(1-e^{-\frac{T_p}{T}}\right)}\left(e^{j\omega T_p}-e^{-\frac{T_p}{T}}\right) \tag{13.50}$$

The locus of the gain in the interval $0 \leqslant \omega \leqslant \frac{\omega_p}{2}$ is a semicircle in the upper half-plane, shown as a dotted line in Fig. 13.8.

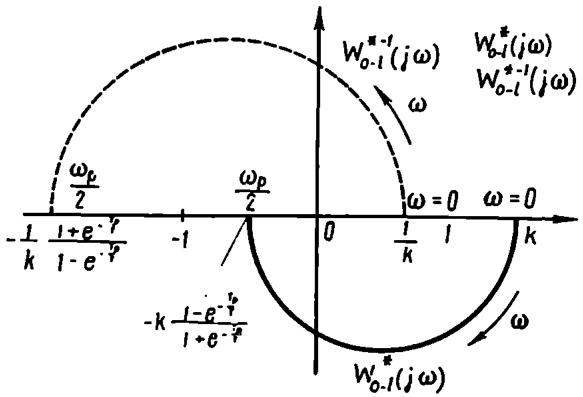

Fig. 13.8

The locus of $W^*_{o\text{-}l}(j\omega)$ obtained by inverting that of $W^{*-1}_{o\text{-}l}(j\omega)$ is also a semicircle but it is located in the lower half-plane and supported by the real axis in the points

$$\left.\begin{array}{ll} k & \text{at } \omega=0 \\ -k\dfrac{1-e^{-\frac{T_p}{T}}}{1+e^{-\frac{T_p}{T}}} & \text{at } \omega=\dfrac{\omega_p}{2} \end{array}\right\} \tag{13.51}$$

This locus is shown in Fig. 13.8 as a solid line.

Example 13.2. Let us find the transfer function $W^*_{o-l}(p)$ for the digital servo system of Sec. 12.1. The reduced continuous part transfer function has been found for it in Example 12.1 (see Eq. (12.9))

$$W_{RCP}(p) = W_{sh}(p) W_{CP}(p) = \frac{1-e^{-pT_p}}{p} \frac{k}{p(1+pT)}$$

As in the preceding example, we represent $W^*_{o-l}(p)$ in the form

$$W^*_{o-l}(p) = (1-e^{-pT_p}) W^*_{o-l1}(p)$$

where $W^*_{o-l1}(p)$ corresponds to the transfer function

$$W_{RCP1}(p) = \frac{k}{p^2(1+pT)}$$

Unlike the previous example, Eq. (13.32) cannot be used here directly because it is valid for simple roots only, whereas in the case under consideration the denominator of $W_{RCP1}(p)$ has a double zero root. Let us expand W_{RCP1} into simple fractions

$$W_{RCP1}(p) = \frac{C_1}{p} + \frac{C_2}{p^2} + \frac{C_3}{1+pT} = \frac{(C_1T+C_3)p^2 + (C_1+C_2T)p + C_2}{p^2(1+pT)}$$

whence, determining the coefficients $C_1 = -kT$, $C_2 = k$, $C_3 = kT^2$, we have

$$W_{RCP1}(p) = k\left(-\frac{T}{p} + \frac{1}{p^2} + \frac{T^2}{1+pT}\right) \tag{13.52}$$

Turning now to Table 12.1 and finding the images of discrete signals corresponding to the respective addends in Eq. (13.52), we get

$$W^*_{o-l1}(p) = k\left[-\frac{Te^{pT_p}}{e^{pT_p}-1} + \frac{T_p e^{pT_p}}{(e^{pT_p}-1)^2} + \frac{Te^{pT_p}}{e^{pT_p} - e^{-\frac{T_p}{T}}}\right] \tag{13.53}$$

Thence

$$W^*_{o-l}(p) = \frac{e^{pT_p}-1}{e^{pT_p}} k\left[\frac{-Te^{pT_p}}{e^{pT_p}-1} + \frac{T_p e^{pT_p}}{(e^{pT_p}-1)^2} + \frac{Te^{pT_p}}{e^{pT_p} - e^{-\frac{T_p}{T}}}\right] =$$

$$= k\left[-T + \frac{T_p}{e^{pT_p}-1} + \frac{T(e^{pT_p}-1)}{e^{pT_p} - e^{-\frac{T_p}{T}}}\right] =$$

$$= k\frac{[T_p - T(1-e^{-\frac{T_p}{T}})]e^{pT_p} + T(1-e^{-\frac{T_p}{T}}) - T_p e^{-\frac{T_p}{T}}}{(e^{pT_p}-1)(e^{pT_p} - e^{-\frac{T_p}{T}})} \tag{13.54}$$

or

$$W^*_{0\text{-}l}(p) = k\frac{[T_p - T(1-e^{-\frac{T_p}{T}})]e^{pT_p} + T(1-e^{-\frac{T_p}{T}}) - T_p e^{-\frac{T_p}{T}}}{e^{2pT_p} - (1+e^{-\frac{T_p}{T}})e^{pT_p} + e^{-\frac{T_p}{T}}} \qquad (13.55)$$

The complex gain is obtained by substituting $p = j\omega$ into Eq. (13.54). It can be conveniently expressed as

$$W^*_{0\text{-}l}(j\omega) = k\left[-T + \frac{T_p}{e^{j\omega T_p}-1} + \frac{T(e^{j\omega T_p}-1)}{e^{j\omega T_p} - e^{-\frac{T_p}{T}}}\right] =$$

$$= \frac{kT_p}{e^{j\omega T_p}-1} - \frac{kT(1-e^{-\frac{T_p}{T}})}{e^{j\omega T_p} - e^{-\frac{T_p}{T}}} \qquad (13.56)$$

The locus of the first addend (Fig. 13.9) is the straight line *1*. which is parallel to the imaginary axis and located in the lower half-plane; it ends at $\omega = \frac{\omega_p}{2}$ on the real axis in the point $-\frac{kT_p}{2}$. This follows from the fact that the locus of the inverse component $\frac{1}{kT_p}(e^{j\omega T_p} - 1)$ is a semicircle with centre on the real axis and passing through the origin of coordinates (it is shown as the dotted line *1'* in Fig. 13.9).

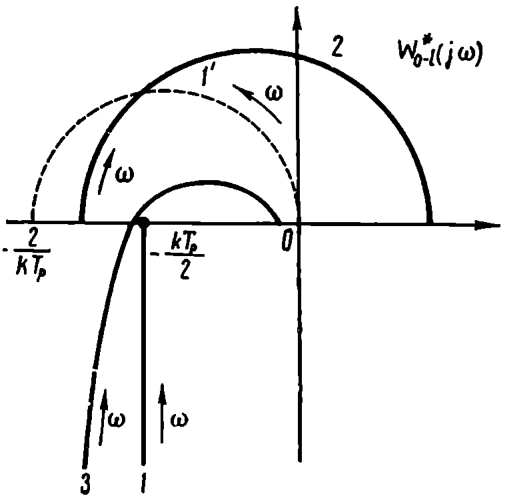

Fig. 13.9

As shown in the preceding example, the locus of the second addend is semicircle *2* located in the upper half-plane and supported by the real axis in the points

$$\left.\begin{array}{ll} -kT & \text{at } \omega = 0 \\ kT\dfrac{1-e^{-\frac{T_p}{T}}}{1+e^{-\frac{T_p}{T}}} & \text{at } \omega = \dfrac{\omega_p}{2} \end{array}\right\} \qquad (13.57)$$

The overall locus of the complex gain $W^*_{0\text{-}l}(j\omega)$ obtained by vectorial summation of loci *1* and *2* is given by curve *3* in the same figure.

At $T = 0$ the transfer function of the continuous part is

$$W_{CP}(p) = \frac{k}{p} \tag{13.58}$$

and that of the reduced continuous part is

$$W_{RCP}(p) = \frac{k(1-e^{-pT_p})}{p^2}$$

The transfer function of the open-loop sampled-data system is in this case obtained from Eq. (13.55) by substituting $T = 0$

$$W^*_{o-l}(p) = k\frac{T_p e^{pT_p}}{e^{2pT_p} - e^{pT_p}} = \frac{kT_p}{e^{pT_p} - 1} \tag{13.59}$$

The complex gain is

$$W^*_{o-l}(j\omega) = \frac{kT_p}{e^{j\omega T_p} - 1} \tag{13.60}$$

The locus of the complex gain is represented by curve *1* in Fig. 13.9.

13.3. COMPLEX GAINS AND TRANSFER FUNCTIONS OF CLOSED-LOOP SAMPLED-DATA SYSTEMS

Results obtained for complex gains and transfer functions of open-loop sampled-data systems can be used independently in specific cases for analysis of open-loop systems. We propose to discuss here closed-loop sampled-data control systems. The basic characteristics of closed-loop systems (complex gains and transfer functions) can be expressed in terms of the appropriate characteristics of open-loop systems.

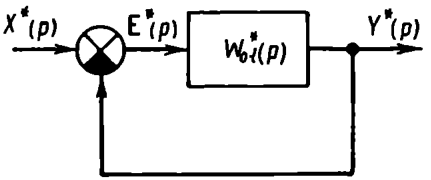

Fig. 13.10

The structural diagram of the closed-loop sampled-data control system of Fig. 13.3*b* can be reduced to the form of Fig. 13.10 and is a replica of the structural diagram for continuous control systems. The complex gain of a closed-loop sampled-data system, which is defined as the ratio of the spectra of the discrete signals $y^*(t)$ and $x^*(t)$ at the output and input, is thus expressed in terms of $W^*_{o-l}(j\omega)$ as in continuous systems

$$W^*_{cl-l}(j\omega) = \frac{Y^*(j\omega)}{X^*(j\omega)} = \frac{W^*_{o-l}(j\omega)}{1 + W^*_{o-l}(j\omega)} \tag{13.61}$$

The closed-loop transfer function is obtained by replacing $j\omega$ by p in Eq. (13.61)

$$W^*_{cl\text{-}l}(p) = \frac{W^*_{o\text{-}l}(p)}{1+W^*_{o\text{-}l}(p)} \tag{13.62}$$

Substituting $W^*_{o\text{-}l}(p) = \frac{K^*(p)}{D^*(p)}$, we have

$$W^*_{cl\text{-}l}(p) = \frac{K^*(p)}{K^*(p)+D^*(p)} = \frac{K^*(p)}{A^*(p)} \tag{13.63}$$

where $A^*(p)$ is the characteristic polynomial of a closed-loop system

$$A^*(p) = K^*(p) + D^*(p) \tag{13.64}$$

The basic results for complex gains and transfer functions of open-loop systems automatically extend to similar characteristics of closed-loop systems. Let us dwell on some of these.

If the reduced continuous part of a sampled-data system has a passband limited by a frequency ω_{b1} and if the inequality $\omega_{b1} \leqslant \leqslant \frac{\omega_p}{2}$ holds, then Eqs. (13.26) and (13.63) lead to

$$W^*_{cl\text{-}l}(j\omega) = \frac{\frac{1}{T_p} W_{RCP}(j\omega)}{1+\frac{1}{T_p} W_{RCP}(j\omega)} \tag{13.65}$$

in the frequency range $-\frac{\omega_p}{2} < \omega \leqslant \frac{\omega_p}{2}$.

In practice this equality holds if the largest time constant is much greater than T_p.

If at the same time the input signal spectrum is limited by the frequency ω_b, which is less than $\frac{\omega_p}{2}$, then the closed-loop sampled-data system behaves exactly as a closed-loop continuous system with an open-loop complex gain $\frac{1}{T_p} W_{RCP}(j\omega)$.

If the condition $\omega_b \leqslant \frac{\omega_p}{2}$ is not valid, then those stroboscopic properties of the sampled-data system begin to manifest themselves which depend on the periodic character of the complex gain $W^*_{cl\text{-}l}(j\omega)$. The behaviour of the sampled-data system then differs substantially from that of a similar continuous system.

The identity condition for a sampled-data control system and a continuous system with a complex gain $\frac{1}{T_p} W_{RCP}(j\omega)$ in the open-loop state can be formulated in a more general form in terms of Eq. (13.5)

$$\omega_p \geqslant \omega_b + \omega_{b1} \tag{13.66}$$

where ω_b = boundary frequency of the input signal spectrum
ω_{b1} = passband boundary frequency of the reduced continuous part.

The transfer functions of closed-loop sampled-data control systems are periodic in the p plane of the complex variable along the imaginary axis and are therefore studied in the band $-\frac{\omega_p}{2} < \operatorname{Im} p \leqslant \frac{\omega_p}{2}$ (see Fig. 12.14).

Transfer functions of closed-loop sampled-data control systems are fractional rational functions of e^{pT_p}. The degree of the characteristic polynomial $A^*(p)$ is equal to that of the continuous part, n, if the latter does not include delay elements and poles differing by $jk\omega_p$.

In systems with a delay τ at $(k-1)\,T_p < \tau \leqslant kT_p$ the degree of $A^*(p)$ is $n+k$.

The numerator order of the transfer function $W^*_{cl-l}(p)$ in systems without delay is $n-1$, in systems with delay, n.

Example 13.3. Determine the transfer function $W^*_{cl-l}(p)$ of the system discussed in Example 13.1. Substitution of Eq. (13.48) into Eq. (13.62) gives

$$W^*_{cl-l}(p) = \frac{k\left(1-e^{-\frac{T_p}{T}}\right)}{e^{pT_p}+k-(k+1)\,e^{-\frac{T_p}{T}}} \tag{13.67}$$

Example 13.4. Determine the transfer function $W^*_{cl-l}(p)$ of the digital servo system discussed in Example 13.2. It is found by substituting Eq. (13.55) into Eq. (13.62)

$$W^*_{cl-l}(p) = \frac{k\left[T_p - T\left(1-e^{-\frac{T_p}{T}}\right)\right]e^{pT_p} + k\left[T\left(1-e^{-\frac{T_p}{T}}\right) - T_p e^{-\frac{T_p}{T}}\right]}{e^{2pT_p} + \left\{k\left[T_p - T\left(1-e^{-\frac{T_p}{T}}\right)\right] - \left(1+e^{-\frac{T_p}{T}}\right)\right\}e^{pT_p} + k\left[T\left(1-e^{-\frac{T_p}{T}}\right) - T_p e^{-\frac{T_p}{T}}\right] + e^{-\frac{T_p}{T}}} \tag{13.68}$$

At $T=0$

$$W^*_{cl-l}(p) = \frac{kT_p}{e^{pT_p}-1+kT_p} \tag{13.69}$$

The nature of changes in the error of a sampled-data control system can be studied by using the transfer function relating the input to the error

$$W^*_{\varepsilon}(p) = \frac{E^*(p)}{X^*(p)} = \frac{W^*_{cl-l}(p)}{W^*_{o-l}(p)} = \frac{1}{1+W^*_{o-l}(p)} = \frac{D^*(p)}{K^*(p)+D^*(p)} \tag{13.70}$$

Example 13.5. Determine the transfer function $W_\varepsilon^*(p)$ relating the input to the error for the system of Example 13.1. It is found by substituting Eq. (13.48) into Eq. (13.70)

$$W_\varepsilon^*(p) = \frac{e^{pT_p} - e^{-\frac{T_p}{T}}}{e^{pT_p} + k - (k+1)\,e^{-\frac{T_p}{T}}} \tag{13.71}$$

Example 13.6. Determine the transfer function $W_\varepsilon^*(p)$ for a digital servo system (see Example 13.2). By Eq. (13.54)

$$W_\varepsilon^*(p) = \frac{(e^{pT_p}-1)(e^{pT_p} - e^{-\frac{T_p}{T}})}{e^{2pT_p} + \{k[T_p - T(1-e^{-\frac{T_p}{T}})] - (1+e^{-\frac{T_p}{T}})\}e^{pT_p} + k[T(1-e^{-\frac{T_p}{T}}) - T_p e^{-\frac{T_p}{T}}] + e^{-\frac{T_p}{T}}} \tag{13.72}$$

At $T=0$

$$W_\varepsilon^*(p) = \frac{e^{pT_p}-1}{e^{pT_p} - 1 + kT_p} \tag{13.73}$$

On certain occasions, it is useful to know the nature of changes in some intermediate value y_1 in the continuous part of the system

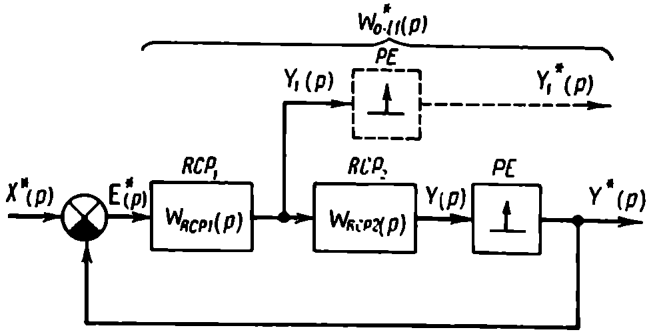

Fig. 13.11

(Fig. 13.11). Introducing in this case a dummy PE at the output we are interested in (shown as a dotted line in the figure) gives

$$W_{cl-1}^*(p) = \frac{Y_1^*(p)}{X^*(p)} = \frac{W_{o-1}^*(p)\,E^*(p)}{X^*(p)} = \frac{W_{o-1}^*(p)}{1+W_{o-1}^*(p)} \tag{13.74}$$

where $W_{o-1}^*(p)$ is the transfer function of an open-loop sampled-data system which corresponds to the part of the system between the

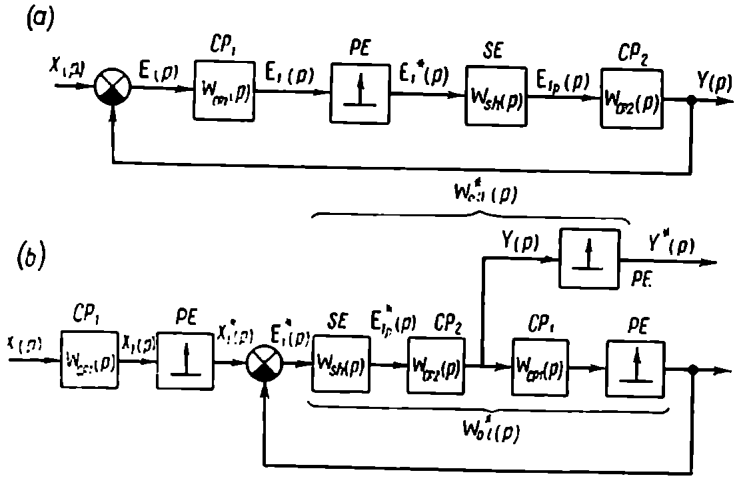

Fig. 13.12

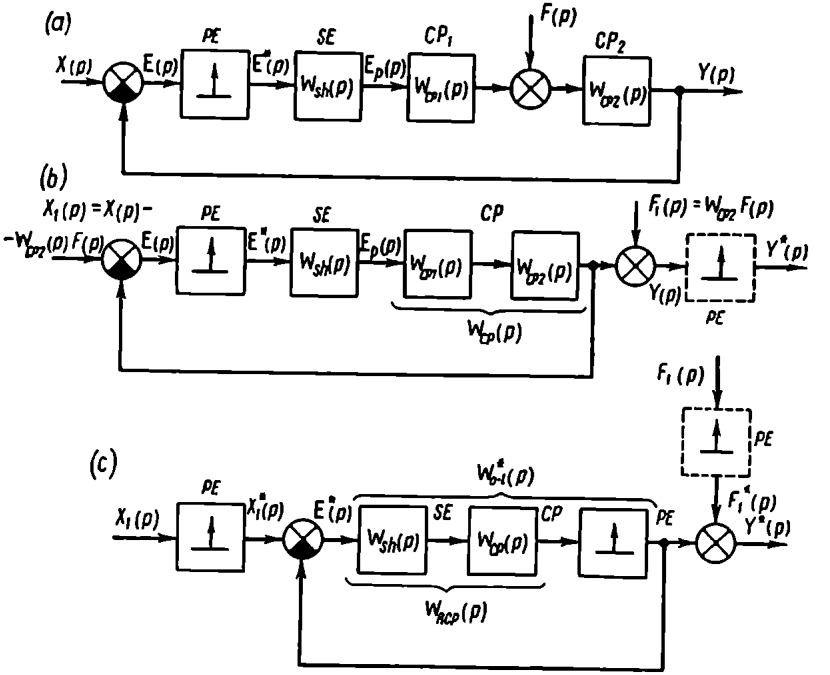

Fig. 13.13

comparator and the output under study having the transfer function $W_{RCP1}(p)$. $W^*_{o\text{-}11}(p)$ can be obtained from $W_{RCP1}(p)$ or $w_{RCP1}(t)$ via Eq. (13.28) or (13.29).

When studying structural diagrams of sampled-data control systems (see Fig. 12.7) we assumed that a PE is connected directly after the comparator. However, practically, an element with a transfer function $W_{CP1}(p)$ can be included between them (Fig. 13.12*a*). In the general case the CP_1 and PE cannot be simply interchanged. Equivalent transformations can reduce the structural diagram of Fig. 13.12*a* to the form of Fig. 13.12*b*. Then the image of the output quantity $Y^*(p)$ can be obtained from the expressions

$$\left.\begin{aligned} Y^*(p) &= W^*_{cl\text{-}11}(p)\, X^*_1(p) \\ W^*_{cl\text{-}11}(p) &= \frac{W^*_{o\text{-}11}(p)}{1+W^*_{o\text{-}l}(p)} \\ X_1(p) &= W_{CP1}(p)\, X(p) \end{aligned}\right\} \qquad (13.75)$$

The transfer function $W^*_{n\text{-}l}(p)$ represents a continuous part with a transfer function $W_{CP1}(p)\, W_{CP2}(p)$.

If a sampled-data control system is subject to a disturbance $f(t)$ (the image $F(p)$ in Fig. 13.13*a*), the system structural diagram can be conveniently reduced to the form of Fig. 13.13*b* and *c*. In this case the image of the output variable is

$$Y^*(p) = \frac{W^*_{o\text{-}l}(p)}{1+W^*_{o\text{-}l}(p)}\,[X^*(p) - F^*_1(p)] + F^*_1(p) \qquad (13.76)$$

where $F^*_1(p)$ is the image of a discrete signal obtained in time sampling of the signal $f_{CP1}(t)$, which in turn is obtained when the disturbance $f(t)$ propagates through an element with a transfer function $W_{CP2}(p)$

$$f_1(t) = L^{-1}[F(p)\, W_{CP2}(p)] \qquad (13.77)$$

Chapter XIV

SAMPLED-DATA CONTROL SYSTEMS. STABILITY, TRANSIENT AND STEADY-STATE PROCESSES

14.1. STABILITY OF SAMPLED-DATA CONTROL SYSTEMS

Conditions for stability of sampled-data systems. The image $Y^*(p)$ of a signal at the output of a sampled-data control system, subjected to an arbitrary signal with an image $X^*(p)$ at the input, is presented as

$$Y^*(p) = W^*_{cl\text{-}l}(p)\, X^*(p) = \frac{K^*(p)}{A^*(p)} X^*(p)$$

If the image $Y^*(p)$ is known the output signal discrete values can be obtained, by virtue of Eq. (12.48), as a sum of residues of the product $Y^*(p)\, e^{p(l-1)T_p}$ relative to its poles

$$y(lT_p) = \sum_{\nu} \operatorname{Res}_{ep_\nu T_p} [Y^*(p)\, e^{p(l-1)T_p}] =$$

$$= \sum_{\nu} \operatorname{Res}_{ep_\nu T_p} [W^*_{cl\text{-}l}(p)\, X^*(p)\, e^{p(l-1)T_p}] \qquad (14.1)$$

The output signal can be represented as a sum of the forced and transient components

$$y(lT_p) = y_{fo}(lT_p) + y_t(lT_p) \qquad (14.2)$$

The forced component is the sum of residues (see Eq. (14.1)) relative to the poles of the input signal image $X^*(p)$ in the band $-\frac{\omega_p}{2} < \operatorname{Im} p \leqslant \frac{\omega_p}{2}$; the transient component is the sum of residues relative to the poles of the transfer function $W^*_{cl\text{-}l}(p)$ in the same band. The poles of the transfer function (which are a fractional rational function of e^{pT_p}, as was shown in Sec. 13.2) can be found from the equation

$$A^*(p) = a_n e^{npT_p} + a_{n-1} e^{(n-1)pT_p} + \ldots + a_0 = 0 \qquad (14.3)$$

which is called the *characteristic equation of a closed-loop system* and has n roots in the band under review. If these roots are simple, then the transient component can be given as a sum of exponents

(Eq. (12.49))

$$y_t(lT_p) = \sum_{\nu=1}^{n} g_\nu e^{p_\nu l T_p} \qquad (14.4)$$

where p_ν = roots of the characteristic equation
g_ν = coefficients.

If all roots of the characteristic equation have negative real parts, i.e. are located in the left-hand half of the band $-\frac{\omega_p}{2} < \operatorname{Im} p \leqslant \frac{\omega_p}{2}$, then as $l \to \infty$ all addends in Eq. (14.4) tend to zero, the transient component decays, and the process $y(lT_p)$ converges to the forced component. A sampled-data system of this kind is *stable*.

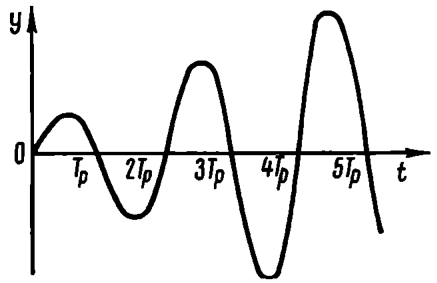

Fig. 14.1

If at least one root of the characteristic equation is in the right-hand part of the band, the corresponding addend in Eq. (14.4) increases infinitely in magnitude. Such a system is *unstable*. If one or several roots are on the imaginary axis, the sampled-data system is *neutral*.

Consequently, the necessary and sufficient condition for stability of sampled-data control systems is that all roots of the characteristic equation for a closed-loop system remain in the left-hand half of the band $-\frac{\omega_p}{2} < \operatorname{Im} p \leqslant \frac{\omega_p}{2}$ in the complex p plane.

This position of the roots of Eq. (14.3) makes a sampled-data system stable only at discrete sampling instants and does not exclude the possibility of unstable behaviour between these instants. Concealed oscillations may arise in such a system if, for instance, the reduced continuous part has a transfer function with poles in the right half-plane, and the imaginary part of these poles is a multiple of halved frequency ω_p of a *PE*. A closed-loop system in this case may have all roots of the characteristic equation (14.3) in the left-hand side, but diverging oscillations may generate in the reduced continuous part. With the proper phase they will not affect the system owing to time sampling (Fig. 14.1).

Concealed oscillations are rare in sampled-data control systems and arise only if ω_p is of the same order as the natural frequencies of the continuous part elements. In practice ω_p is well in excess of these frequencies.

Any attempts at estimating the stability of a sampled-data control system by direct calculation of the characteristic equation roots

encounter the same difficulties as in the case of continuous systems. Therefore the stability criteria obtained for continuous systems can be usefully extended to sampled-data systems.

Hurwitz stability criterion for sampled-data systems. Let us apply the Hurwitz algebraic criterion of stability to analysis of sampled-data systems. For this purpose substitute $e^{pT_p} = z$ in the characteristic equation of the closed-loop sampled-data system

$$A^*(p) = a_n e^{npT_p} + a_{n-1} e^{(n-1)pT_p} + \ldots + a_0 = 0$$

Then

$$A(z) = a_n z^n + a_{n-1} z^{n-1} + \ldots + a_0 = 0 \qquad (14.5)$$

This substitution maps the half-band $\operatorname{Re} p < 0$, $-\frac{\omega_p}{2} < \operatorname{Im} p \leqslant \frac{\omega_p}{2}$ of the p plane on a unit radius circle $|z| \leqslant 1$ in the z plane;

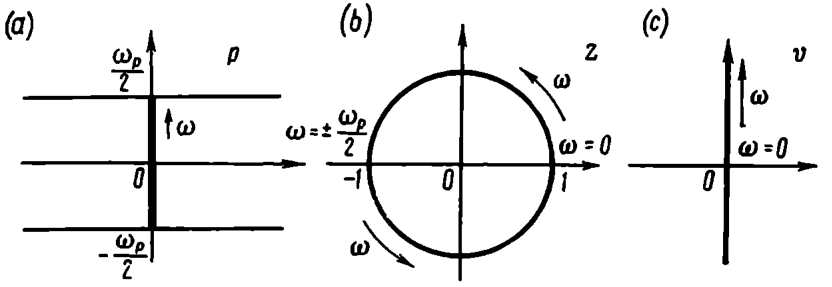

Fig. 14.2

here the segment of the imaginary axis from $-\frac{\omega_p}{2}$ to $\frac{\omega_p}{2}$ is transformed into a circumference of unit radius (Fig. 14.2*a* and *b*).

Substituting the variables in $A(z)$:

$$z = \frac{1+v}{1-v} \qquad (14.6)$$

$$v = \frac{z-1}{z+1} \qquad (14.7)$$

$$v = \frac{e^{pT_p}-1}{e^{pT_p}+1} \qquad (14.8)$$

We will transform the circumference of unit radius in the z plane into an imaginary axis in the v plane. Consequently, the specified segment of the imaginary axis in the p plane turns into the entire imaginary axis in the v plane (Fig. 14.2*c*)

$$v = \frac{e^{j\omega T_p}-1}{e^{j\omega T_p}+1} = j \tan \frac{\omega T_p}{2} \qquad (14.9)$$

The interior of a unit circle in the z plane (and the left half-band $\operatorname{Re} p < 0$, $-\frac{\omega_p}{2} < \operatorname{Im} p \leqslant \frac{\omega_p}{2}$ in the p plane) then corresponds to the left half of the v plane.

The system characteristic equation then takes the form

$$a_n \left(\frac{1+v}{1-v}\right)^n + a_{n-1} \left(\frac{1+v}{1-v}\right)^{n-1} + \ldots + a_0 = 0$$

or

$$a_n (1+v)^n + a_{n-1} (1+v)^{n-1} (1-v) + \ldots + a_0 (1-v)^n = 0 \tag{14.10}$$

or

$$a'_n v^n + a'_{n-1} v^{n-1} + \ldots + a'_0 = 0$$

where a'_i = new coefficients of the equation.

For the characteristic equation (14.10), the Hurwitz criterion can be used and the stability of a sampled-data system estimated by the signs of Hurwitz determinants (see Ch. VII) obtained from the coefficients a'_i.

Example 14.1. Let us consider the characteristic equation of a digital servo system which can be obtained from Eq. (13.68) (see Example 13.4)

$$e^{2pT_p} + a_1 e^{pT_p} + a_0 = 0 \tag{14.11}$$

where

$$\left.\begin{aligned} a_1 &= k\left[T_p - T\left(1 - e^{-\frac{T_p}{T}}\right)\right] - \left(1 + e^{-\frac{T_p}{T}}\right) \\ a_0 &= k\left[T\left(1 - e^{-\frac{T_p}{T}}\right) - T_p e^{-\frac{T_p}{T}}\right] + e^{-\frac{T_p}{T}} \end{aligned}\right\} \tag{14.12}$$

or, substituting $z = e^{pT_p}$, we obtain

$$z^2 + a_1 z + a_0 = 0 \tag{14.13}$$

Substituting $z = \frac{1+v}{1-v}$ and grouping terms of equal power gives

$$(1 - a_1 + a_0) v^2 + 2(1 - a_0) v + 1 + a_1 + a_0 = 0 \tag{14.14}$$

According to the Hurwitz criterion the necessary and sufficient condition for stability of second-order systems is that the characteristic equation coefficients be positive

$$\left.\begin{aligned} 1 + a_1 + a_0 &> 0 \\ 1 - a_0 &> 0 \\ 1 - a_1 + a_0 &> 0 \end{aligned}\right\} \tag{14.15}$$

Substituting a_1 and a_0 from Eq. (14.12) into Eq. (14.15) gives the stability conditions

$$kT_p\left(1 - e^{-\frac{T_p}{T}}\right) > 0 \tag{14.16}$$

$$k < \frac{1-e^{-\frac{T_p}{T}}}{T\left(1-e^{-\frac{T_p}{T}}\right)-T_p e^{-\frac{T_p}{T}}} = k_{lim1} \qquad (14.17)$$

$$k < \frac{2\left(1+e^{-\frac{T_p}{T}}\right)}{T_p\left(1+e^{-\frac{T_p}{T}}\right)-2T\left(1-e^{-\frac{T_p}{T}}\right)} = k_{lim2} \qquad (14.18)$$

The first of these inequalities can be rewritten as

$$k > 0 \qquad (14.19)$$

The second and the third inequalities signify that the continuous part gain k should be below the lesser of the two limit values, k_{lim1} and k_{lim2}. These values can be expressed in the following way

$$k_{lim1} = \frac{1}{T_p} \frac{\frac{T_p}{T}\left(1-e^{-\frac{T_p}{T}}\right)}{1-\left(1+\frac{T_p}{T}\right)e^{-\frac{T_p}{T}}} \qquad (14.20)$$

$$k_{lim2} = \frac{1}{T_p} \frac{2\frac{T_p}{T}\left(1+e^{-\frac{T_p}{T}}\right)}{\frac{T_p}{T}\left(1+e^{-\frac{T_p}{T}}\right)-2\left(1-e^{-\frac{T_p}{T}}\right)} \qquad (14.21)$$

The plots of the dimensionless values $k_{lim1}T_p$ and $k_{lim2}T_p$, which depend on the dimensionless ratio $\frac{T_p}{T}$, are given in Fig. 14.3 (Ref. 81). They show that at small $\frac{T_p}{T}$ the former is the lesser and at large $\frac{T_p}{T}$ the latter is the lesser. At $0 < \frac{T_p}{T} \leqslant 0.5$, $k_{lim1}T_p \approx 2$, and therefore for these $\frac{T_p}{T}$ the limit value of the system gain is

$$k_{lim} \approx \frac{2}{T_p} = \frac{1}{\pi}\omega_p \qquad (14.22)$$

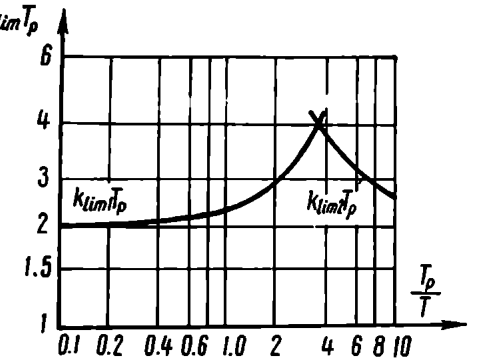

Fig. 14.3

The servo system gain is thus proportional to the PE frequency in a sufficiently wide range.

As $\omega_p \to \infty$ the system becomes continuous and $k_{lim} \to \infty$, as should indeed be the case in a continuous second-order system.

In a particular case where $T = 0$, k_{lim1} becomes infinite, and the stability condition takes the form

$$0 < k < k_{lim2} = \frac{2}{T_p} = \frac{1}{\pi_j^i}\omega_p \qquad (14.23)$$

Table 14.1 gives the stability conditions expressed in terms of the coefficients of the closed-loop characteristic equation (14.3) according to the Hurwitz criterion.

Table 14.1

Characteristic Equation Power n	Stability Conditions
1	$a_1+a_0>0$ $a_1-a_0>0$
2	$a_2+a_1+a_0>0$ $a_2-a_1+a_0>0$ $a_2-a_0>0$
3	$a_3+a_2+a_1+a_0>0$ $a_3-a_2+a_1-a_0>0$ $a_3(a_3-a_1)-a_0(a_0-a_2)>0$ $3(a_3+a_0)-a_2-a_0>0$
4	$a_4+a_3+a_2+a_1+a_0>0$ $a_4-a_3+a_2-a_1+a_0>0$ $(a_4-a_0)^2(a_4-a_2+a_0)+(a_3-a_1)(a_4a_1-a_3a_0)>0$ $2(a_4-a_0)-a_3+a_1>0$ $2(a_4-a_0)+a_3-a_1>0$

Mikhailov criterion for sampled-data systems. Let us first determine the changes in the argument of a closed-loop system characteristic vector $A^*(j\omega)$ when ω varies from $-\frac{\omega_p}{2}$ to $+\frac{\omega_p}{2}$. This can be conveniently done by substituting $z = e^{pT_p}$ into the characteristic polynomial of a closed-loop system

$$A(z) = a_n z^n + a_{n-1}z^{n-1} + \ldots + a_0$$

and expanding it into

$$A(z) = a_n (z - z_1)(z - z) \ldots (z - z_n) \qquad (14.24)$$

where z_i are the roots of the equation $A(z) = 0$ which correspond to the roots p_i of the characteristic equation $A^*(p) = 0$.

Then assume that $z = e^{j\omega T_p}$ and find the changes in the argument of one of the multipliers included in $A(z)$

$$\Delta \arg (e^{j\omega T_p} - z_i)$$

$$-\frac{\omega_p}{2} < \omega \leqslant \frac{\omega_p}{2}$$

Two cases must be treated: the characteristic equation root z_i is (1) inside and (2) outside a circle of unit radius in the z plane.

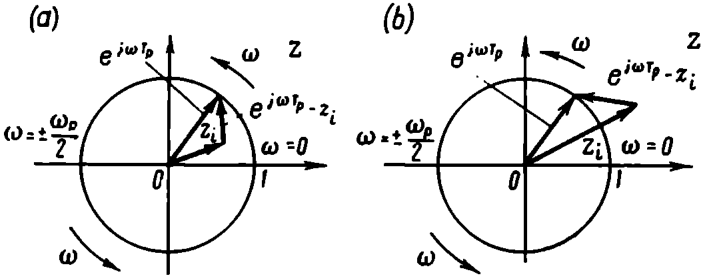

Fig. 14.4

The former case implies the location of the appropriate root p_i in the left-hand half of the band $-\frac{\omega_p}{2} < \operatorname{Im} p \leqslant \frac{\omega_p}{2}$ in the p plane and the latter, its location in the right-hand half. Figure 14.4*a* and *b* represents the respective cases.

The ends of the vectors $z = e^{j\omega T_p}$ and $e^{j\omega T_p} - z_i$ slide along the circle of unit radius counterclockwise with ω varying from $-\frac{\omega_p}{2}$ to $\frac{\omega_p}{2}$. In the former case the argument changes as

$$\Delta \arg (e^{j\omega T_p} - z_i) = 2\pi$$

$$-\frac{\omega_p}{2} < \omega \leqslant \frac{\omega_p}{2}$$

and in the latter case,

$$\Delta \arg (e^{j\omega T_p} - z_i) = 0$$

$$-\frac{\omega_p}{2} < \omega \leqslant \frac{\omega_p}{2}$$

If we assume that the characteristic equation of the system $A^*(p) = 0$ has k roots in the left half of the band $-\frac{\omega_p}{2} < \operatorname{Im} p \leqslant \frac{\omega_p}{2}$, then the overall change of the argument of the characteristic vector

(the sum of multiplier argument changes for all the roots) is

$$\Delta \arg A^*(j\omega) = \Delta \arg A(e^{j\omega T_p}) = 2k\pi \qquad (14.25)$$

$$-\frac{\omega_p}{2} < \omega \leqslant \frac{\omega_p}{2}$$

Since

$$\begin{aligned} \operatorname{Re} e^{j\omega T_p} &= \operatorname{Re} e^{-j\omega T_p} \\ \operatorname{Im} e^{j\omega T_p} &= -\operatorname{Im} e^{-j\omega T_p} \end{aligned} \qquad (14.26)$$

whence it follows that the complex vectors $A^*(j\omega)$ and $A^*(-j\omega)$ are conjugate. The result of Eq. (14.25) can be written then for the halved band of ω

$$\Delta \arg A^*(j\omega) = k\pi \qquad (14.27)$$

$$0 \leqslant \omega \leqslant \frac{\omega_p}{2}$$

For a stable sampled-data control system the number of roots in the left half of the band is n. Therefore the Mikhailov criterion

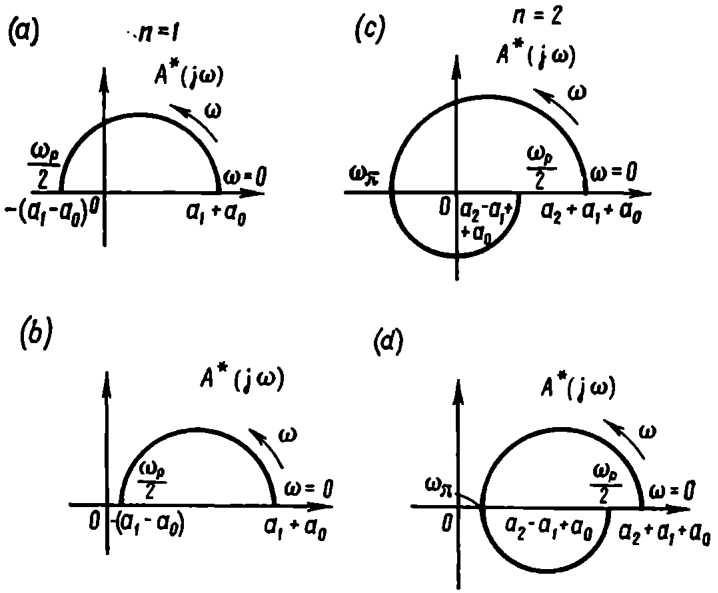

Fig. 14.5

can be formulated as follows. *For a sampled-data control system to be stable it is necessary and sufficient that with* ω *varying from* 0 *to* $\frac{\omega_p}{2}$ *the characteristic vector* $A^*(j\omega)$ *be turned by an angle* $n\pi$, *where* n *is the order of the characteristic equation*; in other words, that

with ω *increasing from* 0 *to* $\frac{\omega_p}{2}$ *the locus* $A^*(j\omega)$ *intersect* $2n$ *quadrants successively in the positive direction.*

Figure 14.5 represents the loci of the characteristic vector $A^*(j\omega)$ for stable (*a* and *c*) and unstable (*b* and *d*) first- and second-order systems. These loci differ from the corresponding loci of continuous systems in that they end as well as start on the imaginary axis at $\omega = \frac{\omega_p}{2}$. Unlike continuous systems, not only second- but even first-order sampled-data systems can be unstable at positive coefficients of the characteristic equation, which is also seen in Table 14.1.

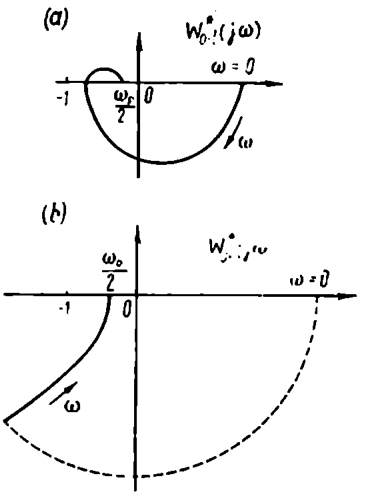

Fig. 14.6

Nyquist criterion for sampled-data systems. The Nyquist criterion can be derived by studying the variations of the vector $1 + W^*_{o\text{-}l}(j\omega)$ argument as was done for continuous systems (see Sec. 7.3). Without repeating the argumentation, we will give the Nyquist criterion in terms of direct amplitude-phase responses of open-loop sampled-data systems for two cases, a stable and a neutral open-loop system.

In the first case *for a closed-loop system to be stable it is necessary and sufficient that with* ω *varying from* 0 *to* $\frac{\omega_p}{2}$ *the amplitude-phase response* $W^*_{o\text{-}l}(j\omega)$ *of an open-loop system should not encircle the point* $-1, j0$; in other words, *that with* ω *varying from* 0 *to* $\frac{\omega_p}{2}$ *the difference between the number of positive and negative transitions of the amplitude-phase response* $W^*_{o\text{-}l}(j\omega)$ *over the segment* $(-\infty, -1)$ *of the real axis be zero* (Fig. 14.6*a*).

The stability of an open-loop sampled-data system can be estimated from the stability of its continuous part because the open-loop system transfer function poles coincide with an accuracy to their imaginary part with the poles of the transfer function of the continuous part (see Sec. 13.2). If the continuous part of the system is stable, neutral or unstable, then the open-loop sampled-data system is stable, neutral or unstable, respectively.

A possible exception is the case where the reduced continuous part is unstable and two or more poles of $W_{CP}(p)$ in the right half-plane of the variable p differ only in their imaginary parts, the difference being $jk\omega_p$, where k is an integer.

Such cases are rare, as has been noted above.

If the reduced continuous part (and hence an open-loop sampled-data system) is neutral and contains ν integrators connected in series (the zeroth ν-tuple pole), then by virtue of Eq. (13.44) the transfer function and the complex gain have the form

$$W^*_{o\text{-}l}(p) = \frac{K^*(p)}{(e^{pT_p}-1)^\nu D_1^*(p)} \tag{14.28}$$

$$W^*_{o\text{-}l}(j\omega) = \frac{K^*(j\omega)}{(e^{j\omega T_p}-1)^\nu D_1^*(j\omega)} \tag{14.29}$$

The amplitude-phase response $W^*_{o\text{-}l}(j\omega)$ at low ω starts at infinity (Fig. 14.6*b*). If at low ω we regard $W^*_{o\text{-}l}(j\omega)$ as

$$W^*_{o\text{-}l}(j\omega) = \lim_{\beta\to 0} \frac{K^*(j\omega)}{(e^{j\omega T_p}-1+\beta)^\nu D_1^*(j\omega)} \tag{14.30}$$

then it is possible to show (as was done for continuous systems) that the above formulation of the Nyquist criterion is applicable to neutral open-loop sampled-data systems provided that the amplitude-phase response is complemented with a circle of infinitely large radius starting on the imaginary axis (see Fig. 14.6*b*).

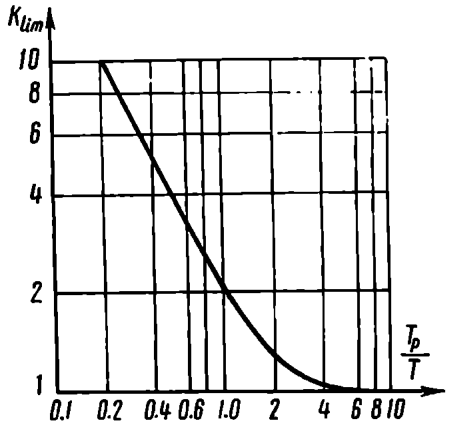

Fig. 14.7

Example 14.2. Let us analyze the stability of the system of Example 13.1 whose complex gain in the open-loop state is

$$W^*_{o\text{-}l}(j\omega) = \frac{k\left(1-e^{-\frac{T_p}{T}}\right)}{e^{j\omega T_p}-e^{-\frac{T_p}{T}}}$$

The locus of $W_{o\text{-}l}(j\omega)$ is shown in Fig. 13.8. For a closed-loop system to be stable in terms of the Nyquist criterion $k > 0$, it is necessary and sufficient that the following inequality obtained from (13.51) be valid

$$k < \frac{1+e^{-\frac{T_p}{T}}}{1-e^{-\frac{T_p}{T}}} = k_{llm} \tag{14.31}$$

Figure 14.7 portrays the variation of k_{llm} as a function of the dimensionless value $\frac{T_p}{T}$. As $T_p \to 0$ the system becomes continuous,

and k_{lim} becomes infinitely large, which is natural. With increasing T_p the limit gain decreases.

Example 14.3. Let us take up the stability of a digital servo system whose complex gain (see Example 13.2) is

$$W^*_{o\text{-}l}(j\omega) = \frac{kT_p}{e^{j\omega T_p} - 1}$$

Its locus is shown in Fig. 13.9 (curve *1*).

The only stability condition at $k > 0$ is

$$W^*_{o\text{-}l}\left(j\frac{\omega_p}{2}\right) = -\frac{kT_p}{2} > -1$$

whence

$$k < \frac{2}{T_p} = \frac{1}{\pi}\omega_p$$

which coincides with Eq. (14.23).

The examples of this section reveal that a reduction in the frequency of PE (increase in T_p) normally leads to reduced limit gain and

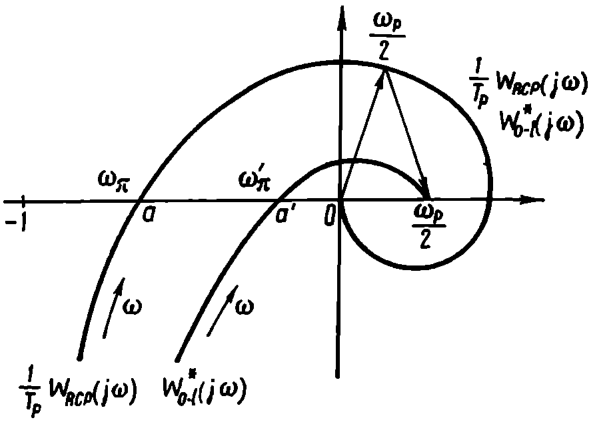

Fig. 14.8

deteriorated dynamic properties of a sampled-data system. In the design of sampled-data control systems, therefore, T_p must be so selected that it is much below the main time constant of the continuous part. As noted in Sec. 13.3, with input signals having a limited spectrum a sampled-data system behaves practically as a continuous one with $W_{o\text{-}l}(p) = \frac{1}{T_p} W_{RCP}(p)$.

There is, however, a case where the largest gain in a sampled-data system is obtained with a nonzero T_p. This happens when the amplitude-phase response of the reduced continuous part of the system is of the form given in Fig. 14.8. The amplitude-phase response $\frac{1}{T_p} W_{RCP}(j\omega)$ traverses the first and fourth quadrants, retaining

large enough values there. This is typical of systems whose continuous part includes delays.

Figure 14.8 also illustrates an amplitude-phase response $W^*_{o\text{-}l}(j\omega)$, which is plotted according to Eq. (13.25). If in a sampled-data system of the type in question T_p is selected so that the frequency $\frac{\omega_p}{2}$ is in the first quadrant, as shown in the figure, then $W^*_{o\text{-}l}(j\omega)$ intersecting the real axis to the right of $\frac{1}{T_p} W_{RCP}(j\omega)$ can be obtained. The sampled-data system limit gain then exceeds that of the corresponding continuous system.

In conclusion we will note that the relative estimate of the applicability of stability criteria given in Sec. 7.5 is also valid for sampled data systems.

14.2. DETERMINING SIGNAL VARIATION LAWS IN SAMPLED-DATA CONTROL SYSTEMS

Methods for finding discrete values of signals in sampled-data systems. The image of the output signal in a sampled-data control system can be given in terms of a closed-loop system transfer function in the following way

$$Y^*(p) = W_{cl\text{-}l}(p)\, X^*(p)$$

Here $X^*(p)$ is understood as the image of some generalized discrete signal which in the general case is made up of the setpoint and disturbance signals, both may be first propagated through linear elements (see Figs. 13.12, 13.13 and Eqs. (13.75), (13.76), and (13.77)). In a particular case this signal coincides with the setpoint.

We will consider methods for determining the processes of variation of discrete values of signals in sampled-data systems.

The core of *the first method* is the use of difference equations related to transfer functions. If the transfer function of a closed-loop sampled-data control system (which is equal to the ratio of the images $Y^*(p)$ and $X^*(p)$ at zero initial conditions) is of the form (13.63)

$$W^*_{cl\text{-}l}(p) = \frac{Y^*(p)}{X^*(p)} = \frac{k_m e^{mpT_p} + k_{m-1} e^{(m-1)pT_p} + \ldots + k_0}{a_n e^{npT_p} + a_{n-1} e^{(n-1)pT_p} + \ldots + a_0}$$

the delay theorem leads to a relation for the discrete signals $y^*(t)$ and $x^*(t)$ and then for discrete values of the signals y and x

$$a_n y^*[(l+n)T_p] + a_{n-1} y^*[(l+n-1)T_p] + \ldots + a_0 y^*(lT_p) = k_m x^*[(l+m)T_p] + k_{m-1} x^*[(l+m-1)T_p] + \ldots + k_0 x^*(lT_p) \quad (14.32)$$

$$a_n y[(l+n)T_p] + a_{n-1} y[(l+n-1)T_p] + \ldots + a_0 y(lT_p) = k_m x[(l+m)T_p] + k_{m-1} x[(l+m-1)T_p] + \ldots + k_0 x(lT_p) \quad (14.32a)$$

This relation is known as the difference equation of a closed-loop sampled-data control system (and can be expressed in terms of finite difference of the functions y and x formed from discrete values corresponding to sampling points; hence the term difference equation). A difference equation can be derived for an open-loop sampled-data system as well.

Difference equations can be deduced by the following simple rule. A relation of the type (13.63) for the system in question is written in one line, the parentheses removed, and in the left-hand part of the resulting equality $Y^*(p)$ is replaced by $y(lT_p)$, $e^{pT_p}Y^*(p)$ by $y[(l+1)T_p]$, . . ., and $e^{npT_p}Y^*(p)$ by $y[(l+n)T_p]$.

Similar substitutions should be made in the right-hand part of the equality for $X^*(p)$, $e^{pT_p}X^*(p)$, . . ., and $e^{mpT_p}X^*(p)$.

If a difference equation is given, the transfer function of the sampled-data system can be obtained by the reverse transformation.

Having rearranged Eq. (14.32) as

$$y[(l+n)T_p] = \frac{1}{a_n}\{k_m x[(l+m)T_p] + \ldots + k_0 x(lT_p) - \\ - a_{n-1}y[(l+n-1)T_p] - \ldots - a_0 y(lT_p)\} \qquad (14.33)$$

the difference equation can be regarded as a recurrence relation which permits finding discrete values of the sampled-data system output signal at the $(l+n)$th sampling point from the values of signals at the input and output at preceding sampling instants starting with the lth one. The value of the input signal x at $t=(l+n)T_p$ is not included in the recurrence relation since the power of the transfer function numerator is below that of the denominator.

Example 14.4. Let us consider a digital servo system with the transfer function $W^*_{cl\text{-}l}(p)$ obtained in Example 13.4 (Eq. 13.68)

$$W^*_{cl\text{-}l}(p) = \frac{k_1 e^{pT_p} + k_0}{e^{2pT_p} + a_1 e^{pT_p} + a_0}$$

where a_i and k_i are given by the expressions

$$\left.\begin{aligned} a_1 &= k\left[T_p - T\left(1-e^{-\frac{T_p}{T}}\right)\right] - \left(1+e^{-\frac{T_p}{T}}\right) \\ a_0 &= k\left[T\left(1-e^{-\frac{T_p}{T}}\right) - T_p e^{-\frac{T_p}{T}}\right] + e^{-\frac{T_p}{T}} \\ k_1 &= k\left[T_p - T\left(1-e^{-\frac{T_p}{T}}\right)\right] \\ k_0 &= k\left[T\left(1-e^{-\frac{T_p}{T}}\right) - T_p e^{-\frac{T_p}{T}}\right] \end{aligned}\right\} \qquad (14.34)$$

The difference equation for this system is of the form

$$y[(l+2)T_p] + a_1 y[(l+1)T_p] + a_0 y(lT_p) = \\ = k_1 x[(l+1)T_p] + k_0 x(lT_p) \qquad (14.35)$$

whence it follows that

$$y[(l+2)T_p] = k_1 x[(l+1)T_p] + k_0 x(lT_p) - \\ - a_1 y[(l+1)T_p] - a_0 y(lT_p) \qquad (14.36)$$

The recurrence relation (14.36) permits computing the discrete values of the output signal from its values and those of the input signal at the two preceding sampling points. It holds both for positive and negative values of l. The calculations should be started with $l = -2$ to find $y(0)$ equal to zero, since the input and output signals are normally zero at negative t. The subsequent values are

$$\left.\begin{aligned} y(T_p) &= k_1 x(0) \\ y(2T_p) &= k_1 x(T_p) + k_0 x(0) - a_1 y(T_p) \\ y(3T_p) &= k_1 x(2T_p) + k_0 x(T_p) - a_1 y(2T_p) - a_0 y(T_p) \\ &\ldots\ldots\ldots\ldots\ldots\ldots\ldots\ldots \end{aligned}\right\} \qquad (14.37)$$

The number of addends needed to obtain $y(lT_p)$ is constant. It is equal to four starting with $l = 1$ in the example under study and increases with the order of the systems (there are $2n$ addends for a continuous part of the nth order).

The *second method* of calculating processes in sampled-data control systems uses Eq. (13.10) obtained by the superposition principle. Substituting $\varepsilon(iT_p) = x(iT_p) - y(iT_p)$ gives the recurrence relation

$$y(lT_p) = \sum_{i=0}^{l} x(iT_p)\, w_{RCP}[(l-i)T_p] - \\ - \sum_{i=0}^{l} y(iT_p)\, w_{RCP}[(l-i)T_p] \qquad (14.38)$$

The calculations should be started with $l = 0$. But since $w_{RCP}(0) = 0$, $y(0)$ is also zero. The subsequent values are

$$\left.\begin{aligned} y(T_p) &= x(0)\, w_{RCP}(T_p) \\ y(2T_p) &= x(0)\, w_{RCP}(2T_p) + x(T_p)\, w_{RCP}(T_p) - \\ &\quad - y(T_p)\, w_{RCP}(T_p) \\ y(3T_p) &= x(0)\, w_{RCP}(3T_p) + x(T_p)\, w_{RCP}(2T_p) + \\ &\quad + x(2T_p)\, w_{RCP}(T_p) - y(T_p)\, w_{RCP}(2T_p) - \\ &\quad - y(2T_p)\, w_{RCP}(T_p) \\ &\ldots\ldots\ldots\ldots\ldots\ldots\ldots\ldots \end{aligned}\right\} \qquad (14.39)$$

etc.

The necessary number of addends for obtaining $y(lT_p)$ is $2l-1$; it increases with l, which hinders the calculation. True, in practice the maximal number of addends is limited with decaying weighting functions $w_{RCP}(t)$.

For the case where the image $Y^*(p)$ is a fractional rational function of e^{pT_p} (which occurs when the input signal image $X^*(p)$ is a fractional rational function), the *third method* of finding the discrete values of $y(lT_p)$ based on expanding $Y^*(p)$ into a power series of e^{-pT_p} may be recommended. Since by Eq. (12.12)

$$Y^*(p)=\sum_{l=0}^{\infty} y(lT_p)\,e^{-plT_p}$$

the discrete values of $y(lT_p)$ are coefficients in the power series of e^{-pT_p}. The power series expansion may be done by writing the numerator and denominator of $Y^*(p)$ in the decreasing order of the powers of

$$Y^*(p)=\frac{B^*(p)}{A^*(p)}=\frac{b_m e^{mpT_p}+b_{m-1}e^{(m-1)pT_p}+\ldots+b_0}{a_n e^{npT_p}+a_{n-1}e^{(n-1)pT_p}+\ldots+a_0}$$

by Eqs. (9.53) or directly, by dividing the numerator by the denominator according to the rules of polynomial division.

The division generally results in an infinite series the coefficients of which are the desired discrete values of the output signals.

All these tools are applicable to analysis of processes in closed-loop and open-loop sampled-data control systems. In the second case the relation (14.38) simplifies because the addends in the right-hand part containing the output signal values are not present.

Transient function and weighting function of sampled-data systems. The dynamic properties of sampled-data systems (both closed-loop and open-loop) can be described by the transient function $h(t)$ and the weighting function $w(t)$, which have the same meaning as in the case of continuous systems. Their discrete values $h(lT_p)$ and $w(lT_p)$ are the easiest to find by using the equivalent diagram of the sampled-data system shown in Fig. 14.9*a*, $h(lT_p)$ may be found from the system response to a discrete unit function $1\overset{*}{(t)}$ at the input (Fig. 14.9*b*). The discrete values of the weighting function $w(lT_p)$ depend on the system response to a unit input pulse (Fig. 14.9*c*).

In open-loop sampled-data systems $h(t)$ and $w(t)$ are the transient and the weighting function, respectively, of the reduced continuous part, $h_{RCP}(t)$ and $w_{RCP}(t)$.

With the sampled-data system weighting function known it is possible to find the discrete values of the system output signal when the system is subjected to arbitrary inputs. The formula can be obtained by the superposition principle as was done in Sec. 13.2

when deriving Eq. (13.9)

$$y(t) = \sum_{i=0}^{l} x(iT_p)\, w(t - iT_p) \tag{14.40}$$

or for discrete sampling times

$$y(lT_p) = \sum_{i=0}^{l} x(iT_p)\, w[(l-i)T_p] = \sum_{i=0}^{l} x[(l-i)T_p]\, w(iT_p) \tag{14.41}$$

The second part of Eq. (14.41) is obtained by substituting i for $l - i$ in the first one and by changing the order of summation.

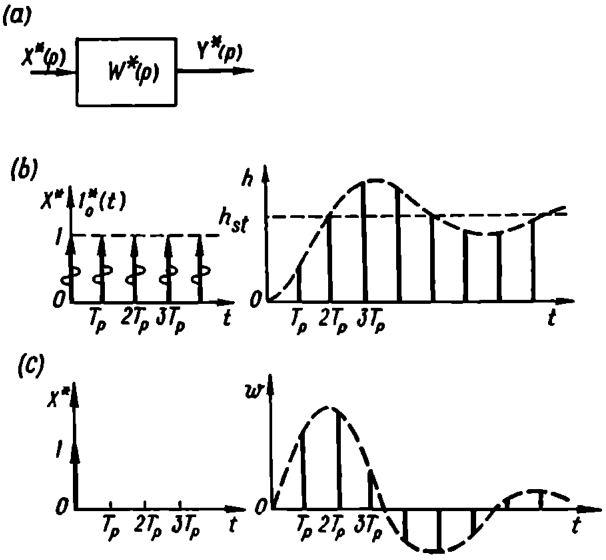

Fig. 14.9

This approach may be used along with the other devices of this section.

Equation (14.41) is easily seen to be similar to Eq. (2.67) for continuous systems; in Eq. (2.67) the output signal is found by integration, and in Eq. (14.41), by summation since control requires the use of time-sampled signals.

Substituting $x(iT_p) = 1$ into Eq. (14.41) gives the transient function at discrete times $h(lT_p)$ expressed in terms of the weighting function

$$h(lT_p) = \sum_{i=0}^{l} w[l-i)T_p] = \sum_{i=0}^{l} w(iT_p) \tag{14.42}$$

The inverse relation is

$$w(lT_p) = \sum_{i=0}^{l} w(iT_p) - \sum_{i=0}^{l-1} w(iT_p) =$$
$$= h(lT_p) - h[(l-1)T_p] = \nabla h(lT_p) \qquad (14.43)$$

where $\nabla h(lT_p)$ is the so-called *descending first-order difference of discrete values of the transient function h.*

Equations (14.42) and (14.43) are similar to Eq. (2.31) for continuous systems, which relates the transient and weighting functions.

The images of discrete signals $h^*(t)$ and $w^*(t)$ generated from transient and weighting functions of a sampled-data system are related as follows

$$H^*(p) = W^*(p) \frac{e^{pT_p}}{e^{pT_p} - 1} \qquad (14.44)$$

The discrete values of $h(lT_p)$ and $w(lT_p)$ can be found by using the tools of this section. Also, transfer functions can lead to them through the expansion formula (12.49).

If the transfer function is $W^*(p) = \frac{K^*(p)}{A^*(p)}$, then

$$h(lT_p) = \sum_{\nu=1}^{n+1} \frac{K^*(p_\nu) e^{p_\nu T_p}}{\frac{d}{d(e^{pT_p})}[A^*(p)(e^{pT_p} - 1)]|_{p=p_\nu}} e^{p_\nu (l-1) T_p} \qquad (14.45)$$

where p_ν are the roots of the polynomial $A^*(p)(e^{pT_p} - 1)$ ($A^*(p)$ has a degree n).

If we single out the addend representing the known root $p = 0$, then

$$h(lT_p) = \frac{K^*(0)}{A^*(0)} + \sum_{\nu=1}^{n} \frac{K^*(p_\nu)}{(e^{p_\nu T_p} - 1)\dot{A}^*(p_\nu)} e^{p_\nu lT_p} \qquad (14.46)$$

where

$$\dot{A}^*(p) = \frac{dA^*(p)}{d(e^{pT_p})}$$

(p_ν = roots of the characteristic equation $A^*(p) = 0$ of a sampled-data system, $\nu = 1, 2, \ldots, n$).

This addend is the steady-state value of the transient function

$$h_{st} = \frac{K^*(0)}{A^*(0)} = W^*(0) \qquad (14.47)$$

The second component, which contains a sum of discrete exponents, is a transient component and decays in stable sampled-data control systems where all the roots of the characteristic equation are to the left of the imaginary axis.

By the expansion formula the weighting function discrete values are

$$w(lT_p) = \sum_{\nu=1}^{n} \frac{K^*(p_\nu)}{e^{p_\nu T_p} \dot{A}^*(p_\nu)} e^{p_\nu l T_p} \tag{14.48}$$

In a stable sampled-data system $w(lT_p)$ decays as $l \to \infty$.

Example 14.5. Find the discrete values of the transient function for a digital servo system with a transfer function

$$W^*_{cl\text{-}l}(p) = \frac{kT_p}{e^{pT_p} - 1 + kT_p}$$

obtained in Example 13.4.

The system characteristic equation is

$$e^{pT_p} - 1 + kT_p = 0$$

whence the single root is

$$e^{p_1 T_p} = 1 - kT_p \tag{14.49}$$

Calculating $h(lT_p)$ for this value by Eq. (14.46), we have

$$h(lT_p) = 1 + \frac{kT_p}{-kT_p \cdot 1}(1 - kT_p)^l = 1 - (1 - kT_p)^l \tag{14.50}$$

Ultimately $h_{st} = 1$.

Let us see how discrete values of the weighting function can be obtained by expanding $W^*(p)$ into a power series of e^{-pT_p}.

$$W^*(p) = \frac{K^*(p)}{A^*(p)} = \frac{k_m e^{mpT_p} + k_{m-1} e^{(m-1)pT_p} + \ldots + k_0}{a_n e^{npT_p} + a_{n-1} e^{(n-1)pT_p} + \ldots + a_0} =$$

$$= w[(n-m)T_p] e^{-(n-m)pT_p} +$$

$$+ w[(n-m+1)T_p] e^{-(n-m+1)pT_p} + \ldots \tag{14.51}$$

If a sampled-data control system is such that

$$\left.\begin{aligned} a_{n-1} = a_{n-2} = \ldots = a_0 = 0 \\ A^*(p) = a_n e^{npT_p} \end{aligned}\right\} \tag{14.52}$$

the series (14.51) is finite

$$W^*(p) = \frac{1}{a_n}[k_m e^{-(n-m)pT_p} + k_{m-1} e^{-(n-m+1)pT_p} + \ldots + k_0 e^{-npT_p}] \tag{14.53}$$

and all other terms are zero.

This means that the weighting function (its discrete values) becomes zero within a finite number of periods T_p equal to the system order n. Then the transient discrete components in a sampled-data system subject to arbitrary actions vanish within n periods of T_p.

Indeed, by virtue of (14.41),

$$y(lT_p) = \sum_{i=0}^{l} x[(l-i)T_p]\, w(iT_p) =$$

$$= \sum_{i=0}^{\infty} x[(\infty - i)T_p]\, w(iT_p) - \sum_{i=l+1}^{\infty} x[(\infty - i)T_p]\, w(iT_p) \quad (14.54)$$

The first sum in Eq. (14.54) is the forced component of the discrete values of the output signal, the second is the transient component. If the conditions (14.52) are valid, then at $l \geqslant n$ the transient component is zero and a forced process sets in.

This phenomenon was not observed in continuous control systems where transient processes at arbitrary inputs vanish as a rule for $t \to \infty$ only.

Observance of the finite-duration conditions (14.52) makes a sampled-data system speed-optimal since in any other case, all other conditions being equal, the transient processes will be longer. Such systems are sometimes described as *infinite stability systems* because with Eqs. (14.52) valid the characteristic equation

$$a_0 e^{npT_p} = 0 \quad (14.55)$$

has n roots equal to ∞.

Note that in order to arrive at optimal control laws for sampled-data systems very big control signals (especially at small T_p) may be needed which cannot be obtained owing to the constraints in the system amplifiers.

Example 14.6. Find conditions for finite duration of transient processes in a digital servo system with the transfer function obtained in Example 13.4. At $T = 0$

$$W^*_{cl\text{-}l}(p) = \frac{kT_p}{e^{pT_p} - 1 + kT_p}$$

whence the finite-duration condition is

$$kT_p = 1, \quad k = \frac{1}{T_p} \quad (14.56)$$

When the condition (14.56) holds, the transfer function is

$$W^*_{cl\text{-}l}(p) = e^{-pT_p} \quad (14.57)$$

The weighting function $W_{cl\text{-}l}$ has just one nonzero discrete value at $t = T_p$. Figure 14.10*a*, *b* shows the discrete values of the system weighting and transient functions.

The finite duration of transient processes in sampled-data systems cannot always be attained by mere selection of their parameters and may sometimes involve system rearrangement by introducing compensating elements, feedbacks, etc.

Determining the law for variations of the output signal of a sampled-data system between samplings. The above methods yield a law for variation of a sampled-data control system output only at discrete times (sampling points 0, T_p, $2T_p$, $3T_p$, . . .). Very often the data on the system behaviour at discrete times proves sufficient for estimating its behaviour between samplings. This is the case when the continuous part has a passband limited by the frequency ω_{b1} and the frequency of the PE is so high that $\omega_p \geqslant 2\omega_{b1}$. Then the

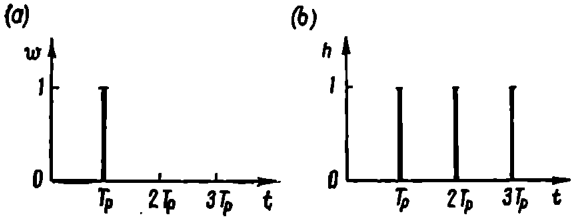

Fig. 14.10

sampled-data system output signal satisfies the conditions of the pulse theorem (see Sec. 12.2) and can therefore be reconstructed with the use of discrete values.

A smooth envelope passed through the obtained discrete values of the output signal gives a sufficiently true characteristic of the system behaviour between samplings provided that the pulse period T_p is much less than the main time constant of the continuous part.

Sometimes, however, the knowledge of discrete values of signals in sampled-data systems does not give a sufficiently clear idea of the signal behaviour. The problem then is to determine the law for signal variations between samplings.

The image of the continuous signal $y(t)$ at the output of a sampled-data control system can be obtained by Eq. (13.6) if the image of the discrete misalignment $\mathrm{E}^*(p)$ is known

$$Y(p) = W_{RCP}(p)\,\mathrm{E}^*(p)$$

where $\mathrm{E}^*(p)$ can be found from Eq. (13.70) so that

$$Y^*(p) = W_{RCP}(p)\,\frac{X^*(p)}{1+W^*_{o\text{-}l}(p)} \tag{14.58}$$

The original $y(t)$ may be obtained by using the image multiplication theorem

$$y(t) = \int_0^t \varepsilon^*(\tau)\, w_{RCP}(t-\tau)\, d\tau \tag{14.59}$$

Substituting

$$\varepsilon^*(\tau) = \sum_{i=0}^{\infty} \varepsilon(iT_p)\,\delta(\tau - iT_p)$$

gives

$$y(t) = \sum_{i=0}^{l} \varepsilon(iT_p)\, w_{RCP}(t - iT_p) \qquad (14.60)$$

where l = integral part of the number $\frac{t}{T_p}$

$w_{RCP}(t)$ = weighting function of the reduced continuous part.

Equation (14.60) coincides with Eq. (13.9) obtained by using the superposition principle and leads to a law for variation of y between samplings provided the discrete values of the misalignment are found in advance by one of the above methods.

Example 14.7. Consider a digital servo system at $T = 0$ (Examples 13.2, 14.5). The weighting function corresponding to $W_{RCP}(p) = \frac{k}{p}$ is

$$w_{RCP}(t) = \begin{cases} kt & \text{at } 0 \leqslant t < T_p \\ kT_p & \text{at } T_p \leqslant t \end{cases} \qquad (14.61)$$

It is plotted in Fig. 14.11*a*. In the intervals between samplings the signal $y(t)$ varies by a linear law; therefore the discrete values of $y(lT_p)$ can be connected by straight lines. In particular, the system transient function whose discrete values were obtained in Example 14.5 (Eq. 14.50) is of the form given in Fig. 14.11*b*. The weighting and transient functions of this system, the finite-duration conditions being satisfied, are shown in Fig. 14.11*c* and *d* (the discrete values were shown in Fig. 14.10*a* and *b*).

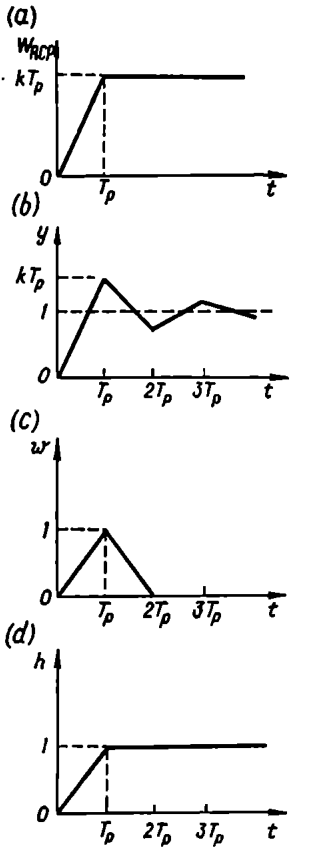

Fig. 14.11

The methods developed for the determination of signal discrete values in sampled-data control systems at sampling points can be extended to discrete values of signals between samplings. For this purpose an equivalent circuit should have a dummy delay element with a delay τ which can be varied between 0 and T_p (Fig. 14.12). Then, assuming different values of delay, the output signal in the intervals between samplings can be studied. The discrete value of the output signal taken from the delay element at the lth sampling

time is obviously equal to the value of the real signal at the system output at the time $t = lT_p - \tau$ (Fig. 14.13).

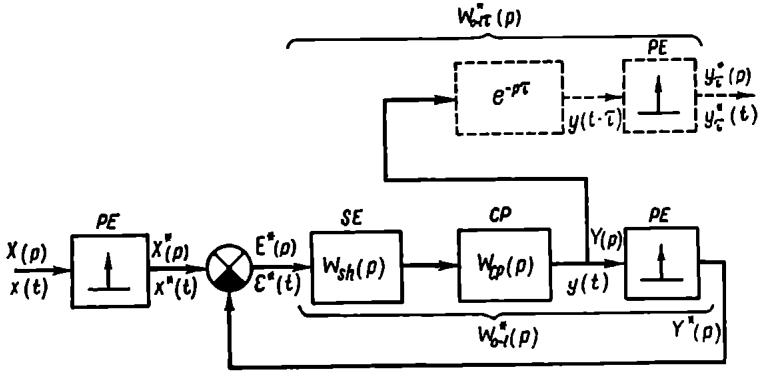

Fig. 14.12

The signal image at the delay element output is

$$Y^*_\tau(p) = \frac{W^*_{o\text{-}l\,\tau}(p)}{1 + W^*_{o\text{-}l}(p)} X^*_{o\text{-}l} = W^*_{cl\text{-}l\,\tau}(p)\, X^*(p) \qquad (14.62)$$

where $W^*_{o\text{-}l\tau}(p)$ is the transfer function of an open-loop sampled-data system with a delay which can be obtained by Eq. (13.34) or from tables (Ref. 73).

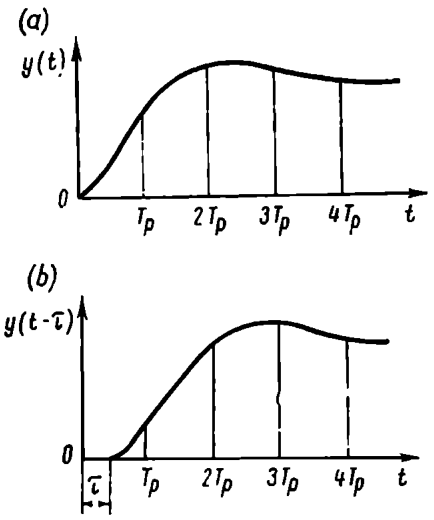

Fig. 14.13

The transformation of the image to discrete values of the original $y(lT_p - \tau)$ can be performed by any of the above-described techniques.

The above methods of analysis applied to signal behaviour between samplings can also be used for open-loop sampled-data systems; the formulae then simplify.

Steady-state processes in sampled-data systems. Consider the steady-state values of discrete signals in sampled-data control systems subject to standard actions. We will first show that the steady-state value of a certain discrete signal sequence $x(lT_p)$ can be found from the image $X^*(p)$. For this purpose we represent $x(lT_p)$ as a sum of increments (differences) for all sampling times starting with

$t = 0$

$$x(lT_p) = x(0) + [x(T_p) - x(0)] + \ldots + \{x(lT_p) - x[(l-1)T_p]\} = \sum_{i=0}^{l} \nabla x(iT_p) \tag{14.63}$$

The steady-state value to which the sequence $x(lT_p)$ tends can be obtained from (14.63) as $l \to \infty$

$$x_{st} = \sum_{l=0}^{\infty} \nabla x(iT_p) \tag{14.64}$$

The sum of all discrete values of a quantity $f(lT_p)$ can be obtained via the image

$$F^*(p) = \sum_{l=0}^{\infty} f(lT_p)\, e^{-plT_p}$$

if $p = 0$ is substituted into $F^*(p)$

$$F^*(0) = \sum_{l=0}^{\infty} f(lT_p) \tag{14.65}$$

Therefore

$$x_{st} = \lim_{p \to 0} \nabla X^*(p) \tag{14.66}$$

where $\nabla X^*(p)$ is the image of the sequence of the pulse differences $\nabla x^*(t) = x^*(t) - x^*(t - T_p)$:

$$\nabla X^*(p) = X^*(p) - e^{-pT_p} X^*(p) = (1 - e^{pT_p})\, X^*(p) \tag{14.67}$$

Consequently

$$x_{st} = \lim_{p \to 0} (1 - e^{-pT_p})\, X^*(p) = \lim_{p \to 0} \frac{e^{lpT_p} - 1}{e^{pT_p}} X^*(p) \tag{14.68}$$

The theorem proved is an analog of the final value theorem for continuous quantities.

Let us now find the expression for the steady-state misalignment in a sampled-data control system subject to the action of a unit function, at its setpoint (input). For images the following equality is true

$$E^*(p) = W_\varepsilon^*(p)\, 1_0^*(p) = W_\varepsilon^*(p) = \frac{e^{pT_p}}{e^{pT_p} - 1} =$$

$$= \frac{1}{1 + W_{o-l}^*(p)} \frac{e^{pT_p}}{e^{pT_p} - 1} = \frac{D^*(p)}{K^*(p) + D^*(p)} \frac{e^{pT_p}}{e^{pT_p} - 1} \tag{14.69}$$

where $\frac{e^{pT_p}}{e^{pT_p} - 1}$ is the image of a unit discrete signal $1_0^*(t)$.

Then we have the steady-state misalignment

$$\varepsilon_{st} = \lim_{p \to 0} W_\varepsilon^*(p) = \lim_{p \to 0} \frac{D^*(p)}{K^*(p) + D^*(p)} \tag{14.70}$$

The system will be setpoint-astatic if $\varepsilon_{st} = 0$, which can be valid only if the transfer function $W_{\varepsilon}^{*}(p)$ has a zero of at least the first order in the point $p = 0$. In other words, the open-loop transfer function denominator should contain the factor $e^{pT_p} - 1$, i.e.

$$D^{*}(p) = (e^{pT_p} - 1)\, D_1^{*}(p) \tag{14.71}$$

Section 13.2 shows this to be true if the continuous part of a sampled-data system includes an integrator connected in series (see Eq. (13.43)).

If the input of a sampled-data control system is a power function $x = t^n$, then its image, according to Table 12.1, is

$$X^{*}(p) = \frac{T_p^n e^{pT_p}}{(e^{pT_p} - 1)^{n+1}} R_n^{*}(p) \tag{14.72}$$

where $R_n^{*}(p)$ is a polynomial of the $(n-1)$th degree in e^{pT_p} without zero roots.

In this case we have

$$E^{*}(p) = W_{cl\text{-}l\,\varepsilon}^{*}(p) \frac{T_p^n e^{pT_p}}{(e^{pT_p} - 1)^{n+1}} R_n^{*}(p) =$$

$$= \frac{D^{*}(p)}{K^{*}(p) + D^{*}(p)} \frac{T_p^n e^{pT_p}}{(e^{pT_p} - 1)^{n+1}} R_n^{*}(p) \tag{14.73}$$

$$\varepsilon_{st} = \lim_{p \to 0} W_{cl\text{-}l\,\varepsilon}^{*}(p) \frac{T_p^n R_n^{*}(p)}{(e^{pT_p} - 1)^n} = \lim_{p \to 0} \frac{D^{*}(p)}{K^{*}(p) + D^{*}(p)} \frac{T_p^n R_n^{*}(p)}{(e^{pT_p} - 1)^n} \tag{14.74}$$

If $D^{*}(p)$ contains $(e^{pT_p} - 1)^{n+1}$ as a factor, then $\varepsilon_{st} = 0$. In this case we have a *setpoint-astatic system of the* $(n+1)$*th order*, which can be physically realized by series connection of $(n+1)$ integrators in the continuous part.

In a static sampled-data control system the steady-state value of misalignment with a unit signal at the input is

$$\varepsilon_{st} = W_{cl\text{-}l\,\varepsilon}^{*}(0) = \frac{1}{1 + W_{o\text{-}l}^{*}(0)} \tag{14.75}$$

which is similar to Eq. (9.15) for continuous systems. Constant discrete values of misalignment for arbitrarily shaped control pulses $s(t)$ make the sampled-data system output oscillate about a mean value. Figure 14.14 portrays the variations of the discrete ε^{*}, control pulses ε_p, and the output signal y in a sampled-data control system the continuous part of which has a transfer function $W_p(p) = \frac{k}{1 + pT}$ and whose input signal is of constant value. Pulses acting on the continuous part are rectangular in shape and their duty factor $\gamma < 1$.

If we make $\gamma = 1$, preserving the rectangular pulse shape, there will be no oscillation.

The steady-state values of signals between samplings can be found by using the dummy delay as described in this section.

Discrete values of a dynamic error in a sampled-data control system subjected to a harmonic signal $Ae^{j\omega t}$ at the input can be found by the formula

$$\varepsilon(lT_p) = \operatorname{Im} W_{\varepsilon}^{*}(j\omega) A e^{j\omega l T_p} \quad (14.76)$$

Example 14.8. Find the steady-state value of misalignment when there is a unit signal at the input of a sampled-data system (see Example 13.1) with a transfer function

$$W_{o\text{-}l}^{*}(p) = \frac{k\left(1 - e^{-\frac{T_p}{T}}\right)}{e^{pT_p} - e^{-\frac{T_p}{T}}}$$

By virtue of Eq. (14.75),

$$\varepsilon_{st} = \frac{1}{1+k} \quad (14.77)$$

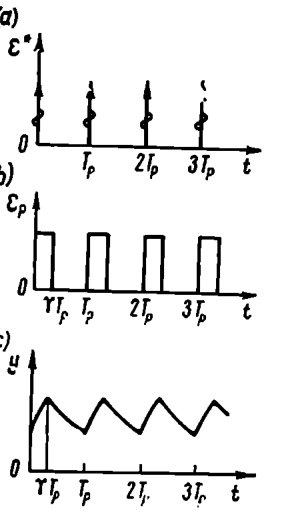

Fig. 14.14

Example 14.9. The steady-state misalignment when there is a unit signal at the input of a digital servo system (see Example 13.2) is zero since the continuous part includes an integrator. Find the steady-state misalignment in the case of a linearly increasing input signal $x = vt$. The image $X^{*}(p)$ is found from Table 12.1

$$X^{*}(p) = \frac{vT_p e^{pT_p}}{(e^{pT_p} - 1)^2}$$

The misalignment image is

$$E^{*}(p) = \frac{(e^{pT_p} - 1)\left(e^{pT_p} - e^{-\frac{T_p}{T}}\right)}{k_1 e^{pT_p} + k_0 + (e^{pT_p} - 1)\left(e^{pT_p} - e^{-\frac{T_p}{T}}\right)} \cdot \frac{vT_p e^{pT_p}}{(e^{pT_p} - 1)^2} \quad (14.78)$$

where k_1 and k_0 are found from Eq. (14.34).

The steady-state misalignment

$$\varepsilon_{st} = vT_p \frac{1 - e^{-\frac{T_p}{T}}}{k_0 + k_1} = \frac{v}{k} \quad (14.79)$$

14.3. INDIRECT METHODS OF PERFORMANCE ESTIMATION, AND SYNTHESIS OF SAMPLED-DATA CONTROL SYSTEMS

The basic definitions of process performances for continuous control systems given in Ch. IX hold for sampled-data systems. The latter are characterized by the same five performance indices related to the transfer function: the static deviation h_{stat}, control time t_c, maximal overshoot σ, maximal overshoot time t_{max}, the number N of overshoots within the control time. The only difference is that in sampled-data systems these indices are normally found on the basis of transfer function discrete values because these are rather easy to come by. In most practical sampled-data control systems the frequency ω_p of a PE is selected high enough, so that the system

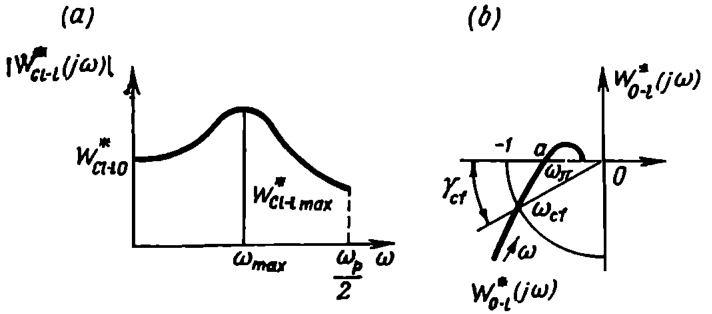

Fig. 14.15

properties are close to those of continuous systems; the discrete values of signals on the plots are in this case connected by smooth curves. Consequently the performance may be estimated by using discrete data. If the laws for signal variations between samplings can be found, the performance can be estimated on the basis of complete data.

The performance indices can be found by calculating the transient function $h(lT_p)$ using one of the tools of the preceding section. This problem is rather unwieldy and so indirect methods have been developed both for continuous and sampled-data systems, namely frequency, cumulative (similar to integrals) and root methods.

Frequency methods. As in the case of continuous systems, the performance of sampled-data control systems can be estimated using the oscillation index M, phase-stability margin γ_{cf}, gain-stability margin L_{mr} (db), and the cutoff frequency ω_{cf}.

The oscillation index is found from the closed-loop system amplitude-frequency response (Fig. 14.15*a*)

$$M = \frac{W^*_{cl\text{-}l\,max}}{W^*_{cl\text{-}l0}}$$

The stability margins are determined in the complex $W^*_{o\text{-}l}(j\omega)$ plane. Figure 14.15*b* shows γ_{cf}; L_{mr} is found from the value of $|W^*_{o\text{-}l}(j\omega_\pi)|$ (segment *Oa* in Fig. 14.15*b*)

$$L_{mr} = 20 \log \frac{1}{|W^*_{o\text{-}l}(j\omega_\pi)|}$$

For a sampled-data control system to operate well, in particular, for the maximal overshoot σ to be kept within 0.15 to 0.3, the oscillation index and the stability margin must have the same values as in continuous systems, i.e. $M = 1.2$ to 1.5, $\gamma_{cf} = 30°$ to 50°, $L_{mr} = 8$ to 12 db. This is especially true for sampled-data systems with a low T_p the properties of which are close to those of continuous systems.

Example 14.10. A first-order digital servo system has the following transfer function in the open-loop state

$$W^*_{o\text{-}l}(p) = \frac{kT_p}{e^{pT_p} - 1}$$

The transient function for this system was found in Examples 14.5 and 14.7 and shown in Fig. 14.11. The maximal overshoot in the system is seen to be related to its parameter in a straightforward way:

$$\sigma = kT_p - 1 \qquad (14.80)$$

The relation of the oscillation index and the system parameters may be found from Fig. 14.16*a*, which displays the open-loop system

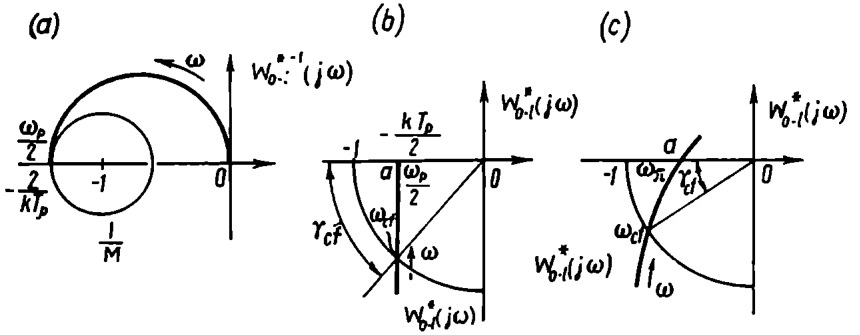

Fig. 14.16

inverse complex gain locus shown earlier in Fig. 13.9 (curve *1'*)

$$W^{*-1}_{o\text{-}l}(j\omega) = \frac{e^{j\omega T_p} - 1}{kT_p}$$

The same figure exhibits a circle of equal M values, which is tangential to the locus of $W^{*-1}_{o\text{-}l}(j\omega)$ in the point $-\frac{2}{kT_p}$, $j0$. This circle

has the centre in the point $-1, j0$, its radius is $\frac{1}{M}$. Thence it follows that

$$\frac{1}{M} = \frac{2}{kT_p} - 1$$

$$M = \frac{kT_p}{2 - kT_p}$$

or, with an allowance for Eq. (14.80),

$$M = \frac{1+\sigma}{1-\sigma} \tag{14.81}$$

The reverse relation is of the form

$$\sigma = \frac{M-1}{M+1} \tag{14.82}$$

The stability margins can be found by using the locus of $W^*_{0.1}(j\omega)$ shown in Fig. 14.16*b* whence it follows that

$$\left.\begin{aligned} \gamma_{cf} &= \arccos \frac{kT_p}{2} \\ L_{mr} &= 20 \log \frac{2}{kT_p} \end{aligned}\right\} \tag{14.83}$$

These formulae simplify the calculation of kT_p, M, γ_{cf}, and L_m for the extreme values of σ

$\sigma = 0.15$	$\sigma = 0.30$
$kT_p = 1.15$	$kT_p = 1.30$
$M = 1.35$	$M = 1.86$
$\gamma_{cf} = 55°$	$\gamma_{cf} = 50°$
$L_{mr} = 4.8$ db	$L_{mr} = 3.8$ db

The values of γ_{cf} and M in this example are unduly high and L_{mr}, unduly low against the above recommendations owing to the nontypical shape of the first-order system locus.

A typical shape of a higher-order system locus for medium frequencies is given in Fig. 14.16*c*. In systems having such a locus and the same values of M as in Example 14.10 the phase margin is seen to be below and the gain margin above those of a first-order servo system. The values of the oscillation index for higher-order systems should be within the above range ($M = 1.2$ to 1.5); the maximal overshoot σ will be within 0.15 to 0.3. To support this statement, Fig. 14.17 shows a plot of σ as a function of M calculated with due regard for output variations between samplings. This plot corresponds to a sampled-data servo system the continuous part

of which has a transfer function

$$W_{CP}(p) = \frac{k}{p(1+pT)}$$

the control pulses are of rectangular form and their duty factor $\gamma = 1$. This relation is given by $n = 2$. The relations for the above first-order sampled-data system ($n = 1$) and for a continuous second-order servo system are also presented for comparison (Ref. 31).

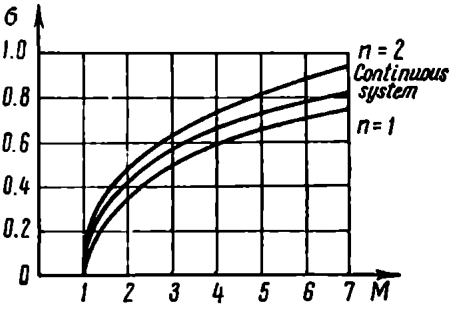

Fig. 14.17

Synthesis of compensating units in sampled-data systems. The performance of sampled-data control systems can be improved by introducing into their continuous parts (in series or in parallel) some compensating elements which would reshape the frequency responses of the reduced continuous part in a desired way. Since the complex gain of the reduced continuous part depends on $W_{sh}(j\omega)$, or

$$W_{RCP}(j\omega) = W_{sh}(j\omega)\, W_{CP}(j\omega)$$

the compensation may also be achieved by shaping the control pulses $s(t)$ so as to reshape the locus $W_{sh}(j\omega)$, and, consequently, $W_{RCP}(j\omega)$ (pulse-shape compensation).

Sampled-data systems can also be compensated by using specific pulse compensating units which are implemented most readily with

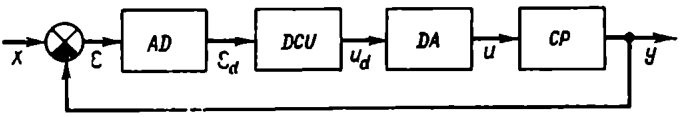

Fig. 14.18

the aid of digital computers. The compensating unit is introduced as shown in Fig. 14.18, where *AD* is an analog-to-digital converter, *DA* a digital-to-analog converter, *DCU* a digital computing unit, and *CP* the continuous part.

The *DCU* receives discrete values of the misalignment signal $\varepsilon(lT_p)$, performs the computations and delivers a discrete sequence of digits $u_d(lT_p)$, which enforces a certain control law. In the *DA* these digits are converted into pulses u, which then act on the continuous part.

The *DCU* can also compare the output and input; in that case analog-to-digital converters should be incorporated into the loops of these signals.

The program for the *DCU* may be compiled so that the output signal u_d is a solution to a linear difference equation of the form

$$u_d(lT_p) = \sum_{i=0}^{n} k_{n-i} e_d[(l-i)T_p] - \sum_{i=1}^{n} d_{n-i} u_d[(l-i)T_p] \quad (14.84)$$

where k_i and d_i are constant factors.

In this case the output signal is a linear combination of discrete input and output signals for several sampling points; these values are stored in the *DCU* memory.

If we assume that the *DCU* inputs and outputs are discrete signals which are in fact sequences of modulated unit pulses with the modulation law given by Eq. (14.84), then

$$u_d^*(t) = \sum_{i=0}^{n} k_{n-i} e_d^*(t-iT_p) - \sum_{i=1}^{n} d_{n-i} u_d^*(t-iT_p) \quad (14.85)$$

Thence follows an equation for images

$$U_d^*(p) = \sum_{i=0}^{n} k_{n-i} E_d^*(p) e^{-piT_p} - \sum_{i=1}^{n} d_{n-i} U_d^*(p) e^{-piT_p} \quad (14.86)$$

and for the transfer function of the compensating *DCU*

$$W_{com}^*(p) = \frac{U_d^*(p)}{E_d^*(p)} = \frac{\sum_{i=0}^{n} k_{n-i} e^{-piT_p}}{1 + \sum_{i=1}^{n} d_{n-i} e^{-piT_p}} =$$

$$= \frac{k_n e^{npT_p} + k_{n-1} e^{(n-1)pT_p} + \ldots + k_0}{e^{npT_p} + d_{n-1} e^{(n-1)pT_p} + \ldots + d_0} \quad (14.87)$$

The power of the numerator of $W_{com}^*(p)$ is found to be equal to that of the denominator, n, because the right-hand part of the difference equation includes a discrete value of the input signal at the time lT_p. *DCU* can supply the input data to the output with a very short delay.

An equivalent diagram of a sampled-data control system is portrayed in Fig. 14.19. *AD* and *DA* converters act as proportional elements (rounding-off error is neglected), and their gains may be included into $W_{com}^*(p)$ or $W_{RCP}(p)$.

In practice a continuous element may be connected between the comparator and the *DCU*, but by using equivalent transformations (see Sec. 13.3) in this case one can obtain the diagram of Fig. 14.19.

The transfer function of a compensated open-loop system which relates the images $E^*(p)$ and $Y^*(p)$ is expressed as

$$W^*_{o\text{-}l\,com}(p) = W^*_{com}(p)\, W^*_{o\text{-}l}(p) \tag{14.88}$$

where $W^*_{o\text{-}l}(p)$ is the uncompensated open-loop system transfer function, which is equal to $\frac{Y^*(p)}{U^*(p)}$.

The transfer function of a closed-loop system is

$$W^*_{cl\text{-}l}(p) = \frac{W^*_{o\text{-}l\,com}(p)}{1 + W^*_{o\text{-}l\,com}(p)}$$

If for some reason or other the desired transfer function $W^*_{cl\text{-}l}(p)$ of a closed-loop system and the transfer function $W^*_{o\text{-}l}(p)$ of a system

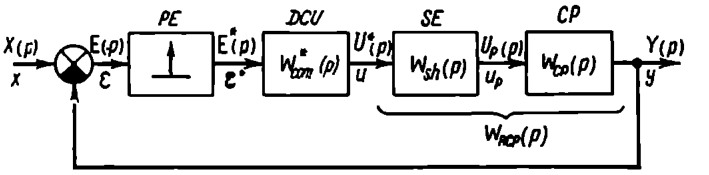

Fig. 14.19

without compensation are given, then the transfer function of the compensating *DCU* is

$$W^*_{com}(p) = \frac{W^*_{o\text{-}l\,com}(p)}{W^*_{o\text{-}l}(p)} \tag{14.89}$$

where

$$W^*_{o\text{-}l\,com}(p) = \frac{W^*_{cl\text{-}l}(p)}{1 - W^*_{cl\text{-}l}(p)} \tag{14.90}$$

Digital computers can effectively improve compensation of sampled-data control systems. Thus, astatic properties of any order can be obtained by introducing a factor $e^{pT_p} - 1$ of the desired power into the denominator $D^*(p)$. To obtain a first-order astatic system the transfer function must be of the form

$$W^*_{com}(p) = \frac{1}{e^{pT_p} - 1} \tag{14.91}$$

The appropriate difference equation is

$$u[(l+1)\,T_p] - u(lT_p) = \varepsilon(lT_p)$$

or

$$u[(l+1)\,T_p] = \varepsilon(lT_p) + u(lT_p)$$

i.e.

$$
\begin{aligned}
&u(0) = 0\\
&u(T_p) = \varepsilon(0)\\
&u(2T_p) = \varepsilon(T_p) + u(T_p) \; = \varepsilon(0) + \varepsilon(T_p)\\
&\cdots\cdots\cdots\cdots\cdots\cdots\cdots\cdots\\
&u[(l+1)T_p] = \sum_{i=0}^{l} \varepsilon(iT_p)
\end{aligned}
$$

Consequently, the *DCU* in this case is an adder of discrete input values (a discrete integrator) with a delay equal to one period T_p.

There are, of course, other ways to compensate control systems, e.g. disturbance compensation. For more details on the design of compensating units see Ref. 81.

Chapter XV

NONLINEARITIES IN CONTROL SYSTEMS. GENERAL

15.1. INTRODUCTION

The previous chapters were concerned with control systems that can be described by linear differential equations to a certain degree of accuracy. For continuous systems these equations have constant coefficients, while for sampled-data systems the coefficients of equations which describe pulse elements are discrete time functions. The superposition principle was used extensively.

This description of control systems is by no means applicable to all of them. There are many systems which cannot be described by linear differential equations and so nonlinear differential equations have to be used.

Nonlinearities may be either inherent in real characteristics of system elements or introduced intentionally to improve system performance.

In the former case the nonlinearities are allowed for to evaluate their effect on the control performance and eliminate this effect if it is undesirable.

In the latter case the goal is to increase the control performance or to obtain essentially new control algorithms by introducing additional nonlinear elements. This serves to improve the system response and accuracy, reduce the overshoot or offset the adverse effect of inherent nonlinearities.

Also, nonlinear plants with nonmonotonic extremal characteristics are controlled by special control circuits that automatically maintain the optimal operating mode of the plant. In this case nonlinear plants are controllable either by linear or by nonlinear elements.

While linear systems are operative only if they are stable and increasing oscillations are regarded there as inadmissible, the problem of nonlinear system stability is considered in a somewhat different light.

There are many nonlinear self-oscillating control systems where oscillations are a property of normal operation. In these cases stable system operation implies stable self-oscillations in an unstable

(from the linear theory point of view) system. The definition of stability itself is modified in this case. A linear system is stable when the system returns to the initial state as the external action decreases to zero.

This is known as *asymptotic stability*, or *stability in a point*. The same concept can also be used to characterize nonlinear systems.

In nonlinear systems, however, stability in a certain region is of greater importance—a system returns into a specified region when the external action drops to zero. To estimate stability of both kinds the concepts of stability in the small, in the large and in the whole are used which were introduced when discussing processes in nonlinear systems (see Ch. I). All these kinds of stability will be dealt with in analyzing specific control systems by various techniques.

The superposition principle is inapplicable to studies of nonlinear systems because the process initiated by a complex action in a system is not a sum of processes resulting from each constituent of the action, a fact which greatly hinders qualitative analysis of nonlinear control systems.

The mathematical tools employed in analysis of nonlinear systems require studies of nonlinear differential equations the theory of which has many specific methods applicable to different types of equations. The complexity of solving nonlinear differential equations calls for development of approximate methods evaluating the nature of processes observed in a system. Nonlinear characteristics of actual elements are replaced by idealized approximate characteristics which depend both on the nature of the nonlinear element and the analysis method employed.

Consequently, an analysis of processes in an actual system involves two stages of approximation, viz. derivation of nonlinear differential equations approximately describing the system, and approximate solution of these equations.

If an accurate solution to equations obtained at the first stage is found, we speak of an accurate solution of the overall problem. If, however, there are two stages of approximation, i.e. the nonlinear equations obtained are solved by using some simplifications, we speak of an approximate solution of the problem.

Apart from analytical and graphical methods, analog computer simulation and numerical methods implemented by means of digital computers are used extensively to solve nonlinear equations.

15.2. EXAMPLES OF INHERENT NONLINEARITIES

Chapter I showed that many plants such as a generator, a motor, aircraft, etc. are described by nonlinear differential equations and that only in the case of small deviations of the variables from the rated values can the system be approximately treated as a linear one.

Also, in all mechanical systems such essentially nonlinear phenomena as Coulomb friction and the effects of gaps, limiters and stops in transmission systems were disregarded. In the case of large disturbances and more detailed study of processes in these systems, however, nonlinear characteristics must be allowed for.

Consider examples of control systems where the nonlinearity of characteristics cannot be neglected.

Automatic stabilization of a d.c. generator voltage. The schematic of a static system for a d.c. generator voltage stabilization is shown in Fig. 15.1*a*. The approximate linear equations for this system have been treated in Ch. VI. If nonlinear characteristics of the generators and amplifier are allowed for, the equations of this system composed according to the diagram of Fig. 15.1*a*, with an allowance for the inertia of amplifier A, have the form

$$\left.\begin{aligned}
&k_A x = u_x + T_A \frac{du_x}{dt}\\
&u_A = u_A(u_x)\\
&u_A = r_e i_A + w_e \frac{d\Phi_e}{dt} = r_e i_A + T_e \frac{de_e}{dt}\\
&e_e = a_e \Phi_e = e_e(r_e i_A)\\
&e_e = r_g i_e + w_g \frac{d\Phi_g}{dt} = r_g i_e + T_g \frac{de_g}{dt}\\
&e_g = a_g \Phi_g = e_g(r_g i_e)\\
&u_l = e_g - r_{arm} i_l\\
&x = E_0 - k u_l
\end{aligned}\right\} \qquad (15.1)$$

where $T_e = \frac{w_e}{a_e}$ and $T_g = \frac{w_g}{a_g}$. The notation is as follows: i=current, u=voltage, x=misalignment voltage, e = e.m.f., Φ=magnetic flux, r = resistance, T = time constant, w = number of turns, a and k = proportionality factors, while the subscripts e, g, A, l, and *arm* stand for exciter, generator, amplifier, load, and armature, respectively.

In this system of equations the nonlinear relations $u_A(u_x)$, $e_e(i_A)$, $e_g(i_e)$ are represented by the curves of Fig. 15.1*b*, *c*, and *d*. If the hysteresis of the generator response is disregarded, the relation is single-valued (Fig. 15.1*c* and *d*); if not, the response $e_g(i_e)$ will be ambiguous.

The structural diagram of a system described by Eqs. (15.1) is displayed in Fig. 15.1*e*.

The geometrical interpretation of the system of equations (15.1) may be given either as a structural diagram or as a directed graph (Fig. 15.1*f*). The vertices of the graph represent the physical quantities which describe the process, the arcs representing relations between these quantities. Each arc describes a certain transformation

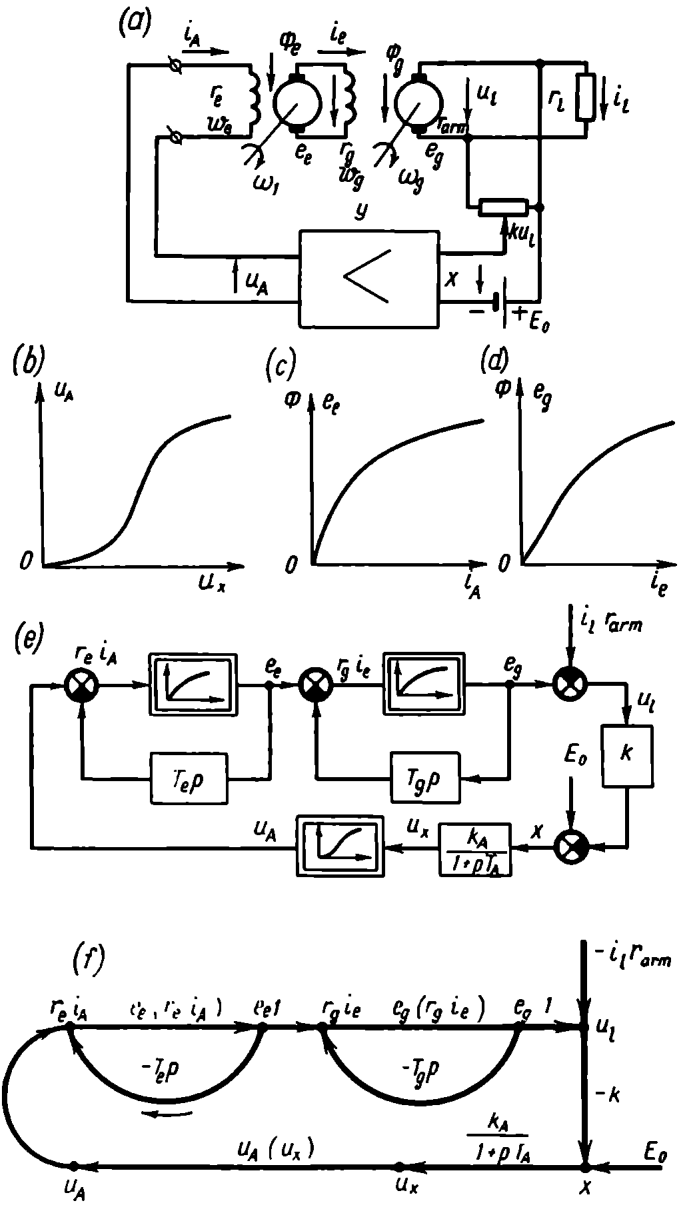

Fig. 15.1

of the value transmitted and corresponds to an element in the structural diagram.

The transformation operators are shown in the graph at the corresponding arcs. Where an arc represents signal transmission without

transformation the transformation operator is unity. For linear relations the operator is described by a transfer function and for nonlinear inertialess relations, by a certain function. Several arcs reaching the same vertex express summation of the quantities.

It is evident from the structural diagram and the directed graph (Fig. 15.1*e*, *f*) that they are completely equivalent and are just different ways of expressing the same structure described by a system of equations.

Both structural diagrams and directed graphs are used to describe processes in systems. In further discussion we will use structural diagrams, bearing in mind that each of these can be represented as a directed graph.

A servo system. An astatic servo system is shown in Fig. 15.2*a*. Approximate linear equations of such a system have been discussed in Ch. VI. In a more detailed discussion one should allow for the nonlinearity in the meter-converter unit, amplifier, and the mechanical transmission system.

The misalignment angle between the input, θ_1, and the output, θ_2, shafts of a servo system is measured by selsyns acting as transformers as well as by potentiometric sensors discussed in Ch. XVIII. The three-beam windings of selsyn stators are interconnected so that the appearance of a pulsed magnetic field in a selsyn-sensor generates currents in the stator windings of the selsyn-receiver; as a result, the magnetic fields in the selsyn-receiver and selsyn-sensor are similarly oriented.

The pulsed field in the selsyn-sensor is generated by the armature winding fed from a sine-current source. If the selsyn-receiver armature axis makes an angle of 90° with the selsyn-sensor axis, there will be no e.m.f. in the armature winding of the selsyn-receiver since the magnetic field is normal to the armature winding axis. Any deflection of this angle from 90° will generate an e.m.f. in the armature winding of the selsyn-receiver. The e.m.f. is at its greatest if the angle between the axes is either zero or 180°.

With the two perpendicular axes *I-I* and *II-II* assumed as the reference for the position of the armatures of both selsyns and denoting the rotation angles of the armatures as θ_1 and θ_2, respectively, we have the following expression for the voltage across the selsyn-receiver armature winding

$$u_\theta = U_m \sin(\theta_1 - \theta_2) \sin \omega t \qquad (15.2)$$

This voltage is fed to the phase-sensitive amplifier-rectifier A, which converts the modulating voltage

$$u_1 = U_m \sin(\theta_1 - \theta_2) \qquad (15.3)$$

into the motor d.c. voltage u_M.

The supply of the amplifier and the selsyn-sensor from the same source makes it possible to allow for the phase sign of the voltage u_θ.

If the amplifier receives at its input the compensation (correction) voltage u_{com} supplied by a tachometric generator, the output u_M

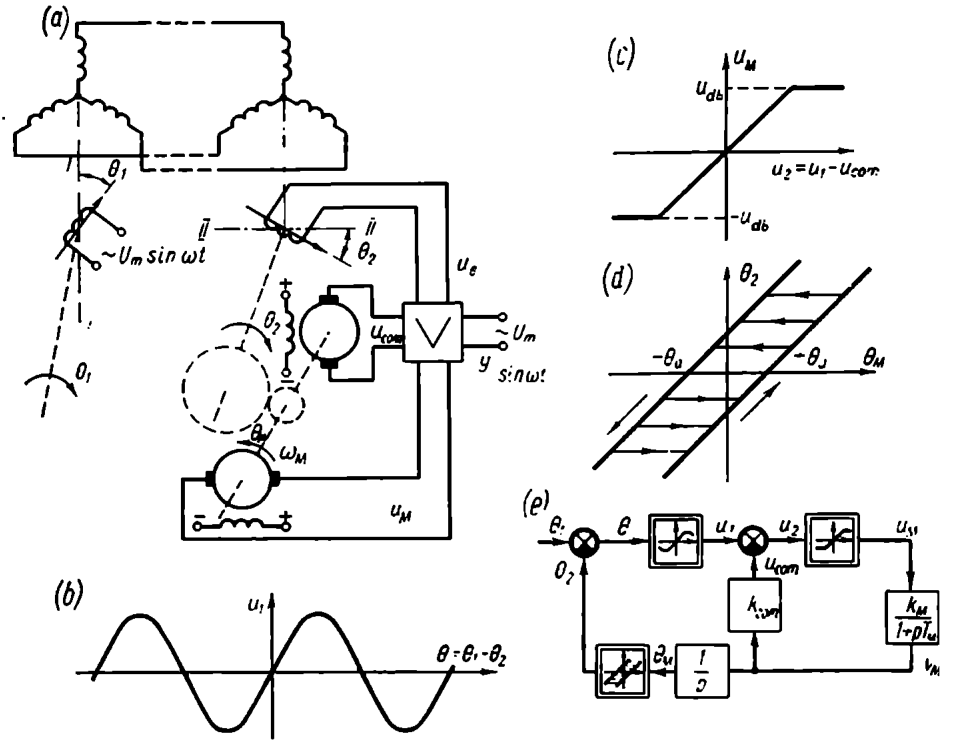

Fig. 15.2

depends on the difference $u_1 - u_{com}$, which should be regarded as the signal u_2 fed to the amplifier input.

In accordance with Eq. (15.3) the selsyn transmission response u_1 $(\theta_1 - \theta_2)$ is expressed as a nonlinear relation (Fig. 15.2*b*), as is also the response of a phase-sensitive amplifier u_M (u_2) shown schematically in Fig. 15.2*c*.

With an allowance for gaps in the mechanical transmission from the motor shaft to the output shaft of the servo system the response of the reduction gear 0_2 (θ_M) differs from that of a proportional element and has an ambiguous form (Fig. 15.2*d*). For $\frac{d\theta_2}{dt} > 0$ this relation is given as a straight line shifted rightwards from the origin

of coordinates by a certain amount θ_a, and for $\frac{d\theta_2}{dt} < 0$, as a straight line shifted leftwards by the same amount.

Any changes of rotation direction lead to idle run for a certain time as the angle θ_M changes by $2\theta_a$ in either direction. This time is known as *play elimination time.*

The structural diagram of a servo system with the above nonlinearities allowed for is shown in Fig. 15.2*e*.

Course stabilization system. The course of ships, torpedoes or aircraft is stabilized by an automatic rudder control system. One of the simplest stabilization systems is pictured in Fig. 15.3*a*. The plant is shown schematically as ship *1* the axis of which makes an angle of ψ with the desired course ψ_0 given by gyroscopic compass *2*. The deviation from course, $\psi_0 - \psi_1$, acts through the compass amplifier on rudder control actuator *3*. The latter turns rudder *4* by the angle δ via an appropriate transmission device.

Figure 15.3*b* displays the pneumatic rudder control drive. The flapper regulating air supply to the motor working cylinder turns by an angle of γ, thus causing an air pressure drop in the cylinder and the shift y of the piston. The movement of the piston is limited by stops and can vary in the range $-y_b \leqslant y \leqslant +y_b$.

The relation of the piston rate $v = \frac{dy}{dt}$ and the position γ of the control flapper is plotted in Fig. 15.3*c*. At any value of y in the range from $-y_b$ to $+y_b$ this relation is maintained and is a symmetrical curve with dead and saturation zones. As soon as the piston reaches a stop, however, it ceases to move, and if subsequent variations of γ act to press the piston against the stop, the piston rate remains zero at any value of γ.

The velocity v of the piston is thus a function of two variables $v(\gamma, y)$ and is given by the following equations

$$v = \begin{cases} \varphi(\gamma) \begin{cases} \text{at} -y_b \leqslant y < +y_b & \text{for} \quad \gamma > 0 \\ \text{at} -y_b < y \leqslant +y_b & \text{for} \quad \gamma < 0 \end{cases} \\ 0 \begin{cases} \text{at} \quad y = +y_b & \text{for} \quad \gamma > 0 \\ \text{at} \quad y = -y_b & \text{for} \quad \gamma < 0 \end{cases} \end{cases} \tag{15.4}$$

The transition from the curve $\varphi(\gamma)$ to the straight line $v = 0$ is made in one step at $y = \pm y_b$ (the dotted lines in Fig. 15.3*c*).

The transmission from the rudder control actuator to the rudder blade may have gaps contributing to the ambiguity of $\delta(y)$ of the type shown in Fig. 15.2*d*.

Consequently, even a simplified analysis of a course stabilization system reveals two nonlinearities caused by stops and gaps in the transmission system.

The structural diagram of the system in question is shown in Fig. 15.3*d*, where the plant is presumed to be described by inertial integrating element *1*, and the gyro amplifier and the rudder position

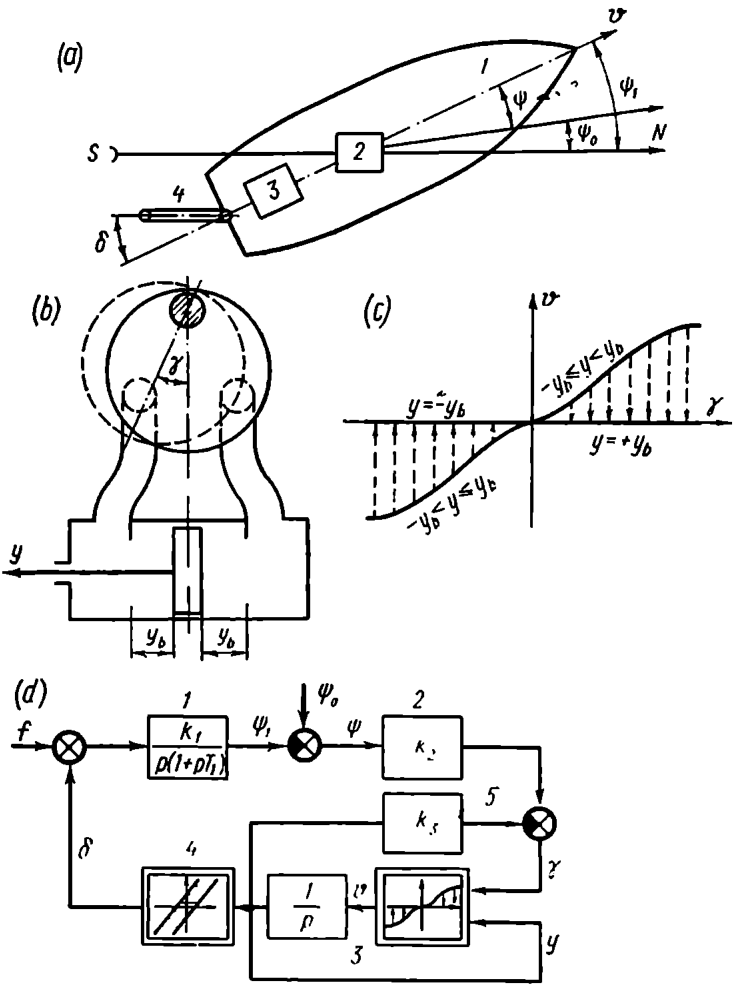

Fig. 15.3

compensating feedback, by proportional elements *2* and *5* with the gains k_2 and k_3. The rudder control system is described by nonlinear elements *3* and *4*.

Random disturbances reduced to the rudder rotation angle are denoted as *f*.

The structural diagrams of Figs. 15.1*e*, 15.2*e*, and 15.3*d* can be described by nonlinear equations, whose linearization may lead to

very crude approximations and whose solutions do not accurately reflect the processes in actual systems. For example, gaps in the transmission system rule out any judgement as to asymptotic stability, since after the external action ceases the operational points may occupy different positions on the curve (Fig. 15.2*d*) depending on the sign of the external action. The ambiguity of this response may cause self-oscillations, which are not observed in linear systems. If the saturation in the amplifier reponses is disregarded, the estimates of overshoot may grossly overstate the actual values. Consequently, intrinsic nonlinearities can either improve or deteriorate the system performance data as compared with an analysis of a linearized problem.

15.3. SYSTEMS WITH DELIBERATELY INTRODUCED NONLINEARITIES

In discussing linear systems we considered methods for improving the performance of transient processes by introducing linear compensating (correcting) units. Nonlinear elements introduced into control systems offer great possibilities for improving the system transient performance. Elements of this kind are nonlinear continuous and relay amplifiers, multi-input functional converters, digital computers with analog-to-digital and digital-to-analog converters.

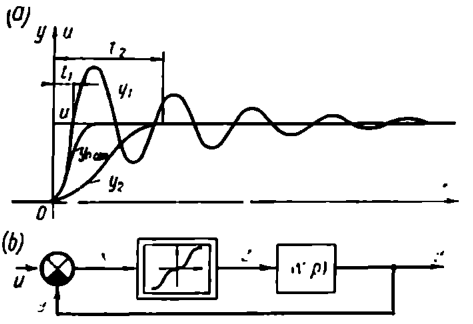

Fig. 15.4

Insertion of relay amplifiers in a control circuit may result in a small-self-oscillation mode, which will improve the speed of response and reduce overshoot in the case of stepwise actions.

Consider some simple examples of systems including nonlinear elements incorporated with the specific purpose of improving the transient performance.

Nonlinear compensation (correction) of continuous systems. In order to familiarize ourselves with the principle of nonlinear correction let us consider responses of a primitive servo system to a jerk, $u\,(t)$, at two different gain values (see Fig. 15.4*a*).

At a large gain (curve $y_1\,(t)$) the process is pronouncedly oscillatory, the overshoot is large, and the time t_1 required for equalization of y_1 and u is short. At a low gain (curve $y_2\,(t)$) the process is aperio-

dic, there is no overshoot, and misalignment or compensation time t_2 is long. Naturally, a system is sought which would feature a high gain at large misalignments $x = u - y$ and reduce the gain with decreasing misalignment. In this case the transient process should be given by the curve $y_{tr}(t)$. The reduction of gain is achieved by introducing a nonlinear amplifier with a response as in Fig. 15.4*b*.

The mechanism is protected from overloads at high values of control action by means of saturated amplifiers the response of which has a break at large values of the input signal (see Fig. 15.4*b*).

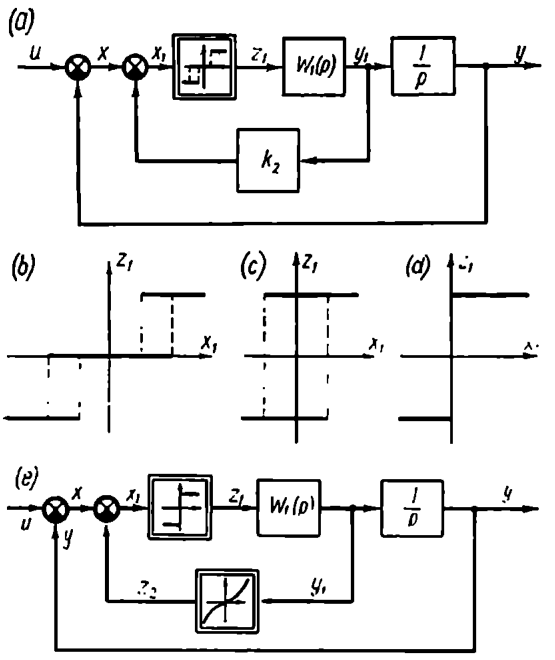

Fig. 15.5

Relay control systems. Continuous nonlinear amplifiers (Fig. 15.4*b*) can be replaced by relay amplifiers of different types. The structural diagram of the resulting control system is shown in Fig. 15.5*a*. The relay amplifier response can be three- or two-positional (Fig. 15.5*b* and *c*, *d*, respectively). In the former case the system has a dead zone where the misalignment $x = u - y$ can vary without closing the loop of the control system. In the latter case the system is self-oscillatory. The self-oscillations in the operating condition depend on the dynamic responses of the linear part and on the width of the relay response hysteresis loop (see Fig. 15.5*c*). Any change of the control action u causes an oscillatory process of misalignment reduction, which may take less time than in continuous systems.

As in linear systems, the performance of a relay system is improved by a compensating feedback, which may be either linear (see Fig. 15.5*a*) or nonlinear (Fig. 15.5*e*). In the latter case a speed-optimal transient process can be obtained by appropriate choice of the relation $z_2(y_1)$, provided there is no hysteresis in the relay response (Fig. 15.5*d*). A compensating unit of this type was suggested by D. I. Maryanovsky and D. V. Svecharnik in 1935.

Variable structure systems. Figure 15.6 is the diagram of a simple variable structure system suggested by S. V. Yemelyanov (Ref. 20). Consider the diagram without the part contoured by a dotted line. This is an inherently unstable system with an open-loop transfer function $\frac{k_1 k_2}{p^2}$.

The system is stabilized, its performance improved, and the sensitivity to parameter variations reduced by incorporating a relay unit,

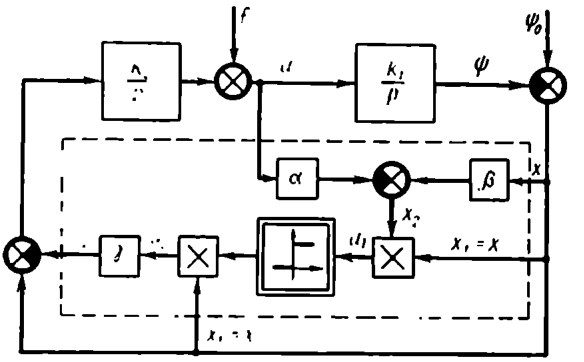

Fig. 15.6

which makes the feedback gain a function of the control signal x and of its time derivative $\frac{dx}{dt} = \dot{x}$.

In Fig. 15.6 this unit is delimited by a dotted line. Here $u = -\frac{\dot{x}}{k_1}$ and $u_1 = x\left[\alpha x + \frac{\beta}{k_1}\dot{x}\right]$ at $\psi_0 = \text{const}$; u_1 is positive if $x > 0$ and $\left[\alpha x + \frac{\beta}{k_1}\dot{x}\right] > 0$ or $x < 0$ and $\left[\alpha x + \frac{\beta}{k_1}\dot{x}\right] < 0$ (α and β are proportionality factors). Under these conditions the relay element transmits the signal $u_2 = x$ additionally through the unit γ. Then the open-loop transfer function is

$$W_{o\text{-}l} = \frac{k_1 k_2 (1-\gamma)}{p^2} \tag{15.5}$$

If u_1 is negative, which is the case when $x > 0$ and $\left[\alpha x + \frac{\beta}{k_1}\dot{x}\right] < 0$ or $x < 0$ and $\left[\alpha x + \frac{\beta}{k_1}\dot{x}\right] > 0$, then $u_2 = 0$, and the signal does not pass to the control system through the unit γ. Then

$$W_{o\text{-}l} = \frac{k_1 k_2}{p^2} \tag{15.6}$$

Since normally $\gamma > 1$, the feedback sign and the system structure depend on the sign of x. It will be shown in Ch. XVII that such a change in the structure of a system during its operation improves the performance as well as stabilizing the system.

A variable structure relay unit is incorporated both in servo systems (see Fig. 15.2) and in controllers (see Fig. 15.3) instead of compensating units k_{com} and elements k_3.

Digital servo system. Digital elements are even more helpful in control systems. Let us illustrate their effect using a servo system as an example.

A digital servo system converts digital signals, e.g. from a digital control computer, into linear or angular mechanical displacements.

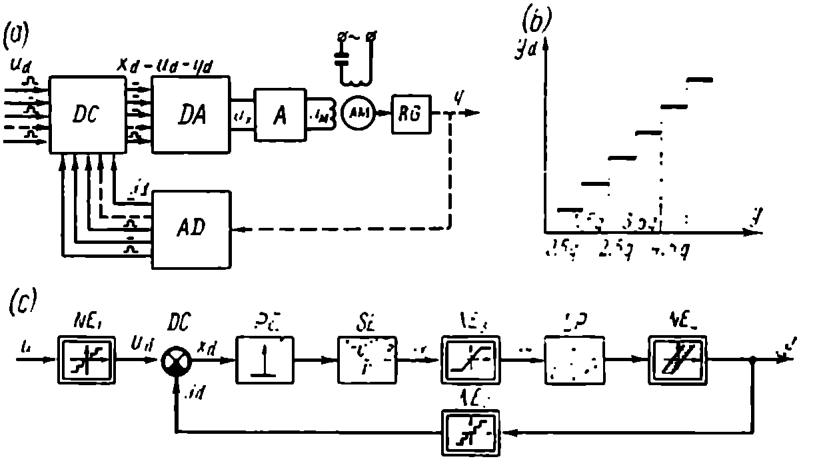

Fig. 15.7

The functional diagram of a digital servo system is shown in Fig. 15.7*a*, and its functioning was discussed in Ch. XII. The following notation is adopted: *DC* is a digital comparator; *AD* and *DA* are analog-to-digital and digital-to-analog converters; *A* is an amplifier; *AM* is an actuating motor; *RG* is a reduction gear; u_d is the input digital signal to be converted; y is output displacement; y_d is the result of the output displacement measurement given in the digital form; x_d is the digital misalignment; u_x is the analog misalignment voltage; u_{AM} is the voltage controlling the actuating motor.

The mathematical description of the digital servo system allows for time quantization of signals, which makes the system a sampled-data one, although remaining linear; no allowance is made, however, for the fact that digital signals are quantized in level, i.e. can only assume a number of discrete values. The level quantization is

performed by the AD, whose static response is a ladder curve having numerous disruptions and horizontal segments between them. The curve is shown in Fig. 15.7*b*, where q denotes one quantum of the system output y.

When y changes by q the digital signal y_d changes by a unit of the junior digit.

The digital input signal u_d can also be represented as a result of transformation of the analog signal u performed by the analog-to-digital converter with the ladder response. Therefore the structural diagram of the digital servo system shown in Fig. 15.7*c* incorporates two nonlinear elements, NE_1 and NE_2, with ladder responses. The linear portion, LP, of the system in the diagram allows for the time constant T and for the integrating properties of the motor. The circuit also includes a PE and a shaping elements SE (see Ch. XII) and two nonlinear elements allowing for the saturation in the amplifier (NE_3) and the play in the reduction gear (NE_4).

A digital servo system is an example of a nonlinear sampled-data control system.

Sometimes a digital servo system does not perform time quantization. This is due to the fact that AD converters and digital comparators can ensure continuous delivery and transmission of signals. Then the two nonlinear elements NE_1 and NE_2 in he circuit of Fig. 15.7*c* are replaced by one nonlinear element inserted in place of PE and SE. Such a system is an example of a nonlinear continuous control system.

A more sophisticated digital comparator (see Fig. 15.7*a*) can perform additional calculations and correct the signal x_d fed to the control loop. For example, it can handle computations corresponding to the action of the nonlinear elements $z_1(x)$ and $z_2(y)$ in the circuits of Figs. 15.4*b* and 15.5*a* and *e*, and offset the effect of nonlinearity NE_4 in the diagram of Fig. 15.7*c*.

15.4. EXAMPLES OF SYSTEMS CONTROLLING PLANTS WITH NONMONOTONIC (EXTREMAL) RESPONSES

Control of plants with a nonlinear extremal response varying arbitrarily in the course of time requires maintaining the controlled variable at the extremum point. This problem is solved by using continuous and sampled-data hardware. Consider examples of simple solutions and the characteristic nonlinearities involved.

A continuous self-oscillating extremal control system. To maintain the value of the controlled variable near the optimal point, extremal control systems include nonlinear elements with still more complicated responses.

Figure 15.8*a* displays the functional diagram of the extremal control system with continuous trial motion developed by

V.V. Kazakevich. The plant with unobservable action f is denoted as *1*. The control system consists of unit *2*, which stores the extremum

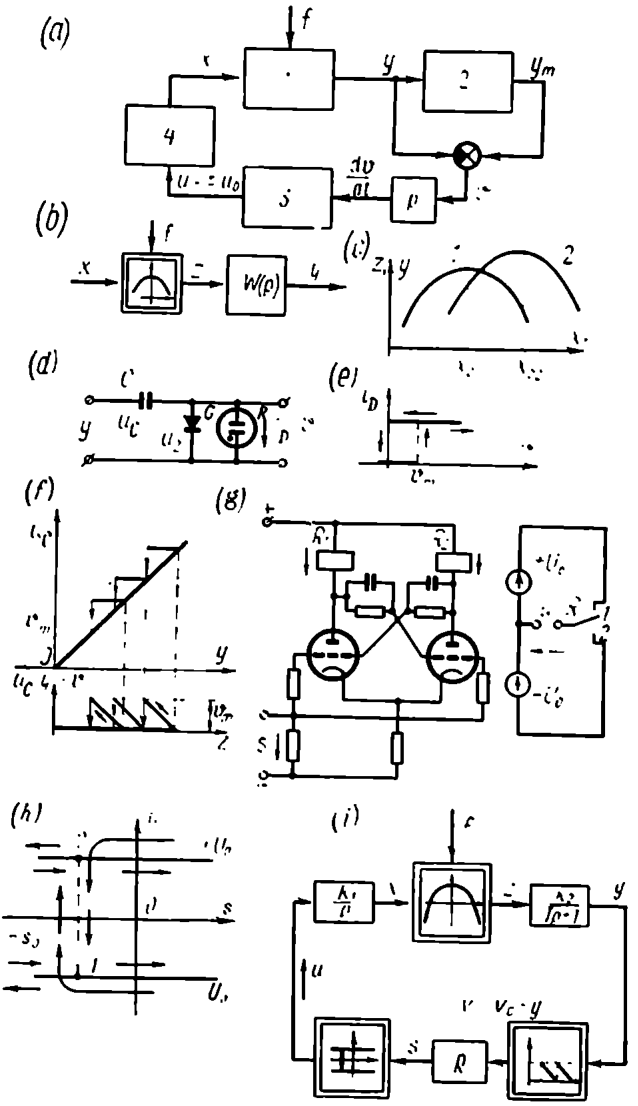

Fig. 15.8

y_m and determines the deviation from it, $y_m - y = v$; static symmetrical flip-flop *3*, which responds when the deviation from the extremum reaches a specified maximal value; and flip-flop-operated

actuator *4*. Unit *2* and flip-flop *3* are nonlinear as is the plant itself. Let us consider these elements in detail.

Plant. The plant may be any installation with an extremal response $y(x)$, where x is the control variable and y is the objective function reflecting the process performance. The goal of control is to maintain y at a maximal (or minimal) level. The relation between x and y generally depends on the rate at which x changes and may be rather involved.

In simpler cases this relation can be represented as the response of a nonlinear and a linear element connected in series. In one case it is represented by a nonlinear element $z(x)$ and a linear element with z at the input and y at the output; in another, by a linear element with x at the input and y at the output and a nonlinear element $z(y)$. Figure 15.8*b* shows a structural diagram corresponding to the first case; Fig. 15.8*c* depicts examples of nonlinear responses $z(x)$. The two responses, *1* and *2*, correspond to different values of f and, consequently, to different coordinates of the extremum points x_{01} and x_{02}. In further discussion the value x will be understood as deviation from the extremum point coordinate, $x = x_1 - x_{01}$ with the value of x_{01} fixed. The simplest linear element is a first-order inertial element, or a delay. The extremum point will be the maximum of y. Similar reasoning is applicable to the minimum of this function.

Maximum storage unit. The maximum of the objective function y may be stored by mechanical, electromechanical or electrical units, depending on the measurement technique. Figure 15.8*d* shows an electric circuit where the capacitor C is charged to the voltage y via the gate G. With increasing value of y the voltage u_C across the capacitor is invariably equal to y and the gate voltage $u_2 = v$ is 0. With decreasing y, however, the voltage $u_C = y_m$ and the difference $y - y_m$ is applied to the gate G.

When the voltage $u_2 = v_m$ is achieved at the gate, the discharger D passes the current and the gate voltage reduces to zero due to the capacitor discharge via the discharger circuit (current i_D). The discharger response is given in Fig. 15.8*e*.

For the system under discussion the nonlinear responses $u_C(y)$ and $v(y)$ are shown in Fig. 15.8*f*, where the response $u_C \cdot y$ corresponds to $\frac{dy}{dt} > 0$. If $\frac{dy}{dt} < 0$, then at $v < v_m$ the equalities $u_C = y_m$ and $v = y_m - y$ hold. At $v = v_m$ the capacitor discharges to y, and the equality $y = u_C$ (i.e. $v = 0$) is restored.

A symmetrical static flip-flop. A symmetrical static flip-flop with electronic tubes is shown in Fig. 15.8*g*; it triggers when negative pulses s exceed s_0. The anode circuits of the flip-flop tubes include windings of the differential polarized relay R_1 and R_2 so that at each triggering the contact of the relay R is switched over and the voltage u changes from $+U_0$ to $-U_0$, or vice versa.

The response of a symmetrical flip-flop as a nonlinear element is given in Fig. 15.8*h*, where jumpwise transitions from point *1* to point *2* and back occur as the voltage s decreases to $-s_0$.

The system structural diagram including all the three nonlinear elements under consideration is given in Fig. 15.8*i*. The linear part of the plant is assumed to be representable as an inertial element with a time constant T connected after the nonlinear element $z(x)$, the actuating motor being described by the integrating element $\frac{k_1}{p}$.

The symmetrical flip-flop receives pulses obtained by differen-

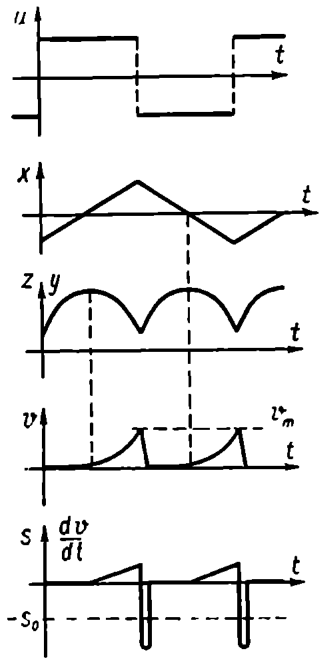

Fig. 15.9

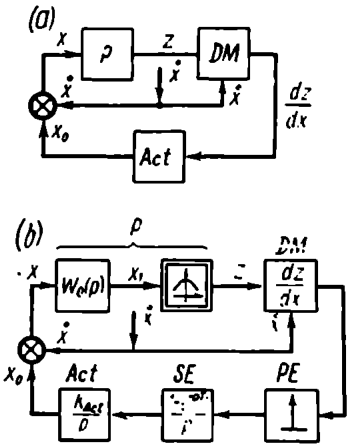

Fig. 15.10

tiating the quantity v in the maximum storage circuit.

The time diagram of each element operation is shown in Fig. 15.9 for the case where $T = 0$, or for an inertialess plant. One can see that in normal operation the motor reverses (and y again approaches the maximum) periodically when the deviation from the maximum reaches v_m. Any change of the plant response and of the maximum point coordinates caused by the action f is automatically accompanied with a transition of the system to the region of a new maximum point.

A sampled-data extremal control system. In a sampled-data extremal control system, whose functional diagram is shown in Fig. 15.10*a*, the value of the derivative $\frac{dz}{dx}$ of the plant nonlinear static response $z(x)$ is measured periodically at intervals of T_p. In the figure, *P*

is the plant; *DM* is the derivative meter; *Act* is the actuator. The derivative meter is a computing unit which measures $\frac{dz}{dx}$ on the basis of variations in the signals z and x. The time T_0 required to measure the increments of z and x and compute $\frac{dz}{dx}$ is a portion of the overall period T_p.

The *DM* can have most diverse implementations but its most widespread version is a synchronous detector. In this case an additional periodic trial signal $\dot{x} = X_{tr\,m} \sin \omega_{tr}\, t$ is delivered to the input of the plant P and of the *DM*, and the product $z\dot{x}$ is computed; the integration of this product in the *DM* over the time T_0 then yields a constant component, which is proportional to $\frac{dz}{dx}$. The measured discrete values of the derivative are fed to the *Act*, which changes the coordinate x_0 within T_{op} (op = operational) at a rate proportional to the value of $\frac{dz}{dx}$. In all cases $T_0 + T_{op} \leqslant T_p$. If one digital computer controls n plants, then

$$\sum_{i=1}^{n} (T_0 + T_{op})_i \leqslant T_p \tag{15.7}$$

The system equilibrium state equation is

$$\frac{dz}{dx} = 0$$

which coincides with the extremum condition.

Figure 15.10*b* displays the structural diagram of a sampled-data extremal system where the plant P is represented as a series connection of the linear part with a transfer function $W_0(p)$ and an element with a nonlinear extremal response $z(x_1)$. The discrete nature of the system is given by the introduction of a pulse element *PE* and a shaping element *SE* with a transfer function

$$W_s(p) = \frac{1 - e^{-pT_{op}}}{p} \tag{15.8}$$

which corresponds to the rectangular shape of the control pulses. The *Act* contains an integrator with a transfer function $\frac{k_{Act}}{p}$

Note that the period T_p and the time T_{op} are often selected such that the transient processes in the linear part of the plant practically complete within T_p. Then the plant transfer function $W_0(p)$ can be assumed equal to $k_0 = W_0(0)$ in studying the process in the main control loop.

Depending on the relation of the trial signal period $T_{tr} = \frac{2\pi}{\omega_{tr}}$, the time T_0, and the plant time constants, the dynamic responses of the plant may affect the system operation.

The system in question has two nonlinear elements, the plant and the *DM* containing a multiplier.

This system of extremal control is an example of a nonlinear sampled-data system maintaining the optimal value of the controlled parameter.

15.5 NONLINEAR ELEMENTS OF CONTROL SYSTEMS

The above control systems exhibit nonlinearities of most different forms. We will denote each nonlinearity by the appropriate function $z = z(x)$, assuming that there is one-dimensional nonlinearity, or that the variable z is a function of just one variable, x. There may also be multidimensional nonlinearities where the variable z is a function of several variables. An example of a two-dimensional nonlinearity is the element of Sec. 15.2 (Fig. 15.3), where the velocity v of the piston is a function of γ and y. In what follows we will deal with one-dimensional nonlinearities, while some multidimensional nonlinearities will be reduced to a combination of one-dimensional nonlinear responses.

Nonlinear elements can be classified in different ways: by symmetry, smoothness, unambiguity of responses. Let us consider each of these.

Symmetry. Two types of symmetry for nonlinear responses can be specified:

1) If the function $z(x)$ satisfies the condition

$$z(x) = z(-x) \tag{15.9}$$

the response is known as *symmetrical with respect to the y-axis* or *even-symmetrical*. In case of a single-valued relation such responses can be represented as a series with even powers of x

$$z(x) = \sum_{i=0}^{\infty} C_{2i} x^{2i}$$

where C is a constant factor.

2) If the function $z(x)$ satisfies the condition

$$z(x) = -z(-x) \tag{15.10}$$

the response is referred to as *symmetrical relative to the origin of coordinates*, or *odd-symmetrical*. If $z(x)$ is single-valued, such responses can be represented as a series with odd powers of x

$$z(x) = \sum_{i=0}^{\infty} C_{2i+1} x^{2i+1}$$

Responses which do not satisfy either condition are termed *asymmetrical.*

Sometimes asymmetrical responses may be made symmetrical by shifting the origin of coordinates, which is equivalent to introduction of some supplementary addends at the element input and output. Thus for an asymmetrical response $z_1(x_1)$ (Fig. 15.11*a*, *b*) the substitution $x_1 = x_0 + x$ makes the response $z(x) = z_1(x)$ symmetrical relative to the y-axis. This transformation of coordinates is equivalent to introducing the signal x_0 at the element input and transition from the asymmetrical response $z_1(x_1)$ to the even-symmetrical response $z(x)$ (Fig. 15.11*c*, *d*).

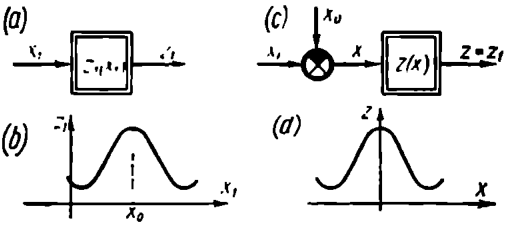

Fig. 15.11

In a similar way the response $z_1(x_1)$ of Fig. 15.12*a*, *b* can be replaced with an odd-symmetrical response $z(x)$ by substituting $x_1 = x_0 + x$ and $z_1 = z_0 + z$. The structural diagram and the response $z(x)$ corresponding to this transformation of coordinates are given in Fig. 15.12*c* and *d*.

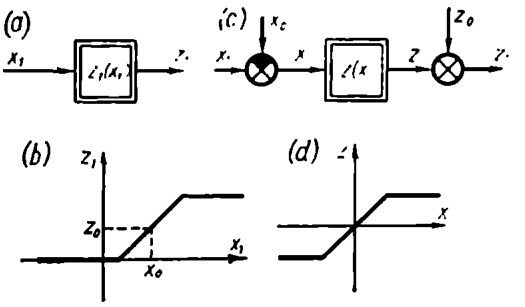

Fig. 15.12

The extremal responses of Fig. 15.8*c*, for instance, can be made even-symmetrical. The plots of Figs. 15.2*c*, *d*; 15.3*c*; 15.5*b*, *c*, *d* are odd-symmetrical responses. The selsyn response (Fig. 15.2*b*) may be either odd-, or even-symmetrical, depending on the x_0 selected. The graphs of Figs. 15.1*b*; 15.8*f*, *h*, etc. illustrate asymmetrical responses.

Smoothness. If a derivative $\frac{dz}{dx}$ exists at any point of the response $z(x)$, the response is *smooth.* If a response has breaks where the derivative is disrupted, the response is known as *broken.* A large group of broken responses are *piecewise-linear* responses consisting of segments of straight lines.

Examples of smooth responses are given in Figs. 15.1*b*, *c*, *d*, and 15.2*b*. Piecewise-linear responses are shown in Fig. 15.2*c*, *d*, etc. A broken response can be either continuous (Fig. 15.2*c*, *d*) or discontinuous (Fig. 15.5*c*, *d*). Sometimes smooth responses can be

approximated by piecewise-broken ones to facilitate calculations. Thus, by appropriate approximation and coordinate transformation the response of Fig. 15.1*b* can be reduced to a broken piecewise-linear form (Fig. 15.2*b*).

Unambiguity. If each value of x is associated with one specific value of z, the response is *unambiguous*, or *single-valued*; if it is associated with more values of z depending on the operating conditions prior to the particular instant, the response is referred to as *multivalued*, or *ambiguous*. In this case the number of the possible z values ranges from 2 to ∞.

Examples of unambiguous nonlinear responses are given in Figs. 15.1*b*, *d*; 15.2*b*, *c*; 15.5*d*; two-valued responses are shown in Figs. 15.5*b*, *c*; 15.8*e*, *h*. Nonlinear elements whose responses are given in Figs. 15.2*d* and 15.8*f* are multivalued.

Consider some widely used standard elements the responses of which, when properly simplified, are symmetrical with respect to the origin of coordinates (odd-symmetrical) and can be sufficiently well approximated by piecewise-linear curves.

Elements with more complicated responses which are not widely used will be referred to as *nonstandard*, or *singular*. These also include elements where nonlinearities are introduced intentionally in order to satisfy certain requirements.

15.6. STANDARD NONLINEAR ELEMENTS

Standard nonlinear elements may have both single-valued and multivalued responses, which can readily be reduced to a normalized dimensionless form by changing the scale of the input, x, and output, z, variables. If the response $z(x)$ is known, a normalized nonlinear response $\zeta(\xi)$ in relative units can be obtained by transformations $\xi = k_x x$ and $z = k_z \zeta$, which represent the change of scale. This transformation is illustrated by structural diagrams of Fig. 15.13*a*, *c*, where $x_0 k_x = 1$ and $x_0 k = k_z$. Standard nonlinear elements and their normalized responses were originally introduced by L.S. Goldfarb in 1947 for approximate analysis of control systems.

Consider basic nonlinear elements which are responsible for most typical nonlinearities of automatic systems.

Elements with single-valued continuous responses. *An element with a dead zone (threshold element).* Responses of this element are shown in Fig. 15.13*b*, *d* and are typical of some electronic, magnetic, and hydraulic amplifiers at low input signals. A simple mechanical model of a threshold element is a coupling system for two shafts with spring-operated return of the driven shaft to the neutral position when there is a play in the transmission system. This coupling is shown schematically in Fig. 15.13*e*. The play of the driving shaft is $2x_0$. The element response (see Fig. 15.13*b*) is given by the following

equations

$$z=\begin{cases} 0 & \text{at } |x|\leqslant x_a \\ k(x-x_a) & \text{at } x>x_a \\ k(x+x_a) & \text{at } x<-x_a \end{cases} \qquad (15.11)$$

Introducing the variables $\xi=\frac{x}{x_a}$ and $\zeta=\frac{z}{kx_a}$ we get the normalized response

$$\zeta=\begin{cases} 0 & \text{at } |\xi|\leqslant 1 \\ \xi-1 & \text{at } \xi>1 \\ \xi+1 & \text{at } \xi<-1 \end{cases} \qquad (15.12)$$

Saturation element. The responses of a saturation element are given in Fig. 15.11*b*, *d* and are valid for practically all actual amplifiers (electronic, magnetic, pneumatic, hydraulic) with a limited power

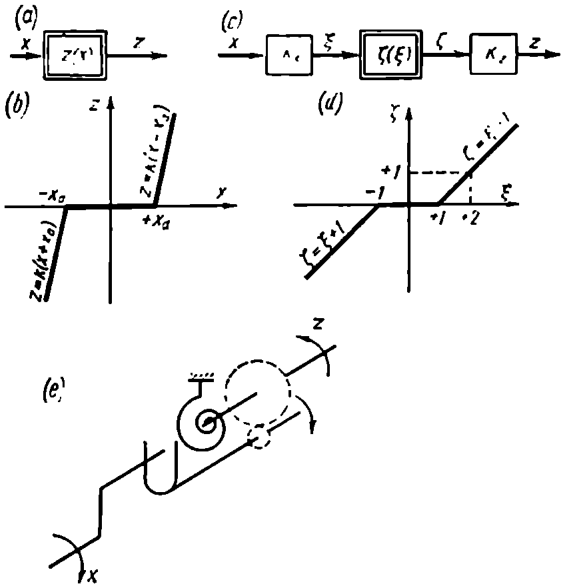

Fig. 15.13

in the range of large input signals. A simple mechanical model of a saturation element is two shafts connected by an elastic spring with stops or limiters in the system of the driven shaft.

This model is shown schematically in Fig. 15.14*a*, where the working feed of the driven shaft is equal to $2z_b$.

The response of this element (Fig. 15.14*b*) is expressed as

$$z=\begin{cases} kx & \text{at } |x|\leqslant x_b \\ z_b \operatorname{sign} x & \text{at } |x|>x_b \end{cases} \qquad (15.13)$$

By introducing the variables $\xi=\frac{x}{x_b}$ and $\zeta=\frac{z}{kx_b}$ we obtain the normalized response

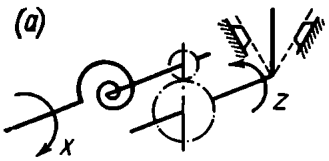

$$\zeta=\begin{cases} \xi & \text{at } |\xi|\leqslant 1 \\ \operatorname{sign}\xi & \text{at } |\xi|>1 \end{cases} \qquad (15.14)$$

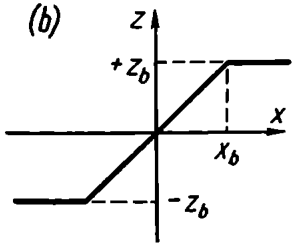

Fig. 15.14

A saturation element with a dead zone. Many control system elements are described by a nonlinear relation which includes both a dead zone and a saturation. The response of an element combining the two types of nonlinearity is given in Fig. 15.15*a*. At low input signals the element acts as a dead zone element and at large signals, as a saturation element.

The response of the element is described by the following equations

$$z=\begin{cases} 0 & \text{at } |x|\leqslant x_a \\ k(x-x_a) & \text{at } x_b>x>x_a \\ k(x+x_a) & \text{at } -x_b<x<-x_a \\ z_b \operatorname{sign} x & \text{at } |x|>x_b \end{cases} \qquad (15.15)$$

By introducing the notation $\xi=\frac{x}{x_a}$, $\zeta=\frac{z}{kx_a}$, $m=\frac{x_b}{x_a}$ we have the normalized response

$$\zeta=\begin{cases} 0 & \text{at } |\xi|\leqslant 1 \\ \xi-1 & \text{at } m>\xi>1 \\ \xi+1 & \text{at } -m<\xi<-1 \\ (m-1)\operatorname{sign}\xi & \text{at } |\xi|>m \end{cases} \qquad (15.16)$$

The potentiometric model of the element is given in Fig. 15.15*b*. The element represents a sufficiently general case of a single-valued continuous nonlinearity.

Elements with single-valued discontinuous responses. *A two-positional hysteresisless relay.* A single-valued response of a two-positional

polarized relay is shown in Fig. 15.16*a*. With the input signal magnitude $|x| < x_b$ the relay contacts are opened and nothing is known

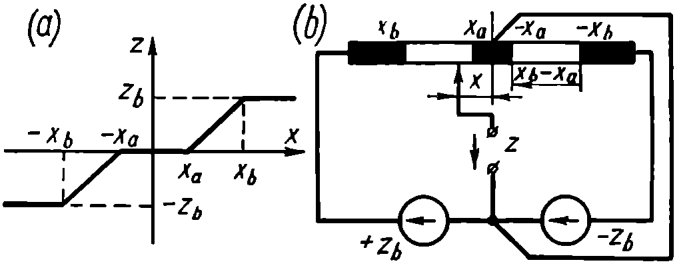

Fig. 15.15

about the voltage z picked up at the relay contact. The value of z is not related to the value of the input signal, x, so in this range of x

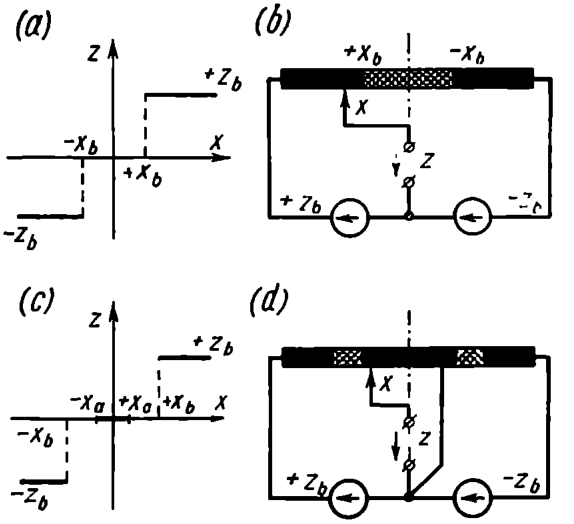

Fig. 15.16

there is no function $z(x)$. At $|x| \geqslant x_b$, z takes on the value $+z_b$ or $-z_b$ depending on the sign of x, and the function $z(x)$ can be expressed as a sign function.

Consequently, the nonlinear element response in the entire range of x is expressed as

$$z = \begin{cases} z_b \operatorname{sign} x & \text{at} \quad |x| \geqslant x_b \\ \text{inexistent} & \text{at} \quad |x| < x_b \end{cases} \qquad (15.17)$$

Figure 15.16*b* is an example of a potentiometric system where this relation holds. Here, at $|x| < x_b$ the potentiometer slide moves along the insulator and the output voltage z is uncertain.

A three-positional hysteresisless relay. A single-valued discontinuous response of a three-positional hysteresisless polarized relay is shown in Fig. 15.16*c*.

This response can be expressed analytically as

$$z = \begin{cases} z_b \operatorname{sign} x & \text{at} \quad |x| \geqslant x_b \\ 0 & \text{at} \quad |x| \leqslant x_a \\ \text{inexistent} & \text{at} \quad x_a < |x| < x_b \end{cases} \tag{15.18}$$

Figure 15.16*d* is an example of a corresponding potentiometric circuit.

In analysis and synthesis of different relay control systems use is often made of idealized responses of a two-positional relay as shown in Fig. 15.5*d*. This response can be obtained by limit transition from one of the responses of Figs. 15.14*b* and 15.15*a* or 15.16*a* and *c* as $x_a \to 0$ and $x_b \to 0$. At $x = 0$, however, the resultant responses have different values.

Thus, assuming in Eq. (15.13) that $x_b \to 0$ and $k \to \infty$ at $kx_b = z_b$, we have

$$z = \begin{cases} z_b \operatorname{sign} x & \text{at} \quad |x| > 0 \\ -z_b < z < z_b & \text{at} \quad x = 0 \end{cases} \tag{15.19}$$

A similar limit transition in Eq. (15.17) gives

$$z = \begin{cases} z_b \operatorname{sign} x & \text{at} \quad |x| > 0 \\ \text{inexistent} & \text{at} \quad x = 0 \end{cases} \tag{15.20}$$

For Eq. (15.15) or (15.18) the limit transition yields

$$z = \begin{cases} z_b \operatorname{sign} x & \text{at} \quad |x| > 0 \\ 0 & \text{at} \quad x = 0 \end{cases} \tag{15.21}$$

Sometimes in analysis of feedback relay circuits attention must be given to differences in the system operating conditions at $x = 0$ in each of the three cases. In further discussion a nonlinearity of the "sign" type will be understood as the response expressed by Eq. (15.19).

This response can be analytically given by and odd-power parabola $2n + 1$ as $n \to \infty$

$$z = z_b \operatorname{sign} x = z_b \lim_{n \to \infty} x^{(2n+1)-1} \tag{15.19a}$$

The inverse relation $x(z)$ will be denoted as

$$x = \operatorname{asign} \frac{z}{z_b} = \lim_{n \to \infty} \left(\frac{z}{z_b} \right)^{2n+1} \tag{15.19b}$$

Hysteresisless analog-to-digital converter. Elements which convert an analog quantity into a digital one by level sampling have a ladder response belonging to the class of single-valued discontinuous responses.

Such a response is shown in Fig. 15.17*a* and is analytically expressed as

$$\zeta = E\left(\xi + \frac{1}{2}\operatorname{sign}\xi\right) \tag{15.22}$$

where $E(t)$ is the integral part of t.

Such responses describe units which introduce an analog signal into a digital computer (see Fig. 15.7*b*). In potentiometric instruments, when taking into account voltage jumps on the rheostat slide as it moves from one turn to another (Fig. 15.17*b*), we obtain a similar relation between the position of the slide and the output voltage. The voltage jump u_0 is equal to the voltage across one turn. Then

$$z = u_0 E\left(\frac{x}{\Delta} + 0.5\operatorname{sign}x\right) \tag{15.23}$$

where Δ is the thickness of the rheostat wire.

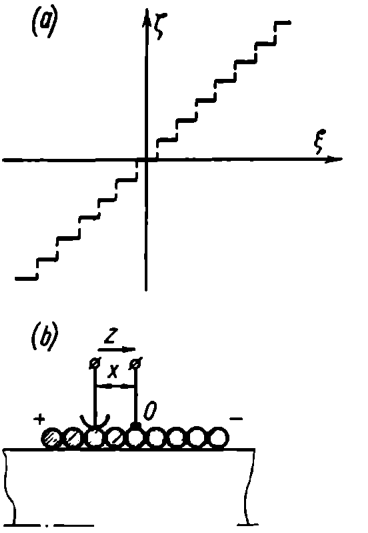

Fig. 15.17

Elements with two-valued responses. *Two-positional relay with hysteresis.* The above single-valued relay responses imply a certain idealization of the real systems. The value of the input signal at which the output quantity z jumps is in fact different for contact switching in the forward and reverse directions. For instance, in a two-positional polarized relay, which is symmetrically adjusted, the contact is switched in one direction at a certain voltage, and in the reverse direction, at the same voltage, but of the opposite sign.

The two-positional relay response (a backlash) is shown in Fig. 15.18*a* and is expressed analytically as follows

$$z = \left\{\begin{array}{ll} +z_b & \text{at } -x_a < x < \infty \\ -z_b & \text{at } -\infty < x < +x_a \end{array}\right\} \tag{15.24}$$

In the range $-x_a < x < x_a$ the quantity z is either $+z_b$ or $-z_b$ depending on the preceding values of x. The conditions for a jump from the lower to the upper branch are described as $x = x_a$, $z =$

$= -z_b$, $\frac{dx}{dt} > 0$ and for a jump in the opposite direction, as $x = -x_a$, $z = z_b$, $\frac{dx}{dt} < 0$.

Such properties are characteristic of amplifiers with a positive feedback and a saturation (see Fig. 15.14*a*). In this case the response is a continuous curve (Fig. 15.18*b*).

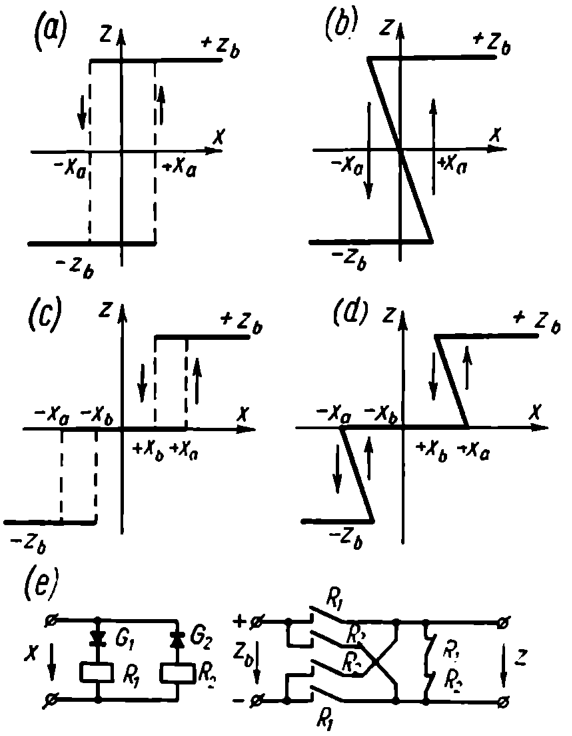

Fig. 15.18

The part of the response at $-x_a < x < x_a$ has a negative slope for $-z_b < z < z_b$ and is usually unstable. Thus, although at $-x_a < x < x_a$ each value of x has three corresponding values of z, only two of these, z_b and $-z_b$, represent a stable state of the system, and consequently the response (see Fig. 15.18*b*) is reduced to the above two-valued response (see Fig. 15.18*a*).

The equivalence of the above two types of response can help in analysis of relay control systems.

Three-positional relay with hysteresis. If we allow for differences in the values of the input quantity which correspond to contact switchings in both directions, the three-positional relay responses become ambiguous.

Thus, if transition from $z = 0$ to $z = z_b$ occurs at $x = x_a$ and return, at $x = x_b$, the response takes the form of Fig. 15.18*c*. Analytically this is expressed as

$$z = \begin{cases} z_b \operatorname{sign} x & \text{at } |x| > x_b \\ 0 & \text{at } |x| < x_a \end{cases} \qquad (15.25)$$

The quantity z has two values in the range $x_b < |x| < x_a$.

A similar response is obtained when an amplifier with a dead zone and a saturation (see Fig. 15.15*a*) has a positive feedback. In this case the continuous response (Fig. 15.18*d*) includes two parts with a negative slope which are usually found to be unstable and represent the jump zone. If jumpwise transitions in the response are allowed for, we obtain the conditions for its equivalence to the response of a three-positional relay with hysteresis. This problem is treated in more detail in Sec. 16.4.

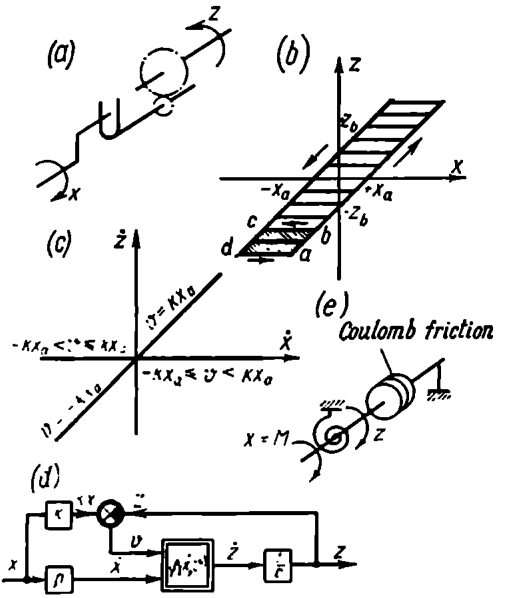

Fig. 15.19

The response of Fig. 15.18*c* can be obtained by using an electric circuit (Fig. 15.18*e*) consisting of two electromagnetic relays R_1 and R_2 connected via gates G_1 and G_2. The relays close the circuit between the supply with a voltage z_b and output terminals so that, depending on the value of x, the voltage z at the terminals takes on the value $-z_b$ or 0 or $+z_b$ as defined by the response (see Fig. 15.18*c*).

Elements with multivalued responses. *Play-type elements.* Nonlinearities in mechanical systems are often caused by gaps in the transmission system. One such nonlinearity was dealt with in examples of Sec. 15.2, it may occur when in a dead-zone mechanical model (see Fig. 15.13*e*) we remove the spring which returns the driven shaft to zero position (Fig. 15.19*a*).

In this case the relation between the position x of the driving and position z of the driven shaft is ambiguous. The response expressing the relation between the positions of the shafts is shown in Fig. 15.19*b*. Each position x of the driving shaft is associated with a set of positions z of the driven shaft in the range $k(x - x_a) \leqslant$

$\leqslant z \leqslant k(x + x_a)$. The selection of a particular position depends on the maximal or minimal deflection of z which preceded the particular moment.

The response of a play-type element is expressed analytically as

$$\dot{z} = \begin{cases} k\dot{x} \begin{cases} \text{at } \dot{x} > 0 \text{ and } v = kx_a \\ \text{at } \dot{x} < 0 \text{ and } v = -kx_a \end{cases} \\ 0 \begin{cases} \text{at } \dot{x} > 0 \text{ and } -kx_a \leqslant v < kx_a \\ \text{at } \dot{x} < 0 \text{ and } -kx_a < v \leqslant kx_a \end{cases} \end{cases} \tag{15.26}$$

where $\dot{x} = \frac{dx}{dt}$, $\dot{z} = \frac{dz}{dt}$, $v = kx - z$.

The relation $\dot{z}$ versus $\dot{x}$ expressed by Eq. (15.26) is shown in Fig. 15.19*c* for different values of v.

By introducing the notation $\varphi(\dot{x}, v)$ for the element which converts the signals $\dot{x}$ and v into the signal $\dot{z}$, a structural diagram can be obtained for a play-type element (Fig. 15.19*d*).

Play-type responses are inherent in systems both with a gap and with Coulomb friction. The latter case is shown in simplified form in Fig. 15.19*e*. The torque M is balanced by the spring moment αz (α is a proportionality factor) and by the Coulomb friction moment $\pm x_a$ the sign of which depends on the sign of $\dot{z}$. In this system the input action is the torque $x = M$ and the output, the angle of rotation, z, of the shaft. The moment equation is

$$x = M = \alpha z \pm x_a$$

or, by denoting $k = \frac{1}{\alpha}$,

$$z = k(x \mp x_a) \tag{15.27}$$

which corresponds to the plot of Fig. 15.19*b* and Eq. (15.26).

Besides

$$\frac{dz}{dt} = 0 \quad \text{at} \quad |x - \alpha z| < x_a \tag{15.28}$$

If the model allows for the viscous friction moment $\frac{\beta dz}{dt}$ or the moment caused by the inertia $\frac{\gamma d^2z}{dt^2}$ (β and γ are proportionality factors), as well as the spring moment, the equation for the system is more complicated and the model cannot be reduced to a play-type element. In this case the effect of the Coulomb friction moment should be isolated as a nonlinear feedback of a linear element. This nonlinearity will be discussed below.

Stop-type element. The motion of the driven part of mechanical systems may be limited in two directions, whereas the driving part can move unboundedly. This is exemplified by the mechanism of Fig. 15.20*a*. The driving shaft is coupled with the driven part by means of a friction clutch which disengages as soon as the resistance moment exceeds a certain threshold. The driven part has stops on two sides; consequently, when it reaches the stop and causes a large friction moment, the clutch disengages and the driving shaft continues turning while the driven part remains motionless. If the driving shaft rotation is reversed, the clutch reengages, and the driven part moves with the driving shaft.

If the rotation angles of the driving and driven shafts are denoted as x and z, their relation is expressed by the plot of Fig. 15.20*b*.

Each position x of the driving shaft is associated with a set of positions of the driven shaft in the range $-z_b \leqslant z \leqslant +z_b$.

Analytically, the response of such an element is given as

$$\dot{z} = \begin{cases} k\dot{x} \begin{cases} \text{at } \dot{x} > 0 \text{ and } -z_b \leqslant z < z_b \\ \text{at } \dot{x} < 0 \text{ and } -z_b < z \leqslant z_b \end{cases} \\ 0 \begin{cases} \text{at } \dot{x} > 0 \text{ and } z = z_b \\ \text{at } \dot{x} < 0 \text{ and } z = -z_b \end{cases} \end{cases} \tag{15.29}$$

The relation of $\dot{z}$ versus $\dot{x}$ as expressed by Eq. (15.29) is shown in Fig. 15.20*c*. The structural diagram corresponding to this equation is shown in Fig. 15.20*d*.

The nonlinear responses representing the stop-type element describe the processes in systems with pneumatic and hydraulic amplifiers (see Fig. 15.3) and with electric motors for rudder servos with end switches (ES) in the armature circuit.

Assume that with the armature circuit closed (see Fig. 15.20*e*, where one of the parallel branches, contact ES_1-gate G_1 or contact ES_2-gate G_2, is closed) the rate $\dot{z}$ of the motor is proportional to the voltage u across the armature, or $\dot{z} = ku$. When the motor shaft turns to touch one of the stops, the contact is opened and the motor is cut off, $\dot{z} = 0$. If the overrun of the motor is neglected, the relation between $u = \dot{x}$ and $\dot{z}$ is expressed by the plot of Fig. 15.20*c*, and the system of Fig. 15.20*e* is represented by a stop-type nonlinearity.

Let us now compare the nonlinear responses of the play- and stop-type elements. For responses of both types any cyclic change in x entails a similar change in z, so $z(x)$ is expressed by a certain closed curve. Such curves are shown as *abcd* cycles in Figs. 15.19*b* and 15.20*b*. Note the different directions of movement along these cycles,

which is counterclockwise for the play-type element and clockwise for a stop-type element. For responses of the play type as well as the relay hysteresis type (see Fig. 15.18)

$$\oint z\,dx < 0 \quad (15.30)$$

whereas for the stop-type response

$$\oint z\,dx > 0 \quad (15.31)$$

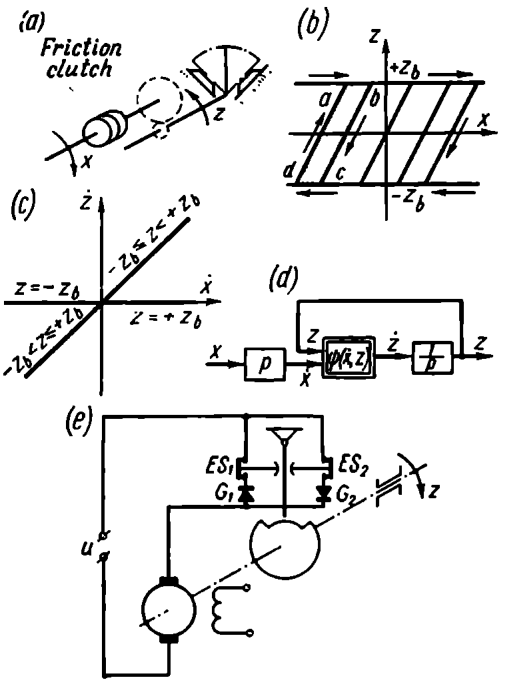

Fig. 15.20

With gains in play- and stop-type elements going to infinity their responses become rectangular (Fig. 15.21*a*, *b*).

The response of a stop-type element with an infinitely high gain is exemplified by the effect of Coulomb friction in the mechanical transmission system if the input action x is the rotation of the shaft while the output z is the friction moment, e.g. in the mechanism of Fig. 15.21*c*. In this case the torque M is balanced by the moments of the spring αx, viscous friction $\frac{\beta dx}{dt}$, Coulomb friction $z(\dot{x}) = \pm z_b$, and inertia $\frac{\gamma d^2x}{dt^2}$. Under these conditions

$$z = z_b \operatorname{sign} \dot{x} \quad (15.32)$$

and

$$M - z = \alpha x + \frac{\beta\,dx}{dt} + \frac{\gamma\,d^2x}{dt^2} \quad (15.33)$$

The structural diagram which fits the latter equation is shown in Fig. 15.21*d*, where

$$W(p) = \frac{1}{\alpha + \beta p + \gamma p^2} \quad (15.34)$$

The feedback loop described by the nonlinear element $z(\dot{x})$ has the response of Fig. 15.21*b* and corresponds to series connection of a differentiatingel ement and a nonlinearity of the "sign" type.

Magnetic hysteresis elements. Magnetic memories are often characterized by nonlinear responses, where hysteresis loops are given

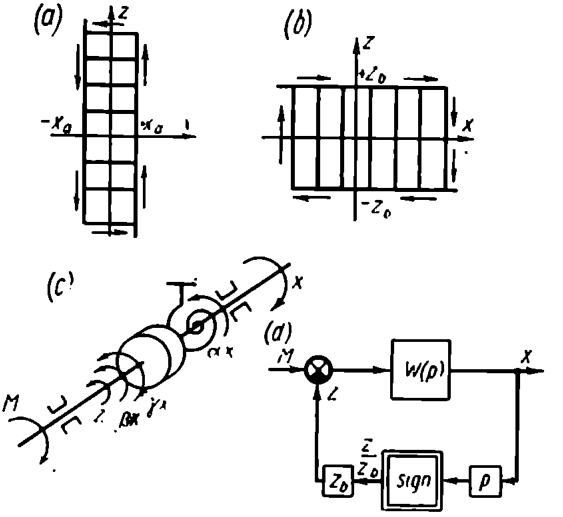

Fig. 15.21

as piecewise-linear closed curves. An example of such a response is given in Fig. 15.22*a*. The response can be described by the following equations

$$\left.\begin{aligned} z &= \mu_1 (x \pm x_a) \\ z &= \mu_2 x + C \end{aligned}\right\} \quad (15.35)$$

where $-z_b < C < z_b$, while μ_1 and μ_2 are constants.

Depending on the initial conditions, inside the loop z can take on any value from $z = \mu_2 x - z_b$ to $z = \mu_2 x + z_b$.

As $\mu_1 \to \infty$ and $\mu_2 \to 0$ the hysteresis loop becomes rectangular (Fig. 15.22*b*). This response differs from that of a play-type element as $k \to \infty$ (see Fig. 15.21*a*) in that the value of z is restricted to the range from $-z_b$ to $+z_b$.

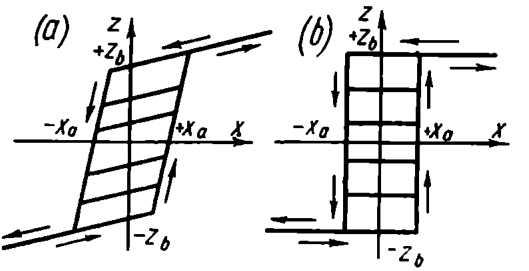

Fig. 15.22

15.7. LINEARIZATION OF STANDARD NONLINEAR ELEMENTS BY PERIODIC OSCILLATIONS (VIBRATIONAL LINEARIZATION)

One way to offset the undesirable effect of dead-zone and play-type nonlinearities is to impose an additional periodic signal at the input of a nonlinear element and to filter it out at the output. Thus,

if such a rapidly changing component $\overset{\circ}{x}$ is added to a constant or a slowly changing signal x_0, the resultant signal at the input, $x = x_0 + \overset{\circ}{x}$, will cause an output signal z, which in turn can be represented as a sum of a constant or slowly changing component z_0 and a rapidly changing component $\overset{\circ}{z}$ (Fig. 15.23).

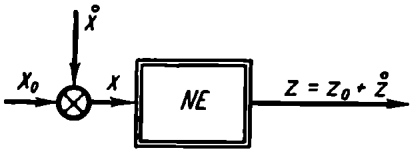

Fig. 15.23

Since the superposition principle is inapplicable to nonlinear systems, the variable component $\overset{\circ}{x}$ affects the relation z_0 versus x_0.

Let us see how the response of a dead-zone-type element to a constant component x_0 and z_0 changes when an additional periodic

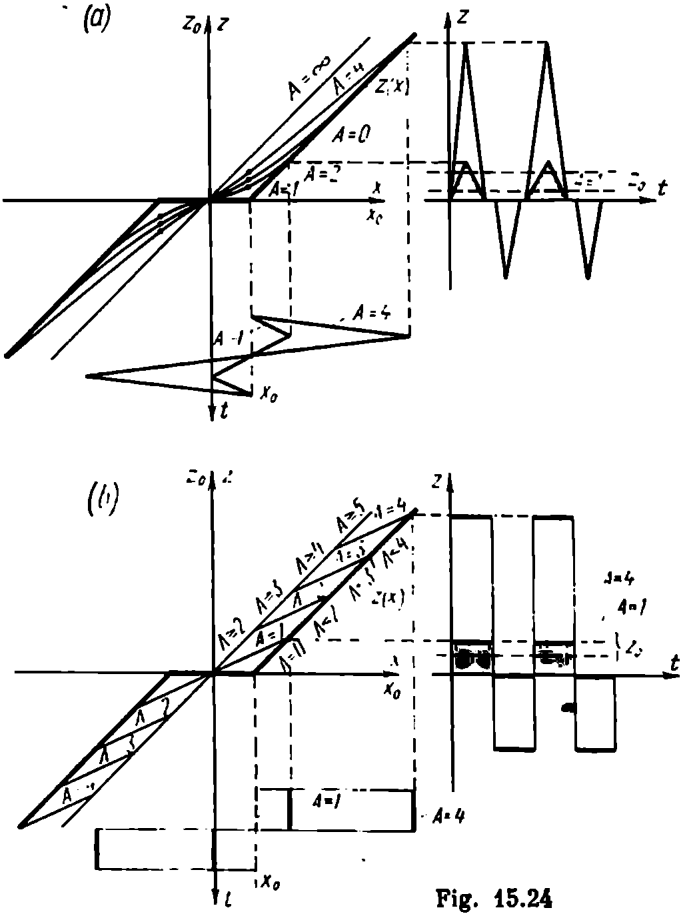

Fig. 15.24

signal $\dot{x}$ is introduced. The action of the periodic signal depends on its shape. Consider two extreme cases where the variable signal is either triangular or rectangular. In the case of a sinusoidal signal the solution is somewhere between the results for the above two cases.

In Fig. 15.24*a* the heavy line denotes the nonlinear response $z\,(x)$, which coincides with the response $z_0\,(x_0)$ at $\dot{x} = 0$.

With increasing $\dot{x}$ the response $z_0\,(x_0)$ changes, approaching a straight line with increasing amplitude A of the signal $\dot{x}$. The

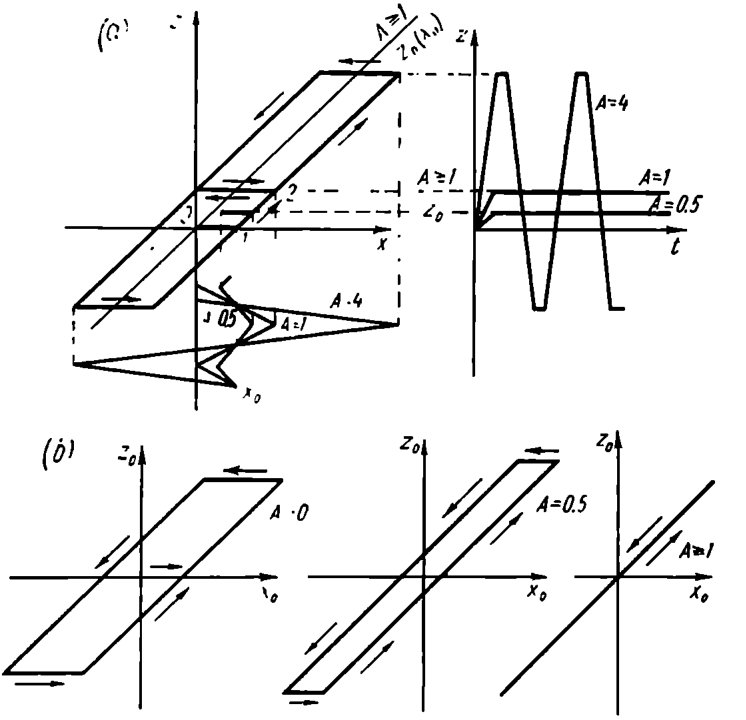

Fig. 15.25

plot of the relation $z_0\,(x_0)$ for a triangular variable component is shown in Fig. 15.24*a*. This corresponds to the most important point $x_0 = 1$ for $A = 1$ and $A = 4$. With increasing A, z_0 is seen to increase in the vicinity of the initial dead zone, and as $A \to \infty$ the relation $z_0\,(x_0)$ becomes a straight line traversing the origin of coordinates.

A rectangular component (Fig. 15.24*b*) linearizes the response to an even greater extent.

For a dead-zone-type nonlinearity the addition to the input of a rectangular component with an amplitude n times the half-width

of the dead zone linearizes the response in a range of width $(n - 1)$ times that of the dead zone.

The effect of linearization is even more amazing with a play-type element. In this case the addition of a triangular (or rectangular) signal ensures linearization provided its amplitude exceeds the half-width of the play zone.

Plotting for this case is illustrated in Fig. 15.25*a* and the responses $z_0 (x_0)$ at different values of A are shown in Fig. 15.25*b*.

The addition of a variable component is seen to reduce the nonlinearities of responses of dead-zone and play-type elements; at certain, sufficiently high, values of the amplitude A this imparts to nonlinear elements properties of proportional linear elements. This effect is called *vibrational linearization*. For stop- and saturation-type nonlinearities this linearization widens the linear zone, which is accompanied by gain reduction in this part of the response.

Studies of vibrational linearization lead to the conclusion that control circuits with small self-oscillations are effective. If stable, these can improve transient performance and offset certain objectionable nonlinearities.

15.8. NONSTANDARD (SINGULAR) ELEMENTS OF NONLINEAR SYSTEMS

The above examples by no means cover the entire variety of nonlinear system elements. It is sufficient to discuss the examples of Secs. 15.2, 15.3, and 15.4 to discern many nonlinear elements not covered by Sec. 15.6.

Of special importance among the elements of linear and nonlinear systems is the multiplier. Depending on the method of connection this element can be present both in linear and nonlinear systems.

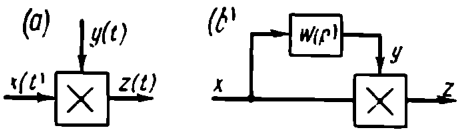

Fig. 15.26

If a multiplier receives independent input signals, then it functions without disturbing the linearity of the system and just characterizes parameter variations. An ideal pulse element (see Ch. XII) is an example of such a multiplier. It multiplies the signal $x(t)$ by a sequence of δ-functions.

The system uses the superposition principle and remains linear. The structural diagram of multiplication of independent signals $z = xy$ is shown in Fig. 15.26*a*.

The situation is different when the signals x and y are interrelated. Then the system becomes nonlinear even if all other elements are linear (Fig. 15.26*b*).

An example of a nonlinear element with a parabolic even response $z = x^2$ (Fig. 15.27*a*) implemented by a multiplier is shown in Fig. 15.27*b*. Such responses are discussed when studying extremal control systems (see Fig. 15.8*b*, *c*, *i*).

A multiplier and simpler nonlinear elements with piecewise-linear responses can be used to obtain an element with an odd-parabolic response

$$z = x \mid x \mid = x^2 \operatorname{sign} x \tag{15.36}$$

Figure 15.28*a* represents this response and Fig. 15.28*b*, the structural diagrams which should be employed to obtain an element with

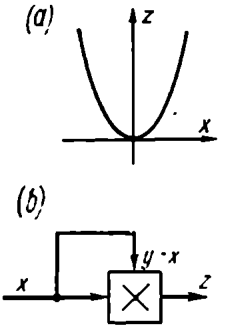

Fig. 15.27

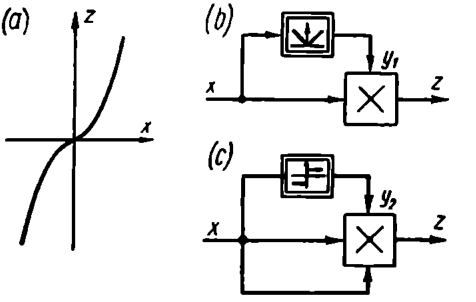

Fig. 15.28

this response by connecting the multiplier and nonlinear elements with responses

$$y_1 = \mid x \mid \tag{15.37}$$

or

$$y_2 = \operatorname{sign} x \tag{15.38}$$

Nonlinear elements with an odd-parabolic response (15.36) lead to speed-optimal systems (see Fig. 15.5*e*).

A multiplier is also included in more complicated nonlinearities where the output is a function of two or more inputs.

Thus, if a static nonlinear plant with n inputs $x_1, x_2, \ldots, x_n$ and one output z has a continuous response $z(x_1, x_2, \ldots, x_n)$, the response can be given by the relation

$$z = \sum_{i=1}^{n} a_i x_i + \sum_{\substack{i=1 \\ i \leqslant j}}^{n} \sum_{j=1}^{n} b_{ij} x_i x_j + \sum_{\substack{i=1 \\ i \leqslant j \leqslant k}}^{n} \sum_{j=1}^{n} \sum_{k=1}^{n} c_{ijk} x_i x_j x_k \tag{15.39}$$

where a_i, b_{ij}, c_{ijk} are constant factors, while at $i > j$, $b_{ij} = 0$ and at $i > j$ or $j > k$, $c_{ijk} = 0$.

Such plants are dealt with in multidimensional optimization problems. Equation (15.39) represents a connection of proportional, multiplying, and adding elements.

Certain relay elements perform multiplication as well as signal conversion. Such elements are often simpler to implement than a separate multiplier.

Consider a relay converter whose structural diagram is shown in Fig. 15.29*a*.

Here

$$z = z(x_1, x_2) = x_1 1_0(x_2) \tag{15.40}$$

and the output signal is nonzero and equal to the signal x_1 at the input only when x_2 is positive. The spatial representation of the relay

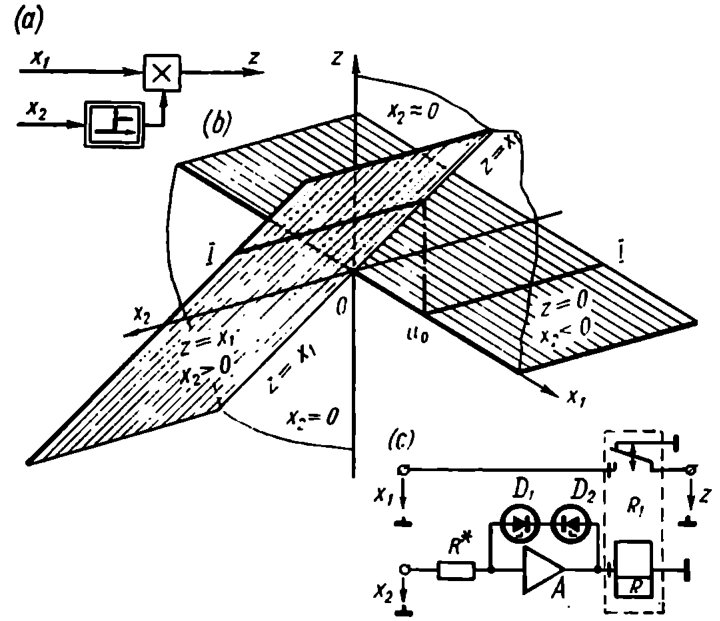

Fig. 15.29

converter response is given in Fig. 15.29*b*. The response $z(x_1, x_2)$ is shown as two flat surfaces $z = x_1$ at $x_2 > 0$ and $z = 0$ at $x_2 < 0$. If $x_1 = \text{const} = U_0$, the cross section *I-I* of these surfaces gives the relay response $z = U_0 1_0(x_2)$.

A circuit with such a response is shown in Fig. 15.29*c*. The coil of the polarized relay R_1 is supplied by the operational amplifier A controlled by the signal x_2; the amplifier output is limited by two

reference diodes D_1 and D_2 in the feedback loop D_1D_2R. Consequently, the current through the winding of the relay R_1 is proportional to sign x_2, and the relay closes the lower contact at a positive value

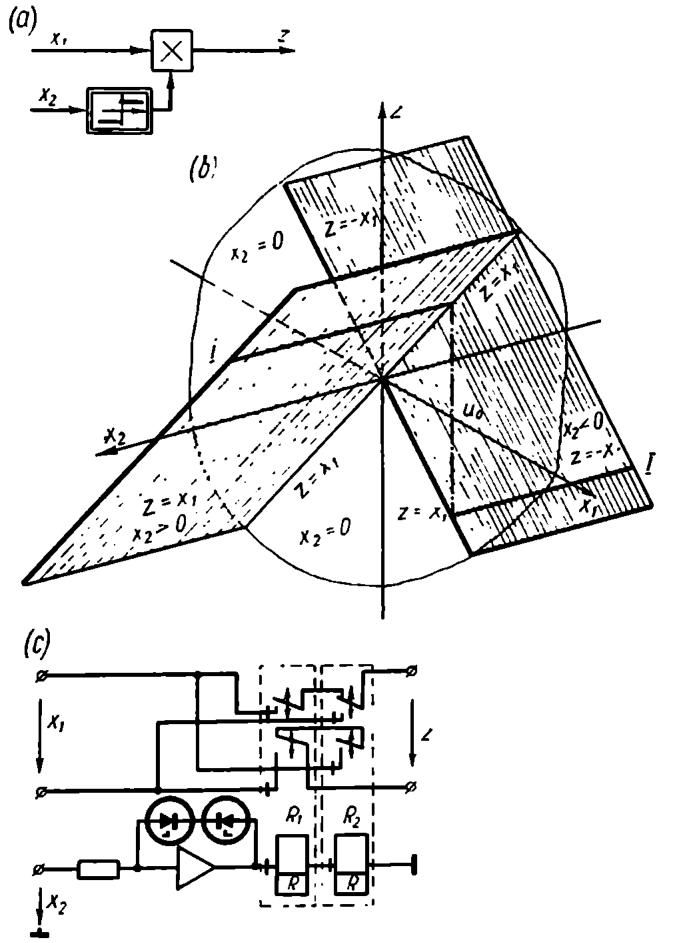

Fig. 15.30

of x_2. The signal z at the output is equal to the input signal x_1 at $x_1 > 0$ and to zero at $x_1 < 0$.

An element with the structural diagram of Fig. 15.30*a* and response

$$z = z(x_1, x_2) = x_1 \operatorname{sign} x_2 \tag{15.41}$$

is more difficult to obtain. In this case the response of Fig. 15.30*b* can be implemented if the two relays, R_1 and R_2, close the contacts

at different signs of the signal x_2 (Fig. 15.30*c*). The sign of x_1 fed to the circuit z is changed in accordance with the sign of x_2 by the switching contacts of relays R_1 and R_2. To prevent a short circuit in case the two relays act simultaneously by mistake, the break

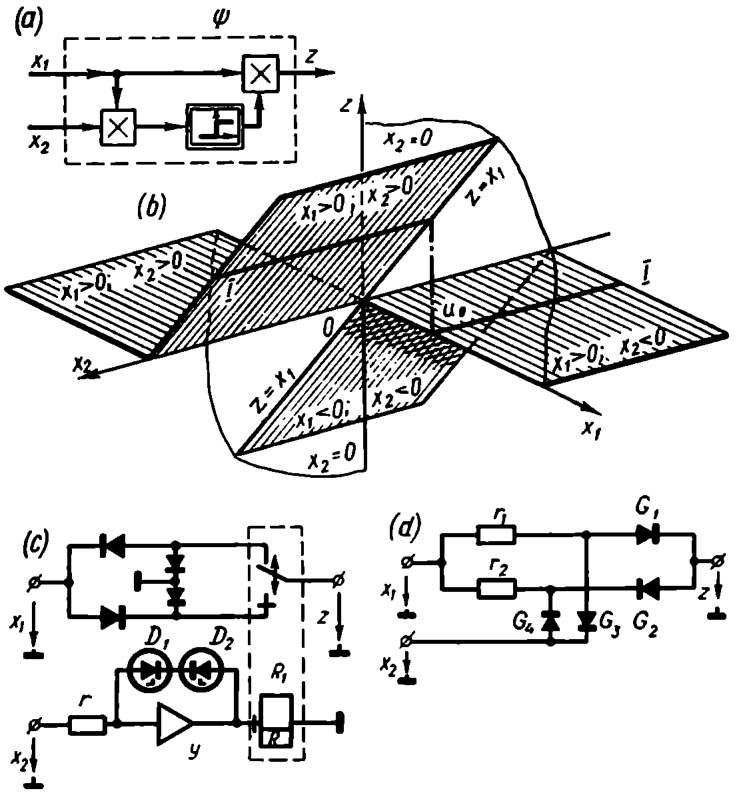

Fig. 15.31

contacts of the relays are connected in series into the circuit. At $x_1 = \text{const} = U_0$ the response is a discontinuous curve I-I, which corresponds to $z = U_0 \operatorname{sign} x_2$ (Fig. 15.30*b*).

Variable structure systems (Sec. 15.3, Fig. 15.6) include relay elements performing the conversion

$$u_2 = z = z(x_1, x_2) = x_1 1_0(x_1 x_2) \qquad (15.42)$$

The structural diagram of this element is shown in Fig. 15.31*a*. The spatial representation of the response (Fig. 15.31*b*) has the form of four flat portions of two surfaces, $z = x_1$ and $z = 0$ touching at the point 0. As in the circuit of Fig. 15.29*a*, the cross section representing $x_1 = U_0$ gives the relay response $z = U_0 1_0(x_2)$.

The element performing the conversion (15.42) is used in variable structure systems and is known as a ψ-element. In the adopted notation $\psi = \frac{z}{x_1} = 1_0 (x_1 x_2)$.

There are different ways of obtaining ψ-elements, two of which are shown in Fig. 15.31c and *d*.

In the first version (Fig. 15.31*c*) a polarized relay R_1 is used with contacts connected in a bridge gate circuit so that when x_1 is positive, this signal passes through the lower gate to the circuit z only at $x_2 > 0$, and when x_1 is negative, connection to the circuit z is achieved through the upper gate and only at $x_2 < 0$. In the second version no relays are used and the diagram is still simpler (Fig. 15.31*d*). In this case, when the signal x_1 is positive, the signal transmission through the resistor r_1 and gate G_1 to the circuit z can only take place at positive x_2. The second circuit is then closed through gate G_4. Otherwise the circuit is closed through gate G_3, and $z = 0$. When x_1 is negative, it is transmitted along the lower branch through the resistor r_2 and gate G_2 only at negative x_2. The resistors r_1 and r_2 are assumed to be equal and to limit the power transmitted to the circuit z. The output circuit of z is usually a power amplifier.

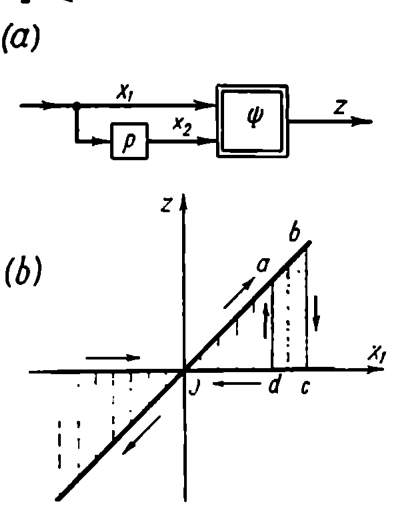

Fig. 15.32

Figure 15.6 illustrates an example of connecting a ψ-element into a control circuit. Assuming that $\beta = 0$ the ψ-element input will be the signal x_1 and its derivative $x_2 = \frac{dx_1}{dt}$ (Fig. 15.32*a*). In this case the ψ-element with a differentiator combine into a nonlinear element, which converts the input signal x_1 into the signal z. The element response is shown in Fig. 15.32*b*. The straight line $z = x_1$ represents the condition $x_1 \dot{x}_1 > 0$ and the straight line $z = 0$, the condition $x_1 \dot{x}_1 < 0$. A jump from one straight line to the other occurs at $x_1 \dot{x}_1 = 0$.

Similarly to a stop-type element the resultant element $z(x_1)$ with a multivalued response has inverse (negative) hysteresis since here we have $\oint z\, dx_1 > 0$ (e.g. the cycle *abcd* in Fig. 15.32*b*).

Other nonlinear elements with negative hysteresis may be implemented with the use of relay elements. For example, responses similar to those shown in Fig. 15.18*a* for a two-positional relay with

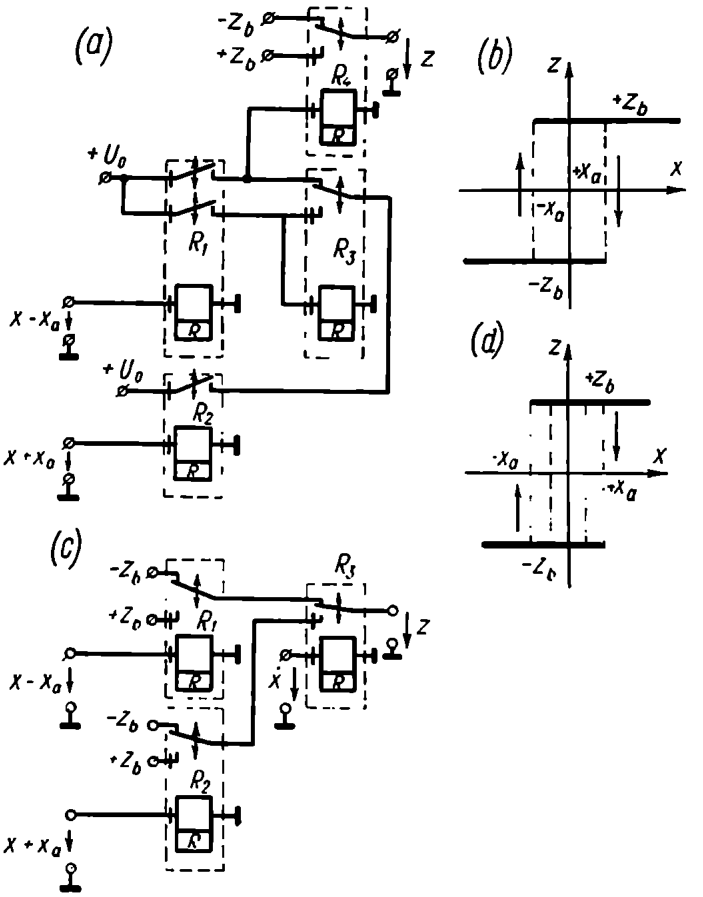

Fig. 15.33

positive hysteresis can be obtained but they will have negative hysteresis.

Figure 15.33*a*, *c* shows two ways of obtaining a relay response with negative hysteresis by using polarized relays R_1, R_2, R_3, and R_4. In both cases the response is expressed by Eq. (15.24) but the conditions for a jump in the ambiguity zone are different. In the first case the jump from the lower to the upper branch is given by the condition $x = \pm x_a$, $z = -z_b$, and $\frac{dx}{dt} > 0$ and from the upper to

the lower branch, by the condition $x = \pm x_a$, $z = +z_b$, and $\frac{dx}{dt} < 0$ (Fig. 15.33*b*). In the second case the jump also takes place when the sign of $\frac{dx}{dt}$ changes at any point of the ambiguity zone. The jump from the lower to the upper branch occurs at $\frac{d^2x}{dt^2} > 0$ and $\frac{dx}{dt} = 0$. At $\frac{d^2x}{dt^2} < 0$ and $\frac{dx}{dt} = 0$ the jump occurs in the opposite direction (Fig. 15.33*d*).

The both systems of relay elements with negative hysteresis are employed to improve control performance. Three-positional relays with negative hysteresis can be obtained in a similar way.

Nonlinear systems of Secs. 15.2, 15.3, and 15.4 included other elements as well. Thus practical servo systems also include (see Fig. 15.2) nonlinear elements with a sinusoidal response

$$z = k \sin\left(\frac{2\pi x}{x_T}\right) \tag{15.43}$$

where x_T is the sinewave period.

Extremal control systems include multivalued elements with a saw-tooth response (see Fig. 15.8*f*), which ensure extremum memorization, and symmetric flip-flops with a double-valued response (see Fig. 15.8*g*, *h*), which convert a variable input signal into a signal with a frequency half that of the input signal.

Chapter XVI

NONLINEAR SYSTEM STATICS. CONNECTION AND TRANSFORMATION OF NONLINEAR ELEMENTS

16.1. SPECIFIC FEATURES OF RESPONSE OF NONLINEAR ELEMENT CONNECTIONS

In nonlinear systems signal conversion is generally described by a differential or integral nonlinear equation and can be expressed by a certain conversion operator Λ. If the input signal is $x(t)$ and the output signal is $z(t)$, then

$$z(t) = \Lambda\{x(t)\} \tag{16.1}$$

Depending on the nature of the nonlinearity and on the element's dynamic properties, the operator Λ may have a rather complex expression. In some particular cases, signal conversion in a nonlinear element can be represented as sequential action of a linear operator $W(p)$ reflecting the element's dynamic properties, and of a nonlinear operator f expressing static conversion of the signal.

This representation corresponds to an equivalent circuit consisting of a linear dynamic and a nonlinear static element connected in series.

A signal can be converted in different ways depending on the sequence in which the linear and the nonlinear operators act. Thus, if

$$\left.\begin{aligned} z_1(t) &= \Lambda_1\{x(t)\} = f\langle L^{-1}\{W(p)\,L[x(t)]\}\rangle \\ z_2(t) &= \Lambda_2\{x(t)\} = L^{-1}\langle W(p)\,L\{f[x(t)]\}\rangle \end{aligned}\right\} \tag{16.2}$$

then, in the general case,

$$z_2(t) \neq z_1(t)$$

L and L^{-1} are the direct and inverse Laplace transforms.

Equivalent circuits corresponding to the two kinds of transformation are shown in Fig. 16.1*a* and *b*.

Since $z_2(t) \neq z_1(t)$, then in case of series connection the nonlinear static and the linear dynamic elements cannot change places. The only exception is the delay τ, for which $W(p) = e^{-p\tau}$ and

$$L^{-1}\{e^{-p\tau}L[x(t)]\} = x(t-\tau)$$

In this case

$$z_1(t) = f[x(t-\tau)] = z_2(t \tag{16.3}$$

and interchanging the positions of the delay and the nonlinear static element $f(x)$ does not affect the properties of the system.

In order to write down the solution to Eq. (16.1) with respect to the variable $x(t)$, an inverse operator Λ^{-1} is introduced to represent the condition

$$\Lambda^{-1}\{\Lambda[x(t)]\} = x(t)$$

Then

$$x(t) = \Lambda^{-1}\{z(t)\} \tag{16.4}$$

provided, of course, that there is a solution to Eq. (16.2) for a given

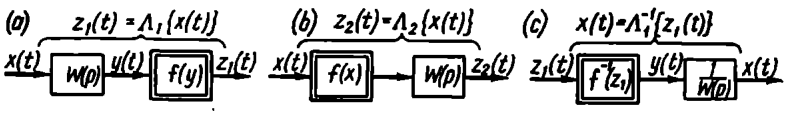

Fig. 16.1

$z(t)$. If Λ_1 is a direct operator of a series connection of a linear dynamic and a nonlinear static element

$$\Lambda_1\{x(t)\} = f\{L^{-1}\{W(p)\, L[x(t)]\}\}$$

then the inverse operator is

$$\Lambda_1^{-1}\{z(t)\} = L^{-1}\left\{\frac{1}{W(p)} L\{f^{-1}[z(t)]\}\right\} \tag{16.5}$$

Here the symbol f^{-1} denotes a nonlinear function, which is inverse to f. Then $f^{-1}\{f(x)\} = x$. Equivalent circuits representing the direct (Λ_1) and inverse (Λ_1^{-1}) operators are given in Fig. 16.1*a*, *c*.

In studying the statics of nonlinear systems the signals x and z do not depend on time, and the linear element can be regarded as a proportional element $W(0)$ and be combined with the nonlinear static element. Static problems are very important in nonlinear systems and are the essence of this chapter.

In deriving equivalent responses of different connections of nonlinear static elements, as was done in the case of linear elements (see Ch. V), we will cover three types of connection:

(a) series connection;
(b) parallel feedforward connection;
(c) parallel feedback connection.

In all cases we assume that the elements are unilateral and their connection does not affect individual responses. We will now discuss the specific features of each connection, illustrating them with examples.

16.2. SERIES CONNECTION

In series connection of nonlinear elements, as in the case of linear ones, the output of one element is the input of another.

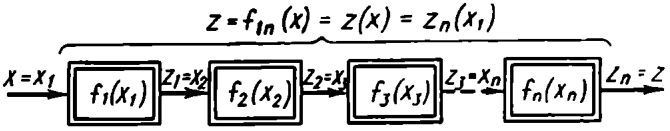

Fig. 16.2

If n elements are connected in series (Fig. 16.2), then

$$x_{i+1} = z_i \tag{16.6}$$

and since $z_i = f_i(x_i)$, then

$$x_{i+1} = f_i(x_i) \tag{16.7}$$

Solving simultaneously n nonlinear equations of this type we will have for series connection of n elements the following nonlinear function expressing the response $z(x) = z_n(x_1)$

$$z(x) = f_{1n}(x) = \overbrace{= f_n\{f_{n-1} \ldots [f_1(x)]\}}^{n-1} \tag{16.8}$$

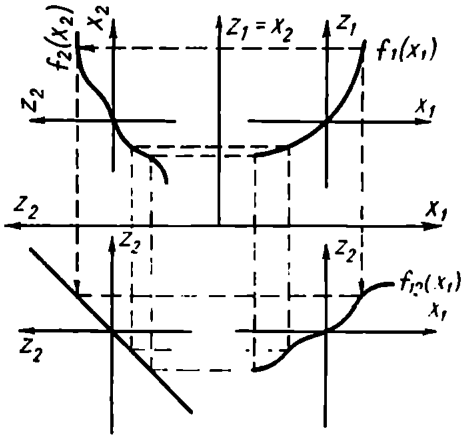

Fig. 16.3

The determination of the overall response $z(x)$ can be reduced to $(n - 1)$ successive calculations of equivalent responses of two series-connected elements and finding $z_2(x_1)$, $z_3(x_1)$, etc., up to $z_n(x_1)$ inclusive.

Given $f_1(x_1)$ and $f_2(x_2)$ the plotting of $f_{12}(x_1)$ is illustrated in Fig. 16.3. When plotting is performed in four quadrants, the use of the third quadrant with the line $z_2(z_2)$ facilitates the transition from the z_2-axis related to the response $z_2(x_2)$ to the z_2-axis related to the response $z_2(x_1)$. Repeating this plotting n times can give the resulting response $z_n(x_1) = f_{1n}(x_1)$.

Plotting for specific cases leads to the conclusion that changes in the order of connection of the elements usually lead to changes in the resultant response.

Example 16.1. Find the response of a series connection of nonlinear elements of the dead-zone type, $z_1 = f_1(x_1)$, and of the saturation type, $z_2 = f_2(x_2)$, for different sequences of their connection.

Figure 16.4 shows two versions of response construction. Figure 16.4*b* gives the plotting of $z_2(x_1) = f_2[f_1(x_1)]$ for the circuit of Fig. 16.4*a*, and Fig. 16.4*d*, the plotting of $z_1(x_2) = f_1[f_2(x_2)]$ for the circuit of Fig. 16.4*c*.

In both cases a saturation element with a dead zone is obtained, but the output values associated with saturation, z_c, and the input values associated with the dead zone, x_c, are found to be different.

In the first case they coincide with the values for initial nonlinearities: $z_c = z_b$ and $x_c = x_a$, and in the second case they differ considerably: $z_c = z_b - x_a$ and $x_c = \frac{x_a}{k_2}$. At $z_b \leqslant x_a$ the second connection breaks the signal transmission circuit.

Example 16.2. Reduce two nonlinear elements to one in a series connection of a nonlinear element with a single-valued response, an integrating element and a stop-type element (Fig. 16.5*a*). This problem can be solved by introducing the concept of an element whose response expresses the relation between the signal derivatives or time integrals as well as between the signals themselves.

If the response of a stop-type element is represented as the structural diagram of Fig. 15.20*d*, we will get an equivalent circuit shown in Fig. 16.5*c* by replacing the element $z(x)$ in Fig. 16.5*a* with the circuit of Fig. 16.5*b*, keeping in mind that an integrating and a differentiating element connected in series compensate each other. The nonlinear elements $\dot{x}(\gamma)$ and $\dot{z}(\dot{x}, z)$ connected in series can be replaced by one nonlinear element (shown in Fig. 16.5*d*) with a response $\dot{z}(\gamma, z)$.

The response $\dot{z}(\gamma, z)$ is plotted in Fig. 16.6.

Comparing Fig. 16.5*a* and Fig. 15.3*d* it is easy to see that the circuit resulting from the transformations (Fig. 16.5*d*) corresponds to the rudder servo of Sec. 15.2 (Fig. 15.3*b*, *c*, *d*). Consequently, the series connection of the three elements shown in Fig. 16.5*a* expresses the relation between the positions of the nozzle throttle and the piston in a pneumatic rudder servo.

When two nonlinear elements with responses f and f^{-1} are series connected, the resultant response may prove to be linear and the system gain, to be equal to one. Two nonlinear elements whose series connection forms a proportional element with unit gain will be termed *mutually inverse*.

For two mutually inverse nonlinear elements with responses $z_1 = f(x_1)$ and $z_2 = f^{-1}(x_2)$ the following equality is valid

$$f^{-1}[f(x_1)] = x_1 \tag{16.9}$$

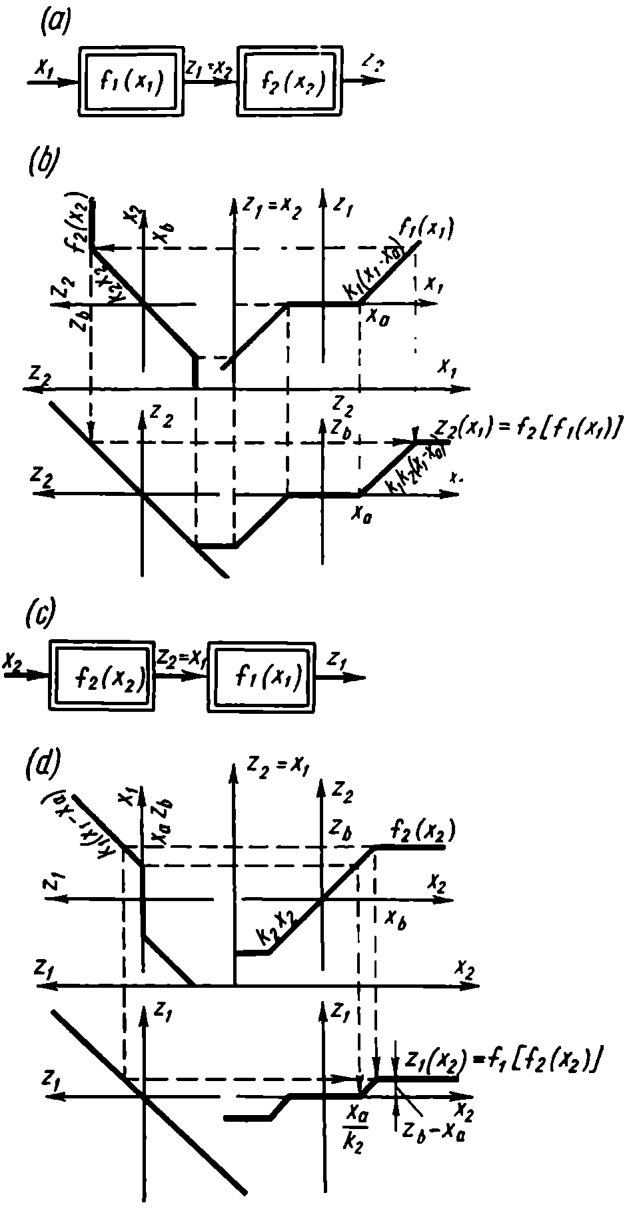

Fig. 16.4

It is easy to show that if such elements are interchanged, the overall response of the system remains unchanged, i.e. the commutative law is applicable to these elements:

$$f\,[f^{-1}\,(x_2)] = x_2 \qquad (16.10)$$

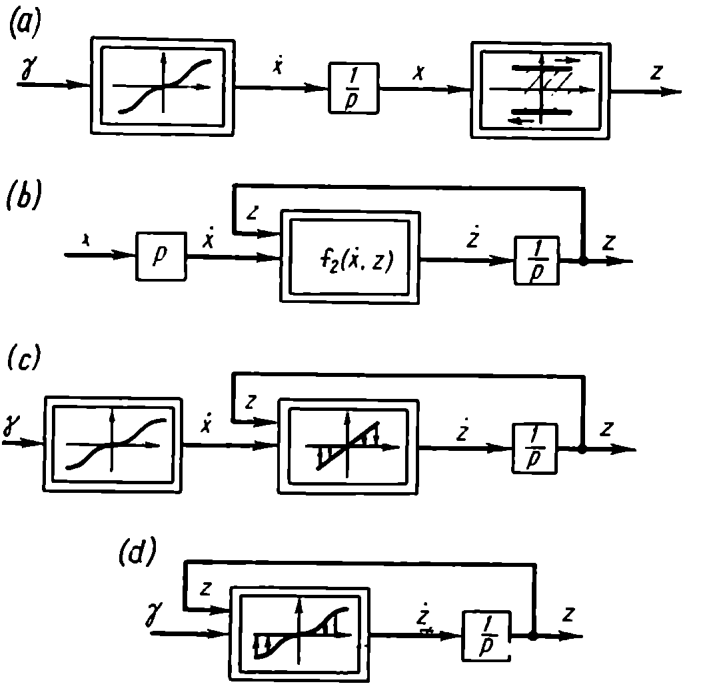

Fig. 16.5

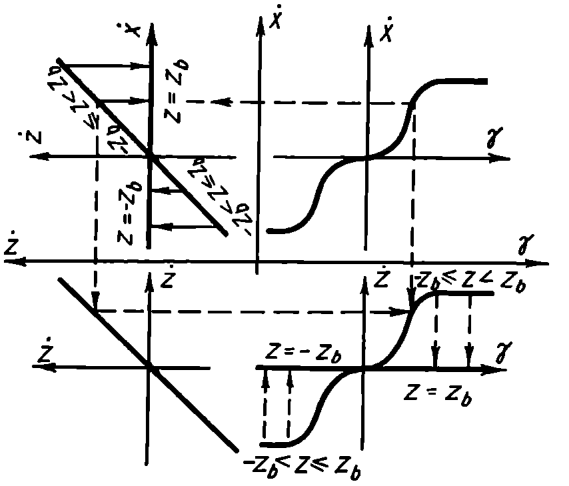

Fig. 16.6

Indeed, if the condition (16.9) is valid, then

$$f\{f^{-1}[f(x_1)]\} = f(x_1)$$

But since $f(x_1) = x_2$, this expression coincides with Eq. (16.10). This property is valid only for monotonic responses without horizontal or vertical portions. In the presence of a zone where $\frac{dz_1}{dx_1} = 0$ and $\frac{dz_2}{dx_2} = \infty$, interchanging the nonlinearities $f(x_1)$ and $f^{-1}(x_2)$ changes the overall response of the connection.

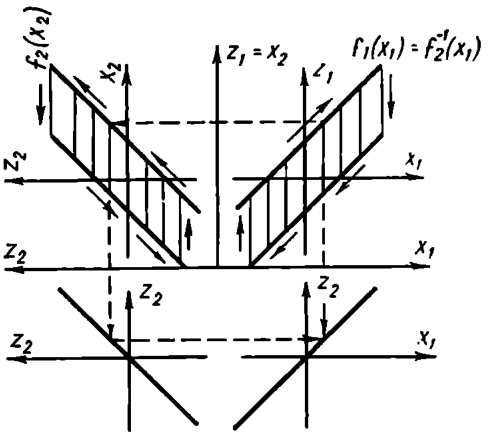

Fig. 16.7

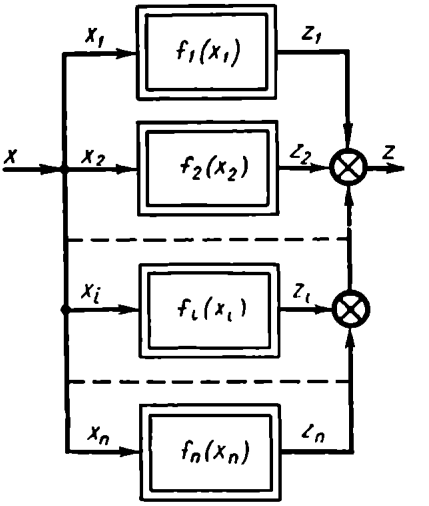

Fig. 16.8

Example 16.3. Find the response of the nonlinear element $z_1 = f_1(x_1)$ which is to be connected in series with the play-type element $z_2 = f_2(x_2)$ so that the resultant response of the series connection is linear and expressed by the straight line $z_2(x_1) = x_1$.

The response $z_1 = f_1(x_1)$ can be found by reversing the procedure for the plotting of the known responses $z_2 = f_2(x_2)$ and $z_2(x_1) = x_1$ (Fig. 16.7). The plotting shows that for the condition $z_2(x_1) = x_1$ to be valid the responses $z_1 = f_1(x_1)$ and $z_2 = f_2(x_2)$ in two quadrants of the coordinates x_1, $z_1 = x_2$, z_2 should be curves mirror-symmetrical with respect to the axis $z_1 = x_2$.

The resultant curve $z_1 = f_1(x_1)$ is inverse to the play-type response and

$$z_1 = f_1(x_1) = f_2^{-1}(x_1)$$

An element with such a response can be applied to offset the adverse effect of a play-type nonlinearity.

16.3. PARALLEL FEEDFORWARD CONNECTION

In parallel feedforward connection of nonlinear elements their inputs receive the same quantity while the outputs are summed with the appropriate signs.

If n elements are connected in parallel, the input is

$$x = x_1 = x_2 = \ldots = x_n \tag{16.11}$$

while the output is

$$z = f(x) = \sum_{i=1}^{n} f_i(x) \tag{16.12}$$

The latter expression shows that the response of a parallel feedforward connection of a set of nonlinear elements can be obtained by direct summation of the appropriate ordinates of the constituent responses.

Such a connection is shown in Fig. 16.8.

Example 16.4. Find the response of a parallel feedforward connection of nonlinear elements of the dead-zone type, z_1 and z_2,

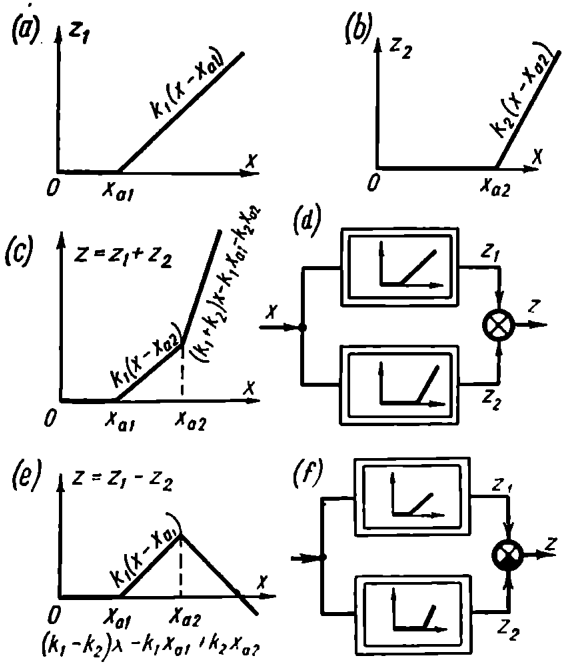

Fig. 16.9

with dead zones x_{a1} and x_{a2} and slopes k_1 and k_2, respectively (Fig. 16.9*a*, *b*).

Figure 16.9*c* is the plot of the response $z(x) = z_1 + z_2$ in the case where the signals z_1 and z_2 are summed with like signs in the summing unit (Fig. 16.9*d*). Figure 16.9*e* is the response $z(x) = z_1 - z_2$ when they are summed with different signs (Fig. 16.9*f*).

The portion of the response for $x > x_{a2}$ (Fig. 16.9*e*) demonstrates that if $k_1 = k_2$, the response slope is zero and the response represents a dead-zone-type element with saturation.

Example 16.5. Represent an element with the response $z_1(x_1)$ of Example 16.3 (see Fig. 16.7) as a parallel feedforward connection of two simpler standard elements.

One can easily see that parallel connection of a stop-type element with a rectangular response (see Fig. 15.21*b*) and a proportional

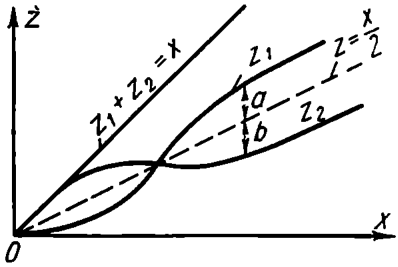

Fig. 16.10

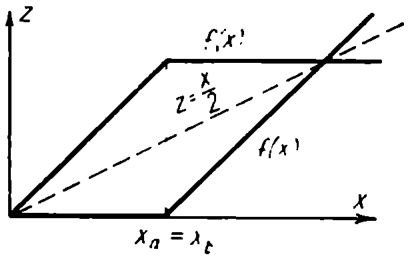

Fig. 16.11

element with unit gain comprises an element with the desired response $z_1(x_1)$.

Parallel feedforward connection of two nonlinear elements with the appropriate choice of their responses may produce a linear resultant response and a unit gain. Such two nonlinear elements will be referred to as *complementary*. Their switch-over will not change anything.

Two complementary elements can be described by the equality

$$f_1(x) + f_2(x) = x \tag{16.13}$$

or

$$f_1(x) - \frac{x}{2} = \frac{x}{2} - f_2(x) \tag{16.14}$$

From the latter equality it follows that the responses $z_1 = f_1(x)$ and $z_2 = f_2(x)$ are complementary when distances a and b from these responses to the straight line $z = \frac{x}{2}$ (Fig. 16.10) along the z-axis are equal. This is called the *equidistance* condition.

If the nonlinear response $f(x)$ is given, the complementary response will be denoted as $\overline{f}(x)$. Equation (16.13) for the two complemen-

tary responses then takes the form

$$f(x) + \bar{f}(x) = x \qquad (16.15)$$

Example 16.6. Find the response $\bar{f}(x)$ complementary to the response $f(x)$ of a saturation element with a linear zone $x_b = \frac{1}{2}$ and a unit slope.

By tracing the straight line $z = \frac{x}{2}$ (the dotted line in Fig. 16.11) we obtain the desired response $\bar{f}(x)$ from the condition of equidistance along the axis z relative to this line. This response describes a dead zone-type element with $x_a = x_b = \frac{1}{2}$.

Consequently, at $x_a = x_b$ and a unit slope, dead-zone- and saturation-type elements have complementary responses.

16.4. PARALLEL FEEDBACK CONNECTION

In a parallel feedback connection of two elements (Fig. 16.12) the output signal of the first (feedforward) element is fed to the input of the second (feedback) one and the output signal of the second element, with the appropriate sign, is summed with the common input signal and fed to the input of the first element. The common output signal is the output of the feedforward element. Depending on the sign of the signal fed to the adder, the feedback can be either negative or positive.

The closing equations have the form

$$x_1 = x \pm z_2 \qquad (16.16)$$

where the plus sign corresponds to a positive feedback and the minus sign, to a negative feedback.

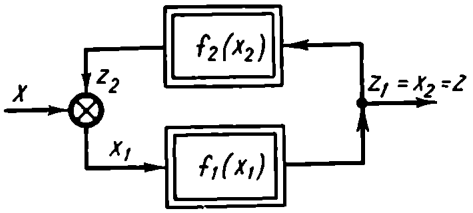

Fig. 16.12

The output signal

$$z = z_1 = x_2 \qquad (16.17)$$

The overall response $z(x)$ of a parallel feedback connection is plotted by considering Eqs. (16.16) and (16.17) simultaneously with responses $f_1(x_1)$ and $f_2(x_2)$ of nonlinear elements.

Then, transforming Eq. (16.16) with an allowance for Eq. (16.17), we have

$$x = f_1^{-1}(z) \pm f_2(z) \qquad (16.18)$$

where the minus denotes positive and the plus, negative feedback.

The overall response $z(x)$ or $x(z)$ is easily obtained through Eq. (16.18).

Let the responses $f_1(x_1)$ and $f_2(x_2)$ have the form of plots as given in Fig. 16.13*a*, *b*. Then $z(x)$ is obtained by first plotting the curves $f_1(x_1) = z(x_1)$, $f_2^{-1}(z_2) = z(z_2)$ and then algebraically adding up

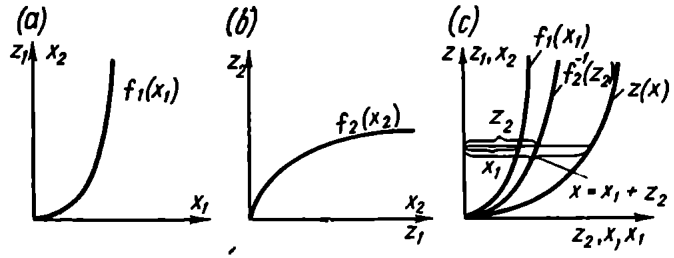

Fig. 16.13

the abscissas of these curves according to Eq. (16.18). This procedure is illustrated for a negative feedback by Fig. 16.13*c*.

Example 16.7. Construct the response of a saturation-type element with a dead zone $z_1 = f_1(x_1)$ having a negative (Fig. 16.14*a*) or a positive (Fig. 16.14*b*) proportional feedback with a gain k_0.

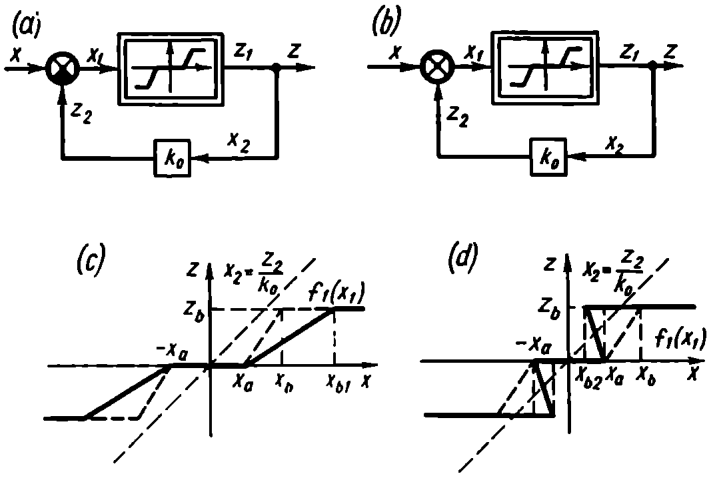

Fig. 16.14

In this case the feedback response is linear, $z_2 = k_0 x_2$ or $x_2 = \frac{z_2}{k_0}$. The plotting of the resultant response is shown for both cases in Fig. 16.14*c*, *d*.

In the first case the resultant response is seen to be single-valued and corresponds to a stop-type element with a dead zone. The linear

range extends from $x_b - x_a$ to $x_{b1} - x_a$, where $x_{b1} = x_b + z_b k_0$. In the second case the resultant response at $k_0 z_b > x_b - x_a$ ceases to be single-valued and represents a three-positional relay with hysteresis (see Sec. 15.5). The width of the hysteresis loop is equal to $x_a - x_{b2} = k_0 z_b - x_b + x_a$.

Example 16.8. Solve the problem of Example 16.7, but this time for a two-positional relay without hysteresis whose response is expressed by Eq. (15.20).

Constructions similar to those of Example 16.7 clearly indicate that with a negative feedback and at $-k_0 z_b < x < k_0 z_b$ there is no definite value of z for each value of x.

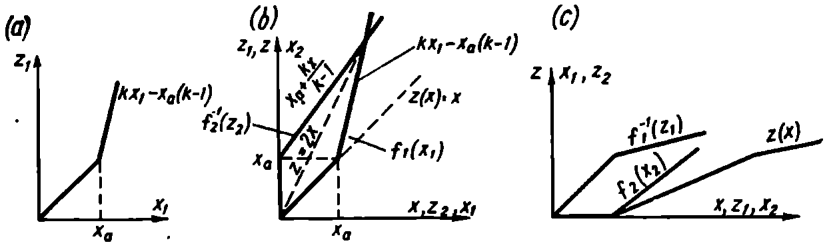

Fig. 16.15

The relay continuously switches at a frequency depending on the parasitic parameters of the system. The constant component of the output signal may coincide with the linear law $z = \frac{x}{k_0}$ with sufficient accuracy.

This condition is known as the vibrational mode.

With a positive feedback the overall response becomes double-valued and takes the form of Fig. 15.18*a*, for which $x_a = k_0 z_b$.

As in the above cases, it may be asked, what kind of nonlinearity the feedback circuit $z_2(x_2)$ should have so that the gain is equal to one or $z(x) = x$. We will assume that the feedback is negative.

Then Eq. (16.18) takes the form

$$x = z = f_1^{-1}(z) + f_2(z) \tag{16.19}$$

or, by virtue of Eq. (16.15),

$$f_2(z) = z - f_1^{-1}(z) = \bar{f}^{-1}(z) \tag{16.20}$$

Example 16.9. Let the feedforward nonlinear response $z_1 = f_1(x_1)$ be expressed by the relation (Fig. 16.15*a*)

$$z_1 = \begin{cases} x_1 & \text{at } x_1 \leqslant x_a \\ kx_1 - (k-1)x_a & \text{at } x_1 \geqslant x_a \end{cases} \tag{16.21}$$

Find the response of a nonlinear feedback which compensates for the nonlinearity of the feedforward path, i.e. makes the system linear ($z = x$).

Figure 16.15*b* depicts the response $x_2 = f_2^{-1}(z_2)$ obtained by Eq. (16.20). It is constructed by using the response $f_1(x_1)$ and the condition of equidistance along the axis x relative to the straight line $z = 2x$. This response is given by the equation

$$z_2 = \begin{cases} 0 & \text{at} \quad x_2 \leqslant x_a \\ \dfrac{k-1}{k}(x_2 - x_a) & \text{at} \quad x_2 \geqslant x_a \end{cases} \qquad (16.22)$$

Unlike parallel feedforward connection, interchanging nonlinearities in the feedforward and feedback paths changes the system response substantially. For example, in the above case an overall response obtained after switching over the feedforward and feedback nonlinearities will be as shown in Fig. 16.15*c*. The resultant response $z(x)$ differs considerably from the straight line $z(x) = x$ (Fig. 16.15*b*) obtained earlier.

16.5. STEADY-STATE MISALIGNMENT (SSM) OF NONLINEAR CONTROL SYSTEMS

Using the above methods one can easily plot the relation between the SSM of a control system and the external action. We will consider an automatic voltage stabilization system of a d.c. generator as an example (see Sec. 15.2, Fig. 15.1).

A static continuous control system in a steady state can be represented as a connection of a feedforward and a feedback elements. Then the structural diagram of the control system (see Fig. 15.1*e*) has the form shown in Fig. 16.16*a*, where $z(x)$ is the total response of nonlinear elements corresponding to an amplifier $u_A(x)$, exciter $e_e(u_A)$, and generator $z = e_g(e_e)$ connected in series. The voltage drop caused by the load current $r_{arm} i_l = f$ is an external disturbance, which is subtracted from the generator e.m.f., $z = e_g$. The difference $z - f = u_l$ is a controlled variable, which is fed to the voltage divider with a gain k to be transformed into $y = ku_l$ and then compared with the setpoint voltage E_0. The misalignment $x = E_0 - y$ is the input signal of the feedback circuit.

The calculation of the control system SSM requires the determination of the relation $y(f)$, which represents the effect of the load on the controlled variable.

This relation is found as the response of a parallel feedback connection of a linear, k, and a nonlinear, $z(x)$, elements.

The plot is shown in Fig. 16.16*b* and *c*. The way of plotting follows directly from the closing equation $u_l = \frac{y}{k} = z(y) - f$ a

$y = E_0 - x$. The plot y (f) is obtained by summation of the abscissas of the feedforward, $y = -kf$, and feedback, y (z), responses, f being found as $z(y) - \frac{y}{k}$. The relation y (f) obtained is shown separately in Fig. 16.16*d*.

The misalignment is seen to be rather large even if there is no external action ($f = 0$).

In this case, by appropriate choice of the setpoint E_0 or the gain k, the discrepancy δ between the desired (reference) value of the controlled variable y_0 and the actual value of y can be reduced and will be

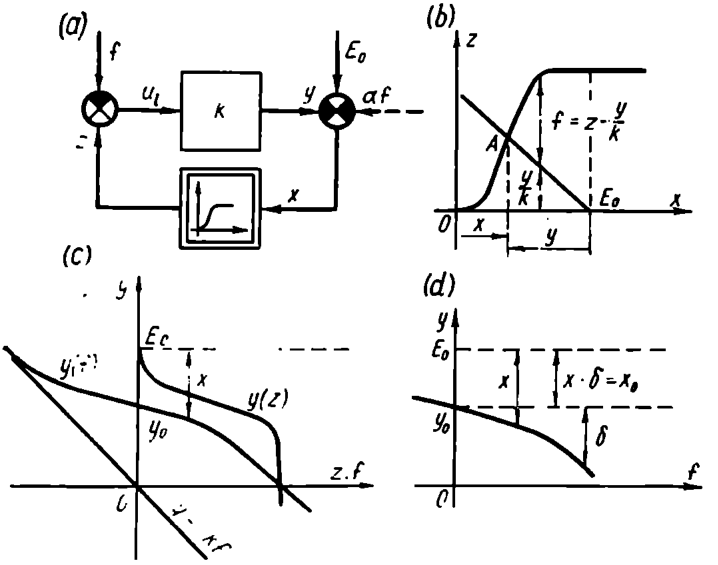

Fig. 16.16

zero at a certain specified value of f. Thus, at $f = 0$ the condition $y = y_0$ can always be obtained by appropriate choice of k or E_0. Figure 16.16*d* shows the plot of y (f) and the values of the SSM, $x = E_0 - y$, and the error $\delta = y_0 - y$.

By selecting the operating point on the steepest part of the response z (x) at $f = 0$ (Fig. 16.16*b*) the desired accuracy can be ensured for a range of f.

The effect of f on the controlled variable y can be reduced by feeding into the comparator an additional compensating signal αf, given as a dotted line in Fig. 16.16*a*. With $\alpha = k$ the compensating signal offsets the effect of f in the plant circuit, and the controlled variable becomes independent of the action f. In this case the response y (f) is a horizontal straight line $y = y_0$, and the SSM $x = x_0$ is independent of the load. This kind of generator control compensation is known as *compounding*.

If the feedback circuit includes an integrator and at $x = 0$ the feedback gain is not zero, the response $z(x)$ is vertical and passes through the point $x = 0$.

In this case the plot is a straight line $y = E_0$, and the SSM is zero. This should have been expected by virtue of the linear theory described in Ch. IX.

16.6. TRANSFORMATION OF NONLINEAR SYSTEM STRUCTURAL DIAGRAMS

Transformation of structural diagrams of linear systems was described in Sec. 6.2. Although the introduction of linear elements somewhat reduces the scope of structural transformations, they are still very important for the design and construction of models.

Recall the rules for transformation of linear systems and see whether they can be extended to nonlinear systems.

There are four kinds of transformation:

(1) transposition of an adder and a fanning node;
(2) transposition of a linear element and a fanning node;
(3) transposition of a linear element and an adder;
(4) transposition of two linear elements.

The rules of structural transformation cannot be extended to nonlinear systems because these do not meet two requirements, the superposition principle and the commutative law. The former prevents the use of the third transformation and the latter, of the fourth one. The first two transformations do not clash with these two requirements and so can be used in transformation of nonlinear systems.

Two rules for transposition of an adder and a fanning node are fully applicable to nonlinear systems.

First Rule. If an adder is moved over a fanning node along the direction of fanning (or along the signal propagation direction), similar adders should be introduced into the outgoing branches of the fanning node.

Second Rule. If an adder is moved over a fanning node in the direction opposite to fanning (or to signal propagation), adders differing from the one in question in the signs of addends should be introduced into the branches.

Neither of these rules is related to the nonlinearity conditions, and their application was described in detail when discussing linear systems.

As applied to nonlinear systems, the rules for transposing a nonlinear element and a fanning node can be formulated as follows.

Third Rule. If an element is moved over a fanning node along the direction of fanning (of signal propagation), the outgoing branches should include elements having the same operator.

Fourth Rule. If an element is moved over the fanning node against the direction of fanning (of signal propagation), the outgoing branches should include elements whose operators are the inverse of the initial one.

Example 16.10. Transpose an inertialess nonlinear element $z(x)$ over a fanning node along the direction of fanning.

Figure 16.17*a*, *b* shows the application of the third rule for transposing a nonlinear element with a piecewise-linear response.

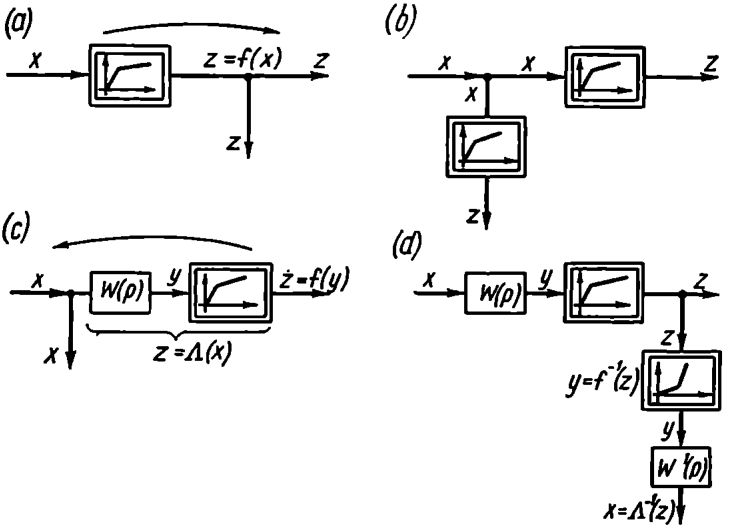

Fig. 16.17

Example 16.11. Transpose an inertial nonlinear element consisting of a linear, $W(p)$, and a nonlinear, $z = f(y)$, element connected in series over a fanning node against the direction of fanning.

The application of the fourth rule for this purpose is demonstrated in Fig. 16.17*c*, *d*.

Here the nonlinear response $y = f^{-1}(z)$ is inverse to $z = f(y)$, and $W^{-1}(p) = \frac{1}{W(p)}$.

The concept of inverse operators can be used to show that a circuit with the feedforward Λ_1 and feedback Λ_2 paths of Fig. 16.18*a* is equivalent to one (Fig. 16.18*b*) made up of inverse operators Λ_1^{-1} and Λ_2^{-1} if the element Λ_1^{-1} is used in place of Λ_2 and the element Λ_2^{-1}, in place of Λ_1.

Indeed, by writing down the closing equation

$$z = \Lambda_1 [x - \Lambda_2 (z)] \qquad (16.23)$$

or

$$\Lambda_1^{-1}(z) = x - \Lambda_2(z) \tag{16.24}$$

after elementary transformations we have

$$z = \Lambda_2^{-1}[x - \Lambda_1^{-1}(z)] \tag{16.25}$$

which corresponds to the circuit of Fig. 16.18*b*.

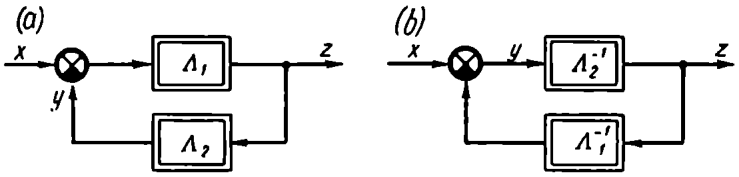

Fig. 16.18

The introduction of inverse operators thus leads to one more rule, which is equally applicable to linear and nonlinear structural diagrams.

Fifth Rule. In negative feedback systems the elements connected into feedforward and feedback circuits can be interchanged with inversion of the element operators.

This rule is important where unimplementable or hard-to-implement structural diagrams are to be replaced by implementable circuits.

Example 16.12. For a circuit of Fig. 16.19*a* consisting of a proportional element k with a feedback responding to the sign of the

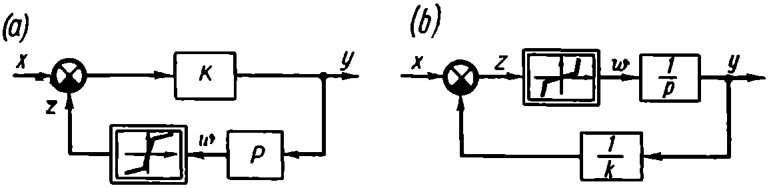

Fig. 16.19

derivative, i. e. implemented by a differentiating element p and a nonlinear element $z(w)$ connected in series, find an easier-to-implement equivalent circuit consisting of elements with inverse responses.

The application of the fifth rule leads to the equivalent circuit of Fig. 16.19*b*.

The nonlinear responses $w(z)$ and $z(w)$ can be described by the piecewise-linear relations

$$w = \begin{cases} \alpha z & \text{at } |z| \leqslant z_a \\ \alpha z_a + \beta(z - z_a) & \text{at } z \geqslant z_a \\ -\alpha z_a + \beta(z + z_a) & \text{at } z \leqslant -z_a \end{cases} \tag{16.26}$$

and

$$z = \begin{cases} \frac{w}{\alpha} & \text{at } |w| \leqslant \alpha z_a \\ z_a + \frac{w - \alpha z_a}{\beta} & \text{at } w \geqslant \alpha z_a \\ -z_a + \frac{w + \alpha z_a}{\beta} & \text{at } w \leqslant -\alpha z_a \end{cases} \tag{16.27}$$

As $\alpha \to 0$ and $\beta \to \infty$ this response becomes $z = z_a$ sign w.

Since an integrator can be implemented more accurately than a differentiator, the circuit of Fig. 16.19*b* is more convenient.

16.7. EQUIVALENT CIRCUITS OF MULTIVALUED NONLINEARITIES

Section 16.4 demonstrated that the most widespread double-valued nonlinearities can be represented by an equivalent circuit which is a parallel feedback connection of inertialess elements with linear and single-valued nonlinear responses. For multivalued nonlinearities, e.g. play- and stop-type ones, equivalent circuits can also be obtained. These consist of linear and nonlinear elements with single-valued responses. In such cases the multivalued nature of nonlinear responses increases the order of the differential equation describing the element and leads to the appearance of one more integration constant reflecting the system's case history and expressing the ambiguity of the nonlinear response.

Thus, in the structural diagrams of the play- and stop-type nonlinearities of Figs. 15.19*d* and 15.20*d* the ambiguity of the response is expressed by integrators. These structural diagrams, however, are not the only possible way of representing nonlinear equations (15.26) and (15.29), especially because these circuits contain nonlinear elements implementing the function of two variables, which can be represented as a connection of simpler elements. These equations can lead to several structural diagrams consisting of linear and single-valued nonlinear elements.

The circuits of Figs. 16.20*a* and 16.21*a* are obtained by representing a play and a stop as a connection of a linear proportional and an integrating element and a nonlinear element "asign" x whose gain $\frac{dz}{dx}$ tends to zero or infinity, depending on the magnitude of the input signal.

In the former case this nonlinear element acts as a discontinuity in the circuit, which corresponds to multivalued parts of the response attributable to the value of the integration constant C at the output of the integrating element $\frac{1}{p}$.

For a play (Fig. 16.20*a*)

$$z_1 = C_1$$

and for a stop (Fig. 16.21*a*)

$$z_1 = \frac{k}{x_1 - C}$$

In the latter case a nonlinear element combines with a linear circuit to form an ideal servo system which in the case of a play follows up the incrementation of the input signal $x_1 - \frac{z_1}{k_1} = \pm x_a$ and in the case of a stop outputs the misalignment $z_1 = \pm z_b$ and ensures the constancy of the signal at the output under input variations.

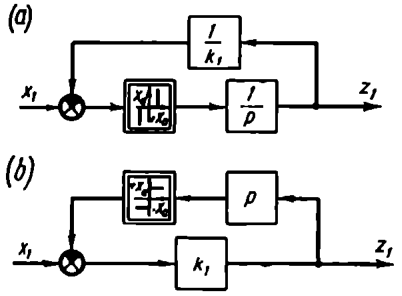

Fig. 16.20

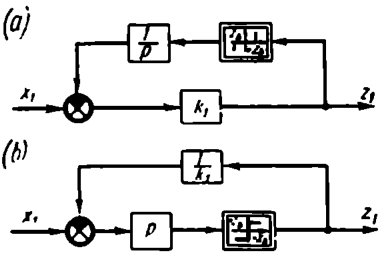

Fig. 16.21

The fifth rule for transformation of nonlinear structural diagrams permits easy transition from circuits *a* to circuits *b* (see Figs. 16.20 and 16.21). Both equivalent circuits accurately represent the initial nonlinearities only in ideal conditions where it can be safely assumed that the tangent of the slope angle in different parts of the response tends to zero or to infinity. Allowance for the actual values of gains makes it possible to estimate the errors in transition from ideal to actual systems. Small parasitic parameters are of special importance in limit cases and in transition from calculated circuits to their implementation.

16.8. SMALL PARAMETERS OF ACTUAL INERTIALESS ELEMENTS

When discussing proportional and differentiating elements we noted that in all actual unilateral elements the output is always somewhat behind the input. If the input frequency is low enough,

this delay can be neglected and in static elements the output can be presumed to follow the input immediately. At high frequencies, however, this assumption ceases to be valid, and wrong conclusions may be made if the delay is neglected.

In linear systems small parameters are usually accounted for by the condition $\lim_{\omega\to\infty} W(j\omega) = 0$, which indicates that the order of the numerator in $W(p)$ is below that of the denominator, and therefore the transfer function $W(p)$ allows for the delay.

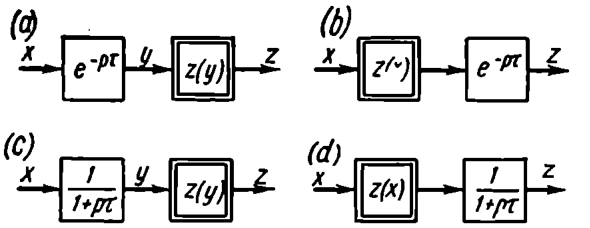

Fig. 16.22

In studying nonlinear systems it is usually undesirable to increase he order of the differential equation, and in setting up an approximate equation small parameters of substantial importance may be omitted inadvertently.

If a nonlinear static element is described by the equation

$$z(t) = z[y(t)] \tag{16.28}$$

an allowance for small delay τ makes it possible to represent this equation as

$$z(t) = z[x(t-\tau)] \tag{16.29}$$

The structural diagrams associated with this equation are shown in Fig. 16.22*a* and *b*. The two diagrams are equivalent (see Sec. 16.1) and express the delay τ of the output signal in relation to the signal in the case of a static nonlinearity.

Using the series

$$e^{p\tau} = 1 + p\tau + \frac{(p\tau)^2}{2} + \ldots \tag{16.30}$$

and neglecting the higher-order terms, the delay τ can be approximated by an inertial element with a time constant τ connected either before or after the inertialess element $z(y)$ (Fig. 16.22*c*, *d*).

Now the circuits of Fig. 16.22*c* and *d* are not equivalent, but with τ sufficiently small each can serve to allow for the small parameter of a unilateral element.

Disregarding small parameters may result in erroneous conclusions concerning the stability of different linear and particularly nonlinear

circuits. The effect of small parameters on the stability of nonlinear systems was first theoretically analyzed by A.A. Andronov and S.E. Khaikin in 1935.

Example 16.13. A nonlinear element with an inertialess response $z(x)$ has a positive feedback with a transfer function $W(p) = \frac{1+pT_1}{1+pT_2}$ (Fig. 16.23*a*).

Find the values of the coordinates x and z at equilibrium points for $f = 0$ and decide whether they are stable.

Since in a steady state $y = x = z$, the coordinates of the equilibrium points are found as intersection points *1*, *2*, *3* of the curve

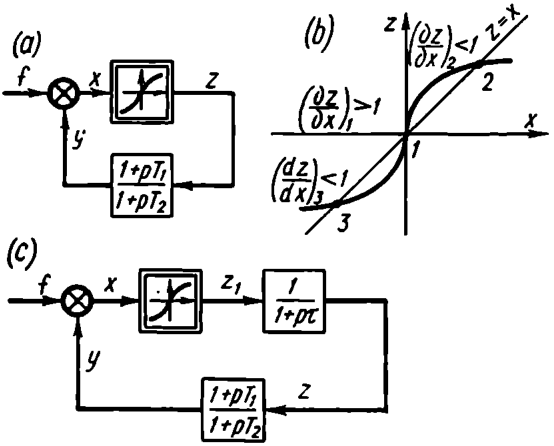

Fig. 16.23

$z(x)$ and the straight line $z = x$ (Fig. 16.23*b*). Calculating $\left(\frac{\partial z}{\partial x}\right)_i$ at the three intersection points ($i = 1, 2, 3$), one can easily derive the characteristic equation for a linearized system in the vicinity of the equilibrium points

$$1 - \frac{1+pT_1}{1+pT_2}\left(\frac{\partial z}{\partial x}\right)_i = 0 \qquad (16.31)$$

or

$$1 - \left(\frac{\partial z}{\partial x}\right)_i + pT_2\left[1 - \frac{T_1}{T_2}\left(\frac{\partial z}{\partial x}\right)_i\right] = 0 \qquad (16.32)$$

From this equation it follows that for the coefficients of the characteristic equation to have the same signs and, consequently, for the system to have no positive roots, the following inequalities should hold simultaneously

$$\left(\frac{\partial z}{\partial x}\right)_i < 1 \quad \text{and} \quad \frac{T_1}{T_2}\left(\frac{\partial z}{\partial x}\right)_i < 1 \qquad (16.33)$$

or

$$\left(\frac{\partial z}{\partial x}\right)_i > 1 \quad \text{and} \quad \frac{T_1}{T_2}\left(\frac{\partial z}{\partial x}\right)_i > 1 \tag{16.34}$$

With the proper choice of $\frac{T_1}{T_2}$ this condition will hold in all the three equilibrium points but this by no means implies that stability can be ensured in all of them.

An allowance for the small parameter, no matter how small it is, results in an additional multiplier, $1 + p\tau$, in the linear part transfer function denominator (Fig. 16.23*c*).

With due regard for the small parameter τ the characteristic equation takes the form

$$1 - \frac{1 + pT_1}{(1 + pT_2)(1 + p\tau)}\left(\frac{\partial z}{\partial x}\right)_i = 0 \tag{16.35}$$

or, since $\tau \ll T_2$

$$1 - \left(\frac{\partial z}{\partial x}\right)_i + pT_2\left[1 - \frac{T_1}{T_2}\left(\frac{\partial z}{\partial x}\right)_i\right] + p^2\tau T_2 = 0 \tag{16.36}$$

In this case the system is stable if the following two inequalities ensuring the positive value of all the coefficients of the characteristic equation hold

$$\left(\frac{\partial z}{\partial x}\right)_i < 1 \quad \text{and} \quad \frac{T_1}{T_2}\left(\frac{\partial z}{\partial x}\right)_i < 1 \tag{16.37}$$

Thence point *1* is always unstable because the first of these inequalities is not satisfied there. Depending on the value of $\frac{T_1}{T_2}$, points *2* and *3* can be either stable or unstable.

This example demonstrates how neglecting small delays may lead to the wrong conclusion concerning the stability of the equilibrium state.

If small parameters are properly allowed for in the circuits of Figs. 16.20*a*, *b* and 16.21*a*, *b*. then the circuits will prove to be nonequivalent, and elements of low inertia will appear in the feedback loop which affect the operating mode in different parts of the responses. The circuits of these figures will not be described by mutually inverse operators and their behaviour in actual conditions will differ somewhat.

16.9. MODELS OF NONLINEAR ELEMENTS

In Sec. 5.7 we discussed models of standard linear elements obtained by connecting different linear resistors into the circuit of an operational amplifier. This principle can also be used in simulating nonlinear elements.

If the circuit of an operational amplifier (Fig. 16.24*a*) includes nonlinear two-terminals *1* and *2*, for which the voltage vs current relation is expressed by a certain operator Λ which generally depends on the process time variation $i(t) = \Lambda[u(t)]$, this circuit can be employed to simulate all kind of nonlinearities.

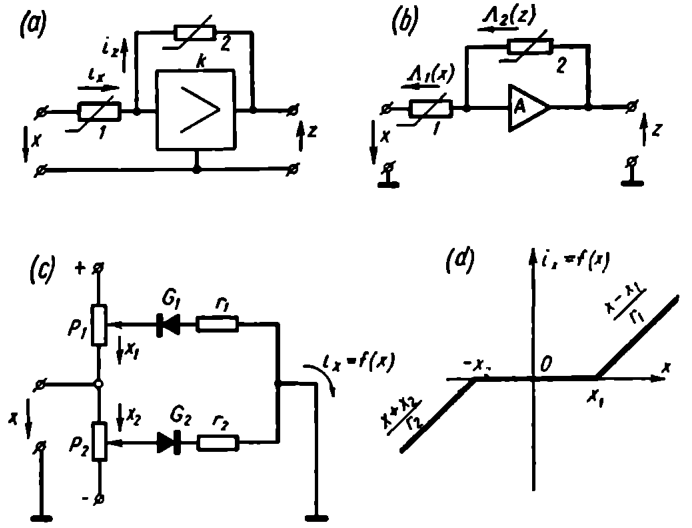

Fig. 16.24

Thus, if the gain of an ideal operational amplifier is $k \to \infty$ and its input resistance is infinitely high, the input i_x and feedback i_z currents (see Fig. 16.24*a*) can be expressed as

$$i_x = \Lambda_1(x) = i_z = \Lambda_2(z) \tag{16.38}$$

whence

$$z = \Lambda_2^{-1}[\Lambda_1(x)] \tag{16.39}$$

Consequently, by selecting nonlinear two-terminals with appropriate responses we can obtain an operational amplifier A reproducing the specified function. This amplifier is normally depicted as in Fig. 16.24*b*.

Example 16.14. Let a nonlinear two-terminal be given by the circuit of Fig. 16.24*c*. The response $i_x = f(x)$ depends on the reference voltages x_1 and x_2 across the potentiometers P_1 and P_2 and has the form of Fig. 16.24*d*. It consists of three parts representing different conditions for the passage of current through the gates G_1 and G_2.

The two-terminal is connected into circuit *1* (see Fig. 16.24*b*) and feedback loop *2* includes a resistor r_3.

Since $i_x = f_1(x) = f(x)$ and $i_z = f_2(z) = \frac{z}{r_3}$, Eq. (16.39) gives

$$z = r_3 f(x) \tag{16.40}$$

and, consequently, the response corresponds to a dead-zone-type element.

At $x_1 = x_2$ and $r_1 = r_2$ the response is symmetrical and its slope in the pass range

$$\frac{dz}{dx} = k_n = \frac{r_3}{r_1} = \frac{r_3}{r_2} \tag{16.41}$$

As $k_n \to \infty$ the response represents an element of the "asign" type (see Eq. (15.19b)).

If the two-terminal is connected into circuit *2* of the feedback loop and the resistor r_3 into circuit *1*, then $i_x = \frac{x}{r_3}$ and $i_z = f_2(z) = f(z)$. Equation (16.39) then gives

$$z = f^{-1}\frac{x}{r_3} \tag{16.42}$$

At $x_1 = x_2$, $r_1 = r_2$, and $\frac{r_1}{r_3} = \frac{r_2}{r_3} \to 0$ the response represents a "sign"-type element (see Eq. (15.19a)).

Different nonlinear two-terminals connected in the circuit of an operational amplifier yield models of most diverse nonlinearities. Models of nonlinear elements are widely used in studying nonlinear control systems by means of analog hardware.

Chapter XVII

NONLINEAR SYSTEM DYNAMICS. PHASE PLANE

17.1. EQUATIONS OF NONLINEAR DYNAMIC SYSTEMS. STATE SPACE

Dynamic systems are physical systems whose behaviour in the course of time t can be described by a system of differential equations

$$\varphi_i\left(y_1, \frac{dy_1}{dt}, \ldots, \frac{d^r y_1}{dt^r}, y_2, \frac{dy_2}{dt}, \ldots, \frac{d^s y_2}{dt^s}, \ldots, y_m, \frac{dy_m}{dt}, \ldots, \frac{d^p y_m}{dt^p}, t\right) = 0 \qquad (17.1)$$

whose number m is finite.

In Sec. 1.1 through 1.4 it was shown that a control system can be regarded as a plant (Fig. 17.1*a*) whose m controlled variables $y_1, y_2, \ldots, y_m$ are related with external actions—control signals $\mathbf{u} = (u_1, u_2, \ldots, u_n)$, observable disturbances (load) $\mathbf{z} = (z_1, z_2, \ldots, z_r)$, and unobservable disturbances (noises) $\mathbf{f} = (f_1, f_2, \ldots, f_h)$—through a system of m differential equations. Since in each specific case the external actions $\mathbf{u}$, $\mathbf{z}$, and $\mathbf{f}$ are definite (although not always known in advance) functions of time, the system satisfies the mathematical description (17.1). Systems with distributed parameters and a delay are generally an exception, but in some practically important cases their analysis can also be reduced to studying a system of the type (17.1).

The system (17.1) can be transformed into an equivalent system of first-order differential equations

$$\varphi_j\left(\frac{dy_j}{dt}, y_1, y_2, \ldots, y_N, t\right) = 0 \qquad (j = 1, 2, \ldots, N) \qquad (17.2)$$

where the number of equations $N = r + s + \ldots + p$ is equal to the sum of the equation orders for each of the m controlled variables. This concept is illustrated in Fig. 17.1*b*.

From the numerous examples of mathematical descriptions given above it follows that the system of equations (17.2) is obtained directly from mathematical descriptions of the control system elements and can easily be fitted to its structural diagram, whereas

the derivation of a system of m nonlinear equations (17.1) is rather difficult (Ref. 1). Equations (17.2) are as a rule solvable for the derivatives $\frac{dy_j}{dt}$ and can be written in the form

$$\dot{y}_j = \frac{dy_j}{dt} = P_j(y_1, y_2, \ldots, y_j, \ldots, y_N, t) \qquad (17.3)$$

or in the vectorial (matrix) notation

$$\mathbf{v} = \dot{\mathbf{y}} = \mathbf{P}(\mathbf{y}, t) = \mathbf{P}(\mathbf{y}_s) \qquad (17.3a)$$

where $\mathbf{v} = \dot{\mathbf{y}} = \{\dot{y}_1, \dot{y}_2, \ldots, \dot{y}_N\}$ is the phase rate vector, and $\mathbf{P}$ is the vector function of the system state vector $\mathbf{y}_s$.

This notation is known as the *normal Cauchy form.*

The geometrical theory of differential equations (dynamic systems), some results of which are used as a basis for further discussion,

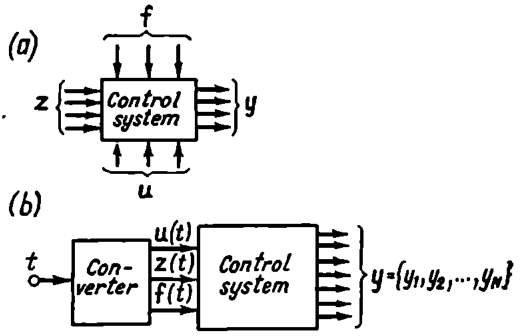

Fig. 17.1

deals specifically with systems of the type (17.3). This notation is presumed to be the standard form for accurate mathematical description of a nonlinear control system.

Example 17.1. Using the general description of nonlinear element responses given in Sec. 15.2 and the structural diagram of Fig. 15.3, derive Eq. (17.3) for an automatic course stabilization system.

Introduce standard notation for the basic variables

$$y_1 = \psi_1, \qquad y_2 = \dot{\psi}_1 = \frac{d\psi_1}{dt}, \qquad y_3 = y$$

and replace the transfer function of linear unit *1* (see Fig. 15.3) by its differential equation

$$T_1 \frac{d^2\psi_1}{dt^2} + \frac{d\psi_1}{dt} = k_1 [f(t) + \delta(y)]$$

Then Fig. 15.3*d* can be used to write directly

$$\frac{dy_1}{dt} = P_1(y_2)$$

$$\frac{dy_2}{dt} = P_2(y_2, y_3, t)$$

$$\frac{dy_3}{dt} = P_3(y_1, y_3, t)$$

where

$$P_1(y_2) = y_2, \quad P_2(y_2, y_3, t) = \frac{1}{T_1}\{-y_2 + k_1[f(t) + \delta(y_3)]\}$$

$$P_3(y_1, y_3, t) = v\{-k_2[y_1 - \psi_0(t)] - k_3 y_3, y_3\} \quad (N = 3)$$

A multivalued play-type nonlinearity $z = \delta(y_3)$ is discussed in detail in Sec. 15.5a, while the complex nonlinear response of a gyro motor (Fig. 15.3*b*) $v(\gamma, y_3)$, $\gamma = \gamma(y_1, y_3, t) = k_2[\psi_0(t) - y_1] - k_3 y_3$ is given in Fig. 15.3*c*.

If the right-hand parts of Eq. (17.3) $P_j(y_1, y_2, \ldots, y_j, \ldots, y_N, t)$ are continuous and precisely specified, the state of the system and the further course of the control process can be assumed *unambiguously defined* provided the values of N dependent variables y_j at a fixed instant $t = t_i$ are known. These values can be regarded as coordinates $\{y_0 = t, y_1, y_2, \ldots, y_N\}$ of a point referred to as the *describing point* in an $N + 1$-dimensional state space of the system under study, or as the position of the state vector $\mathbf{y}_s$. A change in the state in the course of the control process is associated with changes in the coordinates of the describing point, or with its motion along a certain line, which is the *trajectory in the state space*. The system (17.3) defines the relation between the system state vector $\mathbf{y}_s$ and the components $\frac{dy_j}{dt} = \frac{dy_j}{dy_0}$ of the change rate vector $\mathbf{v} = \frac{dy_s}{dt} = \frac{dy_s}{dy_0}$. The solution (integral) of the system (17.3), which can always be found by existing digital or analog computers, gives numerical values of the trajectory coordinates.

The main difficulty in studying nonlinear dynamic systems lies, not in the cumbersome computations involved in the solution of the differential equations, but in the fact that these solutions may be qualitatively dependent on the initial state. Here is a simple example: when the pendulum of a wound clock is stopped, the clock will stand still for an infinitely long time despite the slight vibration of its base. But if the pendulum is deflected by a finite angle exceeding a certain boundary value and then released, the clock starts and will continue working for an infinite period, provided it is rewound in due time.

This behaviour is impossible in a linear system, and the above example proves that calculation of specific processes in a nonlinear system without previous deliberate study is pointless, as a rule.

Further, the requirement for the functions P_j to be continuous is too strict even in Example 17.1, and the conditions for transition beyond their points of discontinuity should be specified by physical reasoning.

In studying these problems, geometric representation of solutions to the system (17.3) as trajectories of the describing point in the state space has unquestionable advantages. The first advantage is gained in studying the system in the absence of variable external actions or parameter variations in the course of time.

In this case of study of an *autonomous dynamic system* time is not included explicitly into the right-hand parts of the differential equations $P_j = P_j(y_1, y_2, \ldots, y_N)$, and transition to the state space reduces the number of equations in the system (17.3) by unity. Indeed, considering the coordinate y_1 as an independent variable one can obtain a system

$$y'_k = \frac{dy_{k+1}}{dy_1} = \frac{P_{k+1}(y_1, y_2, \ldots, y_N)}{P_1(y_1, y_2, \ldots, y_N)} = F_k(y_1, y_2, \ldots, y_N) \quad (17.4)$$

$$(k = 1, 2, \ldots, N-1)$$

which contains $N - 1$ first-order differential equations, by merely dividing the second and subsequent equations of the system (17.3) by the first one.

In vectorial notation Eq. (17.4) is given as

$$\mathbf{y}' = \mathbf{P}(\mathbf{y}) \quad (17.4a)$$

The system (17.4) is referred to as a *system of equations of integral curves in the N-dimensional phase space*, while the trace of the describing point in this space, which unambiguously defines time variations of the system state, as a *phase trajectory*.

Another, equally important advantage of the phase space is the possibility of clearly separating regions in each of which the behaviour of the system is qualitatively unchanged, i.e. the system reaches the same steady state after some time. Steady states are independent of the initial state. The equilibrium (rest) states are associated with isolated singular points in space, and periodic modes, with closed isolated trajectories along which the describing point can move for an infinitely long time.

It should also be indicated that all variables defining the state of an actual system are physically bounded. Therefore there is no practical need to consider remote regions of the phase space. At the same time one can impose artificial constraints on physical variables (rates, accelerations, voltages, currents, etc.) for reasons of safety and provide for protective and interlocking units to ensure the implementation of these constraints.

Example 17.2. Derive Eqs. (17.4) for the integral curves of a course stabilization system (see Example 17.1) in autonomous navigation, $\psi_0(t) = \psi_0 = \text{const}$; $f(t) = 0$.

Determine the dimension and configuration of phase space constraints.

Under given conditions the system of differential equations for phase trajectories obtained in Example 17.1 takes the form

$$\left.\begin{aligned} \frac{dy_1}{dt} &= y_2 \\ \frac{dy_2}{dt} &= \frac{1}{T_1}\left[-y_2 + k_1\delta(y_3)\right] \\ \frac{dy_3}{dt} &= v\left[k_2(\psi_0 - y_1) - k_3 y_3,\ y_3\right] \end{aligned}\right\}$$

Dividing the second and third equations of this system by the first yields a system of two equations

$$\frac{dy_2}{dy_1} = \frac{1}{T_1}\,\frac{\left[-y_2 + k_1\delta(y_3)\right]}{y_2}$$
$$\frac{dy_3}{dy_1} = \frac{v\left[k_2(\psi_0 - y_1) - k_3 y_3,\ y_3\right]}{y_2}$$

The phase space is three-dimensional, $y = \{y_1, y_2, y_3\}$ (Fig. 17.2). Since a deviation from the course by an integral number of revolutions returns the plant to the initial position, we can consider, in the phase space, a region bounded by the vertical planes $y_1 = \psi_0 + \pi$ and $y_1 = \psi_0 - \pi$ such that when the describing point arrives at one of these it should be transferred to the other without changing the coordinates y_2 and y_3 and should keep on moving.

The coordinate y_3 is limited by rigid stops: $-y_b \leqslant y_3 \leqslant y_b$ (see Fig. 15.3*b*); therefore the phase space is bounded by the horizontal planes $y_3 = y_b$ and $y_3 = -y_b$ so that when the describing point reaches one of these it can only move along the plane until it returns inside the bounded space.

The plant rotation rate y_2 is not rigidly constrained but if we consider only that plant movement which is caused by the rudder deflection $\delta(y_3)$, then by virtue of the constraint imposed on y_3 this coordinate will also be found constrained, $k_1\delta(-y_b) \leqslant y_2 \leqslant k_1\delta(y_b)$.

The limited phase space of the system is sketched in Fig. 17.2.

The fundamentals of the geometric theory of dynamic systems as a mathematical subject were expounded in the famous memoirs of Henri Poincare.

The application of this tool to physical systems was pioneered by Academician L.I. Mandelshtam. His disciples Academicians A.A. Andronov, L.S. Pontryagin, A.A. Witt, G.S. Gorelik,

S.E. Khaikin (Refs. 3, 4, 47), B.V. Bulgakov made an important contribution to the theory of oscillation.

The most prominent foreign researchers in the field are N. Minorski, S. Lefschetz (Ref. 41), I. Flügge-Lotz (Ref. 25), and V. Cunningham (Ref. 19).

In the theory of nonlinear control systems the most notable results were obtained by A.A. Feldbaum (Refs. 23, 24), A.I. Lurye

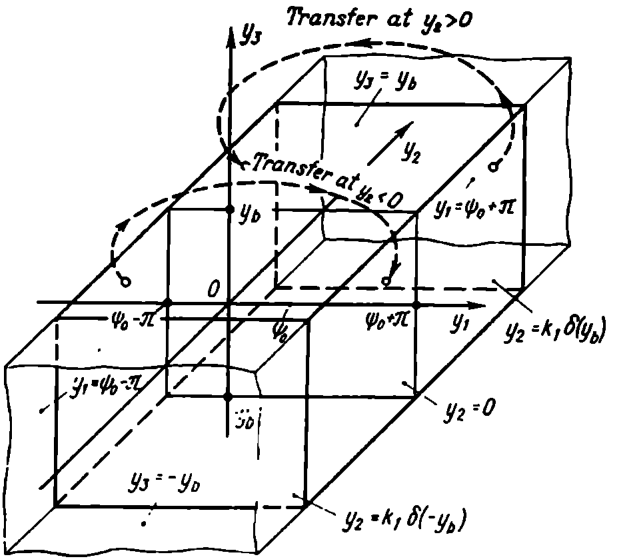

Fig. 17.2

(Ref. 43), M.A. Aizerman and F.R. Gantmacher (Refs. 1, 2), G.M. Ulanov (Ref. 76).

Essentially new achievements in improving the performance of control systems through the use of nonlinear control methods were attained by A.A. Feldbaum (Ref. 22), L.S. Pontryagin and his followers (Ref. 66), and by S.V. Yemelyanov (Ref. 20).

The illustrative value of geometrical representation falls rapidly with increasing dimension of the space under investigation. At the same time analysis becomes increasingly cumbersome.

Classical (Refs. 3, 4), accurate methods of studying dynamic systems described by a nondegenerate third-order differential equation, $N = 3$, are of great theoretical and cognitive importance, but accurate study of dynamic systems at $N \leqslant 2$ is of doubtless practical value. In the latter case the system of equations of integral curves (17.4) degenerates either into a *single differential equation* or into a *set of independent first-order differential equations.*

These systems are discussed in the subsequent sections.

17.2. THE PHASE PLANE AND ITS PROPERTIES

Accurate geometric methods give important practical results provided they are applied to systems whose study reduces to analysis of a set of first-order differential equations confined to one independent variable

$$y_k' = \frac{dy_2}{dy_1} = \frac{P_{2k}(y_1, y_2)}{P_{1k}(y_1, y_2)} \quad (k = a, b, \ldots, r) \tag{17.5}$$

In this case the state space degenerates into r two-dimensional surfaces (sheets) whose boundaries are interconnected in a specified way. The resulting surface is known as a *two-dimensional multisheet surface.*

The law of motion of the describing point within each sheet is given by that relation from the set (17.5) which corresponds to the ordinal number of the sheet under consideration, in other words, by the integral curve equation. The surface geometry, boundaries of sheets and conditions for transition from one sheet to another are given by additional equations resulting from physical considerations.

The simplest form of such systems is a system studied in the phase plane.

Within each *flat* sheet the equation of integral curves has the form*

$$\frac{dy_2}{dy_1} = \frac{P_2(y_1, y_2)}{P_1(y_1, y_2)} \tag{17.6}$$

where P_1 and P_2 are single-valued continuous functions differentiable with respect to both variables, y_1 and y_2, over the entire sheet.

Such systems include systems described by a first-order differential equation ($y_1 = t$) and systems described by a second-order differential equation which does not contain specified time functions (autonomous second-order systems).

With special selection of phase variables, systems (17.6) can describe second-order systems in certain simple specified nonautonomous operational modes under pulse, steplike, constant and monoharmonic input actions.

The motion of the describing point along the phase trajectory should correspond unambiguously to changes of a system state in time, $y_1 = y_1(t)$; $y_2 = y_2(t)$.

In the parametric form the integral curve equation (17.6) is represented as a system of differential equations describing phase

* The traditional (Ref. 4) notation is somewhat different: x and y, and $P(x, y)$ and $Q(x, y)$, respectively.

trajectories

$$\left.\begin{aligned}\frac{dy_1}{dt} &= P_1(y_1, y_2)\\ \frac{dy_2}{dt} &= P_2(y_1, y_2)\end{aligned}\right\} \tag{17.7}$$

or, in the vectorial form,

$$\mathbf{v} = \frac{d\mathbf{y}}{dt} = \mathbf{P}(\mathbf{y}) \tag{17.7a}$$

where the vector of the phase rate may be given by its components

$$\mathbf{v} = \frac{d\mathbf{y}}{dt} = P_1(y_1, y_2)\,\mathbf{i} + P_2(y_1, y_2)\,\mathbf{j}$$

or by the magnitude $v = \frac{ds}{dt} = \sqrt{P_1^2 + P_2^2}$ and the direction $\alpha = \operatorname{arc\,tan} \varkappa$; $\varkappa = \frac{P_2}{P_1}$.

The system (17.7) is more informative than Eq. (17.6). Together with its solutions (phase trajectories) it yields unambiguous and direct estimates of the direction and nature of the motion of the describing point and, consequently, permits correct judgement of the stability and performance of processes in the system.

From Eq. (17.6) it follows that in any common point of the phase plane the direction of the tangent to the integral curve $\varkappa = \frac{dy_2}{dy_1}$ is unique; therefore *phase trajectories never intersect.*

In singular points of the phase plane both functions P_1 and P_2 vanish simultaneously. Their coordinates (y_{1s}, y_{2s}) $(s = a, b, \ldots, m)$ can be calculated by solving the set of algebraic or transcendental equations

$$\left.\begin{aligned}P_1(y_1, y_2) &= 0\\ P_2(y_1, y_2) &= 0\end{aligned}\right\} \tag{17.8}$$

The number of singular points m depends on the specific form of Eqs. (17.8). For the linear system

$$\left.\begin{aligned}P_1(y_1, y_2) &= k_{10} + k_{11}y_1 + k_{12}y_2\\ P_2(y_1, y_2) &= k_{20} + k_{21}y_1 + k_{22}y_2\end{aligned}\right\} \tag{17.9}$$

in a limited region of the phase plane there exists just one singular point whose coordinates y_{1s} and y_{2s} are calculated by Eq. (17.67).

From Eq. (17.7) it follows that both phase rate components vanish simultaneously in singular points, i.e. $\frac{dy_1}{dt} = \frac{dy_2}{dt} = 0$. This means that the describing point does not move and the state of the system cannot change when it is not subjected to external actions.

Consequently, *singular points correspond to the equilibrium positions (states) of the control system under investigation.*

Each singular point is a separate (so-called trivial) solution of the system of differential equations (17.7)

$$y_1(t) = y_{1s} = \text{const}$$
$$y_2(t) = y_{2s} = \text{const}$$

and should be regarded as a *separate phase trajectory.*

A field of directions of a tangent to the integral curves can be readily constructed. The equation for an isocline, the locus of points where the slope angle $\alpha = \arctan \frac{dy_2}{dy_1}$ of the phase rate vector is constant and

$$\varkappa = \frac{dy_2}{dy_1} = \frac{P_2(y_1, y_2)}{P_1(y_1, y_2)} = \text{const} \tag{17.10}$$

follows from differential equation (17.6) if the right-hand part of the latter is equated to the given value of the family parameter $\varkappa$. For convenience, in some points of the isocline the appropriate direction of the tangent is marked by tracing a short line at an angle $\alpha = \arctan \varkappa$ to the x-line. By repeating this procedure for consecutively specified values of the parameter, a family of isoclines and a field of directions are constructed. The density of field lines depends on the specific research problems and the desired accuracy of their solution.

Since the functions P_1 and P_2 are single-valued within one sheet of the phase plane, the isoclines intersect only in singular points.

The x-line of the phase plane usually corresponds to the main variable y_1 of the system, and the y-line to the rate of change of this variable, $y_2 = \frac{dy_1}{dt} = \dot{y}_1$. An example of characteristic trajectories in the phase plane of this type is shown in Fig. 17.3. The law of the motion of the describing point becomes especially simple in this case:

$$y_2' = \frac{dy_2}{dy_1} = \frac{P_2(y_1, y_2)}{y_2} \tag{17.11}$$

or

$$\left.\begin{aligned} \frac{dy_1}{dt} &= y_2 \\ \frac{dy_2}{dt} &= P_2(y_1, y_2) \end{aligned}\right\} \tag{17.12}$$

For this phase plane the following simple rules are valid (see Fig. 17.3).

1. According to Eq. (17.11) the isocline corresponding to vertical tangents coincides with the x-line $y_2 = 0$, the phase trajectories

intersect it at right angles, and the deviation $y_1(t)$ of the describing point takes an extremal value on that axis.

2. Singular points lie only on the x-line where this line meets the isocline corresponding to horizontal tangents $P_2(y_1, y_2) = 0$.

3. Because the positive values of the rate $y_2 = \dot{y}_1 > 0$ are associated with the growth of the variable y_1 and the negative values, with its fall, the describing point moves with the time t in the upper

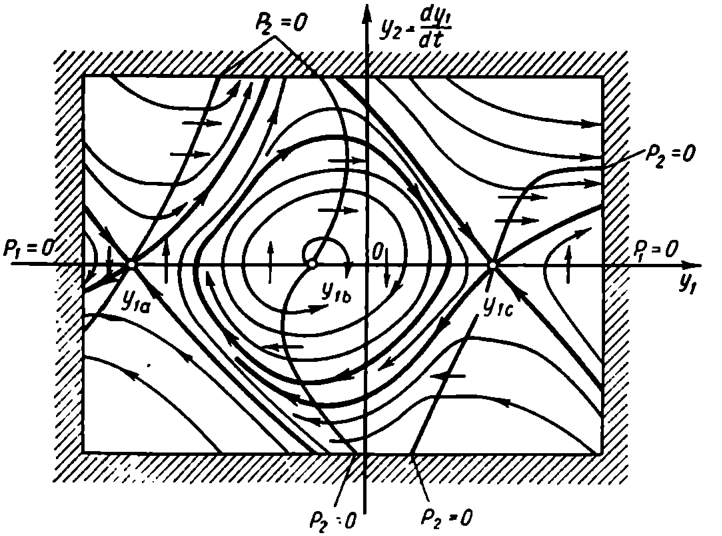

Fig. 17.3

half-plane (see Fig. 17.3) rightwards and in the lower half-plane, leftwards. The closed trajectories or turns of a spiral are traced clockwise.

These rules establish an unambiguous correspondence between the integral curves $y_2 = f(y_1, y_{10}, y_{20})$ resulting from integrating Eq. (17.11) and changing the state of the dynamic system under study in the course of time.

But if another set of phase variables is preferable, for convenience of studies or for the sake of physical illustrativeness, then the direction in which the describing point moves should be determined from the system of differential equations (17.7). Neither Eq. (17.6) of integral curves with time eliminated nor its solutions $y_2(y_1, y_{10}, y_{20})$ give these data.

Example 17.3. Derive equations describing changes in the state of the servo system whose structural diagram and nonlinear responses are given in Fig. 15.2 assuming reduction gear play negligibly small ($\theta_a \approx 0$).

Determine at what control actions $\theta_1(t)$ the system can be analyzed in the phase plane. Find the singular points.

Let us use, in place of transfer functions of linear elements, their differential equations

$$k_M u_M = T_M \frac{d\omega_M}{dt} + \omega_M, \qquad \omega_M = \frac{d\theta_M}{dt} \tag{17.13}$$

where ω_M = motor angular velocity, θ_M = rotation angle, both reduced to the output shaft.

Since the play θ_a is negligibly small, $\theta_M = \theta_2$.

Introduce the dimensionless time $\tau = \frac{t}{T_M}$; then

$$\frac{d\omega_M}{dt} = \frac{1}{T_M}\frac{d\omega_M}{d\tau} \quad \text{and} \quad \omega_M = \frac{1}{T_M}\frac{d\theta_M}{d\tau}$$

Assume the phase variables to be the system misalignment $y_1 = \theta = \theta_1 - \theta_2$ and the normalized dimensionless rate of its change

$$y_2 = \frac{1}{k_M U_{Mb} T_M}\frac{d\theta}{d\tau} = \frac{1}{\Omega_m}\frac{dy_1}{d\tau} = \frac{1}{\Omega_m}\left(\frac{d\theta_1}{d\tau} - T_M\omega_M\right)$$

$$\Omega_m = k_M U_{Mb} T_M = \omega_{Mm} T_M \tag{17.14}$$

whence

$$\omega_M = \frac{1}{T_M}\frac{d\theta_1}{d\tau} - k_M U_{Mb} y_2$$

The first differential equation in the phase plane is

$$\frac{dy_1}{d\tau} = \Omega_m y_2 = P_1(y_2)$$

Let us write down analytical expressions for nonlinear responses of the measuring unit (see Fig. 15.2*b*)

$$f_1 = u_1 = U_{1m}\sin\theta = U_{1m}\sin y_1 = f_1(y_1) \tag{17.15}$$

and of the electronic amplifier (see Fig. 15.2*c*)

$$f_2(u_2) = \frac{u_M}{U_{Mb}} = \begin{cases} -1, & u_2 < -1 \\ u_2, & -1 \leqslant u_2 \leqslant 1 \\ 1, & u_2 > 1 \end{cases} \tag{17.16}$$

where

$$u_2 = \frac{u_1 - u_{com}}{U_{Mb}} = \frac{U_{1m}}{U_{Mb}}\sin y_1 - \frac{k_{com}}{U_{Mb}}\omega_M =$$

$$= \frac{U_{1m}}{U_{Mb}}\sin y_1 + k_{com}k_M y_2 - \frac{k_{com}}{U_{Mb}T_M}\frac{d\theta_1}{d\tau}$$

if there is a proportional rate feedback.

With due regard for equalities (17.13)-(17.16)

$$k_M u_M = -k_M U_{Mb}\frac{dy_2}{d\tau} + \frac{1}{T_M}\frac{d^2\theta_1}{d\tau^2} - k_M U_{Ml} y_2 + \frac{1}{T_M}\frac{d\theta_1}{d\tau}$$

or

$$\frac{u_M}{U_{Mb}} = f_2\left(A_1 \sin y_1 + k_{com}k_M y_2 - \frac{k_{com}k_M}{k_M U_{Mb}} \cdot \frac{1}{T_M}\frac{d\theta_1}{d\tau}\right) = \\ = -\frac{dy_2}{d\tau} - y_2 + \frac{1}{k_M U_{Mb} T_M}\left(\frac{d^2\theta_1}{d\tau^2} + \frac{d\theta_1}{d\tau}\right)$$

where $A_1 = \frac{U_{1m}}{U_{Mb}}$.

Let us solve the resultant equation for the derivative

$$\frac{dy_2}{d\tau} = -y_2 - f_2\left(A_1 \sin y_1 + k_{ss}y_2 - \frac{k_{ss}}{\Omega_m}\frac{d\theta_1}{d\tau}\right) + \\ + \frac{1}{\Omega_m}\left(\frac{d^2\theta_1}{d\tau^2} + \frac{d\theta_1}{d\tau}\right) = P_2(y_1, y_2, \tau)$$

where $k_{ss} = k_{com}k_M$, "ss" standing for "servo system".

Consequently, a change in the misalignment angle of a servo system with a proportional rate compensating feedback under any control action $\theta_1(\tau) = \theta_1\left(\frac{1}{T_M}t\right)$ corresponds to a change in the coordinates $\{y_0 = \tau, y_1, y_2\}$ of the describing point given by a *non-autonomous* system of two differential equations

$$\left.\begin{aligned} \frac{dy_1}{d\tau} &= P_1(y_2) \\ \frac{dy_2}{d\tau} &= P_2(y_1, y_2, \tau) \end{aligned}\right\} \qquad (17.17)$$

in the state space.

In order to study the system of equations directly in the phase plane, the function

$$P_2 = -y_2 - f_2\left(A_1 \sin y_1 + k_{ss}y_2 - k_{ss}\frac{1}{\Omega_m}\cdot\frac{d\theta_1}{d\tau}\right) + \\ + \frac{1}{\Omega_m}\left(\frac{d^2\theta_1}{d\tau^2} + \frac{d\theta_1}{d\tau}\right)$$

should be explicitly independent of time. This condition is met when responding to the specified misalignment and then continuing with a steady follow-up $\theta_1 = a_0 + \Omega_m a_1 \tau$ since in this case $\frac{d^2\theta_1}{d\tau^2} = 0$ and $\frac{d\theta_1}{d\tau} = \Omega_m$, $a_1 = \text{const}$.

Consequently

$$P_2(y_1, y_2, \tau) = \\ = -(y_2 - a_1) - f_2[A_1 \sin y_1 + k_{ss}(y_2 - a_1)] = P_2(y_1, y_2)$$

The rate $\Omega_m a_1$ of the input axis is included into differential equations of phase trajectories as the fixed parameter a_1.

The system of equations discribing phase trajectories

$$\left.\begin{aligned}\frac{dy_1}{d\tau} &= \Omega_m y_2 \\ \frac{dy_2}{d\tau} &= -\{f_2[A_1 \sin y_1 + k_{ss}(y_2 - a_1)] + (y_2 - a_1)\}\end{aligned}\right\} \quad (17.17a)$$

and the integral curve equation

$$\frac{dy_2}{dy_1} = -\frac{f_2[A_1 \sin y_1 + k_{ss}(y_2 - a_1)] + (y_2 - a_1)}{\Omega_m y_2} \quad (17.17b)$$

belong to the types (17.11) and (17.12). Moreover, the right-hand part of Eq. (17.17a) is y_1-periodical, therefore it is sufficient to

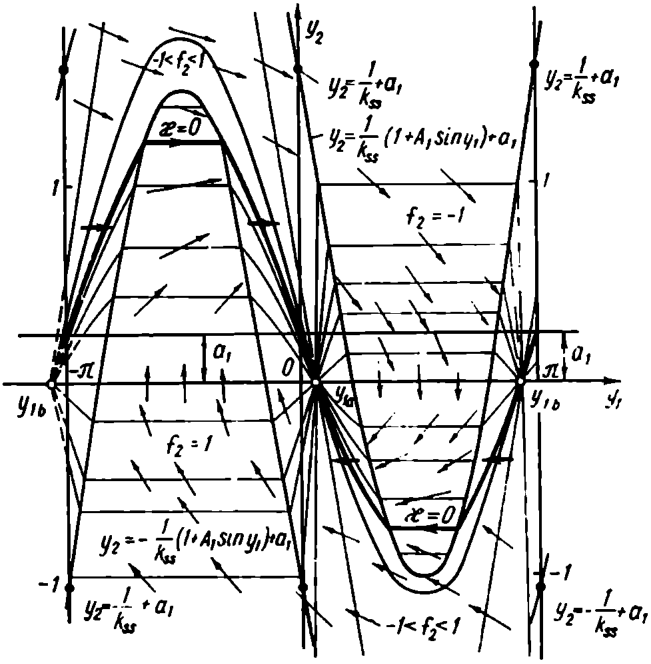

Fig. 17.4

deal with the range $-\pi \leqslant y_1 \leqslant \pi$ in the phase plane (Fig. 17.4). The describing point is transferred from one of the vertical boundaries to another without changing the ordinate y_2.

The isocline corresponding to horizontal tangents $P_2 = 0$ (see Fig. 17.4)

$$y_2 - a_1 = f_2[-A_1 \sin y_1 - k_{ss}(y_2 - a_1)]$$

intersects the isocline corresponding to vertical tangents $y_2 = 0$ in the singular points y_{1s} found from the equation

$$a_1 = f_2(A_1 \sin y_{1s} - k_{ss} a_1)$$

The functions f_2 and $\sin y_1$ are restricted and the latter equation imposes a constraint on feasible rates of steady follow-up

$$|a_1| \leqslant \begin{cases} \frac{A_1}{1+k_{ss}}; & \frac{A_1}{1+k_{ss}} \leqslant 1 \\ 1; & \frac{A_1}{1+k_{ss}} > 1 \end{cases} \tag{17.18}$$

Figure 17.4 shows the singular points y_{1a} and y_b and a family of isoclines corresponding to $A_1 = 2.0$, $k_{ss} = 0.75$, $\Omega_m = 2$ and a follow-up with the dimensionless rate $a_1 = 0.25$.

Practical servo systems fall into two classes. Most are systems with high gain (figure of merit); $U_{Mb} \ll U_{1m}$ and the limitation of f_2 represents small deviations of the misalignment angle from 0 and 180°. These systems can be regarded as piecewise linear since $|\sin y_1| \approx y_1$ at $|y_1 + k\pi| < \frac{\pi}{6}$. Their analysis is given in Examples 17.4 and 17.7.

The other class includes systems with a low voltage gain (with no amplification or with power amplification). Such are systems for slow synchronous angle tracking and some systems of phase frequency adjustment. These are further studied in Example 17.5.

17.3. SYSTEM BEHAVIOUR AT SMALL DEFLECTIONS FROM EQUILIBRIUM

If the conditions imposed in Sec. 17.2 on the right-hand part of Eq. (17.6) are met, the system operation in a small vicinity of each of m equilibrium positions can as a rule be characterized by linearized differential equations with sufficient accuracy. This fact, proved (as applied to stability estimates) by Lyapunov, justifies the practical use of the theory of linear systems in estimating the behaviour of a nonlinear system "in the small".

In doing so at least as many linearized equations should be derived and analyzed as there are singular points (y_{1s}, y_{2s}) $s = a, b, \ldots, m$ resulting from the solution of the system of equations (17.8).

In each of the m cases the phase variables are replaced:

$$y_1 = y_{1s} + x_1$$

$$y_2 = y_{2s} + x_2$$

which is equivalent to the transfer of the reference to the singular point under study (Fig. 17.5).

Expanding the right-hand part of Eq. (17.7) and confining ourselves to linear terms as described in Sec. 2.3, a system of linear differential equations is obtained for *increments* of phase variables y_1 and

y_2 relative to the singular point

$$\left.\begin{aligned}\frac{dx_1}{dt} &= k_{11}x_1 + k_{12}x_2\\ \frac{dx_2}{dt} &= k_{21}x_1 + k_{22}x_2\end{aligned}\right\} \tag{17.19}$$

where

$$k_{11} = \left.\frac{\partial P_1}{\partial y_1}\right|_{\substack{y_1=y_{1s}\\ y_2=y_{2s}}}, \qquad k_{12} = \left.\frac{\partial P_1}{\partial y_2}\right|_{\substack{y_1=y_{1s}\\ y_2=y_{2s}}},$$

$$k_{21} = \left.\frac{\partial P_2}{\partial y_1}\right|_{\substack{y_1=y_{1s}\\ y_2=y_{2s}}}, \qquad k_{22} = \left.\frac{\partial P_2}{\partial y_2}\right|_{\substack{y_1=y_{1s}\\ y_2=y_{2s}}}$$

For systems of the type (17.12), $k_{11} = 0$, $k_{12} = 1$ at all times. The linear system (17.19) is conveniently solved by the operator method subject to the condition that at the initial moment $t_1 = t - t_0 = 0$ the increments of the phase coordinates take on the

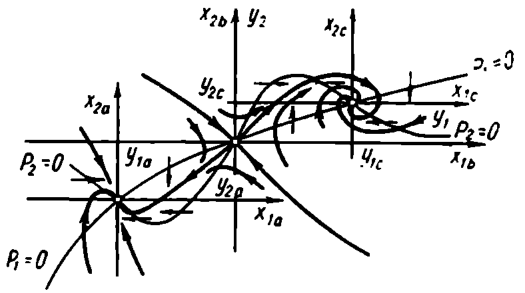

Fig. 17.5

values $x_1(t_0) = x_{10}$ and $x_2(t_0) = x_{20}$. Apply Laplace transformation to (17.19) (allowing for the initial conditions)

$$\left.\begin{aligned}pX_1(p) - x_{10} &= k_{11}X_1(p) + k_{12}X_2(p)\\ pX_2(p) - x_{20} &= k_{21}X_1(p) + k_{22}X_2(p)\end{aligned}\right\}$$

or

$$\left.\begin{aligned}(p-k_{11})X_1(p) - k_{12}X_2(p) &= x_{10}\\ -k_{21}X_1(p) + (p-k_{22})X_2(p) &= x_{20}\end{aligned}\right\}$$

whence follow two equations in terms of images

$$[p^2 - (k_{11} + k_{22})p + (k_{11}k_{22} - k_{12}k_{21})]X_1(p) = (p-k_{22})x_{10} - k_{12}x_{20}$$
$$[p^2 - (k_{11} + k_{22})p + (k_{11}k_{22} - k_{12}k_{21})]X_2(p) = (p-k_{11})x_{20} - k_{21}x_{10}$$

which are evidence that the both phase variables x_1 and x_2 satisfy a homogeneous second-order differential equation

$$\frac{d^2x}{dt^2} - \sigma\left(\frac{dx}{dt}\right) + \Delta x = 0 \tag{17.20}$$

where

$$\sigma = k_{11} + k_{22}, \qquad \Delta = \begin{vmatrix} k_{11}, & k_{12} \\ k_{22}, & k_{22} \end{vmatrix} = k_{11}k_{22} - k_{12}k_{21}$$

The images of solutions to the system (17.19) in the explicit form are

$$\left.\begin{aligned} X_1(p) &= \frac{(p-k_{22})\,x_{10} + k_{12}x_{20}}{(p-p_1)(p-p_2)} \\ X_2(p) &= \frac{k_{21}x_{10} + (p-k_{11})\,x_{20}}{(p-p_1)(p-p_2)} \end{aligned}\right\} \qquad (17.21)$$

where p_1 and p_2 are the roots of the characteristic equation

$$p^2 - \sigma p + \Delta = 0$$

calculated by the formula

$$p_{1,2} = \frac{\sigma \pm \sqrt{\sigma^2 - 4\Delta}}{2} = \frac{(k_{11}+k_{22}) \pm \sqrt{(k_{11}-k_{22})^2 + 4k_{12}k_{21}}}{2} \qquad (17.22)$$

In what follows the index 1 always denotes a root of smaller magnitude.

Using inverse transformation gives a parametric equation of the phase trajectory

$$\left.\begin{aligned} x_1 &= \frac{x_{10}}{p_1 - p_2}\left[(p_1 - k_{22})\,e^{p_1(t-t_0)} - (p_2 - k_{22})\,e^{p_2(t-t_0)}\right] + \\ &+ \frac{k_{12}x_{20}}{p_1 - p_2}\left[e^{p_1(t-t_0)} - e^{p_2(t-t_0)}\right] \\ x_2 &= \frac{k_{21}x_{10}}{p_1 - p_2}\left[e^{p_1(t-t_0)} - e^{p_2(t-t_0)}\right] + \\ &+ \frac{x_{20}}{p_1 - p_2}\left[(p_1 - k_{11})\,e^{p_1(t-t_0)} - (p_2 - k_{11})\,e^{p_2(t-t_0)}\right] \end{aligned}\right\} \qquad (17.23)$$

which relates the current coordinates of the describing point with the initial ones.

If p_1 and p_2 are complex-conjugate roots, $p_{1,2} = -\alpha \pm j\omega$; $\alpha = -\frac{\sigma}{2}$; $\omega = \frac{1}{2}\sqrt{4\Delta - \sigma^2}$, then for the systems (17.12) the expression

$$\left.\begin{aligned} x_1 &= e^{-\alpha(t-t_0)}\left[x_{10}\cos\omega(t-t_0) + \frac{\alpha x_{10} + x_{20}}{\omega}\sin\omega(t-t_0)\right] \\ x_2 &= e^{-\alpha(t-t_0)}\left[x_{20}\cos\omega(t-t_0) - \frac{\Delta x_{10} + \alpha x_{20}}{\omega}\sin\omega(t-t_0)\right] \end{aligned}\right\} \qquad (17.23a)$$

is more convenient.

For a nonlinear system these equations describe the pattern of phase trajectories "*in the small*" at small deviations from the singular point under consideration. For a linear system they are valid over

the whole phase plane. This fact will be used below in Sec. 17.5 in analysis of piecewise linear systems.

Stability and performance of a system "*in the small*" depend on the roots of the characteristic equation, which are functions of the coefficients σ and Δ, according to Eq. (17.22).

Decompose the plane of these coefficients into the regions which correspond to qualitatively different behaviour of the system under

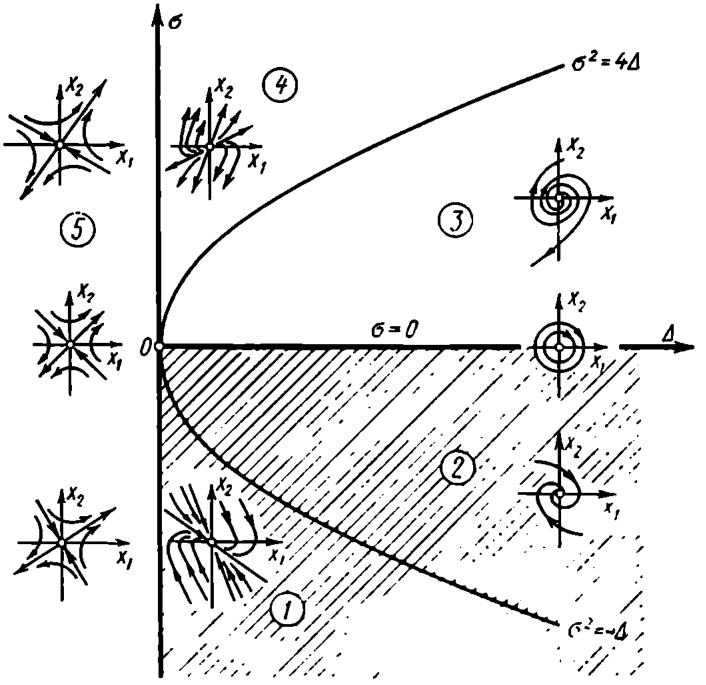

Fig. 17.6

investigation (Fig. 17.6) and have a closer look at processes taking place in each of these regions.

$\Delta = k_{11}k_{22} - k_{12}k_{21} > 0$ is the right half-plane (see Fig. 17.6). Denote in this case $\Delta = \omega_0^2$; $\sigma = -2\zeta\omega_0$, after which differential equation (17.20) takes the familiar (Sec. 3.4) form of the oscillator equation

$$\frac{d^2x}{dt^2} + 2\zeta\omega_0\frac{dx}{dt} + \omega_0^2 x = 0$$

The oscillator is represented by the damping ratio $0 \leqslant \zeta \leqslant 1$. We propose to study solutions of the above equation at $-\infty < \zeta < \infty$.

We will simplify the analysis by introducing dimensionless time $\tau = \omega_0 t$; then

$$\frac{d^2x}{d\tau^2} + 2\zeta \frac{dx}{d\tau} + x = 0 \tag{17.24}$$

The phase variables selected for studies "*in the small*" are the deflection x_1 and the dimensionless rate of its change $x_2 = \frac{dx_1}{d\tau}$. Note that

$$\frac{d^2x_1}{d\tau^2} = \frac{dx_2}{d\tau} = \frac{dx_2}{dx_1}\frac{dx_1}{d\tau} = x_2\frac{dx_2}{dx_1}$$

Substituting this value of the second derivative into Eq. (17.24) yields

$$x_2\frac{dx_2}{dx_1} + 2\zeta x_2 + x_1 = 0$$

Consequently, the integral curve equation

$$\frac{dx_2}{dx_1} = -\frac{2\zeta x_2 + x_1}{x_2} \tag{17.25}$$

and the system of differential equations for phase trajectories

$$\left.\begin{aligned}\frac{dx_1}{d\tau} &= x_2\\ \frac{dx_2}{d\tau} &= -x_1 - 2\zeta x_2\end{aligned}\right\} \tag{17.26}$$

belong to the types (17.11) and (17.12); therefore all the rules given in Sec. 17.2 for such systems are also valid in this case, while the roots of the characteristic equation

$$q^2 + 2\zeta q + 1 = 0, \qquad q = \frac{1}{\omega_0}p$$

depend only on the damping ratio ζ.

Region *1*. Start with large positive values of the damping ratio $\zeta > 1$. Here we have $\sigma < -2\omega_0 = -2\sqrt{\Delta} < 0$. The values of coordinates in the plane (σ, Δ) (see Fig. 17.6) belong to region *1* situated in the fourth quadrant below the parabola $\sigma^2 = 4\Delta$.

In this case the characteristic equation roots are

$$q_1 = -\zeta + \sqrt{\zeta^2 - 1} = \frac{1}{\omega_0 T_1} \quad \text{and} \quad q_2 = -\zeta - \sqrt{\zeta^2 - 1} = \frac{1}{\omega_0 T_2},$$

$$q_1 q_2 = 1$$

Then, as shown in Example 5.2, the system is equivalent to series connection of two inertial elements whose time constants ratio

$$\frac{T_1}{T_2} = \frac{\zeta + \sqrt{\zeta^2 - 1}}{\zeta - \sqrt{\zeta^2 - 1}} = (\zeta + \sqrt{\zeta^2 - 1})^2 = \zeta^2\left(1 + \sqrt{1 - \frac{1}{\zeta^2}}\right)^2$$

grows rapidly with ζ (Fig. 17.7). At $\zeta \geqslant 1.75$ the time constant T_1 is more than 10 times as great as the time constant T_2. In this case the system behaves as an inertial element with $W(p) \approx \frac{1}{T_1 p + 1}$

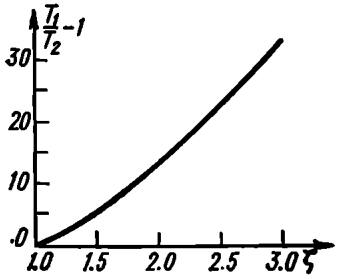

Fig. 17.7

The isocline equation

$$\varkappa = -\frac{x_1 + 2\zeta x_1}{x_2}$$

represents a family of straight lines

$$x_2 = -\frac{1}{\varkappa + 2\zeta} x_1 \qquad (17.27)$$

passing through the origin of coordinates in the phase plane (x_1, x_2) (Fig. 17.8).

The x-line is the isocline corresponding to vertical tangents with $\varkappa = \infty$, the y-line is the isocline with $\varkappa = -2\zeta$, while the isocline $x_2 = -\left(\frac{1}{2\zeta}\right) x_1$, which corresponds to horizontal tangents, intersects the second and fourth quadrants. With increasing damping ratio the angle between the latter isocline and the x-line decreases.

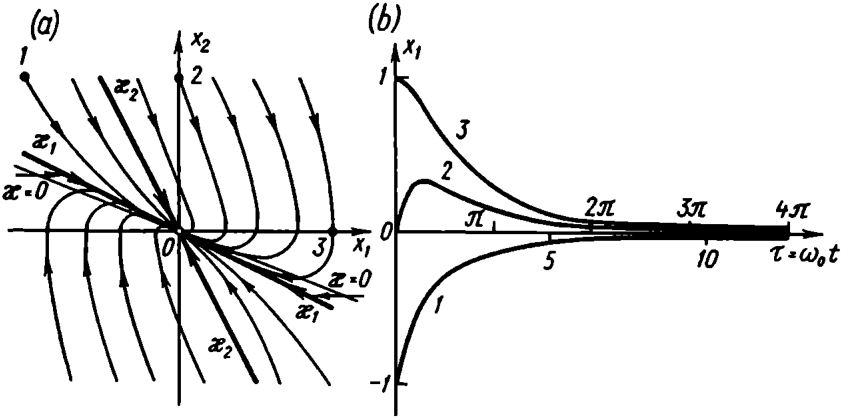

Fig. 17.8

Figure 17.8*a* portrays the phase plane for

$$\zeta = 1.25, \qquad \frac{T_1}{T_2} = 4$$

Since the roots q_1 and q_2 are real, the isoclines with $\varkappa_1 = q_1$ and $\varkappa_2 = q_2$ are at the same time phase trajectories of the system (17.26), which is easily seen by substituting any of these singular values

into Eq. (17.27), e.g. $\varkappa_1 = q_1$. Indeed,

$$x_2 = -\left(\frac{1}{q_1+2\zeta}\right) x_1 = \frac{1}{q_2} x_1 = q_1 x_1 = \varkappa_1 x_1$$

and, consequently, the phase rate vector is directed along this isocline.

The phase plane of the general form (17.19) also includes similar singular directions for which the values of the angular coefficient $\varkappa$ should simultaneously satisfy the isocline equation

$$\varkappa = \frac{dx_2}{dx_1} = \frac{k_{21}x_1 + k_{22}x_2}{k_{11}x_1 + k_{12}x_2} \tag{17.28}$$

and the straight line equation $x_2 = \varkappa x_1$.

Simultaneous solution of these equations yields the quadratic equation

$$k_{12}\varkappa^2 + (k_{11} - k_{22})\,\varkappa - k_{21} = 0$$

whose roots

$$\varkappa_{1,2} = \frac{-(k_{11}-k_{22}) \pm \sqrt{(k_{11}-k_{22})^2 + 4k_{12}k_{21}}}{2k_{12}} \tag{17.29}$$

are related with those of the characteristic equation (17.22a) as

$$\varkappa_1 = \frac{k_{22}-p_2}{k_{12}} = -\frac{k_{11}-p_1}{k_{12}}, \qquad \varkappa_2 = \frac{k_{22}-p_1}{k_{12}} = -\frac{k_{11}-p_2}{k_{12}}$$

Singular directions exist if the roots p_1 and p_2 are real.

Let us write down the solution of differential equations (17.26) at the initial conditions $x_1 = x_{10}$, $x_2 = x_{20}$, $\tau = 0$ in the parametric form

$$\left.\begin{aligned} x_1 &= \frac{x_{20}-q_2x_{10}}{q_1-q_2} e^{q_1\tau} - \frac{x_{20}-q_1x_{10}}{q_1-q_2} e^{q_2\tau} \\ x_2 &= \frac{q_1}{q_1-q_2}(x_{20}-q_2x_{10}) e^{q_1\tau} - \frac{q_2}{q_1-q_2}(x_{20}-q_1x_{10}) e^{q_2\tau} \end{aligned}\right\} \tag{17.30}$$

Since in this case the roots q_1 and q_2 are negative, the deviations x_1 and x_2 go to zero as $\tau \to \infty$, and we have the *asymptotic stability* of the equilibrium "*in the small*".

The slope of the tangent vector

$$\varkappa = \frac{dx_2}{dx_1} = \frac{1}{x_2}\frac{dx_2}{d\tau} = \frac{q_1^2(x_{20}-q_2x_{10}) e^{q_1\tau} - q_2^2(x_{20}-q_1x_{10}) e^{q_2\tau}}{q_1(x_{20}-q_2x_{10}) e^{q_1\tau} - q_2(x_{20}-q_1x_{10}) e^{q_2\tau}} \tag{17.31}$$

tends to the value $\varkappa_1 = q_1$ with increasing τ, irrespective of the initial conditions x_{10} and x_{20}. Consequently, the tangent common to all phase trajectories in the vicinity of the singular point is the isocline $x_2 = \varkappa_1 x_1$.

One exception is the points on the second singular direction $x_2 = \varkappa_2 x_1$ for which, according to Eq. (17.31),

$$\varkappa = \frac{dx_2}{dx_1} = \varkappa_2 = q_2 = \text{const}$$

This is the value to which the slope of phase trajectories tends asymptotically when receding from the singular point ($\tau \to -\infty$). In points remote from the origin of coordinates in the plane (x_2, x_1) the phase trajectories are thus practically parallel to the isocline $x_2 = \varkappa_2 x_1$.

The resemblance of the resulting picture (phase portrait) of Fig. 17.8*a* with a strand of threads tied in the middle led to the term *node* for a singular point of this kind. Figure 17.8*b* shows processes which correspond to phase trajectories *1*, *2*, and *3* (see Fig. 17.8*a*) as functions of dimensionless time τ.

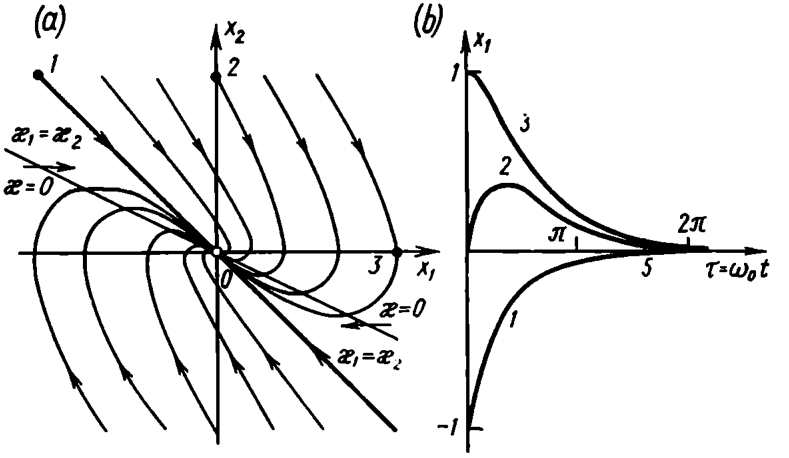

Fig. 17.9

The aforesaid leads to the conclusion that *Region 1 in the plane* (σ, Δ) *is associated with stable equilibriums and with nonoscillatory transient processes. Such singular points are known as stable nodes.*

The phase portrait in the vicinity of the point whose parameters meet the condition $\sigma = -2\omega_0 = -2\sqrt{\Delta}$, i.e. are on the boundary between Regions *1* and *2* (see Fig. 17.6), is given in Fig. 17.9. In this case $\zeta = 1$, the roots $q_1 = q_2 = -1$, and the system is equivalent to two series-connected similar inertial elements.

The isocline corresponding to horizontal tangents has a slope $\alpha = -\text{arc tan}\,\frac{1}{2}$, and the singular directions $x_2 = \varkappa_1 x_1$ and $x_2 = \varkappa_2 x_1$ coincide with the bisector of the second and fourth quadrants. The phase trajectories in the vicinity of the singular point are tangential to this straight line and become parallel to it with increasing distance. This angular point, which is referred to as a *degenerate stable node*, represents the conditions of critical damping of a dynamic system.

The transient processes here are as in Fig. 17.9*b*.

Region 2. In Region *2* (see Fig. 17.6) $0 > \sigma > -2\omega_0 = -2\sqrt{\Delta}$, the damping ratio is $1 > \zeta > 0$, and the system is equivalent to the oscillator the standard processes in which, including their representation in the phase plane (h, w), are described in Sec. 3.4.

In this case the characteristic equation roots are complex-conjugate with the negative real part

$$q_1 = -\zeta + j\Omega, \quad q_2 = -\zeta - j\Omega, \quad \Omega = \sqrt{1-\zeta^2} = \frac{\omega_t}{\omega_0}$$

and $\omega_t = \omega_0\sqrt{1-\zeta^2}$ is the circular frequency of damped oscillations.

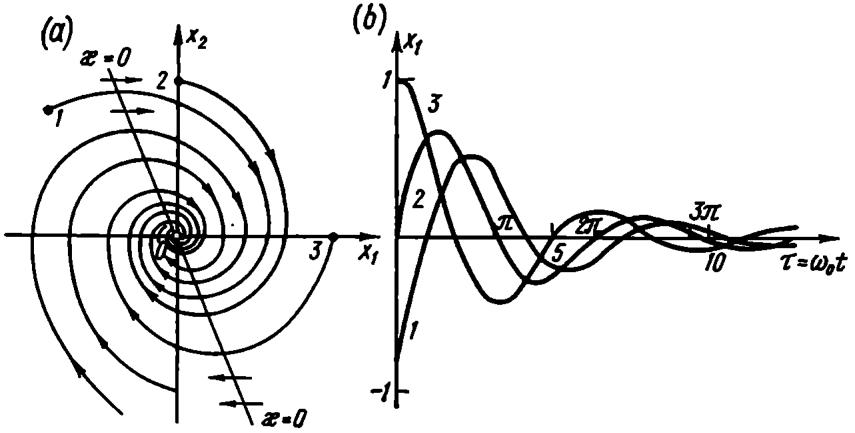

Fig. 17.10

Substituting these data into the parametric equation of phase trajectories (17.30) and performing simple transformations gives

$$\left.\begin{aligned} x_1 &= e^{-\zeta\tau}\left[x_{10}\cos\Omega\tau + \frac{x_{20}+\zeta x_{10}}{\Omega}\sin\Omega\tau\right] \\ x_2 &= e^{-\zeta\tau}\left[x_{20}\cos\Omega\tau - \frac{\zeta x_{20}+x_{10}}{\Omega}\sin\Omega\tau\right] \end{aligned}\right\} \qquad (17.32)$$

With an increase in time $t = \frac{\tau}{\omega_0}$ the deviation x_1 and its rate of variation $x_2 = \frac{dx_1}{d\tau}$ tend to zero and undergo damped oscillations, whose period $T = \frac{2\pi}{\omega_t}$ corresponds to the changes in the parameter τ within a complete revolution $\Delta\varphi = \Delta(\Omega\tau) = 2\pi$ of spiral phase trajectories (Fig. 17.10*a*) around their *focus* ($x_1 = 0$, $x_2 = 0$).

These are logarithmic spirals because the logarithm of the relative change in deviation per revolution is constant:

$$\ln \frac{x_1(2k\pi)}{x_1[2(k+1)\pi]} = \frac{\zeta}{\Omega} = \frac{\zeta}{\sqrt{1-\zeta^2}} = \text{const}$$

The maximum of the ordinate x_2 is achieved in intersecting the isocline $x_2 = -\left(\frac{1}{2}\zeta\right) x_1$ corresponding to horizontal tangents which passes through the second and fourth quadrants $\left(-\frac{1}{2} > -\frac{1}{2}\zeta > -\infty\right)$ as before. Figure 17.10*b* represents the respective transient processes $x_1(\tau)$ at $\zeta = 0.25$.

Region 2 of the plane (σ, Δ) *is associated with stable equilibrium points and oscillatory transient processes. These singular points are referred to as stable foci.*

On the right half of the x-line in the plane (σ, Δ) the damping ratio ζ is zero. The characteristic equation roots are purely imaginary, $q_1 = j$, $q_2 = -j$, and the system is an ideal oscillatory circuit

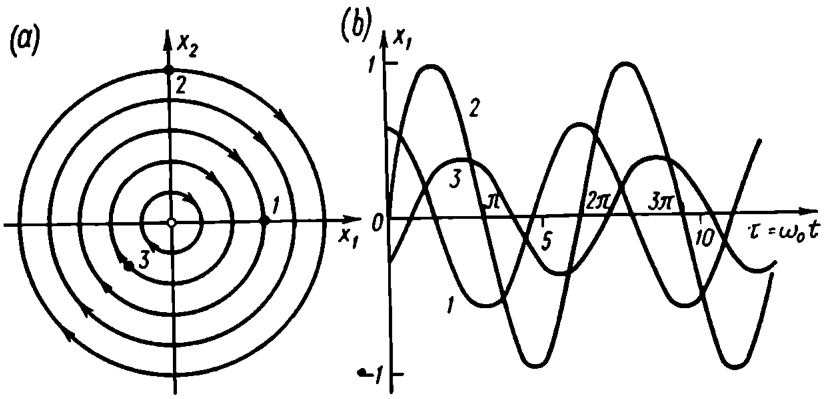

Fig. 17.11

simulated by closing two integrating elements by means of a negative feedback.

The phase plane (x_1, x_2) is given in Fig. 17.11*a*. The isocline corresponding to horizontal tangents coincides with the y-line $x_1 = 0$. From Eq. (17.32) and since $\zeta = 0$, $\Omega = 1$

$$\left.\begin{aligned} x_1 &= x_{10}\cos\tau + x_{20}\sin\tau \\ x_2 &= x_{20}\cos\tau - x_{10}\sin\tau \end{aligned}\right\} \qquad (17.33)$$

The phase trajectories are a family of concentric circles

$$x_1^2 + x_2^2 = x_{10}^2 + x_{20}^2 = r^2 \qquad (17.34)$$

whose radius depends on the initial conditions. The use of the type (17.19) phase plane just stretches the circles into ellipses.

The singular point $x_{1s} = 0$, $x_{2s} = 0$, which is referred to as the *centre*, is associated with neutral equilibrium; the distance of the describing point $x_1(t)$, $x_2(t)$ from the centre does not change in the course of time on any initial deflections.

Consequently, *the right half of the x-line in the plane of* Fig. 17.6, *where* $\sigma = 0$; $\Delta > 0$, *is associated with neutral singular points of the centre type.*

The change of the deflection $x_1(\tau)$ is shown in Fig. 17.11*b*.

It is noteworthy that the equation (17.19) does not give in this case an idea of stability or behaviour of the *nonlinear* system under

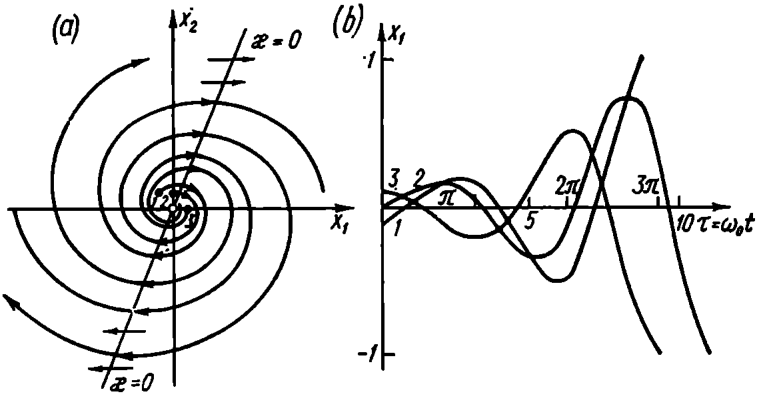

Fig. 17.12

study. Nonlinear terms are of essential importance in decomposition of the functions $P_1(y_1, y_2)$ and $P_2(y_1, y_2)$. *According to A. A. Andronov* (Ref. 4) *such systems are not insensitive and so their behaviour depends on small parameters.*

Region *3*. At $0 < \sigma < 2\omega_0 = 2\sqrt{\Delta}$ the damping ratio ζ becomes negative. Therefore in Region *3* (see Fig. 17.6) the real parts of both complex-conjugate roots of the characteristic equation are positive

$$q_1 = \alpha + j\Omega, \quad q_2 = \alpha - j\Omega, \quad 1 > \alpha = -\zeta > 0 \tag{17.35}$$

The phase trajectory equation

$$\left.\begin{aligned} x_1 &= e^{\alpha\tau}\left[x_{10}\cos\Omega\tau + \frac{x_{20} - \alpha x_{10}}{\Omega}\sin\Omega\tau\right] \\ x_2 &= e^{\alpha\tau}\left[x_{20}\cos\Omega\tau + \frac{\alpha x_{20} - x_{10}}{\Omega}\sin\Omega\tau\right] \end{aligned}\right\} \tag{17.36}$$

is here geometrically represented as a family of diverging logarithmic spirals (Fig. 17.12*a*). The isocline $x_2 = \left(\frac{1}{2}\alpha\right)x_1$ corresponding

to horizontal tangents passes through the first and third quadrants, $\infty > \frac{1}{2}\alpha > \frac{1}{2}$. With increasing time $t = \frac{\tau}{\omega_0}$ the phase trajectories recede from their focus ($x_1 = 0$, $x_2 = 0$). The system equilibrium is unstable. The transient processes are oscillations with an exponentially increasing amplitude (Fig. 17.12*b*).

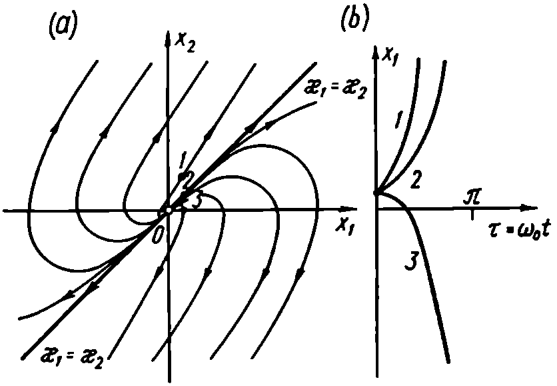

Fig. 17.13

Singular points for which the values of the coefficients σ *and* Δ *belong to Region 3 are known as unstable foci.*

The upper branch $0 < \sigma = 2\omega_0 = 2\sqrt{\Delta}$ of the boundary between Regions *3* and *4* (see Fig. 17.6) is associated with an *unstable degenerate node*. The phase portrait and the plots of transient processes are shown in Fig. 17.13*a* and *b*, respectively.

Region *4*. The phase portrait in the vicinity of the unstable node (Fig. 17.14*a*) for which the values of the coefficients σ and Δ lie in Region *4* (see Fig. 17.6) is the mirror image of the stable node vicinity (see Fig. 17.8) relative to the coordinate axis x_1 with a changed direction of movement of the describing point along the phase trajectory. The values of the damping ratio are $-1 > \zeta > -\infty$, the roots of the characteristic equation are real and positive

$$q_1 = \alpha - \sqrt{\zeta^2 - 1}, \qquad q_2 = \alpha + \sqrt{\zeta^2 - 1}, \qquad \alpha = -\zeta > 0$$

The phase trajectory parametric equation is obtained by substituting these values into Eq. (17.30). The increase of x_1 as a function of time is shown in Fig. 17.14*b*.

Region *5*. The left half of the plane (see Fig. 17.6) corresponds to $\Delta = k_{11}k_{22} - k_{12}k_{21} < 0$. In the left half of the plane (σ, Δ) the free term of the characteristic equation (17.22) becomes negative, $\Delta < 0$. Denoting $-\Delta = \omega_0^2 > 0$ and reducing to dimensionless time,

we have, in place of Eq. (17.24),

$$\frac{d^2x_1}{d\tau^2}+2\zeta\frac{dx_1}{d\tau}-x_1=0 \qquad (17.37)$$

The roots of the characteristic equation

$$q_1=-\zeta+\sqrt{\zeta^2+1}>0, \qquad q_2=-\zeta-\sqrt{\zeta^2+1}<0 \qquad (17.38)$$

are real, irrespective of the value of ζ (and consequently, of σ), and have different signs.

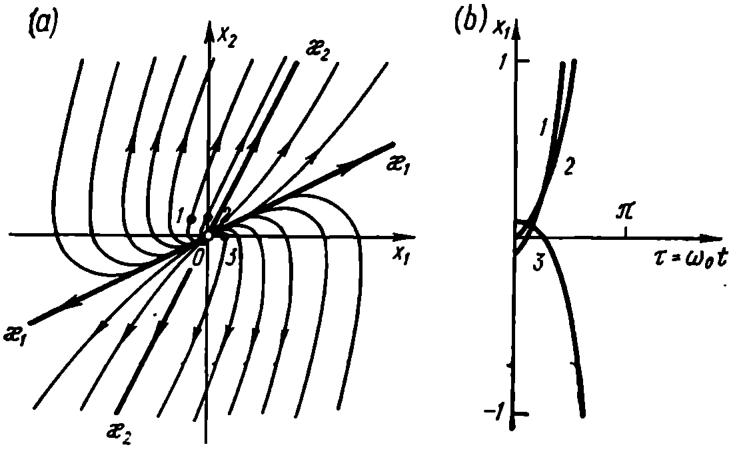

Fig. 17.14

The equilibrium position ($x_{1s}=0$, $x_{2s}=0$) is always unstable. The singular directions

$$x_2=q_1x_1=\varkappa_1x_1, \qquad x_2=q_2x_1=\varkappa_2x_1 \qquad (17.39)$$

pass through different quadrants of the phase plane ($\zeta>0$) (Fig. 17.15*a*), ($\zeta=0$) (Fig. 17.16*a*), and ($\zeta<0$) (Fig. 17.17*a*). The isoclines corresponding to horizontal and vertical tangents are always on different sides of isoclines (17.39).

The phase portrait looks like a topographic map of a mountain saddle, therefore the unstable singular points in whose vicinity the parameters σ and Δ belong to Region *5* (see Fig. 17.6) are called *saddles*.

It follows from the parametric equation (17.30) for phase trajectories, with an allowance for Eq. (17.38), that with increasing time $t=\frac{1}{\omega_0\tau}$ any phase trajectory asymptotically tends to the straight line $x_2=q_1x_1$. The phase variables increase ($x_1\to\infty$, $x_2\to\infty$) or decrease ($x_1\to-\infty$, $x_2\to-\infty$) unboundedly depending on the

position of the describing point relative to the singular direction $x_2 = q_2 x_1$ at any arbitrary time instant (in particular, at $t = t_0$).

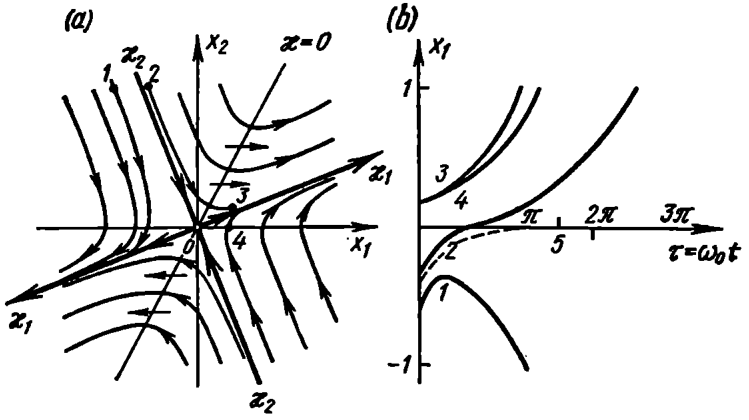

Fig. 17.15

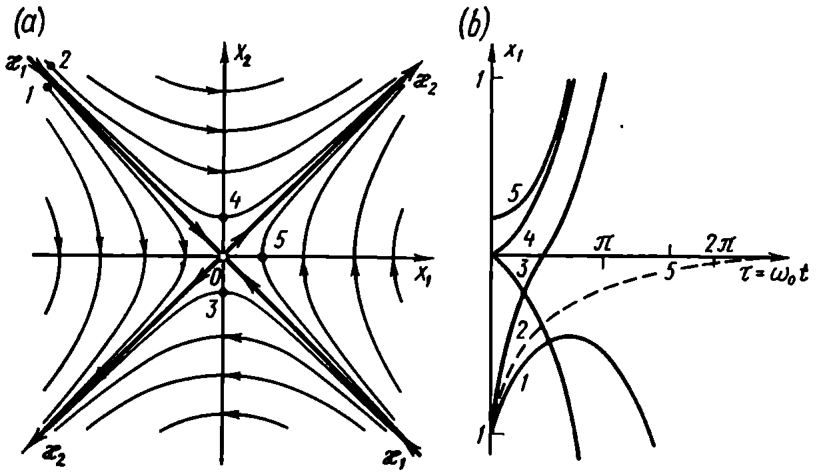

Fig. 17.16

Indeed, at high τ

$$x_1 \approx \frac{x_{20} - q_2 x_{10}}{q_1 - q_2} e^{q_1 \tau}, \quad \text{while} \quad x_2 \approx \frac{q_1}{q_1 - q_2} (x_{20} - q_2 x_{10}) e^{q_1 \tau}$$

the value of x_2 is positive at $x_{20} > q_2 x_{10}$ (the describing point is above and to the right of the straight line $x_2 = q_2 x_1$) and negative at $x_{20} < q_2 x_{10}$ (the describing point is to the left of and below the

straight line $x_2 = q_2 x_1$). *The singular direction* $x_2 = q_2 x_1$ *is a separating line* (*separatrix*) *of phase trajectories*; on both sides of it the describing point moves away from the saddle asymptotically along

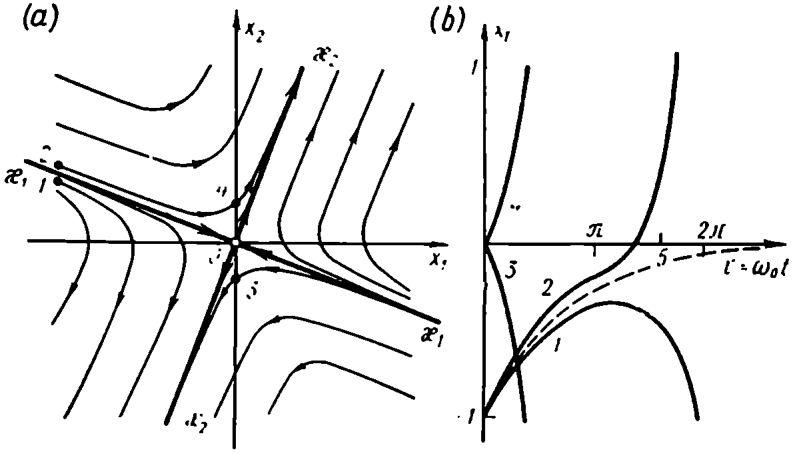

Fig. 17.17

the second separatrix in diametrically opposite directions, $x_2 = q_1 x_1 > 0$ and $x_2 = q_1 x_1 < 0$. Moving along the separatrix $\varkappa_2 = q_2$ itself the describing point approaches the equilibrium position

$$x_1 = \frac{q_1 x_{10} - x_{20}}{q_1 - q_2} e^{-(\zeta + \sqrt{\zeta^2+1})\,\tau}$$

$$x_2 = \frac{q_2}{q_1 - q_2}(q_1 x_{10} - x_{20})\, e^{-(\zeta + \sqrt{\zeta^2-1})\,\tau}$$

but the *separatrix per se is unstable* because every, however small, deflection from it increases unboundedly in the course of time.

In the particular case when $\zeta = 0$ or the coordinates x_1 and x_2 of the system (17.19) are selected so that $k_{11} = -k_{22}$, the equation of integral curves becomes especially simple, $\frac{dx_2}{dx_1} = \frac{x_1}{x_2}$, whence

$$\int_{x_{20}}^{x_2} x_2\, dx_2 = \int_{x_{10}}^{x_1} x_1\, dx_1$$

and integral curves are constructed as the family of symmetrical hyperbolas

$$x_2^2 - x_1^2 = x_{20}^2 - x_{10}^2 = \text{const}$$

shown in Fig. 17.16*a*.

The aperiodic unstable transient processes in a zone where the linear approximation is valid are shown in Figs. 17.15*b*, 17.16*b*, and 17.17*b*.

The degenerate case $\Delta = 0$. Now let us have a look at points that are on the y-line of the diagram (see Fig. 17.6) where, for physical reasons, $\Delta = k_{11}k_{22} - k_{12}k_{21} = 0$.

In this case equation (17.20) takes the form

$$\frac{d^2x}{dt^2} - \sigma \frac{dx}{dt} = 0 \tag{17.40}$$

The system is equivalent to a series connection of the inertial and integrating elements (one each) which were treated in detail in Example 5.1.

Denoting $x_1 = x$, $x_2 = \frac{dx}{dt}$, write down a system of differential equations for phase trajectories

$$\left.\begin{aligned} \frac{dx_1}{dt} &= x_2 \\ \frac{dx_2}{dt} &= \sigma x_2 \end{aligned}\right\} \tag{17.41}$$

whence follows that the *x-line* $x_2 = 0$ *here consist only of singular points.*

Since $k_{11} = k_{21} = 0$, $k_{12} = 1$ and $k_{22} = \sigma$, the roots of the characteristic equation are $p_1 = 0$, $p_2 = \sigma$.

The parametric equation (17.23) of phase trajectories is given in the form

$$\left.\begin{aligned} x_1 &= x_{10} + \frac{1}{\sigma} x_{20} [1 - e^{\sigma (t-t_0)}] \\ x_2 &= x_{20} e^{\sigma (t-t_0)} \end{aligned}\right\} \tag{17.42}$$

Determining the value of $e^{\sigma(t-t_0)} = \frac{x_2}{x_{20}}$ from the second equation, substitute it into the first one. The phase variables are then found to be related by the straight line equation

$$x_2 - x_{20} = \sigma (x_1 - x_{10}) \tag{17.43}$$

At $\sigma < 0$ the describing point (Fig. 17.18*a*) moves towards the x-line to each it in the point $x_{1s} = x_{10} + \left(\frac{1}{\sigma}\right) x_{20}$. Consequently, *the points of this axis represent the positions of stable equilibrium of the system under investigation.*

At $\sigma > 0$ the phase coordinates increase unboundedly (Fig. 17.18*b*). *The relevant points of the x-line represent the positions of unstable equilibrium.*

Note that the study of degenerate dynamic systems is of interest only where the condition

$$\Delta = k_{11}k_{22} - k_{12}k_{21} = 0$$

follows from physical considerations rather than from a numerical (and necessarily approximate) relation of the coefficients $k_{11}k_{22} = k_{12}k_{21}$ belonging to linear terms of the expansion of the functions $P_1(x_1, x_2)$ and $P_2(x_1, x_2)$ into a power series. In this latter case

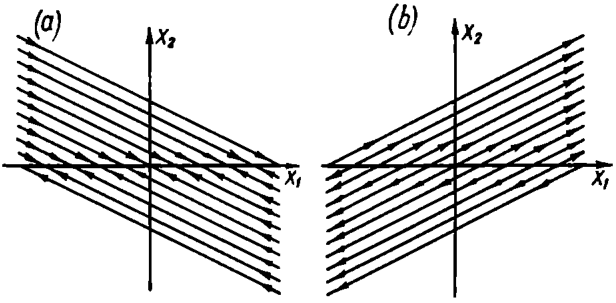

Fig. 17.18

the system is noninsensitive and its behaviour should be estimated at those nonzero values of Δ that are obtained with an allowance for possible design or maintenance differences causing variations of the system parameters.

Example 17.4. Study the operation of the servo system treated in Example 17.3 under small deflections from the singular points

$$y_{1s} = \arcsin \frac{1+k_{ss}}{A_1} a_1, \quad y_{2s} = 0$$

Linearize the system of phase trajectory differential equations (17.17)

$$\left.\begin{aligned} \frac{dy_1}{d\tau} &= \Omega_m y_2 = P_1(y_2) \\ \frac{dy_2}{d\tau} &= -\{(y_2 - a_1) + f_2[A_1 \sin y_1 + k_{ss}(y_2 - a_1)]\} = P_2(y_1, y_2) \end{aligned}\right\}$$

in the vicinity of the singular points y_{1s} by Eq. (17.19) with an allowance for the constraint on the follow-up rate a_1 specified by Eq. (17.18)

$$k_{11} = \frac{\partial P_1}{\partial y_1} = 0, \qquad k_{12} = \frac{\partial P_1}{\partial y_2} = \Omega_m,$$

$$k_{21} = \frac{\partial P_2}{\partial y_1}_{y_1 = y_{1s}} = -A_1 \cos y_{1s} = -A_1 \cos \arcsin \frac{1+k_{ss}}{A_1} a_1 =$$

$$= \mp \sqrt{A_1^2 - (1+k_{ss})^2 a_1^2}$$

Here the negative value represents the singular points

$$-\frac{\pi}{2}\pm 2k\pi\leqslant y_{1a}\leqslant\frac{\pi}{2}\pm 2k\pi \quad (k=0,\ 1,\ 2,\ \ldots)$$

and the positive value, the singular points

$$\frac{\pi}{2}\pm 2k\pi\leqslant y_{1b}\leqslant\frac{3}{2}\pi\pm 2k\pi$$

Finally,

$$k_{22}=\frac{\partial P_2}{\partial y_2}=-(1+k_{ss})$$

Consequently, the system (17.19) takes the form

$$\left.\begin{aligned}\frac{dx_1}{d\tau}&=\Omega_m x_2\\ \frac{dx_2}{d\tau}&=\mp\sqrt{A_1^2-(1+k_{ss})^2 a_1^2}\,x_1-(1+k_{ss})\,x_2\end{aligned}\right\}$$

In each band $-\pi\leqslant y_1\leqslant\pi$ two singular points should be distinguished. Consider them separately

(1) $$-\frac{\pi}{2}\leqslant y_{1a}=\arcsin\frac{1+k_{ss}}{A_1}a_1\leqslant\frac{\pi}{2}.$$

The value of the misalignment angle (kinetic error) depends on the steady follow-up rate and vanishes when responding to the specified constant angle ($a_1 = 0$). Substituting the values of A_1, k_{ss} and a_1 from Example 17.3 yields

$$y_{1a}=\theta_{kin}=\arcsin\frac{1+k_M k_{com}}{k_M U_{1m} T_M}\frac{d\theta_1}{d\tau}=\arcsin\frac{1+k_{ss}}{k_{as}}\omega_1$$

$k_{as}\left(\frac{1}{\text{sec}}\right)$ = the figure of merit of the servo system

$\omega_1\left(\frac{1}{\text{sec}}\right)$ = the input axis rotation rate.

The roots of the characteristic equation in the vicinity of this equilibrium point are

$$q_{1,2}=T_M p_{1,2}=\frac{-(1+k_{ss})\pm\sqrt{(1+k_{ss})^2-4\Omega_m\sqrt{A_1^2-(1+k_{ss})^2 a_1^2}}}{2}$$

The system is stable with a negative rate feedback $k_{ss} > 0$.

Repolarization of the feedback, $k_{ss}\leqslant -1$, may lead to instability.

(2) $$\frac{\pi}{2}\leqslant y_{1b}=\pi-\arcsin\frac{1+k_{ss}}{A_1}a_1\leqslant\frac{3}{2}\pi.$$

The valuo of the misalignment angle is about 180°. Then the roots of the characteristic equation are

$$q_{1,2}=T_M p_{1,2}=\frac{-(1+k_{ss})\pm\sqrt{(1+k_{ss})^2+4\Omega_m\sqrt{A_1^2-(1+k_{ss})^2 a_1^2}}}{2}$$

The singular point is the saddle the angular coefficient of whose separatrixes is, by virtue of Eq. (17.29),

$$\varkappa_{1,2} = \frac{1}{\Omega_m} q_{1,2} = \frac{-(1+k_{ss}) \pm \sqrt{(1+k_{ss})^2 + 4\Omega_m \sqrt{A_1^2 - (1+k_{ss})^2 a_1^2}}}{2\Omega_m}$$

Figure 17.19*a* shows the shape of phase trajectories near the first singular point y_{1a} which represents stable follow-up. The parameter

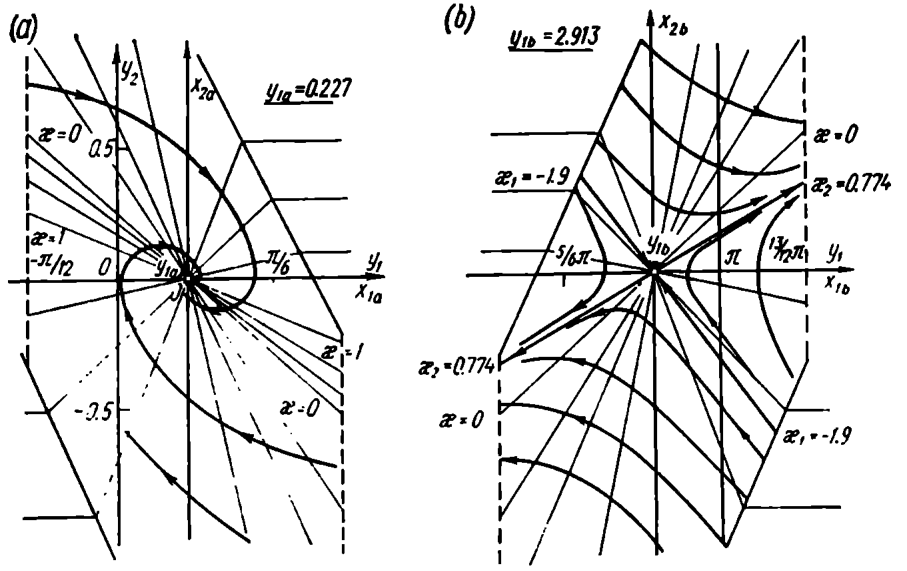

Fig. 17.19

values are the same as in Example 17.3: $A_1 = 2$, $k_{ss} = 0.75$, $\Omega_m = 2$, and $a_1 = 0.25$. Then $y_1 = \theta_{kin} = 0.227$, the boundaries of the linear zone are given by the straight lines $|y_1| \leqslant \frac{\pi}{6}$ and by portions of the saturation region boundaries $|f_2| = 1$ (see Fig. 17.4).

Figure 17.19*b* gives a linear region in the vicinity of the unstable singular point $y_{1b} = 2.913$ for the same parameter values.

The separatrix equations for this case are

$$y_2 = \varkappa_1 (y_1 - y_{1b}) = -1.9 (y_1 - 2.913) = -1.9y_1 + 5.52$$

and

$$y_2 = \varkappa_2 (y_1 - y_{1b}) = 0.774 (y_1 - 2.913) = 0.774y_1 - 2.25$$

17.4. SYSTEM BEHAVIOUR AT LARGE DEFLECTIONS. SELF-OSCILLATIONS

Once the singular points have been found on a sheet of the phase plane and the nature of processes near each equilibrium has been ascertained ("*in the small*"), the following problem of nonlinear system study can be formulated.

Determine what kind of steady states apart from the equilibria are possible and what are the conditions ensuring invariant operation in each of these steady states.

The first part of the problem is solved by determining the periodic oscillatory modes which in the phase plane are associated with special stable closed trajectories, the *stable limit cycles.*

In order to solve the second part those regions of values should be established for the describing point coordinates in each of which just one possible steady state mode is achieved in the course of time. The boundaries of such regions, referred to as mode *attraction regions*, are formed by special unstable trajectories, the *unstable limit cycles* and the *separatrixes of the saddles.*

The technical difficulty at this stage of research is the labour consumed in construction and analysis of the large phase trajectory curves. The analytical approach is applicable here only to piecewise-linear systems the methods of study for which have been expounded in Sec. 17.5.

In other cases graphical and numerical methods are used. Digital computers and system simulation by operational amplifiers are especially advantageous.

Consider now simple graphical techniques for construction of the phase trajectory and the process as a function of time.

The method of isoclines. The parameter of isoclines $\varkappa = \frac{dy_2}{dy_1} = \frac{\Delta y_2}{\Delta y_1}$ (Fig. 17.20*a*) calculated by Eq. (17.10) is equal to the tangent of the phase trajectory slope angle α if both phase plane coordinate axes are given in the same scale.

However, this selection of scale may sometimes prove inadmissible for graphical construction because if the scale is the same, the phase portrait contracts along one of the axes, and so a scale ratio different from unity (m, for example) should be selected. Then

$$\tan \alpha = \frac{\Delta y_{2b}}{\Delta y_{1b}} = \frac{m_2 \Delta y_2}{m_1 \Delta y_1} = m\varkappa \qquad (17.44)$$

because in the plot $y_{1b} = m_1 y_1$ cm and $y_{2b} = m_2 y_2$ cm.

In graphical construction of phase trajectories by the method of isoclines their family is constructed so that the difference of the angles corresponding to any two adjacent isoclines is about the same:

$$\Delta\alpha_i = \text{arc tan } m\varkappa_{i+1} - \text{arc tan } m\varkappa_i \approx \text{const}$$

What value of $\Delta\alpha$ is selected depends on the desired accuracy of construction and on the scale of the plot, quality of the drafting facilities, experience, time and manpower available. The usual selection is $10° \leqslant \Delta\alpha \leqslant 30°$.

Once a family of isoclines is constructed (Fig. 17.20*b*), two rays are traced at angles $\alpha_0 = \arctan m\varkappa_0$ and $\alpha_1 = \arctan \varkappa m_1$ from

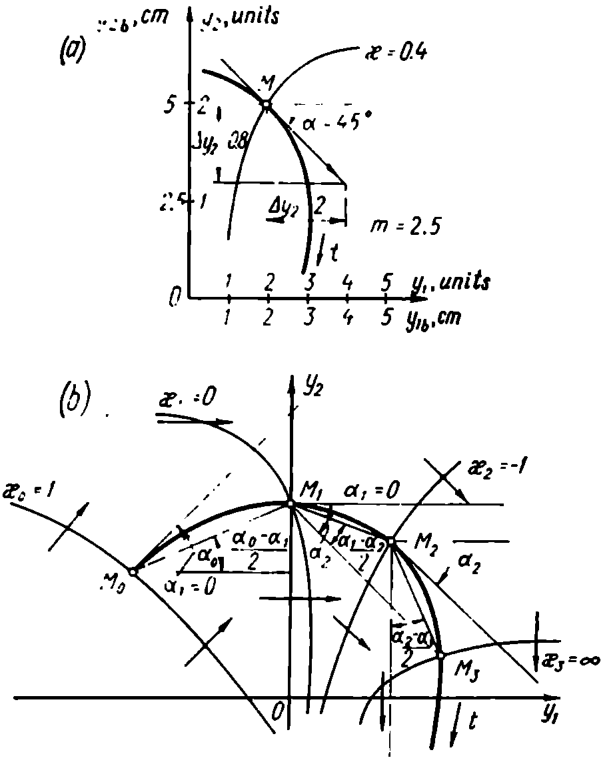

Fig. 17.20

the initial point M_0 lying on one of them, $\varkappa = \varkappa_0$. The angle between these rays $\Delta\alpha_1$ is halved and the point M_1 at the intersecton of the resulting bisectrix and the next isocline $\varkappa = \varkappa_1$ is assumed to be the new calculated point of the phase trajectory.

Then the process is reiterated as shown in Fig. 17.20*b*. The points M_i $(i = 0, 1, 2, \ldots, N)$ are connected by a smooth curve.

The Lienard and the delta techniques. To construct the phase trajectories of widespread systems whose differential equation has the form

$$\frac{d^2y_1}{dt^2} + F_1\frac{dy_1}{\partial t} + \omega_0^2 y_1 = 0 \qquad (17.45)$$

Lienard proposed a convenient graphical method in 1928 (Fig. 17.21).

Using for simplicity the dimensionless time $\tau = \omega_0 t$ and denoting $y_2 = \frac{dy_1}{d\tau}$ write the equation of integral curves equivalent to the initial equation (17.45)

$$\frac{dy_2}{dy_1} = -\frac{y_1 + F(y_2)}{y_2} \tag{17.46}$$

Since $F(y_2)$ is a function with a limited derivative we can assume that in the vicinity of the specified point M_i with coordinates $y_1 = y_{1i}$, $y_2 = y_{2i}$, $F(y_2) \approx F(y_{2i}) = \text{const}$.

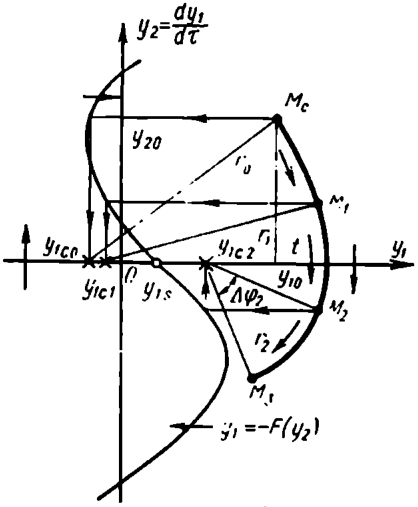

Fig. 17.21

Let us separate the variables and integrate Eq. (17.46)

$$\int_{y_{2i}}^{y_2} y_2\, dy_2 + \int_{y_{1i}}^{y_1} [F(y_{2i}) + y_1]\, dy_1 = 0$$

whence

$$y_2^2 + [F(y_{2i}) + y_1]^2 = y_{2i}^2 + [F(y_{2i}) + y_{1i}]^2 = r_i^2 \tag{17.47}$$

This is evidently the equation of an arc of the circle traced through the specified point M_i with centre in a point with coordinates $y_{2c} = 0$, $y_{1ci} = -F(y_{2i})$. Noting that $y_1 = -F(y_2)$ is the equation of the isocline corresponding to horizontal tangents we have an iterative graphical procedure for constructing a phase trajectory which can be initiated by obtaining a single isocline of horizontal tangents $\varkappa = 0$. From the given initial point $M_0(y_{10}, y_{20})$ (see Fig. 17.19) a horizontal line is then traced until it intersects the isocline. The normal from the intersection point to the x-line gives the centre $y_{1c0} = -F(y_{20})$ of the circle to which the first arc belongs. The arc is drawn from the point M_0 in the direction of the describing point motion corresponding to $\tau \to \tau_0$. Taking the end M_1 of the arc as the next given point of the trajectory the process of construction is reiterated.

In finding the length of individual arcs (M_i, M_{i+1}) one proceeds from the assumption that the angle $\Delta\varphi_i$ subtended by each such arc may increase when the associated slope of the isocline $\varkappa = 0$ to the y-line decreases.

Indeed, if $F(y_2) = \text{const}$ and $\frac{dF}{dy_2} = 0$, the phase trajectories of systems described by Eq. (17.45) become a family of concentric circles.

The ease and the elegance of the Lienard technique are responsible for the fact that starting with 1952 or 1953 a similar construction is also used for purposes other than study of phase trajectories of the system described by Eq. (17.45).

The so-called delta technique (δ-technique) permits construction of integral curves for the systems described by Eq. (17.11) and for the nonautonomous systems whose integral curve equation can be written in the form

$$\frac{dy_2}{dy_1} + \frac{F(y_1, y_2, t)}{y_2} = 0 \qquad (17.48)$$

The method is based on the fact that if the function $F(y_1, y_2, t)$ is single-valued, continuous and differentiable in any point of a chosen sheet of the plane (y_1, y_2) and also is continuous and differentiable with respect to time, then the function $\delta(y_1, y_2, t)$ resulting from identical transformation of Eq. (17.48)

$$\frac{dy_2}{dy_1} + \frac{y_1}{y_2} = -\frac{F(y_1, y_2, t) + y_1}{y_2} = -\frac{\delta(y_1, y_2, t)}{y_2} \qquad (17.49)$$

into Eq. (17.49) also has these properties. The exceptions are, of course, equilibrium states, singular points $y_{2s} = 0$, $y_{1s} = -\delta(y_1, y_2, t)$, but in the vicinity of these points the system can be studied in a different way, as shown in Sec. 17.3. Hence in the vicinity of the specified nonequilibrium state $y_1 = y_{1i}$, $y_2 = y_{2i}$, $t = t_i$ the function δ can be assumed approximately constant, $\delta \approx \delta_i = \text{const}$.

Separating the variables and integrating Eq. (17.49)

$$\int_{y_{2i}}^{y_2} y_2\, dy_2 + \int_{y_{1i}}^{y_1} [\delta(y_{1i}, y_{2i}, t_i) + y_1]\, dy_1 = 0$$

gives an equation similar to Eq. (17.47):

$$y_2^2 + (\delta_i + y_1)^2 = y_{2i}^2 + (\delta_i + y_{1i})^2 = r_i^2 \qquad (17.50)$$

for the arc of the circle passing through the point M_i whose centre lies in the point $y_{1ci} = -\delta_i$, $y_{2c} = 0$.

The essential difference between Eqs. (17.50) and (17.47) is that the value of δ_{i+1} for the subsequent stage of construction cannot be directly obtained by purely graphical means and is instead calculated grapho-analytically using coordinates of the end of the arc $y_1 = y_{1(i+1)}$, $y_2 = y_{2(i+1)}$ and the respective value of $t = t_{i+1}$ which

can be determined as shown below since $y_2 = \frac{dy_1}{dt}$. The complexity of calculations depends on the specifically given function δ. In many cases the method of successive approximations has to be applied.

Determining the time of the describing point motion. Constructing processes as functions of time. The relation of changes in the coordinates of the describing point and the time of its motion is generally defined by the system (17.17).

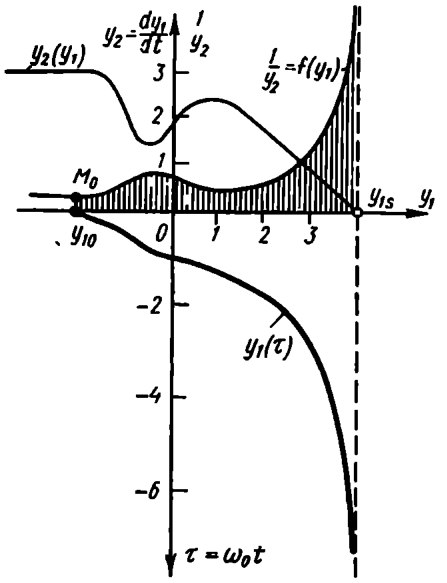

Fig. 17.22

The equation for the arc of the phase trajectory which does not contain the singular points

$$f(y_1, y_{10}, y_2, y_{20}) = 0 \quad (17.51)$$

permits us to essentially eliminate the variable y_1 from the right-hand part of the first equation of system (17.7) or the variable y_2 from the right-hand part of the second equation, following which the interval of the motion time is found by integration

$$\Delta t = t - t_0 = \int_{y_{10}}^{y_1} \frac{dy_1}{P_1(y_1)} = \int_{y_{20}}^{y_2} \frac{dy_2}{P_2(y_2)} \quad (17.52)$$

For small changes of coordinates the approximate relation can be written down

$$\Delta t \approx \frac{\Delta y_1}{P_1(y_{1av}, y_{2av})} = \frac{\Delta y_2}{P_2(y_{1av}, y_{2av})}, \quad f(y_{1av}, y_{2av}) = 0 \quad (17.53)$$

The solution is considerably simplified for systems (17.12) since here $\frac{dy_1}{dt} = P_1(y_1, y_2) = y_2$. The phase trajectory expresses y_2 as an explicit function of y_1, therefore the integral (17.52) can be given in the form

$$t - t_0 = \int_{y_{10}}^{y_1} \frac{1}{y_2(y)}\, dy_1 \quad (17.54)$$

and its determination is reduced to calculating the area under the curve $f(y_1) = \frac{1}{y_2(y_1)}$ reconstructed from the phase trajectory (Fig. 17.22). This operation can be done mechanically using a planimeter.

The time of the describing point motion along the circular arc is especially easy to find. In this case, i.e. at $\zeta = 0$, $\Delta = -k_{12}k_{21} > 0$, the dimensionless phase rate components, as shown in Sec. 17.3, are

$$\left.\begin{aligned} \frac{dy_1}{d\tau} &= -(y_2 - y_{2s}) \\ \frac{dy_2}{d\tau} &= (y_1 - y_{1s}) \end{aligned}\right\} \tag{17.55}$$

where y_{1s}, y_{2s} are coordinates of the *centre*, $\tau = \omega_0 t$.

The integral curve equation

$$\frac{dy_2}{dy_1} = -\frac{y_1 - y_{1s}}{y_2 - y_{2s}}$$

permits separation of variables and integration resulting in

$$(y_1 - y_{1s})^2 + (y_2 - y_{2s})^2 = r^2 = \text{const} \tag{17.56}$$

where

$$r^2 = (y_{10} - y_{1s})^2 + (y_{20} - y_{2s})^2$$

The rate of the describing point motion

$$\frac{ds}{dt} = \omega_0 \frac{ds}{d\tau} = \omega_0 \sqrt{\left(\frac{dy_1}{d\tau}\right)^2 + \left(\frac{dy_2}{d\tau}\right)^2} =$$

$$= \omega_0 \sqrt{(y_1 - y_{1s})^2 + (y_2 - y_{2s})^2} = \omega_0 r = \text{const}$$

is constant and proportional to the radius of the circle, while the time of motion

$$\Delta t = t - t_0 = \frac{1}{\omega_0 r} \int_{s_0}^{s} ds = \frac{1}{\omega_0} (\varphi - \varphi_0) = \frac{\Delta\varphi}{\omega_0}$$

is proportional to the respective increment of the central angle

$$\Delta t = \frac{1}{\omega_0} \Delta\varphi \tag{17.57}$$

The time of scanning the entire circle $\Delta\varphi = 2\pi$ is, as expected, equal to the period of undamped oscillations

$$T = \frac{2\pi}{\omega_0} \tag{17.58}$$

We will now show that if in the phase plane $y_1 = m_1 u$, $y_2 = m_2 \frac{du}{dt}$ (Fig. 17.23*a*) there is a closed trajectory which resembles an ellipse, one of whose axes of symmetry $AB = 2y_{1m}$ lies on the x-axis and the other $CD = 2y_{2m}$ is parallel to the y-axis, then the following *approximate* relations are valid:

$$\left.\begin{aligned} y_1 - y_{1s} &= y_{1m} \sin \omega_0 t = m_1 U_m \sin \omega_0 t \\ y_2 &= y_{2m} \cos \omega_0 t = m_2 \omega_0 U_m \cos \omega_0 t \end{aligned}\right\}$$

whence

$$\omega_0 \approx \frac{m_1}{m_2} \frac{y_{2m}}{y_{1m}}$$

and

$$T = \frac{2\pi}{\omega_0} \approx 2\pi \frac{m_2}{m_1} \frac{y_{1m}}{y_{2m}} = 2\pi m \frac{AB}{CD} \tag{17.59}$$

It should always be remembered that Eq. (17.59) is valid for a trajectory similar to a symmetric ellipse, but not to any oval. So for

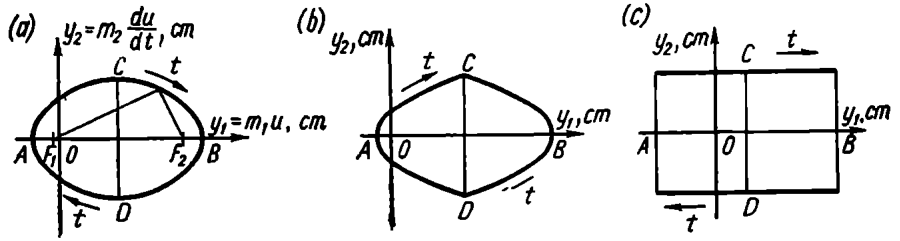

Fig. 17.23

a trajectory consisting of two parabolic segments (Fig. 17.23*b*)

$$T = 8 \frac{m_2}{m_1} \frac{y_{1m}}{y_{2m}} = 8m \frac{AB}{CD}$$

and for a rectangle (Fig. 17.23*c*)

$$T = 4 \frac{m_2}{m_1} \frac{y_{1m}}{y_{2m}} = 4m \frac{AB}{CD}$$

which is quite distinct from Eq. (17.59).

When studying dynamic systems in the phase plane, simple graphical techniques should be preferred whereby the trajectory can be tagged so that the describing point passes along the arc between any adjacent tags within the same specified time interval $\Delta t = c = \text{const}$. Having trajectories so tagged, the phase portrait can easily give, for example, the plots of $y_1(t)$ or $y_2(t)$ starting with the specified value of y_{10} or y_{20}. If necessary, this construction can be effected simultaneously with the tagging.

The method of inscribed isosceles triangles is one of the convenient ways to tag the phase trajectories of the systems described by Eqs. (17.12).

A study of the above methods for constructing phase trajectories of a system described by Eqs. (17.12) leads to the conclusion that the arc (M_i, M_{i+1}) can be represented with sufficient accuracy by an arc of the circle whose centre is on the x-line of the phase plane (Fig. 17.24). Trace from the points M_i and M_{i+1} two secants so

that they intersect on the x-line and make equal angles with the normal to the x-line passed through the intersection point. The angle α_i formed by these secants is always equal to the central angle $\Delta\varphi_i$ subtended by the arc (M_i, M_{i+1}) irrespective of the radius r of the approximating circle and the shift y_{1ci} of its centre.

This signifies that if a sequence of isosceles triangles with the apex angle $\alpha = \text{const}$ (Fig. 17.25*a*) is inscribed between the phase trajectory and the x-axis, then by virtue of Eq. (17.57) the time within which the describing point moves between the apexes of adjacent triangles is constant

$$\Delta t_i = \frac{1}{\omega_0}\alpha = \text{const} \quad (17.60)$$

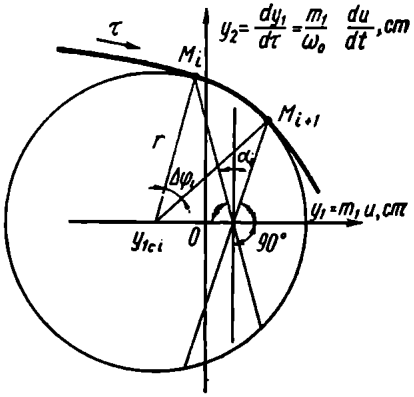

Fig. 17.24

The tagging procedure should now be completed so that the time of motion between the apex of the last triangle on one side of the x-line and the first apex on the other is also described by Eq. (17.60).

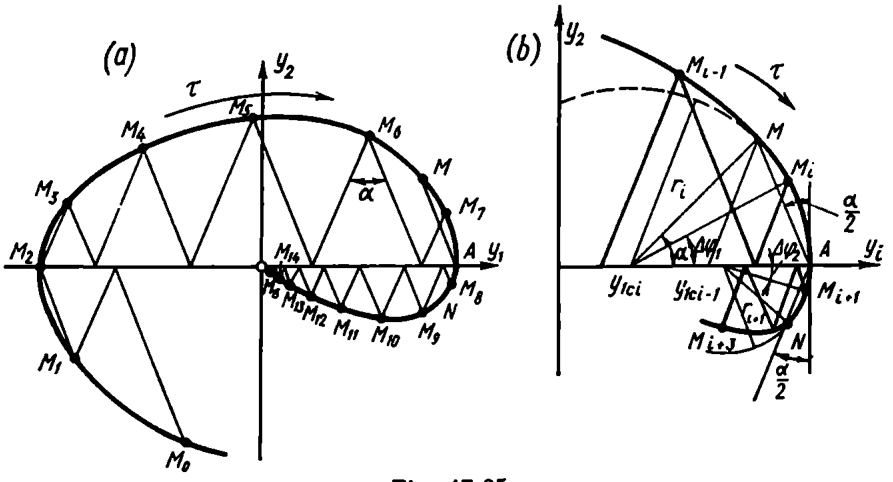

Fig. 17.25

Consider Fig. 17.25*b* where the portion of construction we are interested in is shown in detail. The arcs of the phase trajectory on both sides of the intersection point A can be approximated by the respective circular arcs MA and AN which subtend the equal central angles α. The arc between the points A and M_i resulting from the previous stages of construction subtends the central angle $\Delta\varphi_1 < \alpha$.

From Eq. (17.57) it follows that the arc AM_{i+1} should be constructed so that $\Delta\varphi_1 + \Delta\varphi_2 = \alpha$.

But

$$\frac{\Delta\varphi_1}{\alpha} = \frac{M_iA}{MM_i + M_iA}$$

whence

$$\frac{\Delta\varphi_2}{\alpha} = \frac{\alpha - \Delta\varphi_1}{\alpha} = \frac{MM_i}{MM_i + M_iA}$$

On the other hand,

$$\frac{\Delta\varphi_2}{\alpha} = \frac{AM_{i+1}}{AN}$$

and

$$AM_{i+1} = AN\frac{MM_i}{MM_i + M_iA} \tag{17.61}$$

Therefore when the process has reached the stage of construction of a triangle whose base extends beyond the intersection with the x-line, we should trace from this point A two secants at an angle $\frac{\alpha}{2}$ to the vertical line, find the ratio of the arc MM_i between the end of the secant M and the last point M_i of the tagging to the complete arc MA of the segment and divide the arc AN of the second segment in this ratio. Since the angle α is selected small enough (20° to 40°), in calculations by Eq. (17.61) the arcs can be replaced by chords.

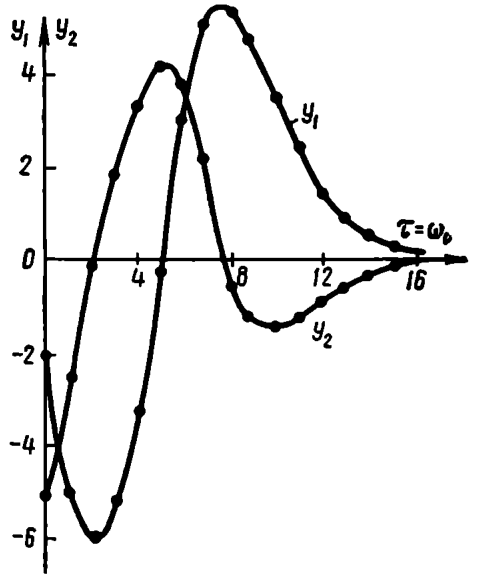

Fig. 17.26

The resultant point M_{i+1} meets the condition (17.60) and permits continuation of the tagging as shown in Fig. 17.25. Figure 17.26 represents plots of $y_1(\tau)$ and $y_2(\tau)$ which are associated with Fig. 17.25*a*.

Let us now analyze the characteristic modes of nonlinear systems using specific examples.

Example 17.5. Study a servo system with a low figure of merit (a pendulum with a constant moment, Ref. 4).

From Example 17.3 it follows that without a rate feedback ($k_{ss} = 0$) and at $A_1 \leqslant 1$ the constraint introduced by the nonlinear element f_2 does not affect the operation of the servo system, and so the differential equations of its phase trajectories (17.17) take

the form

$$\left.\begin{aligned}\frac{dy_1}{d\tau} &= \Omega_m y_2\\ \frac{dy_2}{d\tau} &= -A_1 \sin y_1 - (y_2 - a_1)\end{aligned}\right\} \qquad (17.62)$$

The system misalignment scale $y_1 = \theta$ looks as shown in Fig. 17.27. After an integral number of revolutions it is reset to the initial position.

The cylindrical surface (see Fig. 17.27), however, is not convenient for the construction of phase trajectories or, even more so, for their time tagging. Normally the cylinder is developed into a strip in the phase plane, observing the rule of describing point transfer as shown in Examples 17.1 and 17.3.

In a detailed study of the angle response and follow-up the section line can be conveniently drawn along the generatrix $\pm 180°$ (see Fig. 17.27).

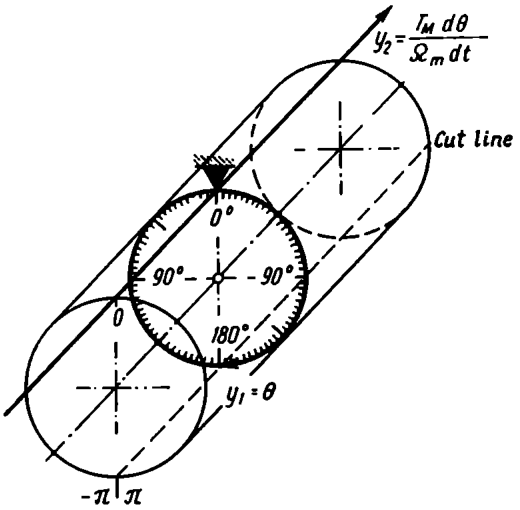

Fig. 17.27

Use the method of isoclines to construct the phase trajectories at different rates of uniform follow-up:

$$a_1 = \frac{1}{\Omega_m}\frac{d\theta_1}{d\tau} = \frac{T_M}{\Omega_m}\frac{d\theta_1}{dt}$$

Equating the right-hand part of the integral curve equation to the given parameter

$$\frac{dy_2}{dy_1} = -\frac{A_1 \sin y_1 + (y_2 - a_1)}{\Omega_m y_2} = \varkappa$$

we have an equation for a family of isoclines

$$y_2 = -\frac{1}{1+\Omega_m \varkappa}(A_1 \sin y_1 - a_1) \qquad (17.63)$$

The isoclines (Fig. 17.28) are sinusoids intersecting in the singular points $y_{2s} = 0$, $y_{1a} = \arcsin \frac{a_1}{A_1}$, $y_{1b} = \pi - \arcsin \frac{a_1}{A_1}$ (see Example 17.4) in whose vicinity the linearized equations of phase trajectories in deviations $x_2 = y_2$, $x_1 = y_1 - y_{1s}$ are

$$\left.\begin{aligned}\frac{dx_1}{d\tau} &= k_{12}x_2 = \Omega_m x_2\\ \frac{dx_2}{d\tau} &= k_{21}x_1 + k_{22}x_2 = -A_1 \cos y_{1s} x_1 - x_2 = \mp\sqrt{A_1^2 - a_1^2}\, x_1 - x_2\end{aligned}\right\}$$

The negative value of the coefficient k_{21} corresponds to the smaller misalignment y_{1a} since

$$A_1 \cos\left(\arcsin\frac{a_1}{A_1}\right) = \sqrt{A_1^2 - a_1^2}$$

and the positive value, to the misalignment y_{1b} because

$$A_1 \cos\left(\pi - \arcsin\frac{a_1}{A_1}\right) = -\sqrt{A_1^2 - a_1^2}$$

The extremal values of isoclines are:

$$y_{2ext} = \frac{A_1 + a_1}{1 + \Omega_m \varkappa} \quad \text{at} \quad y_1 = -\frac{\pi}{2}$$

and

$$y_{2ext} = \frac{a_1 - A_1}{1 + \Omega_m \varkappa} \quad \text{at} \quad y_1 = \frac{\pi}{2}$$

At $a_1 = 0$ (Fig. 17.28) the singular points are located diametrically opposite at the zero and $\pm\pi$ points of the system misalignment scale. The family of isoclines

$$y_1 = -\frac{A_1}{1 + \Omega_m \varkappa} \sin y_1 \tag{17.63a}$$

and the phase portrait are symmetrical relative to the origin of coordinates. Response to the specified misalignment in the position of rest $y_{20} = 0$, $y_1 = y_{10}$, i.e. in points of the x-line, proceeds along the shortest distance with a rotation of the output shaft by not more than $180° + \Delta h_m$, where Δh_m is the maximal overshoot.

The separatrices y_{1b}, a, y_{1a} and y_{1b}, b, c, d of the saddle divide the phase plane into Regions *I*, *II*, *III* of the initial values of the misalignment angle y_{10} and of the rate y_{20} of its change. From these regions the servo system reaches the same stable state $y_{1s} = y_{2s} = 0$ owing to the clockwise rotation of the output shaft by $\theta_{21} \leqslant -(\pi + \Delta h_m)$, $\theta_{21I} \leqslant -2\pi$, $\theta_{21II} \leqslant -4\pi$, respectively. The system response to initial conditions from symmetrical regions *I'*, *II'*, *III'*, ... of the lower half-plane is the counterclockwise rotation of the output shaft. Consequently, at $a_1 = 0$ the system arrives at the origin of coordinates irrespective of the initial conditions, and in this case the origin is referred to as an *absolutely stable* point.

For any actual system the values $y_{20} = \frac{T_M}{\Omega_m}\frac{d\theta_{20}}{dt}$ of the initial drive rates are limited. An open-loop system driven by its own motor cannot ensure an initial rate in excess of $|y_{20}| = A_1$, which corresponds to the amplitude of isocline associated with horizontal tangents (see Fig. 17.28).

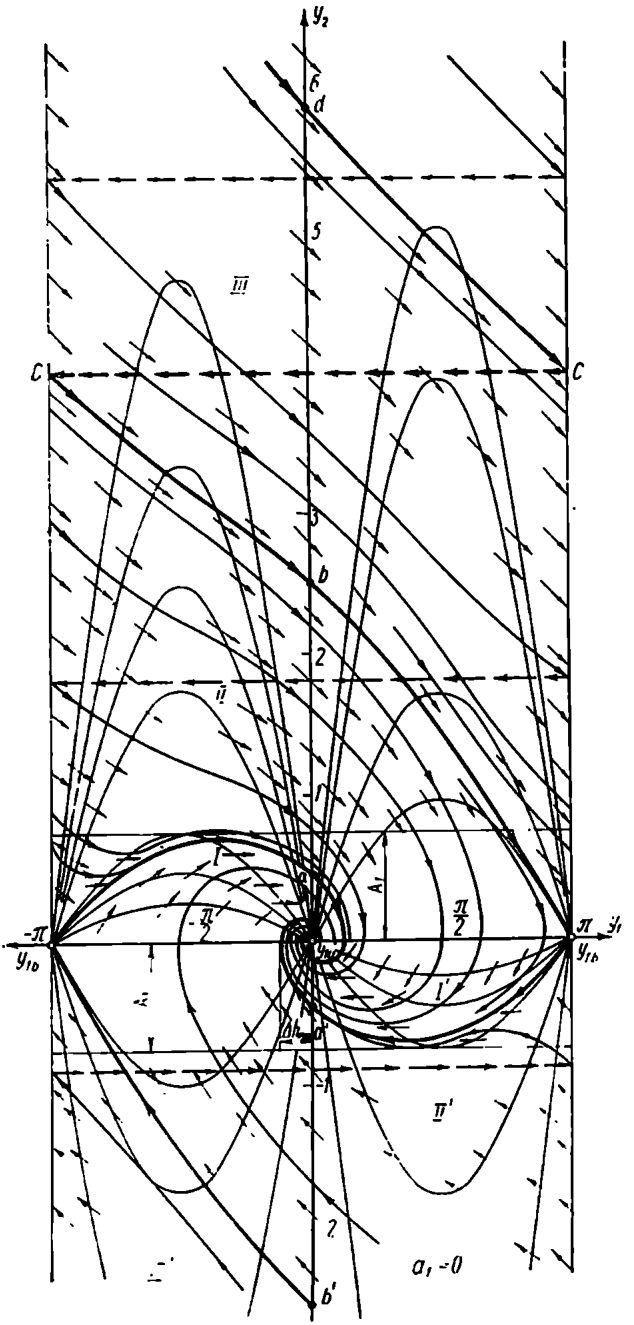

y_2
6
d
5
III
C
C
3
b
2
II
1
I
A_1
$\frac{\pi}{2}$
$-\frac{\pi}{2}$
$-\pi$
y_{1b}
π
y_1
y_{1b}
I'
Δh
a'
-1
II'
2
$a_1 = 0$
b'

Fig. 17.28

The phase portraits of Figs. 17.28-17.30 are constructed for $A_1 = 0.75$, $\Omega_m = 1.75$ at different values of a_1.

At specified rates a_1 of uniform follow-up appreciably below the boundary value $a_1 = A_1$, the system operation (Fig. 17.29*a*) does not change qualitatively.

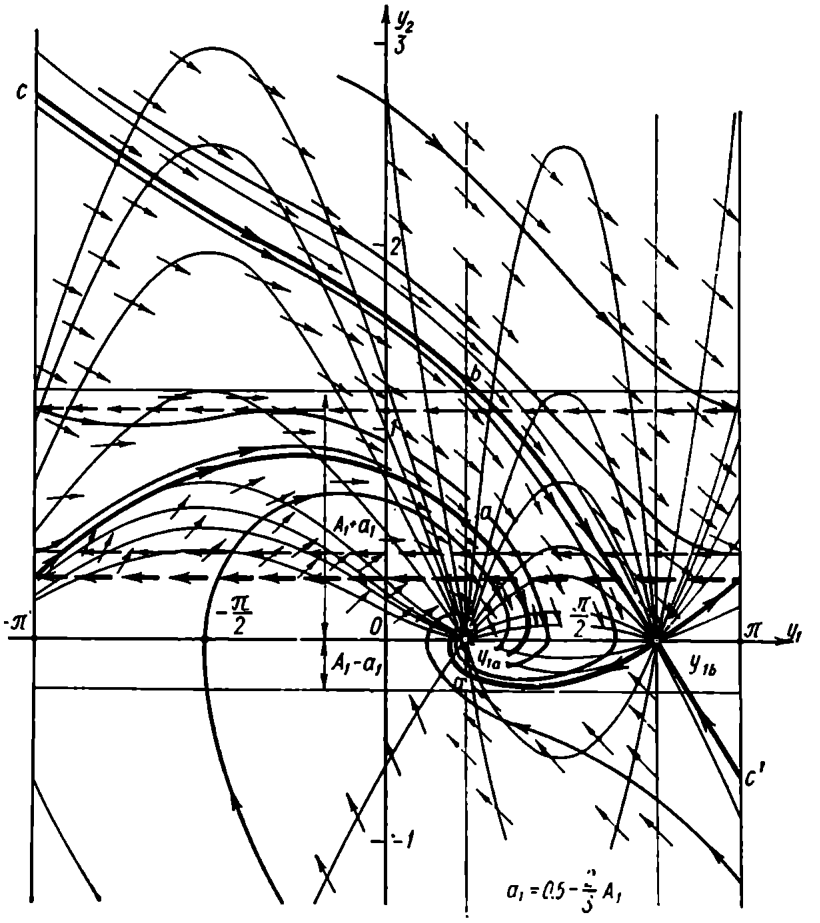

Fig. 17.29*a*

Quantitative changes are characterized by the fact that the singular points y_{1a} and y_{1b} get closer together and tend to the limit value $|y_{1s}| = \frac{\pi}{2}$. The phase portrait becomes asymmetrical.

In the vicinity of the stable singular point y_{1a} the system behaviour depends on the characteristic equation roots. Here we have

$$q^2+q+\Omega_m\sqrt{A_1^2-a_1^2}=0, \quad q=T_M p$$

$$q_{1,2}=\frac{-1\pm\sqrt{1-4\Omega_m\sqrt{A_1^2-a_1^2}}}{2}$$

So the roots are complex if $4\Omega_m\sqrt{A_1^2-a_1^2}=4A>1$.

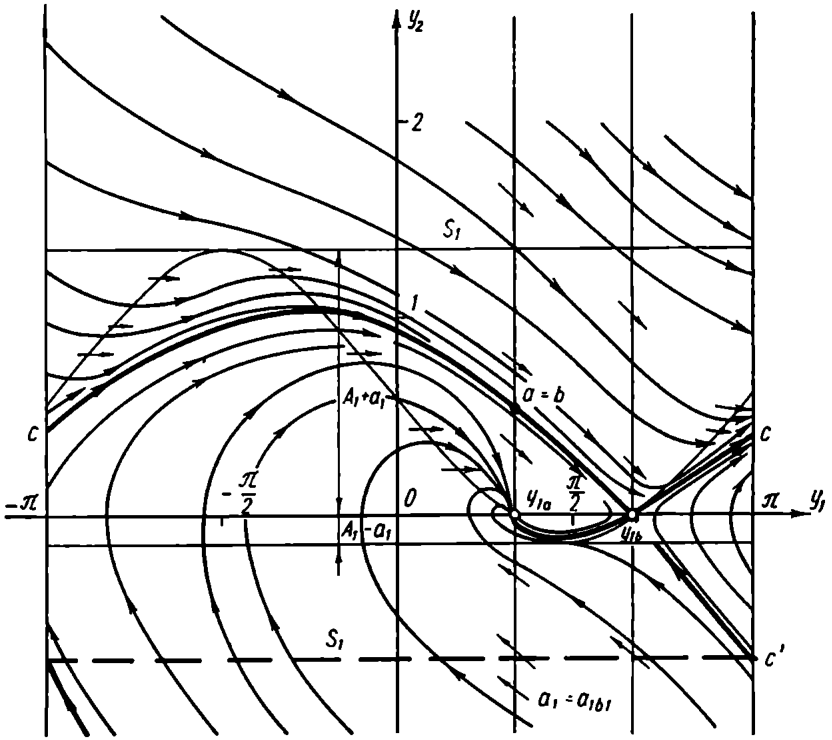

Fig. 17.29*b*

The transient processes are oscillatory but their damping ratio

$$\zeta=\frac{1}{2\sqrt{\Omega_m\sqrt{A_1^2-a_1^2}}}=\zeta_0\frac{1}{\sqrt{1-\frac{a_1^2}{A_1^2}}}$$

increases relatively slowly as compared with the damping ratio ζ_0 found when the system responds to the constant misalignment $a_1=0$.

The unstable singular point is a saddle the initial slope of whose separatrices is, by virtue of Eq. (17.29),

$$\varkappa_{1,2}=\frac{-1\pm\sqrt{1+4\Omega_m\sqrt{A_1^2-a_1^2}}}{2\Omega_m}$$

Figure 17.29*a* is constructed for $a_1 = 0.5 = \frac{2}{3}A_1$.

A comparison of Figs. 17.28 and 17.29*a* shows that the separatrices $y_{1b}\,ay_{1a}$ ($\varkappa_1 > 0$) and $y_{1b}bc$ ($\varkappa_2 < 0$) come closer together in the zone *ab* of the upper half of the phase plane $y_2 > 0$. At a certain boundary value of the parameter a_1 which, according to A. A. Andronov, is *bifurcational* ($a_1 = a_{1b1}$), these lines merge (Fig. 17.29*b*).

Starting with this rotation rate of the input shaft the system behaviour changes qualitatively. The system can no longer respond to the initial misalignments associated with the points *c*, *a*, y_{1b}, *c* above the boundary and consequently steps out of the follow-up mode (goes out of synchronism).

Consider Fig. 17.30*a* plotted for the value $a_1 \approx 0.739 = 0.985A_1$, which is greater than a_{1b1}. The singular point coordinates are

$$y_{1a}=\arcsin 0.985=\frac{8}{18}\pi=80^\circ$$

$$y_{1b}=\pi-y_{1a}=\frac{10}{18}\pi=100^\circ$$

The stable singular point y_{1a} is a node in whose vicinity [see Eq. (17.29)] the common tangent to all phase trajectories is a straight line with an angular coefficient

$$\varkappa_{11}=\frac{-1+\sqrt{1-4\Omega_m\sqrt{A_1^2-a_1^2}}}{2\Omega_m}=-0.2$$

The second singular direction in the vicinity of the node is $\varkappa_{12} = -0.372$.

The saddle separatrices have an initial slope of

$$\varkappa_{21}=\frac{-1+\sqrt{1+4\Omega_m\sqrt{A_1^2-a_1^2}}}{2\Omega_m}=0.109$$

and

$$\varkappa_{22} = -0.639$$

The region of synchronization S_1 is confined by the curve $abcdy_{1b}f$. The latter contains just one asymptotically stable point $y_{1s} = y_{1a}$, $y_{2s} = 0$, to which the describing point tends in the course of time from any initial position belonging to the region S_1. The transient processes are not oscillatory.

Outside the region S_1 all phase trajectories tend to the trajectory ABA, which represents the periodic solution of the system of equations (17.62), a stable limit cycle.

The plots of misalignment change $y_1(\tau)$ and of the rotation of the system's input, $\theta_1(\tau)$, and output, $\theta_2(\tau)$, shafts are constructed

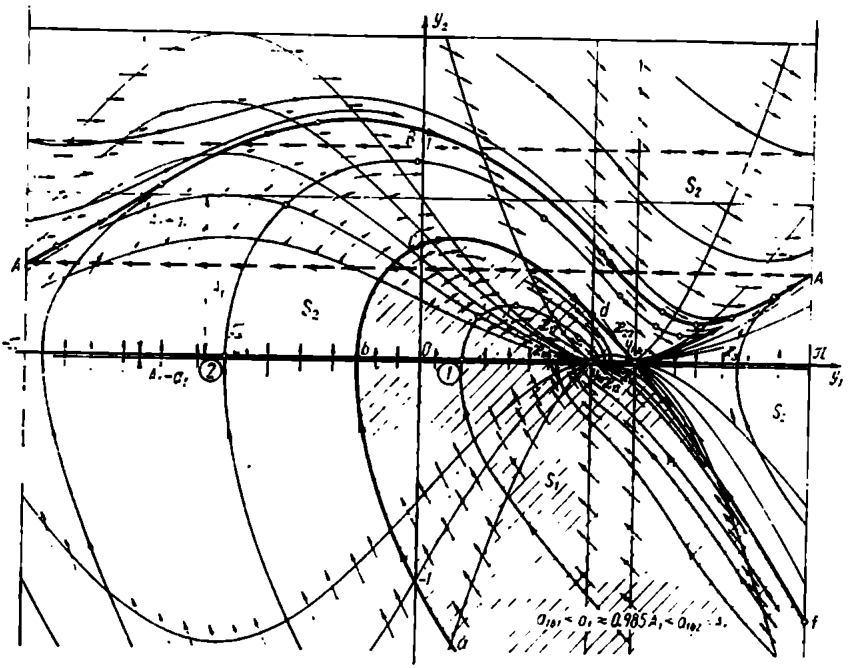

Fig. 17.30*a*

using two tagged trajectories (see Fig. 17.30*a*) and are represented in Fig. 17.31*a* for initial conditions *1* from the region S_1 and in Fig. 17.31*b* for initial conditions *2* outside this region.

Finally, if the rotation rate of the input shaft exceeds the limit value $a_1 = a_{1b2} = A_1$, the system is completely outside the follow-up mode and the only steady-state condition of its operation corresponds to the limit cycle (Fig. 17.30*b*). The system rotates, continuously lagging behind the input shaft, and the rate of this rotation fluctuates periodically about a constant average value. Figure 17.30*b* is plotted for $a_1 = 1 > A_1$.

This example shows that, depending on the specified values of the uniform follow-up rate (parameter a_1), the system (17.62) may exhibit the following modes of operation that are also characteristic of other nonlinear systems.

1. At $|a_1| < a_{1b1} < A_1$ there is, on the phase surface, only one stable singular point $y_1 = y_{1a}$, $y_2 = 0$ characterizing synchronous uniform follow-up. Sooner or later this mode is set up at any initial deflections; consequently, its attraction region covers the entire phase surface.

2. At $a_{1b1} < |a_1| < a_{1b2} = A_1$ there are, on the phase surface, simultaneously a stable singular point $y_1 = y_{1a}$, $y_2 = 0$, whose

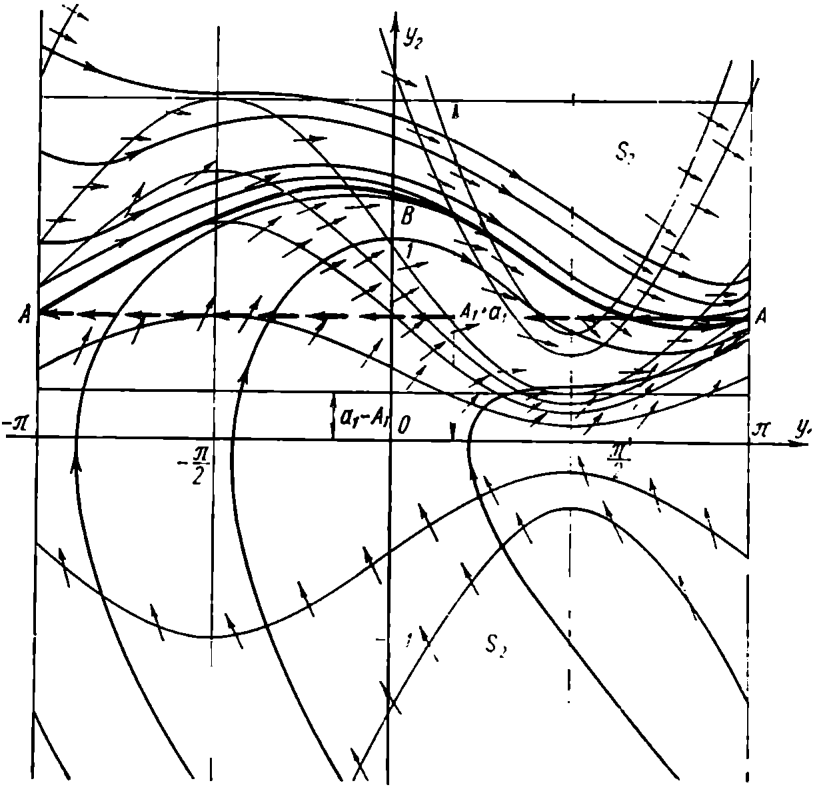

Fig. 17.30*b*

attraction region S_1 is limited by the separatrix of the saddle (see Fig. 17.30*a*), and a stable limit trajectory ABA, which corresponds to periodic oscillations of the rotation rate about its mean value. The amplitude and the period of these oscillations depend on the system parameters and the value of the external action a_1. They are independent of the initial conditions provided these belong to the region S_2 of the limit cycle attraction. The transients for both modes are represented in Fig. 17.31*a* (synchronization) and in Fig. 17.31*b* (asynchronous periodic condition).

3. At $|a_1| > a_{1b2} = A_1$ there exists, on the phase surface, only one stable limit trajectory y_1^c, y_2^c (cycle) ABA, whose attraction region covers the entire phase surface (see Fig. 17.30*b*).

Example 17.6. Study a model of a course stabilization system (autopilot, Ref. 4).

The model is described in Sec. 15.2 and its structural diagram is given in Fig. 15.3. It is assembled of operational amplifiers as in Fig. 17.32*a*, so that the nonlinearity of the pneumatic amplifier is neglected, whereas that of the compensating feedback amplifier is allowed for. The goal is to ascertain the effect of the linear feedback gain specified by the resistance r at the summing input A.

The response z_1 (u_{in}) of the amplifiers is given in Fig. 17.32*b* and the response z_2 (u_{in}) of the nonlinear unit NU of the model in Fig. 17.32*c*.

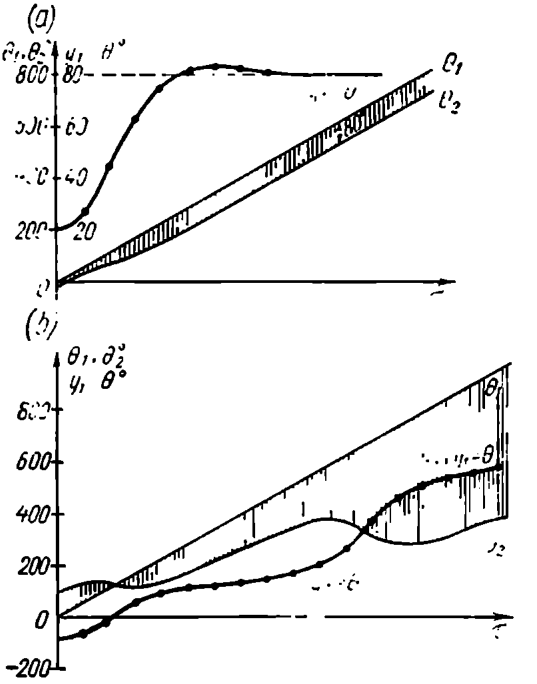

Fig. 17.31

Owing to the saturation of the operational amplifiers, $|z_1| \leqslant \leqslant 100$ V, the phase variables are rigidly constrained, and the phase plane is a square (Fig. 17.33).

On the linear section z_1 the gain $|k| = 10^5 \gg 1$ and, as shown in Sec. 5.7, these amplifiers can integrate differential equations (simulate elements of dynamic systems).

From the circuit of Fig. 17.32*a* it follows directly that the model solves the equation

$$\frac{d^2y_1}{dt^2} = z_2 \frac{dy_1}{dt} + k\frac{dy_1}{dt} - y_1, \quad k = \frac{1}{r}\,\text{Mohm} \tag{17.64}$$

at the initial conditions

$$y_1 = y_{10}, \qquad y_2 = \frac{dy_1}{dt} = y_{20}$$

The resultant equation is reducible to Eq. (17.45) assuming that $F(y_2) = z_2(y_2) - ky_2$, $\omega_0 = 1$. Let us use the Lienard technique to construct the phase portrait.

If the describing point intersects the isocline corresponding to horizontal tangents before or after intersecting the vertical axis $y_1 = 0$, then the deflection of the describing point from the origin

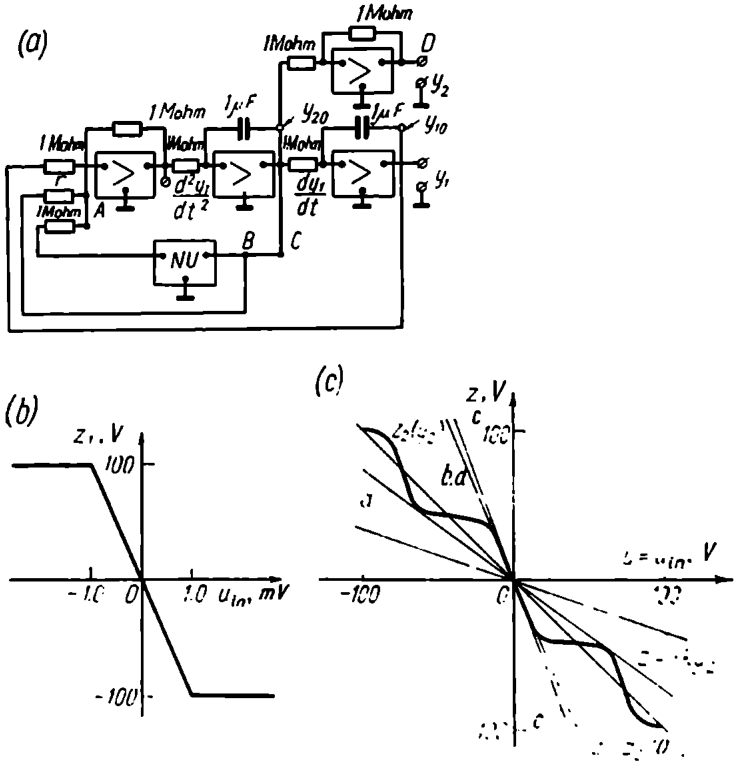

Fig. 17.32

of coordinates decreases or increases, respectively. The regions where this occurs are denoted as *I* or *II* in Fig. 17.33.

At comparatively large initial values of r the straight line $z = -ky_2$ intersects the curve $z_2(y_2)$ only in the origin of coordinates (see Fig. 17.32*c*). In this case the isocline $y_1 = ky_2 - z_2(y_2)$ corresponding to horizontal tangents lies within the second and fourth quadrants of the phase plane.

Figure 17.33*a* is the phase portrait for $k = 0.75$, $r = 1.34$ Mohm when the straight line z touches the curve z_2 (portion *a* in Fig. 17.32*c*). The sole steady state of the system is seen to correspond to the stable equilibrium point at $y_{1s} = y_{2s} = 0$. In the vicinity of this point the system acts according to the linearized equation

$$\frac{d^2y_1}{dt} + 2\zeta\frac{dy_1}{dt} + y_1 = 0$$

where

$$\zeta = -\frac{1}{2}\left(\frac{dz_2}{dy_2}_{y_2=0} + k\right) = \frac{1}{2}(2.5-0.75) = 0.875 < 1$$

The system is analogous to a stable oscillatory element with strong damping.

The situation is quite different at $k = 1$, $r = 1$ Mohm, which corresponds to the position b of the straight line z (see Fig. 17.32c).

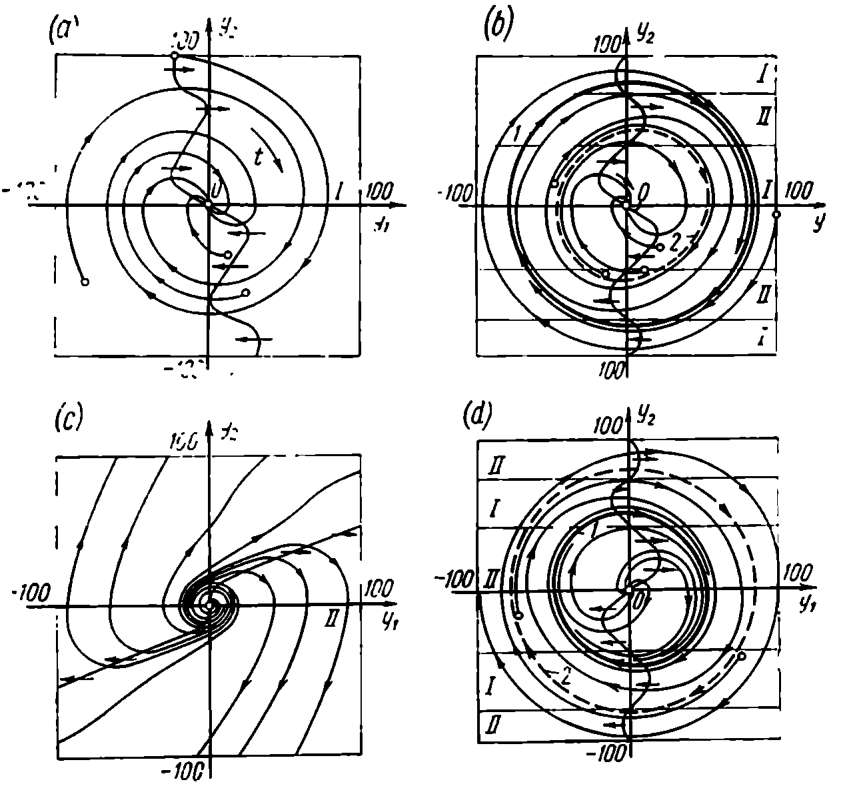

Fig. 17.33

In this case the isocline corresponding to a horizontal tangent (Fig. 17.33b) repeatedly intersects the y-axis of the phase plane. Apart from the stable equilibrium (rest) state at the point $y_{1s} = y_{2s} = 0$, the system is seen to be able to perform undamped oscillations whose amplitude and frequency do not depend on the initial conditions provided that the latter are inside the attraction region of stable limit cycle *1*. This operational condition is known as *self-oscillations* and the system itself is *self-oscillatory*. In the case in

question it is important that self-oscillations cannot arise unless the system is given the initial deflection taking it out of unstable limit cycle *2*, which has the equilibrium attraction area inside it. This generation of self-oscillations is known as *rigid*, or *hard*.

In further reduction of the resistance r the straight line $z = -ky_2$ (see Fig. 17.32*c*) rotates clockwise, the isocline corresponding to horizontal tangents (Fig. 17.33) is shifted to the first and third quadrants, the amplitude of stable, *1*, and unstable, *2*, cycles increases. Once this straight line coincides with the line $z = \frac{ydz}{dy}\Big|_{y=0}$ the entire isocline $\varkappa = 0$ shifts to the other side of the y-axis and the stability of the equilibrium is disturbed. The system acts as shown in Fig. 17.33*c* constructed for $k = 5$, $r = 0.2$ Mohm (position *c* in Fig. 17.32*c*).

A model of a self-oscillating system with soft excitation is obtained if the signal fed to the nonlinear element z_2 and the resistor r is inverted, i.e. the input B is connected to the point D (see Fig. 17.32*a*).

Then the differential equation (17.64) takes the form

$$\frac{d^2y_1}{dt^2} = -z_2\frac{dy_1}{dt} - k_1\frac{dy_1}{dt} - y_1 \qquad (17.65)$$

and the isocline $y_1 = -F(y_2)$ corresponding to horizontal tangents changes sign. Figure 17.33*d* represents the phase portrait for $r = 1$ Mohm, $k = 1$ (position *d* in Fig. 17.32*c*). The singular point is an unstable focus, curve *1* is a stable limit cycle. Outside unstable cycle *2* the system is unstable and the processes therein depend on constraints on the amplifier responses $z_1 = 100$ V.

This example shows that, given proper parameters, undamped oscillations may arise in an autonomous nonlinear system. The shape and period of these does not depend on the initial conditions if they belong to the attraction region of this mode and are a function of the system responses alone. These modes are known as self-oscillations and systems where they are observed are self-oscillatory.

17.5. PIECEWISE-LINEAR SYSTEMS

The preceding sections and the examples cited there lead to the conclusion that processes in the nonlinear system (17.6) can be constructed with the required accuracy if functions P_1 and P_2 are numerically defined.

Major difficulties arise in solving the basic problems of control system design and calculation:

—system analysis, i.e. studies of the dependence of operational modes on the element parameters;

—system synthesis, i.e. selection of the system structure and values of the element parameters so as to ensure the desired or the best (in a specified sense) performance.

Tangible results have been obtained for two specific classes of dynamic systems:

1. For generators of undamped harmonic oscillations (such systems include, in particular, the system of Example 17.6). They are discussed in detail in the theory of oscillations (Ref. 4) and special technical courses on development and use of periodic signal generators.

2. For systems whose nonlinear element characteristics can be represented as segments of straight lines (piecewise-linear systems). These systems are of special interest in the theory and practice of automatic control.

As shown in Sec. 15.4 a broken piecewise-linear response can be obtained in approximating the smooth response $z(x)$. Thus, a single-valued response of an electronic amplifier may lead to a saturation-type nonlinearity (see Fig. 15.2), and a family of experimental cycles, in which a ferromagnetic core is remagnetized, can lead to a magnetic-hysteresis-type nonlinearity (see Fig. 15.22). It will be remembered that such approximation should not affect the system performance analysis. In other words, the number and type of singular points, the qualitative picture of the boundaries of their attraction regions, the presence and stability of limit cycles should not change in approximating; a powerful tool for checking the admissibility of the adopted piecewise-linear approximation is comparison of analysis results and results of simulation of the original system.

It is important that in most essentially nonlinear control systems the piecewise-linear mathematical description is not obtained from approximation of smooth curves but follows from the physical nature of the elements used in the systems. Such are elements with abruptly changing mechanical (play, stop) or electric (relay, switch) contact and contactless circuits with similar responses (semiconductor relay, gate, flip-flop).

A discontinuous piecewise-linear response is a natural representation of experimental properties of such elements (see Sec. 15.5).

Let us see how piecewise-linear element responses affect the system phase plane. Each linear portion of the responses $z_i(y_1)$ and $z_j(y_2)$ of elements incorporated into the system which does not contain break and discontinuity points is associated with a separate area or sheet $k = a, b, c, \ldots$, within which the right-hand parts of the differential equation system (17.7) are linear for both phase variables. Thus,

$$\left.\begin{aligned} \frac{dy_1}{dt} &= k_{10} + k_{11}y_1 + k_{12}y_2 \\ \frac{dy_2}{dt} &= k_{20} + k_{21}y_1 + k_{22}y_2 \end{aligned}\right\} \qquad (17.66)$$

where $k_{10} = P_{1k}(y_1 = 0, y_2 = 0) = P_{1k}(0)$ and $k_{20} = P_{2k}(0)$.

The coordinates of the singular point $\frac{dy_1}{dt} = \frac{dy_2}{dt} = 0$ are

$$y_{1s} = \frac{-k_{10}k_{22} + k_{20}k_{12}}{k_{11}k_{22} - k_{12}k_{21}} \quad \text{and} \quad y_{2s} = \frac{k_{10}k_{21} - k_{20}k_{11}}{k_{11}k_{22} - k_{12}k_{21}} \tag{17.67}$$

Because a sheet is limited, the singular point is often found outside it. Moreover, it is not the system equilibrium point, and its vicinity is inaccessible to the describing point moving along the phase trajectory.

Since, from Eq. (17.66), $k_{10} = -(k_{11}y_{1s} + k_{12}y_{2s})$ and $k_{20} = -(k_{21}y_{1s} + k_{22}y_{2s})$, the differential equations of phase trajectories can be simplified to suit Eq. (17.19)

$$\left.\begin{aligned} \frac{dy_1}{dt} &= k_{11}(y_1 - y_{1s}) + k_{12}(y_2 - y_{2s}) \\ \frac{dy_2}{dt} &= k_{21}(y_1 - y_{1s}) + k_{22}(y_2 - y_{2s}) \end{aligned}\right\} \tag{17.68}$$

The difference between Eqs. (17.68) and (17.19) is that the singular point is shifted from the origin of coordinates to the point with the coordinates (17.67), and hence the entire analysis given in Sec. 17.3 is applicable to each sheet of the phase plane for the piecewise-linear system.

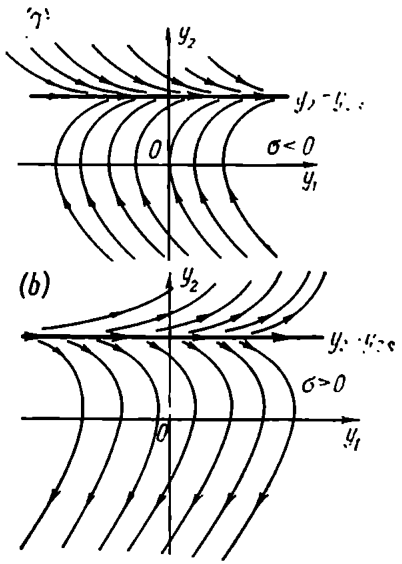

Fig. 17.34

One special degenerate case is $\Delta = 0$. In particular, at

$$\left.\begin{aligned} \frac{dy_1}{dt} &= y_2 \\ \frac{dy_2}{dt} &= \sigma(y_2 - y_{2s}) \end{aligned}\right\} \tag{17.69}$$

which is different from Eq. (17.41) only in the presence of the constant component $k_{20} = P_2(0) = -\sigma y_{2s}$, the phase portrait is not akin to Fig. 17.20.

The equation of integral curves in this case is of the form

$$\frac{dy_2}{dy_1} = \sigma \frac{y_2 - y_{2s}}{y_2} \tag{17.70}$$

The isoclines are the straight lines

$$y_2 = -\frac{\sigma y_{2s}}{\varkappa - \sigma} \tag{17.71}$$

parallel to the x-line, while the isocline corresponding to horizontal tangents, $\varkappa = 0$ $y_2 = y_{2s}$ (Fig. 17.34). is at the same time the limit phase trajectory of the system.

Integrating the second equation (17.69) and then the first one gives a parametric expression for the family of phase trajectories

$$\left.\begin{aligned} y_2 - y_{2s} &= (y_{2k} - y_{2s})\, e^{\sigma(t-t_k)} \\ y_1 - y_{1k} &= \frac{1}{\sigma}(y_{2k} - y_{2s})\,(e^{\sigma(t-t_k)} - 1) + y_{2s}\,(t - t_k) \end{aligned}\right\} \quad (17.72)$$

The system (17.72) permits elimination of the parameter t; following this, y_1 is expressed as an explicit function of y_2:

$$\sigma\,(y_1 - y_{1k}) = (y_2 - y_{2k}) + y_{2s} \ln \left| \frac{y_2 - y_{2s}}{y_{2k} - y_{2s}} \right| \quad (17.73)$$

The shape of phase trajectories at $\sigma < 0$ (a neutral system) is shown in Fig. 17.34*a* and at $\sigma > 0$ (an unstable system), in Fig. 17.34*b*.

At $\sigma = 0$

$$\left.\begin{aligned} \frac{dy_1}{dt} &= y_2 \\ \frac{dy_2}{dt} &= C \end{aligned}\right\} \quad (17.74)$$

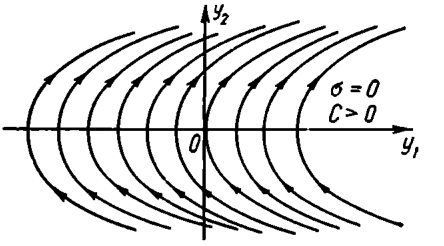

Fig. 17.35

In this strongly degenerate case of two integrating elements connected in series, the phase trajectories are a family of parabolas, equidistant along the x-line

$$y_1 - y_{1k} = \frac{1}{2C}(y_2 - y_{2k})^2 \quad (17.75)$$

plotted in Fig. 17.35.

A break or rupture in the piecewise-linear response $z_l\,(y)$ at the point of conjugation of adjacent linear parts represents the boundary of a phase sheet.

We will consider two types of intersheet transition:

(a) transition with preservation of continuity in the right-hand part of differential equations (17.66) and thus of the phase rate components. This is typical of continuous piecewise-linear systems;

(b) transition with a rupture of phase rate component values but with preservation of continuity of phase trajectories. This is typical of piecewise-linear systems with switching.

Continuous piecewise-linear systems. Since the functions $P_1\,(y_1, y_2)$ and $P_2\,(y_1, y_2)$ change while preserving continuity, the isoclines of the system (17.66) are also continuous polygonal lines. The phase trajectories have no inflections. A characteristic example is a servo system with a limited rate of the actuating motor.

Example 17.7. Study the response of a servo system to the specified constant misalignment $\theta_1 = \text{const}$ if $A_1 = 2$, $\Omega_m = 1$, $k_{ss} = 0$.

From Example 17.3 it follows that the system of differential equations of phase trajectories is

$$\left.\begin{aligned} \frac{dy_1}{d\tau} &= y_2 \\ \frac{dy_2}{d\tau} &= -f_2(2\sin y_1) - y_2, \quad |f_2| \leqslant 1 \end{aligned}\right\}$$

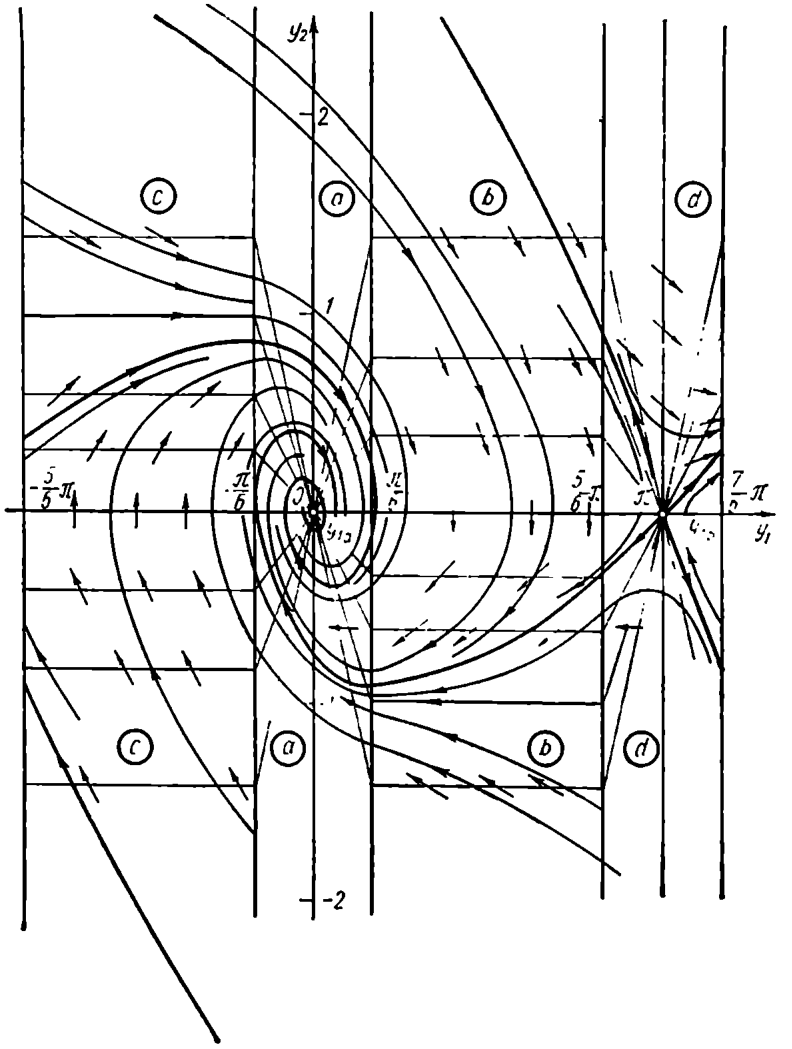

Fig. 17.36

The phase plane is divided into four sheets (Fig. 17.36).

Sheet *a*. The linear zone of small angles is

$$|2 \sin y_1| \leqslant 1, \qquad \frac{d \sin y_1}{dy_1} > 0$$

The sheet boundaries are the vertical straight lines $y_1 = \arcsin -\frac{1}{2} = -\frac{\pi}{6}$ and $y_1 = \arcsin \frac{1}{2} = \frac{\pi}{6}$. Within these values of the argument it can be approximately assumed that $\sin y_1 = y_1$, whence

$$\left.\begin{aligned} \frac{dy_1}{d\tau} &= y_2 \\ \frac{dy_2}{d\tau} &= -y_1 - y_2 \end{aligned}\right\}$$

The singular point $y_{1s} = y_{2s} = 0$ is a stable focus; the transient processes are oscillatory with the damping ratio $\zeta = \frac{1}{2}$.

Sheet *b*. The positive saturation area $f_2 = 1$. $\frac{\pi}{6} < y_1 < \pi - \frac{\pi}{6} = \frac{5}{6}\pi$, whence

$$\left.\begin{aligned} \frac{dy_1}{d\tau} &= y_2 \\ \frac{dy_2}{d\tau} &= -y_2 - 1 \end{aligned}\right\}$$

which corresponds to Eq. (17.69) at $\sigma = -1$, $y_{2s} = -1$.

From Eq. (17.71) it follows that the family of isoclines is $y_{2b} = -(1 + \varkappa)^{-1}$. By virtue of Eq. (17.72), a parametric equation of the phase trajectory is

$$\left.\begin{aligned} y_2 + 1 &= (y_{2b} + 1)\, e^{-(\tau - \tau_b)} \\ y_1 - y_{1b} &= (y_{2b} + 1)\,[1 - e^{-(\tau - \tau_b)}] - (\tau - \tau_b) \end{aligned}\right\} \qquad (17.76)$$

and from Eq. (17.73) follows an equation with the parameter τ eliminated

$$y_1 - y_{1b} = y_{2b} - y_2 + \ln \left| \frac{y_2 + 1}{y_{2b} + 1} \right| \qquad (17.77)$$

The phase trajectories in areas of amplifier positive saturation, when the linear part of the system is under constant action, are equidistant along the x-line and tend in the course of time to the singular straight line $y_2 = -1 = \text{const}$, which represents uniform motor rotation.

Sheet *c*. The area of negative saturation is

$$f_2 = -1, \quad -\frac{5}{6}\pi < y_1 < \frac{\pi}{6}$$

Then

$$\left.\begin{aligned}\frac{dy_1}{d\tau}&=y_2\\ \frac{dy_2}{d\tau}&=-y_2+1\end{aligned}\right\}$$

whence $\sigma=-1$, $y_{2s}=1$. The isocline equation is then $y_2=-(1-\varkappa)^{-1}$.

The phase trajectories of Sheet *c*

$$\left.\begin{aligned}y_2-1&=(y_{2c}-1)\,e^{-(\tau-\tau_c)}\\ y_1-y_{1c}&=(y_{2c}-1)\,[1-e^{-(\tau-\tau_c)}]+(\tau-\tau_c)\end{aligned}\right\} \qquad (17.78)$$

as shown in Fig. 17.36, are symmetrical to phase trajectories of Sheet *b*. In the explicit form

$$y_1-y_{1c}=y_{2c}-y_2-\ln\left|\frac{y_2-1}{y_{2c}-1}\right| \qquad (17.79)$$

Sheet *d*. The linear zone of angles close to π is

$$|2\sin y_1|\leqslant 1, \quad \frac{d\sin y_1}{dy_1}<0$$

The boundaries of the sheet are the verticals

$$y_1=\arcsin\frac{1}{2}=\pi-\frac{\pi}{6}=\frac{5}{6}\pi \text{ and } y_1=\arcsin\left(-\frac{1}{2}\right)=\pi+\frac{\pi}{6}=\frac{7}{6}\pi$$

Within these values of y_1 it can be approximately assumed that $\sin y_1\approx\pi-y_1$, whence

$$\left.\begin{aligned}\frac{dy_1}{d\tau}&=y_2\\ \frac{dy_2}{d\tau}&=y_1-y_2+\pi\end{aligned}\right\}$$

The singular point $y_{1s}=\pi$, $y_{2s}=0$ is a saddle the slope of whose separatrices is

$$\varkappa_{1,2}=\frac{-1\pm\sqrt{5}}{2}$$

and the separatrix equations are

$$y_2=-\frac{1+\sqrt{5}}{2}(y_1-\pi)\approx-1.618\,(y_1-\pi)$$

and

$$y_2=\frac{\sqrt{5}-1}{2}(y_1-\pi)\approx 0.618\,(y_1-\pi)$$

respectively.

Smoothness of the phase trajectory transition from one sheet to another and continuity of isoclines are demonstrated in Fig. 17.36.

Piecewise-linear systems with discontinuous nonlinearities. The boundaries of sheets in crossing which the right-hand part of differential equations (17.66) is disrupted are called *switching lines.*

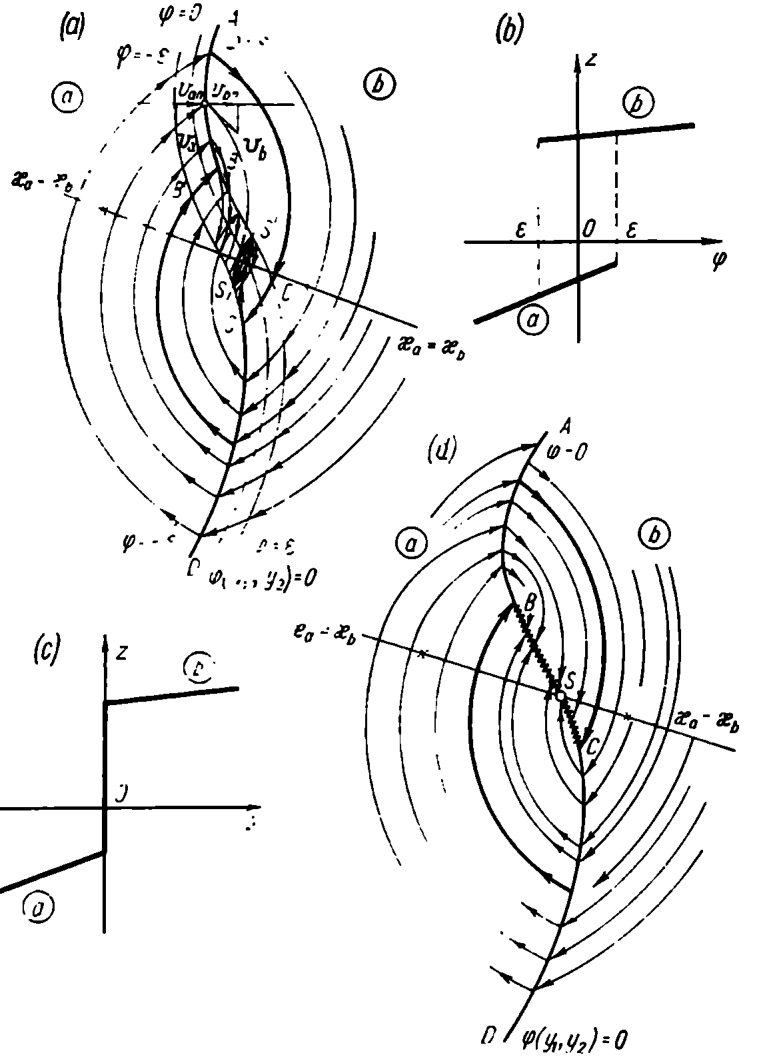

Fig. 17.37

The direction of the phase trajectory on one side of a switching line generally does not coincide with the direction on the other side.

Figure 17.37*a* demonstrates the transition from Sheet *a* to Sheet *b* of the phase plane corresponding to switching with hysteresis 2ε as defined by the response (Fig. 17.37*b*) of the switching element.

Once it reaches the line $\varphi(y_1, y_2) = \varepsilon < 0$ on the interval AB the describing point passes to Sheet b as a result of the switching. This transition is possible because the vector $\mathbf{v}_a$ of the phase rate before switching is directed to the switching line and the vector $\mathbf{v}_b$ after switching, away from it. The projections of the phase rate vectors v_{an} and v_{bn} onto the normal to the switching line have the same sign. The phase trajectory leaves the hysteresis strip, breaks and passes on to Sheet b.

The picture changes if the vector $\mathbf{v}_b$ of the phase rate is directed to the switching line (see the interval BC). The projections v_{an} and v_{bn} have opposite signs and the phase rate vectors $\mathbf{v}_a$ and $\mathbf{v}_b$ are directed towards each other. Following the switching, the describing point is shifted inside the hysteresis strip $-\varepsilon < \varphi(y_1, y_2) < \varepsilon$. The rate of its motion along that strip depends on the difference of shifts corresponding to each two switchings or, approximately, the difference of phase vector tangential projections in the switching points.

If at the ends of the strip $BB'CC'$ the vectors of this difference are directed towards each other, there is at least one stable limit cycle SS' to which the describing point tends and which is related to a self-oscillating condition whose frequency and amplitude *completely depend on the switching element parameters* (the hysteresis loop width) and the *adjustment of the element* (the switching line slope). Note that the symmetry axis of the limit cycle is the common isocline $\varkappa_a = \varkappa_b$ of Sheets a and b.

If the hysteresis loop width is negligibly small ($\varepsilon \to 0$) and the switching element response can be regarded as ideal (hysteresisless) (Fig. 17.37*c*), then the strip $-\varepsilon < \varphi < \varepsilon$ contracts into the switching line $\varphi = 0$ (Fig. 17.37*d*) with portions of attraction (switching) AB and CD and portions of repulsion, the *sliding mode*, BC, where the switching element (relay) acts in *vibrational conditions*. The switching frequency depends on the parameters of the relay itself and is so high that the plant responds only to variations of the signal mean value. The limit cycle SS' shrinks into the singular point S of the sliding mode which lies at the intersection of the switching line $\varphi = 0$ with the common isocline $\varkappa_a = \varkappa_b$ of the phase plane sheets. If this singular point is stable as in Fig. 17.37*d*, then it represents steady stabilization of the plant in the vibrational high-frequency switching mode of the control unit.

Chapters XV and XVI were concerned with possible functions of a relay switch. Consider its operation in switching a signal acting on a plant with constant parameters.

Example 17.8. Study the response to a specified initial misalignment $-\frac{\pi}{2} \leqslant \theta_0 \leqslant \frac{\pi}{2}$ in a servo system whose amplifier is a three-positional relay with hysteresis the response of which was

discussed in Sec. 15.6 and shown in Fig. 15.18c. A structural diagram of such a system is shown in Fig. 17.38a.

According to Eqs. (17.13), (17.15), and (15.25)

$$k_M u_M = T_M \frac{d\omega_M}{dt} + \omega_M, \quad \omega_M = \frac{d\theta_2}{dt},$$

$$u_1 = f_1(\theta) = U_{1m} \sin \theta = U_{1m} \sin (\theta_1 - \theta_2),$$

$$u_2 = u_1 - u_{com}, \quad u_{com} = k_{com}\omega_M,$$

$$u_M = f_2(u_2) = \begin{cases} z_b \operatorname{sign} u_2 & \text{at} \quad |u_2| > x_b \\ 0 & \text{at} \quad |u_2| < x_a \end{cases}$$

The system is supposed to respond to a limited initial misalignment θ_0. Also, for a relay of sufficiently high sensitivity $x_a \leqslant x_b \ll U_{1m}$. These constraints lead to the assumption that $\theta = -\theta_2$, $u_2 \approx U_{1m}\theta + k_{com}\frac{d\theta}{dt}$.

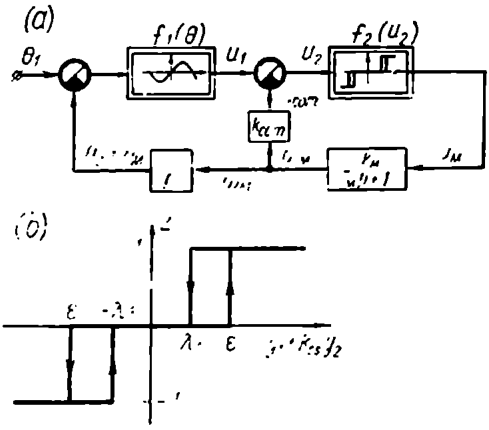

Fig. 17.38

Let us introduce dimensionless time $\tau = \frac{1}{T_M} t$ and phase variables $y_1 = \frac{1}{k_M z_b T_M}\theta$, $y_2 = \frac{dy_1}{d\tau}$. Then the system of differential equations of phase trajectories takes the form

$$\left.\begin{aligned} \frac{dy_1}{d\tau} &= y_2 \\ \frac{dy_2}{d\tau} &= -z(y_1 - k_{ss}y_2) - y_2 \end{aligned}\right\} \tag{17.80}$$

where the function

$$z = \begin{cases} \operatorname{sign}(y_1 - k_{ss}y_2), & |y_1 - k_{ss}y_2| > \lambda\varepsilon \\ 0, & |y_1 - k_{ss}y_2| < \varepsilon \end{cases}$$

as shown in Fig. 17.38b. With an allowance for the scale selected

$$k_{ss} = \frac{k_{com}}{U_{1m}}, \qquad \varepsilon = \frac{x_a}{k_M U_{1m} z_b T_M}, \qquad \lambda = \frac{x_b}{x_a}$$

Each of the three constant values, 0, 1, and -1, of the function z is associated with a sheet of the phase plane (Fig. 17.39).

The dead zone ($z = 0$) is represented by Sheet a confined by two straight switching lines

$$y_2 = -\frac{y_1 - \varepsilon}{k_{ss}} \quad \text{and} \quad y_2 = -\frac{y_1 + \varepsilon}{k_{ss}}$$

The system of differential equations for phase trajectories

$$\left.\begin{aligned} \frac{dy_1}{d\tau} &= y_2 \\ \frac{dy_2}{d\tau} &= -y_2 \end{aligned}\right\} \tag{17.81}$$

coincides with Eqs. (17.41) at $\sigma = -1$. The phase trajectories on this sheet are, according to Eqs. (17.42) and (17.43), straight lines

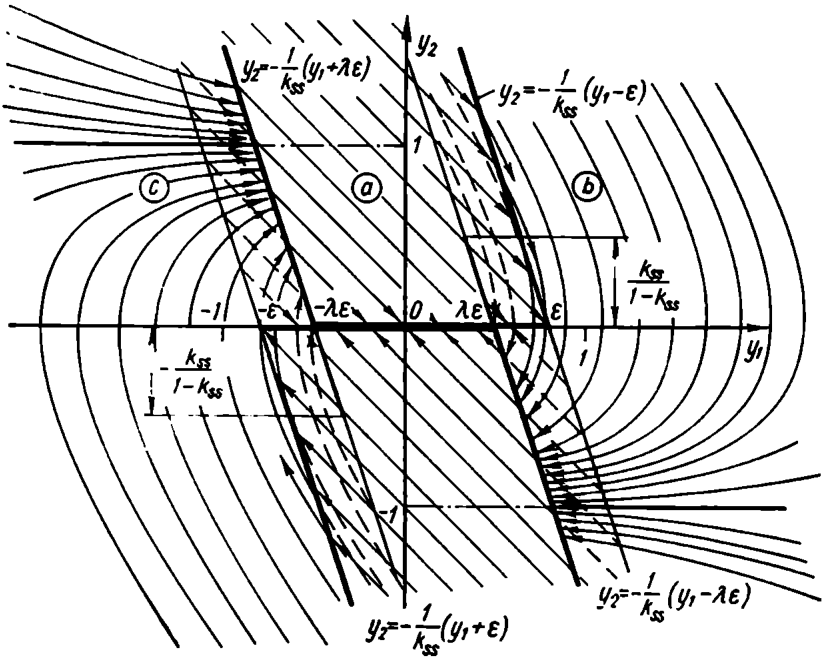

Fig. 17.39

inclined at an angle of $-45°$ to the x-line; along these lines the describing point tends to the segment of rest $-\varepsilon \leqslant y_1 \leqslant \varepsilon$. Owing to hysteresis the neighbouring sheets partially overlap this one.

Sheet b corresponds to the positive value $z = 1$. The differential equations of phase trajectories

$$\left.\begin{aligned} \frac{dy_1}{d\tau} &= y_2 \\ \frac{dy_2}{d\tau} &= -y_2 - 1 \end{aligned}\right\} \tag{17.82}$$

coincide with Eqs. (17.69) at $\sigma = -1$, $y_{2s} = -1$. The family of phase trajectories satisfies equalities (17.76) and (17.77) and is identical with the one constructed on Sheet *b* (see Fig. 17.36). The behaviour of the relay system with the relay switched on is similar to that of a continuous system in the amplifier saturation zone.

The switching line is the straight line $y_2 = -\frac{y_1 - \lambda_\varepsilon}{k_{ss}}$ which is parallel to the right-hand switching line of Sheet *a* and at $1 > \lambda > 0$ it passes between this line and the origin of coordinates.

The negative value $z = -1$ is associated with Sheet *c* within which

$$\left.\begin{aligned} \frac{dy_1}{d\tau} &= y_2 \\ \frac{dy_2}{d\tau} &= -y_2 + 1 \end{aligned}\right\} \qquad (17.83)$$

and the phase trajectories calculated by Eqs. (17.78) and (17.79) are symmetrical to phase trajectories of Sheet *b* relative to the origin of coordinates.

Consider several specific cases.

1. A system without rate feedback (Fig. 17.40*a*, *b*, *c*).

At $k_{ss} = 0$ the switching lines are vertical. Depending on the ratio of the dead-zone width ε to the parameter λ the system operation can be stable when all phase trajectories end on the segment of rest (Fig. 17.40*a*) or self-oscillatory when at sufficiently large initial deflections (outside the hatched stagnation zone *S*) the phase trajectories tend to the stable limit cycle, $ABA'B'$ (Fig. 17.40*b*).

The boundary of these two conditions corresponds to the critical ratio of the parameters $\lambda = \lambda_{cr}$, $\varepsilon = \varepsilon_{cr}$ at which the limit cycle and the boundaries of *S* coincide (Fig. 17.40*c*).

Let us determine the boundary relation between the parameters directly from Fig. 17.40*c*. The leg $y_{2a} = AC$ of the isosceles rectangular triangle ABC is equal to $\lambda_{cr} \cdot \varepsilon_{cr} + \varepsilon_{cr} = (1 + \lambda_{cr})\, \varepsilon_{cr}$. On the other hand, the coordinates of the point A should satisfy Eq. (17.79) of the phase trajectory whose initial point B' lies on the x-line $y_{2c} = 0$ at a distance of $y_{1c} = -\varepsilon_{cr}$ from the origin of coordinates. Substitute these values into Eq. (17.79)

$$-\lambda_{cr} \cdot \varepsilon_{cr} + \varepsilon_{cr} = -(1 + \lambda_{cr})\, \varepsilon_{cr} - \ln \left| \frac{(1+\lambda_{cr})\, \varepsilon_{cr} - 1}{-1} \right|$$

Thence

$$-2\varepsilon_{cr} = \ln [1 - (1 + \lambda_{cr})\, \varepsilon_{cr}]$$

or

$$1 + \lambda_{cr} = \frac{1}{\varepsilon_{cr}} (1 - e^{-2\varepsilon_{cr}}) \qquad (17.84)$$

2. With relatively small rate feedback the picture does not change qualitatively. We allow for the negative slope of the switching line in determining the critical values of the parameters. Figure 17.40*d*

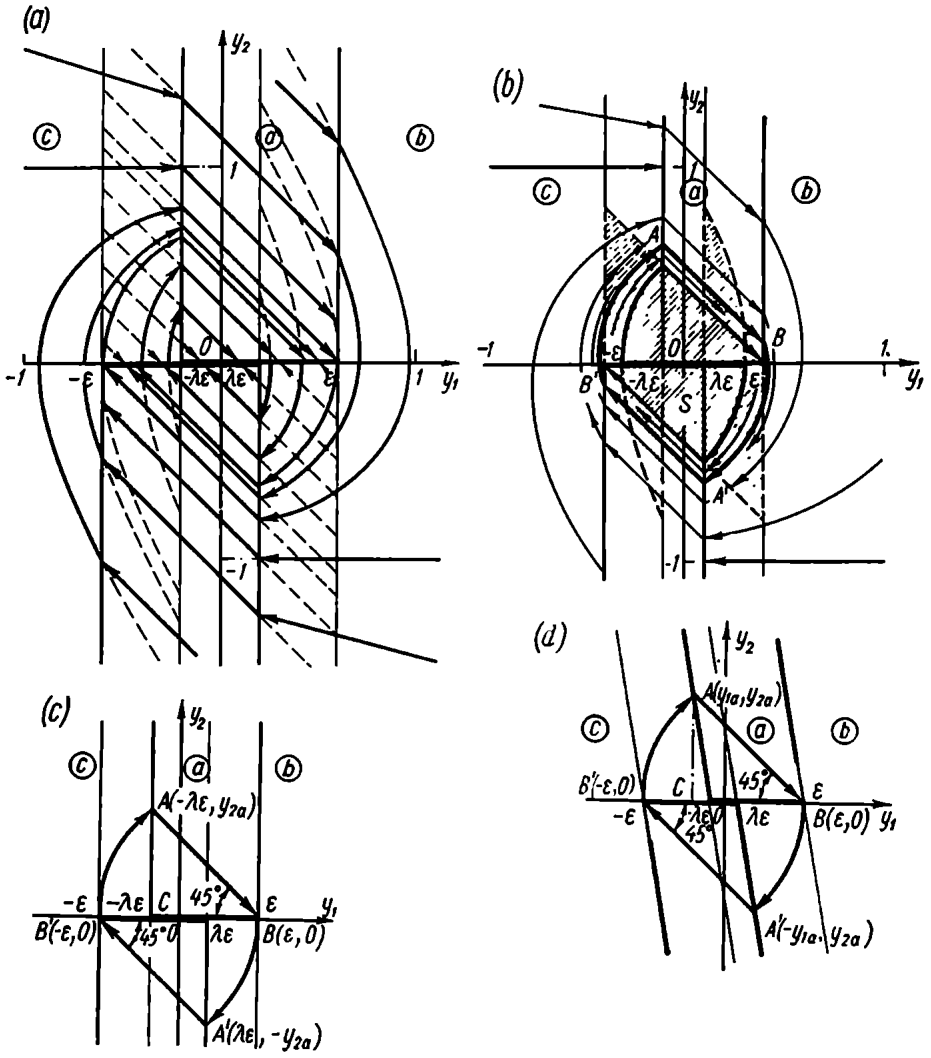

Fig. 17.40

represents the boundary case with feedback. The coordinates of the point A are determined from the condition for intersection of the straight line AB as given by the equation

$$y_2 = -y_1 + e_{cr}$$

with the switching line of Sheet c

$$y_2 = -\frac{1}{k_{ss}}(y_1 + \lambda_{cr}\varepsilon_{cr})$$

Simultaneous solution of these equations yields

$$\left.\begin{aligned} y_{1a} &= -\frac{\lambda_{cr}+k_{ss}}{1-k_0}\varepsilon_{cr} \\ y_{2a} &= \frac{1+\lambda_{cr}}{1-k_{ss}}\varepsilon_{cr} \end{aligned}\right\} \qquad (17.85)$$

Substituting these data into Eq. (17.79) gives

$$-\frac{\lambda_{cr}+k_{ss}}{1-k_{ss}}\varepsilon_{cr} + \varepsilon_{cr} = -\frac{1+\lambda_{cr}}{1-k_{ss}}\varepsilon_{cr} - \ln\left|\frac{\frac{1+\lambda_{cr}}{1-k_{ss}}\varepsilon_{cr}-1}{-1}\right|$$

whence

$$-2\varepsilon_{cr} = \ln\left|1-\frac{1+\lambda_{cr}}{1-k_{ss}}\varepsilon_{cr}\right|$$

or

$$\frac{1}{\varepsilon_{cr}}(1-e^{-2\varepsilon_{cr}}) = \frac{1}{1-k_{ss}}(1+\lambda_{cr}) \qquad (17.86)$$

Equation (17.84) is evidently a particular case of Eq. (17.86) at $k_{ss} = 0$.

Since the left-hand part of Eq. (17.86) depends only on ε_{cr} and the right-hand part, only on λ_{cr}, k_{ss} being the parameter, this equation can be simply solved graphically as shown in Fig. 17.41*a*. Thence it follows, in particular, that at $k_{ss} \geqslant 0.5$ and $0 \leqslant \lambda$ no self-oscillation can exist in the system.

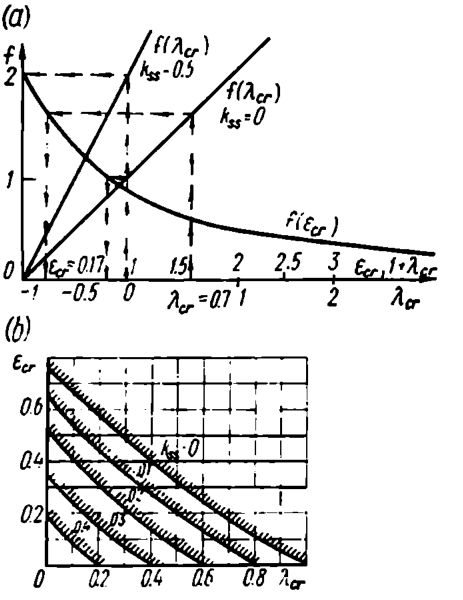

Fig. 17.41

Figure 17.41*b* represents a family of curves for different values of $0 \leqslant k_{ss} \leqslant 0.5$. Systems whose parameters ε and λ lie below the appropriate boundary curve are self-oscillatory; if they lie above it, the systems are stable.

3. In the case of very large feedback ($k_{ss} > 1$) the slope of the switching line becomes less than that of the phase trajectories in Sheet *a*. The response to the negative initial deflections $y_1 < -\varepsilon$, $y_2 = 0$ after the first reset to zero involves the vibrational mode of one relay contact, the response to the positive ones $y_1 > \varepsilon$, $y_2 = 0$,

the vibrational mode of the other contact. The relay is not observed to switch from the position $z = 1$ to the position $z = -1$ at all. The phase portrait of such a system is shown in Fig. 17.42.

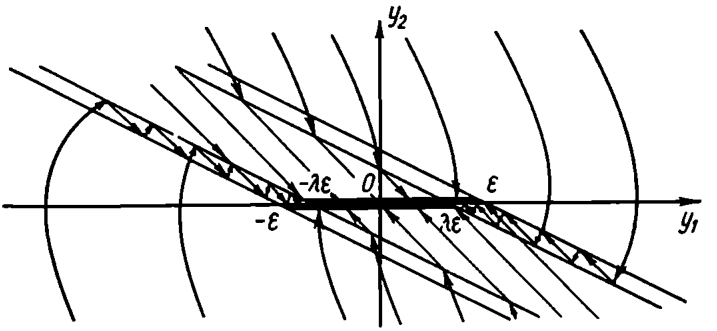

Fig. 17.42

Chapter XV discussed the operation of a relay as an element performing more complicated functions, switching the links between system elements depending on the signal fed to the control winding (see Sec. 15.8).

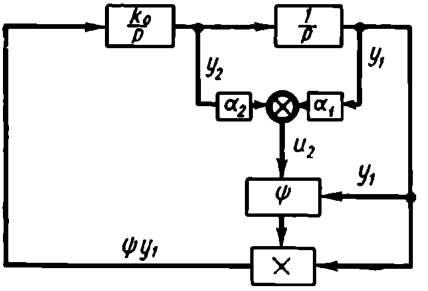

Fig. 17.43

Variable structure systems of Sec. 15.3 are built of such elements.

Consider a simple structural diagram where a relay with a response as given in Fig. 15.5*a* switches the sign of feedback connecting two integrating elements as a function of the linear combination of phase coordinates $u_2 = \alpha_1 y_1 + \alpha_2 y_2$ (Fig. 17.43).

The function ψ fed to the multiplying element of the structural diagram takes the values $+1$ or -1 as shown in the plane (y_1, y_2) (Fig. 17.44*a*) giving two switching lines $y_1 = 0$ and $y_2 = -ky_1$, where $k = \frac{\alpha_1}{\alpha_2}$ is the adjustable parameter of the ψ-unit.

Assume initially that $k_0 = 1$. Then at $\psi = -1$ the differential equations of the system phase trajectories are

$$\left.\begin{aligned} \frac{dy_1}{dt} &= y_2 \\ \frac{dy_2}{dt} &= -y_1 \end{aligned}\right\} \qquad (17.87)$$

As shown in Sec. 17.3 in the origin of coordinates (Fig. 17.44*b*) lies a singular point of the centre type; the system is oscillatory with zero damping.

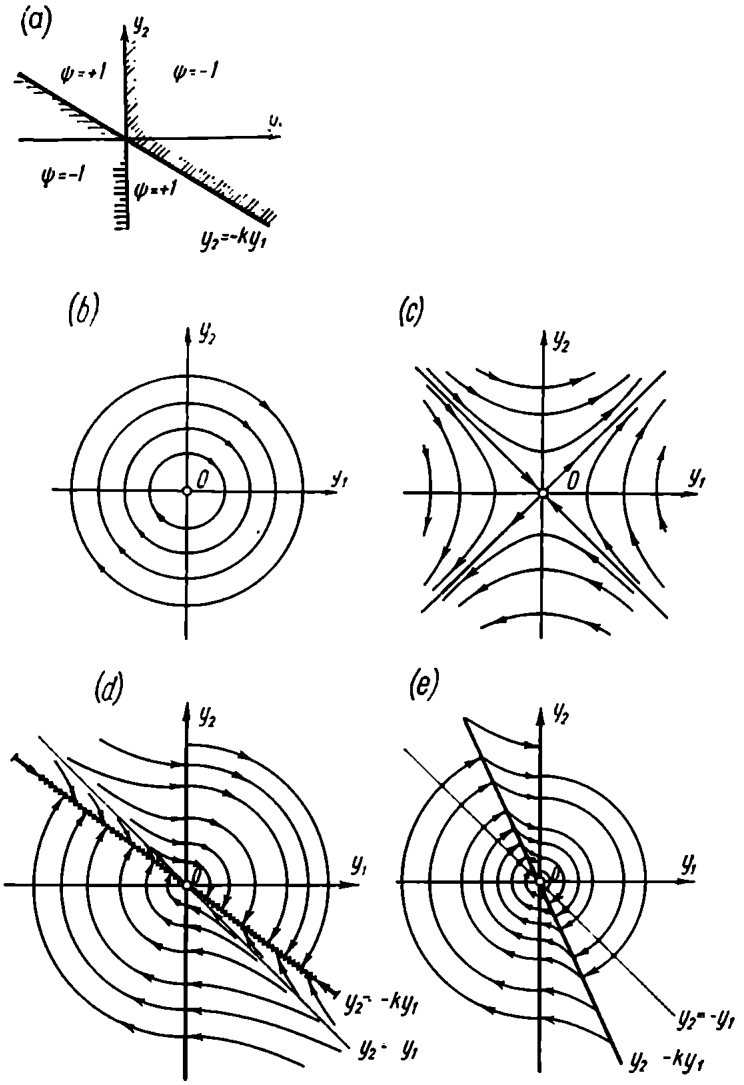

Fig. 17.44

At $\psi = 1$ the phase trajectory differential equations are

$$\left.\begin{aligned}\frac{dy_1}{dt} &= y_2\\ \frac{dy_2}{dt} &= y_1\end{aligned}\right\} \qquad (17.87a)$$

In the origin of coordinates (Fig. 17.44*c*) lies a symmetrical saddle with the separatrices $y_2 = -y_1$ and $y_2 = y_1$, and the system is unstable.

Figure 17.44*d* portrays a phase plane when the ψ-unit is switched and $0 < k < 1$. A sliding mode along the switching line $y_2 = ky_1$ is observed in the system, the sole *stable* point being in the origin of coordinates of the phase plane. The rate of transient processes in such systems increases with the slope of the switching line, in other words, with k approaching unity. But if $k > 1$ and the switching line is raised above the separatrix $y_2 = -y_1$, the system at once becomes oscillatory (Fig. 17.44*e*) and the transient process caused by restructuring drastically deteriorates. The system stability is preserved, however, even with this kind of adjustment.

Consequently, a variable structure system permits obtaining a stable control system which at different time intervals is described by linear equations of a neutral (oscillatory with zero damping) or an unstable system.

If the factor k_0 differs from unity, then the phase trajectories (see Fig. 17.44*b* and *c*) are families of ellipses and nonsymmetric hyperbolas. The nature of the sliding mode (see Fig. 17.44*d*) remains unchanged. Variations of k_0 within a certain range do not affect the transient process and the system is insensitive to parameter variations. This advantage of variable structure systems explains their wide practical application (Ref. 20).

17.6. POINT TRANSFORMATION METHOD

The method of point transformations (mappings) developed by A. A. Andronov and associates (Ref. 3) is very important in investigating the periodic operation of nonlinear systems and especially in a detailed study of stability of such modes and the boundaries of their attraction areas.

Assume that in the phase plane (Fig. 17.45) a segment of the curve *OA not containing points of contact with phase trajectories* can be found and the phase trajectories intersect the segment OA in the same direction.

Let us consider the phase trajectory passing through an arbitrary point M_0 (see Fig. 17.45). If the shape of this trajectory can be traced and the point M_1 where it returns to the segment OA can be found, then the point transformation T of the segment OA is understood as an operator expressing the single-valued relation $M_1 = T\{M_0\}$. Consequently the transformation T maps a point of the segment which does not contain contact or singular points onto a subsequent point of the same segment. The same operator T can transform the point M_1 to the point M_2

$$M_2 = T\{M_1\} = T^2\{M_0\} \tag{17.88}$$

and so on.

If there is a point M^c which is transformed into itself by the operator T without changing the position of the point on the line OA, $M^c = T\{M^c\}$, then the point lies on a closed phase trajectory, the *limit cycle.*

The question of stability in a periodic condition so defined is thus solved by applying the transformation T to points adjacent to the

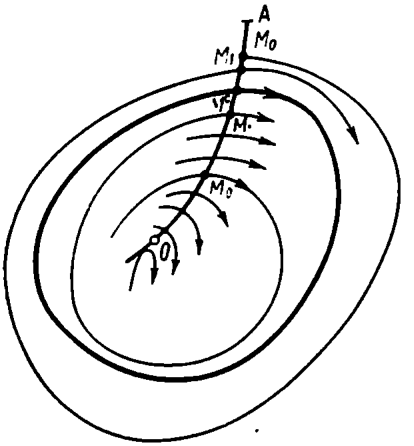

Fig. 17.45

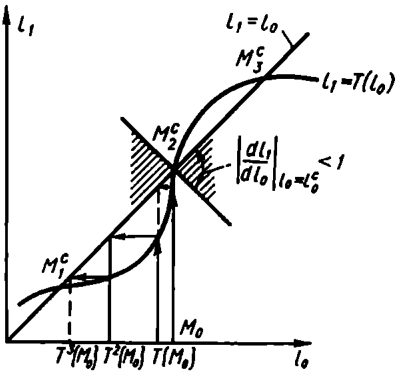

Fig. 17.46

immovable point M^c. If successive point transformation brings them closer to M^c, then the limit cycle is stable, if it does not, the cycle is unstable.

Assume that in a particular case the transformation T was found to be simple and the dependence of the coordinate l_1 of the point M_1 on the coordinate l_0 of the point M_0 was constructed as the graph

$$l = T(l_0) \tag{17.89}$$

which is known as the *Koenigs-Lamereille diagram* (Fig. 17.46). A second transformation T as defined by Eq. (17.88) may be performed in an illustrative way.

From the initial point M_0 on the axis l_0 a perpendicular is erected to intersect the curve (17.89). The resultant coordinate l_1 is transferred to the bisectrix $l_1 = l_0$ of the coordinate angle; in this way the abscissa of the next point to be transformed is obtained.

The limit cycles in the Koenigs-Lamereille diagram in this and more involved versions (see Examples 17.9, 17.10) are associated with points whose coordinates do not change in this construction. In Fig. 17.46 these are the points in which the curve (17.89) and the straight line $l_1 = l_0$ intersect. The immovable points M_1^c and M_3^c are stable and M_2^c is unstable, which is defined by the slope k^c of the

curve (17.89) in the intersection point in question. The limit cycle is stable if $|k^c| < 1$ and the curve intersects the straight line in the zone shaded in Fig. 17.46, and unstable if $|k^c| > 1$ and the intersection is outside the shaded zone.

In practical use of this method a number of difficulties arise.

1. An analytical relation between two points of the same phase trajectory is generally established only for piecewise-linear systems.

2. In the case of piecewise-linear systems the transformation T decomposes into several transformations $T = T_a, T_b, \ldots, T_r$ whose number is equal to that of the sheets pierced by the describing point while moving from one point of the line under transformation to another.

3. On each sheet the relation between the initial and current points is generally expressed by a transcendental parametric function.

4. The relation between the coordinates of the point to be transformed, $M(y_{1M}, y_{2M})$, as given by the equation $\varphi(y_{1M}, y_{2M}) = 0$ of the OA line, should permit elimination of one coordinate in the course of transformation.

In view of this, point transformation of one straight line into another is used in practical studies of piecewise-linear systems with typical nonlinearities described in Ch. XV.

More complicated problems can be solved with the aid of computers.

Now, let us take up specific systems.

Example 17.9. Determine the parameters and self-oscillation stability of a servo system without rate feedback and with a two-positional relay amplifier whose response is given in Fig. 15.18*a*.

In line with Example 17.8 the differential equations for phase trajectories are

$$\left.\begin{aligned} \frac{dy_1}{d\tau} &= y_2 \\ \frac{dy_2}{d\tau} &= -z(y_1) - y_2 \end{aligned}\right\}$$

where

$$z(y_1) = \begin{cases} 1, & y_1 > \varepsilon \\ -1, & y_1 < -\varepsilon \end{cases}$$

The system phase plane (see Fig. 17.47*a*) consists of two Sheets b ($z = 1$) and c($z = -1$) filled with symmetrical phase trajectories (17.76) and (17.78).

The segment without contact points will be the straight vertical switching line $y_1 = \varepsilon$, $y_2 > 0$. The transformation T mapping the point y_{20} of this line into the point y_{22} of the same line consists of two consecutive transformations, T_b transforming y_{20} into y_{21} and T_c transforming y_{21} into y_{22}, $T = T_b T_c$. Due to the symmetry of phase

trajectories in Sheets *b* and *c* either of the components can be considered separately instead of the complete transformation.

Let us consider the transformation T_b which, in the parametric form, is expressed by formula (17.76) if we substitute

$$y_{1b} = \varepsilon, \qquad y_1 = -\varepsilon, \qquad \tau - \tau_b = \tau_1, \qquad y_{2b} = y_{20}$$

In order to construct a Koenigs-Lamereille diagram in the first rather than in the fourth quadrant, assume that $y_{21} = -y_{2c} > 0$. Then

$$\left.\begin{aligned} 1 - y_{21} &= (1 + y_{20})\, e^{-\tau_1} \\ -2\varepsilon &= (1 + y_{20})\,(1 - e^{\tau_1}) - \tau_1 \end{aligned}\right\}$$

Determining y_{20} from the second equation and substituting it into the first gives the parametric expression

$$\left.\begin{aligned} y_{21} &= 1 - \frac{\tau_1 - 2\varepsilon}{1 - e^{-\tau_1}}\, e^{-\tau_1} > 0 \\ y_{20} &= \frac{\tau_1 - 2\varepsilon}{1 - e^{-\tau_1}} - 1 \geqslant 0 \end{aligned}\right\} \qquad (17.90)$$

The minimal value of the parameter τ_1, dimensionless time of motion along the trajectory in Sheet *b* (see Fig. 17.47*a*), is obtained from the condition $y_{20} = 0$. Then

$$\frac{\tau_{1min} - 2\varepsilon}{1 - e^{-\tau_{1min}}} - 1 = 0 \quad \text{or} \quad \tau_{1min} - 2\varepsilon = 1 - e^{-\tau_{1min}}$$

which graphically corresponds to the abscissa of the point where exponent *1* intersects straight line *2* (Fig. 17.47*b*). It is evident that τ_{1min} monotonically increases with ε; $\tau_{1min} = 0$ at $\varepsilon = 0$. Substituting the values of τ_{1min} into Eq. (17.90) reveals that

$$y_{21}(\tau_{1min}) = 1 - e^{-\tau_{1min}} > 0$$

Now, y_{20} increases infinitely while y_{21} tends to unity as $\tau_1 \to \infty$. This reasoning explains the Koenigs-Lamereille diagram of Fig. 17.47*c*. The intersection point of curve (17.90) with the straight line $y_{21} = y_{20}$ determines the maximal value of the dimensionless rate y_2 in the limit cycle (see Fig. 17.47*a*). Self-oscillations are stable.

The self-oscillation period $T = 2\tau_1^c$ can be found by equating the values y_{20} and y_{21} in Eq. (17.90). The resultant transcendental equation is known as an *equation of periods*. In this specific case its form is rather simple

$$\frac{\tau_1^c - 2\varepsilon}{1 - e^{-\tau_1^c}}\,(1 + e^{-\tau_1^c}) = 2$$

and it expresses the relation $T(\varepsilon)$ as given by the graph of Fig. 17.47*d*.

Example 17.10. Study a servo system (see Fig. 15.2) with a considerable play of the reducing gear. Confine yourself to analysis of small initial misalignments $|\theta_0| \leqslant \frac{\pi}{6}$.

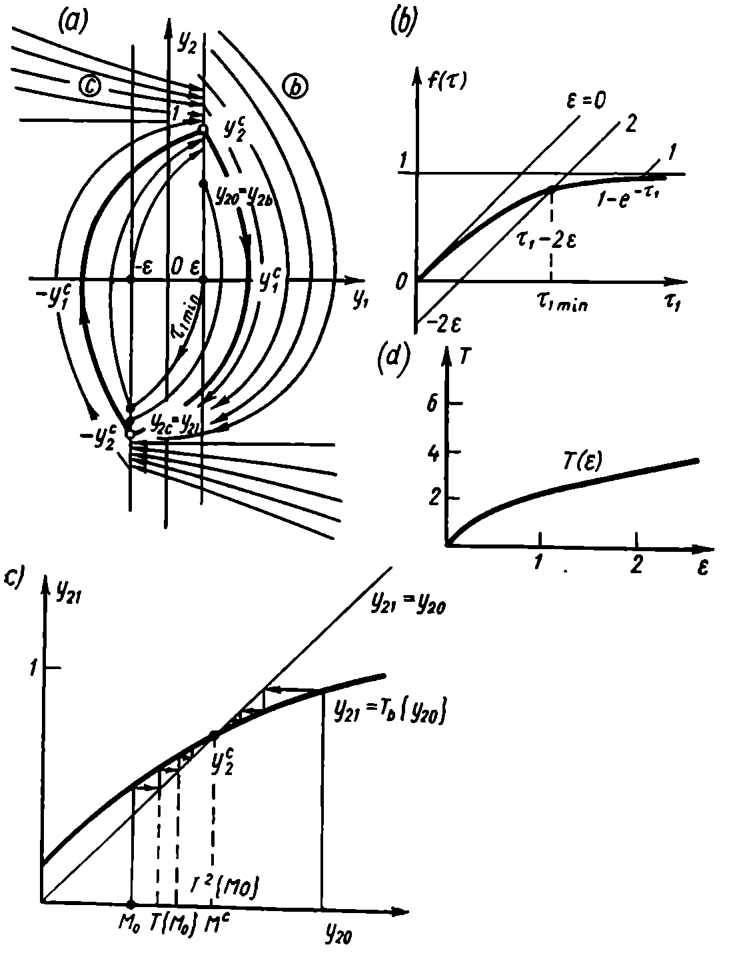

Fig. 17.47

As shown in Examples 17.3 and 17.7, in the zone of small misalignments, the responses of the measuring unit (selsyn pair) and the amplifier can be regarded as linear

$$u_1 = f_1 = U_{1m} \sin\theta \approx U_{1m}\theta, \quad u_M = U_{Mb} f_2 = U_{1m}(\theta - k_{com}\omega_M)$$

Let us write down the equation of the system in accord with Fig. 15.2 and Eq. (17.13)

$$T_M \frac{d\omega_M}{dt} + \omega_M = k_M u_M, \qquad \omega_M = \frac{d\theta_M}{dt}$$

The sign of misalignment angle θ variation is opposite to the sign of the motor angle θ_M variation reduced to the load (output) axis; these angles are interrelated via the nonlinear response of play in the reducing gear

$$\theta = -z(\theta_M, \omega_M)$$

The multivalued piecewise-linear function z is given by Eq. (15.26). The above relations are reduced to the equation

$$T_M \frac{d^2\theta}{dt^2} + \frac{d\theta_M}{dt} = -k_M U_{1m}\left[z\left(\theta_M, \frac{d\theta_M}{dt}\right) + k_{com}\frac{d\theta_M}{dt}\right]$$

or

$$\frac{d^2\theta_M}{dt^2} + \frac{1 + k_M k_{com} U_{1m}}{T_M}\frac{d\theta_M}{dt} + \frac{k_M U_{1m}}{T_M} z(\theta_M, \omega_M) = 0 \quad (17.91)$$

Now the dimensionless time is

$$\tau = (1 + k_M k_{com} U_{1m})\frac{t}{T_M}$$

Then Eq. (17.91) takes the form

$$\frac{d^2\theta_M}{d\tau^2} + \frac{d\theta_M}{d\tau} + \frac{T_M k_M U_{1m}}{(1 + k_M k_{com} U_{1m})^2} z = 0$$

Taking the play width $\Delta = 2x_a$ as the base of normalization, introduce dimensionless phase variables

$$y_1 = \frac{1}{2x_a} z, \qquad y_2 = \frac{1}{2x_a}\theta_M,$$

$$y_3 = \frac{1}{2x_a}\frac{d\theta_M}{d\tau} = \frac{dy_2}{d\tau}$$

Let us now write the corresponding system of equations for phase trajectories

$$\left.\begin{aligned} \frac{dy_2}{d\tau} &= y_3 \\ \frac{dy_3}{d\tau} &= -Ay_1 - y_3 \end{aligned}\right\} \quad (17.92)$$

where

$$A = \frac{T_M k_M U_{1m}}{(1 + k_{com} k_M U_{1m})^2} = \frac{k}{(1 + k_{ss})^2}$$

By virtue of Eq. (15.26) and Fig. 17.48*a*, the system eliminates the play in the range $-\frac{1}{2} < y_1 - y_2 < \frac{1}{2}$. The misaligment signal θ remains unchanged, whence $\frac{dy_1}{d\tau} = 0$ and $y_1 = y_{1k} = \text{const}$.

In the case of leftward, $y_2 = y_1 + \frac{1}{2}$, $y_3 > 0$, or rightward, $y_2 = y_1 - \frac{1}{2}$, $y_3 < 0$, play elimination, the mechanical couplings remain intact, therefore $\frac{dy_1}{d\tau} = \frac{dy_2}{d\tau} = y_3$.

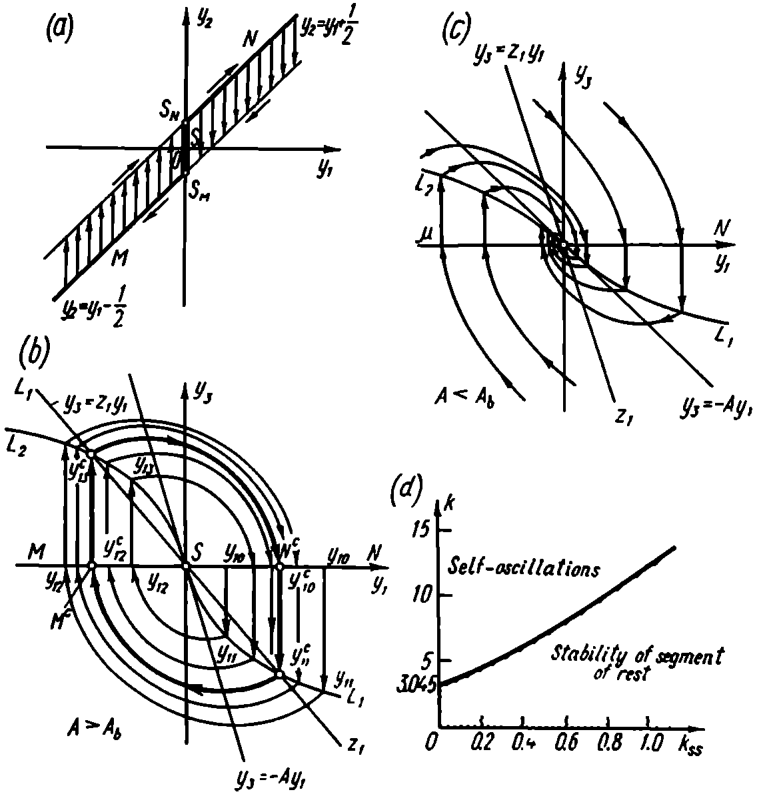

Fig. 17.48

The system enters the range of play when the rotation is reversed, $y_3 = \frac{dy_2}{d\tau} = \frac{dy_1}{d\tau} = 0$. Let us start analysis with this instant. To be more specific, assume that directly before the reversal $y_3 > 0$. This signifies that in the initial state the describing point is on the straight line N (Fig. 17.48*a*), where $y_{20} = y_{10} + \frac{1}{2}$; $y_{30} = 0$.

System (17.92) in the range of play takes the form

$$\left.\begin{aligned}\frac{dy_2}{d\tau} &= y_3\\ \frac{dy_3}{d\tau} &= -(y_3 + Ay_{10})\end{aligned}\right\} \qquad (17.92a)$$

which coincides with Eqs. (17.69). Coordination of subscripts and substitution of the values $\sigma = -1$, $y_{3s} = -Ay_{10}$, $t - t_k = \tau$, $y_{20} = y_{10} + \frac{1}{2}$, $y_{30} = 0$ in Eq. (17.72) yields a parametric equation for current coordinates of the phase trajectory:

$$\left.\begin{aligned}y_3 &= -Ay_{10}(1 - e^{-\tau})\\ y_2 &= y_{10} + \frac{1}{2} - Ay_{10}(e^{-\tau} + \tau - 1)\end{aligned}\right\}$$

At the time $\tau = \tau_1$ and at $y_2 = y_{21} = y_{10} - \frac{1}{2}$ the system eliminates the play. By denoting $y_3(\tau_1) = y_{31}$ we obtain the relation between the coordinates of the final points y_{31} and $y_{11} = y_{10}$ of the phase trajectory part under consideration and the parameter τ_1:

$$\left.\begin{aligned}y_{31} &= \frac{e^{-\tau_1} - 1}{e^{-\tau_1} + \tau_1 - 1}\\ y_{11} &= \frac{1}{A(e^{-\tau_1} + \tau_1 - 1)}\end{aligned}\right\} \qquad (17.93)$$

This expression determines the points of the curve L_1 in Fig. 17.48*b*.

Subsequent motion of the system satisfies Eq. (17.92) at $y_3 = \frac{dy_2}{dt} = \frac{dy_1}{d\tau}$

$$\left.\begin{aligned}\frac{dy_1}{d\tau} &= y_3\\ \frac{dy_3}{d\tau} &= Ay_1 - y_3\end{aligned}\right\} \qquad (17.92b)$$

The parametric equation of a phase trajectory can be written as Eq. (17.23) at $A < \frac{1}{4}$ or (17.23a) at $A > \frac{1}{4}$. In this example more tangible results are obtained through direct solution on the integral curve equation

$$\frac{dy_3}{dy_1} = -\frac{Ay_1 + y_3}{y_3}$$

This is a homogeneous differential equation. By substituting $z = \frac{y_3}{y_1}$, $\frac{dz}{dy_1} = \frac{\left(\frac{dy_3}{dy_1}\right) y_1 - y_3}{y_1^2}$ it is reduced to the equation

$$y_1\left(\frac{dz}{dy_1}\right) = -\frac{z^2 + z + A}{z}$$

which permits separation of the variables

$$\frac{dy_1}{y_1} = -\frac{z\,dz}{z^2+z+A} \tag{17.94}$$

Note that the points for which $z = z_h = \text{const}$ are on the straight line $y_3 = z_h y_1$. Integrate Eq. (17.94)

$$\int_{y_{11}}^{y_{12}} \frac{dy_1}{y_1} = -\int_{z_1}^{z_2} \frac{z\,dz}{z^2+z+A}$$

At $A > \frac{1}{4}$, $\sqrt{4A-1} > 0$ and integration leads to the expression

$$\ln|y_1|\Big|_{y_{11}}^{y_{12}} = -\frac{1}{2}\ln|z^2+z+A| + \\ + \frac{1}{\sqrt{4A-1}} \arctan\frac{2z+1}{\sqrt{4A-1}}\Big|_{z_1}^{z_2}$$

The upper limit of integration will be the horizontal straight line M (see Fig. 17.48*b*) in whose points $y_{22} = y_{12} - \frac{1}{2} < 0$, $y_{32} = z_2 = 0$ the system is reversed and reenters the range of play. Use as the lower limit the line $y_{31} = z_1 y_{11}$ for which $|y_{12}| = |y_{11}|$. Substituting these values gives

$$0 = \frac{1}{\sqrt{4A-1}}\left[\arctan\frac{1}{\sqrt{4A-1}} - \arctan\frac{2z_1+1}{\sqrt{4A-1}}\right] + \\ + \frac{1}{2}\ln\frac{z_1^2+z_1+A}{A}$$

or, transforming the difference of arc tangents, we have

$$\ln\frac{z_1^2+z_1+A}{A} = \frac{2}{\sqrt{4A-1}} \arctan\frac{z_1\sqrt{4A-1}}{2A+z_1}$$

whence we obtain the transcendental equation

$$z_1^2+z_1+A = Ae^{\frac{2}{\sqrt{4A-1}}\arctan\frac{z_1\sqrt{4A-1}}{2A+z_1}} \tag{17.95}$$

whose first negative root $0 < \arctan\frac{z_1\sqrt{4A-1}}{2A+z_1} < \pi$ determines the slope of the straight line z_1 as a function of the parameter A.

Let us have a look at the transformation T_1 of the point $y_1 = y_{10} > 0$ belonging to the straight line N (see Fig. 17.48*b*) to the point $y_1 = y_{12} < 0$ of the straight line M.

If the point under study is to the left of the normal y_{10}^c passing through the intersection of the straight line z_1 and the curve L_1, then by the time of reversal on the line M it will be found that $|y_{12}| > |y_{10}|$. Because of the symmetry, each subsequent point

transformation T_k increases the magnitude of the coordinate y_{1k}, which tends to the value y_{10}^c.

If $y_{10} > y_{10}^c$, then (see Fig. 17.48*b*) the transformation T_1 results in $|y_{12}| < y_{10}$. Further transformations T_k again lead to a sequence converging to y_{10}^c. If the straight line z_1 intersects the curve L_1 at $y_1 > 0$, then the sole stable mode of a servo system with play proves to be self-oscillations with an amplitude $\theta^c = 2ay_{10}^c$ proportional to the value of gear play.

The intersection of z_1 and L_1 at $y_{10}^c > 0$ takes place if $z_1 > \frac{dy_{31}}{dy_{11}|_{y_{11}=0}} = -A$. If $z_1 < -A$, then the single intersection point (Fig. 17.48*c*) will be the state of rest $S\left(y_1 = y_3 = 0, -\frac{1}{2} \leqslant y_2 \leqslant \frac{1}{2}\right)$. The system is stable, there are no self-oscillations.

Find the boundary value A_b by substituting $z_1 = -A_b$ into Eq. (17.95). The numerical solution of the resultant equation

$$\ln A_b = \frac{2}{\sqrt{4A_b - 1}} \arctan \sqrt{4A_b - 1}$$

gives $A_b = 3.045$.

The stability boundary in the plane k, k_{ss} is plotted in Fig. 17.48*d*.

Example 17.11. Determine the steady-state parameters of the extremal controller of Sec. 15.4 shown in Fig. 15.8*i*.

In accordance with the structural diagram the control system equations are

$$\frac{1}{k_1}\left(\frac{dx}{dt}\right) = f\left(v, \frac{dx}{dt}\right) =$$

$$= \begin{cases} U_0, & v < v_m, \ \frac{dx}{dt} > 0 \\ -U_0, & v < v_m, \ \frac{dx}{dt} < 0 \end{cases}$$

$$z(x) = z_0 - k_0 x^2$$

$$T_2\left(\frac{dy}{dt}\right) + y = k_2 z$$

From these equations it follows that the phase plane consists of two sheets; at $u = U_0$ the scanning goes rightwards and at $u = -U_0$, leftwards, transition from the phase trajectory of one sheet to that of another occurs at $y_m - y = v_m$ in accordance with the flip-flop switching logic.

Let us now use the dimensionless equation in deviations

$$\eta_2 \pm \frac{d\eta_2}{d\eta_1} = -\eta_1^2 \qquad (17.96)$$

where

$$\eta_1 = \frac{x}{T_2 k_1 U_0} \quad \text{and} \quad \eta_2 = \frac{y - k_2 z_0}{k_0 k_2 (T_2 k_1 U_0)^2}$$

In the second term of Eq. (17.96) the sign changes whenever

$$\eta_{2max} - \eta_2 = \frac{v_m}{k_0 k_2 (T_2 k_1 U_0)^2} = \delta \tag{17.97}$$

Consequently, we have a two-sheet phase plane where the transition from one sheet to another occurs at the time when $\eta_{2max} - \eta_2 = \delta$.

The equation of the first sheet $\left(\frac{dx}{dt} = k_1 U_0 = \text{const} > 0\right)$ is

$$\eta_2 + \frac{d\eta_2}{d\eta_1} = -\eta_1^2 \tag{17.98}$$

while the equation of the second sheet $\left(\frac{dx}{dt} = -k_1 U_0 = \text{const} < 0\right)$ is

$$\eta_2 - \frac{d\eta_2}{d\eta_1} = -\eta_1^2 \tag{17.99}$$

Unlike the above examples, here the relation between the phase coordinates η_2 and η_1 is not expressed by straightforward differentiation, but is of a more involved nonlinear nature. This relation follows from Eq. (17.96):

$$T_2 \left(\frac{d\eta_2}{dt}\right) = \frac{d\eta_2}{d\tau} = -\eta_1^2 - \eta_2 \tag{17.100}$$

The phase trajectories of processes can easily be obtained in the coordinates η_1 and η_2 through isoclines which, as follows from Eqs. (17.98) and (17.99), are a family of equidistant parabolas. The isocline corresponding to horizontal tangents for both sheets is the parabola

$$\eta_2 = -\eta_1^2$$

It coincides with the locus of extremal values of η_2, where $\frac{d\eta_2}{d\tau} = \frac{d\eta_2}{d\eta_1} = 0$.

Examples of isoclines and phase trajectories for the first and second sheets are given in Fig. 17.49*a* and *b* which also shows the points *A* and *B*, where $\eta_{2max} - \eta_2$ reaches the value δ and thus a transition from one sheet to another occurs.

Depending on the initial conditions the transient process consists of several transitions from one sheet to another and ends in steady self-oscillations represented by an ∞-shaped trajectory in the phase plane (Fig. 17.49*c*).

In order to determine the parameters of steady self-oscillations Eq. (17.98) or (17.99) should be integrated and then the equation of periods solved which establishes a correlation between the initial and the final positions of the describing point on each sheet with due regard for the flip-flop switching conditions.

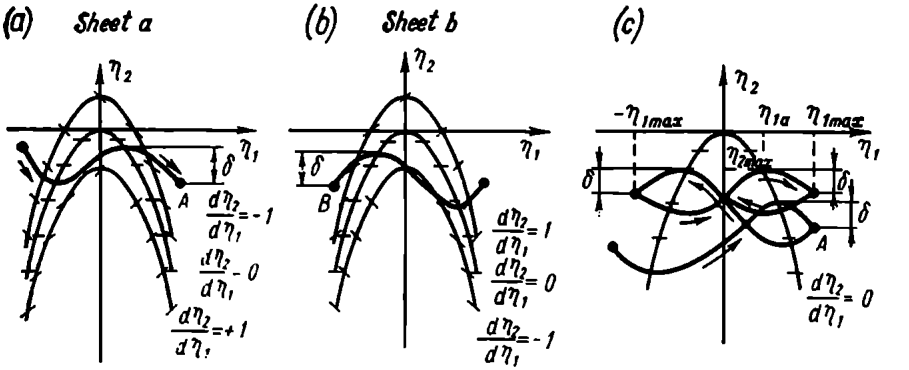

Fig. 17.49

The symmetrical steady self-oscillations can be characterized by the abscissas η_{1a} of the maximum point η_{2max} and by the maximal value of the deviation η_{1max} at $\eta_{2max} - \eta_2 = \delta$.

The equations relating these coordinates may be written as

$$\eta_2(\eta_{1max}) = \eta_2(-\eta_{1max}) \tag{17.101}$$

and

$$\eta_2(\eta_{1a}) - \eta_2(\eta_{1max}) = \delta \tag{17.102}$$

To solve these equations the relation $\eta_2(\eta_1)$ should be obtained explicitly through integration of, say, Eq. (17.98).

The solution of the nonhomogeneous linear equation (17.98) can be represented as a sum of a free and a forced component

$$\eta_{2fr} = Ae^{-\eta_1}, \qquad \eta_{2fo} = -(\eta_1 - 1)^2 - 1 \tag{17.103}$$

Substituting $\eta_2 = \eta_{2fr} + \eta_{2fo}$ into Eqs. (17.101) and (17.102) and keeping in mind that $\eta_2(\eta_{1a}) = -\eta_{1a}^2$, after transformations and elimination of the constant $A = \frac{2\eta_{1max}}{\sinh \eta_{1max}}$ we have

$$\left.\begin{aligned} \frac{\eta_{1max}}{\sinh \eta_{1max}} &= (1-\eta_{1a})\, e^{\eta_{1a}} \\ \eta_{1a}^2 &= (\eta_{1max}1)^2 - \frac{2\eta_{1max}}{\sinh \eta_{1max}}\, e^{\eta_{1max}} + 1 - \delta \end{aligned}\right\} \tag{17.104}$$

The graphical solution of Eqs. (17.104) for different values of δ is shown in Fig. 17.50*a*.

Considering δ as an argument, the solution obtained can be conveniently represented as the curve $\eta_{1max}(\delta)$ (Fig. 17.50*b*). Knowing

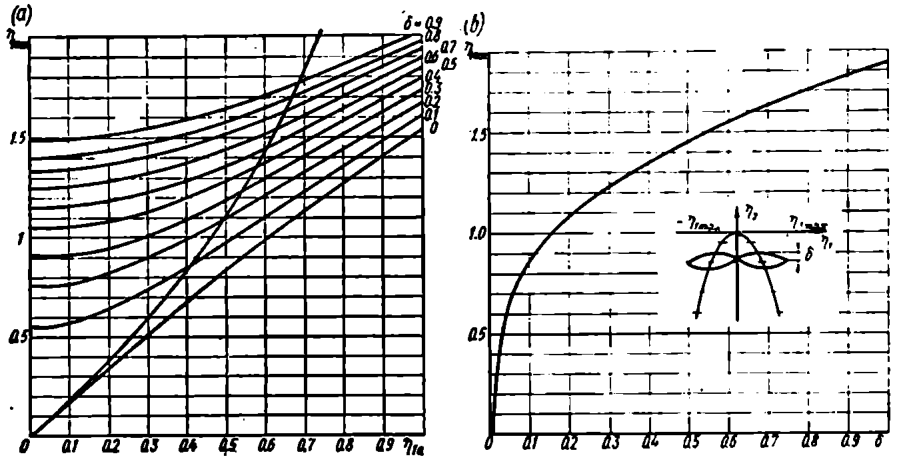

Fig. 17.50

η_{1max}, the period of oscillations in the system can easily be found. Since $\left|\frac{dx}{dt}\right| = k_1 U_0 = \text{const}$, then for symmetrical self-oscillations

$$T = \frac{4x_m}{k_1 U_0} = 4\eta_{1max} T_2 \tag{17.105}$$

Consequently, with η_{1max} known, the oscillation period and frequency can easily be found

$$\omega^c = \frac{2\pi}{T} = \frac{\pi}{2\eta_{1max} T_2} \tag{17.106}$$

The value of $x_m = k_1 U_0 T_0 \eta_{1max}$ gives the losses due to hunting in the vicinity of the extremum

$$\Delta y_{av} = -\frac{1}{2x_m} \int_{-x_m}^{x_m} (x - k_2 z_0)\, dx =$$

$$= -\frac{k_2 k_0 (T_2 k_1 U_0)^2}{2\eta_{1max}} \int_{-\eta_{1max}}^{\eta_{1max}} \eta_2\, d\eta_1 =$$

$$= \frac{k_2 k_0 (T_2 k_1 U_0)^2}{3} \eta_{1max}^2$$

The losses due to hunting Δy_{av} express the reduction in the average value of the controlled quantity y relative to the maximal value in the extremum point in the absence of external actions $f(t)$.

Let us determine the values of ω^c and x_m if $k_0 = 10^4$ deg/m^2, $k_1 = 5 \times 10^{-4}$ m/V·sec, $k_2 = 1$ V/deg, $T_2 = 1$ sec, $U_0 = 36$ V, and $v_m = 1$ V.

We determine

$$\delta = \frac{v_m}{k_0 k_2 (T_2 k_1 U_0)^2} = \frac{1}{10^4 (1.8 \times 10^{-2})^2} = 0.31$$

from the plot of Fig. 17.50*b* and find $\eta_{1max} = 1.23$.

By Eq. (17.106)]

$$\omega^c = \frac{\pi}{2\eta_{1max} T_2} = \frac{\pi}{2 \times 1.23 \times 1} = 1.28 \frac{1}{\text{sec}}$$

and

$$x_m = \eta_{1max} T_2 k_1 U_0 = 2.2 \times 10^{-2} \text{m}$$

Chapter XVIII

HARMONIC LINEARIZATION

18.1. THE METHOD OF HARMONIC LINEARIZATION. GENERAL

The most widespread method in studying high-order ($n > 2$) nonlinear control systems is the approximate method of harmonic linearization (or of harmonic balance) with the use of frequency-domain concepts developed in the theory of linear systems. Based on the works of N.M. Krylov and N.N. Bogolyubov, the method of harmonic linearization was proposed by L.S. Goldfarb in 1940 (Ref. 50) and used by him in analysis of control systems. Much later several versions of this method were worked out by scientists of other countries.

The essence of the method is as follows. Let a closed-loop autonomous (without external actions) nonlinear system consist of a nonlinear inertialess element *NE* and a stable or neutral linear part *LP* connected in series (Fig. 18.1*a*).

In order to say whether monoharmonic undamped oscillations can exist in this system, a harmonic sine signal $x(t) = X_m \sin \omega t$ is assumed to act at the input of the nonlinear element (Fig. 18.1*b*). The output signal $z(t) = z[x(t)]$ contains a spectrum of harmonic components with amplitudes, Z_{m1}, Z_{m2}, Z_{m3}, etc. and frequencies ω, 2ω, 3ω, etc. It is presumed that the signal $z(t)$, which goes through the linear part $W_{LP}(j\omega)$, is filtered so that in the linear part output $y(t)$ we may neglect all higher harmonics Y_{m2}, Y_{m3}, etc. and consider that $y(t) \cong Y_{m1} \sin(\omega t + \varphi)$.

The latter assumption is known as the *filter hypothesis* whose validity is a necessary condition for harmonic linearization.

The condition for equivalence of the circuits given in Fig. 18.1*a* and *b* can be formulated as the equality

$$x(t) + y(t) = 0 \tag{18.1}$$

When the filter hypothesis holds, $y(t) = Y_{m1} \sin(\omega t + \varphi)$ and Eq. (18.1) decomposes into two

$$X_m = Y_{m1} \tag{18.2}$$

and

$$\varphi = \pi \tag{18.3}$$

These two equations are known as *harmonic balance equations*; the former expresses the balance of amplitudes, the latter, the balance of phases. Thus, for undamped harmonic oscillations to exist in the system in question, the conditions (18.2) and (18.3) should be satisfied when the filter hypothesis is valid.

In order to see whether this hypothesis holds, take the frequency spectra of the signals $x(t)$, $z(t)$, and $y(t)$ in an open-loop circuit (Fig. 18.1*b*). With a monoharmonic signal $x(t)$ the spectra of $z(t)$ and $y(t)$ include higher harmonics Z_{mk} and Y_{mk} as well as the main harmonic Z_{m1} and Y_{m1}. Depending on the form of the nonlinearity

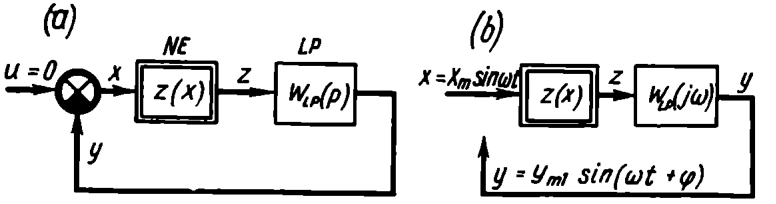

Fig. 18.1

$z(x)$ the amplitudes of higher harmonics in $z(t)$ are greater or smaller. The relative content of higher harmonics in the signal $y(t)$ is different. If the linear part has the properties of a low-pass filter, then the relative importance of higher harmonics is less in the signal $y(t)$ than in $z(t)$. The truth of the filter hypothesis is reflected in the response of the linear part $W_{LP}(j\omega)$ such that all harmonics except the first decay to negligible values when passing through it.

Quantitatively this condition may be expressed as

$$\frac{Z_{mk}}{Z_{m1}}\left|\frac{W_{LP}(jk\omega)}{W_{LP}(j\omega)}\right| \ll 1 \qquad (18.4)$$

where k is the ordinal number of the harmonic studied.

In a general case the condition (18.4) should hold for any integer $k \geqslant 2$. Where the oscillations are symmetrical, there are no even harmonics in the signal $y(t)$ and the condition (18.4) should be applied to $k \geqslant 3$. The harmonic linearization method aids in solving two basic groups of problems:

(a) study of self-oscillations in nonlinear closed-loop systems;

(b) study of conditions for absence of monoharmonic self-oscillations in nonlinear closed-loop systems.

In the former case the condition (18.4) should hold for the frequency ω of presumed self-oscillations, in the latter case, in the whole frequency range $0 \leqslant \omega < \infty$. Since usually $\frac{Z_{mk}}{Z_{m1}} < 1$ at $k \geqslant 2$, the condition (18.4) can be softened for approximate calculations and reformulated as follows: the slope of the logarithmic frequency response of the linear part should be at least -20 to -40 db/dec.

At the slope of —20 db/dec

$$\left|\frac{W_{LP}(j2\omega)}{W_{LP}(j\omega)}\right|=\frac{1}{2} \quad \text{and} \quad \left|\frac{W_{LP}(j3\omega)}{W_{LP}(j\omega)}\right|=\frac{1}{3}$$

while at the slope of —40 db/dec

$$\left|\frac{W_{LP}(j2\omega)}{W_{LP}(j\omega)}\right|=\frac{1}{4} \quad \text{and} \quad \left|\frac{W_{LP}(j3\omega)}{W_{LP}(j\omega)}\right|=\frac{1}{9}$$

Depending on whether the self-oscillations are symmetrical or not, the approach to their study differs. If they are nonsymmetrical, the constant component of the signal is of importance, while at odd nonlinearities and no external action ($u(t) = 0$ in Fig. 18.1*a*) symmetrical self-oscillations are of greatest interest.

The validity of the filter hypothesis in the form of strong inequality (18.4) is a relatively rare case in practical problems. Therefore harmonic linearization is far from always strictly justified. But even so the method yields satisfactory approximation of actual processes and is one of the simplest. In each case where the hypothesis is not valid the solution obtained needs experimental or theoretical verification with the use of a mathematical or physical model.

18.2. COMPLEX GAIN OF A NONLINEAR ELEMENT

A nonlinear element with a harmonic signal at the input can be described by a complex gain which depends on the input amplitude.

This characteristic of a nonlinear element is sometimes referred to as a *describing function.*

Consider an inertialess nonlinear element with the static response $z = z(x)$ of Fig. 18.2*a*. If the input is a harmonic signal $x = X_m \sin \omega t = \operatorname{Im} X_m e^{j\omega t}$, the periodic signal $z(t)$ at the output (Fig. 18.2*b*) can be represented as a Fourier series

$$z(t) = Z_0 + \sum_{k=1}^{\infty} Z_{Pk} \sin k\omega t + \sum_{k=1}^{\infty} Z_{Qk} \cos k\omega t \qquad (18.5)$$

where the coefficients Z_{Pk} and Z_{Qk} are given by the formulae

$$Z_{Pk} = \frac{1}{\pi} \int_0^{2\pi} z(X_m \sin \omega t) \sin k\omega t \, d(\omega t) \qquad (18.6)$$

$$Z_{Qk} = \frac{1}{\pi} \int_0^{2\pi} z(X_m \sin \omega t) \cos k\omega t \, d(\omega t) \qquad (18.7)$$

Let us take up for the time being those nonlinear responses for which the constant component in the given mode is zero ($Z_0 = 0$).

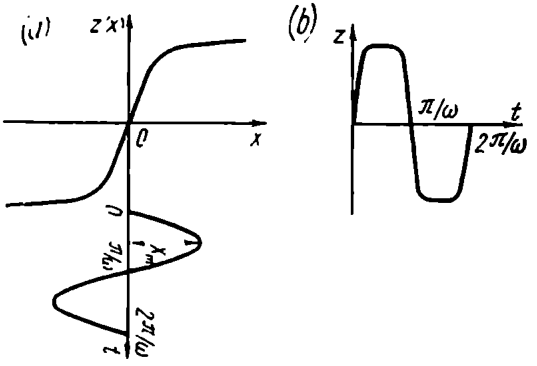

Fig. 18.2

This condition is often met in practice, e.g. at odd responses $z(x)$. Such are, for instance, the typical nonlinear responses of Ch. XV.

In harmonic linearization the periodic signal $z(t)$ is approximated by its first harmonic.

$$z(t) \approx Z_{P1} \sin \omega t + Z_{Q1} \cos \omega t \tag{18.8}$$

or, in the complex form,

$$z(t) \approx \operatorname{Im} (Z_{P1} + jZ_{Q1})\, e^{j\omega t} \tag{18.9}$$

where

$$Z_{P1} = \frac{1}{\pi} \int_0^{2\pi} z(X_m \sin \omega t) \sin \omega t \, d(\omega t) \tag{18.10}$$

$$Z_{Q1} = \frac{1}{\pi} \int_0^{2\pi} z(X_m \sin \omega t) \cos \omega t \, d(\omega t) \tag{18.11}$$

A complex gain of a nonlinear element is the complex ratio of the basic output harmonic to the basic input harmonic

$$\hat{W}_n(X_m) = P_n(X_m) + jQ_n(X_m) = \frac{Z_{P1}}{X_m} + j\frac{Z_{Q1}}{X_m} = |\hat{W}_n| e^{j\varphi_n} \tag{18.12}$$

$$P_n(X_m) = \frac{Z_{P1}}{X_m} = \frac{1}{\pi X_m} \int_0^{2\pi} z(X_m \sin \omega t) \sin \omega t \, d(\omega t) \tag{18.13}$$

$$Q_n(X_m) = \frac{Z_{Q1}}{X_m} = \frac{1}{\pi X_m} \int_0^{2\pi} z(X_m \sin \omega t) \cos \omega t \, d(\omega t) \tag{18.14}$$

$$|\hat{W}_n| = \frac{Z_{m1}}{X_m} = \frac{\sqrt{Z_{P1}^2 + Z_{Q1}^2}}{X_m}, \qquad \varphi_n = \arctan \frac{Z_{Q1}}{Z_{P1}} \tag{18.15}$$

A complex gain shows the relation of amplitudes and phases of the input and output first harmonics and resembles in this respect the linear element complex gain, but it depends, in the case of an inertialess nonlinear element, on the amplitude of the input signal X_m rather than on the frequency. The complex gain components $P_n(X_m)$ and $Q_n(X_m)$ are *harmonic linearization coefficients.*

It is easy to show that only in the case of multivalued nonlinearity does a harmonic signal shift in phase while propagating through a nonlinear element. Let us write the imaginary component of $\tilde{W}_n(X_m)$ in the form

$$Q_n(X_m) = \frac{1}{\pi X_m} \int_0^{2\pi} z(X_m \sin \omega t) \cos \omega t \, d(\omega t) =$$

$$= \frac{1}{\pi X_m^2} \oint z(X_m \sin \omega t) \, d(X_m \sin \omega t) = \frac{1}{\pi X_m^2} \oint z(x) \, dx \qquad (18.16)$$

Figure 18.3 portrays a multivalued hysteresis response with branches scanned counterclockwise. The integration in Eq. (18.16) is performed from $x=0$ $(t=0)$ to $x=X_m\left(t=\frac{\pi}{2\omega}\right)$ and then from $x=X_m$ to $x=-X_m\left(t=\frac{3\pi}{2\omega}\right)$, and from $x=-X_m$ to $x=0\times$ $\times\left(t=\frac{2\pi}{\omega}\right)$. The result of integration in the appropriate scale is easily seen to be equal to the area S of the hysteresis loop with the negative sign (the sign depends on the direction of scanning the multivalued curve). The imaginary component of the complex gain is thus expressed as

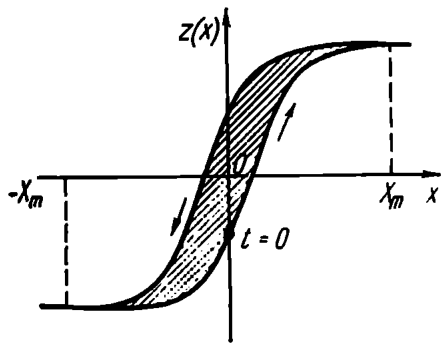

Fig. 18.3

$$Q_n(X_m) = -\frac{S}{\pi X_m^2} \qquad (18.17)$$

and is zero in the case of a single-valued nonlinearity.

Example 18.1. Determine the complex gain of a relay element with the multivalued response of Fig. 18.4*a*. The set point of the relay element is x_a and the reset is x_b; the output of the actuated relay element is $\pm z_a$.

At small input signals $X_m < x_a$ the output is zero, therefore $\tilde{W}_n(X_m) = 0$. At $X_m \geqslant x_a$ the output signals are rectangular pulses (Fig. 18.4*b*). The set time t_a is given by the condition

$$X_m \sin \omega t_a = x_a \qquad (18.18)$$

or

$$\sin \omega t_a = \frac{x_a}{X_m} \tag{18.19}$$

The reset time is given as

$$X_m \sin \omega \left(\frac{\pi}{\omega} - t_b \right) = x_b \tag{18.20}$$

or

$$\sin (\pi - \omega t_b) = \frac{x_b}{X_m} \tag{18.21}$$

Using Eq. (18.13) and allowing for oddness of the nonlinearity $z(x)$,

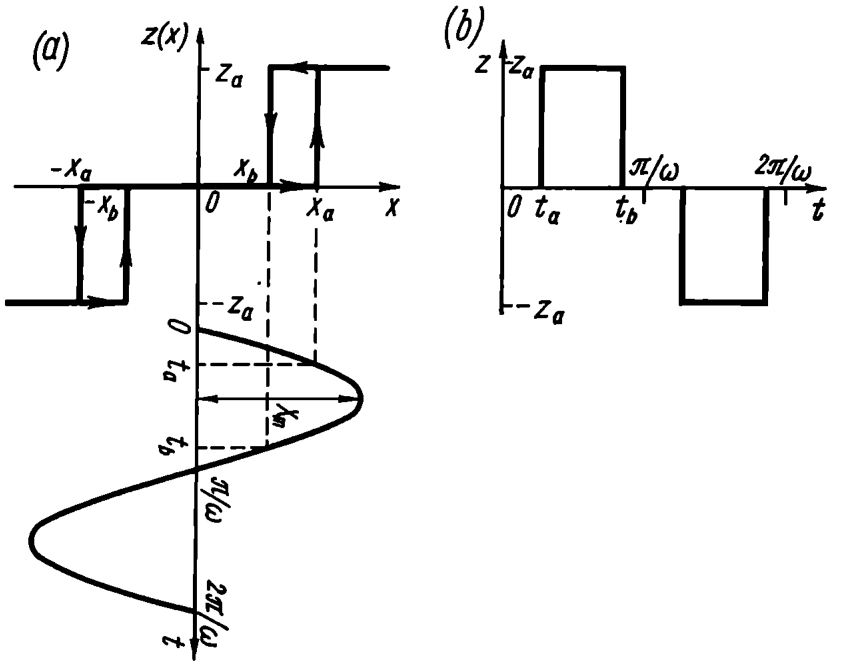

Fig. 18.4

we have for the real component

$$P_n(X_m) = \frac{2}{\pi X_m} \int_{t_a}^{t_b} z_a \sin \omega t \, d(\omega t) = \frac{2z_a}{\pi X_m} [\cos \omega t_a - \cos \omega t_b] \tag{18.22}$$

By virtue of Eqs. (18.19) and (18.21)

$$\cos \omega t_a = \sqrt{1 - \left(\frac{x_a}{X_m} \right)^2} \tag{18.23}$$

$$\cos \omega t_b = -\sqrt{1 - \left(\frac{x_b}{X_m} \right)^2} \tag{18.24}$$

therefore

$$P_n(X_m)=\frac{2za}{\pi X_m}\left[\sqrt{1-\left(\frac{x_a}{X_m}\right)^2}+\sqrt{1-\left(\frac{x_b}{X_m}\right)^2}\right] \quad (18.25)$$

By Eq. (18.17) the imaginary component of $\tilde{W}_n(X_m)$ is

$$Q_n(X_m)=-\frac{2z_a(x_a-x_b)}{\pi X_m^2} \quad (18.26)$$

The overall expression for the complex gain of the relay is

$$\tilde{W}_n(X_m)=\frac{2z_a}{\pi X_m}\left[\sqrt{1-\left(\frac{x_a}{X_m}\right)^2}+\sqrt{1-\left(\frac{x_b}{X_m}\right)^2}\right]-j\frac{2z_a(x_a-x_b)}{\pi X_m^2} \quad (18.27)$$

Figure 18.5*a* shows the relationship between the harmonic linearization coefficients P_n, Q_n and the amplitude X_m. They have discontinuities at $X_m = x_a$ because in this case a finite-duration pulse is obtained at once at the output.

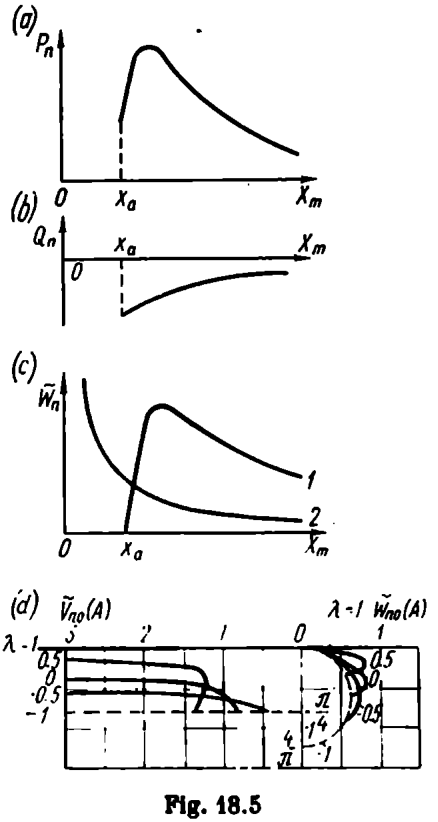

Fig. 18.5

For a single-valued relay response $x_a = x_b$, $Q_n(X_m) = 0$ the complex gain is equal to the real coefficient of harmonic linearization

$$\tilde{W}_n(X_m)=\frac{4z_a}{\pi X_m}\sqrt{1-\left(\frac{x_a}{X_m}\right)^2} \quad (18.28)$$

The plot of $\tilde{W}_n(X_m)$ for this case is shown in Fig. 18.5*c* (curve *1*).

At $x_a = 0$ the relay is made two-positional and Eq. (18.28) takes the form

$$\tilde{W}_n^*(X_m)=\frac{4z_a}{\pi X_m} \quad (18.29)$$

and is represented by curve *2* in Fig. 18.5*c*.

Sometimes the normalized form of a complex gain is convenient. For this purpose certain characteristic values of the input and output signals are isolated in the nonlinear element response $z(x)$ and then used to normalize the harmonic linearization coefficients. For the relay element these

values may be x_a and z_a, and then Eqs. (18.25) and (18.26) take the form

$$P_n(X_m) = \frac{z_a}{x_a}\frac{2x_a}{\pi X_m}\left[\sqrt{1-\left(\frac{x_a}{X_m}\right)^2} + \sqrt{1-\left(\frac{x_b}{X_m}\right)^2}\right] \quad (18.30)$$

$$Q_n(X_m) = -\frac{z_a}{x_a}\frac{2(x_a-x_b)x_a}{\pi X_m^2} \quad (18.31)$$

Introducing the notation:

$\lambda = \frac{x_b}{x_a}$ = reset coefficient; $N = \frac{z_a}{x_a}$ = normalizing factor; $A = \frac{X_m}{x_a}$ = dimensionless amplitude; $\tilde{W}_{n0}(A) = P_{n0}(A) + jQ_{n0}(A)$ = normalized gain, we can write

$$\tilde{W}_n(A) = N\tilde{W}_{n0}(A) \quad (18.32)$$

where

$$\tilde{W}_{n0}(A) = \frac{2}{\pi A^2}\left[\sqrt{A^2-1} + \sqrt{A^2-\lambda^2} - j(1-\lambda)\right] \quad (18.33)$$

At $A = 1$

$$\tilde{W}_{n0}(1) = \frac{2}{\pi}\left[\sqrt{1-\lambda^2} - j(1-\lambda)\right]$$

and

$$P_{n0}(1) = \frac{2}{\pi}\sqrt{1-\lambda^2}, \qquad Q_{n0}(1) = -\frac{2}{\pi}(1-\lambda)$$

For coefficients of harmonic linearization

$$P_{n0}^2(1) + Q_{n0}^2(1) = -\frac{4}{\pi}Q_{n0}(1) \quad (1)$$

or

$$P_{n0}^2(1) + \left[Q_{n0}(1) + \frac{2}{\pi}\right]^2 = \left(\frac{2}{\pi}\right)^2$$

Consequently, the locus of the points of $W_{n0}(A)$ corresponding to $A = 1$ at different values of λ is a circle (more specifically, its right-hand part) whose centre is on the imaginary axis at the point $\left(0, -j\frac{2}{\pi}\right)$ and which passes through the origin of coordinates at $\lambda = 1$.

A family of loci $\tilde{W}_{n0}(A)$ at different λ for this example is shown in Fig. 18.5*d*. In graphical calculations of nonlinear systems, reverse loci with the negative sign $-\tilde{W}_{n0}^{-1}(A) = \tilde{V}_{n0}(A)$ are convenient. In this particular case a family of such loci is shown in Fig. 18.5*d*.

Table 18.1

Name	Form of nonlinearity	$\tilde{W}_n(A) = P_n(A) + jQ_n(A)$	Loci
Dead zone	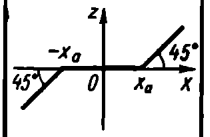	$P_n = 1 - \frac{2\alpha + \sin 2\alpha}{\pi}$ $Q_n = 0$ $\sin \alpha = \frac{1}{A}$	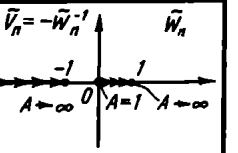
Saturation	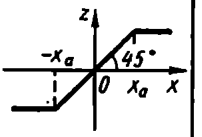	$P_n = \frac{2\alpha + \sin 2\alpha}{\pi}$ $Q_n = 0$ $\sin \alpha = \frac{1}{A}$	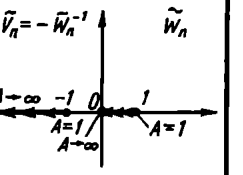
Play	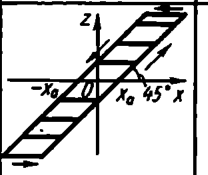	$P_n = \frac{1}{2} - \frac{\alpha}{\pi} + \frac{\sin 2\alpha}{2\pi}$ $Q_n = -\frac{\cos^2 \alpha}{\pi}$ $\sin \alpha = \frac{2}{A} - 1$	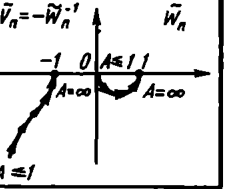
Stop	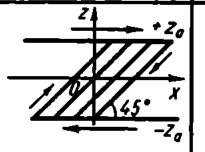	$P_n = \frac{1}{2} + \frac{\alpha}{\pi} - \frac{\sin 2\alpha}{2\pi}$ $Q_n = \frac{\cos^2 \alpha}{\pi}$ $\sin \alpha = \frac{2z_a}{X_m} - 1$	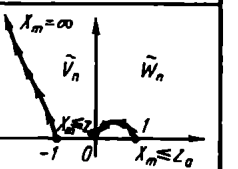
Coulomb friction	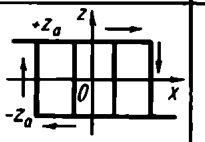	$P_n = 0$ $Q_n = \frac{4z_a}{\pi X_m}$	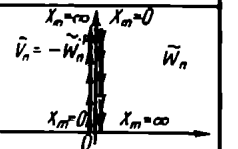
Two-positional relay with positive hysteresis	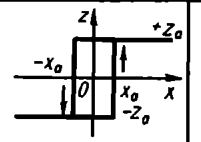	$P_n = \frac{4z_a}{\pi A X_a} \cos \alpha$ $Q_n = -\frac{4z_a}{\pi A X_a} \sin \alpha$ $\sin \alpha = \frac{1}{A}$	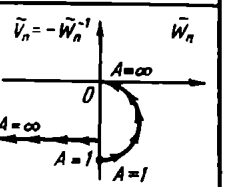

Two-positional relay with constant-width negative hysteresis	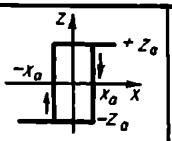	$P_n = \frac{4 z_0}{\pi A x_0} \cos\alpha$ $Q_n = \frac{4 z_0}{\pi A x_0} \sin\alpha$ $\sin\alpha = \frac{1}{A}$	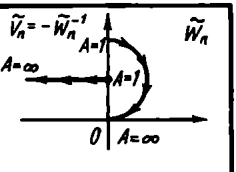
Two-positional relay with variable-width negative hysteresis	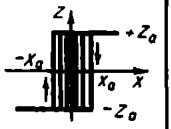	$P_n = 0, \quad Q_n = \frac{4 z_0}{\pi A x_0}$ for $\lvert x\rvert \ll x_0$; $P_n = \frac{4 z_0}{\pi A x_0} \cos\alpha, \quad Q_n = \frac{4 z_0}{\pi A x_0} \sin\alpha$ for $\lvert x\rvert > x_0$; $\sin\alpha = \frac{1}{A}$	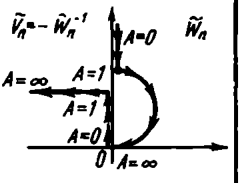
Three-positional relay with positive hysteresis	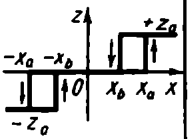	$P_n = \frac{2 z_0}{\pi A x_0} (\cos\alpha_1 + \cos\alpha_2)$ $Q_n = -\frac{2 z_0}{\pi A x_0} (\sin\alpha_1 - \sin\alpha_2)$ $\sin\alpha_1 = \frac{1}{A}, \quad \sin\alpha_2 = \frac{\lambda}{A}$ $\lambda = \frac{x_b}{x_0}$	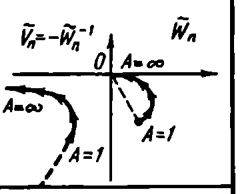
Hysteresisless three-positional relay	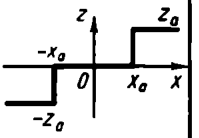	$P_n = \frac{4 z_0}{\pi A x_0} \cos\alpha$ $Q_n = 0$ $\sin\alpha = \frac{1}{A}$	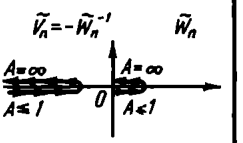
Variable structure	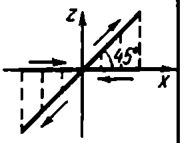	$P_n = \frac{1}{2}$ $Q_n = \frac{1}{\pi}$	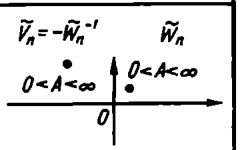
Analog-to-digital converter	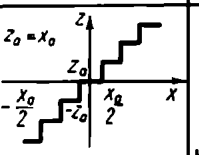	$P_n = \frac{2}{\pi A} \sum_{i=1}^{k} \sqrt{4 - \left(\frac{1}{A}\right)^2 (2i-1)^2}$ $Q_n = 0$ $k = E(A + 0.5)$, where E = integral part	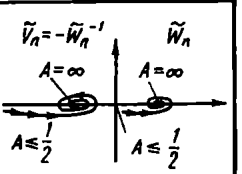

Since

$$\tilde{W}_{n0}^{-1} = \frac{1}{P_{n0}+jQ_{n0}} = \frac{P_{n0}-jQ_{n0}}{P_{n0}^2+Q_{n0}^2} =$$

$$= \frac{\pi A^2}{4} \frac{(\sqrt{A^2-1}+\sqrt{A^2-\lambda^2})+j(1-\lambda)}{A^2-\lambda^2+\sqrt{(A^2-1)(A^2-\lambda^2)}} \qquad (18.34)$$

then at $A=1$

$$\tilde{W}_{n0}^{-1}(1) = \frac{\pi}{4} \frac{\sqrt{1-\lambda^2}+j(1-\lambda)}{1-\lambda} = \frac{\pi}{4}\left[\sqrt{\frac{1+\lambda}{1-\lambda}}+j\right]$$

Consequently, the locus of points of $-\tilde{W}_{n0}^{-1}(A)$ for $A=1$ at different values of λ is the straight line parallel to the x-line and situated in the third quadrant at a distance of $\frac{\pi}{4}$ from the x-line.

As in Example 18.1 the complex gain may be found for different nonlinearities of Ch. XV. The formulae and loci of $\tilde{W}_n(A)$ and $\tilde{V}_n(A)$ for different nonlinearities are given in Table 18.1. A logarithmic scale can usefully be applied to harmonic linearization coefficients (Ref. 84).

18.3. ANALYSIS OF SYMMETRICAL SELF-OSCILLATIONS IN NONLINEAR SYSTEMS

In discussing a control system with a nonlinear element and a linear part (see Fig. 18.1) it was noted that a harmonic balance of oscillations at the input of a nonlinear element and the output of the comparator is the necessary condition for self-oscillations in a system. The equation of harmonic balance in terms of a complex gain is

$$\tilde{W}_n(A)\, W_{LP}(j\omega) = -1 \qquad (18.35)$$

Symmetrical self-oscillations are presumed to be studied without a constant component, which is the case if responses of the nonlinear element are odd and $u=0$.

Expression (18.35) can be regarded as an equation in unknown frequency and amplitude of self-oscillations, the amplitude being determined at the input to the nonlinear element. The equation splits into two (it is written for complex variables) and the real solutions, if they exist, give the frequency and amplitude of possible self-oscillations in the system.

According to L.S. Goldfarb the self-oscillation equation can be conveniently solved graphically as follows*. Write Eq. (18.35)

* There are also other ways to solve self-oscillation equations (see e.g. Ref. 68).

in the form

$$W_{LP}(j\omega) = -\frac{1}{\tilde{W}_n(A)} = -\tilde{W}_n^{-1}(A) = \tilde{V}_n(A) \qquad (18.36)$$

Figure 18.6 illustrates frequency response loci of the linear part and loci of the inverse harmonic linearization coefficient taken with the negative sign $\tilde{V}_n(A) = -\tilde{W}_n^{-1}(A)$. These loci intersect in two points, *1* and *2*, which determine the self-oscillating modes. The self-oscillation frequencies and amplitudes ω_1^c, A_1^c and ω_2^c, A_2^c can be read out from the associated loci in the intersection points.

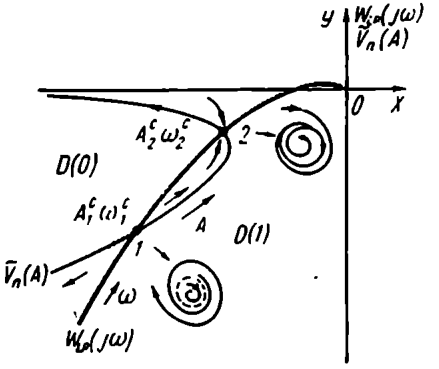

Fig. 18.6

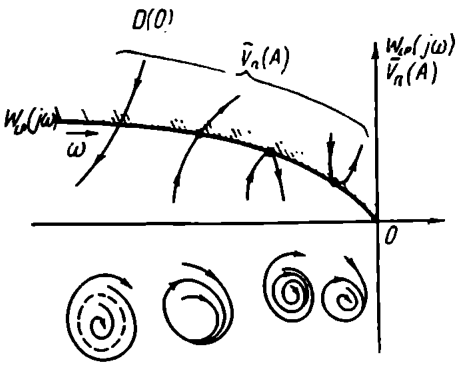

Fig. 18.7

Note that not all the solutions found correspond to stable self-oscillations or oscillations which are restored if there is a short-term disturbance.

To judge the stability of self-oscillations we will regard $\tilde{V}_n(A)$ as a certain complex parameter of a D-decomposition (see Ref. 50 and Sec. 8.4). In this case Eq. (18.35) can be regarded as the condition for the locus $\tilde{V}_n(A)$ to belong to some region of D-decomposition of the plane

$$\tilde{V}_n = W_{LP}(j\omega) = X + jY \qquad (18.37)$$

After hatching the $W_{LP}(j\omega)$ plane accounting for the complex parameter $\tilde{V}_n$, we take up the entire (X, Y) plane, not the real axis alone as in Sec. 8.4. If the whole locus $\tilde{V}_n(A)$ lies within the region D (0), there are no monoharmonic self-oscillations in the system. If it lies within the region D (1), the system is unstable and only diverging processes can arise there. If it intersects the boundary of the region D (0), then near-harmonic oscillations may generate in the system and in order to assess the stability of these more reasoning is necessary (Ref. 50).

Consider, for instance, point *1* where the loci $\tilde{V}_n(A)$ and $W_{LP}(j\omega)$ intersect in Fig. 18.6. Assume that for some reason or other the self-oscillation amplitude has increased and we have moved along the locus $\tilde{V}_n(A)$ in the direction of increasing A. In doing so we move from point *1* to region D (1). The presence of the root with a positive real part should lead to a further increase of the amplitude A and to a disturbance of the mode associated with point *1* (see the respective arrow in Fig. 18.6). If we assume that the self-oscillation amplitude has decreased, then we move along the locus to the region D (0) where all oscillations should decay and the amplitude reduce accordingly.

Consequently, at any changes of the oscillation amplitude in point *1* there is a process characterized by an increasing or vanishing

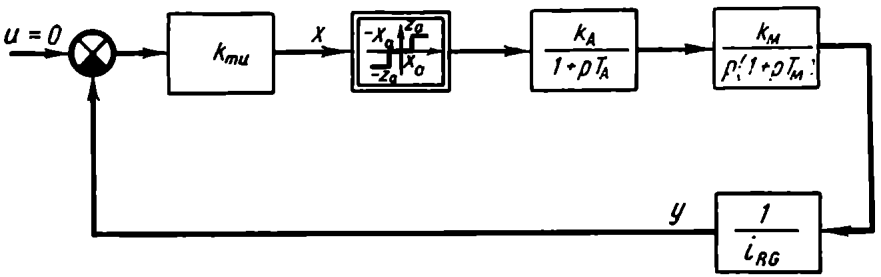

Fig. 18.8

amplitude. This leads to the conclusion that self-oscillations in point *1* are unstable.

Similar reasoning indicates that deviation from the mode in point *2* towards increasing A leads to the region D (0) and will be accompanied by a decrease in A. This will, conversely, lead to the region D (1) and cause an increase in oscillations and a return to point *2*. Consequently, point *2* represents stable self-oscillations.

The above considerations lead to the following rule for judging the stability of self-oscillations: self-oscillations are stable if, while moving along the response of the nonlinear element towards higher amplitudes, we pass from the unstable to the stable region of D-decomposition. Conversely, self-oscillations are unstable if, while moving along the same response, we come to the unstable region of D-decomposition.

Point *1* corresponds to an unstable and point *2*, to a stable limit cycle in the phase space.

Unilaterally unstable oscillations are also possible if a random increase of the amplitude disturbs the mode, while amplitude reduction does not affect the mode, or, conversely, if amplitude reduction

disturbs the mode, while its increase does not. These cases correspond to the tangential points of the amplitude, $\tilde{V}_n(A)$, and frequency, $W_{LP}(j\omega)$, loci.

The four possible types of self-oscillations and the respective phase portraits are shown in Fig. 18.7.

Example 18.2. Find the parameters of symmetric self-oscillations in a relay servo system with a structural diagram of Fig. 18.8 and having the following characteristics: the measuring unit gain $k_{mu} = 1$ V/deg; the relay set voltage $x_a = 0.1$ V; the relay output voltage $z_a = 6$ V; the amplifier gain and time constant $k_A = 5$ and $T_A = 0.2$ sec; the rate gain and the motor time constant $k_M = 300$ deg/(V·sec) and $T_M = 2$ sec; the transmission ratio of the reduction gear is $i_{RG} = 7{,}500$.

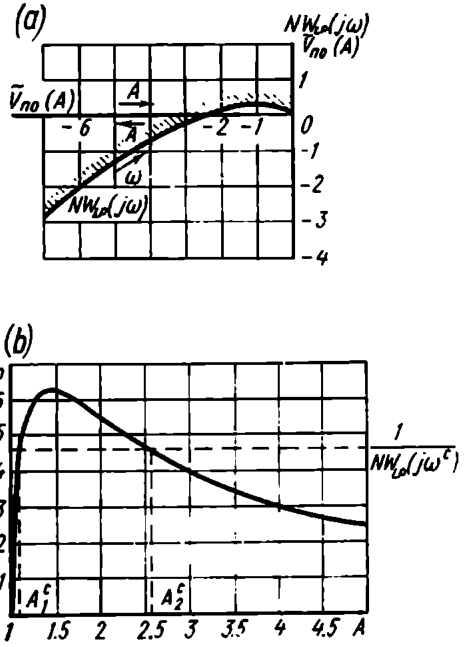

Fig. 18.9

The linear part frequency response is given in the form

$$M_{LP}(j\omega) = \frac{k}{j\omega(1+j\omega T_A)(1+j\omega T_M)} \tag{18.38}$$

where $k = k_{mu}k_A k_M \left(\frac{1}{i_{RG}}\right) = 0.2\,\frac{1}{\text{sec}}$ is the overall gain of the servo system.

The normalizing factor is $N = \frac{z_a}{x_a} = 60$.

The product $NW_{LP}(j\omega)$ with substituted values of the constants is

$$NW_{LP}(j\omega) = \frac{12}{j\omega(1+j\cdot 0.2\omega)(1+j\cdot 2.0\omega)} \tag{18.39}$$

Figure 18.9*a* shows the relative positions of the loci $NW_{LP}(j\omega)$ and $\tilde{V}_{n0}(A)$. These loci have two intersection points at the same frequency $\omega_1^c = \omega_2^c = \omega_3^c$, which can be found from the condition

$$\arg W_{LP}(j\omega^c) = -\pi$$

or

$$\frac{\pi}{2} + \arctan 0.2\omega^c + \arctan 2.0\omega^c = \pi \tag{18.40}$$

whence

$$\omega^c = 1.58 \text{ sec}^{-1}$$

The two self-oscillation amplitudes A_1^c and A_2^c can be found conveniently from the plot of $\tilde{W}_{n0}(A)$ (Fig. 18.9*b*), where the horizontal line is traced at the level $\frac{1}{|NW_{LP}(j\omega^c)|} = 0.458$, which corresponds to representing the self-oscillation equation in the form

$$W_{n0}(A) = -\frac{1}{N} W_{LP}^{-1}(j\omega) \qquad (18.41)$$

The smaller amplitude $A_1^c = 1.10$ corresponds to unstable, and the greater amplitude $A_2^c = 2.59$, to stable self-oscillations, which follows from the above rule for estimating the stability of self-oscillations. In terms of degrees the amplitude of stable self-oscillations is equal to

$$A_2^c \left(\frac{|x_a}{k_{mu}}\right) = 2.59 \times \frac{0.1}{1} = 0.259 \text{ deg}$$

If initially there are no self-oscillations and $x = 0$, then for self-oscillations to generate in the system an initial pulse is required whose values should exceed the smaller amplitude. Only then will stable self-oscillations arise in the system. This phenomenon is referred to as *rigid excitation.*

To solve the same problem for a two-positional relay ($x_a = 0$, all other parameters remain unchanged) no graphical construction is necessary if Eq. (18.29) is used. The conditions of phase balance and the self-oscillation frequency remain the same: $\omega^c = 1.58 \text{ sec}^{-1}$. At this frequency the self-oscillation equation takes the form

$$\frac{4z_a}{\pi X_m^c} W_{LP}(j\omega^c) = -1 \qquad (18.42)$$

or

$$\frac{4 \times 6}{\pi X_m^c}(-0.0364) = -1$$

whence

$$X_m^c = 0.278 \text{ V}$$

i.e., in terms of degrees,

$$\frac{X_m^c}{k_{mu}} = 0.278 \text{ deg}$$

To verify the applicability of the filter hypothesis to the problem under consideration let us find the linear element filtration coefficient at the frequency ω^c of self-oscillations. Since the relay response is odd-symmetrical, only odd harmonics are possible in the system.

Then after substituting $\omega^c = 1.58$ sec^{-1} into Eq. (18.38) we have

$$\left|\frac{W_{LP}(j3\omega^c)}{W_{LP}(j\omega^c)}\right| = \frac{1}{3}\sqrt{\frac{[1+(0.2\times 1.58)^2][1+(2\times 1.58)^2]}{[1+(0.6\times 1.58)^2][1+(6\times 1.58)^2]}} \approx 0.09$$

which demonstrates satisfactory observance of the filter hypothesis (see Sec. 18.1).

Example 18.3. Find the self-oscillation parameters in a second-order structurally unstable astatic system with a stop-type nonlinearity. The structural diagram of the system is shown in Fig. 18.10*a*.

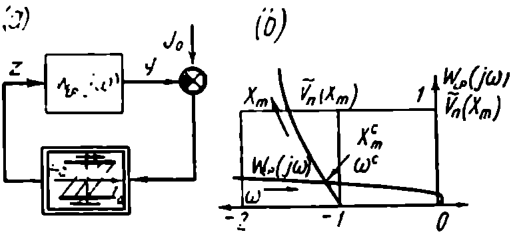

Fig. 18.10

The response of the linear part is

$$W_{LP}(j\omega) = \frac{k}{(j\omega)^2(1+j\omega T_1)(1+j\omega T_2)} \qquad (18.43)$$

where $k = 0.35$ sec^{-2}, $T_1 = T_2 = 0.2$ sec.

Once the frequency locus $W_{LP}(j\omega)$ and the amplitude locus $\tilde{V}_n(X_m)$ (Fig. 18.10*b*) are constructed, find the intersection point of the loci for which $X_m^c = 1.25z_a$ and $\omega^c = 0.55\ \frac{1}{\text{sec}}$.

Here $2z_a$ is the range of the input nonlinearity coordinate.

18.4. ANALYSIS OF NONSYMMETRICAL SELF-OSCILLATIONS IN NONLINEAR SYSTEMS

Aside from the above symmetrical self-oscillations without a constant component, nonsymmetric oscillations also generate in nonlinear systems, and in this case the constant component is very important*. Here too, the nonlinear element can be harmonically linearized, but the harmonic linearization coefficients now depend on the signal constant component as well as on the harmonic component.

If the input of a nonlinear element with a response $z(x)$ is $x = X_0 + X_m \sin \omega t$, then, according to the filter hypothesis, with

* The constant component can be generated either by an external constant signal or by the nonsymmetrical response of the nonlinear element (see Sec. 15.5).

higher harmonic components neglected and the index 1 deleted the output signal can be given in a manner similar to Eq. (18.8)

$$z(t) = Z_0 + Z_m \sin(\omega t + \varphi) = Z_0 + Z_P \sin \omega t + Z_Q \cos \omega t \tag{18.44}$$

or, in the complex form,

$$z(t) = Z_0 + \operatorname{Im}(Z_P + jZ_Q)\, e^{j\omega t} \tag{18.45}$$

where

$$Z_0 = \frac{1}{2\pi} \int_0^{2\pi} z(X_0 + X_m \sin \omega t)\, d(\omega t) \tag{18.46}$$

$$Z_P = \frac{1}{\pi} \int_0^{2\pi} z(X_0 + X_m \sin \omega t) \sin \omega t\, d(\omega t) \tag{18.47}$$

$$Z_Q = \frac{1}{\pi} \int_0^{2\pi} z(X_0 + X_m \sin \omega t) \cos \omega t\, d(\omega t) \tag{18.48}$$

For a nonlinear element two gains may then be introduced: the constant component gain

$$k_n = \frac{Z_0}{X_0} \tag{18.49}$$

and the harmonic component gain

$$\tilde{W}_n = \frac{Z_P + jZ_Q}{X_m} = P_n + jQ_n = |\tilde{W}_n|\, e^{j\varphi_n} \tag{18.50}$$

For a multivalued nonlinearity $Z_Q \neq 0$, $\tilde{W}_n$ is a complex quantity.

Both gains depend on the constant X_0, and on the amplitude of the harmonic, X_m, components of the input

$$k_n = k_n(X_0, X_m) \quad \text{and} \quad \tilde{W}_n = \tilde{W}_n(X_0, X_m) \tag{18.51}$$

The dependence of the harmonic linearization coefficients k_n, P_n, and Q_n on the two quantities, X_0 and X_m, complicates the calculation of self-oscillations in the system, but the techniques applicable to symmetrical self-oscillations are suitable here, with some modifications.

Let us consider the structural diagram of a nonlinear closed-loop system (Fig. 18.11*a*).

Assuming, on the basis of the filter hypothesis, that the signal x consists of two components, $x = X_0 + X_m \sin \omega t$, the closing equations can be considered for each of them:

for the constant component

$$X_0 = U_0 - Z_0(X_0, X_m)\, W_{LP}(0) \tag{18.52}$$

for the harmonic component

$$-X_m = X_m \tilde{W}_n(X_0, X_m)\, W_{LP}(j\omega) \tag{18.53}$$

Use of different equations for the constant and the harmonic component is equivalent to decomposition of a nonlinear element

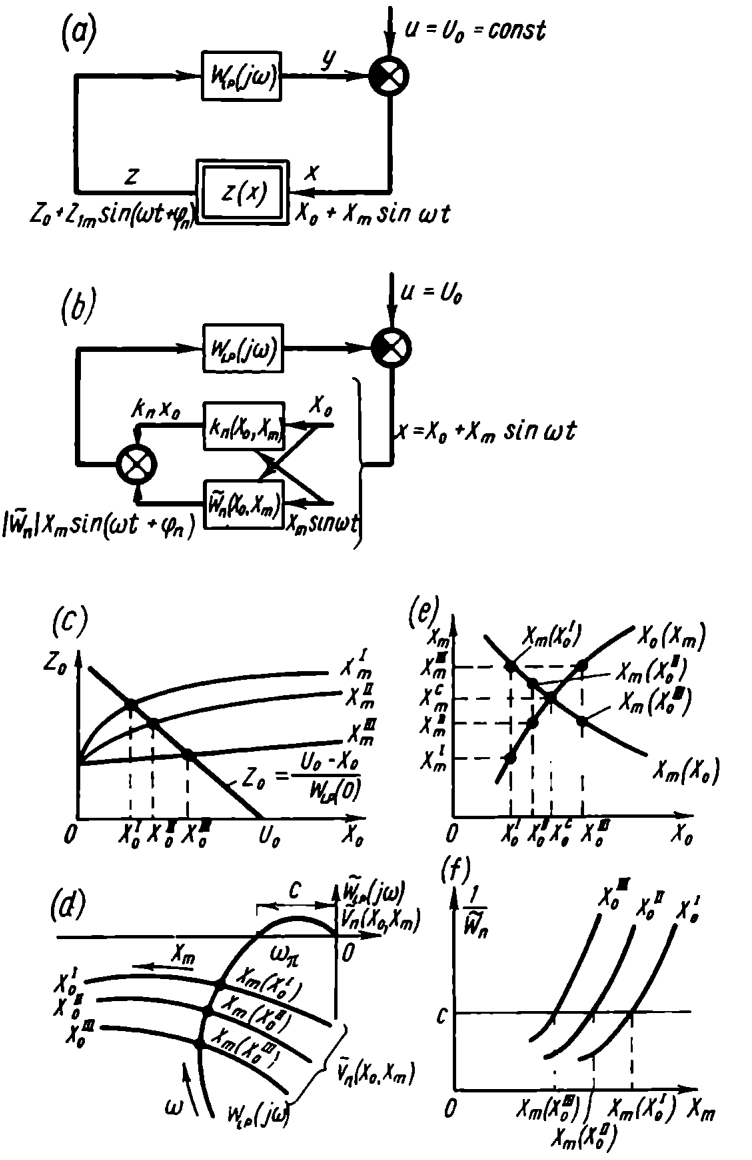

Fig. 18.11

into two parallel different quasilinear elements with gains $k_n(X_0, X_m)$ and $\tilde{W}_n(X_0, X_m)$. The constant component passes

through one of these elements, the harmonic component through the other. The structural diagram corresponding to this representation is shown in Fig. 18.11*b*.

Equations (18.52) and (18.53) can be easily solved simultaneously in a graphical way. To do this, a family of curves $Z_0 (X_0)$ is constructed for different values of X_m (Fig. 18.11*c*). This construction is completely analogous to vibrational linearization of nonlinear responses (see Sec. 15.7). The intersections of the responses with the straight line

$$Z_0 = \frac{U_0 - X_0}{W_{LP}(0)}$$

obtained from Eq. (18.52) give the relation $X_0 (X_m)$.

On the other hand, a family of loci $\bar{V}_n (X_0, X_m) = -\bar{W}_n^{-1}(X_0, X_m)$ can be constructed for different values of X_0 (Fig. 18.11*d*). The intersections with the locus $W_{LP} (j\omega)$ as given by Eq. (18.53) and rearranged as $-\frac{1}{\bar{W}_n (X_0, X_m)} = W_{LP} (j\omega)$ yield the relation $X_m (X_0)$. Simultaneous solution of the equations $X_m = X_m (X_0)$ and $X_0 = X_0 (X_m)$ supplies the desired parameters of self-oscillations: $X_0 = X_0^c$ and $X_m = X_m^c$ (Fig. 18.11*e*).

For single-valued nonlinearities, a family of loci $\bar{V}_n (X_0, X_m)$ is hard to obtain since they all lie on the real axis. In this case it is convenient to plot $-\bar{V}_n = \bar{W}_n^{-1}$ as a function of X_m at different values of X_0 (Fig. 18.11*f*) and use the intersection of these curves with the straight line $\bar{W}_n^{-1} = -W_{LP} (j\omega_n) = C$, where ω_n is the intersection frequency (see Fig. 18.11*d*), to determine the relation $X_m (X_0)$.

The self-oscillation frequency ω^a is found from the point of intersection of $W_{LP} (j\omega)$ with the locus $\bar{V}_n (X_0, X_m)$ at $X_0 = X_0^c$. For a single-valued nonlinearity the self-oscillation frequency is ω_n.

The stability of self-oscillations is found by using the rule of Sec. 18.3 for symmetrical oscillations.

Example 18.4. Find the self-oscillation parameters of a vibrational controller in a d.c. generator voltage stabilizer (see Sec. 15.2) if the amplifier has a nonsymmetric nonlinear response $z (x)$ which coincides with that of a two-positional relay with hysteresis (Fig. 18.12*a*). The system parameters are

$$W_{LP} (j\omega) = \frac{k}{(1 + j\omega T_1)(1 + j\omega T_2)}$$

where $k = 50$, $T_1 = 1$ sec, $T_2 = 4$ sec, $U_0 = 30$ V, $z_a = 1$V, $x_a = 2.0$ V, $\Delta = 0.5$ V.

Equation (18.46) gives the relation $Z_0 (X_0, X_m)$ at different values of X_m. The plots of these relations and their intersection with

the straight line $Z_0 = \frac{U_0 - X_0}{k} = 0.6 - 0.01\left(\frac{X_0}{\Delta}\right)$ are presented in Fig. 18.12*b*.

The intersection points yield curve *2* (Fig. 18.12*d*). The loci $\tilde{V}_n(X_0, X_m)$ calculated by Eqs. (18.47) and (18.48) for the values

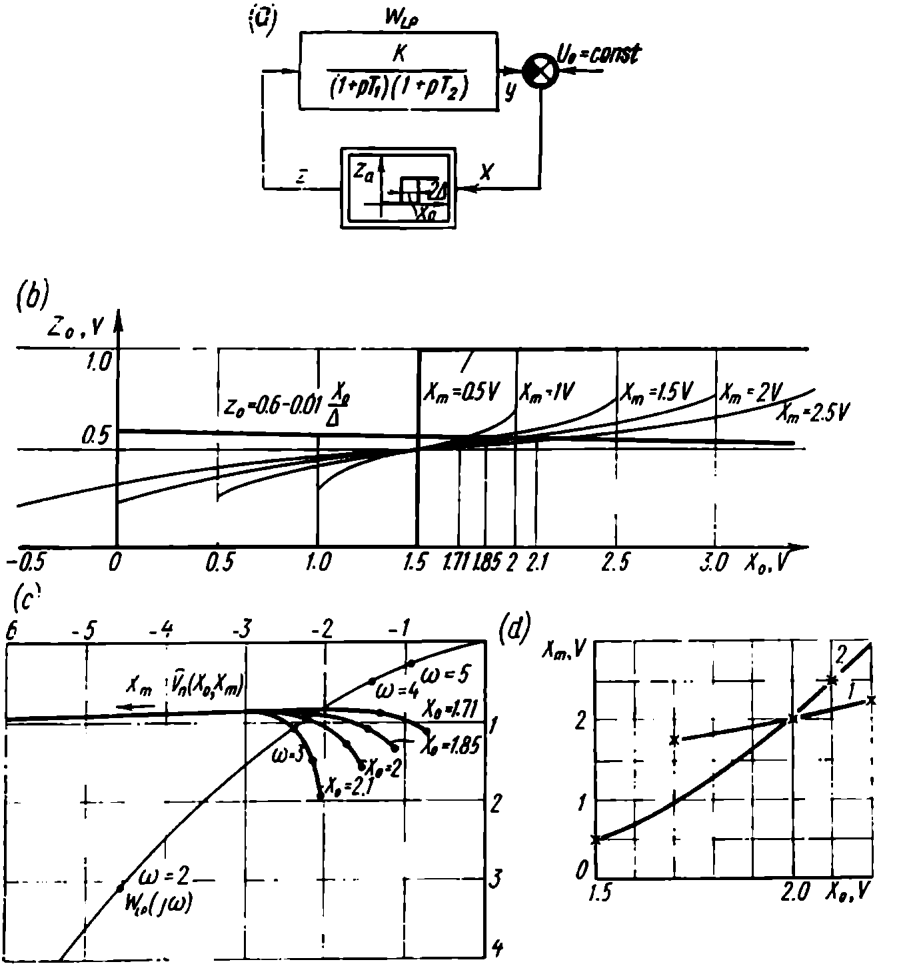

Fig. 18.12

of X_0 obtained from Fig. 18.12*b* are shown in Fig. 18.12*c*. The points of intersection of the loci $\tilde{V}_n(X_0, X_m)$ with the response $W_{LP}(j\omega)$ give curve *1* shown in Fig. 18.12*d*.

Intersection of curves *1* and *2* indicates the values $X_m^c = 2V$ and $X_0^c = 2$ V, which characterize the self-oscillations in the system. The intersection of the loci $\tilde{V}_n(2, X_m)$ (Fig. 18.12*c*) and $W_{LP}(j\omega)$ gives the value of the self-oscillation frequency $\omega^c = 3.15 \frac{1}{\text{sec}}$. Since with increasing amplitude X_m the point of the locus $\tilde{V}_n(2, X_m)$ at this frequency passes from the unstable region to the stable one, the resultant self-oscillations are found to be stable. Because the frequency thus found exceeds $\frac{1}{T_1} = 1\,\text{sec}^{-1}$ and $\frac{1}{T_2} = 0.25\ \text{sec}^{-1}$, the slope of the linear element frequency response is about —40 db/dec, and the filtration conditions necessary for harmonic linearization are thus observed.

18.5. CONDITIONS FOR ABSENCE OF MONOHARMONIC SELF-OSCILLATIONS IN NONLINEAR SYSTEMS

As has been shown above, for a nonlinear control system (we will confine ourselves to systems with a stable or neutral linear part) to be free of monoharmonic oscillations, at $0 \leqslant A < \infty$ the locus $\tilde{V}_n$ should belong to the region D (0), and the filter hypothesis should hold for all points of the region boundary. Since at all frequencies the filter hypothesis is valid only if there is at least one integrating element, the above conditions are applicable only to astatic systems.

This rule is analogous to the Nyquist criterion, in which the critical point —1, *j*0 has been transformed into a complete critical curve, the locus $\tilde{V}_n(A) = -\tilde{W}_n^{-1}(A)$. It should be remembered that this rule is not a strict stability criterion for nonlinear systems because the harmonic linearization method is approximate.

An example of mutual arrangement of the loci $W_{LP}(j\omega)$ and $\tilde{V}_n(A)$ is shown in Fig. 18.13*a* for a system with no self-oscillations. These loci can be replaced by $NW_{LP}(j\omega)$ and $V_{n0}(A)$.

Example 18.5. Find conditions for the absence of monoharmonic self-oscillations in a control system shown in Fig. 18.13*b* with a nonlinearity corresponding to a hysteresisless three-positional relay when there is no external signal ($u = 0$)

(a) $W_{LP}(j\omega) = \dfrac{k_a}{(j\omega)^2(1+j\omega T)}$

(b) $W_{LP}(j\omega) = \dfrac{k_b}{j\omega(1+j\omega T)^2}$

Figure 18.13*c* shows the relative positions of the loci $W_{LP}(j\omega)$ and $\tilde{V}_n(A)$; in the case *a* the system is unstable at any values of the parameters; in the case *b* the condition for absence of monoharmonic

self-oscillations is the inequality

$$\frac{\pi r_a}{2z_a} > -W_{LP}(j\omega_\pi) = \frac{k_b T}{2} \qquad (18.54)$$

Example 18.6. Using the harmonic linearization method determine the limit gain k_{lim} of a linear part with a transfer function $W_{LP}(p) = \frac{k}{T_p(1+pT)}$ if the nonlinear element is of the play (backlash) type.

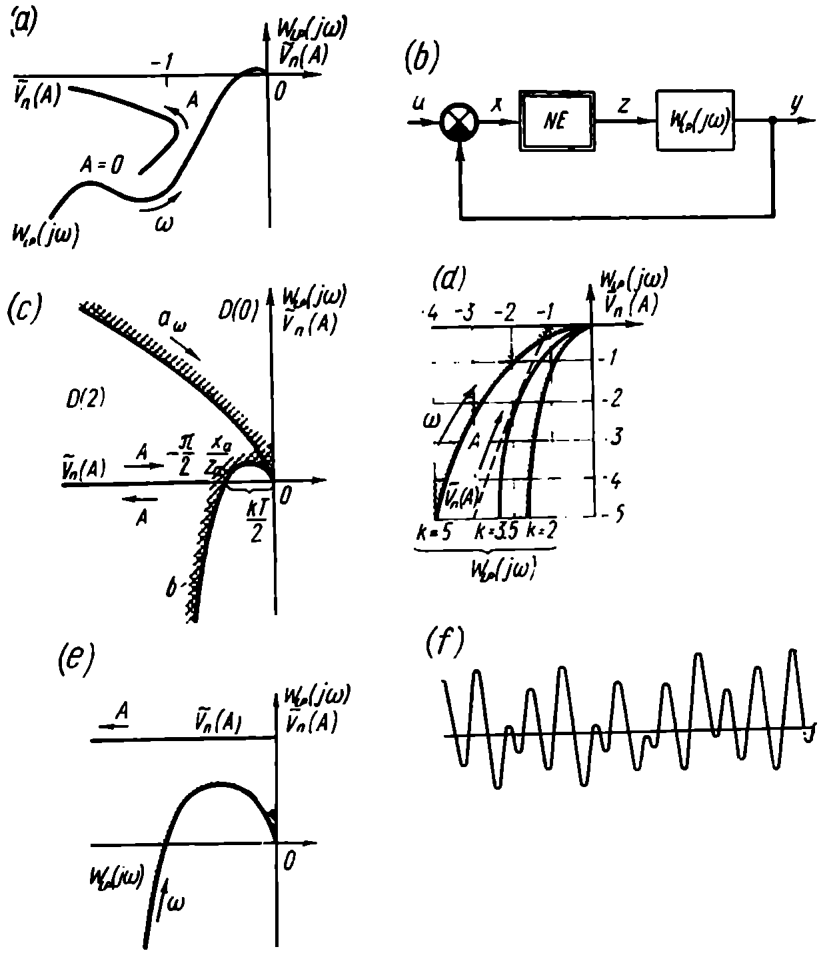

Fig. 18.13

Once the response $\tilde{V}_n(A)$ and a family of responses $W_{LP}(j\omega)$ are constructed for the play-type element at different k values (Fig. 18.13*d*), it can be noted that at $k < 3.5$ all responses $W_{LP}(j\omega)$

do not enclose the locus $\tilde{V}_n(A)$ and, consequently, there are no monoharmonic self-oscillations in the system. At $k > 3.5$ the response $W_{LP}(j\omega)$ intersects the locus $\tilde{V}_n(A)$ and thus monoharmonic oscillations are possible in the system. Consequently $k_{lim} = 3.5$.

If this result is compared against accurate calculations made by the phase plane method, which gives $k_{lim} = 3.04$ (see Example 17.12), then harmonic linearization leads to a somewhat exaggerated value of k_{lim}, a fact attributable to inadequate filtration properties of the linear part and the pronounced effect of higher harmonics.

Example 18.7. Investigate conditions for the absence of monoharmonic oscillations in a system consisting of a two-positional relay circuit with constant-width negative hysteresis (Fig. 15.33 and Table 18.1) and a linear part $W_{LP}(p) = \frac{k}{Tp(1+Tp)^2}$.

Figure 18.13*e* displays the loci $W_{LP}(j\omega)$ and $\tilde{V}_n(A)$ for this case. The condition for the absence of monoharmonic self-oscillations is that the straight line $\tilde{V}_n(A)$ should pass above the locus $W_{LP}(j\omega)$. A more accurate analysis shows, however, that in this case polyharmonic self-oscillations are present whose oscillogram is shown in Fig. 18.13*f*. In other words, the system is unstable, although the entire locus $\tilde{V}_n(A)$ lies in the region $D(0)$.

18.6. IMPROVEMENT OF HARMONIC LINEARIZATION ACCURACY

Harmonic linearization, as noted above, is an approximate method inevitably resulting in errors. Thus, in systems with single-valued nonlinearities for which the loci $\tilde{V}_n(A)$ are positioned on the negative real half-axis, according to harmonic linearization the self-oscillation frequency should remain constant while the linear part gain varies (see Example 18.2), whereas in fact it changes.

A quantitative idea of such errors can be obtained from the plots of Fig. 18.14*a*, *b*, which represent the calculation and simulation results for self-oscillations in the relay servo of Example 18.2.

Figure 18.14*a* shows variations of the dimensionless amplitude A^c, and Fig. 18.14*b*, variations of the self-oscillation frequency ω^c with variations of the product Nk, where N is a normalizing factor and k is the linear part gain. The solid curve shows the calculated data and the dots, the simulated results. The extreme left calculated and experimental points represent the limit value $(Nk)_{lim}$ to the left of which self-oscillations terminate; the calculated value is 8.6 sec^{-1}, the experimental one is 6.3 sec^{-1}.

Unfortunately, calculation yields an exaggerated value of $(Nk)_{lim}$ (see also Example 18.6); this means that at sufficient initial deflections self-oscillations can generate in the system, whereas the harmonic linearization theory asserts their absence.

From Fig. 18.14 the self-oscillation amplitude and frequency are seen to increase with (Nk) and the mismatch of the calculated and actual values of A^c and ω^c reduces noticeably.

Errors in harmonic linearization are attributed to the effect of unallowed-for higher harmonics at the nonlinear element output which increases with reduction of the self-oscillation frequency because in this case the slope of the logarithmic amplitude frequency response of the linear part decreases and its filtering action reduces. That is why the greatest errors in the above example were observed

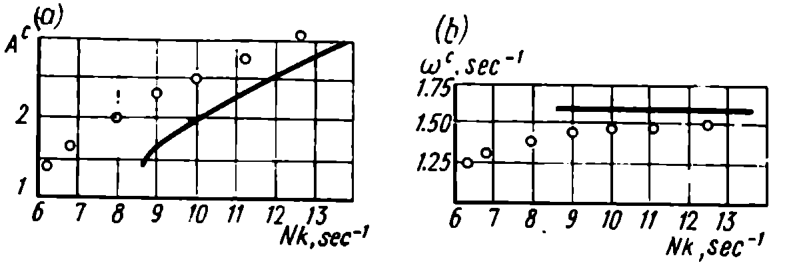

Fig. 18.14

at the limit value of (Nk) when the self-oscillation frequency reduced abruptly. With increasing (Nk) the self-oscillation frequency increases and the errors diminish.

The above example permits assessment of the credibility of results obtained in different applications of the harmonic linearization method. The best results are obtained in determining the parameters of self-oscillation conditions in systems in which these conditions are inherent due to the nature of their operation, e.g. in systems of extremal control or systems with vibrational controllers. Less reliable results are obtained in determining the conditions for the absence of self-oscillations in a system. Nevertheless, the simplicity and illustrativeness of the method, its kinship to the conventional frequency concepts explain its wide practical application.

The accuracy of the method can be improved by partial allowance for the effect of higher harmonics. In the case of single-valued odd nonlinearities the greatest effect is exerted by the third harmonic at the output of the nonlinear element. This effect can be accounted for as follows. Assume that using the conventional procedure we have found the frequency ω and the dimensionless amplitude A of self-oscillations at the input to the nonlinear element (see Fig. 18.1). The amplitude and the phase shift of the third harmonic at the output of the nonlinear element can be found as a function of the amplitude A of the harmonic signal at the input. The frequency response of the linear part can lead to the amplitude and phase of the third harmonic at the input of the nonlinear element; the resultant ampli-

tude and phase shift will be functions of the frequency ω as well as of the amplitude A. Add the third harmonic to the harmonic signal at the input of the nonlinear element and consider propagation of the resultant periodic signal through the nonlinear element. The first harmonic of the output signal will be different from the first harmonic obtained through a conventional procedure as a first approximation. Variations in the parameters of the first harmonic are a function of A and ω and can be allowed for by appropriate variation of

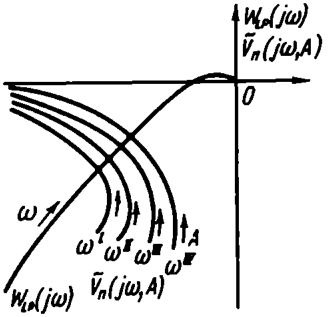

Fig. 18.15

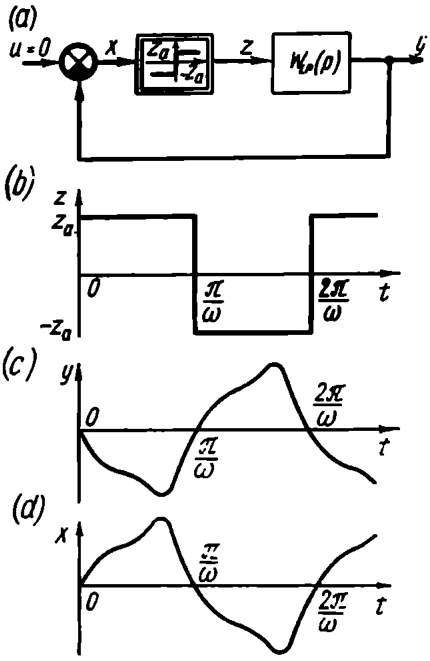

Fig. 18.16

the harmonic linearization coefficient, which is now a function of the frequency ω as well as of the amplitude A.

Then an updated harmonic balance equation is obtained

$$\tilde{W}_n(j\omega, A)\, W_{LP}(j\omega) = -1 \qquad (18.55)$$

or

$$W_{LP}(j\omega) = -\tilde{W}_n^{-1}(j\omega, A) = \tilde{V}_n(j\omega, A) \qquad (18.56)$$

It can be solved graphically by constructing a family of loci $\tilde{V}_n(j\omega, A)$ at different values of ω (Fig. 18.15). The solution is found as the intersection of the frequency response $W_{LP}(j\omega)$ with that curve of the family $\tilde{V}_n(j\omega, A)$ whose frequency coincides with the frequency at the specified point of the locus $W_{LP}(j\omega)$.

Note that in this method the shape of the responses $\tilde{V}_n(j\omega, A)$ depends on the linear part frequency response as well as on the nonli-

near element static response. This rules out a tentative calculation of $\hat{W}_n$ and $\hat{V}_n$ for typical nonlinearities. The method cited above was first proposed and described in detail by E.P. Popov (Ref. 68). He also studied possibilities of accounting for an arbitrary number of higher harmonics, which, however, involves still greater difficulties.

In the particular case of a relay nonlinear response higher harmonics can be allowed for in a simpler way. The linear part of a relay system is generally subject to the action of constant-height rectangular pulses whose sign, duration and relative positions depend on the state of the system's linear part and external actions. An analysis of a relay control system thus reduces to an analysis of the behaviour of the linear part subjected to such pulses. In this sense relay systems are the simplest class of nonlinear systems.

Ya.Z. Tsypkin (Ref. 82) suggested an accurate method for determining the conditions for the existence of self-oscillations and self-oscillation parameters in relay control systems. The basic idea can be illustrated by a system with a relay without a dead zone and hysteresis (Fig. 18.16*a*).

Let us consider the conditions of symmetrical self-oscillations at which the durations of the positive and negative pulses are equal to $\frac{\pi}{\omega}$ each (Fig. 18.16*b*). A periodical sequence of these pulses at the input of the linear part (the time reference point coincides with the positive front) can be represented by a Fourier series

$$z(t) = \frac{4z_a}{\pi} \sum_{k=1}^{\infty} \frac{1}{2k-1} \sin(2k-1)\omega t \tag{18.57}$$

If the linear part frequency response is

$$W_{LP}(j\omega) = |W_{LP}(j\omega)| e^{j\varphi_{LP}(\omega)} = P_{LP}(\omega) + jQ_{LP}(\omega) \tag{18.58}$$

the output can be given as

$$y(t) = \frac{4z_a}{\pi} \sum_{k=1}^{\infty} \frac{|W_{LP}[j(2k-1)\omega]|}{2k-1} \sin\{(2k-1)\omega t + \varphi_{LP}[(2k-1)\omega]\} \tag{18.59}$$

The shape of the signal $y(t)$ is shown in Fig. 18.16*c*. The signal $x(t)$ differs from it only in sign (Fig. 18.16*d*). The condition for the existence of self-oscillations is the balance of phases of the oscillatory processes $y(t)$ and $x(t)$.

The conditions for the existence of self-oscillation can be written as

$$y\left(\frac{\pi}{\omega}\right)=0 \tag{18.60}$$

$$y\left(\frac{\pi}{\omega}\right)>0 \tag{18.61}$$

Observance of the condition (18.60) ensures that the relay switches at $t=\frac{\pi}{\omega}$, and observance of the condition (18.61) leads to switching in the desired direction.

From Eq. (18.59)

$$y\left(\frac{\pi}{\omega}\right)=-\frac{4z_a}{\pi}\sum_{k=1}^{\infty}\frac{|W_{LP}[j(2k-1)\omega]|}{2k-1}\sin\varphi_{LP}[(2k-1)\omega]=$$

$$=-\frac{4z_a}{\pi}\sum_{k=1}^{\infty}\frac{Q_{LP}[(2k-1)\omega]}{2k-1} \tag{18.62}$$

The derivative of $y(t)$ with respect to t is

$$\dot{y}(t)=\omega\frac{4z_a}{\pi}\sum_{k=1}^{\infty}|W_{LP}[j(2k-1)\omega]|\times$$

$$\times\cos\{(2k-1)\omega t+\varphi_{LP}[(2k-1)\omega]\} \tag{18.63}$$

which at $t=\frac{\pi}{\omega}$ yields

$$\dot{y}\left(\frac{\pi}{\omega}\right)=-\omega\frac{4z_a}{\pi}\sum_{k=1}^{\infty}|W_{LP}[(2k-1)\omega]|\cos\varphi_{LP}[(2k-1)\omega]=$$

$$=-\omega\frac{4z_a}{\pi}\sum_{k=1}^{\infty}P_{LP}[(2k-1)\omega] \tag{18.64}$$

The determination of the self-oscillation frequency through the conditions (18.60) and (18.61) is facilitated by the concept of the relay system response

$$\tilde{W}_{rel}(\omega)=-\frac{1}{\omega}\dot{y}\left(\frac{\pi}{\omega}\right)-jy\left(\frac{\pi}{\omega}\right) \tag{18.65}$$

which is a complex function dependent on the frequency ω according to Eqs. (18.62), (18.64), and (18.65) and can be represented by a locus akin to the loci for common frequency responses (Fig. 18.17).

With the locus $\tilde{W}_{rel}(\omega)$ known, the self-oscillation frequency is easily found as the intersection point of $\tilde{W}_{rel}(\omega)$ with the negative real half-axis. Indeed, the following relations hold for this point ($\omega^c = \omega_\pi$)

$$\operatorname{Im} \tilde{W}_{rel}(\omega_\pi) = -y\left(\frac{\pi}{\omega_\pi}\right) = 0$$

$$\operatorname{Re} \tilde{W}_{rel}(\omega_\pi) = -\frac{1}{\omega} \dot{y}\left(\frac{\pi}{\omega_\pi}\right) < 0$$

which coincides with Eqs. (18.60) and (18.61).

With the self-oscillation frequency ω^c known, the shape of self-oscillation can be found by Eq. (18.59); in doing so, the absence of extra relay switchings within a half-period should be verified.

If the linear part frequency response is such that all harmonics at the output of the linear part, starting with 3ω, are negligible, then we have the harmonic output signal

$$y(t) = \frac{4z_a}{\pi} |W_{LP}(j\omega)| \sin[\omega t + \varphi_{LP}(\omega)] \qquad (18.66)$$

The relay system response in this case coincides with $W_{LP}(j\omega)$ to within the proportionality factor

$$\tilde{W}_{rel}(\omega) = \frac{4z_a}{\pi} W_{LP}(j\omega) \qquad (18.67)$$

and the self-oscillation frequency $\omega^c = \omega_\pi$ is found as the intersection point of $W_{LP}(j\omega)$ with the negative real half-axis. The self-oscillation amplitude is found from Eq. (18.66) as

$$X_m = \frac{4z_a}{\pi} \left| W_{LI}\ j\omega_\pi) \right| \qquad (18.68)$$

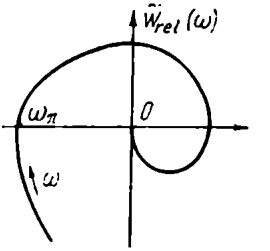

Fig. 18.17

These solutions coincide with the results obtained in Example 18.2 by the method of harmonic linearization.

The problem of self-oscillations in systems in which the relay has hysteresis and a dead zone is solved in a similar way. In the case of a dead zone (with or without hysteresis) the rectangular pulses at the relay output have a duty factor $\gamma < 1$; therefore two families of responses have to be constructed for different γ. One of these describes relay switchings at $t = \frac{\pi}{\omega}$, and the other at $t = \frac{\gamma\pi}{\omega}$. This is a hindrance in practice, especially in cases where the conditions for absence of self-oscillations in a relay control system are to be determined.

18.7. APPLICATION OF THE HARMONIC LINEARIZATION METHOD IN THE PRESENCE OF SEVERAL NONLINEARITIES

Take up self-oscillations in a system with two nonlinear elements divided by linear parts (Fig. 18.18). If the signal at the input of the

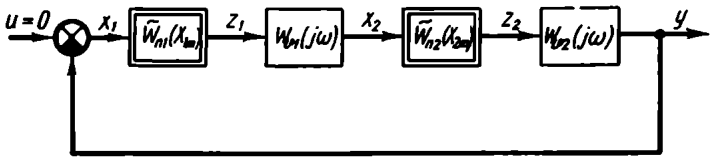

Fig. 18.18

first nonlinear element is

$$x(t) = X_{1m} \sin \omega t = \operatorname{Im} X_{1m} e^{j\omega t} \tag{18.69}$$

then the complex image of the first harmonic at the output is equal to

$$\dot{Z}_{1m} = \tilde{W}_{n1}(X_{1m})\, X_{1m} \tag{18.70}$$

and at the input of the second nonlinear element

$$\dot{X}_{2m} = \tilde{W}_{n1}(X_{1m})\, W_{LP1}(j\omega)\, X_{1m} \tag{18.71}$$

The amplitude X_{2m} of the first harmonic depends on the amplitude X_{1m} and frequency

$$X_{2m}(\omega, X_{1m}) = |\tilde{W}_{n1}(X_{1m})|\, |W_{LP1}(j\omega)|\, X_{1m} \tag{18.72}$$

Then we obtain the expressions for complex images of the first harmonics at the output of the second nonlinear and linear elements

$$\dot{Z}_{2m} = \tilde{W}_{n1}(X_{1m})\, W_{LP}(j\omega)\, \tilde{W}_{n2}[X_{2m}(\omega, X_{1m})]\, X_{1m} \tag{18.73}$$

$$\dot{Y}_m = \tilde{W}_{n1}(X_{1m})\, W_{LP1}(j\omega)\, \tilde{W}_{n2}[X_{2m}(\omega, X_{1m})]\, W_{LP2}(j\omega)\, X_{1m} \tag{18.74}$$

and the self-oscillation equation is

$$\tilde{W}_{n1}(X_{1m})\, \tilde{W}_{n2}[X_{2m}(\omega, X_{1m})]\, W_{LP}(j\omega) = -1 \tag{18.75}$$

where

$$W_{LP}(j\omega) = W_{LP1}(j\omega)\, W_{LP2}(j\omega)$$

Equation (18.75) can be solved graphically by finding the intersections of the inverse frequency response $\tilde{W}_{LP}^{-1}(j\omega)$ with a family defined by

$$-\tilde{W}_{n1}(X_{1m})\, \tilde{W}_{n2}[X_{2m}(\omega, X_{1m})]$$

which can be regarded as the single complex gain $-\bar{W}_n(j\omega, X_{1m})$ dependent on ω and X_{1m}. The self-oscillation frequency on the locus $W_{LP}(j\omega)$ should coincide with the frequency specified in the family of loci $-\bar{W}_n(j\omega, X_{1m})$ as in the case of the responses $W_{LP}(j\omega)$ and $\bar{V}_n(j\omega, A)$ in Fig. 18.15.

Note that the self-oscillations are determined in a similar way if there is one nonlinear element whose output signal depends not only on the input signal but on its derivatives (in other words, the nonlinear element is not inertialess and its behaviour is described by a nonlinear differential equation).

The problem is greatly simplified if $W_{LP1}(j\omega) = 1$ or $W_{LP2}(j\omega) = 1$. In this case the harmonic linearization coefficients of two nonlinear elements connected in series should not be multiplied; instead they should be reduced to one element with a common nonlinear response (see Sec. 16.2) and a common complex gain. The problem then boils down to the conventional version shown in Fig. 18.1 and discussed in detail earlier.

One example of a closed-loop system with two nonlinearities separated by linear dynamic elements is a self-oscillating, extremal control system with extremum memorization described in Sec. 15.4. The steady-state self-oscillations for this system in the case of first-order linear elements were discussed with reference to the phase plane in Sec. 17.6.

A simplified structural diagram of this system based on Fig. 15.8*i* and composed to suit the harmonic linearization method is shown in Fig. 18.19*a*.

The both nonlinearities $z(x)$ and $u(y)$ are nonsymmetric. Depending on the values of x_0 and z_m the response $z(x)$ of the plant can be anywhere in the plane of coordinates, while the nonlinearity $u(y)$ at $|u| = U_0$ represents the alternation of the sign of u whenever y deviates from the maximal value y_m by a specified value v_m (see Sec. 15.4).

The nonlinear element $u(y)$ denoted as *Flip-flop* includes also units which memorize the extremum and differentiate the signal controlling the flip-flop.

The linear elements $W_{LP1}(p)$ and $W_{LP2}(p)$ can generally be anything.

Assume that the response of the plant's inertialess part is given as a quadratic parabola

$$z = z_m - k(x + x_0)^2 \tag{18.76}$$

In considering the symmetrical self-oscillations near the extremum x_0 is assumed zero. When the sine signal $x = X_m \sin \omega t$ is fed to the nonlinear plant's input the signal $z(t)$ contains only the first and second harmonics apart from the constant component; at $x_0 = 0$

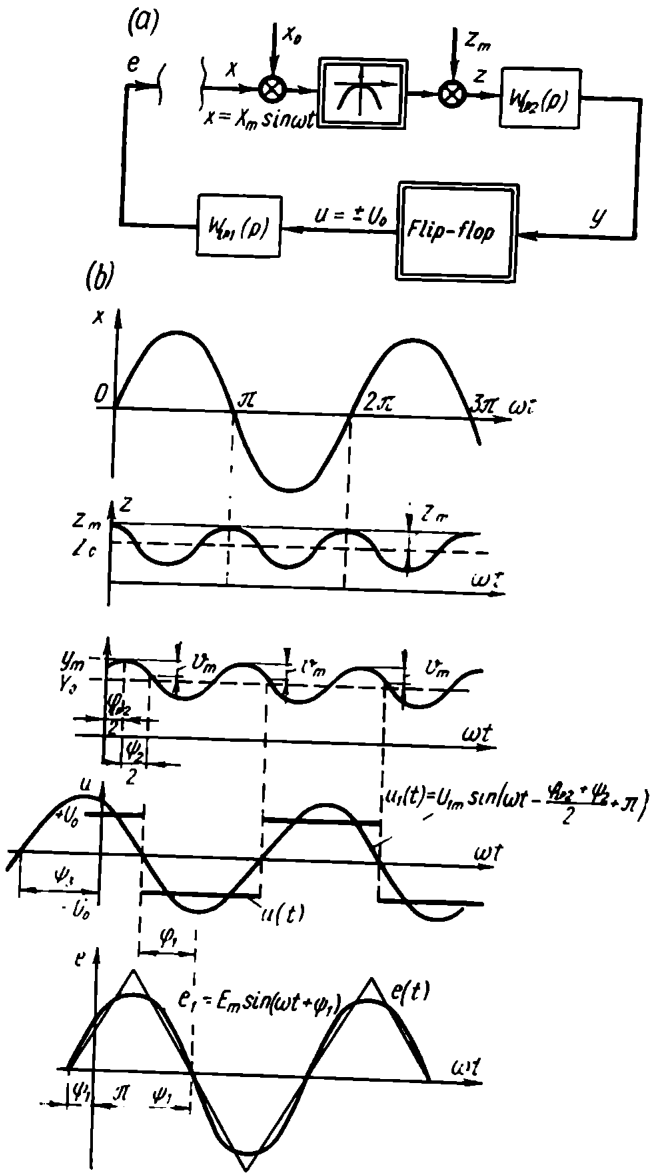
(a)
e
x
x_0
z_m
z
$x = X_m \sin\omega t$
$W_{p2}(p)$
$W_{p1}(p)$
$u = \pm U_0$
Flip-flop
y
(b)
x
0
π
2π
3π
ωt
z
z_m
l_c
ωt
y_m
Y_0
φ_{p2}
ψ_2
ωt
u
$+U_0$
$-U_0$
ψ_1
$u_1(t)=U_{1m}\sin(\omega t - \frac{\varphi_{p2}+\psi_2}{2}+\pi)$
ωt
u(t)
φ_1
e
$e_1 = E_m \sin(\omega t + \varphi_1)$
e(t)
ωt
ψ_1
π
ψ_1

Fig. 18.19

the first harmonic vanishes, and the output signal

$$z(t) = Z_0 + (z_m - Z_0)\cos 2\omega t \tag{18.77}$$

is a sine wave with doubled frequency. Besides

$$Z_m = z_m - Z_0 = \frac{kX_m^2}{2} \tag{18.78}$$

Once it has propagated through the linear element $W_{LP2}(p)$ and affected the second nonlinear element $u(y)$ *Flip-flop*, this signal converts into the rectangular signal $u(t)$ of frequency ω. The plots characterizing the conversions of the signal $x = X_m \sin \omega t$ into $z(t)$, $y(t)$, $u(t)$ and $e(t)$ are shown in Fig. 18.19*b*.

The characteristic feature of this example is the double conversion of the main signal frequency in its propagation through the system. The element with the parabolic response doubles and the flip-flop halves the frequency.

If $x_0 = 0$, harmonic linearization does not require the application of the filter hypothesis to the element $W_{LP2}(p)$ since the signal $z(t)$ includes just one harmonic component and the element $W_{LP2}(p)$ should not have the properties of a filter eliminating undesired harmonics. In contrast the element $W_{LP1}(p)$ should meet all the filter requirements because the signal $u(t)$ at the input of this element differs greatly from a sinusoid. The plots of the first harmonics $u_1(t)$ and $e_1(t)$ of the signals $u(t)$ and $e(t)$ are presented in Fig. 18.19*b*.

The harmonic balance conditions are formulated for this problem as follows: at $x = X_m \sin \omega t$ the first harmonic of the output signal $e_1 = E_m \sin(\omega t + \psi_1)$ should ensure a balance of amplitudes ($E_m = X_m$) and of phases ($\psi_1 = 0$).

Because the signal $u(t)$ is rectangular and has an amplitude U_0, its first harmonic has an amplitude $U_{1m} = \frac{4U_0}{\pi}$.

The balance of amplitudes is, in this case,

$$E_m = \frac{4U_0}{\pi} |W_{LP1}(j\omega)| = X_m \tag{18.79}$$

In formulating the conditions for the balance of phases, a time shift of signals propagating through all the elements of the circuit should be taken into consideration. Analyzing the propagation of the signal $z(t)$ given by Eq. (18.77) through the linear element $W_{LP2}(j2\omega)$ gives the phase lag of $y(t)$ relative to $z(t)$

$$\varphi_{LP2} = -\arg W_{LP2}(j2\omega) \tag{18.80}$$

at the amplitude of this signal

$$Y_m = Z_m |W_{LP2}(j2\omega)| \tag{18.81}$$

The switching time of the flip-flop is given by the phase ψ_2 and is described by the equation

$$Y_m \cos \psi_2 = Y_m - v_m \tag{18.82}$$

whence

$$\psi_2 = \arccos \frac{Y_m - v_m}{Y_m} \tag{18.83}$$

The first harmonic of $u(t)$ is consequently given by the equation

$$u_1(t) = U_{1m} \sin(\omega t + \psi_3) \tag{18.84}$$

where

$$\psi_3 = \pi - \frac{\varphi_{LP2} + \psi_2}{2} \tag{18.85}$$

Once the signal has propagated through the element $W_{LP1}(j\omega)$, the phase takes on the value

$$\psi_1 = \psi_3 + \arg W_{LP1}(j\omega) \tag{18.86}$$

and the equation of the balance of phases is

$$\psi_1 = \pi + \frac{1}{2} \arg W_{LP2}(j2\omega) + \arg W_{LP1}(j\omega) - \\ - \frac{1}{2} \arccos \frac{Y_m - v_m}{Y_m} = 0 \tag{18.87}$$

where

$$Y_m = \frac{kX_m^2}{2} |W_{LP2}(j2\omega)|$$

Solving Eqs. (18.79) and (18.87) simultaneously can give the amplitude X_m^c and the frequency ω^c of self-oscillations in the system. Since these equations do not include the displacement z_m of the response $z(x)$ along the vertical axis, the self-oscillation parameters do not depend on the response drift along the z-axis.

Example 18.8. Determine the self-oscillation parameters in an extremal system if $W_{LP1}(j\omega) = \frac{k_1}{j\omega}$ and $W_{LP2}(j\omega) = \frac{k_2}{(1 + j\omega T_2)}$, $k = 10^{-4}$ deg/m^2, $k_1 = 5 \times 10^{-4}$ m/(V·sec), $k_2 = 1$ V/deg, $T_2 = 1$ sec, $U_0 = 36$ V, $v_m = 1$ V.

Substituting the values of W_{LP1} and W_{LP2} into Eqs. (18.79) and (18.47) gives

$$4U_0 k_1 = \pi X_m \omega \tag{18.88}$$

and

$$\arccos \frac{Y_m - v_m}{Y_m} + \arctan 2\omega T_2 = \pi \tag{18.89}$$

where

$$Y_m = \frac{kX_m^3 k_2}{2\sqrt{1+(\omega T_2)^2}} \tag{18.90}$$

or, after substitution of X_m from Eq (18.88),

$$Y_m = \frac{8kk_1^3 k_2 U_0^3}{\pi^2 \omega^2 \sqrt{1+(\omega T_2)^2}} \tag{18.91}$$

Denoting $\omega T_2 = \Omega$ and

$$\frac{\pi^2 v_m}{8kk_1^2 k_2 U_0^3 T_2^3} = \lambda \tag{18.92}$$

and substituting (18.91) and (18.92) into (18.89) give the following transcendental equation

$$\arccos\left[1-\lambda\Omega\sqrt{1+\Omega^2}\right] + \arctan 2\Omega = \pi \tag{18.93}$$

Solution of this equation gives the relation $\Omega(\lambda)$, shown in Fig. (18.20). With λ calculated, the plot readily yields the self-oscillation frequency Ω^c and $\omega^c = \frac{\Omega^c}{T_2}$, and by Eq. (18.88) the self-oscillation amplitude is

$$X_m^c = \frac{4U_0 k_1 T_2}{\pi \Omega^c} \tag{18.94}$$

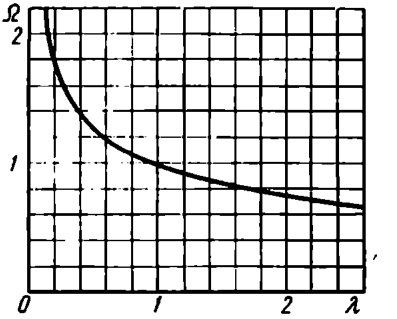

Fig. 18.20

Calculations for the specified parameters gives $\lambda = 0.38$, and the plot of $\Omega(\lambda)$, $\Omega^c = 1.4$. Consequently, $\omega^c = \frac{\Omega^c}{T_2} = 1.4$ sec^{-1} and

$$X_m^c = \frac{4 \times 36 \times 5 \times 10^{-4}}{3.14 \times 1.4} \approx 1.6 \cdot 10^{-2} \text{ m}$$

Certain disagreement with the results of Example 17.11 (Ch. XVII) are attributable to insufficient filtering properties of the element $W_{LP1}(p)$.

18.8. THE USE OF THE HARMONIC LINEARIZATION METHOD IN THE STUDIES OF NONLINEAR SAMPLED-DATA SYSTEMS

Let us consider a nonlinear sampled-data amplitude-modulated (*AM*) control system where (Fig. 18.21) the inertialess nonlinear element, *NE*, is connected into the misalignment circuit before the simple pulse element, *PE*, and the reduced continuous part, *RCP*, with a shaping element, *SE*, and a continuous part, *CP* (see Sec. 12.2). These elements combine to form a linear sampled-data part, *LSDP*.

The characteristic feature of nonlinear sampled-data systems is that the periodic modes at $u = 0$, if generated at all, are normally synchronized by a pulse element. Owing to the periodic

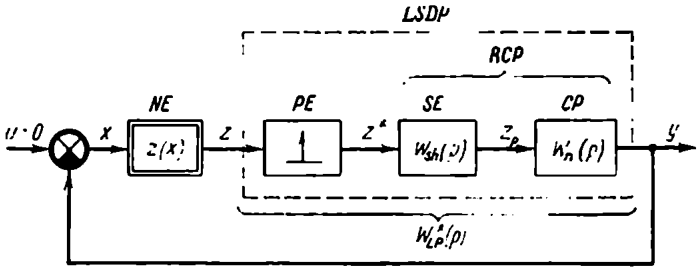

Fig. 18.21

disconnection of the system loop by the pulse element, the periodic mode frequencies ω are related to the frequency of the pulse element by the condition

$$\frac{\omega_p}{\omega} = n \geqslant 2 \tag{18.95}$$

where n is an integer.

For this reason the term self-oscillations is not applicable to periodic modes at $u = 0$ although the case in question seems to be akin to self-oscillations in nonlinear continuous systems. It is noteworthy

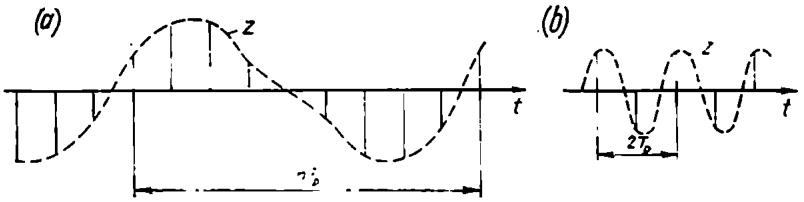

Fig. 18.22

that in certain cases the condition (18.95) is not observed and complex nonperiodic oscillations generate in nonlinear sampled-data systems. This happens, for instance, in relay sampled-data systems whose linear part is either unstable or contains more than two integrating elements connected in series. We will not dwell on such cases.

Since the pulse element responds only to discrete input values, we will deal with these alone. The periodic mode is completely described by n discrete values of the signal at the nonlinear element output sampled sequentially over the oscillation period (Fig. 18.22*a*). The maximal possible frequency of oscillations in the periodic mode is $\frac{\omega_p}{2}$ (at $n = 2$) (Fig. 18.22*b*).

From harmonic analysis a periodic discrete function is known to be representable as a trigonometric polynomial with a finite number of harmonics

$$z(lT_p) = \sum_{k=0}^{n_1} \left(Z_{Ph} \sin k \frac{2\pi}{nT_p} lT_p + Z_{Qk} \cos k \frac{2\pi}{nT_p} lT_p \right) =$$

$$= \sum_{k=0}^{n_1} \left(Z_{Ph} \sin k \frac{2\pi}{n} l + Z_{Qk} \cos k \frac{2\pi}{n} l \right) \qquad (18.96)$$

where $\frac{2\pi}{nT_p}$ = oscillation frequency in the periodic mode

n_1 = number of harmonics equal to

$$n_1 = \begin{cases} \frac{n}{2} & \text{if } n \text{ is even} \\ \frac{(n-1)}{2} & \text{if } n \text{ is odd} \end{cases}$$

and the coefficients are

$$Z_{Q0} = \frac{1}{n} \sum_{l=0}^{n-1} z(lT_p) \qquad (18.97)$$

$$Z_{Ph} = \frac{2}{n} \sum_{l=0}^{n-1} z(lT_p) \sin k \frac{2\pi}{n} l \qquad (18.98)$$

$$Z_{Qk} = \frac{2}{n} \sum_{l=0}^{n-1} z(lT_p) \cos k \frac{2\pi}{n} l \qquad (18.99)$$

The frequency of the senior harmonic, which is equal to $n_1 \left(\frac{2\pi}{nT_p} \right)$, is in the case of an even n equal to $\frac{\pi}{T_p} = \frac{\omega_p}{2}$ and in the case of an odd n, to

$$\frac{n-1}{n} \frac{\pi}{T_p} < \frac{\omega_p}{2}$$

The discrete harmonic components (denoted as z_k) propagate through the *LSDP*, each producing a discrete harmonic component Y_k at the output. The relation between the harmonic components $\dot{Z}_{mk}$ and $\dot{Y}_{mk}$ has been shown in Sec. 13.2 to depend on the complex value of the *LSDP* frequency response $W^*_{LP}(j\omega)$

$$\dot{Y}_{mk} = W^*_{LP}(jk\omega)\, \dot{Z}_{mk} \qquad (18.100)$$

The frequency response of the *LSDP* in the range from 0 to $\frac{\omega_p}{2}$ decreases, which means that in this range the *LSDP* is a low-pass

filter. True, the decrease does not reach zero as in continuous systems, but it still takes place. The high frequency discrete harmonic components the frequencies of which are within this range and whose amplitudes are usually below that of the first harmonic weaken again when propagating through the *LSDP*. This fact and the finite number of discrete harmonics permit us to neglect higher discrete harmonic components at the input of the nonlinear element, as is done in continuous systems.

If $n = 2$ or $n = 3$ $\left(\text{the periodic modes of the highest frequency } w = \frac{\omega_p}{2},\ \omega = \frac{\omega_p}{3}\right)$ the sum in Eq. (18.98) contains just one harmonic component with a frequency ω. In these cases the method will give accurate, not approximate, results. This is also valid for symmetric oscillations at $n = 4$. The relevant reasoning is given in an example below.

Let us now take up periodic modes in which the constant component at the nonlinear element output is zero. Under this condition a discrete harmonic signal can be assumed at the input of the nonlinear element

$$x(lT_p) = X_m \sin\left(\frac{2\pi}{n} l + \psi\right) \tag{18.101}$$

In the complex form we have

$$\dot{X}_m = X_m e^{j\psi} \tag{18.102}$$

The phase shift ψ varies in the range $-\frac{\pi}{n} < \psi \leqslant \frac{\pi}{n}$, which at the frequency $\frac{2\pi}{nT_p}$ is associated with a time shift ranging from $-\frac{T_p}{2}$ to $\frac{T_p}{2}$ and covering all possible cases since at shifts of large magnitude the time reference can always be shifted by the appropriate integral number of periods T_p so that the phase shift falls within this range.

The first harmonic of a discrete periodic signal at the nonlinear element output is

$$z_1(lT_p) = Z_{P1} \sin\frac{2\pi}{n} l + Z_{Q1} \cos\frac{2\pi}{n} l \tag{18.103}$$

where in accordance with Eqs. (18.98) and (18.99)

$$Z_{P1} = \frac{2}{n} \sum_{l=0}^{n-1} z(lT_p) \cos\frac{2\pi}{n} l \tag{18.104}$$

$$Z_{Q1} = \frac{2}{n} \sum_{l=0}^{n-1} z(lT_p) \cos\frac{2\pi}{n} l \tag{18.105}$$

The expressions for the coefficients Z_{P1} and Z_{Q1} at different n values are given in Table 18.2; for brevity the value of $z(lT_p)$ is denoted as z_l ($l = 0, 1, 2, \ldots, 7$).

Table 18.2

n	Z_{P1}	Z_{Q1}
2	0	$\frac{z_0 - z_1}{2}$
3	$\frac{z_1 - z_2}{\sqrt{3}}$	$\frac{2z_0 - z_1 - z_2}{3}$
4	$\frac{z_1 - z_3}{2}$	$\frac{z_0 - z_2}{2}$
5	$0.3804(z_1 - z_4) + 0.2351(z_2 - z_3)$	$0.4z_0 + 0.1236(z_1 + z_4) - 0.3236(z_2 + z_3)$
6	$\frac{\sqrt{3}}{6}(z_1 + z_2 - z_4 - z_5)$	$\frac{1}{6}(2z_0 + z_1 - z_2 - 2z_3 - z_4 + z_5)$
7	$0.2234(z_1 - z_2) + 0.2785(z_2 - z_5) + 0.1239(z_3 - z_4)$	$0.2857z_0 + 0.1781(z_1 + z_6) - 0.6360(z_2 + z_5) - 0.2574(z_3 + z_4)$
8	$\frac{\sqrt{2}}{8}(z_1 + z_3 - z_5 - z_7) + \frac{1}{4}(z_2 - z_6)$	$\frac{1}{4}(z_0 - z_4) + \frac{\sqrt{2}}{8}(z_1 - z_3 - z_5 + z_7)$

The complex expression for the signal z_l (lT_p) is

$$\dot{Z}_{lm} = \sqrt{Z_{P1}^2 + Z_{Q1}^2}\, e^{j \arctan \frac{Z_{Q1}}{Z_{P1}}} \qquad (18.106)$$

The ratio of $\dot{Z}_{lm}$ to $\dot{X}_m$ is referred to as a *complex gain of a nonlinear element in a sampled-data system*

$$\bar{W}_n^*(X_m, n, \psi) = \frac{\dot{Z}_{lm}}{\dot{X}_m} = \frac{\sqrt{Z_{P1}^2 + Z_{Q1}^2}}{X_m} e^{j(\varphi_n - \psi)} \qquad (18.107)$$

where $\varphi_n = \arctan \frac{Z_{Q1}}{Z_{P1}}$.

The complex gain in a sampled-data system depends on the relative period of oscillations n and on the phase shift ψ of the input signal as well as on the amplitude.

The effect of the phase shift ψ on $\tilde{W}_n^*$ can be illustrated by a two-positional relay response.

Example 18.9. Find the complex gain if there is a two-positional hysteresisless relay response (Fig. 18.23). For this response the condition that the constant component Z_{Q0} be zero holds only for even n. Figure 18.24 shows discrete input and output signals of the nonlinear element at $n = 2$ and different signs of ψ. At $\psi > 0$ (Fig. 18.24*a*) the coefficients Z_{P1} and Z_{Q1} found by the formulae of Table 18.2 are: $Z_{P1} = 0$; $Z_{Q1} = z_a$.

For this case $\varphi = \frac{\pi}{2}$ and the complex gain is

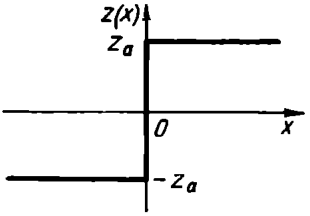

Fig. 18.23

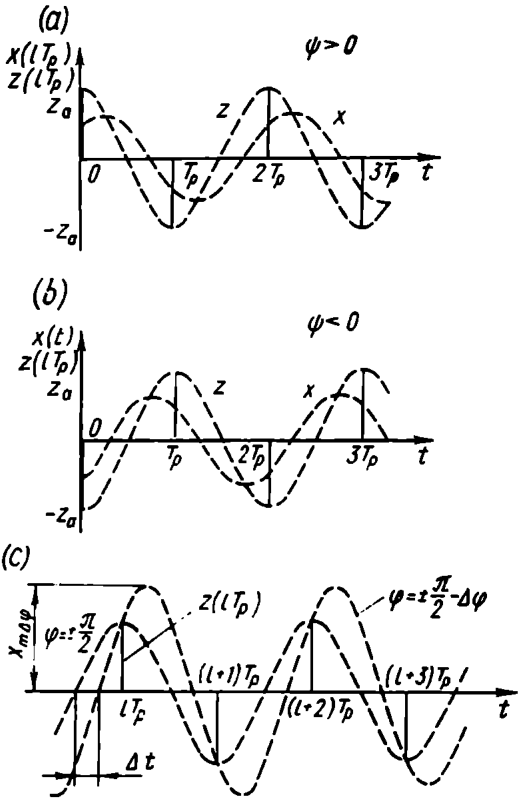

Fig. 18.24

$$\tilde{W}_n^*(X_m, 2, \psi) = \frac{z_a}{X_m} e^{j\left(\frac{\pi}{2} - \psi\right)} \qquad (18.108)$$

At $\psi < 0$ (Fig. 18.24*b*) the following values are obtained

$$Z_{P1} = 0, \qquad Z_{Q1} = -z_a, \qquad \varphi = -\frac{\pi}{2}$$

and the complex gain is

$$\tilde{W}_n^*(X_m, 2, \psi) = \frac{z_a}{X_m} e^{-j\left(\frac{\pi}{2} + \psi\right)} \qquad (18.109)$$

Note that if $n = 2$ there is an infinite number of harmonic envelopes of discrete signals (this also refers to systems other than this one). Figure 18.24*c* shows two possible envelopes of which

one is obtained by formulae of Table 18.2 and has $\varphi = \pm \frac{\pi}{2}$, and the other one is shifted by $\Delta\varphi = \frac{\Delta l 2\pi}{T_p\left(-\frac{\pi}{2} < \Delta\varphi < \frac{\pi}{2}\right)}$. It is easy to see that the formulae of Table 18.2 produce an envelope with the least amplitude equal to $|z(lT_p)|$, whereas at $\varphi = \pm\frac{\pi}{2} - \Delta\varphi$ the amplitude is

$$X_{m\Delta\varphi} = \frac{|z(lT_p)|}{\sin\left(\frac{\pi}{2} - \Delta\varphi\right)} = \frac{|z(lT_p)|}{\cos\Delta\varphi} \qquad (18.110)$$

Table 18.3 gives expressions for the complex gain of a two-positional hysteresisless relay at different n obtained as in the case of $n = 2$. The same figure shows families of loci of the responses W_n^* and $V_n^* = -\bar{W}_n^{*-1}$ (without specifying the values of amplitudes). The loci are enclosed within the angle of $\pm\frac{\pi}{n}$ around the real axis. They are symmetrical relative to this axis for different signs of ψ. At $\psi = 0$ they are at the maximal distance from the real axis (by an angle of $\pm\frac{\pi}{n}$), while at $\psi = \pm\frac{\pi}{n}$ they are on the real axis. As $n \to \infty$ all the loci tend to the real axis; this corresponds to transition to the continuous case.

The equation for determining the parameters of periodic modes in sampled-data control systems is composed by using the harmonic balance for envelopes of discrete signals and is akin to the equation for self-oscillations in continuous systems

$$\bar{W}_n^*(X_m, n, \psi)\, W_{LP}^*\left(j\frac{\omega_p}{n}\right) = -1 \qquad (18.111)$$

Because this equation, which splits into two, for the real and the imaginary part, includes three unknowns, it can be satisfied by different combinations of X_m, n and ψ representing different oscillatory modes. A great diversity of these is indeed observed in practical sampled-data control systems.

Equation (18.111) can be conveniently rewritten as

$$\bar{W}_{LP}^*\left(j\frac{\omega_p}{n}\right) = \bar{V}_n^*(X_m, n, \psi)$$
$$\bar{V}_n^*(X_m, n, \psi) = -\bar{W}_n^{*-1}(X_m, n, \psi) \qquad (18.112)$$

and solved graphically by constructing in the same plane a family of inverse responses $\bar{V}_n^*(X_m, n, \psi)$ for a fixed n and different ψ and

Table 18.3

n	$\widetilde{W}_n^*(X_m, n, \psi)$		$\widetilde{W}_n^*$	$\widetilde{V}_n^*$
2	$\frac{\pi}{2} > \psi > 0$	$\frac{z_a}{X_m} e^{j\left(\frac{\pi}{2} \cdot \psi\right)}$	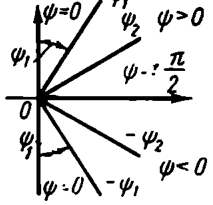	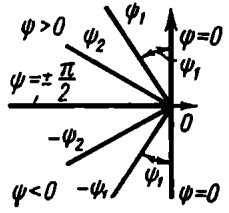
	$-\frac{\pi}{2} < \psi < 0$	$\frac{z_a}{X_m} e^{-j\left(\frac{\pi}{2} + \psi\right)}$		
4	$\frac{\pi}{4} > \psi > 0$	$\frac{\sqrt{2}z_a}{X_m} e^{j\left(\frac{\pi}{4} \cdot \psi\right)}$	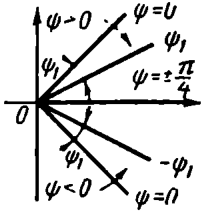	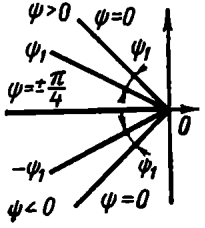
	$-\frac{\pi}{4} < \psi < 0$	$\frac{\sqrt{2}z_a}{X_m} e^{-j\left(\frac{\pi}{4} + \psi\right)}$		

6	$\frac{\pi}{6} > \psi > 0$	$\frac{4z_a}{3X_m} e^{j\left(\frac{\pi}{6} - \psi\right)}$	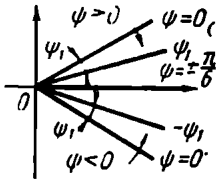	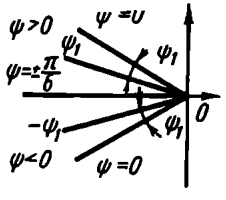
	$-\frac{\pi}{6} < \psi < 0$	$\frac{4z_a}{3X_m} e^{-j\left(\frac{\pi}{6} + \psi\right)}$		
8	$\frac{\pi}{8} > \psi > 0$	$\frac{z_a\sqrt{1+\frac{\sqrt{2}}{2}}}{X_m} e^{j\left(\frac{\pi}{8} - \psi\right)}$	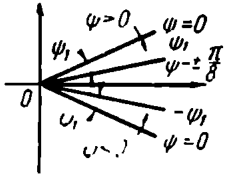	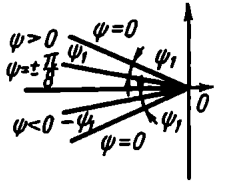
	$-\frac{\pi}{8} < \psi < 0$	$\frac{z_a\sqrt{1+\frac{\sqrt{2}}{2}}}{X_m} e^{-j\left(\frac{\pi}{8} + \psi\right)}$		

the frequency response $\tilde{W}^*_{LP}(j\omega)$. If at any one value of ψ the response $\tilde{V}^*_n$ intersects the frequency response W^*_{LP} at $\omega = \frac{\omega_p}{n}$, a periodic mode with these frequency and phase can exist in the system. The

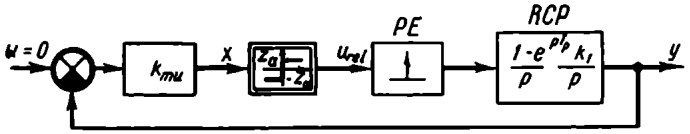

Fig. 18.25

amplitude X_m can be read off the locus $\tilde{V}^*_n$. If at a specified n the intersections do not take place, another n is taken and in this way all possible periodic modes are found in sequence.

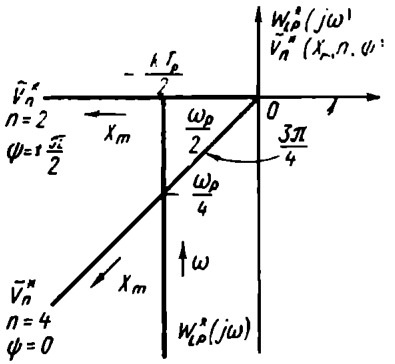

Fig. 18.26

Lack of solutions for periodic modes may be evidence of absolute stability of the system but in passing the final judgement even greater caution should be exercised than in the case of continuous systems.

Example 18.10. Find possible periodic modes in a relay sampled-data servo system (Fig. 18.25) containing a measuring unit with a gain k_{mu}, a relay with an output voltage $\pm z_a$, a pulse element and a reduced continuous part with rectangular pulses having a duty factor equal to 1 and including an integrating element with the gain k_1 in the continuous part. The frequency response of the linear sampled-data part was obtained in Example 13.2 and, with an allowance for the measuring element, is

$$W^*_{LP}(j\omega) = \frac{kT_p}{e^{j\omega T_p} - 1} \tag{18.113}$$

where $k = k_{mu}k_1$.

The locus $W^*_{LP}(j\omega)$ is shown in Fig. 18.26.

The phase shift in the linear part can easily be shown to depend on frequency as follows

$$\varphi_{LP}(\omega) = -\frac{1}{2}(\pi + \omega T_p) \tag{18.114}$$

The reader can obtain this formula by using the inverse response $W^{*-1}_{LP}(j\omega)$ (see Fig. 13.9).

For the possible frequencies $\omega = \frac{\omega_p}{n}$ the phase shift is

$$\varphi_{LP} = -\frac{1}{2}\left(\pi + \frac{\omega_p T_p}{n}\right) = -\frac{1}{2}\left(\pi + 2\frac{\pi}{n}\right) = -\left(\frac{1}{2} + \frac{1}{n}\right)\pi \quad (18.115)$$

On the other hand, by virtue of Table 18.3 the loci $\tilde{V}_n^*(X_m, n, \psi)$ are situated in the sector $\pm\frac{\pi}{n}$ around the real negative half-axis. The condition for a periodic mode is

$$-\varphi_{LP} \geqslant \left(\pi - \frac{\pi}{n}\right) \quad (18.116)$$

or, substituting Eq. (18.115), we have

$$\left(\frac{1}{2} + \frac{1}{n}\right)\pi \geqslant \left(1 - \frac{1}{n}\right)\pi, \qquad \frac{1}{n} \geqslant \frac{1}{4}, \qquad n \leqslant 4$$

Thence it follows that irrespective of z_a, k and T_p, two periodic modes can exist in the system: $n = 2\left(\omega = \frac{\omega_p}{2}\right)$ and $n = 4\left(\omega = \frac{\omega_p}{4}\right)$. Figure 18.26 shows the position of the loci W_{LP}^* and $\tilde{V}_n^*$ for these cases; at $n = 2$ the phase shift ψ is seen to be $\pm\frac{\pi}{2}$ and at $n = 4, \psi = 0$. Increase of the gain k or the period T_p shifts the frequency response $W_{LP}^*(j\omega)$ leftwards and increases the amplitude of oscillation. An increase in z_a changes the values of amplitudes on the locus $\tilde{V}_n^*$ and also leads to increased amplitudes of oscillation. Changes in T_p, while leaving n constant, give a new value to the oscillation frequency $\omega = \frac{2\pi}{nT_p}$.

The amplitude of oscillation can be found by using the formulae of Table 18.3. At $k_{mu} = 1$ V/deg, $z_a = 6$ V, $k_1 = 0.2$ deg/(V·sec), $T_p = 0.5$ sec the abscissa of the frequency response $W_{LP}^*(j\omega)$ is

$$-\frac{kT_p}{2} = -\frac{k_{mu}k_1 T_p}{2} = -0.1$$

whence it follows that at $n = 2$ and $\psi = \pm\frac{\pi}{2}$

$$\tilde{V}_n^* = -\frac{X_m}{z_a} = -0.1$$

or

$$X_m = 0.1, \qquad z_a = 0.6 \text{ V}$$

The amplitude at the input of the measuring unit is then

$$\frac{X_m}{k_{mu}} = \frac{0.6}{k_{mu}} = 0.6 \text{ deg}$$

At $n=4$, $\psi=0$

$$-\frac{X_{m1}}{\sqrt{2}\,z_a}\cos\frac{\pi}{4}=-\frac{X_m}{2z_a}=-0.1$$

or

$$X_m=0.2z_a=1.2\ \text{V},\qquad \frac{X_m}{k_{mu}}=1.2\ \text{deg}$$

It has already been shown that the solution found for $n=2$ is accurate. In this case the symmetry of oscillations can be shown to preclude discrete higher harmonics at $n=4$ as well; consequently, for $n=4$ the solution is also accurate.

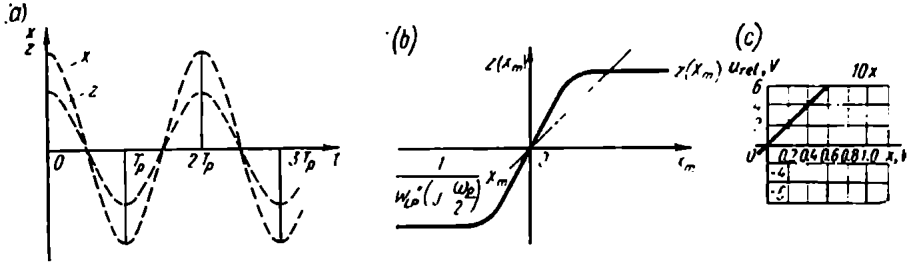

Fig. 18.27

As shown above, at $n=2$ the problem has a set of solutions which differ in amplitude as given by Eq. (18.110). The value of 0.6 deg is minimal.

It should be noted that the highest frequency mode ($n=2$) can be determined in a simpler way than in Example 18.10. Because $W^*_{LP}\left(\frac{j\omega_p}{2}\right)$ takes on real (usually negative) values, Eq. (18.111) of harmonic balance can be satisfied only with real $\tilde{W}^*_n(X_m, 2, \psi)$. Therefore, if a periodic mode with $n=2$ does exist in the system, then the envelopes of discrete signals at the input and output of a nonlinear element are in phase (provided that $W^*_{LP}\left(\frac{j\omega_p}{2}\right)<0$). If the condition $Z_0=0$ is met, the mode is symmetrical and consequently by the formulae of Table 18.2 there is a phase shift of $\pm\frac{\pi}{2}$ relative to the sampling times. Figure 18.27*a* shows the shape of the harmonic envelopes of the signals x and z. If the amplitude of the envelope x is X_m, then, the envelopes being in phase, the amplitude of z becomes $z(X_m)$, the response of the nonlinear element. Thence the value of the complex gain satisfying Eq. (18.111) is

$$\tilde{W}^*_n=\frac{z(X_m)}{X_m} \qquad (18.117)$$

and the equation of harmonic balance takes the form

$$\frac{z(X_m)}{X_m} W^*_{LP}\left(\frac{j\omega_p}{2}\right) = -1$$

or

$$z(X_m) = -\frac{1}{W^*_{LP}\left(\frac{j\omega_p}{2}\right)} X_m \qquad (18.118)$$

This equation is readily solved by plotting the relation $z(X_m)$ and the straight line $-\frac{1}{W^*_{LP}\left(\frac{j\omega_p}{2}\right)} X_m$ on the same graph and finding their intersection (Fig. 18.27*b*). If they do not intersect, there is no periodic mode with $n = 2$.

Example 18.11. Find the amplitude of oscillation in the system of Fig. 18.10 where $W^*_{LP}\left(\frac{j\omega_p}{2}\right) = -0.1$.

Figure 18.27*c* shows the response of a relay and a straight line with a slope of $-\frac{1}{(-0.1)} = 10$. Their intersection gives the amplitude of U_x equal to 0.6 V, which confirms the above result.

The formulae and loci for complex gains of sampled-data systems in the case of a relay response with a dead zone and hysteresis and also of a stepwise response are available in the literature (Ref. 50). They can be used to determine periodic modes in relay and digital control systems.

Chapter XIX

STABILITY OF NONLINEAR SYSTEMS

19.1. CONCEPT OF STABILITY IN NONLINEAR SYSTEMS

As shown in previous sections, any transient process taking place in a linear system can be represented as a sum of a transient (or free) and a forced component. A linear system is stable if the transient component goes to zero as $t \to \infty$.

In nonlinear systems stability is a much more involved problem since the superposition principle is inapplicable and so the process cannot be divided into the two components. Possible self-oscillations further aggravate the problem.

For nonlinear systems there are several stability concepts depending on the regions of possible deviations from the equilibrium state and on the presence or absence of external actions.

Some of these concepts were introduced in Examples of Chs. XVII and XVIII. Accurate judgements on the nature of processes, however, were achieved only for low-order systems (Ch. XVII), while in the case of higher-order systems approximate methods were applied (Ch. XVIII).

This Chapter will generalize certain stability concepts and list more rigorous methods of judging sifficient conditions for system stability without limiting the order of differential equations describing the systems.

The founder of the stability theory for nonlinear systems was A.M. Lyapunov, who stated in 1892 the general problem of motion stability (Ref. 44) and formulated the concept of stability both for linearized systems (see previous sections) and for essentially nonlinear systems. He had a number of followers (Refs. 16, 43, 2).

Depending on the presence or absence of external actions all control systems can be classified into *autonomous* and *nonautonomous*. The former are subjected to no external actions. Any continuous system of Ch. XV subjected to a constant external action can be reduced to an autonomous system. Nonautonomous systems are under the effect of time-dependent external actions and include sampled-data systems in which external actions lead to periodic closure of

the system loop and continuous systems subjected to external actions varying in time.

For autonomous systems two different concepts of stability are used, stability of equilibrium and stability of self-oscillations.

For nonautonomous systems there is a concept of stability of a process generated by an external action.

Attempts to use, in analysis of nonlinear systems, methods similar to those applied to linear systems have led to the concepts of disturbed and undisturbed system motion. The former is associated with a certain particular solution, and the latter, with a set of other feasible (complete) solutions.

Undisturbed motion is one of the possible calculated motions of a system under definite initial conditions and under a specified external action. Any other motion is referred to as *disturbed*. Any disturbed motion results from a short-term external action at $t = 0$.

The equilibrium state and steady state oscillations can be regarded as important particular cases of undisturbed motions of an autonomous system.

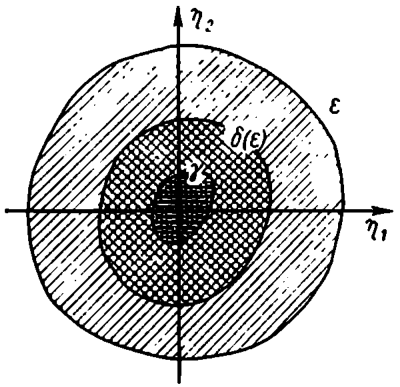

Fig. 19.1

Let us take up the motion of a continuous system in the phase space of the vector $\mathbf{y} = \{y_1, y_2, \ldots, y_k, \ldots, y_n\}$.

An undisturbed motion is expressed as the vectorial function $\mathbf{y}^u(t)$ or a set of n functions $y_k^u(t)$. A disturbed motion is described by the vectorial function $\mathbf{y}(t)$ or by a set of n functions $y_k(t)$. The process variation is described by the vector $\boldsymbol{\eta}(t)$ or by a set of n functions $\eta_k(t)$

$$\boldsymbol{\eta}(t) = \mathbf{y}(t) - \mathbf{y}^u(t) \tag{19.1}$$

$$\eta_k(t) = y_k(t) - y_k^u(t) \tag{19.2}$$

and expresses the difference of disturbed and undisturbed motion.

A general idea of the stability of motion is given by the stability concept introduced by M. A. Lyapunov: *motion is stable if for any given infinitesimal area* ε *of permissible deviations* η_k *from the point* $\eta_k = 0$ *a region of initial values* $\delta(\varepsilon)$ *inside the area* ε *can be specified whose one property is that no disturbed motion originating within the region* δ *will ever reach the boundary of the area* ε. *If there is no such region, the motion is unstable.*

The area ε and region δ in the η_1, η_2 plane are shown in Fig. 19.1.

Besides ε and δ the stability may conveniently be characterized by the concept of the area γ of steady-state values of the difference

between disturbed and undisturbed motion. As $t \to \infty$

$$\eta \in \gamma \tag{19.3}$$

The shape of the area γ depends on the area of initial deviations of δ and in the general case its dimension is equal to that of the system, i.e. n. Two practically important particular cases of areas γ should be noted. In the first case $\gamma = 0$, or

$$\lim_{t\to\infty} \eta_k(t) = 0 \tag{19.4}$$

This motion is called *asymptotically stable*. If for Eq. (19.4) to hold the region of initial deviations δ must be small enough, we speak of asymptotic stability in the small; if δ has finite dimensions, we speak of asymptotic stability in the large. If, finally, the equality holds at infinitely large deviations, we speak of asymptotic stability in the whole.

In the other particular case the area γ is a segment of the axis η_1, the equality (19.4) does not hold at infinitesimal deviations from equilibrium, and the stability is nonasymptotic.

All the above definitions of stability can be related to stability of equilibrium, self-oscillations and forced processes.

Stability of self-oscillations is assessed by using the concept of *orbital stability*.

Periodic motion (self-oscillations) is represented in the phase space by a closed curve Γ. By representing any phase trajectory as a locus of the head of a vector $\mathbf{y}(t)$, the shortest distance $\rho[y(t), \Gamma]$ from the head of the vector $\mathbf{y}(t)$ to the curve Γ can be determined at any time instant t.

An *orbital asymptotically stable* periodic motion of an autonomous system (self-oscillations) is a motion for which

$$\lim_{t\to\infty} \rho[y(t), \Gamma] = 0 \tag{19.5}$$

This condition can be expressed in terms of the concept of undisturbed motion with an allowance for a possible phase shift τ between $\mathbf{y}^u(t)$ and $\mathbf{y}(t)$.

Denoting

$$\eta_k(t, \tau) = y_k(t) - y_k^u(t - \tau) \tag{19.6}$$

the condition for orbital asymptotic stability can be formulated as follows: there are such positive real values $\tau = \tau_0$ for which

$$\lim_{t\to\infty} \eta_k(t, \tau_0) = 0 \tag{19.7}$$

If the condition (19.5) or (19.7) is not met, the orbital asymptotic stability is disturbed.

The conditions of self-oscillation stability given in Chs. XVII and XVIII correspond to orbital asymptotic stability.

Now let us see how the above definitions agree with the phenomena in linear control systems studied earlier in the book.

Variational equations for these systems are linear and homogeneous, therefore motions in linear systems are asymptotically stable as a whole if all roots of the characteristic equations have negative real parts. If at least one root of the characteristic equation has

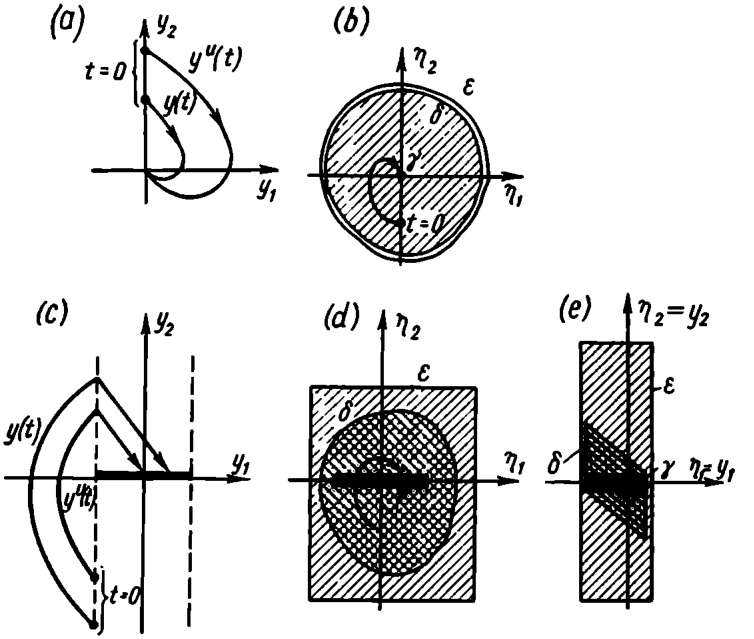

Fig. 19.2

a positive real part, then any motion in the system is unstable. If one root is zero (the system is neutral), then the motions in the system are Lyapunov-stable, but not asymptotically stable. The attraction area of γ in this case is a segment of the axis η_1. If there is a pair of imaginary roots, then γ is an area containing the closed phase trajectory $\eta(t)$ corresponding to a steady periodic misalignment to which $\eta(t)$ tends as $t \to \infty$.

Consider certain examples of autonomous and nonautonomous systems and characterize the stability of processes taking place therein.

Example 19.1. Determine the nature of motion stability in Examples 17.5 and 17.8 represented by Figs. 17.30*a* and 17.39.

For the first case (see Fig. 17.30*a*) the process phase trajectories $y^u(t)$ and $y(t)$ are portrayed in Fig. 19.2*a*. Using now the coordinates, $\eta_1 = y - y^u$ and $\eta_2 = \frac{d\eta_1}{dt}$, the respective trajectory $\eta(t)$

(Fig. 19.2*b*) can be obtained for each phase trajectory $y(t)$. Assuming a certain area ε, a region δ can always be found within it such that no motion started in δ ever reaches the boundary of the region ε. All motions end at the origin of coordinates and are thus Lyapunov-stable and asymptotically stable. The area γ consists of a single point which is the origin of coordinates.

For the second case (see Fig. 17.39) the phase trajectories of an undisturbed, $y^u(t)$, and a disturbed, $y(t)$, process are shown in Fig. 19.2*c*. The undisturbed motion is taken to be represented by a phase trajectory which, as $t \to \infty$, approaches the origin of coordinates. Using the coordinates η_1 and η_2 gives trajectories ending on the rest line corresponding to the area γ (Fig. 19.2*d*). Assuming the area ε the region δ ensuring Lyapunov stability can always be found.

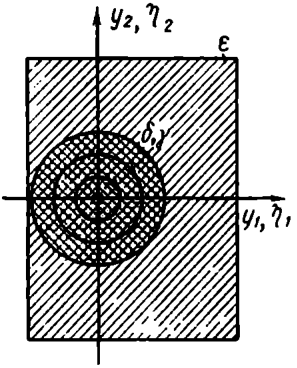

Fig. 19.3

The regions ε, δ and γ (see Fig. 19.2) correspond to the case where the undisturbed motion is the state of rest represented by the origin of coordinates. In this case $y_1^u = y_2^u = 0$, while $\eta_1 = y_1$ and $\eta_2 = y_2$.

Both motion and equilibrium are thus Lyapunov-stable, but not asymptotically stable.

Example 19.2. Assess the Lyapunov stability of a centre-type equilibrium point for a second-order linear conservative system and find the regions δ and γ for the area ε specified by the inequalities $-a < y_1 < 2a$ and $-2a < y_2 < 2a$, where a is an arbitrary number.

Considering the phase trajectories for this case (see Sec. 17.3), we conclude that if the radius-vector of a point representing the initial conditions always remains inside a circle with centre at the origin of coordinates, then the motion will never reach the boundary of the area ε. The motion will proceed along the circle as long as desired.

Consequently, the area δ coincides with the area γ. The equilibrium is Lyapunov-stable, but not asymptotically stable. The areas ε, δ and γ for this case are shown in Fig. 19.3.

Example 19.3. Assess Lyapunov stability for self-oscillations expressed by limit cycles of Fig. 17.33*b* and *d*.

If the undisturbed motion $y^u(t)$ is described by a motion along the limit cycle and the disturbed motion $y(t)$ is selected so that it differs by some small value from the disturbed motion at the initial instant $t = 0$, in the coordinates η_1, η_2 the process may be seen to diverge for unstable cycles, while for stable cycles it converges, although not to the origin of coordinates but to a certain orbit

depending on the initial conditions as is the case of centre-type neutral equilibrium. This can easily be verified by considering two time-shifted motions along the stable limit cycle $y^{u}(t)$ and $y(t) = y^{u}(t-\tau)$.

A plot of the variation $\eta(t) = y(t) - y^{u}(t)$ in the phase plane gives a periodic motion with an amplitude depending on τ. At τ equal to the halved self-oscillation period the diameter of the limit cycle of $\eta(t)$ is twice that of the limit cycle of $y(t)$ and $y^{u}(t)$.

Stable self-oscillations are thus Lyapunov-stable but not asymptotically stable. On the other hand, disturbed and undisturbed motions end in motions along the same orbit; therefore self-oscillations are orbitrally asymptotically stable processes.

Example 19.4. Consider stability of forced processes in a simple first-order relay system with hysteresis at the external signal $u(t) = At$. The structural diagram of the system is shown in Fig. 19.4*a*.

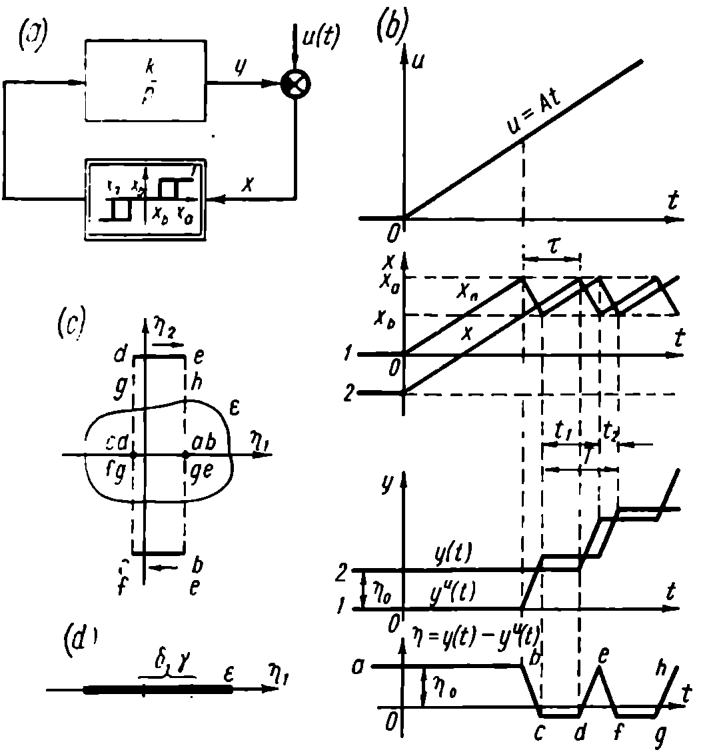

Fig. 19.4

Figure 19.4*b* demonstrates $x(t)$ and $y(t)$ for two different initial conditions: 1) for $y(0) = 0$ and 2) for $y(0) = \eta_0$. The first case is assumed to be undisturbed and the second, disturbed motion.

The both processes lead to oscillations with equal periods. Because the latter take place in a nonautonomous system and depend on the external action $u(t)$, they cannot be called self-oscillations.

The oscillation period consists of two time intervals, $T = t_1 + t_2$, where $t_1 = \frac{(x_a - x_b)}{A}$ is the time within which the external signal changes by the width of the hysteresis loop while $t_2 = \frac{(x_a - x_b)}{k - A}$ is the period over which the servo system responds to the misalignment, provided that the external signal continues increasing. The lag of the disturbed process from the undisturbed one, $\tau = \frac{\eta_0}{A}$, depends on the initial conditions of the disturbed process. To judge the process stability, let us determine the variation $\eta(t) = y(t) - y^u(t)$. This relation is plotted in Fig. 19.4*b*. By the time $t_a = \frac{(\eta_a - x_a)}{A}$ the process becomes periodical with a period of $T = t_1 + t_2 = \frac{k(x_a - x_b)}{A(k - A)}$.

The range of $\eta(t)$ depends on the initial conditions η_0

$$\Delta\eta \leqslant k\tau = \frac{k\eta_0}{A}$$

and cannot exceed $kt_2 = \frac{k(x_a - x_b)}{k - A}$.

Figure 19.4*c* is the phase portrait of the process $\eta(t)$ in the coordinates $\eta_1 = \eta$ and $\eta_2 = \frac{d\eta}{dt}$.

The coordinate η_2 does not change continuously and the phase trajectory is discontinuous. If points a, b, c, d, e, f, g, h for different time instants are set on the curve $\eta(t)$ the corresponding points can be mapped on the phase portrait. The motion of the describing point in the phase plane can be traced as follows: rest at the point ab, jerk $b \to b$, uniform motion along the line bc, jerk $c \to c$, rest at the point cd, jerk $d \to d$, uniform motion along the line de, jerk $e \to e$, continuous motion ef, etc. The motion consists of intervals of rest, uniform motion and jerks and ends in a discontinuous limit cycle of width $\Delta\eta$. Since the system under study is described by a first-order differential equation ($n = 1$), then to judge the system stability one should use a phase straight line with a single coordinate η_1 rather than a phase plane.

On this straight line (see Fig. 19.4*d*), with the area ε given, an area δ required to assess the Lyapunov stability can always be isolated.

For this example the area δ coincides with the area γ within which the system oscillates. No attempt to denote the area ε and look for the area δ in the phase plane for our example (see Fig. 19.4*c*) will shed any light on the system's Lyapunov stability because the second

phase coordinate η_2 does not agree with the equation order and is superfluous for assessment of stability.

All definitions given in this section for stability of processes in control systems hold also for sampled-data systems if the discrete processes are the object of our studies.

19.2. LYAPUNOV'S DIRECT METHOD

A method was proposed by A.M. Lyapunov which determines sufficient conditions for stability of nonlinear control systems. This method, known as the *Lyapunov's direct method* (Refs. 44, 42), will be discussed as applied to analysis of equilibrium stability.

Consider an autonomous nonlinear system whose motion is described by the set (17.3) of nonlinear first-order differential equations

$$\left.\begin{aligned} \frac{dy_1}{dt} &= P_1(y_1, y_2, \ldots, y_n \\ &\cdots\cdots\cdots\cdots \\ \frac{dy_n}{dt} &= P_n(y_1, y_2, \ldots, y_n) \end{aligned}\right\} \tag{19.8}$$

or, in shorter notation,

$$\frac{dy_i}{dt} = P_i(y_1, y_2, \ldots, y_n) \qquad (i = 1, 2, \ldots, n) \tag{19.9}$$

where $y_1, y_2, \ldots, y_n$ are variables describing the system state, and P_i are known functions specified in the space of these variables (phase space).

Examples of representing motion equations in the form (19.8) were given in Ch. XVII.

The equilibrium is defined by a set of equations

$$P_i(y_1, y_2, \ldots, y_n) = 0 \qquad (i = 1, 2, \ldots, n) \tag{19.10}$$

Assume now for simplicity that set (19.10) has a single solution in the origin of coordinates, i.e. $y_1 = 0, y_2 = 0, \ldots, y_n = 0$.

By the Lyapunov's direct method a special function $V(y_1, y_2, \ldots, y_n)$ is introduced in the phase space which has the following properties:

1. It is continuous with all its first-order partial derivatives in a certain open region containing the origin of coordinates.

2. In the origin of coordinates the function $V(y_1, y_2, \ldots, y_n)$ is zero.

3. In the whole region except the origin of coordinates the function $V(y_1, y_2, \ldots, y_n)$ is nonzero and has the same sign. Such functions are known as *definite sign functions*. Besides, there are *constant sign functions*, which can be zero not only in the origin of coordinates while in the other points the sign is retained.

A.M. Lyapunov proved the following assertion (Ref. 44): if differential equations (19.9) of motion are such that one can find the definite sign function $V(y_1, y_2, \ldots, y_n)$ whose derivative $\frac{dV}{dt}$, by virtue of the equations, would be either a constant sign function with a sign opposite to that of V or identically zero, the system is in stable equilibrium in the origin of coordinates.

If the derivative $\frac{dV}{dt}$ is a definite sign function with a sign opposite to that of V, then the system equilibrium in the origin of coordinates is asymptotically stable.

Stability (or asymptotic stability) of the equilibrium, with the conditions of the Lyapunov theorem observed, is related to the fact

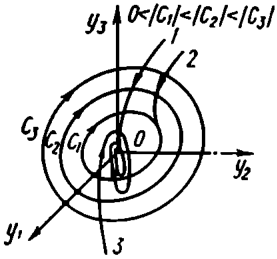

Fig. 19.5

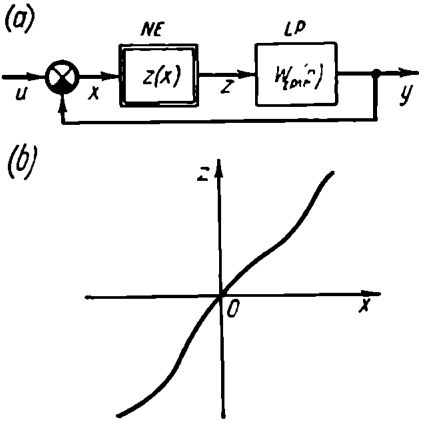

Fig. 19.6

that for a V-function featuring the above properties a family of closed surfaces with the same values of V can be constructed in a certain vicinity of the origin of coordinates. These surfaces are described by the equation

$$V(y_1, y_2, \ldots, y_n) = C \qquad (19.11)$$

and enclose the origin of coordinates. With decreasing $|C|$ the surfaces shrink to the origin of coordinates (Fig. 19.5).

Figure 19.5 shows three types of phase trajectories. On trajectory *1* the derivative $\frac{dV}{dt}$ is of a definite sign which is opposite to that of V. If all phase trajectories belong to type *1*, the equilibrium is asymptotically stable.

Phase trajectory *2* represents the case of a constant sign of the derivative $\frac{dV}{dt}$ and, hence, the case of Lyapunov stability (but not

asymptotic stability). The phase trajectories may "stick" in those points of the phase space where the derivative $\frac{dV}{dt}$ vanishes or may even close on the surface $V = C$ (see Fig. 19.5). With an appropriate choice of the initial point the limit point or the phase trajectory will always remain in a specified vicinity of the equilibrium.

Phase trajectory *3* represents asymptotic stability of equilibrium although it does not satisfy the conditions of the Lyapunov theorem. The possibility of such motion confirms that the observance of the conditions of the Lyapunov theorem is not necessary for stability of control systems.

The theorem covers stability of equilibrium "*in the small*", but if a V-function can be selected whose surfaces of equal values existing in a finite region include the origin of coordinates and have values of C increasing in magnitude with the distance from the origin of coordinates, then a conclusion can be made concerning the asymptotic stability "*in the large*" within the region, provided $\frac{dV}{dt}$ has a definite sign which is opposite to that of V. If these conditions are met over the entire phase space the equilibrium is asymptotically stable "*in the whole*". As in the case of stability in the small the conditions in which such Lyapunov functions exist are sufficient conditions for stability.

If a Lyapunov V-function has been selected, then in order to find the sign of its derivative there is no need to solve Eq. (19.9) of the system motion. Indeed, since

$$\frac{dV(y_1, y_2, \ldots, y_n)}{dt} = \sum_{i=1}^{n} \frac{\partial V(y_1, y_2, \ldots, y_n)}{\partial y_i} \frac{dy_i}{dt} \qquad (19.12)$$

then, by virtue of Eq. (19.9),

$$\frac{dV(y_1, y_2, \ldots, y_n)}{dt} = \sum_{i=1}^{n} \frac{\partial V(y_1, y_2, \ldots, y_n)}{\partial y_i} P_i(y_1, y_2, \ldots, y_n) \qquad (19.13)$$

Selection of V-functions is very difficult in practical use of the Lyapunov's direct method. Unfortunately, there are no unambiguous techniques for construction of these functions and one should largely rely on intuition. This fact is a serious limitation on the application of the method.

For control systems whose structure is represented in Fig. 19.6*a* with a nonlinear element response satisfying the conditions $xz(x) > 0$, $z(0) = 0$ (Fig. 19.6*b*), the V-functions can be selected in the form proposed by A.I. Lurye, and V.N. Postnikov (Ref. 43)

$$V(y_1, y_2, \ldots, y_n) = L(y_1, y_2, \ldots, y_n) + \beta \int_0^x z(\xi)\, d\xi \qquad (19.14)$$

where $L(y_1, y_2, \ldots, y_n)$ is the quadratic form of the phase coordinates

$$L(y_1, y_2, \ldots, y_n) = \sum_{i=1}^{n} \sum_{j=1}^{n} \alpha_{ij} y_i y_j \tag{19.15}$$

α_{ij} and β are constant factors, and $\alpha_{ij} = \alpha_{ji}$.

The surfaces of equal values of Lyapunov functions taken in this form can be shown to enclose the origin of coordinates, the values of C increasing in magnitude with the distance from the origin of coordinates. These surfaces fill the entire phase space and with an appropriate choice of the coefficients α and β can serve to judge the equilibrium stability "*in the whole*".

V-functions of this type help solve many practical problems involving stability analysis for nonlinear control systems.

Example 19.5. Verify the stability of equilibrium in the system (see Fig. 19.6*a*) containing an inertial element in the linear part

$$W_{LP}(p) = \frac{k}{1+pT} \tag{19.16}$$

The system motion equations can be written in the form

$$\left.\begin{aligned} T\frac{dy}{dt} + y &= z(x) \\ x &= u - y \end{aligned}\right\} \tag{19.17}$$

At $u = 0$, $y = -x$ the system motion can be represented by a single first-order equation

$$\frac{dx}{dt} = -\frac{x}{T} - \frac{k}{T} z(x) \tag{19.18}$$

Take a Lyapunov function in the Lurye-Postnikov form

$$V = \frac{1}{2} x^2 + \int_0^x z(\xi)\, d\xi \tag{19.19}$$

then its derivative is

$$\frac{dV}{dt} = \left(\frac{dV}{dx}\right)\left(\frac{dx}{dt}\right) = [x + z(x)]\frac{dx}{dt} = -[x + z(x)]\left[\frac{x}{T} + \frac{k}{T} z(x)\right] =$$

$$= -\left[\frac{x^2}{T} + \frac{k}{T} z^2(x) + \frac{1+k}{T} xz(x)\right] \tag{19.20}$$

At $xz(x) > 0$ the derivative is negative over the entire phase space if $k > 0$. Consequently, the sufficient condition for asymptotic stability "*in the whole*" of a first-order system with an inertial element is the positive sign of the linear part gain. The response of the

nonlinear element can then be of any shape and should remain within the first and the third quadrants (Fig. 19.7). It can also be discontinuous but must be single-valued.*

Example 19.6. Verify the stability of equilibrium in a system (Fig. 19.6*a*) whose linear part transfer function is

$$W_{LP}(p) = \frac{1}{p^2} \qquad (19.21)$$

The system motion equations have the form

$$\left.\begin{aligned} \frac{d^2y}{dt^2} &= z(x) \\ x &= u - y \end{aligned}\right\} \qquad (19.22)$$

or, at $u = 0$,

$$\frac{d^2x}{dt^2} = -z(x) \qquad (19.23)$$

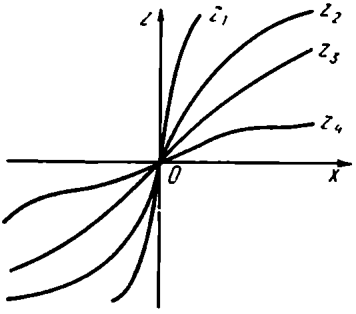

Fig. 19.7

Now we will use the normal form by introducing a new variable, $x_1 = \frac{dx}{dt}$. Then Eq. (19.23) is replaced by a system of two first-order equations

$$\left.\begin{aligned} \frac{dx}{dt} &= x_1 \\ \frac{dx_1}{dt} &= -z(x) \end{aligned}\right\} \qquad (19.24)$$

Take the Lyapunov function in the form

$$V = \frac{1}{2}x_1^2 + \int_0^x z(\xi)\,d\xi \qquad (19.25)$$

The V-function derivative is then

$$\frac{dV}{dt} = \left(\frac{\partial V}{\partial x}\right)\left(\frac{dx}{dt}\right) + \left(\frac{\partial V}{\partial x_1}\right)\left(\frac{dx_1}{dt}\right) = z(x)\frac{dx}{dt} + x_1\frac{dx_1}{dt} =$$

$$= z(x)x_1 - x_1 z(x) = 0 \qquad (19.26)$$

The derivative $\frac{dV}{dt}$ is identically zero over the entire phase space which signifies that the equilibrium is Lyapunov-stable, not asymptotically stable. The system in question is represented in the phase plane by a family of nonintersecting closed curves (one enclosing another). The equilibrium corresponds to a centre-type point.

More complicated examples of applying Lyapunov's direct method are given in Ref. 43.

* Such systems are referred to as absolutely stable (see Sec. 19.3).

19.3. THE CRITERION FOR ABSOLUTE STABILITY OF EQUILIBRIUM

Absolute stability is asymptotic stability of the system equilibrium "*in the whole*" for nonlinearities belonging to a certain class. The most widespread approach, proposed by M.A. Aizerman in 1946, is to consider nonlinear responses contained within an angle made by the

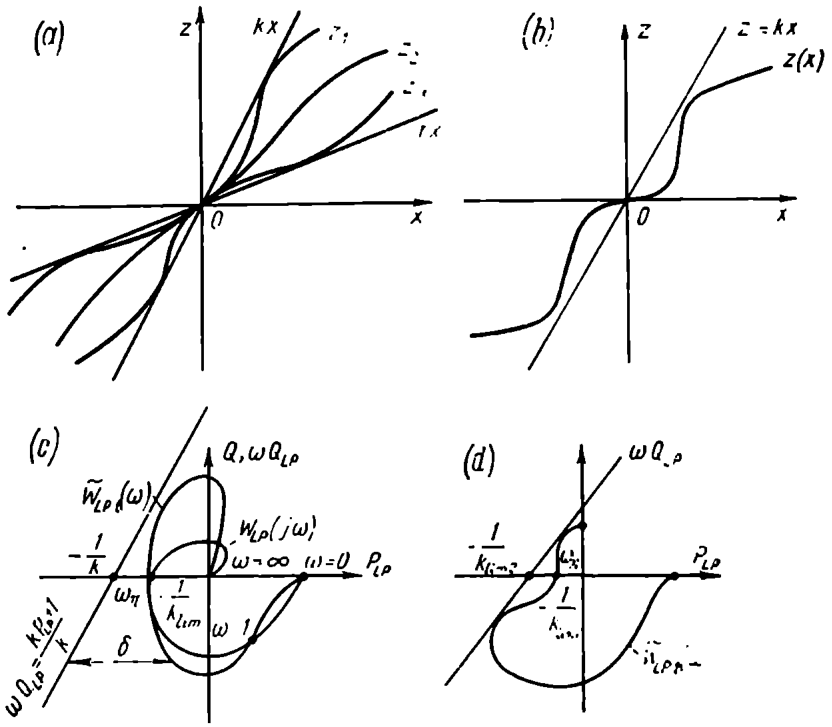

Fig. 19.8

straight lines $z = kx$ and $z = rx$ $(r < k)$ in the first and third quadrants (Fig. 19.8*a*). Responses of this kind are said to be contained within the sector $[r, k]$.

An example of a system absolutely stable in the sector $[0, \infty]$, i.e. for all responses contained in the first and third quadrants, was obtained in the preceding section (see Example 19.5) by Lyapunov s direct method. Incidentally, the problem of absolute stability originated in connection with the use of this method.

In 1959 V.M. Popov, a Roumanian mathematician, proposed a very simple and illustrative frequency criterion for absolute stability of control systems.

The absolute stability criterion is formulated as follows: *if a closed-loop system* (see Fig. 19.6*a*) *consists of a stable linear part with a transfer function* $W_{LP}(p)$ *all poles of which are in the left half-plane and a single-valued nonlinearity* $z(x)$ *contained in an angle* $0 \leqslant \frac{z(x)}{x} \leqslant k$ (*sector* $[0, k]$, Fig. 19.8*b*), *a sufficient condition for stability is the validity of the equation*

$$\operatorname{Re}[(1+jq\omega)W_{LP}(j\omega)]+\frac{1}{k}=\delta>0 \qquad (19.27)$$

where q *is an arbitrary real number.*

It is presumed that $k<\infty$ and $\lim\limits_{\omega\to\infty} W_{LP}(j\omega)=0$. The latter condition follows from proper allowance for small parameters of nonlinearity (see Sec. 16.8) or insensitivity of the system in question (see Sec. 17.4).

The absolute stability criterion can be given a convenient geometrical interpretation. Substituting into Eq. (19.27) the expression

$$W_{LP}(j\omega)=P_{LP}(\omega)+jQ_{LP}(\omega) \qquad (19.28)$$

gives

$$P_{LP}(\omega)-q\omega Q_{LP}(\omega)+\frac{1}{k}=\delta>0 \qquad (19.29)$$

Introduce the concept of a transformed frequency response of the linear part

$$\tilde{W}_{LP\,t}(\omega)=P_{LP}(\omega)+j\omega Q_{LP}(\omega) \qquad (19.30)$$

If we plot the locus $\tilde{W}_{LP\,t}(\omega)$ and trace a straight line described by the equation

$$P_{LP}(\omega)=-\frac{1}{k}+q\omega Q_{LP}(\omega) \qquad (19.31)$$

then the condition for the validity of the inequality (19.29) is the location of the locus $\tilde{W}_{LP\,t}(\omega)$ to the right of this straight line (Fig. 19.8*c*).

Consequently, the absolute stability criterion can be reformulated as follows: a system is absolutely stable if with the linear part stable a straight line can be traced through the point $-\frac{1}{k}$, $j0$ so that the locus $\tilde{W}_{LP\,t}(\omega)$ is on its right. A straight line satisfying this condition is termed the *Popov straight line.*

We will now note specific properties of the response $\tilde{W}_{LP\,t}(\omega)$ which distinguish it from $\tilde{W}_{LP}(\omega)$. Firstly, the former includes an imaginary part which is an even function of ω since $Q_{LP}(\omega)$ is an odd function of frequency. Consequently, the locus $W_{LP\,t}(\omega)$ is not symmetric relative to the real axis at frequencies of different signs. Secondly, if $W_{LP}(p)$ has one zero pole (the applicability of

the criterion of absolute stability to such systems will be treated below), i. e.

$$W_{LP}(p) = \frac{K(p)}{pD_1(p)} \tag{19.32}$$

then

$$W_{LP}(j\omega) = \frac{K(j\omega)}{j\omega D_1(j\omega)} = \frac{1}{\omega} \operatorname{Im} \frac{K(j\omega)}{D_1(j\omega)} - j \frac{1}{\omega} \operatorname{Re} \frac{K(j\omega)}{D_1(j\omega)} \tag{19.33}$$

whence

$$P_{LP}(\omega) = \frac{1}{\omega} \operatorname{Im} \frac{K(j\omega)}{D_1(j\omega)} \tag{19.34}$$

$$Q_{LP}(\omega) = -\frac{1}{\omega} \operatorname{Re} \frac{K(j\omega)}{D_1(j\omega)} \tag{19.35}$$

Expressions for the imaginary and real components of $\frac{K(j\omega)}{D_1(j\omega)}$ may be obtained through the standard procedure of multiplying $D_1(j\omega)$ by the conjugate complex value. This gives fractional-rational functions of ω whose identical denominators contain ω raised to even powers (including the compulsory free term since $W_{LP}(p)$ has just one zero pole) while the numerator of $\operatorname{Im} \frac{K(j\omega)}{D_1(j\omega)}$ contains ω raised to odd powers and that of $\operatorname{Re} \frac{K(j\omega)}{D_1(j\omega)}$, ω raised to even powers (including the compulsory free term).

Therefore the factor $\frac{1}{\omega}$ in Eqs. (19.34) and (19.35) will be cancelled from $P_{LP}(\omega)$ and will remain in $Q_{LP}(\omega)$, and so the locus $W_{LP}(j\omega)$ goes unboundedly downwards from the origin of coordinates as $\omega \to 0$. The locus $\tilde{W}_{LP\,t}(\omega)$ will start at $\omega = 0$ from the terminal point of the complex plane because

$$\operatorname{Im} \tilde{W}_{LP\,t}(\omega) = \omega Q_{LP}(\omega) \quad -\operatorname{Re} \frac{K(j\omega)}{D_1(j\omega)} \tag{19.36}$$

Similar reasoning reveals that if $\lim_{\omega \to \infty} W_{LP}(j\omega) = 0$, then $W_{LP\,t}(\omega)$ also tends either to zero or to a finite limit as $\omega \to \infty$.

Since they have similar real parts, the responses $W_{LP}(j\omega)$ and $\tilde{W}_{LP\,t}(\omega)$ intersect the real axis in the same points. If the locus $\tilde{W}_{LP\,t}(\omega)$ is convex, the absolute stability criterion coincides with the Nyquist criterion (see Sec. 7.3) when the nonlinear response is replaced by the straight line $z = kx$. Indeed, in this case the condition that the locus $kW_{LP}(j\omega)$ does not enclose the point $-1, j0$ coincides with the condition for absolute stability.

Such nonlinear systems are termed *stable in the Hurwitz angle*, the latter being understood as the angle between the straight line $z = k_{lim}\, x$, where k_{lim} is the limit gain of the linear part, and the

horizontal axis (in the general case, the straight line $z = r_{llm}\, x$, where r_{llm} is the lower extreme value of the linear system gain).

With a more complicated shape of the locus $\tilde{W}_{LP\,t}(\omega)$ the absolute stability criterion is more rigorous than the Nyquist criterion (Fig. 19.8*d*). In the figure the limit value $\frac{1}{k_{llm}}$ according to Nyquist $\left(\frac{1}{k_{llm\,1}}\right)$ is less than the one according to Popov $\left(\frac{1}{k_{llm\,2}}\right)$. Consequently, $k_{llm\,1} > k_{llm2}$.

L.P. Smolnikov has shown that the locus $\tilde{W}_{LP\,t}(\omega)$ is convex for systems whose linear part contains any number of inertial and

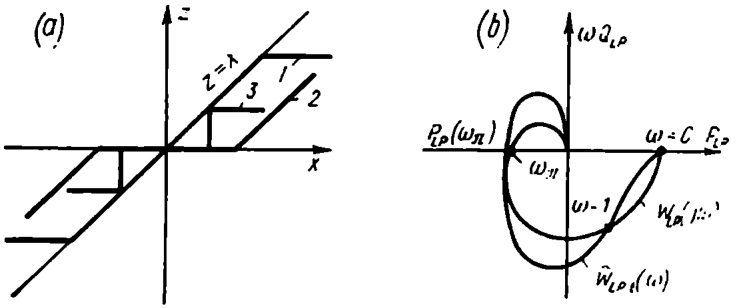

Fig. 19.9

oscillating elements and at most one integrating element, all connected in series. The damping ratio of the oscillatory elements should be at least $\frac{\sqrt{2}}{2}$.

Example 19.7. Let $W_{LP}(p) = \frac{k}{(1+pT_1)(1+pT_2)(1+pT_3)}$.

Determine the value of k_{lim} at which the system with any single-valued nonlinearity contained in the sector [0, 1] is absolutely stable. This nonlinearity may be either saturation (curve *1* in Fig. 19.9*a*) or a dead zone (curve *2*), or a relay response (curve *3*), or any other single-valued nonlinearity.

Because the curve $\tilde{W}_{LP\,t}(\omega)$ is convex (Fig. 19.9*b*), the Nyquist criterion is applicable to the problem. The condition for stability is the inequality $-W_{LP}(j\omega_\pi) = -P_{LP}(\omega_\pi) < 1$. Using the results of Example 7.4 gives

$$k_{lim} = (T_1 + T_2 + T_3)\left(\frac{1}{T_1} + \frac{1}{T_2} + \frac{1}{T_3}\right) - 1 \qquad (19.37)$$

If the linear part is neutral or unstable, the absolute stability criterion cannot be used directly. The system can, however, be trans-

formed so as to make the linear part stable. This transformation can be effected by introducing two similar proportional elements of opposite sign (Fig. 19.10*a*). The gain of the proportional element, r, is selected so that the linear part $W_{LP}(p)$ with a proportional negative feedback is stable. In this case the system can be represented as a stable equivalent linear part $W_{LP\,eq}(p)$ with an internal

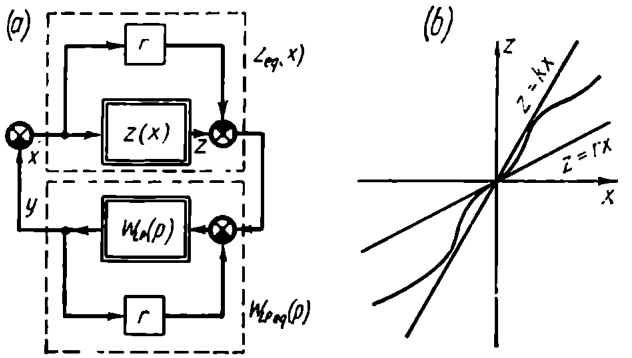

Fig. 19.10

feedback $-r$ and an equivalent nonlinear part with an internal feedforward $-r$. For this system the condition that the nonlinear response $z_{eq}(x)$ should belong to the sector $[0, k]$ means that the original linear element response $z(x)$ belongs to the sector $[r, k+r]$ (Fig. 19.10*b*).

Then

$$W_{LP\,eq}(p) = \frac{W_{LP}(p)}{1 + rW_{LP}(p)} \tag{19.38}$$

and

$$z_{eq}(x) = z(x) - rx \tag{19.39}$$

If the system is neutral and has one zero root, then introduction of an infinitesimal feedback $r \to 0$ leads to conditions where the absolute stability criterion is applicable.

Example 19.8. What conditions should be met by the nonlinear response $z(x)$ of an element in a system with a transfer function $W_{LP}(p) = \frac{1}{(pT_1 - 1)(1 + pT_2)}$ so that the closed-loop system is absolutely stable?

Equation (19.38) gives

$$W_{LP\,eq}(p) = \frac{1}{p^2 T_1 T_2 + p(T_1 - T_2) - 1 + r}$$

For the linear part to be stable the inequalities $T_1 > T_2$, $r > 1$ should hold.

The locus $W_{LP\,eq}(j\omega)$ of a second-order system is completely contained in the lower half-plane and so is the locus of the transformed frequency response $W_{LP\,eq\,t}(\omega)$. Since in this case the Popov straight line can be traced through any point of the negative real axis including the origin of coordinates, the absolute stability condition at $T_1 > T_2$ is

$$0 \leqslant \frac{z_{eq}}{x} \leqslant \infty$$

and, consequently, $1 \leqslant \frac{z}{x} \leqslant \infty$.

At $T_1 < T_2$ the system is unstable at any nonlinearity.

Example 19.9. What conditions should be met by the nonlinear response in a system with a transfer function $W_{LP}(p) = \frac{N}{pT(1+pT)} - M$ so that the closed-loop system is absolutely stable? The transfer function in question does not meet the conditions of the absolute stability criterion for two reasons: (1) it is neutral because it has one zero pole, and (2) it does not tend to zero as $\omega \to \infty$.

To make the criterion applicable, introduce two small parameters α and β (see Sec. 16.8). Then

$$W_{LP\,eq}(p) = \frac{W_{LP}(p)}{(1+\alpha p)+\beta W_{LP}(p)} = \\ = \frac{N - MpT(1+pT)}{pT(1+\alpha p)(1+pT)+\beta[N - MpT(1+pT)]} \approx \frac{N - MpT(1+pT)}{\alpha T^2 p^3 + T^2 p^2 + pT + \beta N} \tag{19.40}$$

The smallness of the parameters $\alpha \ll T$ and $\beta \ll 1$ is allowed for.

It is easy to see that both obstacles to applying the criterion have been removed because the system has all the roots of $W_{LP\,eq}$ in the left half-plane and $W_{LP\,eq}(j\omega) \to 0$ as $\omega \to \infty$.

The locus $W_{LP\,eq}(j\omega)$ is plotted in Fig. 19.11*a* and consists of three distinct parts. At low frequencies, where the higher powers of ω are negligible and $W_{LP\,eq}(j\omega) \approx \frac{N}{\beta N + j\omega T}$, it is a circle of radius $R = \frac{1}{\beta}$ which goes to infinity as $\beta \to 0$.

At medium frequencies where small terms containing the multipliers α and β can be neglected

$$W_{LP\,eq}(j\omega) \approx \frac{N}{j\omega T(1+j\omega T)} - M$$

and the locus shape is characteristic of an inertial integrating element biased by $-M$. At high frequencies, where the lower powers of ω can be neglected,

$$W_{LP\,eq}(j\omega) = -\frac{M}{1+j\omega\alpha}$$

and the locus is a semi-circle of radius $0.5M$ lying in the second quadrant.

The transformed locus is obtained by multiplying the imaginary component of $W_{LP\,eq}(j\omega)$ by ω (Fig. 19.11*b*). The arc of a circle of infinite radius becomes a straight line going from the point $-N-M$, $-j\frac{N}{T}$ to infinity parallel to the real axis. The response of the inertial integrating element becomes a segment of a straight

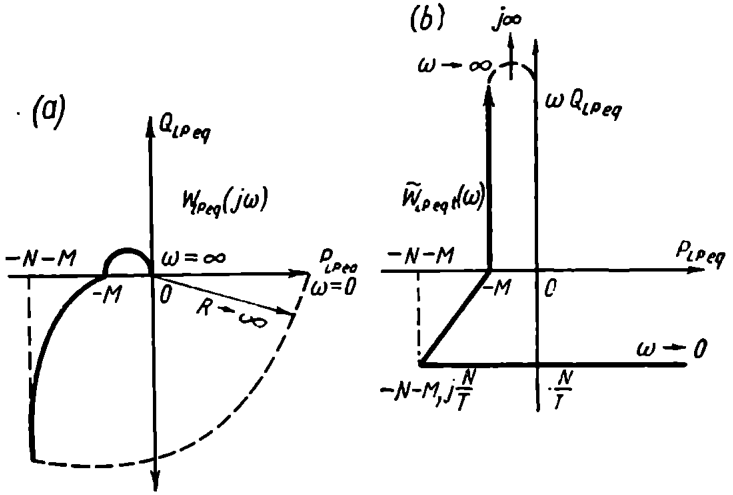

Fig. 19.11

line, and the circle of radius $0.5M$ transforms into a straight line going to infinity from the point $-M$ parallel to the imaginary axis.

The Popov straight line can be traced only to the left of the point $-M-N$, $j0$. Consequently, the condition for absolute stability is

$$0<\frac{z_{eq}}{x}<\frac{1}{M+N} \quad \text{or} \quad \beta<\frac{z}{x}<\frac{1}{M+N} \tag{19.42}$$

where β is infinitesimal.

When the problem is Nyquist-solved, it follows directly from Fig. 19.11*a* that

$$0\leqslant\frac{z_{eq}}{x}\leqslant\frac{1}{M}$$

because the locus $W_{LP\,eq}(j\omega)$ intersects the real axis in the point $-M$, $j0$. In the respective angle nonlinearities can be selected so that the system is unstable.

It is interesting that if the condition $\lim\limits_{\omega\to\infty} W_{eq}(j\omega)=0$ is neglected, then wrong conclusions may be drawn concerning the system stability.

The Popov absolute stability criterion and Lyapunov's direct method are interrelated. In particular, if the Popov criterion is met, there is Lyapunov's V-function in the Lurye-Postnikov form which has a definite sign derivative $\frac{dV}{dt}$ over the entire phase space, with a sign opposite to that of V (Refs. 2, 87). This makes the Popov criterion preferable in practical analysis of stability in nonlinear control systems with one nonlinearity because it is expressed in convenient terms of frequency.

In practical use of the absolute stability criterion, logarithmic notation is preferable (Ref. 84).

19.4. EXTENSION OF THE ABSOLUTE STABILITY CRITERION TO CERTAIN MULTIVALUED NONLINEARITIES

Absolute stability criteria for systems with several nonlinearities, multivalued nonlinearities and distributed parameters are outside the scope of this textbook. Certain problems involved in the analysis of systems with multivalued nonlinearities can, however, be reduced to problems with single-valued nonlinearities by structural transformations and be easily studied by the above methods, as discussed in Sec. 16.7. We will adduce some examples to show how in these cases the criterion helps ascertain the sufficient conditions for stability of systems with typical multivalued nonlinearities.

Example 19.10. Determine the conditions for stability of a relay system with hysteresis. Assume that the linear part transfer function is $W_{LP}(p) = \frac{N}{pT(1+pT)}$ while the nonlinearity is of a relay hysteresis type (see Fig. 19.12*a*).

As shown in Sec. 16.7 this nonlinearity can be represented as an equivalent circuit containing a single-valued relay-type (Fig. 19.12*b*) nonlinearity with a positive feedback depending on the hysteresis loop width M. The system circuit is portrayed in Fig. 19.12*c*. Relating the linear feedback to the linear part gives the structural diagram of Fig. 19.12*d*.

In this diagram the nonlinearity is single-valued and remains in the sector $\left[0, \frac{1}{r_a}\right]$ while the linear part transfer function is

$$W_{LP1} = \frac{N}{pT(1+pT)} - M \tag{19.43}$$

The problem has thus been reduced to Example 19.9. Using the results of the preceding example, we conclude that stability is ensured at

$$\frac{1}{(M+N)} > \frac{1}{r_a} \tag{19.44}$$

or

$$N < x_a - M = x_b \tag{19.45}$$

The response $z(x)$ should not invade the infinitesimal area near the x-line.

The equilibrium absolute stability condition for the system in question thus reduces to the condition that the response $z(x)$

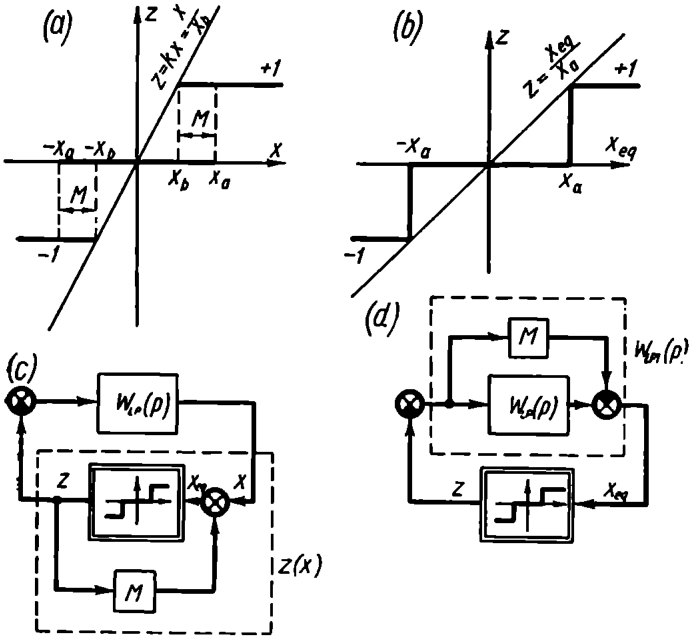

Fig. 19.12

(see Fig. 19.12*a*) belongs to the angle

$$\beta = \frac{z}{x} \leqslant k = \frac{1}{x_b} < \frac{1}{N}$$

Thence

$$k_{lim} = \frac{1}{N} \tag{19.46}$$

These conditions are much more stringent than results of the Nyquist analysis for the specified angle.

Example 19.11. Analyze the stability of a system containing the linear part $W_{LP}(p)$ from Example 19.10 and a play-type nonlinearity.

Representing the play-type nonlinearity $z(x)$ by an equivalent circuit (see Sec. 16.7, Fig. 16.21*a*) gives the circuit of Fig. 19.13*a*.

Taking separately the linear part

$$W_{LP1}(p) = \frac{1}{p[1+W_{LP}(p)]} \tag{19.47}$$

and a nonlinearity of the asign type (Fig. 19.13*b*) leads to the assum-

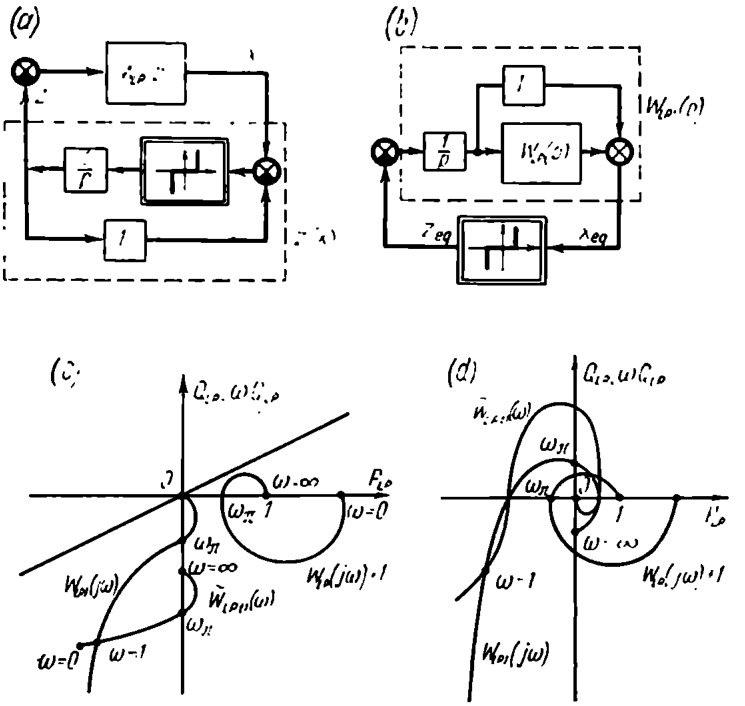

Fig. 19.13

tion that the nonlinear part is single-valued and belongs to the angle

$$\beta \leqslant \frac{z_{eq}}{x_{eq}} < k = \infty$$

In this case $\frac{1}{k} = 0$, and the absolute stability condition is reduced to the requirement that the Popov line can be traced through the origin of coordinates.

Figure 19.13*c* illustrates the locus $\tilde{W}_{LP\,1}(\omega)$ for the case where the locus $W_{LP}(j\omega) + 1$ stays in the right half-plane, and Fig. 19.13*d*, the case where this locus reaches into the left half-plane. The Popov line is seen to be plottable only in the case *c*.

Consequently, the condition for absolute stability of a system with play is reduced to the inequalities

$$\operatorname{Re}[W_{LP}(j\omega) + 1] > 0 \tag{19.48}$$

or

$$\operatorname{Re} W_{LP}(j\omega) > -1 \tag{19.49}$$

Example 19.12. Determine the stability conditions for a system with a stop and containing the linear element from Example 19.10.

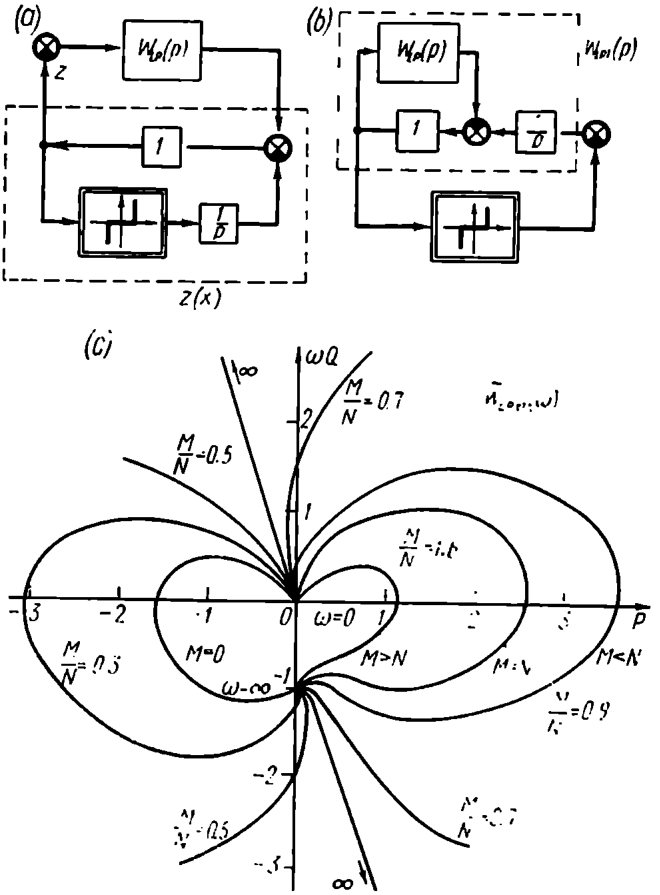

Fig. 19.14

The reasoning applied to the system with play can be used here. The equivalent circuits for this case are shown in Fig. 19.14*a*, *b*. Now, for the transformed circuit

$$W_{LP1}(p) \quad \frac{1}{p}\frac{1}{1+W_{LP}(p)} \tag{19.50}$$

and since the conditions for $1+W_{LP}(j\omega)$ and $\frac{1}{|1+W_{LP}(j\omega)|}$ to belong to the right half-plane coincide the absolute stability conditions for the system with a stop coincide with the conditions (19.48) and (19.49) for a system with play.

A specific example is the transfer function $W_{LP}(p) = \frac{1}{p}\left[\frac{N}{pT(1+pT)}+M\right]$ which represents a compensated course stabilization system (see Sec. 15.2). For this case the position of the locus $W_{LP}(j\omega)$ depends on the relation of M and N. At $N>M$ the locus is in the second and third quadrants while at $M>N$ it is within the third quadrant. The sufficient condition (19.49) is unduly stringent and does not hold.

The required conclusions can be made from the plots of transformed loci $\tilde{W}_{LP\,tl}(\omega)$ for different ratios $\frac{M}{N}$ which are shown in Fig. 19.14*c*. As seen in the loci, the Popov line can go through the origin of coordinates only for $\frac{M}{N}>1$ and, consequently, only in this case the absolute stability conditions expressed by the inequality

$$N<M \tag{19.51}$$

are met.

19.5. ABSOLUTE STABILITY OF PROCESSES

Absolute stability of equilibrium proves in many cases insufficient to ensure normal operation of a nonlinear control system at different setting and disturbing actions. The processes in a nonlinear system caused by different external actions should also be made stable. Sec. 19.1 gave a definition of the asymptotically stable process which, when disturbed, asymptotically returns to the condition existing in the system prior to the disturbance. Absolute stability takes place only when the process is asymptotically stable for a class of nonlinear element responses in the system.

The sufficient condition for absolute stability of processes in the original system at constrained input actions was found by B. N. Naumov and Ya. Z. Tsypkin. For a general system with an unstable linear part it is of the form

$$\operatorname{Re}\frac{W_{LP}(j\omega)}{1+rW_{LP}(j\omega)}+\frac{1}{k-r}=\delta\geqslant 0 \tag{19.52}$$

where r is a factor which ensures stability of the linear part with negative feedback.

The nonlinear response derivative should then belong to the range

$$r+\beta\leqslant\frac{dz(x)}{dx}\leqslant k+\beta \tag{19.53}$$

where β is an infinitesimal positive value.

In the case of a stable linear part with $r = 0$ in Eq. (19.52) we have

$$\operatorname{Re} W_{LP}(j\omega) + \frac{1}{k} \geqslant 0 \tag{19.54}$$

or

$$k \operatorname{Re} W_{LP}(j\omega) + 1 \geqslant 0 \tag{19.55}$$

To formulate the absolute stability criterion for processes in the general case transform inequality (19.52) by introducing the notation $\frac{k}{r} = A$,

$$\operatorname{Re} \frac{kW_{LP}(j\omega)}{A + kW_{LP}(j\omega)} + \frac{1}{A-1} \geqslant 0 \tag{19.56}$$

where

$$kW_{LP}(j\omega) = kP_{LP}(\omega) + jkQ_{LP}(\omega) \tag{19.57}$$

Find in the (kP_{LP}, kQ_{LP}) plane the locus corresponding to the equality sign in expression (19.56). Substituting Eq. (19.57) into the left-hand part of Eq. (19.56) gives an equation for the desired curves

$$\left[kP_{LP} + \frac{1}{2}(A+1)\right]^2 + (kQ_{LP})^2 = \frac{1}{4}(A-1)^2 \tag{19.58}$$

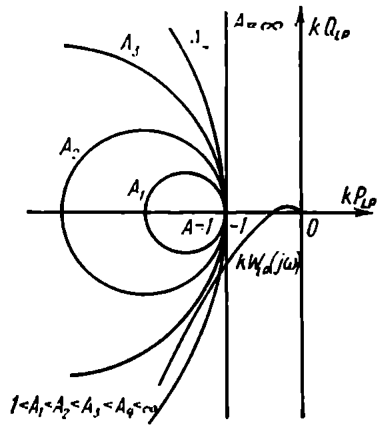

Fig. 19.15

Equation (19.58) defines a family of circles passing through the point -1, $j0$ having a radius $R = \frac{A-1}{2}$ and located to the left of the straight line $kP_{LP} = -1$ (Fig. 19.15). Each of these circles is associated with its own value of $A = \frac{k}{r} \geqslant 1$.

Inequality (19.56) will hold outside the A-circles, which is easily verified assuming $P_{LP} = Q_{LP} = 0$ at $k > 0$, $r > 0$. The condition (19.56) and consequently the condition for stability of the equivalent linear part is valid if the locus of the frequency response is outside the appropriate A-circle.

It is noteworthy that the grids of A-circles coincide with circular diagrams used in plotting the real frequency responses of closed-loop systems from amplitude-phase responses of open-loop systems (see Section 9.5).

If $A = \infty$ (i.e. $k = \infty$ or $r = 0$), the associated circle in Fig. 19.15 becomes a vertical straight line passing through the point -1, $j0$. If the condition for absolute stability holds at $A = \infty$, it also holds at any A.

If in a system with a stable linear part the nonlinear response $z(x)$ is such that $\frac{dz(x)}{dx} > r + \beta$, the absolute stability criterion for processes may be used in the form of Eq. (19.56). The location of a frequency response locus $kW_{LP}(j\omega)$ is compared with a circle at $A = \frac{k}{r} < \infty$. Then the condition for absolute stability is not so stringent.

At $A = 1$ the circle degenerates into a point $-1, j0$ and the sufficient condition for nonlinear system absolute stability becomes a necessary and sufficient condition for linear system stability at $k = r$.

If the frequency criterion of absolute stability is met, the equilibrium will evidently be stable as well. In this sense the class of nonlinear systems has a property akin to that of linear systems.

Conditions for absolute stability of processes in nonlinear systems are more rigorous than those for stability of equilibrium, they impose additional constraints on the nonlinear response derivative and represent a particular case of the V. M. Popov condition at $q = 0$ (Popov's vertical straight line).

In analysis of absolute process stability when the nonlinear response $z(x)$ is given, the problem reduces to verification of the location of the frequency response $kW_{LP}(j\omega)$ relative to the circle with A defined from a specified nonlinear response and to selection of the linear part parameters such that the response $kW_{LP}(j\omega)$ is outside this circle.

Conversely, if the frequency response $W_{LP}(j\omega)$ is given, the admissible value of r can be determined as a function of k by assuming different values of k, plotting $kW_{LP}(j\omega)$ and determining a circle tangential to it. With A and k known for this circle the value of r is found.

19.6. ABSOLUTE STABILITY OF SAMPLED-DATA SYSTEMS

For a nonlinear sampled-data system in which the nonlinear element *NE* is connected before the pulse element *PE* (Fig. 19.16*a*), sufficient conditions for stability can be based either on Lyapunov's direct method or on Popov's frequency criterion. The latter is more widespread.

The early papers on this subject include Ya. Z. Tsypkin's article proving that a sufficient condition for absolute stability of a sampled-data system with a nonlinear response belonging to the sector $[0, k]$ is the inequality

$$\operatorname{Re} W_{LP}^{*}(j\omega) + \frac{1}{k} > 0 \qquad (19.59)$$

where $W^*_{LP}(j\omega)$ is the frequency response of the linear sampled-data part *LSDP* of a system which is presumed stable. The nonlinear response belonging to the sector [0, k] can be discontinuous, multivalued and even nonstationary.

By this criterion, absolute stability is ensured if the entire frequency response locus $W^*_{LP}(j\omega)$ is to the right of the vertical line

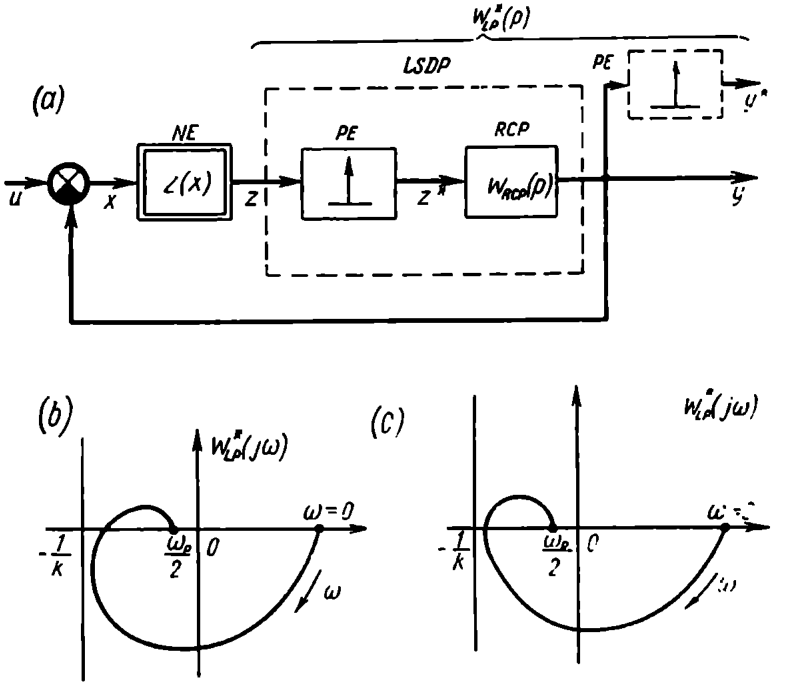

Fig. 19.16

passing through the point $-\frac{1}{k}$, $j0$ (Fig. 19.16*b*). This condition is necessary as well as sufficient if the real part of the frequency response has a minimum at the intersection point with the real axis (Fig. 19.16*c*). In this case the extreme value of the coefficient k in a linear system where the nonlinear element is replaced with a linear one whose gain is k, which is found by the Nyquist criterion, coincides with the limit boundary of the sector [0, k] determined by the Tsypkin criterion.

Such situations are, however, relatively rare; in most cases the criterion (19.59) imposes excessive requirements on the system parameters. Thus, there must be a vertical straight line with respect to which the position of the frequency response $W^*_{LP}(j\omega)$ is analyzed.

Recall that in the basic formulation of the Popov criterion for continuous systems Popov's straight line going through the point $-\frac{1}{k}$, $j0$ may have any slope. Here, the limit values of k for the upper sector boundary are clearly seen to exceed those corresponding to Popov's vertical line.

The absolute stability criterion for nonlinear sampled-data systems is reinforced by imposing additional constraints on nonlinearities in the system; an example is an analog of the Popov criterion formulated by Ya. Z. Tsypkin and valid for systems with monotonic nonlinear responses. By this criterion a sufficient condition for stability of a nonlinear sampled-data system with a stable linear part and a monotonic nonlinear response belonging to the sector $[0, k]$ is that the following inequality holds

$$\operatorname{Re}\left[1+q\left(1-e^{-j\omega T_p}\right)\right] W_{LP}^{*}(j\omega)+\frac{1}{k}=\delta\geqslant 0 \qquad (19.60)$$

where q is an arbitrary positive number.

The operator $1-e^{-j\omega T_p}$ represents the first difference and is analogous to the factor $j\omega$ in the Popov inequality for continuous systems.

Introduce a transformed frequency response of the linear sampled-data part

$$W_{LP\,t}^{*}(j\omega)=\operatorname{Re} W_{LP}^{*}(j\omega)+j\left\{\operatorname{Re} e^{-j\omega T_p} W_{LP}^{*}(j\omega)-\operatorname{Re} W_{LP}^{*}(j\omega)\right\} \qquad (19.61)$$

Then the criterion (19.60) is geometrically interpreted in the same way as the Popov criterion for continuous systems. A nonlinear sampled-data system is stable if, with the linear sampled-data part stable, a straight line with an arbitrary positive slope $\frac{1}{q}$ can be passed through the point $-\frac{1}{k}$, $j0$ so that $W_{LP\,t}^{*}(j\omega)$ is to the right of the line.

In the case of a neutral or unstable linear sampled-data part, it can be rearranged with introduction of an internal negative feedback as is done for continuous system in Sec. 19.3. The boundaries of the sector which can contain the nonlinear response vary in exactly the same way as in the case of continuous systems, while the formulation of the criterion remains unchanged.

Ya. Z. Tsypkin proposed a sufficient condition for absolute stability of processes in nonlinear sampled-data control systems which is quite identical to the condition (19.52) for continuous systems

$$\operatorname{Re}\frac{W_{LP}^{*}(j\omega)}{1+rW_{LP}^{*}(j\omega)}+\frac{1}{k-r}=\delta\geqslant 0 \qquad (19.62)$$

with the following constraint on the nonlinear response derivative

$$r+\beta \leqslant \frac{dz(x)}{dx} \leqslant k+\beta, \qquad \beta \to 0 \tag{19.63}$$

Unlike the continuous case the derivative can be nonstationary.

Examples of investigations into absolute stability in nonlinear sampled-data systems are cited, e.g., in Ref. 84.

19.7. COMPARISON OF STABILITY ANALYSIS METHODS IN NONLINEAR SYSTEMS

Of all the above methods of stability analysis in nonlinear systems, the phase space method alone leads to accurate formulation of necessary and sufficient conditions for stability. These conditions can also be obtained approximately, through mathematical simulation, with an accuracy determined by implementation of the model associated with the specific system of equations.

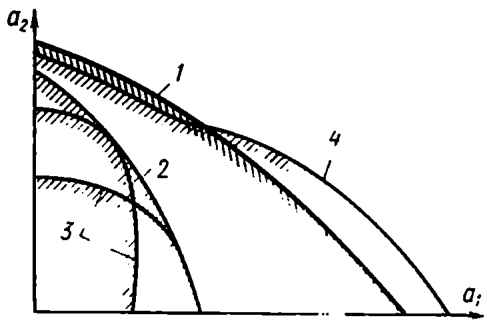

Fig. 19.17

Sufficient, but not necessary, stability conditions are set by the frequency criterion of absolute stability; Lyapunov's direct method with a specific form of the V-function can delineate a narrower region of sufficient stability conditions than Popov's criterion. Both these methods, however, ensure stability in a specified area.

The method of harmonic linearization indicates an approximate value of the stability area, depending on the extent to which the filter hypothesis is satisfied, but does not ensure stability in that area because the area may extend across the stability boundary. Polyharmonic self-oscillations are occasionally possible in this area.

The stability boundaries obtained through different methods are shown in Fig. 19.17, where a_1 and a_2 are some generalized parameters of the specified nonlinear system. The shading denotes stability areas obtained by the different methods. Curve *1* is the actual boundary of the system stability. Curve *2* shows the sufficient stability boundary obtained by using Popov s criterion. Curves *3* schematically show examples of the boundary obtained by Lyapunov's direct method for different V-functions.

Harmonic linearization establishes a boundary (curve *4*) which can extend across the actual stability area.

The general conclusions can be illustrated with the following examples.

Example 19.13. Using the criterion of absolute stability of equilibrium determine the limit gain $(Nk)_{lim}$ of the relay servo system of Example 18.2 and compare this gain with the values obtained by harmonic linearization and experimentally (Fig. 18.14). The linear part transfer function is

$$W_{LP}(p) = \frac{k}{p(1+0.2p)(1+2p)} \tag{19.64}$$

The frequency at which the locus $W_{LP}(j\omega)$ intersects the negative real half-axis was found in Example 18.2 to be equal to 1.58 sec^{-1}. At this frequency the magnitude of the frequency response $W_{LP}(j\omega) = 0.182k$. Assuming that the relay response (Table 18.1) is contained, in the sector $[r, N]$, where r is a positive infinitesimal and $N = \frac{z_a}{x_a}$ is the normalizing factor of the harmonic linearization method, and bearing in mind that the locus $W_{LP}(j\omega)$ for this system is convex, we have, according to the criterion, the condition for absolute stability

$$0.182k < \frac{1}{N}$$

whence

$$(Nk)_{lim} = \frac{1}{0.182} = 5.5 \text{ sec}^{-1}$$

According to Fig. 18.14 the exact value of $(Nk)_{lim} = 6.3$ sec^{-1}, according to the harmonic linearization method $(Nk)_{lim} = 8.6$ sec^{-1}.

All the results obtained correspond to the parameter a_1 in Fig. 19.17.

Example 19.14. Determine in different ways the limit value of the coefficient N in the transfer function of the linear part, $W_{LP}(p) = \frac{N}{pT(1+pT)}$ if the nonlinear response represents a three-positional relay with hysteresis and lies in the sector $k = \frac{1}{x_b}$ with a relative width of the hysteresis loop equal to M (see Example 19.10).

Once this problem is solved by using the phase plane (see Example 17.10), we have the exact value of N_{lim}, which is the solution of the transcendental equation

$$e^{-\frac{2}{N_{lim}}} = 1 - \frac{1}{N_{lim}} \frac{1+2Mk}{1+Mk}$$

For the particular case where $M = 0.5$ and $k = 2$ we have $N_{lim} = 3.15$.

Solving this problem with the aid of the absolute stability criterion (see Example 19.10) gives the condition

$$N_{lim} = \frac{1}{k} = 0.5$$

When the problem is solved by the harmonic linearization method (without adjusting it for relay responses) we can obtain, for the specified parameters, $N_{lim} = 6.4$.

All the three solutions correspond to the parameter a_1 in Fig. 19.17.

Example 19.15. Determine the limit value of the coefficient N for $W_{LP}(p) = \frac{N}{pT(1+pT)}$ if the nonlinearity has a response of the play type.

The exact solution is given in Example 17.12. The plot of Fig. 17.49*d* shows that in this case $N_{lim} = 3.04$.

Solution obtained by the method of absolute stability (see Example 19.11) produces the condition (19.49) which, after the calculation of $\lim_{\omega \to \infty} \operatorname{Re} W_{LP}(j\omega) = -N$, leads to the value $N_{lim} = 1$.

Following the appropriate constructions of $W_{LP}(j\omega)$ and $\tilde{V}_n(A)$ harmonic linearization yields $N_{lim} = 3.5$ (see Example 18.6).

All the values of N_{lim} thus obtained correspond to the parameter a_1 in Fig. 19.17.

Chapter XX

CONTROL PERFORMANCE IN NONLINEAR SYSTEMS

20.1. SPECIFIC FEATURES OF NONLINEAR SYSTEM PERFORMANCE

The problem of obtaining the required performance in nonlinear systems is as important as in linear systems. The performance of nonlinear systems can be assessed by the same characteristics as linear ones (see Ch. IX), although to analyze nonlinear system performance is more difficult (see Ch. XVII). Nonlinear systems, however, hold a better promise for achieving good performance, processes there can be made optimal in one sense or another, e.g. in terms of speed.

This chapter discusses the basic methods of analyzing transient processes and performance in nonlinear control systems and certain problems of nonlinear systems synthesis.

As in the case of linear systems the methods of analyzing the performance of nonlinear control systems can be classified into direct and indirect ones. The direct methods require implementation of the process under study. The basic direct methods are discussed in Secs. 20.1 through 20.3. The indirect methods deal with some indirect indices associated with the nature of control. These methods are considered in Secs. 20.4 and 20.5.

Detailed information on all these methods can be found in Refs. 68, 82, 76.

20.2. THE METHOD OF "PASSING SOLUTIONS" IN CONSTRUCTION OF TRANSIENT PROCESSES IN NONLINEAR SYSTEMS

If the response of a nonlinear element in the system (Fig. 20.1*a*) can be approximated by a polygonal line (Fig. 20.1*b*), the behaviour of the resulting piecewise-linear system can be described by a set of linear differential equations replacing each other successively in the conjugation points. The transient process is expressed within certain time intervals by solutions of these differential equations; the final values of solution to the preceding equation and its derivatives are initial conditions for the subsequent solution.

If a linear part is described by a second-order differential equation, then passing solutions in transition from one part of the response

to another can be conveniently performed in the phase plane as was done in examples of Ch. XVII.

Example 20.1. Consider transient processes in the variable-structure system whose schematic is shown in Fig. 17.43 and phase portrait, in Fig. 17.44. Let $k_0 = 1$ and let the slope of the switching

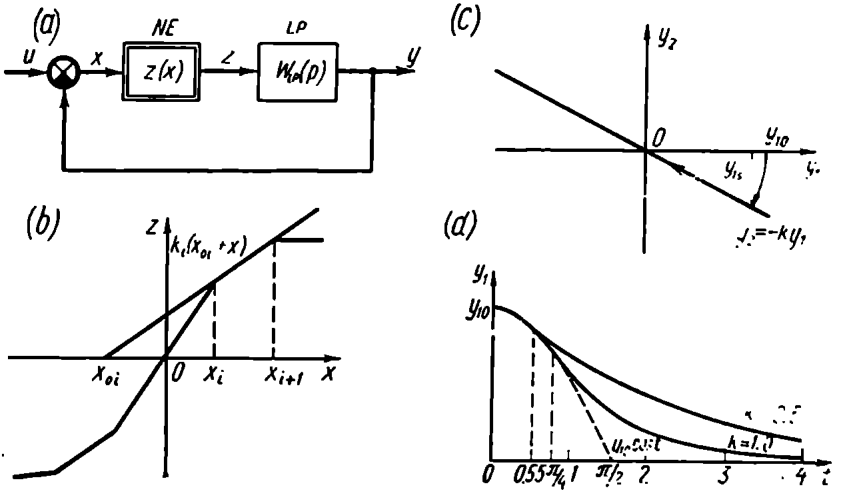

Fig. 20.1

line (Fig. 17.44*d*) have two values: (a) $k = 0.5$; (b) $k = 1.0$. Consider transient processes when the system responds to the initial misalignment: $\tau = 0$, $y_1 = y_{10}$, $y_2 = 0$ (Fig. 20.1*c*).

The motion of the system along the first part of the trajectory (from the horizontal axis to the switching line) can be described in the time domain on the basis of (17.33)

$$\left.\begin{aligned} y_1 &= y_{10}\cos\tau \\ y_2 &= -y_{10}\sin\tau \end{aligned}\right\} \qquad (20.1)$$

The switching line equation is

$$y_2 = -ky_1 \qquad (20.2)$$

Therefore the relative switching time τ_s following the substitution of Eq. (20.2) into the second Eq. (20.1) and term-by-term division of the result by the first equation (20.1) can be found from the expression

$$k = \tan\tau$$

or

$$\tau_s = \operatorname{arc\,tan} k \qquad (20.3)$$

On the second portion of the system trajectory there is a sliding mode on the switching line, $y_2 = -ky_1$, which is described, by virtue of Eq. (17.42), in the parametric form by the equations

$$\left.\begin{aligned} y_1 &= y_{1s}e^{-k(\tau-\tau_s)} \\ y_2 &= y_{2s}e^{-k(\tau-\tau_s)} \end{aligned}\right\} \tag{20.4}$$

where y_{1s} and y_{2s} are values of the system phase coordinates at $\tau = \tau_s$. Figure 20.1*d* shows two versions of transient processes in the system, at $k = 0.5$ and $k = 1$. The switching time will be 0.55 and $\frac{\pi}{4}$, respectively. At $k < 1$ the transient process time exceeds that at $k = 1$.

The application of the passing solutions method to higher-order systems with nonlinear responses consisting of many separate portions generally involves unwieldy calculations.

The method is easiest to apply to relay systems, where relay switching generates pulses of constant height, variable duration and alternating polarity. Owing to this, analysis of processes in a relay control system is reduced to studying the behaviour of the linear part subjected to the action of these pulses. The superposition principle then helps find the overall response of the linear part to any number of pulses merely by summing up responses to each separate action.

Consider now the relay control system of Fig. 20.2*a*. Let the relay element *RE* have the response of Fig. 20.2*b* while the linear part *LP* transient function is $h_{LP}(t)$ (Fig. 20.2*c*). At $t = 0$ the linear part is at rest and $y = 0$ (zero initial conditions). Find system motion at an arbitrary input signal $u(t)$ (Fig. 20.3*a*). At $t = t_1$ we have $x = x_a$, and the relay responds. The input of the linear part is

$$z(t) = z_a 1_0 (t - t_1) \tag{20.5}$$

and the output signal varies according to the law

$$y(t) = y_1(t) = z_a h_{LP}(t - t_1) \tag{20.6}$$

and the misalignment, according to the law

$$\begin{aligned} x(t) &= u(t) - y(t) = u(t) - y_1(t) = \\ &= u(t) - z_a h_{LP}(t - t_1) \end{aligned} \tag{20.7}$$

The plots of $u(t)$, $y(t)$ and $x(t)$ are shown in Fig. 20.3*a*. The misalignment $x(t)$ reduces and at $t = t_2$ becomes equal to x_b; as a result the relay releases, which is equivalent to the linear part receiving a negative jerk $-z_a 1_0 (t - t_2)$ while the action of the signal $z_a 1_0 (t - t_1)$ is maintained (Fig. 20.3*b*). The output signal varies in the following way

$$y(t) = y_1(t) + y_2(t) = z_a h_{LP}(t - t_1) - z_a h_{LP}(t - t_2) \tag{20.8}$$

and the misalignment is given by the expression

$$x(t) = u(t) - y(t) = u(t) - z_a [h_{LP}(t - t_1) - h_{LP}(t - t_2)] \tag{20.9}$$

The plot of $x(t)$ defines the time t_3 at which the relay responds anew; depending on the form of $u(t)$ and $y(t)$ the relay can respond

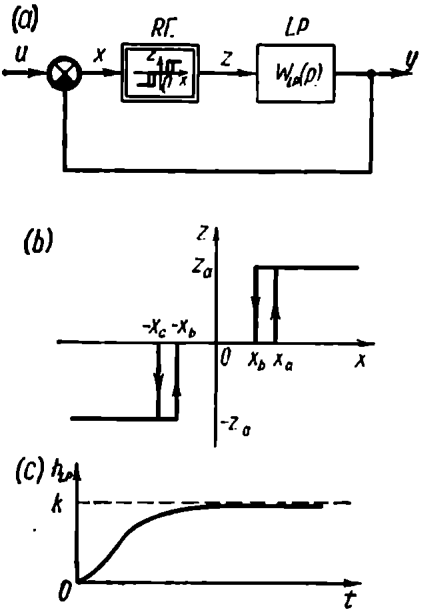

Fig. 20.2

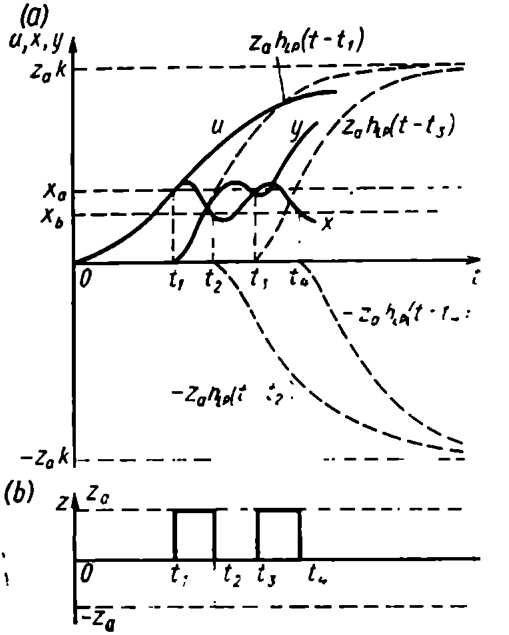

Fig. 20.3

either in the positive, ($x = x_a$) or in the negative, ($x = -x_a$), direction. The general expressions for $y(t)$ and $x(t)$ are of the form

$$y(t) = \sum_{i=1}^{k} \pm z_a h_{LP}(t - t_i) \tag{20.10}$$

$$x(t) = u(t) - y(t) = u(t) - \sum_{i=1}^{k} \pm z_a h_{LP}(t - t_i) \tag{20.11}$$

where k is the number of relay switchings from $t = 0$ up to the current moment t; the sign is positive when responding in the positive and releasing in the negative directions, and negative in the opposite case.

With increasing t the number of addends increases but this does not hinder the plotting since in systems with a static linear part

$h_{LP}(t)$ tends with time to a steady state value, which is equal to the linear part gain k. The steady state values of different signs cancel out, so that the total number of time-dependent addends remains small.

If the linear part contains an integrating element and the transient function $h_{LP}(t)$ grows unboundedly with time t, then the increasing linear part which corresponds to the integrating element should be isolated from it (Fig. 20.4*a*). The sum of the increasing part $h_{LP1}(t)$ and the remaining constrained part $h_{LP2}(t)$ is equal to the transient function.

When plotting the process (Fig. 20.4*b*) two constituents are added with the appropriate sign, $z_a h_{LP1}(t-t_i)$ and $z_a h_{LP2}(t-t_i)$, at each switching time t_i.

The general expression for the signal y takes the form

$$y(t) = \sum_{i=1}^{k} \pm z_a h_{LP1}(t-t_i) + \sum_{i=1}^{k} \pm z_a h_{LP2}(t-t_i) \qquad (20.12)$$

The sum of displaced linear functions is also a linear function. Owing to this, no infinitely increasing components should be plotted; instead, their sum can be represented at once as a polygonal line whose portions have slopes 0, $+z_a k_p$ — $z_a k$. The slopes are changed at the switching times. This sum is supplemented with constrained components with appropriate signs, $\pm z_a h_{LP2}(t-t_i)$. As in the case of a static linear part, the switching times are found while plotting the process itself (Fig. 20.4*b* and *c*).

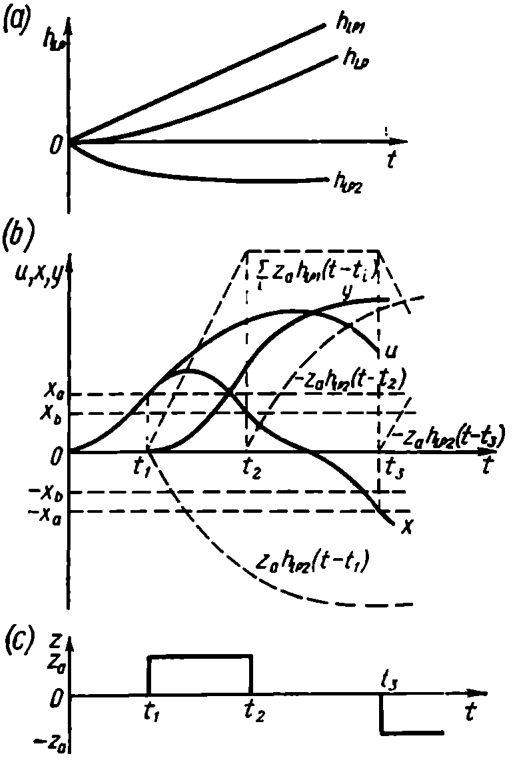

Fig. 20.4

The passing solutions method, as described above, is suitable in calculations of transient processes in digital systems with continuous transmission of signals as well as in relay systems. Such systems have stepwise nonlinearities (see Fig. 15.17).

20.3. DIFFERENCE METHODS OF CONSTRUCTING TRANSIENT PROCESSES IN NONLINEAR SYSTEMS

The basic idea of the difference methods consists in approximate replacement of a nonlinear differential equation by a difference equation, which in itself can be regarded as a ready-made recurrence relation permitting sequential point-by-point process calculations. These calculations can be made on a digital computer; difference methods are easy to program.

The simplest difference method is the Euler technique; to begin with, we will discuss a linear first-order differential equation.

Assume that we have a differential equation

$$\frac{dy}{dt} = f(y, t) \tag{20.13}$$

with an initial condition $y(0) = y_0$.

With the increment Δt sufficiently small construct a grid of equidistant values

$$t_l = l\Delta t \qquad (l = 0, 1, 2, 3, \ldots) \tag{20.14}$$

Replace approximately the differential equation (20.13) on the lth portion by

$$\frac{y[(l+1)\Delta t] - y(l\Delta t)}{\Delta t} = f[y(l\Delta t), l\Delta t] \tag{20.15}$$

whence

$$y[(l+1)\Delta t] = y(l\Delta t) + f[y(l\Delta t), l\Delta t]\,\Delta t \tag{20.16}$$

The latter relation is a nonlinear difference equation which sequentially leads to the discrete values

$$\left.\begin{aligned} y_1 &= y(\Delta t) = y_0 + f(y_0, 0)\,\Delta t \\ y_2 &= y(2\Delta t) = y_1 + f(y_1, \Delta t)\,\Delta t \\ &\cdots\cdots\cdots\cdots\cdots \\ y_{l+1} &= y[(l+1)\Delta t] = y_l + f(y_l, l\Delta t)\,\Delta t \end{aligned}\right\} \tag{20.17}$$

The Euler technique is readily extendable to systems of differential equations in the normal form which describe processes in nonlinear control systems subjected to an external action

$$\frac{dy_i}{dt} = f_i(y_1, y_2, \ldots, y_n, t) \qquad (i = 1, 2, \ldots, n) \tag{20.18}$$

In this case a set of recurrence relations, instead of one relation (20.16), should be written down

$$y_i[(l+1)\Delta t] = y_i(l\Delta t) + f_i[y_1(l\Delta t), y_2(l\Delta t), \ldots, y_n(l\Delta t)]\,\Delta t \tag{20.19}$$

then successive values calculated as in Eq. (20.17).

There are numerous difference methods of solving nonlinear differential equations which use the same basic idea as the Euler technique but are more accurate, namely the Runge-Kutta, Adams, Krylov techniques, etc. All these lead to recurrence relations of the type (20.19), which are used in calculations.

Standard subroutines are available for some of these techniques (e.g. for the Runge-Kutta technique), which greatly facilitate the use of digital computers.

The graphoanalytical methods of A.V. Basharin and of D.A. Bashkirov are closely related to the Euler technique and

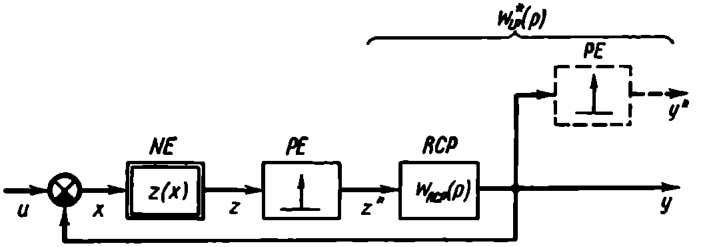

Fig. 20.5

determine a sequence of discrete values of the process through graphical constructions.

Transition from nonlinear differential equations to nonlinear difference equations can be achieved by approximate replacement of the initial nonlinear continuous control system by a sampled-data system. There are several ways to do this, but we will first construct transient processes in nonlinear sampled-data systems.

Let a nonlinear sampled-data system be represented by the structural diagram of Fig. 20.5. The nonlinear element *NE* with a response $z(x)$ is connected before the ideal pulse element *PE*. The reduced continuous part, *RCP*, has a transfer function $W_{RCP}(p)$ which is associated with the transfer function of the linear sampled-data part

$$W^*_{LP}(p) = \frac{Y^*(p)}{Z^*(p)} = \frac{k_m e^{mpT_p} + k_{m-1} e^{(m-1)pT_p} + \ldots + k_0}{d_n e^{npT_p} + d_{n-1} e^{(n-1)pT_p} + \ldots + d_0} \quad (20.20)$$

The latter expression in its turn (see Sec. 14.2) can be rewritten as a difference equation

$$d_n y[(l+n)T_p] + d_{n-1} y[(l+n-1)T_p] + \ldots + d_0 y(lT_p) = k_m z[(l+m)T_p] + k_{m-1} z[(l+m-1)T_p] + \ldots + k_0 z(lT_p) \quad (20.21)$$

Eq. (20.21) is associated with the recurrence relation

$$y[(l+n)T_p] = \frac{1}{d_n}\{k_m z[(l+m)T_p] + \ldots + k_0 z(lT_p) - d_{n-1} y[(l+n-1)T_p] - \ldots - d_0 y(lT_p)\} \quad (20.22)$$

where

$$z(iT_p) = z[x(iT_p)] = z[u(iT_p) - y(iT_p)] \qquad (20.23)$$

The relations (20.22) and (20.23) permit successive calculation of discrete values of processes in a nonlinear sampled-data system at an arbitrary input signal $u(lT_p)$ starting with $l = -n$, exactly as was done in linear sampled-data systems (see Example 14.4). The only difference is that Eq. (20.22) includes the nonlinear relation $z(x)$.

Processes in nonlinear sampled-data systems can also be described by another method which uses the weighting function of the reduced continuous part $w_{RCP}(t)$. Similarly to Eq. (14.41), for a nonlinear system

$$y(lT_p) \sum_{i=0}^{l-1} z[u(iT_p) - y(iT_p)]\, w_{RCP}[(l-i)\,T_p] \qquad (20.24)$$

Then the discrete values of $y(lT_p)$ can be calculated successively starting with $l = 1$ because $w_{RCP}(0) = 0$ (at $m < n$). For the same reason the upper bound in the sum is assumed equal to $l - 1$.

If the weighting function $w_{RCP}(t)$ is not specified it can be found through the response of the reduced continuous part to a unitary pulse or through the transfer function $W^*_{LP}(p)$ as shown in Sec. 14.2.

The merits and demerits of the two methods were noted in Sec. 14.2. The relations (20.22) through (20.24) can easily be used to program a digital computer, which will be useful in handling cumbersome calculations (e.g. at small T_p).

The intermediate values of the output signal in nonlinear sampled-data systems can be found in the same way as in linear systems. Consequently, no essential difficulties are encountered in determining the laws for signal variations in nonlinear sampled-data systems. Now, let us take up the methods for approximate transition from continuous systems to sampled-data ones.

Consider a nonlinear control system (Fig. 20.6*a*) containing a nonlinear element NE and a linear part LP. Assume that the external action $u(t)$ results in a process represented by time diagrams for the signals $z(t)$ and $y(t)$ (Fig. 20.6*b*). The latter signal is the effect of the former signal acting on the linear part of the system. Replace the continuously varying signal $z(t)$ by a sequence of periodic instantaneous pulses so that $y(t)$ remains unchanged (Fig. 20.6*c*). The area of each pulse is assumed equal to the value of the signal $z(t)$ at the pulse time multiplied by the period T_p. At small T_p the areas of instantaneous pulses are approximately equal to those of variable shape pulses into which the real signal $z(t)$ is divided by the sampling times (Fig. 20.6*c* shows this at the lth sampling instant). The smallness of T_p is also a condition for an approximately equal effect of the real and instantaneous pulses on the linear part,

owing to which $y(t)$ remains almost unchanged. The smaller T_p, the better the approximation.

Replacement of a continuous signal by a sequence of modulated instantaneous pulses denotes a transition from a continuous to a sampled-data system (Fig. 20.6*d*), where $Z^*(p) \approx \frac{1}{T_p} Z(p)$ and the transient function of the reduced continuous part is $W_{RCP}(p) = T_p W_{LP}(p)$. The factor T_p acts as the transfer function of the shaping element and should be measured in units used for all time

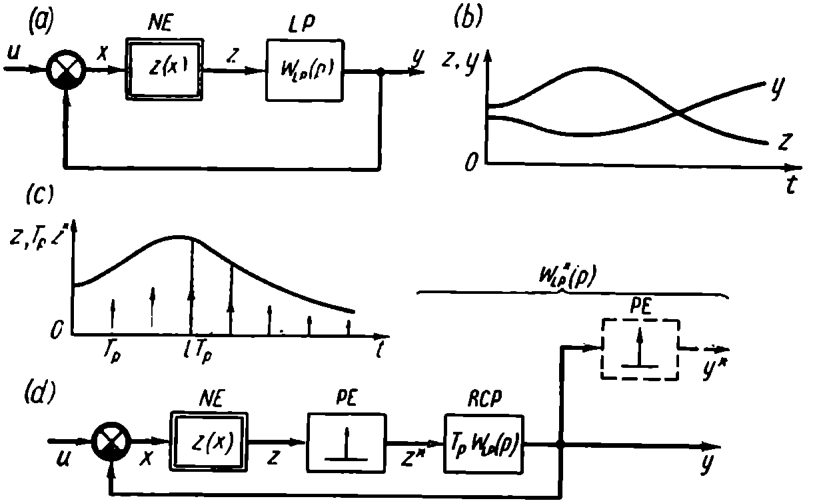

Fig. 20.6

constants in the system. In order to find the transfer function $W^*_{LP}(p)$ of the linear sampled-data part which would be in line with $T_p W_{LP}(p)$, one of the techniques described in Ch. XIII can be used. After that the processes in the resultant nonlinear sampled-data system are to be calculated by one of the methods described above.

Example 20.2. Find the transfer function $W^*_{LP}(p)$ and the recurrence relations for a system with $W_{LP}(p) = \frac{k}{p(1+pT)}$. Using Eq. (12.39) from Example 12.5 and allowing for the factor T_p gives

$$W^*_{LP}(p) = \frac{kT_p\left(1-e^{-\frac{T_p}{T}}\right)e^{pT_p}}{\left(e^{pT_p}-1\right)\left(e^{pT_p}-e^{-\frac{T_p}{T}}\right)} = \frac{kT_p\left(1-e^{-\frac{T_p}{T}}\right)e^{pT_p}}{e^{2pT_p}-\left(1+e^{-\frac{T_p}{T}}\right)e^{pT_p}+e^{-\frac{T_p}{T}}} \tag{20.25}$$

The corresponding difference equation takes the form

$$y[(l+2)T_p]-(1+e^{-\frac{T_p}{T}})y[(l+1)T_p]+e^{-\frac{T_p}{T}}y(lT_p)=$$
$$=kT_p(1-e^{-\frac{T_p}{T}})z[(l+1)T_p] \quad (20.26)$$

whence

$$y[(l+2)T_p]=kT_p(1-e^{-\frac{T_p}{T}})z[(l+1)T_p]+$$
$$+(1+e^{-\frac{T_p}{T}})y[(l+1)T_p]-e^{-\frac{T_p}{T}}y(lT_p) \quad (20.27)$$
$$z[(l+1)T_p]=z\{u[(l+1)T_p]-y[(l+1)T_p]\} \quad (20.28)$$

The weight function of the reduced continuous part can be obtained as discrete values of the linear part response $T_pW_{LP}(p)$ to a unitary pulse. For this example it was found in Example 5.1. Equation (5.11) yields

$$w_{RCP}(lT_p)=kT_p(1-e^{-l\frac{T_p}{T}}) \quad (20.29)$$

Substituting Eq. (20.29) into (20.24) gives

$$y(lT_p)=\sum_{i=0}^{l-1}[u(iT_p)-y(iT_p)]kT_p[1-e^{-(l-i)\frac{T_p}{T}}] \quad (20.30)$$

The real signal $z(t)$ can be replaced by a sequence of instantaneous pulses if the power of the denominator of the transfer function $W_{LP}(p)$ exceeds that of the numerator at least by 2. If the powers are equal ($m = n$) it will signify that in the right-hand part of the relation (20.22) the signal z should be taken at the same instant as y in the left-hand part. As a result the recurrence relation becomes a nonlinear equation.

Complications also arise in this case with the relation (20.24) because $w_{RCP}(0) \neq 0$ at $m = n$. The relation becomes an equality as well.

Instantaneous pulses may be replaced by pulses of a more complex shape ensuring a better approximation. Figure 20.7*a* shows replacement of a continuous signal by rectangular pulses with a duty factor equal to one (stepwise approximation). The linear continuous part associated with this replacement (Fig. 20.7*b*) includes a shaping element with a transfer function

$$W_{sh}(p)=\frac{1-e^{-pT_p}}{p}$$

so that

$$W_{RCP}(p)=\frac{1-e^{-pT_p}}{p}W_{LP}(p) \tag{20.31}$$

Example 20.3. Find the transfer function $W^*_{LP}(p)$ and the recurrence relations associated with stepwise approximation for the system

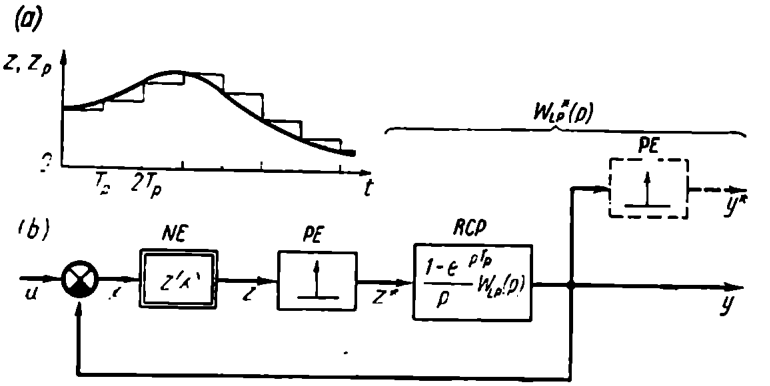

Fig. 20.7

of Example 20.2. For the linear reduced continuous part the transfer function is

$$W_{RCP}(p)=\frac{1-e^{-pT_p}}{p}\,\frac{k}{p(1+pT)} \tag{20.32}$$

The associated transfer function $W^*_{LP}(p)$ can be obtained through Eq. (13.55) of Example 13.2

$$W^*_{LP}(p)=k\,\frac{[T_p-T(1-e^{-\frac{T_p}{T}})]e^{pT_p}+T(1-e^{-\frac{T_p}{T}})-T_pe^{-\frac{T_p}{T}}}{e^{2pT_p}-(1+e^{-\frac{T_p}{T}})e^{pT_p}+e^{-\frac{T_p}{T}}} \tag{20.33}$$

whence

$$\begin{aligned}y[(l+2)T_p]=k[T_p-T(1-e^{-\frac{T_p}{T}})]z[(l+1)T_p]+\\+k[T(1-e^{-\frac{T_p}{T}})-T_pe^{-\frac{T_p}{T}}]z(lT_p)+\\+(1+e^{-\frac{T_p}{T}})y[(l+1)T_p]-e^{-\frac{T_p}{T}}y(lT_p)\end{aligned} \tag{20.34}$$

where $z(iT_p)$ is obtained from Eq. (20.23).

Compare the methods for transition from differential equations to nonlinear difference equations based on the Euler technique (and

similar approximate calculations mentioned above) and on approximate replacement of a continuous system by a sampled-data system.

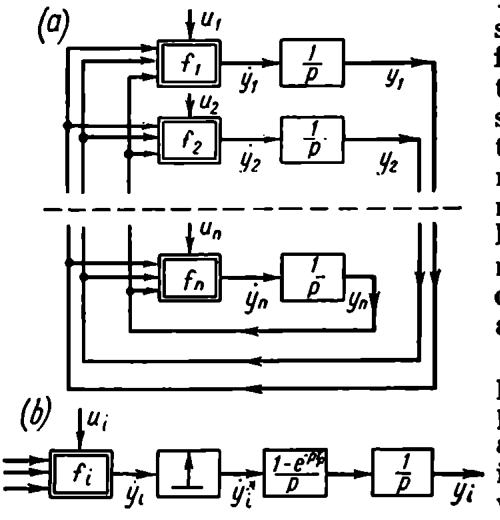

Fig. 20.8

The representation of the system motion in the normal form (20.18) used in the Euler technique corresponds to its structural representation in the form of integrating elements with nonlinear elements at the inputs; the nonlinear elements, which have many inputs, are interconnected and subjected to external actions (Fig. 20.8*a*).

The use of Eq. (20.19) in place of Eq. (20.18) corresponds to connection of pulse and shaping elements producing rectangular pulses between all nonlinear and integrating elements. In Fig. 20.8*b* this is shown for one circuit.

The Euler technique can thus be regarded as an extension of the method discussed in Example 20.2 to a more complicated structure.

Example 20.4. Calculate transient processes in a relay servo (Fig. 20.9*a*) with a linear part having a transfer function

$$W_{LP}(p) = \frac{k}{p(1+pT)}$$

at $k = 4\ \text{sec}^{-1}$, $T = 1$ sec. The linear element response is shown in Fig. 20.9*b*. The input action has the form of $u(t) = 10 \times 1_0(t)$. Use two sampled-data systems (with instantaneous and rectangular pulses).

The recurrence relations may be found by using the results of Examples 20.2 and 20.3. Let $T_p = 0.1T = 0.1$ sec. For a system with instantaneous pulses we find from (20.27) and (20.28)

$$y[(l+2)T_p] = 0.03808\, z[(l+1)T_p] + 1.9048\, y[(l+1)T_p] - 0.9048 y(lT_p) \qquad (20.35)$$

$$z[(l+1)T_p] = z\{u[(l+1)T_p] - y[(l+1)T_p]\} = z\{10 \times 1_0[(l+1)T_p] - y[(l+1)T_p]\} \qquad (20.36)$$

For a system with rectangular pulses at $T_p = 0.1$ sec from Eq. (20.34) we have

$$y[(l+2)T_p] = 0.0192z[(l+1)T_p] + 0.01888z(lT_p) + 1.9048y[(l+1)T_p] - 0.9048\, y(lT_p) \qquad (20.37)$$

where

$$z(iT_p) = z[u(iT_p) - y(iT_p)] = z[10 \times 1_0(iT_p) - y(iT_p)] \quad (20.38)$$
$$(i = l,\ l+1)$$

Figure 20.9*c* illustrates the plots of transient processes (the initial portions associated with the system start-up are not shown) calculated on a digital computer and, for comparison, an accurate plot of the transient process obtained in the same conditions by the passing

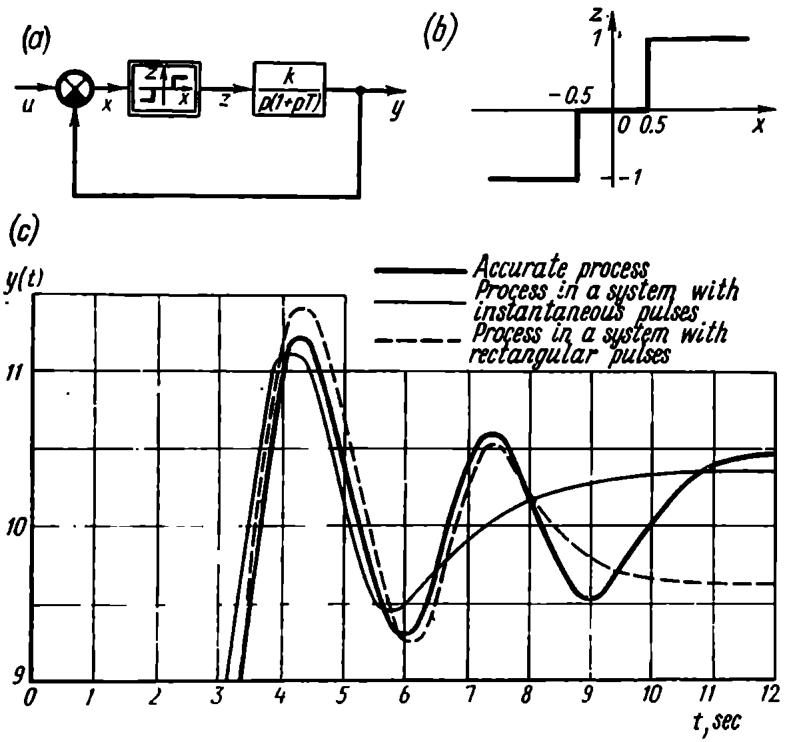

Fig. 20.9

solutions technique. The process in the system with instantaneous pulses is seen to "lead" due to the fact that in replacing the control signal $z(t)$ (see Fig. 20.6*c*) by a sequence of instantaneous pulses the latter act in the beginning of the real pulses $z(t)$. The calculation errors in systems with instantaneous pulses may be reduced by introducing a sequential lag element with a delay time of $\frac{1}{2T_p}$ into the linear part.

The process in the system with rectangular pulses coincides with the exact plot until the entry into the insensitivity zone ($9.5 \leqslant y \leqslant 10.5$).

An increase in the difference between the actual and calculated processes with time indicates accumulation of the error, which is generally typical of difference methods.

Accuracy may be increased by reducing T_p.

An important problem in using the difference methods is a correct choice of the period T_p; an overreduction leads to increased computations, and oversized T_p, to increased errors.

The systems of Fig. 20.6*a* and *d* are completely equivalent if the conditions of the extended Kotelnikov theorem are met (see Sec. 13.1)

$$\omega_b + \omega_{b1} \leqslant \omega_p = \frac{2\pi}{T_p} \tag{20.39}$$

where ω_b is the boundary frequency of the spectrum $z(j\omega)$ of the continuous signal $z(t)$; ω_{b1} is the passband boundary of the reduced continuous part frequency response $W_{RCP}(j\omega)$.

In order to avoid analyzing the spectrum of the signal $z(t)$ (generally a very involved problem) and constructing the frequency responses $W_{RCP}(j\omega)$, the following procedure may be recommended. The processes are calculated with period T_p many (e.g. ten) times shorter than the greatest time constant of the linear part of the system. Then the processes are recalculated at a halved T_p. If the processes in the two calculations are akin, the choice of T_p was correct. Note that the difference methods based on the application of a pulse element may be used in plotting transient processes in linear as well as nonlinear control systems. A pulse element can be connected into the input circuit, and the closed-loop part of the system can be described by a unitary transfer function $W_{cl-l}(p)$. This eliminates the closing equation

$$x_. = u - y \tag{20.40}$$

and the calculations are simplified.

A transition from discrete images to originals can be achieved by any one of the methods described in Ch. XIV for linear sampled-data systems.

20.4. THE EFFECT OF NONLINEARITIES ON TRANSIENT PROCESSES

This section discusses a method which determines the upper estimate of the difference between transient processes in a nonlinear and a certain linear system. The latter is obtained from the initial nonlinear system by replacing the nonlinear response by a linear one close to it. The method can be applied both to continuous and sampled-data control systems.

Consider a continuous nonlinear control system (Fig. 20.10*a*). The nonlinear element $z(y)$ is connected in the middle of the control

circuit between the linear elements with the transfer functions $W_1(p)$ and $W_2(p)$, while the output goes to the comparator, not directly but through an element with a transfer function $W_3(p)$. Consequently the structural diagram in question is rather general.

Figure 20.10*b* portrays the static response of the nonlinear element $z(y)$. Replace the nonlinear element by parallel connection of a linear element with a response $z_{LP}(y) = k_n y$ (see Fig. 20.10*b*)

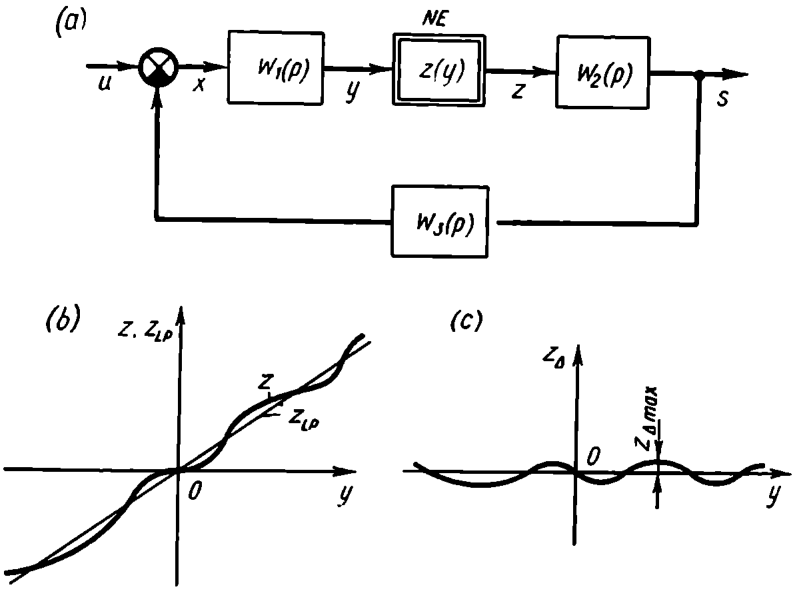

Fig. 20.10

and a nonlinear element with a difference response $z_\Delta(y) = z(y) - k_n(y)$ (Fig. 20.10*c*). The maximal (in magnitude) value of the difference is $z_{\Delta\,max}$; the linear response should be drawn so that $z_{\Delta\,max}$ is minimal.

Fig. 20.11*a* shows the parallel connection of two elements and in Fig. 20.11*b* this part of the diagram is redrawn with disrupted nonlinear relation between the signals y and z_Δ. This means that we will no longer concern ourselves with the actual behaviour of the signal $z_\Delta(t)$ in the course of time. We must only remember that this signal is always weaker than $z_{\Delta\,max}$.

All the transformations result in an equivalent circuit of the system (Fig. 20.11*c*). Apart from the basic signal this linear system is subjected to an additional signal $z_\Delta(t)$, which represents the effect of nonlinearity $z(y)$ on dynamic processes in the control system. The effect of nonlinearity can be ascertained by using the superposition principle to determine the system output signal component

$s_\Delta(t)$ arising under the effect of the additional signal $z_\Delta(t)$. The complete form of this component cannot be determined because the variations of $z_\Delta(t)$ are not known. But the absolute value of this component can be estimated because it is attributable to the action of a signal of limited magnitude.

The effect of constrained signals on linear systems was estimated by B.V. Bulgakov, who coined the term "problem of accumulation", meaning of which will become clear later.

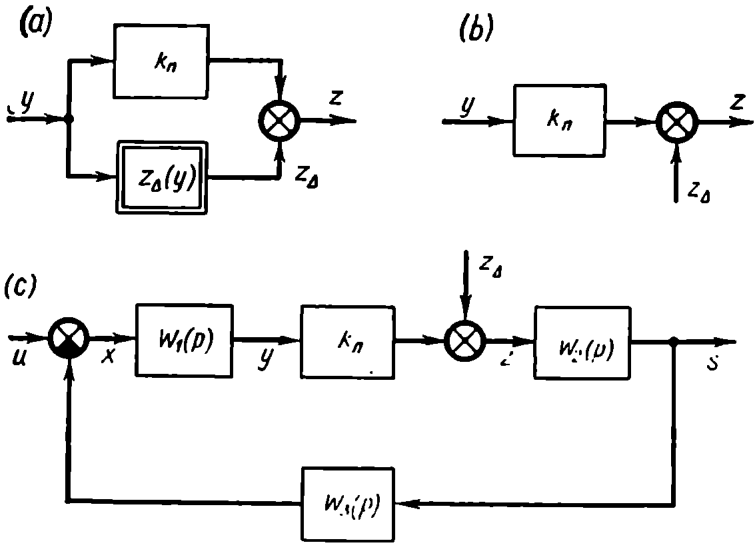

Fig. 20.11

Let us see how Bulgakov's problem is solved in this particular case. Assume that $u = 0$ (the superposition principle) and the system is under zero initial conditions. Assume also that the resultant linear system is stable. For the image of the output signal we have

$$S_\Delta(p) = W_{cl\text{-}l\Delta}(p)\, Z_\Delta(p) \tag{20.41}$$

where

$$W_{cl\text{-}l\Delta}(p) = \frac{W_2(p)}{1 + W_p(p)} \tag{20.42}$$

$$W_{o\text{-}l}(p) = k_n W_1(p)\, W_2(p)\, W_3(p) \tag{20.43}$$

The transfer function $W_{cl\text{-}l\Delta}(p)$ relates the system output with the additional signal $Z_\Delta(p)$.

In the expression (20.41) the originals can be used if we apply the convolution theorem and remember that the original of the transfer

function $W_{cl\text{-}l\Delta}(p)$ is the respective weighting function $w_{cl\text{-}l\Delta}(t)$

$$s_\Delta(t) = \int_0^t w_{cl\text{-}l\Delta}(\tau)\, z_\Delta(t-\tau)\, d\tau \qquad (20.44)$$

Take the magnitude of the right-hand and left-hand parts of Eq. (20.44). Then we have the inequalities

$$|s_\Delta(t)| = \left| \int_0^t w_{cl\text{-}l\Delta}(t-\tau)\, z_\Delta(t-\tau)\, d\tau \right| \leqslant$$

$$\leqslant \int_0^t |w_{cl\text{-}l\Delta}(\tau)| \cdot |z_\Delta(t-\tau)|\, d\tau \leqslant z_{\Delta\, max} \int_0^t |w_{cl\text{-}l\Delta}(\tau)|\, d\tau \qquad (20.45)$$

Consider the latter integral and replace the weighting function by the derivative of the corresponding transient function

$$z_{\Delta\, max} \int_0^t |w_{cl\text{-}l\Delta}(\tau)|\, d\tau = z_{\Delta\, max} \int_0^t \left| \frac{dh_{cl\text{-}l\Delta}(\tau)}{d\tau} \right| d\tau \qquad (20.46)$$

If the integrand did not contain the absolute value symbol, the integral would be equal to $h_{cl\text{-}l\Delta}(t)$ at all times. Because of the symbol, the portions where the derivative has a constant sign ($\gamma \to 0$, Fig. 20.12*a*) should be integrated separately:

$$\int_0^t \left| \frac{dh_{cl\text{-}l\Delta}(\tau)}{d\tau} \right| d\tau = \int_0^{\gamma} \frac{dh_{cl\text{-}l\Delta}(\tau)}{d\tau} d\tau - \int_{\gamma}^{t_1} \frac{dh_{cl\text{-}l\Delta}(\tau)}{d\tau} d\tau +$$

$$+ \int_{t_1}^{t_2} \frac{dh_{cl\text{-}l\Delta}(\tau)}{d\tau} d\tau - \ldots = h_0 - (h_1 - h_0) + (h_2 - h_1) - \ldots$$

As a result the integral (20.46) can generally be expressed as a difference of neighbouring extremal values of $h_{cl\text{-}l\Delta}(t)$

$$\int_0^t \left| \frac{dh_{cl\text{-}l\Delta}(\tau)}{d\tau} \right| d\tau = |h_0| + |h_1 - h_0| + |h_2 - h_1| + \ldots + |h_{cl\text{-}l\Delta}(t) - h_r| \qquad (20.47)$$

where h_r is the last extremum of the transient function before the current instant t.

At any instant t the effect of nonlinearities does not exceed in magnitude the estimates given by the formula

$$\delta(t) = z_{\Delta\, max} [\, |h_0| + |h_1 - h_0| + |h_2 - h_1| + \ldots + |h_{cl\text{-}l\Delta}(t) - h_r|] \qquad (20.48)$$

The plot of the upper estimate is shown in Fig. 20.12*b*. It rises monotonically, which means that the effect of nonlinearity can

accumulate with time, tending to the upper boundary δ_∞, which can serve as the upper estimate for any instant of time

$$\delta_\infty = z_{\Delta\, max} \sum_{i=1}^{\infty} [\,|h_0| + |h_i - h_{i-1}|\,] \qquad (20.49)$$

The estimate δ_∞ can be simply obtained from the plot of the transient function $h_{cl\text{-}l\Delta}(t)$ (see Fig. 20.12*a*) by summing up the magnitudes of successive differences between extrema and can in some cases be expressed in a closed form through the system parameters.

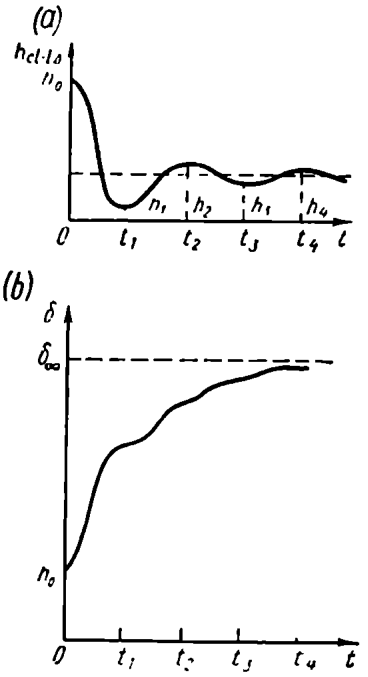

Fig. 20.12

This method permits estimating the difference between dynamic processes in a nonlinear system and a related linear system resulting from replacement of the nonlinear response by a linear one. When the estimate thus found is small enough, processes in the system can be analyzed by well-developed linear tools of the control theory.

The estimates given by Eqs. (20.48), (20.49) are small enough only when $z_{\Delta\, max}$ is small, or when nonlinear responses do not differ greatly from the linear ones. Such nonlinear responses are obtained for play, hysteresis, wire-type and sectioned potentiometers, and analog-to-digital converters (see Figs. 15.17, 15.19, 15.22). The sum in Eqs. (20.48), (20.49) depends on the overshoot and the oscillation properties of the linear approximation of the system.

Example 20.5. Estimate the effect of play on transient processes in a servo system with a second-order linear part (Fig. 20.13*a*). Replacement of the nonlinear element by a linear one with a gain $k_n = 1$ gives an equivalent circuit with an additional signal (Fig. 20.13*b*), which acts directly on the system output, and $z_{\Delta max} = y_a$, as follows from the element response (see Fig. 20.13*a*).

The transfer function $W_{cl\text{-}l\Delta}(p)$ is, according to Eqs. (20.42) and (20.43),

$$W_{cl\text{-}l\Delta}(p) = \frac{1}{1 + \dfrac{k}{p(1+pT)}} = \frac{p(1+pT)}{p(1+pT)+k} = 1 - \frac{1}{1 + \dfrac{1}{k}p + \dfrac{T}{k}p^2} \qquad (20.50)$$

The transient function, according to Eq. (3.92), is of the form

$$h_{cl\text{-}l\Delta}(t) = e^{-\frac{t}{2T}}\left[\cos\frac{\sqrt{4kT-1}}{2T}t + \frac{1}{\sqrt{4kT-1}}\sin\frac{\sqrt{4kT-1}}{2T}t\right] \quad (20.51)$$

Figure 20.14*a* portrays the transient function $h_{cl\text{-}l\Delta}(t)$ for the following values of the system parameters: $k = 14.14$ sec^{-1}, $T = 0.1$ sec. These values ensure a phase margin of 45° in the linear

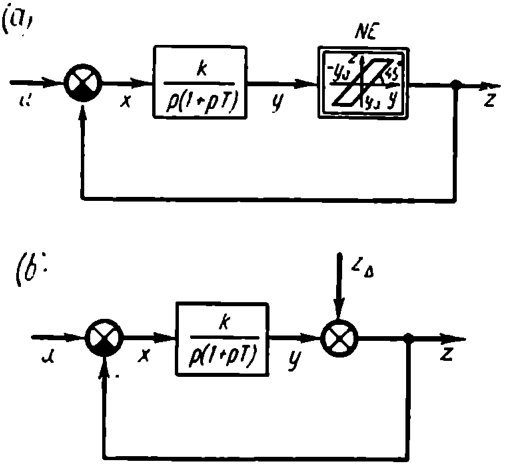

Fig. 20.13

system. Figure 20.14*b* shows the transient processes in the servo system with these parameters for stepwise change of $u(t)$ from 0 to 5 at $t = 0$ and zero initial conditions. The gap $2y_a$ is assumed to be 0.5. Position *1* in Fig. 20.14*b* denotes the process in a linear approximation of the system, position *2*, the transient process in the actual system calculated by the passing solutions method. Figure 20.14*c* exhibits the plots of variation in the difference between processes *2* and *1* (i.e. the values of $z_\Delta(t)$ and the estimates $\delta(t)$ and $-\delta(t)$ plotted according to Fig. 20.14*a* at $z_{\Delta max} = y_a = 0.25$). The curves of δ and $-\delta$ enclose the area of possible variation in the difference $z_\Delta(t)$. In the latter figure the value of $\delta(t)$ is seen to provide a good estimate of the maximal magnitude of the difference between the actual transient processes and those in a linear approximation, in other words, it gives a sufficiently exact upper estimate for the effect of the nonlinear element (of the play-type in this case) on transient processes in the automatic control system.

An expression for the maximal estimate δ_∞ can be found in the closed form in this example. The times of the extrema $t_1, t_2, t_3, \ldots$

for the transient function (20.51) are $\frac{2\pi T}{\sqrt{4kT-1}}$, $\frac{4\pi T}{\sqrt{4kT-1}}$, $\frac{6\pi T}{\sqrt{4kT-1}}$, respectively. The initial value of the transient function is 1, the subsequent extremal values are

$$h_1 = -e^{-\frac{t_1}{2T}} = -e^{-\frac{\pi}{\sqrt{4kT-1}}}$$

$$h_2 = e^{-\frac{t_2}{2T}} = e^{-\frac{2\pi}{\sqrt{4kT-1}}}$$

$$h_3 = -e^{-\frac{t_3}{2T}} = -e^{-\frac{3\pi}{\sqrt{4kT-1}}}$$

Their magnitudes form a decreasing geometrical progression with the initial term 1 and the denominator $e^{-\frac{\pi}{\sqrt{4kT-1}}}$.

By virtue of Eq. (20.49) the maximal estimate δ_∞ is

$$\delta_\infty = z_{\Delta\,max}[h_0 + (h_0 - h_1) + (h_2 - h_1) + (h_2 - h_3) + \ldots] = 2z_{\Delta\,max}\sum_{i=0}^{\infty}|h_i| \quad (20.52)$$

and is computed by the formula of the sum of geometrical progression terms

$$\delta_\infty = 2z_{\Delta\,max}\frac{1}{1-e^{-\frac{\pi}{\sqrt{4kT-1}}}} \quad (20.53)$$

At $k = 14.14$ sec^{-1}, $T = 0.1$ sec, $z_{\Delta max} = 0.25$ we have

$$\delta_\infty = 0.67 = 2.68y_a$$

which indicates a low relative effect of the play given by the factor 2.68.

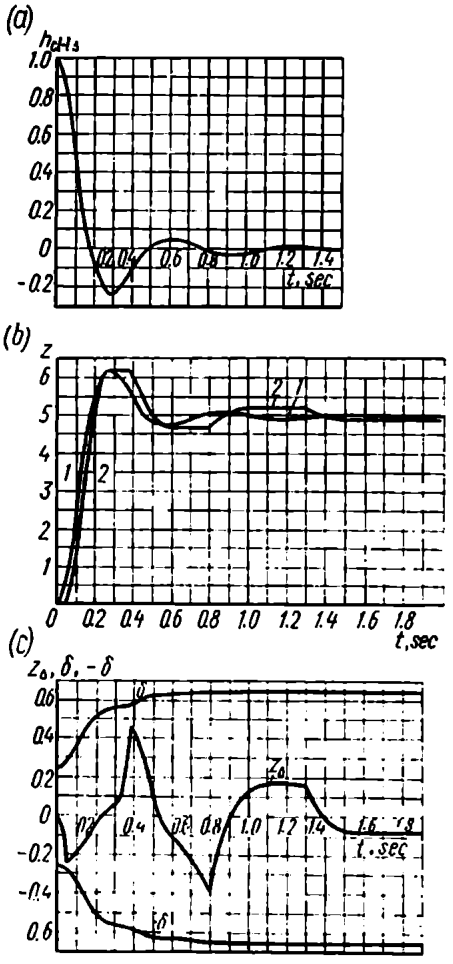

Fig. 20.14

The method of estimates suggests certain conclusions as to the properties of an autonomous (without any external actions) nonlinear system with a near-linear response. If the corresponding linear system is stable, then there are no diverging processes in the nonlinear system. The amplitude of self-oscillations, if any, does not exceed δ_∞.

We will now take up a nonlinear sampled-data control system in which the nonlinear element NE is connected after the comparator and before the pulse element (Fig. 20.15*a*). In other, more involved

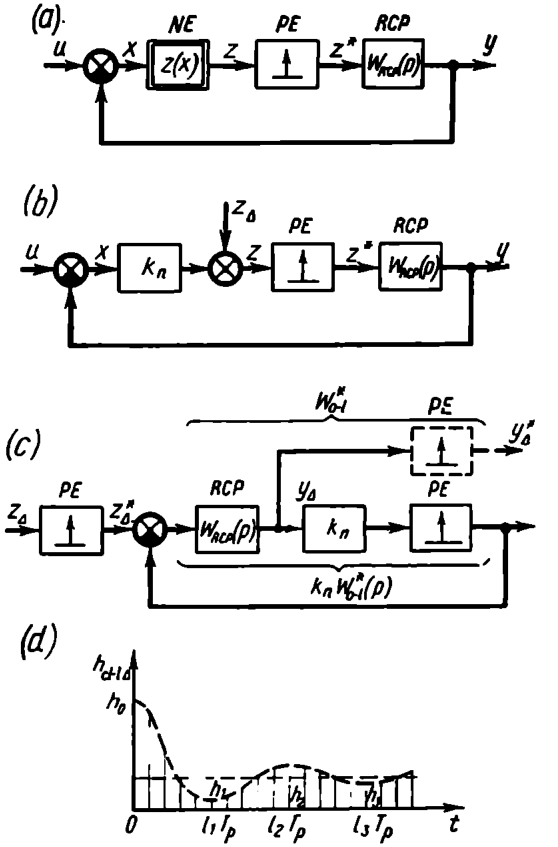

Fig. 20.15

versions of connecting a nonlinear element the circuit should be reduced to the case in question via equivalent transformations. Replacement of a nonlinear element by a linear one with the introduction of an additional signal (see Fig. 20.11) leads to an equivalent circuit of Fig. 20.15*b*. The effect of the additional signal (i.e. of the nonlinearity) is estimated in an equivalent circuit (Fig. 20.15*c*), where u is put at zero, the pulse element PE is transferred from the misalignment circuit to the input and feedback circuits; also, a dummy pulse element (dotted line) is introduced into the output signal circuit.

The transfer function of a closed-loop linear sampled-data system (see Fig. 20.15*c*) is

$$W^*_{cl\text{-}l\Delta}(p) = \frac{W^*_{o\text{-}l}(p)}{1 + k_n W^*_{o\text{-}l}(p)} \tag{20.54}$$

The corresponding weighting function $w_{cl\text{-}l\Delta}(lT_p)$ can be found in any one of the ways described in Ch. XIV. With the weighting function $w_{cl\text{-}l\Delta}(lT_p)$ known, the system output signal (see Fig. 20.15*c*) can be obtained for zero initial conditions using the superposition principle

$$y_\Delta(lT_p) = \sum_{i=1}^{l} w_{cl\text{-}l\Delta}(iT_p)\, z_\Delta[(l-i)T_p] \tag{20.55}$$

The output signal magnitude is estimated as a series of inequalities

$$\begin{aligned} |y_\Delta(lT_p)| &= \Big|\sum_{i=0}^{l} w_{cl\text{-}l\Delta}(iT_p)\, z_\Delta[(l-i)T_p]\Big| \leqslant \\ &\leqslant \sum_{i=0}^{l} |w_{cl\text{-}l\Delta}(iT_p)|\, |z_\Delta[(l-i)T_p]| \leqslant \\ &\leqslant z_{\Delta\,max} \sum_{i=0}^{i} |w_{cl\text{-}l\Delta}(iT_p)| = \delta(lT_p) \end{aligned} \tag{20.56}$$

The latter formula is analogous to the formula (20.45) for continuous systems. Since

$$\sum_{i=1}^{l} w_{cl\text{-}l\Delta}(iT_p) = h_{cl\text{-}l\Delta}(lT_p)$$

then, as in the case of continuous systems, the estimate $\delta(lT_p)$ can be expressed through extremal values of the closed-loop system transient function at sampling times (Fig. 20.15*d*)

$$\begin{aligned} \delta(lT_p) = z_{\Delta max}[\,|h_0| + |h_1 - h_0| + |h_2 - h_1| + \ldots \\ \ldots + |h_{cl\text{-}l\Delta}(lT_p) - h_r|] \end{aligned} \tag{20.57}$$

where h_r is the last extremum of $h_{cl\text{-}l\Delta}(lT_p)$ before the current sampling time (lT_p).

Assuming $l \to \infty$ gives the general upper estimate for any time

$$\delta_\infty = z_{\Delta\,max} \sum_{i=1}^{\infty} [\,|h_0| + |h_l - h_{l-1}|\,] \tag{20.58}$$

This estimate is easily obtained from the closed-loop transient function plot (see Fig. 20.15*d*), which in its turn can be constructed in any one of the ways listed in Ch. XIV.

The remarks on the use of the estimate method for nonlinear systems with continuous signal transmission are valid for nonlinear sampled-data systems.

Example 20.6. Estimate the effect of level quantization on the transient processes in the digital servo system (Fig. 20.16*a*) discussed in Examples 13.2 and 13.4.

The continuous part contains an integrating element; the pulses are rectangular with a duty factor equal to 1. The transfer function of the continuous part (see Eq. (13.59)) is

$$W^*_{o\text{-}l}(p) = \frac{kT_p}{e^{pT_p} - 1} \qquad (20.59)$$

The nonlinear element has the stepwise response of analog-to-digital conversion (Fig. 20.16*b*). Replacement of the nonlinear element by a linear one with the introduction of a "quantization noise" $y_\Delta(t)$ leads to an equivalent linear circuit (Fig. 20.16*c*), where $y_{\Delta\,max} = 0.5y_a$. The transfer function is

$$W^*_{cl\text{-}l\Delta}(p) = -W^*_{cl\text{-}l}(p) = -\frac{W^*_{o\text{-}l}(p)}{1 + W^*_{o\text{-}l}(p)} = -\frac{kT_p}{e^{pT_p} - 1 + kT_p} \qquad (20.60)$$

The weighting function $w_{cl\text{-}l\Delta}(lT_p) = -w_{cl\text{-}l}(lT_p)$ can be found by Eq. (14.48) with an allowance for the fact that the characteristic equation has a single root given by the equation

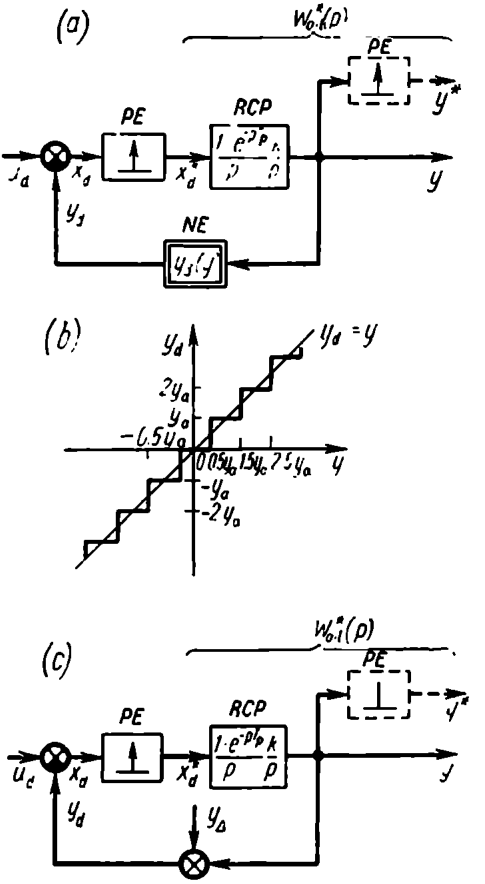

Fig. 20.16

$$e^{pT_p} = 1 - kT_p \qquad (20.61)$$

therefore

$$w_{cl\text{-}l\Delta}(lT_p) = -[kT_p(1 - kT_p)^{l-1}] \qquad (20.62)$$

The magnitudes of discrete values of $w_{cl\text{-}l\Delta}(lT_p)$ form a geometrical progression at $l = 1, 2, 3, \ldots$

$$kT_p, \qquad kT_p\,|1 - kT_p|, \qquad kT_p\,|1 - kT_p|^2, \ldots$$

Their sum gives

$$\delta_\infty = y_{\Delta\, max} \frac{kT_p}{1-|1-kT_p|} \tag{20.63}$$

At $y_{\Delta\, max} = 0.5y_a$ and $kT_p = 1.5$ (note that $kT_p < 2$ from the conditions for stability of the system linear approximation)

$$\delta_\infty = 1.5y_a$$

In actual system the value y_a may be very small, and so is the effect of level quantization on dynamic processes.

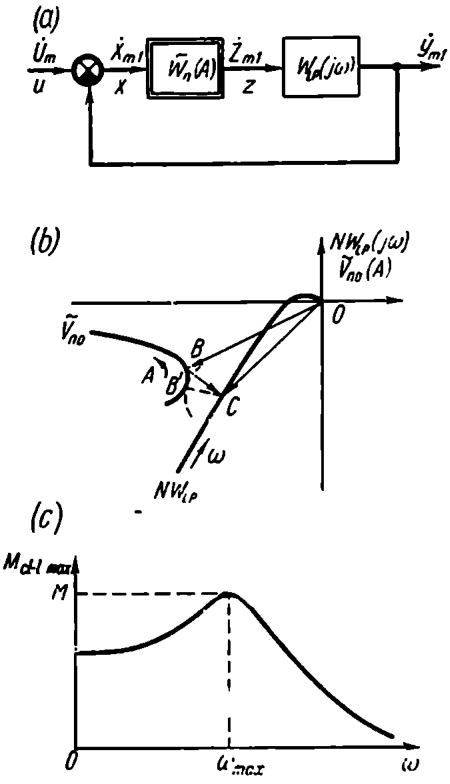

Fig. 20.17

20.5. HARMONIC LINEARIZATION AS A TOOL IN ANALYZING CONTROL PERFORMANCE

The most widespread methods of indirect performance analysis in linear control systems are frequency methods based on the calculation of the oscillation index, phase and gain stability margins, and the cutoff frequency (Ch. X). Harmonic linearization permits extension of these methods to nonlinear systems. The complexity of processes in nonlinear systems which depend both quantitatively and qualitatively on the amplitude of input actions, and the approximate nature of the harmonic linearization method prevent establishing a clear-cut relation between the indirect frequency indices and direct performance indices found from plots of transient processes. Of all the frequency methods based on harmonic linearization, the method based on the computation of the oscillation index is the most popular.

Consider the behaviour of a nonlinear closed-loop system (Fig. 20.17*a*) subjected to the action of a harmonic input disturbance. The frequency response, which is equal here to the ratio of the complex amplitudes $\dot{Y}_{m1}$ and $\dot{U}_m$, is given by

$$W_{cl\text{-}l}(j\omega, A) = \frac{\tilde{W}_n(A)\, W_{LP}(j\omega)}{1+\tilde{W}_n(A)\, W_{LP}(j\omega)} \tag{20.64}$$

or

$$W_{cl\text{-}l}(j\omega, A) = \frac{\tilde{W}_{n0}(A) NW_{LP}(j\omega)}{1+\tilde{W}_{n0}(A) NW_{LP}(j\omega)} \tag{20.65}$$

where A is the dimensionless amplitude of the first harmonic of the signal x at the input of the nonlinear element NE, and N is the normalizing factor.

Equation (20.65) can be conveniently rewritten as

$$W_{cl\text{-}l}(j\omega, A) = \frac{NW_{LP}(j\omega)}{NW_{LP}(j\omega)-[-\tilde{W}_{n0}^{-1}(A)]} = \frac{NW_{LP}(j\omega)}{NW_{LP}(j\omega)-\tilde{V}_{n0}(A)} \tag{20.66}$$

Figure 20.17*b* shows the relative positions of the loci $NW_{LP}(j\omega)$ and $\tilde{V}_{n0}(A)$. At a certain frequency ω and amplitude A the numerator of Eq. (20.62) is represented by the complex vector $\overline{CO}$, and the denominator, by the vector $\overline{CB}$.

If ω is fixed and A varied, the magnitude of the frequency response $W_{cl\text{-}l}(j\omega, A)$ is maximal at the minimal length of $\overline{CB}$, which is equal to the radius of the circle with centre in the point C tangential to the locus $\tilde{V}_{n0}(A)$ (the segment CB' in Fig. 20.17*b*). If there can be several such circles, the minimal radius should be selected. Determining in this way $|W_{cl\text{-}l}(j\omega, A)|_{max}$ at different ω, the plot of $|W_{cl\text{-}l}(j\omega, A)|_{max} = f(\omega)$ can be drawn (Fig. 20.17*c*). The oscillation index M is found at the point $\omega = \omega_M$, where the curve is at its maximum.

Nonlinear control systems have been found (Ref. 50) to perform satisfactorily when $M < 2$.

In order to determine the oscillation index of nonlinear control systems, the lines of equal values of $|W_{cl\text{-}l}(j\omega, A)|$ can be found in the complex plane $NW_{LP}(j\omega)$, $\tilde{V}_{n0}(A)$. Introducting the notation

$$NW_{LP}(j\omega) = P_{LP}(\omega) + jQ_{LP}(\omega) \tag{20.67}$$

$$\tilde{V}_{n0}(A) = R_{n0}(A) + jS_{n0}(A) \tag{20.68}$$

the magnitude $W_{cl\text{-}l}(j\omega, A)$ can be rewritten, according to Eq. (20.66), as

$$|W_{cl\text{-}l}(j\omega, A)| = \frac{\sqrt{P_{LP}^2+Q_{LP}^2}}{\sqrt{(P_{LP}-R_{n0})^2+(Q_{LP}-S_{n0})^2}} \tag{20.69}$$

Assuming $|W_{cl\text{-}l}(j\omega, A)| = c$ we have, after transformations, the equation of a circle

$$\left(P_{LP}-\frac{R_{n0}c^2}{c^2-1}\right)^2+\left(Q_{LP}-\frac{S_{n0}c^2}{c^2-1}\right)^2 = \frac{(R_{n0}^2+S_{n0}^2)^2 c^2}{(c^2-1)^2} \tag{20.70}$$

with centre at the point with coordinates

$$P_{LP} = \frac{R_{n0}c^2}{c^2-1}, \qquad Q_{LP} = \frac{S_{n0}c^2}{c^2-1} \tag{20.71}$$

and with a radius

$$R = \frac{\sqrt{R_{n0}^2 + S_{n0}^2}\,|c|}{|c^2 - 1|} \tag{20.72}$$

At $R_{n0} = -1$, $S_{n0} = 0$ the system becomes linear and Eq. (20.70) coincides with Eq. (10.13) for linear systems.

Assuming a certain c, for each nonlinearity a family of circles can be plotted which would represent different values of R_{n0} and S_{n0} or different values of A. It is easy to see that according to Eqs. (20.71) and (20.72) the centres of the circles lie on a curve similar to $\tilde{V}_{n0}(A)$ (the similarity factor is $\frac{c^2}{(c^2-1)}$), while their radii are proportional to the distances of the points of the locus $\tilde{V}_{n0}(A)$ to the origin of coordinates (the proportionality factor is $\frac{c}{(c^2-1)}$). As $c \to \infty$ the centres of the circles fall on the locus $\tilde{V}_{n0}(A)$, and their radii become zero.

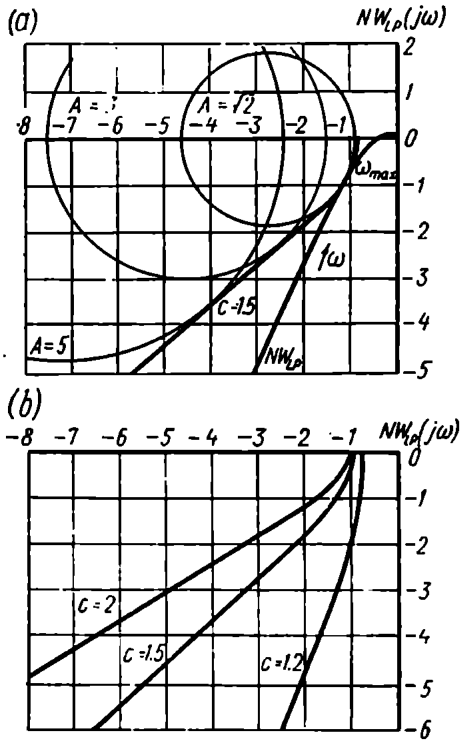

Fig. 20.18

Figure 20.18*a* portrays a family of circles (whose centres are marked with crosses) for the case of a single-valued relay response (see the locus $\tilde{V}_{n0}$ in Table 18.1) at $c = 1.5$. The same figure shows the envelope of these circles. The oscillation index M of the nonlinear system is c (in this case $c = 1.5$) if the locus of the frequency response $NW_{LP}(j\omega)$ touches the envelope at any point. The presence of the point of tangency and intersection of $NW_{LP}(j\omega)$ and $\tilde{V}_{n0}(A)$ result in an infinitely large oscillation index $M = \infty$, which corresponds to the existence of self-oscillations in the system.

Figure 20.18*b* shows the envelopes for a single-valued response at different c values. These families can be conveniently used in the synthesis of linear compensating units which shape $NW_{LP}(j\omega)$ so that the nonlinear system oscillation index is equal to the desired

one. The response $NW_{LP}(j\omega)$ and the envelopes can be represented in the logarithmic scale to facilitate determination of the compensation unit frequency responses.

20.6. CRITERION FOR ABSOLUTE STABILITY AS AN AID IN ANALYZING CONTROL PERFORMANCE

The criteria for absolute stability of equilibrium and processes in nonlinear control systems given in Ch. XIX can be used in estimating the performance of processes in nonlinear systems. In doing so sufficient conditions are studied under which variations of disturbed (by changing the initial conditions) and undisturbed processes decay faster than $M_0 e^{-\lambda_0 t}$, where M_0 is a constant depending on the initial disturbance and λ_0 is the degree of stability. The parameter λ_0 can serve as estimate of transient process duration not exceeding a three-fold time constant of the decaying exponent

$$t_c \leqslant \frac{3}{\lambda_0} \tag{20.73}$$

For the system output variation η

$$\lim_{t\to\infty} \eta e^{\lambda_0 t} = 0$$

Multiplying the original by the exponential factor $e^{\lambda_0 t}$ involves displacement of the complex operator p in the image by $-\lambda_0$, therefore in formulations of conditions for absolute stability the degree of stability should be represented by the biased frequency response $W_{LP}(j\omega - \lambda_0)$ in place of the linear part frequency response $W_{LP}(j\omega)$. As for equilibrium, a sufficient condition ensuring a degree of stability λ_0 for the system of Fig. 19.6*a* ($u = 0$) is fulfilment of the inequality

$$\operatorname{Re}(1 + jq\omega) W_{LP}(j\omega - \lambda_0) + \frac{1}{k} > 0 \tag{20.74}$$

This inequality is similar to the inequality (19.27) in the basic formulation of the absolute stability criterion and implies the same conditions: the piecewise-continuous nonlinear response $z(x)$ lies within the sector bounded by the x-line and the straight line $z = kx$; the linear part with the transfer function $W_{LP}(p)$ is stable; q is an arbitrary positive or negative number. This result is extended to the case of a neutral or unstable linear part by using structural transformations similar to those in Sec. 19.3.

In estimating the degree of stability the biased transformed response of the linear part can be used in place of inequality (20.74)

$$\tilde{W}^t_{LP}(j\omega - \lambda_0) = \operatorname{Re} W_{LP}(j\omega - \lambda_0) + j\omega \operatorname{Im} W_{LP}(j\omega - \lambda_0) \tag{20.75}$$

The desired degree of stability is ensured if the response lies to the right of Popov's straight line traced through the point $-\frac{1}{k}$, $j0$ with a slope of $\frac{1}{q}$ (see Ch. XIX).

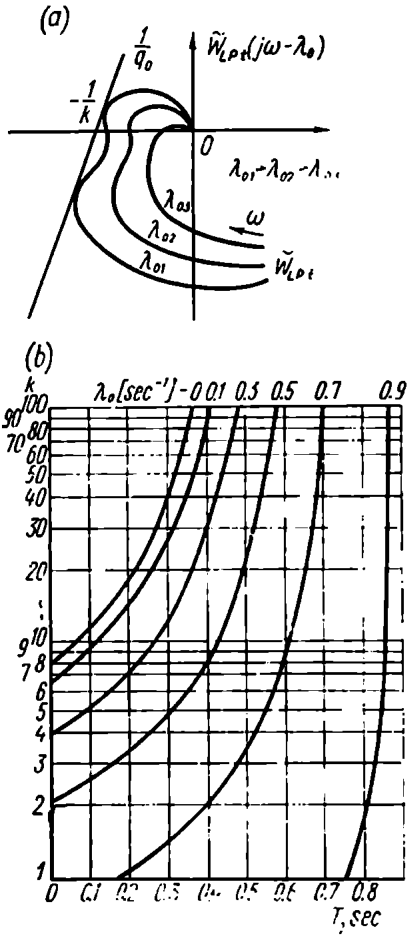

Fig. 20.19

The degree of stability of an actual system is determined by constructing a family of responses $\tilde{W}_{LP}(j\omega-\lambda_0)$ at different λ_0 values. The response, which intersects all Popov's lines with different slopes $\frac{1}{q}$, except the line $\frac{1}{q_0}$ with which it has one or more tangential points (Fig. 20.19*a*), determines the degree of stability. The problem may be inverted: determine the ranges of system parameter values ensuring a degree of stability at least equal to the desired one.

Example 20.7. Determine areas characterized by a degree of stability at least equal to the desired one in the space of parameters of a system with a transfer function

$$W_{LP}(p)=\frac{k(1+pT)}{(1+pT_1)^2} \quad (20.76)$$

The nonlinear element is of the play-type (backlash) (see Table 18.1).

According to the results of Example 19.11 (see inequality (19.49)) the condition for biased response can be written as

$$\operatorname{Re} W_{LP}(j\omega-\lambda_0)>-1 \quad (20.77)$$

Substituting $p=j\omega-\lambda_0$ into Eq. (20.76) and isolating the real part we have at $T_1=1$ sec

$$\operatorname{Re} W_{LP}(j\omega-\lambda_0)=\frac{k[\omega^2(2T-T\lambda_0-1)-T\lambda_0^3]}{[(1-\lambda_0)^2+\omega^2]^2}+$$
$$+\frac{k[\lambda_0^3(2T+1)-\lambda_0(2+T)+1]}{[(1-\lambda_0^2)+\omega^2]^2} \quad (20.78)$$

Equating to zero the derivative of the function (20.78) with respect to ω we find ω_0 at which the function (20.78) is minimal

$$\omega_0^2=\frac{T\lambda_0^3-3\lambda_0^2+(6-3T)\lambda_0-3+2T}{2T-T\lambda_0-1} \quad (20.79)$$

Substituting Eq. (20.79) into (20.78) and further into (20.77), we obtain the condition

$$k < \frac{8(\lambda_0-1)^2(1-T)}{[T(2-\lambda_0)-1]^2} \tag{20.80}$$

Figure 20.19*b* exhibits in the semilogarithmic scale the boundaries of areas ensuring various degrees of stability at different T values.

A sufficient condition ensuring the desired degree of process stability in nonlinear systems is the validity of an inequality similar to (19.52) assuming the same conditions

$$Re\,\frac{W_{LP}(j\omega-\lambda_0)}{1+rW_{LP}(j\omega-\lambda_0)}+\frac{1}{k-r}=\delta\geqslant 0 \tag{20.81}$$

Here we use notation of expression (19.52).

In synthesizing linear compensating units ensuring the fulfilment of conditions (20.74) and (20.81) one may rely on logarithmic frequency responses.

The described methods for estimating processes performance are of course applicable to sampled-data nonlinear control systems. In that case, when estimating the degree of stability the sufficient conditions (19.59) and (19.60) take the form

$$\mathrm{Re}\,W^*_{LP}(j\omega-\lambda_0)+\frac{1}{k}\geqslant 0, \tag{20.82}$$

$$\mathrm{Re}\,[1-q(1-e^{-(j\omega-\lambda_0)T_p})]\,W^*_{LP}(j\omega-\lambda_0)+\frac{1}{k}\geqslant 0 \tag{20.83}$$

The frequency criterion for absolute stability can also be applied to derive estimates of integral performance indices in continuous and sampled-data control systems (Ref. 87).

20.7. SPECIFIC FEATURES OF SYNTHESIS OF NONLINEAR CONTROL SYSTEMS

If processes satisfy the desired performance requirements, nonlinear control systems can be synthesized in different ways:

1. Compensating units may be introduced in the linear part to change the frequency response so as to provide certain indirect performance characteristics, e.g. the desired oscillation index M or degree of stability λ_0. The design methods for linear compensating units are similar to those discussed above for linear systems with an allowance for the specific features introduced into the system by nonlinear elements. These features were discussed in Secs. 20.3 through 20.5. In the synthesis of compensating units logarithmic frequency responses can be used.

Once the circuit and parameters of the compensating unit are found, one of the direct methods can be used which involves plotting transient processes with a view to verifying the operation of compensating units by calculation. Such verification should also be effected in linear control systems and is all the more essential for nonlinear systems for which the indirect methods are either approximate or are based on verification of the sufficient conditions. Naturally, the calculations of transient processes can be replaced by simulation, which is outside the scope of this book.

2. Nonlinear compensating units can be synthesized which are aimed either at weakening the effect of harmful nonlinearities or at improving the performance of processes in the system by introducing useful nonlinearities. The nonlinearities can be compensated for, e.g. with the aid of negative feedbacks in nonlinear elements.

Introduction of useful nonlinearities is very advantageous in designing nonlinear control systems and involves the development of nonlinear control laws. Systems of this kind include variable-structure systems, some of which were discussed in Ch. XVII, and a wide class of optimal control systems, which will be considered in detail in Chs. XXI and XXII.

Chapter XXI

PROBLEMS AND METHODS OF OPTIMAL CONTROL: GENERAL

21.1. STATEMENT OF THE PROBLEM

By an *optimal control system* is meant a system which is *the best* in a certain sense. The optimality criteria on which a system is based can be most diverse and depend on the nature of the problem at hand. They include accuracy of the control system against input signal variations, the transient process time, integral criteria of a transient process, economic efficiency, productivity, complexity of the control system, and other technological and economic indices.

At present there are two well-developed lines in the theory of optimal control systems, the theory of optimal control of the system motion with complete information on the plant and disturbances, and the theory of optimal control at random disturbances.

A great contribution to the former line of research has been made by A.A. Feldbaum, a Soviet scientist (Ref. 22), who stated and solved many problems in this field.

The principles of optimal control are being used on an ever-increasing scale, they have helped in developing new automatic controllers, servos, and other devices considerably improving the efficiency of industrial control systems.

Let us consider optimal control problems with complete data on the plant and disturbances. We assume that the plant is linear, completely described mathematically, and its properties are unchangeable, while the controller can be selected within a certain range and its possibilities are restricted to suit the specific problem. As a rule, constraints are imposed on control actions and on the system phase coordinates, and in most cases are given as systems of inequalities. For control actions such inequalities can be written in the form

$$M_i(\mathbf{u}) = M_i(u_1, \ldots, u_r) \leqslant 0 \qquad (21.1)$$
$$(i = 1, \ldots, r)$$

where

$$u_k = \frac{d^{k-1}u}{dt^{k-1}} \qquad (21.2)$$
$$(k = 1, \ldots, r)$$

In further discussion notation of the type (21.2) will be used.

The control vector **u** satisfying inequalities (21.1) belongs to a certain area Ω (**u**) bounded by the hypersurface M_i (**u**) = 0 ($i = 1, \ldots, r$), i.e.

$$\mathbf{u} \in \Omega(\mathbf{u}) \tag{21.3}$$

Controls satisfying the condition (21.1) or (21.3) are called *feasible*.

For instance, if the control is constrained only in magnitude, $a \leqslant u \leqslant b$, the area of feasible controls is the segment ab (Fig. 21.1*a*).

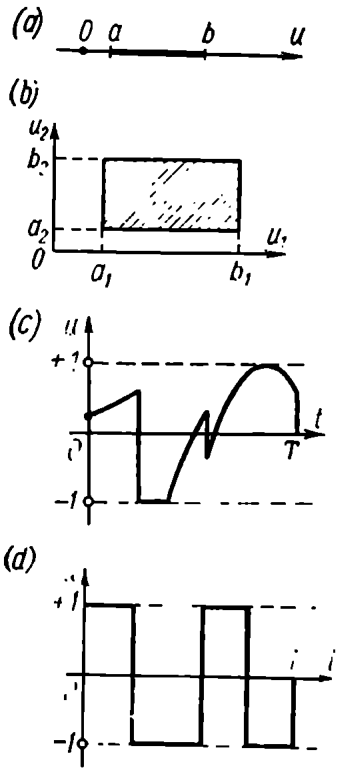

Fig. 21.1

If the value and derivative of control are constrained by inequalities

$$a_1 \leqslant u_1 \leqslant b_1$$
$$a_2 \leqslant u_2 \leqslant b_2$$

then the area of feasible controls is a rectangle (Fig. 21.1*b*). When only the control value is constrained from above and below, then it is convenient to assume hereafter that the constraint on control is given by the inequality

$$|u| \leqslant 1 \tag{21.4}$$

This form of constraints can as a rule be obtained by shifting the reference point and changing the scale of u.

A constraint of the type (21.4) can be satisfied by functions with discontinuities of the first kind. If in the entire time interval $[0, T]$ over which control is performed the number of discontinuities of the function $u(t)$ is finite, the function is referred to as *piecewise-continuous* (Fig. 21.1*c*). A particular case of practical importance is *piecewise-constant functions*, for which $u(t)$ is alternatively $+1$ or -1 (Fig. 21.1*d*). When a piecewise-constant function is to be described, the number of intervals over which it is constant is specified. Thus the function of Fig. 21.1*d* has four *constancy intervals*.

Constraints on controls are chiefly attributable to limited power resources of the system. The phase coordinates are most frequently constrained for the sake of safety, strength, etc. For instance, the angle and rate of rotation of an aircraft rudder are limited by the structural safety and admissible overload on the crew, while the acce-

leration of the rudder is a function of the maximum permissible torque of the rudder system.

Constraints on the phase coordinates will be written, as for controls, in the form of type (21.1) inequalities

$$N_j(\mathbf{y}) = N_j(y_1, \ldots, y_n) \leqslant 0 \tag{21.5}$$

where

$$y_k = \frac{d^{k-1}y}{dt^{k-1}} \qquad (j = 1, \ldots, n)$$

or as conditions of the type (21.3)

$$\mathbf{y} \in \Gamma(\mathbf{y}) \tag{21.6}$$

where $\Gamma(\mathbf{y})$ is the area limited by the hypersurface

$$N_j(\mathbf{y}) = 0 \qquad (j = 1, \ldots, n)$$

Phase coordinates satisfying the conditions (21.5) and (21.6) are called *feasible.*

The most important stage in the development of optimal control systems is setting the optimality criterion, Q, which should depend on a control function. With Q specified the main problem is to provide the extremal value of Q. Thus in developing response- (or speed)-optimal systems which are required to change from one state to another as fast as possible, the transient time may be used as the criterion of optimality. In this case the criterion should naturally be minimized. It should be maximized, for instance, in calculating the program of rocket engine thrust variation if the greatest possible distance is to be covered using a specified amount of propellant.

Consequently, an optimal system requires that

$$Q[\mathbf{u}, \mathbf{y}, t] = \text{extremum at } \mathbf{u} \in \Omega, \ \mathbf{y} \in \Gamma \tag{21.7}$$

By this condition the criterion Q depends on the output coordinate, control, and time, and the optimal-control problem is to find the feasible control $\mathbf{u} \in \Omega(\mathbf{u})$ which would extremize the criterion Q with constraints imposed on the phase coordinates $\mathbf{y} \in \Gamma(\mathbf{y})$.

Note that the value of the criterion Q depends on the time variation law of the function $\mathbf{y}(t)$. Quantities whose values depend on functions are called *functionals.* The mathematical tools for finding functions which extremize a functional are treated in variational calculus. The functions $\mathbf{y}(t)$, $\mathbf{u}(t)$ for which the condition (21.7) is valid are referred to as *extremals.*

The optimality criterion is thus a functional $Q[\mathbf{y}(t), \mathbf{u}(t)]$, and the objective of optimal control is to find the extremals $\mathbf{y}(t)$, $\mathbf{u}(t)$ subject to constraints $\mathbf{u} \in \Omega(\mathbf{u})$ and $\mathbf{y} \in \Gamma(\mathbf{y})$.

A functional is usually specified as a definite integral

$$Q = \int_0^T G[\mathbf{u}(t),\ \mathbf{y}(t)]\,dt \tag{21.8}$$

For instance, in the problem of maximum-speed response, $G \equiv 1$, and the requirement $Q = \min_{u(t)}$ becomes $T = \min$.

The most widespread problem in optimal control is to determine the optimal processes $\mathbf{u}(t)$ and, accordingly, $\mathbf{y}(t)$ as time functions with specified boundary conditions $\mathbf{y}(0)$ and $\mathbf{y}(T)$.

The optimal-control processes $\mathbf{u}(t)$ can be determined and implemented in systems of two kinds. In an open-loop system (Fig. 21.2*a*),

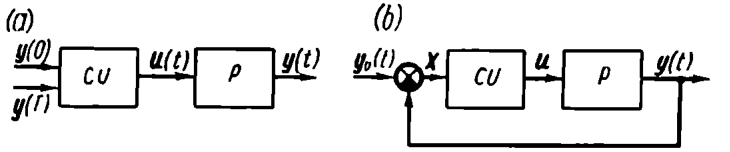

Fig. 21.2

the control unit *CU* implements the desired control law using the boundary conditions, and the current phase coordinates take no part in forming the control. In a closed-loop system current phase coordinates $\mathbf{x} = \mathbf{y}_0 - \mathbf{y}$ are introduced into a *CU* (Fig. 21.2*b*), where $\mathbf{y}_0 = \mathbf{y}_0(t)$ is the assigned control law. Then the control action depends only on the phase coordinates, i.e.

$$\mathbf{u}(t) = \mathbf{u}[\mathbf{x}(t)] \tag{21.9}$$

The final goal of system development is to establish the operational law (21.9) for a closed-loop optimal-control system, or to synthesize the *CU*. In doing so, the optimal processes $\mathbf{u}(t)$ and $\mathbf{x}(t)$ are found and then, by eliminating time, the relation $\mathbf{u}(\mathbf{x})$ is obtained from which the structure and parameters of the *CU* are determined.

21.2. EXAMPLES OF OPTIMAL-CONTROL PROBLEMS

D.c. motor control. Assume that we can control the armature current of a separate-excitation d.c. motor (Fig. 21.3*a*). Assume that the magnetic flux Φ is constant. Then the angle of rotation α of the motor is related to the current through a differential equation of moments balance on the shaft

$$ic\Phi = J\frac{d^2\alpha}{dt^2} + M_r \tag{21.10}$$

where the armature current i = control action, c = a coefficient, Φ = magnetic flux, J = inertia moment of the armature and the

load reduced to the motor shaft, M_r = resistance moment, α = motor rotation angle (a controlled coordinate), and t = real time.

To simplify further reasoning assume that the resistance moment is negligible, or $M_r = 0$. Besides, the real time t is replaced by the relative time $\tau = t\sqrt{\frac{c\Phi}{J}}$. Equation (21.10) then takes the form

$$\frac{d^2\alpha}{d\tau^2} = i \tag{21.11}$$

To suit the accepted notation, where y is the controlled coordinate and u is the control action, replace $i = u$, $\alpha = y$. The final form of the controlled plant equation will then be (Fig. 21.3*b*)

$$\frac{d^2y}{d\tau^2} = u \tag{21.12}$$

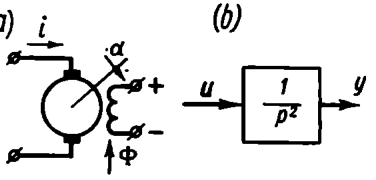

Fig. 21.3

Several optimal-control problems for the motor can now be formulated which differ in optimal-control criteria and in the form of constraints.

Optimal response. In this case the optimal-control criterion is the transient process time T; in other words, the functional is

$$Q = \int_0^T dt = T \tag{21.13}$$

Problem 1. *Find the optimal processes* $u(t)$ *and* $y(t)$ *satisfying Eq.* (21.12) *and minimizing the functional* (21.13) *given that* (1) *a constraint of the form* (21.4) *is imposed on the control, or* $|u| \leqslant 1$, (2) *the angle of rotation is* α_0, *or*

$$\int_0^T \dot{y}(t)\,dt = \alpha_0 \tag{21.14}$$

(3) *the boundary conditions for the shaft rotation rate are*

$$\left.\begin{aligned} \dot{y}(0) &= \omega_0 \\ \dot{y}(T) &= \omega_T \end{aligned}\right\}$$

Assume for simplicity that the initial and final rotation rates are zero, or

$$\dot{y}(0) = \dot{y}(T) = 0 \tag{21.15}$$

Assuming that the objective of the control is to respond precisely to the angle α_0, the boundary conditions along the coordinate y should be specified. Assume in all examples of motor control that

$y(0) = -\alpha_0$, $y(T) = 0$, i.e. y changes by the value of α_0 and completes its motion in the point $y(t) = \dot{y}(T) = 0$.

Problem 2. In this problem constraints are imposed on motor heating or power consumption, i.e. the value of the integral $\int_0^T u^2(t)\,dt$ is specified.

Thus, *find the optimal processes* $u(t)$ *and* $\dot{y}(t)$ *satisfying Eq.* (21.12) *and minimizing the functional* (21.13) *given that the values of the integrals are*

$$\int_0^T \dot{y}(t)\,dt = \alpha_0, \qquad \int_0^T u^2(t)\,dt = q_0 \tag{21.16}$$

and that the rate boundary conditions are zero.

Optimal productivity. In this case the optimal-control criterion is the shaft rotation angle α over a definite time T; the functional thus takes the form

$$Q = \int_0^T \dot{y}(t)\,dt \tag{21.17}$$

Problem 3. *Find the optimal processes* $u(t)$, $\dot{y}(t)$ *satisfying Eq.* (21.12) *and maximizing* (21.17) *given that a constraint of the type* (21.4) *is imposed on the control, i.e.* $|u| \leqslant 1$, *and the rate boundary conditions are zero.*

If the limit power consumption is specified while the magnitude of u is not constrained, another optimal-productivity problem can be formulated.

Problem 4. *Find the optimal processes* $u(t)$ *and* $\dot{y}(t)$ *satisfying Eq.* (21.12) *and maximizing* (21.17) *given that*

$$\int_0^T u^2(t)\,dt = q_0$$

and that the rate boundary conditions are zero.

Optimal economic efficiency. In this case the optimal-control criterion is power consumption over a specified time. The functional has the form

$$Q = \int_0^T u^2(t)\,dt \tag{21.18}$$

Here it is power consumption in motor heating that is to be minimized.

Problem 5. *Find the optimal processes* $u(t)$ *and* $\dot{y}(t)$ *satisfying Eq.* (21.12) *and minimizing Eq.* (21.18) *given that*

$$\int_0^T \dot{y}(t)\,dt = \alpha_0$$

and that the rate boundary conditions are zero.

By varying the conditions, more problems can be formulated, e.g. when both the control and power consumption are constrained.

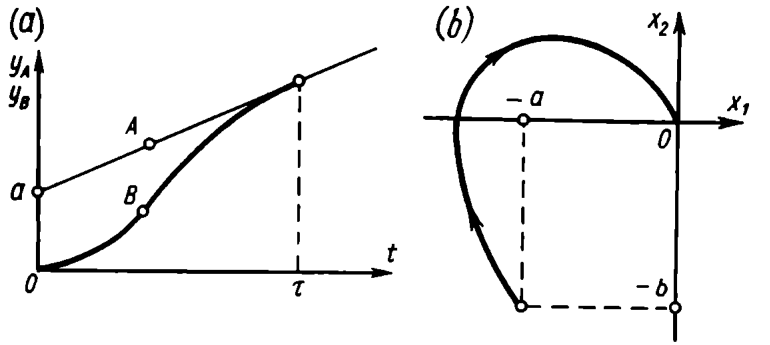

Fig. 21.4

But we will confine ourselves to the above problems because they give a good idea of the practical requirements for optimal control.

Speed-optimal rendez-vous of moving objects. Let a plant A perform a uniform linear motion described by the equation

$$y_A = a + bt \tag{21.19}$$

where y_A is the coordinate of the plant A; a and b are constants; t is time.

A plant B follows it along the same straight line. Variation of the coordinate y_B is described by a second-order equation

$$T\frac{d^2y_B}{dt^2} = \frac{dy_B}{dt} = u \tag{21.20}$$

with initial conditions

$$y_B(0) = \dot{y}_B(0) = 0 \tag{21.21}$$

where T is the time constant of the plant B characterizing its inertial properties.

A constraint of the type (21.4), i.e. $|u| \leqslant 1$ is imposed on the control.

The problem is to change the control $u(t)$ so that within a minimal time the positions and rates of the plants A and B in space coincide. Time variation of the coordinates y_A and y_B is shown in Fig. 21.4*a*.

In practice this problem arises, for instance, in in-flight refuelling of aircraft when the fuel-carrier flies at a constant speed and the aircraft to be refuelled manoeuvres to fly alongside. The control action is then the thrust P of the engine of the plane to be refuelled.

The limit values of the thrust P_{min} and P_{max} are positive, so in order to obtain constraints on control in the form (21.4) P must be replaced by the control

$$u = \frac{2P}{P_{max} - P_{min}} - \frac{P_{max} + P_{min}}{P_{max} - P_{min}}$$

The solution is facilitated by introducing the misalignment of the plant coordinates

$$x = y_B - y_A \tag{21.22}$$

Substituting y_B from Eq. (21.22) and y_A from (21.19) into (21.20) gives

$$T \frac{d^2x}{dt^2} + \frac{dx}{dt} = u - b \tag{21.23}$$

The initial conditions for Eq. (21.23) are found from the given law of plant motion and the coupling equation (21.22) with an allowance for the initial conditions of the motion of the plant B

$$\begin{aligned} x(0) &= y_B(0) - y_A(0) = -a \\ \dot{x}(0) &= \dot{y}_B(0) - \dot{y}_A(0) = -b \end{aligned} \tag{21.24}$$

Introducing now a phase plane for the variable x denoting $x = x_1$, $\dot{x} = x_2$, the control problem for the plant B can be formulated as the problem of the fastest transition of a point in the phase plane from the initial position ($x_1 = -a$, $x_2 = -b$) into the origin of coordinates (Fig. 21.4*b*).

Problem 6. *Find the optimal processes* $u(t)$ *and* $x(t)$ *satisfying Eq.* (21.23) *and minimizing the integral* (21.13), *or* $Q = \int_0^T dt$ *given that the constraint* (21.4) *is imposed on the control, or* $|u| \leqslant 1$; *the initial conditions for the coordinate* x *are given by equalities* (21.24), *and the final conditions are zero, i.e.* $x(T) = \dot{x}(T) = 0$.

Speed-optimal control of a conservative plant. Let the plant equation be of the form

$$\frac{d^2y}{dt^2} + y = u \tag{21.25}$$

All the coefficients in this equation are equal to one, which can always be achieved by normalizing the variables u, y, and t. The constraint $|u| \leqslant 1$ is imposed on the control. The problem is to find the speed-optimal control $u(t)$ which moves the coordinate y from

the initial position

$$y(0) = -1 \qquad (21.26)$$
$$\dot{y}(0) = 0$$

to the final position

$$y(T) = \dot{y}(T) = 0 \qquad (21.27)$$

If we introduce a phase plane with coordinates $y = y_1$, $\dot{y} = y_2$, the problem will be to provide the fastest transition of the describing point from the initial conditions $(-1, 0)$ to the origin of coordinates.

An example of this is the movement of a load suspended on a long rope from a gantry crane winch (Fig. 21.5).

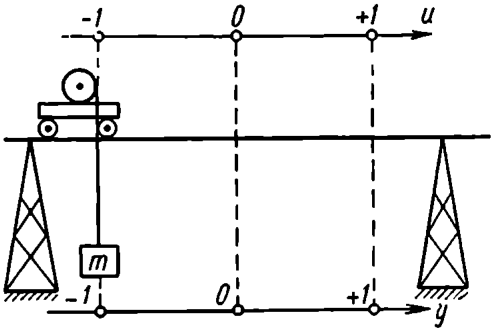

Fig. 21.5

The crane winch, whose position is given by the coordinate u, can move at any speed in the range $-1 \leqslant u \leqslant +1$. The position of the load m is given by the coordinate y. Ignoring the forces which damp the load oscillations (friction and elastic deformations of the rope, air resistance, etc.), the equation relating y to u has the form of Eq. (21.25). It is required to control the position u of the winch so that the load reaches the point $y = 0$ in the shortest possible time; the speed at the end of the motion should be zero.

Note that the problem is rather unusual. Any attempt at carrying the load from $y = -1$ to $y = 0$ (even in a nonoptimal way) by moving the winch from $u = -1$ to $u = 0$ at any (low or high) speed would result in undamped oscillations of the coordinate y. Indeed, a free solution of the conservative plant motion equation, i.e. Eq. (21.25), has the form

$$y(t) = A \sin t$$

where A is the amplitude of oscillations given by the initial conditions of motion (in this case, by the rate of winch movement from $u = -1$ to $u = 0$).

Problem 7. *Find the processes $u(t)$ and $y(t)$ related by Eq.* (21.25) *and minimizing the integral* (21.13), *i.e.* $Q = \int_0^T dt$ *given that a constraint* $|u| \leqslant 1$ *is imposed on the control, and the boundary conditions*

are

$$y(0) = -1, \qquad y(T) = 0$$
$$\dot{y}(0) = 0, \qquad \dot{y}(T) = 0$$

Analytical design of controllers. In all the above examples it was required to find the optimal-control process $u(t)$ whereby the final goal of control (the transient time, productivity, economic efficiency) is extremized. Let us now take up the problem of developing an optimal controller.

In studying the transient performances in linear systems (see Ch. X) various integral performance criteria were introduced whereby the

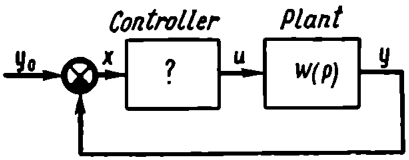

Fig. 21.6

transient process was estimated on an infinite time interval. These criteria were shown to determine the optimal parameters of controllers if the structure of the controllers is specified.

A more general problem can be formulated: find the control law, or the *analytical* function relating the controlled coordinate to the control action and minimizing the integral performance criterion. *This optimal design of a differential equation for a controller via mathematical analysis is known as analytical design of controllers.* The basic results in analytical design were obtained by Soviet scientists A.M. Letov and N.N. Krasovsky (Ref. 35). In terms of solution techniques and statement this problem is akin to those treated above in that it is a variational problem where the required extremal is a function relating $x(t)$ to $u(t)$.

Consider the statement of the analytical design problem. The plant is described by differential equations for deviations, which corresponds, in the operator form, to specification of the transfer function $W(p)$ (Fig. 21.6). Assume that the system is not subjected to external disturbances and there is a transient process caused by the initial conditions

$$\mathbf{x}_0 = \{x_1(0), x_2(0), \ldots, x_n(0)\} \text{ and}$$
$$\mathbf{u}(0) = \{u(0), \dot{u}(0)\} \qquad (21.28)$$

where

$$x_k = \frac{d^{k-1}x}{dt^{k-1}}, \qquad \mathbf{x} = \mathbf{y}_0 - \mathbf{y}$$

In a stable linear system all phase coordinates converge to the zero value as a result of the transient process; in other words, in a steady state the following equality should be valid

$$x_1(\infty) = \ldots = x_n(\infty) = u(\infty) = 0 \tag{21.29}$$

The optimality criterion will be the integral

$$\int_0^\infty V\,dt \tag{21.30}$$

where V is a positive-definite quadratic form, e.g.

$$V = \dot{u}^2 + u^2 + \sum_{k=1}^{n} x_k^2 \tag{21.31}$$

The integral (21.30) characterizes the r.m.s. error of the system. In addition, the term $u^2(t)$ in (21.31) characterizes the cost of control in the transient process (power, heating, etc.), while the term $\dot{u}^2(t)$ ensures the absence of laws unimplementable in the linear controllers whereby the rate of control actions goes to infinity.

In analytical design the problem is to find in the analytical form

$$\Phi(\dot{u}, u, x_1, \ldots, x_n) = 0 \tag{21.32}$$

the control law which, with an allowance for the plant equations and under the boundary conditions (21.28), (21.29), minimizes the integral (21.30).

Our next example will be the problem of analytical design of a controller in a system with a first-order plant.

Problem 8. *Let the plant be described by the equation*

$$\frac{dx}{dt} + x + u = 0 \tag{21.33}$$

All the coefficients of the equation are assumed equal to one, which can always be achieved by normalizing the variables x, u, t.

Find a differential equation relating the variables x and u (both satisfying the plant equation (21.33)) *and minimize the integral*

$$Q = \int_0^\infty [u^2(t) + \dot{u}^2(t) + x^2(t)]\,dt \tag{21.34}$$

21.3. DESIGN OF SIMPLE RESPONSE-OPTIMAL SECOND-ORDER SYSTEMS

We will now consider the solution of the problem of finding the optimal processes and designing the controller, using as an illustration Problem 1 of Sec. 21.2, where optimal-response time is to be

achieved for a plant corresponding to Eq. (21.12) $\frac{d^2y}{dt^2} = u$ with a constraint $|u| \leqslant 1$ and boundary conditions

$$y(0) = -\alpha_0,\ y(T) = 0,$$

$$\dot{y}(0) = 0,\ \dot{y}(T) = 0$$

Optimal-control processes. It would be natural to assume that for achieving the fastest possible response to α_0 the system should first be run up with the maximum permissible acceleration and then at a certain time the control should be switched over from run-up to slow-down, also with the maximum permissible, but negative, acceleration. With the switch-over time properly selected the rate of variation of the coordinate y is zero exactly at the time when y has been shifted by α_0. Because the maximal and the minimal values of control are equal in magnitude, the time intervals taken up by run-up and slow-down are equal and amount to $\frac{T}{2}$, where T is the transient time. The plot of this control process $u(t)$ is shown in Fig. 21.7*a*.

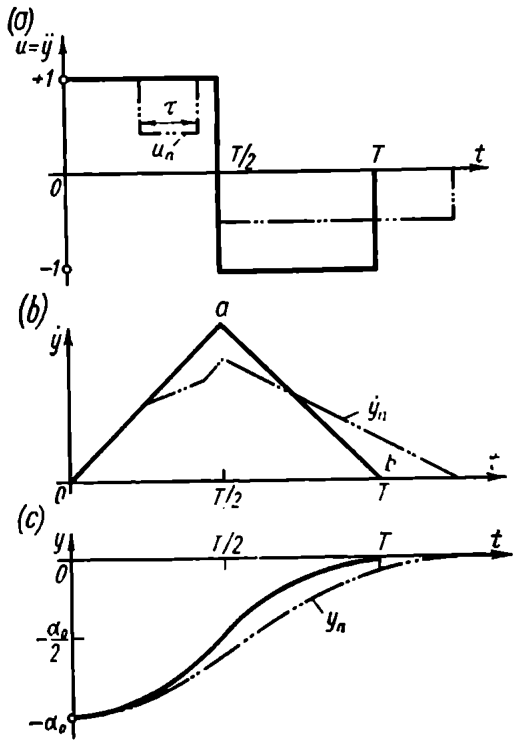

Fig. 21.7

At a positive acceleration $\left(u = +1,\ 0 \leqslant t \leqslant \frac{T}{2}\right)$ the speed increases by the law $\frac{dy}{dt} = t$ (Fig. 21.7*b*).

By the time $t = \frac{T}{2}$ the coordinate y (Fig. 21.7*c*) reaches half of the quantity to be responded to, or

$$y\left(\frac{T}{2}\right) = \int_0^{\frac{T}{2}} \dot{y}(t)\,dt - \alpha_0 = \frac{t^2}{2}\Bigg|_0^{\frac{T}{2}} - \alpha_0 = \frac{T^2}{8} - \alpha_0 = -\frac{\alpha_0}{2} \qquad (21.35$$

Thence the total time of the optimal transient process is

$$T = 2\sqrt{\alpha_0} \tag{21.36}$$

In an open-loop system the optimal process is implemented by using a computer which, with α_0 specified, determines T from Eq. (21.36) and performs the programmed control $u = +1$ over the interval $0 \leqslant t \leqslant \frac{T}{2}$ and $u = -1$ over the interval $\frac{T}{2} < t \leqslant T$ and then $u = 0$ at $t > T$. The optimality of this control can be demonstrated by simple reasoning.

Note that at any control the area under the line $\dot{y}(t)$ should be the same and equal to the specified quantity α_0.

Assume, for instance, that in the time interval $\left[0, \frac{T}{2}\right]$ the equality $u = +1$ was not valid over the period τ. This nonoptimal control is shown in Fig. 21.7*a* as a dot-and-dash line and denoted as $u_n(t)$. The line of the rate $\dot{y}_n(t)$ variation at $t \in \left[0, \frac{T}{2}\right]$ associated with the control $u_n(t)$ will pass below the straight line $0a$ of the optimal rate process and consequently the area under the line $\dot{y}_n(t)$ on the segment $\left[0, \frac{T}{2}\right]$ is found below the value $\frac{\alpha_0}{2}$. In order to cover the desired area α_0 in the subsequent motion of the system, the line $\dot{y}_n(t)$ should partially pass above the line ab. This means that for $t > \frac{T}{2}$ the lines $\dot{y}(t)$ and $\dot{y}_n(t)$ should intersect. They cannot intersect for a second time within the segment $\left[\frac{T}{2}, T\right]$ or at least meet at $t = T$ because, to achieve this, $\dot{y}_n(t)$ should fall steeper than $y(t)$, which is not feasible due to the constraints on u. Thence it follows that the time required for response to α_0 under the control $u_n(t)$ exceeds T.

Consequently, any deflection from the control

$$u(t) = \begin{cases} +1 & \text{at} \quad 0 \leqslant t \leqslant \frac{T}{2} \\ -1 & \text{at} \quad \frac{T}{2} < t \leqslant T \end{cases} \tag{21.37}$$

leads to increased transient time, and so the control (21.37) is optimal. We recall that the function $u(t)$ determined in the form (21.37) is called *piecewise-constant.*

Design of optimal controller. Let us introduce a phase plane with coordinates

$$\left.\begin{aligned} y &= y_1 \\ \frac{dy}{dt} &= \frac{dy_1}{dt} = y_2 \end{aligned}\right\} \tag{21.38}$$

Then the problem in question can be formulated as a problem of the fastest transition of a point in the phase plane (y_1, y_2) from the position ($-\alpha_0$, 0) to the origin of coordinates. Using the notation of Eq. (21.38),

$$\frac{d^2y}{dt^2}=\frac{dy_2}{dt}=\frac{dy_2}{dy_1}\frac{dy_1}{dt}=\frac{dy_2}{dy_1}y_2$$

Substituting this equality into Eq. (21.12) of the plant gives

$$\frac{dy_2}{dy_1}y_2=u \tag{21.39}$$

It is seen from Eq. (21.37) that the optimal control action can assume only two values, $u=-1$, or $u=+1$. Substituting these values into Eq. (21.39), an equation for system phase trajectories can be found. At $u=+1$

$$\frac{y_2^2}{2}=y_1+c \tag{21.40}$$

Here c is an integration constant, whose value can be found by specifying the coordinate of the point on the desired trajectory. For instance, for the trajectory of the family (21.40) passing through the origin of coordinates, $c=0$ and the equation of this trajectory is

$$\frac{y_2^2}{2}=y_1 \tag{21.41}$$

The family of phase trajectories (21.40) at different c values is shown in Fig. 21.8*a*. A trajectory described by Eq. (21.41) is isolated. At $u=-1$

$$\frac{y_2^2}{2}=-y_1+c \tag{21.42}$$

The trajectory passing through the origin of coordinates is given by the equation

$$\frac{y_2^2}{2}=-y_1 \tag{21.43}$$

The family of trajectories (21.42) is shown in Fig. 21.8*b*, where the trajectory (21.43) is isolated.

Because the objective of control is to bring the describing point in the phase plane to the origin of coordinates, the final stage of the motion can occur only along the trajectory (21.41) if $u=+1$ or the trajectory (21.43) if $u=-1$.

It should be remembered that not the entire trajectory (21.41) leads the system to the origin of coordinates, but only its part situated in the fourth quadrant, where $y_2<0$. This part can be described by an equation equivalent to Eq. (21.41) at $y_2<0$

$$y_1=\frac{y_2^2}{2}(-\operatorname{sign} y_2) \tag{21.44a}$$

Similarly, for $u = -1$ only the part of the trajectory (21.43) at $y_2 > 0$ leads to the origin of coordinates. This part can be described

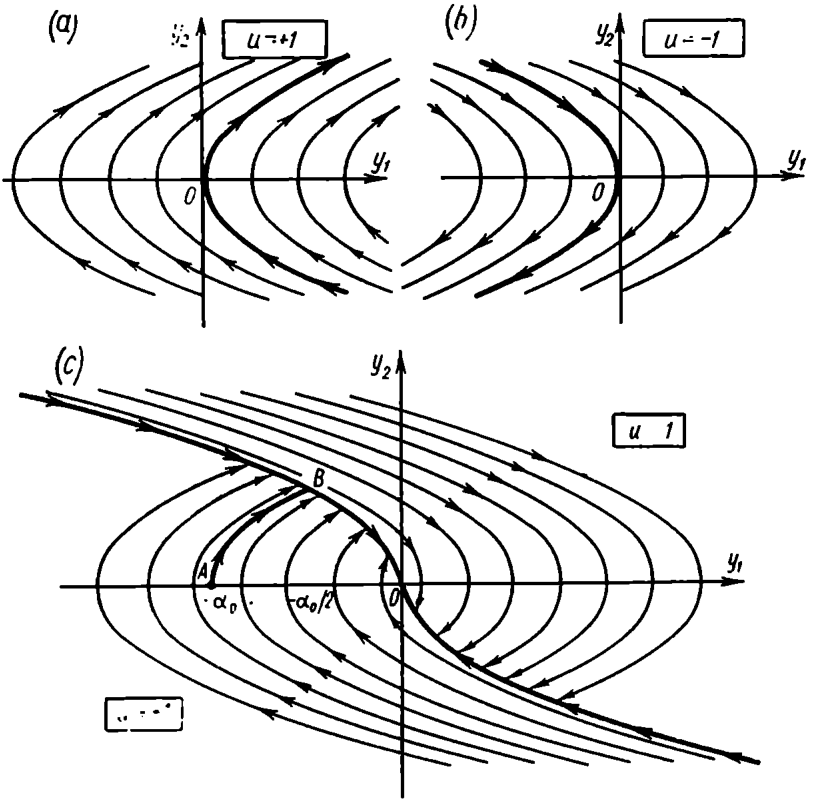

Fig. 21.8

by an equation equivalent to (21.43) at $y_2 > 0$

$$y_1 = -\frac{y_2^2}{2} \operatorname{sign} y_2 \tag{21.44b}$$

Equations (21.44a) and (21.44b) are seen to coincide. Consequently, the system motion over the final time interval is described by the equation

$$y_1 + \frac{y_2^2}{2} \operatorname{sign} y_2 = 0 \tag{21.44}$$

In order to reach the closing portion the motion should occur along the trajectories (21.40) when the initial points lie below the line representing Eq. (21.44), and along the trajectories (21.42) when they lie above the line described by Eq. (21.44) (Fig. 21.8c).

For example, in the problem under study the transition of the describing point from the position $(-\alpha_0, 0)$ starts at $u = +1$ (the portion AB in Fig. 21.8*c*). At the point B the control should change sign, i.e. for further motion $u = -1$ (portion $B0$).

When the describing point reaches the line (21.44) a switch-over from one limit value of control to the other takes place, and therefore the curve (21.44) can be termed the *switching line.*

Let us introduce the function

$$v = -\left(y_1 + \frac{y_2^2}{2} \operatorname{sign} y_2\right) \tag{21.45}$$

which becomes zero on the switching line as follows from Eq. (21.44). For points of the phase plane which are to the right of the switching line (where $u = -1$), $v < 0$. This is easily seen if we move from any point of the switching line rightwards without changing y_2. The addend y_1 has a positive increment, while $\frac{y_2^2}{2} \operatorname{sign} y_2$ remains unchanged. Consequently, with an allowance for the negative sign before the parenthesis in Eq. (21.45), the right-hand part of this expression has a negative increment, and since $v = 0$ on the switching line our assertion is proved. In a similar way, for points to the left of the switching line (where $u = +1$), the function v is seen to be greater than zero.

If, allowing for the behaviour of the function v, the control law is assumed in the form

$$u = \operatorname{sign} v \tag{21.46}$$

the resulting control coincides with the optimal one. Practical implementation of the law (21.46) is relatively simple. The control u should be generated by an ideal two-positional relay which switches over when the sign of the function v changes. Because v controls the switchings of the relay, this function can be referred to as the *switching function.* Note that the expression (21.45) for the switching function differs only in sign from the left-hand part of the switching line equation (21.44).

A controller for an optimal system can be designed on the basis of Eqs. (21.45) and (21.46).

The structural diagram of an optimal system is shown in Fig. 21.9, where the control unit CU is confined within the dotted rectangle. The minus before the parenthesis in Eq. (21.45) is matched by the corresponding sign in the comparator. The misalignment (in our case $x = -y_1$) is fed to the adder, whose other input receives the quantity $-\frac{y_2^2}{2} \operatorname{sign} y_2$ obtained from the derivative signal y_2 by means of three nonlinear converters. The derivative is given by the differentiator p. The output signal of the adder controls the state of the relay acting on the plant.

The above problem suggests the following conclusions:

1. The optimal control action is a piecewise-constant function assuming extreme values (± 1).

2. The optimal control can be obtained by using a two-positional relay whose state depends on the switching function sign.

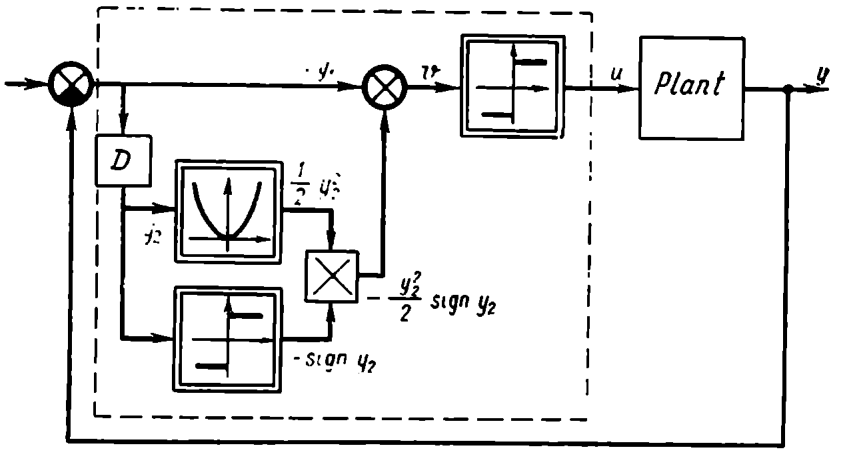

Fig. 21.9

3. The technical implementation of the optimal switching function v is complicated even in a primitive system; therefore practical problems are better solved by finding an equivalent switching function v_{eq} coinciding with v in sign but easier to implement.

21.4. QUASI-OPTIMAL CONTROL TECHNIQUES

Although important results have been obtained in the theory of optimal control the practical use of this theory has been rather limited because control systems for plants described by high-order equations and subject to complex constraints are difficult to implement.

What is required is to develop easily implementable approximate (quasi-optimal) control laws which do not differ much from the optimal ones as regards the criterion adopted. Quasi-optimal systems are also convenient for the following reasons.

1. Any control unit is made up of elements with limited possibilities and, consequently, certain constraints are imposed on selection of the control unit.

2. The mathematical model of the plant on which the control is based is often approximate because the structure and parameters of the plant are not always known in detail.

3. Strictly optimal control systems require detailed data on the system coordinates, input signals and their derivatives, which are very hard to come by in practical work. Thus, for instance, higher derivatives of the controlled coordinate cannot be measured without errors, which are often so large that prevent the use of the derivatives in the control law.

The ways of developing quasi-optimal systems can be classified into two groups: the use of an approximate model of the plant, ignoring the knowledge of strictly optimal control laws for an accurate model, and the use of simple hardware to approximate strictly optimal controls obtained in advance for the accurate model.

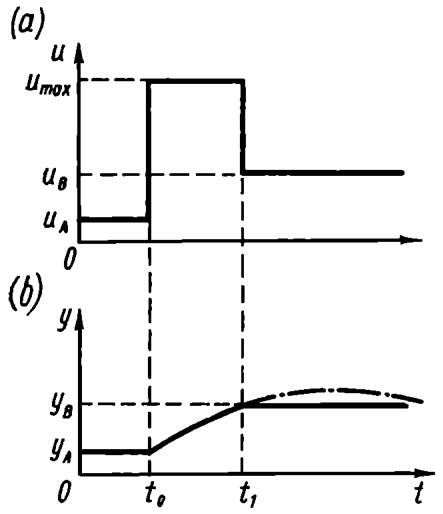

Fig. 21.10.

Simplified mathematical description of a plant. As an example of quasi-optimal control we will consider the following practical problem. A process includes a system used to control the parameter y. A control board carries only an indicator of y and a setpoint unit with its own indicator of u. In this case the setpoint is the control action. To facilitate operation, all controllers are made so that the readings of the indicators of y and u coincide in the steady state. If the controlled variable is to be changed from y_A to y_B, the simplest way to achieve this is to make the setpoint equal to u_B instead of u_A, which was associated with y_A (Fig. 21.10). On completion of the transient process y will be equal to y_B.

However, an experienced operator who wishes to accelerate transition to new conditions acts as follows. Precisely at the time t_0 when the conditions must be changed, the maximal setpoint value $u = u_{max}$ is set (Fig. 21.10*a*). Then $y(t)$ increases sharply. At the time t_1 when y reaches the desired value, or $y(t_1) = y_B$, the setpoint is shifted to $u = u_B$. The time when the control is switched is not calculated in advance and depends on the time taken to reach the desired point $y = y_B$.

A control action of this kind is strictly optimal for a first-order system. Indeed, at $t_0 \leqslant t < t_1$ the coordinate $y(t)$ changed under the effect of the greatest value of control, while at the time t_1 the assignment of the setpoint $u = u_B = y_B$ stopped the change of $y(t)$, i.e. $y(t) = y_B$ at $t \geqslant t_1$. This can easily be verified by substi-

tuting $u = y$ into the equation of the system

$$T\frac{dy}{dt} + y = u$$

Then $\frac{dy}{dt} = 0$; the coordinate $y(t)$ has ceased to change.

For higher-order plants with aperiodic transient processes control of the above type is not strictly optimal because once $u = u_B$, the coordinate $y(t)$ may continue changing (the dotted line in Fig. 21.10*b*). Nevertheless, due to the forced operation in the time interval $[t_0, t_1]$ the transient process in such a system will achieve a steady state sooner than with conventional control given as a step from u_A to u_B.

The application of control which is strictly optimal for first-order systems to higher-order systems may be interpreted as follows: *replacement of the actual equation of the system by a simpler one, determination of an extremal for this simple equation, and implementation of this extremal in order to control the original system.* This approach to quasi-optimal control problems is the essence of simplified mathematical description.

Simplification does not, however, always lead to a first-order equation.

In this case the extremal is a piecewise-constant function taking on the extreme values u_{max} and u_{min}, and the times of switching are found from the solution of the associated variational problem of strictly optimal control.

Quasi-optimal control of an oscillatory plant. The above technique of quasi-optimal control in which the control action takes on extreme values while the times of switching are found from a simplified mathematical model may prove unsatisfactory with oscillatory plants because even small errors in switching times may result in large overshoots in the transient process.

For quasi-optimal control of oscillatory plants, the following techniques can be proposed. If the plant equation is

$$\frac{d^2y}{dt^2} + 2\zeta\frac{dy}{dt} + y = u \qquad (21.47)$$

the plant input should receive a step increment from u_A to u_C at the time t_0 to

$$u_C = u_A + \frac{u_B - u_A}{1+m} \qquad (21.48)$$

to bring the output coordinate y from y_A to y_B. Here m is the transient function overshoot when responding to a unit step.

The function $y(t)$ has an overshoot and at t_1 reaches a value y_B, i.e. $y(t_1) = y_B$ (Fig. 21.11*b*). The time t_1 corresponds to the maximum of the function $y(t)$, therefore $\dot{y}(t_1) = 0$. At $t = t_1$ the input

receives a second step resulting in $u = u_B$. Since at $t = t_1$, $y = u = u_B$ and $\dot{y}(t_1) = 0$, it follows from Eq. (21.47) that $\ddot{y}(t_1) = 0$. The fact that the first and second derivatives are zeroes for a second-order system means that the transient process of $y(t)$ has steadied, or that at $t > t_1$, $y(t) = \text{const} = y_B$. The time interval $[t_1 - t_0]$ corresponds to one half of the period of the oscillations shown in Fig. 21.11*b* by a dotted line and is equal to

$$t_1 - t_0 = \frac{\pi}{\sqrt{1-\zeta^2}} \qquad (21.49)$$

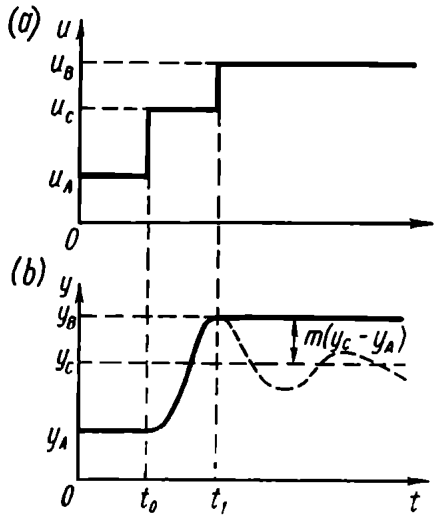

Fig. 21.11

Consequently, the control action $u(t)$ of the form shown in Fig. 21.11 ensures a transient process in an oscillatory plant without an overshoot within the finite time given by (21.49).

In Problem 7 on controlling a conservative plant, $\zeta = 0$ and the overshoot $m = 1$ because a unit step action leads to nondecaying oscillations in the plant. Substituting these values into Eqs. (21.48) and (21.49) leads to a quasi-optimal control law for a conservative plant: at the time t_0 the plant input receives a step whose height is equal to half the quantity to be responded to, and at the time $t_1 = t_0 + \pi$ a second step of the same magnitude is fed. The transient process time is then $T = \pi$.

Approximation of the optimal switching function. As noted in Sec. 21.3, for linear problems of optimal control (where the plant and the functional are linear) with the constraints given as inequalities of the type (21.4) the optimal control action is a piecewise-constant function taking on extreme values. This control action is implemented by means of a relay whose input is the quantity v formed according to the expression for the switching function.

The switching function is as a rule a complicated nonlinear function of the phase coordinates and is implemented with the aid of computers. Even for a simple second-order optimal system the unit which implements the function $v(y_1, y_2)$ (see Fig. 21.9) includes three nonlinear converters. For systems whose plants are described by more involved equations, the shape of the switching lines $v(y_1, y_2) = 0$ in the phase plane may be very intricate and difficult to implement.

For systems of higher-than-second order an equation of the form

$$v(y_1, \ldots, y_n) = 0 \qquad (21.50)$$

determines, in the phase space with coordinates $y_1, \ldots, y_n$, a certain switching hypersurface whose form dictates the complexity of implementation.

If the optimal switching function $v_0(y_1, \ldots, y_n)$ is found, the system engineer has to approximate this function by techologically realizable functions v_r. The chief requirement in approximating the function $v_0(y_1, \ldots, y_n)$ is simplicity of subsequent implementation.

A linear switching function is most convenient in this sense. In the phase space it is associated with a hyperplane, while technical implementation requires only linear amplifiers and an adder. Piecewise-linear and relay functions are also easily implementable.

In approximating the optimal switching function v_0 the qualitative deflections in the system processes should be estimated; in other words, the nature of processes in control systems should be the performance criterion of approximation, and it cannot be replaced by any yardstick of proximity of the functions v_0 and v_r. We will illustrate this with the following example.

Assume that two versions have been proposed for approximation of the optimal switching function (21.45) in a simple second-order optimal system within a limited region of the phase coordinates, $-a \leqslant y_1 \leqslant a$; $-b \leqslant y_2 \leqslant b$. Figure 21.12 shows the optimal switching line given by the equation $v_0 = 0$ (the dotted line) and the switching lines given by the equation $v_{r1} = 0$ (Fig. 21.12*a*, line *ABCD*) and $v_{r2} = 0$ (Fig. 21.12*b*, line *ABCD*).

Assume that the criterion for proximity of the lines $v_0 = 0$ and $v_{ri} = 0$ $(i = 1, 2)$ is the integral

$$I_i = \int_{-a}^{a} \int_{-b}^{b} [v_0(y_1, y_2) - v_{ri}(y_1, y_2)]^2 \, dy_1 \, dy_2 \qquad (21.51)$$

which estimates the area between the lines. Assume also that the approximation made by the function v_{r1} is worse as far as the criterion (21.51) is concerned, or that $I_1 > I_2$. Nevertheless the performance of processes approximated by v_{r1} may prove better than with the use of v_{r2}.

This can be proved by assuming that in a simple optimal system whose structural diagram is shown in Fig. 21.9 and the phase portraits, in Fig. 21.8, the function v_{r1} is implemented and not the optimal switching function. Indeed, Fig. 21.12*a* demonstrates that once the describing point, starting from M_1, reaches the switching line, a sliding mode is generated. Further motion proceeds along the *CD* line until the describing point reaches the optimal switching

line. Then the system moves along the optimal trajectory $v_0 = 0$ from the point C to the origin of coordinates. If the initial conditions were represented by the point M_2, the system, having reached the

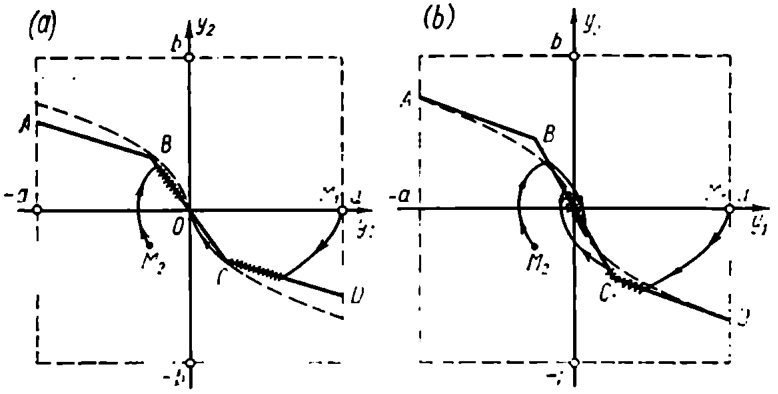

Fig 21.12

switching line, moves in sliding mode along the segment BO. In all cases the transient processes do not oscillate if the switching function v_{r1} is used. The point in the phase plane moves, as a rule, in sliding mode along the switching line $v_{r1} = 0$.

If the switching function v_{r2} is used, all processes generated by the response to the initial conditions oscillate, which follows from Fig. 21.12*b*.

Chapter XXII

THEORETICAL METHODS OF OPTIMAL CONTROL

22.1. GENERAL

The problem of optimal control has been formulated in Ch. XXI as the problem of reaching the extremum of the functional Q [**y** (t), **u** (t)] by selecting the control **u** (t) with due respect for the necessary constraints imposed on controls and phase coordinates. The mathematical tool for finding the extremals is variational calculus.

Three basic methods are employed to solve problems of optimal control: the Euler equation, the maximum principle, and dynamic programming.

Hystorically, the Euler equation method was the first to appear. The basic problems it is intended for have smooth functions as extremals, while the functional to be extremized and the additional conditions are specified by nonlinear functions of the coordinates. The Euler equation is therefore useful in optimal-control problems, where discontinuous functions cannot figure as solutions for physical reasons and where the functional and the coupling equations are essentially nonlinear.

By the mid-1950's the practice of automatic control had proved the expediency of piecewise-continuous control actions in many linear problems. New problems gave rise to a new method based on the maximum principle, which can be applied most effectively to linear problems with constraints imposed on control in the form of inequalities.

Dynamic programming, which stems from the principle of optimal conditions, was developed, also in the 1950's, as a tool for studying multistep optimal solutions in different fields of science and technology including automatic control and has been used most effectively in problems with discrete time and finite difference equations, being a happy combination of the optimality principle and the possibilities of modern computing technology.

22.2. THE EULER EQUATION IN SOLVING OPTIMAL-CONTROL PROBLEMS

The Euler equation for finding the function $x(t)$, which extremizes the functional

$$Q = \int_0^T G[x(t), \dot{x}(t)]\, dt \tag{22.1}$$

has the form

$$G_x - \frac{d}{dt} G_{\dot{x}} = 0 \tag{22.2}$$

where $G_x = \frac{\partial G}{\partial x}$, $G_{\dot{x}} = \frac{\partial G}{\partial \dot{x}}$.

In most applications of variational calculus, functions extremizing the functional are subject to certain additional conditions (to coupling equations).

For control problems these are equations describing a plant in the form

$$\varphi_i[x(t), \dot{x}(t)] = 0 \qquad (i = 1, \ldots, n) \tag{22.3}$$

In this case the variational problem is solved by the method of indefinite Lagrange multipliers the essence of which is that the Euler equation is set up for the auxiliary function

$$F = G[x(t), \dot{x}(t)] + \sum_{i=1}^{n} \lambda_i(t)\, \varphi_i[x(t), \dot{x}(t)] \tag{22.4}$$

where $\lambda_i(t)$ are the Lagrange multipliers to be defined.

The function $x(t)$ and the Lagrange multipliers $\lambda_1(t), \ldots, \lambda_n(t)$ are found from a system of $(n + 1)$ equations: the Euler equations for the function (22.4) and n coupling equations (22.3). The problem of conditional extremum thus formulated is known as the *general Lagrange problem.*

If the conditions to which the desired functions are subjected are given as definite integrals of the form

$$\int_0^T K_i[x(t), \dot{x}(t)]\, dt = Q_i \qquad (i = 1, \ldots, n) \tag{22.5}$$

where Q_i = specified values, the solution is achieved via the auxiliary function

$$F = G[x(t), \dot{x}(t)] + \sum_{i=1}^{n} \lambda_i K_i[x(t), \dot{x}(t)] \tag{22.6}$$

where λ_i are indefinite Lagrange multipliers independent of time. The variational problem under conditions of the form (22.5) is known as the *isoperimetric problem*. The function $x(t)$ and the multipliers λ_i are found, as in the general Lagrange problem, by the Euler equation for the function (22.6) and by n coupling equations (22.5).

Let us see how the Euler equation is used to solve optimal-control problems.

Example 22.1. Consider Problem 5 of Sec. 21.2 on optimal electric drive control with the minimal possible power consumption when the plant equation has the form

$$\frac{d^2y}{dt^2} = u \tag{22.7a}$$

with rate boundary conditions equal to zero

$$\dot{y}(0) = \dot{y}(T) = 0 \tag{22.8a}$$

and the angle to be responded to

$$\int_0^T \dot{y}(t)\,dt = \alpha_0 \tag{22.9a}$$

After introducing the notation

$$\left.\begin{aligned} y &= y_1 \\ \frac{dy_1}{dt} &= \dot{y} = y_2 \end{aligned}\right\}$$

Eqs. (22.7a), (22.8a), (22.9a) can be rearranged as

$$\dot{y}_2 = u \tag{22.7}$$

$$y_2(0) = y_2(T) = 0 \tag{22.8}$$

$$\int_0^T y_2(t)\,dt = \alpha_0 \tag{22.9}$$

The functional to be minimized by selection of the functions $u(t)$ and $y_2(t)$ is the integral

$$Q = \int_0^T u^2(t)\,dt \tag{22.10}$$

Substituting $u(t)$ from (22.7) into (22.10) we have

$$Q = \int_0^T (\dot{y}_2)^2\,dt \tag{22.11}$$

Now we have an isoperimetric problem of minimizing the functional (22.11) provided the integral (22.9) has the given value.

The integrand in the functional to be minimized

$$G = (\dot{y}_2)^2$$

The integrand in the functional whose value is given

$$K_1 = y_2$$

Let us form the function F (see Eq. (22.6))

$$F = G + \lambda_1 K_1 = (\dot{y}_2)^2 + \lambda_1 y_2 \tag{22.12}$$

where λ_1 is an indefinite Lagrange multiplier.

Compose an Euler equation for the function (22.12)

$$F_{y2} = \lambda_1$$

$$F_{\dot{y}2} = 2\dot{y}_2$$

$$\frac{d}{dt} F_{\dot{y}2} = 2\ddot{y}_2$$

In the final form

$$F_{y2} - \frac{d}{dt} F_{\dot{y}2} = \lambda_1 - 2\ddot{y}_2 = 0$$

or

$$\ddot{y}_2 = \frac{\lambda_1}{2} \tag{22.13}$$

After the first integration of Eq. (22.13) we obtain the law for control action variations

$$u = \dot{y}_2 = \frac{\lambda_1}{2} t + C_1 \tag{22.14}$$

Reintegration gives the optimal process

$$y_2(t) = \frac{\lambda_1}{4} t^2 + C_1 t + C_2 \tag{22.15}$$

The three unknowns in Eq. (22.15) (the indefinite multiplier λ_1 and the integration constants C_1, C_2) are found from the two equations for the boundary conditions (22.8) and equality (22.9). Substituting $t = 0$ into Eq. (22.15) and bearing in mind that $y_2(0) = 0$ (by virtue of Eq. (22.8)), we obtain $C_2 = 0$.

Substituting $t = T$ into Eq. (22.15) and bearing in mind that $y_2(T) = 0$ (by virtue of Eq. (22.8)), we get the first equation for determining λ_1 and C_1:

$$\frac{\lambda_1}{4} T^2 + C_1 T = 0 \tag{22.16}$$

Integrating Eq. (22.15) over the range $0 \leqslant t \leqslant T$ and allowing for equality (22.9), we obtain the second equation for determining λ_1 and C_1:

$$\alpha_0 = \int_0^T y_2(t)\,dt = \frac{\lambda_1}{12} T^3 + \frac{C_1}{2} T^2 \qquad (22.17)$$

Solving Eqs. (22.16) and (22.17) simultaneously for C_1 and λ_1 gives

$$\left.\begin{aligned} \lambda_1 &= -\frac{24\alpha_0}{T^3} \\ C_1 &= \frac{6\alpha_0}{T^2} \end{aligned}\right\} \qquad (22.18)$$

Taking into account Eq. (22.18) and $C_2 = 0$, the equation for the optimal processes $u^*(t)$ and $y^*(t)$ can finally be written as

$$\left.\begin{aligned} u^*(t) &= \frac{6\alpha_0}{T^2} - \frac{12\alpha_0}{T^3} t \\ y^*(t) &= \frac{6\alpha_0}{T^2} t - \frac{6\alpha_0}{T^3} t^2 \end{aligned}\right\} \qquad (22.19)$$

The plots corresponding to Eqs. (22.19) are given in Fig. 22.1. As can be seen from Fig. 22.1*a* the control action $u^*(t)$ (the armature

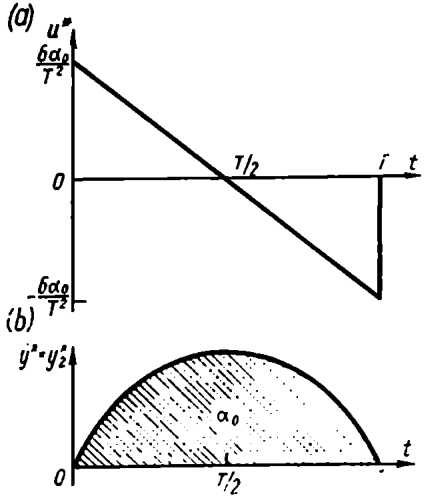

Fig. 22.1

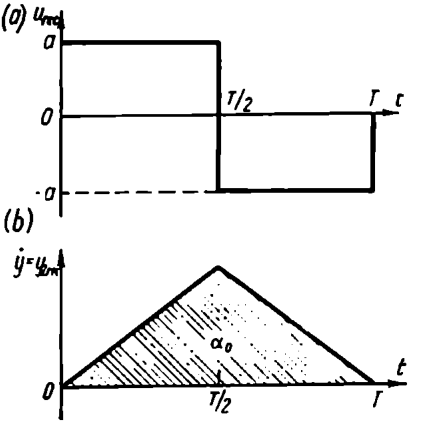

Fig. 22.2

current) should vary by a linear law and the rate $y_2^* = \frac{dy^*}{dt}$, by a parabola (Fig. 22.1*b*).

Once the optimal processes have been found, the optimality of the resultant control can be estimated. For this purpose we compare

power consumptions in optimal control with that in control corresponding to a rectangular diagram (motor start-up and slow-down at a constant armature current). Let us find the parameters of rectangular control (Fig. 22.2*a*) ensuring response to the angle α_0 within the time T. Assume that control takes on the values $u_{rec} = a$ at $0 \leqslant t \leqslant \frac{T}{2}$ and $u_{rec} = -a$ at $\frac{T}{2} < t \leqslant T$. The variation of the output coordinate over the time T obviously depends on the area under the line $y_{2rec}(t)$ (Fig. 22.2*b*). Since positive and negative controls have the same magnitudes, we have

$$\alpha_0 = 2 \int_0^{\frac{T}{2}} y_{2rec}(t)\, dt$$

At $0 \leqslant t \leqslant \frac{T}{2}$, $y_{2rec} = at$ and consequently

$$\alpha_0 = 2 \int_0^{\frac{T}{2}} at\, dt = \frac{aT^2}{4}$$

whence

$$a = \frac{4\alpha_0}{T^2} \tag{22.20}$$

Now write, in the final form, the control law for a rectangular control diagram (this law seems more natural for optimal control problems than a linear law):

$$u_{rec}(t) = \begin{cases} +\frac{4\alpha_0}{T^2} & \text{at } 0 \leqslant t \leqslant \frac{T}{2} \\ -\frac{4\alpha_0}{T^2} & \text{at } \frac{T}{2} < t \leqslant T \end{cases} \tag{22.21}$$

Substituting Eqs. (22.19) and (22.21) into Eq. (22.10) for the functional gives, in the case of optimal control,

$$Q^* = \int_0^T (u^*)^2\, dt = \frac{12\alpha_0^2}{T^3} \tag{22.22}$$

and in the case of a rectangular control diagram

$$Q_{rec} = \int_0^T u_{rec}^2\, dt = \frac{16\alpha_0^2}{T^3} \tag{22.23}$$

The degree of optimality is

$$\varkappa = \frac{Q_{rec}}{Q^*}$$

Substituting the values of power consumption from Eqs. (22.22) and (22.23) gives

$$\varkappa = 1.33$$

i.e. the process in the case of a rectangular control diagram leads to excessive power consumption, which is 33 per cent greater than in the case of optimal control.

Example 22.2. Consider Problem 2 of Sec. 21.2 on response-optimal control of a motor with the proviso that the angle to be responded to is α_0 and the admissible losses are q_0, i.e. that the integrals

$$Q_1 = \int_0^T y_2\, dt = \alpha_0$$

$$Q_2 = \int_0^T (\dot{y}_2)^2\, dt = q_0$$

are given, and the rate boundary conditions are zero. It is required to find such $u(t)$ and $y_2(t)$ that minimize the functional

$$Q = T = \int_0^T dt$$

This is again an isoperimetric problem in which the integrand of the functional to be extremized is $G = 1$, while the integrand functions of functionals with specified values are $K_1 = y_2$ and $K_2 = (\dot{y}_2)^2$.

Now form the function F (see Eq. (22.6)):

$$F = G + \sum_{i=1}^{2} \lambda_i K_i = 1 + \lambda_1 y_2 + \lambda_2 (\dot{y}_2)^2 \qquad (22.24)$$

Compose an Euler equation for the function (22.24):

$$F_{y_2} = \lambda_1, \qquad F_{\dot{y}_2} = 2\lambda_2 \dot{y}_2, \qquad \frac{d}{dt} F_{\dot{y}_2} = 2\lambda_2 \ddot{y}_2$$

In the final form

$$\lambda_1 - 2\lambda_2 \ddot{y}_2 = 0$$

or

$$\ddot{y}_2 = a_0 \qquad (22.25)$$

where $a_0 = \frac{\lambda_1}{2\lambda_2}$.

The first integration results in

$$u(t) = \dot{y}_2 = a_0 t + a_1 \qquad (22.26)$$

Reintegration gives

$$y_2(t) = \frac{a_0}{2} t^2 + a_1 t + a_2 \tag{22.27}$$

The constants a_0, a_1, a_2 in Eq. (22.27) are found from the boundary conditions for y_2, accounting for the integral Q_1 as in Example 22.1.

It can be seen from Eqs. (22.26) and (22.27) that the shape of the optimal process in this problem is the same as in the preceding example.

Example 22.3. Consider Problem 4 of Sec. 21.2 on productivity-optimal control of a d.c. motor when the functional

$$Q = \int_0^T y_2(t)\, dt$$

is to be maximized at a specified magnitude of the integral

$$Q_1 = \int_0^T (\dot{y}_2)^2\, dt = q_0 \tag{22.28}$$

and at known rate boundary conditions.

As in the preceding examples, the variational problem is isoperimetric. To solve it we form the function $F = G + \lambda_1 K_1$, where $G = y_2$; $K_1 = (\dot{y}_2)^2$; and $\lambda_1 =$ indefinite Lagrange multiplier. Consequently,

$$F = y_2 + \lambda_1 (\dot{y}_2)^2 \tag{22.29}$$

Compose an Euler equation for the function (22.29)

$$F_{y_2} - \frac{d}{dt} F_{\dot{y}_2} = 1 - 2\lambda_1 \ddot{y}_2 = 0 \tag{22.30}$$

In this problem the differential equation (22.30) for the extremal coincides with Eqs. (22.25) and (22.13) for extremals in Examples 22.2 and 22.1, respectively. Thence the forms of extremals are the same in all the three problems. The difference can only be found in the coefficients, which are obtained from the boundary conditions and from α_0 or q_0.

The identical shape of optimal processes in all the three examples is attributable to the kinship of the problems, in which the same functionals are considered, while the individuality of a problem consists only in the selection of one of the three functionals for extremization and fixation of the other two.

In the above examples the plant equations were not used explicitly as coupling conditions in shaping the function F, for which the Euler equation was composed. This is explained by the simple nature of the relations between the plant coordinates and control

in these problems owing to which all functionals can simply be represented as functions of $y_2(t)$ for which the variational problem was solved.

When the relation between the plant coordinates is more involved or when processes must be found which are optimal both in terms of phase coordinates and control, the plant equations should be incorporated into the function F. In this case we deal with the general variational Lagrange problem; examples of solution of this problem are discussed below.

Example 22.4. Consider Problem 8 of Sec. 21.2 on analytical controller design. It is required to find the optimal transfer function $W_c(p)$ of a controller which, if connected (in a closed loop) to a plant with a transfer function $W(p) = \frac{1}{1+p}$ (see Fig. 21.6), satisfies the following equation for the transient components x and u

$$\dot{x} + x + u = 0 \tag{22.31}$$

The optimality condition is the minimum of the integral

$$Q = \int_0^\infty [x^2(t) + u^2(t) + \dot{u}^2(t)]\, dt \tag{22.32}$$

at the boundary conditions

$$x(0) = x_0, \qquad x(\infty) = 0$$
$$u(0) = u_0, \qquad u(\infty) = 0$$

For the variational problem of minimizing the functional (22.32) the differential equation (22.31) is a coupling equation and can be given in the form (22.3)

$$\varphi[u, x, \dot{x}] = \dot{x} + x + u = 0 \tag{22.33}$$

Form the function (22.4)

$$F = G + \lambda(t)\,\varphi = x^2 + u^2 + \dot{u}^2 + \lambda(t)(\dot{x} + x + u) \tag{22.34}$$

where $\lambda(t)$ = indefinite Lagrange multiplier, which is not constant as in the isoperimetric problem.

Because in designing the controller the optimal processes at its input and output must be known, compose an Euler equation in the variables $x(t)$ and $u(t)$ for the function F

$$2u + \lambda - 2\ddot{u} = 0$$
$$2x + \lambda - \dot{\lambda} = 0$$

Completing this system with the plant equation (22.33) and placing the variables in the appropriate order, we obtain a system of

equations for a variational problem

$$\begin{aligned} 2(u-\ddot{u}) \qquad\qquad\qquad &+ \lambda &= 0 \\ 2x \qquad\qquad &+ (\lambda - \dot{\lambda}) &= 0 \\ u \qquad + (x+\dot{x}) \qquad\qquad &&= 0 \end{aligned} \tag{22.35}$$

To solve the system (22.35) it is necessary to find the characteristic equation, which is obtained by equating the characteristic determinant to zero, i.e.

$$\begin{vmatrix} 2(1-p^2) & 0 & 1 \\ 0 & 2 & (1-p) \\ 1 & (1+p) & 0 \end{vmatrix} = 0$$

Evaluation of the determinant gives

$$p^4 - 2p^2 + 2 = 0 \tag{22.36}$$

The characteristic equation (22.36) has four roots which correspond to different combinations of plus and minus signs in the following expression

$$p_{1,2,3,4} = \pm\sqrt{1 \mp j} \tag{22.37}$$

The disposition of roots in the complex plane is shown in Fig. 22.3.

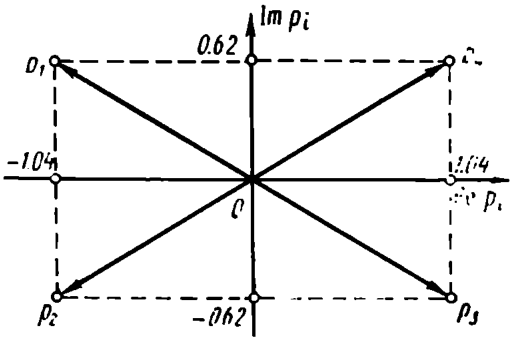

Fig. 22.3

For simple roots of a characteristic equation, the system general solution is the sum of exponents. Thus, for misalignment we can write

$$x = \sum_{i=1}^{4} C_i e^{p_i t} \tag{22.38}$$

The constants C_i can be found from the boundary conditions. Incidentally, from the fact that at infinity $x \to 0$ it follows that the

coefficients of exponents whose powers have a positive real part are zero. It can be seen from Eq. (22.3) that $\operatorname{Re} p_3 = \operatorname{Re} p_4 > 0$ and, consequently, in (22.38) it should be assumed that $C_3 = C_4 = 0$. With this equality in mind rewrite Eq. (22.38) as

$$x = C_1 e^{p_1 t} + C_2 e^{p_2 t}$$

Differentiating and substituting $\dot{x}$ into the plant equation (22.31) gives u. Differentiation can also yield $\dot{u}$. Write the expressions for processes in a system and their derivatives

$$\begin{aligned} x &= C_1 e^{p_1 t} + C_2 e^{p_2 t} \\ \dot{x} &= p_1 C_1 e^{p_1 t} + p_2 C_2 e^{p_2 t} \\ -u &= (1 + p_1) C_1 e^{p_1 t} + (1 + p_2) C_2 e^{p_2 t} \\ -\dot{u} &= p_1 (1 + p_1) C_1 e^{p_1 t} + p_2 (1 + p_2) C_2 e^{p_2 t} \end{aligned} \tag{22.39}$$

Let us analyze this solution. Firstly, the processes in the optimal system can be described by linear differential equations. Thence, with an allowance for the plant linearity, it can be inferred that the optimal controller should also be linear. Secondly, the solution obtained corresponds to an equation of a second order system.

Since the plant is described by an equation of an inertial element, then to obtain a second-order equation for the system the controller transfer function should have a first-order denominator. The numerator may be of any order from 0 to 2.

Assume that the controller is described by the equation

$$A\dot{x} + Bx = C\dot{u} + Du \tag{22.40}$$

Substitution of Eq. (22.39) into Eq. (22.40) for all coordinates and simple transformations result in

$$\begin{aligned} &C_1 e^{p_1 t} [Ap_1 + B + Cp_1 (1 + p_1) + D (1 + p_1)] + \\ &+ C_2 e^{p_2 t} [Ap_2 + B + Cp_2 (1 + p_2) + D (1 + p_2)] = 0 \end{aligned} \tag{22.41}$$

The functions $C_1 e^{p_1 t}$ and $C_2 e^{p_2 t}$ cannot be identically zero at the same time, otherwise we would have $x \equiv 0$, which would mean that the control is ineffective. Consequently, both expressions in brackets in Eq. (22.41) should be zero, i.e.

$$\begin{aligned} Ap_1 + B + Cp_1 (1 + p_1) + D (1 + p_1) &= 0 \\ Ap_2 + B + Cp_2 (1 + p_2) + D (1 + p_2) &= 0 \end{aligned} \tag{22.42}$$

The resultant system of equations leads to the parameters of the optimal controller, i.e. of the optimal control law.

Because there are only two equations but four unknowns, any values can be assumed for two unknowns. Thence the solution obtained

cannot be single-valued. This ambiguity, however, refers only to the selection of parameters (and hence of the structure), but there is just one optimal process, which is determined by the system (22.39).

Let us have a look at certain important solutions which follow from Eqs. (22.42). In the simplest case two unknowns are assumed zero. Then the following structures of controllers are obtained:

1) $A = C = 0$ or $B = D = 0$: a proportional controller with an equation $Bx = Du$ or $A\dot{x} = C\dot{u}$;

2) $B = C = 0$: an ideal differentiating controller with an equation $u = \frac{A}{D}\dot{x}$;

3) $A = D = 0$: an integrating controller (I-controller) with an equation $u = \frac{B}{C}\int_0^t x(\tau)\,d\tau$.

(The combinations $A = B = 0$ or $C = D = 0$ are senseless). Without going into details of application of these controllers, we will note that with any pair of unknowns given as zeros the remaining unknowns also become zeros in solving Eqs. (22.42). This proves that controller structures (1-3) cannot be taken as optimal.

Consider two more combinations of arbitrarily specified unknowns:

4) $A = 0$, $D = 1$. Then the equation of the controller is

$$Bx = (C\dot{u} + u)$$

and the transfer function is of the form

$$W_c(p) = \frac{U(p)}{X(p)} = \frac{B}{Cp+1} \tag{22.43}$$

The resultant controller is seen to be described as an inertial element; it is required to determine its gain and time constant. The obvious disadvantage of this controller is that the resultant system is static;

5) setting $C = 1$ and $D = 0$, we have a controller with an equation $A\dot{x} + Bx = \dot{u}$ and a transfer function

$$W_c(p) = \frac{U(p)}{X(p)} = \frac{Ap+B}{p} = A\left[1 + \frac{1}{\frac{A}{B}p}\right] \tag{22.44}$$

A controller with this transfer function is known as *proportional-plus-integral* (PI-controller); the parameter A is treated as a gain and $\frac{A}{B}$ as a time constant. A system with this controller is astatic, so the optimal controller should have the transfer function (22.44).

Determine the parameters A and B by substituting $C = 1$ and $D = 0$ into Eqs. (22.42)

$$\left.\begin{aligned} Ap_1 + B + p_1(1 + p_1) = 0 \\ Ap_2 + B + p_2(1 + p_2) = 0 \end{aligned}\right\} \tag{22.45}$$

From Eqs. (22.45), with numerical values allowed for, (see Fig. 22.3 and Eq. (22.37)) we have

$$\begin{aligned} A &= -(1 + p_1 + p_2) = 1.08 \\ B &= p_1 p_2 = \sqrt{2} \end{aligned} \tag{22.46}$$

The result obtained in analytical designing of an optimal controller for an inertial plant is of great practical importance. From the solution of the variational problem with a general-type functional

$$Q = \int_0^\infty (x^2 + u^2 + \dot{u}^2)\, dt$$

which allows for performance of processes (the integrand addend x^2), the control cost (the addend u^2) and feasibility ($\dot{u}^2$), it follows that the optimal controller is a PI-controller. The solution also gives the parameters of the controller. This result explains the wide use of PI-controllers in inertial industrial plants.

The use of the Euler equation with constrained controls. In the above examples no constraints were imposed on the desired functions of optimal processes; they can, however be imposed on controls and, sometimes, on phase coordinates, and are usually given as inequalities, e.g. in the form of (21.4) $|x| \leqslant 1$.

Such an inequality limits the freedom of varying the function in search of extremals. The basic necessary condition for an extremum, the Euler equation, is derived under the assumption that if $x(t)$ is an extremal, then $x + \eta$ and $x - \eta$ (where $\eta > 0$) are admissible functions. The value of the functional for the functions $x + \eta$ and $x - \eta$ can then be compared with the one corresponding to the extremal. If the range of $x(t)$ is closed and $x(t)$ passes along the boundary, then one of these functions leaves the admissible region.

Consider one possible way to overcome this difficulty, assuming for simplicity that the extremal is sought near one of the boundaries of the admissible region defined by inequality

$$x \geqslant \varphi(t) \tag{22.47}$$

Thus, for the constraint $|x| \leqslant 1$ the condition (22.47) is written as $x \geqslant -1$, i.e. $\varphi(t) = -1$. Let us replace the variables by introducing a coordinate z, which is determined as

$$z^2 = x - \varphi \tag{22.48}$$

No constraints are imposed on the new variable z, and the boundary of the region to which the variable x belongs is associated with $z = 0$. Now write the functional $Q = \int_{t_0}^{T} G[x, \dot{x}, t]\, dt$ in terms of new variables. From Eq. (22.48) it follows that $x = z^2 + \varphi$, whence

$$\dot{x} = 2z\dot{z} + \dot{\varphi}$$

Substituting these expressions into the functional Q gives

$$Q = \int_{t_0}^{T} G[z^2 + \varphi, 2z\dot{z} + \dot{\varphi}, t]\, dt \tag{22.49}$$

Because no constraints are imposed on z any longer, the extremum of the functional (22.49) can be found with the aid of the Euler equation

$$G_z - \frac{d}{dt} G_{\dot{z}} = 0 \tag{22.50}$$

Calculate the components of Eq. (22.50), expressing x and $\dot{x}$ in terms of z

$$G_z = \frac{\partial G}{\partial z} = \frac{\partial G}{\partial x}\frac{\partial x}{\partial z} + \frac{\partial G}{\partial \dot{x}}\frac{\partial \dot{x}}{\partial z} = G_x 2z + G_{\dot{x}} 2\dot{z}$$

$$G_{\dot{z}} = \frac{\partial G}{\partial \dot{z}} = \frac{\partial G}{\partial x}\frac{\partial x}{\partial \dot{z}} + \frac{\partial G}{\partial \dot{x}}\frac{\partial \dot{x}}{\partial \dot{z}} = G_{\dot{x}} 2z$$

$$\frac{d}{dt} G_{\dot{z}} = 2z\left(\frac{d}{dt} G_{\dot{x}}\right) + G_{\dot{x}} 2\dot{z}$$

With an allowance for the above results Eq. (22.50) is rearranged as

$$G_x 2z + G_{\dot{x}} 2\dot{z} - 2z\frac{d}{dt} G_{\dot{x}} - G_{\dot{x}} 2\dot{z} = 0$$

or

$$2z\left(G_x - \frac{d}{dt} G_{\dot{x}}\right) = 0 \tag{22.51}$$

Equation (22.51) actually decomposes into two: 1) $z = 0$, which represents the boundary of the admissible area, and 2) the Euler equation for the initial functional

$$G_x - \frac{d}{dt} G_{\dot{x}} = 0$$

Consequently, from Eq. (22.51) it follows that if constraints are given in the form of inequalities the extremum of a functional is achieved only on curves made up of pieces of extremals and pieces of the admissible area boundary.

Unfortunately, Eq. (22.51) only indicates the admissibility of boundary values of the control function $u(t)$ as extremals but does not enable one to prove that for a linear problem, e.g. in the case of the constraint $|u| \leqslant 1$, control takes on only boundary values. This can be proved in a simple way by using the maximum principle (see the next Section), and sometimes this follows from physical considerations, as for a simple second-order system (Sec. 21.3).

Where control is known to be a piecewise-constant function taking on boundary values $u = +1$ and $u = -1$, the Euler equation can lead to parameters of this control function, i.e. the number of intervals where controls are constant, and switching times. For this purpose the condition $|u| = 1$ is represented with the use of the integral

$$\int_0^T u^{2m}\,dt = T \tag{22.52}$$

where $m \to \infty$ (an integer).

If $|u| > 1$ at least on a small time interval, then $u^{2m} \to \infty$ as $m \to \infty$ and the integral exceeds the specified values of T. If, conversely, $|u| < 1$ at least on a small time interval, then $u^{2m} \to 0$ and the value of the integral is below T. With $|u| = 1$ replaced by the condition (22.52) the variational problem of finding the extremal of $u(t)$ becomes an isoperimetric problem whose solution has already been discussed.

Example 22.5. Consider Problem 1 of Sec. 21.2 on optimal speed response for a plant with an equation $\ddot{y} = u$ and a constraint on control $|u| \leqslant 1$. The plant equation can be conveniently written as a system of first-order equations, which will later be used as coupling equations. Denoting $y_1 = y$, $y_2 = \dot{y}$, we have

$$\dot{y}_1 = y_2$$
$$\dot{y}_2 = u$$

or

$$\varphi_1 = \dot{y}_1 - y_2 = 0$$
$$\varphi_2 = \dot{y}_2 - u = 0 \tag{22.53}$$

Assuming that the extremal is a piecewise-constant function $|u(t)| = 1$, introduce also the condition (22.52)

$$\int_0^T u^{2m}\,dt = T, \text{ where } m \to \infty$$

The integrand function in the functional to be extremized in the optimal response problem is $G = 1$.

The integrand function in the functional representing the condition is $K_0 = u^{2m}$.

Let us compose the function

$$F = G + \lambda_0 K_0 + \lambda_1(t)\,\varphi_1 + \lambda_2(t)\,\varphi_2 =$$
$$= 1 + \lambda_0 u^{2m} + \lambda_1(t)\,(\dot{y}_1 - y_2) + \lambda_2(t)\,(\dot{y}_2 - u) \quad (22.54)$$

Because the function F includes the differential coupling equations (22.53), the problem thus posed is a variational Lagrange problem. Note that in Eq. (22.54) $\lambda_0 = \text{const}$ is an indefinite Lagrange multiplier in the isoperimetric problem, while $\lambda_1(t)$ and $\lambda_2(t)$ are time functions. The extremals to be found are functions $u(t)$, $y_1(t)$ and $y_2(t)$, therefore set up Euler equations for each of the unknowns

$$F_u - \frac{d}{dt}F_{\dot{u}} = \lambda_0 2mu^{2m-1} - \lambda_2 = 0 \quad (22.55)$$

$$F_{y1} - \frac{d}{dt}F_{\dot{y}1} = -\dot{\lambda}_1 = 0 \quad (22.56)$$

$$F_{y_2} - \frac{d}{dt}F_{\dot{y}_2} = -\lambda_1 - \dot{\lambda}_2 = 0 \quad (22.57)$$

From Eq. (22.55)

$$u = \sqrt[2m-1]{\frac{\lambda_2(t)}{2m\lambda_0}} \quad (22.58)$$

Note that if m is an integer and $m \to \infty$, the following equalities (introduced in Ch. XV (15.19*b*)) are valid for any number A:

$$\sqrt[2m-1]{A} = \begin{cases} +1 \text{ if } A > 0 \\ -1 \text{ if } A < 0 \end{cases}$$

By definition of the function "sign A" these equalities can be rewritten in the form

$$\sqrt[2m-1]{A} = \operatorname{sign} A, \quad \text{where } m \to \infty$$

Then the optimal control law (22.58) will be represented as

$$u(t) = \operatorname{sign}\left(\frac{\lambda_2(t)}{2m\lambda_0}\right) \quad (22.59)$$

Because m and λ_0 are constant numbers, the behaviour of the function $u(t)$ depends only on the variation of $\lambda_2(t)$. From Eq. (22.56) $\lambda_1 = \text{const}$, and from Eq. (22.57)

$$\lambda_2(t) = C_2 - C_1 t \quad (22.60)$$

where C_1 and C_2 are integration constants, which can be found from the boundary conditions of the problem.

Substituting Eq. (22.60) into (22.59) finally gives

$$u(t) = \text{sign}\left(\frac{1}{m(a_2 - a_1 t)}\right)$$

where

$$a_1 = \frac{C_1}{2\lambda_0}, \qquad a_2 = \frac{C_2}{2\lambda_0}, \quad m > 0 \tag{22.61}$$

From Eq. (22.61) it can be seen that the control $u(t)$ cannot change sign more than once, i.e. it can contain no more than two intervals of constancy. This result coincides with the result of Sec. 21.3.

22.3. THE MAXIMUM PRINCIPLE IN SOLUTION OF OPTIMAL CONTROL PROBLEMS

The maximum principle. This method for solving variational problems was developed by a team of Soviet scientists headed by Academician L.S. Pontriagin in the period from 1956 through 1960. The core of the method is the maximum principle originally hypothesized by L. S. Pontriagin and named after him (Refs. 66, 12, 22).

The principle was specifically developed to solve optimal control problems and therefore the statement of the problem and the terminology are much more comprehensible to control engineers than those of Euler equation-based methods. The chief advantage of the method is, however that the class of extremals to be found includes piecewise-continuous functions.

The theorems of the maximum principle are valid for control systems whose behaviour can be described by a system of first-order differential equations

$$\dot{y}_i = f_i(y_1, \ldots, y_n, u_1, \ldots, u_r) \qquad (i = 1, \ldots, n) \tag{22.62}$$

where y_i = phase coordinates of the plant; u_i = controls.

It is required to find the controls $\mathbf{u}(t)$ transferring the system from the state $\mathbf{y}(t_0)$ to the state $\mathbf{y}(T)$ within a period T and extremizing the functional

$$Q = \int_{t_0}^{T} G(\mathbf{y}, \mathbf{u}, t)\, dt$$

The use of a system of equations of the type (22.62) in place of, say, a linear nth-order equation is made possible by substituting $y_k = \frac{d^{k-1}y}{dt^{k-1}}$ into the initial equation. Assume that a plant with one control action u is described by the equation

$$a_0 \frac{d^n y}{dt^n} + a_1 \frac{d^{n-1}y}{dt^{n-1}} + \ldots + a_n y = u$$

Then, denoting $y_1 = y$, $y_2 = \dot{y}$, $y_3 = \ddot{y}$, a system of n first-order equations can be written

$$\dot{y}_1 = y_2$$
$$\dot{y}_2 = y_3$$
$$\dots\dots$$
$$\dot{y}_{n-1} = y_n$$
$$\dot{y}_n = -\frac{1}{a_0}[a_1 y_n + a_2 y_{n-1} + \dots + a_n y_1 - u]$$

The phase coordinates include also a quantity y_0, which characterizes the current value of the functional, i.e.

$$y_0(t) = \int_{t_0}^{t} G[u, \mathbf{y}, t]\, dt, \qquad [y_0(T) = Q]$$

The differential equation for the coordinate y_0 is given as

$$\dot{y}_0 = G[u, \mathbf{y}, t] = f_0(u, \mathbf{y}, t) \tag{22.63}$$

Completing Eq. (22.62) with Eq. (22.63) gives the final system of equations for the optimal control problem

$$\dot{y}_0 = f_0(u, \mathbf{y}, t) = G[u, \mathbf{y}, t]$$
$$\dot{y}_1 = f_1(u, \mathbf{y}, t)$$
$$\dots\dots\dots$$
$$\dot{y}_n = f_n(u, \mathbf{y}, t)$$

or, in the general form,

$$\dot{y}_i = f_i(u, \mathbf{y}, t) \qquad (i = 0, \dots, n) \tag{22.64}$$

An important role in the maximum principle is played by the auxiliary variables $\psi_0(t), \dots, \psi_n(t)$ and the function

$$H = \sum_{i=0}^{n} \psi_i(t) f_i(u, \mathbf{y}, t) \tag{22.65}$$

The functions $\psi_i(t)$ are obtained from the differential equations

$$\frac{d\psi_i}{dt} = -\frac{\partial H}{\partial y_i} \qquad (i = 0, \dots, n) \tag{22.66}$$

It should be emphasized that Eq. (22.66) is essentially a definition of the functions $\psi_i(t)$ and the question "What is the function $\psi_i(t)$?" is completely answered by: "It is a function which satisfies

Eq. (22.66)." If the function H of Eq. (22.65) is substituted into Eq. (22.66), we have

$$\frac{d\psi_i}{dt} = -\sum_{k=0}^{n} \psi_k(t) \frac{\partial f_k(u, \mathbf{y}, t)}{\partial y_i} \qquad (i=0, \ldots, n) \qquad (22.67)$$

This equality can be used as another definition of the functions $\psi_i(t)$.

Incidentally, from Eqs. (22.64) and (22.65)

$$\frac{dy_i}{dt} = \frac{\partial H}{\partial \psi_i} \qquad (i=0, \ldots, n) \qquad (22.68)$$

Indeed, since $\frac{dH}{d\psi_i} = f_i$, Eqs. (22.68) are equivalent to Eqs. (22.64).

If Eqs. (22.68) and (22.66) are written simultaneously

$$\frac{d\psi_i}{dt} = -\frac{\partial H}{\partial y_i}$$

$$\frac{dy_i}{dt} = \frac{\partial H}{\partial \psi_i}$$

a certain symmetry can be observed in the resultant system of equations. Equations of this kind are known as *canonically conjugate.*

Now we will formulate the basic theorem of the method (the maximum principle):

for the control $\mathbf{u}(t)$ *and trajectory* $\mathbf{y}(t)$ *with coordinates* $u_1(t), \ldots, u_r(t)$ *and* $y_1(t), \ldots, y_n(t)$, *respectively, to be optimal there should be a nonzero continuous function* $\boldsymbol{\psi}(t)$ *with coordinates* $\psi_1(t), \ldots, \psi_n(t)$ *and associated with the functions* $\mathbf{u}(t)$ *and* $\mathbf{y}(t)$ *by virtue of Eqs.* (22.66) *such that at any* t $(t_0 \leqslant t \leqslant T)$ *the function* $H[\boldsymbol{\psi}(t), \mathbf{y}(t), \mathbf{u}]$ *of the variable* $\mathbf{u} \in \Omega$ *reaches a maximum at the point* $\mathbf{u} = \mathbf{u}(t)$, i.e.

$$H[\boldsymbol{\psi}(t), \mathbf{y}(t), \mathbf{u}] = \max_{\mathbf{u} \in \Omega}$$

This theorem will be proved in the next section, where the geometrical interpretation of the maximum principle for the problem of optimal-speed response will be given (using the Bellman equation). Here, we will indicate only a specific feature of the method by which its authors derived the principle. We will confine ourselves to a single control $u(t)$.

As in derivation of the Euler equation, the presumed extremal of $u(t)$ is supplemented with the variation $\eta(t)$, the corresponding first variation of the functional δQ is calculated, and from the fact that this variation is zero the conditions necessary to ensure the optimal value of $u(t)$ are obtained. The shape of the variation in deriving the maximum principle is significant (Fig. 22.4). This is a pulse acting at the time τ and having an infinitesimal duration ε but a finite, arbitrary height $u(\tau)$. The only condition imposed on the

value of $u(\tau)$ is that $u(\tau) \in \Omega$. Thus, if $|u| \leqslant 1$, then $-1 \leqslant u(\tau) \leqslant +1$. A variation of this kind is referred to as a *needle type variation*. The latter is essentially distinct from the variations whereby the Euler equation is derived since it is not smooth and has a stepwise form. The use of stepwise variations makes it possible to include

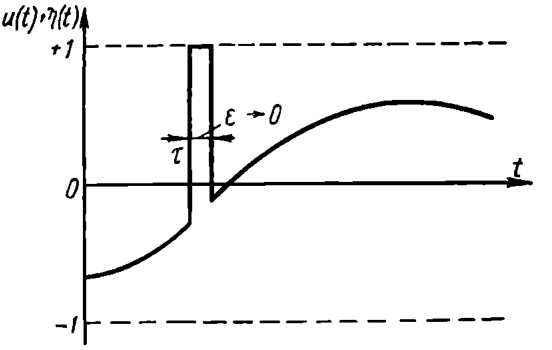

Fig. 22.4

piecewise-continuous functions among the extremals to be found. In the mean time these functions are extremals in many problems of optimal control as we will see from examples which follow.

Before getting down to examples let us outline the procedure of obtaining the solution by the maximum principle.

1. Write a system of first-order differential equations (22.64) of the plant

$$\dot{y}_i = f_i(u, y, t) \qquad (i = 0, \ldots, n)$$

and the equation (22.63) of the functional.

2. Compose the function H

$$H = \sum_{i=0}^{n} \psi_i(t) f_i(u, y, t)$$

3. Determine the value of u maximizing the function H from the system of equations

$$\frac{\partial H}{\partial u_j} = 0 \qquad (j = 1, \ldots, r) \tag{22.69}$$

The maximum of H may be achieved on the boundary of the permissible area of controls; then for some j values equality (22.69) may not hold for the nonzero function $\psi(t)$.

Equations (22.69) defining $u(t)$ have $(2n + r + 2)$ unknowns: $(n + 1)$ functions $y_i(t)$, $(n + 1)$ functions $\psi_i(t)$ and r functions $u_j(t)$. They are defined by r equations (22.69), $(n + 1)$ equations of the initial system (22.64), and now it is required to obtain another $(n + 1)$ equations for the functions $\psi_i(t)$ of the form (22.66).

4. Compose equations (22.66) in order to determine $\psi_i(t)$

$$\frac{d\psi_i}{dt} = -\frac{\partial H}{\partial y_i} \qquad (i = 0, \ldots, n)$$

The optimal control $u(t)$ is found from simultaneous solution of the above $(2n + r + 2)$ equations.

The specific feature of the maximum principle is that the variational problem of finding the function $u(t)$ extremizing the functional Q is replaced by a simpler analytical problem of finding the parameter u maximizing the auxiliary function $H(u)$. Thence the term "the maximum principle".

Example 22.6. Use the maximum principle to solve Problem 1 of Sec. 21.2 on speed-optimal control of a plant described by the equation $\ddot{y} = u$, the control constraint being $|u| \leqslant 1$.

Write a system of first-order equations describing the plant using the notation $y_1 = y$, $y_2 = \dot{y}$:

$$\dot{y}_1 = y_2, \qquad \dot{y}_2 = u \tag{22.70}$$

The functional is the process time $Q = T = \int_0^T dt$, therefore the differential equation for the functional (22.63) has the form

$$\dot{y}_0 = 1 \tag{22.71}$$

Completing Eq. (22.70) with Eq. (22.71) we obtain the initial system of equations for the plant

$$\dot{y}_0 = 1$$
$$\dot{y}_1 = y_2$$
$$\dot{y}_2 = u$$

Compose the function

$$H = \sum_{i=0}^{2} \psi_i f_i = \psi_0 \cdot 1 + \psi_1 y_2 + \psi_2 u \tag{22.72}$$

In this equation only the last addend depends on u, therefore the maximal value of H can be attained by maximizing this addend, i.e. it is necessary that

$$\psi_2(t)\, u = \max_{|u| \leqslant 1} \tag{22.73}$$

The value of u satisfying the condition (22.73) is found from the equation (22.69)

$$\frac{\partial H}{\partial u} = \psi_2(t) = 0$$

which holds only at $\psi_2(t) = 0$. However, the formulation of the maximum principle requires the existence of a nonzero function $\psi(t)$, i.e. the equality $\psi_2(t) = 0$ can not hold for all t. Consequently, the values of u that would ensure the validity of (22.73) should be taken on the boundaries, i.e. $u = +1$ or $u = -1$. At $\psi_2(t) > 0$ we should evidently take $u = +1$, while at $\psi_2(t) < 0$, $u = -1$. This control law can be represented via the sign function

$$u = \operatorname{sign} \psi_2(t) \tag{22.74}$$

The functions $\psi_i(t)$ are determined via differential equations of the type (22.66)

$$\frac{d\psi_0}{dt} = -\frac{\partial H}{\partial y_0} = 0$$

$$\frac{d\psi_1}{dt} = -\frac{\partial H}{\partial y_1} = 0$$

$$\frac{d\psi_2}{dt} = -\frac{\partial H}{\partial y_2} = -\psi_1$$

Solutions of these equations have the form

$$\begin{aligned} \psi_0 &= \text{const} = C_0 \\ \psi_1 &= \text{const} = C_1 \\ \psi_2 &= C_2 - C_1 t \end{aligned} \tag{22.75}$$

Substituting Eq. (22.75) into (22.74) finally gives

$$u = \operatorname{sign}(C_2 - C_1 t) \tag{22.76}$$

Because the function $\psi_2 = C_2 - C_1 t$ can change the sign just once, the optimal control (22.76) is a piecewise-constant function which takes on limit values of $+1$ or -1 and has at most two constancy intervals.

This solution coincides completely with the one obtained in Example 22.5 with the aid of the Euler equation; in this case no assumptions as to the form of optimal control are needed. The same solution was obtained in Ch. XXI when designing a simple optimal system.

This example leads to the conclusion that the function $\dot{y}_0 = f_0$, and hence $\psi_0(t)$, may be omitted from the expression for H if the functional does not include control u explicitly because in this case the addend $\psi_0 f_0$ does not influence the maximization of H.

Example 22.7. Consider Problem 3 of Sec. 21.2 concerned with productivity-optimal control of a plant described by the equation $\ddot{y} = u$ with a constraint $|u| \leqslant 1$. The functional, in this case $Q = y_0(T) = \int_0^T \dot{y}(t)\,dt$, does not explicitly depend on the control u;

for this reason the equation $\dot{y}_0 = f_0$ may be left out of the system of equations for the problem, which can then be represented as

$$\dot{y}_1 = y_2$$
$$\dot{y}_2 = u$$

The H function is

$$H = \sum_{i=1}^{2} \psi_i f_i = \psi_1 y_2 + \psi_2 u$$

The subsequent solution completely, including the notation, repeats that of the preceding example; in other words, the optimal control is again a piecewise-constant function which takes on the extreme values of $+1$ or -1 and has at most two constancy intervals.

Example 22.8. Let us consider Problem 6 of Sec. 21.2 on speed-optimal rendez-vous of two vehicles. The relevant law is represented by the second-order equation (21.23)

$$T\ddot{x} + \dot{x} = u - b$$

with the initial conditions (21.24), which are given as

$$x(0) = -a, \qquad \dot{x}(0) = -b$$

where T = time constant of the controlled vehicle, b = speed of the uncontrolled vehicle, a = initial misalignment of the vehicle positions. All the three quantities are constant.

Because the functional is the time of the process, the equation $\dot{x}_0 = f_0$ is not included in the equations of the problem.

Let us write a system of equations of the type (22.64) denoting $x_1 = x$, $x_2 = \dot{x}$:

$$\dot{x}_1 = x_2$$
$$\dot{x}_2 = \frac{1}{T}(-x_2 + u - b) \tag{22.77}$$

Write the function

$$H = \sum_{i=1}^{2} \psi_i f_i = \psi_1 x_2 + \psi_2 \frac{1}{T}(-x_2 + u - b) =$$
$$= \psi_1 x_2 - \frac{1}{T}\psi_2 x_2 - \psi_2 \frac{b}{T} + \frac{1}{T}\psi_2 u \tag{22.78}$$

In Eq. (22.78) only the last addend depends on control, therefore $H = \max_{|u|\leqslant 1}$, when $\left(\frac{1}{T}\psi_2 u\right) = \max_{|u|\leqslant 1}$. Thence follows the

obvious law of control

$$u = \text{sign}\,[\psi_2(t)] \tag{22.79}$$

Write the differential equations for the functions $\psi_i(t)$:

$$\frac{d\psi_1}{dt} = -\frac{\partial H}{\partial x_1} = 0$$

$$\frac{d\psi_2}{dt} = -\frac{\partial H}{\partial x_2} = -\psi_1 + \frac{1}{T}\psi_2$$

From the first equation it follows that

$$\psi_1 = \text{const} \tag{22.80}$$

and from the second, with an allowance for Eq. (22.80),

$$\psi_2(t) = C_1 + C_2 e^{\frac{t}{T}} \tag{22.81}$$

Substituting Eq. (22.81) into (22.79) write the optimal control law in the final form

$$u = \text{sign}\,(C_1 + C_2 e^{\frac{t}{T}}) \tag{22.82}$$

Figure 22.5 shows plots of the function $\psi_2(t)$ for various combinations of integration constants: curve *1* corresponds to $C_1 > 0$, $C_2 > 0$, curve *2* to $C_1 > 0$, $C_2 < 0$, curve *3* to $C_1 < 0$, $C_2 > 0$, and curve *4* to $C_1 < 0$ and $C_2 < 0$. The function $\psi_2(t)$ is seen to change the sign no more than once; consequently, optimal control contains no more than two constancy intervals.

The physical meaning of the problem indicates that at first the control must ensure acceleration of the vehicle B and then its slowing down (see trajectories of vehicles A and B, Fig. 21.4*a*). Taking into account the result (22.82) and the physical meaning of the problem one can say that the control must consist of two intervals (Fig. 22.6). On the first interval, at $0 \leqslant t \leqslant t_1$, the control $u = +1$, and on the second, at $t_1 < t \leqslant t_2$, $u = -1$. The switching time t_1 and the rendez-vous completion time t_2 are the unknown parameters of the control law. At $t > t_2$ both vehicles will move at the same speed $u = b$. As follows from the rendez-vous law (21.23), $\ddot{x} = \dot{x} = 0$.

Determine t_1 and t_2 using the equations of the system and the boundary conditions. Introducing the normalized time $\tau = \frac{t}{T}$, rewrite the differential equation (21.23) of the rendez-vous law

$$\frac{dx_2}{d\tau} + x_2 = u - b \tag{22.83}$$

The boundary conditions take the form

$$x_1(0) = -a, \quad x_1(\tau_2) = 0, \quad x_2(0) = -b, \quad x_2(\tau_2) = 0 \tag{22.84}$$

Substituting $u = +1$ on the interval $[0, \tau_1]$ into (22.83) gives

$$\dot{x}_2 + x_2 = 1 - b$$

whence

$$x_2 = (1 - b) + Ce^{-\tau} \qquad (0 \leqslant \tau \leqslant \tau_1) \tag{22.85}$$

The integration constant C is found from the initial condition $x_2(0) = -b$. Substituting $\tau = 0$ into Eq. (22.85) gives $C = -1$,

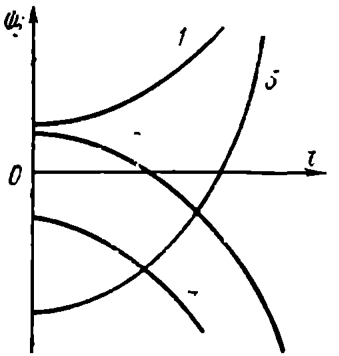

Fig. 22.5

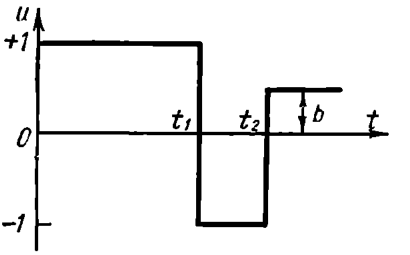

Fig. 22.6

and the law of variation of $x_2(\tau)$ can be rewritten as

$$x_2 = (1 - b) - e^{-\tau} \qquad (0 \leqslant \tau \leqslant \tau_1) \tag{22.86}$$

Integrating Eq. (22.86) with an allowance for the initial conditions $x_1(0) = -a$, define the law for $x_1(\tau)$ on the interval $[0, \tau_1]$

$$x_1(\tau) = -(a + 1) + (1 - b)\tau + e^{-\tau} \qquad (0 \leqslant \tau \leqslant \tau_1) \tag{22.87}$$

Substituting $\tau = \tau_1$ into Eqs. (22.86) and (22.87) calculate $x_1(\tau_1)$ and $x_2(\tau_2)$, which are the initial conditions for the differential equation of motion on the second interval $\tau_1 < \tau \leqslant \tau_2$, where $u = -1$

$$\left.\begin{aligned} x_1(\tau_1) &= -(a+1) + (1-b)\tau_1 + e^{-\tau_1} \\ x_2(\tau_1) &= (1-b) - e^{-\tau_1} \end{aligned}\right\} \tag{22.88}$$

Write the motion equation for $\tau_1 < \tau \leqslant \tau_2$

$$\dot{x}_2 + x_2 = -(1 + b) \tag{22.89}$$

Integrating Eq. (22.89) with an allowance for the initial conditions (22.88), we have

$$x_2(\tau) = -(1+b) + (2-e^{-\tau_1})\, e^{-(\tau-\tau_1)} \qquad (\tau_1 < \tau \leqslant \tau_2) \quad (22.90)$$

The law for $x_1(\tau)$ on the interval $\tau_1 < \tau \leqslant \tau_2$ is found by integrating Eq. (22.90), taking into account the initial conditions (22.88)

$$x_1(\tau) = (1-a+2\tau_1) - (1+b)\,\tau - (2-e^{-\tau_1})\, e^{-(\tau-\tau_1)}$$
$$(\tau_1 < \tau \leqslant \tau_2) \qquad (22.91)$$

By the problem conditions at the completion of the process $x_1(\tau_2) = x_2(\tau_2) = 0$; therefore, substituting $\tau = \tau_2$ into Eqs. (22.90) and (22.91), we get a system of equations for defining the instances τ_1 and τ_2

$$-(1+b) + (2-e^{-\tau_1})\, e^{-(\tau_2-\tau_1)} = 0$$
$$(1-a+2\tau_1) - (1+b)\,\tau_2 - (2-e^{-\tau_1})\, e^{-(\tau_2-\tau_1)} = 0$$

Elementary transformations of this system yield a simpler pair of equations

$$\tau_2 = \frac{2\tau_1 - a - b}{1+b}$$

$$\tau_2 = \tau_1 + \ln\frac{2-e^{-\tau_1}}{1+b} \qquad (22.92)$$

Considering these equations as functions of the form $\tau_2 = \varphi_1(\tau_1)$ and $\tau_2 = \varphi_2(\tau_1)$, the appropriate plots can be constructed in a plane with coordinates τ_1 and τ_2 (Fig. 22.7); their intersection defines the desired instants τ_{1des}, τ_{2des}.

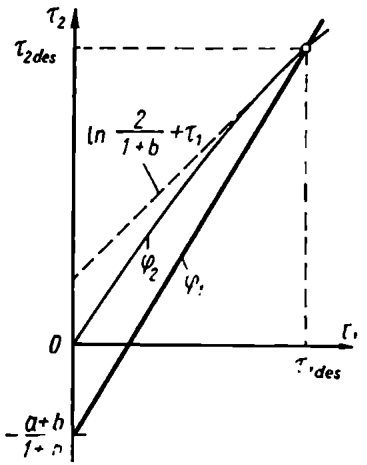

Fig. 22.7

The theorem of n intervals. The specific feature of optimal controls in Examples 22.6-22.8 is that the control action is a piecewise-constant function taking on boundary values and having at most two constancy intervals. It is important to note that all the three problems are linear, i.e. the system equations and the functional are linear and, besides, in all the three problems the characteristic equations of the system have real roots. Indeed, in Examples 22.6 and 22.7 the characteristic equation has the form $p^2 = 0$ and the respective roots are $p_1 = p_2 = 0$; in Example 22.8 the characteristic equation $p(pT+1) = 0$ has roots $p_1 = 0$, $p_2 = -\frac{1}{T}$.

The presence of at most two constancy intervals is a particular case of the optimal control law for linear problems with real roots of the nth-order characteristic equation. This law is called the theorem of n intervals.

For an nth-order linear system in which all roots of the characteristic equation are real and the control is constrained by the inequality $|u| \leqslant 1$, the optimal control $u(t)$ extremizing a linear functional is a piecewise-constant function which takes on boundary values of ± 1 and has at most n constancy intervals.

This theorem was originally formulated and proved by A.A. Feldbaum in 1949 without the use of the variational methods and by reasoning similar to that given in Sec. 21.3 when proving the optimality of piecewise-constant control for a simple second-order system. In the original formulation the roots were to be nonpositive as well as real. This constraint resulted from the presumption that the controlled system is stable, although the theorem also holds for positive roots.

Prove the theorem of n intervals by using the maximum principle. The system is presumed to be described by a linear equation with real roots of the characteristic equation

$$a_0 \frac{d^n y}{dt^n} + a_1 \frac{d^{n-1} y}{dt^{n-1}} + \ldots + a_n y = bu$$

where $a_0, \ldots, a_n$ and b are coefficients, and u is constrained by the inequality $|u| \leqslant 1$.

Assume also that the functional is linear and, for simplicity, is independent of control.

Denoting $y = y_1$, the system of equations for the problem can be given as

$$\begin{aligned} dy/dt &= \dot{y}_1 = y_2 \\ d^2y/dt^2 &= \dot{y}_2 = y_3 \\ &\ldots\ldots\ldots \\ d^n y/dt^n &= \dot{y}_n = \frac{b}{a_0} u - 1/a_0 (a_1 y_n + a_2 y_{n-1} + \ldots + a_n y_1) \end{aligned} \quad (22.93)$$

Write the function

$$\begin{aligned} H = \sum_{i=1}^{n} \psi_i f_i = \psi_1 y_2 + \psi_2 y_3 + \ldots + \psi_{n-1} y_n - \\ - \psi_n \frac{1}{a_0} (a_1 y_n + a_2 y_{n-1} + \ldots + a_n y_1) + \psi_n \frac{b}{a_0} u \end{aligned} \quad (22.94)$$

Only the last addend in Eq. (22.94) depends on the control u, therefore H is at a maximum when

$$\psi_n \frac{b}{a_0} u = \max_{|u| \leqslant 1} \quad (22.95)$$

From the condition (22.95) follows the obvious equality defining the optimal control law

$$u(t) = \operatorname{sign} \psi_n(t) \tag{22.96}$$

i.e. the function $u(t)$ can only be $+1$ or -1 and changes sign as many times as $\psi_n(t)$ intersects the time axis.

The function $\psi_n(t)$ is determined from the corresponding differential equations (22.66)

$$\begin{aligned}
\frac{d\psi_1}{dt} &= -\frac{\partial H}{\partial y_1} = \psi_n \frac{a_n}{a_0} \\
\frac{d\psi_2}{dt} &= -\frac{\partial H}{\partial y_2} = \psi_n \frac{a_{n-1}}{a_0} - \psi_1 \\
&\cdots\cdots\cdots\cdots\cdots \\
\frac{d\psi_n}{dt} &= -\frac{\partial H}{\partial y_n} = \psi_n \frac{a_1}{a_0} - \psi_{n-1}
\end{aligned} \tag{22.97}$$

Subtract from the first equation of the system (22.97) all others, having previously differentiated the second equation once and multiplied it by $(-1)^1$, differentiated the third one twice and multiplied it by $(-1)^2$, and so on; the last equation is differentiated $(n-1)$ times and multiplied by $(-1)^{n-1}$:

$$(-1)^{n-1} \frac{d^n \psi_n}{dt^n} = \frac{a_n}{a_0} \psi_n - (-1) \frac{a_{n-1}}{a_0} \frac{d\psi_n}{dt} - \ldots - (-1)^{n-1} \frac{a_1}{a_0} \frac{d^{n-1}\psi_n}{dt^{n-1}}$$

or

$$(-1)^n a_0 \frac{d^n \psi_n}{dt^n} + (-1)^{n-1} a_1 \frac{d^{n-1}\psi_n}{dt^{n-1}} + \ldots + (-1)^1 a_{n-1} \frac{d\psi_n}{dt} - a_n \psi_n = 0 \tag{22.98}$$

The roots of the corresponding characteristic equation

$$(-1)^n a_0 p^n + (-1)^{n-1} a_1 p^{n-1} + \ldots + (-1)^1 a_{n-1} p - a_n = 0 \tag{22.99}$$

differ, by virtue of the Viet theorem, from those of the system characteristic equation only in the sign, or, in other words, are also real. Assume for simplicity that the roots of Eq. (22.99) are simple; then

$$\psi_n(t) = \sum_{i=1}^{n} C_i e^{p_i t} \tag{22.100}$$

From Eq. (22.100) it is seen that the function $\psi_n(t)$, as a sum of n exponents with real powers, changes sign no more than $(n-1)$ times, therefore the control $u(t) = \operatorname{sign} \psi_n(t)$ has at most n constancy intervals.

If the roots of the characteristic equation are complex-conjugate or the control problem is nonlinear, then the theorem of n intervals is not valid. This can be seen from the following examples.

Example 22.9. Consider Problem 7 of Sec. 21.2 on a speed-optimal control of a conservative plant described by the equation

$$\ddot{y} + y = u$$

where $|u| \leqslant 1$; the boundary conditions are given by the equalities

$$y_1(0) = -1, \qquad y_1(T) = 0$$
$$y_2(0) = 0, \qquad y_2(T) = 0$$

Here T is the duration of the optimal process. We introduce the notation $y_1 = y$, $y_2 = \dot{y}$. The objective thus consists in speed-optimal transfer of the describing point y_1, y_2 from the position -1, 0 to the origin of coordinates.

Write the system of equations for the control problem

$$\dot{y}_1 = y_2, \qquad \dot{y}_2 = u - y_1 \tag{22.101}$$

Write the function

$$H = \sum_{i=1}^{2} \psi_i f_i = \psi_1 y_2 - \psi_2 y_1 + \psi_2 u \tag{22.102}$$

From Eq. (22.102) H is seen to be at a maximum when

$$u = \operatorname{sgn} \psi_2 \tag{22.103}$$

The system of equations for the auxiliary functions ψ_1 and ψ_2 is

$$\left.\begin{aligned} \frac{d\psi_1}{dt} &= -\frac{\partial H}{\partial y_1} = \psi_2 \\ \frac{d\psi_2}{dt} &= -\frac{\partial H}{\partial y_2} = -\psi_1 \end{aligned}\right\} \tag{22.104}$$

Direct Laplace transformation gives

$$\left.\begin{aligned} p\Psi_1(p) - \Psi_1(0) &= \Psi_2(p) \\ p\Psi_2(p) - \Psi_2(0) &= \Psi_1(p) \end{aligned}\right\} \tag{22.105}$$

From Eq. (22.105) we have

$$\Psi_2(p) = \frac{\psi_1(0) + \psi_2(0)}{p^2 + 1}$$

An inverse Laplace transformation gives

$$\psi_2(t) = A \sin(t + \alpha_0) \tag{22.106}$$

and from the first Eq. (22.104)

$$\psi_1(t) = -A \cos(t + \alpha_0)$$

where A and α_0 are constant and satisfy the relations

$$A \sin \alpha_0 = \psi_2 (0)$$
$$-A \cos \alpha_0 = \psi_1 (0)$$

Substituting Eq. (22.106) into (22.103), write the optimal contrc law in the final form

$$u = \text{sign} [\sin (t + \alpha_0)] \qquad (22.107$$

The function $u(t)$ is thus obtained from the function sign (sin equal alternately to $+1$ and -1 on intervals of length π by mean of a shift by the length α_0 (Fig. 22.8).

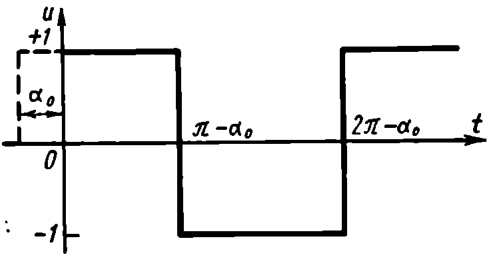

Fig. 22.8

Consider the phase trajectories of the system in optimal control Let $u = +1$; then, substituting this value into the system of plant equations (22.101), write

$$\dot{y}_1 = y_2$$
$$\dot{y}_2 = 1 - y_1 \qquad (22.108)$$

The first equation in (22.108) will not change if we substitute $(y_1 - 1)$ for y_1. Then we have a system of equations

$$\frac{d}{dt}(y_1 - 1) = y_2$$

$$\frac{d}{dt} y_2 = -(y_1 - 1)$$

which is formally identical to Eqs. (22.104) already solved. Consequently

$$y_1 - 1 = A \sin (t + \alpha_0)$$
$$y_2 = -A \cos (t + \alpha_0)$$

whence

$$(y_1 - 1)^2 + y_2^2 = A^2 \qquad (22.109)$$

Equation (22.109) defines, in the phase plane with coordinates y_1, y_2, a family of concentric circles with centre at the point $+1$, 0

(Fig. 22.9*a*). The describing point moves uniformly along the phase trajectory (over the period π it covers exactly half the circle).

At $u = -1$ similar reasoning leads to the equation of phase trajectories

$$(y_1 + 1)^2 + y_2^2 = A^2 \qquad (22.110)$$

which are also concentric circles, but with centre at the point $-1, 0$ (Fig. 22.9*b*).

Assume that on the final time interval of duration β the control $u = +1$. Because the control objective is to reach the origin of coordinates, the motion of the system can be represented by the arc AO

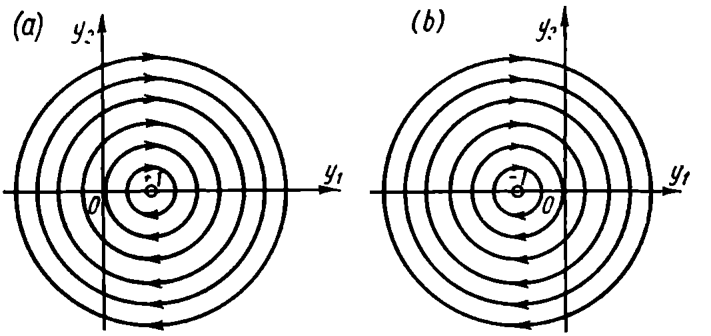

Fig. 22.9

of the circle (22.109) passing through the origin of coordinates (Fig. 22.10). This arc does not exceed one half of the circle because $\beta \leqslant \pi$.

The describing point reaches the point A after moving during a time interval of length π under the effect of a control having the opposite sign, i.e. at $u = -1$. This means that the appropriate portion of the phase trajectory is a half-circle BA with centre at the point $-1, 0$ terminating at point A. The point B is clearly symmetrical to the point A relative to the point $-1, 0$ and is located on the half-circle N_1N_2, which is symmetrical to the half-circle M_1O with the same centre of symmetry.

In a similar way the arc BC, preceding the arc BA and representing a time interval of length π on which $u = +1$, is equal to a half-circle with centre at the point $+1, 0$; therefore the point C lies on the half-circle M_2M_3, which is symmetrical to the half-circle N_1N_2 with centre of symmetry at the point $+1, 0$.

Using the same technique we can obtain system phase trajectories when the control on the final interval is $u = -1$ (not $+1$). Combining both possibilities ($u = +1$ and $u = -1$ on the final time interval) gives a complete picture of phase trajectories (Fig. 22.11). In the figure the appropriate values of control, $+1$ or -1, are speci-

fied. For all phase trajectories located above the line ... ... $M_3M_2M_1ON_1N_2N_3$ ..., made up of an infinite number of half-

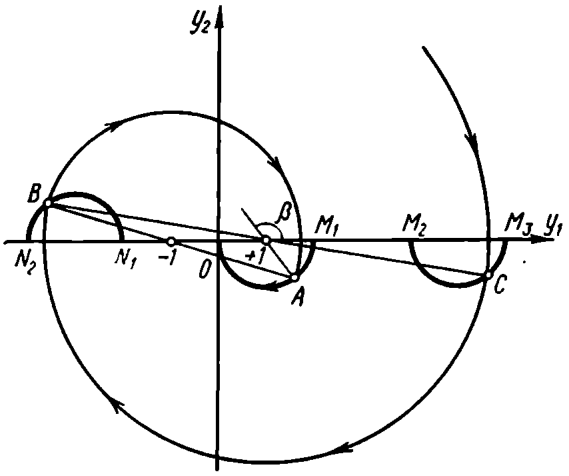

Fig. 22.10

circles of radius 1, the control is seen to be $u = -1$, while for trajectories below that line, $u = +1$.

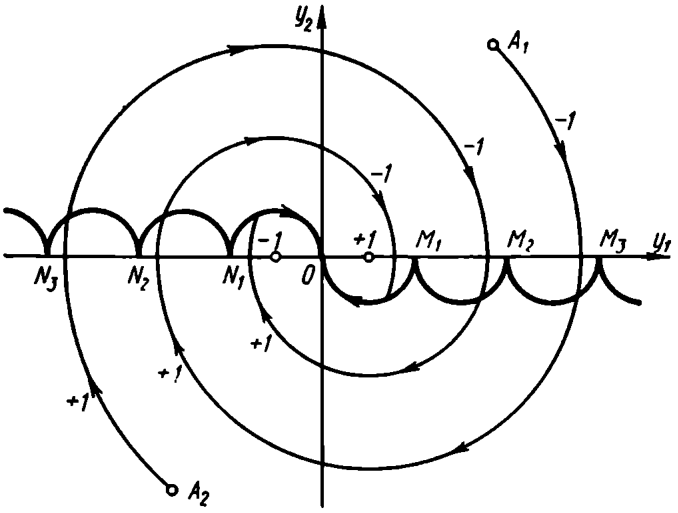

Fig. 22.11

Consequently, the signs of control alternate on that line which was termed the *switching line* in Sec. 21.3.

In the example cited two problems were stated: (1) find the optimal control shifting the system from the point $-1, 0$ to the origin of coordinates, and (2) ascertain that the theorem of n intervals does not hold in the case of complex roots of the characteristic equation.

The characteristic equation of the system $p^2 + 1 = 0$ has a pair of pure imaginary roots $p_{1,2} = \pm j$, while there can be more than two constancy intervals; their number depends entirely on initial conditions. For instance, the optimal processes which take the system from the point A_1 or A_2 into the origin of coordinates are seen (Fig. 22.11) to consist of four such intervals.

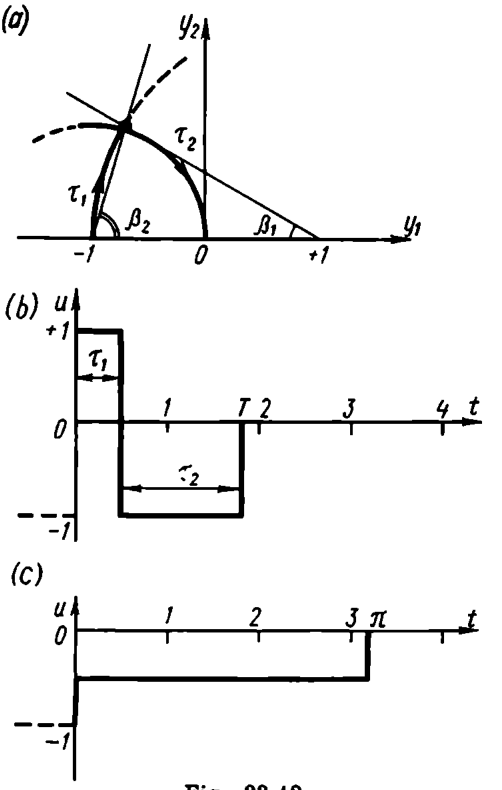

Fig. 22.12

The optimal control taking the system from the point $-1, 0$ to the origin of coordinates of the phase plane (Fig. 22.12*a*) consists of two intervals of duration $\tau_1 (u = +1)$ and $\tau_2 (u = -1)$, respectively. The duration of intervals is determined simply by measuring the angles β_1 and β_2 corresponding to the arcs τ_1 and τ_2 of circles with centres at the points $+1, 0$ and $-1, 0$. Here $\tau_1 = 0.52$ ($\beta_1 = 30°$), $\tau_2 = 1.28$ ($\beta_2 = 73°$), and the overall time of the optimal process is $\tau = \tau_1 + \tau_2 = 1.8$.

The optimal control thus obtained (Fig. 22.12*b*) can be usefully compared with the quasi-optimal control of Sec. 21.4 (Fig. 22.12*c*). The dotted lines for $t < 0$ show that the initial position is associated with the control parameter value $u = -1$. The quasi-optimal control lasts π units of time. The optimal control thus transfers the system from the initial to the final state $\frac{\pi}{1.8} \approx 1.74$ times faster than the quasi-optimal control.

Example 22.10. Let us again take up Problem 5 of Sec. 21.2 on efficiency-optimal control of a plant with an equation $\ddot{y} = u$, which has already been solved in Example 22.1 with the aid of the Euler

equation. In this case the functional $Q = \int_0^T u^2(t)\,dt$ is a nonlinear function of control. Introducing coordinates $y_1 = y$, $y_2 = \dot{y}$ and $y_0 = \int_0^T u^2(t)\,dt$, write a system of equations describing the problem

$$\begin{aligned} \dot{y}_0 &= u^2 \\ \dot{y}_1 &= y_2 \\ \dot{y}_2 &= u \end{aligned} \tag{22.111}$$

Write the function

$$H = \sum_{i=0}^{2} \psi_i \dot{y}_i = \psi_0 u^2 + \psi_1 y_2 + \psi_2 u \tag{22.112}$$

Find the value of u maximizing the function H by solving the equation

$$\frac{\partial H}{\partial u} = 2\psi_0 u + \psi_2 = 0$$

We have

$$u(t) = -\frac{\psi_2(t)}{2\psi_0(t)} \tag{22.113}$$

Write equations for the functions $\psi_i(t)$

$$\frac{d\psi_0}{dt} = -\frac{\partial H}{\partial y_0} = 0$$

$$\frac{d\psi_1}{dt} = -\frac{\partial H}{\partial y_1} = 0$$

$$\frac{d\psi_2}{dt} = -\frac{\partial H}{\partial y_2} = -\psi_1$$

whence

$$\begin{aligned} \psi_0 &= \text{const} = C_0 \\ \psi_1 &= \text{const} = C_1 \\ \psi_2 &= C_2 - C_1 t \end{aligned} \tag{22.114}$$

Substituting the expressions for ψ_0 and ψ_2 from Eqs. (22.114) into the optimal control law (22.113), we find

$$u(t) = -\frac{C_2 - C_1 t}{C_0} = a_1 - a_2 t \tag{22.115}$$

This result coincides with (22.14) obtained in Example 22.1 which also elucidates methods for determining integration constants

It is noteworthy that extremals in problems with nonlinear equations can be functions other than piecewise-constant, which means that the theorem of n intervals is indeed inapplicable.

As can be seen from the examples the maximum principle is the most effective and simple way to find the optimal control law in the case of linear problems with constraints given as inequalities. The effectiveness of this method is even more pronounced in linear problems with several control actions which can not be readily solved by other methods.

Example 22.11. Consider a second-order linear system with two control parameters, u_1 and u_2, subject to constraints $|u_1| \leqslant a$, $|u_2| \leqslant b$. Assume that the system constraints can be represented in the form

$$\begin{aligned} \dot{y}_1 &= f_1(y_1, y_2) + u_1 \\ \dot{y}_2 &= f_2(y_1, y_2) + u_2 \end{aligned} \tag{22.116}$$

Write the function

$$H = \sum_{i=1}^{2} \psi_i \dot{y}_i = \psi_1 f_1 + \psi_1 u_1 + \psi_2 f_2 + \psi_2 u_2 \tag{22.117}$$

Thence it follows that H is at its maximum when

$$\psi_1 u_1 + \psi_2 u_1 = \max_{\substack{|u_1| \leqslant a \\ |u_2| \leqslant b}}$$

Consequently, the optimal control law is

$$\begin{aligned} u_1 &= a \operatorname{sign} \psi_1 \\ u_2 &= b \operatorname{sign} \psi_2 \end{aligned} \tag{22.118}$$

From this equation it follows that the optimal control is represented by the vertices of a rectangle bounding the feasible controls region in the plane with coordinates u_1, u_2. The instants of passing from one vertex to another can be determined once the functions ψ_1 and ψ_2 are found.

Finding the initial values of the functions $\varphi_i(t)$. In all the above examples where the maximum principle is applied we managed to establish the optimal control law. The control action was defined in terms of functions $\psi_i(t)$. The values of coefficients in formulae defining $\psi_i(t)$ were not found, however. Once the form of optimal control was found in the general form, we turned to the initial equations of the problem and to the physical meaning to find the parameters of the control functions.

We did so, however, not for the sake of illustrativeness, but because so far there are unfortunately no formulae for finding the initial values $\psi_i(0)$ of the functions $\psi_i(t)$, and these values have to be known

for a complete solution of the system $\frac{d\psi_i}{dt} = -\frac{dH}{dy_i}$ determining the functions $\psi_i(t)$.

All the available procedures for finding $\psi_i(0)$ (Ref. 12) use successive approximations (iterations) starting with a certain initial set of values $\psi_i^0(0)$ (first approximation) and ending with the final set $\psi_i^*(0)$, the solution of the optimal problem.

Let us consider one of the possible ways to determine the vector $\psi^*(0)$ with coordinates $\psi_i^*(0)$. An arbitrary zero approximation $\psi^0(0)$ gives the corresponding control $u^0(t)$ and the trajectory $y^0(t)$ in the phase space (Fig. 22.13). If $\psi^0(0)$ is taken at random, there is little chance that the trajectory $y^0(t)$ will reach the origin of coordinates. The objective of control is presumed to be transition from the point M to the origin of coordinates. The adopted measure of proximity of the trajectory thus obtained to the desired one is the distance r^0 from the origin of coordinates to that trajectory. The subsequent approximations $\psi^j(0)$ are selected so that the distance r^j reduces from one iteration to another. The desired value $\psi^*(0)$ is clearly associated with $r^* = 0$. The ways to find the parameter values (in our case $\psi_i(0) = 0$) minimizing the relevant function (in this case r) are treated in Ch. XXVI.

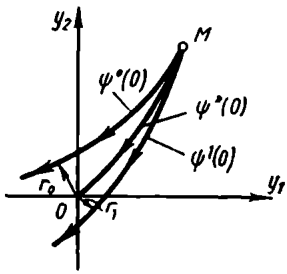

Fig. 22.13

The maximum principle and the Euler equation. The maximum principle is one of the variational methods and gives solutions identical to those obtained by the Euler equation (cf. Examples 22.1 and 22.10 or 22.5 and 22.6). Furthermore, the maximum principle permits including discontinuous (piecewise-continuous) functions in the class of extremals. It is natural to assume that with no constraints on the class of desired extremals the maximum principle gives optimality conditions identical to those given by the Euler equation.

Indeed, assume that a plant is described by the equation

$$\dot{y} = u \tag{22.119}$$

The functional is the definite integral $Q = \int_0^T G[u, y, t]\,dt$. Introducing the notation $y_0 = \int_0^t G[u, y, t]\,dt$, $y_1 = y$, write a system of

equations

$$\left.\begin{aligned}\dot{y}_0 &= G[u, y, t]\\ \dot{y}_1 &= u\end{aligned}\right\} \tag{22.120}$$

Write the function H and a system of equations for the functions ψ_i:

$$H = \psi_0 G[u, y, t] + \psi_1 u \tag{22.121}$$

$$\left.\begin{aligned}\frac{d\psi_0}{dt} &= -\frac{\partial H}{\partial y_0} = 0\\ \frac{d\psi_1}{dt} &= -\frac{\partial H}{\partial y_1} = -\frac{\partial H}{\partial y} = -\psi_0 \frac{\partial G[u, y, t]}{\partial y}\end{aligned}\right\} \tag{22.122}$$

Determine the value of u maximizing the function H

$$\frac{\partial H}{\partial u} = \psi_0 \frac{\partial G[u, y, t]}{\partial u} + \psi_1 = 0 \tag{22.123}$$

From the first equation of the system (22.122) $\psi_0 = \text{const}$. Assume that $\psi_0 = -1$ and substitute this value into Eq. (22.123). Then

$$\psi_1 = \frac{\partial G[u, y, t]}{\partial u} \tag{22.124}$$

On the other hand, substituting $\psi_0 = -1$ into the second equation of the system (22.122) and integrating, we have

$$\psi_1 = C_1 + \int_0^t \frac{\partial G[u, y, \tau]}{\partial y}\, d\tau \tag{22.125}$$

Equating the right-hand parts of (22.124) and (22.125) gives the Euler equation in the integral form

$$\frac{\partial G[u, y, t]}{\partial u} = C_1 + \int_0^t \frac{\partial G[u, y, \tau]}{\partial y}\, d\tau \tag{22.126}$$

Differentiating both parts of Eq. (22.126) with respect to time with $u = \dot{y}$ (see Eq. 22.119) and introducing the notation of Sec. 22.1, $\frac{dG}{dy} = G_y$, $\frac{dG}{d\dot{y}} = G_{\dot{y}}$, gives $G_y - \frac{d}{dt} G_{\dot{y}} = 0$.

This expression coincides with the Euler equation (22.2) with an accuracy to notation.

22.4. DYNAMIC PROGRAMMING AND ITS APPLICATION TO OPTIMAL CONTROL

The principle of optimality. The Bellman equation. Variational calculus may be regarded as an extension of differential calculus to N variables. Indeed, the function $u(t)$ in the functional $Q =$

$= \int_{t_0}^{T} G[u, y, t]\, dt$ can be replaced by a broken line with breakings $u_0 = u(t_0)$, $u_1 = u(t_0 + \Delta t)$, . . ., $u_N = u(t_0 + N\Delta t)$ and the functional, by the sum

$$Q = \sum_{i=0}^{N} G[u_i, y_i, t_i]\, \Delta t$$

where N and Δt are related as $N\Delta t = T - t_0$, $t_i = t_0 + i\Delta t$.

This done, the variational problem can be roughly regarded as a common extremal problem for the function $Q(t_1, \ldots, t_N)$ of N variables. With increasing N the solution of this problem will progressively approach the solution of the variational problem. The process of solution is regarded as a single act and is referred to as a *one-step process.*

The conventional methods of finding the extremum of a function of many variables may prove inapplicable when their number is great, and therefore the values of the functions $u(t_i)$ should be evaluated gradually, step by step, rather than at once, in one step. Such processes are known as *multistep processes.*

Multistep processes can yield solutions to optimization problems in various fields of science, technology, and economy. The mathematical tool used is dynamic programming developed largely by R. Bellman and his associates in the 1950's.

R. Bellman explains the terms (Ref. 6) in these words:

"The title is also derived in this way. The problems we treat are programming problems, to use a terminology now popular. The adjective "dynamic", however, indicates that we are interested in processes in which time plays a significant role and in which the order of operation may be crucial."

To illustrate the use of the method of dynamic programming we will consider speed-optimal transition from the phase state $\mathbf{y}_0$ to $\mathbf{y}_{fin}$. The final phase point $\mathbf{y}_{fin}$ is assumed fixed and the initial point $\mathbf{y}_0$ is chosen from among various points of the phase space.

We assume that for any point y other than $\mathbf{y}_{fin}$ there is an optimal control $\mathbf{u}_y(t)$ which carries the plant from $\mathbf{y}_0$ to $\mathbf{y}_{fin}$. The time of transition is denoted as T (y) and cannot be less than T (y), otherwise $\mathbf{u}_y(t)$ could not be optimal.

Assuming T (y) = const this equation defines, in the phase space y $(y_1, y_2, \ldots, y_N)$, the locus of points for which the time of optimal transition to $\mathbf{y}_{fin}$ is the same. Such loci are called *isochrons.*

In further considerations T (y) can be replaced by the function S (y) which differs only in sign

$$S(\mathbf{y}) = -T(\mathbf{y}) \qquad (22.127)$$

Assume that the function S (y) is continuous and has continuous partial derivatives

$$\frac{\partial S}{\partial y_1}, \ldots, \frac{\partial S}{\partial y_n}$$

everywhere except the point y_{fin}.

If the plant has started its motion from the point $\mathbf{y}_0$ at the time t_0 along an arbitrary phase trajectory, then a certain point $\mathbf{y}(t)$ is reached after the time $(t - t_0)$. If the plant moves from the point $\mathbf{y}(t)$ to $\mathbf{y}_{fin}$ along the optimal trajectory, the motion is completed within the time $T[\mathbf{y}(t)]$. As a result, the time of transition from $\mathbf{y}_0$ to $\mathbf{y}_{fin}$ is $(t - t_0) + T[\mathbf{y}(t)]$. But since the optimal time of motion from $\mathbf{y}_0$ to $\mathbf{y}_{fin}$ is equal to $T[\mathbf{y}(t_0)]$, then

$$T[\mathbf{y}(t_0)] \leqslant (t - t_0) + T[\mathbf{y}(t)] \tag{22.128}$$

Replacing the function T by S (see Eq. (22.127)) and dividing both parts of the inequality by the positive quantity $(t - t_0)$ gives

$$\frac{S[\mathbf{y}(t)] - S[\mathbf{y}(t_0)]}{t - t_0} \leqslant 1$$

or, going to the limit as $t \to t_0$, we get

$$\frac{d}{dt} S[\mathbf{y}(t)]\,|_{t=t_0} \leqslant 1 \tag{22.129}$$

The derivative in the left-hand part of this inequality exists because the functions S (y) and $\mathbf{y}(t)$ are differentiable, and it is computed by the formula of the complete derivative

$$\frac{d}{dt} S[\mathbf{y}(t)] = \sum_{i=1}^{n} \frac{\partial S}{\partial y_i} \dot{y}_i(t)$$

Assuming that the plant motion is described by a system of first-order equations of the form $\dot{y}_i = f_i(\mathbf{u}, \mathbf{y})$, rewrite the inequality (22.129)

$$\sum_{i=1}^{n} \frac{\partial S(\mathbf{y}_0)}{\partial y_i} f_i(\mathbf{u}_0, \mathbf{y}_0) \leqslant 1$$

Here the points $\mathbf{u}_0$ and $\mathbf{y}_0$ are arbitrary, therefore for any point y of the phase space other than $\mathbf{y}_0$ and for any point u of the control region the relation

$$\sum_{i=1}^{n} \frac{\partial S(\mathbf{y})}{\partial y_i} f_i(\mathbf{u}, \mathbf{y}) \leqslant 1 \tag{22.130}$$

holds.

Assume now that $[\mathbf{u}(t), \mathbf{y}(t)]$ is an optimal process which carries the plant from the phase state $\mathbf{y}_0$ to the state $\mathbf{y}_{fin}$ and $t_0 \leqslant t \leqslant t_{fin}$ is the time of this optimal motion; so $\mathbf{y}(t_0) = \mathbf{y}_0$, $\mathbf{y}(t_{fin}) = \mathbf{y}_{fin}$ and $t_{fin} = t_0 + T(\mathbf{y}_0)$. The equation of the associated optimal trajectory is found by the plant equations $\dot{y}_i = f_i(\mathbf{u}, \mathbf{y})$. The motion along this trajectory from the point $\mathbf{y}_0$ to $\mathbf{y}(t)$ is completed within the time $(t - t_0)$, and from the point $\mathbf{y}(t)$ to $\mathbf{y}_{fin}$, within $T[\mathbf{y}(t)]$. Because the overall time of motion from $\mathbf{y}_0$ to $\mathbf{y}_{fin}$ along the optimal trajectory is equal to $T(\mathbf{y}_0)$, we can write

$$T[\mathbf{y}(t_0)] = (t - t_0) + T[\mathbf{y}(t)] \qquad (22.131)$$

This equality seems simple and evident, but it serves as a formal representation of the principle of optimality, which is the core of dynamic programming. Bellman's formulation of the principle of optimality is:

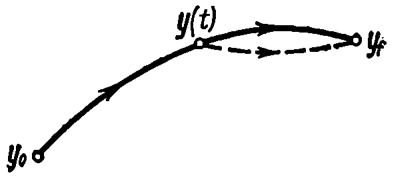

Fig. 22.14

"Principle of optimality. An optimal policy has the property that whatever the initial state and initial decisions are, the remaining decisions must constitute an optimal policy with regard to the state resulting from the first decision."

Thence follows the equality (22.131): if $\mathbf{y}(t)$ is the optimal trajectory for $t_0 \leqslant t \leqslant t_{fin}$, then for any intermediate point $t_0 < t < t_{fin}$ the final portion of the trajectory on the interval t, t_{fin} is also the optimal trajectory. The principle of optimal control in general and the equality (22.131) in particular are easily proved by *reductio ad absurdum*. Indeed, let there exist a trajectory (the dotted line in Fig. 22.14) along which transition from the point $\mathbf{y}(t)$ to the point $\mathbf{y}_{fin}$ is completed within a time less than $T(\mathbf{y}_0) - (t - t_0)$. Then transfer from $\mathbf{y}_0$ to $\mathbf{y}(t)$ within the time $(t - t_0)$, and from $\mathbf{y}(t)$ to $\mathbf{y}_{fin}$ within a time less than $T(\mathbf{y}_0) - (t - t_0) = T[\mathbf{y}(t)]$ would lead to transition from the point $\mathbf{y}_0$ to the point $\mathbf{y}_{fin}$ within a time less than $T(\mathbf{y}_0)$, which contradicts the optimal nature of the process $[\mathbf{y}(t), \mathbf{u}(t)]$.

Equality (22.131) has thus been proved. Replacing T by $-S$ in Eq. (22.131), we have

$$S[\mathbf{y}(t)] = S[\mathbf{y}(t_0)] + t - t_0$$

and differentiation with respect to time gives

$$\sum_{i=1}^{n} \frac{\partial S[\mathbf{y}(t)]}{\partial y_i} f_i[\mathbf{y}(t), \mathbf{u}(t)] = 1 \qquad (22.132)$$

Introduce the notation

$$H(\mathbf{u}, \mathbf{y}) = \sum_{i=1}^{n} \frac{\partial S[\mathbf{y}(t)]}{\partial y_i} f_i[\mathbf{y}(t), \mathbf{u}(t)] \tag{22.133}$$

Then the relations (22.130) and (22.132) may be written as

$$\begin{cases} H(\mathbf{u}, \mathbf{y}) \leqslant 1 \text{ for an arbitrary feasible process} \\ H(\mathbf{u}, \mathbf{y}) = 1 \text{ for an optimal feasible process} \end{cases}$$

Collating these conditions gives

$$\max_{\mathbf{u} \in \Omega} H(\mathbf{u}, \mathbf{y}) = 1$$

or, with an allowance for the notation (22.133),

$$\max_{\mathbf{u} \in \Omega} \sum_{i=1}^{n} \frac{\partial S[\mathbf{y}]}{\partial y_i} f_i(\mathbf{y}, \mathbf{u}) = 1 \tag{22.134}$$

for any point $\mathbf{y} \neq \mathbf{y}_{fin}$.

This expression is known as the *Bellman equation.*

Let us consider the proof of the Pontriagin maximum principle and its geometrical interpretation as a first application of the Bellman equation.

Proof of the maximum principle. We continue our discussion by assuming the function $S(\mathbf{y})$ twice continuously differentiable (everywhere except $\mathbf{y}_{fin}$). Thence the function $H(\mathbf{u}, \mathbf{y})$ (see Eq. (22.133)) has the following continuous derivatives everywhere except the point $\mathbf{y}_{fin}$.

$$\frac{\partial H(\mathbf{y}, \mathbf{u})}{\partial y_j} = \sum_{i=1}^{n} \frac{\partial^2 S(\mathbf{y})}{\partial y_i \partial y_j} f_i(\mathbf{y}, \mathbf{u}) + \sum_{i=1}^{n} \frac{\partial S(\mathbf{y})}{\partial y_i} \frac{\partial f_i(\mathbf{y}, \mathbf{u})}{\partial y_j} \tag{22.135}$$

$$(j = 1, \ldots, n)$$

Since the function $H(\mathbf{y}, \mathbf{u})$ reaches a maximum on the optimal trajectory (see Eq. (22.134)), its partial derivatives with respect to y_j at the point $\mathbf{y}(t)$ on the optimal trajectory vanish

$$\sum_{i=1}^{n} \frac{\partial^2 S[\mathbf{y}(t)]}{\partial y_i \partial y_j} f_i[\mathbf{y}(t), \mathbf{u}(t)] + \sum_{i-1}^{n} \frac{\partial S[\mathbf{y}(t)]}{\partial y_i} \frac{\partial f_i[\mathbf{y}(t), \mathbf{u}(t)]}{\partial y_j} = 0 \tag{22.136}$$

Differentiate the function $\frac{\partial S[\mathbf{y}(t)]}{\partial y_j}$ with respect to time, bearing in mind that $\dot{y}_i = f_i[\mathbf{y}(t), \mathbf{u}(t)]$

$$\left[\frac{d}{dt} \frac{\partial S[\mathbf{y}(t)]}{\partial y_j}\right] = \sum_{i=1}^{n} \frac{\partial^2 S[\mathbf{y}(t)]}{\partial y_j \partial y_i} \dot{y}_i(t) = \sum_{i=1}^{n} \frac{\partial^2 S[\mathbf{y}(t)]}{\partial y_j \partial y_i} f_i[\mathbf{y}(t), \mathbf{u}(t)]$$

With an allowance for this equality rewrite the relation (22.136)

$$\frac{d}{dt}\left[\frac{\partial S[\mathbf{y}(t)]}{\partial y_j}\right]+\sum_{i=1}^{n}\frac{\partial S[\mathbf{y}(t)]}{\partial y_i}\frac{\partial f_i[\mathbf{y}(t),\ \mathbf{u}(t)]}{\partial y_j}=0 \qquad (22.137)$$

Note now that the function $S[\mathbf{y}(t)]$ does not appear in formula (22.137), which only includes the partial derivatives $\frac{\partial S}{\partial y_1}, \ldots, \frac{\partial S}{\partial y_n}$, so introduce the following notation

$$\frac{\partial S[\mathbf{y}(t)]}{\partial y_j}=\psi_j(t) \qquad (j=1, \ldots, n) \qquad (22.138)$$

With an allowance for this notation rewrite Eq. (22.137)

$$\frac{d\psi_j}{dt}=-\sum_{i=1}^{n}\psi_i\frac{\partial f_i[\mathbf{y}(t),\ \mathbf{u}(t)]}{\partial y_j} \qquad (22.139)$$

With an allowance for Eq. (22.138) the expressions (22.133) giving the functions H and (22.139) giving $\frac{d\psi_j}{dt}$ can be rewritten as

$$H=\sum_{i=1}^{n}\psi_i(t)\,f_i[\mathbf{y}(t),\ \mathbf{u}(t)] \qquad (22.140)$$

$$\frac{d\psi_i}{dt}=-\frac{\partial H}{\partial y_j} \qquad (22.141)$$

Turning to the relations (22.130) and (22.132) again, formulate the conditions to be satisfied by the function H

$$H[\mathbf{y}(t),\ \mathbf{u}(t)]=\sum_{i=1}^{n}\psi_i(t)\,f_i[\mathbf{y}(t),\ \mathbf{u}(t)]\leqslant 1 \quad \text{for an arbitrary feasible process}$$

$$H[\mathbf{y}(t),\ \mathbf{u}(t)]=\sum_{i=1}^{n}\psi_i(t)\,f_i[\mathbf{y}(t),\ \mathbf{u}(t)]=1 \quad \text{for an optimal feasible process}$$

whence it follows that for an optimal process

$$H[\mathbf{y}(t),\ \mathbf{u}(t)]=\max_{\mathbf{u}\in\Omega} \qquad (22.142)$$

Thus if $[\mathbf{u}(t),\ \mathbf{y}(t)]$ (where $t_0\leqslant t\leqslant t_{fin}$) is an optimal process, there are functions $\psi_i(t)$ such that the relations (22.142) and (22.141) hold, where the function H is determined by the formula (22.140). This is just the maximum principle which was treated above.

Consider now the geometrical interpretation of the maximum principle. If f_i and ψ_i are assumed to be components of the appropriate vectors $\mathbf{f}$ and $\boldsymbol{\psi}$ the function $H=\mathbf{f}\,\boldsymbol{\psi}$ is their scalar product.

The vector f (Fig. 22.15), whose components are first time derivatives of the phase coordinates $\dot{y}_i$, characterizes the rate of motion of the describing point in the phase space. The vector ψ, whose components are partial derivatives $\frac{\partial S[y(t)]}{\partial y_i} = -\frac{\partial T[y(t)]}{\partial y_i}$ (see Eq. (22.138)), is equal in magnitude to the gradient of the function $T[y(t)]$ and is directed towards reduction in the time of transition from $y(t)$ to y_{fin} (minus sign before $\frac{dT[y(t)]}{dy_i}$), i.e.

$$\psi(t) = -\text{grad } T[y(t)]$$

The requirement of the maximal scalar product $H = f\psi$ at given magnitudes of the rate $|f[y(t)]|$ and the gradient $|\text{grad } T[y(t)]|$ is associated with the requirement of maximal proximity of the directions of the vectors f and ψ.

Consequently, for speed-optimal control problems the maximum principle recommends that the control $u(t)$ be selected so that the point in the phase space move in a direction opposite to that of the gradient of isochrones or in the direction of the fastest reduction of the process time $T(y)$.

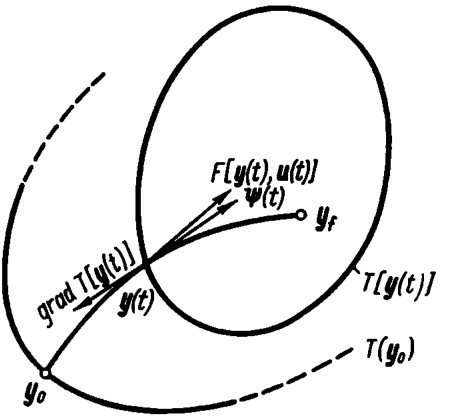

Fig. 22.15

Another illustration of the use of the Bellman equation is an optimal control problem in a simple second-order system.

Example 22.12. Let us consider Problem 1 of Sec. 21.2 on speed-optimal control of a plant with an equation $\ddot{y} = u$ and a constraint on control $|u| \leqslant 1$.

With a notation $y_1 = y$, $y_2 = \dot{y}$ the system of first-order equations describing the plant is of the form

$$\dot{y}_1 = y_2 = f_1(y, u)$$
$$\dot{y}_2 = u = f_2(y, u) \qquad (22.143)$$

Substituting it into Eq. (22.134) we can write

$$\max_{|u| \leqslant 1} \left\{ \frac{\partial S(y_1, y_2)}{\partial y_1} y_2 + \frac{\partial S(y_1, y_2)}{\partial y_2} u \right\} = 1 \qquad (22.144)$$

whence obviously follows

$$u = \text{sign} \frac{\partial S(y_1, y_2)}{\partial y_2} \qquad (22.145)$$

As follows from Eq. (22.145), the optimal process should be a piecewise-constant function which takes on extreme values ± 1, while the switching times are determined by the behaviour of the function $\frac{\partial S(y_1, y_2)}{\partial y_2}$.

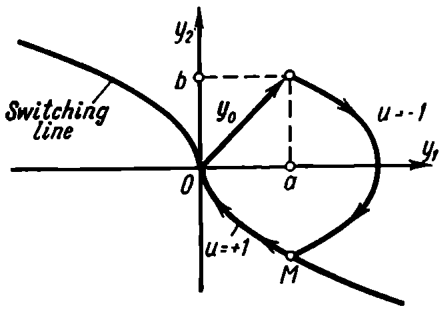

Fig. 22.16

To proceed with the solution, it is necessary to know the function $S(y_1, y_2)$ or the expression for isochrones $T(y_1, y_2) = -S(y_1, y_2)$.

Now turn to the phase plane of a simple optimal system (see Sec. 21.3). Let the point y_0 (Fig. 22.16), where the system starts its motion, be above the switching line. Denote the coordinates of this point as a, b. For the parabola (21.42), which corresponds to $u = -1$ (the equation $\frac{1}{2} y_2^2 = -y_1 + C$), to pass through the point y_0, one should know the coordinates of this point satisfying Eq. (21.42)

$$\frac{1}{2} b^2 = -a + C$$

Thence $C = a + \frac{1}{2} b^2$. Consequently, the parabola (21.42) passing through y_0 is given by the equation

$$y_1 = -\frac{1}{2} y_2^2 + a + \frac{1}{2} b^2 \qquad (22.146)$$

The switching point M (see Fig. 22.16) can be found as the point of intersection of the parabola (22.146) with the switching line, whose equation is (see Eq. (21.41))

$$y_1 = \frac{1}{2} y_2^2 \qquad (22.147)$$

In order to find the intersection point, Eqs. (22.146) and (22.147) should be solved simultaneously. Subtracting Eq. (22.147) from Eq. (22.146), we have $y_2^2 = a + \frac{1}{2} b^2$, whence $y_2 = \pm \sqrt{a + \frac{1}{2} b^2}$. The ordinate of the point M should be negative because it is below the x-line. Thus

$$y_{2M} = -\sqrt{a + \frac{1}{2} b^2} \qquad (22.148)$$

(The abscissa of the point is not needed.)

Since when moving from the point $\mathbf{y}_0$ to the point M the control $u = -1$, the motion equation is of the form $\dot{y}_2 = -1$, and therefore integration gives

$$y_{2M} - b = \int_{t_0}^{t} \dot{y}_2(\tau)\, d\tau = \int_{t_0}^{t} (-1)\, d\tau = t_0 - t \qquad (22.149)$$

where t is the switching time, or the time when the trajectory passes through the point M.

Similarly, when moving from the point M to the origin of coordinates $u = +1$, i.e. $\dot{y}_2 = +1$, and therefore

$$0 - y_{2M} = \int_{t}^{t_{fin}} \dot{y}_2(\tau)\, d\tau = \int_{t}^{t_{fin}} (+1)\, d\tau = t_{fin} - t \qquad (22.150)$$

where t_{fin} is the time of process completion, or of reaching the origin of coordinates.

Subtracting (22.149) from (22.150) and substituting y_{2M} from Eq. (22.148), we have

$$T(y_0) = t_{fin} - t_0 = b - 2y_{2M} = b + 2\sqrt{a + \frac{1}{b}b^2} \qquad (22.151)$$

This formula has been derived for the points $\mathbf{y}_0$ located on or above the switching line.

For points below the switching line the isochrone formula can be obtained by similar reasoning, but it is still simpler to consider a point with coordinates $-a$, $-b$ symmetrical to the point y_0 with respect to the origin of coordinates. Substituting $-a$ for a and $-b$ for b in Eq. (22.151), write

$$T(\mathbf{y}_0) = -b + 2\sqrt{-a + \frac{1}{2}b^2} \qquad (22.152)$$

Remembering that $T(\mathbf{y}_0) = -S(\mathbf{y}_0)$ and also that the initial point $\mathbf{y}_0$ is arbitrary and replacing $a = y_1$, $b = y_2$, write finally

$$S(y_1, y_2) = \begin{cases} -y_2 - 2\sqrt{y_1 + \frac{1}{2}y_2^2} & \text{if the point } (y_1, y_2) \text{ is on or above the switching line} \\ y_2 - 2\sqrt{-y_1 + \frac{1}{2}y_2^2} & \text{if the point } (y_1, y_2) \text{ is on or below the switching line} \end{cases}$$

A family of isochrones plotted for various values of T ($T = 1, 2, 3, 4$) is shown in Fig. 22.17. It only remains to introduce the expression found for $S(y_1, y_2)$ into the control law (22.145) and complete the calculation.

But the fact that the function $S(y_1, y_2)$ is given by different ormulae (22.151) and (22.152) requires additional research. It should

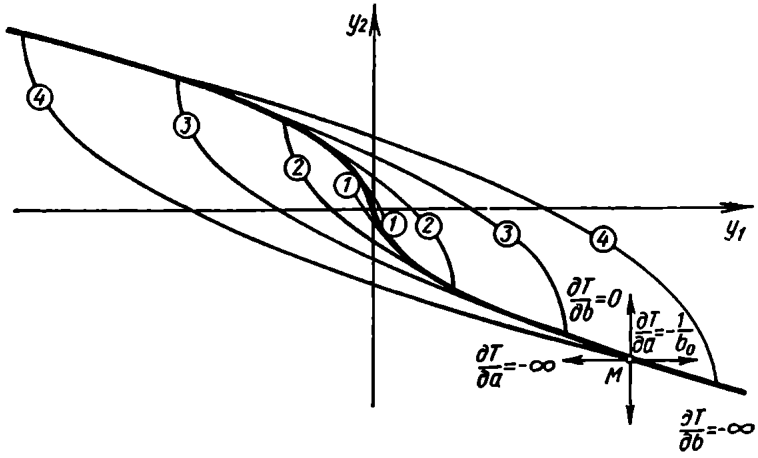

Fig. 22.17

be ascertained that $S(y_1, y_2)$ is a continuous function with continuous partial derivatives $\frac{\partial S}{\partial y_i}$ because the Bellman equation was derived under these assumptions.

Note that if the point $\mathbf{y}_0 = (a, b)$ is on the switching line and $b < 0$, i.e. the equality $a = \frac{1}{b^2}$ holds, the expression (22.151) takes the form $T(\mathbf{y}_0) = b + 2\sqrt{b^2} = b + 2|b|$. Since $b < 0$, then $|b| = -b$ and therefore $T(\mathbf{y}_0) = b + 2(-b) = -b$. The expression (22.152) for the same portion of the switching line $\left(\text{where } a = \frac{1}{2b^2}\right)$ also gives $T(\mathbf{y}_0) = -b$. In other words, in that portion of the switching line where $b < 0$ both formulae for $T(\mathbf{y}_0)$, and thus for $S(\mathbf{y}_0)$, give the same result. In a similar way one can see that in that portion where $b > 0$ both formulae for $S(\mathbf{y}_0)$ will give the same result.

Thence it follows that although the functions $T(\mathbf{y}_0)$ above and below the switching line are described by different formulae, on the line itself these formulae coincide, and so the function $S(\mathbf{y}_0)$ is continuous in the entire plane.

With expressions for the function $T(\mathbf{y}_0)$ at hand we can find out whether it is differentiable. Outside the switching line the function clearly has continuous derivatives with respect to a and b because in the vicinity of any point outside the switching line the function $T(\mathbf{y}_0)$ is given by either one of the formulae (22.151) or (22.152)

and is readily differentiable. What then happens on the switching line itself? Show that at no point of this line has the function $T(y_0)$ continuous derivatives with respect to a and b.

Let M be a certain point of the switching line (see Fig. 22.17) and a_0, b_0, its coordinates. The ordinate $b_0 < 0$; therefore, as follows from Eq. (21.41), $a = \frac{1}{2} b^2$ and

$$\sqrt{a_0 + \frac{1}{2} b_0^2} = \sqrt{b_0^2} = |b_0| = -b_0$$

Find at the point M the derivatives of the function (22.151)

$$\left.\frac{\partial T}{\partial a}\right|_M = \left.\frac{1}{\sqrt{a + \frac{1}{2} b^2}}\right|_{a_0, b_0} = -\frac{1}{b_0}$$

$$\left.\frac{\partial T}{\partial b}\right|_M = 1 + \left.\frac{b}{\sqrt{a + \frac{1}{2} b^2}}\right|_{a_0, b_0} = 1 + \frac{b_0}{-b_0} = 0$$

Now find the derivatives of the function (22.152) at the point M with $a_0 = \frac{1}{2} b_0^2$

$$\left.\frac{\partial T}{\partial a}\right|_M = \left.\frac{-1}{\sqrt{-a + \frac{1}{2} b^2}}\right|_{a_0, b_0} = -\infty$$

$$\left.\frac{\partial T}{\partial b}\right|_M = -1 + \left.\frac{-1}{\sqrt{-a + \frac{1}{2} b^2}}\right|_{a_0, b_0} = -\infty$$

Consequently, at the point M (see Fig. 22.17) the partial derivatives of the function $T(y_1, y_2)$, and hence of the function $S(y_1, y_2)$, are discontinuous and go to infinity. The discontinuity of the derivatives $\frac{\partial S}{\partial y_i}$ can be shown in a similar way for that part of the switching line where $b > 0$.

Thus, the function $S(y)$ is not differentiable everywhere, and the Bellman equation has failed to lead to a complete and well substantiated solution.

It has been shown that even in simplest cases the assumption that the function $S(y)$ is differentiable at all the points of the phase space does not always hold, therefore the use of the Bellman equation is sometimes unjustified. It should also be noted that the Bellman equation is difficult to solve; firstly, it includes the function $S(y)$, which is not known in advance; secondly, it is a partial derivative equation and, finally, it is complicated by the maximum symbol.

These difficulties restrict the practical use of the method in continuous problems.

On the other hand, the method is successfully applied to sampled-data systems because in problems with discrete time which are described by finite difference equations, the principle of optimal control is successfully combined with the achievements of computer technology. The variational problem of optimization with discrete time can be reduced, by using the principle of optimal control, to N simple problems of minimization (or maximization) of a function depending on a small number of variables (controls), where N is the number of time intervals into which the overall control time is divided. It is assumed that inside each interval the control parameter and the system coordinates remain unchanged; this approach is thus similar to that applied to sampled-data systems. The basic difficulties stem from the large amount of computations in minimizing the function of control parameters. These difficulties can only be surmounted by using up-to-date high-speed and large-memory computers.

22.5. COMPARISON OF OPTIMAL CONTROL METHODS

The above methods (the Euler equation, the maximum principle and dynamic programming) are all variational and closely interrelated. Indeed, dynamic programming has led to the maximum principle, while the maximum principle was instrumental in deriving the Euler equation.

Each method, however, has its own specific features and is best applied to a definite type of problem as is evidenced by the examples of this chapter.

The Euler equation is most useful in control problems with nonlinear functionals and with conditions specified in the form of nonlinear functions where, because of the physical nature of the problem, the solution is expected in the form of smooth continuous functions.

The maximum principle is most effective in solving linear problems where the controls (or coordinates) are constrained by inequalities.

Dynamic programming is effective with systems reducible to sampled-data systems. The principle of optimality combined with achievements of computer technology enables one to handle very complicated problems. The application of this method to continuous systems is limited owing to the difficulties involved in solution of the Bellman equation. Also, before the problem is finally solved it is not known whether the requirements imposed in deriving this equation will be met.

Chapter XXIII

RANDOM SIGNALS IN CONTROL SYSTEMS

23.1. GENERAL

The preceding chapters dealt with control systems subjected to entirely definite, deterministic external signals described by specified time functions.

However, control systems have to function in other conditions as well. Furthermore, the very need for control systems arises from the existence of unknown *random* actions which can never be predicted or completely described mathematically and are represented by random functions of time.

For example, the load current of a generator servicing parallel-connected individually controlled users is a random time function. The position of the driving shaft of a tracking system which may switch to different targets is also a random function. Different interferences in an electric control system, supply parameter variations in different versions of the device, noises in elements, gusts of wind in aerodynamic systems, wave shocks in hydrodynamic systems are different examples of random actions, and their effect on the control system requires special consideration.

A simple closed-loop control system which includes units allowing for random signals is of the type shown in Fig. 23.1. Both the signal x and noises h, g as well as variations in the parameters of the controller, δK_1 and plant, δK_2 are random quantities which cannot be described by definite time functions.

Random functions describe both useful actions, such as load variations, and undesirable actions, such as interferences. Besides, in more involved self-adjusting systems the study of component circuits is facilitated by specially introduced random actions which, although of a random nature, are used for system adjustment and are thus useful signals helping to obtain additional data to be used in improving the system performance. In these cases signals having some properties of random functions, while remaining deterministic, may be generated. These are called *pseudorandom signals.*

In studying systems subjected to random signals a *sample set* of each signal given in the form of time functions on the interval $2T$

is analyzed. This sample set is described by certain statistical characteristics which are nonrandom dependences, although they describe a random function.

Random signals can be described by two kinds of methods.

1. Set averaging, which uses different distribution of random values at different time instants. The sample set in this case is described by set-averaged values which can be time functions.

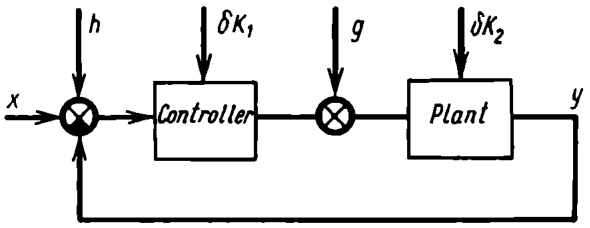

Fig. 23.1

2. Time averaging, which uses different kinds of statistical means to estimate the correlation function and the process spectral densities given one sufficiently large process sample.

Linear systems are chiefly studied by time averaging, nonlinear, by set averaging.

The basic works on the use of probabilistic and statistical methods in control engineering are indicated in the Reference List (71, 75, 33, 61).

Although all actual processes under study are nonstationary, in the investigation of control systems wide use is made of principles following from the assumption that the process is stationary; it is assumed that on the time interval under review a certain variation of time does not affect the statistical characteristics of the signals. These are said to be stationary random signals. Processes for which time and set averaging gives the same results are called *ergodic*.

All methods for describing random functions of time are presented in special mathematical courses and summarized in the Appendix. In this chapter we will deal only with mathematical description of most typical random signals. We will begin with deterministic signals depending on one random parameter and then describe random signals expressed by random functions of time the sample set of which cannot be described analytically.

A signal x will be described by the following functions: one-dimensional distribution density $p_1(x)$, the correlation function of the set $K_x(\tau)$ or the time $R_x(\tau)$ and the spectral density $S_x(\omega)$.

23.2. EXAMPLES OF RANDOM SIGNALS AND THEIR CHARACTERISTICS

A random quantity, independent of time,

$$x = a \tag{23.1}$$

where a is a random quantity with a specified one-dimensional distribution density $p_1(a)$.

The distribution density $p_1(x)$ is independent of time.

The correlation function is defined by two-dimensional distribution density $p_2(x_1, x_2)$. With various values of a independent (see Appendix 3)

$$p_2(x_1, x_2) = p_1(x_1)\, p_2(x_2) \tag{23.2}$$

Then correlation function of the set is

$$K_x = \int_{-\infty}^{\infty} \int_{-\infty}^{\infty} x_1 x_2 p_1(x_1)\, p_2(x_2)\, dx_1\, dx_2 = m_x^2 = \overline{\overline{(a)}^2} \tag{23.3}$$

If we represent all the samples $x = a$ on the intervals $2T$ as a time sequence and then assume that $T \to \infty$, the correlation function of the time

$$R_x = M\left\{\lim_{T\to\infty} \frac{1}{2T} \int_{-T}^{T} x(t)\, x(t+\tau)\, dt\right\} = M\{a^2\} = \overline{a^2} \tag{23.4}$$

The set and time correlation functions are thus different for the given signal. In a particular case where the signal is deterministic and all its samples have the same value $a = a_0$ we have

$$p_2(x_1, x_2) = \delta(x_1 - a_0)\, \delta(x_2 - a_0) \tag{23.5}$$

and

$$K_x = R_x = a_0^2 \tag{23.6}$$

The spectral density of a signal is found through the Fourier transformation of the time correlation function (see Eq. A4)

$$S_x(\omega) = \int_{-\infty}^{\infty} R_x e^{-j\omega\tau} d\tau = \overline{\overline{a^2}} \int_{-\infty}^{\infty} e^{-j\omega\tau} d\tau \tag{23.7}$$

Since

$$\int_{-\infty}^{\infty} e^{-j\omega\tau} d\tau = 2\pi\delta(\omega) \tag{23.8}$$

then

$$S_x(\omega) = 2\pi \overline{\overline{a^2}} \delta(\omega) \tag{23.9}$$

Figure 23.2 shows the plots of $p_1(x)$, $R_x(\tau)$ and $S_x(\omega)$ for the signal under study. Figure 23.2*a* represents a random signal, and Fig. 23.2*b*, a deterministic one. This is a stationary signal and therefore it is ergodic only at $p_2(x_1, x_2) = \delta(x_1 - a_0)\,\delta(x_2 - a_0)$,

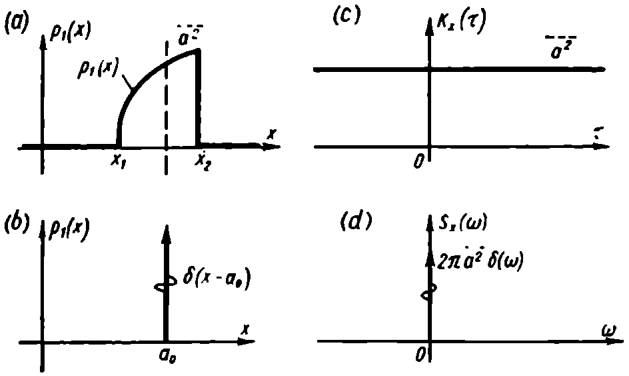

Fig. 23.2

i.e. when it is deterministic rather than random. In all other cases the ergodic hypothesis is not valid and the signal should be classified as nonergodic.

Normally in studying the statistical characteristics of a random stationary ergodic signal the deterministic constant component $\overline{x}$ is subtracted from it and the characteristics R_x and S_x are calculated for the centred signal $\mathring{x} = x - \overline{x}$.

A sine signal with a random phase

$$x = X_m \sin(\omega_0 t + \alpha) \tag{23.10}$$

where the phase is distributed by the uniform law

$$p_1(\alpha)\begin{cases} \dfrac{1}{2\pi} & \text{at} \quad 0 \leqslant \alpha \leqslant 2\pi \\ 0 & \text{at} \quad \alpha > 2\pi \end{cases} \tag{23.11}$$

As follows from the plot $x(\omega_0 t)$ (Fig. 23.3*a*), the probability that x is in the interval dx

$$p_1(x)\,dx = \frac{d\omega_0 t}{\pi} \tag{23.12}$$

From Eq. (23.10)

$$\omega_0 t = \arcsin\frac{x}{X_m} - \alpha \tag{23.13}$$

Differentiation of Eq. (23.13) and substitution into Eq. (23.12) gives

$$p_1(x) = \frac{1}{\pi \sqrt{X_m^2 - x^2}} \tag{23.14}$$

The time correlation function is found as

$$R_x(\tau) = \lim_{T\to\infty} \frac{1}{2T} \int_{-T}^{T} X_m^2 \sin(\omega_0 t + \alpha) \sin[\omega_0 (t+\tau) + \alpha]\, dt = \frac{X_m^2}{2} \cos \omega_0 \tau \tag{23.15}$$

The resultant equation is independent of the random quantity α and thus the set averaging does not affect it. The set correlation

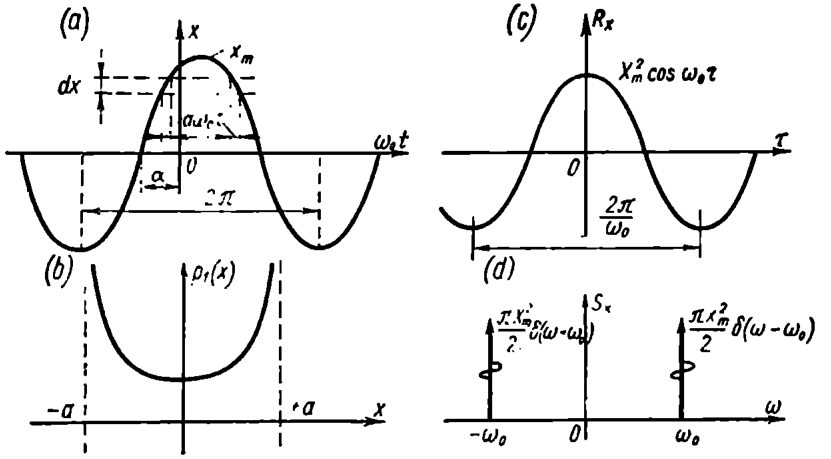

Fig. 23.3

function $K_x(\tau)$ for the given distribution of α coincides with $R_x(\tau)$ and, consequently, the stationary signal is ergodic.

The spectral density is found through the Fourier transformation of $R_x(\tau)$

$$S_x(\omega) = \int_{-\infty}^{\infty} \frac{a^2}{2} \cos \omega_0 \tau e^{-j\omega\tau}\, d\tau =$$

$$= \frac{a^2}{4} \int_{-\infty}^{\infty} [e^{-j(\omega+\omega_0)\tau} + e^{-j(\omega-\omega_0)\tau}]\, d\tau \tag{23.16}$$

Substituting the values of integrals according to Eq. (23.8) we have

$$S_x(\omega) = \left[\frac{\pi a^2}{2}\right] [\delta(\omega+\omega_0) + \delta(\omega-\omega_0)] \tag{23.17}$$

The plots of $p_1(x)$, $R_x(\tau)$, and $S_x(\omega)$ are given in Fig. 23.3*b*, *c* and *d*, respectively.

A single pulse of specified width T_0 at a random instant t_0. The pulse

$$x = a\,[1_0(t - t_0) - 1_0(t - T_0 - t_0)] \tag{23.18}$$

in the case of uniform distribution of the pulse start time t_0 on the interval $-T < t_0 < T - T_0$, i.e.

$$p_1(t_0) = \frac{1}{2T - T_0} \tag{23.19}$$

In this case the distribution density $p_1(x)$ is nonzero only at $x = 0$ and $x = a$ and can be expressed as

$$p_1(x) = \left(1 - \frac{T_0}{2T}\right)\delta(x) + \frac{T_0}{2T}\,\delta(x - a) \tag{23.20}$$

If $T_0 \ll T$ the probability that $x \neq 0$ and $x = a$ is a very small value equal to $\frac{T_0}{2T}$ which goes to zero as $T \to \infty$.

The correlation function is found by time averaging of the product $x(t)\,x(t+\tau)$ over the interval from $-T$ to $+T$.

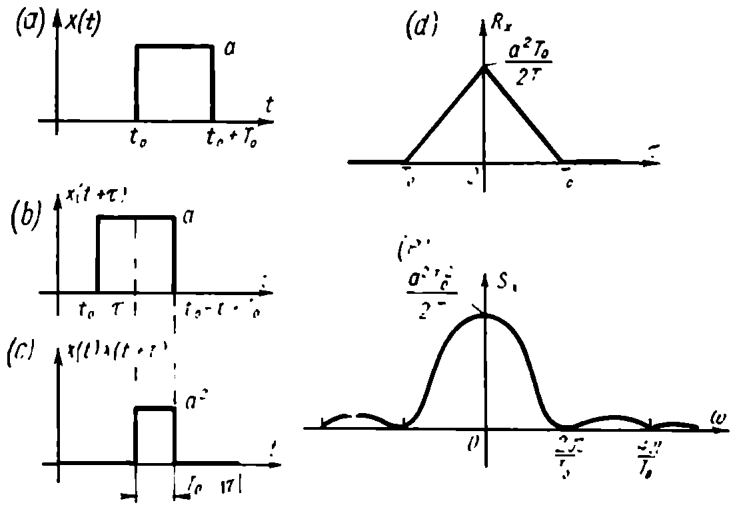

Fig. 23.4

This product is nonzero only at $|\tau| < T_0$, which is clear from Fig. 23.4*a*, *b*, *c*. In that case

$$R_{xT}(\tau) = \frac{a^2}{2T}\int_{-T}^{T} x(t)\,x(t+\tau)\,dt = \frac{a^2}{2T}\begin{cases} T_0 - |\tau| & \text{at } |\tau| < T_0 \\ 0 & \text{at } |\tau| > T_0 \end{cases} \tag{23.21}$$

The Fourier transformation of this equation gives

$$S_{xT}(\omega) = \frac{a^2 T_0^2}{2T}\left(\frac{\sin\frac{\omega T_0}{2}}{\frac{\omega T_0}{2}}\right)^2 \tag{23.22}$$

Using the expression for spectral density in terms of the Fourier transformation $X_T(j\omega)$ of a random signal sample on the interval $2T$

$$S_{xT}(\omega) = \frac{1}{2T}|X_T(j\omega)|^2 \tag{23.23}$$

and substituting

$$X_T(j\omega) = \frac{2a}{\omega}\sin\frac{\omega T_0}{2} \tag{23.24}$$

we obtain, after transformations, the same formula as (23.22).

The plots of $R_{xT}(\tau)$ and $S_{xT}(\omega)$ are shown in Fig. 23.4*d* and *e*.

Equations (23.21), (23.22) and (23.20) do not include the random quantity t_0, and so the resultant functions $p_1(x)$, $R_{xT}(\tau)$ and $S_{xT}(\omega)$ are nonrandom characteristics of a random signal.

Ideal pulses. If in the previous example $a = \frac{1}{T_0}$ as $T_0 \to 0$, we have a unit pulse which acts at a random instant t_0

$$x = \delta(t - t_0) \tag{23.25}$$

For a random signal in the form of a unit pulse acting at a random instant as $T_0 \to 0$ Eqs. (23.21) and (23.22) give the following characteristics

$$R_{xT}(\tau) = \left(\frac{1}{2T}\right)\delta(\tau) \tag{23.26}$$

$$S_{xT}(\omega) = \frac{1}{2T} \tag{23.27}$$

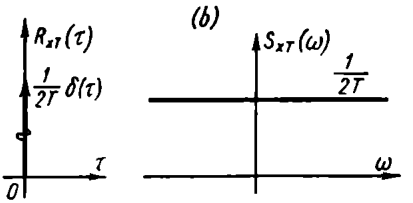

Fig. 23.5

Figure 23.5*a*, *b* exhibits the plots of these characteristics.

Since the spectral density obtained is independent of frequency, this signal is a white noise where the signal energy is distributed uniformly over the entire spectrum.

Consider a random signal which is not a single ideal pulse but a set of random pulses. Assume that the amplitudes as well as the intervals between neighbouring pulses are random values.

Similar manipulations for such a random set of pulses gives the following expressions for the correlation function and the spectral density

$$R_x(\tau) = \dddot{a}^2 f\delta(\tau) \tag{23.28}$$

$$S_x(\omega) = \dddot{a}^2 f \tag{23.29}$$

where $\overline{a^2} = M\{a^2\}$ is the mean square value of the area of each pulse, and $\overline{f} = \frac{1}{T_{av}} = M\{f\}$ is the mean frequency of the pulses. The pulse amplitude distribution laws may vary widely.

Equations (23.28) and (23.29) describe many actual processes with sufficient accuracy. Thus, the useful signal in tracking changing targets by the control system of a gun or a machine-gun can be

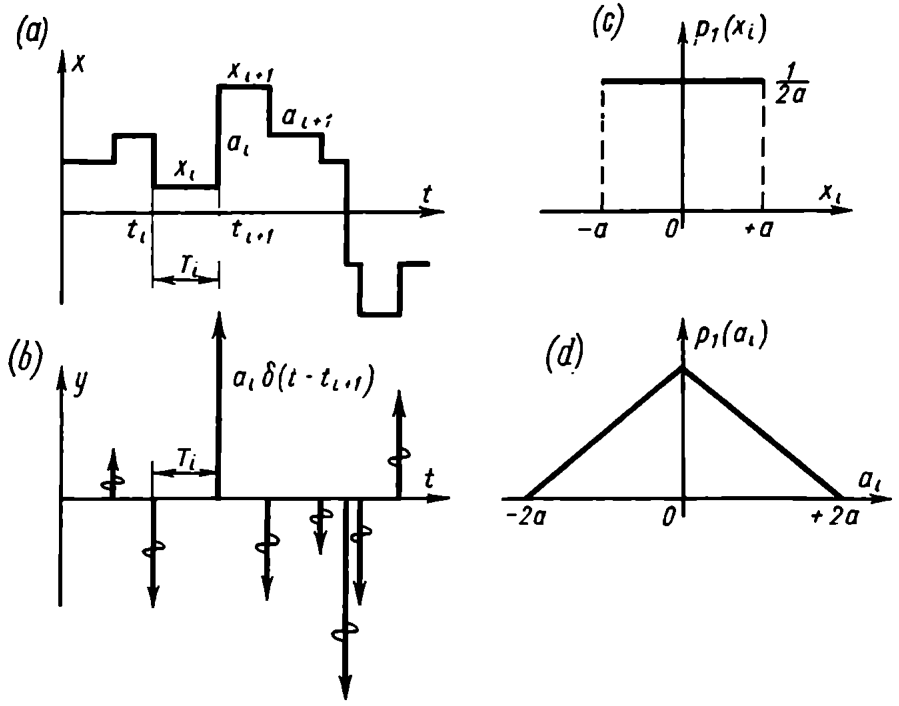

Fig. 23.6

approximately represented by a piecewise-constant stepwise relation where the target switching instants t_i and the target positions x_i are random values.

Figure 23.6*a* is an example of this random relation.

The derivative $y = \frac{dx}{dt}$ of the signal (Fig. 23.6*b*) is a sequence of pulse functions which follow at random time intervals T_i and have random amplitudes a_i

$$\left.\begin{aligned} a_i &= x_{i+1} - x_i \\ T_i &= t_{i+1} - t_i \end{aligned}\right\} \qquad (23.30)$$

In the case of uniform distribution of x_i on the interval $-a < x_i < +a$ (Fig. 23.6c)

$$p_1(x_i) = \begin{cases} \frac{1}{2}a & \text{at } |x_i| < a \\ 0 & \text{at } |x_i| > a \end{cases} \tag{23.31}$$

The distribution density $p_1(a_i)$ (Fig. 23.6d) can be obtained as the distribution density of the difference between two random quantities with uniform distribution densities (see Eq. (A 10a))

$$p_1(a_i) = \begin{cases} \frac{1}{2}a\left(1 - \frac{|a_i|}{2a}\right) & \text{at } |a_i| < 2a \\ 0 & \text{at } |a_i| > 2a \end{cases} \tag{23.32}$$

Any distribution law of the intervals, $p_1(T_i)$, is feasible.

Determining the average values of $\overline{a_i^2}$ and T_i as associated expectations for the random signal

$$y(t) = \sum_{i=0}^{\infty} a_i \delta(t - t_i) \tag{23.33}$$

find the correlation function and the spectral density

$$R_y(\tau) = \overline{a_i^2 f_i} \delta(\tau) = M\{a_i^2\} M\{f_i\} \delta(\tau) \tag{23.34}$$

$$S_y(\omega) = \overline{a_i^2 f_i} = M\{a_i^2\} M\{f_i\} \tag{23.35}$$

where $f_i T_i = 1$. These expressions correspond to (23.28) and (23.29).

Binary white noise. Near-white-noise statistical characteristics can be inherent not only in signals whose instantaneous values are distributed over a certain area (e.g. from $-a$ to $+a$) but also in signals which can take on only two values. Such signals are known as *binary*.

Consider a signal which can take on only values $(+a, -a)$, while its stepwise change can occur only at equal intervals T_0. Assume that at a certain instant, which is taken as a reference, this signal is $+a$. After $\frac{T_0}{2}$ it can either remain $+a$ or change to $-a$ with equal probability. Over the interval $\frac{T_0}{2} < t < \frac{3}{2T_0}$ it remains the same, while at the instant $\frac{3}{2T_0}$ it can again remain the same or change sign with equal probability.

The situation is similar at instants preceding $t = 0$. At $-\frac{T_0}{2}$, $-\frac{3}{2T_0}$, $-\frac{5}{2T_0}$ etc. the probabilities that the sign remains or changes are equal.

The graph of probability that the signal changes sign at instants $t_k = T_0\left(\frac{1}{2}+k\right)$ is shown in Fig. 23.7. The associated arcs denote k versions where the pulse width at $t=0$ is kT_0.

The graph illustrates a certain instant $t = 0$ which is the midpoint of the interval between two sign switching instants t_{-1} and t_0; the sign of the signal x is assumed positive over this interval.

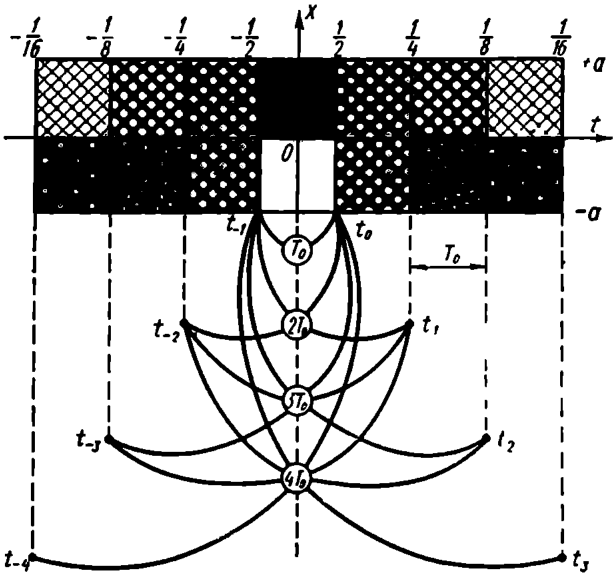

Fig. 23.7

The probabilities that the sign of this pulse will change from positive to negative at the instants t_0, t_1, t_2, etc. are $\frac{1}{2}$, $\frac{1}{4}$, $\frac{1}{8}$, and so on. The probabilities that the opposite change takes place at the instants t_{-1}, t_{-2}, t_{-3}, etc. are also $\frac{1}{2}$, $\frac{1}{4}$, $\frac{1}{8}$ and so on. The values of these probabilities are shown in the upper part of the figure. In the lower part the arcs illustrate the possible versions of pulses of various widths. Thus, a pulse of width T_0 has one version with sign changes at the instants t_{-1} and t_0. A pulse of width $2T_0$ has two versions with switchings at the instants t_{-2}, t_0, and t_{-1}, t_1. With increased pulse width the number of possible versions increases (Fig. 23.7, cases $3T_0$ and $4T_0$).

The shading in the time diagram represents the probability that $x = +a$ or $-a$ at the time t.

The probability that the pulse width is kT_0 can be represented by the formula

$$P_1(kT_0) = k\left(\frac{1}{2}\right)^{k+1} \tag{23.36}$$

and, consequently, the pulse width distribution density is

$$p_1(T_i) = k\left(\frac{1}{2}\right)^{k+1}\delta(t - kT_0) \tag{23.37}$$

Figure 23.8*a* and *b* shows the distribution densities $p_1(x)$ of the signal x and $p_1(T_i)$ of the pulse width T_i.

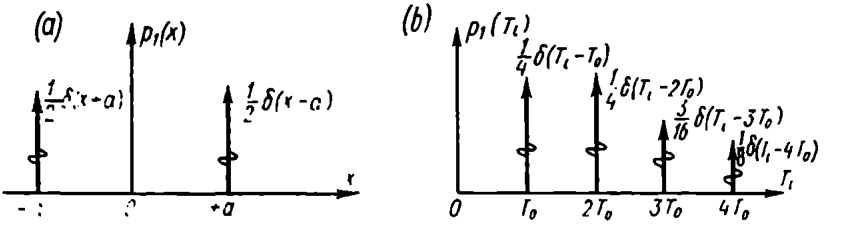

Fig. 23.8

Let us find the correlation function of the signal. With

$$R_x(\tau) = \frac{1}{2}T\int_{-T}^{T} x(t)\,x(t+\tau)\,dt$$

it is easily found that at $\tau = 0$

$$R_x(0) = a^2 \tag{23.38}$$

because $x^2(t) = a^2$ at any time.

At $|\tau| \geqslant T_0$ the probability that $x(t)$ and $x(t+\tau)$ are of the same sign at any time is $\frac{1}{2}$ and consequently $R_x(\tau) = 0$. Considering the mean value of the product $x(t)\,x(t+\tau)$ at $|\tau| \leqslant T_0$ on the interval T_0 for four possible equiprobable versions, when the alternation occurs at t_0 and t_{-1} (Fig. 23.9*a*), t_{-1} and $t > t_0$ (Fig. 23.29*b*), t_0 and $t < t_{-1}$ (Fig. 23.9*c*), $t < t_{-1}$ and $t > t_0$ (Fig. 23.9*d*), one can easily see that it decreases with increasing $|\tau|$ by the linear law. Therefore

$$R_x(\tau) = a^2\begin{cases} 1 - \left|\frac{\tau}{T_0}\right| & \text{at } |\tau| < T_0 \\ 0 & \text{at } |\tau| > T_0 \end{cases} \tag{23.39}$$

The plot of $R_x(\tau)$ is similar to Fig. 23.4*d* and differs only in the scale along the y-axis. The form of the correlation function is thus

the same for a unit pulse of width T_0 and a binary signal with equiprobable sign alternation at intervals T_0.

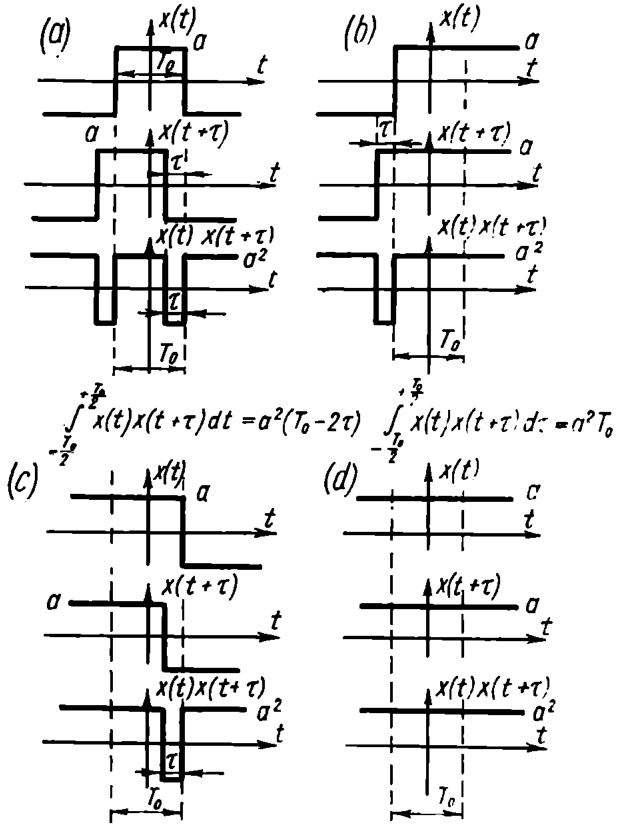

Fig. 23.9

The spectral density is then expressed similarly to (23.22)

$$S_x(\omega) = a^2 T_0 \left(\frac{\sin \frac{\omega T_0}{2}}{\frac{\omega T_0}{2}} \right)^2 \qquad (23.40)$$

The plot of $S_x(\omega)$ differs from Fig. 23.4*e* only in the scale along the y-axis. If $\omega T_0 < 1$, then $S_x(\omega)$ is within 100 to 95% and in this range the signal is a white noise with an accuracy sufficient for practical purposes.

Pseudorandom binary white noise. A source of a binary white noise with purely random equiprobable switchings is difficult to

obtain in practice. A generator of deterministic binary signals whose properties are close to those of a binary white noise is much easier to implement. Such generators can be based on different principles: (1) codes specifying the alternation instants can be precalculated and introduced into a magnetic or photoelectric program unit and (2) the alternation instants can be specified in the generator itself.

A generator operating by the latter principle may have the form of a ring of shift registers closed through a modulo 2 adder (Fig. 23.10).

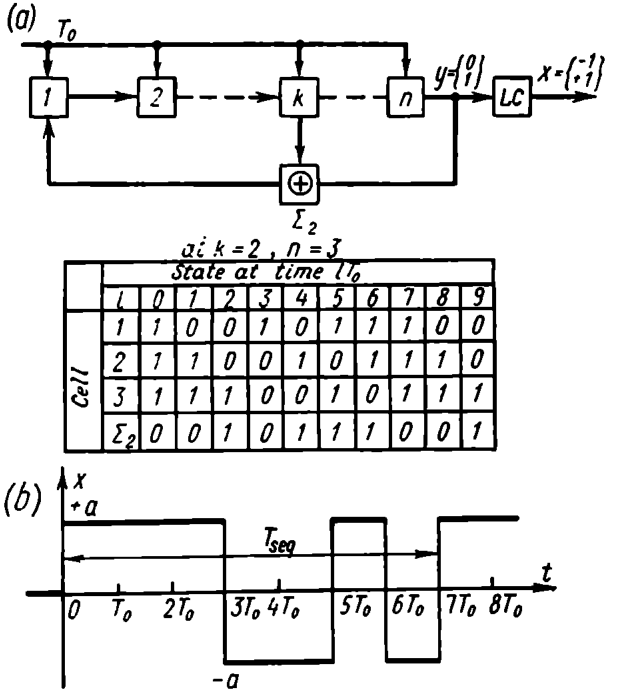

	l	0	1	2	3	4	5	6	7	8	9
Cell	1	1	0	0	1	0	1	1	1	0	0
	2	1	1	0	0	1	0	1	1	1	0
	3	1	1	1	0	0	1	0	1	1	1
	Σ_2	0	0	1	0	1	1	1	0	0	1

Fig. 23.10

The cells $1, 2, \ldots, k, \ldots, n$ denote elements of the shift register; in each element either 0 or 1 can be recorded and at the end of each interval T_0 the record from the ith cell is transferred to the $(i+1)$th. The register ring is closed via the modulo 2 adder where 0 is recorded if elements k and n store the same values (0 and 0 or 1 and 1) and 1 is recorded when the values are different (0 and 1 or 1 and 0).

The linear converter LC at the output converts the input signal y by the law $x = 2y - 1$.

Consider, for instance, the operation of such a generator for the simple case of $n = 3$, $k = 2$.

Assume that originally 1 is stored in all the three elements of the register. Then the adder stores 0. At the end of T_0 this 0 is shifted to element 1, and in the adder a zero will reappear as a modulo 2 sum of two 1's recorded in cells *2* and *3*. Thus, in each cycle T_0 the content of memory cells will alternate, and the first cell will display the result of modulo 2 summation of values stored in cells *2* and *3*.

The table of Fig. 23.10 shows the values stored in cells *1*, *2*, *3* and $\sum_2$ at instants 0, T_0, $2T_0$, $3T_0$, etc. After the interval $7T_0$ the record is seen to repeat itself, and this time is the period of the signal $y(t)$ picked up from the cell $n = 3$, and, hence, of $x(t)$. The plot of $x(t)$ for this case is shown in Fig. 23.10*b*.

With a greater number of cells this period grows. If there are n memory cells, the overall period of a sequence of pulses will be

$$T_{seq} = NT_0 = T_0(2^n - 1) \tag{23.41}$$

Within the period T_{seq} the number of positive cycles is

$$n_+ = \frac{N+1}{2} \tag{23.42}$$

and of negative cycles

$$n_- = \frac{N-1}{2} \tag{23.43}$$

The mean value of the signal over the period T_{seq}

$$\frac{1}{T_{seq}} \int_0^{T_{seq}} x\,dt = \bar{x} = \frac{n_+ - n_-}{N} a = \frac{a}{N} \tag{23.44}$$

The greater N, the closer the signal x to a binary white noise.

The correlation function of such a periodic pseudorandom binary signal is an ordinate-symmetrical periodic curve consisting of triangular pulses with a period T_{seq} (Fig. 23.11*a*).

On the portion $|\tau| < \frac{T_{seq}}{2}$

$$R_x(\tau) = a^2 \begin{cases} \left(1+\frac{1}{N}\right)^2 \left(1-\left|\frac{\tau}{T_0}\right|\right) - \frac{1}{N^2} & \text{at } \left|\frac{\tau}{T_0}\right| \leqslant 1 \\ -\frac{1}{N^2} & \text{at } 1 \leqslant \left|\frac{\tau}{T_0}\right| \leqslant \frac{N}{2} \end{cases} \tag{23.45}$$

Following the Fourier expansion in terms of harmonics $k\omega_{seq}$, where $\omega_{seq} = \frac{2\pi}{T_{seq}}$, we have for a spectrum symmetrical relative to $k = 0$

$$R_x(\tau) = \frac{a^2}{N} \left\{ -1 + \left(1+\frac{1}{N}\right) \sum_{k=-\infty}^{\infty} \left(\frac{\sin \frac{\pi k}{N}}{\frac{\pi k}{N}} \right)^2 \cos k\omega_{seq}\tau \right\} \tag{23.46}$$

Using Eqs. (23.9) and (23.17) to determine the spectral density for each of the correlation function harmonic components, including

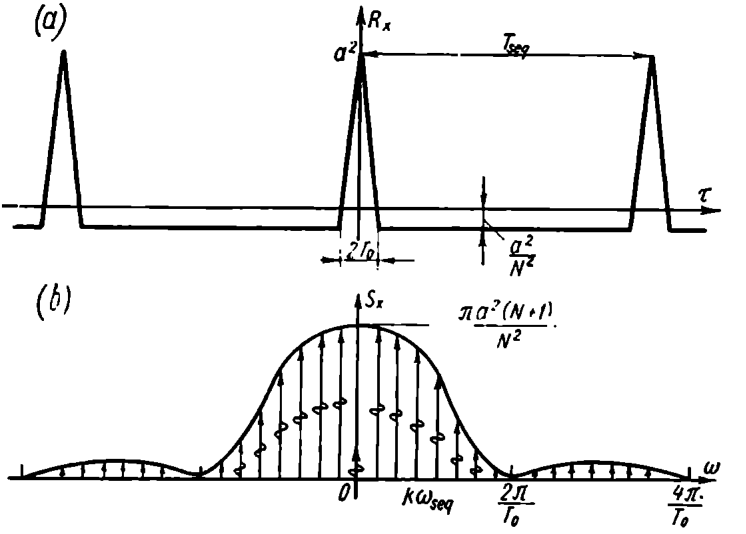

Fig. 23.11

the constant one, we have

$$S_x(\omega) = \frac{\pi a^2}{N}\left\{\left(1+\frac{1}{N}\right)\left(\frac{\sin\frac{\omega T_0}{2}}{\frac{\omega T_0}{2}}\right)^2 1^*(\omega) - \left(1-\frac{1}{N}\right)\delta(\omega)\right\} \quad (23.47)$$

where

$$1^*(\omega) = \sum_{k=-\infty}^{\infty}\delta(\omega - k\omega_{seq}) \quad \text{and} \quad \frac{2\pi}{N\omega_{seq}} = T_0$$

At $N = \frac{T_{seq}}{T_0} \gg 1$, simplifying we get

$$S_x(\omega) = \frac{\pi a^2 T_0}{T_{seq}}\left\{\left(\frac{\sin\frac{\omega T_0}{2}}{\frac{\omega T_0}{2}}\right)^2 1^*(\omega) - \delta(\omega)\right\} \quad (23.48)$$

Equation (23.48) is a discrete power spectrum with an envelope analogous to the spectral density of a unit pulse of width T_0 with an interval between frequencies $\omega_{seq} = \frac{2\pi}{(NT_0)}$ and the band corresponding to the constant component dropped out (for $k = 0$ in the braces the two δ-functions cancel out).

At $\omega T_0 < 1$ the spectral density of such a signal corresponds to a white noise to within 5%, which is sufficient for practical purposes.

Figure 23.11*b* illustrates a plot for the spectral density of the periodic pseudorandom signal in question.

There are also other generators whose distribution density is different from the binary law, e.g. a source where the amplifier circuit is closed by random contacts of balls contained in a rotating drum (Fig. 23.12*a*) or by spraying a conducting liquid (Fig. 23.12*b*).

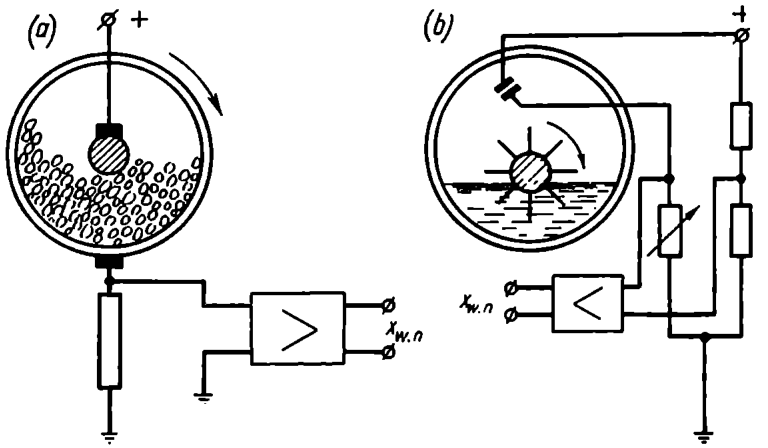

Fig. 23.12

In these cases the source of white noise $x_{w.n}$ has a frequency spectrum which is close to that of a white noise and a distribution density which can be normal, given the proper kind of contact and circuit.

Arbitrary signals. Most signals in technical devices, biological, astrophysical, space and other systems are so complicated that they cannot be represented analytically, but their statistical characteristics, e.g. the correlation function and spectral density, can be obtained.

The most widely used correlation functions describing a random signal are expressed by the following equations

$$R_{x1}(\tau) = ae^{-\alpha|\tau|} \tag{23.49}$$

and

$$R_{x2}(\tau) = ae^{-\alpha|\tau|}\cos\beta\tau \tag{23.50}$$

The former represents a standard random signal at the input of a servo system and the latter may characterize, for instance, a stationary random signal of nonregular ship rolling or the results of electroencephalogram processing.

Direct Fourier transformation makes it possible to use spectral densities instead of correlation functions. Then

$$S_{x1}(\omega) = \frac{2\alpha a}{\alpha^2 + \omega^2} \tag{23.51}$$

$$S_{x2}(\omega) = \alpha a \left(\frac{1}{\alpha^2 + (\beta - \omega)^2} + \frac{1}{\alpha^2 + (\beta + \omega)^2} \right) \tag{23.52}$$

The signal characteristics expressed by Eqs. (23.49) through (23.52) are often found in considering the propagation of a random signal through linear systems.

23.3. MEAN CORRELATION TIME AND MEAN FREQUENCY BAND OF RANDOM SIGNALS

Random signals are sometimes characterized by certain square-wave equivalent characteristics which approximate the correlation function and spectral density. Then it is assumed that within the interval $|\tau| < \tau_0 R_{eq}(\tau) = R(0)$, and at $|\tau| > \tau_0$, $R_{eq}(\tau) = 0$. In a similar way, for spectral density it is assumed that $S_{eq}(\omega) = S(0)$ at $|\omega| \leqslant \omega_0$ and $S_{eq}(\omega) = 0$ at $|\omega| > \omega_0$. The quantities τ_0 and ω_0 can be expressed through known values of $R(0)$ and $S(0)$. Indeed,

$$R(0) = \frac{1}{2\pi} \int_{-\infty}^{\infty} S_{eq}(\omega)\, d\omega = S(0) \frac{\omega_0}{\pi} \tag{23.53}$$

and therefore

$$S(0) = \int_{-\infty}^{\infty} R_{eq}(\tau)\, d\tau = R(0)\, 2\tau_0 \tag{23.54}$$

From these expressions we have

$$\tau_0 = \frac{S(0)}{2R(0)} \tag{23.55}$$

and

$$\omega_0 = \frac{\pi R(0)}{S(0)} \tag{23.56}$$

and

$$\tau_0 \omega_0 = \frac{\pi}{2} = \text{const} \tag{23.57}$$

From the latter equality it follows directly that the wider and flatter the area bounded by the correlation function, the narrower and steeper the curve expressing the spectral density. Conversely, the steeper the correlation function, the flatter the plot of spectral density. This interrelation of the curves representing the direct and inverse Fourier transforms was very pronounced when we dealt with a constant signal and a white noise. In the former case the

correlation function was a horizontal (Fig. 23.2*c*) straight line (maximal flatness), while the spectral density (Fig. 23.2*d*) had the shape of a δ-function (maximal steepness). In the latter case the picture is reversed (Fig. 23.5*a* and *b*).

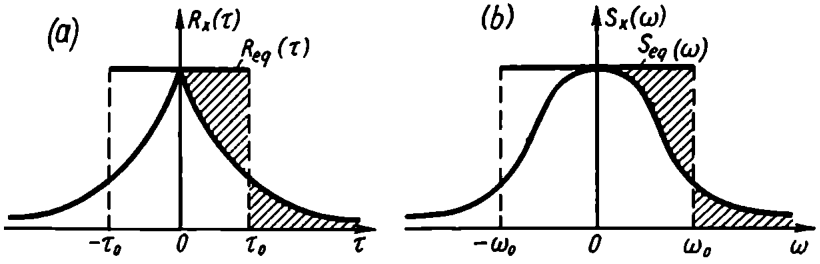

Fig. 23.13

Example 23.1. Find ω_0 and τ_0 for a signal with a correlation function and a spectral density expressed by Eqs. (23.49) and (23.51). In this case $R(0) = a$ and $S(0) = \frac{2a}{\alpha}$.

Consequently, Eqs. (23.55) and (23.56) yield

$$\tau_0 = \frac{1}{\alpha} \quad \text{and} \quad \omega_0 = \frac{\pi\alpha}{2} \tag{23.58}$$

The plots of $R_x(\tau)$, $R_{eq}(\tau)$, and $S_x(\omega)$, $S_{eq}(\omega)$ for this example are shown in Fig. 23.13*a* and *b*, respectively.

23.4. CROSS-CORRELATION FUNCTIONS AND SPECTRAL DENSITIES OF RANDOM SIGNALS

If there are two or more random signals, one must know the interrelationship of two signals which can be expressed by the joint distribution density $p_{xy} = p_2(x_1, t_1; y_2, t_2)$, cross-correlation function $K_{xy}(\tau)$ and cross spectral density (see Appendix).

If the cross-correlation function of two random signals is zero, the signals are referred to as *uncorrelated*, if not, they are said to be *correlated*.

If signals are uncorrelated, then their origin is different and they are probably statistically independent as given by the expression

$$p_2(x_1, t_1; y_2, t_2) = p_x(x_1, t_1)\, p_y(y_2, t_2) \tag{23.59}$$

For stationary random signals

$$\begin{aligned} x_1 &= x(t_1) \\ y_2 &= y(t_1 + \tau) \end{aligned} \tag{23.60}$$

In this case the cross-correlation function given as a mean for the set in terms of joint distribution density is

$$K_{xy}(\tau) = \int_{-\infty}^{\infty} dx_1 \int_{-\infty}^{\infty} x_1 y_2 p_2(x_1, y_2)\, dy_2 \qquad (23.61)$$

The cross-correlation function given as a time mean for stationary random signals x and y is

$$R_{xy}(\tau) = \lim_{T\to\infty} \frac{1}{2T} \int_{-T}^{T} x(t)\, y(t+\tau)\, dt \qquad (23.62)$$

For ergodic processes computations by Eqs. (23.61) and (23.62) give the same result, $R_{xy}(\tau) = k_{xy}(\tau)$.

Example 23.2. Let a stationary random signal $x(t)$ of an ergodic process be tape-recorded and played back with a delay of t_0. Denoting the played-back signal as $y(t) = x(t - t_0)$ one can consider certain properties of cross-correlation functions of two correlated signals x and y.

By Eq. (23.62)

$$R_{yx}(\tau) = \lim_{T\to\infty} \frac{1}{2T} \int_{-T}^{T} x(t)\, x(t+\tau-t_0)\, dt = R_x(\tau - t_0) \qquad (23.63)$$

In this case the cross-correlation function is an auto-correlation function shifted rightwards by t_0 on the time scale. Since the auto-correlation function has a maximum at the argument equal to zero, then the cross-correlation function has a maximum at $\tau = t_0$.

Reversing the order of functions x and y and determining the cross-correlation function $R_{yx}(\tau)$, we have

$$R_{yx}(\tau) = \lim_{T\to\infty} \frac{1}{2T} \int_{-T}^{T} x(t-t_0)\, x(t+\tau)\, dt =$$

$$= \lim_{T\to\infty} \frac{1}{2T} \int_{-T}^{T} x(t)\, x(t+\tau+t_0)\, dt = R_x(\tau + t_0) = R_{xy}(-\tau) \qquad (23.63a)$$

Now the cross-correlation function is an auto-correlation function shifted leftwards by t_0. In this case the curve reaches a maximum at $\tau = -t_0$.

Consequently, cross-correlation functions are associated with an inequality

$$R_{xy}(\tau) \neq R_{yx}(\tau)$$

Using the spectral densities instead of correlation functions, we obtain

$$S_{xy}(j\omega) = e^{-j\omega t_0} S_x(\omega)$$
$$S_{yx}(j\omega) = e^{j\omega t_0} S_x(\omega) \tag{23.64}$$

Example 23.3. Consider two sinusoidal signals with random initial phases and different frequencies, ω_1 and ω_2:

$$x = x_m \sin(\omega_1 t + \alpha)$$
$$y = y_m \sin(\omega_2 t + \beta)$$

Equation (23.62) yields

$$R_{xy}(\tau) = R_{yx}(\tau) = 0$$

and consequently

$$S_{xy}(j\omega) = S_{yx}(j\omega) = 0$$

The latter equalities show that two sinusoidal signals with different frequencies are uncorrelated.

This is also true of two white-noise-like signals which are combinations of pulses (see Sec. 23.2) with random and statistically independent intervals between them.

If auto-correlation and cross-correlation functions of two signals x and y are known, they can be used to express correlation functions of the sum or difference of these signals.

Let

$$z(t) = x(t) \pm y(t) \tag{23.65}$$

Then Eq. (A.30) readily yields after transformations

$$R_z(\tau) = R_x(\tau) + R_y(\tau) \pm R_{xy}(\tau) \pm R_{yx}(\tau) \tag{23.66}$$

Therefore

$$S_z(\omega) = S_x(\omega) + S_y(\omega) \pm S_{xy}(j\omega) \pm S_{yx}(j\omega) = \\ = S_x(\omega) + S_y(\omega) \pm 2\mathrm{Re}\, S_{xy}(j\omega) \tag{23.67}$$

Example 23.4. Find the spectral density of the sum of two signals, $x(t)$ and $y(t) = x(t + t_0)$, shifted in time by t_0 if $S_x(\omega)$ is known. Equation (23.67) combined with (23.64) yields

$$S_z(\omega) = 2S_x(\omega)\left[1 + \frac{e^{-j\omega t_0} + e^{j\omega t_0}}{2}\right] = 2S_x(\omega)[1 + \cos\omega t_0] \tag{23.68}$$

Example 23.5. Find the correlation function of the sum of two uncorrelated signals, $x(t) = a\cos(\omega_0 t + \alpha)$ and $y(t)$, with a correlation function $R_y(\tau) = b^2 e^{-\beta|\tau|}$.

Equation (23.66) combined with (23.15) gives

$$R_z(\tau) = R_x(\tau) + R_y(\tau) = \frac{a^2}{2}\cos\omega_0\tau + b^2 e^{-\beta|\tau|} \tag{23.69}$$

In this expression the second term is seen to decay with increasing τ while the amplitude of the first oscillating term remains unchanged.

If $x(t)$ expresses the useful signal and $y(t)$ the noise, then from Eq. (23.69) it is seen that by measuring the auto-correlation function of the sum z at large values of τ it is possible to filter out a small useful signal x at a high level of noise y.

23.5. DETERMINING STATISTICAL CHARACTERISTICS OF RANDOM SIGNALS BY THEIR SAMPLES ON AN INTERVAL OF LENGTH T_s

We will restrict ourselves to the characteristics of stationary random ergodic processes for which one or several samples on the time

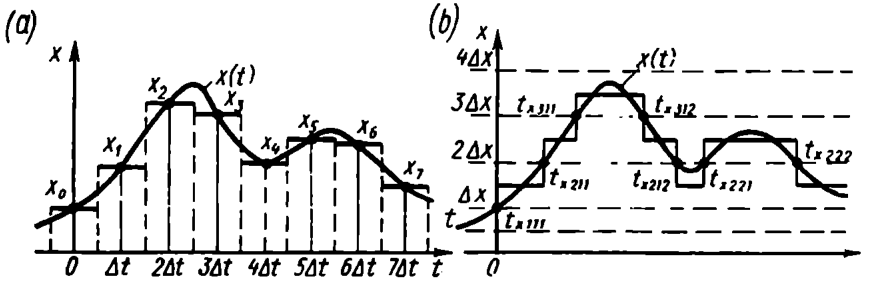

Fig. 23.14

interval $0 < t < T_s$ are known, so that we can calculate approximately the basic characteristics of a random process such as the distribution function, the correlation function and the spectral density.

In order to calculate the characteristics, a continuous sample signal should be represented in discrete form by replacing the smooth curve by a stepwise curve with the use of *time* or *level quantization*.

In the former case the signal is specified as a sequence of its ordinates which follow at equal intervals Δt, and in the latter case by a number of instants which correspond to signals equal to certain values $k\Delta x$.

The reference point for x can be selected so that the condition $x > 0$ is met at any time.

In time quantization (see Fig. 23.14*a*) the signal is represented as a lattice function which is expressed as a sequence of ordinates x_k for instant $k\Delta t$. If the signal is approximated by a stepwise function for which the constant value of the signal over the interval Δt is equal to its true value at the midpoint of the interval, then

$$x(t) \approx \sum_{i=0}^{n} x_i \left\{1_0\left[t-\left(i-\frac{1}{2}\right)\Delta t\right]-1_0\left[t-\left(i+\frac{1}{2}\right)\Delta t\right]\right\} \quad (23.70)$$

In level quantization (Fig. 23.14*b*) the signal is given as n time sequences of the intersections of the curve $x(t)$ and the straight lines $x = k\Delta x$. These instants can be denoted as t_{xkij}, where k indicates the level of the straight line $x = k\Delta x$, i represents the ordinal number of the intersection, and $j = 1$ if the intersection occurs upwards and $j = 2$ if it occurs downwards. These two values $j = 1$ and $j = 2$ clearly alternate.

If the Boolean time function

$$x_{0k}(t) = 1_0[x(t) - k\Delta x] \tag{23.71}$$

is represented for each level the stepwise signal approximating the given function $x(t)$ is

$$x(t) \approx \Delta x\left[\frac{1}{2} + \sum_{k=1}^{n} x_{0k}(t)\right] \tag{23.72}$$

Representing the signal in the form (23.70) or (23.72) its desired statistical characteristics can be obtained by means of a digital computer.

Special-purpose computers can also be used, such as distribution function analyzers, correlators, and spectral analyzers.

Determination of distribution functions. These are conveniently determined by representing the signal in a level-quantized discrete form. In this case the probability that $x(t) > k\Delta x$

$$P_1[x(t) > k\Delta x] = \frac{1}{T_s}\int_0^{T_s} x_{0k}(t)\,dt = \frac{1}{T_s}\sum_{i=1}^{m}(t_{xki2} - t_{xki1}) \tag{23.73}$$

and consequently the distribution function or the probability that $x(t) < k\Delta x$ is

$$P_1(k\Delta x) = 1 - P_1[x(t) > k\Delta x] = \frac{1}{T_s}\int_0^{T_s}(1 - x_{0k})\,dt \tag{23.74}$$

For the mean value of distribution density on the interval Δx we have

$$p_{1m}[(k + 0.5)\,\Delta x] = \frac{1}{T_s\Delta x}\int_0^{T_s}(x_{0k} - x_{0k+1})\,dt \tag{23.75}$$

In time quantization the calculation of distribution functions is somewhat more complicated because in this case the number of ordinates of the lattice function in each interval Δx should be calculated and then related to their total number (Ref. 53).

$P_1(k\,\Delta x)$ and $p_{1m}(x)$ can be obtained with the aid of distribution function analyzers.

The structural diagrams of simple distribution function and distribution density analyzers are shown in Fig. 23.15*a* and *b*, respectively. Both these circuits calculate automatically by Eqs. (23.74) and (23.75). Setting different values of $k\,\Delta x$ we can easily obtain P_1 and $p_{1m} = p_{1\Delta x}$ at the output.

Determination of correlation functions. Correlation functions are most often calculated with the use of time-quantized signals.

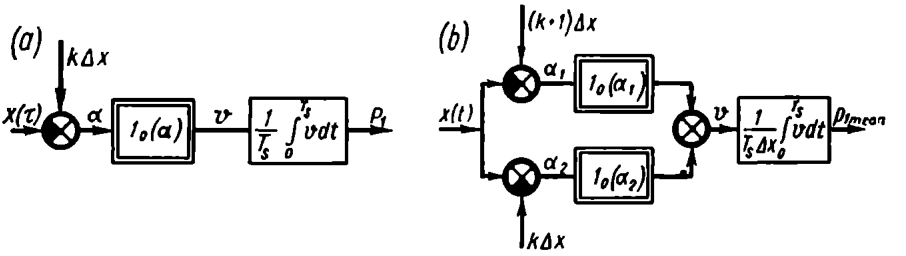

Fig. 23.15

If samples of two signals x and y on the time intervals T_{sx} and T_{sy} are known, the calculation of $R_{xyT}(\tau)$ requires that

$$T_{sx} = 2T \quad \text{and} \quad T_{sy} = 2T + \tau_{max} \tag{23.76}$$

with the origins of these intervals coinciding.

Only in this case can we determine

$$R_{xyT}(\tau) = \frac{1}{2T} \int_{-T}^{T} x(t)\, y(t+\tau)\, dt \tag{23.77}$$

in the specified range $0 < \tau < \tau_{max}$.

The signal steady-state conditions and the substitution of $t = t_1 - \tau$ reshape the integral (23.77) as follows

$$R_{xyT}(\tau) = \frac{1}{2T} \int_{-T}^{T} x(t_1 - \tau)\, y(t_1)\, dt_1 \tag{23.77a}$$

To calculate the correlation function by Eq. (23.77a) it is necessary that

$$T_{sx} = 2T + \tau_{max} \quad \text{and} \quad T_{sy} = 2T \tag{23.76a}$$

In calculation of $R_{yxT}(\tau)$, x and y are interchanged in all expressions (23.76), (23.76a), (23.77) and (23.77a).

All the high frequency components of a signal can be allowed for by so selecting the time quantization step Δt that it is always less than t_{min}, the minimal distance between two adjacent extrema of

the signal $x(t)$ or $y(t)$ (Fig. 23.16). It is recommended that $\Delta t < 0.5t_{min}$.

Once Δt is selected the characteristic $R_{xy}(\tau)$ can be used to calculate the number of points

$$n = \frac{\tau_{max}}{\Delta t} \tag{23.78}$$

and the number of addends for calculation of the correlation function

$$N = \frac{2T}{\Delta t} \tag{23.79}$$

Low-frequency components are much more difficult to account for. In selecting the sample length T_s one should be sure that all low-frequency components are allowed for, and this requires the

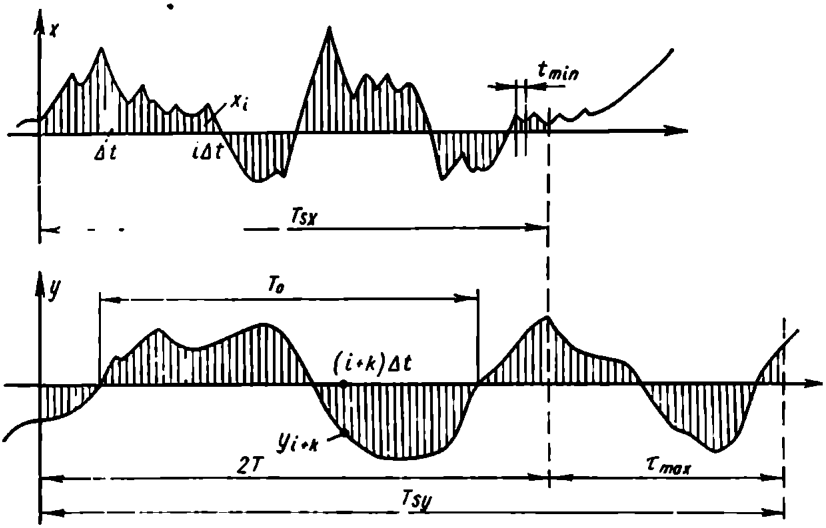

Fig. 23.16

knowledge of a signal sample on an interval greatly exceeding T_s or of *apriori* data on the form of the correlation functions to be determined.

If no such data are available, the sample length is selected approximately, then the correlation functions are calculated, after which the selected length is adjusted.

Even so the necessary information can easily be lost, especially in determining the cross-correlation function. For instance, if x and y are two identical signals shifted by t_0 greatly exceeding the period of the lowest-frequency component of these signals, then in selecting $\tau_{max} < t_0$ one may fail to detect any cross-correlation of signals.

Nevertheless, if no *apriori* information is available, in approximate calculation of the correlation function the low-frequency components are allowed for by selecting a sampling period so that $T > 2T_0$, where T_0 is the period of the largest low-frequency component with τ_{max} selected so that $N > 5n$.

One way to verify the selection of the sampling period is an auxiliary calculation with a greater, say doubled, sampling period. If the accuracy is improved but slightly, it means that the sampling period has been selected well enough.

Knowing N values of x_i and $N + n$ values of y_l on the y-axis and using a sum in place of the integral in Eq. (23.77), we have

$$R_{xyT}(k\Delta t) = \frac{1}{N}\sum_{i=1}^{N} x_i y_{i+k} \tag{23.80}$$

For centred signals $\mathring{x}(t) = x(t) - \dddot{x}$ and $\mathring{y}(t) = y(t) - \dddot{y}$ the correlation function

$$\mathring{R}_{xyT}(k\Delta t) = \frac{1}{N}\sum_{i=1}^{N} x_i y_{i+k} - \dddot{x}\dddot{y} \tag{23.80a}$$

where

$$\dddot{x} = \frac{1}{N}\sum_{i=1}^{N} x_i$$

$$\dddot{y} = \frac{1}{N}\sum_{i=1}^{N} y_{i+k}$$

Equations (23.80) and (23.80a) are normally used to calculate auto- ($x = y$) and cross- ($x \neq y$) correlation functions of signals on the basis of their samples on the interval $2T + \tau_{max}$.

If the signal is quantized in level, its correlation function can also be calculated by convenient formulae.

Correlation functions are also calculated by special devices known as *correlators* or *correlation meters*. The basic elements of correlators are a unit of controlled delay (by a length of time τ), a multiplication unit, and a unit for calculating the mean value over a period $2T$.

Correlators may be magnetic, electronic, and electromechanic, depending on the specific implementation of the units. Since calculation of one ordinate value takes a period of $2T$, correlators are sampled-data instruments with pulse repetition period $T_p = 2T$.

The structure of a simple analog correlator is shown in Fig. 23.17. Since the signal cannot be advanced and can only be delayed, the circuit performs calculations by Eq. (23.77*a*). If there are n such circuits for different values of τ, n ordinate values of the correlation functions necessary for its representation can be determined within

a period $2T$, and the function can be automatically displayed on a cathode ray tube. There are also many digital correlators which

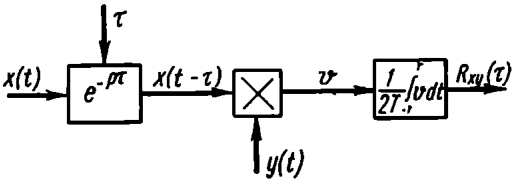

Fig. 23.17

use different procedures of calculating the correlation function from discrete values of the signal.

Calculation of spectral densities. If correlation functions of random signals are known, their spectral densities can be found through direct Fourier transformation of these functions. This calculation can be performed by special-purpose automatic analyzers.

Thus if the cross-correlation function $R_{xy}(\tau)$ is known, then by Eq. (A.44)

$$S_{xy}(j\omega) = \int_{-\infty}^{\infty} R_{xy}(\tau)\cos\omega\tau\, d\tau - j\int_{-\infty}^{\infty} R_{xy}(\tau)\sin\omega\tau\, d\tau = \\ = G_{xy}(\omega) - jQ_{xy}(\omega) \qquad (23.81)$$

$G_{xy}(\omega)$ and $Q_{xy}(\omega)$ can be calculated by an analog or digital device. A block diagram of a simple analog device for automatic calculation of $G_{xy}(\omega)$ and $Q_{xy}(\omega)$ from the correlation function $R_{xy}(\tau)$ given as a time function is presented in Fig. 23.18. It is assumed here that $R_{xy}(\tau) \approx 0$ at $|\tau| > \tau_m$ and integration over τ can be performed on a finite time interval $2\tau_m$. The signals v_1 and v_2 are found by multiplying $R_{xy}(\tau)$ by the sinusoidal signals $\sin\omega\tau$ and $\cos\omega\tau$ received from the generator G.

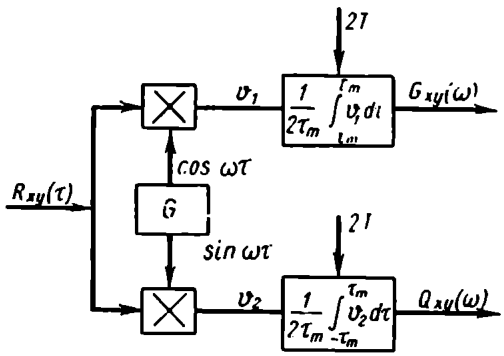

Fig. 23.18

Since there is no imaginary component in the natural spectral density $S_x(\omega)$ one channel $G_x(\omega)$ is sufficient to determine it from $R_x(\tau)$.

If the correlator stores a number of discrete values of $R_{xy}(\tau)$ the time function introduced into the spectral analyzer is found

by a reading system which converts the lattice function $R_{xy}(n\Delta\tau)$ into a stepwise time-quantized curve $R_{xy}(t)$. The determination of the spectral density from the correlation function gives the most accurate results.

On the other hand, with a known sample of the random signal $x(t)$ on the interval T_s, the spectral density can be found directly. To obtain unambiguous results, the signal should be adjusted for the entire time interval outside T_s. This problem can be approached in two different methods. In one of them $x(t)$ is assumed zero outside T_s, i.e. the signal has a continuous frequency spectrum. In the other it is assumed that $x(t) = x(t + kT_s)$, i.e. the signal repeats with a period of T_s. In this case the signal has a discrete spectrum with the main harmonic frequency $f_0 = \frac{1}{T_s}$.

The calculation and automatic analysis depend on the approach used. Consider both approaches in determining natural spectral densities.

In the first case the signal power is represented as a sum of partial powers (see Eq. (A.43)).

$$\overline{x^2(t)} = \frac{1}{\pi}\int_0^\infty S_x(\omega)\,d\omega \tag{23.82}$$

If the signal spectrum is confined to the frequencies $\left(\omega_1 = \omega - \frac{\Delta\omega}{2}\right.$ and $\left.\omega_2 = \omega + \frac{\Delta\omega}{2}\right)$ the mean power in the band $\Delta\omega$ around the frequency ω is

$$\overline{x_\omega^2(t)} = \frac{1}{\pi}\int_{\omega-\frac{\Delta\omega}{2}}^{\omega+\frac{\Delta\omega}{2}} S_x(\omega)\,d\omega = \frac{\overline{S_x(\omega, \Delta\omega)}\,\Delta\omega}{\pi} \tag{23.83}$$

With the value $\Delta\omega$ sufficiently small

$$S_x(\omega) \approx \overline{S_x(\omega, \Delta\omega)} = \frac{\overline{\pi x_\omega^2(t)}}{\Delta\omega} \tag{23.84}$$

The spectral density is thus seen to be obtainable by measuring the mean power of the signal in a known narrow frequency band, i.e. by cutting out a narrow spectrum band of the process under study and measuring the mean power of the resultant stationary random signal.

An instrument performing this operation should incorporate a narrow pass band filter with a controlled pass frequency, a quadratic detector and an integrator isolating the constant component of the signal over the integration period $2T$ (Fig. 23.19). Here F is

a narrow pass band filter isolating a band of width $\Delta\omega$ in the vicinity of the frequency ω. By using n such units tuned to frequencies $\omega = k\,\Delta\omega$ at $1 < k < n$ over a time $2T$ we will have n discrete values of spectral density $\overline{S_x(k\Delta\omega, \Delta\omega)}$ necessary to characterize the signal.

Selection of a frequency band $\Delta\omega$ and a sampling period is usually dictated by the condition $2T\Delta\omega \gg 1$, which follows from an analysis of the operational accuracy of the unit.

The larger $2T\Delta\omega$, the better the accuracy of determining $\overline{S_x(\omega, \Delta\omega)}$. The reasoning behind selection of an integration period $2T$ is the same as in calculating the correlation function.

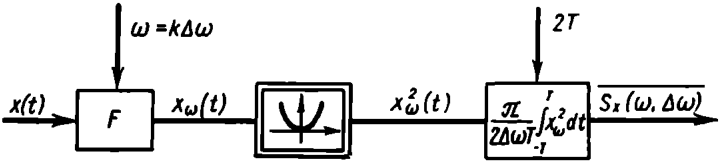

Fig. 23.19

This is discussed in detail in Ref. 53 and others.

In the second case a recorded (say, taped) and repeatedly played back signal $x(t)$ of a given sample forms a periodic signal $x(t + 2nT)$ with a frequency of $\omega_0 = \frac{\pi}{T}$, which can be decomposed into harmonic components X_{mk} by using a spectral analyzer and represented in the form

$$x(t+2nT) = \sum_{k=-\infty}^{\infty} X_{mk} \sin(k\omega_0 t + \psi_k) \qquad (23.85)$$

For each of the harmonic components we have, by virtue of Eq. (23.18),

$$S_{xk}(\omega) = \frac{\pi X_{mk}^2}{2} [\delta(\omega + k\omega_0) + \delta(\omega - k\omega_0)] \qquad (23.86)$$

Since the cross-correlation function of different harmonics is zero, then $S_{xkl}(\omega) = 0$ (see Eq. (23.67)), and the sum of different harmonics is represented by the sum of their spectral densities. Thus, for the signal $x(t)$

$$S_x(\omega) = \frac{\pi}{2} \sum_{k=-\infty}^{\infty} X_{mk}^2 [\delta(\omega + k\omega_0) + \delta(\omega - k\omega_0)] \qquad (23.87$$

If the discrete spectral density is now replaced by a continuous one by averaging the discrete value over the entire interval ω_0 it is associated with, we have a stepwise function

$$S_x(\omega) = \frac{\pi X_{mk}^2}{2\omega_0} = \frac{TX_{mk}^2}{2} \qquad (23.88)$$

Figure 23.20 shows the plot of $S_x(\omega)$ for discrete and continuous representation of the spectral density.

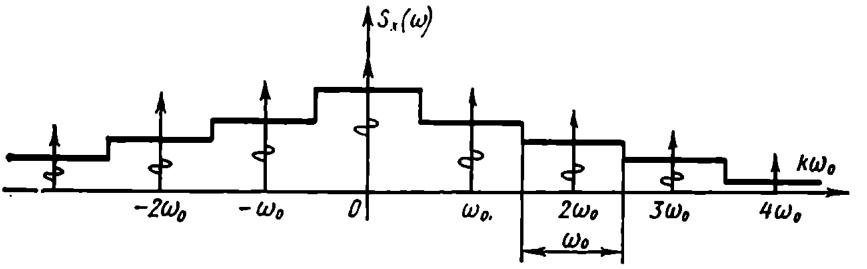

Fig. 23.20

An instrument for determining $S_x(\omega)$ by this method should incorporate a spectral analyzer, e.g. a synchronous detector with a filter and a quadratic detector. Such an instrument for one channel $k\omega_0$ is shown in Fig. 23.21.

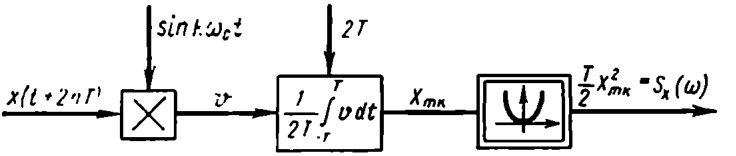

Fig. 23.21

Comparing the two methods one can see that the former is much faster in obtaining current data, but the latter is more accurate. Apart from the above-described analog spectral analyzers there are some digital instruments yielding the spectral density to the desired accuracy on the basis of a signal sample. $S_x(\omega)$ can also be obtained by digital computers by using discrete values of $x(t)$.

$S_{xy}(j\omega)$ is found in a similar way; however, as in calculating $S_{xy}(j\omega)$ from the correlation function R_{xy}, phases of the harmonic signal components should be allowed for and the imaginary component $S_{xy}(j\omega)$ should be found as well as the real one.

Chapter XXIV

LINEAR SYSTEMS SUBJECTED TO RANDOM STATIONARY SIGNALS

24.1. A RANDOM SIGNAL PROPAGATING THROUGH A LINEAR ELEMENT

We have described heretofore different methods of studying th transformation of deterministic signals in linear systems. All thes methods are also applicable to certain samples of random signals

If the signal $x(t)$ at the input of a linear element (Fig. 24.1*a* with a weighting function $w(t)$ is known, the signal $y(t)$ at th

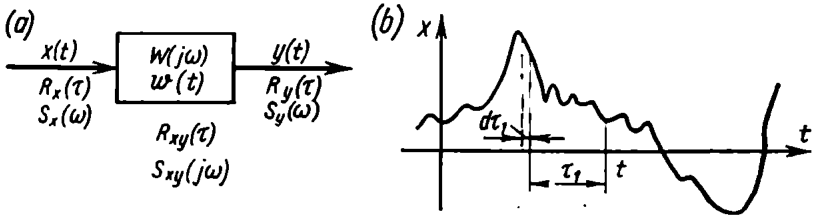

Fig. 24.1

output can be obtained as the element response to a set of pulse $x(t-\tau_1)$ of width $d\tau_1$ (Fig. 24.1*b*). The output of a linear elemer is then

$$y(t) = \int_0^\infty w(\tau_1)\, x(t-\tau_1)\, d\tau_1 \qquad (24.$$

The frequency spectrum at the output is

$$Y(j\omega) = W(j\omega)\, X(j\omega) \qquad (24.$$

where $X(j\omega)$ and $Y(j\omega)$ are Fourier transforms of $x(t)$ and $y(t$

If the system input is a random stationary signal with know statistical characteristics $R_x(\tau)$ and $S_x(\tau)$, Eqs. (24.1) and (24. can give the statistical characteristics of the output signal.

Transformation of correlation functions. The auto-correlation function of a stationary random signal at the linear element output is

$$R_y(\tau) = \lim_{T\to\infty} \frac{1}{2T} \int_{-T}^{T} y(t)\, y(t+\tau)\, dt$$

and, following the substitution of $y(t)$ as given by Eq. (24.1) and a change in the order of integration, it is expressed as

$$R_y(\tau) = \lim_{T\to\infty} \frac{1}{2T} \int_{-T}^{T} \int_{0}^{\infty} w(\tau_1)\, x(t-\tau_1)\, d\tau_1 \int_{0}^{\infty} w(\tau_2)\, x(t-\tau_2+\tau)\, d\tau_2\, dt =$$

$$= \int_{0}^{\infty} w(\tau_1)\, d\tau_1 \int_{0}^{\infty} w(\tau_2)\, R_x(\tau+\tau_1-\tau_2)\, d\tau_2 \qquad (24.3)$$

Here the auto-correlation function of the input stationary random signal is

$$R_x(\tau-\tau_1-\tau_2) = \lim_{T\to\infty} \frac{1}{2T} \int_{-T}^{T} x(t-\tau_1)\, x(t+\tau-\tau_2)\, dt \qquad (24.4)$$

For the cross-correlation function we will have, similarly,

$$R_{xy}(\tau) = \lim_{T\to\infty} \frac{1}{2T} \int_{-T}^{T} x(t)\, dt \int_{0}^{\infty} w(\tau_1)\, x(t+\tau-\tau_1)\, d\tau_1 =$$

$$= \int_{0}^{\infty} w(\tau_1)\, R_x(\tau-\tau_1)\, d\tau_1 \qquad (24.5)$$

Equations (24.3) and (24.5) permit finding the correlation functions of the output signal on the basis of the input signal correlation function.

Equation (24.5) leads to a very important practical conclusion that if the linear element input is a unitary white noise, the cross-correlation function $R_{xy}(\tau)$ is equal to the linear element weighting function $w(t)$. Indeed, in accordance with Eq. (23.29), by substituting $R_x(\tau-\tau_1) = \delta(\tau-\tau_1)$ into Eq. (23.5) we have

$$R_{xy}(\tau) = w(\tau) \qquad (24.6)$$

Example 24.1. Find $R_y(\tau)$ and $R_{xy}(\tau)$ of the signal at the output of an inertial element with

$$w = \left\{ \begin{array}{ll} \frac{1}{T_0} e^{-\frac{t}{T_0}} & \text{at } t \geqslant 0 \\ 0 & \text{at } t < 0 \end{array} \right\}$$

if its input signal is a white noise with an auto-correlation function $R_x(\tau) = a^2\delta(\tau)$. In this case, by Eq. (24.3)

$$R_y(\tau) = \frac{a^2}{T_0^2}\int_0^\infty e^{-\frac{\tau_1}{T_0}}d\tau_1 \int_0^\infty e^{-\frac{\tau_2}{T_0}}\delta(\tau+\tau_1-\tau_2)\,d\tau_2 =$$

$$= \frac{a^2}{T_0^2}\int_0^\infty e^{-\frac{\tau_1}{T_0}}\left\{\begin{matrix} e^{-\frac{\tau_1+\tau}{T_0}} & \text{at} & \tau+\tau_1\geqslant 0 \\ 0 & \text{at} & \tau+\tau_1<0 \end{matrix}\right\}d\tau_1 =$$

$$= \frac{a^2}{T_0^2}\left\{\begin{matrix} \int_0^\infty e^{-\frac{2\tau_1+\tau}{T_0}}d\tau_1 & \text{at} & \tau>0 \\ \int_{-\tau}^\infty e^{-\frac{2\tau_1+\tau}{T_0}}d\tau_1 & \text{at} & \tau<0 \end{matrix}\right\} =$$

$$= \frac{a^2}{2T_0}\left\{\begin{matrix} e^{-\frac{\tau}{T_0}} & \text{at} & \tau>0 \\ e^{\frac{\tau}{T_0}} & \text{at} & \tau<0 \end{matrix}\right\} = \frac{a^2}{2T_0}e^{-\left|\frac{\tau}{T_0}\right|} \qquad (24.7)$$

By Eq. (24.5) or (24.6) we have for the cross-correlation function

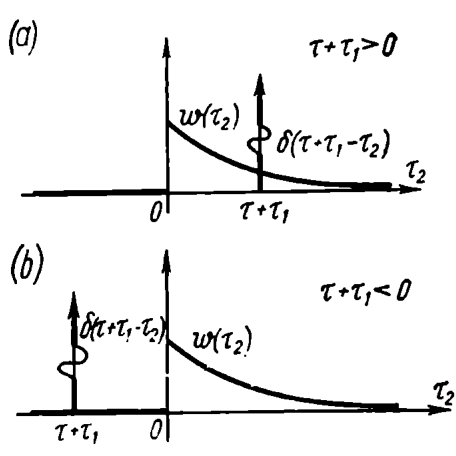

Fig. 24.2

$$R_{xy}(\tau) = \frac{a^2}{T_0}\int_0^\infty e^{-\frac{\tau_1}{T_0}}\delta(\tau-$$

$$-\tau_1)\,d\tau_1 = \frac{a^2}{T_0}e^{-\frac{\tau}{T_0}} \qquad (24.8$$

The plots of $\delta(\tau+\tau_1-\tau_2$ and $w(\tau_2)$ at $\tau+\tau_1>0$ an $\tau+\tau_1<0$ are shown in Fig 24.2*a* and *b*, respectively.

Thus, by measuring the cross correlation function of the sig nals at the linear element inpu and output with the input bein a near-white noise, the elemen weighting function can b found.

Example 24.2. Find $R_y(\tau)$ of the signal at the output of an ine tial element with a weighting function

$$w = \left\{\begin{matrix} \alpha e^{-\alpha t} & \text{at} & t\geqslant 0 \\ 0 & \text{at} & t<0 \end{matrix}\right\}$$

if tho input is a signal with a correlation function

$$R_x(\tau) = \beta b e^{-\beta|\tau|}$$

By Eq. (24.3) at $\tau > 0$ we have

$$R_y(\tau) = \beta b\alpha^2 \int_0^\infty e^{-\alpha\tau_1} d\tau_1 \int_0^\infty e^{-\alpha\tau_2} e^{-\beta|\tau+\tau_1-\tau_2|} d\tau_2 =$$

$$= \beta b\alpha^2 e^{-\beta\tau} \int_0^\infty e^{-(\alpha+\beta)\tau_1} d\tau_1 \int_0^{\tau+\tau_1} e^{(\alpha-\beta)\tau_2} d\tau_2 +$$

$$+ \beta b\alpha^2 e^{\beta\tau} \int_0^\infty e^{-(\alpha-\beta)\tau_1} d\tau_1 \int_{\tau+\tau_1}^\infty e^{-(\alpha+\beta)\tau_2} d\tau_2$$

The plot of $R_x(\tau + \tau_1 - \tau_2)$ as a function of τ_2 for this case at $\tau + \tau_1 > 0$ is shown in Fig. 24.3.

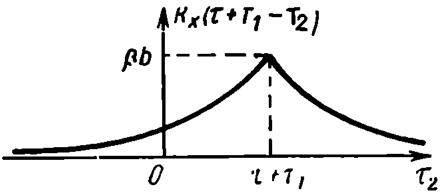

Fig. 24.3

Integration with the necessary transformations gives

$$R_y(\tau) = \frac{\beta b\alpha^2}{\alpha^2-\beta^2}\left[e^{-\beta\tau} - \frac{\beta}{\alpha}e^{-\alpha\tau}\right]$$

Similar calculations for $\tau < 0$ show that the expression of $R_y(\tau)$ differs only in the signs of the factors of τ. Therefore for $-\infty < \tau < \infty$ we can write

$$R_y(\tau) = \frac{\beta b\alpha^2}{\alpha^2-\beta^2}\left[e^{-\beta|\tau|} - \frac{\beta}{\alpha}e^{-\alpha|\tau|}\right] \qquad (24.9)$$

With $\beta \to \infty$, or with $R_x(\tau)$ tending to the δ-function we have

$$R_y(\tau) = \alpha b e^{-\alpha|\tau|} \qquad (24.10)$$

which represents the solution (24.7) in Example 24.1. Here $b = \frac{a^2}{2}$ and $\alpha = \frac{1}{T_0}$.

Of great practical interest is the case where $\beta \gg \alpha$.

The analysis of this case can be facilitated by representin Eq. (24.9) as

$$R_y(\tau) = \alpha b e^{-\alpha|\tau|}\left\{\left[\frac{1}{1-\left(\frac{\alpha}{\beta}\right)^2}\right]\left[1-\frac{\alpha}{\beta}e^{-(\beta-\alpha)|\tau|}\right]\right\} \quad (24.11$$

The first multiplier before the braces is the auto-correlatio function of the output signal with a white noise at the system input The second multiplier (in braces) represents a correction necessitate by the difference of the input signal from the ideal white noise at $\beta \gg \alpha$ this multiplier tends to unity. Thus, with $\beta \gg \alpha$ th actual input signal can be approximated by a white noise with a accuracy sufficient for practical purposes. If $\frac{\beta}{\alpha} = 100$, the erro does not exceed 1%.

Conversion of spectral densities. Let the frequency spectra of th signals $x(t)$, $y(t)$, $u(t)$ and $f(t)$ be related as

$$\left.\begin{aligned} Y(j\omega) &= W_1(j\omega)X(j\omega) \\ U(j\omega) &= W_2(j\omega)F(j\omega) \end{aligned}\right\} \quad (24.12$$

For each signal the set of its samples on an interval $2T$ denote $x_T(t)$, $y_T(t)$, $u_T(t)$ and $f_T(t)$ or $X_T(j\omega)$, $Y_T(j\omega)$, $U_T(j\omega)$ an $F_T(j\omega)$, respectively, is known.

The spectral cross-density of the signals y and u specified on th intervals $2T$ can be expressed through the correlation function a

$$S_{yuT}(j\omega) = \int_{-\infty}^{\infty} e^{-j\omega\tau}R_{yu}(\tau)\,d\tau =$$

$$= \int_{-\infty}^{\infty} e^{-j\omega\tau}M\left\{\frac{1}{2T}\int_{-T}^{T} y_T(t)\,u_T(t+\tau)\,dt\right\}d\tau \quad (24.13$$

Placing the integral under the symbol of mathematical expectatio and changing the order of integration, after the multiplication o the integrand by $e^{-j\omega t}e^{j\omega t} = 1$ we obtain

$$S_{yuT}(j\omega) = \frac{1}{2T}M\left\{\int_{-T}^{T} y_T(t)\,e^{j\omega t}\,dt\int_{-\infty}^{\infty} u_T(t+\tau)\,e^{-j\omega(t+\tau)}\,d(t+\tau)\right\} =$$

$$= \frac{1}{2T}M\{Y_T(-j\omega)\,U_T(j\omega)\} \quad (24.14$$

Expressing $Y_T(-j\omega)$ and $U_T(j\omega)$ by Eq. (24.12) and keepin in mind that Eq. (24.14) is valid for the signals x and f we hav

$$S_{yuT}(j\omega) = W_1(-j\omega)\,W_2(j\omega)\frac{1}{2T}M\{X_T(-j\omega)\,F_T(j\omega)\} =$$

$$= W_1(-j\omega)\,W_2(j\omega)\,S_{xfT}(j\omega) \quad (24.15$$

Since $\lim_{T\to\infty} S_{xyT}(j\omega) = S_{xy}(j\omega)$, then

$$S_{yu}(j\omega) = W_1(-j\omega)\, W_2(j\omega)\, S_{xf}(j\omega) \qquad (24.16)$$

Equation (24.16) can be obtained in a more rigorous way by representing the correlation function $R_{yu}(\tau)$ in Eq. (24.13) in a form similar to Eq. (24.5) and by subsequent transformation of integrals.

Assuming that $W_1(j\omega) = W_2(j\omega) = W(j\omega)$, $x(t) = f(t)$ and $y(t) = u(t)$, we have

$$S_y(\omega) = |W|^2 S_x(\omega) \qquad (24.17)$$

Assuming that $W_1(j\omega) = W(j\omega)$, $u(t) = x(t)$, $W_2(j\omega) = 1$, $f(t) = x(t)$ we get

$$\left.\begin{aligned} &S_{yx}(j\omega) = W(-j\omega) S_x(\omega) \\ \text{or}\quad &\\ &S_{xy}(j\omega) = S_{yx}(-j\omega) = W(j\omega) S_x(\omega) \end{aligned}\right\} \qquad (24.18)$$

In Eqs. (24.17) and (24.18) $S_x(\omega) = S_{xx}(j\omega)$ and $S_y(\omega) = S_{yy}(j\omega)$.

The mean power of the linear element input and output signals is

$$\overline{x^2(t)} = R_x(0) = \frac{1}{2\pi}\int_{-\infty}^{\infty} S_x(\omega)\, d\omega = \frac{1}{\pi}\int_0^{\infty} S_x(\omega)\, d\omega \qquad (24.19)$$

$$\overline{y^2(t)} = R_y(0) = \frac{1}{2\pi}\int_{-\infty}^{\infty} S_y(\omega)\, d\omega = \frac{1}{\pi}\int_0^{\infty} S_x(\omega)\, |W(j\omega)|^2\, d\omega \qquad (24.20)$$

The latter expression is very important for computation of r.m.s. errors in different control systems. In this case $W(j\omega)$ relates the system input and the error signal.

Example 24.3. Find $S_y(\omega)$ and $S_{xy}(j\omega)$ at the output of an inertial element with $W(j\omega) = \frac{1}{1+j\omega T_0}$ if its input is a white noise with a spectral density $S_x(\omega) = a^2$. In this case Eqs. (24.17) and (24.18) give

$$S_y(\omega) = \frac{a^2}{1+\omega^2 T_0^2} \quad \text{and} \quad S_{xy}(j\omega) = \frac{a^2}{1+j\omega T_0} \qquad (24.21)$$

Applying the inverse Fourier transformation to Eq. (24.21), we obtain Eqs. (24.7) and (24.8).

The signal power can be determined by Eq. (24.20). Then

$$\left.\begin{aligned} &\overline{x^2(t)} = R_x(0) = a^2\delta(0) \to \infty \\ &\overline{y^2(t)} = R_y(0) = \frac{a^2}{2T_0} \end{aligned}\right\} \qquad (24.22)$$

Thence the ideal white noise power is infinitely large becaus a white noise with a correlation function in the form of a δ-functio is a mathematical abstraction which can to some degree or othe be approached by actual signals. It is found that the power of a signa obtained when a white noise propagates through an inertial elemen and its mean frequency range are finite values and agree with actuall observed signals.

24.2. PROBLEMS INVOLVED IN STUDY OF LINEAR SYSTEMS SUBJECTED TO STATIONARY RANDOM SIGNALS

Let us consider a linear system of Fig. 24.4 with a transfer func tion $W(p)$. The input is $x(t)$, which is the sum of the main operatin signal $u(t)$ in normal functioning and an additional noise $f(t)$ The resultant output signal is $y(t)$.

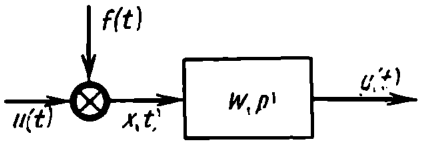

Fig. 24.4

The system may face different problems. The most widespreac are: (a) plant identification and (b) filtering out the noise witl signal conversion.

Identification is the development of a plant mathematical mode in order to estimate its responses (static and dynamic).

In the case of dynamic responses the problem is reduced to findin $W(p)$ through $y(t)$ with a given $f(t)$.

In the case of filtering out the noise with conversion of the operatio nal signal the problem is reduced to selection of linear elemen parameters at which the output signal $y(t)$ is as close as possibl to the converted operational signal given in the statement of th problem. If the frequency spectrum of the operational signal i $U(j\omega)$, the required transformation law can be written as

$$Z(j\omega) = W_{ref}(j\omega)\, U(j\omega)$$

where $Z(j\omega)$ is the frequency spectrum of the desired output signal and $W_{ref}(j\omega)$ the operator of the specified reference conversion

If the only objective is filtration and the signal does not hav to be converted, then $W_{ref}(j\omega) = 1$. If a derivative of the operatio nal signal is sought, then $W_{ref}(j\omega) = j\omega$. In the case of integratin conversion $W_{ref}(j\omega) = \frac{1}{j\omega}$. To obtain an output signal leadin the input signal by τ_0 it is assumed that $W_{ref}(j\omega) = e^{j\omega\tau_0}$. Othe conversion rules may also be stipulated.

In identifying dynamic responses, the noise $f(t)$ fed to the system input is the useful signal, while the operational signal $u(t)$ introduces an error in determining the system parameters. Therefore in the case of identification the effect of the operational signal should be reduced. In the case of filtration with signal conversion the operational signal is useful, whereas the noise brings about an additional error in signal conversion, therefore the effect of noise is to be reduced.

Let us have a closer look at each problem and its solutions.

Identification of linear plant dynamic responses. Two approaches are possible: (1) direct determination of the plant weighting function

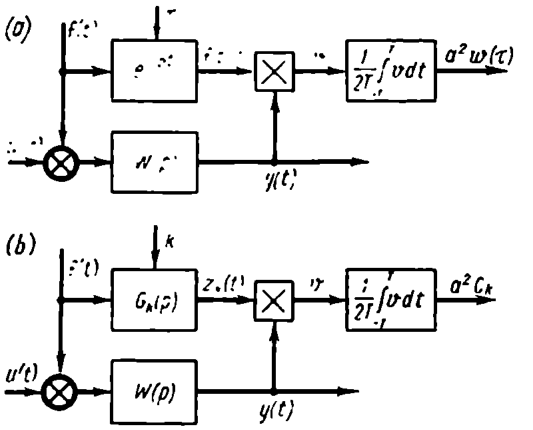

Fig. 24.5

and (2) obtaining the weighting function as factors of decomposition of the function into orthogonal functions.

In the first case the weighting function is sought through the expression (24.6), according to which the input-output cross-correlation function with a white noise at the input coincides with the weighting function to within a constant factor. Consequently, the plant may be identified using a variety of a correlator (see Fig. 23.17) shown schematically in Fig. 24.5*a*. The effect of $u(t)$ on $w(t)$ can be eliminated if $f(t)$ is a white noise, uncorrelated with the operational signal $u(t)$.

This intentionally introduced "noise" can be a pseudorandom binary white noise.

Since in this case $f(t)$ and hence $f(t-\tau)$ can take on but two values, $\pm a$, the multiplier in the correlator can be very simple, in the form of a relay changing the polarity of the signal $y(t)$.

The binary signal can be delayed by $\tau = kT_0$ by picking up the signal from one of the $n-1$ registers of the circuit (see Fig. 23.11).

In the second case a weighting function decomposed into orthogonal components can be obtained by selecting a specific kind of orthogonal g_k functions. Once the functions have been selected, elements $G_k(p)$ which generate these functions with pulse signals at the inputs can be used in the circuit of Fig. (24.5*b*) to automatically calculate the factors C_k for the decomposition of $w(t)$ into these orthogonal functions. As in the preceding case, $f(t)$ is a binary white noise and the integration is completed within a period of $2T = T_{seq} = NT_0$.

In identifying plants with inertial responses Laguerre functions can be conveniently used. A kth-order Laguerre function $l_k(\gamma t)$ is described as

$$l_k(\gamma t) = e^{-\gamma t} \sum_{i=0}^{k} \frac{2^{k-i} k! (-1)^i}{i! [(k-i)!]^2} (\gamma t)^{k-i} \qquad (24.23)$$

$$l_0(\gamma t) = e^{-\gamma t} \quad \text{at} \quad k=0, \quad l_1(\gamma t) = e^{-\gamma t}[2\gamma t - 1] \quad \text{at} \quad k=1$$

where γ is a scaling factor.

The plots of Laguerre functions for $k = 0, 1, 2, 3$ are shown in Fig. 24.6*a*. These functions are seen to describe an aperiodic process with multiple real roots; as $t \to \infty$ they tend to zero in the region of positive values, while the number of sign alterations is k; they are orthogonal and absolutely integrable.

Direct Fourier transformation of the Laguerre function (see Eq. (24.23)) yields

$$L_k(j\Omega) = L_k\left(j\frac{\omega}{\gamma}\right) = \int_{-\infty}^{\infty} l_k(\gamma t)\, e^{-j\omega t}\, dt = \frac{\gamma(\gamma - j\omega)^k}{(\gamma + \gamma\omega)^{k+1}} =$$

$$= |L_0(j\Omega)| \exp\{(2k+1)\, j \arg L_0(j\Omega)\} \qquad (24.24)$$

which is associated with a nonminimal-phase $(k+1)$th-order inertial element. The loci

$$L_k(j\Omega) = |L_0(j\Omega)| \exp\{(2k+1)\, j \arg L_0(j\Omega)\}$$

at $0 < \Omega < \infty$ are shown in Fig. 24.6*b*.

With Laguerre elements whose transfer functions are $L_k\left(\frac{p}{\gamma}\right)$ acting as generators $G_k(p)$ in Fig. 24.5*b*, the output of this circuit can directly give the factors for decomposition of the weighting function into Laguerre functions. Represent the unknown transfer function as a series

$$W(p) = \sum_{k=0}^{m} C_k L_k\left(\frac{p}{\gamma}\right) \qquad (24.25$$

and, accordingly, the weighting function as

$$w(t) = \sum_{k=0}^{m} C_k l_k(\gamma t) \tag{24.26}$$

Assume that the signal $f(\gamma t)$ is a unit pulse uncorrelated with the operational signal $u(t)$. Then the component of the signal $y(t)$

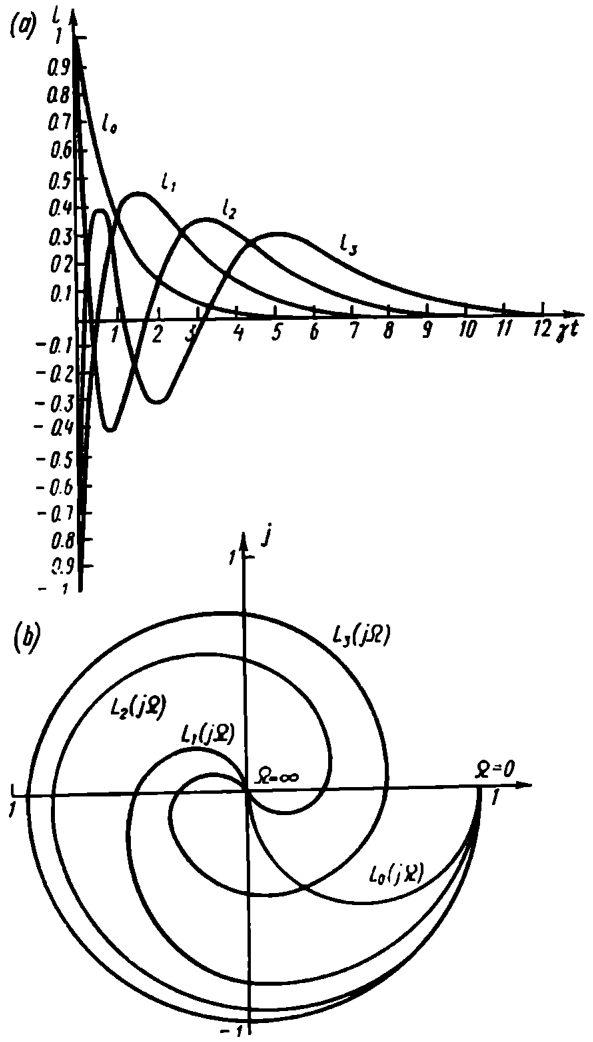

Fig. 24.6

uncorrelated with $u(t)$ is expressed by the function $w(t)$ as given by Eq. (24.26). The signal sent from the generator $G_k(p)$ to the multiplier is $l_k(\gamma t)$.

Since Laguerre functions are orthogonal, it follows that

$$2\int_0^\infty w(t)\, l_k(\gamma t)\, dt = C_k \qquad (24.27)$$

and, consequently, with a long enough averaging time the signal picked up from the multiplier (Fig. 24.5*b*) is proportional to the associated factor C_k.

If the signal $f(t)$ is a set of pulses with a spectral density $S_f(\omega) = a^2$, as in the case of a binary white noise, the signal picked up from the multiplier after integration is proportional to $a^2 C_k$. Thus, with m generators corresponding to different available values of k in the Laguerre functions integration yields the values of m factors C_k of the weighting function decomposition into the Laguerre functions.

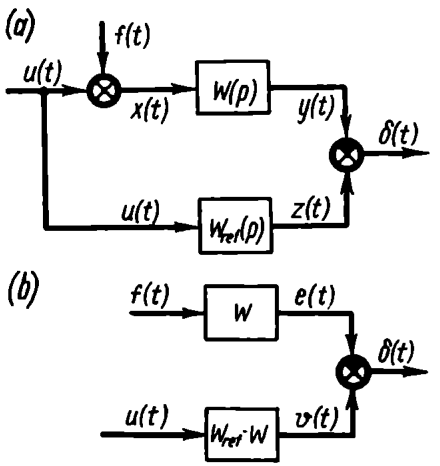

Fig. 24.7

Comparing the two methods of plant identification (see Fig. 24.5*a* and *b*) we see that both lead to dynamic responses of a normally operating plant at the rated value of $u(t)$.

The first method gives a set of weighting function ordinates at various τ, while the second yields the factors C_k of the weighting function decomposition into the Laguerre functions.

The latter is very convenient in constructing a plant model described by Eq. (24.25) and is readily implementable with known values of C_k.

Noise filtration with signal conversion. As in the analysis of linear system performance (see Ch. IX), in this case a structural diagram can be composed (Fig. 24.7*a*) consisting of an actually existing system $W(p)$ to be analyzed (the upper portion) and an imaginary ideal reference system $W_{ref}(p)$ (the lower portion).

The difference between the desired result $z(t)$ and the actual output signal $y(t)$ characterizes the system error.

In Ch. XI this problem was discussed for the case where the noise $f(t)$ and the operational signal $u(t)$ were deterministic. Now let us consider the case where these signals are of a random nature and only their statistical characteristics are known. Then two formulations of the problem are possible, depending on the degree of determinacy of the plant responses $W(p)$.

In the first case the expression for $W(p)$ is known; using $W_{ref}(p)$ and statistical characteristics of the signals $u(t)$ and $f(t)$, the r.m.s. error $\overline{\delta^2(t)}$ should be found and minimized by varying the plant parameters.

In the second case the plant response $W(p)$ is not constrained and should be so synthesized that using $W_{ref}(p)$ and statistical characteristics of the signals $u(t)$ and $f(t)$ $\overline{\delta^2(t)}$ is minimal.

The first formulation is associated with analysis and the second, with synthesis.

Here we will confine ourselves to the first one and find the expression for $\overline{\delta^2(t)}$.

The system error $\delta(t)$ (see Fig. 24.7) can be given in the operator form as

$$\Delta(p) = Z(p) - Y(p) = W_{ref}(p)\,U(p) - W(p)\,[U(p) + F(p)]$$
$$= [W_{ref}(p) - W(p)]\,U(p) - W(p)\,F(p) \qquad (24.28)$$

This expression describes the circuit of Fig. 24.7*b*.

Regarding the spectrum of the signal $\Delta(j\omega)$, by virtue of Eq. (24.28), as the difference of two signal spectra $V(j\omega) = [W_{ref}(j\omega) - W(j\omega)]\,U(j\omega)$ and $E(j\omega) = W(j\omega)\,F(j\omega)$, the spectral density can be given, according to Eq. (23.67), as

$$S_\delta(\omega) = S_v(\omega) + S_e(\omega) - 2\mathrm{Re}\,S_{ve}(j\omega) \qquad (24.29)$$

Expressing $S_v(\omega)$, $S_e(\omega)$ and $S_{ve}(j\omega)$ through $S_u(\omega)$, $S_f(\omega)$, $S_{uf}(j\omega)$, $W_{ref}(j\omega) - W(j\omega)$ and $W(j\omega)$ according to Eq. (24.28) and using Eqs. (24.16) and (24.17) gives

$$S_\delta(\omega) = |W_{ref}(j\omega) - W(j\omega)|^2 S_u(\omega) + |W(j\omega)|^2 S_f(\omega) -$$
$$- 2\mathrm{Re}\,[W_{ref}(j\omega) - W(j\omega)]\,W(-j\omega)\,S_{fu}(j\omega) \qquad (24.30)$$

If the signals $u(t)$ and $f(t)$ are uncorrelated, then $S_{fu}(j\omega) = 0$ and

$$S_\delta(\omega) = S_u(\omega)\,|W_{ref}(j\omega) - W(j\omega)|^2 + S_f(\omega)\,|W(j\omega)|^2 \qquad (24.31)$$

The first term is caused by signal distortion in the element $W(j\omega)$ due to the difference of this element from the reference, and the second one, by the noise.

If $W_{ref}(j\omega) = 1$, the first term of Eq. (24.31) is the spectral density of the misalignment signal component due to the operational signal $u(t)$, and the second one is the spectral density of the output signal component caused by the noise $f(t)$.

Equations (24.30) and (24.31) provide a simple device for calculating the r.m.s. error in signal conversion and filtration

$$\overline{\delta^2(t)} = \frac{1}{2\pi}\int_{-\infty}^{\infty} S_\delta(\omega)\,d\omega \qquad (24.32)$$

Since for linear systems $S_\delta(\omega)$ is usually a fractional rational real function, the calculation of the integral in (24.32) is reduced to finding the sum of integrals of the form

$$J_0 = \frac{1}{2\pi} \int_{-\infty}^{\infty} \frac{b(j\omega)\, b(-j\omega)}{c(j\omega)\, c(-j\omega)}\, d\omega \qquad (24.33)$$

given in Table A3.

Example 24.4. Find the r.m.s. error $\overline{\delta^2(t)}$ for the case where $S_f(\omega) = a^2$, $S_u(\omega) = \frac{1}{1+\omega^2}$, $W_{ref} = 1$, $W = \frac{k}{1+j\omega T_0}$ given that $S_{fu}(j\omega) = 0$.

Equation (24.31) yields

$$S_\delta(\omega) = \frac{1}{1+\omega^2}\left|1 - \frac{k}{1+j\omega T_0}\right|^2 + a^2\left|\frac{k}{1+j\omega T_0}\right|^2 =$$

$$= \frac{[(1-k)+j\omega T_0][(1-k)-j\omega T_0]}{[(1+j\omega)(1+j\omega T_0)][(1-j\omega)(1-j\omega T_0)]} + \frac{a^2k^2}{(1+j\omega T_0)(1-j\omega T_0)} \qquad (24.34)$$

The first addend is a product of two conjugate fractions with a second-order denominator

$$c_I(j\omega) = c_2(j\omega)^2 + c_1 j\omega + c_0 = T_0(j\omega)^2 + (T_0 + 1)\, j\omega + 1$$

and a first-order numerator

$$b_I(j\omega) = b_1 j\omega + b_0 = T_0 j\omega + (1 - k)$$

The integral (24.33) with the first addend as the integrand is

$$J_{0I} = \frac{b_1^2 c_0 + b_0^2 c_2}{2c_0 c_1 c_2} = \frac{T_0^2 + (1-k)^2 T_0}{2T_0(T_0+1)} = \frac{T_0 + (1-k)^2}{2(T_0+1)} \qquad (24.35)$$

The second addend of (24.34) is a product of two conjugate fractions with a first-order denominator

$$c_{II}(j\omega) = c_1 j\omega + c_0 = T_0 j\omega + 1$$

and a zero-order numerator

$$b_{II}(j\omega) = b_0 = ak$$

The integral (24.33) with the second addend as the integrand is

$$J_{0II} = \frac{b_0^2}{2c_0 c_1} = \frac{a^2k^2}{2T_0} \qquad (24.36)$$

We finally have

$$\overline{\delta^2(t)} + J_{0I} + J_{0II} = \frac{T_0 + (1-k)^2}{2(T_0+1)} + \frac{a^2k^2}{2T_0} \qquad (24.37)$$

The first addend of the error is caused by the element inertia and cutting off signal high-frequency components, and the second one, by the noise.

Example 24.5. Using the conditions of Example 24.4 find the values of T_0 and k ensuring the minimal r.m.s. error.

Because at $k < 1$ the first term of Eq. (24.37) decreases and the second one increases with increasing k, there exists an optimal value of k at which the error is minimal.

The value k_{opt} is found from Eq. (24.37)

$$\frac{\overline{\partial \delta^2(t)}}{\partial k} = 0 = -\frac{1-k}{1+T_0} + \frac{a^2 k}{T_0} \tag{24.38}$$

whence

$$k = k_{opt} = \frac{T_0}{a^2(1+T_0)+T_0} \tag{24.39}$$

The value of $T_{0\,opt}$ is found in a similar way from the equation

$$\frac{\overline{\partial \delta^2(t)}}{\partial T_0} = 0 = \frac{k(2-k)}{(1+T_0)^2} - \frac{a^2 k^2}{T_0^2}$$

Solving this equation for T_0 gives

$$T_0 = T_{0\,opt} = \frac{ak}{\sqrt{k(1-k)} - ak} \tag{24.40}$$

The optimal values of T_0 and k are found by simultaneous solution of Eqs. (24.39) and (24.40).

Transformations yield

$$k_{opt} = 1 - T_{0\,opt} \tag{24.41}$$

where

$$T_{0\,opt} = \frac{a}{\sqrt{1+a^2}}$$

For the particular case where the levels of noise and useful signal are the same, or $a = 1$, we have

$$k_{opt} = 1 - \frac{1}{\sqrt{2}} = \frac{1}{2+\sqrt{2}}, \qquad T_{0\,opt} = \frac{1}{\sqrt{2}}$$

If there is no noise $a = 0$ and

$$k_{opt} = 1 \quad \text{and} \quad T_{0\,opt} = 0$$

which represents a proportional element with a unit gain.

24.3. FINDING THE PARAMETERS OF AN OPTIMAL (IN TERMS OF MINIMAL R.M.S. ERROR) SERVO SYSTEM

The expressions obtained for the r.m.s. error ((24.32) and (23.30)) permit analysis of servo system accuracy with given statistical characteristics of the control signal $u(t)$ and noise $f(t)$.

Indeed, once the noise is reduced to the input (see Sec. 9.1) the structural diagram of a servo system can be represented as the circuit bounded by the dotted line in Fig. 24.8*a*.

Since the basic requirement for a servo system is the most accurate possible reproduction of the control signal at the output, it follows that for a servo system $W_{ref} = 1$, and the structural diagram facilitating error calculation can be represented as in Fig. 24.8*a* or (following transformations similar to those shown in Fig. 24.7*a* and *b*) as in Fig. 24.8*b*.

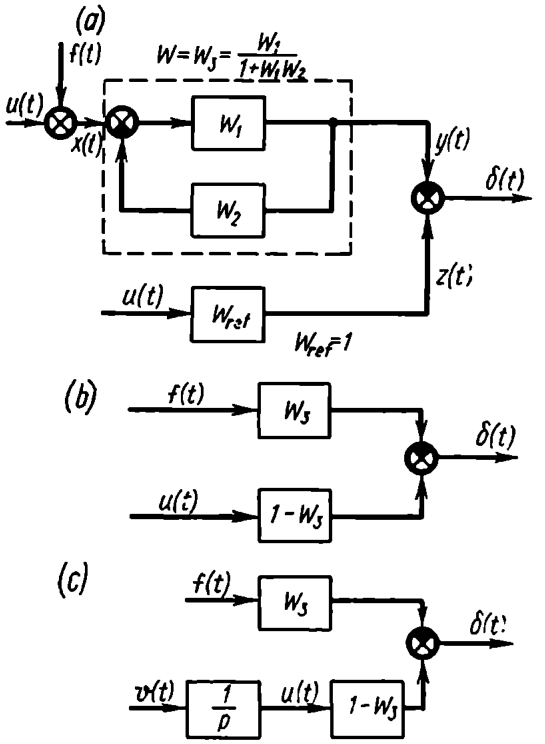

Fig. 24.8

In this case Eqs. (24.32) and (24.30) can be directly applied with $W_{ref} = 1$, $W = W_{cl\text{-}l} = \frac{W_1}{1+W_1W_2}$, and the statistical characteristics of the control signal $u(t)$ and the noise $f(t)$ are given.

If (as is often the case in servo systems) the statistical characteristics of the derivative $v(t) = \frac{du}{dt}$ rather than those of the control signal $u(t)$ are known, the structural diagram is converted to the form shown in Fig. (24.8*c*), and the error spectral density is given as

$$S_\delta(\omega) = S_v(\omega)\left|\frac{1-W_{cl\text{-}l}(j\omega)}{j\omega}\right|^2 + S_f(\omega)\,|W_{cl\text{-}l}(j\omega)|^2 - 2\,\mathrm{Re}\left[\frac{1-W_{cl\text{-}l}(j\omega)}{j\omega}\right] W_{cl\text{-}l}(-j\omega)\,S_{fv}(j\omega) \qquad (24.42)$$

The first term represents the system error, the second one, the error due to the noise, and the last term, the error caused by the cross-impact of the noise and the control signal.

If Eq. (24.42) is used for determining the system r.m.s. error by Eq. (24.32), the accuracy-optimal values of the servo system parameters a_i can be determined by varying the parameters a_i (e.g. k and T) and finding the conditions for a minimal r.m.s. error

$$\frac{\partial\overline{\delta^2(t)}}{\partial a_i} = 0 \qquad (24.43)$$

Example 24.6. A servo system has $W_1 = \frac{k_1}{p}$ and $W_2 = k_2$. Find the optimal values of k_1 and k_2 ensuring a minimal value of $\overline{\delta^2(t)}$ if the spectral densities of the noise and of the control signal are as in Examples 24.4. and 24.5.

The closed-loop transfer function is

$$W_{cl\text{-}l} = \frac{W_1}{1+W_1W_2} = \frac{k_1}{p+k_1k_2} = \frac{\frac{1}{k_2}}{1+\frac{p}{k_1k_2}} \tag{24.44}$$

and, consequently, for

$$W_{cl\text{-}l} = W = \frac{k}{1+pT_0}$$

we have $k = \frac{1}{k_2}$ and $T_0 = \frac{1}{k_1k_2}$, or $k_2 = \frac{1}{k}$ and $k_1 = \frac{k}{T_0}$.

Thus, the conditions are reduced to Example 24.5, for which the optimal values of k and T_0 expressed by Eq. (24.41) have been found. Substituting these values into the expressions for k_2 and k_1, we have

$$k_{2\,opt} = \frac{1}{k_{opt}} = 1 + a^2 + a\sqrt{1+a^2}$$

$$k_{1\,opt} = \frac{k_{opt}}{T_{0\,opt}} = \frac{\sqrt{1+a^2}}{a} - 1$$

If $a = 1$, then $k_{1\,opt} = \sqrt{2}-1$ and $k_{2\,opt} = 2+\sqrt{2}$.

At $a = 0$ we have $k_{1\,opt} \to \infty$ and $k_{2\,opt} = 1$.

Example 24.7. A servo system has $W_1 = \frac{k_1}{p(1+pT_1)}$ and $W_2 = 1$. Find the optimal value of k_1 which ensures a minimum of $\overline{\delta^2(t)}$ if there is a white noise $S_f(\omega) = a^2$ and the rate $v = \frac{du}{dt}$ at which the control signal changes is characterized by a spectral density $S_v(\omega) = \frac{\alpha^2}{\alpha^2+\omega^2}$. The noise and control action are uncorrelated, $S_{fu}(j\omega) = 0$.

Equation (24.42) gives

$$S_\delta(\omega) = \frac{\alpha^2(1+\omega^2T_1^2)}{(\alpha^2+\omega^2)[(k_1-T_1\omega^2)^2+\omega^2]} + \frac{a^2k_1^2}{(k_1-T_1\omega^2)^2+\omega^2} =$$

$$= \frac{\alpha^2(1+j\omega T_1)(1-j\omega T_1)}{(\alpha+j\omega)[(k_1-T_1\omega^2)+j\omega](\alpha-j\omega)[(k_1-T_1\omega^2)-j\omega]} +$$

$$+ \frac{a^2k_1^2}{[(k_1-T_1\omega^2)+j\omega][(k_1-T_1\omega^2)-j\omega]} \tag{24.45}$$

Calculating the integrals of the form (24.36) by the formulae of Table A3, we have

$$\overline{\delta^2(t)} = \frac{\alpha[1+\alpha T_1(1+k_1T_1)]}{2k_1[\alpha^2T_1+\alpha+k_1]} + \frac{a^2k_1}{2} \qquad (24.46)$$

The first term here is $\overline{\delta_u^2(t)}$, the error caused by the control action and reducing with increasing k_1, and the second term is $\overline{\delta_f^2(t)}$, the noise-induced error, which increases with k_1.

Finding the optimal value of k_1 in the general form by differentiation of Eq. (24.43) is a rather cumbersome process because it involves the solution of fourth-order equations. Therefore the problem is usually solved numerically for specific values of parameters. An example showing the dependence of $\overline{\delta_u^2}$, $\overline{\delta_f^2}$ and $\overline{\delta^2}$ on k_1 for $a_1 = \alpha = 1$ and $T_1 = 2$ is shown in Fig. 24.9.

24.4. SYNTHESIS OF ACCURACY-OPTIMAL SYSTEMS SUBJECTED TO STATIONARY RANDOM ACTIONS

We have thus far dealt with the problems of finding optimal parameters for a linear system in the first version, where the structure of an expression for $W(p)$ is known and the parameter values are determined through an analysis of the r.m.s. error.

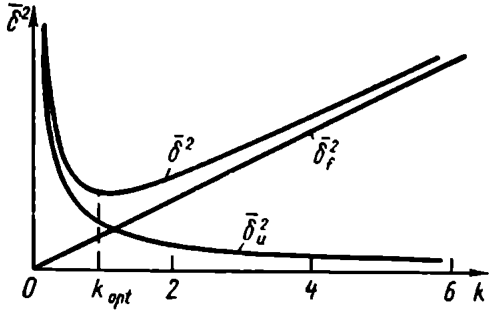

Fig. 24.9

We will now consider a more general synthesis problem where the statistical characteristics of signals and $W_{ref}(j\omega)$ are known and an expression for $W(j\omega)$ which minimizes $\overline{\delta^2(t)}$ is to be found.

The results of Kolmogorov and Wiener as applied to the problem of noise filtration with signal conversion are described below.

Considering the diagram of Fig. 24.7*a* we have for the frequency spectrum $\Delta(j\omega)$, similarly to Eq. (24.28),

$$\Delta(j\omega) = W_{ref}(j\omega)\,U(j\omega) - W(j\omega)\,X(j\omega) \qquad (24.47)$$

Using the spectral densities, as in Eq. (24.33), gives

$$S_\delta(\omega) = |W(j\omega)|^2 S_x(\omega) - 2\mathrm{Re}\,W_{ref}(j\omega)\,W(-j\omega) \times \\ \times S_{xu}(j\omega) + |W_{ref}(j\omega)|^2 S_u(\omega) \qquad (24.48)$$

Completing the first two terms to the squared magnitude of the difference between the two complexes by adding

$$|W_{ref}(j\omega)|^2 \frac{|S_{xu}(j\omega)|^2}{S_x(\omega)}$$

we have, after transformations,

$$S_\delta(\omega) = \left|W(j\omega) - \frac{W_{ref}(j\omega) S_{xu}(j\omega)}{S_x(\omega)}\right|^2 S_x(\omega) + \\ + |W_{ref}(j\omega)|^2 \left(1 - \frac{|S_{xu}(j\omega)|^2}{S_x(\omega) S_u(\omega)}\right) S_u(\omega) \qquad (24.49)$$

The minimization of $S_\delta(\omega)$ and, hence, of $\delta^2(t)$ is achieved by selecting $W(j\omega)$ so that the first addend is minimal.

The second addend is real and positive and independent of $W(j\omega)$.

Since the first addend is a positive real number, the minimization condition is that it be zero.

Consequently, the optimal value is

$$W(j\omega) = W_{opt}(j\omega) = \frac{W_{ref}(j\omega) S_{xu}(j\omega)}{S_x(\omega)} \qquad (24.50)$$

If the noise and signal are uncorrelated and $S_{fu}(j\omega) = 0$, then $S_{xu}(j\omega) = S_u(\omega)$, while $S_x(\omega) = S_u(\omega) + S_f(\omega)$.

In this case Eq. (24.50) takes the form

$$W(j\omega) = W_{opt}(j\omega) = \frac{W_{ref}(j\omega) S_u(\omega)}{S_u(\omega) + S_f(\omega)} \qquad (24.51)$$

Consequently, if there are no constraints on selection of $W(j\omega)$, $W(j\omega)$ should be selected with the use of Eq. (24.50) or (24.51) for the system to be optimal in terms of the minimal r.m.s. error. The mathematical solution, however, is found to contradict the conditions for physical realization. In most practical cases $W(j\omega)$ values found by these formulae lead to physically unrealizable values of parameters.

Example 24.8. Find the optimal value of $W(j\omega)$ if

$$W_{ref}(j\omega) = 1, \qquad S_u(\omega) = \frac{1}{1+\omega^2}$$

$$S_f(\omega) = 1, \qquad S_{fu}(j\omega) = 0$$

Equation (24.51) yields

$$W_{opt}(j\omega) = \frac{1}{2+\omega^2} = \frac{1}{(\sqrt{2}+j\omega)(\sqrt{2}-j\omega)} \qquad (24.52)$$

This equation represents a series connection of two inertial elements of which one is unstable and unimplementable in practical hardware.

The unrealizability of the condition (24.52) becomes especially apparent when changing over from $W_{opt}(j\omega)$ to the weighting function

$$w_{opt}(t) = \frac{1}{2\pi}\int_{-\infty}^{\infty} \frac{1}{2+\omega^2} e^{j\omega t}\, d\omega = \frac{1}{2\sqrt{2}} e^{-|t|\sqrt{2}} \qquad (24.53$$

The plot of the system response $y(t) = w_{opt}(t)$ to a unit pulse $x = \delta(t)$ (Fig. 24.10*a*) for this case is shown in Fig. 24.10*b*. To obtain the desired weighting function, the signal at the output should begin increasing long before the appearance of the pulse at the input.

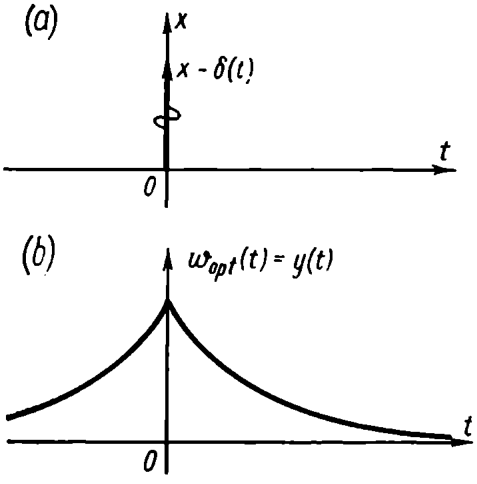

Fig. 24.10

Processes in which the effect precedes the cause are clearly out of the question in practice.

To find the optimal value of $W(j\omega)$ taking into account the conditions for practical realizability, the expression for $W_{opt}(j\omega)$ may be represented as two addends of which one is realizable and the other is unrealizable and represents a component of the error spectral density.

In further discussion this technique, which has been derived from the Kolmogorov-Wiener theory, is given without proof.

Suppose we know $W_{opt}(j\omega)$ expressed by Eq. (24.50); then $S_x(\omega)$ can be given as a product of two conjugate functions, $\Psi(j\omega)$ and $\Psi(-j\omega)$, the former having poles in the upper half-plane and the latter, in the lower one

$$S_x(\omega) = \Psi(j\omega)\,\Psi(-j\omega) \qquad (24.54$$

The function $\Psi(j\omega)$ represents a realizable stable linear element which transforms a white noise into a signal $x(t)$ at the input of the linear system to be designed. The function $\Psi(-j\omega)$ represents the unrealizable part.

The representation of $S_x(\omega)$ as the product $\Psi(j\omega)\,\Psi(-j\omega)$ and the isolation of the multiplier $\Psi(j\omega)$ is usually referred to as *factorizing*.

Consequently

$$W_{opt}(j\omega) = \frac{1}{\Psi(j\omega)} \frac{W_{ref}(j\omega)\, S_{xu}(j\omega)}{\Psi(-j\omega)} \qquad (24.55$$

The isolation of the multiplier $\frac{1}{\Psi(j\omega)}$ is in fact the reduction of the input signal to a white noise followed by an analysis of the white noise effect on an unrealizable element with a response $\frac{W_{ref}(j\omega)\,S_{xu}(j\omega)}{\Psi(-j\omega)}$.

The other operation is known as *splitting*; the function $\Psi(j\omega)\,W_{opt}(j\omega)$ is split into $R(j\omega)$ and $N(-j\omega)$ with poles in the upper and the lower half-planes

$$\Psi(j\omega)\,W_{opt}(j\omega)=\frac{W_{ref}(j\omega)\,S_{xu}(j\omega)}{\Psi(-j\omega)}=R(j\omega)+N(-j\omega) \qquad (24.56)$$

The first of these addends corresponds to the realizable and the second, to the unrealizable transfer function. Ignoring the unrealizable part we will have for the realizable response

$$W_{opt\,r}(j\omega)=\frac{R(j\omega)}{\Psi(j\omega)} \qquad (24.57)$$

This formula is known as the Kolmogorov-Wiener formula and serves to obtain the optimal parameters.

If $W(j\omega)$ has been obtained by Eq. (24.57), the error spectral density found by Eq. (24.49) is given as

$$S_\delta(\omega)=\left|\frac{N(-j\omega)}{\Psi(j\omega)}\right|^2 S_x(\omega)+|W_{ref}(j\omega)|^2\left[S_u(\omega)-\frac{|S_{xu}(j\omega)|^2}{S_x(\omega)}\right] \qquad (24.58)$$

Example 24.9. Find the optimal value of $W(j\omega)$ in Example 24.8 with the realizability conditions met.

Factorize by Eq. (24.54) and determine

$$S_x(\omega)=S_u(\omega)+S_f(\omega)=\frac{2+\omega^2}{1+\omega^2}=\left(\frac{\sqrt{2}+j\omega}{1+j\omega}\right)\left(\frac{\sqrt{2}-j\omega}{1-j\omega}\right)=$$
$$=\Psi(j\omega)\,\Psi(-j\omega) \qquad (24.59)$$

Split by Eq. (24.56)

$$\frac{W_{ref}(j\omega)\,S_{xu}(j\varphi)}{\Psi(-j\omega)}=\frac{(1-j\omega)}{(1+\omega)^2(\sqrt{2}-j\omega)}=\frac{1}{(1+j\omega)(\sqrt{2}-j\omega)}=$$
$$=R(j\omega)+N(-j\omega)=\frac{A}{1+j\omega}+\frac{B}{\sqrt{2}-j\omega} \qquad (24.60)$$

To determine the factors A and B, solve the equation

$$A(\sqrt{2}-j\omega)+B(1+j\omega)=1 \qquad (24.61)$$

whence

$$A=B=\frac{1}{1+\sqrt{2}} \quad \text{and} \quad R(j\omega)=\frac{1}{(1+\sqrt{2})(1+j\omega)} \qquad (24.62)$$

Equation (24.57) finally gives

$$W_{opt\,r}(j\omega)=\frac{1}{(1+\sqrt{2})(\sqrt{2}+j\omega)}=\frac{1}{(2+\sqrt{2})\left(1+j\frac{\omega}{\sqrt{2}}\right)} \quad (24.63)$$

Comparing the solution obtained with the results of Example 24.5 for $a=1$ we have complete agreement.

The structure of an inertial element obtained in Example 24.5 is thus optimal for the problem conditions at hand.

24.5. TRANSFORMATION OF A DISTRIBUTION LAW BY A LINEAR ELEMENT

Not only spectral characteristics of random signals but also their distribution functions change in propagation through a linear dynamic element. It is generally very difficult to establish the output signal distribution law with known statistical characteristics of the input (Ref. 62).

This problem has a simple solution only in two particular, although important, practical cases.

1. The signal $x(t)$ has a normal distribution. In this case, as will be shown, a linear transformation also leads to a normal distribution. The parameters completely determining this distribution are two moments: the first, $M[y(t)]$, is defined by multiplying the first moment $M[x(t)]$ of the input signal by the element gain, and the second, $M[y^2(t)]$, is found by Eq. (24.20).

2. The signal $x(t)$ is a harmonic signal with a random phase. In this case the output signal $y(t)$ is also harmonic, that is the shape of the distribution is preserved, and only the amplitude, the numerical parameter, undergoes a change

$$Y_m=|W(j\omega)|X_m \quad (24.64)$$

where ω is the harmonic random signal frequency, $W(j\omega)$ the element complex gain and X_m the input signal amplitude.

Consider now one property of a linear transformation which greatly facilitates the problem in many theoretically important cases.

Consider the convolution integral (24.1)

$$y(t)=\int_0^\infty w(\tau)x(t-\tau)\,d\tau$$

Divide the integration interval into subintervals

$$(0, \tau_1), (\tau_1, \tau_2), \ldots, (\tau_k, \tau_{k+1})$$

and use the mean value theorem.

Then

$$y(t)=\sum_{k=0}^{\infty} x(t-\tau_k^*)\int_{\tau_k}^{\tau_{k+1}} w(\tau)\,d\tau=\sum_{k=0}^{\infty}\xi_k \qquad (24.65)$$

where

$$\xi_k=x(t-\tau_k^*)\int_{\tau_k}^{\tau_{k+1}} w(\tau)\,d\tau \qquad (24.66)$$

$$\tau_k\leqslant\tau_k^*\leqslant\tau_{k+1},\qquad \tau_0=0$$

Let the subintervals be selected so that the random quantities $x(t-\tau_k^*)$ and, hence, the quantities ξ_k are statistically independent. Then $y(t)$ is a sum of an infinite number of statistically independent random quantities.

Among other things Eq. (24.65) corroborates the above statement that if $x(t)$ is distributed normally, the process $y(t)$ is normal as well, because a sum of normally distributed random quantities also has a normal distribution (Ref. 85).

Furthermore, the central limit theorem (the Lyapunov theorem) states that the distribution of a sum of a great number of uncorrelated random quantities approaches the normal law even if the distribution of each individual quantity differs from a normal one.

The conditions under which this statement is true are basically reducible to the requirement that the quantities to be added up have dispersions of approximately equal order.

These conditions are apparently met if a sufficiently large number, N, of subintervals of statistical independence ($\Delta\tau_k=\tau_{k+1}-\tau_k$) is selected so that over a period from 0 to τ_N the value of the weighting function is not unduly low.

In other words, if a signal with an arbitrary distribution $p_1(x)$ propagates through a linear element, the output distribution $p_1(y)$ is normalized, or approaches the normal law if the plant weighting function $w(\tau)$ decays slowly and the input signal correlation function $R_x(\tau)$ decays rapidly.

Let us have an example of normalizing the distribution law of a random signal at the output of a linear element.

Example 24.10. The input signal of an inertial element with a transfer function

$$W(p)=\frac{1}{1+pT} \qquad (24.67)$$

is a binary white noise with an amplitude a and a cycle duration T_0.

If $T=0$, then the probability distribution $p_1(y)$ of the output signal is made up of two δ-functions (Fig. 24.11*a*) because in this case $y(t)=x(t)$.

If in Eq. (24.67) $T \neq 0$, $y(t)$ cannot change stepwise from one level to another as the input signal does, but takes on all the values

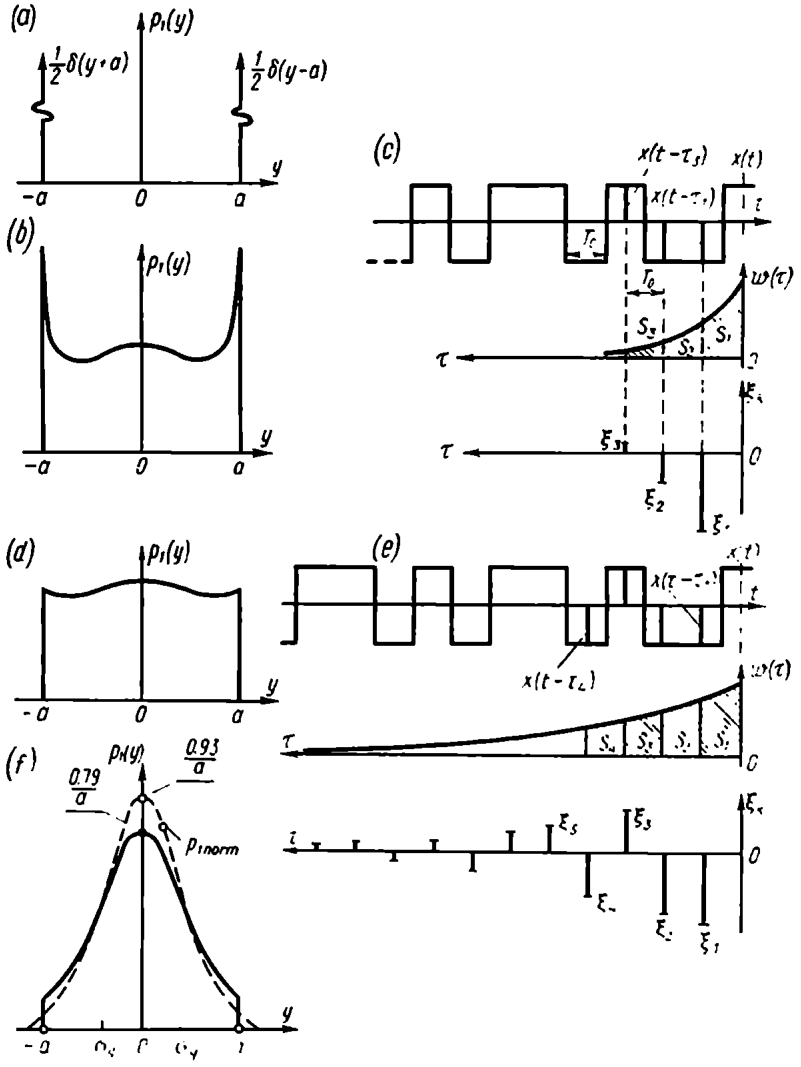

Fig. 24.11

in the interval $(-a, a)$. In this case, for the entire range $-a \leqslant y \leqslant a$ the probability distribution $p_1(y)$ is nonzero.

In order to find the distribution law $p_1(y)$ at various values of the time constant T, the propagation of a binary white noise through

an inertial element was simulated on a digital computer. The function $p_1(y)$ was calculated by a technique built around Eq. (23.75).

Figure 24.11*b* shows the probability distribution for the signal $y(t)$ when $T = T_0$. This distribution is still far from normal, it being attributable to the small number of addends, ξ_k, in the sum (24.65) with this time constant. Figure 24.11*c* illustrates the formation of these addends. As follows from Eq. (23.39), for $\tau \geqslant T_0$ the values $x(t)$ and $x(t-\tau)$ of the binary white noise are uncorrelated. Therefore the axis of the variable τ is divided into subintervals $\Delta\tau = T_0$. The values $x(t+\tau_1)$, $x(t-\tau_2)$, . . . of the input signal multiplied by the areas S_1, S_2, . . . bounded by the weighting function on the appropriate subintervals $S_k = \int_{\tau_{k-1}}^{\tau_k} w(\tau)\,d\tau$ represent the addends ξ_1, ξ_2, . . . of the sum (24.65). Figure 24.11*c* shows only three quantities ξ_k (ξ_1, ξ_2, ξ_3) because the magnitude of the subsequent quantities is less than one-twentieth of that of the first one.

Figure 24.11*d* shows the distribution $p_1(y)$ with $T = 4T_0$, which appears to be closer to uniform. Figure 24.11*e* shows as many as 12 values of ξ_k. Starting with $k = 13$, the values of ξ_k amount to less than 5% of ξ_1.

At $T = 8T_0$ the distribution $p_1(y)$ is given in Fig. 24.11*f*, which shows the r.m.s. deviation σ_y found from Eq. (24.20) on the basis of the complex gain (see Eq. (24.67)) and from the spectral density of the binary white noise (see Eq. (23.40))

$$\sigma_y^2 = \frac{1}{\pi}\int_0^\infty \left|\frac{1}{1+j\omega T}\right|^2 a^2 T_0 \left(\frac{\sin\frac{\omega T_0}{2}}{\frac{\omega T_0}{2}}\right)^2 d\omega =$$

$$= \frac{a^2}{T_0}\left[T_0 - T\left(1-e^{-\frac{T_0}{T}}\right)\right] \qquad (24.68)$$

For $T = 8T_0$ Eq. (24.68) gives

$$\sigma_y^2 = 0.35a \qquad (24.69)$$

The normal distribution law for this value of σ_y, $p_{1\,norm}$ is denoted by the dotted line. The distribution $p_1(y)$ for $T = 8T_0$ is seen to be relatively close to normal.

To normalize the distribution of a signal propagating through a linear element, all values of ξ_k (see Eq. (24.66)) which add up to the output signal should be indeed random, otherwise the distribution law can even recede from normal.

This is illustrated by the following example.

Example 24.11. At the input of an integrating element (Fig. 24.12a the signal is of a saw-tooth waveform (Fig. 24.12*b*); T_1 is the signal period and A is the amplitude. The distribution law for a saw-tooth signal is apparently uniform $p_1(x) = \frac{1}{2A}$, over the interval $-A \leqslant x \leqslant A$ (Fig. 24.12*c*). The output coordinate $y(t)$ is found by integrating the signal $x(t)$ over the time intervals $0 \leqslant t \leqslant \frac{T_1}{2}$ and $\frac{T_1}{2} \leqslant t \leqslant T_1$:

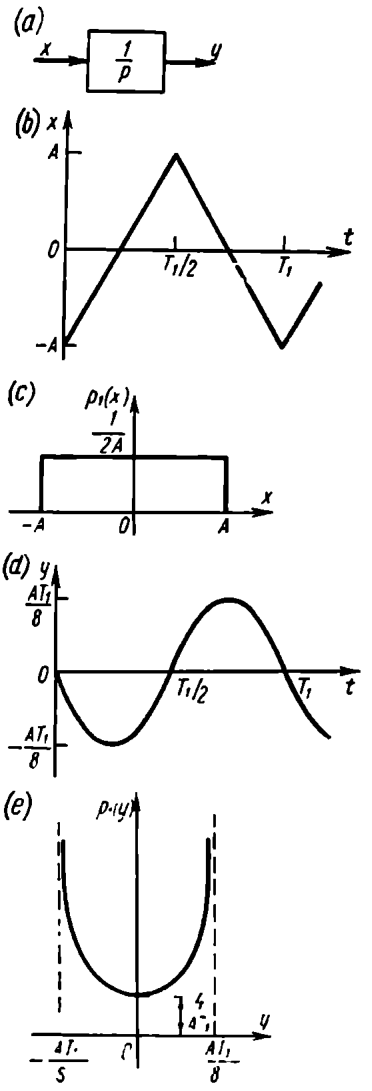

Fig. 24.12

$$y(t) = \begin{cases} \frac{2A}{T_1} t^2 - At & \text{for } 0 \leqslant t \leqslant \frac{T_1}{2} \\ 3At - \frac{2A}{T_1} t^2 - AT_1 & \text{for } \frac{T_1}{2} \leqslant t \leqslant T_1 \end{cases} \tag{24.70}$$

The plot $y(t)$ is shown in Fig 24.12*d*.

By virtue of Eq. (23.75) the distribution density $p_1(y)$ can be found as a relative time of being in the interval $(y, y + \Delta y)$. Since $y(t)$ is periodic and each such interval is swept out twice within a half-period we have

$$p_1(y)\,\Delta y = \frac{2\Delta t}{\frac{T_1}{2}} = \frac{4\Delta t}{T_1} \tag{24.71}$$

where Δt is the time period associated with Δy.

Making Δy go to zero, we have from Eq. (24.71)

$$p_1(y) = \frac{4}{T_1} \frac{dt}{dy} \tag{24.72}$$

Expressing t through y from Eq. (24.70) and taking into account that $y < 0$ for $0 < t < \frac{T_1}{2}$ and $y > 0$ for $\frac{T_1}{2} < t < T_1$, we get from

Eq. (24.72)

$$p_1(y) \cdot \begin{cases} \dfrac{4}{AT_1\sqrt{1+\dfrac{8}{AT_1}y}} & \text{at} \quad -\dfrac{8}{AT_1} < y \leqslant 0 \\ \dfrac{4}{AT_1\sqrt{1-\dfrac{8}{AT_1}y}} & \text{at} \quad \dfrac{8}{AT_1} > y \geqslant 0 \end{cases} \tag{24.73}$$

The plot of the function (24.73) is displayed in Fig. 24.12*e*.

Comparing Figs. 24.12*c* and 24.12*e*, we can see that the signal $y(t)$ at the output of a linear element (incidentally, with the non-decaying weighting function $\omega(t) = 1$) subjected to a deterministic signal $x(t)$ at the input has a distribution $p_1(y)$, which is still farther from normal than the distribution $p_1(x)$ of the input signal.

Chapter XXV

NONLINEAR SYSTEMS SUBJECTED TO RANDOM STATIONARY SIGNALS

25.1. RANDOM SIGNAL PROPAGATION THROUGH A NONLINEAR ELEMENT

Random signal propagation through a linear element was studied by using time-averaging methods (correlation functions and spectral densities); in studying nonlinear elements, set-averaging methods (distribution laws) are used.

As with nonlinear systems subjected to deterministic actions, the methods for studying random signal propagation through a nonlinear element are more complicated and diverse than those used for linear systems.

Since accurate solutions are either complicated or unattainable approximate methods are most widely used. These methods may differ greatly depending on whether the nonlinear response is single or multivalued, inertial or otherwise, and on whether the system is closed- or open-loop. The most developed methods are those for a nonlinear element with a single-valued inertialess response.

Let us first consider the change of the distribution law for a random signal at a fixed instant and, hence, the change of its mathematical expectation and dispersion (first- and second-order moments). Then we shall see how the signal correlation function and spectral density are transformed and how we can apply the results thus obtained to approximate calculation of processes in control systems.

25.2. DISTRIBUTION DENSITY TRANSFORMATION

Consider an inertialess nonlinear element (Fig. 25.1*a*) with a monotonically increasing response $z(x)$ (Fig. 25.1*b*) whose input receives a random signal $x(t)$ with a sample set 1, 2, 3, . . ., n having a distribution density $p_1(x)$ at any time t_1 (Fig. 25.1*c*).

In this case the distribution density $p_1(z)$ of the output signal $z(t)$ with the sample set 1, 2, 3, etc. at the same instant t_1 (Fig. 25.1*c*) can be found from the condition of equal probability that the input signal belongs to the region $x_1 < x < x_1 + dx$ and the output signal belongs to the region $z_1 < z < z_1 + dz$ (Fig. 25.1*b*), where $z_1 =$

$= z(x_1)$ and $dz = \frac{dz}{dx}\, dx$; then

$$p_1(x)\, dx = p_1(z)\, dz \tag{25.1}$$

$$p_1(z) = \left(\frac{dx}{dz}\right) p_1[x(z)] \tag{25.2}$$

This expression permits obtaining $p_1(z)$ from $p_1(x)$ and $z(x)$ with $z(x)$ monotonically increasing.

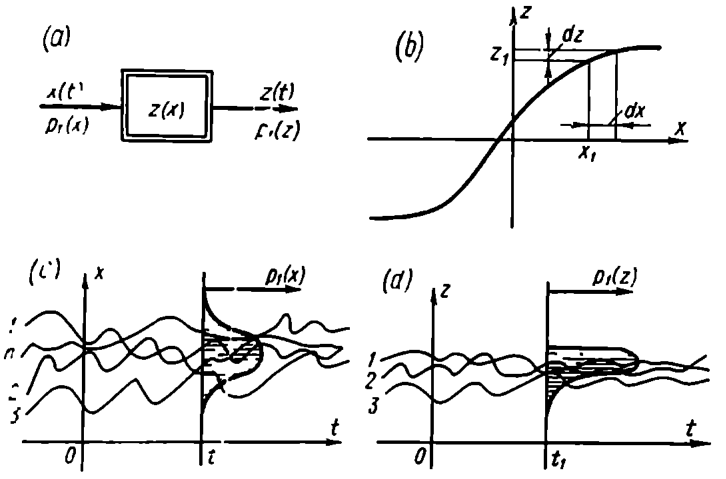

Fig. 25.1

Example 25.1. A signal x with a uniform distribution

$$p_1(x) = \begin{cases} \frac{1}{2}a & \text{at } |x| \leqslant a \\ 0 & \text{at } |x| > a \end{cases}$$

propagates through a nonlinear element with a response $z = x^3$ or $x = z^{\frac{1}{3}}$. Determine $p_1(z)$.

For the region $|z| < a^3$ we have by Eq. (25.2)

$$p_1(z) = \frac{1}{2a}\frac{dx}{dz} = \frac{1}{6a} z^{-\frac{2}{3}}$$

For the region $|z| > a^3$ we have $p_1(z) = 0$.

The plots $p_1(x)$, $z(x)$ and $p_1(z)$ are given in Fig. 25.2*a*, *b*, *c*.

Example 25.2. A signal x with a normal distribution (Fig. 25.3*a*)

$$p_1(x) = \frac{1}{\sigma_x \sqrt{2\pi}} \exp\left[\frac{(x - m_x)^2}{2\sigma_x^2}\right] \tag{25.3}$$

passes through a saturation-type nonlinear element with a response (Fig. 25.3*b*)

$$z = \begin{cases} x & \text{at} \quad |x| \leqslant x_b = z_b \\ x_b \operatorname{sign} x & \text{at} \quad |x| > x_b = z_b \end{cases}$$

Determine $p_1(z)$.

For the region $|z| < x_b$ Eq. (25.2) gives

$$p_1(z) = \frac{1}{\sigma_x \sqrt{2\pi}} \exp\left[-\frac{(z-m_x)^2}{2\sigma^2}\right]$$

For $|z| = x_b$ we have $\frac{dz}{dx} = 0$ and, consequently, $p_1(z) \to \infty$. So in the points $z = \pm z_b$ the distribution density $p_1(z)$ (Fig. 25.3*c*) is expressed by pulse functions $S_1\delta(z - z_b)$ and $S_2\delta(z + z_b)$.

The values of S_1 and S_2 are obtained from the conditions

$$S_1 = \int_{x_b}^{\infty} p_1(x)\,dx \quad \text{and} \quad S_2 = \int_{-\infty}^{-x_b} p_1(x)\,dx \qquad (25.4)$$

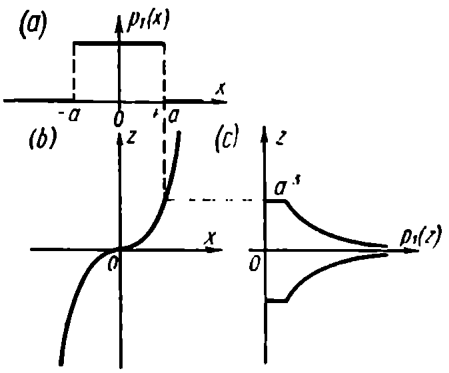

Fig. 25.2

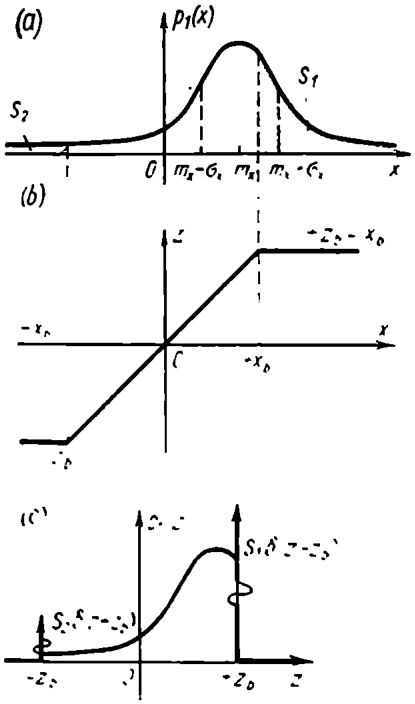

Fig. 25.3

which follow directly from Eq. (25.1) after its integration.

Here S_1 and S_2 are the probabilities of z being equal to $+z_b$ and $-z_b$. These probabilities are equal to areas bounded by the curve $p_1(x)$ on the intervals $-\infty < x < -x_b$ and $x_b < x < \infty$ (see Fig. 25.3*a*).

For the normal distribution law (25.3)

$$\int_{-\infty}^{m_x} p_1(x)\,dx = \int_{m_x}^{\infty} p_1(x)\,dx = \frac{1}{2}$$

and these probabilities will thus be

$$S_1 = \frac{1}{2} - \int_0^{x_b - m_x} p_{10}(x)\,dx = \frac{1}{2} - \Phi\left(\frac{x_b - m_x}{\sigma_x}\right)$$
$$S_2 = \frac{1}{2} - \int_0^{x_b + m_x} p_{10}(x)\,dx = \frac{1}{2} - \Phi\left(\frac{x_b + m_x}{\sigma_x}\right) \tag{25.5}$$

where

$$p_{10}(x) = \frac{1}{\sigma_x \sqrt{2\pi}} \exp\left(-\frac{x^2}{2\sigma_x^2}\right) \tag{25.6}$$

$$\Phi\left(\frac{x}{\sigma_x}\right) = \int_0^x p_{10}(x)\,dx \tag{25.7}$$

The integral $\Phi(t) = \frac{1}{2\pi} \int_0^t e^{-\frac{t^2}{2}}\,dt$ is a probability integral. Tables of such integrals are readily available.

The plot of $\Phi(t)$ is given in Fig. 25.4.

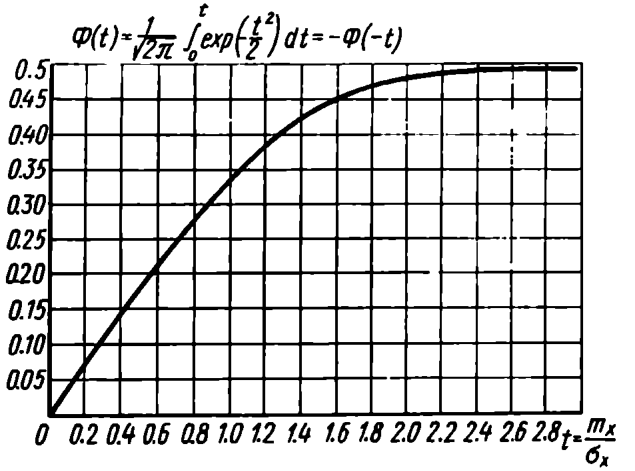

Fig. 25.4

Example 25.3. The signal x considered in Example 25.2 propagates through a nonlinear element with a relay response

$$z = z_b \operatorname{sign} x \tag{25.8}$$

In this case $p_1(z) = 0$ at $|z| \neq z_b$, while at $|z| = z_b$ the distribution density $p_1(z)$ is expressed by the pulse functions $S_1\delta(z - z_b)$ and $S_2\delta(z + z_b)$, where

$$S_1 = \int_0^\infty p_1(x)\,dx = \frac{1}{2} + \Phi\left(\frac{m_x}{\sigma_x}\right)$$

$$S_2 = \int_{-\infty}^0 p_1(x)\,dx = \frac{1}{2} - \Phi\left(\frac{m_x}{\sigma_x}\right) \tag{25.9}$$

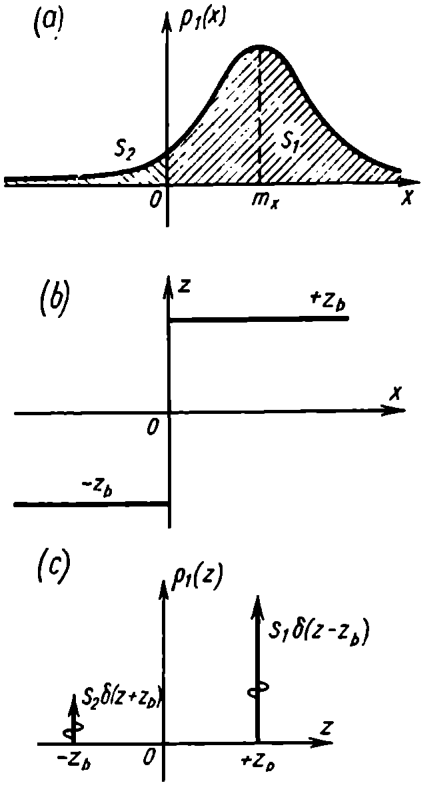

Fig. 25.5

The plots $p_1(x)$, $z(x)$ and $p_1(z)$ for this case are shown in Fig. 25.5*a*, *b*, *c*, respectively.

When a nonlinear response is multivalued, the distribution density at the output of a nonlinear element is much more difficult to determine. For a relay with hysteresis, a play- or step-type element there are no such simple methods as for nonlinearities with a single-valued response.

The signal distribution density at the output of nonlinear elements with a multivalued response depends on the probabilistic characteristics of the input signal time derivative as well as on the input signal distribution density. For a random signal, one should specify the distribution densities $p_1(x)$ and $p_1(\dot{x})$ for the signal itself and its derivative, respectively, and the joint distribution density $p_2(x, \dot{x})$ of the signal and its derivative. Let us see now how the output signal distribution is obtained for a nonlinear element with a multivalued response; as an example we will use a nonlinearity $z(x)$ of the type "two-positional relay with hysteresis" (Fig. 25.6). For this nonlinearity

$$z(x) = \begin{cases} +z_b & \text{at} \quad -x_a < x < \infty \\ -z_b & \text{at} \quad -\infty < x < +x_a \end{cases} \tag{25.10}$$

and at any input signal characteristics the distribution density of the output signal can be expressed by a relation similar to tha

of Example 25.3

$$p_1(z) = S_1\,\delta(z - z_b) + S_2\delta(z + z_b) \tag{25.11}$$

This time, however, determination of the probabilities S_1 and S_2 is more complicated.

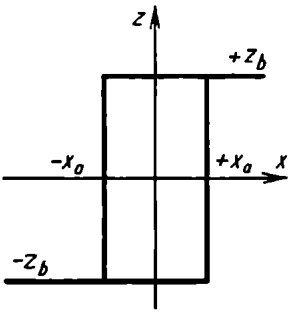

Fig. 25.6

The probability that $z = +z_b$, which is expressed by S_1, is made up of S_{11} (the probability that x belongs to the range $x > x_a$) and $S_{10} = S_0\mu_1$ (the probability that x belongs to the region $-x_a < x < x_a$ multiplied by the factor μ_1 which is equal to the probability that the upper part of the multivalued response $z = +z_b$ is reached). Similarly, the quantity S_2 is made up of S_{21} (the probability that $x < x_a$) and $S_{20} = S_0\mu_2$ (the probability that x belongs to the region $-x_a < x < x_a$ multiplied by the factor μ_2 which is equal to the probability that the lower part of the multivalued response $z = -z_b$ is reached)

$$\left.\begin{aligned} S_1 &= S_{11} + S_{10} = S_{11} + \mu_1 S_0 \\ S_2 &= S_{21} + S_{20} = S_{21} + \mu_2 S_0 \end{aligned}\right\} \tag{25.12}$$

where

$$S_{11} = \int_{x_a}^{\infty} p_1(x)\,dx, \quad S_{21} = \int_{-\infty}^{-x_a} p_1(x)\,dx \quad \text{and} \quad S_0 = \int_{-x_a}^{x_a} p_1(x)\,dx$$

The most difficult step is computing the factors μ_1 and μ_2, which depend on the probabilistic characteristics of the signal derivative $\dot{x}$ as well as of the signal itself.

This problem can be tackled by any one of the several proposed approximate methods, depending on the assumptions as to the nature of the signal (Ref. 62). We will discuss one of these methods.

Whether the upper or the lower part of the response is reached in the ambiguity zone depends on the probability of the positive or negative sign of $\dot{x}$ at $x = \pm x_a$.

The distribution density at $x = -x_a$ for $\dot{x} > 0$ can be represented as

$$p_1(\dot{x} > 0,\ x = -x_a) = \int_0^{\infty} p_2(-x_a, \dot{x})\,d\dot{x}$$

Similarly

$$p_1(\dot{x} < 0,\ x = +x_a) = \int_{-\infty}^{0} p_2(+x_a, \dot{x})\,d\dot{x} \tag{25.13}$$

It can be assumed that

$$\left.\begin{aligned}\mu_1 &= \frac{p_1(\dot{x}<0,\ x=+x_a)}{p_1(\dot{x}<0,\ x=+x_a)+p_1(\dot{x}>0,\ x=-x_a)}\\ \mu_2 &= \frac{p_1(\dot{x}>0,\ x=-x_a)}{p_1(\dot{x}<0,\ x=+x_a)+p_1(\dot{x}>0,\ x=-x_a)}\end{aligned}\right\} \qquad (25.14)$$

In a particular case where the distributions of x and $\dot{x}$ are independent and $p_2(x, \dot{x}) = p_1(x)\, p_1(\dot{x})$, Eqs. (25.13) are simplified to

$$p_1(\dot{x}<0,\ x=+x_a) = p_1(x_a)\int\limits_{-\infty}^{0} p_1(\dot{x})\, d\dot{x}$$

$$p_1(\dot{x}>0,\ x=-x_a) = p_1(-x_a)\int\limits_{0}^{\infty} p_1(\dot{x})\, d\dot{x}$$

and Eqs. (25.14) take the form

$$\left.\begin{aligned}\mu_1 &= \frac{p_1(x_a)\int\limits_{-\infty}^{0} p_1(\dot{x})\, d\dot{x}}{p_1(x_a)\int\limits_{-\infty}^{0} p_1(\dot{x})\, d\dot{x}+p_1(-x_a)\int\limits_{0}^{\infty} p_1(\dot{x})\, d\dot{x}}\\ \mu_2 &= \frac{p_1(-x_0)\int\limits_{0}^{\infty} p_1(\dot{x})\, d\dot{x}}{p_1(x_a)\int\limits_{-\infty}^{0} p_1(\dot{x})\, d\dot{x}+p_1(-x_a)\int\limits_{0}^{\infty} p_1(\dot{x})\, d\dot{x}}\end{aligned}\right\} \qquad (25.15)$$

Example 25.4. Assume that a stationary random ergodic signal is given as a saw-tooth curve with a random tooth width T_i and a constant rise time-fall time ratio $\frac{\alpha}{1-\alpha}$ (Fig. 25.7*a*).

Find the distribution density of the signal $z(t)$ at the output of a nonlinear element $z(x)$ of the type "two-positional relay with hysteresis" (see Fig. 25.6).

With a known sample of $x(t)$ the response $z(x)$ can lead directly to a sample of $z(t)$, which can in turn yield the distribution density $p_1(z)$. Figure 25.7*b* shows a curve of $z(t)$ for specified $x(t)$ and $z(x)$. Since z can only take on the values $+z_b$ or $-z_b$, it follows that $p_1(z)$ is expressed by Eq. (25.11), where S_1 and S_2 are equal to relative time periods over which $z = +z_b$ and $z = -z_b$.

These relative time periods can easily be found from the plots of Fig. 25.7*a* and *b*.

$$\left.\begin{aligned} S_1 &= \alpha\frac{x_1-x_a}{x_1+x_2}+(1-\alpha)\frac{x_1+x_a}{x_1+x_2}=\frac{x_1+x_a-2\alpha x_a}{x_1+x_2}\\ S_2 &= 1-S_1=\frac{x_2-x_a+2\alpha x_a}{x_1+x_2}\end{aligned}\right\} \qquad (25.16)$$

The same results can be obtained by using more general expressions (25.12)-(25.15). Indeed, for saw-tooth curves (see Fig. 25.7*a*)

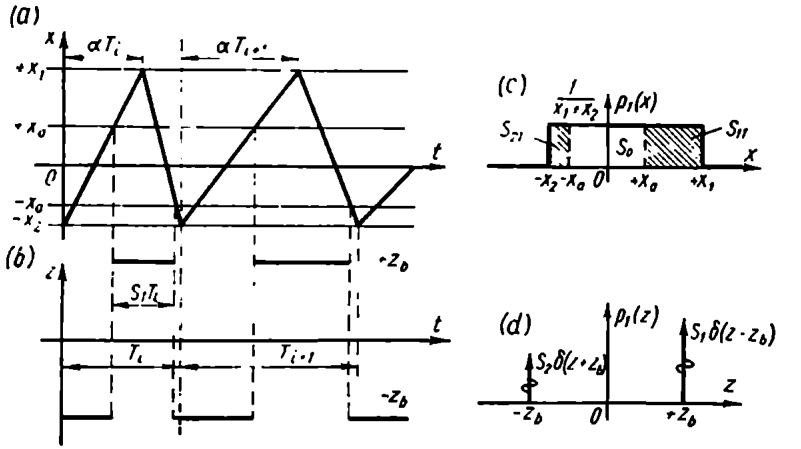

Fig. 25.7

with any distribution law of T_i the distribution density $p_1(x)$ is uniform (Fig. 25.7*c*)

$$p_1(x)=\begin{cases}\dfrac{1}{x_1+x_2} & \text{at} \quad -x_2<x<x_1\\ 0 & \text{at} \quad \begin{cases} x<x_2\\ x>x_1\end{cases}\end{cases} \qquad (25.17)$$

In this case Eqs. (25.12) yield

$$S_{11}=\frac{x_1-x_a}{x_1+x_2}, \qquad S_{21}=\frac{x_2-x_a}{x_1+x_2} \quad \text{and} \quad S_0=\frac{2x_a}{x_1+x_2}$$

In order to determine μ_1 and μ_2 we should know $p_2(x, \dot{x})$. Since in this case x and $\dot{x}$ are independent and for any distribution law of T_i the condition

$$\int_0^{\infty} p_1(\dot{x})\,d\dot{x}=\alpha \quad \text{and} \quad \int_{-\infty}^{0} p_1(\dot{x})\,d\dot{x}=1-\alpha$$

holds good, then by Eqs. (25.15)

$$\mu_1 = 1 - \alpha \quad \text{and} \quad \mu_2 = \alpha$$

Substituting the values found into Eqs. (25.12) we have values of S_1 and S_2 coinciding with (25.16). The distribution law $p_1(z)$ is expressed by Eq. (25.11) (see Fig. 25.7*d*).

25.3. TRANSFORMATION OF MEAN VALUE (FIRST ORDER MOMENT OR MATHEMATICAL EXPECTATION)

If the distribution density of the nonlinear element output is known, then its mathematical expectation, or first-order moment, is easy to determine

$$\overline{z} = m_z = M\{z(t)\} = \int_{-\infty}^{\infty} z p_1(z)\, dz = \int_{-\infty}^{\infty} z(x)\, p_1(x)\, dx \qquad (25.18)$$

Since the first-order moment of the input signal

$$\overline{x} = m_x = M\{x(t)\} = \int_{-\infty}^{\infty} x p_1(x)\, dx \qquad (25.19)$$

is known, the transformation of this moment by a nonlinear element is thus defined.

The relation between the first-order moments of the input and output signals of a nonlinear element is multivalued and depends on the nature of the input signal distribution function.

The most common problem is analysis of the transformation of a normally distributed signal (Eq. (25.3)). In that case the law of first-order moment transformation depends only on the nonlinear response $z(x)$ and σ_x as a parameter

$$m_z = m_z(m_x, \sigma_x) \qquad (25.20)$$

where all quantities can be either dependent on or independent of time t (stationary process). The relation (25.20) expresses the first-order moment transformation law.

Example 25.5. Find the law of first-order moment transformation for a saturation-type nonlinearity with a normally distributed input signal.

Substituting the results of Example 25.2 into Eq. (25.18) gives

$$m_z = \frac{1}{\sigma_x \sqrt{2\pi}} \int_{-z_b}^{z_b} z \exp\left[-\frac{(z-m_x)^2}{2\sigma_x^2}\right] dz + z_b(S_1 - S_2) \qquad (25.21$$

where

$$S_1 - S_2 = \Phi\left(\frac{x_b + m_x}{\sigma_x}\right) - \Phi\left(\frac{x_b - m_x}{\sigma_x}\right) \tag{25.22}$$

Integration and transformations yield

$$m_z = \frac{\sigma_x}{\sqrt{2\pi}}\left\{\exp\left[-\frac{(x_b - m_x)^2}{2\sigma_x^2}\right] - \exp\left[-\frac{(x_b - m_x)^2}{2\sigma_x^2}\right]\right\} +$$

$$+ (x_b + m_x)\,\Phi\left(\frac{x_b + m_x}{\sigma_x}\right) - (x_b - m_x)\,\Phi\left(\frac{x_b - m_x}{\sigma_x}\right) \tag{25.23}$$

In relative units this relation can be represented in the form

$$\frac{m_z}{x_b} = \Psi_1\left(\frac{m_x}{x_b},\ \frac{\sigma_x}{x_b}\right) \tag{25.24}$$

Figure 25.8 depicts the relation $\Psi_1\left(\frac{m_x}{x_b}\right)$ for different $\frac{\sigma_x}{x_b}$. The nonlinearity of the initial response corresponding $\sigma_x = 0$ is seen to be smoothed out and the linear zone expands with increasing random component σ_x. The constant component gain on the linear portion $k_0 = \frac{m_z}{m_x}$ decreases with increasing σ_x.

The effect of the random component is similar to that of the variable component in vibrational linearization (see Sec. 15.6).

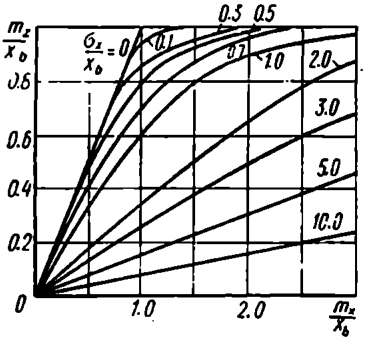

Fig. 25.8

Example 25.6. The problem is the same as in Example 25.5 with the additional condition that for a single-valued relay-type nonlinearity $z = z_b \operatorname{sign} x$.

Substituting the results of Example 25.3 into Eq. (25.18) gives

$$m_z = 2z_b\Phi\frac{m_x}{\sigma_x} \tag{25.25}$$

This relation is expressed by the plot of Fig. 25.4, where the response is seen to be practically linear at $m_x < 0.5\sigma_x$.

25.4. TRANSFORMATION OF DISPERSION (SECOND-ORDER MOMENT)

Second-order moments of input and output signals of a nonlinear element are determined as

$$\overline{z^2} = M\{z^2(t)\} = \int_{-\infty}^{\infty} z^2 p_1(z)\,dz = \int_{-\infty}^{\infty} z^2(x)\,p_1(x)\,dx \tag{25.26}$$

and

$$\overline{x^2} = M\{x^2(t)\} = \int_{-\infty}^{\infty} x^2 p_1(x)\,dx \qquad (25.27$$

A dispersion of input and output signals may be expressed in terms of the first- and second-order moments

$$\left.\begin{aligned} D_z &= M\{(z-m_z)^2\} = \overline{z^2} - m_z^2 \\ D_x &= M\{(x-m_x)^2\} = \overline{x^2} - m_x^2 \end{aligned}\right\} \qquad (25.28$$

If the distribution densities are known, Eqs. (25.26)-(25.28 can be used to obtain expressions for the transformation of a random signal dispersion in a nonlinear element.

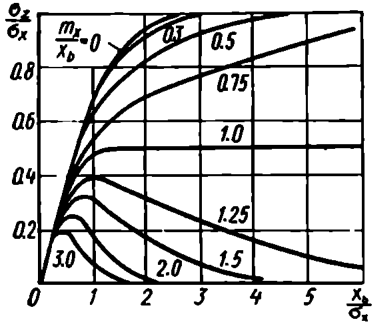

Fig. 25.9

This transformation depends on m and on the nature of the signal distribution function.

With a normally distributed input signal (Eq. (25.3)) the law of second-order moment transformation depends on σ_x and m_x as a parameter

$$D_z = \sigma_z^2 = D_z(D_x, m_x) = D_z(\sigma_x^2, m_x) \qquad (25.29$$

All these quantities can either vary or remain constant in the course of time.

Example 25.7. Find the dispersion transformation law for the conditions of Examples 25.2 and 25.5. Substituting the results of Example 25.2 into Eq. (25.26) we have

$$\overline{z^2} = D_z + m_z^2 = \frac{1}{\sigma_x\sqrt{2\pi}} \int_{-z_b}^{z_b} z^2 \exp\left[-\frac{(z-m_x)^2}{2\sigma_x^2}\right] dz + z_b^2 (S_1 + S_2) \qquad (25.30$$

where

$$S_1 + S_2 = \Phi\left(\frac{z_b + m_x}{\sigma_x}\right) + \Phi\left(\frac{z_b - m_x}{\sigma_x}\right)$$

The calculation of the integral obtained is unwieldy, and the result of integration contains a number of terms expressed through specially tabulated functions (Ref. 24).

The calculation may, however, be facilitated by using convenient plots expressing the relation (25.30) in relative units

$$\frac{\sigma_z}{\sigma_x} = \Psi_2\left(\frac{x_b}{\sigma_x}, \frac{m_x}{x_b}\right) \qquad (25.3$$

These plots (Ref. 62) are given in Fig. 25.9.

Example 25.8. Find the law of dispersion transformation for the conditions of Examples 25.3 and 25.6.

Substitute the results of Example 25.3 into Eq. (25.26) to obtain

$$D_z + m_z^2 = z_b^2$$

whence by virtue of Eq. (25.25)

$$D_z = z_b^2 - m_z^2 = z_b^2\left[1 - 4\Phi^2\left(\frac{m_x}{\sigma_x}\right)\right] \qquad (25.32)$$

Here, as before, $\Phi\left(\frac{m_x}{\sigma_x}\right)$ is expressed by the plot of Fig. 25.4.

To calculate the law of dispersion transformation by a nonlinear element, use is also made of the formulae for correlation function transformation which follow below.

25.5 TRANSFORMATION OF CORRELATION FUNCTIONS

Let us take up the general case (Fig. 25.10) with two signals $x(t_1)$ and $y(t_2)$ which are transformed by two single-valued nonlinearities $z_x(x)$ and $z_y(y)$. The joint distribution density of the signals

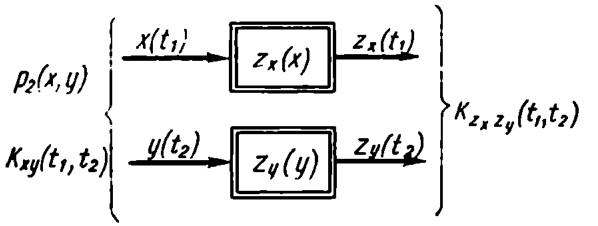

Fig. 25.10

x and y is given by the function $p_2(x, y)$. Then the cross-correlation function of z_x and z_y at the output is

$$K_{z_x z_y}(t_1, t_2) = M\{z_x(t_1)\, z_y(t_2)\} = \int_{-\infty}^{\infty}\int_{-\infty}^{\infty} z_x(x)\, z_y(y)\, p_2(x, y)\, dx\, dy \qquad (25.33)$$

On finding the cross-correlation function of the signals at the input

$$K_{xy}(t_1, t_2) = M\{x(t_1)\, y(t_2)\} = \int_{-\infty}^{\infty}\int_{-\infty}^{\infty} xy\, p_2(x, y)\, dx\, dy \qquad (25.34)$$

the law governing the transformation of correlation functions by nonlinear elements can be derived.

In a particular case where $x(t) = y(t)$ and $z_x(x) = z_y(y) = z(x)$ the expressions (25.33) and (25.34) give the auto-correlation functions of signals at the output and input of the nonlinear element $z(x)$.

Consider the case where the signals x and y have a normal distribution expressed by the joint distribution density

$$p_2(x, y) = \frac{1}{2\pi\sigma_x\sigma_y\sqrt{1-\rho_{xy}^2}} \exp\left\{-\frac{1}{2(1-\rho_{xy}^2)} \times \right.$$
$$\left. \times \left[\frac{(x-m_x)^2}{\sigma_x^2} + \frac{(y-m_y)^2}{\sigma_y^2} - \frac{2\rho_{xy}(x-m_x)(y-m_y)}{\sigma_x\sigma_y}\right]\right\} \qquad (25.35)$$

where ρ_{xy} is a centred normalized cross-correlation function of the input signals x and y

$$\rho_{xy}(t_1, t_2) = \frac{1}{\sigma_x\sigma_y}\mathring{K}_{xy}(t_1, t_2) = \frac{M\{(x-m_x)(y-m_y)\}}{\sigma_x\sigma_y} \qquad (25.36)$$

For stationary processes, m_x, m_y, σ_x and σ_y are independent of time. If the random component alone is stationary, the mathematical expectation m_x may be a function of time. In this case

$$m_x = m_x(t_1), \qquad m_y = m_y(t_2)$$

The computation of the integral (25.33) can be simplified by expanding $p_2(x, y)$ into a Tchebyshev-Hermite polynomials series. In that case Eq. (25.35) takes the form

$$p_2(x, y) = \frac{1}{2\pi\sigma_x\sigma_y} \exp\left\{-\frac{1}{2}\left[\left(\frac{x-m_x}{\sigma_x}\right)^2 + \right.\right.$$
$$\left.\left. + \left(\frac{y-m_y}{\sigma_y}\right)^2\right] \sum_{n=0}^{\infty} \frac{1}{n!}\rho_{xy}^n H_n\left(\frac{x-m_x}{\sigma_x}\right) H_n\left(\frac{y-m_y}{\sigma_y}\right)\right\} \qquad (25.37)$$

where $H_n(t)$ are polynomials given by the relation

$$H_n(t) = (-1)^n \exp\left(\frac{t^2}{2}\right) \frac{d^n}{dt^n}\left[\exp\left(-\frac{t^2}{2}\right)\right] \qquad (25.38)$$

$H_n(t)$ can be conveniently found from the recurrence relation

$$H_{n+1}(t) = tH_n(t) - nH_{n-1}(t) \qquad (25.39)$$

with

$$H_0(t) = 1, \qquad H_1(t) = t$$

The Tchebyshev-Hermite polynomials $H_n(t)$ are orthogonal with a weight $\exp\left(-\frac{t^2}{2}\right)$ on the straight line $-\infty < t < \infty$, i.e.

$$\int_{-\infty}^{\infty} H_n(t) H_m(t) \exp\left(-\frac{t^2}{2}\right) = \begin{cases} \sqrt{2\pi n!} & \text{at} \quad m = n \\ 0 & \text{at} \quad m \neq n \end{cases} \qquad (25.40)$$

Thanks to this property the substitution of Eq. (25.37) into (25.33) yields a simple enough expression for the cross-correlation function of the signals z_x and z_y

$$K_{z_x z_y}(t_1, t_2) = \sum_{n=0}^{\infty} \rho_{xy}^n a_{xn} a_{yn} \tag{25.41}$$

where

$$a_{xn} = a_{xn}(m_x, \sigma_x) = \frac{1}{\sqrt{2\pi n!}} \int_{-\infty}^{\infty} z(x) H_n\left(\frac{x-m_x}{\sigma_x}\right) \times$$

$$\times \exp\left[-\frac{1}{2}\left(\frac{x-m_x}{\sigma_x}\right)^2\right] dx \tag{25.42}$$

The factor a_{yn} is expressed in a similar way and can be obtained from Eq. (25.42) by substituting y for x. The factors a_{xn} and a_{yn} decrease with increasing n. Consequently, in calculating the correlation function one may sometimes restrict oneself to several terms of the series (25.41).

In determining the auto-correlation function of a stationary process, $x = y$, $z_x = z_y$, $\rho_{xy} = \rho_x$, $m_x = m_y$ and $a_{xn} = a_{yn} = a_n$. In that case Eq. (25.41) takes the form

$$K_z(\tau) = \sum_{n=0}^{\infty} \rho_x^n a_n^2 \tag{25.43}$$

Since $H_0(t) = 1$ and $\rho_x^0 = 1$, the first term of the series (25.43) is in fact the squared mathematical expectation of the signal at the nonlinear element output

$$m_z^2 = a_0^2 \tag{25.44}$$

In this case the centred correlation function is

$$\mathring{K}_z(\tau) = K_z(\tau) - m_z^2 = \sum_{n=1}^{\infty} \rho_x^n a_n^2 \tag{25.45}$$

Knowing the nonlinear response and the input signal distribution function, the relation between the correlation functions of input and output signals of a nonlinear element can be found through Eqs. (25.41)-(25.45).

Equation (25.45) determines the dispersion of the signal at the output of a nonlinear element

$$D_z = \sigma_z^2 = \mathring{K}_z(0) = \sum_{n=1}^{\infty} a_n^2 \tag{25.46}$$

Example 25.9. For the normal distribution law (25.35) and the correlation function $\rho_x|\tau| = \frac{K_x(\tau)}{\sigma_x^2} = e^{-\alpha|\tau|}$ of the signal at the input of a nonlinear element with a response $z = z_b \operatorname{sign} x$ find the output signal correlation function.

Knowing $H_0(t) = 1$ and $H_1(t) = t$, we can use Eq. (25.39) to determine the values of the following Tchebyshev-Hermite polynomials

$$H_2(t) = t^2 - 1, \quad H_3(t) = t^3 - 3T, \quad H_4(t) = t^4 - 6t^2 + 3, \text{ etc.}$$

Substituting these expressions into Eq. (25.42) and integrating we have

$$a_0 = 2z_b\Phi\left(\frac{m_x}{\sigma_x}\right) \tag{25.47}$$

$$a_1 = z_b\sqrt{\frac{2}{\pi}}\exp\left[-\frac{1}{2}\left(\frac{m_x}{\sigma_x}\right)^2\right] \tag{25.48}$$

$$a_2 = -\frac{m_x}{\sigma_x\sqrt{2}}a_1 \tag{25.49}$$

$$a_3 = \frac{1}{\sqrt{6}}\left[\left(\frac{m_x}{\sigma_x}\right)^2 - 1\right]a_1 \tag{25.50}$$

etc.

The plots of $\frac{a_n}{z_b}\frac{m_x}{\sigma_x}$ representing Eqs. (25.47)-(25.50) are shown in Fig. 25.11*a*. It is obvious that $m_z = a_0$ and that Eq. (25.47) coincides with Eq. (25.25) of Example 25.6.

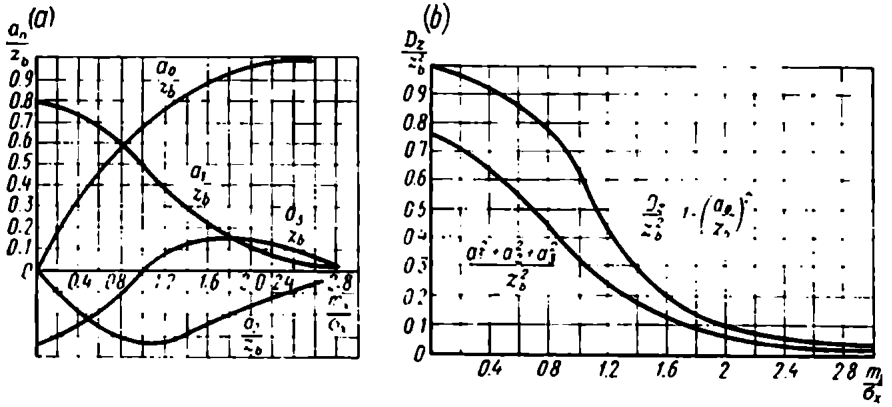

Fig. 25.11

Important conclusions can be drawn from collating the dispersion D_z obtained from Eq. (25.46) using three terms of the sum with the calculation by Eq. (25.32)

$$D_z = z_b^2 - a_0^2 \tag{25.51}$$

The calculation results are shown in Fig. 25.11*b*. If calculated only with three terms of the series, D_z is below the true value and the deviation grows relatively with increasing m_x.

With the factors a_n known, according to Eq. (24.45) the correlation function is

$$K_z(\tau) = a_0^2 + a_1^2 e^{-\alpha|\tau|} + a_2^2 e^{-2\alpha|\tau|} + a_3^2 e^{-3\alpha|\tau|} + \ldots \quad (25.52)$$

Using the nonlinear element input and output correlation functions it is easy to obtain spectral densities of these signals with the aid of direct Laplace transformation.

25.6 INPUT-OUTPUT CROSS-CORRELATION FUNCTION FOR A NONLINEAR ELEMENT

Let us now consider the case where only the signal $y(t)$ is subjected to nonlinear transformation, or where $z_x(x) = x = x(t_1)$ and $z_y(y) = z(y) = z(t_2) = z$ (Fig. 25.12).

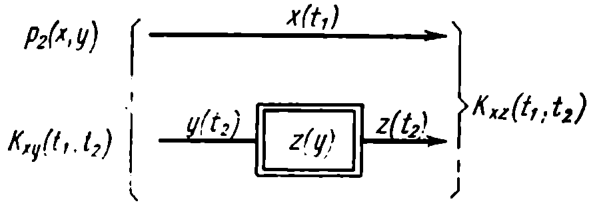

Fig. 25.12

In this case Eq. (25.41) can yield the cross-correlation function of the signals x and z with normal distribution of the signals

$$K_{xz}(t_1, t_2) = \sum_{n=0}^{\infty} \rho_{xy}^n a_{xn} a_{yn} \quad (25.53)$$

where

$$a_{xn} = \frac{1}{\sqrt{2\pi n!}} \int_{-\infty}^{\infty} x H_n\left(\frac{x - m_x}{\sigma_x}\right) \exp\left[-\frac{1}{2}\left(\frac{x - m_x}{\sigma_x}\right)^2\right] dx \quad (25.54)$$

and a_{yn} is given by Eq. (25.42), where x is replaced by y.

Here, the factors a_{xn} with due regard for the equalities

$$H_0\left(\frac{x - m_x}{\sigma_x}\right) = 1 \quad \text{and} \quad \sigma_x H_1\left(\frac{x - m_x}{\sigma_x}\right) = x - m_x$$

have the following values: $a_{x0} = m_x$, $a_{x1} = \sigma_x$ and $a_{xn} = 0$ at $n \geqslant 2$.

Consequently Eq. (25.53) takes the following form

$$K_{xz}(t_1, t_2) = m_x a_{y0} + \sigma_x a_{y1} \rho_{xy} \quad (25.55)$$

Since according to Eq. (25.44) $a_{y0} = m_z$, then

$$\mathring{K}_{xz}(t_1, t_2) = K_{xz}(t_1, t_2) - m_x m_z = \sigma_x a_{y1} \rho_{xy} = \left(\frac{a_{y1}}{\sigma_y}\right) \mathring{K}_{xy}(t_1, t_2) \quad (25.56)$$

or

$$\mathring{K}_{xy}(t_1, t_2) = \left(\frac{\sigma_y}{a_{y1}}\right) \mathring{K}_{xz}(t_1, t_2) \qquad (25.57)$$

The resultant expression is very important in practical work because it shows that in determining the cross-correlation function of two normally distributed signals any single-valued nonlinear transformation of one of them changes only the scaling factor, not the shape of the function.

This fact lies at the basis of relay correlators, where the multiplying element is a polarized relay which changes the sign of the signal propagating along one channel depending on the polarity of

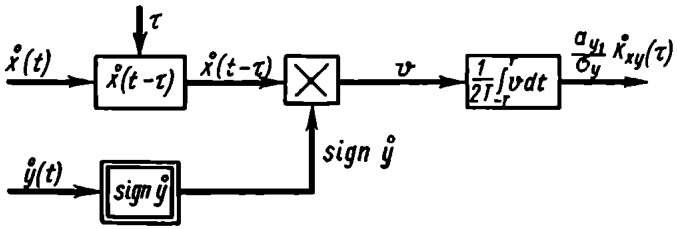

Fig. 25.13

the other signal. The structural diagram of a relay correlator is given in Fig. 25.13. The replacement of a multiplier (see Fig. 23.18) by a polarized relay (see Sec. 15.8) greatly simplifies the correlator design.

Example 25.10. The input-output cross-correlation function of a nonlinear element with a response $z = z_b \operatorname{sign} x$ takes the form $K_{xz}(\tau) = Be^{-\alpha|\tau|}$, where B and α are constant.

Find the input signal auto-correlation function if it is known to have a normal distribution.

Finding by Eq. (25.48) the factor $a_{y1} = a_1$ and substituting it into Eq. (25.57) we have for $y = x$

$$K_x(\tau) = \sigma_x \left(\frac{B}{z_b}\right) \sqrt{\frac{\pi}{2}} \exp\left[\frac{1}{2}\left(\frac{m_x}{\sigma_x}\right)^2\right] \exp(-\alpha|\tau|) \qquad (25.58)$$

25.7 STATISTICAL LINEARIZATION OF NONLINEAR ELEMENTS

Analysis of random as well as regular processes in nonlinear systems is greatly improved by finding an approximate description of the system which would enable the application of well-developed linear theory methods. This is achieved, in particular, by using the method of harmonic linearization (see Ch. XVIII) whereby under regular signals nonlinear elements are replaced by quasilinear ele-

ments whose parameters are dependent on the input signal amplitude. Equivalence is attained when the output first harmonic coincides with a desired one at a harmonic input.

The same ideas were developed in the theory of random processes and were implemented in statistical linearization of nonlinear elements (Ref. 33).

The essence of statistical linearization is in replacement of a a nonlinear element by a linear one preserving some probabilistic characteristics of the output signal. These are commonly the mean value and dispersion. Sometimes the equivalence is judged by the

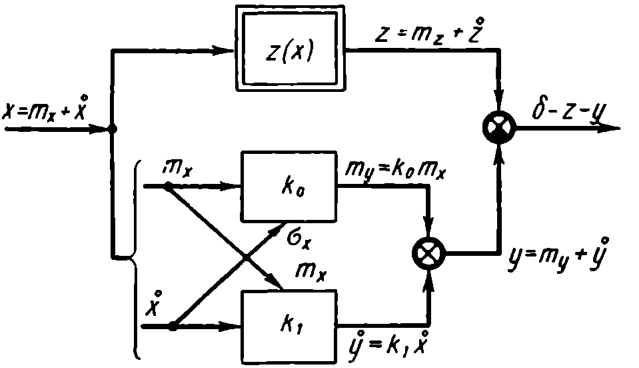

Fig. 25.14

minimal r.m.s. error, assuming a certain law for the nonlinear element input signal distribution. Usually a normal law is adopted. Sometimes this is justified, but more often it is not; nevertheless the law is tentatively assumed normal and approximate calculations are made.

The resultant parameters of the linear element depend on the probabilistic characteristics of the input signal and on the element nonlinear response.

Assume that the nonlinear response is

$$z = z(x) \tag{25.59}$$

and the input signal is

$$x(t) = m_x + \mathring{x}(t) \tag{25.60}$$

where m_x is generally a time-varying mathematical expectation of the signal $x(t)$ and $\mathring{x}(t)$ is its centred component for which the expectation is zero.

To linearize the nonlinear response, the components m_x and $\mathring{x}(t)$ are presumed to branch out into two different channels (Fig. 25.14)

with gains k_0 and k_1, and the output signal, to be the sum of two linearly transformed signals

$$y = k_0 m_x + k_1 \overset{\circ}{x}(t) \tag{25.61}$$

In selecting k_0 and k_1 for a linear system two conditions of equivalence can be used.

In the first case the equivalence criterion is formulated as follows

$$m_y = k_0 m_x = m_z, \qquad D_y = k_1^2 D_x = k_1^2 \sigma_x^2 = D_z \tag{25.62}$$

and in the second case it is the minimum of the r.m.s. error $\sqrt{\overline{\delta^2}}$ (see Fig. 25.14)

$$\frac{\partial \overline{\delta^2}}{\partial k_0} = 0 \quad \text{and} \quad \frac{\partial \overline{\delta^2}}{\partial k_1} = 0 \tag{25.63}$$

where $\delta = z - y$.

The parameters k_0 and k_1 are sometimes found as mean values of those given by the above conditions.

Example 25.11. Determine the equivalent parameters k_0 and k_1 of the linearized element $z = z_b$ sign x if the input signal x is normally distributed (Eq. (25.3)).

First version. Using the results of Examples 25.6 and 25.8, we get

$$m_z = 2z_b \Phi\left(\frac{m_x}{\sigma_x}\right) \quad \text{and} \quad D_z = z_b^2\left[1 - 4\Phi^2\left(\frac{m_x}{\sigma_x}\right)\right] \tag{25.64}$$

Then from Eq. (25.62)

$$k_0 = \frac{m_z}{m_x} = \left(\frac{2z_b}{m_x}\right) \Phi \frac{m_x}{\sigma_x} \tag{25.65}$$

and

$$k_1 = \sqrt{\frac{D_z}{D_x}} = \frac{z_b}{\sigma_x} \sqrt{1 - 4\Phi^2\left(\frac{m_x}{\sigma_x}\right)} \tag{25.66}$$

Second version. Since

$$\delta = z - y = (m_z - k_0 m_x) + (\overset{\circ}{z} - k_1 \overset{\circ}{x}) = m_\delta + \overset{\circ}{\delta}$$

then

$$\overline{\delta^2} = m_\delta^2 + D_\delta$$

where

$$m_\delta = m_z - k_0 m_x, \quad D_\delta = M\{(\overset{\circ}{z} - k_1 \overset{\circ}{x})\}^2 = D_z + k_1^2 D_x - 2k_1 M\{\overset{\bullet\bullet}{z x}\}.$$

From Eqs. (25.63) it follows that $k_0 = \frac{m_z}{m_x}$ and its value is identical to the solution of Eq. (25.65), and

$$k_1 = \frac{M\{\overset{\circ}{z}\overset{\circ}{x}\}}{D_x}$$

In order to determine $M\{\overset{\circ}{z}\overset{\circ}{x}\}$ use Eq. (25.56) for $t_1 = t_2$ and $x = y$. Then

$$M\{\overset{\circ}{z}\overset{\circ}{x}\} = \overset{\bullet}{k}_{xz}(0) = \sigma_x a_{x1} \rho_x(0) = \sigma_x a_{x1}$$

With a nonlinear response specified by Eq. (25.48)

$$a_{x1} = z_b \sqrt{\frac{2}{\pi}} \exp\left[-\frac{1}{2}\left(\frac{m_x}{\sigma_x}\right)^2\right]$$

and, consequently,

$$k_1 = \frac{z_b}{\sigma_x} \sqrt{\frac{2}{\pi}} \exp\left[-\frac{1}{2}\left(\frac{m_x}{\sigma_x}\right)^2\right] \tag{25.67}$$

A comparison of Eqs. (25.66) and (25.67) shows that in the second version the value of k_1 is smaller.

25.8 STATISTICAL LINEARIZATION OF NONLINEAR FEEDBACK SYSTEMS

Nonlinear feedback systems with linear dynamic (usually inertial) as well as nonlinear inertialess elements are the most challenging problem.

The structural diagram of such a system (Fig. 25.15*a*) corresponds to a servo system with a nonlinear element $z(x)$ and a linear part

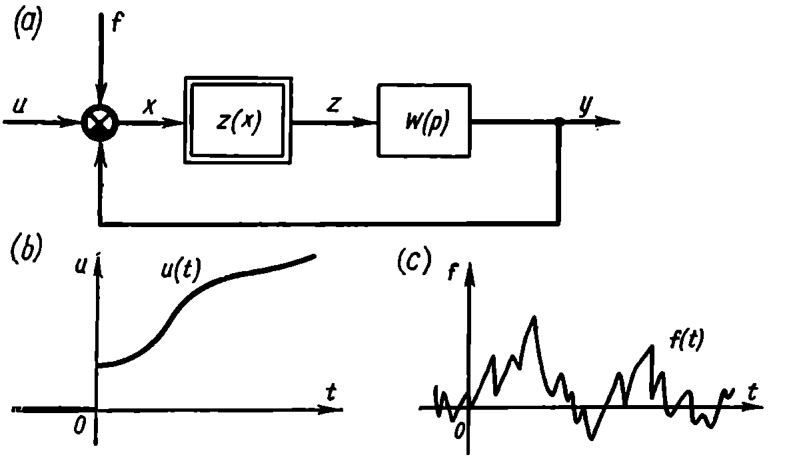

Fig. 25.15

$W(p)$ whose input consists of the operational signal $u(t)$ and the noise $f(t)$.

Take up the case where the operational signal (Fig. 25.15*b*) is deterministic and changes relatively slowly in the course of time, $[u(t) = m_u(t)]$.

The noise $f(t)$ (Fig. 25.15*c*) does not contain a constant component ($m_f = 0$) and changes quickly enough. It is a stationary random quantity, it is described by the correlation function $K_f(\tau)$ and spectral density $S_f(\omega)$ and is distributed normally.

Consequently, the servo system input signal $u(t) + f(t)$ is also normally distributed, and the mean m_u is a given time function.

Statistical linearization of the circuit described results in the structure of Fig. (25.16), where a nonlinear element is represented

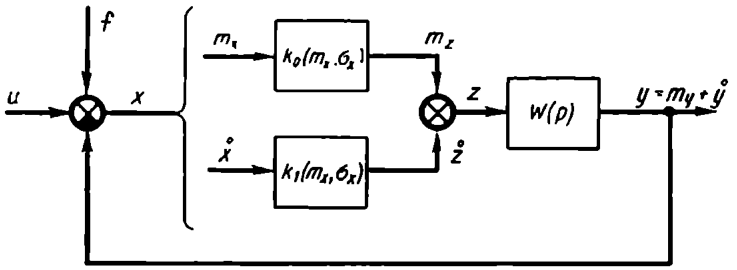

Fig. 25.16

as two channels with k_0 and k_1 depending on the probabilistic characteristics of the signal, $x = u + f - y$. One channel carries the slow regular component, the other the fast random component.

To justify statistic linearization the input signal x of the nonlinear element should be normally distributed. This signal is, however, the difference of the signal $u + f$ with a given normal distribution law and the signal y resulting from the propagation of the signal x through the linear element $W(p)$.

Since the nonlinear element output is not distributed normally, the normal distribution of the signal y can be questioned. The closeness of the distribution of the signal y to the normal one depends on frequency responses of the linear element $W(p)$. The order of the transfer function numerator is always less than that of the denominator, and the linear part acts as a low-pass filter. In this case the input of the linear part $W(p)$, whose distribution is other than normal causes an output signal with a near-normal distribution law (see Sec. 24.5).

This permits formulating the filter hypothesis (by analogy with the harmonic linearization method) as applied to statistical linearizations: if the distribution of the linear part input signal differ from a normal one, the output signal is normally distributed.

We will confine ourselves to cases where $W(p)$ is compatible with this hypothesis. Then the signal x represents the difference of signal satisfying a normal law and thus it is also normally distributed

Consequently, the above rules of statistical linearization based on the assumption of normal distribution of the input signal are fully applicable to feedback systems (see Fig. 25.15*a*); thus, the use of the diagram shown in Fig. 25.16 is justified.

Consider now equations of a deterministic low-frequency and a statistical high-frequency channel of the equivalent circuit resulting from statistical linearization.

For the deterministic channel we have

$$X(p) = U(p)\, W_{cl\text{-}l0}(p) = \frac{U(p)}{1 + k_0 W(p)} \tag{25.68}$$

where $U(p)$ is the operator image of the signal $u(t)$ and $W_{cl\text{-}l0}(p)$ is the first-channel closed-loop transfer function.

According to the limit value theorem the steady state value of $m_x(t)$ as $t \to \infty$ is

$$m_x(\infty) = \lim_{p \to 0} pX(p) = \lim_{p \to 0} \frac{pU(p)}{1 + k_0 W(p)}$$

Since normally $W(p)$ includes an integrating element and $W(p) \to \infty$ as $p \to 0$, the unity in the denominator can be neglected, and for a stationary process

$$m_x = \lim_{p \to 0} p \frac{U(p)}{k_0 W(p)} \tag{25.69}$$

The equation of the signal spectral densities for the second channel of random signal transmission is

$$S_{\overset{\circ}{x}}(\omega) = S_f(\omega)\, |W_{cl\text{-}l1}(j\omega)|^2 \tag{25.70}$$

where $S_{\overset{\circ}{x}}$ and S_f are the spectral densities of random signals $\overset{\circ}{x}$ and f, and $W_{cl\text{-}l1}(p) = \dfrac{1}{1 + k_1 W(p)}$ is the second channel closed-loop transfer function.

The dispersion of x is found from its spectral density

$$D_x = \sigma_x^2 = \frac{1}{2\pi} \int_{-\infty}^{\infty} S_x(\omega)\, d\omega \tag{25.71}$$

Equations (25.69) and (25.71) lead to two equations

$$\left.\begin{aligned} m_x &= m_x(k_0) \\ \sigma_x &= \sigma_x(k_1) \end{aligned}\right\} \tag{25.72}$$

Since there are four unknowns in these equations (m_x, σ_x, k_0, and k_1) two more equations are necessary to obtain a solution.

These equations are found by studying the propagation of a normally distributed signal x through a nonlinear element $z(x)$. Using

one of the above methods of statistical linearization (25.62) or (25.63), we get two equations

$$\left.\begin{aligned} k_0 &= k_0(m_x, \sigma_x) \\ k_1 &= k_1(m_x, \sigma_x) \end{aligned}\right\} \tag{25.73}$$

Solving Eqs. (25.72) and (25.73) simultaneously we will have values of m_x and σ_x expressing the probabilistic characteristics of the misalignment x in the servo system.

Since the noise f has no constant component ($m_f = 0$), the resultant value m_x represents the steady state error of a servo system subjected to the noise $f(t)$.

The random component of the error is found as in Eq. (24.34) from the spectral density of the output signal component due to the noise

$$S_y(\omega) = S_f(\omega)\,|W_{yf}(j\omega)|^2 \tag{25.74}$$

where

$$W_{yf}(p) = \frac{k_1 W(p)}{1 + k_1 W(p)}$$

Finding $D_y = \sigma_y^2$ with the aid of the integral (25.71) it is easy to obtain the system r.m.s. error

$$\overline{\delta^2}(t) = m_x^2 + \sigma_y^2 \tag{25.75}$$

The formula (25.75) reveals that the servo system error in the presence of a deterministic useful signal and a random stationary noise with a zero mathematical expectation can be expressed as the sum of the error x component caused by the useful signal $u(t)$ and the signal y component caused by the error $f(t)$, as in expression (24.31).

Example 25.12. Determine the steady-state error $\delta^2(t)$ of a servo system under the conditions: $u = Bt$

$$S_f(\omega) = \frac{2\sigma_f^2\omega_0}{\omega^2 + \omega_0^2}, \quad z = z_b \operatorname{sign} x, \quad W(p) = \frac{k}{p}$$

The signal $f(t)$ is normally distributed. Besides

$$\frac{\omega_0}{k} = 1, \qquad \frac{B}{kz_b} = 0.5, \qquad \frac{\sigma_f}{z_b} = 2$$

According to Eq. (25.69), for $U(p) = \frac{B}{p^2}$

$$m_x = \lim_{p \to 0} \frac{pB}{p^2 \dfrac{k_0 k}{p}} = \frac{B}{k_0 k} \tag{25.76}$$

By Eq. (25.70)

$$S_x^{\circ}(\omega) = \frac{2\sigma_f^2\omega_0}{\omega^2+\omega_0^2}\left|\frac{j\omega}{j\omega+kk_1}\right|^2$$

and, following substitution into Eq. (25.71) and integration, we have

$$D_x = \sigma_x^2 = \frac{\sigma_f^2\omega_0}{\omega_0+kk_1}$$

or

$$\sigma_x = \frac{\sigma_f}{\sqrt{1+\frac{kk_1}{\omega_0}}} \tag{25.77}$$

The two equations (25.73) coincide with the results of Example 25.11. In the first version of calculation, Eqs. (25.65) and (25.66) give

$$k_0 = \frac{2z_b}{m_x}\Phi\left(\frac{m_x}{\sigma_x}\right) \tag{25.78}$$

$$k_1 = \frac{z_b}{\sigma_x}\sqrt{1-4\Phi^2\left(\frac{m_x}{\sigma_x}\right)} \tag{25.79}$$

Solving Eqs. (25.76)-(25.79) simultaneously we have

$$\sigma_x = -\frac{\alpha}{2}+\sqrt{\sigma_f^2+\left(\frac{\alpha}{2}\right)^2} \tag{25.80}$$

where

$$\alpha = \frac{\sqrt{k^2z_b^2-B^2}}{\omega_0} \tag{25.81}$$

and

$$\Phi = \frac{m_x}{\sigma_x} = \frac{B}{2z_bk} \tag{25.82}$$

From Eq. (25.82) and the plot of Fig. 25.14 we have

$$\beta = \frac{m_x}{\sigma_x} \tag{25.83}$$

and with the value of σ_x found from Eq. (25.80) we obtain

$$m_x = \beta\sigma_x \tag{25.84}$$

According to Eq. (25.74) we have

$$S_y^{\circ}(\omega) = S_x^{\circ}(\omega)\left|\frac{k_1k}{j\omega}\right|^2 = \frac{2\sigma_f^2\omega_0}{\omega^2+\omega_0^2}\left|\frac{k_1k}{j\omega+k_1k}\right|^2 \tag{25.85}$$

and, following substitution into Eq. (25.71) and integration, we ge

$$D_y = \sigma_y^2 = \frac{\sigma_f^2kk_1}{\omega_0+kk_1} \tag{25.86}$$

and

$$\overline{\delta^2(t)} = m_x^2 + \sigma_y^2 \tag{25.87}$$

Substituting the numerical values into the resultant equations (25.76)-(25.87) gives

$$\frac{\alpha}{z_b} = \sqrt{1-0.25} = 0.866$$

$$\frac{\sigma_x}{z_b} = \frac{-\alpha}{2z_b} + \sqrt{\left(\frac{\sigma_f}{z_b}\right)^2 + \left(\frac{\alpha}{2z_b}\right)^2} = 1.6$$

$$\Phi\left(\frac{m_x}{\sigma_x}\right) = \frac{B}{2kz_b} = 0.25$$

From the plot of Fig. 25.4, $\beta = \frac{m_x}{\sigma_x} = 0.71$ and $\frac{m_x}{z_b} = \frac{\beta\sigma_x}{z_b} = 1.16$. Then, using Eqs. (25.79) and (25.86), we have $k_1 = \frac{1}{1.6}\sqrt{1-0.25} = 0.54$, $\frac{\sigma_y^2}{z_b^2} = 1.4$. The relative r.m.s. error is $\frac{\overline{\delta^2(t)}}{z_b^2} = 1.16^2 + 1.4 = 2.74$.

In steady state the relay element output includes a constant component $m_z = \frac{B}{k}$. The relay is periodically switched so as to maintain this quantity even if there is no noise. These switchings are treated in Example 19.4. The noise further complicates the process. The above approximate analysis nevertheless enables one to determine the nature of the relations thus observed. A more accurate analysis of the problem is given in Ref. 33.

Chapter XXVI

ADAPTIVE CONTROL SYSTEMS

26.1 BASIC CONCEPTS, DEFINITIONS, CLASSIFICATION

In many processes and plants (jet planes, some missiles, catalytic reactors, etc.) the dynamic and static responses change unpredictably over a wide range. The lack of *apriori* data on plant properties has led to the need for adaptive automatic systems. Advances in this field are facilitated by the development of new hardware in electronics, computing technology, control theory, and bioengineering.

Adaptive control systems are systems where control action parameters or control algorithms are varied automatically and purposefully so as to achieve a plant control optimal in a specified sense, while the plant responses or environmental actions can change unpredictably.

Since the basic purpose of any control system is to achieve the desired objective under conditions which are not definitely determined in advance, or with incomplete *apriori* data necessary to provide good control (in a specified sense), all automatic control systems can be divided into two classes.

Class I. Systems in which the lack of data required to achieve good control in a specified sense does not greatly impair the attainment of the control objective and therefore automatic updating may be unnecessary. These include conventional stabilization, program control, and servo systems described in the preceding chapters.

Class II. Systems which cannot achieve the control objective with the initial information alone. A natural solution would be automatic updating in the course of operation. This is the class of *adaptive* systems. The process of updating necessary to provide good control in a specified sense is referred to as *adaptation*.

We will assume that an adaptive system can achieve the control objective when the desired complete data is provided. The extent of completeness can be indicated by a certain performance criterion, which is usually directly related to the adaptation characteristics.

One type of adaptive system are learning systems where the lacking information is obtained in the course of learning. As a rule, learning is performed by correction of the system functional algorithm

by a man or by a special automatic unit according to a specified law for optimal functioning in a given situation.

The most widespread type of adaptive system are self-adjusting systems (SAS) without learning elements. This chapter will cover some of the most popular self-adjusting systems.

The operation of a SAS can broadly be described as automatic measurement of basic performance characteristics and automatic adjustment of the control unit with a view to achieving a specified objective. The block diagram of a SAS is shown in Fig. 26.1, where a characteristics measurement and adjustment unit *CMAU* is shown, which supplements the usual plant *P* and control unit *CU*. All the observable variables, x, y, u, may serve as the input variables of the *CMAU*.

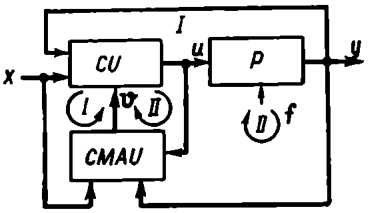

Fig. 26.1

The figure shows control loop *I* and adjustment loops *II*. Actual systems may operate without some loops, while the control unit and a unit of characteristics measurement and adjustment can each be regarded as a SAS incorporating the same functional units.

CMAU compute the performance criterion in the presence of the noise f and compare it with the desired one or the one found earlier following which a command v is generated to change the setpoints, parameters or structure of the *CU* or to perform other operations. The method in which a SAS is adjusted is also important and may be *searching*, *searchless* and *combined*. Searching systems perform special trial steps so as to reveal possible ways to improve the system operation. Searchless systems involve dynamic plant models. Combined systems use both dynamic models and trial steps.

26.2 SEARCHING SYSTEMS. GENERAL

Searching self-adjusting systems are systems which solve the problem of optimal control with incomplete *apriori* data by using *automatic search*, by which is meant a process in a closed-loop control system where the control unit generates trial input signals, analyzes their results, and sets up a specified mode of plant operation. The relation of the required control action to the controlled variable and observed disturbances is not known to the full extent, whereas in conventional control systems the data on the state of the plant may be sufficient for generation of the necessary control actions.

Automatic search is used most often in control systems where the plant static responses have extrema and the objective of control is to find and maintain the control actions ensuring the extremal

value of the controlled variable. When automatic search is used in plants with extremal responses, the associated searching systems are usually referred to as *extremal*. The basic works on such systems have been written by V.V. Kazakevich, a Soviet scientist (Ref. 76).

The concept of automatic search can be illustrated by the following example. It is required to determine a control action $u = u^*$ which provides an extremum (say, the maximum) for the output variable $y = y^*$ of a one-dimensional plant with a static response $y(u)$. The value of y at one point of the plant static response (Fig. 26.2) is insufficient to determine the trend of u which agrees with the desired trend of y. If the current state of the system is associated with the point A on the left-hand branch of the response, the value of u should be increased; if it is associated with the point B, then u should be decreased. Assume that the system is at the point A. To determine the correct direction of motion, the control unit may, for instance, first measure and store the value of $y(u_A)$, then increase u by Δu and remeasure and store y at $u = u_A + \Delta u$. Then, determining $\Delta y = y(u_A + \Delta u) - y(u_A)$, the control unit generates a control action which changes the plant state in the desired direction.

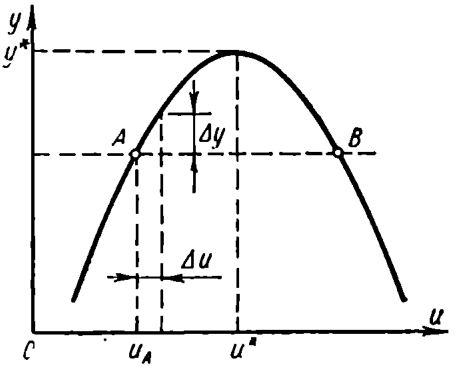

Fig. 26.2

In automatic control practice there are numerous problems in which an extremal value of the plant output has to be maintained. Let us consider some of them.

Example 26.1. One rather common problem is to adjust a loop in resonance (see Fig. 1.13 and pp. 33-34). This problem arises in automatic tuning of receivers for maximal amplification, automatic adjustment of transmitters for maximal efficiency, adjustment of the Q-meter, which measures the figure of merit of an inductor. The parameter to be adjusted is the capacity and the controlled variable is the voltage across the loop; at the resonance value of the capacity the loop voltage is maximal.

Example 26.2. In radar tracking stations TS the control coordinates for the aerial (Fig. 26.3*a*) are the elevation and azimuthal angles u_1 and u_2, while the controlled variable is the echo signa intensity y. The relation $y(u_1, u_2)$ has a clearly defined maximum (Fig. 26.3*b*). When the target moves, the values of u_1 and u_2 maximizing y change. The form of $y(u_1, u_2)$ also changes with the range.

Besides, the value of y determined by the tracking system is a random function of statics and jammings.

Example 26.3. In gas furnaces (Fig. 26.4*a*) the intensity of burning and, consequently, the temperature ϑ in the heating zone

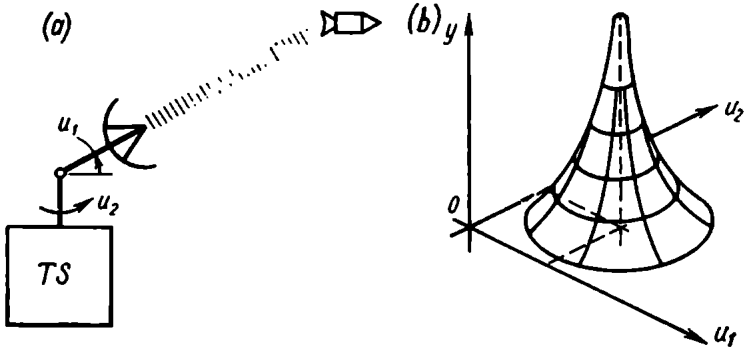

Fig. 26.3

with a specified fuel consumption q depends on the air flow u. The relation of the controlled parameter (thermometer readings y) to the control parameter u has a maximum at $u = u^*$ (Fig. 26.4*b*). The

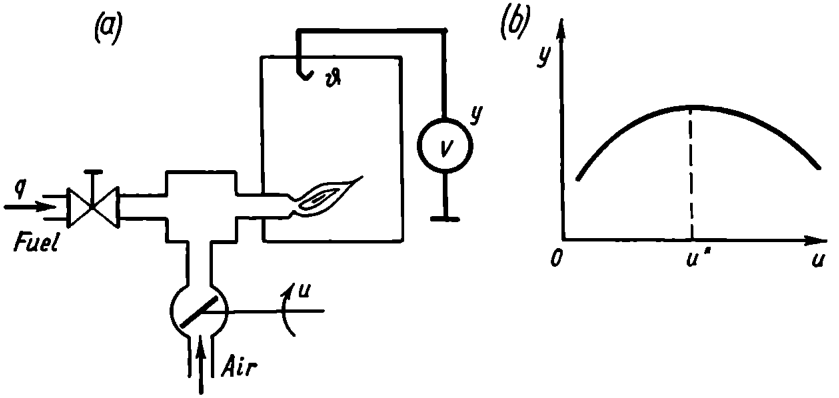

Fig. 26.4

shape of the relation $y(u)$ and the position of the maximum are greatly affected by disturbances: the fuel, air, and ingot temperature, etc. The controlled parameter is measured with errors; this means that y may vary randomly, not only with variations of u. Unlike the previously discussed plants, this one is largely dynamic in that the mixing of air and fuel is inertial, and the ingot and thermometer also exhibit inertial properties.

Example 26.4. In many problems the controlled variable is the performance criterion of a control system, while the controlling variables are the adjustment parameters. Figure 26.5*a* portrays a system controlling the thickness of rolled metal. The slab thickness H before the rolls is measured by the sensor S_1 incorporated in the disturbance compensation control system, which also includes the compensator C and the actuating motor AM using the screw Sc to change the position of the mill rolls. The thickness h of the strip after the rolls is measured by the sensor S_2, and the readings are

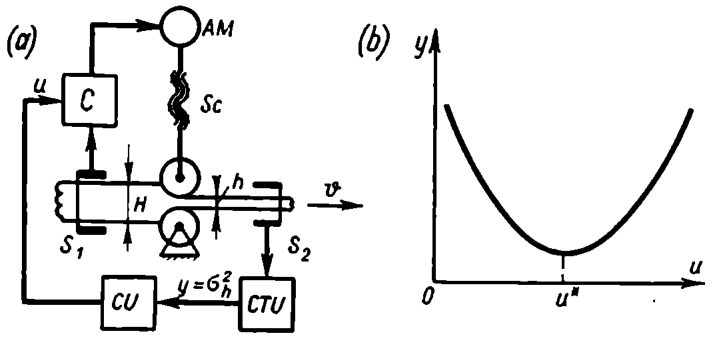

Fig. 26.5

processed in the computer CTU, whose output y is the dispersion σ_h^2 of deviations of h from the desired value. The value of y is fed to the input of the control unit CU, whose output u determines the adjustment of the compensating loop. The static relation $y(u)$ for this system has a minimum (Fig. 26.5*b*), whose position (or the value u^*) heavily depends on a number of disturbances (mechanical properties, temperature, dispersion σ_H^2 of the strip thickness H), and may vary during operation. The value of y can be affected by errors of the sensor and the computing unit. The structural diagram describing the dynamic relation of variations in u and y should allow for the delay (which depends on the speed of movement v of the slab) in addition to the integrating and inertial elements which represent the actuating motor AM.

Generalization of the above examples leads to the structural diagram of an extremal system given in Fig. 26.6. The plant may have several control inputs, therefore the control action is given as a vector **u**. The action **u** is subjected to dynamic transformations, which are described by a matrix of weighting functions $\| w_i(t) \|$ and is fed to the input of an inertialess element with an extremal response z (**v**) as a vector **v** with coordinates $v_1, v_2, \ldots, v_i, \ldots, v_n$. The output value of the nonlinear element passes through a dynamic element with a weighting function $w_2(t)$. The output signal of this

element is supplemented with a noise f_2 caused by errors in meters and by various disturbances. The resultant signal y is a controlled variable fed to the control unit input.

Aside from f_2, the plant is affected by the noise f_1 caused by random disturbances leading to a drift of the plant extremal response. Unobservable disturbances which upset optimal operation are in fact the main reason for the development of extremal systems, whose chief purpose is to find and maintain the extremal values

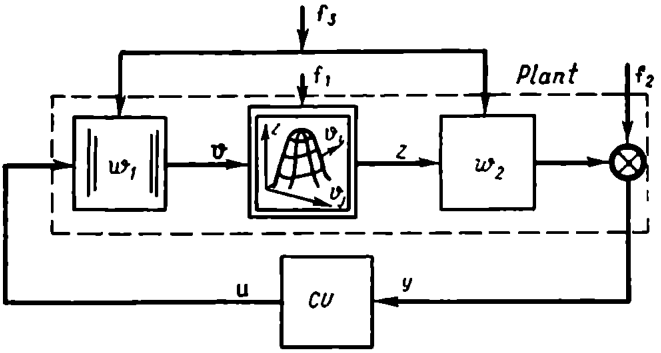

Fig. 26.6

of the controlled parameter. The third kind of disturbances, f_3, includes unobservable variations in linear element dynamic properties, e.g. in the transport delay.

The controlled variable which is in extremal relation to the control may have most diverse physical and techno-economical characteristics such as voltage, temperature, productivity, efficiency, etc. In most cases their values represent the actual optimality of plants; therefore the extremal plant output is often referred to as the *optimality index.*

It is also important to know that the range of control parameters can be subjected to constraints, generally in the form of the inequality

$$H(u_1, u_2, \ldots, u_n) \leqslant 0 \tag{26.1}$$

Methods of automatic search generally originate in computational mathematics (Ref. 89), where one of the most common problems is minimizing a function, known as the objective function, of one or more variables. The necessary condition for the extremum of the function $y = y(u_1, \ldots, u_n)$ is known to be the equality

$$\text{grad } y = 0 \tag{26.2}$$

where

$$\text{grad } y = \frac{\partial y}{\partial u_1} \mathbf{u}_1^0 + \ldots + \frac{\partial y}{\partial u_n} \mathbf{u}_n^0$$

Here $\mathbf{u}_i^0$ are unit vectors in the u_i coordinate space where the function y is determined.

For the condition (26.2) to be valid, the gradient of the objective function y should be determined and control actions leading to the extremum are performed in agreement with the gradient measured (operational actions). Actions aimed at determining the gradient are called *trial actions.*

26.3 METHODS TO DETERMINE THE OBJECTIVE FUNCTION GRADIENT

In determining the gradient, the coordinate decomposition of the plant response to trial actions can be performed by time or frequency separation of the trial actions.

Gradient estimation with time separation of the trial actions. In systems of this type trial actions may be implemented as trial steps along each input variable in succession. Assume that in the initial position the vector $\mathbf{u}$ has coordinates $u_1, \ldots, u_n$. Let us increase the first coordinate by c_1. Once $y(u_1 + c_1, u_2, \ldots, u_n)$ is measured and stored, the same coordinate is incremented by $-c_1$, and then $y(u_1 - c_1, u_2, \ldots, u_n)$ is measured. The smaller is c_1, the closer the relation

$$\frac{y(u_1+c_1, u_2, \ldots, u_n) - y(u_1-c_1, u_2, \ldots, u_n)}{2c_1} \approx \frac{\partial y}{\partial u_1} \qquad (26.3)$$

is to the true value of the derivative. In a similar way all other partial derivatives can be found in succession. The values of the trial steps in each of the channels (c_i) chiefly depend on the sensitivity of the meters measuring the optimality index and on the intensity of noises.

Trial steps as means of study are widely used owing to the ease of their technical implementation and the simplicity of filtering out any noises superimposed on the optimality index. When the quantity $y(t)$ fed to the extremal controller contains also a high-frequency noise f_2, the noises can be filtered out by usual averaging of y with a low-pass filter.

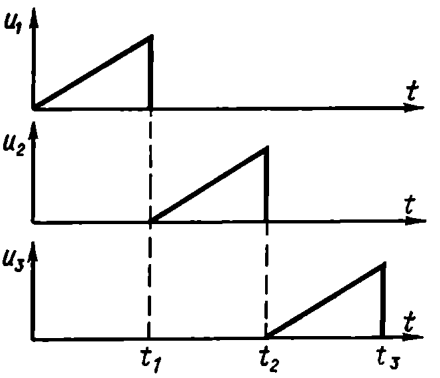

Fig. 26.7

Trial actions can be of different forms. In Fig. 26.7 they are linear functions fed in succession to an inertialess plant input (Ref. 34).

The complete time derivative for this plant is

$$\frac{dy}{dt}=\frac{\partial y}{\partial u_1}\frac{du_1}{dt}+\ldots+\frac{\partial y}{\partial u_n}\frac{du_n}{dt} \tag{26.4}$$

At each instant all but one control variable derivatives are zero, while the one which is not has quite a definite constant value b_i. Say, for $t_1 < t < t_2$ (see Fig. 26.7)

$$\frac{du_1}{dt}=\frac{du_3}{dt}=0, \qquad \frac{du_2}{dt}=b_2 \tag{26.5}$$

With the condition (26.5) substituted into (26.4) for $t_1 < t < t_2$

$$\frac{dy}{dt}=\frac{\partial y}{\partial u_2}\,b_2$$

Thus, by measuring the optimality index time derivative it is easy to find the associated partial derivative.

These methods are simple enough to implement which is a great advantage, but the search consumes much time, and the differentiation inevitably deteriorates the noise-immunity of the method.

Gradient estimation with frequency separation of trial actions. The most popular method is synchronous detection whereby the gradient components are determined with simultaneous variations of the control parameters. The method is only applicable where the plant output is continuously observed and the input admits continuous trial signals.

Assume that the trial signal at the input of a one-dimensional inertialess extremal control plant (Fig. 26.8*a*) is given by the generator G and has the form

$$u_{tr}(t) = X_m \sin \omega_0 t$$

Representing the plant output $y = y(x)$ in the vicinity of the operational point $x = u$ as a Taylor series we have for small X_m

$$y(u + X_m \sin \omega_0 t) = y(u) + \frac{\partial y}{\partial x}\Big|_{x=u} X_m \sin \omega_0 t + \\ + \frac{1}{2}\left(\frac{\partial^2 y}{\partial x^2}\right)\Big|_{x=u} (X_m \sin \omega_0 t)^2 + \ldots$$

which shows that the first harmonic amplitude at the plant output is proportional to the derivative $\frac{dy}{dx}$ at the operational point. When the sign of the derivative changes to the negative one, the phase of the first harmonic shifts by an angle of $\varphi = \pi$. Figure 26.8*b* shows plots of the plant output signals at different positions of the operational point u_i relative to the extremum position u^*. At $u^* > u_1$ the harmonic phases of $u_{tr}(t)$ and $y(t)$ are seen to coincide while at $u^* < u_2$, when $\frac{\partial y}{\partial x} < 0$ the phase difference is π. When $u = u^*$, the frequency of the output signal is $2\omega_0$.

If the plant response y (x) can be described by a second-order curve

$$y = a_0 + a_1 x + a_2 x^2$$

the amplitude of the first harmonic at the plant output is exactly

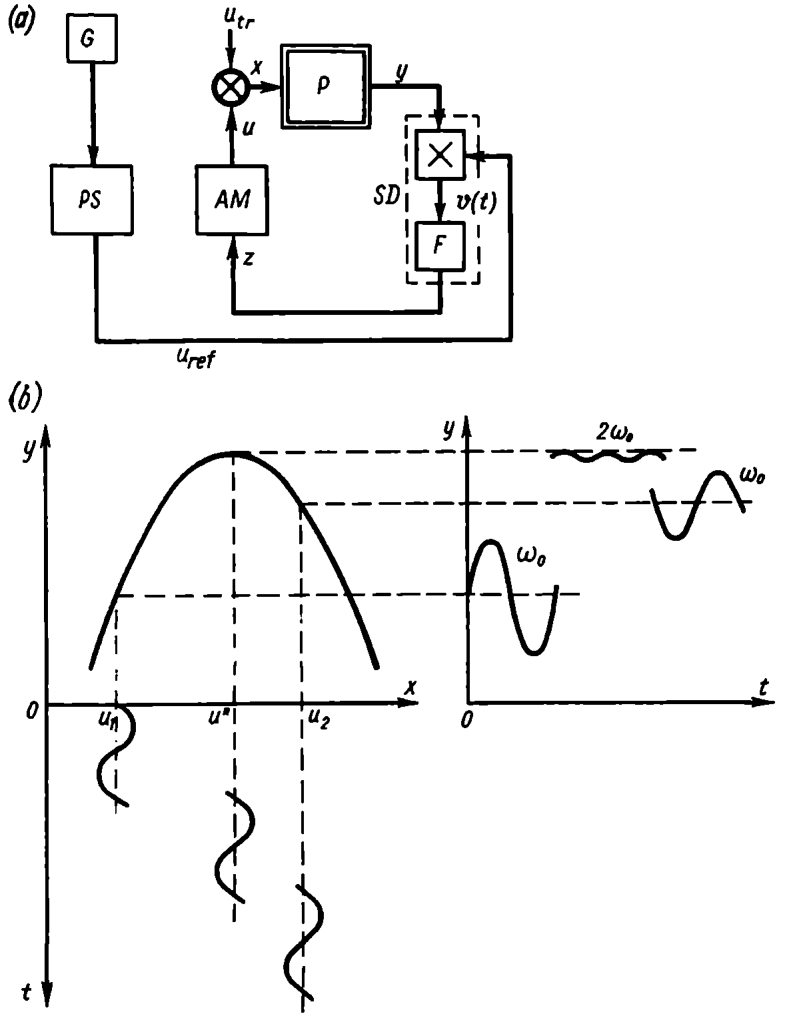

Fig. 26.8

proportional to the derivative $\frac{dy}{dx}$. This is easy to prove by finding the factor of the first term in the expansion of the function y (t)

into the Fourier series

$$Y_{1m} = \frac{\omega_0}{\pi} \int_{t-\frac{2\pi}{\omega_0}}^{t} y\,(u + X_m \sin \omega_0 t) \sin \omega_0 t\, dt =$$

$$= X_m (a_1 + 2a_2 u) = X_m \left(\frac{\partial y}{\partial x}\right)\Big|_{x=u} \qquad (26.6)$$

As follows from Eq. (26.6), the derivative $\frac{\partial y}{\partial x}$ can be found by current averaging over the period of the output signal $y\,(t)$ times the harmonic $\sin \omega_0 t$.

The procedure described by Eq. (26.6) is known as *synchronous* (or *coherent*) *detection* and is performed by a multiplier which receives

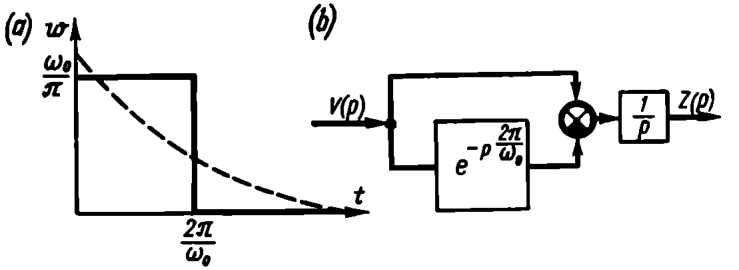

Fig. 26.9

a signal $y\,(t)$ from the plant output and a reference signal, $u_{ref} = \sin(\omega_0 t + \psi)$, picked up from the phase-shifter PS. The multiplier output is connected to the input of the filter F (see Fig. 26.8*a*), which performs current averaging. The output signal $z\,(t)$ of the filter, which is the output of the synchronous detector SD, controls the operation of the actuating motor AM, which changes the coordinate u until the condition $z\,(t) = 0$ is met.

Note that in performing an operational cycle the extremal system acts as a usual control system reducing the error $\left(\text{in our case the quantity } z = \frac{\partial y}{\partial x}\right)$ to zero. The only specific feature of the extremal system is the search operation, i.e. finding the derivative.

The filter which performs the current averaging has a weighting function $w\,(t)$ (solid line in Fig. 26.9*a*) and can be obtained in the form of the unit shown in Fig. 26.9*b*. This unit is seen to require an element of pure delay, which is very difficult to build.

For practical purposes a common low-pass filter will suffice; it may be an inertial element with a weighting function shown in Fig. 26.9*a* as a dotted line. The filter detects the signal proportional

to the derivative $\frac{\partial y}{\partial x}$ because the multiplier output has just one constant component and a set of harmonics which are multiples of ω_0 and are suppressed by the filter. The constant component of the multiplier output is proportional to $\frac{\partial y}{\partial x}\Big|_{x=u}$ which may be proved by simple trigonometrical transformations of the function $v(t) = y(t)\, u_{ref}(t)$.

If the extremal control plant is not inertialess, the output signal first harmonic which carries the data on the first derivative is displaced in phase by an angle of $\varphi(\omega_0)$ from the trial signal. If the reference signal at the second input of the synchronous detector is in phase with the searching signal, i.e. if $u_{ref} = \sin \omega_0 t$, the *SD* output signal is given by the expression

$$z = X_m \left(\frac{\partial y}{\partial x}\right) \cos \varphi(\omega_0) \tag{26.7}$$

It is seen from Eq. (2.67) that with a phase shift close to $\frac{\pi}{2}$ the synchronous detector output is near zero. At $\frac{\pi}{2} < \varphi(\omega_0) < \pi$ the feedback changes its sign; as a result the system moves away from the extremal point. The harmful effect of the phase shift is offset by a phase-shifter, *PS*, introduced into the reference signal channel (see Fig. 26.8*a*). The reference signal $u_{ref} = \sin(\omega_0 t + \psi)$, while the synchronous detector output depends on the cosine of the phase difference

$$z = X_m \left(\frac{\partial y}{\partial x}\right) \cos [\varphi(\omega_0) - \psi] \tag{26.8}$$

The best operational mode is clearly given as

$$\varphi(\omega_0) - \psi = 0 \tag{26.9}$$

The equations (26.6)-(26.8) for the synchronous detector output variable were derived under the assumption that the operational component $u(t)$ changes much slower than the trial signal. Conditions in which the frequency spectra of the signals $u(t)$ and $u_{ref}(t)$ differ greatly are known as *quasi-stationary* (Ref. 34).

One great advantage of the method is the simplicity of search for the extremum in multidimensional plants *P*, where searching signal frequencies are different in different channels (Fig. 26.10), due to which each synchronous detector *SD* calculates the partial derivative for the relevant variable.

In synchronous detection the searching signal (trial and reference) need not be sinusoidal, and other periodical signals can be used

such as a meander

$$u_{tr\,i} = A \text{ sign } [\sin \omega_i t] \qquad (26.10)$$
$$u_{ref\,i} = \text{sign } [\sin (\omega_i t + \varphi_i)]$$

With this searching signal the synchronous detector output is given by the expression

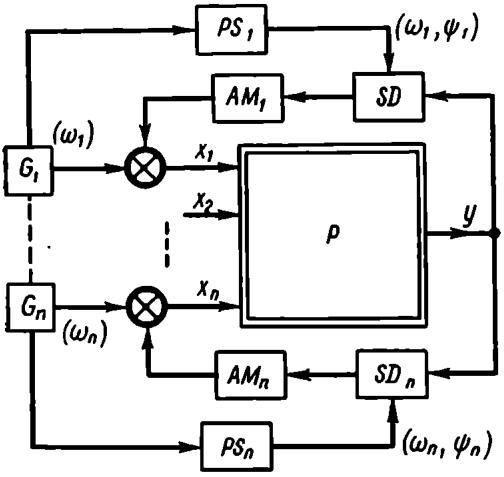

Fig. 26.10

$$z_i = A \frac{\partial y}{\partial x} \left| \frac{\pi}{2} - [\varphi(\omega_i) - \psi_i] \right| \qquad (26.11)$$

Random observable changes in the plant input coordinates can also be used as searching signals. In this case the detector is a correlator which measures the cross-correlation factor R_{yx} of the plant output $y(t)$ and the input variable $x(t)$.

Note that the synchronous detector in fact calculates the cross-correlation factor of the plant input and output harmonics

$$\frac{\partial y}{\partial x} = kR_{yx}$$

where k is a factor depending on the statistical properties of random variations in $x(t)$.

Thanks to averaging, synchronous detection is highly noise-immune as contrasted to time separation of trial actions, which requires differentiation of the plant output.

26.4 SEARCH METHODS WITH SEPARATION OF TRIAL AND OPERATIONAL STEPS

After the partial derivatives are found and the direction and magnitude of the gradient are determined, the system performs an operational action (operational step). There are many ways of moving to the extremum with the partial derivatives known (Ref. 89). Let us take up some of them.

The gradient method. In this method the operational step $\Delta \mathbf{u}$ is proportional to the gradient

$$\Delta \mathbf{u} = a \text{ grad } y(\mathbf{u}) \qquad (26.12$$

where a is a factor; in other words, in each of the control channels the operational action is proportional to the associated partial derivative.

The method can be conveniently illustrated by considering the case of two control parameters on a plane where the lines of constant value (level lines) of the function to be optimized are traced. The level lines are closed curves; lines representing the higher value of y (for the case of the maximum) are inside those for lower values.

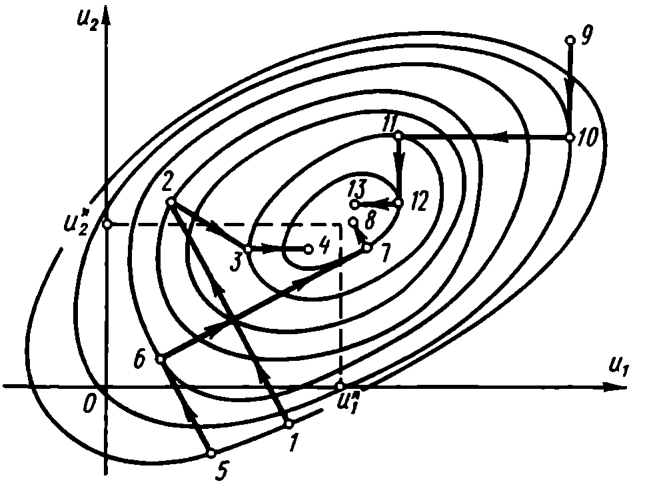

Fig. 26.11

Figure 26.11 shows the trajectory of search by the gradient method (*1-2-3-4*) in the plane of the control variables u_1 and u_2. In each of the points *1*, *2*, *3* the gradient is calculated and an operational step is made in the sequence *1-2*, *2-3*, *3-4*. The direction of the operational step coincides with the normal to the level lines, and its value increases with the gradient magnitude. In Fig. 26.11 greater gradients are seen to be associated with more closely spaced level lines (see steps *1-2* and *3-4*).

The steepest descent (ascent) method. The operational step is performed in the direction of the gradient; its value, however, depends not on the gradient magnitude, but on the condition for achieving the extremum in this direction. Figure 26.11 shows the trajectory of search by the steepest descent method (*5-6-7-8*). The direction of the operational step *5-6*, for instance, coincides with a normal to the level line; this step is completed at the extremum point associated with the direction under consideration, and this is equivalent to the operational step line being tangential to the associated level line. Step *6-7* is seen to be much greater than step *5-6*, although

the gradient magnitude is greater for point *5* than for point *6*, which can be judged by the distance between the level lines.

The coordinate optimization (Gauss-Seidel) method. This method is most frequently used in systems where multiparametric optimization (search for the extremum when plants have several control inputs) is obtained through the use of single-channel extremal controllers which lead to the extremum of a function of one variable. In this method of search one control parameter varies (with others constant) until the extremum for this parameter is reached. Then a similar search is begun for another variable with all others being constant. The path of search is shown in Fig. 26.11 (*9-10-11-12-13*). First u_2 is seen to change at $u_1 = \text{const}$ until the path touches the level line (point *10*) where the condition $\frac{\partial y}{\partial u_2} = 0$ is met, then the variable u_1 is changed in a similar way, etc.

It should be noted that the Gauss-Seidel method is not a gradient method because the search does not proceed in the direction of the gradient. It is discussed here solely because it can be conveniently compared with gradient techniques.

A comparison of these three methods reveals that some vicinity of the extremal point can be reached in a minimal number of steps by using the steepest descent method. We imply the number of steps obtained by averaging for various search paths over a certain region of initial conditions.

The method of stochastic approximation. Random disturbances, which interfere with the measurement of partial derivatives, necessitate the use of noise-immune methods for automatic search. There are search procedures which ensure finding the optimum even in the presence of noises. They are known as *stochastic approximation methods* (Refs. 89, 80). In this case the term approximation signifies that the extremum is found approximately on the basis of previous experiments, while the word stochastic implies the random nature of measurement errors. Stated in the most general terms, the stochastic approximation problem consists in finding the point $\mathbf{u}^*$ in the space of $u_1, \ldots, u_n$ for which the condition

$$M\{\psi(\mathbf{u}^*)\} = 0 \tag{26.13}$$

is observed; here M = mathematical expectation, ψ = a function depending on the nature of the problem at hand.

For extremum search problems the function ψ is given by Eq. (26.2): $\psi(\mathbf{u}) = \text{grad } y(\mathbf{u})$; in other words, for extremal systems the method of stochastic approximation is reduced to the condition

$$M\{\text{grad } y(\mathbf{u}^*)\} = 0 \tag{26.14}$$

The idea of the stochastic approximation method will be illustrated by finding the value of a constant parameter measured with

a random error. Let u^* be the true value of a certain quantity and u_i (where $i = 1, \ldots, k$), a sequence of experimentally determined values of this quantity which differ from the true one because of the additive noise f_i, i.e.

$$u_i = u^* + f_i$$

Then the problem of stochastic approximation is formulated as

$$M\{u - u^*\} = 0$$

and the function

$$\psi(u) = u - u^* \tag{26.15}$$

If the mean value of the noise is zero, the best approximation to the true value of the parameter after k measurements is the arithmetical mean

$$u_k^* = \frac{1}{k} \sum_{i=1}^{k} u_i \tag{26.16}$$

where u_k^* is the value of u^* after k experiments.

Perform simple transformations of Eq. (26.16) with the aim of expressing u_k^* in terms of the preceding estimate u_{k-1}^* and the subsequent experimental value u_k

$$u_k^* = \frac{(u_1 + \ldots + u_{k-1}) + u_k}{k} = \frac{1}{k} \frac{k-1}{k-1} \sum_{i=1}^{k-1} u_i + \frac{1}{k} u_k =$$

$$= \frac{k-1}{k} u_{k-1}^* + \frac{1}{k} u_k \tag{26.17}$$

In this equation the preceding estimate is seen to have a weight of $\frac{k-1}{k}$, while the new experimental value u_k has a weight of $\frac{1}{k}$; with increasing number of observations the effect of new data diminishes. This idea of weighing new measurements in proportion to $\frac{1}{k}$ expresses the rule of rational behaviour in the presence of noises: the greater is the amount of data stored, the smaller are the changes in the final result introduced by new measurements. Let us rearrange Eq. (26.17)

$$u_k^* = u_{k-1}^* + \frac{1}{k} [u_k - u_{k-1}^*] \tag{26.18}$$

A block diagram with a discrete integrator D implementing formula (26.18) is shown in Fig. 26.12*a*. The adder which receives the new value u_k and the current estimate u_{k-1}^* generates the current value of the function ψ_k in accordance with Eq. (26.15).

This diagram leads to the general block diagram of stochastic approximation (Fig. 26.12*b*)

$$u_k^* = u_{k-1}^* + \gamma_k \psi(u_k) \tag{26.19}$$

where γ_k is a sequence of numbers depending on the ordinal number k of the experiment.

For extremal systems, with an allowance for Eq. (26.14), Eq. (26.19) is given as

$$\mathbf{u}_k^* = \mathbf{u}_{k-1}^* + \gamma_k \operatorname{grad} y(\mathbf{u}_k) \tag{26.20}$$

This differs from Eq. (26.12), which corresponds to the above-discussed gradient method, in that the gradient factor γ_k depends

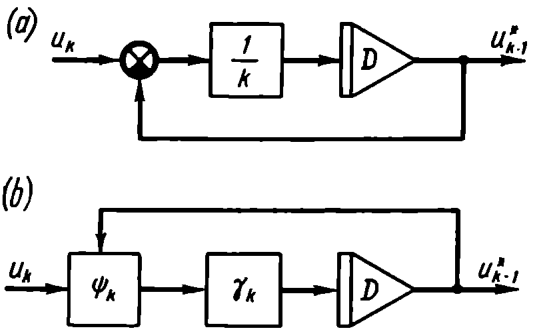

Fig. 26.12

on the ordinal number of the step. Consider the conditions which should be satisfied by a sequence of numbers γ_k for $\mathbf{u}_k^*$ to tend to $\mathbf{u}^*$ with a unit probability as $k \to \infty$:

$$\text{(a)} \quad \gamma_k > 0 \tag{26.21a}$$

is the condition for the correct direction of compensation, and for structural diagrams of stochastic approximations this is the condition for the correct sign of the feedback;

$$\text{(b)} \quad \lim_{k\to\infty} \gamma_k = 0 \tag{26.21b}$$

is the condition ensuring the asymptotic accuracy of the method. Since estimates of the gradient, even at large k, are not zero due to random noises, the magnitude of compensations (corrections) will fall to zero owing to reduction in γ_k;

$$\text{(c)} \quad \sum_{k=1}^{\infty} \gamma_k^2 < \infty \quad \text{or} \quad \lim_{m\to\infty} \sum_{k=m}^{\infty} \gamma_k^2 = 0 \tag{26.21c}$$

is the condition which guarantees the filtration of noises if their dispersion is finite. To prove this we write Eq. (26.20) as

$$\mathbf{u}_k^* - \mathbf{u}_{k-1}^* = \gamma_k \operatorname{grad} y(\mathbf{u}_k) \tag{26.22}$$

In the presence of noises the gradient estimate consists of two components, a regular one, grad $y_0(\mathbf{u}_k)$, and a random one, δ_k, i.e.

$$\text{grad } y(\mathbf{u}_k) = \text{grad } y_0(\mathbf{u}_k) + \delta_k$$

Then we rewrite Eq. (26.22)

$$\mathbf{u}_k^* - \mathbf{u}_{k-1}^* = \gamma_k \text{ grad } y_0(\mathbf{u}_k) + \gamma_k \delta_k \tag{26.23}$$

Substituting $k = \infty$ and $k = m$ into Eq. (26.20) with an allowance for Eq. (26.23) we have

$$\mathbf{u}_\infty^* - \mathbf{u}_m^* = \sum_{k=m}^{\infty} \gamma_k \text{ grad } y_0(\mathbf{u}_k) + \sum_{k=m}^{\infty} \gamma_k \delta_k \tag{26.24}$$

The second addend in this equation expresses the random component of the deviation of the extremum point's asymptotical position at the mth step. The dispersion of this component is

$$M\left\{\sum_{k=m}^{\infty} (\gamma_k \delta_k)^2\right\} = \sigma_\delta^2 \sum_{k=m}^{\infty} \gamma_k^2 \tag{26.25}$$

If the dispersion σ_δ^2 of the gradient measurement errors is finite, then from the conditions (26.21c) and (26.25) it follows that as $m \to \infty$ the effect of errors due to noises tends to zero.

$$\text{(d)} \sum_{k=1}^{\infty} \gamma_k = \infty \tag{26.21d}$$

is the condition ensuring the convergence of the search to the true maximum even if the initial point is far enough from the extremum because the total correction may be of any magnitude.

All the above conditions (26.21a)-(26.21d) are satisfied by the sequence

$$\gamma_k = \frac{1}{k} \tag{26.26}$$

which first appeared in the example illustrating the estimation of the mean value via general physical concepts (see Eq. (26.17)). This sequence $\left(1, \frac{1}{2}, \frac{1}{3}, \ldots\right)$ is known as *harmonic* and is widely used in most diverse iterative procedures.

In studying stochastic approximation as applied to the problem of search for the extremum we did not touch upon the methods for measuring the gradient components. The basic method is the use of trial steps, or estimation of partial derivatives by increments of the function to be optimized with the aid of the expression (26.3). The specific feature of stochastic approximation is that the value of the trial step is not constant but depends on the ordinal number of the step. In the course of time, or with $k \to \infty$, the step value c_{ik} tends to zero ($i = 1, \ldots, n$) so as to ensure steady-state conditions as close to the extremum point as possible. At the same time,

to provide convergence to the extremum point with a unit probability (Refs. 80, 14) the step value c_{ik} should decrease slower than the coefficient γ_k and this is given by the conditions

$$\sum_{k=1}^{\infty} \frac{\gamma_k^2}{c_{ik}^2} < \infty \tag{26.27a}$$

$$\sum_{k=1}^{\infty} c_{ik}\gamma_k < \infty \tag{26.27b}$$

Assuming that $\gamma_k = \frac{1}{k}$ the conditions (26.27) are satisfied by the sequence

$$c_{ik} = \frac{1}{\sqrt[3]{k}} \tag{26.28}$$

26.5 SEARCH METHODS WITH COMBINED TRIAL AND OPERATIONAL STEPS

In many automatic search methods an operational step is also a trial one. One of them (extremum storage) was described in Sec. 15.4 when extremal control systems were discussed. In this system the lacking data on the position of the extremum are obtained owing to self-oscillations, whose parameters (amplitude and frequency) depend on the properties of the plant and the controller (see Examples 17.11 and 18.8). The dynamic properties of this method are similar to those of the stepping method with output signal differentiation and a constant rate of change of the control variable.

Stepping method. Having incremented the control variable by Δu_k (where k is the ordinal number of the step), the system measures the output parameter y_k and compares it with the value y_{k-1} stored at the preceding step. The direction of the next step Δu_{k+1} depends on the sign of the increment $\Delta y_k = y_k - y_{k-1}$. Thus, for instance, in seeking the maximum

$$u_{k+1} = c \operatorname{sign} (\Delta y_k) \tag{26.29}$$

where c is the value of the step.

Figure 26.13*a* shows the variation of the coordinates in a system where the frequency of steps is specified in advance and is independent of the plant responses. Figure 26.13*b* represents the same diagrams for a system where the frequency of steps depends on the slope of the plant static response. The structural diagram of a system where this method of search is used is shown in Fig. 26.13*c*. The value $\Delta y_k = y_k - y_{k-1}$ is obtained by subtracting the value y_{k-1}, generated at the output of the log L, from the current value y_k. The integrator I, whose output is connected to the logical unit LU, receives Δy_k. The logical unit controls the actuating motor AM,

which responds to the steps Δu_k according to the law

$$\Delta u_k = \begin{cases} +c \quad \text{at} \quad \int\limits_{T_{k-1}}^{T_k} \Delta y_k \, dt > \delta \\ -c \quad \text{at} \quad \int\limits_{T_{k-1}}^{T_k} \Delta y_k \, dt < -\delta \end{cases} \tag{26.30}$$

where δ is the logical element threshold; $(T_k - T_{k-1})$ is the time between the $(k-1)$th and the kth steps.

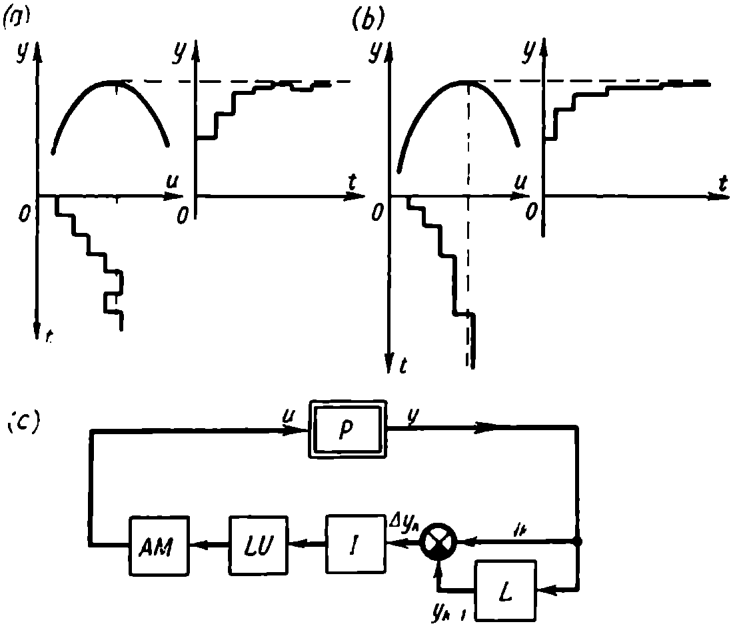

Fig. 26.13

It is seen from Eq. (26.30) that the system makes a subsequent step when $\left| \int\limits_{T_{k-1}}^{T_k} \Delta y_k \, dt \right|$ reaches δ. The farther is the system from the extremum, the greater is Δy_k and the smaller $(T_k - T_{k-1})$, therefore the steps are more frequent.

The advantage of this system is its noise-immunity achieved by integrating the increment Δy_k. The closer is the system to the extremum, the smaller is Δy_k and the greater the effect of noises. In this case, however, with decreasing Δy_k the integration time T_k increases, thereby facilitating noise suppression.

Simplex method. In the above stepping methods of search the procedure of changing the control coordinate was the simplest; the subsequent coordinate u_{k+1} is defined by the end of a straight line segment whose other end is at the current point u_k. The orientation of the segment at the $(k+1)$th step depends on the values of the function to be extremized at the ends of the preceding step, u_{k-1} and u_k, in accordance with (26.29) or (26.30).

Geometrically, a straight line segment is the simplest figure (simplex) in a one-dimensional space. The rise of simplices for the purpose

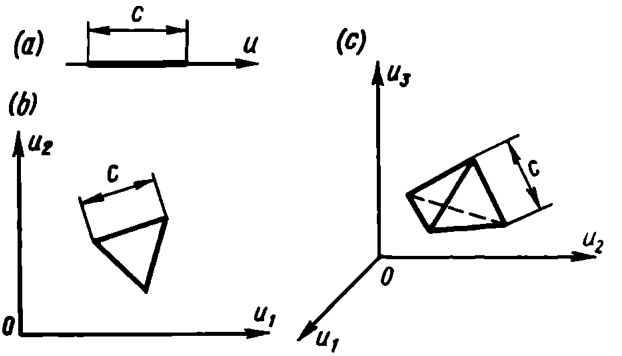

Fig. 26.14

of search in multidimensional spaces eliminates the necessity of determining the gradient, and this greatly simplifies the search procedure. Figure 26.14 shows simplices: one-dimensional—a straight line segment (Fig. 26.14*a*); two-dimensional—a triangle (Fig. 26.14*b*); and three-dimensional—a tetragonal pyramid (Fig. 26.14*c*).

A two-dimensional problem (Fig. 26.15*a*) conveniently illustrates the idea of the simplex method. As before, the function to be optimized which has a maximum is represented in a plane by level lines. At three points (*1*, *2*, *3*) of the initial area which are the simplex vertices, the associated values of the function, y_1, y_2, y_3, are determined. The next point, *4*, is found as the mirror image of the simplex vertex with the least value of the function relative to the opposite edge. Then a new simplex is formed.

In Fig. 26.15*a* $y_1 < y_2 < y_3$ (which follows from the position of the points with reference to the level lines), therefore the subsequent simplex uses the points *2*, *3*, and point *4* is the mirror image of point *1*. The next vertex, *5*, is the mirror image of point *2* because $y_2 < y_3 < y_4$. The search proceeds in a similar way and point *12* leads the system close enough to the extremum. Then at step *13* the system leaves the extremum and at step *14* reaches the point where it was at step *10*. The next step (*15*) takes the system to where

it was at step *13* and self-oscillations will arise around the optimum, bringing the system from point *13* to point *10* and back. These may be eliminated if, right after the first cycle (oscillation from point *13* to point *10* and again to point *13*), we reduce the simplex edge c in accordance with the harmonic sequence law, i.e.

$$c_k = \frac{c_0}{k-l} \qquad (k > l) \tag{26.31}$$

where c_k is the simplex edge length at the kth step; c_0 is the simplex edge length at the start of the search; l is the ordinal number of the step at which it was decided to reduce the simplex.

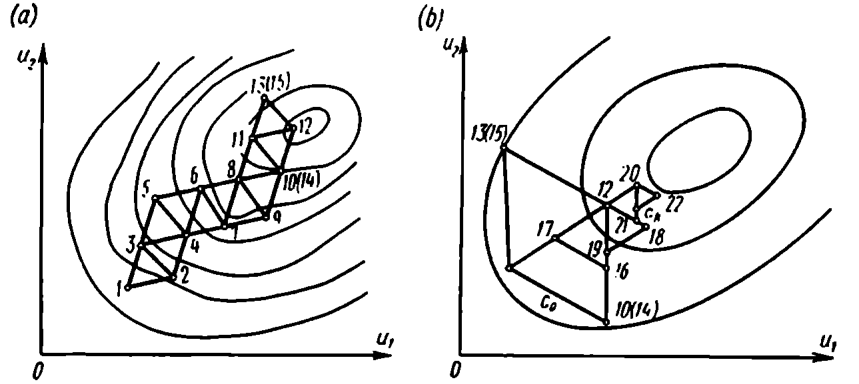

Fig. 26.15

At this stage the vertex with the greatest value of y should remain one of the vertices for new simplices.

Figure 26.15*b* shows the procedure of search with an allowance for Eq. (26.31) starting with the tenth step. This version of search combines the simplex method and stochastic approximation.

The simplex method solves the optimization problem in most complicated situations where a quantitative estimate of the function to be minimized is hampered and only qualitative estimates, such as "at this point the value of y is at its worst", can be obtained because for further search it is mportant to specify just one worst point.

The disadvantage of simplex methods is the relatively complex technical implementation in multidimensional problems where computers have to be used to find the simplex vertices.

Random search. The last group of methods to be discussed in this section are random search techniques which are used to advantage (Ref. 72) only in problems with a large number of variables ($n > 5$).

Thus, in one random search method the system makes a step of constant length in a random direction in the space of variables.

If the function to be optimized increases as a result of this step, the system makes the next step in the same way; if it decreases, the system returns to the initial point and then again changes the control coordinate vector in a random direction. In multidimensional systems the number of steps leading to the optimum in random search is commensurate with that of the steepest descent and the gradient method which are among the regular search methods.

We note in conclusion that the number of automatic search methods taking account of the specific features of the plant and of technical implementations, and different constraints is great and we have discussed only the most popular ones.

26.6 EXTREMAL SYSTEM DYNAMICS

In steady state a correctly calculated system should perform oscillatory motions (sometimes of a rather complicated shape) in the vicinity of the extremum. The oscillations, natural or forced, reflect the specific features of searching systems and are necessary to update the information on the system position in relation to the extremum. The amplitude of steady oscillations of the control coordinate vector is often referred to as the *value of hunting*.

Searching systems are nonlinear control systems aimed at tracking, in the space of control coordinates, a point for which the gradient of the function to be optimized is zero (condition (26.2)). The dynamics study problems in these systems (steady-state motion stability, transient performance) can be solved by using the methods employed in analysis of linear and nonlinear systems. For instance, determining the parameters of self-oscillations in a continuous system with extremum storage by the phase plane method and by harmonic linearization is treated in Chs. XVII and XVIII.

In some cases two nonlinearities which are associated with the plant and the facility computing the gradient compensate each other and the entire system can be reduced to a linear one. Thus if the plant static response is expressed as a quadratic parabola $y = bx^2$ and if the gradient computation is reducible to the determination of $\frac{\partial y}{\partial x} = 2bx$, then a series connection of the plant and the gradient-computing facility is equivalent to a linear proportional element with an input variable x and an output variable $\frac{\partial y}{\partial x}$. For most practical problems in steady state where the searching system is in the neighbourhood of the extremum the plant static response can be accurately enough approximated by a parabola; this assumption is thus well justified.

Example 26.5. Let the plant have an extremal static response $y(x) = bx^2 + y_0$ (Fig. 26.16*a*). After the derivative $\frac{\partial y}{\partial x} = z(x)$ i

determined, the searching system makes an operational step Δx by the law (26.6), i.e.

$$\Delta x_k = -az(x_k)$$

Assume that the time interval T between the operational steps is large enough for the steadying of transient processes in the plant and controller dynamic parts. If this assumption is valid, the search depends only on parameters of the static response and the gain a. Since in this case $z(x) = \frac{\partial y}{\partial x} = 2bx$, then in the initial structural diagram the series connection of the plant and the computing unit may be replaced by a linear element. This results in a linear first-order sampled-data system (Fig. 26.16*b*) the processes in which are described by the equation $\Delta x_k = -2abx_k$. Obviously, the optimal condition of search when the system reaches the extremum within one step, will be given by the equality $\Delta x_k = -x_k$; then

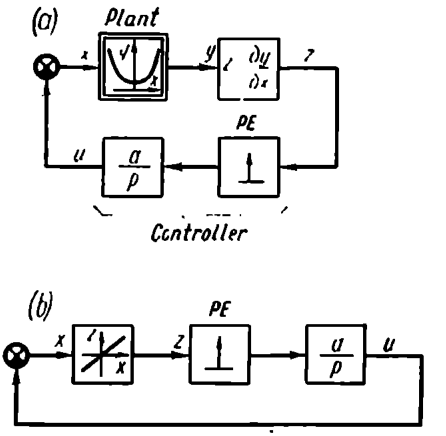

Fig. 26.16

$$2ba = 1 \qquad (26.32)$$

At $0 < 2ba < 1$ the search is monotonic, i.e. the system will approach the extremum without overshoot. Figure 26.17*a* shows search for this case in planes with coordinates $\frac{\partial y}{\partial x}$, x and x, t. If the system is at the point x_0 at the start of the search, after the first operational step Δx_1 it will reach the point x_1, that is $\Delta x_1 = x_1 - x_0$. The straight lines *1-2*, *3-4*, etc. in Fig. 26.17*a* make an angle α with the vertical line (α = arc tan a). The next step is $|\Delta x_2| < |\Delta x_1|$ because $\left|\frac{\partial y}{\partial x}\Big|_{x2}\right| < \left|\frac{\partial y}{\partial x}\Big|_{x1}\right|$.

At $1 < 2ba < 2$ the search is oscillatory, and the system is stable. The relevant construction is shown in Fig. 26.17*b*. As in the preceding case, the auxiliary straight lines *1-2*, *3-4*, etc. make an angle α with the vertical line (α = arc tan a).

If $2ba = 2$, there are oscillations in the system, their amplitude depending on the initial conditions (Fig. 26.17*c*). At $2ba > 2$ the search is unstable, and the system performs oscillatory diverging motions (Fig. 26.17*d*).

In this example, for the conditions of stability to be valid the factor a should satisfy the inequality

$$a < \frac{1}{b} \tag{26.33}$$

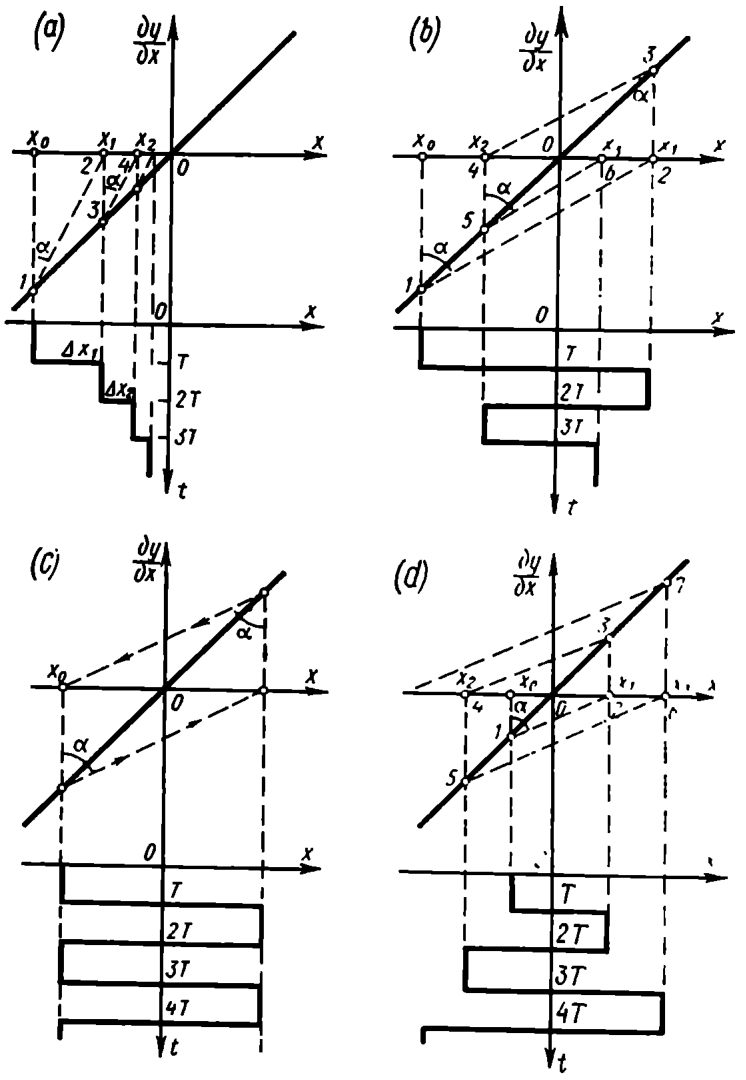

Fig. 26.17

Multiplying the numerator and denominator of the right-hand part of inequality (26.33) by $2x$ and bearing in mind that $2bx =$

$= z(x)$, we can write

$$|z(x)| < \left|\frac{2x}{a}\right| \qquad (26.34)$$

This condition is valid for any form of $z(x)$ and permits selecting the gain a of the gradient system so as to guarantee the stability of search. Figure 26.18 illustrates a method for determination of a ensuring the stability of the system with a response $y(x)$ (Fig. 26.18*a*) different from a parabola. In the plane where the plant response $\frac{\partial y}{\partial x} = z(x)$ is constructed (Fig. 26.18*b*) a straight line, kx, is traced so that $z(x)$ is in the sector between this line and the x-line. From Eq. (26.34)

$$a < \frac{2}{k} \qquad (26.35)$$

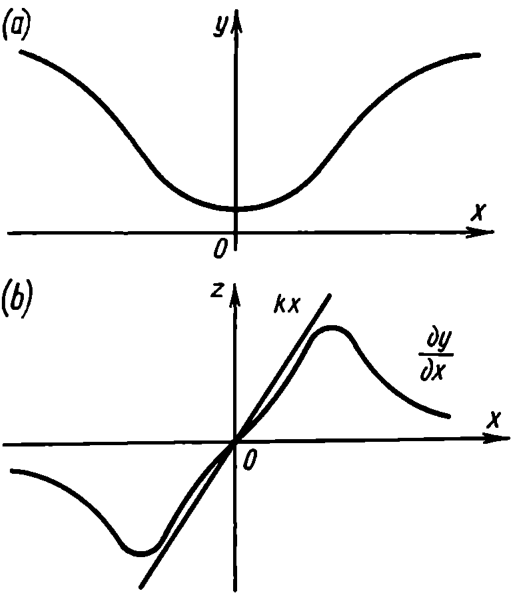

Fig. 26.18

Example 26.5 described a stationary case of search where the plant response was assumed invariable and known, whereas in most cases the study of searching systems in steady state involves analysis of a system subjected to random disturbances which change the plant responses. Several basic disturbances (see Fig. 26.6) have already been indicated, first of all, unobservable changes in the coordinates of the extremum f_1.

For searching systems these changes are a sort of a setting signal because the problem consists in searching and tracking the extremum. Also, the parameters of the plant static and dynamic responses may change randomly. The control unit can also be subjected to random disturbances, e.g. noise f_2 superimposed on the coordinate to be optimized.

The objective of system analysis under random disturbances is as a rule to determine the optimal parameters or structures of the control part of the system. Typical problems will be illustrated by two examples where the object of study is a one-dimensional system containing a synchronous detector (see Fig. 26.8) and operating in a quasi-stationary mode. Recall that a quasi-stationary mode takes place (Ref. 34) when the frequency of periodic searching signals

greatly exceeds that of operational signals. The effect of trial signals on the searching dynamics is disregarded.

Example 26.6. Assume that in a system containing a synchronous detector (Fig. 26.19*a*) the plant is inertialess with an extremal response of the form

$$y=\frac{1}{2}(x-f_1)^2 \quad (26.36)$$

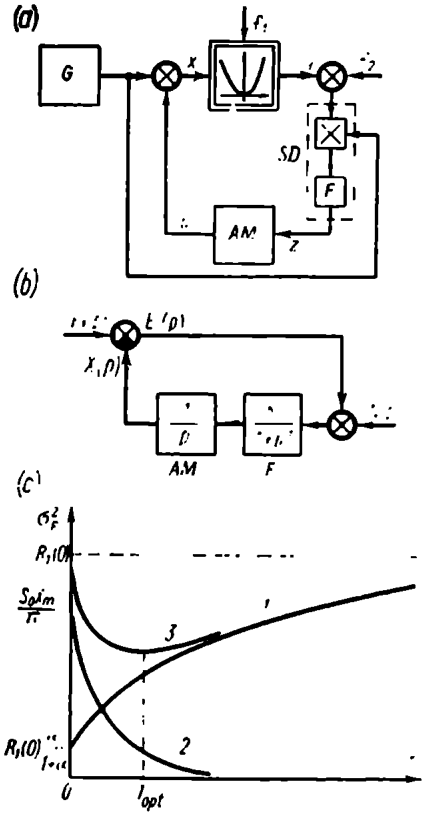

Fig. 26.19

where f_1 is a random disturbance causing a drift of the response and having an auto-correlation function

$$R_{f1}(\tau) = R_1(0)\, e^{-\alpha|\tau|} \quad (26.37)$$

where $R_1(0)$ = the dispersion of the extremum drift and α = the drift velocity statistic characteristic.

Assume that the plant output is subjected to a noise f_2 which is a high-frequency white noise with a spectral density S_0 at $\omega > \omega_2$ and 0 at $\omega \leqslant \omega_2$. Assume also that f_1 and f_2 are not correlated. The synchronous detector SD thus receives the sum $y + f_2$. The noise f_2 leads to distortions in the magnitude of the derivative $\frac{\partial y}{\partial x}$ computed in the SD. In the synchronous detector the multiplier is followed by an averaging low-pass filter F with a transfer function

$$W(p)=\frac{1}{1+Tp} \quad (26.38)$$

The actuating motor AM is represented in the structural diagram (Fig. 26.19*b*) as an integrating element.

In addition to suppression of the searching signal higher harmonics, the filter reduces the effect of f_2 on the accuracy of search: the greater the time constant T of the filter, the better is noise filtration and the smaller the fraction of the component due to f_2 in the overall error. On the other hand, the greater is T, the slower the system follows up the extremum drift and the greater is the component due to f_1 in the overall error.

Now we are facing the problem of selecting the optimal time constant for the filter. Here the optimality criterion is the minimum

of the system overall error for which we may take the dispersion σ_ε^2 of the deviation $\varepsilon = f_1 - x$ from the extremum during the search.

Let us have a look at the system structural diagram (see Fig. 26.19*b*). A plant with a response $y(x)$ and a synchronous detector may be replaced by an element represented as a subtracting unit with a response $\frac{\partial y}{\partial x} = z(x) = f_1 - x$. The filter F is retained as an inertial element because it affects the system dynamics. The generator G of searching signals and the multiplier are deleted because they are only required to determine $\frac{\partial y}{\partial x}$. The noise $n(t) = f(t) X_m \sin \omega_0 t$, which has propagated through a multiplier, will still be a white noise, except that the spectral density will change in proportion to the squared amplitude of the reference signal. The spectral density of the transformed noise $N(p)$ at $\omega_0 \ll \omega_2$ is

$$X_m^2 \frac{S_0}{2} \tag{26.39}$$

The factor $\frac{X_m^2}{2}$ represents the change in the specific power of noise f_2 when it is multiplied by the reference signal in the multiplying unit of the synchronous detector ($X_m \sin \omega_0 t$).

The deviation $\varepsilon = f_1 - x$ from the extremum is of a random nature because of the randomness of the signals $f_1(t)$ and $n(t)$. In this case the system accuracy may be characterized by the dispersion σ_ε^2. Since f_1 and f_2 are uncorrelated and the problem posed is linear, the dispersion of the error σ_ε^2 can be given as the sum of two components

$$\sigma_\varepsilon^2 = \sigma_1^2 + \sigma_2^2 \tag{26.40}$$

where σ_1^2 is the dispersion of the component caused by the drift f_1, and σ_2^2 is the dispersion of the component caused by the noise f_2. The addend σ_1^2 is found from the known statistical characteristics of the signal f_1 and the transfer function $W_1(p) = \frac{E(p)}{F_1(p)}$, which relates the drift and the error, with the use of Eq. (24.15):

$$\sigma_1^2 = \frac{1}{\pi} \int_0^\infty |W_1(j\omega)|^2 S_1(\omega)\, d\omega \tag{26.41}$$

From Fig. 26.19*b* it follows that

$$W_1(j\omega) = \frac{j\omega(1 + j\omega T)}{j\omega(1 + j\omega T) + 1} \tag{26.42}$$

The spectral density for a signal with a correlation function (26.37) (see Eqs. (23.49) and (23.51)) is of the form

$$S_1(\omega) = \frac{2R_1(0)\alpha}{\alpha^2 + \omega^2} \tag{26.43}$$

Substitute Eqs. (26.42) and (26.43) into (26.41)

$$\sigma_1^2(T)=\frac{2R_1(0)\alpha}{\pi}\int_0^\infty \frac{\omega^2(\omega^2T^2+1)}{[(1-\omega^2T)^2+\omega^2](\alpha^2+\omega^2)}d\omega$$

$$\sigma_1^2(0)=R_1(0)\frac{\alpha}{1+\alpha} \quad \text{at} \quad T=0$$

$$\sigma_1^2(\infty)=R_1(0)\left(1+\frac{1}{\alpha}\right) \quad \text{as} \quad T\to\infty$$

The function $\sigma_1^2(T)$ is shown in Fig. 26.19*c* (curve *1*).
Let us find the dispersion of the error component due to f_2

$$\sigma_2^2=\frac{1}{\pi}\int_0^\infty |W_2(j\omega)|^2 S_2(\omega)\,d\omega \tag{26.44}$$

where

$$W_2(j\omega)=\frac{E(j\omega)}{N(j\omega)}=\frac{1}{j\omega(1+j\omega T)+1} \tag{26.45}$$

while $S_2(\omega)$ is found from Eq. (26.39).
Substituting Eqs. (26.45) and (26.39) into (26.44) we have

$$\sigma_2^2(T)=\frac{X_m^2S_0}{2\pi}\int_{\omega_2}^\infty \frac{d\omega}{\omega^4T^2+\omega^2(1-2T)+1}$$

$$\sigma_2^2(0)\approx\frac{S_0X_m^2}{4} \quad \text{at} \quad T=0,\ \omega_2\ll 1$$

$$\sigma_2^2(\infty)=0 \quad \text{at} \quad T\to\infty$$

The function $\sigma_2^2(T)$ is shown in Fig. 26.19*c* (curve *2*). The overall dispersion of the error $\sigma_\varepsilon^2(T)=\sigma_1^2(T)+\sigma_2^2(T)$ obviously has a minimum (curve *3* in Fig. 26.19*c*). The value $T=T_{opt}$ at which $\sigma_\varepsilon^2=\min$ can be found by computational mathematics methods from the condition $\frac{d\sigma_\varepsilon^2}{dT}=0$.

Example 26.7. Consider a method of automatic adjustment of an optimal parameter in systems with synchronous detection where the plant dynamic properties change considerably under the action of unobservable disturbances. If the plant is not inertialess, then the output signal $z(t)$ of the synchronous detector depends on the phase shift $[\varphi(\omega_0)-\psi]$ between the search component of the plant output signal (the first harmonic) and the reference signal u_{ref1} as given by Eq. (26.8), or

$$z_1=X_m\left(\frac{\partial y}{\partial x}\right)\cos[\varphi(\omega_0)-\psi]$$

where ω_0 is the searching signal frequency. As shown in Sec. 26.3, the highest possible level of the synchronous detector output at a specified value of the derivative $\frac{\partial y}{\partial z}$ is maintained by keeping the phase difference $[\varphi(\omega_0) - \psi]$ down to zero (Eq. (26.9)).

When the plant dynamic properties change under the effect of disturbances, the phase shift of the signal searching component $[\varphi(\omega_0)]$ also varies. The condition (26.9) is satisfied by automatic monitoring of $\varphi(\omega_0)$, e.g. by means of an additional synchronous detector whose one input receives the plant output signal and the other, the reference signal of the doubled searching frequency. The output of the additional synchronous detector is given by the expression

$$z_2 = B\left(\frac{\partial^2 y}{\partial x^2}\right)\sin 2\varphi(\omega_0) \tag{26.46}$$

where B is a coefficient depending on the amplitude of the signals fed to the SD.

This is verified by using a simple example where the plant has a quadratic static response $y = av^2$, and a linear dynamic element (LP) with a transfer function $W(p) = \frac{V(p)}{X(p)}$ is connected before a nonlinear element (Fig. 26.20*a*). The linear part parameters change under the action of the random disturbances f_3. The trial signal $u_{tr} = X_m \sin \omega_0 t$ changes its amplitude and phase in the dynamic element, therefore the searching signal at the input of the nonlinear element can be written in the form

$$v_{tr} = V_m(\omega_0)\sin[\omega_0 t + \varphi(\omega_0)]$$

where

$$V_m(\omega_0) = X_m |W(j\omega_0)|$$
$$\varphi(\omega_0) = \arg W(j\omega_0)$$

Assuming that the reference signal in the SD_2 is $u_{ref2} = \sin 2\omega_0 t$ and filtration is ideal, i.e. it is performed by averaging over the period $\left(\frac{2\pi}{\omega_0}\right)$, we determine the output z_2 of the second synchronous detector

$$z_2 = \frac{1}{\pi}\int_0^{2\pi} a\{V_m(\omega_0)\sin(\omega_0 t + \varphi)\}^2 \sin 2\omega_0 t\, d\omega_0 t = \frac{2aV_m^2(\omega_0)}{4}\sin 2\varphi \tag{26.47}$$

It can be seen that the output signal of SD_2 actually has the function $\sin 2\varphi$ as a multiplier, while the other multiplier is $2a = \frac{d^2}{dv^2} av^2$.

When the plant static response and the amplitude-frequency response are known and do not change, the value of the output signal z_2 of the second synchronous detector can serve as a clue to the value

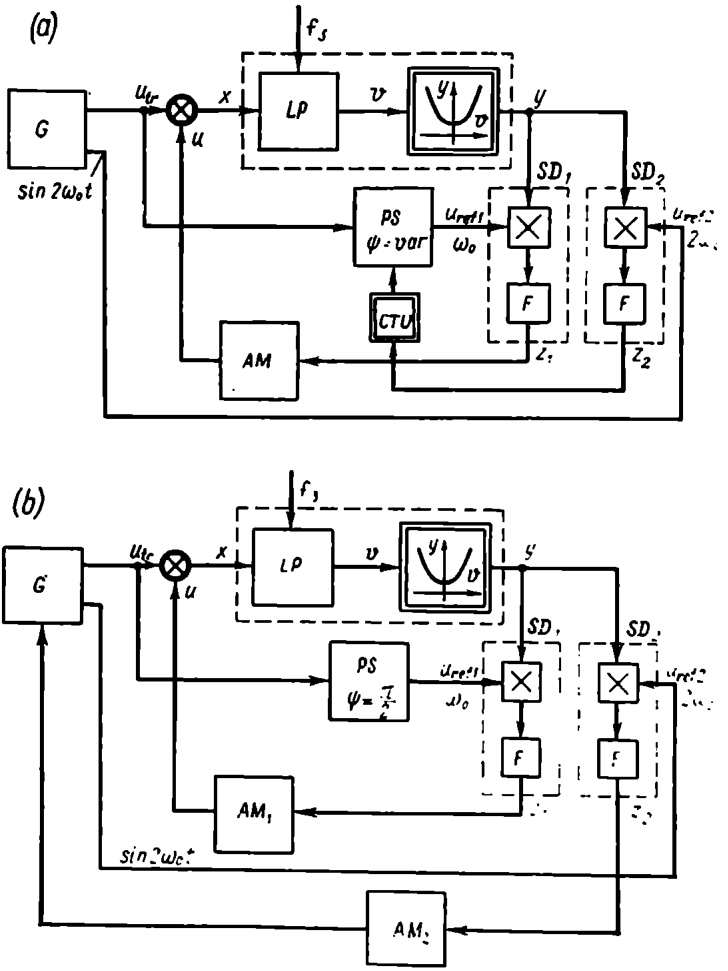

Fig. 26.20

of the plant phase shift $\varphi(\omega_0)$. With the value $\varphi(\omega_0)$ found, the phase shifter PS in the channel of the reference signal can be adjusted by setting $\varphi = \psi$. Figure 26.20*a* illustrates a version of such a use of the SD_2 output signal. Here the computer determines the necessary action on the PS using the value of z_2. This type of zero phase difference adjustment requires extensive information on the plant responses because to compute φ (see Eq. (26.46)) one must

know the second derivative $\frac{\partial^2 y}{\partial x^2}$ and the coefficient B depending on the plant amplitude-frequency properties.

Zero phase difference adjustment can also be achieved by another method. As follows from Eq. (26.46), the output signal z_2 of the synchronous detector with a doubled reference frequency is zero at $\varphi = \frac{m\pi}{2}$, where m is an integer at any values of B and $\frac{\partial^2 y}{\partial x^2}$. If the searching signal frequency ω_0 is increased from small values when $\varphi(\omega_0)$ is near zero, then z_2 vanishes at the frequency ω_0, for which $\varphi(\omega_0) = \frac{\pi}{2}$ (it is assumed that $\frac{\partial^2 y}{\partial x^2} \neq 0$).

Consequently, maintaining $z_2 = 0$ by controlling the searching signal frequency the plant phase shift can be kept constant, $\varphi(\omega_0) = \frac{\pi}{2}$. To hold the phase difference down to zero, it remains to set a constant phase shift in the channel of the reference signal $\psi = \frac{\pi}{2}$. The structural diagram of a system implementing this procedure is given in Fig. 26.20*b*, where the plant, the synchronous detector SD_1 with a reference frequency ω_0, and the actuating motor AM_1 form the main adaptation loop ensuring that the condition $\frac{\partial y}{\partial x} = 0$ is met in steady state. The synchronous detector SD_2 with a reference frequency $2\omega_0$ controls the frequency of the generator G through the actuating motor AM_2, thereby ensuring, in steady state, the condition $\varphi - \psi = 0$ under which the main adaptation loop has the greatest possible gain.

26.7. GENERAL CHARACTERISTICS OF SYSTEMS WITH MODELS

When self-adjusting systems are employed in optimization o dynamic modes of control systems, the plant dynamic propertie (dynamic model) should be determined. Moreover, the necessary setpoints of the control unit should be defined in terms of a specified performance criterion and their observance ensured.

An important stage in constructing such a SAS is elaboration of a dynamic model of the plant, i.e. the identification of the plant (system) dynamic response in normal operation.

At present two methods for using models in control problems can be visualized, namely: they may be applied as correcting units and as sensors of the plant dynamic state.

Figure 26.21 exhibits a generalized diagram of a SAS with the use of a model. For illustrativeness the model M incorporated into the control unit CU is shown separately.

In this figure $\mathbf{u}_M$ is the vector of actions controlling the model, $\mathbf{y}_M$ the vector of model outputs, $\mathbf{v}_M$ the vector of model setpoints, and $\mathbf{x}$ the vector of external actions.

The use of a model as a correcting (compensating) unit permits changing the system characteristics in the desired direction, and its use as a sensor of the plant dynamic state provides information on the actual or desired dynamic state of the system at a current moment or in the future and permits utilization of these data for setting the optimal control parameters.

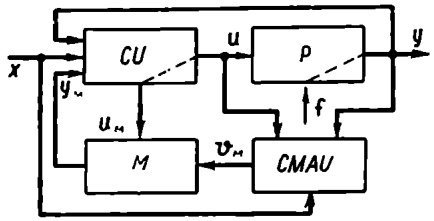

Fig. 26.21

Example 26.8. An example of a model acting as a sensor of the plant dynamic state is its use for compensation of a plant delay affecting control stability (Fig. 26.22). The plant with a delay is connected in parallel to its dynamic model and a delay D; the outputs of the plant and of the model with the delay are mutually compensated, and the system is closed by using the undelayed model

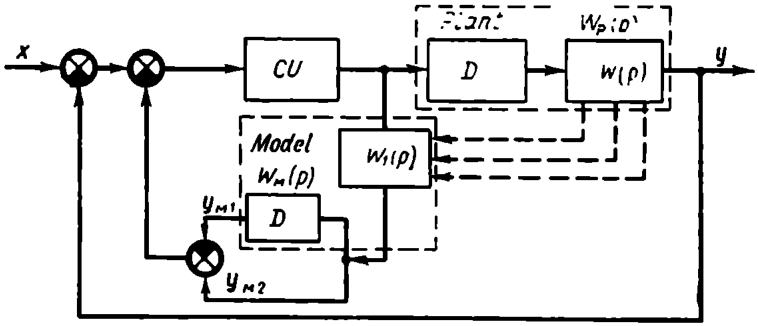

Fig. 26.22

output. The system is stable when the conditions $W_M(p) = W_P(p) = W_1(p)\,e^{-p\tau_1}$ are met and the delays of the plant, τ_P, and of the model, τ_1, are equal.

When the plant responses $W_P(p)$ change, the model must be adjusted so as to ensure $W_M(p) = W_P(p)$.

A very promising approach is to use models as sensors of the dynamic state so as to predict the system behaviour under specified disturbances and different types of control and to select the optimal control functions. This can be achieved using two-scale systems (Fig. 26.23). *Apriori* data or identification are used to build a plant model, which operates on a compressed time scale. All data obtained in plant identification are automatically fed into the model through the Data Input. The plant control function is related to the fast part

of the system, which includes models of the plant and of the control unit operating in the mode of periodic control problem solution. The current control law (best in a specified sense), which is found with an allowance for the future behaviour of the plant, is transmitted through the Data Output for implementation in the plant.

One promising approach is to use the principle of a two-scale system with a mode to control a plant whose output is inaccessible

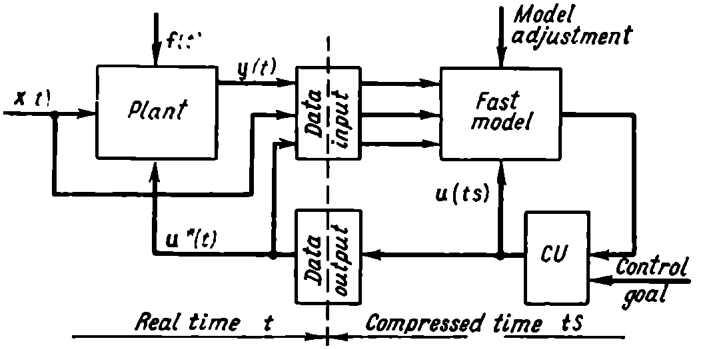

Fig. 26.23

for on-line measurements. Such plants include processes whose output characteristics are monitored or estimated by instruments which deliver data at discrete instants of time and with a considerable delay; examples are some gas mixture analyzers in chemical and heat-engineering equipment, *IR* spectrographs, humidity meters for solid and friable materials, etc. In such systems the plant model is based on *apriori* data and is periodically adjusted to the changing conditions. The model may lead to optimal control data which can then be implemented in the plant.

Practical control systems with models can be classified into SAS with a reference model and SAS with an adjustable model.

26.8 SYSTEMS WITH A REFERENCE MODEL

Such systems normally contain (Fig. 26.24) a model of a closed-loop control system (a reference model) simulating the optimal characteristics of the system under study, a correspondence criterion computer *CCC* and a control unit *CU* to change the parameters (and possibly the structure) of the system compensator *C*. The correspondence criterion should contain data on the plant dynamic responses, and its computation involves a rather complicated analysis. In certain cases the determination of these responses (identification) is possible by using additional test signals (see Ch. XXIII). The

basic requirement imposed on the test signals is that they should not disrupt the normal functioning of the system. Consequently, their intensity should be low enough. We will consider some examples of SAS with models.

Example 26.9. Take up a system with a reference model connected in parallel to the plant (Fig. 26.25). Several widely used versions of this system ensure insensitivity of the system transfer function to variations in the plant dynamic responses. This problem arises,

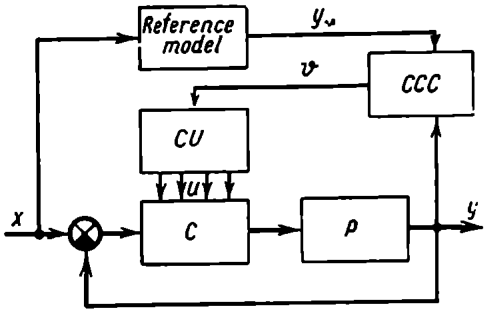

Fig. 26.24

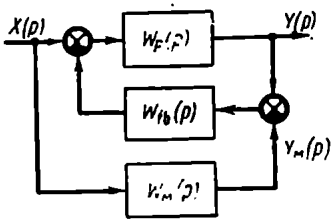

Fig. 26.25

say, in designing manned high-speed high-altitude aircraft. The aircraft should be equally controllable in all flight conditions. This is achieved by introducing into the control loop a reference model connected to the main control system. The model transfer function $W_M(p)$ is selected so that it is optimal in terms of ease of control. The aircraft output coordinate (e.g. the pitch angle) is measured and compared with the model output signal. The difference between them is fed into the feedback loop and is subtracted from the output control signal acting on the aircraft.

The transfer function of the entire system is (see Fig. 26.25)

$$W(p)=\frac{Y(p)}{X(p)}=\frac{W_P(p)\,[1+W_M(p)\,W_{fb}(p)]}{1+W_{fb}(p)\,W_P(p)}$$

where $W_P(p)$ = the plant transfer function and $W_{fb}(p)$ = the feedback loop transfer function.

With a large feedback gain

$$W(p)\approx W_M(p)$$

and the aircraft output coordinate depends only on the model dynamic properties.

Example 26.10. Consider a system with automatic adjustment of the gain of the compensator C (Fig. 26.26). The system uses a small-

amplitude trial signal u_{tr} given by the sine-wave generator G

$$u_{tr} = U_m \sin \omega_0 t$$

where U_m = the trial signal amplitude and ω_0 = the trial signal frequency.

The signal is fed simultaneously to the closed-loop control system and to the plant model M. The system output has a resonance filter

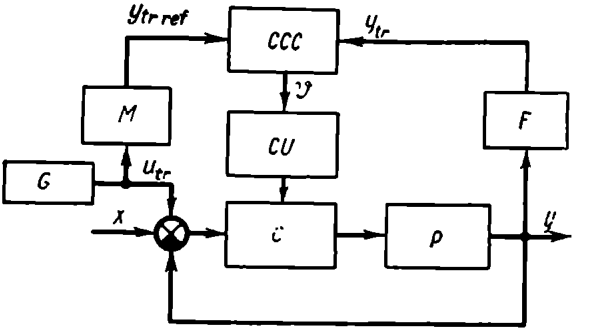

Fig. 26.26

F, which isolates from the output signal the system response to the trial signal (the search component) in the form

$$y_{tr} = Y_m \sin (\omega_0 t + \varphi)$$

where φ = the phase shift and Y_m = the output signal amplitude.

The reference model output will be

$$y_{tr\,ref} = Y_{m\,ref} \sin (\omega_0 t + \varphi_{ref})$$

The correspondence criterion computer in this case generates a control action v proportional to the difference

$$\mathrm{v} = \mathrm{y}_{tr} - \mathrm{y}_{tr\,ref}$$

and controlling the closed-loop control system gain.

26.9 SYSTEMS WITH AN ADJUSTABLE MODEL

SAS with an adjustable model are employed in optimal control of dynamic plants. One effective way to solve this problem is to use a two-scale system which presumes the presence of a dynamic plant model. Since the plant dynamic responses can change in the course of time, high control performance is achieved by periodic tracking of the changes and by automatic correction of the model parameters so as to maintain the correspondence of the model to the plant. Consequently, self-adjusting models (SAM) should be developed.

These fall into two types, searching and searchless. The principle underlying the design of SAM often depends on the nature of the correspondence criterion selected.

In searching-type SAM this criterion may be the minimal r.m.s. error between the plant and model responses to the same input signal.

Searching SAM are normally representable by the diagram of Fig. 26.27*a*, where the control unit *CU* varies the model parameters so as to obtain the least value of the criterion. These are closed-loop SAM. In searchless self-adjusting models self-adjustment is done by a computing unit which analyses the plant input and output signals (Fig. 26.27*b*). These are open-loop SAM.

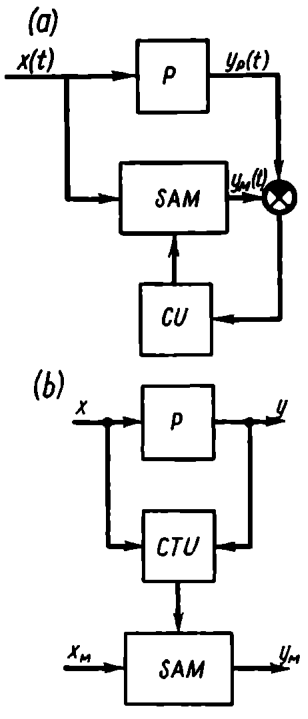

Fig. 26.27

With all their valuable properties, such as high accuracy of adjustment and noise-immunity, searching self-adjusting models require much time for adjustment, and the more so, the greater the number of parameters to be adjusted.

In searchless SAM the data needed for adjustment result from processing a much larger body of plant data than in searching SAM. The adjustment time, however, is shorter here and is independent of the number of parameters.

The problem of SAM design can be subdivided into two stages:

1) analysis, or obtaining data on a functioning plant;

2) synthesis, or implementation of the resultant model by using computers, in particular, analog ones.

For simplicity, only linear plants with one input and one output will be treated in further discussion.

The problem of analysis of the plant dynamic responses is formulated as follows: proceeding from the readings of the input, $x(t)$, and output, $y(t)$, signals of the plant determine a model of the pulse response $w_M(t)$ minimizing the squared error ε^2 with the analysis time limited and in the presence of noises. The information on the dynamic response should be obtained in a form suitable for use in an analog computer

$$\varepsilon^2 = \int_0^\infty [w(t) - w_M(t)]^2 \, dt \qquad (26.48)$$

where $w(t)$ is the plant weighting function.

Example 26.11. Consider a dynamic response analyzer (e.g. АДХ-2 developed at the Moscow Power Institute). In Sec. 24.2 we discussed a method of identifying dynamic responses using decomposition of an unknown weighting function of the plant into a system of orthogonal functions. The same section showed that when the plant transient process is aperiodic or mildly oscillatory, Laguerre functions can conveniently serve as the basic orthogonal functions. Representation of the model weighting function in the form of (24.26), or as

$$w_M(t) = \sum_{k=0}^{m} C_k l_k(t)$$

where $l_k(t)$ are pulse responses of Laguerre elements, satisfies the requirement of simple analog implementation because these responses are described by simple transfer functions Eq. (24.24). Besides, this representation of $w_M(t)$ ensures good accuracy for most industrial plants with a small number, m, of the expansion terms.

The simplest approach to estimating coefficients C_k was discussed in Ch. XXIV (see Fig. 24.5*b*). The plant input is a binary white noise. The plant output signal $y(t)$ is fed to a multiplier whose second input receives the response of the appropriate Laguerre element (z_k) to the binary white noise. After the product is averaged by the filter, C_k is estimated with an accuracy to a constant multiplier a^2, i.e.

$$C_k = \frac{1}{2Ta^2} \int_{-T}^{T} y(t) z_k(t)\, dt \qquad (26.49)$$

where $2T$ is the averaging time.

In practice, this kind of computation for plants with lengthy transient processes is complicated by the fact that Laguerre elements with large time constants and multiplier are difficult to implement.

The formula (26.49) can be simplified if the probability distribution of $z_k(t)$ is near normal. Since for $T \to \infty$ the coefficient C_k is the value of the cross-correlation function of $y(t)$ and $z_k(t)$ at zero shift, then by virtue of Eq. (25.57) the expression (26.49) can be replaced by an equivalent one

$$C_k = B_k \frac{1}{2T} \int_{-T}^{T} y(t) \operatorname{sign} z_k(t)\, dt \qquad (26.50)$$

where B_k is a coefficient depending on dispersions of the signals y and z_k (see Sec. 25.6).

From Eq. (26.50) it follows that multiplication by $z_k(t)$ can be replaced by multiplication by ± 1; in other words, C_k can be found by merely integrating $y(t)$ with an allowance for the sign of $z_k(t)$.

Recall that Eq. (26.50) is valid at normal distribution of $z_k(t)$. This condition is met if the cycle time of the binary white noise T_0, is much shorter than the Laguerre elements time constants (see Sec. 24.5).

Formula (26.50) is easily realizable if the trial signal consists of pseudorandom binary sequences (PRBS) of the maximal period. The properties of PRBS are discussed in detail in Ch. XXIII.

The frequency properties of PRBS depend on the cycle duration T_0 and the number of cycles in the period T_{tr}. The PRBS spectrum lies largely in the band

$$\omega_{max} = \frac{2\pi}{T_0}$$
$$\omega_{min} = \frac{2\pi}{T_{tr}} \qquad (26.51)$$

In analyzing plants with transfer functions of the form

$$W(p) = \frac{K}{\prod_{i=1}^{N} (1+pT_i)}$$

a PRBS-type trial signal should have such parameters (cycle duration T_0, period T_{tr}) that the signal frequency band (see Eq. (26.51)) overlap the plant passband.

With a PRBS used as a trial signal, the dispersion of estimates of C_k is the lowest for the formula (26.50) if the estimates are read at time instants T_j multiple of the period of the trial signal, i.e.

$$T_j = jT_{tr} \qquad (j = 1, 2, \ldots)$$

The dispersion of the estimate does not exceed 5% if the following conditions are met

$$T_{tr} = 1{,}023T_0, \qquad T_a \approx (15 \text{ to } 25)T$$

where T is the transient time of the plant and T_a is the continuous analysis time.

Formula (26.50) using a PRBS with a period of 1,023 T_0 is implemented in the АДХ-2 device mentioned above which determines the dynamic responses of complex plants with the aid of using two interdependent channels with a transient time from 2 to 300 min. For simplicity sake the instrument dispenses with a generator of a trial signal and elements implementing Laguerre functions. The signal is obtained by reading a sample of a PRBS of finite length recorded in the program unit (Fig. 26.28). The use of PRBS permits further simplifying of implementation of formula (26.50). The necessary values of sign $z_k(t)$, which are sign-valued responses of the elements l_k to a test signal, are pre-calculated and recorded in the program unit together with the PRBS.

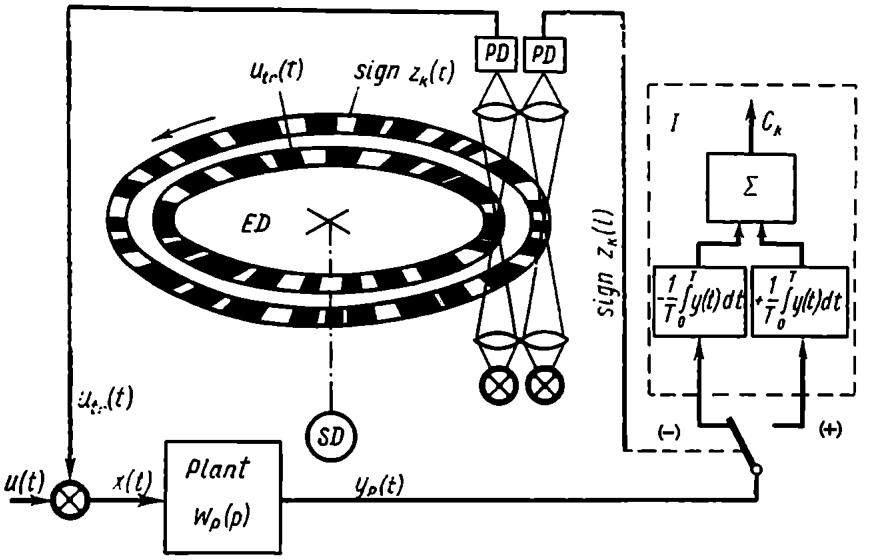

Fig. 26.28

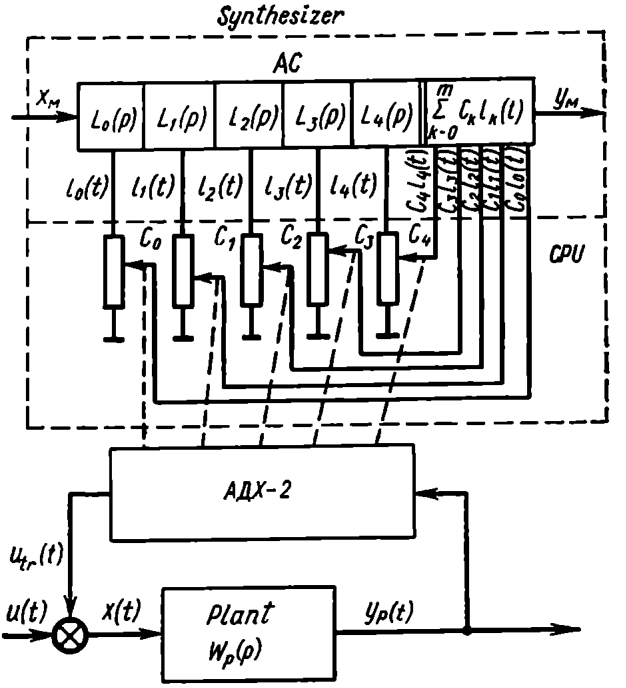

Fig. 26.29

The program unit consists of an encoding disk *ED* with optical data reading effected by photo diodes *PD*. The integration required by Eq. (26.50) is performed by a digital integrator *I*. The АДХ-2 has been used as the basis for a system which automatically obtains a compressed time (fast) self-adjusting model in practical operation (Fig. 26.29). The system also includes an analog computer *AC* and a coupling unit *CPU*. A system of dynamic elements $L_k(p)$ necessary for synthesizing a fast model is easily obtained by means of the *AC*. The *CPU* ensures automatic adjustment of the model on the basis of the coefficients C_k. The *CPU* stores the value and sign of C_k and performs the multiplication $C_k l_k(T)$.

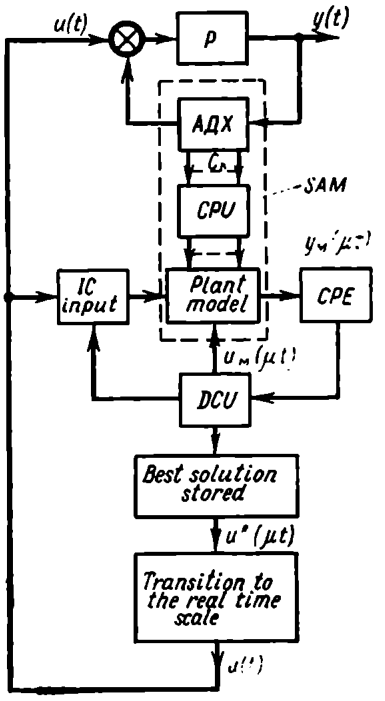

Fig. 26.30

The *CPU* automatically adjusts the model to the current value of C_k determined by the АДХ-2.

The self-adjusting model implemented by the analog computer is part of a two-scale hybrid system HS, which consists of analog and digital computing units intended for handling optimal control problems (Fig. 26.30).

The analog computer reproduces a plant model which operates on a compressed time scale (μt, $\mu > 1$).

The digital computing unit *DCU* generates certain algorithms of admissible control and implements them in the model.

In this way, the HS easily solves the problem of linear plant control near optimal in terms of the speed of response.

The model operating on a compressed time scale receives a control signal generated by the *DCU* from a class of piecewise-constant functions with an allowance for the constraints imposed. Prior to that, initial conditions (*IC* input) are introduced into the model which allow for the effect of the input signal during the transient period preceding the search for control.

Each implemented version of control is estimated against a selected optimality criterion (e.g. minimal time of the process) by a control performance estimator *CPE*. Each estimate can be obtained within a short enough time. Examination of all permissible controls u from a certain closed set Ω generated in the *DCU* permits finding

and storing a near-optimal version for its further implementation in the plant. Finding near-optimal control in terms of the speed of response amounts to finding switching times t_i ($i = 1, 2, \ldots, n$). The process of search for near-optimal control u^* can proceed in the HS as follows.

The transient process time is found by using the model. For given constraints (e.g. $|u| \leqslant 1$) and coordinates of the initial and final points in the phase space of the plant a certain search interval of duration t^0 ($0 < t^0 \leqslant T$) is specified such that

$$t^* < t^0 \leqslant T \tag{26.52}$$

where t^* is the duration of strictly optimal control, t^0 the initial estimate of control duration and T the transient time under a unit disturbance.

The searching interval t^0 is divided into m discrete switching times. All feasible controls are generated on the interval (26.52) and are then estimated in the model. Their number is $N = 2^{m+1}$.

Since the switching times are discrete with a step of $\Delta t = \frac{t^0}{m}$, the error of search for each optimal switching time is

$$\delta t_i \leqslant \frac{t^0}{2m}$$

where

$$\delta t_i = |t_i^* - t_i|$$

while t_i is a discrete instant of control switching.

The number of versions to be examined is seen to depend on the accuracy of estimating the interval t^0 and the admissible error. Since an accurate estimate of t^0 is rather hard to obtain, a sequential procedure can be arranged for generation of feasible controls which would ensure successive updating of the estimate of t^0 with simultaneous reduction of the search error.

APPENDIX

MATHEMATICAL DESCRIPTION OF RANDOM SIGNALS (DEFINITIONS AND NOTATION)

A random signal is characterized by a sample set over a specified time interval. Its mathematical description involves the following characteristics which are non-random functions: a) distribution function and density, (b) correlation function, c) spectral density.

Random signal distribution laws. A one-dimensional integral distribution law $P_1(x_1, t_1)$ of a random signal or a distribution function is the probability that at the time $t = t_1$ the value of $x < x_1$.

A one-dimensional differential distribution law dP_1 of a random signal is the probability that at the time $t = t_1$ the value of x is between x_1 and $x_1 + dx_1$

$$dP_1 = p_1(x_1, t_1)\, dx_1 \tag{A 1}$$

Here $p_1 = \frac{dP_1}{dx_1}$ is a one-dimensional probability density or a one-dimensional distribution density.

Therefore

$$P_1(x_1, t_1) = \int_{-\infty}^{x_1} p_1(x_1, t_1)\, dx_1 \tag{A 1a}$$

Since

$$\lim_{x_1 \to \infty} P_1(x_1, t_1) = 1$$

then

$$\int_{-\infty}^{\infty} p_1(x_1, t_1)\, dx_1 = 1$$

A two-dimensional integral distribution law $P_2(x_1, t_1; x_2, t_2)$ of a random signal, or a two-dimensional distribution function is the probability that $x < x_1$ at the time t_1, while $x < x_2$ at the time t_2. A two-dimensional differential distribution law d^2P_2 of a random signal is the probability that at the time t_1 the value of x is somewhere between x_1 and $x_1 + dx_1$ and at the time t_2. between x_2 and $x_2 + dx_2$;

$$d^2P_2 = p_2(x_1, t_1; t_2, x_2)\, dx_1\, dx_2 \tag{A 2}$$

Here $p_2 = \frac{d^2P_2}{dx_1\, dx_2}$ is the two-dimensional probability density or the two-dimensional distribution density of two random signals, x and y.

Therefore

$$P_2(x_1, t_1; x_2, t_2) = \int_{-\infty}^{x_1}\int_{-\infty}^{x_2} p_2(x_1, t_1; x_2, t_2)\, dx_1\, dx_2 \qquad \text{(A 2a)}$$

Since

$$\lim_{\substack{x_1\to\infty \\ x_2\to\infty}} P_2(x_1, t_1; x_2, t_2) = 1$$

then

$$\int_{-\infty}^{\infty}\int_{-\infty}^{\infty} p_2(x_1, t_1; x_2, t_2)\, dx_1\, dx_2 = 1$$

n-dimensional functions and distribution densities are introduced in the same way

$$P_n(x_1, t_1; x_2, t_2; \ldots; x_n, t_n)$$
$$p_n(x_1, t_1; x_2, t_2; \ldots; x_n, t_n)$$

Simple examples of processes

1. An independent process. Such a process can be completely described by a one-dimensional probability density

$$p_n(x_1, t_1; x_2, t_2; \ldots; x_n, t_n) = p_1(x_1, t_1)\, p_1(x_2, t_2) \ldots p_1(x_n, t_n) \qquad \text{(A 3)}$$

2. A stationary random process, an analog of a steady-state process

$$p_n(x_1, t_1; x_2, t_2; \ldots; x_n, t_n) = p_n(x_1, t_1 + t_0; x_2, t_2 + t_0; \ldots; x_n, t_n + t_0) \qquad \text{(A 4)}$$

for a one-dimensional distribution density

$$p_1(x_1, t_1) = p_1(x_1) \qquad \text{(A 5)}$$

for a two-dimensional distribution density

$$p_2(x_1, t_1; x_2, t_2) = p_2(x_1, t_1 + t_0; x_2, t_2 + t_0)$$

at $t_2 - t_1 = \tau$ and $t_1 = -t_0$

$$p_2(x_1, t_1; x_2, t_2) = p_2(x_1, x_2, \tau) \qquad \text{(A 6)}$$

In the presence of two random signals $x(t)$ and $y(t)$

$$d^2P_2 = p_2(x_1, t_1; y_2, t_2)\, dx_1\, dy_2 \qquad \text{(A 7)}$$

is the probability that at the time t_1 the value of x is somewhere between x_1 and $x_1 + dx_1$, while at t_2 the value of y is between y_2 and $y_2 + dy_2$.

If

$$p_2(x_1, t_1; y_2, t_2) = p_2(x_1, t_1 + t_0; y_2, t_2 + t_0) = p_2(x_1, y_2, \tau) \qquad \text{(A 8)}$$

the processes are stationary dependent.

Examples of distribution densities

1. The most widespread distribution law is the normal Gaussian law

$$p_1(x) = \frac{1}{\sigma_x\sqrt{2\pi}} \exp\left[-\frac{(x - x_0)^2}{2\sigma_x^2}\right] \qquad \text{(A 9)}$$

2. Uniform (rectangular) distribution

$$p_1(x)=\begin{cases}\dfrac{1}{x_2-x_1} & \text{at } x_1\leqslant x\leqslant x_2\\ 0 & \text{at } x<x_1 \text{ and } x\geqslant x_2\end{cases} \tag{A 10}$$

3. Exponential distribution

$$p_1(x)=\begin{cases}\alpha e^{-\alpha x} & \text{at } x\geqslant 0\\ 0 & \text{at } x<0.\end{cases} \tag{A 11}$$

4. Rayleigh distribution

$$p_1(x)=\begin{cases}x\exp\left(\dfrac{-x^2}{2}\right) & \text{at } x>0\\ 0 & \text{at } x<0\end{cases} \tag{A 12}$$

5. Cauchy distribution

$$p_1(x)=\frac{1}{\pi\alpha}\,\frac{1}{1+\left(\dfrac{x-x_0}{\alpha}\right)^2} \tag{A 13}$$

6. Laplace distribution

$$p_1(x)=\frac{1}{2\beta}\,e^{-\frac{|x-x_0|}{\beta}} \tag{A 14}$$

7. Poisson distribution

$$p_1(x)=\frac{\xi^x}{x!}\,e^{-\xi}1_0^*(x) \tag{A 15}$$

where x is a positive integer. Only in this case will $1_0^*(x)\cdot\sum_{k=0}^{\infty}\delta(x-k)$ be nonzero (see Ch. XII)

8. Two-dimensional normal distribution law

$$p_2(x,\ y)=\frac{1}{2\pi\sigma_x\sigma_y\sqrt{1-\rho_{xy}^2}}\exp\left\{-\frac{1}{2(1-\rho_{xy}^2)}\left[\left(\frac{x-x_0}{\sigma_x}\right)^2+\right.\right.$$
$$\left.\left.+\left(\frac{y-y_0}{\sigma_y}\right)^2-2\rho_{xy}\frac{(x-x_0)(y-y_0)}{\sigma_x\sigma_y}\right]\right\} \tag{A 9a}$$

where

$$x=x(t_1);\quad y=y(t_2),\quad \rho_{xy}=\rho_{xy}(t_1,\ t_2)=\frac{1}{\sigma_x\sigma_y}M\{(x-x_0)(y-y_0)\}$$

For the independent processes x and y, $\rho_{xy}=0$.

9. Distribution of a sum (difference) of two independent processes

$$z(t)=x(t)\pm y(t)$$

(a) normal distribution

$$p_1(x)=\frac{1}{\sigma_x\sqrt{2\pi}}\exp\left[-\frac{(x-x_0)^2}{2\sigma_x^2}\right]$$

$$p_1(y)=\frac{1}{\sigma_y\sqrt{2\pi}}\exp\left[-\frac{(y-y_0)^2}{2\sigma_y^2}\right]$$

$$p_1(z)=\frac{1}{\sigma_z\sqrt{2\pi}}\exp\left[-\frac{(z-z_0)^2}{2\sigma_z^2}\right]$$

where

$$z_0 = x_0 \pm y_0, \qquad \sigma_z^2 = \sigma_x^2 + \sigma_y^2 \tag{A 9b}$$

(b) uniform (rectangular) distribution

$$p_1(x) = \begin{cases} \dfrac{1}{2\Delta_x} \text{ at } x_0 - \Delta x < x < x_0 + \Delta_x \\ 0 \quad \text{at} \begin{cases} x < x_0 - \Delta_x \\ x > x_0 + \Delta_x \end{cases} \end{cases}$$

$$p_1(y) = \begin{cases} \dfrac{1}{2\Delta_y} \text{ at } y_0 - \Delta_y < y < y_0 + \Delta_y \\ 0 \quad \text{at} \begin{cases} y < y_0 - \Delta_y \\ y > y_0 + \Delta_y \end{cases} \end{cases}$$

$$p_1(z) = \begin{cases} 0 \qquad\qquad \text{at } z < z_0 - \Delta_z \\ \dfrac{1}{\Delta_z^2}(z - z_0 + \Delta_z) \text{ at } z_0 - \Delta_z < z < z_0 \\ \dfrac{1}{\Delta_z^2}(z_0 + \Delta_z - z) \text{ at } z_0 < z < z_0 + \Delta_z \\ 0 \qquad\qquad \text{at } z > z_0 + \Delta_z \end{cases} \tag{A 10a}$$

where $z_0 = x_0 \pm y_0$, $\Delta_z = \Delta_x + \Delta_y$.

The distribution of the sum (difference) of two interdependent signals with a normal distribution law (A 9a) is also normal.

The mathematical expectation of the function $x(t_1)$ ***(the original first-order moment)***

$$m_x(t_1) = \ddot{x}(t_1) = M\{x(t_1)\} = \int_{-\infty}^{\infty} x_1 p_1(x_1, t_1)\, dx_1 \tag{A 16}$$

A centred signal is

$$\mathring{x}(t_1) = x(t_1) - m_x(t_1) \tag{A 16a}$$

For the distribution laws (A 9), (A 10), (A 13), (A 14)

$$m_x(t_1) = x_0$$

The average value of the squared function $x(t)$ ***(the original second-order moment)***

$$\dddot{x}^2(t_1) = [\ddot{x}(t_1)]^2 = M\{x^2(t_1)\} = \int_{-\infty}^{\infty} x_1^2 p_1(x_1, t_1)\, dx_1 \tag{A 17}$$

For stationary random processes $\ddot{x}$ and $\dddot{x}^2$ are independent of time.

Dispersion (central second-order moment)

$$(\mathring{x})^2 = \sigma_x^2 = D\{x(t)\} = M\{[x(t) - M\{x(t)\}]^2\} = M\{\mathring{x}(t)\} \tag{A 18}$$

at $m_x = M\{x(t)\} = 0$

$$\sigma_x^2 = D\{x(t)\} = M\{x^2(t)\} \tag{A 19}$$

at $m_x \neq 0$

$$\sigma_x^2 = \overline{x^2} - (\overline{x})^2 = M\{x^2(t)\} - m_x^2$$

For a normal distribution $\sigma_x^2 = D\{x\}$ and $m_x = x_0$

$$\overline{x^2} = \sigma_x^2 + m_x^2$$

The central nth-order moment is

$$(\mathring{x})^n = (\overline{x - \overline{x}})^n = M\{(x - \overline{x})^n\} = \int_{-\infty}^{\infty} (x - x)^n p_1(x)\, dx \tag{A 20}$$

Time average value. On a finite interval $2T$

$$\overline{x}_T = \frac{1}{2T} \int_{-T}^{T} x(t)\, dt \tag{A 21}$$

On an infinite interval

$$\overline{x} = \lim_{T \to \infty} \int_{-T}^{T} x(t)\, dt \tag{A 22}$$

The average signal power is

$$\overline{x^2(t)} = \lim_{T \to \infty} \frac{1}{2T} \int_{-T}^{T} x^2(t)\, dt \tag{A 23}$$

The time average value of the product of two functions is

$$\overline{x(t)\, y(t+\tau)} = \lim_{T \to \infty} \int_{-T}^{T} x(t)\, y(t+\tau)\, dt \tag{A 24}$$

In *ergodic* processes the set average value is equal to the time average value

$$\overline{x} = \overline{x} = M\{x(t)\} = m_x = x_0$$

or

$$\int_{-\infty}^{\infty} x_1 p_1(x_1)\, dx_1 = \lim_{T \to \infty} \frac{1}{2T} \int_{-T}^{T} x(t)\, dt \tag{A 25}$$

For ergodic processes one sample of the process on the interval $T \to \infty$ is equivalent to the entire set of the process samples.

For ergodic processes

$$[\overline{x^2(t)}] = M\{x^2(t)\} = \overline{x}^2 \tag{A 26}$$

or

$$\int_{-\infty}^{\infty} x^2 p_1(x)\,dx = \lim_{T\to\infty} \frac{1}{2T} \int_{-T}^{T} x^2(t)\,dt$$

and

$$\overline{x(t)\,y(t+\tau)} = M\{x(t)\,y(t+\tau)\} = \overline{x(t)\,y(t+\tau)}$$

or

$$\int_{-\infty}^{\infty}\int_{-\infty}^{\infty} x_1 y_2 p_2(x_1, y_2, \tau)\,dx_1\,dy_2 = \lim_{T\to\infty} \frac{1}{2T} \int_{-T}^{T} x(t)\,y(t+\tau)\,dt \quad (A\text{-}27)$$

Random signal correlation functions. Correlation functions expressing the relation of random signals at different times

$$K_{xy}(t_1, t_2) = M\{x(t_1)\,y(t_2)\} = \int_{-\infty}^{\infty}\int_{-\infty}^{\infty} x_1 y_2 p_2(x_1, t_1; y_2, t_2)\,dx_1\,dy_2 \quad (A\ 28)$$

are termed *cross-correlation functions of the signals* x and y and express the relation between the signal x at time t_1 and the signal y at time t_2.

If $x(t)$ and $y(t)$ are stationary dependent (see (A 8)), K_{xy} depends only on τ

$$K_{xy}(\tau) = M\{x(t_1)\,y(t_1+\tau)\} = \int_{-\infty}^{\infty}\int_{-\infty}^{\infty} x_1 y_2 p_2(x_1, y_2, \tau)\,dx_1\,dy_2 \quad (A\ 29)$$

The centred correlation function $\mathring{K}_{xy}(t_1, t_2)$ is the mathematical expectation of the product of the centred signals $\mathring{x}(t_1)$ and $\mathring{y}(t_2)$

$$\mathring{K}_{xy}(t_1, t_2)\,M\{\mathring{x}(t_1)\,\mathring{y}(t_2)\} = M\{[x(t_1) - m_x(t_1)]\,[y(t_1) - m_y(t_2)]\} =$$

$$= \int_{-\infty}^{\infty}\int_{-\infty}^{\infty} (x_1 - m_{x_1})(y_2 - m_{y_2})\,p_2(x_1, t_1; y_2, t_2)\,dx_1\,dy_2 \quad (A\ 28a)$$

For stationary dependent signals

$$\mathring{K}_{xy}(\tau) = M\{\mathring{x}(t_1)\,\mathring{y}(t_1+\tau)\} \quad (A\ 29a)$$

The time correlation function for stationary dependent signals $x(t)$ and $y(t)$ is

$$R_{xy}(\tau) = \lim_{T\to\infty} \frac{1}{2T} \int_{-T}^{T} x(t)\,y(t+\tau)\,dt = R_{yx}(-\tau) \quad (A\ 30)$$

The centred time correlation function is

$$\mathring{R}_{xy}(\tau) = \lim_{T\to\infty} \frac{1}{2T} \int_{-T}^{T} [x(t) - \overline{x}]\,[y(t+\tau) - \overline{y}]\,dt \quad (A\ 30a)$$

For ergodic processes

$$R_{xy}(\tau) = K_{xy}(\tau)$$

$$\mathring{R}_{xy}(\tau) = \mathring{K}_{xy}(\tau)$$

If $x(t) = y(t)$, then the correlation function is known as the *auto-correlation function* [$K_{xx}(\tau)$ or $K_x(\tau)$; $R_{xx}(\tau)$ or $R_x(\tau)$].

A normalized auto-correlation function is

$$\rho_x(t_1, t_2) = \frac{K_x(t_1, t_2)}{\sqrt{K_x(t_1, t_1)\, K_x(t_2, t_2)}} = \frac{K_x(t_1, t_2)}{\sqrt{M\{x^2(t_1)\}\, M\{x^2(t_2)\}}} \quad \text{(A 31)}$$

For stationary random processes

$$\rho_x(\tau) = \frac{K_x(\tau)}{K_x(0)} \quad \text{(A 32)}$$

A normalized cross-correlation function is

$$\rho_{xy}(t_1, t_2) = \frac{K_{xy}(t_1, t_2)}{\sqrt{K_x(t_1, t_1)\, K_y(t_2, t_2)}} \quad \text{(A 33)}$$

For stationary random processes

$$\rho_{xy}(\tau) = \frac{K_{xy}(\tau)}{\sqrt{K_x(0)\, K_y(0)}} \quad \text{(A 34)}$$

Properties of correlation functions

1. $K_x(t_1, t_2) = K_x(t_2, t_1)$ (A 35)
2. Evenness of the characteristic $K_x(\tau) = K_x(-\tau)$ (A 36)
3. $\rho_x(t_1, t_2) \leqslant 1$; $\rho_{xy}(t_1, t_2) \leqslant 1$ (A 37)
4. For stationary random ergodic processes $K_x(0) = R_x(0) = \overline{x^2} = \ddot{\bar{x}}^2$ (A 38)
5. $\ddot{\bar{x}} = \bar{x} = \sqrt{R_x(\infty)} = \sqrt{K_x(\infty)}$ (A 39)
6. $D\{x\} = \overline{\dot{x}^2} - (\dot{\bar{x}})^2 = R_x(0) - R_x(\infty)$ (A 40)

Spectral density of random signals. *The spectral density* is a Fourier transform of the correlation function

$$S_x(\omega) = \int_{-\infty}^{\infty} R_x(\tau)\, e^{-j\omega\tau}\, d\tau \quad \text{(A 41)}$$

The inverse transform is

$$R_x(\tau) = \frac{1}{2\pi} \int_{-\infty}^{\infty} S_x(\omega)\, e^{j\omega\tau}\, d\omega \quad \text{(A 42)}$$

where $S_x(\omega)$ is a real even function of ω.

The r.m.s. value of $x(t)$ in time is

$$\overline{x^2(t)} = \lim_{T\to\infty} \frac{1}{2T} \int_{-T}^{T} x^2(t)\, dt = R_x(0) =$$

$$= \frac{1}{2\pi} \int_{-\infty}^{\infty} S_x(\omega)\, d\omega = \frac{1}{\pi} \int_{0}^{\infty} S_x(\omega)\, d\omega \quad \text{(A 43)}$$

The spectral density expresses the partial power of the signal $\frac{1}{\pi} S_x \, d\omega$.

The *cross spectral density* is a Fourier transform of the cross-correlation function

$$S_{xy}(j\omega) = \int_{-\infty}^{\infty} R_{xy}(\tau) \, e^{-j\omega\tau} \, d\tau \tag{A 44}$$

The inverse transform is

$$R_{xy}(\tau) = \frac{1}{2\pi} \int_{-\infty}^{\infty} S_{xy}(j\omega) \, e^{j\omega\tau} \, d\omega \tag{A 45}$$

$S_{xy}(j\omega)$ and $R_{xy}(\tau)$ may be odd functions of ω and τ; in contrast to $S_x(\omega)$, $S_{xy}(j\omega)$ can contain an imaginary part. This is reflected in the notation of the argument $(j\omega)$.

For the signals x and y

$$\overline{x(t)\, y(t)} = \lim_{T\to\infty} \frac{1}{2T} \int_{-T}^{T} x(t)\, y(t)\, dt = R_{xy}(0) = \frac{1}{2\pi} \int_{-\infty}^{\infty} S_{xy}(j\omega)\, d\omega \tag{A 43a}$$

The spectral density can be expressed in terms of the frequency spectrum of the signal $X_T(j\omega)$.

Knowing samples of the signal $x(t)$ on the interval $2T$ and of their frequency spectra $X_T(j\omega)$, we get

$$S_x(\omega) = \lim_{T\to\infty} \frac{1}{2T} M\{|X_T(j\omega)|^2\} \tag{A 46}$$

where

$$X_T(j\omega) = \int_{-T}^{T} x(t)\, e^{-j\omega t}\, dt \tag{A 47}$$

is the frequency spectrum of each component of the sample set. From Eq. (A 46) $S_x(\omega)$ is never negative.

For two signals, $x(t)$ and $y(t)$, the cross spectral density is expressed in terms of $X_T(j\omega)$ and $Y_T(j\omega)$ as follows

$$S_{xy}(j\omega) = \lim_{T\to\infty} \frac{1}{2T} M\{X_T(-j\omega)\, Y_T(j\omega)\} = S_{yx}(-j\omega) \tag{A 48}$$

Examples of correlation functions and spectral densities of deterministic and random signals are given in Table A 1.

$K_x(\tau) = R_x(\tau)$		
	Formula	**Plot**
1	a^2	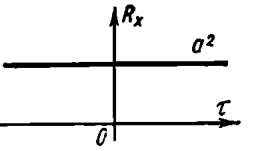
2	$a^2 \cos \omega_0 \tau$	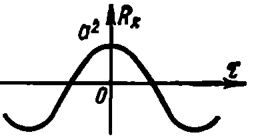
3	$a^2 \begin{cases} 1 - \left\lvert \frac{\tau}{T_0} \right\rvert, & \lvert\tau\rvert < T_0 \\ 0, & \lvert\tau\rvert > T_0 \end{cases}$	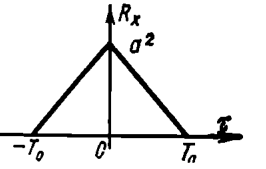
4	$a^2 \begin{cases} 1, & \lvert\tau\rvert < T_0 \\ 0, & \lvert\tau\rvert > T_0 \end{cases}$	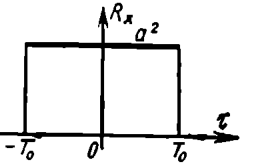
5	$a^2 \delta(\tau)$	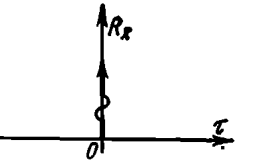

Table A1

$S_x(\omega)$

Formula	Plot
$2\pi a^2\delta(\omega)$	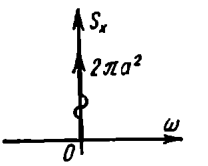
$\frac{\pi a^2}{2}[\delta(\omega+\omega_0)+\delta(\omega-\omega_0)]$	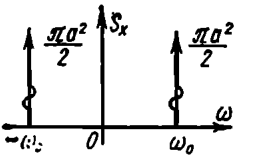
$a^2T_0\left(\frac{\sin\frac{\omega T_0}{2}}{\frac{\omega T_0}{2}}\right)^2$	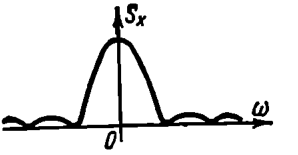
$2T_0a^2\left(\frac{\sin\omega T_0}{\omega T_0}\right)$	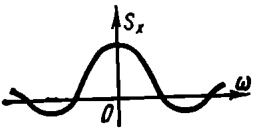
a^2	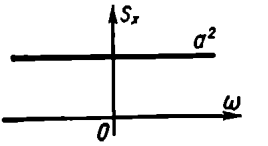

$K_x(\tau) = R_x(\tau)$		
	Formula	**Plot**
6	$\frac{a^2}{N}\sum_{k=-\infty}^{\infty}\left(\frac{\sin\frac{\pi k}{N}}{\frac{\pi k}{N}}\right)\cos\omega_s(\tau)$, $\omega_s=\frac{2\pi}{NT_0}$	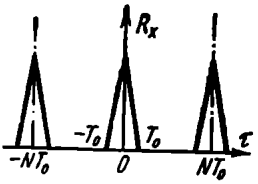
7	$a^2e^{-\alpha\lvert\tau\rvert}$	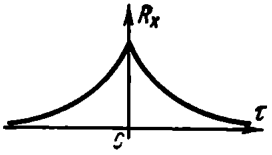
8	$\alpha^2e^{-\alpha\lvert\tau\rvert}\cos\beta\tau$	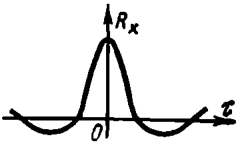
9	$a^2e^{-\alpha\lvert\tau\rvert}\sin\beta\lvert\tau\rvert$	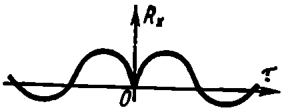
10	$\frac{S_0\omega_0}{\pi}\left(\frac{\sin\omega_0\tau}{\omega_0\tau}\right)$	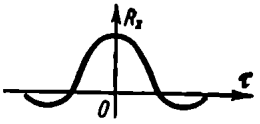

Note. The correlation functions and spectral densities of items 4 and 9 denote com form 3, 5, 7, 8, etc. For the resultant signal $S_x(\omega)$ is always greater than zero.

Table A1 (cont'd)

$S_x(\omega)$

Formula	Plot
$\frac{\pi a^2}{N}\left\{\left(\frac{\sin\frac{\omega T_0}{2}}{\frac{\omega T_0}{2}}\right)^2 1^*\omega+\delta(\omega)\right\}$ $1^*(\omega)=\sum_{k=-\infty}^{\infty}\delta(\omega-k\omega_s)$	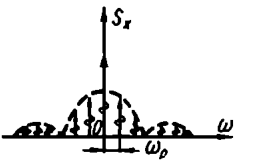
$\frac{2\alpha a^2}{\alpha^2+\omega^2}$	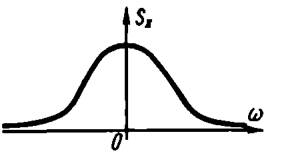
$\frac{\alpha a^2}{\alpha^2+(\beta-\omega)^2}+\frac{\alpha a^2}{\alpha^2+(\beta+\omega)^2}$	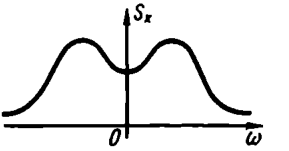
$\frac{a^2(\beta+\omega)}{a^2+(\beta+\omega)^2}+\frac{a^2(\beta-\omega)}{a^2+(\beta-\omega)^2}$	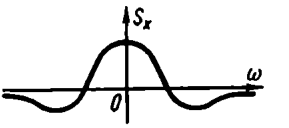
$S_0, \quad \lvert\omega\rvert\leqslant\omega_0$ $0, \quad \lvert\omega\rvert<\omega_0$	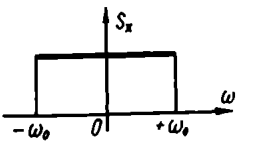

ponents of these functions and are found only as addends together with functions of the

Table A2. ***h*-Functions**

	0.00	0.05	0.10	0.15	0.20	0.25	0.30	0.35	0.40	0.45
0.0	0.000	0.000	0.000	0.000	0.000	0.000	0.000	0.000	0.000	0.000
0.5	0.138	0.165	0.176	0.184	0.192	0.199	0.207	0.215	0.223	0.231
1.0	0.310	0.325	0.340	0.356	0.371	0.386	0.402	0.417	0.432	0.447
1.5	0.449	0.469	0.494	0.516	0.538	0.560	0.594	0.603	0.617	0.646
2.0	0.571	0.560	0.628	0.655	0.682	0.709	0.732	0.761	0.785	0.810
2.5	0.674	0.707	0.739	0.771	0.802	0.833	0.862	0.891	0.917	0.943
3.0	0.755	0.792	0.828	0.863	0.895	0.928	0.958	0.986	1.013	1.038
3.5	0.815	0.853	0.892	0.928	0.963	0.994	1.024	1.050	1.074	1.095
4.0	0.856	0.898	0.937	0.974	1.008	1.039	1.066	1.090	1.110	1.127
4.5	0.883	0.923	0.960	0.998	1.029	1.057	1.084	1.104	1.120	1.129
5.0	0.895	0.939	0.977	1.012	1.042	1.067	1.087	1.102	1.112	1.117
5.5	0.900	0.940	0.986	1.015	1.042	1.063	1.079	1.088	1.092	1.096
6.0	0.903	0.945	0.981	1.013	1.037	1.054	1.065	1.070	1.068	1.062
6.5	0.904	0.943	0.980	1.009	1.029	1.043	1.050	1.049	1.043	1.033
7.0	0.904	0.945	0.978	1.006	1.024	1.034	1.037	1.033	1.023	1.009
7.5	0.907	0.945	0.980	1.005	1.021	1.027	1.027	1.020	1.005	0.989
8.0	0.911	0.951	0.983	1.007	1.020	1.024	1.021	1.011	0.998	0.982
8.5	0.918	0.956	0.989	1.010	1.021	1.024	1.018	1.007	0.993	0.978
9.0	0.925	0.966	0.996	1.016	1.025	1.025	1.017	1.006	0.992	0.978
9.5	0.932	0.972	1,004	1.020	1.028	1.026	1.018	1.006	0.993	0.982
10.0	0.939	0.980	1.009	1.025	1.030	1.027	1.018	1.005	0.994	0.985
10.5	0.946	0.985	1.013	1.028	1.031	1.026	1.016	1.004	0.994	0.989
11.0	0.947	0.988	1.015	1.028	1.030	1.024	1.013	1.002	0.993	0.990
11.5	0.949	0.988	1.016	1.027	1.028	1.021	1.010	0.998	0.991	0.991
12.0	0.950	0.990	1.015	1.025	1.024	1.015	1.004	0.994	0.988	0.990
12.5	0.950	0.989	1.013	1.022	1.019	1.010	0.998	0.990	0.986	0.989
13.0	0.950	0.989	1.012	1.019	1.015	1.004	0.993	0.986	0.984	0.989
13.5	0.950	0.990	1.011	1.016	1.011	1.000	0.990	0.983	0.984	0.989
14.0	0.951	0.990	1.010	1.015	1.008	0.997	0.987	0.983	0.985	0.991
14.5	0.954	0.990	1.011	1.014	1.008	0.996	0.986	0.984	0.987	0.994
15.0	0.956	0.993	1.012	1.014	1.006	0.995	0.987	0.986	0.991	0.998
15.5	0.959	0.995	1.013	1.014	1.006	0.995	0.989	0.989	0.995	1.002
16.0	0.961	0.998	1.015	1.014	1.006	0.995	0.990	0.992	0.999	1.007
16.5	0.964	0.999	1.016	1.015	1.005	0.996	0.992	0.995	1.002	1.009
17.0	0.965	1.001	1.016	1.014	1.005	0.996	0.993	0.998	1.005	1.011
17.5	0.966	1.002	1.016	1.013	1.003	0.995	0.994	0.999	1.007	1.011
18.0	0.966	1.002	1.015	1.012	1.002	0.994	0.994	1.000	1.007	1.010
18.5	0.966	1.001	1.014	1.010	1.000	0.993	0.994	1.001	1.007	1.009
19.0	0.966	1.002	1.013	1.008	0.998	0.992	0.994	1.001	1.006	1.006
19.5	0.967	1.001	1.012	1.006	0.996	0.991	0.994	1.001	1.005	1.004
20.0	0.967	1.001	1.011	1.004	0.995	0.991	0.994	1.001	1.004	1.001
20.5	0.968	1.002	1.010	1.003	0.994	0.991	0.995	1.001	1.003	1.000
21.0	0.968	1.002	1.010	1.003	0.994	0.991	0.996	1.002	1.003	0.999
21.5	0.969	1.003	1.010	1.002	0.994	0.992	0.999	1.004	1.003	0.998
22.0	0.971	1.004	1.011	1.002	0.994	0.994	1.000	1.005	1.004	0.998
22.5	0.973	1.005	1.011	1.002	0.995	0.995	1.002	1.006	1.004	0.998
23.0	0.973	1.006	1.011	1.002	0.995	0.997	1.003	1.006	1.004	0.998
23.5	0.975	1.006	1.011	1.002	0.995	0.998	1.004	1.006	1.003	0.998
24.0	0.975	1.006	1.010	1.001	0.995	0.998	1.005	1.006	1.002	0.998
24.5	0.975	1.006	1.009	1.000	0.995	0.999	1.005	1.005	1.000	0.997
25.0	0.975	1.006	1.008	0.999	0.995	0.999	1.004	1.004	0.999	0.996
25.5	0.975	1.006	1.007	0.998	0.994	0.999	1.004	1.002	0.997	0.996
26.0	0.975	1.006	1.006	0.997	0.994	0.999	1.003	1.001	0.996	0.996

r Trapezia (Ref. 76)

.50	0.55	0.60	0.65	0.70	0.75	0.80	0.85	0.90	0.95	1.00
.000	0.000	0.000	0.000	0.000	0.000	0.000	0.000	0.000	0.000	0.000
.240	0.248	0.255	0.259	0.267	0.275	0.282	0.290	0.297	0.304	0.314
.461	0.476	0.490	0.505	0.519	0.534	0.547	0.561	0.575	0.590	0.602
.665	0.685	0.706	0.722	0.740	0.758	0.776	0.794	0.813	0.832	0.844
.831	0.856	0.878	0.899	0.919	0.938	0.957	0.974	0.991	1.008	1.022
.967	0.995	1.010	1.030	1.050	1.067	1.084	1.090	1.105	1.120	1.133
.061	1.081	1.100	1.116	1.131	1.143	1.154	1.162	1.169	1.175	1.177
.115	1.132	1.145	1.158	1.165	1.170	1.174	1.174	1.175	1.176	1.175
.141	1.151	1.158	1.162	1.163	1.161	1.156	1.150	1.141	1.132	1.119
.138	1.141	1.141	1.138	1.132	1.127	1.111	1.099	1.085	1.071	1.053
.117	1.114	1.107	1.097	1.084	1.069	1.053	1.036	1.019	1.003	0.987
.090	1.076	1.064	1.050	1.032	1.016	0.994	0.979	0.962	0.951	0.932
.051	1.036	1.020	1.001	0.984	0.956	0.949	0.934	0.922	0.914	0.907
.018	1.001	0.982	0.965	0.948	0.936	0.920	0.910	0.906	0.904	0.905
.992	0.975	0.957	0.941	0.927	0.917	0.911	0.909	0.911	0.917	0.926
.974	0.956	0.944	0.931	0.922	0.919	0.920	0.927	0.934	0.946	0.962
.966	0.952	0.941	0.934	0.932	0.936	0.944	0.955	0.970	0.986	1.002
.964	0.954	0.948	0.948	0.951	0.958	0.974	0.990	1.006	1.023	1.041
.968	0.962	0.961	0.967	0.976	0.990	1.006	1.023	1.038	1.051	1.060
.975	0.972	0.977	0.987	1.000	1.015	1.033	1.048	1.059	1.065	1.066
.982	0.984	0.993	1.006	1.020	1.036	1.049	1.059	1.063	1.062	1.056
.988	0.994	1.005	1.019	1.033	1.046	1.054	1.058	1.055	1.048	1.033
.993	1.001	1.014	1.027	1.039	1.047	1.048	1.044	1.034	1.021	1.005
.996	1.006	1.017	1.029	1.037	1.039	1.034	1.024	1.010	0.994	0.977
.997	1.007	1.018	1.026	1.029	1.025	1.015	1.000	0.984	0.970	0.958
.997	1.007	1.015	1.019	1.017	1.010	0.995	0.980	0.965	0.955	0.950
.997	1.006	1.012	1.012	1.005	0.993	0.980	0.965	0.955	0.952	0.955
.998	1.005	1.008	1.004	0.995	0.982	0.968	0.958	0.954	0.958	0.970
.999	1.005	1.005	0.998	0.987	0.975	0.965	0.961	0.965	0.976	0.991
.002	1.005	1.003	0.994	0.983	0.970	0.969	0.971	0.981	0.997	1.010
.005	1.006	1.002	0.994	0.983	0.977	0.978	0.987	1.001	1.018	1.032
.008	1.007	1.001	0.992	0.985	0.984	0.991	1.003	1.019	1.032	1.048
.010	1.008	1.001	0.994	0.990	0.993	1.003	1.018	1.031	1.040	1.039
.011	1.008	1.001	0.995	0.995	1.001	1.014	1.027	1.035	1.037	1.028
.012	1.007	1.000	0.996	0.999	1.008	1.020	1.030	1.032	1.026	1.012
.009	1.005	0.998	0.997	1.002	1.012	1.023	1.027	1.023	1.013	0.994
.008	1.001	0.997	0.997	1.004	1.014	1.020	1.018	1.008	0.993	0.978
.005	0.999	0.995	0.997	1.005	1.012	1.014	1.007	0.993	0.978	0.969
.001	0.995	0.993	0.997	1.004	1.009	1.006	0.995	0.981	0.970	0.967
.998	0.992	0.992	0.997	1.003	1.005	0.998	0.985	0.973	0.967	0.973
.995	0.991	0.992	0.998	1.003	1.001	0.991	0.980	0.972	0.975	0.986
.994	0.991	0.994	0.999	1.002	0.998	0.987	0.978	0.977	0.990	1.001
.993	0.992	0.996	1.001	1.002	0.996	0.987	0.982	0.989	1.001	1.015
.994	0.995	0.999	0.995	1.002	0.995	0.988	0.988	0.998	1.013	1.025
.995	0.997	1.000	1.004	1.002	0.995	0.991	0.997	1.010	1.024	1.029
.996	1.000	1.005	1.005	1.002	0.996	0.996	1.006	1.018	1.028	1.028
.997	1.002	1.007	1.007	1.002	0.997	1.001	1.011	1.022	1.025	1.016
.998	1.003	1.008	1.006	1.001	0.998	1.004	1.015	1.021	1.016	1.002
.999	1.004	1.007	1.004	1.999	0.999	1.007	1.015	1.016	1.006	0.990
.000	1.004	1.006	1.002	0.998	0.999	1.007	1.012	1.007	0.995	0.979
.000	1.004	1.004	0.999	0.996	1.000	1.007	1.008	0.998	0.984	0.975
.000	1.003	1.002	0.997	0.995	1.000	1.005	1.001	0.989	0.978	0.977
.000	1.002	0.999	0.995	0.995	1.000	1.002	0.997	0.984	0.978	0.983

Table A3. **Values of the Integral J_0 for n from 1 through 6 (Ref. 57)**

$$J_0 = \frac{1}{2\pi j} \int_{-j\infty}^{j\infty} \frac{b(p)\, b(-p)}{c(p)\, c(-p)}\, dp$$

where

$$b(p) = b_{n-1}p^{n-1} + \ldots + b_0$$
$$c(p) = c_n p^n + \ldots + c_0$$

For

$$n=1 \quad J_0 = \frac{b_0^2}{2c_0c_1}$$

$$n=2 \quad J_0 = \frac{b_1^2c_0 + b_0^2c_2}{2c_0c_1c_2}$$

$$n=3 \quad J_0 = \frac{b_2^2c_0c_1 + (b_1^2 - 2b_0b_2)\, c_0c_3 + b_0^2c_2c_3}{2c_0c_3\,(-c_0c_3 + c_1c_2)}$$

$$n=4 \quad J_0 = \frac{b_3^2\,(-c_0^2c_3 + c_0c_1c_2) + (b_2^2 - 2b_1b_3)\, c_0c_1c_4 + (b_1^2 - 2b_0b_2)\, c_0c_3c_4}{2c_0c_4\,(-c_0c_3^2 - c_1^2c_4 + c_1c_2c_3)} +$$
$$+ \frac{b_0^2\,(-c_1c_4^2 + c_2c_3c_4)}{2c_0c_4\,(-c_0c_3^2 - c_1^2c_4 + c_1c_2c_3)}$$

$$n=5 \quad J_0 = \frac{1}{2\Delta_5}\,[b_4^2m_0 + (b_3^2 - 2b_2b_4)\, m_1 +$$
$$+ (b_2^2 - 2b_1b_3 + 2b_0b_4)\, m_2 + b_1^2 - 2b_0b_2)\, m_3 + b_0^2m_4]$$

where

$$m_0 = \frac{1}{c_5}\,(c_3n_1 - c_1m_2) \qquad m_3 = \frac{1}{c_0}\,(c_2m_2 - c_4m_0)$$

$$m_1 = -c_0c_3 + c_1c_2 \qquad m_4 = \frac{1}{c_0}\,(c_2m_3 - c_4m_2)$$

$$m_2 = -c_0c_5 + c_1c_4 \qquad \Delta_5 = c_0\,(c_1m_4 - c_3m_3 + c_5m_2)$$

$$n=6 \quad J_0 = \frac{1}{2\Delta_6}\,[b_5^2m_0 + (b_4^2 - 2b_3b_5)\, m_1 + (b_3^2 - 2b_2b_4 + 2b_1b_5)\, m_2 +$$
$$+ (b_2^2 - 2b_1b_3 + 2b_0b_4)\, m_3 + (b_1^2 - 2b_0b_2)\, m_4 + b_0^2m_5]$$

where

$$m_0 = \frac{1}{c_6}\,(c_4n_1 - c_2m_2 + c_0m_3)$$
$$m_1 = -c_0c_1c_5 + c_0c_3^2 + c_1^2c_4 - c_1c_2c_3$$
$$m_2 = c_0c_3c_5 + c_1^2c_6 - c_1c_2c_5$$
$$m_3 = c_0c_5^2 + c_1c_3c_6 - c_1c_4c_5$$
$$m_4 = \frac{1}{c_0}\,(c_2m_3 - c_4m_2 + c_6m_1)$$
$$m_5 = \frac{1}{c_0}\,(c_2m_4 - c_4m_3 + c_6m_2)$$
$$\Delta_6 = c_0\,(c_1m_5 - c_3m_4 + c_5m_3)$$

REFERENCES

1. *Aizerman M. Theory of Automatic Control.* Addison-Wesley, 1963.
2. *Aizerman M., Gantmacher F. Absolute Stability of Regulator Systems.* Holden-Day, 1964.
3. *Andronov A. A. Sobrantye trudov* (Collected works). USSR Academy of Sciences, 1956.
4. *Andronov A. A., Witt A. A., Chaikin C. Theory of Oscillations.* Princeton University Press, 1949.
5. *Avtomatizatsiya proizvodstva i promyshlennaya elektronika* (Industrial automation and electronics). Berg A. I. and Trapeznikov V. A. eds. Entsiklopediya, Moscow, 1962-65.
6. *Bellman R. Dynamic Programming.* (Princeton University Press, Princeton, N.J.), 1967.
7. *Bellman R. Introduction to the Mathematical Theory of Control Processes.* Academic Press, 1967.
8. *Beneš, Jiri. Statistical Dynamics of Automatic Control Systems.* Iliffe Books Ltd., London, 1967.
9. *Bessekersky V. A. et al. Proyectirovaniye sistem maloy moshchnosti* (Design of low-capacity servo systems). Sudpromgiz, 1958.
10. *Bessekersky V. A., Popov Ye. P. Teoriya sistem avtomaticheskogo regulirovaniya* (Theory of automatic control systems). Nauka, 1972.
11. *Bode H. W. Network Analysis and Feedback Amplifier Design.* New York, V. Nostrand, 1945.
12. *Boltyansky V. G. Matematicheskiye metody optimalnogo upravleniya* (Mathematical methods of optimal control). Nauka, 1969.
13. *Butenin N. V. Elements of the Theory of Nonlinear Oscillations.* Blaisdell, 1965.

13a. *Chalam V. V., Misra D. N. Stability Investigations of Control Systems with Stop-Type Nonlinearity.* "J. Inst. Eng. (India). Electron and Telecommun. Eng. Div.", 1972, 52, N7, 204-207.

14. *Chang S.S.L. Synthesis of Optimum Control Systems.* New York, McGraw-Hill, 1961.
15. *Chestnut H. and Mayer R. W. Servomechanisms and Regulating System Design.* New York, John Wiley and Sons, 1951, 1959.
16. *Chetaev N. G. The Stability of Motion.* Pergamon Press, 1961.
17. *Cooper G. R , McGillem C. D. Methods of Signal and System Analysis.* Holt, Rinehard and Winston, Inc., New York, Toronto, London, 1967.
18. *Csaki F., Korszerü. Szabályozáselmélet.* Akademial kiado, 1970.
19. *Cunningham W. J. Introduction to Nonlinear Analysis.* McGraw-Hill, New York, 1958.
20. *Emelyanov S. V. Sistemy avtomaticheskogo upravleniya s peremennoy strukturoy* (Variable-structure automatic control systems). Nauka, 1967.
21. *Fateyev A. V. Osnovy lineynoy teorii avtomaticheskogo regulirovaniya* (Fundamentals of the linear theory of control). Gosenergoizdat, 1959.
22. *Feldbaum A. A. Optimal Control Systems.* Academic Press, 1965.
23. *Feldbaum A. A. Vychislitelnyie ustroystva v avtomaticheskikh sistemakh* (Computing facilities in automatic systems). Fizmatgiz, 1959.

24. *Feldbaum A. A. et al. Teoreticheskiye osnovy svyazi i upravleniya* (Theoretical fundamentals of communication and control). Fizmatgiz, 1963.
24a. *Findeisen W. Technika Regulacji Automatyczneyj.* Warszava, 1965. PWN.
25. *Flügge-Lotz I. Discontinuous Automatic Control.* Princeton University Press, 1953 (McGraw-Hill), New York, 1968.
26. *Gibson J. E. Nonlinear Automatic Control.* McGraw-Hill, New York, 1963.
27. *Gille J. C., Pelegrin M., Decaulne P. Théorie et technique des asservissements.* Dunod, 1956.
28. *Goode H. H., Machol B. E. System Engineering.* McGraw-Hill, New York, 1957.
29. *Hsu J. C., Meyer A. V. Modern Control Principles and Applications.* New York (McGraw-Hill), 1968.
30. *James H. M., Nichols N. B. Phillips R. S. Theory of Servomechanisms.* McGraw-Hill, New York, 1947.
31. *Jury E. I. Sampled-Data Control Systems.* John Wiley and Sons, New York, 1958.
32. *Kaczorek T. Podstawy automatyki.* C.II. Warszawa, 1968.
33. *Kazakov I. Ye. Staticheskiye metody proyektirovaniya sistem upravleniya* (Statistical methods in design of control systems). Mashinostroyeniye, 1969.
34. *Krasovsky A. A. Dinamika nepreryvnykh samonastraivayushchikhsya sistem* (The dynamics of continuous self-adjusting systems). Fizmatgiz, 1963.
35. *Krasovsky N. N. Teoriya upravleniya dvizheniyem* (Theory of motion control). Nauka, 1968.
36. *Krasovsky A. A., Pospelov G. S. Osnovy avtomatiki i tekhnicheskoy kibernetiki* (Fundamentals of automation and control engineering). Gosenergoizdat, 1962.
37. *Kryloff N., Bogoluboff N. Introduction to Nonlinear Mechanics.* Princeton University Press, 1947.
38. *Kaljača K. Teorija automatske regulacije.* Zagreb, 1970.
39. *Laning J. H., Battin R. H. Random Processes in Automatic Control.* McGraw-Hill, New York, 1956.
40. *Lauer H. R. et al. Servomechanisms Fundamentals.* McGraw-Hill, New York, 1960.
41. *Lefschetz S. Stability of Nonlinear Control Systems.* Academic Press, 1965.
42. *Letov A. M. Stability in Nonlinear Control Systems.* Princeton University Press, 1961.
43. *Lur'e A. I. Some Nonlinear Problems in the Theory of Automatic Control.* Her Majesty's Stationary Office, London, 1957.
44. *Lyapunov A. M. Obshchaya zadacha ob ustoychivosti dvizheniya* (The general problem of motion stability). Kharkov, 1892. See also *Lyapunov A. M. Sobraniye sochineniy* (Collected works). Vol. 2. USSR Academy of Sciences Press, 1956.
45. *Maccol R. A. Fundamental Theory of Servomechanisms.* V. Nostrand, New York, 1945.
46. *Macmillan R. H., Higgins T. J., Naslin P. Progress in Control Engineering.* Heywood Scientific Book, 1966.
47. *Mandelshtam L. I. et al. Novyie issledovaniya v oblasti nelineynykh kolebaniy* (New studies in the field of nonlinear oscillations). Radioizdat, 1936.
48. *Meerov M. V. Introduction to the Dynamics of Automatic Regulating of Electrical Machines.* Butterworths, 1961.
49. *Meerov M. V. Sistemy mnogosvyaznogo regulirovaniya* (Multivariable control systems). Fizmatgiz, 1965.
50. *Metod Goldfarba v teorii regulirovaniya* (The Goldfarb method in control theory, a collection of articles). Gosenergoizdat, 1962.
51. *Metody optimizatsii avtomaticheskikh sistem* (Automatic system optimization methods, a colletion of articles in memory of A. A. Feldbaum). Energiya, 1972.

52. *Minorsky N. Theory of Nonlinear Control Systems.* McGraw-Hill, New York, 1969.
53. *Mirsky G. Ya. Apparaturnoye opredeleniye kharakteristik sluchaynykh protsessov* (Hardware for determination of random process responses). Energiya, 1967.
54. *Mishkin E., Braun L. Adaptive Control Systems.* McGraw-Hill, New York, 1961.
55. *Naplatanov N. Teoriya na avtomatichnoto regulirane* (Theory of automatic control). D.I. Tekhnika, Sofia, 1970.
56. *Naumov B. N. Teoriya nelineynykh avtomaticheskikh sistem* (Theory of nonlinear automatic systems). Nauka, 1972.
57. *Newton G. C., Gould L. A., Kaiser J. F. Analytical Design of Linear Feedback Controls.* John Wiley and Sons, New York, 1967.
58. *Oleinikov V. A. et al. Osnovy optimal'nogo i ekstremal'nogo upravleniya* (Fundamentals of optimal and extremal control). Higher School Publ. House, 1969.
59. *Oppelt W. Kleines Handbuck technischer Regelvorgänge.* Verlag Chemie, 1972.
60. *Pámyati A. A. Andronova.* (*Collection of articles in memory of A. A Andronov*). USSR Academy of Sciences Press, 1954.
61. *Pelegrin M. Calcul statistique des systèmes asservies.* Paris. 1953.
62. *Pervozvankij A. A. Random Processes in Nonlinear Control Systems.* Academic Press, 1965.
63. *Petrov Yu. P. Variatsionnyie metody teorii optimal'nogo upravleniya* (Variational methods of optimal control theory). Energiya, 1965.
64. *Petrov B. N., Rutkovsky V. Yu. et al. Printsipy postroyeniya i proyektirovaniya samonastraivayushchikhsya sistem upravleniya* (Principles of self-adjusting control systems construction and design). Mashinostroyeniye, 1972.
65. *Polivanov K. M. Teoreticheskiye osnovy elektrotekhniki* (Theoretical fundamentals of electrical engineering). Energiya, 1965, 1972.
66. *Pontryagin L., Boltyansky V., Gamkrelidze R., Misczenko E. The Mathematical Theory of Optimal Processes.* John Wiley and Sons, 1962.
67. *Popov E. The Dynamics of Automatic Control Systems.* Addison-Wesley, 1962.
68. *Popov Ye. P., Pal'tov I. P. Priblizhonnyie metody issledovaniya nelineynykh avtomaticheskikh sistem* (Approximate methods of investigating nonlinear automatic systems). Fizmatgiz, 1960.
69. *Popov Ye. P., Nelepin R. A., Topcheev Yu. I. et al. eds. Nelineynyie sistemy avtomaticheskogo upravleniya* (Nonlinear systems of automatic control). In six volumes. Mashinostroyeniye, 1970-1971.
70. *Pugachev V. S. ed. Osnovy avtomaticheskogo upravleniya* (Fundamentals of automatic control). Fizmatgiz, 1963.
71. *Pugachev V. S. Teoriya sluchaynykh funktsiy i yeyo primeneniye k zadacham avtomaticheskogo upravleniya* (Theory of random functions and its application to control problems). Fizmatgiz, 1960.
72. *Rastrigin L. A. Sluchaynyi potsk* (Random search). Zinante, 1965.
73. *Rotach V. Ya. Impul'snyie sistemy avtomaticheskogo regulirovaniya* (Sampled-data systems of automatic control). Energiya, 1964.
74. *Shatalov A. S. Strukturnyie metody v teorii upravleniya i elektroavtomatike* (Structural methods in theory of control and electrical automation). Gosenergoizdat, 1962.
75. *Solodovnikov V. V. Introduction to the Statistical Dynamics of Automatic Control Systems.* Dover, 1960.
76. *Solodovnikov V. V. ed. Tekhnicheskaya kibernetika. Teoriya avtomaticheskogo regulirovaniya* (Control engineering. Automatic control theory). Books 1-3. Mashinostroyeniye, 1967-1969.
77. *Strejc V., Salamon M., Kotek Z., Balda M. Zaklady teorie samocinni regulace.* Technike Literatury, Praha, 1958.

78. *Thaler G. F., Pastel M. P. Analysis and Design of Nonlinear Feedback Control Systems.* McGraw-Hill, New York, 1955.
79. *Truxal I. B. Automatic Control System Synthesis.* McGraw-Hill, New York, 1955.
80. *Tsypkin Ya. Z. Adaptatsiya, obucheniye i samoobucheniye v avtomaticheskikh sistemakh* (Adaptation, teaching and learning in automatic systems). Nauka, 1968.
81. *Tsypkin Ya. Z. Teoriya lineynykh impul'snykh sistem* (Theory of linear sampled-data systems). Fizmatgiz, 1963.
82. *Tsypkin Ya. Z. Teoriya releynykh sistem avtomaticheskogo regulirovaniya* (Theory of relay control systems). Gostekhizdat, 1955.
83. *Uderman E. G. Metod kornevogo godografa v teorii avtomaticheskikh sistem* (The root locus method in automatic control theory). Nauka, 1972.
84. *Vavilov A. A. Chastotnyie metody raschota nelineynykh sistem* (Frequency methods of nonlinear system calculation). Energiya, 1970.
85. *Ventsel Ye. S. Teoriya veroyatnostey* (The probability theory). Nauka, 1969.
86. *Virág L. Sza Bályozáselmélet.* Tankönyvkiado, Budapest, 1970.
87. *Voronov A. A. Osnovy teorii avtomaticheskogo upravleniya* (Fundamentals of automatic control theory). P.P. I-III. Energiya, 1965-1970.
88. *Wiener N. Nonlinear Problems in Random Theory.* John Wiley and Sons, 1958.
89. *Wilde D. J. Optimum-Seeking Methods.* Prentice-Hall, Inc., Englewood Cliffs, N. J., 1964.
90. *Yurevich E. I. Teoriya avtomaticheskogo upravleniya* (Theory of automatic control). Energiya, 1969.
91. *Zeveke G., Ionkins P., Netushil A., Strakhov S. Analysis of Electric Circuits.* Mir Publishers, Moscow, 1969.
92. *Zimmermann H. I., Masson S. I. Electronic Circuit Theory.* John Wiley and Sons, 1960.

SUBJECT INDEX

A

Accuracy 31, 39, 189, 191, 194, 203
  dynamic 188, 197, 198
  static 191
Action
  control 15ff, 127, 189, 202
  controlled 124
  external 15ff, 123, 126, 129
  step 263
  trial 707, 747
  unobservable 21, 32
Actuating motor 263, 266
Actuator 35, 36, 38, 121, 126
Adaptation 14
Adder 28, 35, 130, 132, 392
Amplifier 35, 122
  operational 118, 119, 265, 372, 400, 451
  saturated 346
Astatic order 204, 206, 207, 245
Asymptotes 73, 104, 105

B

Bellman equation 653

C

Characteristic equation 62, 85, 92, 99ff
Characteristic polynomial 151, 153, 155, 310
Comparator 35, 40, 123, 127, 266, 575
  digital 349
Compensating loop 38, 127
Compensating circuit 40, 225
Compensation
  cascade (series) 241, 246
  disturbance 39, 243
  nonlinear 345
  parallel 241, 242, 243, 251, 254
Compensator 241
"Complement at infinity" 159, 160, 165
Component
  forced 62
  transient (or free) 62
Compounding 391
Conditions 553
  astatic 192
  boundary 26
  equidistance 386
  initial 26
  stability 142, 143f, 191, 206, 310, 315
  for stability 549
Connection
  feedback 115
  feedforward 112
  parallel 137
  parallel feedback 379, 387
  parallel feedforward 379, 385
  series 103f, 379, 380
Control 14
  automatic 30
  autonomous 136, 139
Optimal 591, 607, 618, 619, 645
  program 30, 31, 32
  proportional 32, 39
  dual 34
Control engineering 13
Controller 31f, 164, 183, 204
  differentiating 624
  extremal 33
  integrating 624
  level 36
  PI 624, 625
  proportional 624
Converter 130, 132, 133, 134
Criteria (Criterion)
  frequency 150
  of Hurwitz 145, 149, 169
  of Mikhailov 151, 169
  of Mikhailov and of Nyquist 143
  of Nyquist 143, 154, 155ff, 314, 556
  optimality 593, 601
  Popov 557, 558
  of Routh and of Hurwitz 143ff
  for sampled-data systems 307, 310, 313
  stability 143, 170, 307

Cycles
limit 471, 472, 535
stable limit 434
unstable limit 434

D

Damping coefficient 85
Damping ratio 81, 84, 218, 239, 420, 426, 447
Decade 48
Decibles 48
D-decomposition 170, 178, 179, 180, 181, 182, 495, 496
Delay 25, 100, 101ff
Delay time 25, 166, 168
Density
distribution 662, 727
spectral 662, 665ff
Diagram
functional 27ff
Koenigs Lamereille 471, 473
structural diagram 27ff
time 352
Differentiator 28, 69, 77
Distribution
Cauchy 784
exponential 784
Laplace 784
normal 710, 711, 713, 717, 719, 729, 731
Poisson 784
Rayleigh 784
uniform (rectangular) 717, 785
Disturbances 14, 15, 191, 192
external 38, 42, 54, 55, 127
unobservable 31
Duhamel integral 43
Duty factor 260, 328, 333
Dynamic programming 613, 649, 660

E

Element
asymptotic lead 110
complex linear 63
delay 98
elastic differentiating 78
elastic integrating 78
first-order 70
inertial (lag) 70ff
inertial-differentiating 75, 77, 105, 117
inertial-integrating 117, 118, 126
integrating 95
irrational 86, 91
lag-lead 77, 105, 115
Element
lead element 74, 109, 111, 115
linear 46, 47, 51, 53, 60, 142
minimal-phase 57, 59, 89, 104, 110, 113
multivariable 49
neutral 52
nonlinear 28, 29, 349, 354ff
nonminimal-phase 58, 64, 86, 104
oscillating 82, 83
play-type 363, 370
proportional 64, 65, 66, 117, 119, 129
pulse 266, 517, 518
quasi-inertial 89
saturation 357, 387
saturation with a dead zone 358
semi-inertial 95, 96, 98
semi-integrating 95
shaping 268, 293, 353, 517, 569, 570
simple 64
stable 57
standard 109
stop-type 365
threshold 356
transcendental 86
unilateral 42, 103, 397
unstable 86, 89, 90, 156
unstable quasi-inertial 90
Equilibrium 432, 539
neutral 425
unstable 430
Equilibrium state 56, 142, 353, 399, 405, 437
Equivalent circuit 66, 107, 108, 111, 136, 378, 575
Error 32ff
constant 207
digital 262
dynamic 196, 198, 243, 245, 329
forced 202, 203, 204
kinetic 194, 195, 196, 432
maximal 188
r.m.s. 188, 701f
static 188, 189, 190, 191, 192, 206
steady-state 188, 194, 738
Estimate
integral 229
linear integral 230, 232
quadratic integral 232, 233, 235 238
Euler equation 613ff
Euler technique 566, 571
Extremal 16, 593, 609, 613

F

Fanning 130ff
Feedback 103ff
  compensating 346
  differentiating 117
  integrating 117
  negative 115, 116, 140, 218, 387, 388, 546, 557
  nonlinear 390
  positive 115, 362, 387, 398
  proportional 116, 118, 253, 388
  proportional rate 412
  rate 255, 442, 466
Feedforward 103, 207
Figure of merit 195, 220, 432, 442
Filtration 700, 701
Flip-flop 350, 351, 516
Fourier series 43
Fourier transform 43, 270, 690
Frequency
  boundary 301
  carrier 66
  conjugation 247, 248, 251
  cutoff 219, 225f
  damping 226
  intersection 154, 158, 160, 165, 168, 502
  natural 85, 306
  oscillation 220
  passband boundary 301
  resonance 81, 84, 218, 226, 294
  sampling 261, 285
Function
Auto-correlation 679, 691, 692, 694, 729, 732
  closed-loop transfer 300
  correlation 662f
  cross-correlation 678f, 727f
  describing 486
  distribution 682
  inverse transfer 133
  irrational transfer 164
  Laguerre 698, 700, 777
  open-loop transfer 160
  pulse-transient 192
  switching 606, 610, 611
  transfer 46ff
  transient 46ff
  weighting 46ff
  δ-function 44, 70, 678, 693, 698, 711

G

Gain 64, 65, 115, 270, 391
  complex 46ff
  inverse complex 296, 331
Gain
  limit 153, 155, 162, 164, 165, 315, 316
  open-loop 247
Goal of control 14, 351

H

Hunting 762
Hurwitz determinants 147, 148, 149, 308
Hurwitz table 145, 147
Hysteresis 375
  negative 375, 377
  positive 376

I

Identification 696, 697, 773
Integrator 28, 66, 104f
Isochrones 650, 655, 657
Isocline 420f, 462, 480
Indices of performance 183, 189, 217, 330

L

Laplace image 50, 270
Laplace transformation table 99
Lienard technique 437, 451
Linearization
  harmonic 484f, 558, 559, 584, 732, 762
  statistical 732, 735, 736, 737, 738
  vibrational 367, 370, 502
Locus 47, 48, 96, 114, 152, 167, 314
  asymptotic root 173, 175, 177
  of the complex gain 65
  frequency 68, 82, 95, 111, 223
  frequency-gain 47, 48
  inverse 104, 106
  Mikhailov 151, 153
  root 170, 171, 173, 174

M

Margin
  gain 225, 226, 227
  gain-stability 330
  phase 225, 227, 244, 246, 247, 249, 579
  phase-stability 330
  stability 244, 331, 332
Method
  difference 566, 574
  of error coefficient 199, 232
  frequency 187, 217, 584

Method
Gauss-Seidel 754
gradient 752, 753
of harmonic linearization 558
indirect 217
of isoclines 434
Lyapunov's direct 537, 558
operator 187
of "passing solutions" 561
point transformation 470
root locus 170
simplex 760
steepest descent (ascent) 753
stochastic approximation 754
Misalignment 35, 185, 345, 563, 564
discrete 324
steady-state 186, 192, 329, 390
system 185, 192, 198
Model
adjustable 775
reference 773
Motion
continuous 536
disturbed 534
undisturbed 531, 532, 534
uniform 536
Multiplier 28, 370, 371

N

Noise 15, 129, 130
binary white 669, 697, 712, 777
Nonlinearities 337, 354, 356
deliberately introduced 345
inherent 338
multivalued 395, 549
single-valued 502, 549
static 397

O

Open-loop state 157, 166
Optimality index 746
Oscillation 762, 763
concealed 306
damped 423
diverging 306
free damping 226
near-harmonic 495
periodic 450
symmetrical 502
undamped 226, 439, 454, 599
Oscillation index 218f, 330, 331, 332, 584
Oscillator 81, 84, 106, 118, 119, 218, 226, 294
Overshoot 211, 220, 345, 609, 610

P

Performance 32, 330
control 217, 561, 584
transient 34, 40, 191, 221, 228, 229, 345
Phase portrait 446, 451, 452, 468, 497, 536, 562, 611
Phase space 405, 531, 540, 541, 655, 781
Phase trajectory 405ff
Plane
phase 85, 402ff
p-plane 53
root 170
Plant 14, 121, 351
multivariable 136
neutral 17
nonlinear 371
simple 18
stable 17, 20, 24, 26
two-variable 135, 136
unstable 17, 142
Point
breakaway 174, 175, 177
breaking 110
describing 406ff
sampling 260, 261, 286, 317, 318, 324, 334
singular 425f
Poles 49, 53, 55, 58, 61, 63, 89, 293
Principle
argument 150, 151, 156
maximum 613, 629, 631, 633, 648, 654, 660
of optimality 649, 652
superposition 44, 118, 243, 318, 563
Pulse
control 260, 266, 291, 294, 353
ideal 667
unit 286

R

Random 40
Random search 761
Reference shaft 39
Regulation 14
Regulators 13
Relay
three-positional hysteresisless 360
three-positional with hysteresis 363
two-positional hysteresisless 358, 361
two-positional with hysteresis 361

Response
amplitude-frequency 58, 100, 217, 218, 221, 223, 227
amplitude-phase 47, 90, 289, 314, 316
asymmetrical 355
asymptotic 73, 76, 80, 84, 97, 98, 108, 109, 111
asymptotic logarythmic amplitude-frequency 228
complementary 386, 387
complex frequency 47, 48
continuous 371
control 20, 21, 27
direct 74
dynamic 31, 354, 697
extremal 26, 349, 355, 745, 766
frequency 68ff
inverse 72, 74, 82, 87, 95, 96
ladder 349, 361
logarithmic 80, 110, 111, 163, 198
logarithmic amplitude-frequency 48, 58, 97, 244
logarithmic amplitude-phase 110
multivalued 363, 720, 721
nonlinear 369, 733
phase-frequency 58, 100, 227
piecewise-linear 355, 393
pulse 20, 22, 233
real frequency 209, 211, 213, 214
relay 719
saw-tooth 377
single-valued 720
sinusoidal 377
static 17, 192
stepwise 583
transient 24, 77, 211
Roots 51, 99, 143
complex 81, 171
complex-conjugate 417
multiple 51, 279
real 53
Rotation angle 39, 104, 126, 365
Rotation rate 40, 128
Routh table 145

S

Saddles 427, 433, 448, 470
Self-adjustment 14, 30, 33, 34, 41
Self-oscillations 337, 434, 513, 586
monoharmonic 506
nonsymmetrical 499
polyharmonic 558
stable 496
symmetrical 509, 513
Separatrix 429, 433, 450, 460
Setpoint 34, 139, 192, 200, 316, 391
Signal
feedback 115
harmonic 43, 82, 116
input 42, 46, 47, 60
output 42, 46, 47, 60
random 661, 716, 787
regular 42, 43
trial 354
Singular direction 427, 428, 429
Stability 40, 142, 243, 305, 409
in the large 532
in the small 532
in the whole 532, 540
of self-oscillations 531
absolute 542, 553, 555, 587
aperiodic 149
asymptotic 338, 421, 538, 539
of equilibrium 531
of nonlinear systems 530
orbital 532
oscillatory 149
structural 164
Stability boundary 154, 162, 167, 558
Stability region 179, 181
Stabilization 30, 31, 33, 41
State space 402, 404
Static deviation 330
Steady state 62, 183, 405
Switching lines 461f, 562, 606, 659
Synchronuous detection 748, 750, 751
System
adaptive 741, 742
astatic 194
automatic cotrol 14, 30
autonomous 531
closed-loop 30, 126, 214
closed-loop sampled-data 299
control 13ff
digital servo 261, 302, 348
dynamic 402, 440
extremal 750
feedback 735, 736, 737
limit 166
linear 44, 58, 690, 696, 734
minimal-phase 227, 228
neutral 164, 193
nonautonomous 536
nonlinear 40, 338, 716
null 41
open-loop 30, 130, 154, 158, 205, 206, 214, 226
optimal 185
piecewise-linear 454
program control 33
relay 35

System
sampled data 101, 276, 284
sampled-data extremal cotrol 352
sampled-data servo 526
searching 742, 762, 765
self-adjusting 771
self-learning 34
servo 32ff
speed-optimal 371
stable 160, 193
static 191, 205
unstable 160
variable structure 35, 347, 374, 468, 562

T

Taylor series 45
Theorem
of automatic control 14
of n intervals 638
central limit 711
delay 316
final value 195, 232
Kotelnikov 278, 574
limit value 190, 737
mean value 710
pulse 282
residue 282
Time
control 34, 186, 330
delay 25, 99, 573
limit delay 168, 169
Time constant 81, 107, 246, 269, 300, 574
Transformation
of structural diagrams 130
Transformation
direct Laplace 46, 54, 55, 56, 57, 123, 641
discrete Laplace 270
Gilbert 58
inverse Fourier 187, 208, 695
inverse Laplace 50, 76, 98, 189, 193, 641
structural 392, 587
z-transformation 270
Transient process 26, 62ff
Transition
negative 163
positive 163
Transposition 392

U

Unit
compensating (correcting) 35, 223, 586, 589, 590
computing 32
control 35
measuring 35, 36, 122, 123
regulating 14
setpoint 35
shaping 286

V

Variable
control 15, 19, 20, 37, 38, 54
cotrolled (output) 15f, 123, 128 129, 130, 184
observable 15, 19, 21
unobservable 15, 19, 21

Z

Zeroes 49, 57, 58, 63, 89, 100

TO THE READER

Mir Publishers would be grateful for your comments on the content, translation and design of this book. We would also be pleased to receive any other suggestions you may wish to make.

Our address is:
USSR, 129820, Moscow I-110, GSP
Pervy Rizhsky Pereulok, 2
MIR PUBLISHERS

Printed in the Union of Soviet Socialist Republics

OTHER BOOKS ON ELECTRICAL ENGINEERING FROM MIR PUBLISHERS

APPLIED ELECTRICITY FOR ENGINEERS

L. A. Bessonov, D. Sc.

A student-oriented book for courses in applied electricity and magnetism designed on a self-teaching approach. Contains over 200 worked-out problems in all topics covered, with the material so organized as to enable the student to master it with little assistance from instructor or tutor.
Coverage includes: d.c. and a.c. linear and non-linear circuits, sinusoidal steady-state performance, transient analysis, four-terminal networks and locus diagrams, elementary topology, complex frequency concept, Fourier and Laplace transforms, three-phase circuit analysis, electrostatic field, magnetism, electromagnetic induction, and electromagnetic radiation.

REMOTE CONTROL SYSTEMS

V. A. Ilyin, D. Sc.

A textbook providing a compact and systematic exposition of current ideas, techniques, and apparatus for remote checking and telecontrol. Suitable for courses in telemechanics. Will interest all who are engaged in the automation of production and development of means of automatic control. Describes methods and equipment for the automatic transmission of data in industrial systems, and presents the results of studies of optimal structures and coding. Much attention is paid to digital and combined control systems, and to their compatibility with digital computers.

Mir Publishers
Also Offer:

V. I. UTKIN
SLIDING MODES
AND THEIR APPLICATION
IN VARIABLE STRUCTURE
SYSTEMS

M. KOSTENKO
AND L. PIOTROVSKY
ELECTRICAL MACHINES
Vol. I and Vol. II

V. P. POLUKHIN
MATHEMATICAL SIMULATION
AND COMPUTER ANALYSIS
OF THIN-STRIP ROLLING
MILLS

The book has been written by a group of authors with the participation and under the general editorship of Professor Anatoly Netushil, D.Sc., Head of the Chair of Electrical Engineering and Electronics at the Moscow Institute of Fine Chemical Technology.

The principal lines of scientific activity of A. Netushil are electrical engineering and automation. He has written a number of monographs on high-frequency electrothermics. The monograph *High-Frequency Heating of Dielectrics and Semiconductors* has been published and reprinted in Russian and then published in Prague in Czech translation. The textbook on theoretical principles of electrical engineering *Analysis of Electric Circuits*, in which he is a co-author, has been published and reprinted in English by our House.

Professor Netushil is the author of over 180 contributions, he has about 20 patent author's certificates and is an Ho[illegible] Doctor of the Slovak Polytechnical Institute in Bratislava.